

2014

Space-time statistical analysis of malaria morbidity incidence cases in Ghana: A geostatistical modelling approach

Simon K. Appiah
Edith Cowan University

Follow this and additional works at: <https://ro.ecu.edu.au/theses>



Part of the [Bioinformatics Commons](#), [Immunology and Infectious Disease Commons](#), and the [Infectious Disease Commons](#)

Recommended Citation

Appiah, S. K. (2014). *Space-time statistical analysis of malaria morbidity incidence cases in Ghana: A geostatistical modelling approach*. <https://ro.ecu.edu.au/theses/1398>

This Thesis is posted at Research Online.
<https://ro.ecu.edu.au/theses/1398>

Edith Cowan University

Copyright Warning

You may print or download ONE copy of this document for the purpose of your own research or study.

The University does not authorize you to copy, communicate or otherwise make available electronically to any other person any copyright material contained on this site.

You are reminded of the following:

- Copyright owners are entitled to take legal action against persons who infringe their copyright.
- A reproduction of material that is protected by copyright may be a copyright infringement.
- A court may impose penalties and award damages in relation to offences and infringements relating to copyright material. Higher penalties may apply, and higher damages may be awarded, for offences and infringements involving the conversion of material into digital or electronic form.

**SPACE-TIME STATISTICAL ANALYSIS OF MALARIA
MORBIDITY INCIDENCE CASES IN GHANA:
A Geostatistical Modelling Approach**

SIMON KOJO APPIAH
MSc, BSc (Mathematics)

**A thesis
submitted in fulfilment of the requirements
for the award of**

DOCTOR OF PHILOSOPHY

**FACULTY OF HEALTH, ENGINEERING AND SCIENCE
EDITH COWAN UNIVERSITY,
WESTERN AUSTRALIAN**

AUGUST, 2014

USE OF THESIS

This copy is the property of Edith Cowan University. However, the literary rights of the author must also be respected. If any passage from this thesis is quoted or closely paraphrased in a paper or written work prepared by the user, the source of the passage must be acknowledged in the work. If the user desires to publish a paper or written work containing passages copied or closely paraphrased from this thesis, which passages would in total constitute an infringing copy for the purpose of the Copyright Act, he or she must first obtain the written permission of the author to do so.

ABSTRACT

Malaria is one of the most prevalent and devastating health problems worldwide. It is a highly endemic disease in Ghana, which poses a major challenge to both the public health and socio-economic development of the country. Major factors accounting for this situation include variability in environmental conditions and lack of prevention services coupled with host of other socio-economic factors. Ghana's National Malaria Control Programme (NMCP) risk assessment measures have been largely based on household surveys which provided inadequate data for accurate prediction of new incidence cases coupled with frequent incomplete monthly case reports. These raise concerns about annual estimates on the disease burden and also pose serious threats to efficient public health planning including the country's quest of reducing malaria morbidity and mortality cases by 75% by 2015.

In this thesis, both geostatistical space-time models and time series seasonal autoregressive integrated moving average (SARIMA) predictive models have been studied and applied to the monthly malaria morbidity cases from both district and regional health facilities in Ghana. The study sought to explore the spatio-temporal distributions of the malaria morbidity incidence and to account for the potential influence of climate variability, with particular focus on producing monthly spatial maps, delimiting areas with high risk of morbidity. This was achieved by modelling the morbidity cases as incidence rates, being the number of new reported cases per 100,000 residents, which together with the climatic covariates were considered as realisations of random processes occurring in space and/or time.

The SARIMA models indicated an upward trend of morbidity incidence in the regions with strong seasonal variation which can be explained primarily by the effects of rainfall, temperature and relative humidity in the month preceding incidence of the disease as well as the morbidity incidence in the previous months. The various space-time ordinary kriging (STOK) models showed varied spatial and temporal distributions of the morbidity incidence rates, which have increased and expanded across the country over the years. The space-time semivariogram models characterising the spatio-temporal continuity of the incidence rates indicated that the occurrence of the malaria morbidity was spatially and temporally correlated within spatial and temporal ranges varying between 30 and 250 km and 6 and 100 months, respectively. The

predicted incidence rates were found to be heterogeneous with highly elevated risk at locations near the borders with neighbouring countries in the north and west as well as the central parts towards the east. The spatial maps showed transition of high risk areas from the north-west to the north-east parts with climatic variables contributing to the variations in the number of morbidity cases across the country. The morbidity incidence estimates were found to be higher during the wet season when temperatures were relatively low whilst low incidence rates were observed in the warm weather period during the dry seasons.

In conclusion, the study quantified the malaria morbidity burden in Ghana to produce evidence-based monthly morbidity maps, illustrating the risk patterns of the morbidity of the disease. Increased morbidity risk, delimiting the highest risk areas was also established. This statistical-based modelling approach is important as it allows short-term prediction of the malaria morbidity incidence in specific regions and districts and also helps support efficient public health planning in the country.

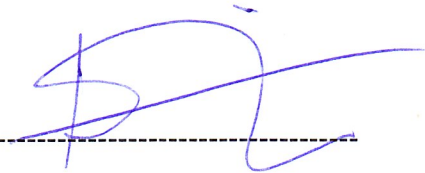
DECLARATION

I certify that this thesis does not, to the best of my knowledge and belief:

- (i) incorporate without acknowledgement any material previously submitted for a degree or diploma in any institution of higher education;
- (ii) contain any material previously published or written by another person except where due reference is made in the text; or
- (iii) contain any defamatory material.

I also grant permission for the Library at Edith Cowan University to make duplicate copies of my thesis as required.

Signed : _____



Date : _____

11/08/2014

ACKNOWLEDGEMENTS

The thesis has been accomplished with the support of and significant contributions received from many others. I am particularly most grateful to Edith Cowan University (ECU), Perth of Western Australia and Kwame Nkrumah University of Science and Technology (KNUST), Kumasi of Ghana for funding the research and also providing me with the necessary financial assistance for my living expenses whilst in Perth to undertake the research. I also acknowledge the staff of Centre for Health Information and Management (CHIM) of Ghana Health Service (GHS) who kindly assisted me for collection of the available malaria morbidity data in the national database without much difficulty and the Ghana Meteorological Agency (GMet) for the provision of the climatic data.

I am extremely indebted to my two supervisors, Associate Professor Ute Mueller and Associate Professor Jim Cross, who did not only guide me but also taught and encouraged me through to a successful completion of the research. I thank them for their constructive criticisms and comments coupled with the numerous useful suggestions which really helped improve the study.

Further thanks and appreciations go to all my colleagues and friends, both in Perth and Ghana for their moral and financial support. My special heart-felt gratitude goes to Derrick Asamoah Owusu, Dr. E. Prempeh and Professor I.K. Dontwi of Department of Mathematics, KNUST, who had always shown their concerns and kept the faith in me. I have also enjoyed the generous hospitality and good company of Henry Okrah, Dr. Patrick Aboagye-Sarfo, Francis Atta Kuranchie, Kwasi Frimpong and Eric Nimako Aidoo. Hey guys, my many thanks to you for your enormous support and encouragement whilst with you in Perth.

Finally to my family Esther, Bernard and Edwin, I could not have done it without their affectionate support. I acknowledge with deep gratitude the love and forbearance that sustained me throughout the study. Jack, my love, thanks and admiration cannot be rightfully expressed to you. I owe you so much. Boys, you have really been of great inspiration to me and I dedicate this thesis to you.

TABLE OF CONTENTS

Use of Thesis.....	ii
Abstract.....	iii
Declaration.....	v
Acknowledgements.....	vi
Table of Contents.....	vii
List of Tables.....	xi
List of Figures.....	xiii
Acronyms and Notations.....	xvii
CHAPTER 1: INTRODUCTION.....	1
1.1 BACKGROUND.....	1
1.1.1 Malaria Situation in Ghana.....	2
1.1.2 Malaria Transmission.....	5
2.2 MALARIA EPIDEMIOLOGICAL STUDIES.....	7
2.2.1 Spatial Epidemiology of Malaria.....	9
2.2.2 Methodological Approaches.....	11
2.2.3 Spatial Statistical Studies in Malaria.....	13
2.2.4 Time Series Analysis of Malaria Epidemics.....	15
2.2.5 Malaria Studies in Ghana.....	17
1.3 RESEARCH PROBLEM AND OBJECTIVES.....	21
1.4 THESIS OUTLINE.....	23
CHAPTER 2: SPATIAL AND TEMPORAL STATISTICAL MODELLING ...	26
2.1 INTRODUCTION.....	26
2.2 BASIC CONCEPTS OF SPATIAL ANALYSIS.....	27
2.2.1 Spatial Models.....	28
2.2.2 Types of Spatial Data.....	29
2.2.3 Stationarity and Spatial Dependency Measures.....	30
2.3 GEOSTATISTICAL SPATIAL ANALYSIS.....	31
2.3.1 Random Function and Stationarity Properties.....	33
2.3.2 Semivariogram and Covariance Functions.....	36
2.3.3 Permissible Models of Covariance and Semivariogram Function.....	38
2.3.4 Semivariogram Estimation and Fitting.....	42
2.3.5 Linear Model of Regionalisation (LMR).....	44
2.3.6 Modelling Coregionalisation.....	45
2.4 GEOSTATISTICAL SPATIAL OPTIMAL PREDICTION.....	51
2.4.1 Assumptions of Best Linear Estimators (BLUE).....	51
2.4.2 Ordinary Kriging.....	53
2.4.3 Ordinary Co-kriging.....	55
2.5 TIME SERIES ANALYSIS.....	57

2.5.1 Smoothing Techniques.....	58
2.5.2 Seasonal ARIMA Predictive Models	59
2.5.3 Box-Jenkins SARIMA Modelling	61
2.6 CHAPTER SUMMARY	63
CHAPTER 3: GEOSTATISTICAL SPACE-TIME ANALYSIS.....	64
3.1 INTRODUCTION.....	64
3.2 GEOSTATISTICAL SPACE-TIME MODELLING.....	65
3.2.1 Space-time Random Function (STRF).....	66
3.2.2 Space-time Covariance and Semivariogram	70
3.2.3 Space-time Permissible Models	73
3.2.4 Model Parameter Estimation.....	79
3.3 GEOSTATISTICAL SPACE-TIME KRIGING.....	81
3.3.1 Space-time Ordinary Kriging (STOK).....	82
3.3.2 Space-time Lognormal Ordinary Kriging (SLTOK).....	83
3.3.3 Space-time Ordinary Co-Kriging (STOCK)	84
3.3.4 Prediction Uncertainty and Accuracy	86
3.4 CONCEPTUAL MODELLING APPROACHES OF STRF	88
3.4.1 Modelling of Space-time Trend Component.....	89
3.4.2 Optimal Prediction of STRF	90
3.5 CHAPTER SUMMARY	90
CHAPTER 4: EXPLORATORY DATA ANALYSIS	92
4.1 INTRODUCTION.....	92
4.1.1 Study Area.....	92
4.1.2 Data Description.....	95
4.2 EXPLORATORY TIME SERIES ANALYSIS OF REGIONAL DATA	97
4.2.1 Descriptive Summary of Morbidity Data.....	97
4.2.2 Time Sequence Plots of MIR	101
4.2.3 Smoothing Analysis of MIR	105
4.3 EXPLOATORY ANALYSIS OF SPACE-TIME MIR DATA	111
4.3.1 Descriptive Summary of Space-time Data.....	112
4.3.2 Distribution of Space-time Data.....	113
4.3.3 Distribution of Climate Covariates	120
4.4 MULTIVARIATE REGRESSION ANALYSIS OF THE DATA	121
4.4.1 Multivariate Linear Regression Analysis of Regional Data	122
4.4.2 Correlation Analysis of Space-time Data.....	129
4.5 SEASONAL ARIMA MODELS OF GLOBAL MIR.....	131
4.5.1 Autocorrelation Analysis of the Detrended Incidence Rates	132
4.5.2 Multiplicative SARIMA Models of Malaria Incidence Rates	135

4.5.3 SARIMA Predictive Model Forecast of MIR and Validation	142
4.6 CHAPTER SUMMARY	146
CHAPTER 5: SPACE-TIME ANALYSIS OF THE MALARIA MORBIDITY	
INCIDENCE RATES	148
5.1 INTRODUCTION.....	148
5.2 ANALYSIS OF SPACE-TIME GLOBAL TREND MODEL OF MIR	150
5.2.1 Estimation of the Trend Model at District Locations	151
5.2.2 Regionalisation of Trend Model Coefficients.....	155
5.2.3 Estimation of Trend Surfaces of MIR.....	159
5.3 STRUCTURAL ANALYSIS OF MORBIDITY INCIDENCE RATES	162
5.3.1 Variography of Log-transformed Space-time MIR Data	162
5.3.2 Variography of Space-time Residuals	164
5.3.3 Product-Sum Semivariogram Modelling of MIR	166
5.3.4 Neighbourhood Selection for the Space-time Models	168
5.4 APPLICATIONS OF SPACE-TIME KRIGING TECHNIQUES TO	
MORBIDITY INCIDENCE RATES	170
5.4.1 Space-time Lognormal Ordinary Kriging of MIR	171
5.4.2 Space-time Ordinary Kriging of Residuals	174
5.4.3 Space-time Ordinary Kriging of Residuals using Product-Sum Model.....	177
5.5 SPACE-TIME PREDICTION OF THE MIR ACCOUNTING FOR	
CLIMATIC EFFECT	180
5.5.1 Interpolation of Climatic Covariates	180
5.5.2 Linear Coregionalisation Models of MIR with Climate	184
5.5.3 Neighbourhood Selection for LMC Semivariograms	188
5.5.4 Space-time Ordinary Co-kriging of MIR.....	189
5.6 COMPARISON AND VALIDATION OF KRIGING ESTIMATES	194
5.6.1 Summary Statistics of Kriging Estimates	194
5.6.2 Validation of Kriging Estimates	195
5.7 MALARIA MORBITY RISK IN BRONG AHAFO REGION	200
5.7.1 Estimation of Trend Surfaces of MIR.....	200
5.7.2 Space-time Ordinary Kriging of MIR.....	204
5.7.3 Validation of Kriging Estimates	208
5.8 MALARIA MORBITY RISK IN THE VEGETATION ZONE	209
5.8.1 Product-sum Semivariogram Models of MIR	209
5.8.2 Space-time Ordinary Kriging of MIR in the Northern Zone	212
5.9 CHAPTER SUMMARY.....	215
CHAPTER 6: CONCLUSIONS AND RECOMMENDATIONS.....	216
6.1 SUMMARY OF ANALYSIS AND FINDINGS	216

6.1.1 Seasonal Analysis of MIR at Regions	217
6.1.2 Structural Analysis of Space-time MIR at District Locations	218
6.1.3 Prediction of Space-time MIR at District Locations.....	219
6.1.4 Discussion of Results	221
6.2 LIMITATIONS	226
6.3 RECOMMENDATIONS FOR FURTHER WORK	227
6.4 CONTRIBUTIONS TO KNOWLEDGE.....	228
REFERENCES.....	231
APPENDICES	248

LIST OF TABLES

Table 4.2.1: Summary statistics of monthly morbidity incidence rates computed for the grand total cases including that of the males and females in the ten regions of Ghana	98
Table 4.2.2: Summary statistics of monthly morbidity incidence rates computed for the grand total cases of age group (0-4) years in the ten regions of Ghana	99
Table 4.2.3: Holt-Winters' smoothing parameters and model coefficients of malaria incidence rates for total and 0-4 year group in the regions	110
Table 4.3.1: Summary statistics for the sampled morbidity incidence rates at district-month locations for 2000-2010. Dataset involving cases reported on all districts in Ghana, only districts in Brong Ahafo Region and districts in each of the three vegetation zones are hereafter referred to as national, BAR and vegetation types (northern, forest and coastal), respectively	113
Table 4.3.2: Summary statistics for the seasonal morbidity incidence rates observed at the district-month locations for each calendar month during 2000-2010	113
Table 4.3.3: Summary statistics of the climatic covariates values obtained at the district-month locations over the whole study area in Ghana	120
Table 4.4.1: Cross-correlation analysis results of morbidity incidence rates (total) and their residuals with climatic covariates	124
Table 4.4.2: Cross-correlation analysis results of morbidity incidence rates for 0-4 year group and their residuals with climatic covariates	125
Table 4.4.3: Multiple regression analysis results for the detrended incidence rates (total) with climatic covariates at lags 0 and 1 in the regions. All predictor variables are retained at p – value < 0.05	127
Table 4.4.4: Multiple regression analysis results for the detrended incidence rates (0-4) with climatic covariates at lags 0 and 1 in the regions. All predictor variables are retained at p – value < 0.05	128
Table 4.4.5: Correlation analysis of residuals of the observed the morbidity incidence rates with the climatic covariates observed at the district-month locations over the whole the study area in Ghana	130
Table 4.5.1: Summary results of multiplicative SARIMA and SARIMAX predictive models of morbidity incidence rates (total) for the ten regions of Ghana with the potential exogenous variables(X); Also indicated are the AIC (and RMSE) values obtained for the models.....	137
Table 4.5.2: Summary results of multiplicative SARIMA and SARIMAX predictive models of morbidity incidence rates (0-4) for the ten regions of Ghana with the potential exogenous variables(X); Also indicated are the AIC (and RMSE) values obtained for the models.....	138
Table 4.5.3: Forecasted MIR values for 2011 (and 2012 for BAR), compared with the observed sample and measures of prediction accuracy for the regional (total) incidence rates data	143
Table 4.5.4: Forecasted MIR values for 2011 (and 2012 for BAR), compared with the observed sample and measures of prediction accuracy for the 0-4 year group incidence rates data	143
Table 5.2.1: Spatial semivariogram model parameters of the regionalised trend model coefficients of morbidity incidence rates for the national study involving all the district locations	156

Table 5.3.1: Space-time semivariogram model parameters of log-transformed malaria incidence rates data for the for the national study.....	164
Table 5.3.2: Space-time semivariogram model parameters of residuals of observed morbidity incidence rates for the national study.....	165
Table 5.3.3: Parameters of the marginal semivariograms and product-sum semivarigram models of the detrended and deseasonlised (residuals) of the observed morbidity incidence rates for the national study.....	167
Table 5.3.4: Cross-validation estimates of the semivariogram models for different moving neighbourhoods within a period of 5 months with number of samples per angular sector for national study area	169
Table 5.5.1: Parameters of space-time linear models of coreginalination of detrended morbidity incidence rates with lagged one month rainfall and maximum temperature for the national data set study	185
Table 5.5.2: Cross-validation estimates of the space-time ordinary co-kriging models for different moving neighbourhoods within a period of 5 months with number of samples per angular sector for national study area.	188
Table 5.6.1: Summary statistics of kriging estimates morbidity incidence rates together with their prediction standard deviations compared with the observed incidence data	195
Table 5.6.2: Prediction estimates for 2011 compared with the sample data and their measures of prediction accuracy in the national study.....	196
Table 5.7.1: Spatial semivariogram model parameters of the regionalised trend model coefficients of morbidity incidence rates for BAR	201
Table 5.7.2: Parameters of the marginal semivariograms and product-sum semivarigram models of the detrended malaria incidence rates (residuals) for the study in BAR.....	205
Table 5.7.3: Summary statistics of kriging estimates of morbidity incidence rates together with their prediction standard deviations compared with the observed incidence data	208
Table 5.7.4: Prediction estimates of MIR for 2011 compared with the sample data and their measures of prediction accuracy in BAR.	208
Table 5.8.1: Parameters of the marginal semivariograms and product-sum semivarigram models of the detrended morbidity incidence rates (residuals) for the vegetation zones	209

LIST OF FIGURES

Figure 1.1.1: Geographic distribution of malaria risk in the WHO endemic regions and malaria-free areas world-wide (Bell et al., 2006)	3
Figure 2.3.1: Relationship between semivariogram and covariance function (left) and the theoretical semivariogram showing the nugget effect, sill and the range which characterise spatial dependence of an attribute (right).....	36
Figure 4.1.1: Figure 4.1.1: Map of Ghana showing the ten administrative regions (left), and digital elevation model (DEM) of Ghana, obtained from IntraSearch (2011)	93
Figure 4.1.2: Data locations of study area (plus signs) indicating the three malaria epidemiological zones as classified by vegetation types (left map) (NMCP/GHS, 2009): northern savannah (N), tropical rainforest (F) and coastal and mangrove swamps (C); the map on the right shows the location of Brong Ahafo Region and its districts within Ghana (insert map)	94
Figure 4.2.1: Time sequence plots of morbidity incidence rates of grand total (black), male (green) and female (red) cases observed in the selected regions: Upper West and Northern (top), Brong Ahafo and Ashanti (middle) and Greater Accra and Central (bottom)	102
Figure 4.2.2: Time sequence plots of morbidity incidence rates of total (black), male (green) and female (red) cases observed for the 0-4 year age group in the selected regions: Upper West and Northern (top), Brong Ahafo and Ashanti (middle) and Greater Accra and Central (bottom)	103
Figure 4.2.3: Time sequence plots of morbidity incidence rates of grand total (black) and age groupings observed for the regions, Upper East and Northern (top); Brong Ahafo and Ashanti (middle); Greater Accra and Western (bottom) ...	104
Figure 4.2.4: 6-point and 12-point moving average smoothing of malaria incidence rates observed for the selected regions: Upper West and Northern (top), Brong Ahafo and Ashanti (middle) and Greater Accra and Western (bottom)	108
Figure 4.2.5: 6-point and 12-point moving average smoothing of morbidity incidence rates observed for the 0-4 year group f the selected regions: Upper West and Northern (top), Brong Ahafo and Ashanti (middle) and Greater Accra and Western (bottom)	109
Figure 4.2.6: Seasonal plots derived from Holt-Winter’s smoothing for the morbidity incidence rates (total, shown left) and 0-4 year group (left) for regions.....	110
Figure 4.3.1: Histograms of observed morbidity incidence rates (MIR) and logMIR for National (top) and Brong Ahafo Region (BAR) (bottom) data sets	114
Figure 4.3.2: Histograms of the observed morbidity incidence rates (MIR) and logMIR for the three vegetation zones, northern (top), forest (middle) and coastal (bottom)	115
Figure 4.3.3: Variogram map (left) and number of pairs (right) of the observed malaria incidence rates for the whole study area (national).....	116
Figure 4.3.4: Temporal profiles of the morbidity incidence rates superimposed with 6- and 12-point moving averages smoothing at some district locations selected across the study area, namely, BolgaM, TamaleM (northern); Berekum, ObuasiM (forest); Accra metropolitan area (AMA), NzemaE (coastal).....	117
Figure 4.3.5: Post-plots of monthly morbidity incidence rates distribution observed nationally at the sampled district locations for the selected months in 2010 (where Months 121–132 correspond to January to December)	118

Figure 4.3.6: Post-plots of monthly morbidity incidence rates distribution at the sampled locations in the Brong Ahafo Region for the selected months in 2010 (where Months 145–156 correspond to January to December)	119
Figure 4.3.7: Histogram of the observed climatic covariates values at the district-month locations over whole study area in Ghana	121
Figure 4 5.1: Time sequence and QQ plots (left), ACFs and PACFs (right) of residuals in Upper West, Northern (top), Brong Ahafo, Ashanti (middle), Greater Accra and Western (bottom) regions for regional total incidence rates	133
Figure 4 5.2: Time sequence and QQ plots (left), ACFs and PACFs (right) of residuals in Upper West, Northern (top), Brong Ahafo, Ashanti (middle), Greater Accra and Western (bottom) regions for the 0-4 year group	134
Figure 4 5.3: SARIMA model diagnostics of the incidence rates (total) by the Lyung_box Q-test indicating the standardised residuals (top), ACF of residuals (middle) and the p-values (bottom) for Upper West, Northern, Brong Ahafo, Ashanti, Greater Accra and Central regions	140
Figure 4 5.4: SARIMA model diagnostics of the incidence rates (0-4) by the Lyung_box Q-test indicating the standardised residuals (top), ACF of residuals (middle) and the p-values (bottom) for Upper West, Northern, Brong Ahafo, Ashanti, Greater Accra and Central regions	141
Figure 4 5.5: SARIMA model forecast of monthly incidence rates (total) for 2011–2013/2014 in Upper West, Northern, Brong Ahafo, Ashanti, Greater Accra and Central regions	144
Figure 4 5.6: SARIMA model forecast monthly incidence rates (0-4) for 2011–2013/2014 in Upper West, Northern, Brong Ahafo, Ashanti, Greater Accra and Central regions	145
Figure 5.2.1: Temporal profiles of the morbidity incidence rates superimposed with the estimated trend model (5.2.1) at some district locations selected across the study area, Bolgantaga and Tamale municipals in Northern zone, Berekum and Kumasi (KMA) in forest zone and Nzema East and Accra (AMA) in coastal zone	153
Figure 5.2.2: Base maps of coefficients of determination (r^2), being proportions of the observed incidence variations explained due to the basis functions (top left) and coefficients of the trend model (b_0, b_1, b_2, b_3 and b_4).....	154
Figure 5.2.3: Spatial experimental semivariograms (dotted green) with fitted variogram models of trend model parameters (coefficients) of the morbidity incidence rates for the national study.....	157
Figure 5.2.4: Spatial interpolated surfaces of trend model coefficients as computed by the optimal linear predictor (5.2.2)	158
Figure 5.2.5: Estimated trend surfaces of the morbidity incidence rates for the selected months: March, July, October and December (from top to bottom) for years 2000 (left), 2002 (middle) and 2004 (right).....	160
Figure 5.2.6: Estimated trend surfaces of the morbidity incidence rates for the selected months: March, July, October and December (from top to bottom) for years 2006 (left), 2008 (middle) and 2010 (right)	161
Figure 5.3.1: Space-time experimental semivariograms (dotted green) fitted with variogram models showing spatial (left) and temporal (right) autocorrelation of log-transformed morbidity incidence rates for national study	164
Figure 5.3.2: Space-time experimental semivariograms (dotted green) with fitted variogram models of residuals of observed morbidity incidence rates for national study	165

Figure 5.3.3: Marginal spatial and temporal semivariograms models (top) and space-time experimental semivariogram and its product-sum models (bottom) of detrended MIR (residuals) for the national study	167
Figure 5.4.1: Malaria morbidity incidence rates estimated by space-time log-normal ordinary kriging (STLOK) for the selected months March, July, October and December (from top to bottom) for years 2000 (left), 2002 (middle) and 2004 (right)	172
Figure 5.4.2: Malaria morbidity incidence rates estimated by space-time lognormal ordinary (STLOK) for the selected months March, July, October and December (from top to bottom) for years 2006 (left), 2008 (middle) and 2010 (right).in 2000 (left) and 2005 (right).....	173
Figure 5.4.3: Malaria incidence rates estimated by the space-time ordinary kriging of residuals (STROK) for the selected months March, July, October and December (from top to bottom) for years 2000 (left), 2002 (middle) and 2004 (right)	175
Figure 5.4.4: Malaria incidence rates estimated by space-time ordinary kriging of residuals (STROK) for the selected months March, July, October and December (from top to bottom) for years 2006 (left), 2008 (middle) and 2010 (right)	176
Figure 5.4.5: Malaria incidence rates estimated by the product-sum modelling of residuals (STOK_PS) for the selected months March, July, October and December (from top to bottom) for years 2000 (left), 2002 (middle) and 2004 (right)	178
Figure 5.4.6: Malaria incidence rates estimated by the product-sum modelling of residuals (STOK_PS) for the selected months March, July, October and December (from top to bottom) for years 2006 (left), 2008 (middle) and 2010 (right)	179
Figure 5.5.1: Spatial maps of rainfall for March, July, October and December in 2000, 2005 and 2010.....	182
Figure 5.5.2: Spatial maps of maximum temperature for March, July, October and December in 2000, 2005 and 2010	183
Figure 5.5.3: Space-time linear model of coregionalisation of detrended morbidity incidence rates (residuals) with lagged one month rainfall showing spatial (top) and temporal (bottom) correlations for the national study.....	186
Figure 5.5.4: Space-time linear model of coregionalisation of detrended malaria incidence rates (residuals) with maximum temperature showing spatial (top) and temporal (bottom) correlations (bottom) for the national study.....	187
Figure 5.5.5: Selected monthly spatial maps of morbidity incidence rates estimated by space-time ordinary cokriging, incorporating the effect of rainfall lagged one month (STOCK_Rain) for 2000-2004	190
Figure 5.5.6: Selected monthly spatial maps of morbidity incidence rates estimated by space-time ordinary cokriging, incorporating the effect of rainfall lagged one month (STOCK_Rain) for 2006-2010	191
Figure 5.5.7: Selected monthly monthly spatial maps of malaria incidence rates estimated by space-time ordinary cokriging (STOCK_MaxT), incorporating the effect of maximum temperature 2000-2004	192
Figure 5.5.8: Selected monthly monthly spatial maps of malaria incidence rates estimated by space-time ordinary cokriging (STOCK_MaxT), incorporating the effect of maximum temperature 2006-2010	193

Figure 5.6.1: Posting of the observed morbidity incidence rates (left) compared with the trend with periodic cycles (as shown in the middle) and STROK (right) estimates.....	197
Figure 5.6.2: Posting of the observed morbidity incidence rates (left) compared with STLOK (middle) and STOK_PS (right) estimates	198
Figure 5.6.3: Posting of the trend (without period cyclest) of the observed malaria incidence rates (left) compared with STOCK_MaxT (middle) and STOCK_Rain (right) estimates	199
Figure 5.7.1: Estimated trend surfaces of the morbidity incidence rates for the selected Months: March, July, October and December in 2000, 2004	202
Figure 5.7.2: Estimated trend surfaces of the morbidity incidence rates for the selected Months: March, July, October and December in 2008 and 2010	203
Figure 5.7.3: Marginal spatial and temporal semivariogram models of the residuals incidence rates (top) and space-time experimental semivariogram surfaces together with their product-sum models (bottom) for the study in Brong Ahafo Region.....	205
Figure 5.7.4: Monthly spatial maps of malaria morbidity risk estimated by space-time ordinary kriging by the generalised product-sum modelling of residuals (STROK_PS) in BAR for some selected months in 2000 and 2002.....	206
Figure 5.7.5: Monthly spatial maps of malaria morbidity risk estimated by space-time ordinary kriging by the generalised product-sum modelling of residuals (STROK_PS) in BAR for some selected months in 2008 and 2010.....	207
Figure 5.8.1: Marginal spatial and temporal semivariogram models of the residuals (top) and space-time experimental semivariogram surfaces together with their product-sum models (bottom) for the northern and forest zones	210
Figure 5.8.2: Marginal spatial and temporal semivariogram models of the residual (top) and space-time experimental semivariogram surfaces together with their product-sum models (bottom) for the coastal	211
Figure 5.8.3: Monthly spatial maps of malaria risk estimated by space-time ordinary kriging by the generalised product-sum modelling of residuals (STROK_PS) in northern zone for some selected months in 2000 and 2002	213
Figure 5.8.4: Monthly spatial maps of malaria risk estimated by space-time ordinary kriging by the generalised product-sum modelling of residuals (STROK_PS) in northern zone for some selected months in 2008 and 2010	214

ACRONYMS

ACF	Autocorrelation function
ACT	Artemisinin (or artesunate-based) combination therapy
AIC	Akaike information criterion
S(ARIMA)	Seasonal (Autoregressive moving average)
BAR	Brong Ahafo Region
BLUE	Best linear unbiased estimator
BHM	Bayesian hierarchical modelling
CHIM	Centre for Health Information and Management
DEM	Digital elevation model
DHS	Demographic Health Survey
GHS	Ghana Health Services
GLM	Generalised linear models
GMet	Ghana Meteorological Agency
GPS	Generalised product-sum
GSS	Ghana Statistical Service
IS	Intrinsic stationary
ITN	Insecticide treated nets
LMC	Linear model of coregionalisation
MAE	Mean absolute error
MAP	Malaria Atlas Project
MARA	Mapping Malaria in Africa
ME	Mean error
MEWS	Malaria early warning system
MICS	Multiple Indicator Cluster Survey
MDG	Millennium Development Goals
MIR	Morbidity incidence rates
MLE	Maximum likelihood estimation
NMCP	National Malaria Control Programme
PACF	Partial autocorrelation function
STRF	Space-time random function
SK	Simple kriging
OCK	Ordinary kriging
OLS	Ordinary least squares
OK	Ordinary co-kriging
OPD	Outpatient Department
RBM	Roll Back Malaria
RF	Random function
RMSE	Root mean squared error
SEA	South-East Asia
SSA	Sub-Saharan African
SOS	Second order stationary
STLOK	Space-time lognormal ordinary kriging

STOK	Space-time ordinary kriging
STOCK	Space-time ordinary co-kriging
STROK	Space-time residuals ordinary kriging
UTM	Universal Transverse Mercator
WHO	World Health Organisation

NOTATIONS

\mathbf{u}	Spatial referenced location
\mathbf{D}	Spatial domain (study area)
\mathbf{T}	Time domain (time period)
\mathbf{h}	Spatial lag separation vector
$Z(\mathbf{u})$	Spatial random variable
$\{Z(\mathbf{u}) : \mathbf{u} \in \mathbf{D}\}$	Spatial random function or field
$C(\mathbf{h})$	Spatial covariance function value at spatial lag \mathbf{h}
$\hat{C}(\mathbf{h})$	Experimental spatial covariance function value at spatial lag \mathbf{h}
$C(\mathbf{0})$	Covariance function a lag value $\mathbf{0}$ (variance of $Z(\mathbf{u})$)
$\gamma(\mathbf{h})$	Spatial semivariogram value at spatial lag separation distance \mathbf{h}
$\hat{\gamma}(\mathbf{h})$	Experimental spatial semivariogram value at spatial lag \mathbf{h}
(\mathbf{u}, t)	Space-time referenced location
$\mathbf{D} \times \mathbf{T}$	Space-time domain (study area over time period)
(\mathbf{h}_s, h_t)	Space-time covariance function value at separation lag vector (\mathbf{h}_s, h_t)
$C(\mathbf{0}, 0)$	Spatio-temporal (global) sill
$Z(\mathbf{u}, t)$	Space-time random variable
$\{Z(\mathbf{u}, t) : (\mathbf{u}, t) \in \mathbf{D} \times \mathbf{T}\}$	Space-time random function (\mathbf{h}_s, h_t) on or field
$\{Z(\mathbf{u}_\alpha, t_j) : \alpha = 1, 2, \dots, n; j = 1, 2, \dots, T\}$	Space-time observed data at locations (\mathbf{u}_α, t_j)
$\hat{Z}(\mathbf{u}, t)$	Estimates of the data at unobserved location (\mathbf{u}, t)
$n(\mathbf{h})$	Number of data pairs separated by the lag vector \mathbf{h}
$n(\mathbf{h}_s, h_t)$	Number of data pairs separated by space-time lag vector (\mathbf{h}_s, h_t)
$\gamma(\mathbf{h}_s, h_t)$	Space-time semivariogram
$\hat{\gamma}(\mathbf{h}_s, h_t)$	Experimental space-time semivariogram
$MC_t(\mathbf{u}_\alpha)$	Malaria morbidity cases reported from district/region α for month t
$I_t(\mathbf{u}_\alpha)$	Malaria incidence rates observed at district/region α for month t
$\{I(\mathbf{u}, t) : (\mathbf{u}, t) \in \mathbf{D} \times \mathbf{T}\}$	Malaria incidence rates in the space-time domain
$\{I(\mathbf{u}_\alpha, t) : \alpha = 1, 2, \dots, n; t = 1, 2, \dots, T\}$	Space-time (district-month) malaria incidence rates
$\hat{I}(\mathbf{u}, t)$	Estimate of the malaria incidence rates at unobserved location (\mathbf{u}, t)

Chapter 1

Introduction

1.1 Background

Malaria is a mosquito-borne infectious disease which is one of the most prevalent and devastating health problems worldwide, particularly in Sub-Saharan Africa (SSA) and South-East Asia (SEA). It has wide global distribution, although its risk and disease burden have always been geographically specific and biased towards SSA (Chatterjee & Sarkar, 2009; Gallup & Sachs, 2001; Okafor & Amzat, 2007; WHO, 2008). Approximately half of the world's population (3.3 billion) is exposed to the risk of malaria transmission; currently, the World Health Organisation (WHO) considers 104 countries and territories to be malaria endemic and has classified them into six endemic regions, namely, African; Americas, European, South-East Asia, Eastern Mediterranean and Western Pacific (WHO, 2011, 2012). Bell, Wongsrichanalai, and Barnwell (2006) provide the spatial distribution pattern of malaria risk in 109 countries and territories in endemic regions, as shown in Figure 1.1.1. It is estimated that globally, there are 200–300 million new clinical cases and 0.655–1.238 million deaths annually; about 80% of the new cases and 90% of the deaths occur in developing countries in the WHO-African region, with children under five years of age and pregnant women being the most severely affected (Cibulskis, Aregawi, Williams, Otten, & Dye, 2011; Cibulskis et al., 2007; Hay et al., 2010; Murray et al., 2012; WHO, 2008, 2011, 2012). According to the World Malaria Report 2011, India, which is in the second highest endemic region (SEA), together with six other African countries (Nigeria, Democratic Republic of the Congo, Tanzania, Uganda, Mozambique and Cote d'Ivoire) accounts for nearly 60% of the estimated total malaria disease case-burden; however, Nigeria and the Democratic Republic of the Congo account for over 40% of the global deaths (WHO, 2011).

In SSA, malaria is the single most important infectious disease in children, causing 25% of all childhood deaths (Chatterjee & Sarkar, 2009; Goodman, Coleman, & Mills, 2000; WHO, 2003). Pregnant women are particularly susceptible to the disease and malaria during pregnancy often causes severe anaemia, miscarriage, stillbirth, and maternal death. In most endemic countries, malaria may account for up to 40% of

preventable low birth weight cases among new-borns (Brabin, 1991; Guyatt & Snow, 2004), and is the greatest risk factor for neonatal death (McCormick, 1985; Schantz-Dunn & Nawal, 2009; Steketee, 2001).

Doubts are often expressed about the reliability of estimates for the high-burden SSA countries which lack credible reporting systems and facilities for diagnostic analysis of cases of the disease. Often reports of incidence of morbidity and death cases are based on the clinically diagnosed treatments in only the public sector facilities (Agyepong & Kangeya-Kayonda, 2004; Cibulskis et al., 2011; Doudou et al., 2012; WHO, 2012), and these limitations tend to affect progress in the global fight against malaria. Malaria interventions in Africa face challenges due to the complexity of the disease and lack of effective development of comprehensive strategies, especially in the high prevalence areas. These contributed to the failure of the earlier global effort in the 1950's to eradicate the disease in the region (AMMREN, 2008) and still seriously impede the slow socio-economic progress as malaria still remains a leading cause of morbidity and mortality (Okafor & Amzat, 2007; Okorosobo, Okorosobo, Mwabu, Orem, & Kirigia, 2011; WHO, 2008, 2012). The current renewed efforts, unlike the previous attempts in the continent, make use of new tools such as insecticides, medications and vaccines as well as effective health care systems coupled with massive support of the community and international development partners. These eradication programmes have been greatly enhanced by Roll Back Malaria (RBM), a global partnership initiated by WHO, UNDP, UNICEF and the World Bank in 1998. RBM seeks to work with governments, other development agencies including, non-governmental organisations (NGOs) and private sector companies to reduce the human and socio-economic burden of malaria by 75% by the year 2015, using 2010 as the baseline (UNICEF, 2008; WHO, 2011). Using Ghana as a case study, this study is undertaken to estimate the malaria morbidity incidence cases and to describe its distribution pattern over space and time.

1.1.1 Malaria Situation in Ghana

In Ghana, malaria is not only the burden of the health sector but it also permeates every aspect of the social as well as economic lives of her people (GHS, 2011). The entire population is at risk of the disease (WHO, 2012) with the most vulnerable being children under 5 years of age and expectant mothers who together account for 20% of the population (GHS, 2011; NMCP/GHS, 2010). Malaria is the leading cause of both

Global Distribution of Malaria Risk

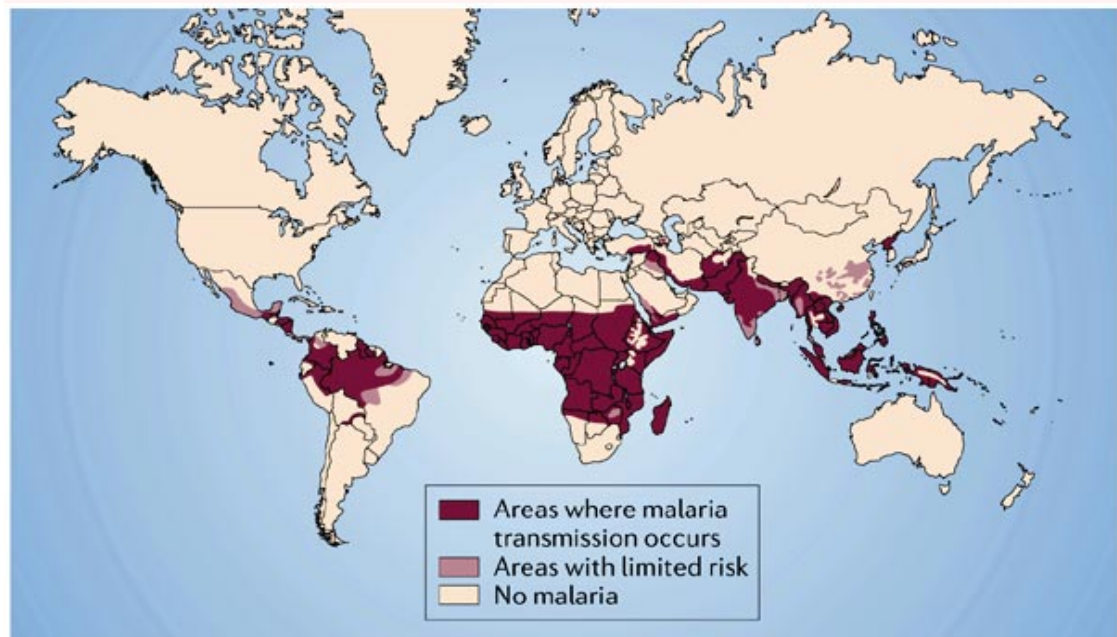


Figure 1.1.1: Geographic distribution of malaria risk in the WHO endemic regions and malaria-free areas world-wide (Bell et al., 2006).

morbidity and mortality cases in Ghana, accounting for about 38% of all out-patient illness, 36% of all admissions, and 33% of all deaths in children under 5 years (GHS, 2007, 2011; NMCP, 2008; PMI, 2009, 2012; WHO/UNICEF, 2005). Between 3 and 4 million clinical cases of malaria per year have variously been reported by public health centres or estimated over the period 2000–2011 of which nearly 1 million cases are children of less than 5 years of age (GHS, 2011; WHO, 2008, 2012). The World Malaria and Ghana Health Service (GHS) annual reports estimate that up to 20,000 children under 5 years die from malaria in Ghana each year, and in the case of pregnant women, out of the total number of those reporting at health institutions (GHS, 2007; WHO, 2008; WHO/UNICEF, 2005), 13.8% suffer from malaria and 9.4% of deaths in pregnant women are a result of the disease (GSS, NMIMR, & Macro, 2004a). Other major effects of the malaria burden in Ghana include poverty, low productivity, school and work absenteeism, and high treatment cost. It is also the leading cause of workdays lost due to illness, contributing more to potential income loss than any other disease (NDPC & IMF, 2005; Okorosobo et al., 2011). It was also found that about 50% of Ghanaians spend money on mosquito control products such as coils, sprays, fly proof nets and mosquito repellent whilst almost every household spends money on the curative treatment of malaria (GSMF, 2004). Several factors which account for this worrisome state of affairs may include poor environmental conditions (Chinery,

1999b); inappropriate medication and lack of adequate medical care to manage cases; access to effective treatment and prevention services; climate variability; and a host of socio-economic factors (NMCP, 2007; NMCP/GHS, 2009; RBM/NMCP/GHS, 2010).

Prompt access to effective treatment of malaria saves lives and is critical element of malaria control (WHO/UNICEF, 2003). Ghana perceives the principles of the WHO global effort to combat malaria, the RBM Initiative, as being consistent with the overall goal of the National Malaria Control Strategy 2008-2015 (NMCP/GHS, 2010). The initiative seeks to reduce malaria morbidity and mortality by 75% by 2015 through improved prevention, better access to care (early detection and rapid treatment of cases), higher quality and efficiency in service delivery, and increased partnership in the context of overall sector-wide development. Thus, Ghana is to facilitate human development by reducing the malaria disease burden in the country by 75% (using 2010 as baseline) through overall health sector development, improved strategic investments in malaria control, and increased coverage of malaria treatment and prevention interventions, especially at the community level. The principles also accord with the objectives of the medium term health strategy of the Ministry of Health (MOH): increasing access, improving quality and efficiency in service delivery and building partnerships in the context of overall sector-wide development (RBM/NMCP/GHS, 2010). The National Malaria Control Programme (NMCP) of the Ghana Health Service (GHS) spearheads the campaign against malaria. Its malaria control interventions include: case management at health facility and community levels, using artemisinin-based combination therapies (ACTs) as first line treatment of uncomplicated cases due to the increasing resistance of the chloroquine; personal protection including chemoprophylaxis in pregnancy; and environmental management through the use of insecticide treated nets (ITNs) and indoor residual spraying (IRS), which are implemented essentially in an integrated fashion.

Malaria has been identified as the national priority disease for control in the medium term policy. However, the coverage of malaria control in the country has been constrained by limited geographical and financial access to basic health services in both public and clinical cure services; inadequate funding of health services; inefficient allocation of resources; and poor community, intersectional and private sector participation. In spite of the partnerships with the RBM and other donors, including the Global Fund, President's Malaria Initiative (PMI), UNICEF and World Bank, to

mobilise resources and rapidly scale-up these intervention activities, the number of new incidence cases being reported annually is alarming (GHS, 2011; WHO, 2012). Ghana's NMCP and WHO annually present reports evaluating these multi-interventional activities toward the malaria reduction burden. This study among others, seeks to provide information for independent assessment of the likelihood for achieving the set target by 2015 through seasonal forecast of the malaria morbidity incidence cases, and also contribute to knowledge on malaria prevalence in Ghana, stimulating further research.

1.1.2 Malaria Transmission

Malaria is the most wide-spread vector-borne disease mainly transmitted through the bites of female *Anopheles* mosquitos, one of the most capable vectors which feed on human blood. The disease is caused by five species of *Plasmodium* protozoa, namely *Plasmodium falciparum*, *Plasmodium vivax*, *Plasmodium ovale*, *Plasmodium malariae* and *Plasmodium falciparum knowlesi*, which infect the human hosts alternatively. Among these species, *Plasmodium falciparum* accounts for the majority of the infections and is by far the most lethal, accounting for almost all malaria deaths and more than 90% of child mortality in SSA (Chatterjee & Sarkar, 2009; Crawley, Chu, Mtove, & Nosten, 2010; Holding & Snow, 2001; WHO, 2012; WHO/UNICEF, 2003). There are many species of *Anopheles* mosquitoes which transmit to human hosts; some feed indoors, some outdoors and others almost exclusively on humans, making them effective malaria vectors; whilst others feed on a number of different vertebrate hosts making them less effective vectors. Each mosquito species has its own breeding site preferences and will respond differently to changing environmental conditions. *Anopheles gambiae*, *Anopheles arabiensis* and *Anopheles funetus* are the most common species, which dominate the SSA landscape and transmit to mostly humans. However, *Anopheles gambiae* is the primary malaria vector; this is attributed to its relatively long life, and strong tendencies to target humans for blood meals and to enter and rest inside houses of would-be victims. The adult mosquitoes emerge to feed at night and their larvae tend to develop in relatively clean temporary bodies of water such as those typically found near agricultural sites, empty containers (cans, tins, tyres, etc.), trees trunks, pools or excavations, drainages or flooded areas. Increased rainfall creates standing waters that favour these *Anopheles* mosquitoes, making them successful vectors (Coetzee, Craig, & le Sueur, 2000; Holt, 2002). However, heavy

down pour of rain tends to sweep away and kills the mosquito larvae to reduce transmission of the disease (Huang, Zhou, Zhang, Wang, & Tang, 2011).

In Ghana, the proportions of people who test positive for malaria parasites in survey areas (crude parasite rates) range from 10 to 70%; *Plasmodium falciparum* accounts for 85–90% of all malaria infections including health life-years lost whilst approximately 10–15% of the infections can be attributed to *Plasmodium malariae* and *Plasmodium ovale* (Crookston et al., 2010; MICS, 2006, 2011). The major vectors include *Anopheles gambiae* complex and *Anopheles funestus* which are commonly found respectively in the rural and peri-urban areas; *Anopheles melas* and *Anopheles arabiensis* are also found in the mangrove swamps of the south-west and in savannah areas of northern Ghana (de Souza, Kelly-Hope, Lawson, Wilson, & Boakye, 2010; NMCP/GHS, 2009). The numerous factors which may increase transmission can be classified as natural and man-made. Both are principally linked or led to environmental changes such like ecological, societal, economical and political (Reiter, 2008), which favour the vectors that transmit the malaria parasite. Human activities such as poor sanitation environment, irrigation and urbanisation can lead to predictable increases in malaria transmission. In contrast, climatic variations, natural disasters, and other disturbances can lead to unexpected outbreaks; sometimes, these changes are accompanied by large-scale population movements which may also foster epidemics (Baragatti et al., 2009; Montalvo & Reynal-Querol, 2007; Small, Goetz, & Hay, 2003). This often happens, for example, during civil wars when health services degrade, surveillance within the control services becomes deficient and control measures are lacking (Montalvo & Reynal-Querol, 2007; Tumwiine, Mugisha, & Luboobi, 2010).

Studies have strongly linked malaria to poverty as estimated incidence rates are highest in countries with a lower gross national income (GNI) per capita (Gallup & Sachs, 2001; Sachs & Malaney, 2002). The majority of people in such countries, whose daily income is less than 1.25 US dollars are not only at increased risk of malaria infection or death, but they are also unable to afford preventive measures or seek prompt effective treatment (Adams, Darko, & Accorsi, 2004; Lynch & Hewitt, 2012; WHO, 2012). They usually live in rural settlements where the transmission risk is higher. Malaria episodes often result in significant direct and indirect costs for households and financial constraints for the poor. As there is a vicious cycle between malaria and poverty, lowering the malaria burden yields positive economic benefits at the

household level, improved living standards and increased overall household income (Gallup & Sachs, 2001; Lynch & Hewitt, 2012). Binka et al. (1996) studied the Kassena-Nankana district in the Upper East Region, one of the most deprived of areas in Ghana with high mortality and morbidity rates. They found that the cost of malaria treatment was 34% of the income of poor households whilst it was just 1% of the income of the rich. This supports the fact that access to health services in Ghana is also affected by the “inverse care law” in which people with the greatest overall needs for health care (that is, socially and economically deprived persons) are the least able to obtain it (Hart, 1971; Watt, 2002), a well-known concept in Economics. The estimation of morbidity and mortality of malaria attributable to a single cause may be complicated by its interrelationship with other diseases like anaemia and HIV (Crawley et al., 2010; Sachs & Malaney, 2002). However, anaemia may also be related to several causes including iron deficiency and malnutrition. Age and gender related analysis may also become useful for assessing the possible associations between diseases which tends to show overlapping morbidity patterns. In Ghana, both high peaks of malaria and anaemia in childhood and low incidence cases in older age groups have been reported (Adams et al., 2004; GHS, 2007), thus supporting the hypothesis that anaemia incidence cases are mainly related to malaria in Ghana.

As a result of the severe health and socio-economic cost of malaria both globally and nationally, there is growing interest in epidemiological modelling of the disease. Modelling infectious diseases such as malaria provides a tool to study the mechanisms by which they occur (Daley & Gani, 2005). Various methodologies have been developed for determining the potential risk factors and areas for estimating the disease’s burden. These studies have been conducted worldwide and at continental, national and local levels, yielding different spatial and temporal distribution patterns of the malaria incidence. They also establish the most favourable risk factor(s) responsible for the increased episodes of the disease in each case. A review of such studies is presented in section 1.2. This study will be limited to estimating malaria morbidity burden in space and time accounting for climatic environmental conditions.

1.2 Malaria Epidemiological Studies

Mathematical modelling has contributed immensely to epidemiological studies of malaria by providing insight into the dynamics of malaria transmission and thus

helping with devising effective interventions (Anderson & May, 1991; Mabaso, 2007; McKenzie & Samba, 2004; Murray et al., 2012; Tumwiine et al., 2010; WHO, 2012). Following the first descriptions of the malaria parasite and its life cycle by Sir Ronald Ross in 1897, several mathematical models were developed for malaria transmission. Ross (1855) cited by McKenzie and Samba (2004) described a mathematical model as an abstract way of representing ideas about the underlying mechanisms and interactions that generate the phenomena being investigated. These mathematical models not only helped with understanding the malaria transmission, but also improved the vectorial control strategies by describing the propagation of the disease using the rate at which susceptible members of a population become infected, and the recovery of infected members. They focus on the basic reproductive rate (r_0), the expected number of individuals (secondary cases) caused by an infected individual in a population that has no immunity to the disease, where the disease spreads if $r_0 > 1$ and declines if $r_0 < 1$. In this way, many of the models assist in the design of malaria intervention programmes, providing useful understanding of the complexity of the disease such as predicting future outbreaks and also evaluating strategies to control such epidemics (Buckee & Gupta, 2009; Daley & Gani, 2005; Gaudart et al., 2009; Reiner et al., 2013).

Mathematical modelling now plays a key role in policy making, including health-economic aspects; emergency planning and risk assessment; control-programme evaluation; and monitoring of surveillance data. In research, it is essential in study design, inferential analysis (such as parameter estimation and hypothesis testing) and interpretation for implementation. Public health and pharmaceutical industry professionals, policy makers and infectious disease researchers increasingly need to understand the transmission pattern and to interpret and critically evaluate both epidemiological data, and the findings of mathematical modelling studies. Recently, several statistical models have been developed and applied to malaria risk predictions as herein reviewed in the chapter. They include the generalised linear regression (GLR) models, seasonal autoregressive integrated moving average (SARIMA) models (for time series forecasting) and space-time statistical models (using geostatistical analysis). The SARIMA and geostatistical space-time statistical models, as applied in this thesis, can also incorporate risk factors such as environmental (including climatic conditions), socio-economic, biological, demographical, anthropogenic (land use)

change, population movement, and poverty related issues or variables as the main determinants of malaria risk. In this study, the focus will be on the potential effect of the climatic covariates of rainfall, temperature and relative humidity on malaria morbidity incidence cases in Ghana as justified by the following review of the literature.

1.2.1 Spatial Epidemiology of Malaria

The malaria disease is preventable and curable. However, in order to prevent or cure the disease in the context of its epidemics in most endemic areas such as the Sub-Saharan African (SSA) including Ghana, decision-makers need to be aware of the risk of epidemic occurring in space and time. Specifically, it is necessary to identify the geographic locations, or areas under their jurisdiction, and the time, when malaria epidemics are most likely to occur (Thomson & Connor, 2001). Spatial epidemiology is the study of the geographical (spatial) distribution of the incidence of a disease and its association with some potential risk factors (Bailey, 2001; Beale, Abellan, Hodgson, & Jarup, 2008). This research field dates back to 1855 with the seminal work of Snow (1855) who mapped the incidence of cholera cases and found that contaminated water caused most of the cases in London (Bingham, Verlander, & Cheal, 2004; Gemperli, 2003). The incidence of malaria varies with the geographical location and time or season if not both. Spatial statistical modelling of the disease can identify areas of high risks (“hot spots”) and assess potential ecological or environmental and socio-economic risk factors which can explain the incidence variations in space and by time. Exploring the relationship between malaria incidence and environmental changes allows prediction of the impact that environmental changes have on malaria risk, including the effect of the global warming and human activities (such as farming, urbanisation, dam construction and irrigation). The environmental impact on malaria provides important information for effective malaria control, focusing not only on the parasite directly, but also on the mosquito vector and its living conditions (de Souza et al., 2010; Gemperli, 2003).

Studying the spatial and temporal distributions of malaria incidence provides better understanding of the crucial questions faced in the health sector of many developing economies. This is often accomplished by applying statistical methods to data collected during disease surveillance and generating a map that describes the variations in risk of the disease in space and by time (Appiah, Mueller, & Cross, 2011; Osnas,

Heisey, Rolley, & Samuel, 2009; Snow, Guerra, Noor, Myint, & Hay, 2005; Zacarias & Anderson, 2011). Thus, spatial statistics provides tools for analysing spatially and/or temporally distributed data by capitalising on the correlation between observations to interpolate the attribute of interest and to delineate areas with high disease risk. A powerful tool of spatial technology that has revolutionised epidemiological research is the geostatistical technique of kriging which is used for making predictions at unobserved locations. Its extensive application in malaria epidemiology has facilitated quantification of spatial features of the disease's transmission to allow its spatial interpolation within the environment (Gething et al., 2007; Gething et al., 2008; Saxena, Nagpal, Srivastava, Gupta, & Dash, 2009). However, its application in malaria control in the WHO African region has been limited.

Geostatistics is a branch of spatial statistics which consists of a set of techniques for analysing and predicting values of a variable distributed in space or time (Ali et al., 2006; Carrat & Valleron, 1992; Webster, Oliver, Munir, & Mann, 1994). Space-time data, as noted earlier, are correlated in both space and time such that observations in close proximity are more likely to be influenced by similar factors and thus affected in a similar way, described as Tobler's first law of geography (Cressie & Kornak, 2003; Tobler, 1970). In the case of malaria prevalence, spatial and temporal correlations are present at both short and large scales, reflecting the transmission of infection by mosquitos which fly over short distances and the effects of environmental factors due to seasonal changes which determine mosquito survival over larger areas (Hellmuth, Moorhead, Thomson, & Williams, 2007). Classical statistical methods assume independence of observations, and when used to analyse spatially correlated data often underestimate the standard errors of the covariate parameters and thus leads to the overestimation of the p -values, which determine the statistical significance of the covariates (Cressie, 1993; Cuzick & Elliott, 1992; Thomson et al., 1999). Of particular interest in this study is the application of concepts and tools of geostatistics to determine whether the observed malaria morbidity cases obtained at the district locations in Ghana display any spatio-temporal dependence (autocorrelation); that is, do nearby observed space-time locations have values of morbidity incidence that are similar, in contrast to locations that are far apart? The space-time (or spatial) correlation structure of the morbidity incidence data (as established in chapter 5) then become important which if ignored leads to inaccurate estimates for the prediction

process (Cressie, 1993; Kleinschmidt, Bagayoko, Clarke, Craig, & Le Sueur, 2000).

1.2.2 Methodological Approaches

The estimation of malaria burden is challenging but is important for efficient public health planning. In most prevalent countries, the systems for tracking the malaria episodes are very poor, which tends to affect the quality of information on the number of cases and deaths. WHO via its World Malaria Report, provides annual estimates of the disease burden globally, regionally and nationally to assist with monitoring progress of national malaria control programmes. This progress will influence the meeting of the United Nations (UN) Millennium Development Goals (MDGs) of reducing poverty in disease-burden countries by 75% by 2015. However, these estimates rely on adjustments due to incompleteness of the national health-facility reporting which leads to large degree of uncertainty. Other efforts to estimate the disease burden have generated criticism because they have often yielded highly variable results (Carneiro, Roca-Feltrer, & Schellenberg, 2005; Dhingra et al., 2010; Lynch et al., 2012). Cibulskis et al. (2007) provides a review of issues for quantifying the burden of malaria whilst Cibulskis et al. (2011) and WHO (2008) summarise the current methodological approaches as being mainly based on:

- (i) The use of surveillance case reports from routine national information systems;
- (ii) The use of population-based surveys of parasite prevalence and risk maps; and
- (iii) The reported deaths, adjusted for incomplete reporting, involve dividing the number of cases by an estimated case fatality rate.

WHO uses a combination of the approaches for modelling and estimating malaria incidence depending upon the region of the endemic country or territory.

The surveillance case reports method estimates the number of malaria cases per year, with lower and upper bounds, using inputs on both confirmed and unconfirmed cases, completeness facility reports and population with suspected malaria (fever) treatments provided by the National Malaria Control Programmes in the respective countries (Cibulskis et al., 2011; WHO, 2008, 2011). The difference between the upper and lower limits reflects the extent to which malaria cases treated are at the health centres. The upper limit represents an estimate of the number of malaria cases assuming all fever cases were likely to be tested positive whilst the lower limit estimates the number of malaria cases if only those with fever cases who seek treatment actually have

malaria. The true number of cases tends to be close to the lower limit in areas where health services are highly accessible and all cases that need treatment actually seek it. It will lie closer to the upper limit in areas where accessibility is poor and many malaria cases are untreated whilst the true value of lies between the two limits (see WHO, 2008 and 2011).

The second method uses an empirical relationship between measures of the malaria transmission risk and incidence rates following the Malaria Atlas Project (MAP), including studies by , Craig, Snow, and le Sueur (1999), Hay et al. (2009), Hay et al. (2010), Korenromp (2005), Patil et al. (2009) and Snow et al.(2005). It is mainly used in the African region where data from routine health information system are considered sufficiently complete, classifying the population in each country as at high, low or no risk of malaria according to climatic suitability (MARA Project, 1998) and the incidence rates are inferred from the risk zones using longitudinal studies carried out in the population without malaria interventions. The incidence rates are then adjusted downwards for each country depending on the expected impact of vector control interventions.

Cibulskis et al. (2011) apply both methods to update the WHO's 2009 estimates for the 99 countries and also provide a critique of the estimates obtained. They compute 225 million cases worldwide with 95% confidence interval of 146–315 million cases and 176 (110–248) million cases in Africa compared with the WHO's of 222 (163–292) and 179 million cases, respectively. Hay et al. (2010) estimated 271 (241–301) million cases in 2007 compared with what WHO computed, 229 (169–304) million cases globally. Recently, Murray et al. (2012), using the database on vital registration and verbal autopsy over the period 1980–2010, developed predictive models including spatio-temporal and mixed models to provide a systematic assessment of malaria mortality for the WHO endemic countries. There have been many concerns about their findings (Lynch et al., 2012). The number of global deaths which occurred in 2010 was estimated at 1.238 (0.929–1.685) million, nearly double the value, provided in the 2012 WHO report (WHO, 2012) of 0.655 (0.537–0.907) million for the same year. Murray and colleagues also found more adults deaths. WHO disputes the use of verbal autopsy for computing malaria deaths as they contend that there is no scientific evidence of establishing the reliability of verbal autopsies of people aged 5 years and over (GMP/WHO, 2012). Nevertheless, the high number of deaths as estimated by

Murray et al. (2012) is consistent with the study of Dhingra et al. (2010) who similarly use verbal autopsy records to obtain 200,000 deaths in India compared to WHO's estimate of 24,000 deaths for the same period. However, some of the models that have been used are considered as too simplistic to generate the required precision of results (Carneiro et al., 2005).

1.2.3 Spatial Statistical Studies in Malaria

There have been a number of research projects in malaria epidemiology that have been done using spatial statistical modelling coupled with time series and GLR models. In the area of spatial statistics, several of these studies have produced risk maps describing the distribution and patterns of the malaria burden both at global and continental (Cibulskis et al., 2011; Hay et al., 2009; Hay, Guerra, Tatem, Noor, & Snow, 2004; Mabaso, 2007; MARA Project, 1998; Noor, Alegana, Gething, & Snow, 2009; Small et al., 2003; Thomson & Connor, 2001) and regional and national (de Souza et al., 2010; Gemperli et al., 2006; Gething et al., 2007; Gething et al., 2006; Gosoniua, Vounatsou, Sgobab, Mairea, & Smith, 2009; Kazembe, Kleinschmidt, Holtz, & Sharp, 2006; Kleinschmidt, Omumbo, et al., 2001; Lin et al., 2009; Nobre, Schmidt, & Lopes, 2005) levels. These studies describe spatial and temporal variations of malaria risk across the various landscapes, all in an effort to aid public health-care decision making on malaria control. The MARA Collaboration (MARA Project, 1998) which was established in 1996, for example, produces estimates of the malaria risk distribution in Africa. The project defines the theoretical distribution and duration of malaria transmission across the whole African continent based on biological constraints of climate suitability for parasite and vector development (Craig et al., 1999). It also estimates the number of people at risk at a continental level (Snow, Craig, Deichmann, & Marsh, 1999). Gemperli et al. (2006) use a transmission-based models to map Mali, and two sub-regions (West and Central Africa) for different seasons and age groups, unlike the other MARA studies which are limited to a particular season and children under 10 years of age.

Malaria risk maps interpolating estimates of disease occurrence from a regional database to a continuous surface have been constructed using geostatistical kriging techniques, a very powerful spatial technique. Kleinschmidt et al. (2000) and Kleinschmidt (2001) use kriging, coupled with a GLR model to estimate the malaria prevalence data from surveys on childhood populations, to predict malaria risk at the

local level in Mali and West Africa, respectively. Gething et al. (2006, 2008) use space-time kriging to predict the monthly malaria cases seen at the public health facilities in Kenya where records were missing to obtain reliable estimates of the national outpatient malaria treatment burden for accurate quantification for health system planning. In another paper Gething et al. (2007) compare three different methodologies of kriging, ordinary kriging, space-time ordinary kriging, and local space-time ordinary kriging, through cross-validation predictions of the proportion of outpatient treatments for malaria at health facilities within the Kenyan health management and information system. A review, of classes of space-time covariance (semivariogram) models which dominate geostatistical prediction but are limited in malaria epidemiology, is given by De Iaco (2010) in her comparative analysis of the existing models. They include the generalised product-sum model (De Iaco, Myers, & Posa, 2001), which is deemed more general and easily applied. This is one of the models considered in this study for the structural analysis of the malaria incidence rates. Kyriakidis and Journel (1999) give a review of two types of space-time models as presented in Chapter 3. The choice of these models depends on the relative abundance of data in the two-dimensional domains.

Nadine et al. (2010) developed Bayesian geostatistical models to analyse data from Zambia's national malaria indicator survey conducted in 2006, to establish the relationship between the malaria parasitaemia data (quantitative measure of parasite load in the blood) and climatic predictors of the disease. The results led to the production of the first contemporary empirical parasitaemia risk map of malaria incidence for evaluation of malaria interventions in the country. Nobre et al. (2005) used spatio-temporal modelling of Bayesian hierarchical models to model the rainfall effect on malaria incidence, accounting for spatial dependence in counties in the Brazilian state of Pará; they adopted a conditional autoregressive (CAR) model, a generalisation of spatio-temporal prior distributions proposed by Besag, York, and Mollié (1991). Kazembe et al. (2006) applied a model-based geostatistical approach with variograms based on logit to explore spatial correlation and prediction of malaria prevalence in Malawi, computing the parameters of the model using the maximum likelihood and Bayesian approaches.

Baragatti et al. (2009) contribute to better understanding of spatial analysis of malaria epidemiology in their study in urban areas of Ouagadougou in Burkina Faso by using a

generalised linear mixed (GLM) model nested with random effects. Malaria prevalence was observed heterogeneous due to the spatial and temporal distributions of vector larval breeding sites. The results also indicated low urban malaria transmission with marked seasonality and high prevalence of malaria risk among children who lived in sparsely populated and irregularly built-up areas. In addition, children in poorer households were found to be at greater risk of malaria infection, independent of bed-net use, and that travel outside the city increases the risk of being exposed to malaria transmission and high parasitaemia.

1.2.4 Time Series Analysis of Malaria Epidemics

Time series analysis, coupled with generalised linear regression (GLR) models, has proved to be a very powerful warning tool for predicting malaria epidemics particularly when vulnerability variables such as environmental factors are included. An autoregressive integrated moving average (ARIMA), coupled with generalised least squares regression modelling, has been applied to monthly incidence of malaria with climatic variables in Shuchen County, China for the period 1980-1991 (Bi, Tong, Donald, Parton, & Ni, 2003). The study indicated temperature, relative humidity, and precipitation to be possible predictors for regions with similar geographic, environmental, or socio-economic conditions to those of Shuchen County. The regression analysis results showed significant effect of monthly mean minimum temperature and total monthly rainfall with a one-month lag effect, as well as seasonality. There was also a declining long-term but non-periodic trend in the incidence of malaria and it was suggested that the above variables could be included in a model as possible predictors of this incidence. A similar study by Tian et al. (2008) also established the potential impact of climate variability on malaria transmission in a tropical rainforest of Mengla County, China. The study in Rwanda proved that monthly malaria incidence in high-altitude regions was related to changes in minimum temperature whereas in low-altitude zones, rainfall and mean temperature were the most significant climatic factors (Loevinshn, 1994). Gomez-Elipe, Otero, van Herp, and Aguirre-Jaime (2007) developed an ARIMA model using data for the period 1997–2003 to predict the expected malaria incidence based on the observed malaria incidence rates and a combination of climatic factors (rainfall, temperature and vegetation index) for the month. Small et al. (2003) fitted an autoregressive AR(p) model to time series malaria incidence data for 1911–1995 in their analysis of climate

suitability of malaria transmission in Africa, testing for the autocorrelation using an ADF test (Dickey & Fuller, 1979) in an attempt to address the concerns of effect of seasonal noise on long-term trend analysis.

Several authors have also established a strong correlation between the malaria incidence rates and variations in environmental variables during several preceding months or season (Craig, Kleinschmidt, Nawn, Le Saour, & Sharp, 2004; Loevinsohn, 1994; Thomson, Mason, Phindela, & Connor, 2005). The model by Loevinsohn (1994), for an unstable malaria transmission area in Rwanda, which did not take into account the influence of the malaria incidence rate in the preceding month, included minimum temperature in the preceding one and two months, and rainfall in the preceding two and three months whilst Thomson et al. (2005), using historical rainfall data and malaria incidence data from Botswana, linked higher rainfall totals with increased malaria incidence several weeks later. Malaria transmission was found to be complex, being influenced by other factors besides climate, but when trends in non-climatic factors were quantified and accounted for, variability in rainfall was found to explain more than two-thirds of the incidence variation. This means that rainfall monitoring can give several lead weeks or months warning of possible epidemics; malaria incidence is also linked to sea surface temperatures which affect continental rainfall and are used for seasonal forecasting. Subsequent analysis confirmed that seasonal forecasts can provide useful indications of the likelihood of an epidemic several months in advance (Thomson et al., 2006). This led to the development of the malaria early warning and response system (MEWS) by the partners of the RBM initiative (which includes the national ministries of health) to gather adequate information on when and where epidemics are most likely to occur. MEWS has five components: vulnerability assessment and monitoring; seasonal climate forecasting; environmental monitoring; sentinel case surveillance; and planning, preparedness and response. It was piloted in several epidemic-prone countries in Southern Africa and holds promise for use in other malarial endemic areas in Asia and Latin America (Hellmuth et al., 2007). Seasonal climate forecasting is of great interest to this study as it seeks to establish a link between climate and malaria morbidity incidence cases to provide a reliable forecasting method that can help predict epidemics. Seasonal analysis gives seasonal trend patterns and lead time forecast to allow effective control and other measures to be implemented (Silal, Barnes, Kok, Mabuza, & Little, 2013).

1.2.5 Malaria Studies in Ghana

Epidemiological research currently available in Ghana can be classified according to three main factors of malaria transmission, as presented by the following findings:

Climate suitability and vegetation Cover: The seasonal variation in climatic conditions, coupled with differences in vegetation cover, directly affects mosquito habitats and thus potential for malaria transmission. Studies in Ghana on the impact of climate variability on malaria incidence or prevalence establish a link, notwithstanding the numerous limitations highlighted in this chapter. Danuor et al. (2010) establish a link between malaria incidence and variability of rainfall, temperature and relative humidity, using correlation and regression analyses to predict the occurrence of the disease but their study was limited to only two public centres located in the forest vegetation zone. They highlighted the need for monthly time series data for at least 10 years, covering more health facilities to obtain a clear picture of the malaria pandemic and to allow comparison of seasonal variability of the disease which should underpin the rationale for seasonal forecasts an efficient malaria early warning system. de Souza et al. (2010) geo-referenced and mapped study sites, of available survey data on *Anopheles gambiae* species, widely spread in Ghana. The GLR model used produced varied distribution of vectors across the country, driven mainly by different environmental factors such as elevation, vegetation cover, precipitation, temperature and humidity obtained via remote-sense satellite sources.

Non-climatic environmental conditions: Non-climatic environmental factors which promote mosquito breeding are mainly due to human activities including poor sanitation conditions resulting from poor design and construction of drainage and sewerage systems, lack of garbage disposal facilities (Osei, Duker, Augustijn, & Stein, 2010), urbanization via road/building and dams for irrigation and hydroelectricity (Jobin, 2004) and farming activities (Chinery, 1999b; Klinkenberg et al., 2005). Malaria is the most wide-spread of the water-associated diseases in the tropics; the association is that it is transmitted by *Anopheles* mosquitos which must have access to stagnant water-bodies for egg-laying. If the water stands for more than a week, the eggs of these blood-sucking insects have time to develop and hatch (Jobin, 2004). Jobin (2004) discusses the health hazards of ten well documented hydro-dams including Akosombo Dam in Ghana, indicating that dams and their reservoirs play three roles in the transmission of tropical diseases. Firstly, the reservoirs can serve as

breeding habitats for the aquatic insects and snails which transmit the tropical diseases. Secondly, the reservoirs attract large numbers of people because of the potential for fishing or other economic activities related to water. Lastly, the dams often displace people from the flooded zone of reservoirs, requiring construction of large resettlement centres, most of which are poorly constructed. Careful siting and selection of simple changes in the design of dams can reduce the risks of lethal tropical diseases such as malaria and cholera, as he suggested.

Asenso-Okyere (1994)'s study based on four districts in the Greater Accra region revealed that poor environmental conditions and other variables including excessive heat, mosquitoes, malnutrition, fatigue, and unsafe drinking water were perceived to be the most important factors for contributing to malaria outbreaks. He also found that almost all the adolescents at that time had no idea of how the disease is transmitted. Symptoms of clinical malaria were also frequently considered to be yellowish eyeballs, chills and shivering headache, a bitter taste, body weakness and yellowish urine. Rapid urbanisation increases artificial mosquito breeding-water habitats as well as eliminating or modifying many natural mosquito-breeding waters (Chinery, 1999a; Klinkenberg et al., 2005). Klinkenberg et al. (2005) used a GLM model to investigate malaria prevalence in children living in an urban area of Ghana; the associated risk factors were low haemoglobin concentration, low socioeconomic status, and higher age. A high parasitemia level of 14.9 (6–22)% was also found, contrary to what is usually associated with most urban communities in Africa, with high population densities, for example, 8.8 (2–14)% for Pikine in Senegal (Vercruyse, Jancloes, & Van de Velden, 1983).

Socio-economic factors: Lack of social amenities coupled with socio-economic factors such as poor nutrition, poverty, low level of education, inappropriate medication and access to health care have been considered as major causes for infection by water-associated diseases such as malaria and cholera. Most communities in Africa including Ghana lack or have limited sewage and sanitation facilities. The surface run-off from waste dump sites contaminates water bodies and causes stagnation and increases organic nutrients, putting inhabitants at risk of these water-borne diseases (Chinery, 1999b; Osei et al., 2010). Osei et al. (2010) uses spatial statistical modelling to determine the dependency of prevalence of other infectious disease on contaminated surface water bodies and establish association between the

spatial distribution of the disease prevalence and proximity to contaminated surface water bodies. Malnutrition impacts on both the manifestation of and susceptibility to malaria. Research has shown that malnutrition increases susceptibility to malaria whilst other studies indicate that malaria increases the likelihood of a child having poor nutritional outcomes (Caulfield, Richard, & Black, 2004; Nyakeriga, Troye-Blomberg, Chemtai, Marsh, & Williams, 2004). Malaria is the most significant human parasitic disease and is the chief cause of anaemia (Crookston et al., 2010) as most episodes of uncomplicated malaria in Ghana can cause mild anaemia. Crookston et al. (2010) use a logistic regression model to explore the relationship between chronic malnutrition and asymptomatic malaria in children under five years in a community in Kumasi, Ghana. The study did not show any significant association between chronic malnutrition as measured by stunting (mild, moderate, or severe) and presence of asymptomatic malaria. However, the results indicate that children who experience anaemia and an increased spleen size are more likely to be positive for malaria without symptoms (a moderate association found between asymptomatic parasitaemia and malnutrition).

An investigative study of the economic burden malaria causes in six African countries including Ghana was recently conducted by Okorosobo et al. (2011). They used econometric models to establish a significant impact of malaria (as indicated by morbidity incidence rate per 100,000 people) on economic growth in Ghana, indicated by gross domestic product (GDP). A decline in GDP growth of 0.435% per year was found for every unit increase of the malaria burden. This confirms the earlier work of Gallup and Sachs (2001) who obtained a higher decrease of 1.3% and a much closer value for SSA (0.55%) as reported in McCarthy et al. (2000). Agyepong and Kangeya-Kayonda (2004) contribute to the estimation of malaria burden issue through a case study in rural communities in the Dangme East and West districts with their findings suggesting under-utilisation of health facilities. They found that for every febrile case of illness treated at a public health facility, there were 4 or 5 others who never had the opportunity to receive treatment. This contradicts the conclusions of a similar study in Niger (Doudou et al., 2012) which overestimates the suspected cases of malaria reported at formal health facilities, thus highlighting the inadequacies in the national health management and information system. In a very recent study, it was found that malaria among children decreased with increasing socio-economic status of families as classified by principal component analysis in Krefis et al. (2010). Higher malaria risk

was further established in highly endemic rural communities with limited use of protective measures where socio-economic differences are not much different.

Biological factors: These include propensity and frequency of mosquito bites; abundance of *Anopheles* species and their susceptibility to the human parasite and the rate at which the parasite develops in mosquitoes, persistence of suitable aquatic habitats until maturity of the mosquitoes, which in turn largely depends on climate variability (Baird et al., 2002; de Souza et al., 2010; Klinkenberg et al., 2005; Obiri-Danso, Weobong, & Jones, 2005; Ofori et al., 2009). Appawu et al. (2004) studied malaria transmission dynamics in a proposed site for testing malaria vaccines at the Kassena-Nankana district of Northern Ghana, using data from a one-year sampling survey on mosquitoes collected via human landing catches in the three micro-ecological sites (irrigated, low and rocky highlands). A highly seasonal malaria transmission was established, mostly occurring between the months of June and October. Malaria transmission intensity was observed to be higher for people in the irrigated communities, whilst approximately 60% of the transmission in the district occurred indoors during the dawn hours. Earlier studies conducted in the same district produced similar patterns of malaria risk (Baird et al., 2002; Binka et al., 1996). Specifically, Baird et al. (2002) estimated that malaria prevalence accounts for over 25% of the under-five mortality in the whole northern part of the country. Furthermore, Binka et al. (1996) indicated intense malaria transmission of approximately 4–7 infections/person-year, mostly in the wet season, and relatively low risk of infection if the rates of severe anaemia among children were low. The use of insecticide treated nets (ITNs) provides significant individual protection; however, the direct and indirect effects on malaria transmission of treated and untreated nets in a community of bed net users and non-users need much insight, despite the recent progress (MICS, 2011). Randomised clinical trials in different malaria transmission regions examined the spatial effect of ITNs on mortality of children. In the Northern Ghana the estimated mortality risk in individuals without insecticide nets increased by 6.7% with every 100 metres movement from the nearest home where treated nets are used (Binka, Indome, & Smith, 1998). Ofori et al. (2009) characterised pregnancy associated with malaria in a rural community along the coast of Greater Accra Region, linking high prevalence of placental malaria parasite infection to low haemoglobin and observed women in their first and second pregnancies were highly at risk.

1.3 Research Problem and Objectives

In spite of Ghana's NMCP numerous intervention strategies to contain the malaria burden for the last decade, the disease remains the country's most prevalent health problem (GMAG, 2007; NMCP, 2008; PMI, 2012). The proportion of the total outpatient department (OPD) cases attributed to malaria continues to increase whilst geographic variation in morbidity cases still persists due to various environmental and socio-economic factors (GHS, 2011; MICS, 2011). This emphasizes the need for accurate quantification of the disease burden and its distribution pattern across Ghana as this should assist effective malaria control. Environmentally-driven studies of the malaria risk and population maps, as reviewed above, have proved to be useful for describing and/or explaining the public burden of the disease (Craig et al., 1999; Gosoni, Vounatsou, Sogoba, & Smith, 2006; WHO/UNICEF, 2003). Numerous efforts, as enshrined in the nation's malaria interventions, include focused research to reduce the disease's burden but little attention is paid to a spatial statistical model-based approach to malaria epidemiology. Most available health research in Ghana focuses solely on biological aspects and characteristics of the people contracting the disease (Obiri-Danso, Okore-Hanson, & Jones, 2003; Osei et al., 2010), but neglects the spatial (Osei & Duker, 2008) and temporal patterns of incidence. Though these studies have been useful, they cannot establish the potential risk factors and also identify areas, with high prevalence of the disease, that require health policy interventions (Osei & Duker, 2008). Periodic risk measures reported on Ghana were based on household surveys, largely from the Demography and Health Surveys (DHS) and Multiple Indicator Cluster Surveys (MICS), which are conducted at limited sentinel sites and through public health information systems. It should also be noted that, expert opinion is sometimes sought. These national surveys are not conducted annually (or regularly), and do not provide sufficient data for accurate prediction of new and future incidence cases, as well as the rate of change in prevalence in different areas. In addition, many health facilities in the country never report or report intermittently resulting in spatially and temporally incomplete data in the CHIM data base. This greatly limits the planning and management of relevant health care delivery systems in the country.

The study is motivated by efforts such as MAP and MEWS, which specifically link malaria incidence rates to climate characteristics through spatial statistical and time

series seasonal predictive models. The current malaria prevalence model for Ghana was obtained by Kleinschmidt, Omumbo, et al. (2001), based on parasite survey data. That study was part of the MARA Project (1998), which produced a malaria risk map for the West African Region. Most countries in the survey region, including Ghana, were poorly covered. A lack of adequate survey-referenced points and wide spacing of the study locations resulted in inaccurate prediction of the malaria risk for these countries. Since this first study, no attempt has been made to update the malaria risk map of Ghana despite the abundance of both published and unpublished data on incidence cases of malaria for all districts. In addition, their study was based only on population prevalence surveys on children less than 10 years of age, which might not be representative enough for estimation of the actual malaria risk burden in the country.

The geographical and seasonal variations of malaria transmission in Ghana are widely attributed to differences in climate and vegetation, which have direct links to mosquito habitats (Chinery, 1999b; Danuor et al., 2010; de Souza et al., 2010; WHO/VBCD, 1989). Spatio-temporal modelling, coupled with adequate data, has been shown to better define the public burden of the disease, providing risk maps to describe the incidence variation in space and by time and also identifying high risk areas (“hot spots”) for relevant policy decisions and implementation. In spite of its wide application in environmental and air pollution studies, not much is seen in West Africa and for that matter Ghana. The studies by Gething (2008, 2007 and 2006) in Kenya appeared to be the first application of geostatistical space-time kriging methodology to malaria epidemiology in Africa. The studies by Gething and colleagues did neither account for any environmental effect nor did they consider all people at data locations at risk of the disease.

The thesis seeks to explore the spatio-temporal distribution of the malaria morbidity incidence and the potential influence of climate variability, which can be used to predict malaria risk by location and time using monthly available data by district and region over the period 1998-2011. This is achieved by applying the geostatistical methodology of space-time kriging, coupled with time series SARIMA predictive models, to the monthly morbidity cases reported on disease data from health facilities; and population and climatic data at the district and regional levels. The data for the study covered all districts and regions in the country. The ultimate aim of the study is

to produce monthly evidence-based risk maps of malaria, estimating its incidence rates and describing the distributional patterns over space and time that incorporate climatic data for rainfall, temperature and relative humidity, with particular focus on delineating areas with high risk of malaria morbidity incidence. Modelling the malaria morbidity cases observed as incidence rates, the specific objectives of the study are as follows:

- (i) To perform seasonal analysis to establish temporal distributional patterns of the morbidity incidence rates in the regions which can be used to provide predictive forecasts of malaria risk. This will have various benefits including assessing progress of meeting the NMCP's target of reducing malaria cases by 75% by the year 2015. Thus, various smoothing analyses coupled with the multiplicative SARIMA model forecasting of the malaria morbidity incidence rates at each region are performed.
- (ii) To characterise the correlation structure of the space-time (district-month) morbidity incidence rates at the district and time locations in the whole country (nationally), Brong Ahafo Region, and the three epidemiological zones. This is achieved via construction of the space-time semivariogram models that describe the spatial and temporal correlations of the morbidity incidence rates for each study area.
- (iii) To obtain optimal predictions of morbidity incidence rates at the unsampled locations, where data are missing for each of the three study areas, based on monthly the malaria risk maps using ordinary kriging and space-time ordinary kriging techniques.
- (iv) To establish the potential effect of the climatic covariates (rainfall, temperature and relative humidity) on the morbidity incidence rates using SARIMAX modelling and space-time co-kriging. The SARIMAX is applied to the regional incidence rates data whereas a linear model of coregionalisation (LMC) is used for the space-time incidence data at the district-month locations.

1.4 Thesis Outline

The thesis concerns the spatio-temporal distribution of monthly malaria morbidity cases as based on disease reports from district and regional health facilities in Ghana. This chapter, being the introduction to the study, gives the background information on

the malaria burden, its control and transmission worldwide and in Ghana. It also reviews malaria epidemiological studies, including the spatial epidemiology, methodological approaches for estimating malaria burden and spatial as well as temporal statistical studies in malaria transmission. Finally, the research problem and objectives of the study are delineated. The rest of the study is structured into five chapters as indicated as follows:

Chapter 2 focuses on the theoretical frameworks for analysing the data using spatial and time series models. It outlines the concepts of spatial statistics and specifically geostatistics in relation to the analysis of geographical distribution of the malaria incidence rates data. It then presents the semivariogram and covariance functions and their estimation; fitting of linear models of regional and linear models of coregionalisation (as multivariate analysis in spatial statistics) for characterising spatial correlations and accounting for exogeneous variables; and geostatistical spatial kriging, being the technique for optimal predictions at unsampled district locations of the malaria incidence data. Finally, time series analysis of smoothing techniques and the use of multiplicative SARIMA predictive models for forecasting are presented.

Chapter 3 covers the geostatistical space-time statistical modelling, which represents the second theoretical framework for studying the morbidity incidence rates, considered as a realisation of a random function distributed in space and time. This chapter is structured into three main sections, covering the space-time semivariogram and covariance functions, permissible models and their estimation; geostatistical space-time kriging techniques; and space-time conceptual modelling approaches.

Chapter 4 provides exploratory analysis of the research data. It establishes the distributional properties of the malaria morbidity cases, which are modelled as incidence rates, (defined as the number of new reported morbidity cases per unit resident population of 10,000). It first presents the background information for the study area and description of the research data collection. Time-plots and smoothing analysis of the regional data are provided, followed by the post plots (spatial maps) of the space-time incidence data. Multiple linear regression analysis of the morbidity incidence rates with the climatic covariates is also performed to establish the potential effects of the covariates. The chapter ends with the multiplicative SARIMA predictive future forecasts of malaria risk in each of the ten regions in Ghana.

Chapter 5 applies the theoretical concepts in chapters 2 and 3 to the space-time malaria morbidity cases, modelled as incidence rates. The analysis includes the global trend modelling, which involves detrending and deseasonalising the space-time morbidity incidence rates and further analysis of the trend model coefficients. It also comprises structural analysis and optimal predictions of morbidity incidence rates. The former explores the spatial and/or temporal correlations of the observed spatial and space-time incidence study data, including the generalised product-sum semivariogram model of the incidence data and linear model of coregionalisation (LMC) with the covariates to establish climatic effect on the morbidity incidence rates. The latter, via space-time ordinary kriging techniques, leads to the predictions of morbidity incidence rates at the unsampled district-month locations resulting in production of the monthly risk maps of the malaria morbidity. Finally, the results of the analyses are summarised and discussed.

The study is concluded in Chapter 6, which summarises and discusses the findings; highlights the limitations; characterises the contributions to knowledge made ; and provides recommendations for future work.

Chapter 2

Spatial and Temporal Statistical Modelling

2.1 Introduction

Statistical modelling, as noted in chapter 1, plays an indispensable role in malaria epidemiological studies, providing better understanding of the dynamics of the malaria epidemics and other infectious diseases. In this chapter, the concepts of both spatial and time series predictive modelling approaches employed to analyse the malaria morbidity incidence in this study are outlined. Spatial statistics specifically deals with geographically referenced data, and unlike the classical statistical modelling which assumes independence, it obeys Tobler's first law of Geography, that nearby observations in space tend to be more alike than those farther apart (Tobler, 1970). This dependency assumption extends spatial statistics, dealing with data correlated in space and time as well. Spatial statistics is a relatively new development within Statistics, having progressed slowly from various areas of applications, including mining engineering, which subsequently led to the development of geostatistics (Matheron, 1963); agriculture with spatial consideration informed by the thinking of Fisher (1935) via his concepts on randomisation and blocking; and forestry, as appeared in a seminal PhD dissertation of Bertil Matérn (Matérn, 1960). The last two decades have seen some remarkable achievements in spatial statistical modelling with an explosion of interest in space and space-time problems which has facilitated the collection of large spatial and spatio-temporal data sets across many fields of study (Christakos, 2012; Cressie & Wikle, 2011; Gelfand, Diggle, Fuentes, & Guttorp, 2010). In the process, spatial statistics has been brought into the mainstream of statistical research with several state-of-the-art works including the texts by Chilès and Delfiner (2012), Cressie and Wikle (2011), Goovaerts (1997), Gelfand et al. (2010) and Kyriakidis, Shortbridge, and Goodchild (1999). This is the new scientific phase of statistical modelling of data according to Cressie & Wikle (2011).

Time series analysis provides useful tools or scientific techniques for analysing and interpreting processes which vary over time. A time series is sequence of data points z_t generating from a process or event, which are measured successively at a specific time t , and often at a uniform time interval. Time series analysis comprises of methods

that attempt to understand such time series, often either the underlying context of the data points (where did z_t come from, and what generated them?), or to make forecasts (predictions). The time series forecasting uses a model to forecast future events based on known past events (that is, to forecast the future values z_t based on previous z_{t-1} values). The forecasting models considered in this study included multiplicative ARIMA processes for modelling non-stationary data, which can be extended to account for seasonality and exogenous variables. These models were used to establish seasonality patterns, fit the climatic covariates to determine whether an association exists and forecast the malaria risk at regional level of the country. Modelling with ARIMA models forecast methodology involves the estimation of a series of parameters to account for the inherent dynamics in the time series, including the trends and autoregressive and moving average processes. The ARIMA models were first introduced by Box and Jenkins (1976) and explicitly includes differencing for stationarity to be achieved.

In the following sections an outline is presented of concepts of both spatial and time series seasonal predictive models used for analysing the malaria morbidity incidence in this study.

2.2 Basic Concepts of Spatial Analysis

In many scientific disciplines including health, environmental and geology, spatial statistical studies are becoming more and more common due to the availability of low cost spatial technology with user-friendly interfaces (Cressie & Kornak, 2003) for the understanding of data distributed in space and time as well. Spatial technology coupled with other integrated programs allows the spatial visualisation of attributes such as incidence of diseases or mineral deposits in a region using maps. Apart from the visual perception of a spatial distribution, it is useful to translate the existing patterns into objective and measurable quantities, for example, in the following contexts:

- (i) Data collected on the occurrence of diseases: Does the distribution of cases of a disease form pattern in space? Is there an association with the environment? Is there any evidence of contagion, if so does it vary with time?
- (ii) Estimation of mineral resources in an exploration region based on sample data: Can those observed samples be used to estimate the mineral distribution in that

region?

- (iii) Investigation of the spatial concentration in the distribution of criminal activities: Are crimes that occur in certain areas of a community correlate with socio-economic characteristics of the areas under study?

These problems form part of spatial analysis of geographical data. The emphasis of spatial analysis is to measure properties and relationships, taking into account the spatial location of the phenomenon being studied in a direct way. When a spatial dimension is present in a phenomenological process as in epidemiology (or health sciences) there is the need to create a modelling framework within which inferences on process parameters can be carried out. Spatial dependency when incorporated into the statistical analysis leads to improved and efficient inferential results.

2.2.1 Spatial Models

The ultimate goal of spatial statistical study is data description, extending bounds to further characterise the sampled population. The key aspect of this process is the application of a quantitative modelling approach to the observed spatial data over the study region. In statistics, mathematical models are used to represent the reality (or unknown) of the phenomenon being studied. Though unique, the reality may have several possible representations, depending on the information available and the aim of the study. The phenomenon being studied (for example, occurrence of a disease, mineral deposits, or rainfall), denoted Z is called an *attribute*, the location of the observation or measurement, \mathbf{u} where $\mathbf{D} \subseteq \mathbb{R}^d$ is d -dimensional Euclidean space and $Z(\mathbf{u})$ is the spatial observation over the study area (or region) \mathbf{D} , called *domain*.

In modelling the attribute over the domain \mathbf{D} steps are taken:

- (i) To ensure that all relevant information (for example spatial continuity) is incorporated;
- (ii) To employ a simple model yet realistic to infer from based on limited sample data; and
- (iii) To use an appropriate model (with a causative component) directed towards the aims and objectives of the study (Cressie, 1993; Goovaerts, 1997).

Statistical models are classified as either being *deterministic* or *probabilistic (random or stochastic)*, depending on whether the representation is unique and deemed exact or the model consists of a set of alternative representations of the uncertainty about the

unknown observations (Goovaerts, 1997). In view of the uncertainties about measurements at data locations we assume probabilistic models in analysing spatial data rather than the deterministic models which provide a single estimate for the unknown $Z(\mathbf{u})$ without further inferences. The choice of such models reflects our imperfect knowledge of the unsampled value $z(\mathbf{u})$ and, more generally of the distribution of Z within the study area.

If randomness is incorporated into the behaviour of the observational process across the study area, $Z(\mathbf{u})$ is considered as a random variable whose particular realisation or outcome is $z(\mathbf{u})$. The set of (usually dependent) random variables $Z(\mathbf{u})$, one for each location \mathbf{u} in the domain \mathbf{D} , $\{Z(\mathbf{u}) : \mathbf{u} \in \mathbf{D}\}$ is called *random function* (or *field*). The attribute of interest Z is a stochastic process with domain (or index set) \mathbf{D} which itself is a subset of \mathbb{R}^d . Thus, given a set of spatially distributed data $\{z(\mathbf{u}_\alpha); \alpha = 1, \dots, n\}$ of an attribute Z at n locations across a study area, $\mathbb{R}^d \in \mathbf{D}$ where \mathbf{u} is a vector of spatial coordinates, Z becomes a random function whose values are the random variables $Z : \mathbf{D} \rightarrow \{Z(\mathbf{u}) : \mathbf{u} \in \mathbf{D}\}$. Usually \mathbf{D} is assumed to be a fixed (non-random) subset of \mathbb{R}^d but a more general assumption is that it is a random set, a measurable mapping from a probability space onto a measure space of (closed) subset of \mathbb{R}^d (Cressie, 1993). In addition, we may assume that \mathbf{D} as well as Z vary from one realisation to another. It is also possible (as the case of this study) to allow for spatially and temporally (spatio-temporally) distributed data by considering the random variable $Z(\mathbf{u}, t)$, but in this section it will be assumed that data are purely spatial either aggregated over time or considered at a fixed instant time. We must note here that the spatial data: $Z(\mathbf{u}_1), \dots, Z(\mathbf{u}_n)$, should not be misconstrued as the same variable Z observed n times over: Z_1, \dots, Z_n , as in time series analysis, rather the variables $\{Z(\mathbf{u}_\alpha); \alpha = 1, \dots, n\}$ are observed once at a point.

2.2.2 Types of Spatial Data

Spatial statistical problems are modelled based upon type of the sampled spatial data. The data may be continuous or discrete, spatial aggregations or observations at points in space; their spatial locations may be regular or irregular, and those locations may be from a spatial continuum or a discrete set. As noted in the preceding section, a stochastic modelling approach is the ideal way to summarise the scale or predict

unobserved data. The spatial data can be thought of as resulting from observations in a stochastic process. If the domain \mathbf{D} is a fixed (non-random) subset of \mathbb{R}^d that contains a d -dimensional rectangle of positive volume and $Z(\mathbf{u})$ is a random vector at location $\mathbf{u} \in \mathbf{D}$, then we obtain *geostatistical data*. In this case the spatial index \mathbf{u} varies continuously throughout the domain \mathbf{D} . The number of locations at which observations and predictions can be made is not countable. Thus, between any two sample locations \mathbf{u}_α and \mathbf{u}_β infinitely many additional samples can be observed. Geostatistical data are also regarded as spatial data with continuous variation due to the continuity of \mathbf{D} (Cressie, 1993). This is irrespective of whether the attribute Z is discrete or continuous; for example, parasites' presence/absence or count cases of a disease (discrete), rainfall precipitation or soil PH (continuous) are geostatistical data unless there is only a countable number of sample locations or the domain changes from one realisation to another realisation of the random function at random (Cressie, 1993).

The other types of data are *lattice* and *point patterns*, which arise if \mathbf{D} is fixed and discrete (regular or irregular) collection of countably many points of or a point process in \mathbb{R}^d . Spatial statistical modelling using lattice or geostatistical data focuses on the $Z(\cdot)$ process (since the domain is not random), in contrast to point pattern data analysis where the attention is on the domain \mathbf{D} . This thesis considers a particular case of geostatistical data where aggregated data from various health facilities are reported on a number of districts and used as point-referenced locations.

2.2.3 Stationarity and Spatial Dependency Measures

Suppose that $z(\mathbf{u})$ and $z(\mathbf{u} + \mathbf{h})$ are two observations at locations \mathbf{u} at $\mathbf{u} + \mathbf{h}$ respectively, the vector \mathbf{h} (called *lag*) is the displacement by which we move from \mathbf{u} to $\mathbf{u} + \mathbf{h}$. If the random function is replicating, the stochastic properties of $Z(\mathbf{u})$ and $Z(\mathbf{u} + \mathbf{h})$ should be similar, and to estimate the correlation between locations distance \mathbf{h} apart, we might consider all pairs $(Z(\mathbf{u}_i), Z(\mathbf{u}_i + \mathbf{h}))$ in the estimation process, regardless of where \mathbf{u}_i is located. In simple terms, stationarity is the absence of an origin, the spatial process has reached a state of equilibrium (Schabenberger & Pierce, 2002). Stationarity assumption is also made for time series data where the concept is considered in terms of time shift. In the spatial context, stationarity means the lack of

importance of absolute coordinates. A stationary random function in which the orientation (angle) of coordinate differences is not of consequence is called *isotropic*. Three important properties of stationarity are *strict*, *second-order* and *intrinsic stationarity*. These are detailed in section 2.3.

Spatial dependence is a key concept for understanding and analysing a spatial phenomenon. The presence of a spatial pattern in an attribute can be investigated using various graphical and/or numerical tools. The computational expression of the concept of spatial dependence is the spatial autocorrelation. This stems from the statistical concept of correlation, used to measure the relationship between two random variables. The preposition “auto” indicates that the measurement of the correlation is done with same random variable, measured in different places in space. There are different indicators used to measure the spatial autocorrelation, all of them being based on the same idea of verifying how the spatial dependency varies by comparing the variation of the sample observations and their neighbours. They include Moran’s index for testing for geographical areas; *D*-statistic, a non-parametric method (Walter, 1992) and semivariogram (or covariance) function. The semivariogram (or covariance) is a very important indicator of spatial dependence. It provides a measure of spatial correlation by describing how sample data are related to distance and direction. The semivariogram computes the square of the difference of the values to $Z(\mathbf{u}_\alpha)$ and $Z(\mathbf{u}_\alpha + \mathbf{h})$ as defined in (2.3.16). It is extensively used in this thesis to characterise the spatial as well as temporal dependence of the malaria morbidity incidence cases in Ghana. This is studied further in sections 2.3.4 and 3.2.2.

2.3 Geostatistical Spatial Analysis

Geostatistics originated from the concept of a regionalised variable distributed in space and assumed spatially auto-correlated such that samples closer in space are more alike than those further apart (Isaaks & Srivastava, 1989; Matheron, 1963). Its development in the 1960’s resulted from the need for a methodology to evaluate the recoverable reserve in mining deposits, and until the late 1990’s, it was essentially viewed as a means to describe spatial patterns and interpolate the value of the attribute of interest at unsampled locations. Geostatistics is a powerful spatial technology which contributes immensely to prediction of random processes distributed in space or time (Ali et al., 2006; Carrat & Valleron, 1992; Webster, Atteia, & Dubios, 1994). Nowadays,

geostatistics is not only used to analyse point data, but also increasingly in combination of various geographic information system (GIS) data sources, for example, to explore spatial variation in remote sensing data (Hengl, 2009) to improve digital elevation model (DEM) generation and for simulations (Hengl & Reuter, 2008; Kyriakidis et al., 1999), and has also been extensively applied in epidemiological studies facilitating quantification of spatial features of disease's transmission to allow its spatial interpolation accounting for effect of the environmental conditions (Kleinschmidt et al., 2000; Saxena et al., 2009). Geostatistics is increasingly being used to model the uncertainty about unknown values through the generation of alternative images (realisations) that all honour the data and reproduce aspects of the patterns of spatial dependence or other statistics deemed consequential for the problem at hand; stochastic imaging is one of the most vibrant and promising areas of research in geostatistics (Goovaerts, 1997).

Typical questions which often arise in geostatistical analysis include (Hengl, 2009): How does an attribute vary in space and time?; Where to locate samples and to describe their spatial variability?; What controls its variations in space and time?; What is the value of the variable at some new location/time?; What is the uncertainty of the estimated values? The answers to these questions address the three main scientific objectives of geostatistics proposed in Diggle and Ribeiro Jr. (2007):

- (i) Model estimation (the inference about the variogram model parameters);
- (ii) Prediction of unobserved values of target variable (often resulting in generation of spatial maps or images);
- (iii) Hypothesis testing (which concerns the uncertainty associated with the decision of spatial prediction).

Wackernagel (2003) presents a framework for a geostatistical study through *data description*, which need to be visually explored for spatial, temporal and multivariate structure; *interpretation*, evaluation of graphical displays from numerical statistics, thus interpretation of spatial/temporal structure, association and causal relations; *estimation*, the objective being to estimate values of phenomenon under study at various scales and at locations different from sample points. These methods are usually based on the least squares estimation techniques and need to be adapted to a wide variety of model formulations in different situations and for different problems encountered in practice.

In this section various procedures of characterising spatial continuity of a random process are presented, whilst the the spatial optimal prediction techniques are considered in section 2.4.

2.3.1 Random Function and Stationarity Properties

Geostatistical techniques assume a stochastic process in modelling the spatial continuity of the attribute being studied which is based on the concept of a random function. The concepts of probability models for the spatial random variable that varies continuously over the domain $\mathbf{D} \subseteq \mathbb{R}^d$ (where $d = 2$ -dimensional Euclidean space) are herein presented.

Let $Z(\mathbf{u})$ be a random variable of the attribute Z at location \mathbf{u} . Then the collection of random variables as defined as in section 2.2.1:

$$\{Z(\mathbf{u}) : \mathbf{u} \in \mathbf{D} \subseteq \mathbb{R}^d\} \quad (2.3.1)$$

(called a random function) has a well-defined joint distribution. For each sample location \mathbf{u}_α , the sample value $z(\mathbf{u}_\alpha)$ is regarded as a particular realisation of the random variable $Z(\mathbf{u}_\alpha)$, whilst $z(\mathbf{u})$ at an unknown or unsampled location \mathbf{u} can be thought of as one realisation of the random variable $Z(\mathbf{u})$. The random variable $Z(\mathbf{u})$ is characterised by its cumulative distribution function (cdf) for all $z = Z(\mathbf{u})$, which models the uncertainty of the sample value $z(\mathbf{u})$:

$$F(z; \mathbf{u}) = P[Z(\mathbf{u}) \leq z] \quad (2.3.2)$$

where $\{z(\mathbf{u}) : \mathbf{u} \in \mathbf{D} \subseteq \mathbb{R}^d\}$ is a realisation of the spatial random function (2.3.1). The observed data are considered as one such realisation. The distribution of the random function $\{Z(\mathbf{u}) : \mathbf{u} \in \mathbf{D} \subseteq \mathbb{R}^d\}$ is given by its associated collection of the finite-dimensional joint distributions:

$$F(z_1, \dots, z_n; \mathbf{u}_1, \dots, \mathbf{u}_n) = P[Z(\mathbf{u}_1) \leq z_1, \dots, Z(\mathbf{u}_n) \leq z_n] \quad (2.3.3)$$

for every collection $\mathbf{u}_1, \dots, \mathbf{u}_n$ in \mathbf{D} . Equation (2.3.3) models the joint uncertainty of the unsampled values $z(\mathbf{u}_1), \dots, z(\mathbf{u}_n)$. If $\mathbf{Z}(\mathbf{u})$ is considered as a vector of random

variables, then the concept is extended to the multivariate spatial stochastic process applied in linear model of coregionalisation and cokriging (as presented in sections

2.3.6 and 2.4.3, respectively). The random function (2.3.1) characterised by its finite dimensional joint distributions (2.3.3), $F(Z(\mathbf{u}_1), \dots, Z(\mathbf{u}_n) : \mathbf{u}_1, \dots, \mathbf{u}_n \in \mathbf{D})$ is invariant under translation of the coordinates \mathbf{u}_α by \mathbf{h} if the joint distribution of $Z(\mathbf{u}_1), \dots, Z(\mathbf{u}_n)$ is identical to the joint distribution of $Z(\mathbf{u}_1 + \mathbf{h}), \dots, Z(\mathbf{u}_n + \mathbf{h})$ for each separation vector \mathbf{h} , and it is said to be *strictly stationary*. Thus, for all $\mathbf{h} \in \mathbb{R}^d$,

$$\left\{ \begin{array}{l} P(Z(\mathbf{u}_1) \leq z_1, \dots, Z(\mathbf{u}_n) \leq z_n) = P(Z(\mathbf{u}_1 + \mathbf{h}) \leq z_1, \dots, Z(\mathbf{u}_n + \mathbf{h}) \leq z_n), \\ \text{or} \\ F(z_1, \dots, z_n; \mathbf{u}_1, \dots, \mathbf{u}_n) = F(z_1, \dots, z_n; \mathbf{u}_1 + \mathbf{h}, \dots, \mathbf{u}_n + \mathbf{h}) \end{array} \right. \quad (2.3.4)$$

In practice (2.3.4) is impossible to test due to data limitations so we rely on a weaker assumption of *second order stationary* (SOS) by considering the cdfs involving just two locations at a time. The assumption of SOS requires that the first moment of the random variables $Z(\mathbf{u})$ exists and is invariant within \mathbf{D} and that the spatial covariance of all pairs of random variables (second moment) exists and depends only on the separation distance \mathbf{h} :

$$\left\{ \begin{array}{l} m = E[Z(\mathbf{u})] = E[Z(\mathbf{u} + \mathbf{h})], \quad \forall \mathbf{u} \in \mathbf{D} \\ C(\mathbf{h}) = \text{Cov}(Z(\mathbf{u}), Z(\mathbf{u} + \mathbf{h})) = E[(Z(\mathbf{u}) - m)(Z(\mathbf{u} + \mathbf{h}) - m)], \\ \forall \mathbf{u} \in \mathbf{D} \text{ and } \forall \mathbf{h} \in \mathbb{R}^d \end{array} \right. \quad (2.3.5)$$

where m is the mean and $C(\mathbf{h})$ is called the covariance function. The conditions under SOS are often not satisfied and so we assume the intrinsic hypothesis which considers the increments $Z(\mathbf{u} + \mathbf{h}) - Z(\mathbf{u})$ as SOS:

$$\left\{ \begin{array}{l} m = E[Z(\mathbf{u})] = E[Z(\mathbf{u} + \mathbf{h})], \quad \forall \mathbf{u} \in \mathbf{D} \\ 2\gamma(\mathbf{h}) = \text{Var}(Z(\mathbf{u} + \mathbf{h}) - Z(\mathbf{u})) = E[(Z(\mathbf{u} + \mathbf{h}) - Z(\mathbf{u}))^2], \\ \forall \mathbf{u} \in \mathbf{D} \text{ and } \forall \mathbf{h} \in \mathbb{R}^d \end{array} \right. \quad (2.3.6)$$

If the random function (2.3.1) satisfies the conditions of the intrinsic hypothesis (2.3.6) it is called *intrinsic stationary* (IS). It should be noted that SOS implies IS, but the converse is not true. The function $\gamma(\mathbf{h})$ is called *semivariogram* (or *variogram* for $2\gamma(\mathbf{h})$) which is the main structural tool used in modelling a random function and an important component of optimal spatial linear prediction (kriging), discussed in section

2.3.4. From the stationarity assumptions in (2.3.5) the following properties of covariance function and semivariogram are obtained:

- $C(\mathbf{0}) = E[(Z(\mathbf{u}) - m)(Z(\mathbf{u} + \mathbf{0}) - m)] = E[(Z(\mathbf{u}))^2] - m^2 = \text{Var}(Z(\mathbf{u})) = \sigma^2$,

the variance of $Z(\mathbf{u})$ which is referred to as the *sill* of the semivariogram. It describes the observational error in potentially repeated measurements at location \mathbf{u}_α .

- $C(\mathbf{h})$ is an even function and satisfies the Schwartz's inequality for an SOS:

$$\begin{cases} C(-\mathbf{h}) = E[Z(\mathbf{u})Z(\mathbf{u} - \mathbf{h})] - m^2 = E[Z(\mathbf{v} + \mathbf{h})Z(\mathbf{v})] - m^2 = C(\mathbf{h}) \\ |C(\mathbf{h})| \leq C(\mathbf{0}) \end{cases}$$

- For an SOS process, $\gamma(\mathbf{h}) = C(\mathbf{0}) - C(\mathbf{h})$ (see Figure 2.3.1 for this relationship):

$$\begin{aligned} 2\gamma(\mathbf{h}) &= E[(Z(\mathbf{u} + \mathbf{h}) - Z(\mathbf{u}))^2] = E[(Z(\mathbf{u} + \mathbf{h}) - m + m - Z(\mathbf{u}))^2] \\ &= E[(Z(\mathbf{u} + \mathbf{h}) - m)^2] + E[(Z(\mathbf{u}) - m)^2] - 2E[(Z(\mathbf{u} + \mathbf{h}) - m)(Z(\mathbf{u}) - m)] \\ &= \text{Var}(Z(\mathbf{u} + \mathbf{h})) + \text{Var}(Z(\mathbf{u})) - 2\text{Cov}(Z(\mathbf{u} + \mathbf{h}), Z(\mathbf{u})) \\ &= 2C(\mathbf{0}) - 2C(\mathbf{h}), \end{aligned}$$

since $\text{Var}(Z(\mathbf{u} + \mathbf{h})) = \text{Var}(Z(\mathbf{u}))$. If $C(\mathbf{h}) \rightarrow 0$ as $\|\mathbf{h}\| \rightarrow \infty$, then $\gamma(\mathbf{h}) \rightarrow C(\mathbf{0})$.

- For intrinsic stationarity, we have: $\lim_{\|\mathbf{h}\| \rightarrow \infty} \frac{\gamma(\mathbf{h})}{\|\mathbf{h}\|^2} = 0$. Also, $\gamma(\mathbf{0}) = 0$, but there

could be a discontinuity just after $\mathbf{h} = \mathbf{0}$, and $\gamma(\mathbf{h}) = \gamma(-\mathbf{h}) \geq 0$.

Definition 3.3.1 (Smoothness property):

A spatial random process $\{Z(\mathbf{u}) : \mathbf{u} \in \mathbf{D} \subseteq \mathbb{R}^d\}$ is said to be mean square continuous if $E[(Z(\mathbf{u}) - Z(\mathbf{u} + \mathbf{h}))^2] \rightarrow 0$ as $\|\mathbf{h}\| \rightarrow 0$. For an SOS process $E[(Z(\mathbf{u}) - Z(\mathbf{u} + \mathbf{h}))^2] = 2(C(\mathbf{0}) - C(\mathbf{h}))$. Thus, the mean square continuity is equivalent to the covariance function being continuous at the origin (and for that matter elsewhere), though such a process need not have continuous sample paths and vice versa (Banerjee & Gelfand, 2003; Gelfand et al., 2010).

There may be several reasons which account for the superiority of IS over SOS and hence the general use of the semivariogram instead the covariance function. They include the following (Cressie & Grondona, 1992; Sherman, 2011):

- IS is a more general assumption than SOS making the variogram adapt more easily to non-stationary observations.
- The estimation of the variogram does not depend on the mean unlike the covariance function.
- The estimation of the variogram is easier (that is, the common moment estimator is more accurate in most cases). In particular, the natural moment estimator of variogram is unbiased under IS whilst that for the covariance function is biased.

2.3.2 Semivariogram and Covariance Functions

The semivariogram and the covariance function are the two main tools for inferring the spatial structure of a random process but as noted above, the former is often used. The semivariogram measures how values of the random function differ as the separation distance (\mathbf{h}) between locations increases and also differ with direction. The theoretical semivariogram, as seen in Figure 2.3.1, is monotonic non-decreasing function as the separation distance increases; its shape can be characterised by three main parameters namely, the nugget, sill and range (see Figure 2.3.1 (right)).

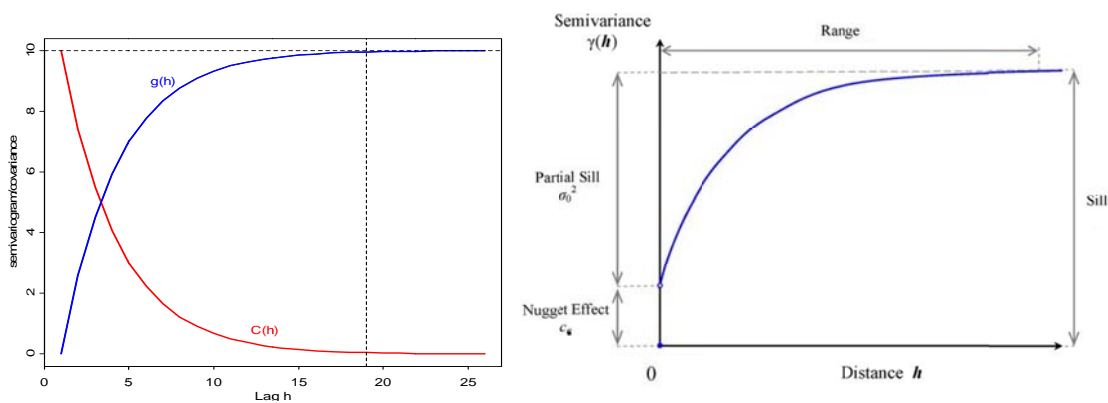


Figure 2.3.1: Relationship between semivariogram and covariance function (left) and the theoretical semivariogram showing the nugget effect, sill and the range which characterise spatial dependence of an attribute (right).

As the semivariogram reaches its limiting value being the sill, $c = C(\mathbf{0})$, it is said to be *transitive (or bounded)*. The distance at which the sill is reached is called the *range* (r), beyond this point there is no longer any correlation between the observations in the samples. The *nugget effect* (c_0) is the measurement of error, representing complete absence of spatial auto-correlation and the difference between the sill and nugget,

$C(\mathbf{0}) - c_0$ is called the *partial sill*. The range and actual magnitude of the sill can depend on direction, a property known as *anisotropy*. The characteristics of the semivariogram plots and models can provide the following additional information (Christakos, 1992):

- The investigation of the semivariogram variation in different directions provides information about the anisotropy structure of the random process.
- The semivariogram also indicates the neighbourhoods of influence from any given location.
- The behaviour of the semivariogram at large distances provides information about the stationarity of the data. Asymptotic behaviour is a strong indication of stationarity. However, under IS hypothesis, the semivariogram could be unbounded which is not characterised by the presence of a sill.
- The behaviour of the semivariogram close to and at the origin indicates the degree of short-scale variability in the process. Three types of behaviour can be observed at the origin, namely nugget effect, linear, and parabolic. The nugget effect represents the discontinuity (at the origin) arising from the erratic behaviour or noise in the data. A linear form is indicative of continuity at the origin and the semivariogram does not present erratic behaviour and abruptly changes at small distances. The parabolic behaviour is indicative of very regular and smooth spatial variation as it is twice differentiable at the origin (Gómez-Hernández, 1996).
- Proportion of the total variance of the random function (spatial variability) that is not accounted for due to spatial variability defined as the ratio of nugget effect to the total sill (relative nugget effect).

The theoretical semivariogram and covariance function are inferred from their respective experimental (or sample) semivariogram and covariance function, which are computed under second order stationarity (2.3.6) and intrinsic stationarity (2.3.5) conditions, respectively. A natural estimator of the semivariogram is based on the method of moments by Matheron (1962-1963), as defined by (2.3.16) in section 2.3.4.

Definition 3.3.1 (Anisotropy and Isotropic Process):

If the covariance or the semivariogram function varies jointly with distance and its direction then it is together with the random process are *anisotropic*. However, when

the spatial dependence is the same in all directions the process is *isotropic* resulting in the relation:

$$C(\mathbf{h}) = \psi(\|\mathbf{h}\|), \mathbf{h} \in \mathbb{R}^d \quad (2.3.7)$$

for some continuous function $\psi : [0, \infty) \rightarrow \mathbb{R}$ with $\psi(0) = 1$ and $C(0) = 1$. The contours produced from an isotropic process (2.3.7) are concentric circles or spheres around the origin which we compute the covariance while contours of an anisotropic process are instead ellipses or ellipsoids.

There are two types of anisotropy. A *geometric* anisotropy is defined in terms of semivariograms that have same sill c and different ranges r for the different spatial directions. If the semivariogram or covariance function is anisotropic, then the observed spatial data along a specific direction may be more highly correlated than those along other directions. The concentric ellipses about the origin have the major axis which indicates the direction of greater continuity (that is, more gradual change in this direction) and the minor axis indicates the direction of least continuity (more rapid change in the direction). However, if the sill depends on the spatial direction, then the anisotropy is known as *zonal*.

2.3.3 Permissible Models of the Semivariogram and Covariance Function

The principal concern of inference of the semivariogram or covariance function using the experimental semivariogram or the experimental covariance function is the choice of the theoretical semivariogram or covariance function deemed to be permissible (or valid). This is subject to two very critical requirements of conditional negative-definiteness and positive-definiteness that the semivariogram and the covariance function must adhere to, respectively. In this study the model fitting procedures are discussed in terms of the semivariogram. However, given stationary data, fitting a covariance function model can be performed following the relation (2.3.8):

$$\gamma(\mathbf{h}) = C(0) - C(\mathbf{h}) \quad (2.3.8)$$

Theorem 2.3.1 (Cressie, 1993; Goovaerts, 1997; Schabenberger & Pierce, 2002; Wackernagel, 2003):

Let Z be a second-order stationary random function, with covariance function $C(\mathbf{h})$

and semivariogram $\gamma(\mathbf{h})$ be defined in (2.3.5) and (2.3.6), respectively. Then for any finite collections of spatial locations $\{\mathbf{u}_\alpha : \alpha = 1, \dots, n\}$ and real numbers $\{\lambda_\alpha : \alpha = 1, \dots, n\}$ the variance of the finite linear combination of the random variables $Z(\mathbf{u}_\alpha)$, $\alpha \in \mathbf{D}$; $i = 1, \dots, n$ is non-negative if and only if:

(i) $C(\mathbf{h})$ is positive-definite, satisfying the condition:

$$\text{Var}\left(\sum_{\alpha=1}^n \lambda_\alpha Z(\mathbf{u}_\alpha)\right) = \sum_{\alpha=1}^n \sum_{\beta=1}^n \lambda_\alpha \lambda_\beta C(\mathbf{u}_\alpha - \mathbf{u}_\beta) \geq 0 \quad (2.3.9)$$

(ii) $\gamma(\mathbf{h})$ is conditionally negative-definite satisfying the condition:

$$\text{Var}\left(\sum_{\alpha=1}^n \lambda_\alpha Z(\mathbf{u}_\alpha)\right) = -\sum_{\alpha=1}^n \sum_{\beta=1}^n \lambda_\alpha \lambda_\beta \gamma(\mathbf{u}_\alpha - \mathbf{u}_\beta) \geq 0, \quad \alpha \neq \beta \quad (2.3.10)$$

such that the sum of weights in 2.3.10) is zero: $\sum_{\alpha=1}^n \lambda_\alpha = 0$ (further reading and proof of theorem can be found in Cressie (1993), Goovaerts (1997) and Wackernagel (2003)).

Theorem 2.3.2 (Cressie, 1993):

If $\gamma(\mathbf{h})$ is continuous function on \mathbb{R}^d satisfying the condition $\gamma(\mathbf{0}) = 0$, then the following three properties are equivalent:

- (i) $2\gamma(\mathbf{h})$ is conditionally negative-definite.
- (ii) For all $\lambda > 0$, $\exp(-\lambda\gamma(\mathbf{h}))$ is positive-definite.
- (iii) $2\gamma(\mathbf{h})$ is of the form:

$$2\gamma(\mathbf{h}) = Q(\mathbf{h}) + \int_{-\infty}^{\infty} \dots \int_{-\infty}^{\infty} \frac{1 - \cos(\omega^T \mathbf{h})}{\|\omega\|^2} G(d\omega) \quad (2.3.11)$$

where $Q(\mathbf{h}) \geq 0$ is a quadratic form and $G(\bullet)$ is a positive symmetric measure continuous at the origin that satisfies $\int_{-\infty}^{\infty} \dots \int_{-\infty}^{\infty} 1 + \cos(\|\omega\|^2)^{-1} G(d\omega) < \infty$ (see Cressie (1993) for further reading and proof of the theorem).

A simple way of modelling a semivariogram (or covariance function) is to infer from the graphical representation of the experimental semivariogram $\hat{\gamma}(\mathbf{h})$ or covariance function $\hat{C}(\mathbf{h})$. Properties including stationarity, anisotropy and definiteness conditions and the three parameters (sill, range and nugget effects) should be taken into account when deciding which model to fit to the data. Any function used to fit the

semivariogram or covariance function needs to satisfy the condition of the negative semi-definiteness though we do not need to check this property for every basic model involved in the fitting. We usually restrict ourselves to a list of semivariogram or covariance models for which the condition of non-negative positive definite has been established. Basically, fitting a parametric model to the experimental semovariogram is to ensure smoothness for accurate prediction at unsampled locations. Gelfand et al. (2010) provide three reasons for smoothing the experimental semivariogram. Firstly, it is too rough so smoothing reduces the noise, increasing our understanding of the spatial dependence in the data. Secondly, the conditionally non-negative definite property must be met to ensure that the error or estimation variance in the prediction is non-negative for all locations in \mathbf{D} . Finally, the prediction at some unobserved locations requires estimates of the semivariogram at lags not included among the chosen h_1, \dots, h_k nor do they exist between data locations, smoothing can provide these needed estimates.

To smooth the experimental semivariogram, a valid or permissible parametric model and a method for fitting that model need to be selected. The selection of a suitable model among the collection of valid semivariogram models is informed by examination of the experimental semivariogram and other considerations such as prior knowledge, computational simplicity and sufficient flexibility (Gelfand et al., 2010). The following conditions are necessary and sufficient for a semivariogram model to be permissible if and only if, for all $\boldsymbol{\theta} = (c_0, c, r) \in \Theta$, where Θ is the parameter space for $\boldsymbol{\theta}$:

$\boldsymbol{\theta}$:

- (i) $\gamma(\mathbf{0}; \boldsymbol{\theta}) = 0$, (i.e., vanishing at 0).
- (ii) $\gamma(-\mathbf{h}; \boldsymbol{\theta}) = \gamma(\mathbf{h}; \boldsymbol{\theta})$, (i.e., evenness).
- (iii) $\sum_{\alpha=1}^n \sum_{\beta=1}^n \lambda_{\alpha} \lambda_{\beta} \gamma(\mathbf{u}_{\alpha}, \mathbf{u}_{\beta}) \leq 0$, for all n , $\mathbf{u}_1, \dots, \mathbf{u}_n$ and $\lambda_1, \dots, \lambda_n$ such that $\sum_{\alpha=1}^n \lambda_{\alpha} = 0$
(conditionally negative definiteness).

There are several models which satisfy the above validity requirements (in \mathbb{R}^d , where $d = 2$ or $d = 3$) including the monotonicity and isotropy following the construction (2.3.10) and elsewhere by Christakos (1984), Journel and Huijbregts (1978) and Yaglom (1957) but we present the following, being the most frequently used (Cressie,

1993; Gelfand et al., 2010; Goovaerts, 1997; Schabenberger & Pierce, 2002; Sherman, 2011), including the three basic models (spherical, exponential and exponential-cosine) used in this study to characterise the malaria morbidity incidence rates:

(i) **Nugget effect** (c_0 is obtained as $h \rightarrow \infty$):

$$\gamma_{nug}(h; \theta) = \begin{cases} 0, & h = 0 \\ c_0, & h \neq 0 \end{cases} \quad (2.3.12)$$

where $\theta = c_0 > 0$, which represents the microscale variation causing the discontinuity at origin (white-noise).

(ii) **Spherical model** (valid in \mathbb{R}^d , $1 \leq d \leq 3$):

$$\gamma_{sph}(h; \theta) = \begin{cases} 0 & h = 0 \\ c_0 + c_1 \left\{ (3/2)(h/r) - (1/2)(h/r)^3 \right\}, & 0 < h \leq r \\ c_0 + c_1 & h \geq r \end{cases} \quad (2.3.13)$$

where $\theta = (c_0, c_1, r)^T$ and $c_0, c_1, r \geq 0$. The spherical model is very popular for fitting SOS random processes. It has a linear behaviour near the origin; beyond r there exists no spatial correlation.

(iii) **Exponential model** (valid in \mathbb{R}^d , $d \geq 1$):

$$\gamma_{exp}(h; \theta) = \begin{cases} 0, & h = 0 \\ c_0 + c_1 \left\{ 1 - \exp(-3h/r^1) \right\}, & h > 0 \end{cases} \quad (2.3.14)$$

where $\theta = (c_0, c_1, r^1)^T$, $c_0, c_1, r^1 > 0$ and $r^1 = 3r$, called the *practical* (or *effective*) *range*. This is another most useful fitting model with linear behaviour near the origin and whose spatial correlation decays to zero. If the sill exists, then the range becomes the smallest value of h for this $\gamma_{exp}(h; \theta)$ is equal to its sill. However, if the range does not exist, then practical range is defined, as the smallest value of h for which $\gamma_{exp}(h; \theta)$ reaches 95% of its sill (i.e., $\gamma_{exp}(3r) = 0.95$).

(iv) **Exponential-cosine model** (valid in \mathbb{R}^d , $1 \leq d \leq 3$):

$$\gamma_{expcos}(h; \theta) = \begin{cases} 0, & h = 0 \\ c_0 + c_1 \left\{ 1 - \exp(-3h/r) \cos(bh) \right\}, & h > 0 \end{cases} \quad (2.3.15)$$

where $\theta = (c_0, c_1, r)^T$; $c_0, c_1, r > 0$ and $b = 2\pi/\lambda$, called angular frequency and

λ is the wavelength or period of the function, which is very useful for modelling periodic cycles or seasonal patterns in the data.

In most practical situations two or more basic models are combined to form a nested model to fit the semivariogram. When this happens the sill of the nested semivariogram model is the sum of the structural components of each constituent models. The ratio of the nugget to the sill, termed the *relative nugget effect*, is an indicative of the proportion of the total variance of the random function that is not due to spatial variability.

2.3.4 Semivariogram Estimation and Fitting

The semivariogram is frequently used for structural analysis of spatially (and temporally) distributed data. There are several procedures which have been proposed for its estimation and also model fitting (Armstrong & Delfiner, 1980; Chilès & Delfiner, 1999; Cressie, 1985, 1993; Cressie & Hawkin, 1980; Journel & Huijbregts, 1978; Matèrn, 1960; Matheron, 1963; Miller, 1974; Webster & Oliver, 1992). The estimator of the semivariogram proposed by Matheron (1962-1963) is the most widely used. It is defined by

$$\hat{\gamma}(\mathbf{h}) = \frac{1}{2|n(\mathbf{h})|} \sum_{n(\mathbf{h})} (Z(\mathbf{u}_\alpha) - Z(\mathbf{u}_\beta))^2, \mathbf{u}_\beta = \mathbf{u}_\alpha + \mathbf{h} \quad (2.3.16)$$

where $n(\mathbf{h}) = \{(\alpha, \beta) : \mathbf{u}_\beta - \mathbf{u}_\alpha = \mathbf{h}\}$, denotes the sample of pairs lagged by vector \mathbf{h} and $|n(\mathbf{h})|$ is the number of distinct elements of $n(\mathbf{h})$. It is an unbiased estimator but can hardly satisfy the conditionally negative definiteness property. This can be resolved by fitting valid parametric models to smoothen the experimental estimates. If the random function is isotropic, \mathbf{h} is replaced by $\|\mathbf{h}\|$. The estimator (2.3.16) is known as *classical semivariogram estimator* due to Matheron (1962-1963) and also called the *Matheron's estimator*. The precision of an empirical estimator at a given lag depends on enough pairs used for averaging. There have been various suggestions for an appropriate unique number of pairs to be available for every lag vector \mathbf{h} or distance $|\mathbf{h}|$ but Webster and Oliver (1992) proposed at least 200–300 observed pairs after their simulation study as the most reliable to estimate the semivariogram as opposed to 50 and 30 proposed by Chilès and Delfiner (1999) and Journel and Huijbregts (1978), respectively (Schabenberger & Pierce, 2002). Cressie (1985) shows that the variance

of Matheron's estimator (2.3.16) can be approximated by:

$$\text{Var}(\hat{\gamma}(\mathbf{h})) \approx \frac{2\gamma^2(\mathbf{h}; \boldsymbol{\theta})}{|n(\mathbf{h})|} \quad (2.3.17)$$

The goal of semivariogram estimation is not to estimate the empirical semivariogram estimators (2.3.16) and others but to estimate the unknown parameters $\boldsymbol{\theta}$ of the theoretical semivariogram model $\gamma(\mathbf{h}; \boldsymbol{\theta})$. If the semivariance (2.3.16) is computed at lags h_1, \dots, h_{k_1} , then $\hat{\gamma}(h_1), \dots, \hat{\gamma}(h_{k_1})$ serve as the data to which the semivariogram model is fit. This is an indirect approach to the semivariogram estimation since an empirical estimate is obtained first which then serves as the data. However, choosing more lag classes can increase the size of this set (Schabenberger & Pierce, 2002). The methods for fitting the semivariogram models are presented as follows.

A semivariogram is a measure of spatial dependence and the idea behind its model fitting is to search for a valid theoretical model that is able to mimic the spatial dependence present in the data (Cressie, 1993). The space of all valid semivariograms is a very large set which may be impossible to search from so we usually choose from a parametric family of valid semivariogram models $P = \{\gamma(\mathbf{h}; \boldsymbol{\theta}) : \boldsymbol{\theta} \in \Theta\}$ as the ones in (2.3.12)–(2.3.15). The characterisation of correlation structure of spatial data set is a very critical process prior to kriging at unsampled locations. In geostatistics the usual procedure is to adopt a goodness-of-fit criterion coupled with visual or manual fitting (initial guess of possible models and parameters) all aiming to provide statistically sound model which can incorporate field-specific knowledge of the user (Zimmerman & Zimmerman, 1991). The goodness-of-fit criteria seek to find best elements of a parametric family of valid semivariogram models $P = \{\gamma(\mathbf{h}; \boldsymbol{\theta}) : \boldsymbol{\theta} \in \Theta\}$. There are several of these methods but the most commonly used in geostatistics are the least squares and likelihood-based methods notwithstanding their computational issues widely raised in the literature (Chilès & Delfiner, 1999; Cressie, 1993; Gelfand et al., 2010; Jian, Olea, & Yu, 1996; Miller, 1974; Schabenberger & Pierce, 2002; Vecchia, 1988; Zimmerman & Zimmerman, 1991). These methods are automatic model-fitting procedures for the selection of the parameters and models. They provide a more objective modelling procedure for different users to obtain same results. In addition, they become very useful when numerous semivariograms are to be modelled on a regular basis. Their main criticisms are that not all the models selected are permissible,

a condition required for the unique solution of kriging system; many permissible (nested) models can be fitted, which requires several models to be selected from. The least squares methods are usually preferred to the likelihood-based techniques, which rely heavily on Gaussian distributional assumptions and also provide seriously biased estimates due to data limitation (Cressie, 1993; Jian et al., 1996).

In this study, manual fitting coupled with automatic sill fitting was used due to the erratic behaviour of most of the computed experimental semivariograms. The automatic fitting procedure using the least squares methods choose the most valid model minimising the weighted sum of squares (WSS). Thus, they are based on the concept of closeness measured by the sum of squares of differences between the estimator $\hat{\gamma}(\mathbf{h})$ and the model $\gamma(\mathbf{h};\boldsymbol{\theta})$ (Cressie, 1993; Schabenberger & Pierce, 2002).

2.3.5 Linear Model of Regionalisation (LMR)

In structural analysis of spatial dependence, two or more basic models can be combined to form a *nested* model to fit the experimental semivariogram (or covariance), though not such all combinations can result in a permissible semivariogram (or covariance) function. One possible way of achieving this is through a random function. A *linear model of regionalisation* (LMR) builds a random function $Z(\mathbf{u})$ as a linear combination of $(p+1)$ independent random functions $y^l(u)$, each with mean zero and basic covariance functions:

$$c_l(\mathbf{h}): Z(\mathbf{u}) = \sum_{l=0}^p y^l(\mathbf{u}) + m, \quad (2.3.18)$$

where $m = E[Z(\mathbf{u})]$ and $E[y^l(\mathbf{u})] = 0, \forall l$; and

$$c_l(\mathbf{h}) = \begin{cases} Cov(y^l(\mathbf{u}), y^l(\mathbf{u} + \mathbf{h})), & l = l_1 \\ 0, & \text{if otherwise} \end{cases} \quad (2.3.19)$$

from which we can have:

$$\begin{aligned} C(\mathbf{h}) &= Cov(Z(\mathbf{u}), Z(\mathbf{u} + \mathbf{h})) \\ &= \sum_{l=0}^p \sum_{l_1=0}^p a^l a^{l_1} Cov(y^l(\mathbf{u}), y^{l_1}(\mathbf{u} + \mathbf{h})) \\ &= \sum_{l=0}^p a^l a^l c_l(\mathbf{h}) = \sum_{l=0}^p b^l c_l(\mathbf{h}), \quad b^l = (a^l)^2 \geq 0 \end{aligned} \quad (2.3.20)$$

where (since $y^l(\mathbf{u})$'s are independent) b^l is the sill of the basic covariance model $c_l(\mathbf{h})$

and (b^0) is the nugget effect, for $l=0$. The sufficient conditions for $C(\mathbf{h})$ to be a linear covariance model are that the basic functions $c_l(\mathbf{h})$ are permissible covariance models; and the sill b^l of each covariance model $c_l(\mathbf{h})$ is positive (Goovaerts, 1997). Applying the concept of LMR to semivariogram, we let $g_l(\mathbf{h})$ denote the semivariogram of the random function $y^l(\mathbf{u})$, with the cross semivariogram between any two different random functions $y^l(\mathbf{u})$ and $y^{l_1}(\mathbf{u})$ equal to zero:

$$g_l(\mathbf{h}) = \begin{cases} E\left[\left(y^l(\mathbf{u}) - y^l(\mathbf{u} + \mathbf{h})\right)\left(y^{l_1}(\mathbf{u}) - y^{l_1}(\mathbf{u} + \mathbf{h})\right)\right], & l = l_1 \\ 0, & \text{if otherwise} \end{cases} \quad (2.3.21)$$

The semivariogram model $\gamma(\mathbf{h})$ is then expressed as a positive linear combination of the basic semivariogram models $g_l(\mathbf{h})$:

$$\gamma(\mathbf{h}) = \frac{1}{2} E\left[\left(Z(\mathbf{u}) - Z(\mathbf{u} + \mathbf{h})\right)^2\right] = \sum_{l=0}^p b^l g_l(\mathbf{h}), \quad b^l = (a^l)^2 \geq 0 \quad (2.3.22)$$

where the positive coefficient b^l is the variance contribution of the corresponding basic semivariogram model $g_l(\mathbf{h})$.

In fitting the experimental semivariogram one must decide whether to use isotropic or anisotropic model and to be sure that the model chosen is permissible and how many of such basic models $g_l(\mathbf{h})$ to use. Additional information such as physical knowledge of the phenomenon being studied and robust measures must be utilized. Over fitting of the semivariogram must be avoided, and also the parameters (nugget, sill and range) for each model used must properly be identified to ensure accuracy. The measurement error and microscale variations (that is, the extent of nugget effect and large amount of variation) if can be distinguished should be modelled using a transition models with a finite range shorter than the shortest sampling interval (Goovaerts, 1997; Goovaerts & Chiang, 1993).

2.3.6 Modelling Coregionalisation

The concepts of spatial modelling presented in the previous sections view the regionalised variable $Z(\mathbf{u})$ as a realisation of a random function $\{Z(\mathbf{u}) : \mathbf{u} \in \mathbf{D}\}$. A generalisation can be considered which is a multivariate spatial process for which $Z(\mathbf{u})$ is a random vector, denoted \mathbf{Z} . Modelling such a random process called,

coregionalisation, is to infer $k(k+1)/2$ direct and cross semivariogram (or covariance) models. The models are built dependently in order to satisfy the established non-negativity conditions of variance of any linear combinations of random variables ((2.3.9) or (2.3.10)). This extends the linear model of regionalisation concept to the multivariate version known as linear model of coregionalisation (LMC). In this section the properties of the random vector functions and construction of the LMC are presented.

Let $\mathbf{Z}(\mathbf{u}) = [\mathbf{Z}_1(\mathbf{u}), \dots, \mathbf{Z}_k(\mathbf{u})]^T$ be a random vector of k random variables observed at location \mathbf{u} . Then the multivariate random function defined over the domain \mathbf{D} whose components are vectors of random functions is given by (2.3.23):

$$\mathbf{Z} : \mathbf{D} \rightarrow \{\mathbf{Z}_1(\mathbf{u}), \dots, \mathbf{Z}_k(\mathbf{u}) : \mathbf{u} \in \mathbf{D}\} \quad (2.3.23)$$

Given the set of locations $\{\mathbf{u}_\alpha : \alpha = 1, \dots, n\} \subset \mathbf{D}$, we define the marginal cumulative distribution function (cdf) as:

$$F_t(\mathbf{u}_1, \dots, \mathbf{u}_n; \mathbf{z}_{t1}, \dots, \mathbf{z}_{tn}) = P[\mathbf{Z}_t(\mathbf{u}_1) \leq \mathbf{z}_{t1}, \dots, \mathbf{Z}_t(\mathbf{u}_n) \leq \mathbf{z}_{tn}], \quad (2.3.24)$$

(for $t = 1, \dots, k$), whilst the joint cumulative distribution functions are given by

$$\begin{aligned} & F_{it}(\mathbf{u}_1, \dots, \mathbf{u}_n; (\mathbf{z}_{i1}, \dots, \mathbf{z}_{in}), \dots, (\mathbf{z}_{k1}, \dots, \mathbf{z}_{kn})) \\ &= P[\mathbf{Z}_i(\mathbf{u}_1) \leq \mathbf{z}_{i1}, \dots, \mathbf{Z}_i(\mathbf{u}_n) \leq \mathbf{z}_{in}, \dots, \mathbf{Z}_k(\mathbf{u}_1) \leq \mathbf{z}_{k1}, \dots, \mathbf{Z}_k(\mathbf{u}_n) \leq \mathbf{z}_{kn}], \end{aligned} \quad (2.3.25)$$

(for $i, t = 1, \dots, k$), which characterises the uncertainty of the n – unobserved vectors of $\mathbf{z}(\mathbf{u}) = [\mathbf{z}_1(\mathbf{u}), \dots, \mathbf{z}_k(\mathbf{u})]^T$. The set of n – point cumulative distributions of the k – variates, for every possible choice of locations in \mathbb{R} constitutes the spatial law of multivariate random vector (2.3.23), which we will infer, just like the univariate case in (2.3.1); this then requires the approximation of the first and second moments via the stationarity assumptions. The random vector function \mathbf{Z} is said to be strictly stationary if for every separation vector $\mathbf{h} \in \mathbf{D}$ for the two random vectors of random variables $\{\mathbf{Z}(\mathbf{u}_1), \dots, \mathbf{Z}(\mathbf{u}_n)\}$ and $\{\mathbf{Z}(\mathbf{u}_1 + \mathbf{h}), \dots, \mathbf{Z}(\mathbf{u}_n + \mathbf{h})\}$ is invariant under the translation:

$$F(\mathbf{u}_1, \dots, \mathbf{u}_n; \mathbf{z}_{11}, \dots, \mathbf{z}_{nk}) = F(\mathbf{u}_1 + \mathbf{h}, \dots, \mathbf{u}_n + \mathbf{h}; \mathbf{z}_{11}, \dots, \mathbf{z}_{nk}), \quad (2.3.26)$$

for all $\mathbf{u}_1, \dots, \mathbf{u}_n$ and $\mathbf{h} \in \mathbf{D}$. Under the joint second order stationarity for all the k random functions, we define the mean vector and the covariance matrix by (2.3.27):

$$\begin{cases} \mathbf{m}(\mathbf{u}) = E[\mathbf{Z}(\mathbf{u})] \\ \mathbf{C}(\mathbf{h}) = E[(\mathbf{Z}(\mathbf{u}) - \mathbf{m}(\mathbf{u}))(\mathbf{Z}(\mathbf{u} + \mathbf{h}) - \mathbf{m}(\mathbf{u}))^T] \end{cases} \quad (2.3.27)$$

where $\mathbf{m}(\mathbf{u}) = [m_1(\mathbf{u}), \dots, m_k(\mathbf{u})]^T$, the mean vector and $\mathbf{C}(\mathbf{h})$ is the matrix of covariance functions $C_{it}(\mathbf{h})$ for all pairs $(i, t) = 1, \dots, k$. The function $C_{it}(\mathbf{h})$ is called direct covariance function for $i = t$ and when $i \neq t$, it is referred to as cross covariance function which can either be even or odd depending on the order of the variables. Thus, $C_{it}(\mathbf{h}) = C_{it}(-\mathbf{h})$, however $C_{it}(\mathbf{h}) \neq C_{ti}(\mathbf{h})$ and $C_{it}(\mathbf{h}) \neq C_{it}(-\mathbf{h})$. The intrinsic stationarity assumption is evoked if the SOS is not met. In this case the increments $\mathbf{Z}(\mathbf{u} + \mathbf{h}) - \mathbf{Z}(\mathbf{u})$ are considered as SOS:

$$\begin{cases} E[\mathbf{Z}(\mathbf{u} + \mathbf{h}) - \mathbf{Z}(\mathbf{u})] = \mathbf{0} \\ \mathbf{\Gamma}(\mathbf{h}) = \frac{1}{2} E[(\mathbf{Z}(\mathbf{u} + \mathbf{h}) - \mathbf{Z}(\mathbf{u}))(\mathbf{Z}(\mathbf{u} + \mathbf{h}) - \mathbf{Z}(\mathbf{u}))^T] \end{cases} \quad (2.3.28)$$

where $\mathbf{\Gamma}(\mathbf{h})$ is the matrix of semivariogram functions $\gamma_{it}(\mathbf{h})$ for all pairs $(i, t) = 1, \dots, k$. If $i \neq t$, $\gamma_{it}(\mathbf{h})$ is called cross semivariogram function and for $i = t$, it is known as direct semivariogram function. The semivariogram is even function and is symmetric. The existence of $\mathbf{C}(\mathbf{h})$ under the SOS implies existence of the finite priori variance: $Var(\mathbf{Z}_t(\mathbf{u})) = E[(\mathbf{Z}_t(\mathbf{u}) - m_t(\mathbf{u}))^2] = C_{tt}(\mathbf{0})$, which leads to the following relationship:

$$\mathbf{\Gamma}(\mathbf{h}) = \mathbf{C}(\mathbf{0}) - \mathbf{C}(\mathbf{h}) \quad (2.3.29)$$

where $\mathbf{C}(\mathbf{0})$ is the variance-covariance matrix of k random variable provided if it exists. In practice the asymmetry property of $\mathbf{C}(\mathbf{h})$ is usually ignored, the reasons being that $\mathbf{\Gamma}(\mathbf{h})$ is often used for structural analysis based on its symmetric property and also the difficulty (if not impossibility) of verifying the presence of a lag effect due to lack of adequate data (Goovaerts, 1997). In this thesis we adopt the semivariogram matrix $\mathbf{\Gamma}(\mathbf{h})$ as the main structural tool to characterise the spatial dependence of malaria morbidity incidence in Ghana and its potential risk factors.

The degree of correlation between the pair $\mathbf{Z}_i(\mathbf{u} + \mathbf{h})$ and $\mathbf{Z}_t(\mathbf{u})$ for all $i, t = 1, \dots, k$ usually decreases as $|\mathbf{h}|$ increases. Hence $C_{it}(\mathbf{h}) \rightarrow 0$ as $|\mathbf{h}| \rightarrow \infty$, and $C_{it}(\mathbf{h}) \rightarrow 0$; $\gamma_{it}(\mathbf{h}) \rightarrow C_{it}(\mathbf{0})$ as $|\mathbf{h}| \rightarrow \infty$, called priori covariance. This limiting value is the sill and the distance at which this value is reached is the range (denoted by c_s and r_s ,

respectively in this thesis). The correlation function (correlogram) of the random function is defined as:

$$\rho_{it}(\mathbf{h}) = \frac{C_{it}(\mathbf{h})}{\sqrt{C_{ii}(\mathbf{0})C_{tt}(\mathbf{0})}}, \quad (2.3.30)$$

which is bounded as $|\rho_{it}| \leq 1$. The vector \mathbf{h} accounts for both distance and direction. If the covariance function exhibits the same spatial behaviour in all direction for all \mathbf{h} then $\mathbf{C}(\mathbf{h}) = \mathbf{C}(|\mathbf{h}|)$ and the function is said to be isotropic and is called anisotropic, if otherwise. Under the assumption of SOS the functions $\mathbf{C}(\mathbf{h})$, $\mathbf{\Gamma}(\mathbf{h})$ and $\boldsymbol{\rho}(\mathbf{h})$ depend only on the separation vector \mathbf{h} , and not functions of the location \mathbf{u} . Each pair of values $[\mathbf{Z}_i(\mathbf{u}_\alpha), \mathbf{Z}_i(\mathbf{u}_\beta)]$ separated by the vector \mathbf{h} can be considered as a different realisation of the pair of random variables $[\mathbf{Z}_i(\mathbf{u}_\alpha), \mathbf{Z}_i(\mathbf{u}_\beta)]$, for all $i, t = 1, \dots, k$ and $\alpha \neq \beta$. This provides the many realisations of the random function necessary to made the required statistical inferences.

The permissible model version conditions of $\mathbf{C}(\mathbf{h})$ and $\mathbf{\Gamma}(\mathbf{h})$ are obtained as follows: Let $\{\mathbf{Z}_t(\mathbf{u}); t = 1, \dots, k\}$ be a set of k interdependent random functions, $\mathbf{u}_\alpha; \alpha = 1, \dots, n$ be n data locations and Y be a linear combination of finite random variables $\mathbf{Z}_t(\mathbf{u}_\alpha); \mathbf{u}_\alpha \in \mathbf{D}$; for $t = 1, \dots, k$. Then

$$Y = \sum_{t=1}^k \sum_{\alpha=1}^n \lambda_{\alpha t} \mathbf{Z}_t(\mathbf{u}_\alpha), \quad (2.3.31)$$

where:

$$\text{Var}(Y) = \text{Var}\left(\sum_{t=1}^k \sum_{\alpha=1}^n \lambda_{\alpha t} \mathbf{Z}_t(\mathbf{u}_\alpha)\right) = \sum_{\beta=1}^n \sum_{\alpha=1}^n \boldsymbol{\lambda}_\alpha^T C(\mathbf{u}_\alpha - \mathbf{u}_\beta) \boldsymbol{\lambda}_\beta \geq 0 \quad (2.3.32)$$

$\boldsymbol{\lambda}_\alpha = (\lambda_{\alpha 1}, \dots, \lambda_{\alpha k})^T$ and $C(\mathbf{u}_\alpha - \mathbf{u}_\beta) = [C_{ij}(\mathbf{u}_\alpha - \mathbf{u}_\beta)]$, a $k \times k$ matrix. To satisfy the condition (2.3.32), the matrix of auto and cross covariance models must be positive semi-definite. Then from (2.3.29) we have:

$$\left\{ \begin{array}{l} \text{Var}(Y) = \sum_{\beta=1}^n \sum_{\alpha=1}^n \boldsymbol{\lambda}_\alpha^T C(\mathbf{u}_\alpha - \mathbf{u}_\beta) \boldsymbol{\lambda}_\beta \\ = C(\mathbf{0}) \sum_{\alpha=1}^n \boldsymbol{\lambda}_\alpha^T \sum_{\alpha=1}^n \boldsymbol{\lambda}_\beta - \sum_{\beta=1}^n \sum_{\alpha=1}^n \boldsymbol{\lambda}_\alpha^T \mathbf{\Gamma}(\mathbf{h}) \boldsymbol{\lambda}_\beta \geq 0, \\ = - \sum_{\beta=1}^n \sum_{\alpha=1}^n \boldsymbol{\lambda}_\alpha^T \mathbf{\Gamma}(\mathbf{h}) \boldsymbol{\lambda}_\beta \geq 0; \quad \sum_{\alpha=1}^n \boldsymbol{\lambda}_\alpha = \mathbf{0} \end{array} \right. \quad (2.3.33)$$

which ensures the non-negativity condition of the variance of Y , where the matrix of semivariogram models must be conditionally negative semi-definite subject to the sum of vectors λ_α being the null vector. The multivariate semivariogram inference then provides a set of matrices $\hat{\mathbf{\Gamma}}(\mathbf{h}_t) = [\hat{\gamma}_{ij}(\mathbf{h}_t)]$ for a finite number of lags, $\mathbf{h}_t; t = 1, \dots, k$, and directions:

$$\hat{\gamma}_{ij}(\mathbf{h}) = \frac{1}{2n(\mathbf{h})} \sum_{\alpha=1}^{n(\mathbf{h})} (\mathbf{Z}_i(\mathbf{u}_\alpha + \mathbf{h}) - \mathbf{Z}_i(\mathbf{u}_\alpha)) (\mathbf{Z}_j(\mathbf{u}_\alpha + \mathbf{h}) - \mathbf{Z}_j(\mathbf{u}_\alpha))^T \quad (2.3.34)$$

for $t = 1, \dots, k$, where $n(\mathbf{h})$ is the number of pairs of sample locations separated by the lag vector \mathbf{h} . The difficulty of this modelling lies in the fact that the $k+1$ semivariograms cannot be built independently from one another. The simplest approach consists of modelling the $k+1$ semivariograms as a linear combinations of the same set of basic semivariograms model, called linear models of coregionalisation (LMC) (Goovaerts, 1999). A permissible combination of functions can be built through the use of LMC.

In the multivariate sense LMC accounts for the spatial dependence between the k attributes from the inference of $k(k+1)/2$ direct and cross experimental semivariograms in (2.3.34), providing the experimental matrices $\hat{\mathbf{\Gamma}}(\mathbf{h}_t)$ for the separation distances h_t to which models are then fitted. Inferring from the univariate case (2.3.18), the multivariate random function \mathbf{Z} , consisting of k interrelated random functions in (2.3.31), can be decomposed into spatially independent components $Y_t^l(\mathbf{u}); t = 1, \dots, k$, each having a mean zero and basic covariance function $C_l(\mathbf{h})$:

$$\begin{cases} \mathbf{Z}_t(\mathbf{u}) = \sum_{l=0}^k Y_t^l(\mathbf{u}) + m_t \\ \text{Cov}(Y_t^l(\mathbf{u}), Y_t^{l_1}(\mathbf{u} + \mathbf{h})) = \begin{cases} C_{ii}^l(\mathbf{h}), & l = l_1 \\ 0 & , l \neq l_1 \end{cases} \end{cases} \quad (2.3.35)$$

where $E[\mathbf{Z}_t(\mathbf{u})] = m_t$, $E[Y_t^l(\mathbf{u})] = 0$, $\forall l, t = 1, \dots, k$, and each components C_{ii}^l of the cross covariance matrix $C_{ii}^l(\mathbf{h})$ is a product of the coefficient b_{ii}^l (partial sills) and the corresponding covariance function $C^l(\mathbf{h})$. The cross covariance function for the pair (Y_i, Y_t) is given as:

$$C_{it}(\mathbf{h}) = \sum_{l=0}^k b_{it}^l C^l(\mathbf{h}), \quad \forall i, t \quad (2.3.36)$$

which defines the linear model of coregionalisation (LMC); the $k \times k$ matrix $\mathbf{B}=[b_{it}^l]$, called coregionalisation matrix, is symmetric from which we can obtain the matrix valued covariance functions as:

$$\mathbf{C}(\mathbf{h}) = \sum_{l=0}^k \mathbf{B}_l C_l(\mathbf{h}) \quad (2.3.37)$$

The conditions sufficient for the constructed model (2.3.37) to be permissible are that $C_l(\mathbf{h})$ are permissible covariance models and that $(k+1)$ coregionalisation matrices \mathbf{B}_l are all positive semi-definite. A similar construction leads to the LMC in terms of the semivariogram models $g_l(\mathbf{h})$ following (2.3.22):

$$\gamma_{it}^l(\mathbf{h}) = \sum_{l=0}^k b_{it}^l g^l(\mathbf{h}), \quad \forall i, t \quad (2.3.38)$$

$$\Gamma(\mathbf{h}) = \sum_{l=0}^k \mathbf{B}_l C_l(\mathbf{h}) \quad (2.3.39)$$

where under SOS, the value of the basic model $C_l(\mathbf{h})=1$ at $|\mathbf{h}|=0$, $\mathbf{C}(\mathbf{0}) = \sum_{l=0}^k \mathbf{B}_l$, and provided $g_l(\mathbf{h})$ are permissible models and \mathbf{B}_l are positive semi-definite, then (2.3.38) is by construction permissible. A particular case of LMC is when $k=1$ which is the linear model of regionalisation (LMR) in section 2.3.5.

The LMC is convenient when employed for fitting a semivariogram (or covariance function) because we are able to verify the permissibility of the models during the process. The models $g_l(\mathbf{h})$ models, as already noted, are selected from a list of functions known to be conditionally non-negative definite and the sill matrices \mathbf{B}_l are required to be positive semi-definite. However, satisfying this can be challenging in view of the number of variables jointly to be modelled coupled with limitations imposed on the choice of basic models. When a basic model b_{it}^l is selected to model a cross semivariogram $\gamma_{it}(\mathbf{h})$ it must be present in the models of both direct semivariograms $\gamma_{ii}(\mathbf{h})$ and $\gamma_{tt}(\mathbf{h})$ where $b_{ii}^l \neq 0$ and $b_{tt}^l \neq 0$ for all $i=1, \dots, k$. This means that if the basic model is absent in the direct semivariogram it must also be absent in the cross semivariogram associated with the variable. However, it is not necessary for each direct and cross semivariogram to include all basic structures. If a structure appears on both direct semivariograms $\gamma_{ii}(\mathbf{h})$ and $\gamma_{tt}(\mathbf{h})$, it need not be present in the

cross semivariogram $\gamma_{it}(\mathbf{h})$, that is, if $b_{ii}^l \neq 0$ and $b_{tt}^l \neq 0$. In addition, it is not necessary for each structure to be present in each direct semivariogram models, that is, b_{it}^l may be equal to zero for some l . However, basic models common to all direct semivariograms are typically chosen as having one or more of the b_{it}^l equal to zero impedes derivation of the positive definite coregionalisation matrices. In practice, the modelling is performed in two steps: The direct semivariograms are modelled as linear combinations of selected basic structures $g_l(\mathbf{h})$, which are then used to fit the cross semivariograms under the conditions that the coefficients $b_{it} \geq 0$ and that $|b_{it}^l| \leq \sqrt{b_{ii}^l \times b_{tt}^l}$, $\forall l, t$ and i .

2.4 Geostatistical Spatial Optimal Prediction

Spatial dependence, if it exists, allows prediction of values of the random function at unsampled locations and, in some cases estimation of the unknown mean across all realisations of the random process. There are several models developed for optimal spatial predictions. One of such class of techniques is the geostatistical methodology of kriging, a family of generalised least squares regression algorithms used for estimating or predicting attributes values at unobserved locations (Goovaerts, 1997; Olea, 1999). Kriging, in geostatistics means optimal prediction, a generic name adopted by Matheron (1963) in recognition of the pioneering work of the South African mining engineer D.G. Krige in quantification of ore reserves (Cressie, 1993; Gelfand et al., 2010; Goovaerts, 1997; Hengl, 2009; Olea, 1999). The kriging techniques seek to minimise the variance of the prediction error under the condition that the prediction error is unbiased with expectation zero; hence they are considered as best linear unbiased estimators (BLUE). In this section we present the kriging techniques, specifically the assumptions underlying optimal spatial prediction and the various types of kriging used for the malaria risk prediction in this study.

2.4.1 Assumptions of Best Linear Unbiased Estimators (BLUE)

The main goal of geostatistical data analysis is spatial prediction of the attribute of the random function $Z(\mathbf{u})$ using the sampled observations $\{Z(\mathbf{u}_\alpha : \alpha = 1, \dots, n)\}$, where $Z(\mathbf{u})$ varies continuously throughout the study region (domain) \mathbf{D} . This leads to

production of a map for the attribute predicting locations \mathbf{u}_0 in the study region where data were missing or unavailable. This process involves various steps but not limited to the following (Schabenberger & Pierce, 2002):

- (i) Using exploratory techniques, prior knowledge and assuming a model of possibly non-stationary mean including SOS or IS error for $Z(\mathbf{u})$ process that generated the data.
- (ii) Estimate the mean function for example, by OLS to detrend the data. If the mean is stationary this step is not necessary. These methods for detrending employed at this step usually do not take auto correlation into account.
- (iii) Using the residuals obtained in step (ii) (or original data if the mean is stationary) fit a semivariogram model $\gamma(\mathbf{h};\boldsymbol{\theta})$ by one of the methods in section 2.3.4.
- (iv) Using statistical estimates of the spatial dependence in hand (from step (iii)), return to step (ii) to re-estimate the parameters of the mean function, now taking into account the spatial autocorrelation.
- (v) Obtain new residuals from step (iv) and iterate steps (ii)–(iv), if necessary.
- (vi) Predict the attribute Z at an unobserved location \mathbf{u} and calculate the corresponding mean square prediction errors to assess the prediction accuracy.

Spatial data exhibit autocorrelations which are functions of the proximity of observations. Let $Z(\mathbf{u}_\alpha); \alpha = 1, \dots, n$ be the attribute values observed at locations $\mathbf{u}_1, \dots, \mathbf{u}_n$ and \mathbf{u}_0 the target location where the prediction is desired. If the observations are spatially correlated then $Z(\mathbf{u}_0)$ is also correlated with the observations unless the target location \mathbf{u}_0 is further removed from the observed locations than the spatial range. In this case we seek to find which function of the data $Z_p(\mathbf{u}_0)$ best predicts $Z(\mathbf{u}_0)$ and how to measure the mean square prediction error. To solve this problem we need to define what “best” means. Kriging methods are solutions to the prediction problem where the predictor is said to be *best linear unbiased estimator* (BLUE) $Z_p(\mathbf{u}_0)$, if and only if, it minimises the mean square predictor error. It is a linear combination of the observed values $Z(\mathbf{u}_\alpha); \alpha = 1, \dots, n$; and it is unbiased in the sense that the mean of the predicted value at \mathbf{u}_0 of $Z(\mathbf{u})$.

There are various types of kriging techniques for determining the optimal spatial predictor $Z_p(\mathbf{u}_0)$, all depending on the model assumption for the random function $Z(\mathbf{u})$, which decomposes into the trend $m(\mathbf{u})$ and residual (or error) $R(\mathbf{u})$ under SOS and IS (Cressie, 1993; Goovaerts, 1997; van Beers & Kleijnen, 2003):

$$Z(\mathbf{u}) = m(\mathbf{u}) + R(\mathbf{u}) \quad (3.4.1)$$

where $Var(R(\mathbf{u})) = Var(Z(\mathbf{u})) = \Sigma$ is the covariance matrix, $E[Z(\mathbf{u})] = m(\mathbf{u})$ and $R(\mathbf{u}) \sim N[\mathbf{0}, \Sigma(\boldsymbol{\theta})]$. In this study we limit ourselves to ordinary kriging and its multivariate version called ordinary co-kriging, the most commonly used spatial kriging predictors, which coupled with other space-time techniques (in chapter 3) were used to estimate the malaria morbidity incidence rates at the various district locations in Ghana.

2.4.2 Ordinary Kriging

The ordinary kriging (OK) considers the trend (mean) $m(\mathbf{u})$ to be locally constant, but unknown. In this way we are able to account for the local variation of the mean, limiting stationarity to only the local neighbourhood $H(\mathbf{u})$ centred at the estimation location \mathbf{u} . The linear estimator then becomes:

$$\begin{cases} Z_p(Z(\mathbf{u}_0)) = \sum_{\alpha=1}^{n(\mathbf{u})} \lambda_{\alpha} [Z(\mathbf{u}_{\alpha}) - m(\mathbf{u}_{\alpha})] + m(\mathbf{u}) \\ = \sum_{\alpha=1}^{n(\mathbf{u})} \lambda_{\alpha} Z(\mathbf{u}_{\alpha}) + \left(1 - \sum_{\alpha=1}^{n(\mathbf{u})} \lambda_{\alpha}\right) m(\mathbf{u}) \end{cases} \quad (2.4.2)$$

Now to ensure unbiasedness of the OK predictor $m(\mathbf{u})$ is filtered from (2.4.2) (since it is explicitly unknown) so that the weights λ_{α}^{ok} sum to one, yielding:

$$Z_p^{ok}(\mathbf{u}) = \sum_{\alpha=1}^{n(\mathbf{u})} \lambda_{\alpha}^{ok} Z(\mathbf{u}_{\alpha}) \quad \text{subject to} \quad \sum_{\alpha=1}^{n(\mathbf{u})} \lambda_{\alpha}^{ok} = 1 \quad (2.4.3)$$

The minimisation of the error variance $\sigma_p^2 = Var(Z_p(\mathbf{u}_0) - Z(\mathbf{u}))$ subject to the unbiasedness condition: $E[Z_p(\mathbf{u})] = Z(\mathbf{u}) = m(\mathbf{u})$ leads to:

$$L(\lambda_{\alpha}^{ok}; \mu_{ok} : \alpha = 1, \dots, n(\mathbf{u})) = \sigma_{pok}^2 - 2\mu_{ok} \left(\sum_{\alpha=1}^{n(\mathbf{u})} \lambda_{\alpha}^{ok} - 1 \right), \quad (2.4.4)$$

a Lagrangian function of the OK weights λ_{α}^{ok} and Lagrange multiplier μ_{ok} where σ_{pok}^2

can be written in terms of the covariance function $C(\cdot)$ and the semivariogram $\gamma(\cdot)$ as in (2.4.5):

$$\left\{ \begin{aligned} \sigma_{pok}^2 &= E \left[\left(Z_p^{ok}(\mathbf{u}_0) - \sum_{\alpha=1}^{n(\mathbf{u})} \lambda_{\alpha}^{ok} Z(\mathbf{u}_{\alpha}) \right)^2 \right] \\ &= \sum_{\alpha=1}^{n(\mathbf{u})} \sum_{\beta=1}^{n(\mathbf{u})} \lambda_{\alpha}^{ok} \lambda_{\beta}^{ok} C(\mathbf{u}_{\alpha} - \mathbf{u}_{\beta}) - 2 \sum_{\alpha=1}^{n(\mathbf{u})} \lambda_{\alpha}^{ok} C(\mathbf{u}_{\alpha} - \mathbf{u}) + C(\mathbf{0}) \\ &= - \sum_{\alpha=1}^{n(\mathbf{u})} \sum_{\beta=1}^{n(\mathbf{u})} \lambda_{\alpha}^{ok} \lambda_{\beta}^{ok} \gamma(\mathbf{u}_{\alpha} - \mathbf{u}_{\beta}) + 2 \sum_{\alpha=1}^{n(\mathbf{u})} \lambda_{\alpha}^{ok} \gamma(\mathbf{u}_{\alpha} - \mathbf{u}) \end{aligned} \right. \quad (2.4.5)$$

Rewriting (2.4.4) in terms $\gamma(\cdot)$ we to obtain (2.5.6):

$$\begin{aligned} L(\lambda_{\alpha}^{ok}; \mu_{ok}) &= - \sum_{\alpha=1}^{n(\mathbf{u})} \sum_{\beta=1}^{n(\mathbf{u})} \lambda_{\alpha}^{ok} \lambda_{\beta}^{ok} \gamma(\mathbf{u}_{\alpha} - \mathbf{u}_{\beta}) \\ &\quad + 2 \sum_{\alpha=1}^{n(\mathbf{u})} \lambda_{\alpha}^{ok} \gamma(\mathbf{u}_{\alpha} - \mathbf{u}_{\beta}) - 2 \mu_{ok} \left(\sum_{\alpha=1}^{n(\mathbf{u})} \lambda_{\alpha}^{ok} - 1 \right) \end{aligned} \quad (2.4.6)$$

Taking $n(\mathbf{u})+1$ partial derivatives of (2.4.6) with respect to λ_{β}^{ok} and μ_{ok} and equating to zero results the following OK system:

$$\left\{ \begin{aligned} \sum_{\beta=1}^{n(\mathbf{u})} \lambda_{\alpha}^{ok} \gamma(\mathbf{u}_{\alpha} - \mathbf{u}_{\beta}) + \mu_{ok} &= \gamma(\mathbf{u}_{\alpha} - \mathbf{u}_{\beta}); \alpha = 1, \dots, n(\mathbf{u}) \\ \sum_{\beta=1}^{n(\mathbf{u})} \lambda_{\beta}^{ok} &= 1 \end{aligned} \right. \quad (2.4.7)$$

The solution of the system (2.4.7), by partitioning, is given by:

$$\left\{ \begin{aligned} \lambda_{ok}^T &= \Gamma^{-1} \boldsymbol{\gamma} = \Gamma^{-1} \left(\boldsymbol{\gamma} + \mathbf{I} \frac{(1 - \mathbf{I}^T \Gamma^{-1} \boldsymbol{\gamma})}{\mathbf{I}^T \Gamma^{-1} \mathbf{I}} \right)^T \\ \mu_{ok} &= - \frac{(1 - \mathbf{I}^T \Gamma^{-1} \boldsymbol{\gamma})}{\mathbf{I}^T \Gamma^{-1} \mathbf{I}} \end{aligned} \right. \quad (2.4.8)$$

where Γ is a $n(\mathbf{u}) \times n(\mathbf{u})$ matrix whose elements are $\gamma(\mathbf{u}_{\alpha} - \mathbf{u}_{\beta})$; $\alpha, \beta = 1, \dots, n(\mathbf{u})$; $\boldsymbol{\gamma}$ denotes the vector $(\gamma(\mathbf{u}_0 - \mathbf{u}_1), \dots, \gamma(\mathbf{u}_0 - \mathbf{u}_{n(\mathbf{u})}))^T$ and \mathbf{I} is a vector with entries 1. The optimal weights in (2.4.8) result in the OK estimator of the local mean with minimum prediction variance given respectively by

$$\left\{ \begin{aligned} \mu_{ok}^* &= \sum_{\alpha=1}^{n(\mathbf{u})} \lambda_{\alpha}^{ok} Z(\mathbf{u}_{\alpha}) \\ \sigma_{pok}^2 &= \sum_{\alpha=1}^{n(\mathbf{u})} \lambda_{\alpha}^{ok} \gamma(\mathbf{u}_0 - \mathbf{u}_{\alpha}) + \mu_{ok} = \boldsymbol{\lambda}_{ok}^T \boldsymbol{\gamma} \end{aligned} \right. \quad (2.4.9)$$

The semivariogram is highly sensitive to strong positive skewness in data resulting from extremely large or small values. The skewness may be reduced by a variance stabilising transformation such as the logarithmic or Box-Cox power transformation (Box & Cox, 1964). In the case of a logarithmic transformation, the observed data $\{Z(\mathbf{u}_\alpha); \alpha = 1, \dots, n\}$, then follow the lognormal distribution and lognormal ordinary kriging (LOK) serves an alternative to OK to offer a better estimation (Journal & Huijbregts, 1978). Equation (2.4.3) is therefore modified for the interpolation of $Z(\mathbf{u})$ using the LOK estimator (Journal, 1980; Rivoirard, 1990) as given by (2.4.10):

$$Z_{lok}(\mathbf{u}) = \exp\left\{Y_p^{ok}(\mathbf{u}_\alpha) + 0.5\sigma_{ok}^2 - \mu_{ok}\right\} \quad (2.4.10)$$

where $Y(\mathbf{u}_\alpha) = \ln(Z(\mathbf{u}_\alpha))$, σ_{ok}^2 is the kriging variance, μ_{ok} is the Lagrange multiplier of the system (2.4.7) in log scale, and $0.5\sigma_{lok}^2 - \mu_{ok}$ is the non-bias term, according to (Journal, 1980). The space-time version of the LOK which is implemented in this study is presented in chapter 3.

2.4.3 Ordinary Co-kriging

In most real situations it may be inadequate to limit stationarity within each neighbourhood $H(\mathbf{u})$ as the case in OK which considers $m(\mathbf{u})$ as locally constant though unknown. The trend of the non-stationary model can be appropriately and alternatively modelled as a smoothly varying function of spatial coordinates or secondary variables (covariates). This leads to a variety of kriging predictors including ordinary cokriging (OCK). Co-kriging incorporates the spatial continuity of the secondary variables into the spatial prediction. It particularly becomes useful if the covariates are not exhaustively sampled but there exists good correlation between the primary variable and the covariates. Cokriging adheres to rather stricter model assumptions to ensure a minimised prediction error variance. It is implemented as follows:

Let $Z_1(\mathbf{u})$ be the primary variable with sampled values $\{z_1(\mathbf{u}_\alpha); \alpha = 1, \dots, n_1(\mathbf{u})\}$ and correlating spatially with $\{Z_i(\mathbf{u}); i = 2, \dots, k\}$, a $k-1$ covariates whose observed values are $\{z_i(\mathbf{u}_{\alpha_i}); \alpha_i = 1, \dots, n_i(\mathbf{u}); i = 2, \dots, k\}$ at locations \mathbf{u}_{α_i} . The linear optimal predictor of $Z_1(\mathbf{u}_0)$ is expressed as a linear combination of all data values of k random variables:

$$\begin{cases} Z_{p1}(\mathbf{u}) = \sum_{i=1}^k \sum_{\alpha_i=1}^{n_i(\mathbf{u})} \lambda_{\alpha_i} Z_i(\mathbf{u}_{\alpha_i}) \\ Z_{p1}(\mathbf{u}) - m_1(\mathbf{u}) = \sum_{\alpha_1=1}^{n_1(\mathbf{u})} \lambda_{\alpha_1} (Z_1(\mathbf{u}_{\alpha_1}) - m_1(\mathbf{u}_{\alpha_1})) + \sum_{i=2}^k \sum_{\alpha_i=1}^{n_i(\mathbf{u})} \lambda_{\alpha_i} (Z_i(\mathbf{u}_{\alpha_i}) - m_i(\mathbf{u}_{\alpha_i})) \end{cases} \quad (2.4.11)$$

where λ_{α_1} is the weight for the primary variable data $z_1(\mathbf{u}_{\alpha_1})$ and $\lambda_{\alpha_i}, i > 1$ are the weights for the covariates data $z_i(\mathbf{u}_{\alpha_i})$. Let the expected values of the random variables $Z_1(\mathbf{u})$ and $Z_i(\mathbf{u}_{\alpha_i})$ be $m_1(\mathbf{u})$ and $m_i(\mathbf{u}_{\alpha_i})$, respectively. Then the cokriging estimator is required to be unbiased and to minimise the prediction error variance σ_{p1}^2 :

$$\begin{cases} E[Z_{p1}(\mathbf{u}) - Z_1(\mathbf{u})] = 0 \\ \sigma_{p1}^2(\mathbf{u}) = \text{Var}(Z_{p1}(\mathbf{u}) - m_1(\mathbf{u})) = E[(Z_{p1}(\mathbf{u}) - m_1(\mathbf{u}))^2] \end{cases} \quad (2.4.12)$$

The random function $Z_i(\mathbf{u})$ is also decomposed as in (2.4.1) into trend $m_i(\mathbf{u})$ and residuals $R_i(\mathbf{u})$ components:

$$Z_i(\mathbf{u}) = m_i(\mathbf{u}) + R_i(\mathbf{u}); \quad i = 1, \dots, k \quad (2.4.13)$$

where $R_i(\mathbf{u})$ is then modelled as stationary random function with mean zero and covariance function $C_{r_i}(\mathbf{h})$. We consider all the trends $m_i(\mathbf{u})$ as locally constants but unknown, which becomes the multivariate version of OK, ordinary cokriging (OCK). The ordinary co-kriging BLUE is thus obtained by minimising:

$$\sigma_{p1}^2 = E \left[\left(Z_{p1}^{ck}(\mathbf{u}_0) - \sum_{i=1}^k \sum_{\alpha_i=1}^{n_i(\mathbf{u})} \lambda_{\alpha_i} Z_i(\mathbf{u}_{\alpha_i}) \right)^2 \right], \text{ subject to:} \quad (2.4.14)$$

$$\sum_{\alpha_1=1}^{n_1(\mathbf{u})} \lambda_{\alpha_1} = 1 \text{ and } \sum_{\alpha_i=1}^{n_i(\mathbf{u})} \lambda_{\alpha_i} = 0; \quad i = 2, \dots, k \quad (2.4.15)$$

The system of $n(\mathbf{u})+1$ equations in terms of the covariance functions $C_{ij}(\cdot)$ is as below:

$$\begin{cases} \sum_{i=1}^k \sum_{\beta_i=1}^{n_i(\mathbf{u})} \lambda_{\beta_i} C_{ij}(\mathbf{u}_{\alpha_i} - \mathbf{u}_{\beta_j}) + \mu_i(\mathbf{u}) = C_{i1}(\mathbf{u}_{\alpha_i} - \mathbf{u}); \quad \alpha_i = 1, \dots, n_i(\mathbf{u}); \quad j = 1, \dots, k \\ \sum_{\beta_i=1}^{n_i(\mathbf{u})} \lambda_{\beta_i} = \delta_{i1}; \quad j = 1, \dots, k \end{cases} \quad (2.4.16)$$

where $\delta_{i1} = 1$, for $i = 1$, and $\delta_{i1} = 0$, otherwise.

In most instances the true means are unknown, IS is implied hence (2.4.16) in terms of semivariograms $\gamma_{ij}(\cdot)$, following the relation: $C_{ij}(\mathbf{h}) = C_{ij}(\mathbf{0}) - \gamma_{ij}(\mathbf{h})$; $i, j = 1, 2$, as in (2.3.29), we have the system (2.4.17):

$$\left\{ \begin{array}{l} \sum_{j=1}^k \sum_{\beta_j=1}^{n_j(\mathbf{u})} \lambda_{\beta_j} \gamma_{ij}(\mathbf{u}_{\alpha_i} - \mathbf{u}_{\beta_j}) - \mu_i(\mathbf{u}) = \gamma_{i1}(\mathbf{u}_{\alpha_i} - \mathbf{u}); \alpha_i = 1, \dots, n_i(\mathbf{u}); j = 1, \dots, k \\ \sum_{\alpha_1=1}^{n_1(\mathbf{u})} \lambda_{\alpha_1} = 1 \\ \sum_{\alpha_i=1}^{n_i(\mathbf{u})} \lambda_{\alpha_i} = 0; j = 2, \dots, k \end{array} \right. \quad (2.4.17)$$

from which the optimal cokriging weights are derived.

Cokriging can also be performed in terms of the residuals $R_i(\mathbf{u})$ in (2.4.13) by detrending each time series for the different attributes at each location. This approach is explored in space-time modelling in chapter 3 and applied to the district-month morbidity incidence rates data with the climatic covariates.

2.5 Time Series Analysis

Time series models will generally reflect the fact that observations close together in time will be more closely related than observations further apart, and in addition, they will often make use of the natural one-way ordering of time so that values in the series of observations z_t for a given time t can be expressed as deriving in some way from past values, rather than from future.

The analysis of time series data includes exploration, description, prediction and forecasting. The general exploration is concerned with graphical examination of data series, autocorrelation analysis to examine serial dependence, and spectral analysis to examine cyclic behaviour which need not be related to seasonality. The description looks at separation into components representing trend, seasonality, slow and fast variation, cyclical irregular; and simple properties of marginal distributions. The prediction and forecasting consists of fully-formed statistical models for stochastic simulation purposes to generate alternate version of the time series and representing what might happen over non-specific time-periods in the future (prediction); simple or

fully-formed statistical models to describe the likely outcome of the time series in the immediate future, given knowledge of the most recent outcomes (forecasting).

The two types of techniques used for analysing the trend and seasonal patterns of the times series malaria morbidity data $I(\mathbf{u}_\alpha)$ in the 10 regions of Ghana are presented.

2.5.1 Smoothing Techniques

The incidence of most diseases (like sales of products) is seasonal and as such the trend patterns are expected to be sustained for some period. However, if successful interventions are introduced the incidence cases (or sales) can decrease or increase initially but then stabilises before increasing (or decreasing) as failure of the intervention measures (or competition of the market) sets in; this leads to a change of the level of pattern from one time period to the next, called *trend* (Cowpertwait & Metcalfe, 2009). Seasonal patterns can also change due to variation in the climatic conditions. An exploratory time series analysis can be performed via smoothing of the time sequence plots to study the long-term and seasonal behaviour of z_t . Two useful techniques which can be employed are the moving average smoothing (MAS) and Holt-Winter's method (HWM) (Shumway & Stoffer, 2011).

The MAS estimates the trend in a given time series by using linear filters to obtain the smoothed observation (Brockwell & Davis, 1987; Brockwell & Davis, 2002):

$$m_t = \sum_{i=-k}^k \alpha_i z_{t+i} \quad (2.5.1)$$

where $\alpha_i = \alpha_{-i} \geq 0$ and $\sum_{i=-k}^k \alpha_i = 1$. A simple class of linear filters are the centred moving averages with equal weights: $\alpha_i = 1/\lambda$, where $\lambda = 2k + 1$ and $i = -k, \dots, +k$ for odd value of λ . If λ even, then the weights of the MAS are given by $\alpha_i = 0$ for $|i| > \lambda/2$; $\alpha_i = \alpha_{-i}$ and $\alpha_{\lambda/2} = 0.5/\lambda$; $\alpha_i = 1/\lambda$ for $|i| < \lambda/2$.

The HWM is a generalisation of exponential smoothing with weights that decays exponentially. The method was first introduced by Holt (1957) and later extended by Winters (1960). It uses exponentially weighted moving averages to update the three smoothing estimates of the seasonally adjusted mean (level), trend and seasonality. There are two different algorithms of the method, depending on whether seasonality is treated as an additive or a multiplicative component. The Holt-Winter's multiplicative

algorithm which is applied in this study is given by (2.5.2):

$$\begin{cases} s_0 = z_0 \\ a_t = \alpha(z_t/s_t) + (1-\alpha)(a_{t-1} + b_{t-1}) \\ b_t = \beta(a_t - a_{t-1}) + (1-\beta)b_{t-1} \\ s_t = \gamma(z_t/a_{t-1} + b_{t-1}) + (1-\gamma)s_{t-p} \end{cases} \quad (2.5.2)$$

where a_t , b_t and s_t are the estimated level, trend and seasonal effect at time t ; α , β and γ (all lie between 0 and 1) are the corresponding smoothing parameters and p is the length of period. The forecast value for z_{t+k} after observation at t is:

$$\hat{z}_{t+k|t} = (a_t + kb_t)s_{t+k-p}, \quad k < p \quad (2.5.3)$$

The smoothing parameters of model (2.5.2) can be estimated using the R function **HoltWinters** which minimises the one-step-ahead prediction errors (Cowpertwait & Metcalfe, 2009).

2.5.2 Seasonal ARIMA Predictive Models

Models for time series analysis can have many forms and represent different stochastic processes. When modelling variations in the levels of a process, three broad classes of practical importance are the autoregressive (AR), integrated (I), and moving average (MA) models. These classes depend linearly on previous data points, and combine ideas to produce an autoregressive integrated moving average (ARIMA) model. They will be applied to the seasonally stationary and non-stationary monthly malaria morbidity incidence data $\{I_t(\mathbf{u}_\alpha) : t \in \mathbf{T}\}$ observed in the various regions of the study area for the period 2000–2011. The general representations of the autoregressive model with parameter p , $AR(p)$ and the moving average model with parameter q , $MA(q)$ are given by (2.5.1) and (2.5.2), respectively:

$$Z_t = \phi_1 Z_{t-1} + \phi_2 Z_{t-2} + \cdots + \phi_p Z_{t-p} + \varepsilon_t \quad (2.5.4)$$

$$Z_t = \varepsilon_t + \theta_1 \varepsilon_{t-1} + \theta_2 \varepsilon_{t-2} + \cdots + \theta_q \varepsilon_{t-q} \quad (2.5.5)$$

where Z_t is stationary process; $\phi_i, i = 1, 2, \dots, p$ and $\theta_i, i = 1, 2, \dots, q$ are constants such that $\phi_p \neq 0$ and $\theta_q \neq 0$; and ε_t is Gaussian white noise (WN), denoted $\varepsilon_t \sim WN(0, \sigma_\varepsilon^2)$. Applying the backward shift operator B , we obtain the following:

$$\begin{cases} B^k Z_t = Z_{t-k}; \\ \phi(B) = 1 - \phi_1 B - \phi_2 B^2 - \dots - \phi_p B^p; \\ \theta(B) = \varepsilon_t - \theta_1 B - \theta_2 B^2 - \dots - \theta_q B^q, \end{cases} \quad (2.5.6)$$

for which $\phi(B) \neq 0$ and $|B| \leq 1$. The equations (2.5.4) and 2.5.5) reduce to $\phi(B)Z_t = \varepsilon_t$ and $Z_t = \theta(B)\varepsilon_t$, respectively. Thus, the ARIMA model combines the $AR(p)$ and $MA(q)$ models with additional process of differencing (d) to give an order (p, d, q) . It is denoted by $ARIMA(p, d, q)$ and defined by

$$\phi(B)\nabla^d Z_t = \theta(B)\varepsilon_t \quad (2.5.7)$$

where $\varepsilon_t \sim \text{WN}(0, \sigma_\varepsilon^2)$, $\nabla Z_t = Z_t - Z_{t-1} = (1-B)Z_t$ and d is differencing to obtain stationarity.

If the time series $\{Z_t : t \in \mathbb{Z}^+\}$ is seasonal with period s , as in most epidemiological data and a case of the malaria morbidity incidence rates time series data $\{I_t(\mathbf{u}_\alpha) : t \in \mathbf{T}\}$ in this study, we obtain the multiplicative seasonal ARIMA (SARIMA) model of order $(p, d, q) \times (P, D, Q)$ which is a generalisation of (2.5.7) containing seasonal and non-seasonal components. The SARIMA model is defined by:

$$\Phi(B^s)\phi(B)\nabla_s^D \nabla^d Z_t = \Theta(B^s)\theta(B)\varepsilon_t \quad (2.5.8)$$

where $\nabla_s^D = (1-B^s)^D$ is the seasonal difference; $\Phi(B^s)$ and $\Theta(B^s)$ represent the seasonal components of $AR(P)$ and $MA(Q)$ models, respectively. In this case Z_t becomes causal and invertible process satisfying the conditions $|\Phi| < 1$ and $|\Theta| < 1$, respectively and is identically and independently distributed (iid) as $N(0, \sigma^2)$.

In this study, it is hypothesised that the malaria morbidity incidence time series data is seriously affected by certain external factors, such as the weather and socio-economic conditions (as extensively reviewed in chapter 1) which can cause temporal effects to the morbidity risk at the various regions in the study area. The multiplicative SARIMA technique of Box and Jenkins (1976), as given in (2.5.8), is then extended to examine the impact of the exogenous climate covariates, resulting in a multivariate SARIMAX model (X , indicating effect of the exogenous variables). The details of both SARIMA

and SARIMAX model fitting to the observed time series data $\{Z_t : t \in \mathbb{Z}^+\}$, which subsequently leads to the future forecast values of z_t , are outlined in the following section.

2.5.3 Box-Jenkins SARIMA Model-Building

The Box-Jenkins methodology offers the set modelling procedures for time series seasonal data $\{z_t : t = 1, \dots, T\}$. These include model identification, estimation, diagnostic checking and forecasting (Box & Jenkins, 1976), which are outlined by the following iterative steps:

- (i) **Model Identification (or Specification):** Inspect the time series $\{z_t : t = 1, \dots, T\}$ by transformation or differencing to remove long-term trend and/or further by graphs of autocorrelation function (ACF) and partial autocorrelation function (PACF) to establish stationarity. ACF measures the relation between the earlier values of z_{t-i} and the later z_t whilst PACF illustrates the correlation between z_t and z_{t-i} which has not been explained by the correlation at the lower lags (Zhang, Zhang, Young, & Li, 2014). For example, if the graphs of ACF and PACF cut off fairly after lags P s and Q s and/or die down at lags ks ($k = 1, 2, \dots$), then the time series $\{z_t : t = 1, \dots, T\}$ is considered stationary (Nochai & Nochai, 2006; Shumway & Stoffer, 2011). Then, the tentative model(s) can be identified and patterns and components specified.
- (ii) **Model Estimation:** The model parameters (ϕ , θ and σ_ε^2) are estimated by various statistical criteria including the maximum likelihood principle which allows discrimination between different model specifications by computing Akaike information criterion (AIC) (Akaike, 1974) or Bayesian information criterion (BIC) (Schwarz, 1978). The maximum likelihood method for fitting model (2.5.8) to the time series data $\{z_t : t = 1, \dots, T\}$ is to maximise the likelihood function (2.5.6) with the aim of of estimating the model parameters:

$$\left\{ \begin{aligned} L(z_T, \dots, z_1; \phi, \theta, \sigma_\varepsilon^2) &= \prod_{t=1}^T f(z_t; \phi, \theta, \sigma_\varepsilon^2) \\ &= \left(\prod_{t=p+1}^T f(z_t | z_{t-1}, \dots, z_1; \boldsymbol{\beta}) \right) \times f(z_p, \dots, z_1; \boldsymbol{\beta}) \end{aligned} \right. \quad (2.5.9)$$

where the conditional distribution $f(z_t | z_{t-1}, \dots, z_1; \boldsymbol{\beta})$ is a Gaussian process and the maximum likelihood estimates (MLEs) of the model parameters, denoted $\boldsymbol{\beta} = (\phi_1, \dots, \phi_p, \phi_{p+1}, \dots, \phi_{p+P}; \theta_1, \dots, \theta_q, \theta_{q+1}, \dots, \theta_{p+Q}; \sigma_\varepsilon^2)^T$ are computed by

$$\begin{aligned} \hat{\boldsymbol{\beta}}_{mle} &= \arg \max(\ln L(z_T, \dots, z_1; \boldsymbol{\beta})) \\ &= \arg \max_{\boldsymbol{\beta}} \left(\sum_{t=p+1}^T \ln f(z_t | z_{t-1}, \dots, z_1; \boldsymbol{\beta}) \right) + \ln f(z_p, \dots, z_1; \boldsymbol{\beta}) \end{aligned} \quad (2.5.10)$$

(see Shumway and Stoffer (2011) and Pfaff (2008) for further details of the estimation procedure). The model order, $(p, d, q) \times (P, D, Q)$, is best determined by the least value of AIC (or BIC), which penalises models with too many parameters. AIC as a measure of the goodness of fit of the estimated model in (2.5.8) is calculated by

$$AIC = -2 \ln L(z_T, \dots, z_1; \hat{\boldsymbol{\beta}}_{mle}) + 2k \quad (2.5.11)$$

where $L(z_T, \dots, z_1; \hat{\boldsymbol{\beta}}_{mle})$ is the maximised value of the likelihood function for the estimated model and k , the estimated number of model coefficients in (2.5.10).

- (iii) Model Diagnostic Checking:** Conduct a diagnostic test by examining the residuals from the estimated SARIMA model for randomness, normality and uncorrelatedness (no autocorrelation). The overall check of the model adequacy is provided by the Ljung-Box Q-statistic test (Ljung & Box, 1978). The test statistic is computed by:

$$Q(h) = n(n+2) \sum_{h=1}^m \left(\frac{r_h^2(e)}{n-h} \right) \sim \chi_{m-k}^2 \quad (2.5.12)$$

where $r_h^2(e)$ is the residual autocorrelation at lag h , n is the number of residuals and m is the number of time lags included in the test. If the p -value associated with $Q(h)$, which follows the chi square distribution with degrees of freedom $m-k$, is large (p -value $> \alpha$), then the time series z_t is uncorrelated and the model is considered adequate for forecast.

- (iv) Forecasting with the Model:** Forecast future values of the time series (\hat{z}_{T+l}) for a specified lead time l , once the model adequacy is established. Note the magnitude of the forecast errors by computing the bias or mean error (ME), the mean absolute error (MAE) or mean absolute percentage error (MAPE) and root mean square error (RMSE) as a way of ascertaining accuracy of forecast

values and validating the model.

$$\left\{ \begin{array}{l} ME = \frac{1}{l} \sum_{t=1}^l (\hat{z}_{T+t} - z_{T+t}); MAE = \frac{1}{l} \sum_{t=1}^l |\hat{z}_{T+t} - z_{T+t}|; \\ MAPE = \frac{1}{l} \sum_{t=1}^l \left| \frac{\hat{z}_{T+t} - z_{T+t}}{z_{T+t}} \right| \times 100\%; RMSE = \sqrt{\frac{1}{l} \sum_{t=1}^l (\hat{z}_{T+t} - z_{T+t})^2} \end{array} \right. \quad (2.5.13)$$

Keep track the model performance to detect out of control situation.

2.6 Summary Chapter

In this chapter, two separate theoretical frameworks on geostatistics and time series analysis for analysing the malaria morbidity incidence cases in purely spatial and purely temporal domains have been discussed. Geostatistics is a branch of spatial statistics which deals with the geographical distribution of point-referenced data. It is based on the theory of a regionalised variable which shows spatial auto-correlation such that closer samples in space are more correlated than those further apart. Thus, the attribute being studied is assumed as a realisation of random process distributed in space. Geostatistical spatial analysis, as outlined in the chapter, involves two main procedures. It begins with structural analysis using the semivariograms and covariance functions as the main tools for modelling the spatial continuity or autocorrelation of the attribute subject to the conditions of stationarity and permissible non-negative definiteness. It then follows with an optimal prediction (or kriging), dealing with the techniques which seek to minimise the prediction error variance to obtain optimal predictions at unsampled locations and production of spatial maps. The two commonly used techniques, ordinary kriging (OK) and ordinary co-kriging (OCK), are presented with the latter applied to for account for the effects of exogeneous variables.

Time series analysis is judged as a useful scientific tool for analysing and interpreting random processes which vary over time. Analysis of time series mainly comprises of exploration, for studying the distributional properties of the data; and fully-informed statistical modelling process, which leads to prediction for future forecasting of the data. Two smoothing techniques (moving averages and Holt-Winters's method) used to analyse the long-term trend and seasonal patterns and Box-Jenkins multiplicative seasonal autoregressive integrated moving average (SARIMA) modelling procedure for predictive future forecasting of time series data have been studied. The latter is extended to SARIMAX to account for the effect of exogenous variables(X).

Chapter 3

Geostatistical Space-time Analysis

3.1 Introduction

Space-time (spatio-temporal) modelling provides a joint (composite) analysis of data distributed through space and evolving over time. The concepts for analysing space-time observations can be seen as natural extensions of those developed for strictly spatial data, though most of these are new to the space-time data context. For example, how should the temporal and spatial correlation models interact with each other?; and can or should they interact with each other?. Some space-time models extend the purely spatial or temporal models, while others try to explicitly model space-time effects and interactions (Cressie & Huang, 1999; De Cesare, Myers, & Posa, 2001a; Kyriakidis & Journel, 1998, 1999; Sherman, 2011).

The space-time statistical modelling presented in this chapter extends the spatial analytical tools reviewed in chapter 2 for modelling random processes distributed purely in space by an additional time coordinate to facilitate quantification of spatial variations for optimal prediction of dynamic processes evolving in space and time. This eventually leads to the presentation of a theoretical framework of space-time modelling of phenomena considered as realisation of random fields in $d + 1$ dimensional space (Kyriakidis & Journel, 1999). Thus, time becomes an important component as in many scientific studies, though such an extension can be complex (Buttafuoco, Caloiero, & Coscarelli, 2011; De Iaco, 2010; Griffith & Heuvelink, 2010; Kyriakidis & Journel, 1999; Yu, 2010). For instance, there are fundamental differences between the geographic and time domains that need to be addressed prior to a successful application of geostatistical techniques to the space-time data, which this study seeks to employ to analyse the malaria morbidity cases as public health data. In the following sections, we outline the geostatistical modelling framework for space-time data in the context of the malaria risk data in Ghana as being considered in this thesis. Specifically, we present the space-time random function and its properties, the conceptual modelling approaches of the spatio-temporal continuity along with the possible prediction methods as applied to the space-time malaria morbidity incidence data.

3.2 Geostatistical Space-time Modelling

Space-time geostatistics provides a stochastic modelling framework for joint analysis of data distributed in space and time domains and builds on the extension of established spatial analytical techniques (Kyriakidis & Journel, 1999; Yu, 2010). This results in a new domain $\mathbf{D} \times \mathbf{T}$ defined for the joint study of the regionalised variable dispersed both in space and time, where \mathbf{D} and \mathbf{T} are finite domains in space and time, respectively and are such that $\mathbf{D} \subseteq \mathbb{R}^d$ and $\mathbf{T} \subseteq \mathbb{Z}^+$, the set of positive integers. A space-time (or simply, spatio-temporal) random variable $Z(\mathbf{u}, t)$ is thus defined to take a series of values at the point $\mathbf{u} \in \mathbf{D}$ at the instant time $t \in \mathbf{T}$, according to a probability distribution. For example, as in this study, $Z(\mathbf{u}, t)$ is the monthly count morbidity cases of malaria reported or recorded weather values in each of the n district (county) locations in Ghana at an instant time where $\mathbf{u} \in \mathbf{D} = \{\mathbf{u}_1, \dots, \mathbf{u}_n\}$ is a spatial location recorded in longitude and latitude (measured in kilometres), and \mathbf{T} is subset of positive integers, denoting the number of months. Conceptually, the spatial domain $\mathbf{u} \in \mathbf{D}$ is continuous (but can be regarded as discrete by aggregation of cases from health facilities or measurements in each district) whilst the temporal domain can be discrete or continuous. The discreteness of the temporal dimension is often (although not always) caused by sampling the continuous time coordinate at equally spaced time intervals (Cressie & Wikle, 2011). In addition, it could be that the data are collected based on one type of domain but inference is desired for another type. An example is the problem of upscaling where a spatial variable at coarse resolution is inferred from the underlying process for a much richer spatial resolution (see the change of support problem in Cressie & Wikle (2011), chapters 4 and 7). Spatio-temporal covariance functions or semivariograms offer a succinct but informative summary of random processes in the space-time domain $\mathbf{D} \times \mathbf{T}$. It is very common to consider the covariance function or semivariogram as a characterisation of the random variable $Z(\mathbf{u}, t)$.

The spatio-temporal random variable is defined to include the instant time when the measurement was made, where $\{Z(\mathbf{u}_\alpha, t); t = 1, 2, \dots, T\}$ represents a discrete, equally spaced time series of observations of an attribute Z observed at location \mathbf{u}_α . The set of stochastic random variables measured at n locations and time instant t is given as

$Z(\mathbf{u}_1, t), \dots, Z(\mathbf{u}_n, t)$, where $t = 1, 2, \dots, T$. Time can be expressed in any unit (for example, hours, days, months or years). The random variable $Z(\mathbf{u}, t)$ can therefore take any series of outcomes at any spatial location $\mathbf{u} \in \mathbf{D}$ and any time point $t \in T$. In a complete data set, the total number of measurements is nT . If k attributes are measured at n locations and T time points $t = 1, 2, \dots, T$, then we obtain $\mathbf{Z}(\mathbf{u}_\alpha, t) = [Z_1(\mathbf{u}_\alpha, t), \dots, Z_k(\mathbf{u}_\alpha, t)]^T$, as the vector of the k attributes at location \mathbf{u}_α and time point t . This will be considered in space-time co-kriging in section 3.4 to establish effect of some climatic covariates on the malaria incidence rates.

3.2.1 Space-Time Random Function (STRF)

The space-time observations constitute a time series of length T at each of the n spatial locations and imply the use of a regular temporal scheme (that is, the observations are equally spaced over time at each spatial location). This leads to a family of random variables defined in space-time domain.

Definition 3.2.1 (Space-time random function) (Kyriakidis & Journel, 1999):

- (i) Let $Z(\mathbf{u}, t)$ be a space-time random variable of a phenomenon or attribute Z at location denoted by (\mathbf{u}, t) . Then the collection (or set) of usually dependent random variables as defined in (3.2.1), one for each location in space $\mathbf{u} \in \mathbf{D}$ and instant time $t \in \mathbf{T}$, is called space-time random function or field (STRF),

$$\{Z(\mathbf{u}, t) : (\mathbf{u}, t) \in \mathbf{D} \times \mathbf{T}\} \quad (3.2.1)$$

where $\mathbf{D} \subseteq \mathbb{R}^d$ and $\mathbf{T} \subseteq \mathbb{R}$ which has a well-defined joint probability distribution as defined in (3.2.2b).

- (ii) The random variable $Z(\mathbf{u}, t)$ is characterised by its cumulative distribution function (cdf) defined by

$$F(z; (\mathbf{u}, t)) = P[Z(\mathbf{u}, t) \leq z], \quad (3.2.2a)$$

for all $Z = Z(\mathbf{u}, t)$, which models the uncertainty of the value $z(\mathbf{u}, t)$ at an unsampled spatial location \mathbf{u} and instant time t . A realisation of the STRF is $\{z(\mathbf{u}, t) : (\mathbf{u}, t) \in \mathbf{D} \times \mathbf{T}\}$ a set of realisations of its component; and

- (iii) Let the space-time domain $\mathbf{D} \times \mathbf{T}$ be discretised into nT sets, such that any assigned set corresponds to a vector of nT random variables $\{Z(\mathbf{u}_1, t_1), \dots, Z(\mathbf{u}_n, t_T)\}$, which is characterised by the cumulative function (cdf):

$$\begin{aligned} F(z_{11}, \dots, z_{nT}; (\mathbf{u}_1, t_1), \dots, (\mathbf{u}_n, t_T)) \\ = P[Z(\mathbf{u}_1, t_1) \leq z_{11}, \dots, Z(\mathbf{u}_n, t_T) \leq z_{nT}] \end{aligned} \quad (3.2.2b)$$

which is used to characterise the joint uncertainty about the nT actual values $\{z(\mathbf{u}_1, t_1), \dots, z(\mathbf{u}_n, t_T)\}$. The set of all such nT – cdf's, for all positive integers, n, T and for any choice of space-time locations $(\mathbf{u}_1, t_1), \dots, (\mathbf{u}_n, t_T)$ constitutes the spatio-temporal law of the random function $Z(\mathbf{u}, t)$.

Inference of the spatio-temporal law requires repeated realisations of the component random variables at each space-time location $(\mathbf{u}, t) \in \mathbf{D} \times \mathbf{T}$, which are unavailable in practice. Pooling together pairs of observations separated by the same space-time vector $(\mathbf{h}_s, h_t) \in \mathbf{D} \times \mathbf{T}$, where $\mathbf{h}_s = \mathbf{u} - \mathbf{u}^1$ and $h_t = t - t^1$ which are used as a set of repetitions. This pooling corresponds to the model decision of a “two-point” space-time stationarity using the pairs of random variables $\{Z(\mathbf{u}_\alpha, t), Z(\mathbf{u}_\alpha + \mathbf{h}_s, t + h_t) : \alpha = 1, 2, \dots, n\}$. This provides the necessary number of realisations of the STRF $Z(\mathbf{u}, t)$ to make the required inferential analysis of the random process $Z(\mathbf{u}, t)$. The three types of spatial and space-time stationarity that are identified in geostatistical methodology are the strict, second order and intrinsic stationarity. The stationarity decision allows pooling data over areas that are deemed homogeneous. The spatio-temporal stationarity in $\mathbf{D} \times \mathbf{T} \subseteq \mathbb{R}^{d+1}$ is defined in a similar fashion as the strict, second order and intrinsic, just as in the case of purely spatial in $\mathbf{D} \subseteq \mathbb{R}^d$.

Definition 3.2.2 (Stationarity):

The STRF $Z(\mathbf{u}, t)$ is said to be strictly stationary within $\mathbf{D} \times \mathbf{T}$ if its spatio-temporal law is invariant by the translation vector $(\mathbf{h}_s, h_t) \in \mathbf{D} \times \mathbf{T}$. Thus for any two vectors of the random variables $\{Z(\mathbf{u}_1, t_1), \dots, Z(\mathbf{u}_n, t_T)\}$ and $\{Z(\mathbf{u}_1 + \mathbf{h}_s, t_1 + h_t), \dots, Z(\mathbf{u}_n + \mathbf{h}_s, t_T + h_t)\}$ have the same multivariate cdf, whatever the translation vector $(\mathbf{h}_s, h_t) \in \mathbf{D} \times \mathbf{T}$:

$$\begin{aligned} F(z_{11}, \dots, z_{nT}; (\mathbf{u}_1, t_1), \dots, (\mathbf{u}_n, t_T)) \\ = F[z_{11}, \dots, z_{nT}; (\mathbf{u}_1 + \mathbf{h}_s, t_1 + h_t), \dots, (\mathbf{u}_n + \mathbf{h}_s, t_T + h_t)] \end{aligned} \quad (3.2.3)$$

for all $(\mathbf{u}_1, t_1), \dots, (\mathbf{u}_n, t_n)$ and $(\mathbf{u}_1, t_1), \dots, (\mathbf{h}_s, h_t) \in \mathbf{D} \times \mathbf{T}$. This property is usually difficult to test and cannot be verified using the limited sampled observations as it needs to be justified by considering the family of finite-dimensional distribution functions of the process (Bruno, Guttorp, Sampson, & Cocchi, 2009). This leads to two weaker forms of stationarity: second order stationary and intrinsic stationary as sufficient basis for the modelling of the random function $Z(\mathbf{u}, t)$. The assumption of strict stationarity is then weakened by limiting the decision of stationary to the one-point and two-point cdfs and the two moments of the random function (Kyriakidis & Journel, 1999) which depends only on the separation vector $\mathbf{h}_{st} = (\mathbf{h}_s, h_t)$ between the locations (\mathbf{u}, t) and (\mathbf{u}^1, t^1) . These two less restrictive assumptions of stationarity (defined below) are the second-order stationarity and intrinsic stationarity which account for both distance $|\mathbf{h}_{st}|$ and direction.

Definition 3.2.3 (Second-Order and Intrinsic Stationarity)

- (i) The STRF $\{Z(\mathbf{u}, t) : (\mathbf{u}, t) \in \mathbf{D} \times \mathbf{T}\}$ is said to be second-order stationary (SOS) within the domain $\mathbf{D} \times \mathbf{T}$ if the first moment of the vector of random variables exists and is constant and the covariance function of all pairs of random variables exists and depends only on the separation vector:

$$\begin{cases} m(\mathbf{u}, t) = E[Z(\mathbf{u}, t)], \forall (\mathbf{u}, t) \in \mathbf{D} \times \mathbf{T} \\ C(\mathbf{h}_s, h_t) = E[(Z(\mathbf{u}, t) - m(\mathbf{u}, t))(Z(\mathbf{u} + \mathbf{h}_s, t + h_t) - m(\mathbf{u}, t))], \\ \forall (\mathbf{u}, t) \in \mathbf{D} \times \mathbf{T} \end{cases} \quad (3.2.4)$$

where $m(\mathbf{u}, t)$ is the space-time mean function and $C(\mathbf{h}_{st}) = C(\mathbf{h}_s, h_t)$ is called the space-time covariance function.

- (ii) The STRF $Z(\mathbf{u}, t)$ is said to be intrinsically stationary (IS) within the space-time domain $\mathbf{D} \times \mathbf{T}$ if the mean vector and the variance of the increments $Z(\mathbf{u}, t) - Z(\mathbf{u} + \mathbf{h}_s, t + h_t)$ exist and are translation invariant:

$$\begin{cases} E[Z(\mathbf{u}, t) - Z(\mathbf{u} + \mathbf{h}_s, t + h_t)] = 0, \forall (\mathbf{u}, t) \in \mathbf{D} \times \mathbf{T} \\ 2\gamma(\mathbf{h}_s, h_t) = \text{Var}(Z(\mathbf{u}, t) - Z(\mathbf{u} + \mathbf{h}_s, t + h_t)) \\ = E[(Z(\mathbf{u}, t) - Z(\mathbf{u} + \mathbf{h}_s, t + h_t))^2], \forall (\mathbf{u}, t) \in \mathbf{D} \times \mathbf{T} \end{cases} \quad (3.2.5)$$

where $\gamma(\mathbf{h}_s, h_t)$ is called the space-time semivariogram.

The strictly stationarity in (3.2.3) implies SOS, assuming that the first two moments exist, whereas SOS does not imply strict stationarity. In a Gaussian spatio-temporal process, SOS and strict stationarity coincide, as a Gaussian process which is completely specified by its mean and variance (Bruno & Cocchi, 2004; Denham, 2012). In many cases the assumption of SOS is not met and so the much weaker assumption of IS needs to be relied upon. Intrinsic stationarity is a sufficient condition to define the space-time semivariogram. In the second order stationary case, the space-time semivariogram is related to the covariance and correlation functions by:

$$\begin{cases} \gamma(\mathbf{h}_s, h_t) = C(\mathbf{0}, 0) - C(\mathbf{h}_s, h_t) \\ \rho(\mathbf{h}_s, h_t) = 1 - \gamma(\mathbf{h}_s, h_t) / C(\mathbf{0}, 0) \end{cases} \quad (3.2.6)$$

However, as the separation distance $|\mathbf{h}_s|$ or time $|h_t|$ increases the correlation between two random variables $Z(\mathbf{u}, t)$ and $Z(\mathbf{u} + \mathbf{h}_s, t + h_t)$ generally tends to zero:

$$C(\mathbf{h}_s, h_t) \rightarrow 0 \text{ for } |\mathbf{h}_s| \rightarrow \infty \text{ or } |h_t| \rightarrow \infty, \quad (3.2.7)$$

whilst the sill value of a bounded space-time semivariogram tends towards a priori variance $C(\mathbf{0})$ or $C(\mathbf{0}, 0)$:

$$\gamma(\mathbf{h}_s, h_t) \rightarrow C(\mathbf{0}, 0), \text{ for } |\mathbf{h}_s| \rightarrow \infty \text{ or } |h_t| \rightarrow \infty. \quad (3.2.8)$$

The space-time covariance function $C(\mathbf{h}_s, h_t)$ and semivariogram $\gamma(\mathbf{h}_s, h_t)$ are said to be anisotropic if they depend on both distance and direction. They are, however, isotropic if they depend only on the modulus of \mathbf{h}_s .

One primary constraint of geostatistical interpolation (or simulation) is the lack of (departure from) stationarity – as many real-life problems generate data sets that do not satisfy the SOS or IS assumption. Non-stationarity is often linked to the presence of trend in the data which can be removed resulting in residuals which are stationary (Kyriakidis & Journel, 1999). Then the trend is added back to the interpolated estimates of the residuals or incorporated directly into the interpolation scheme. The trend in the data represents large scale variations in the data while the residual obtained from the detrending is the small-scale fluctuations around the trend (Snepvangers, Heuvelink, & Huisman, 2003). When considering spatial residual kriging the assumption of IS describes the space-time dependence given by the variogram

$$2\gamma(\mathbf{h}_s, h_t) = E \left[\left(r(\mathbf{u}_\alpha + \mathbf{h}_s, t + h_t) - r(\mathbf{u}_\alpha, t) \right)^2 \right] \quad (3.2.9)$$

which is analogous to the purely spatial version in (2.3.6). In this case it is possible to replace the original data series with the residual values in each of the variogram equations discussed in the preceding sections of the chapter without loss of generality. The possible sources of non-stationarity that exist within a data set are a non-constant mean, non-constant variance or spatio-temporally varying covariance function (Elmatzoglou, 2006). However, in many cases natural processes acting over large scales in space and/or time are better represented by non-stationary spatio-temporal models. Non-stationarity is usually limited to the mean (trend) component $m(\mathbf{u}, t)$, which is made dependent on the space location \mathbf{u} or instant time t or both (\mathbf{u}, t) . The non-constant mean can be dealt with by expressing the mean function in terms of the space-time coordinates or other related variables such as the covariates whilst the non-constant variance can be stabilised by various forms of transformation such as logarithm or Box-Cox transformation (Box & Cox, 1964). Kyriakidis et al. (1999) review forms of spatio-temporal trend models including the permissible models of Dimitrakopoulos and Luo (1997), being polynomial and trigonometric functions or combinations of the two types to detrend and/or deseasonalise the data. This mixed form of these functions is applied in this study to model the trend of the morbidity incidence rates. The details of the space-time trend modelling approaches are presented in section 3.4.

3.2.2 Space-time Covariance Function and Semivariogram

The spatio-temporal moments are based on a similar underlying structure as the purely spatial moments, except that the time component must be taken into account. As mentioned in the introduction, the order in which measurements are observed in time plays an important role in interpolation (and simulation). The space-time variogram, covariance and correlogram are based on the same structures as their spatial counterparts when the temporal factor is included. The variability in the data is described by the graphical representation of the variogram as a function of the spatial lag vector (\mathbf{h}_s) and temporal lag distance (h_t). The spatial and temporal distances respectively describe the spatial and temporal continuity between the measurements (De Cesare, Myers, & Posa, 1997; Kyriakidis & Journel, 1999; Rouhani & Wackernagel, 1990). As already noted, geostatistical modelling basically focuses on the inference of the first two moments (the mean and covariance function or

semivariance) of a random function $Z(\mathbf{u}, t)$ which are required by subsequent estimation or simulation procedures (Sherman, 2011). Theoretical models of the spatio-temporal continuity of the random process are therefore required in order to obtain values of the covariance function or the semivariogram vector for any separation $h_{st} = (\mathbf{h}_s, h_t)$. The space-time covariance function and semivariogram moment estimators are defined completely analogously to that in the purely spatial setting in chapter 2. The experimental space-time semivariogram is given by (2.3.10):

$$\hat{\gamma}_{st}(\mathbf{h}_s, h_t) = \frac{1}{2|n(\mathbf{h}_s, h_t)|} \sum_{n(\mathbf{h}_s, h_t)} \left(Z(\mathbf{u}_\alpha, t_j) - Z(\mathbf{u}_\alpha + \mathbf{h}_s, t_j + h_t) \right)^2 \quad (3.2.10)$$

where $n(\mathbf{h}_s, h_t) = \{[\mathbf{u}_\alpha, t_j), (\mathbf{u}_\beta, t_v)]: \mathbf{u}_\alpha - \mathbf{u}_\beta = \mathbf{h}_s \text{ and } |t_j - t_v| = h_t\}$ and $|n(\mathbf{h}_s, h_t)|$ is the number of elements in the set $n(\mathbf{h}_s, h_t)$. The lag values \mathbf{h}_s and h_t describe the spatial and temporal continuity between the observed samples (De Cesare et al., 1997; Kyriakidis & Journel, 1999; Rouhani & Wackernagel, 1990). The experimental space-time semivariogram is the primary tool for inference in geostatistical space-time analysis. In this study we use the semivariogram to perform all the structural analysis of the morbidity incidence rates. The graphical representation of the semivariograms $\hat{\gamma}_{st}(\mathbf{h}_s, h_t)$ becomes a three-dimensional surface plot. The definitions of the range, sills and nugget effect as define in chapter 2 remain unchanged.

In the case of a multivariate random vector function $\mathbf{Z}(\mathbf{u}, t) = [Z_1(\mathbf{u}, t), \dots, Z_k(\mathbf{u}, t)]^T$ we define the space-time cross-variogram and covariance function with their corresponding estimators defined as follows:

The space-time cross-variogram is given by

$$2\gamma_{ij}(\mathbf{h}_s, h_t) = E \left[(Z_i(\mathbf{u}_\alpha, t) - Z_i(\mathbf{u}_\alpha + \mathbf{h}_s, t_j + h_t)) \times \right. \\ \left. (Z_j(\mathbf{u}_\alpha, t_j) - Z_j(\mathbf{u}_\alpha + \mathbf{h}_s, t_j + h_t)) \right], \quad i, j = 1, \dots, k \quad (3.2.11)$$

whilst its the experimental cross-variogram is calculated as:

$$\hat{\gamma}_{kk^1}(\mathbf{h}_s, h_t) = \frac{1}{2|n(\mathbf{h}_s, h_t)|} \sum_{n(\mathbf{h}_s, h_t)} \left((Z_k(\mathbf{u}_\alpha, t_j) - Z_k(\mathbf{u}_\alpha + \mathbf{h}_s, t_j + h_t)) \times \right. \\ \left. (Z_{k^1}(\mathbf{u}_\alpha, t_j) - Z_{k^1}(\mathbf{u}_\alpha + \mathbf{h}_s, t_j + h_t)) \right) \quad (3.2.12)$$

The space-time cross covariance function is defined by

$$\begin{aligned} C_{ij}(\mathbf{h}_s, h_t) &= \text{Cov}\left((Z_i(\mathbf{u}_\alpha, t) - Z_j(\mathbf{u}_\alpha + \mathbf{h}_s, t + h_t))\right) \\ &= E\left[\begin{array}{l} \{(Z_i(\mathbf{u}_\alpha, t) - m_i(\mathbf{u}_\alpha, t))\} \times \\ \{Z_j(\mathbf{u}_\alpha + \mathbf{h}_s, t + h_t) - m_j(\mathbf{u}_\alpha + \mathbf{h}_s, t + h_t)\} \end{array}\right] \end{aligned} \quad (3.2.13)$$

and its sample cross covariance calculated as:

$$\begin{aligned} \hat{C}_{kk^1}(\mathbf{h}_s, h_t) &= \frac{1}{2|n(\mathbf{h}_s, h_t)|} \sum_{n(\mathbf{h}_s, h_t)} ((Z_i(\mathbf{u}_\alpha, t) - m_{-h}(\mathbf{u}_\alpha, t)) \times \\ &\quad (Z_j(\mathbf{u}_\alpha + \mathbf{h}_s, t + h_t) - m_{+h}(\mathbf{u}_\alpha + \mathbf{h}_s, t + h_t))) \end{aligned} \quad (3.2.14)$$

The interpolation process is to fit a model to the scatter plot of the semivariogram. It is necessary to have a model that enables computing a variogram value for any possible separation distance, so continuous functions must be fitted to the experimental values. A theoretical model that best captures the overall features of the experimental semivariogram is then chosen. Only certain functions or combination of functions may be used to model the theoretical covariance function or semivariogram. The semivariogram estimator is unbiased (as in the purely spatial cases) at observed space-time lags, whilst the covariance estimator is slightly biased.

The space-time covariance function and the semivariogram are subject to the non-negativity condition as in the traditional geostatistical analysis. This is given by the following theorem.

Theorem 3.2.1 (Permissible conditions((Gregori, Porcu, Mateu, & Sasvári, 2008)):

Let $Z(\mathbf{u}, t)$ be a second-order stationary STRF, with covariance function $C_{st}(\mathbf{h}_s, h_t)$ and semivariogram $\gamma_{st}(\mathbf{h}_s, h_t)$, as defined in (3.2.4) and (2.3.5), respectively. Then for the finite collections of spatio-temporal locations $A = \{(\mathbf{u}, t)_{|\alpha} : \alpha = 1, \dots, n\}$:

$$(i) \quad \text{Var}\left(\sum_{\alpha=1}^n \lambda_\alpha Z(\mathbf{u}, t)_{|\alpha}\right) = \sum_{\alpha=1}^n \sum_{\beta=1}^n \lambda_\alpha \lambda_\beta C_{st}(\mathbf{u}_\alpha - \mathbf{u}_\beta; t_\alpha - t_\beta) \geq 0 \quad (3.2.15)$$

$$(ii) \quad \text{Var}\left(\sum_{\alpha=1}^n \lambda_\alpha Z(\mathbf{u}, t)_{|\alpha}\right) = -\sum_{\alpha=1}^n \sum_{\beta=1}^n \lambda_\alpha \lambda_\beta \gamma_{st}(\mathbf{u}_\alpha - \mathbf{u}_\beta; t_\alpha - t_\beta) \leq 0 \quad (3.2.16)$$

where $(\mathbf{u}, t)_{|\alpha} \in \mathbb{R}^d \times \mathbb{R}$ and for all $\lambda_\alpha \in \mathbb{R}$ such that $\sum_{\alpha=1}^n \lambda_\alpha = 0$.

As in the purely spatial case, the moment estimators of the covariance and variogram

functions do not satisfy these properties, in general. For this reason, we consider models that are guaranteed to be valid ones. Further, to carry out optimal prediction we require C_{st} and γ_{st} at an unobserved location $(\mathbf{h}_s, t)_0$. Estimates of these covariances or variances through direct empirical estimation are not available. Again, it is desirable to have space-time models. Stationary space-time covariance functions have a spectral representation, in an analogous to the purely spatial and purely temporal stationary covariance functions as was discussed in chapter 2. This representation can simply be viewed as an extension of the Bochner's Theorem in \mathbb{R}^{d+1} by time dimension (see Cressie and Wikle (2011), chapter 6 for further reading).

3.2.3 Space-time Permissible Models

The two most crucial concerns when modelling spatio-temporal dependence are the choice of the model for the covariance function or semivariogram and the estimation of the model parameters. The space-time covariance function (or semivariogram) models must be valid (permissible), satisfying the condition of positive definiteness for the covariance function (or conditionally negative definiteness for the semivariogram), and the chosen model(s) is/are sufficiently flexible to allow fitting to the data through a careful estimation of the model parameters (and also to ensure that the kriging systems in section 3.3 have a unique solution). Although a well-established set of permissible models exists for the semivariograms (Deutsch & Journel, 1998), a more diverse range of models has been developed for modelling of space-time autocorrelation structures (De Iaco et al., 2001; Griffith & Heuvelink, 2010; Kyriakidis & Journel, 1999). These models are classified as either being *separable* (Gneiting, Genton, & Guttorp, 2007) or *non-separable* (De Iaco, 2010; De Iaco et al., 2001; Ma, 2008).

A separable space-time covariance function or semivariogram considers the spatio-temporal process $Z(\mathbf{u}, t)$ as a joint process of two independent processes, one that occurs in space and the other in time, resulting in a purely spatial and temporal components, although the two processes are not observed separately but jointly (Denham, 2012). This formulation allows for computationally efficient estimation and inference procedures which has led to separable covariance models being used even on situations in which they are not physically justifiable (Bruno & Cocchi, 2004; Cressie & Huang, 1999). Separability is restrictive and often requires unrealistic assumptions. Studies have suggested ways of testing for separability (Fuentes, 2006; Li, Genton, &

Sherman, 2007; Mitchell, Genton, & Gumpertz, 2005, 2006). Separable models are characterised by the decomposition of the SOS variable $C_{st}(\mathbf{u}, t)$ into its purely spatial $C_s(\mathbf{h}_s)$ and purely temporal $C_t(h_t)$ components (De Cesare et al., 1997; Rodriguez-Iturbe & Mejia, 1974), which are reassigned in different combinations. The spatial and temporal zonal anisotropic factors are thus respectively included in the purely spatial and purely temporal covariances. Non-separable models are specifically constructed to take into account the interaction between the spatial and temporal characteristics data. In such cases statistical methods, such as Fourier transforms pairs in \mathbb{R}^d are used (Cressie & Huang, 1999). The models are then restricted to a small class of functions for which the closed form solution to the d – variate Fourier integral is known. De Iaco (2010) presents some classes of space-time covariance models that dominate in the literature in her comparative analysis of these existing models. They include a non-separable generalised product-sum model (De Cesare et al., 2001a; De Iaco et al., 2001).

In this study the product-sum class of models is applied, among the other space-time variography approaches, to the malaria morbidity incidence rates for the following reasons (De Iaco et al., 2001):

- (i) It offers a large class of flexible models that impose fewer constraints of symmetry between the spatial and temporal correlation components than other classes; the admissible values for just one parameter are dependent on the sill values of space-time components varying which leads to a necessary and sufficient condition for positive definiteness;
- (ii) It does not require an arbitrary space-time metric to be imposed, and the model can be fitted to data using relatively straight-forward techniques similar to those established for the purely spatial case.

The product-sum models have wide range of applications, though their applications in malaria epidemiological modelling are limited in the literature, as discussed in chapter 1 and the introductory section. Separable models which provide a useful base for deriving non-separable models include the metric model (Armstrong, Chetboun, & Hubert, 1993; Dimitrakopoulos & Luo, 1994), linear model (Christakos & Bogaert, 1996; Rouhani & Hall, 1989); and the product model (De Cesare et al., 1997; Posa,

1993; Rodriguez-Iturbe & Mejia, 1974) . The product-sum model (De Cesare et al., 2001a; De Cesare, Myers, & Posa, 2001b, 2002; De Iaco et al., 2001) is an extension of the product model to include an additional term being the sum of the spatial and temporal covariance models. The two models are presented as follows:

The **product model** is one simple way of modelling the space-time covariance function where the spatial and temporal domains are kept separate by product decomposition as defined by:

$$C_{st}(\mathbf{h}_s, h_t) = k \cdot C_s(\mathbf{h}_s) \cdot C_t(h_t) \quad (3.2.17)$$

where $k \in \mathbb{R}_+$. The space-time semivariogram version of (3.2.17) can be obtained in terms of marginal functions by

$$\gamma_{st}(\mathbf{h}_s, h_t) = k[C_s(\mathbf{0})\gamma_t(h_t) + C_t(0)\gamma_s(\mathbf{h}_s) - \gamma_s(\mathbf{h}_s)\gamma_t(h_t)] \quad (3.2.18)$$

from which the parameter k is obtained by putting both \mathbf{h}_s and h_t to equal to zero in (3.2.17):

$$k = C_{st}(\mathbf{0}, 0) / C_s(\mathbf{0}) \cdot C_t(0) \quad (3.2.19)$$

where $C_{st}(\mathbf{0}, 0)$ is the spatio-temporal (or global) sill and is such that it is equal to both the spatial and temporal sills:

$$\left\{ \begin{array}{l} C_{st}(\mathbf{0}, 0) = \frac{C_{st}(\mathbf{0}, 0)}{C_s(\mathbf{0}) \cdot C_t(0)} \{C_t(0) \cdot C_s(\mathbf{0}) + C_s(\mathbf{0}) \cdot \gamma_t(0) - C_s(\mathbf{0}) \cdot \gamma_t(0)\} \\ \quad = \gamma_{st}(\mathbf{h}_s, 0) \\ C_{st}(\mathbf{0}, 0) = \frac{C_{st}(\mathbf{0}, 0)}{C_s(\mathbf{0}) \cdot C_t(0)} \{C_t(\mathbf{0}) \cdot \gamma_s(\mathbf{0}) + C_s(\mathbf{0}) \cdot C_t(0) - \gamma_s(\mathbf{0}) \cdot C_t(0)\} \\ \quad = \gamma_{st}(\mathbf{0}, h_t) \end{array} \right. \quad (3.2.20)$$

The product-space-time semivariogram (3.2.18) is derived by the relations:

$$\left\{ \begin{array}{l} \gamma_{st}(\mathbf{h}_s, h_t) = C_{st}(\mathbf{0}, 0) - C_{st}(\mathbf{h}_s, h_t) \\ \gamma_s(\mathbf{h}_s) = C_s(\mathbf{0}) - C_s(\mathbf{h}_s) \\ \gamma_t(h_t) = C_t(0) - C_t(h_t) \end{array} \right. \quad (3.2.21)$$

The product model requires only the global sill which equals both the spatial and temporal, in its fitting (Myers, 2004). Like the metric and linear models (Christakos & Bogaert, 1996; Dimitrakopoulos & Luo, 1994), the product model shares similar limitations as the variability in space and time which do not interact. In addition, for

any pair of time points, the cross covariance function of the two spatial processes always has similar shape (3.2.22) just as the same result holds for any pair of spatial locations and the cross-covariance function of the two time series:

$$\begin{cases} C_{st}(\mathbf{h}_{s_1}, h_t) \propto C_{st}(\mathbf{h}_{s_2}, h_t), \text{ fixed spatial lags } \mathbf{h}_{s_1} \text{ and } \mathbf{h}_{s_2} \\ C_{st}(\mathbf{h}_s, h_{t_1}) \propto C_{st}(\mathbf{h}_s, h_{t_2}), \text{ fixed spatial lags } t_{s_1} \text{ and } t_{s_2} \end{cases} \quad (3.2.22)$$

Thus, no allowance is made for the possibility that the structure may change over time. Consequently, the product model was extended to the **product-sum model** to include an additional term being the sum of the marginal spatial and temporal covariance models.

The product-sum model as earlier mentioned belongs to the class of non-separable models. It is defined by:

$$C_{st}(\mathbf{h}_s, h_t) = k_1 C_s(\mathbf{h}_s) C_t(h_t) + k_2 C_s(\mathbf{h}_s) + k_3 C_t(h_t) \quad (3.2.23)$$

and can equivalently be written in terms of the semivariograms as:

$$\gamma_{st}(\mathbf{h}_s, h_t) = [k_2 + k_1 C_t(0)] \gamma_s(\mathbf{h}_s) + [k_3 + k_1 C_s(0)] \gamma_t(h_t) - k_1 \gamma_s(\mathbf{h}_s) \gamma_t(h_t) \quad (3.2.24)$$

where $C_s(\mathbf{h}_s)$ and $C_t(h_t)$ are the valid spatial and temporal covariance functions and $\gamma_s(\mathbf{h}_s)$ and $\gamma_t(h_t)$ are spatial and temporal semivariograms with corresponding sill values $C_s(\mathbf{0})$ and $C_t(0)$.

By the SOS assumption, using the definition, $\gamma_{st}(\mathbf{0}, 0) = \gamma_s(\mathbf{0}) = \gamma_t(0) = 0$, it is sufficient to ensure that the semivariograms are asymptotically bounded and therefore have sills and for positive definiteness it is then sufficient that $k_1 \geq 0$, $k_2 \geq 0$ and $k_3 \geq 0$. It then follows that:

$$\begin{cases} \gamma_{st}(\mathbf{h}_s, 0) = [k_2 + k_1 C_t(0)] \gamma_s(\mathbf{h}_s) = k_s \gamma_s(\mathbf{h}_s) \\ \gamma_{st}(\mathbf{0}, h_t) = [k_3 + k_1 C_s(0)] \gamma_t(h_t) = k_t \gamma_t(h_t) \end{cases} \quad (3.2.25)$$

where k_s and k_t are respectively considered as coefficients of proportionality between the space-time semivariograms $\gamma_{st}(\mathbf{h}_s, 0)$ and $\gamma_{st}(\mathbf{0}, h_t)$, and the spatial and temporal semivariograms, $\gamma_s(\mathbf{h}_s)$ and $\gamma_t(h_t)$ (De Iaco et al., 2001). These two values were

earlier assumed to be equal to 1 in De Cesare et al. (2001b) for easier determination of k_1 , k_2 and k_3 , and fitting of the model. Deducing from (3.2.23), we have:

$$C_{st}(\mathbf{0}, 0) = k_1 C_s(\mathbf{0}) C_t(0) + k_2 C_s(\mathbf{0}) + k_3 C_t(0) \quad (3.2.26)$$

from which together with (3.2.25) we obtain the system:

$$\begin{cases} k_s = k_2 + k_1 C_t(0) \\ k_t = k_3 + k_1 C_s(\mathbf{0}) \end{cases} \quad (3.2.27)$$

which consequently leads to the following theorems on the asymptotic and bounded behaviour of semivariograms.

Theorem 3.2.2 (Asymptotic behaviour of semivariograms (De Iaco et al., 2001)):

Let $Z(\mathbf{u}, t)$ be a SOS space-time random function. Assume that the space-time covariance function C_{st} has the form in (3.2.23) and suppose that is continuous in space-time domain $\mathbf{D} \times \mathbf{T} \subseteq \mathbb{R}^d \times \mathbb{R}$; $d \geq 2$. Then by (3.2.18), the following holds:

$$\begin{aligned} \lim_{h_s \rightarrow \infty} \lim_{h_t \rightarrow \infty} \gamma_{st}(\mathbf{h}_s, h_t) &= C_{st}(\mathbf{0}, 0) \\ \lim_{h_s \rightarrow \infty} \gamma_{st}(\mathbf{h}_s, 0) &= k_s C_s(\mathbf{0}) \\ \lim_{h_t \rightarrow \infty} \gamma_{st}(\mathbf{0}, h_t) &= k_t C_t(0) \end{aligned} \quad (3.2.28)$$

It then follows that:

$$\begin{aligned} \gamma_{st}(\mathbf{h}_s, h_t) &= C_{st}(\mathbf{0}, 0) - C_{st}(\mathbf{h}_s, h_t) \\ \gamma_{st}(\mathbf{h}_s, 0) &= C_{st}(\mathbf{0}, 0) - C_{st}(\mathbf{h}_s, 0) \\ \gamma_{st}(\mathbf{0}, h_t) &= C_{st}(\mathbf{0}, 0) - C_{st}(\mathbf{0}, h_t) \end{aligned} \quad (3.2.29)$$

and that these semivariograms $\gamma_{st}(\mathbf{h}_s, h_t)$, $\gamma_{st}(\mathbf{h}_s, 0)$ and $\gamma_{st}(\mathbf{0}, h_t)$ do not attain the same sill value.

Theorem 3.2.3 (Sufficiency for Admissibility (De Iaco et al., 2001)): Let $Z(\mathbf{u}, t)$ be a SOS STRF with covariance function (3.2.23) and is continuous in the space-time domain $\mathbf{D} \times \mathbf{T} \subseteq \mathbb{R}^d \times \mathbb{R}$; $d \geq 2$. Assume that for the space-time semivariogram defined in (3.2.24) with the value of k as defined in (3.2.32). Then the parameters: $k_1 \geq 0$, $k_2 \geq 0$ and $k_3 \geq 0$ if and only if k satisfies the following inequality:

$$0 < k \leq \frac{1}{\max \{sill[\gamma_{st}(\mathbf{h}_s, 0)]; sill[\gamma_{st}(\mathbf{0}, h_t)]\}} \quad (3.2.30)$$

It also follows that if either $\gamma_{st}(\mathbf{h}_s, 0)$ or $\gamma_{st}(\mathbf{0}, h_t)$ is unbounded, then:

- (i) there is no choice of k , satisfying the inequality (3.2.30) such that (3.2.33) is a valid space-time semivariogram; and
- (ii) space-time semivariogram (3.2.24) is not a valid model for any choice of the coefficients k_1 , k_2 and k_3 .

Following Theorems 3.2.2 and 3.2.3 the coefficients k_1 , k_2 and k_3 are derived in terms of the sills $C_{st}(\mathbf{0}, 0)$, $C_s(\mathbf{0})$ and $C_t(0)$, and the parameters k_s and k_t as defined by:

$$\begin{cases} k_1 = \frac{k_s C_s(\mathbf{0}) + k_t C_t(0) - C_{st}(\mathbf{0}, 0)}{C_s(\mathbf{0}) \cdot C_t(0)} \geq 0 \\ k_2 = \frac{C_{st}(\mathbf{0}, 0) - k_t C_t(0)}{C_s(\mathbf{0})} \geq 0 \\ k_3 = \frac{C_{st}(\mathbf{0}, 0) - k_s C_s(\mathbf{0})}{C_t(0)} \geq 0 \end{cases} \quad (3.2.31)$$

whilst the single parameter k is defined as:

$$k = \frac{k_s C_s(\mathbf{0}) + k_t C_t(0) - C_{st}(\mathbf{0}, 0)}{k_s C_s(\mathbf{0}) k_t C_t(0)} = \frac{k_1}{k_s k_t}, \quad (3.2.32)$$

which must satisfy condition (3.2.30) in Theorem (3.2.3). The space-time semivariogram (3.2.24) is then re-defined in terms of the single parameter (3.2.32) to obtain the generalised product-sum (GPS) model (De Iaco et al., 2001):

$$\gamma_{st}(\mathbf{h}_s, h_t) = \gamma_{st}(\mathbf{h}_s, 0) + \gamma_{st}(\mathbf{0}, h_t) - k \gamma_s(\mathbf{h}_s, 0) \gamma_t(\mathbf{0}, h_t), \quad (3.2.33)$$

which modifies the earlier proposals by De Cesare et al. (2001a, 2001b) to make it more flexible in its general implementation as earlier discussed.

The generalised product-sum model (3.2.33) exhibits some interesting properties as demonstrated by the previous two theorems. Theorem 3.2.2 ensures the strictly positive-definiteness of the model for any class of covariance models since it is related to the sill values of the marginal covariance functions. This is an important

requirement for a unique solution of kriging system during the prediction process. It also requires that the global sill is greater than the spatial and temporal sills, but less than their combined value. It has recently been shown that the generalised product-sum covariance model is strictly positive definite if the marginal functions are strictly positive definite (De Iaco, Myers, & Posa, 2011a, 2011b).

The product-sum model allows for the specification of different types of covariance or semivariogram models for the spatial and temporal directions. It also offers a mechanism for the interaction of dependence between space and time, making its use more flexible (user friendly) than the more simplistic separable models and the other wider class of non-separable models proposed by Cressie and Huang (1999) and Gneiting (2001) which are too complex and difficult to implement. The spatial and temporal marginal structures of the product and product-sum models can be modelled with their own nugget effects. The alternative way is to add a global nugget effect to the models presented (De Iaco, Myers, Palma, & Posa, 2010). As for the spatial and temporal semivariogram models, space-time semivariogram models can be fitted manually or automatically. Statistical criteria, such as weighted least-squares outlined in section 2.3.4 of chapter 2 can be used to help justify the choice of a particular model and its sets of parameters. In this study manual fitting was used to take into account the observed behaviour of the experimental semivariograms.

3.2.4 Model Parameter Estimation

Space-time autocorrelation analysis, as in the strictly spatial context, basically consists of computing the experimental semivariogram (or covariance function) and fitting valid model (or its components) to it through its estimation of parameters. There may be some complications in the process due to anisotropies or non-stationarity, though (De Iaco et al., 2001). In both cases the simplest approach to fitting a spatio-temporal covariance function or semivariogram is to reduce the problem to one similar to those encountered in the strictly spatial (or traditional) case. This procedure is practical because a large class of known valid models is available and additional models can be generated as positive convex combinations of the simpler models (De Iaco et al., 2001). In addition, there are some key basic geometric features which can be looked for in plotting, for example, the experimental semivariogram that can be used to choose the type of model. The problem of choosing valid space-time models has been considered in the previous section. One way of fitting a model to space-time data is to

estimate and model the spatial and temporal semivariogram via the traditional approach, separately from the observed space-time data and then combine, as in the product or product-sum model, to obtain the final space-time model (De Cesare et al., 1997; De Cesare et al., 2001b). The weighted least squares approach (Cressie, 1993) could also be used as a criterion to determine parameters in either or both of the semivariogram components, which also requires determining the model type(s) separately where cross validation can be used to evaluate the resulting fit (Myers, 1991).

The generalised product-sum (GPS) model as presented in the previous section is widely used, including modelling of spatio-temporal dependence of malaria morbidity incidence rates of Ghana in this study. The following outlines its estimation and modelling procedures (De Cesare et al., 2001b; De Iaco et al., 2010; De Iaco et al., 2001; De Iaco, Myers, & Posa, 2003; De Iaco & Posa, 2012):

Let $Z(\mathbf{u}, t)$ be a STRF and $A = \{(\mathbf{u}_\alpha, t_j), \alpha = 1, \dots, n_s; j = 1, \dots, n_t\}$ be a set of space-time sample data satisfying the SOS property. Then the fitting procedure of the model (3.2.33) basically involves estimating and modelling the spatial and temporal marginal semivariograms, $\gamma_{st}(\mathbf{r}_s, 0)$ and $\gamma_{st}(\mathbf{0}, r_t)$, which proceeds as follows:

If $A = \{(\mathbf{u}_\alpha, t_j), \alpha = 1, \dots, n_s; j = 1, \dots, n_t\}$ is a set of space-time sample data locations of STRF $Z(\mathbf{u}, t)$ satisfying the SOS property, then:

- (i) Compute the experimental marginal spatial and temporal semivariograms by (3.2.10), averaging over time for each data time point and averaging over space for each data spatial location:

$$\begin{cases} \hat{\gamma}_s(\mathbf{r}_s) = \frac{1}{2|n(\mathbf{r}_s)|} \sum_{n(\mathbf{r}_s)} (Z(\mathbf{u} + \mathbf{h}_s, t) - Z(\mathbf{u}, t))^2 = \hat{\gamma}_{st}(\mathbf{r}_s, 0) \\ \hat{\gamma}_t(r_t) = \frac{1}{2|m(r_t)|} \sum_{m(r_t)} (Z(\mathbf{u}, t + h_t) - Z(\mathbf{u}, t))^2 = \hat{\gamma}_{st}(\mathbf{0}, r_t) \end{cases} \quad (3.2.34)$$

where \mathbf{r}_s is a vector lag with spatial tolerance δ_s and similarly r_t , a vector lag which has the corresponding temporal tolerance δ_t ; $|n(\mathbf{r}_s)|$ and $|m(r_t)|$ are, respectively the cardinalities of the sets $n(\mathbf{r}_s)$ and $m(r_t)$:

$$\begin{cases} n(\mathbf{r}_s) = \{(\mathbf{u} + \mathbf{h}_s, t) \in A; (\mathbf{u}, t) \in A : \|\mathbf{r}_s - \mathbf{h}_s\| < \delta_s\} \\ m(r_t) = \{(\mathbf{u}, t + h_t) \in A; (\mathbf{u}, t) \in A : \|r_t - h_t\| < \delta_t\} \end{cases} \quad (3.2.35)$$

Usually, the spatial locations need not be on a regular grid, whilst the temporal points are regularly spaced and it is not necessary to use a temporal distance classes.

- (ii) Choose valid/permissible models, $\gamma_{st}(\mathbf{r}_s, 0)$ and $\gamma_{st}(\mathbf{0}, r_t)$ for the estimators in step (i) with the sills estimated values, $k_s C_s(\mathbf{0})$ and $k_t C_t(0)$, respectively.
- (iii) Compute the experimental space-time semivariogram as in (3.2.10):

$$\hat{\gamma}_{st}(\mathbf{r}_s, r_t) = \frac{1}{2|n(\mathbf{r}_s, r_t)|} \sum_{n(\mathbf{r}_s, r_t)} (Z(\mathbf{u} + \mathbf{h}_s, t + h_t) - Z(\mathbf{u}, t))^2 \quad (3.2.36)$$

where $|n(\mathbf{r}_s, r_t)|$ is the cardinality of the set: $n(\mathbf{r}_s, r_t) = \{(\mathbf{u} + \mathbf{h}_s, t + h_t) \in A; (\mathbf{u}, t) \in A: \|\mathbf{r}_s - \mathbf{h}_s\| < \delta_s \text{ and } \|r_t - h_t\| < \delta_t\}$.

- (iv) Estimate the global sill $C_{st}(\mathbf{0}, 0)$. This can be done visually by plotting the experimental space-time surface $\hat{\gamma}_{st}(\mathbf{h}_s, h_t)$. Alternatively, the weighted least squares (WLS) criterion (Cressie, 1993; De Iaco et al., 2001) can be used to fit $\hat{\gamma}_{st}(\mathbf{h}_s, h_t)$ to the generalised product-sum model (3.2.33).
- (iv) Compute the value of k by (3.2.32), making sure that condition (3.2.30) is satisfied. If not, replace it by an admissible value, usually closet to the least squares estimate; that is, the global sill $C_{st}(\mathbf{0}, 0)$ value can be estimated through the mean value of the semivariogram surface in the neighbourhood around the space-time range (corresponding to the spatial and temporal ranges of the marginal semivariograms). Note that if the parameter k is estimated, the global sill is univocally determined and vice versa.

3.3 Geostatistical Space-Time Kriging Techniques

Once statistical dependencies in space-time have been characterised, optimal linear prediction (kriging) is carried out based on the modelled space-time semivariogram (or covariance function). The goal of space-time kriging is to predict $Z(\mathbf{u}, t)$ at unobserved location $(\mathbf{u}, t)_0$, usually based on incomplete and noisy data observed in the neighbourhood of $(\mathbf{u}, t)_0$ (Cressie & Wikle, 2011). As in the case for the traditional method of kriging discussed in chapter 2, an unbiased linear predictor $Z_p(\mathbf{u}, t)_0$ of $Z_{st}(\mathbf{u}, t)$ has the property that its mean square prediction error can be expressed in

terms of the covariance function $C_{st}(\mathbf{h}_s, h_t)$ or semivariogram $\gamma_{st}(\mathbf{h}_s, h_t)$, which satisfies the non-negative condition in (3.2.15 and (3.2.16), respectively. Unlike the parameter estimation during structural analysis, kriging does require a stationarity (Cressie & Wikle, 2011), like ordinary kriging which requires intrinsic stationarity. To develop the space-time kriging based on the covariance function (or semivariogram), assume the STRF can be decomposed into a global trend $m(\mathbf{u}, t)$ and residual component $R(\mathbf{u}, t)$ as: $m(\mathbf{u}, t) + R(\mathbf{u}, t)$, where the residual has a distribution with mean zero and covariance Σ_{st} , where $E[Z(\mathbf{u}, t)] = m(\mathbf{u}, t)$. This allows some degree of robustness for the stationarity to be attained. Then for the observed values $\{Z(\mathbf{u}_\alpha, t_j), \alpha = 1, \dots, n_s; j = 1, \dots, n_t\}$ and following (2.4.1)–(2.4.5), we obtain the space-time linear predictor which is a linear combination of the $n(\mathbf{u}, t)$ random variables $Z(\mathbf{u}, t)$ plus a constant local mean $m(\mathbf{u}, t)$ which leads to the space-time ordinary kriging (STOK) predictor, as obtained in section 3.3.1. Also presented in the following sub-sections, focusing particularly on those applied to the malaria morbidity incidence cases in Ghana, are space-time lognormal ordinary kriging (STLOK) and space-time ordinary co-kriging (STOCK), being the log-transformed and multivariate versions of the STOK technique, respectively.

3.3.1 Space-Time Ordinary kriging (STOK)

As extension of OK, the space-time ordinary kriging (STOK) predicts at specific unsampled locations $(\mathbf{u}, t)_0$ using the $n(\mathbf{u}, t)$ observed samples in space and time made in those neighbourhoods:

$$\left\{ \begin{aligned} \hat{Z}_{stok}(\mathbf{u}, t)_0 &= \sum_{\alpha=1}^{n_s} \sum_{j=1}^{n_t} \lambda_{\alpha j}^{stok} (Z(\mathbf{u}_\alpha, t_j) - m(\mathbf{u}_\alpha, t_j)) + m(\mathbf{u}, t) \\ &= \sum_{\alpha=1}^{n_s} \sum_{j=1}^{n_t} \lambda_{\alpha j}^{stok} Z(\mathbf{u}_\alpha, t_j) + \left(1 - \sum_{\alpha=1}^{n_s} \sum_{j=1}^{n_t} \lambda_{\alpha j}^{stok}\right) m(\mathbf{u}, t) \end{aligned} \right. \quad (3.3.1)$$

To ensure that (3.3.1) is BLUE, the sum of weights must be equal to 1:

$$\left\{ \begin{aligned} \hat{Z}_{stok}(\mathbf{u}, t)_0 &= \sum_{\alpha=1}^{n_s} \sum_{j=1}^{n_t} \lambda_{\alpha j}^{stok} Z(\mathbf{u}_\alpha, t_j) \\ \text{subject to: } &\sum_{\alpha=1}^{n_s} \sum_{j=1}^{n_t} \lambda_{\alpha j}^{stok} = 1 \end{aligned} \right. \quad (3.3.2)$$

where the weights are estimated such that the expected error is zero, thus $E[\hat{Z}_{stok}(\mathbf{u}, t)|_0 - m(\mathbf{u}, t)] = 0$ and the prediction error variance,

$$\begin{cases} \sigma_{stok}^2(\mathbf{u}, t)|_0 = Var(\hat{Z}_{stok}(\mathbf{u}, t)|_0 - Z(\mathbf{u}, t)) \\ = E\left[\left(\hat{Z}_{stok}(\mathbf{u}, t)|_0 - \sum_{\alpha=1}^{n_s} \sum_{j=1}^{n_t} \lambda_{\alpha j}^{stok} Z(\mathbf{u}_\alpha, t_j)\right)^2\right] \end{cases} \quad (3.3.3)$$

is minimised via the Lagrangian function with multiplier $\varphi(u, t)$ which accounts for the constraint on the weights (Christakos & Hristopulos, 1998; Liu & Koike, 2007):

$$L(\lambda_{\alpha j}; \varphi) = \sigma_{stok}^2(\mathbf{u}_o, t_o) - 2\varphi(\mathbf{u}, t) \left(\sum_{\alpha=1}^{n_s} \sum_{j=1}^{n_t} \lambda_{\alpha j}^{stok} Z(\mathbf{u}_\alpha, t_j) - 1 \right) \quad (3.3.4)$$

which under the IS condition is further simplified following the OK procedure in section 2.4.2 and the work of (Christakos & Hristopulos, 1998) to obtain STOK system:

$$\begin{cases} \sum_{\beta=1}^{n_s} \sum_{j=1}^{n_t} \lambda_{\alpha j}^{stok} \gamma_{st}(\mathbf{u}_\alpha - \mathbf{u}_\beta; t_j - t_{j'}) + \varphi(\mathbf{u}, t) = \gamma_{st}(\mathbf{u}_\alpha - \mathbf{u}; t_j - t) \\ \sum_{\alpha=1}^{n_s} \sum_{j=1}^{n_t} \lambda_{\alpha j}^{stok} Z(\mathbf{u}_\alpha, t_j) = 1 \end{cases} \quad (3.3.5)$$

3.3.2 Space-Time Lognormal Ordinary Kriging (STLOK)

The STOK technique can also be applied to highly positively skewed space-time data, as the case of the observed district-month malaria morbidity incidence rates $\{I(\mathbf{u}_\alpha, t) : \alpha = 1, \dots, n; t = 1, \dots, T\}$ in this study in section 4.3.2 of chapter 4. The space-time data is log-transformed to stabilise the variations in the observed data set and also improve the normality assumption (Journel, 1980; Journel & Huijbregts, 1978)}. The STOK predictor $\hat{Z}_{stok}(\mathbf{u}, t)$ in (3.3.2) is thus modified to obtain the optimal space-time lognormal ordinary kriging (STLOK) predictor:

$$\begin{cases} \hat{Z}_{stlok}(\mathbf{u}, t) = \sum_{\alpha=1}^n \sum_{t=1}^T w_{\alpha t}^{stlok} Z(\mathbf{u}_\alpha, t) \\ \text{such that : } \sum_{\alpha=1}^n \sum_{t=1}^T \lambda_{\alpha t}^{stlok} = 1 \end{cases} \quad (3.3.6)$$

where in this case $Z(\mathbf{u}_\alpha, t) = \ln I(\mathbf{u}_\alpha, t)$. The interpolated $\hat{Z}_{stlok}(\mathbf{u}, t)$ values are back-transformed to obtain the STLOK predictor at the unsampled space-time locations (\mathbf{u}, t) :

$$\hat{I}_{stlok}(\mathbf{u}, t) = \exp[\hat{Z}_{stlok}(\mathbf{u}, t) + 0.5\sigma_{stlok}^2 - \mu_{stlok}] \quad (3.3.7)$$

where σ_{stlok}^2 is the kriging variance and μ_{stlok} is the Lagrangian multiplier in log scale.

3.3.3 Space-Time Ordinary Co-kriging (STOCK)

Space-time co-kriging is a multivariate geostatistical kriging technique used for modelling of spatio-temporal continuity multivariate attributes. The multivariate STRF then becomes the real-valued vector function, $\mathbf{Z}(\mathbf{u}, t) = [Z_1(\mathbf{u}, t), Z_2(\mathbf{u}, t), \dots, Z_k(\mathbf{u}, t)]^T$, where $k \geq 2$, $(\mathbf{u}, t) \in \mathbf{D} \times \mathbf{T} \subseteq \mathbb{R}^{d+1}$ denotes the space-time domain and the components assumed to be SOS and the semivariogram matrix, $\mathbf{\Gamma}(\mathbf{h}_s, h_t) = [\gamma_{ij}(\mathbf{h}_s, h_t)]$ exists and does not depend on (\mathbf{u}, t) where $\mathbf{h}_{st} = (\mathbf{h}_s, h_t)$, $\mathbf{h}_s = \mathbf{u} - \mathbf{u}^1$ and $h_t = t - t^1$;

$$\gamma_{ij}(\mathbf{h}_s, h_t) = Cov([Z_i(\mathbf{u} + \mathbf{h}_s, t + h_t) - Z_i(\mathbf{u}, t)], [Z_j(\mathbf{u} + \mathbf{h}_s, t + h_t) - Z_j(\mathbf{u}, t)]) \quad (3.3.8)$$

$i, j = 1, 2, \dots, k$ are the cross-semivariograms between the $Z_i(\mathbf{u}, t)$ and $Z_j(\mathbf{u}, t)$ STRF's, when $i \neq j$ and the direct semivariograms of the STRF's $Z_i(\mathbf{u}, t)$ when $i = j$. Assuming each component of $\mathbf{Z}(\mathbf{u}, t)$ to be a linear combination of uncorrelated SOS random functions:

$$\mathbf{Y}_l(\mathbf{u}, t) = [Y_1(\mathbf{u}, t), Y_1(\mathbf{u}, t), \dots, Y_k(\mathbf{u}, t)]^T, \quad l = 1, \dots, L \quad (3.3.9)$$

from which we obtain:

$$\mathbf{Z}(\mathbf{u}, t) = \sum_{l=1}^L \mathbf{A}_l Y_l(\mathbf{u}, t), \quad (3.3.10)$$

where \mathbf{A}_l is a $(k \times k)$ coefficient matrix for each $l = 1, \dots, L$. The space-time LCM for the semivariogram matrix $\mathbf{\Gamma}(\mathbf{h}_{st})$ can be written as:

$$\mathbf{\Gamma}(\mathbf{h}_s, h_t) = \sum_{l=1}^L \mathbf{B}_l g_l(\mathbf{h}_s, h_t), \quad (3.3.11)$$

where $\mathbf{B}_l = \mathbf{A}_l \mathbf{A}_l^T = [b_{ij}^l]$ and $l = 1, \dots, L$, $i, j = 1, \dots, k$ are positive definite $(k \times k)$ matrices and $g_l(\mathbf{h}_s, h_t)$ are basic space-time semivariograms representing different scales of variability.

The LMC in space-time framework can be extended using a product-sum model, where each basic space-time semivariogram $g_l(\mathbf{h}_s, h_t)$ is modelled as generalised product-sum model (De Iaco, Maggio, Palma, & Posa, 2012; De Iaco et al., 2001, 2003; De Iaco, Palma, & Posa, 2005):

$$g_l(\mathbf{h}_s, h_t) = \gamma_l(\mathbf{h}_s, 0) + \gamma_l(\mathbf{0}, h_t) - k_l \gamma_l(\mathbf{h}_s, 0) \gamma_l(\mathbf{0}, h_t), l = 1, \dots, L \quad (3.3.12)$$

where $\gamma_l(\mathbf{h}_s, 0)$ and $\gamma_l(\mathbf{0}, h_t)$ are spatial and temporal marginal semivariogram models respectively, and $k_l, l = 1, \dots, L$ are the parameters defined by

$$k_l = \frac{sill[\gamma_l(\mathbf{h}_s, 0)] + sill[\gamma_l(\mathbf{0}, h_t)] - sill[g_l(\mathbf{h}_s, h_t)]}{sill[\gamma_l(\mathbf{h}_s, 0)] \times sill[\gamma_l(\mathbf{0}, h_t)]} \quad (3.3.13)$$

which must satisfy the necessary and sufficient condition (3.2.30) (De Iaco et al., 2001) to ensure that $g_l(\mathbf{h}_s, h_t)$ is strictly conditionally negative definite. Substituting (3.3.12) in (3.3.11), the space-time LCM with basic generalised product-sum semivariogram models is determined by the marginal LMC in space and time respectively:

$$\begin{cases} \mathbf{\Gamma}(\mathbf{h}_s, 0) = \sum_{l=1}^L \mathbf{B}_l \gamma_l(\mathbf{h}_s, 0) \\ \mathbf{\Gamma}(\mathbf{0}, h_t) = \sum_{l=1}^L \mathbf{B}_l \gamma_l(\mathbf{0}, h_t) \end{cases} \quad (3.3.14)$$

The diagonal elements of \mathbf{B}_l are determined after modelling marginal direct thesemivariograms whilst the off-diagonal elements are obtained by marginal cross semivariogram models in such a way to ensure positive definiteness of the matrices \mathbf{B}_l (De Iaco et al., 2012; De Iaco et al., 2010).

The space-time ordinary co-kriging (STOCK) then becomes natural extension of spatial OCK to the space-time data (De Iaco et al., 2005) with the optimal predictor taking the form (3.3.15), from (3.3.14):

$$\hat{\mathbf{Z}}_{stok}(\mathbf{u}, t) = \sum_{\alpha=1}^{n(\mathbf{u}, t)} \mathbf{\Lambda}(\mathbf{u}_\alpha, t) \mathbf{Z}(\mathbf{u}_\alpha, t) \quad (3.3.15)$$

where $\mathbf{\Lambda}(\mathbf{u}_\alpha, t); \alpha = 1, 2, \dots, n(\mathbf{u}, t)$ are $(k \times k)$ matrices of weights whose elements $\lambda_{ij}(\mathbf{u}_\alpha, t)$ are the weights assigned to the j th variable at data location (\mathbf{u}_α, t) to predict

the i th variable at the point $(\mathbf{u}, t) \in \mathbf{D} \times \mathbf{T}$. The predicted space-time random vector, $\hat{\mathbf{Z}}_{stok}(\mathbf{u}, t)$ with components $\hat{Z}_i(\mathbf{u}_\alpha, t)$; $i = 1, 2, \dots, k$, is obtained by using all the data available at the points $(\mathbf{u}_\alpha, t) \in \mathbf{D} \times \mathbf{T}$; $\alpha = 1, 2, \dots, n(\mathbf{u}, t)$. The matrices of weights, $\Lambda(\mathbf{u}_\alpha, t)$ are determined by ensuring the unbiased and efficiency conditions for the predictor $\hat{\mathbf{Z}}_{stok}(\mathbf{u}, t)$ by minimising the prediction error variance (Goovaerts, 1997). De Iaco et al. (2010) propose a modified GSLIB routine code ‘‘COK2ST’’ for producing predictions multivariate in space-time domain using the space-time LMC in (3.3.11).

3.3.4 Prediction Uncertainty and Accuracy

The space-time (or spatial) prediction variance, σ_p^2 is used as a criterion for the determination of optimal values for the space-time kriging system. It provides useful information about each kriging procedure. The prediction variance which depends on the semivariogram (or covariance) model and the spatio-temporal configuration of the data in relation to the data locations $\{(\mathbf{u}_\alpha, t_j); \alpha = 1, 2, \dots, n; j = 1, 2, \dots, T\}$ is used as a measure of uncertainty of each prediction made (Gething, 2006). The prediction uncertainty increases with large spatial or spatio-temporal variances and for predictions that are more distant from data location. As the kriging variance is independence of the observed data its use is restricted to a relative measure of uncertainty which permits a relative comparison of uncertainty of the individual predictions and different data configurations estimate (Gething, 2006). After, for example, the predictor (3.3.2) is implemented for interpolation at the q unampled locations $\{(\mathbf{u}_\beta, t); \beta = 1, 2, \dots, q\}$, it worth to assess the closeness of the predicted values to the observed $(Z(\mathbf{u}, t) - \hat{\mathbf{Z}}_{stok}(\mathbf{u}, t))$ as a away of validating the accuracy of the prediction. However, in practice the set of q true values $\{Z(\mathbf{u}_\beta, t); \beta = 1, 2, \dots, q\}$ is by definition unknown for the accuracy of the predictions to be determined with certainty. There are various methods, including the *cross-validation* and *Jackknife* procedures, which can be employed to assess the predictive power of the developed space-time kriging models (Deutsch & Journel, 1998).

Cross-validation allows the prediction method to be tested at the locations of existing observations (Goovaerts, 1997). It proceeds by the removal of one datum $Z(\mathbf{u}_\alpha, t)$ at a time from the data set and re-estimation of this value from the remaining data using the

kriging technique in question, noting the prediction error $e(\mathbf{u}_\alpha, t) = Z(\mathbf{u}_\alpha, t) - \hat{Z}(\mathbf{u}_\alpha, t)$. The removed datum is then replaced and another removed, repeating for all $n \times T$ data locations to provide a complete set of predicted values for comparison with the observed data set. Cross-validation allows for the assessment of the impact of a semivariogram and kriging models used. It is a measure of the performance of the space-time kriging process within the prediction neighbourhood of the data set. It can also detect what might have gone wrong but does not necessarily ensure the procedure will be successful. The interpolated and actual values can be compared to assess the performance of the model by computing the associated error values $e(\mathbf{u}_\alpha, t)$ which must be symmetric, centred on zero mean with minimum spread of which should not show any trend in space or time (Denham, 2012).

Typical measures of kriging accuracy for comparison include correlation coefficient ρ_{ZZ} , indicating the degree of linear association between the observed and predicted data sets. It also measures the variation explained (r^2) in the data and relates the root mean square error (*RMSE*); the mean error (*ME*) which measures the bias of the model prediction and should be as close to zero for unbiasedness; the mean absolute error (*MAE*) and *RMSE* which serve as measures of mean accuracy with smaller values indicating better performance of the kriging estimator. They are defined as follows:

$$MAE = \frac{1}{n \times T} \sum_{\alpha=1}^n \sum_{t=1}^T |Z(\mathbf{u}_\alpha, t) - \hat{Z}(\mathbf{u}_\alpha, t)| \quad (3.3.16)$$

$$RMSE = \sqrt{\frac{1}{n \times T} \sum_{\alpha=1}^n \sum_{t=1}^T (Z(\mathbf{u}_\alpha, t) - \hat{Z}(\mathbf{u}_\alpha, t))^2} = (SSE) \quad (3.3.17)$$

Prediction accuracy assessment by the cross-validation method may be adversely affected by the strictly dependence on the datum to which it is compared (Denham, 2012; Gething, 2006). For example, when a datum is removed temporarily to generate a cross-validation prediction at that point, the semivariogram is not recomputed. However, for large data observations with absence of extreme outliers, the influence of an individual datum on the experimental semivariogram is negligible in most cases. Another limitation is the use of simple arithmetic averages to generate estimates of *ME* and *MAE* which may result in biased estimates when the data are clustered.

The Jackknife method is used to obtain an unbiased prediction estimate and to minimise the risk of overfitting by reducing the estimation variance (Abdi & Williams, 2010). It was originally proposed by Quenouille (1956) as a non-parametric way of minimising the bias of an estimator of a population parameter and further expanded by Tukey (1958) to include estimation of variance of the estimator. The Jackknife evaluation procedure begins by dropping in turn each observation and fitting the model for the remaining set of data. The model is then used to predict the removed observation. Proceeding in this way, each observation is predicted to obtain a new set of data. In the context of this study, the predictive power of the space-time kriging models is assessed by applying the Jackknife procedure to a small portion of the data set which will not be used in the modelling process. The predicted estimates $\hat{Z}(\mathbf{u}_\alpha, t)$ obtained at each space-time location (\mathbf{u}_α, t) are compared with the observed (validation) data set $Z(\mathbf{u}_\alpha, t)$ by computing the prediction accuracy measures as in (3.3.16) and (3.3.17).

3.4 Conceptual Modelling Approaches of STRF

There are two main schools of thought for modelling spatio-temporal data (Kyriakidis & Journel, 1999). In the first view, the space-time data set is considered as a single random function $Z(\mathbf{u}, t)$, integrating both space and time components (Christakos, 1992), where the joint space-time semivariogram model can be used to characterise the spatio-temporal discontinuity. The second conceptual view considers STRF $Z(\mathbf{u}, t)$ as vectors of random functions or time series, depending on which domain has sufficient data. If $Z(\mathbf{u}, t)$ is a vector of random functions, then it is considered as a collection of finite number of T temporally correlated space random functions $Z(\mathbf{u})$, where $Z(\mathbf{u}, t) = [Z_1(\mathbf{u}), \dots, Z_T(\mathbf{u})]^T$ and the spatial maps of the space-time random variable are generated at limited time instants $t = 1, 2, \dots, T$. In the case of $Z(\mathbf{u}, t)$ being vector of time series, then it becomes a collection of finite number of spatially correlated time series (spatial time series) and $Z(\mathbf{u}, t) = [Z_1(\mathbf{u}), \dots, Z_n(\mathbf{u})]^T$, where constructions of the time series are made at the sparse locations $\mathbf{u}_\alpha; \alpha = 1, \dots, n$. In each of these modelling approaches, the STRF $Z(\mathbf{u}, t)$ can be decomposed into the mean $m(\mathbf{u}, t)$ and a stochastic residual component $R(\mathbf{u}, t)$ as was initially indicated in section 3.3. The mean function $m(\mathbf{u}, t)$ models the average variability, being the trend and/or seasonal

cycles, whilst $R(\mathbf{u}, t)$ models the space-time fluctuations around the trend function. There are two types of decompositions which are usually considered, depending on whether the trend function $m(\mathbf{u}, t)$ is deterministic or stochastic (Kyriakidis & Journel, 1999). The modelling of $m(\mathbf{u}, t)$, where $Z(\mathbf{u}, t)$ is considered as vectors of spatially correlated time series, is presented in the following section.

3.4.1 Modelling of Space-Time Trend Component

The deterministic space-time trend $m(\mathbf{u}, t)$ component of the STRF is often, modelled by the function:

$$m(\mathbf{u}, t) = \sum_{l=0}^L \sum_{k=0}^K b_{kl} f_{kl}(\mathbf{u}, t), \quad \forall (\mathbf{u}, t) \in \mathbf{D} \times \mathbf{T}, \quad (3.4.1)$$

which is made up of KL known basis functions $f_{kl}(\mathbf{u}, t)$ chosen to fit the observed space-time data, and b_{kl} , $k = 1, \dots, K$; $l = 1, \dots, L$ are unknown coefficients to be determined. The basis functions $f_{kl}(\mathbf{u}, t)$ can be polynomial or piece-wise continuous functions to model smooth variations or discontinuities in space, whilst periodic functions are used to account for seasonal variations in the temporal domain. Dimitrakopoulos & Luo (1997) proposed various forms of trend models, which include a mix of a polynomial of order n and trigonometric functions and to fit an upward trend as well as the cycles in the space-time data:

$$m(\mathbf{u}_\alpha, t) = b_0(\mathbf{u}_\alpha) + b_1(\mathbf{u}_\alpha)t + \dots + b_n(\mathbf{u}_\alpha)t^n + b_{n+1}(\mathbf{u}_\alpha) \cos(\omega t) + b_{n+2}(\mathbf{u}_\alpha) \sin(\omega t) \quad (3.4.2)$$

where $b_i(\mathbf{u}_\alpha)$; $i = 0, 1, \dots, n$ are the coefficients of the trend component of the model whereas $b_{n+1}(\mathbf{u}_\alpha)$ and $b_{n+2}(\mathbf{u}_\alpha)$ are the coefficients of the periodic component which are linked to the amplitude $a(\mathbf{u}_\alpha)$ and phase $\phi(\mathbf{u}_\alpha)$ of the cycles in the data with angular frequency $\omega = 2\pi/\lambda$ of period λ . The amplitude and the phase are defined by:

$$\begin{cases} a(\mathbf{u}_\alpha) = \sqrt{[b_{n+1}(\mathbf{u}_\alpha)]^2 + [b_{n+2}(\mathbf{u}_\alpha)]^2} \\ \phi(\mathbf{u}_\alpha) = \tan^{-1}[-b_{n+2}(\mathbf{u}_\alpha)/b_{n+1}(\mathbf{u}_\alpha)] \end{cases} \quad (3.4.3)$$

The coefficients $b_i(\mathbf{u}_\alpha)$ of the trend model (3.4.2) are treated as precise data at each

location \mathbf{u}_α and may be computed with the ordinary least squares (OLS) method (Chatterjee & Hadi, 2006; Draper & Smith, 1981). The OLS method minimises the sum of squares of the residuals $[R(\mathbf{u}_\alpha, t)]^T [R(\mathbf{u}_\alpha, t)]$, resulting in the estimation of the trend coefficients:

$$\hat{\beta}_\alpha = [Z^T(\mathbf{u}_\alpha)Z(\mathbf{u}_\alpha)]^{-1} Z^T(\mathbf{u}_\alpha)R(\mathbf{u}_\alpha) \quad (3.4.4)$$

where $\hat{\beta} = [b_0, b_1, \dots, b_n, \dots, b_{n+2}]^T$. If the trend coefficients are modelled as outcomes of random variables, then the basis functions $f_{kl}(\mathbf{u}, t)$ are considered as random and the model (3.4.1) becomes stochastic model. In this case, the coefficients b_{kl} can be spatially estimated by using the simple or ordinary kriging technique (Fernández-Cortes, Calaforra, Jiménez-Espinosa, & Sánchez-Martos, 2006; Oehlert, 1993) to obtain the interpolated surfaces:

$$b_i^{ok}(\mathbf{u}) = \sum_{\alpha_i=1}^{n(\mathbf{u})} \lambda_{\alpha_i}^{ok}(\mathbf{u}) b_i(\mathbf{u}_\alpha), \quad i = 0, 1, \dots, n+2, \quad (3.4.5)$$

for the optimal prediction of the global trend function to be determined by:

$$\hat{m}(\mathbf{u}, t) = \sum_{i=0}^{n+2} \sum_{\alpha_i=1}^{n(\mathbf{u})} [\lambda_{\alpha_i}^{ok}(\mathbf{u}_\alpha) b_i^{ok}(\mathbf{u}_\alpha)] t^i, \quad (3.4.6)$$

for each $t \in \mathbf{T} = \{t = 1, \dots, T\}$.

3.4.2 Optimal Prediction of STRF

The optimal prediction of the space-time random function (STRF) at the unsampled location (\mathbf{u}, t) is obtained through an established link between the two conceptual approaches as discussed above. The optimal trend estimator in (3.4.6) combines with the interpolated residuals $\hat{R}_{stok}(\mathbf{u}, t)$ via the single spatio-temporal random function modelling approach as in (3.3.2), yielding the space-time optimal predictor (3.4.7):

$$\hat{Z}_{stok}(\mathbf{u}, t) = \hat{m}(\mathbf{u}, t) + \hat{R}_{stok}(\mathbf{u}, t), \quad (3.4.7)$$

for each $t \in \mathbf{T}$, from which continuous spatial maps can be generated to illustrate the distributional pattern of the estimated value of the random variable $Z(\mathbf{u}, t)$.

3.5 Summary Chapter

The chapter provided the geostatistical space-time stochastic modelling framework for the joint analysis of data distributed in space and time domains which serves as an extension of those techniques developed for purely spatial analysis presented in chapter 2. It focused on those modelling procedures mainly used to explore the spatio-temporal distribution of the malaria morbidity incidence cases and its potential climatic effect. The space-time random functions and their properties coupled with the modelling approaches of the spatio-temporal continuity including the generalised product-sum model fitting of the space-time semivariograms were covered.

Also outlined in the chapter were the space-time kriging techniques, namely space-time ordinary kriging (STOK) and its two main variants, space-time lognormal ordinary kriging (STLOK) and space-time ordinary co-kriging (STOCK) to account for the highly positive skewed data and effect of exogeneous variables, respectively. Finally, the two conceptual approaches of spatio-temporal modelling were discussed. The first considers space-time data as a joint single random function, integrating both space and time components, whilst the second views the space-time random function (STRF) and as vectors of random functions or time series. The choice between the two depends on the domain with relatively sufficient data.

Chapter 4

Exploratory Data Analysis

4.1 Introduction

This chapter presents the exploratory analysis of the study data as a preliminary step for the spatio-temporal modelling of the malaria morbidity incidence in Ghana. The malaria morbidity cases are modelled as a realisation of random process occurring in space and time and so it is necessary to establish the distributional properties of the data. This will help to make informed decisions concerning which analytical tools best suit the data and prepare the required output for easier interpretation. In the following sections of this chapter an overview of the study area, the data collection process and description will be presented. Sections 4.2 and 4.3 provide the exploratory analysis of the data and additional tools that are used to describe the spatial characteristics of the malaria incidence data. In Section 4.4 we undertake correlation and regression analyses of the data to determine the potential climatic covariates on malaria risk for future forecast and prediction at the regions and unsampled district locations, respectively. Section 4.5 presents the global analysis of the incidence rates observed in the ten regions using the multivariate time series modelling of seasonal autoregressive integrated moving average (SARIMA) for the future forecast and to establish the effect of climate.

4.1.1 Study Area

Ghana is a tropical country in West Africa. It is centrally located in the sub-region, lying within latitudes 4.5° and 11.5° north, and longitudes 1.5° east and 3.5° west, covering a total land surface area of about 238,540 square kilometres with a coastline of approximately 550 kilometres (Baatuwile & Van Leeuwen, 2011; GSS, NMIMR, & Macro, 2004b). It has a maximum north-south extent of about 750 kilometres and a maximum east-west extent of about 500 kilometres. Ghana shares borders with Cote d'Ivoire to the west, Burkina Faso to the north, Togo to the east; and to the south are the Gulf of Guinea and the Atlantic Ocean. The terrain is mostly low plain, with a dissected plateau in the south-central area with approximately half of the country lying less than 152 metres above sea level whilst the highest point of 885 metres is located in the range in the east, close to the border with Togo (see the gridded elevation map in

Figures 4.1.1, right). It has an estimated population of 25.03 million people, with an annual growth rate of approximately 2.7%, and is divided into ten administrative regions (see Figure 4.1.1, left), where each region is also subdivided into decentralised districts to ensure efficient and effective local administration. As at 2005/2006, there were 138 districts, which have since been re-organised by splitting some and others up-graded to the metropolitan or municipal status, bringing the current number to 170 (PSS/GSS, 2009). The population density in the country varies from 31 to 893 per square kilometre in the Northern Region and Greater Accra Region, respectively and 54% of the population live in rural areas (GSS, 2002; PSS/GSS, 2009).

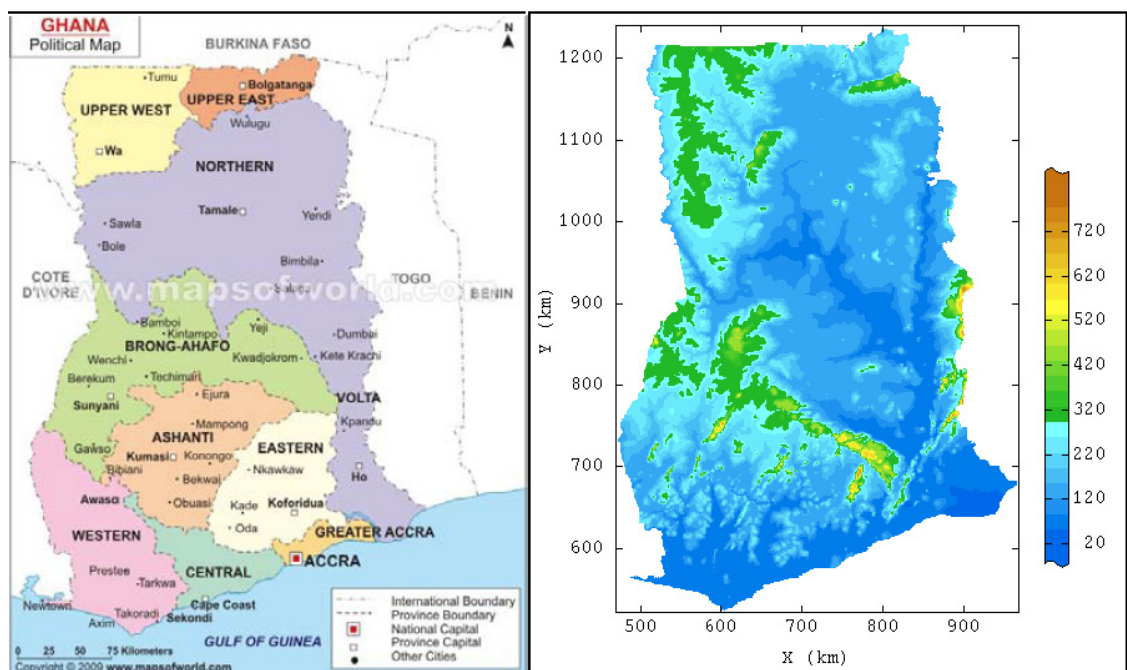


Figure 4.1.1: Map of Ghana showing the ten administrative regions (left), and digital elevation model (DEM) of Ghana, obtained from IntraSearch (2011).

Ecologically the country can be divided into three broad malaria zones, based on the vegetation types in the country, namely the northern savannah, tropical (evergreen/semi-deciduous) rainforest in the central and south-west and the coastal savannah/mangrove swamps (NMCP/GHS, 2009; RMSC/FC, 2011) as shown in Figure 4.1.2 (left). It should also be noted that multiple forest reserves exist in each zone. According to the National Malaria Control Programme (NMCP), each zone exhibits different characteristics in relation to *Anopheles* mosquitoes and the parasites which cause the malaria disease (NMCP/GHS, 2009). *Anopheles gambiae* and *Anopheles arabiensis* are predominant in northern savannah. The former species (the

most efficient vector) breeds in temporary stagnant waters, bites indoors, rests outdoors and is anthropophilic whilst the latter bites and rests outdoors and is more zoophilic. The tropical rainforest zone is dominated by *Anopheles gambiase* and *Anopheles funestus*; the latter breeds throughout the year in permanent stagnant waters and bites and rests indoors, and is anthropophilic. In the coastal zone the *Anopheles gambiase* and *Anopheles funestus* along with the *Anopheles melas* which is anthropophilic and bites and rest indoors. Differences in temperature, rainfall and humidity patterns as well as the ecological characteristics account for these variations (de Souza et al., 2010).

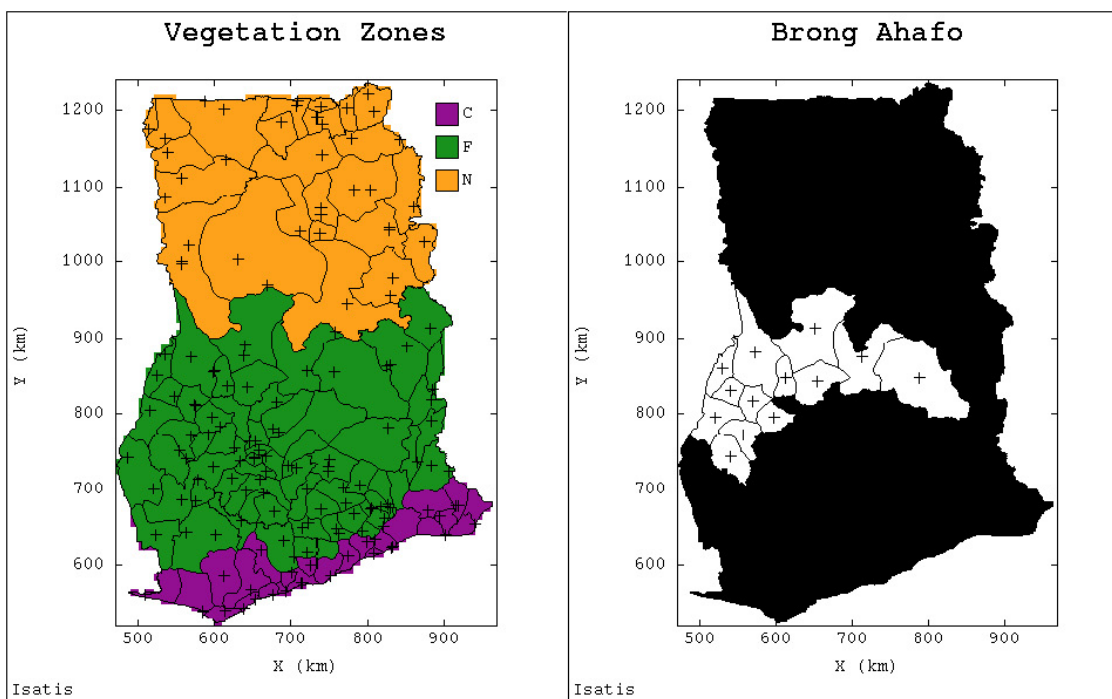


Figure 4.1.2: Data locations of study area (plus signs) indicating the three malaria epidemiological zones as classified by vegetation types (left map) (NMCP/GHS, 2009): northern savannah (N), tropical rainforest (F) and coastal and mangrove swamps (C); the map on the right shows the location of Brong Ahafo Region and its districts within Ghana (insert map).

The climate is warm and relatively dry along the southeast coast and hot and humid in the central and southwest, with a prolonged dry season in the north due to the north-east trade winds from the Sahara desert. There are two main seasons, the rainy season from April to October and dry season from November to March. Temperatures vary relatively little throughout the country, with a mean annual temperature between 26oC and 29oC. Annual average rainfall ranges from about 1,100 mm in the north to 2,100 mm in the southwest, whilst average relative humidity varies from nearly 85% in the south to 70% in the north (Ghana Web, 2013). The transmission of the disease is stable

and takes place all year, although there is a perceptible seasonal variation in the northern savannah zone because of the prolonged dry season from September to April. The normal duration of the intense malaria transmission season in the northern part of the country is around six months beginning May and lasting to September/October.

4.1.2 Data Description

The data on malaria morbidity cases were obtained from the Centre for Health Information and Management (CHIM) and Regional Health Information Units of Ghana Health Services (GHS). The data included monthly morbidity cases reported from the district health facilities at outpatient departments (OPD) based in the 138 districts covering the whole country (see Figure 4.1.2) for the period 1998–2011, comprising 132 (or 168) months with records for several months missing for some districts, especially for the years 1998–2004. Population data over the same period were also collected from the Population Statistics Section (PSS) of Ghana Statistical Service (GSS), and used to compute the monthly reported morbidity incidence rates (MIR) data as defined by (4.2.1). Climatic data on rainfall, temperature, relative humidity and number of sunshine hours were received on 77 districts and for the regions from the Ghana Meteorological Agency (GMet), and a digital elevation model (DEM) of Ghana was obtained from Mapmart IntraSearch (IntraSearch, 2011). The monthly malaria morbidity cases in the districts were point-referenced using coordinates of their capitals in longitudes and latitudes (in degrees) which were transformed to the Universal Transverse Mercator (UTM) coordinate system, easting and northing (in kilometres). The climatic data together with the elevation derived from DEM were used as covariates to establish spatio-temporal correlations to predict the morbidity incidence rates at district locations, thus delineating areas with a high risk of the disease.

The data reporting format of the malaria morbidity cases varied across the districts in the country; whilst some districts reported to CHIM by age and sex, others recorded just the total cases coupled with no recording or misreporting of cases. In view of this inconsistency and differences in the data reporting, the study uses two data sets for the analysis. One is the *regional data*, aggregated cases observed on each of the ten regions structured by sex and into age groups, 0–4, 5–14, 15–59 and 60+ years, to which the time series predictive modelling (SARIMA) is applied for the global forecast of future morbidity incidence rates. The second is the *space-time data*, the

larger data set, consisting of only the total morbidity cases at sampled district locations used to perform the space-time analysis of the disease's incidence at the local level. The spatio-temporal analysis considers this data set not only on all districts in the country which we shall refer to as *national* study, but also the *Brong Ahafo Region (BAR)* and *vegetation types* (coastal savannah/mangrove, tropical rainforest and northern savannah), according to the epidemiologic zones of the disease by Ghana's National Malaria Control Programme (NMCP/GHS, 2009), which in this study are simply referred to as *coastal*, *forest*, and *northern*, respectively. The maps of the vegetation zones and BAR indicating the districts are as shown in Figure 4.1.2.

The interest of a local spatial as well as temporal dependency at a regional level, using BAR, stems from its strategic position in the country (see map in Figure 4.1.2, right). It is centrally located, lying within longitudes 3°W and 0.25°E and latitudes 6.5° and 9°N, and covering an area of approximately 39,560 square kilometres with 19 administrative districts with estimated total population of 2.36 million, each varying between 77,000 and 236,800 (PSS/GSS, 2009). Although the region falls within the tropical rainforest zone, its northern part exhibits characteristics similar to the vegetation type of the northern savannah. Additionally, the region has the most exhaustive data of all the reported cases of the disease for the period 1998–2011 in the temporal domain. Generally, BAR has a tropical climate with high temperatures averaging 25°C and a bimodal rainfall pattern, the annual average total rainfall ranging from 1000 to 1400 millimetres. The study by vegetation zones is informed by the direct links to mosquito habitats due to the differences in climate and vegetation cover which eventually lead to wide spread of malaria transmission (de Souza et al., 2010; Klinkenberg et al., 2005). The indirect effect of vegetation is studied by comparing results of the data analysis for these vegetation types.

The analysis of the monthly count of malaria morbidity cases from the health facilities both at spatial and temporal scales begins with the standardisation of the morbidity cases as incidence rates after which the exploratory behaviour of time series of the observed incidence rates in the regions and at the districts locations is considered. This will ensure proper application of the various temporal and spatio-temporal modelling techniques to be employed to characterise and also predict the morbidity risk patterns as presented in chapter 5.

4.2 Exploratory Time Series Analysis of Regional Data

In this thesis a malaria morbidity case is defined as a diagnosis of simple or severe malaria recorded at an OPD of a health facility in Ghana. In Ghana, most outpatient cases are diagnosed on the basis of clinical symptoms and treatment is presumptive, rather than based on laboratory confirmation (Adams et al., 2004). The whole population is at risk of malaria and, in view of the high incidence of the disease in all the districts, the monthly morbidity case counts reported will be modelled as the incidence rates time series for each district or region, defined as the number of reported morbidity new cases per unit resident population of 10,000 based on PSS/GSS (2009) and following Huang, Zhou, Zhang, Zhang, and Li (2011):

$$I_t(\mathbf{u}_\alpha) = \left(\frac{MC_t(\mathbf{u}_\alpha)}{P_t(\mathbf{u}_\alpha)} \right) \times 10,000, \alpha = 1, 2, \dots, n; t = 1, 2, \dots, T \quad (4.2.1)$$

where $MC_t(\mathbf{u}_\alpha)$ is the number of reported new malaria morbidity cases at district or region α for month t , $P_t(\mathbf{u}_\alpha)$ is the mid-year population for the same month, $n = 138$ is number of districts (or $n = 10$ regions) sampled, and T is the number of consecutive months $MC_t(\mathbf{u}_\alpha)$ is reported at a district (or region) within the study period, 1998–2011. The computation of the morbidity incidence rates (MIR) will be useful to determine the needs for malaria treatments at the various district locations. Such information when made available can be used to compare levels of access to treatment and to constraint resources towards the high priority areas in the country.

4.2.1 Descriptive Summary of the MIR Data

Using the equation (4.2.1) we obtain the monthly malaria MIR observed for 132 consecutive months for each region over the period 2000–2011 (except for Brong Ahafo Region for which there were 168 sampled monthly observations, beginning 1998). The numerical summaries of the MIR data for the regions are reported by sex and the adopted age groupings. In this section only the descriptive statistics for the grand total incidence cases and for 0–4 year old group (children under 5 years of age, the people most severely affected by the disease in the country) are presented; the descriptive summaries for the other age groups are shown in Tables A-1.1–A.1.4 in Appendix A-1. The grand totals are used as proxy for the other age groups as

evidenced by the exploratory time plots in section 4.2.2. Tables 4.2.1 and 4.2.2 present the summary descriptive statistics for the monthly MIR data by region.

Table 4.2.1: Summary statistics of monthly malaria morbidity incidence rates computed for the grand total cases including that of the males and females in the ten regions of Ghana

Region	Data	Min	Max	Mean	Q1	Med	Q3	StD	Skew	Kurt
(Total)	Total	93	264	164	130	161	192	41.28	0.376	-0.674
Ashanti	Male	86	251	149	116	146	175	39.95	0.553	-0.450
	Female	100	322	183	147	177	208	50.09	0.580	-0.240
Brong	Total	105	382	227	186	230	266	56.20	0.114	-0.477
	Male	98	330	203	174	208	234	47.10	0.079	-0.372
Ahafo	Female	112	432	251	201	248	292	66.18	0.168	-0.574
Eastern	Total	74	397	188	130	176	241	73.76	0.667	-0.331
	Male	65	340	159	114	152	197	57.67	0.673	0.008
	Female	82	453	217	146	196	284	90.97	0.671	-0.560
Greater	Total	58	183	104	87	103	101	24.62	0.795	0.650
	Male	49	156	91	76	89	101	21.11	0.788	0.520
	Female	66	211	117	97	115	129	27.29	0.805	0.811
Western	Total	75	358	185	124	161	242	78.43	0.627	-0.748
	Male	64	319	167	114	149	217	69.00	0.492	-0.865
	Female	85	396	201	136	174	263	88.21	0.725	-0.647
Northern	Total	72	346	188	142	180	223	61.19	0.504	-0.529
	Male	65	327	174	131	166	202	56.89	0.509	-0.481
	Female	78	364	202	150	193	246	65.89	0.514	-0.549
Upper	Total	80	624	252	158	222	320	117.21	0.832	0.112
	Male	86	593	241	162	222	298	105.60	0.927	0.512
	Female	72	654	264	156	225	352	129.8	0.761	-0.192
West	Total	102	658	295	193	275	358	147.00	1.347	1.841
	Male	100	735	280	183	250	342	128.90	1.272	1.658
	Female	105	908	321	201	285	374	167.40	1.394	1.880
Upper	Total	63	243	115	84	109	134	37.18	0.906	0.675
	Male	62	225	105	78	98	119	33.21	1.147	1.321
	Female	63	262	125	90	118	152	41.82	0.739	0.205
Central	Total	134	356	196	152	180	225	52.67	0.885	-0.162
	Male	114	286	164	131	152	182	41.09	0.955	-0.023
	Female	148	403	225	174	204	263	62.47	0.751	-0.473
Volta										

Table 4.2.2: Summary statistics of monthly malaria morbidity incidence rates computed for the grand total cases of age group (0-4) years in the ten regions of Ghana

Region (0-4)	Data	Min	Max	Mean	Q1	Med	Q3	StD	Skew	Kurt
Ashanti	Total	181	560	303	235	278	370	88.97	0.793	-0.291
	Male	177	557	302	239	278	358	84.10	0.816	-0.062
	Female	179	563	305	228	305	378	95.45	0.812	-0.397
Brong Ahafo	Total	191	686	410	343	404	471	99.73	0.481	0.005
	Male	207	695	427	360	418	488	99.23	0.422	-0.116
	Female	175	735	394	327	388	452	101.45	0.583	0.322
Eastern	Total	154	662	332	255	312	372	104.20	1.045	0.794
	Male	162	663	335	259	322	376	104.70	1.037	0.875
	Female	143	667	328	258	302	370	106.10	1.042	0.724
Greater Accra	Total	125	445	236	196	229	263	59.50	0.759	0.698
	Male	127	402	242	200	237	270	59.76	0.549	-0.078
	Female	124	511	229	191	222	256	60.32	1.77	2.925
Western	Total	126	719	331	220	293	391	157.20	0.900	-0.255
	Male	124	747	344	228	302	410	164.00	0.896	-0.232
	Female	129	692	319	208	282	396	151.40	0.888	-0.310
Northern	Total	181	710	391	294	377	460	117.20	0.614	-0.301
	Male	170	742	402	310	384	480	125.20	0.601	-0.245
	Female	192	679	380	288	365	444	111.00	0.645	-0.283
Upper West	Total	205	1300	612	426	570	741	225.90	0.872	0.222
	Male	215	1350	610	440	564	745	237.90	0.870	0.260
	Female	190	1370	614	412	551	740	258.20	0.885	0.259
Upper East	Total	284	1940	802	538	704	1010	355.00	0.956	0.586
	Male	280	1900	779	524	698	992	339.10	1.021	0.788
	Female	268	1980	828	539	738	1040	378.00	0.923	0.408
Central	Total	101	443	221	170	208	226	71.01	0.698	-0.408
	Male	98	418	214	159	200	259	69.57	0.637	-0.295
	Female	105	470	229	176	216	274	73.67	0.765	0.210
Volta	Total	228	653	376	288	352	438	112.76	0.804	-0.387
	Male	214	650	367	275	342	432	114.40	0.839	-0.337
	Female	228	657	384	289	356	449	115.20	0.665	-0.599

The reported morbidity incidence rates in the ten regions range from 58 to 658 cases per 10,000 resident people per month with Upper East having the highest mean incidence rate of 295 cases followed by Upper West with a mean rate of 252 cases. Ashanti and Greater Accra, the most populated regions, are among the three regions which recorded the lowest mean incidence rates of 104 and 164 respectively, the third being Central Region with 115 cases. In all regions the incidence among females is higher than that for males. The monthly incidence rates in the regions are positively skewed and appear to be similarly distributed among males and females but with higher variations. As expected, the most vulnerable group (0–4 year olds) recorded the highest incidence rates among all the age groups including the regional total. The total morbidity incidence of the disease in this age group is more variable, ranging from 101 to 1940 with the highest mean of 802 per 10,000 residents in the Upper East Region and lowest mean rate of 221 cases in Central Region (see Table 4.2.2). As the case for the regional total cases, the incidence cases for young children are positively skewed with the female morbidity cases being more variable except in the northern and western regions. It is also observed that occurrence of morbidity of the disease among the children under 5 years of age is approximately equally likely (in terms of the mean rates) between sexes except in Brong Ahafo, Northern and Upper East regions. Brong Ahafo Region is ranked third to the two northern most regions (Upper East and Upper West) with 410 cases but Ashanti, Central and Greater Accra regions consistently have the lowest mean incidence rates of 303, 221 and 236 cases, respectively.

It worth noting that the three northern regions, Northern, Upper East and Upper West which form the northern savannah zone, recorded the highest incidence rates in the country. The environmental conditions coupled with the economic activities in the regions favour the mass breeding of mosquitos which cause the disease. The Upper East and West regions, relatively the most deprived in terms of resources, have high rates of malnutrition and anaemia which are common symptoms of malaria disease in Ghana (Baird et al., 2002). Malaria intervention activities and studies are often carried out in several parts of the regions which could prompt people to visit the health centres regularly to treat the disease. The low incidence rates of the disease in the two densely populated regions (Ashanti and Greater Accra) could be attributed to the numerous health facilities located in and around their regional capitals and other urban centres coupled with much improvement in the health delivery services compared with the

other regions. Also, they have most of the infrastructural developments in the country in addition to hosting the two largest cities, Accra and Kumasi, the former being the capital city of Ghana.

In Ghana, children under 5 years and pregnant women are the people most affected by the malaria disease (GHS, 2011; NMCP, 2008; UNICEF, 2012). The high morbidity incidence rates of these young children and older females confirm the vulnerability of these two categories of people in the country. The incidence within these two groups generally characterises the behaviour of the disease in the regions as exemplified by the time sequence plots and smoothing analysis in sections 4.2.2 and 4.2.3, respectively. In this thesis we shall use the total incidence cases computed for the regions, districts and 0–4 year olds to model the malaria morbidity incidence in Ghana both at global (regional) and local (district) levels. This choice is justified by the time sequence plots of the disease's morbidity incidence for the period 1998-2011 at all regional levels across the country.

4.2.2 Time Sequence Plots of MIR

In this section time sequence plots of the monthly morbidity incidence rates per resident population of 10,000 for the regional total and age groups in the regions for the period 1998–2011 are presented. These plots are produced to visually establish the general trend pattern of the time series data, the series being the monthly morbidity incidence rates. This then leads to the future forecast of the incidence rates at the regions which will be considered in section 4.5. Figures 4.2.1–4.2.3 provide the time sequence plots for some selected regions in each vegetation zone, whilst the plots for the other regions are shown in Appendix A-2.

The examination of the entire regional incidence rates of the disease generally reveals increasing but fluctuating periodic trend patterns in all the regions, which is an indication of non-stationarity. In general, the female incidence rates are slightly higher than that of the males and the regional totals but there appears to be no substantial difference in the incidence between sexes (see Figures 4.2.1 and 4.2.2). The patterns by age groupings (see Figure 4.2.3) are comparable with the patterns for regional total incidence rates, except for the 0-4 years group. For this year group which recorded the highest incidence rates there is some irregular trend behaviour throughout the study period especially in Ashanti, Brong Ahafo, Eastern and Volta regions which fall within

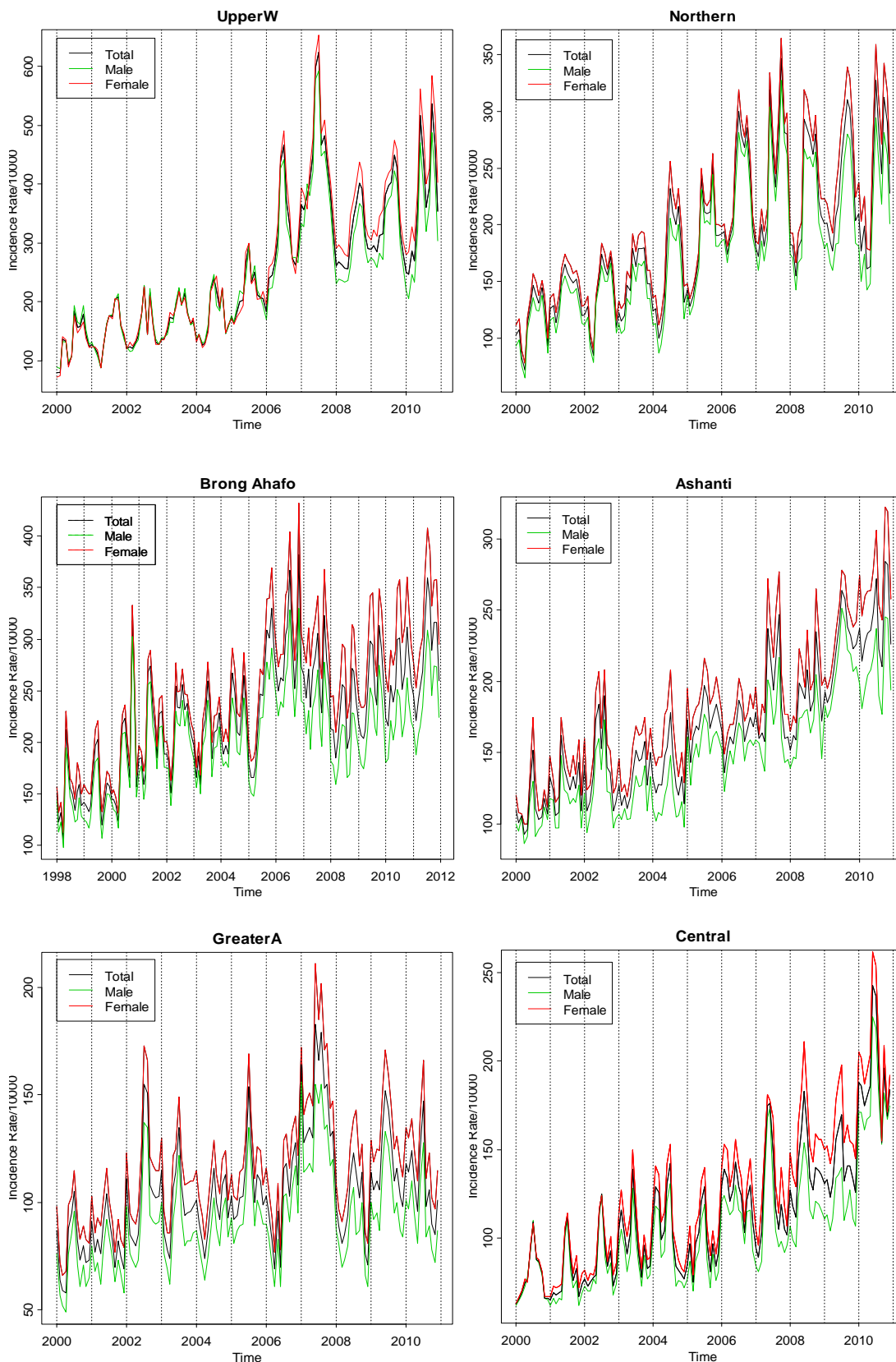


Figure 4.2.1: Time sequence plots of morbidity incidence rates of grand total (black), male (green) and female (red) cases observed in the selected regions: Upper West and Northern (top), Brong Ahafo and Ashanti (middle) and Greater Accra and Central (bottom).

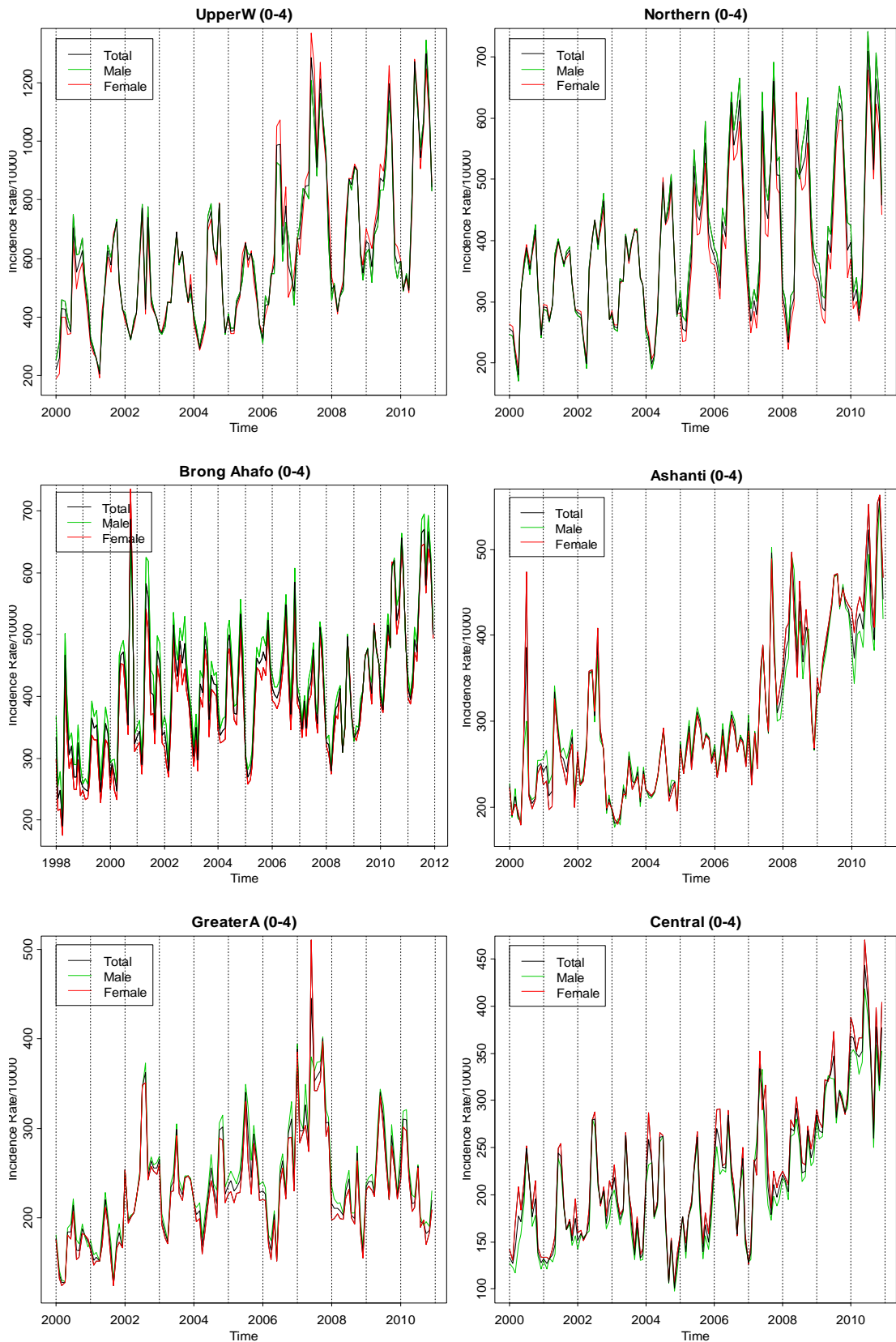


Figure 4.2.2: Time sequence plots of morbidity incidence rates of total (black), male (green) and female (red) cases observed for the 0-4 year age group in the selected regions: Upper West and Northern (top), Brong Ahafo and Ashanti (middle) and Greater Accra and Central (bottom).

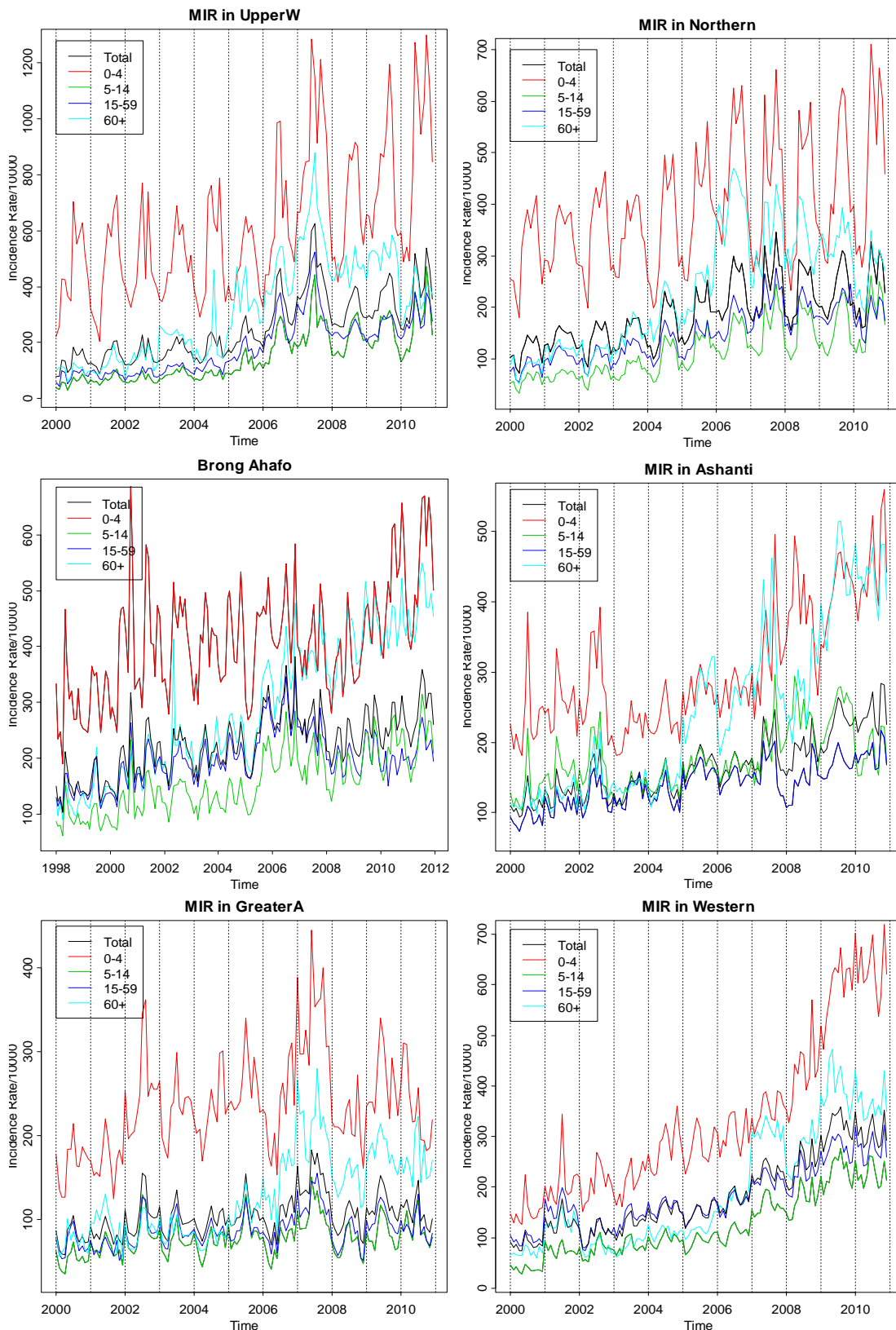


Figure 4.2.3: Time sequence plots of morbidity incidence rates of grand total (black) and age groupings observed for the regions, Upper East and Northern (top); Brong Ahafo and Ashanti (middle); Greater Accra and Western (bottom).

the forest zone. The incidence rates for aged people (60+ years) tend to rise steadily from 2006 or 2007 onwards (particularly in Ashanti, Brong Ahafo and Eastern to equal the incidence cases of children under 5 years old) except in the Upper East Region which consistently appeared to remain the same with the other year groupings throughout the entire study period (see Appendix A-2.2).

The three regions in the northern part of Ghana (Upper East, Upper West and Northern) have very pronounced variations and distinctive seasonal patterns whilst the other regions are observed to experience continuous linear or exponential growth. In particular, the incidence rates in the Greater Accra Region which have the least variation appeared to be mean stationary whereas Western Region increased its incidence of the disease exponentially. All the lowest incidence rates appeared to have occurred in Greater and Central regions whilst the extreme high cases were reported among Brong Ahafo and the two northern most regions (Figures 4.2.2 and 4.2.3) in the northern savannah zone.

4.2.3 Smoothing Analysis of MIR

The moving averages and Holt-Winter's method smoothing models (2.5.1) and (2.5.2) in chapter 2 (section 2.5) were applied to the monthly morbidity incidence rates data in the regions to reduce effects of irregularities and to study the trend and seasonal patterns in the incidence data; this enhances the estimation of quantities such as the standard errors of the mean for an improved future forecast (Cai, 2009; Shumway & Stoffer, 2011). The 12-point moving average smoothing method was applied to establish the long-term trend pattern whilst a 6-point smoothing is used particularly to identify seasonal cycles in the data and help ease prediction of the incidence as presented in section 4.5. The Holt-Winter's method complements the moving averages analysis by computing the trend model coefficients and also seasonal indices. In this section the total monthly incidence rates for the regions and also for the 0–4 year grouping are used instead of a separate study of the male, female and other age groupings incidence rates. This is because of the similarity in the behaviour exhibited by the time sequence plots and also, in all cases, the total monthly incidence rates are either equal or lie between the male and female incidence rates. In addition, they appear more representative of the other age groupings except for the aged whose morbidity incidence rates are observed to be higher, especially for the year 2006 and onwards.

The moving averages smoothing graphs for the total monthly morbidity incidence and 0-4 year group are displayed in Figures 4.2.4 and 4.2.5 (and Appendix A-3). Observation of the smoothing graphs for regional total incidence rates confirms the clear periodicity and generally indicate a steady linear or exponential increase in reports of the disease from onset of the study to the end of 2008 or 2009, after which it seems to be stabilising if not decreasing. In particular, the incidence in the regions in the northern savannah zone (Upper West and Northern) has a gradual growth before reaching its highest peak in 2007 after which it begins to level off. Brong Ahafo and Ashanti regions, in the forest zone, tend to exhibit almost similar behaviour. Critical analysis of both graphs shows an initial linear increase until 2002 after which the growth remains constant only to rise again from 2004 to attain their various peaks in 2006, 2007 and 2009. Each appears to begin to level off in incidence of the disease after 2010. Also noteworthy is Brong Ahafo's incidence reduction of the disease from approximately 300 per 10,000 residents in 2006 to 230 cases in 2008 and Ashanti's increase and decrease reports almost every two years after 2002. In Greater Accra, the only region completely within the coastal zone, the occurrence of the disease follows a trend pattern similar to that of the Brong Ahafo Region, beginning with a constant rate until 2002 at which point it rises sharply and fluctuates between 2003 and 2006 after which there is a sharp rise again to its highest peak in 2007, recording approximately 160 cases per 10,000 people. It then declines to 100 cases in 2008 and rises again in 2009 after which we observe a steady decrease in growth. A very peculiar trend pattern is observed in Western and Central regions which lie within the forest and coastal zones. The incidence trend graphs show a steady rise and fall until 2004 after which they begin to increase exponentially until 2009 and then decrease at the same growth rate after which they begin to level off or increase. The trend patterns of the vulnerable group (0-4 year olds) are similar to the respective regional total except in Ashanti and Brong Ahafo where the incidence rates in young children do not appear to stabilise after 2010.

The varied distributional patterns as in observed in the time sequence and smoothing plots of the morbidity incidence in the regions could be due to several factors including climatic conditions and interventions such as the introduction of the policies on the use of insecticide treated nets (ITNs) and anti-malarial drugs such as Artesunate+ Amodiaquine to treat uncomplicated cases and mass spraying of homes with

insecticides through indoor residual spraying (IRS) to kill the femal *Anopheles* mosquitoes, the main cause of the malaria in the country. The time series forecasting models of the morbidity incidence rates in section 4.5 can be used to assess whether the reduction of the count morbidity cases of the disease can be sustained to achieve the country's NMCP target of 75% reduction by 2015.

Applying the Holt-Winters' method with multiplicative seasonal indices (2.5.2) to the time sequence plots of the morbidity incidence rates results in the seasonal decomposition components, the smoothing parameters and the trend coefficients which establish the level and growth rate of the morbidity incidence of the disease in each region. The plots of seasonal factors (as shown in Figure 4.2.6) indicate that the highest seasonal values of the morbidity incidence of the disease occur during the months May to November and the lowest from December to April (see Figure 4.2.6 and Tables A-4.1 and A-4.2 in Appendix A-4). The high and low peaks incidentally coincide respectively with the wet and dry seasons in Ghana, an indication of climatic influences on the malaria morbidity incidence in the country. This potential study is further explored in the following two sections and in chapter 5.

The Holt-Winters' smoothing parameters and coefficients values are shown in Table 4.2.3. The trend coefficient (b) values are positive for all the regions except in Brong Ahafo which recorded among its young vulnerable age group a monthly slow growth rate of -0.145396, levelling off at a value (a) of 529 cases per 10,000 people. However, the morbidity incidence for the other 0-4 year olds showed higher growth. This negative trend value can be explained as a sign of decline in cases of the disease in the region. Upper East, Eastern, Western and Volta are the top four regions with the highest positive growth rates of approximately 5, but with the incidence in the Upper East levelling off at an extremely high incidence rate of 1,412 whilst the lowest trend coefficient (0.086684) is incidentally computed in the sister region (Upper West) and also stabilising at a very high value of 1,058. For the total incidence rates, the predicted incidence cases per month (3.053145) are highest in the Western Region with an incidence rate of 347 cases as its plateau value. It is then followed by Eastern (1.759470), Volta (1.701900), Ashanti (1.489656) and Upper West (1.350233) regions respectively. The slowest growth rate (0.220134) is observed as expected in BrongAhafo Region at a level of 277 cases whilst the smallest level value (113) occurs

in Greater Accra Region.

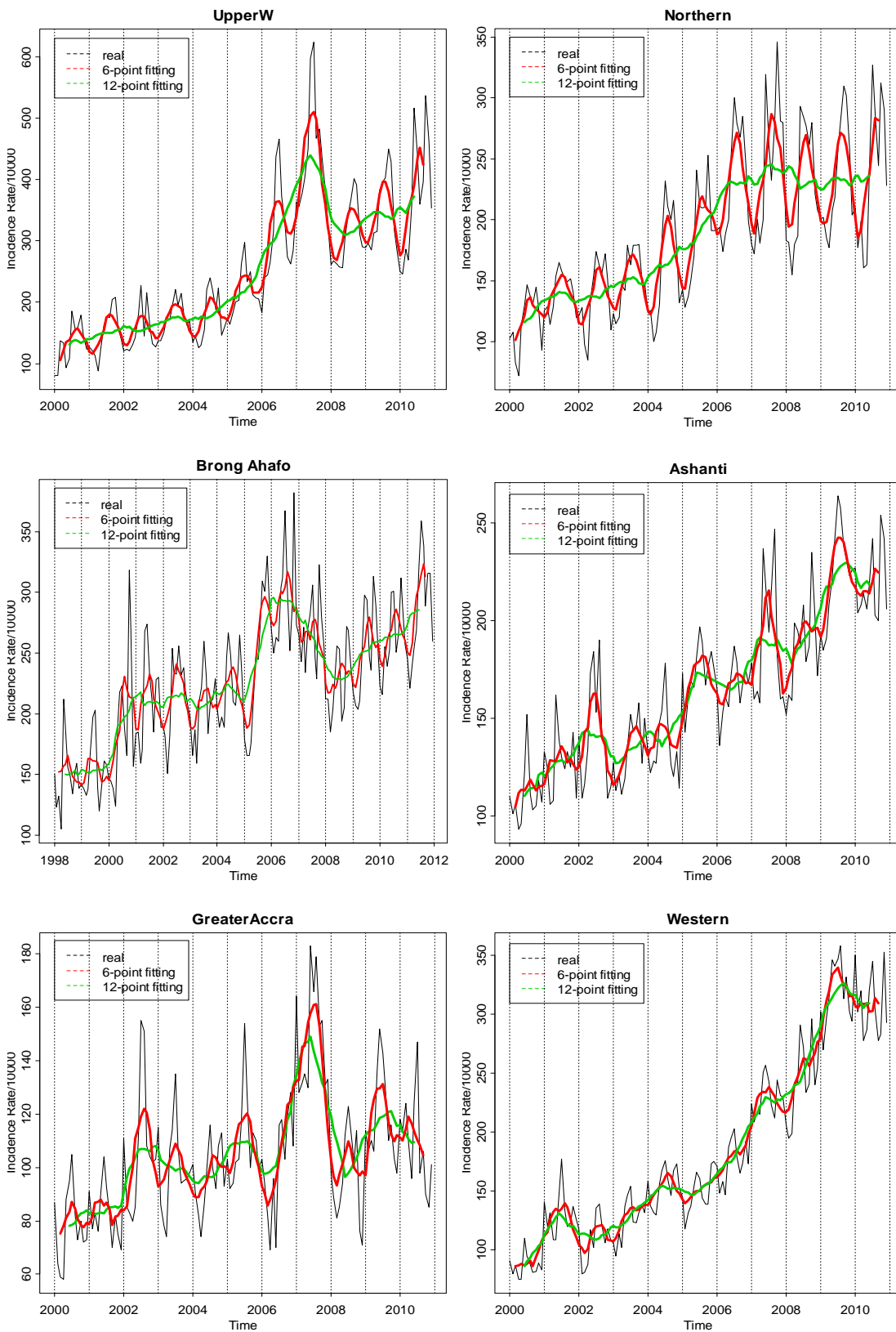


Figure 4.2.4: 6-point and 12-point moving average smoothing of morbidity incidence rates observed for the selected regions: Upper West and Northern (top), Brong Ahafo and Ashanti (middle) and Greater Accra and Western (bottom).

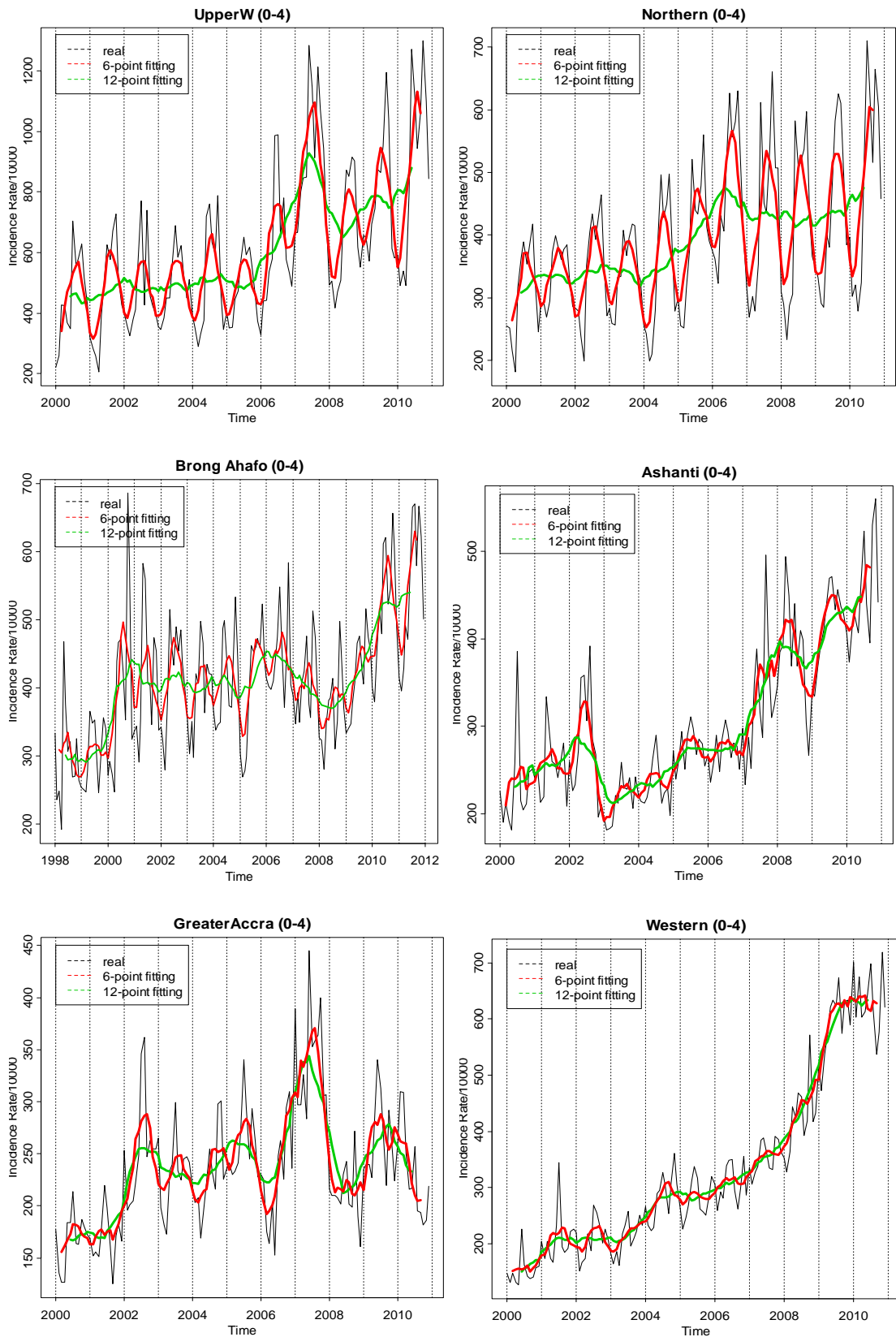


Figure 4.2.5: 6-point and 12-point moving average smoothing of morbidity incidence rates observed for the 0-4 year group of the selected regions: Upper West and Northern (top), Brong Ahafo and Ashanti (middle) and Greater Accra and Western (bottom).

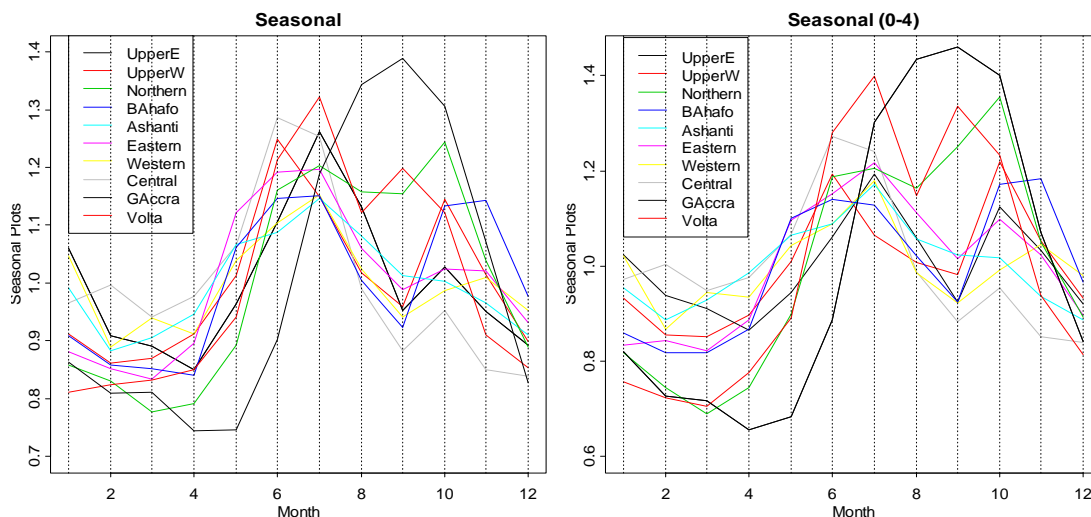


Figure 4.2.6: Seasonal plots derived from Holt-Winter's smoothing of the morbidity incidence rates by region for the total (left) and 0-4 year group (left).

Table 4.2.3: Holt-Winters' smoothing parameters and model coefficients of the morbidity incidence rates by region for the total and 0-4 year group.

Region	Smoothing Parameters			Coefficients	
	Level (α)	Trend (β)	Seasonal (γ)	Level (a)	Trend (b)
(Total)					
Upper West	0.780167	0.000000	1.000000	418.816830	1.350233
Upper East	0.422417	0.000000	0.763038	511.142600	0.499417
Northern	0.168405	0.018941	0.389516	258.024002	1.030066
Brong Ahafo	0.367290	0.000000	0.302486	277.259542	0.220134
Ashanti	0.305577	0.000000	0.425722	239.259304	1.489656
Eastern	0.592064	0.000000	0.475065	343.452058	1.759470
Western	0.505415	0.005414	0.502858	347.253695	3.053145
Central	0.301916	0.008191	0.351282	195.308619	0.708751
Greater Accra	0.660575	0.000000	0.054159	113.120164	0.367716
Volta	0.671337	0.015080	0.547838	307.899566	1.701900
(0-4)					
Upper West	0.332586	0.000000	0.375785	1058.40000	0.086684
Upper East	0.482853	0.010875	0.819571	1411.97588	5.055988
Northern	0.125381	0.000000	0.350017	510.588278	2.310752
Brong Ahafo	0.269060	0.000000	0.394607	529.055489	-0.145396
Ashanti	0.298493	0.000000	0.506730	529.346141	2.220280
Eastern	0.502391	0.007129	0.467830	643.387080	5.039534
Western	0.413002	0.000000	0.339531	680.561930	5.042395
Central	0.217506	0.009589	0.297025	202.942570	0.881647
Greater Accra	0.583546	0.000000	0.083731	212.442700	0.141317
Volta	0.615760	0.032473	0.445411	593.366400	5.092784

The smoothing parameters for seasonal (γ) and level (α) are higher in the northern savannah zone, where the Upper West and Upper East regions have seasonal components of 1 and 0.763038, respectively for the region as whole with corresponding level values of 0.780167 and 0.422417, respectively whilst the seasonal component in the Upper East Region is 0.819571 for the 0–4 age group with a level values of 0.482853. Greater Accra Region records the lowest seasonal smoothing parameters, 0.054159 for the total incidence rates and 0.083731 for the 0–4 year old children whilst the lowest respective level values, 0.168405 and 0.125381, are observed in the Northern Region. The presence of a long-term trend in the incidence data is evidenced by the non-zero β values which predominately occurred in the Central, Northern, Volta and Upper East regions. In particular, the incidence rates in Ashanti and Brong Ahafo regions do not exhibit long-term trend and appear to behave quite similarly in seasonal patterns and level of incidence. However, higher seasonal values are observed in Ashanti for both the total and 0-4 age groups (0.425722 and 0.506730), whilst Brong Ahafo Region records higher level value (0.367290) for its total incidence rates.

4.3 Exploratory Analysis of Space-time MIR Data

The analysis of the space-time (district-month) malaria morbidity incidence rates data, $\{I(\mathbf{u}_\alpha, t) : \alpha = 1, \dots, n; t = 1, \dots, T\}$ involving the 138 districts and 72–168 consecutive months observed at each district location is categorised into three main case studies, national, Brong Ahafo Region (BAR) and vegetation types, based on the morbidity count reports on all the 138 districts across the country, the 19 districts in BAR and the districts in each of the three epidemiologic zones (northern, forest and coastal), respectively. This has been designed for detailed investigation of the spatial dependence of the morbidity incidence at various local scales and to delimit areas of high risk of the disease. The spatial and temporal availability of the morbidity incidence rates $\{I(\mathbf{u}, t) : (\mathbf{u}, t) \in \mathbf{D} \times \mathbf{T}\}$ are regarded as a random process and characterised by the semivariograms presented in chapter 5, which are key elements for the prediction techniques employed in this thesis in that chapter. This section gives the preliminary analysis of the data to explore the spatio-temporal distribution of the malaria morbidity incidence data. Statistical packages used to perform the analyses

include ISATIS (Geovariances, 2013), used in geostatistics and R (R Development Core Team, 2011), an open source programming language for statistical analysis.

4.3.1 Descriptive of Summary of Space-time Data

The summary statistics for the various case studies of the space-time data sets are shown in Tables 4.3.1 and 4.3.2. Nationally, we observe a monthly morbidity incidence range of 42–1574 cases per 10,000 people with a mean of 241 cases and standard deviation of 141.95, which was reported per district whilst the regional case study in BAR recorded a higher mean incidence rates of 288 cases and a standard deviation of 165.68. In the vegetation zones, the northern savannah has the highest mean incidence rate (268 cases) and more variable, whilst the lowest occurred in the coastal savannah/mangrove (186 cases). It is also observed that the mean numbers of incidence cases in the northern and forest zones are greater than that for the national study data but less than what occurred in BAR whilst the mean incidence rates for the coastal zone is lower.

The summaries for each calendar month are also reported based on the national data set (see Table 4.3.2). The statistics indicate higher mean incidence rates between May and November, coinciding with the wettest months across the country and lower incidence rates occur between December and April during which there are two dry seasons in the north and south of Ghana. This suggests the possibility of a climatic effect which we seek to explore in section 4.4. The number of incidence cases reported within the wet season is relatively more variable than that in the other months, probably due to the greater number of incidence cases of the disease observed in the two northern-most regions and BAR during this season.

In all the case studies, the space-time data sets indicate highly positively skewed distributions (as depicted by the histograms in Figures 4.3.1 and 4.3.2) to which a logarithm transformation was applied to reduce variability in the data sets and also approximate to normality for further exploration of autocorrelation and predictions at the unsampled locations. These analyses are performed in sections 5.3 and 5.4 of chapter 5.

Table 4.3.1: Summary statistics for the sampled morbidity incidence rates at district-month locations at the study areas for 2000-2010/2011. Data set involving case study areas were on reported cases in all districts in Ghana, districts in Brong Ahafo Region and districts in each of the three vegetation zones, hereafter referred to as national, BAR and vegetation types (northern, forest and coastal), respectively.

Case Study	No. of Dist.	Min	Q1	Med	Mean	Q3	Max	StD	Skew	Kurt
National	138	42	141	204	241	298	1574	141.95	1.932	6.080
BAR	19	64	174	258	288	350	1275	165.68	1.790	4.480
Coastal	26	45	122	167	186	229	882	96.97	1.873	6.417
Forest	59	42	149	214	246	304	1275	135.66	1.830	5.408
Northern	34	50	143	129	268	342	1574	170.78	1.716	4.575

Table 4.3.2: Summary statistics for the seasonal malaria morbidity incidence rates observed at all district-month locations (national) for each calendar month during 2000-2010.

Month	Min	Q1	Med	Mean	Q3	Max	StD	Skew	Kurt
January	46	126	179	204	260	867	109.56	1.709	4.750
February	42	119	168	194	244	810	104.58	1.622	3.992
March	44	114	163	194	244	895	111.95	1.850	5.116
April	50	120	174	205	260	931	111.69	1.827	4.953
May	52	145	204	236	293	1030	127.79	1.722	4.767
June	50	164	242	276	345	1040	150.87	1.528	3.342
July	55	176	246	286	364	1160	159.98	1.685	4.133
August	57	159	224	264	320	1440	157.14	2.113	7.149
September	51	149	210	254	310	1570	157.38	2.209	8.405
October	52	160	233	277	344	1340	166.49	1.832	4.902
November	46	152	217	256	321	1100	148.65	1.728	4.397
December	45	137	199	227	287	998	127.19	1.771	4.972

4.3.2 Distribution of Space-time Data

The sampled locations as given in Figure 4.1.2 illustrate how the central parts of the country towards south are densely populated compared to the northern parts where they are sparsely inhabited. The space-time morbidity incidence rates for the case studies, namely national, Brong Ahafo Region and the vegetation types, are all found to be highly positively skewed. They have been log-transformed to reduce the effect of high values in the data sets and improve the normality assumption (see Table 4.3.1 and Figures 4.3.1 and 4.3.2) for structural analysis and space-time lognormal kriging to be implemented (Journel, 1980; Journel & Huijbregts, 1978; Lee & Ellis, 1997; Roth,

1998). The variogram maps for the monthly incidence rates (see Figure 4.3.3), calculated using 15 lags at a spacing of 30 km, 36 directions and tolerance of 4 sectors, showed no obvious evidence of anisotropy for short separation distances mostly less than 250 km.

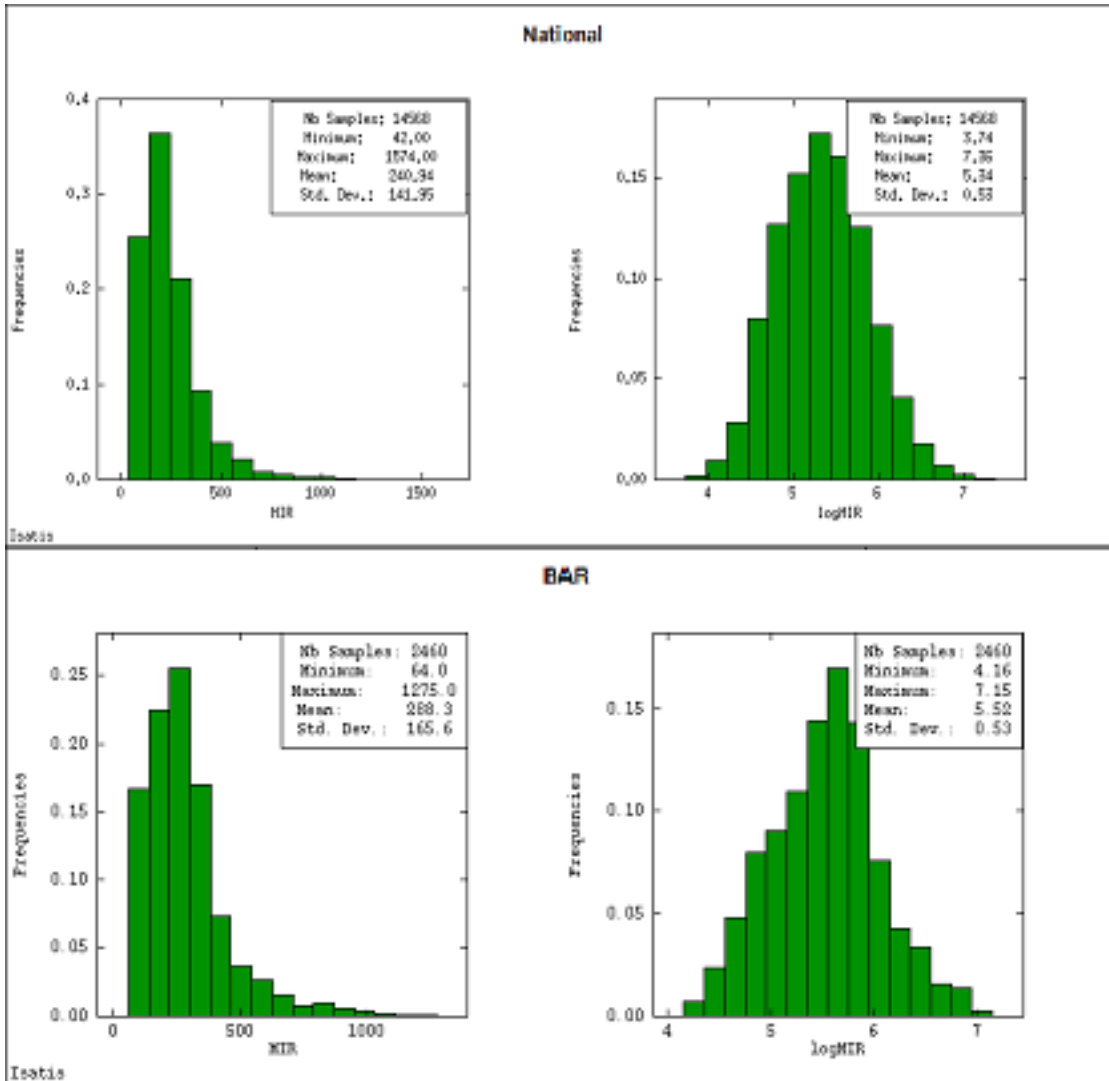


Figure 4.3.1: Histograms of the observed morbidity incidence rates (MIR) and logMIR for National (top) and Brong Ahafo Region (BAR) (bottom) data sets.

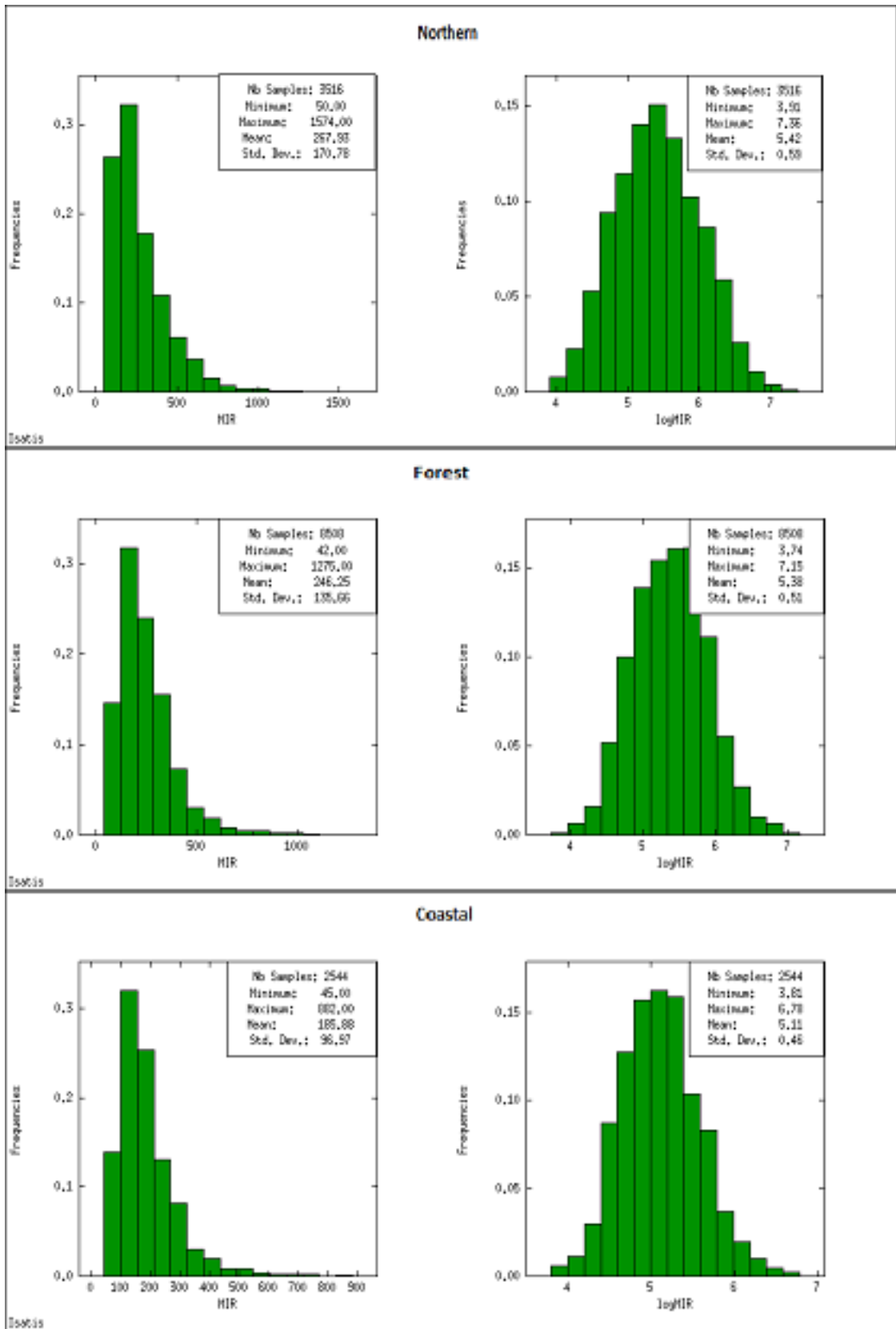


Figure 4.3.2: Histograms of the observed morbidity incidence rates (MIR) and logMIR for the three vegetation zones, northern (top), forest (middle) and coastal (bottom)

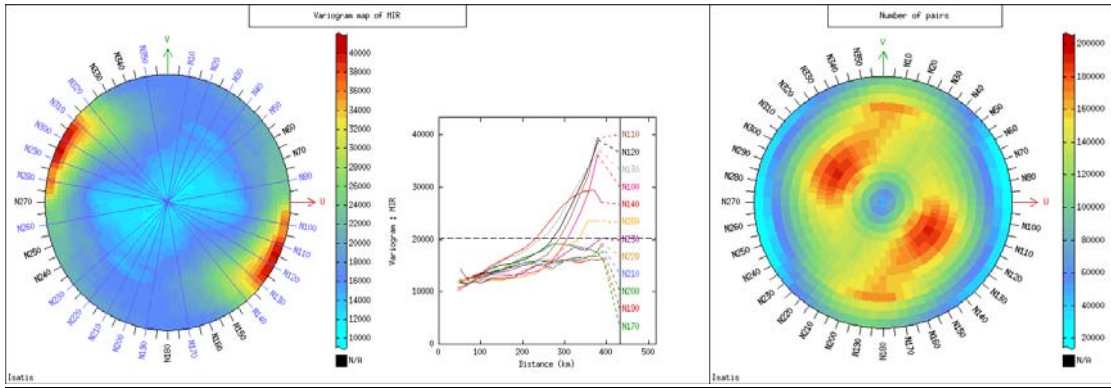


Figure 4.3.3: Variogram map (left) and number of pairs (right) of the observed morbidity incidence rates for the whole study area (national). In the middle is graph of variograms in various directions showing lack of anisotropy for short separation distances.

The temporal profiles of the morbidity incidence rates at some selected district locations (Figure 4.3.4) indicate varied patterns of the disease across the country. After an initial period of stability the districts in the northern savannah zone (for example, Bolgatanga and Tamale) showed continuous rise of morbidity incidence. However, the incidence rates at some locations in the two other zones (for example, Berekum, Obuasi, Accra, and Nzema East) are found to be increasing and/or decreasing. The temporal variability in the data is further studied by the analysis of the trend coefficients in section 5.2 of Chapter 5.

The post-plots of the observed space-time morbidity incidence rates at the various district locations in Ghana are shown in Appendix B-2 whilst Figures 4.3.5 and 4.3.6 present the incidence data observed in 2010 for all the districts and in BAR, respectively. High morbidity incidence rates are observed during months between May and November but tend to be lower from December to April. In addition, there appears to be evidence of spatial heterogeneity as high morbidity incidence values are observed mostly in the northern (northern savannah zone), western and central parts (forest zone) towards the south (coastal zone). Similar seasonal pattern can also be identified in the Brong Ahafo Region where the high risk locations are mostly found in the western parts of the region close to the border with La Cote d'Ivoire, a country with an equally high risk of the malaria disease (WHO, 2008). A critical inspection of the variogram map of the incidence data and its corresponding number of pairs in the spatial domain for the whole study areas show no strong evidence of anisotropy for short lag distances (see Figure 4.3.3). The variography of the morbidity incidence data sets $\{I(\mathbf{u}_\alpha, t); \alpha = 1, \dots, n; t = 1, \dots, T\}$ was performed by calculating and modelling the

semivariograms as isotropic spatially correlated processes. This modelling procedure is implemented in chapter 5, beginning from section 5.3.

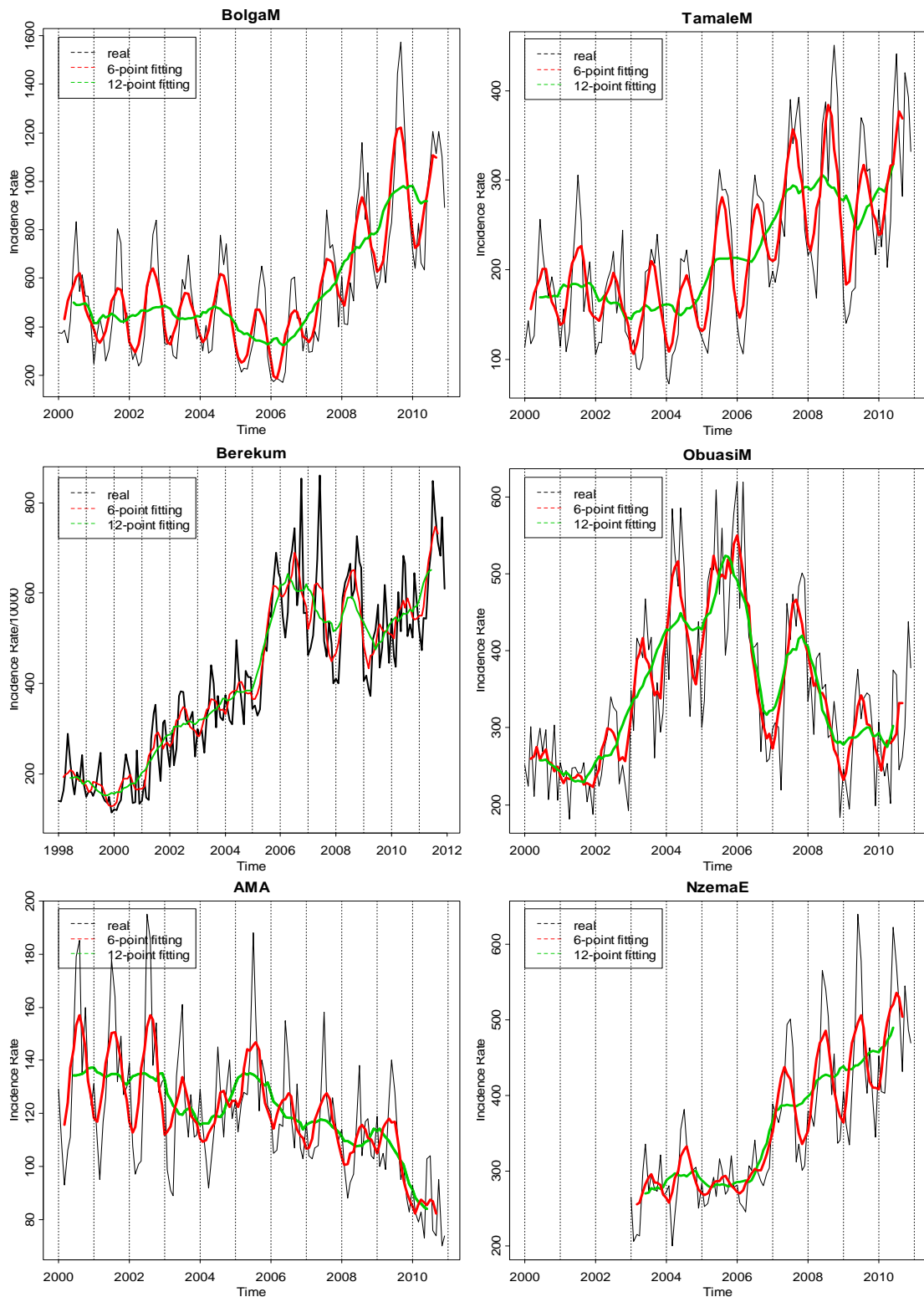


Figure 4.3.4: Temporal profiles of the malaria incidence rates superimposed with 6- and 12-point moving averages smoothing at some district locations selected across the study area, namely, BolgaM, TamaleM (northern); Berekum, ObuasiM (forest); Accra metropolitan area (AMA), NzemaE (coastal

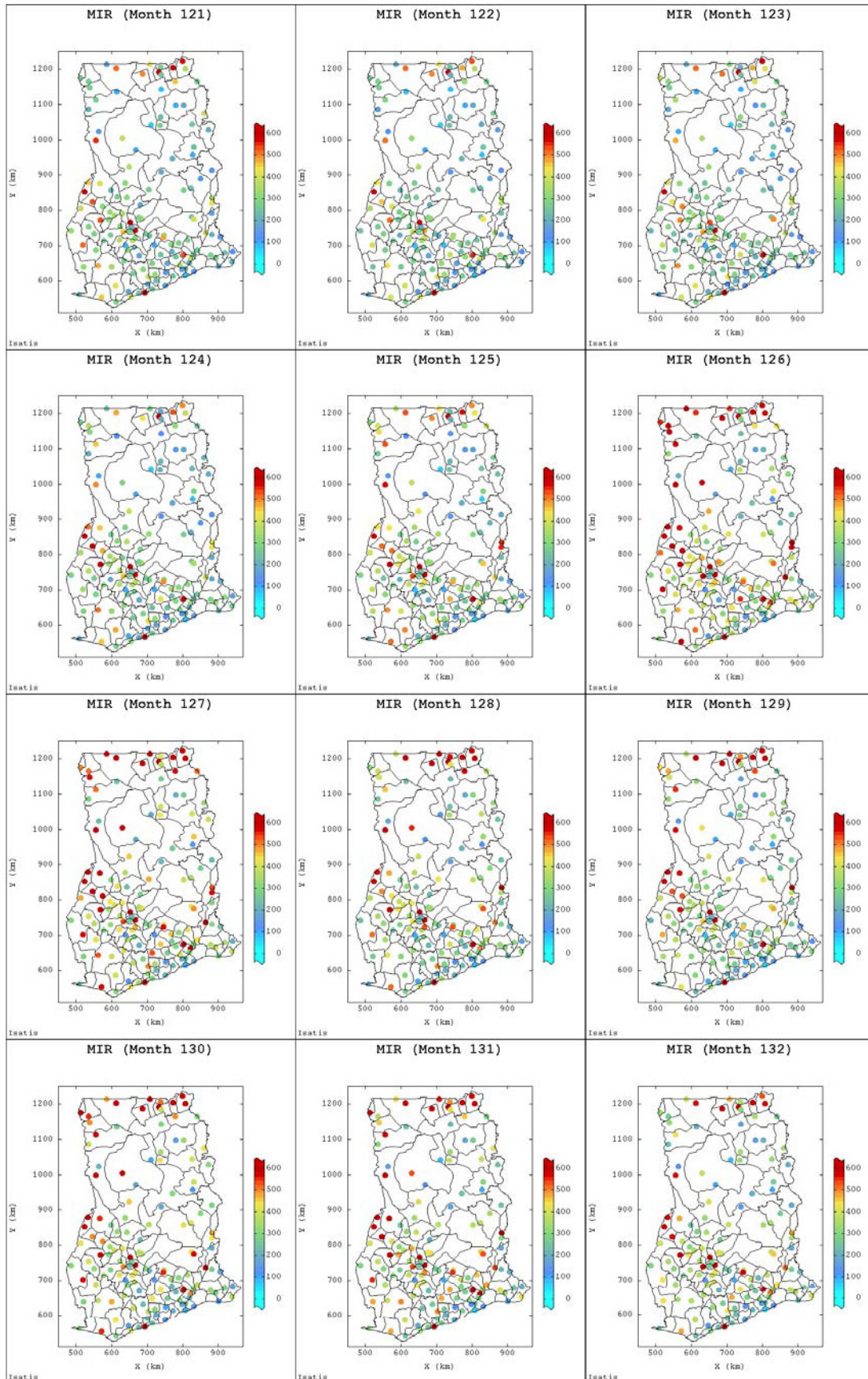


Figure 4.3.5: Post-plots of monthly morbidity incidence rates distribution observed nationally at the sampled district locations for the selected months in 2010 (where Months 121–132 correspond to January to December).

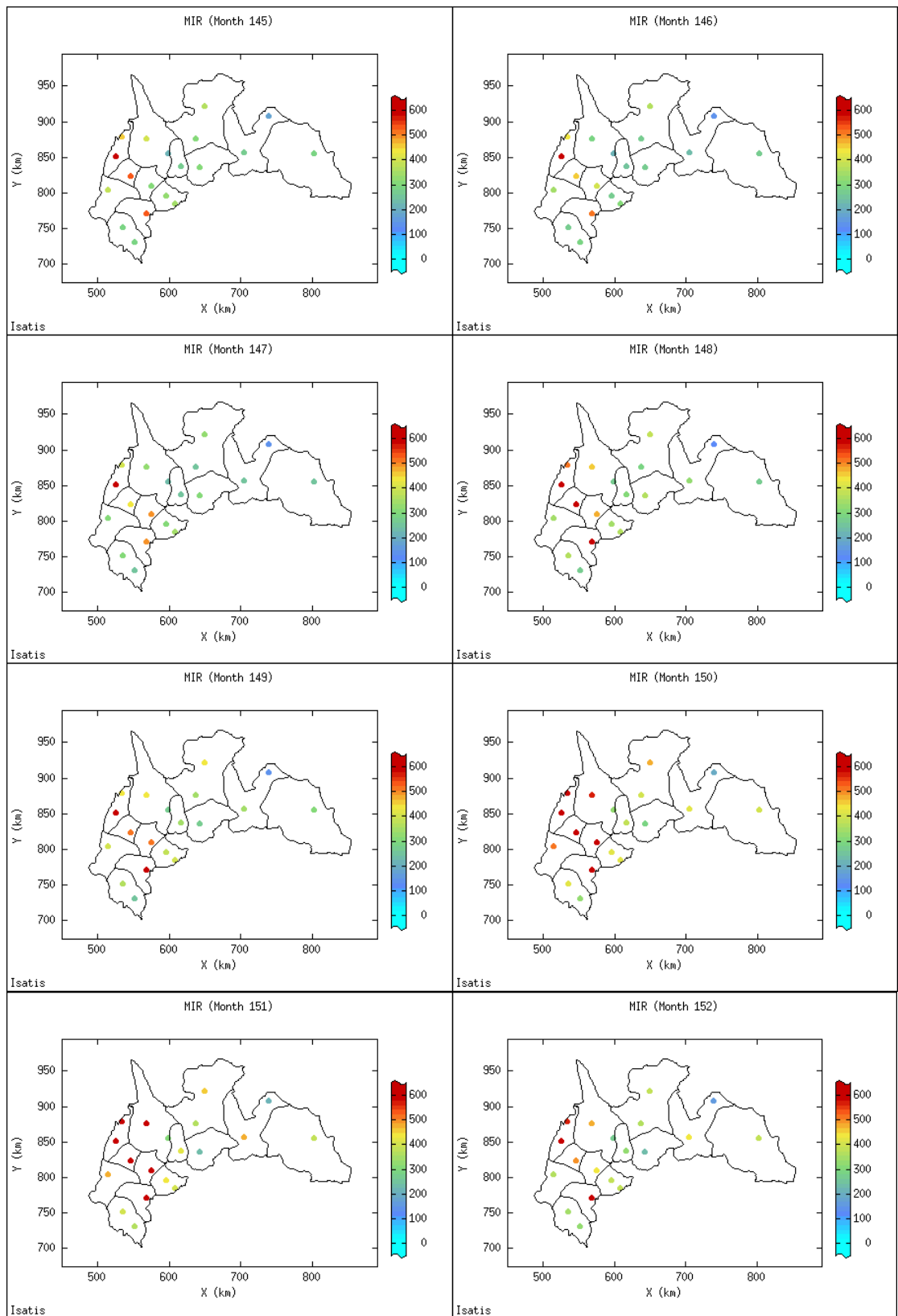


Figure 4.3.6a: Post-plots of monthly morbidity incidence rates distribution at the sampled locations in the Brong Ahafo Region for the selected months in 2010 (where Months 145–152 correspond to January to August).

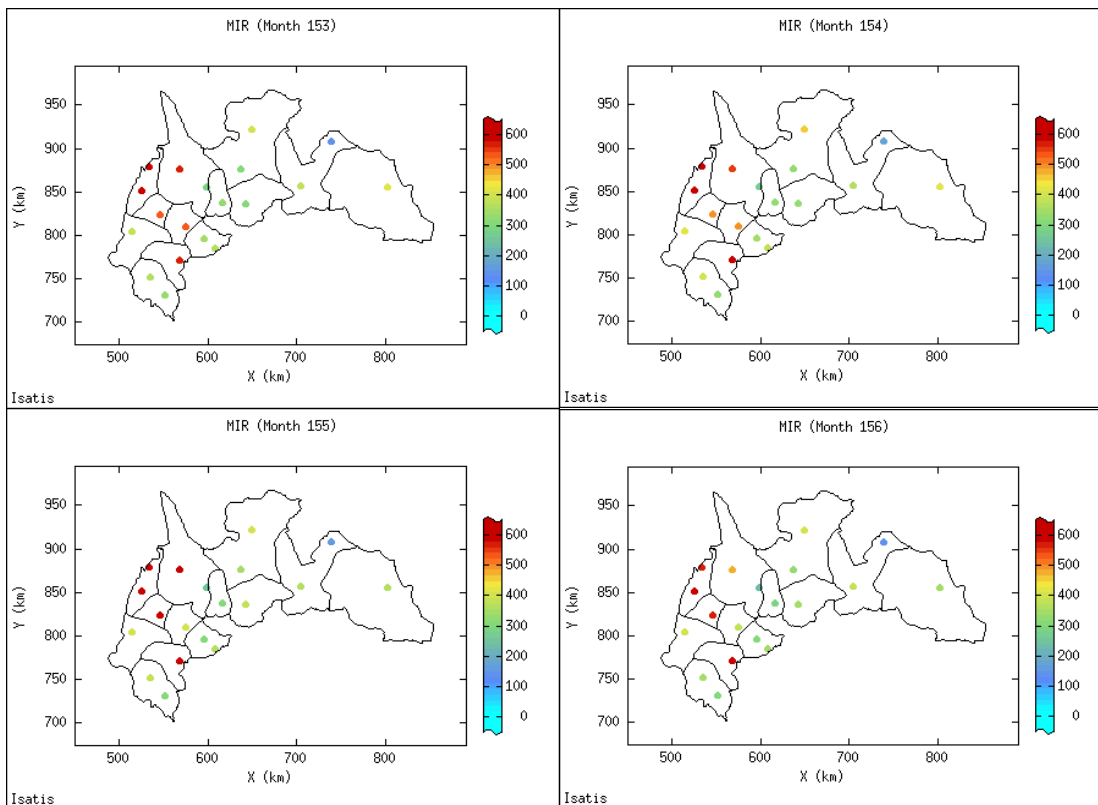


Figure 4.3.6b: Post-plots of monthly morbidity incidence rates distribution at the sampled locations in the Brong Ahafo Region for the selected months in 2010 (where Months 153–156 correspond to September to December).

4.3.3 Distribution of Climate Covariates

Climatic data on rainfall, temperature, relative humidity and number of sunshine hours could not be obtained from all the districts. The observed monthly data from the 77 district locations over the period 1998–2011 are summarised in Table 4.3.3. The climatic data are further illustrated graphically and provided in Figure 4.3.7.

Table 4.3.3: Summary statistics of the climatic covariates values obtained at the district-month locations over the whole study area in Ghana

Covariate	Count	Min	Max	Mean	Median	StDev	CV	Skewness
Rainfall	10164	0	762.8	100.1	84.5	85.273	0.860	1.093
MaxTemp	10164	17.6	41.1	32.0	31.8	2.742	0.086	0.297
MinTemp	10164	13.0	30.1	22.6	22.7	1.746	0.077	-0.621
RH0600	10164	22.0	99.0	89.2	94.0	12.713	0.143	-2.796
RH1500	10164	10.0	89.0	59.5	65.0	16.691	0.281	-1.027
Sunshrs	10164	1.10	10.1	6.40	6.60	1.572	0.246	-0.464

The distributions of these weather values typically depict the seasonal patterns in the country. The monthly rainfall and relative humidity values are more variable and

skewly distributed. Rainfall values averages 100.1 mm, ranging between 0 and 762.2 mm. Relative humidity at 0600 hours has an average of 89%, varying from 22 to 99% whilst the mean and range for the relative humidity at 1500 hours are 59% and 10-89%, respectively. Minimum and maximum temperatures average 22.6° C (13-30.1° C) and 32.0° C (17.1-41.1° C), respectively, whilst the number of sunshine hours is 6.4 (1.1-10.1).

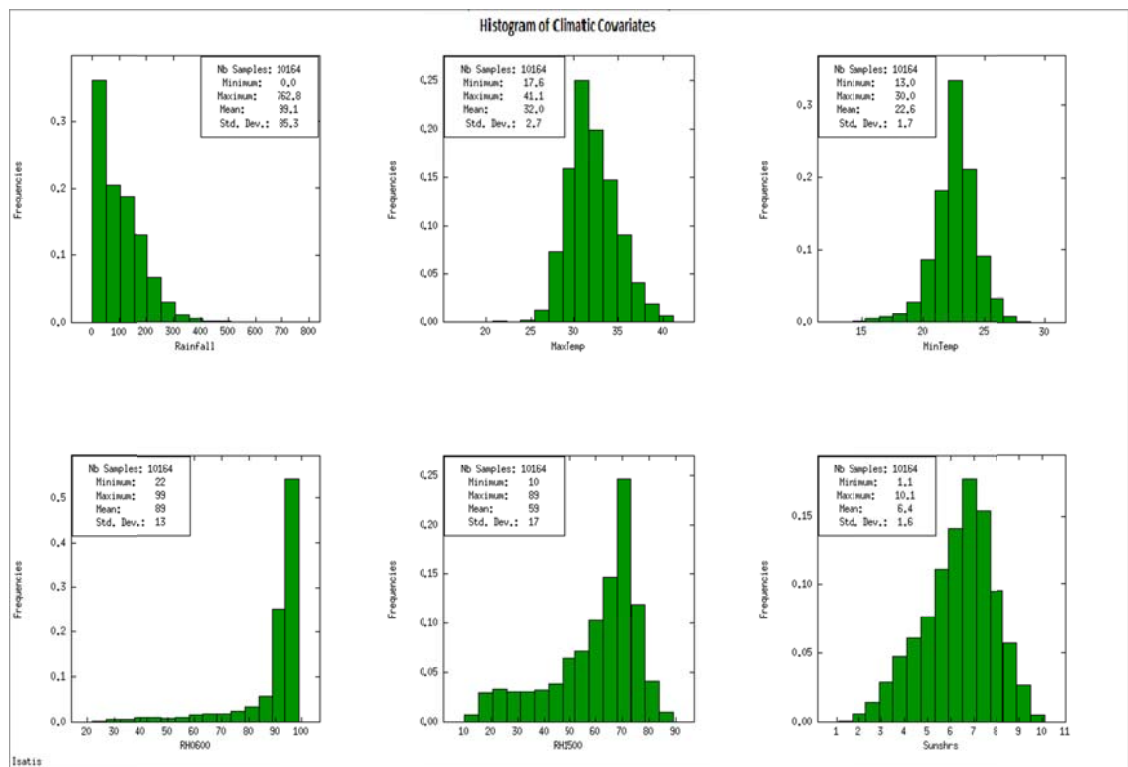


Figure 4.3.7: Histogram of the observed climatic covariates values at the district-month locations over whole study area in Ghana

4.4 Multiple Regression Analysis of the Data

The environmental impact on incidence of malaria provides important information for effective malaria control, focusing not only on the parasites directly, but also on the vector mosquitoes and their living conditions (Gemperli, 2003; Gemperli et al., 2006; Huang, Zhou, Zhang, et al., 2011), which eventually leads to the development of empirical methods for assessing the incidence of the disease (Militino, Dolores, & Ibáñez, 2008). In this section, correlation and regression analyses of the monthly malaria morbidity incidence rates with the covariates are conducted as a first step to establish the potential effect of climatic variability on the morbidity incidence rates as observed in the ten regions and also at the 138 district locations for the period 1998-2011 so as to learn more about the spatial and temporal similarities among regional

and district locations in Ghana. The multiple regression analysis uses the global (regional) incidence rates computed from the monthly reported count morbidity cases of the disease (via equation (4.2.1)) and the observed climatic covariates at each of the ten administrative regions. Cross-correlation analysis of the space-time data, comprising of the monthly total morbidity incidence rates and the observed climatic covariates and elevation data at the district locations is also performed.

4.4.1 Multiple Linear Regression Analysis of Regional Data

Classical multiple linear regression modelling is performed to examine and determine the potential risk factors of the morbidity incidence rates observed in the ten regions. For accurate quantification of the auto-correlations of the morbidity incidence rates and their cross-correlations with the climatic covariates, the upward temporal trends in the morbidity incidence data are eliminated by detrending (Horvatic, Stanley, & Podobnik, 2011). A quadratic function in time t in months (4.4.1), which proved to be more appropriate to account for the varied temporal incidence profiles in the regions (see graphs in sections 4.2.2 and 4.2.3), was chosen:

$$I_t(\mathbf{u}_\alpha) = b_0(\mathbf{u}_\alpha) + b_1(\mathbf{u}_\alpha)t + b_2(\mathbf{u}_\alpha)t^2 + R_t(\mathbf{u}_\alpha) \quad (4.4.1)$$

In this way, the resultant residuals $R_t(\mathbf{u}_\alpha)$ with periodic cycles are able to reveal the true correlations existing with the covariates, which equally exhibit strong seasonality patterns (Horvatic et al., 2011). This paves way for further analysis of the residuals to be considered in section 4.5.1. The detrended incidence data set $\{R_t(\mathbf{u}_\alpha); t = 1, \dots, T\}$ for each region α is cross-correlated with and regressed on the climatic covariates $X_{t,1}(\mathbf{u}_\alpha), \dots, X_{t,6}(\mathbf{u}_\alpha)$, being the data on rainfall, maximum and minimum temperatures, relative humidity at 0600 and 1500 hours and number of sunshine hours, respectively in the month t together with their data in $t-1$ and $t-2$ incidence months (lag $p = 1$ and 2), as predictor variables for each of the $T = 132$ months, beginning from January 2000 to December 2011 except for the BAR which has time sequence data of 168 months starting from January 1998:

$$R_t(\mathbf{u}_\alpha) = X_t^T(\mathbf{u}_\alpha)\beta_\alpha + \varepsilon_t(\mathbf{u}_\alpha), \text{ for each } \alpha = 1, \dots, 10, \quad (4.4.2)$$

where $\mathbf{X}_t^T(\mathbf{u}_\alpha) = [X_{t-p,1}(\mathbf{u}_\alpha), \dots, X_{t-p,6}(\mathbf{u}_\alpha)]$, for $p = 0, 1, 2$ and each $t = 1, 2, \dots, 132$ or 168 is a vector of covariates with components at incidence time lags p ; $\beta_\alpha = [\beta_{\alpha 0}, \beta_{\alpha -p,1}, \dots, \beta_{\alpha -p,6}]^T$ is the vector of regression coefficients; and $\varepsilon_t(\mathbf{u}_\alpha)$, a

vector of residuals of the unobservable random errors with the components $\varepsilon_t(\mathbf{u}_\alpha) \sim N(0, \sigma_\alpha^2)$ as white noise.

The backward stepwise elimination method, an automated iterative regression process based on the ordinary least squares (OLS) method (3.4.4), is employed to sequentially select the potential predictors of morbidity risk in the model (4.4.2) for each region. This iterative process first considers all the predictor variables, and was preferred to forward regression which adds variables progressively and might result in rendering some already included variable(s) non-significant (Draper & Smith, 1981; Lindsey & Sheather, 2010). Interaction terms were ignored so as not to compound the multicollinearity problem between the potential predictors (Jaccard, Wan, & Turrisi, 1990) (further readings on issues of interaction effects can be found in Aiken and West (1991) and Morris, Sherman, and Mansfield (1986)). The OLS method minimising the sum of squares of the residuals, $R_t^T(\mathbf{u}_\alpha)R(\mathbf{u}_\alpha)$, results in the estimation of the regression coefficients:

$$\hat{\beta}_\alpha = [X_t^T(\mathbf{u}_\alpha)X_t(\mathbf{u}_\alpha)]^{-1} X_t^T(\mathbf{u}_\alpha)R_t(\mathbf{u}_\alpha) \quad (4.4.3)$$

with components: $\hat{\beta}_{\alpha_0}$ as the intercepts and $\hat{\beta}_{t-i,1}, \dots, \hat{\beta}_{t-i,k}$, indicating the contributions of the morbidity risk by each of the k selected predictors for its unit change. Detailed results of the multiple regression model in (4.4.2) based on a selection criterion of p -value < 0.05 , prescribed in the R function code for the computations, for all the ten regions are as displayed by Results A-5.2 and A-5.3 in Appendix A-5. Tables 4.4.1 and 4.4.2 show the cross-correlations of the incidence rates and their residuals with the atmospheric covariates in the month t including the previous month ($t-1$) recorded data (lag 1 month) whilst Tables 4.4.3 and 4.4.4 produce the estimated output of model (4.4.3) using the detrended incidence rates data with the same covariates at lags 0 and 1 for some selected regions.

The cross-correlation analysis indicates varied but significant influence of the climatic covariates on the incidence rates (with the p -values mostly being less than 0.01). The detrended incidence data correlate more strongly with the covariates than the actual incidence rates and correlations are also higher when the climatic variables are lagged by 1 or 2 month(s), with the former appearing to be stronger. Generally, morbidity incidence in the regions correlates positively with monthly rainfall and relative humidity (at both 0600 and 1500 hours) and negatively with (maximum and minimum)

Table 4.4.1a: Cross-correlation analysis results of morbidity incidence rates (total) and their residuals with climatic covariates in the month of incidence.

Region	Data (Total)	Rainfall	MaxT	MinT	RH0600	RH1500	Sunshrs
Upper	MIR	0.37517	-0.41299	-0.33456	0.40830	0.41626	-0.28713
East	Residuals	0.51698	-0.68095	-0.22902	0.60715	0.62679	-0.44292
Upper	MIR	0.29325	-0.29108	-0.00606	0.32827	0.32870	-0.23930
West	Residuals	0.40126	-0.47068	-0.05591	0.48821	0.52229	-0.37294
	MIR	0.36101	-0.48360	-0.08874	0.42511	0.45753	0.27157
Northern	Residuals	0.45752	-0.65031	-0.21757	0.50955	0.52660	-0.2049
Brong	MIR	0.15688	-0.25353	-0.09649	0.23809	0.40653	-0.05015
Ahafo	Residuals	0.15053	-0.42017	-0.07398	0.31553	0.40983	-0.14929
	MIR	0.14858	-0.18715	-0.23007	0.08023	0.25167	-0.22743
Ashanti	Residuals	0.23776	-0.44149	-0.07784	0.21189	0.40956	-0.39887
	MIR	0.22215	-0.32198	0.11401	0.04429	0.28893	-0.19682
Eastern	Residuals	0.29221	-0.46909	-0.20356	0.25504	0.47270	-0.31009
	MIR	0.15543	-0.09984	0.02935	0.24307	0.14636	-0.09859
Western	Residuals	0.24507	-0.24988	-0.10537	0.19628	0.22637	-0.22165
	MIR	0.21676	-0.13425	0.22943	0.12558	0.24541	-0.02805
Central	Residuals	0.38345	-0.27906	0.10467	0.12685	0.34065	-0.24029
Greater	MIR	0.15809	-0.40176	-0.25700	0.02224	0.28055	-0.33633
Accra	Residuals	0.13479	-0.45900	-0.40380	-0.0918	0.28419	-0.37415
	MIR	0.20809	-0.32084	-0.00028	0.20879	0.42504	-0.16029
Volta	Residuals	0.47196	-0.58961	-0.18044	0.35642	0.56342	-0.33388

Table 4.4.1b: Cross-correlation analysis results of the total morbidity incidence rates and their residuals with climatic covariates in the month incidence prior to (lag 1).

Region	Data (Total)	Rainf_1	MaxT_1	MinT_1	RH06_1	RH15_1	Sunsh_1
Upper	MIR	0.51606	-0.49244	-0.22680	0.47298	0.52387	-0.39751
East	Residuals	0.72212	-0.79891	-0.07478	0.69590	0.78774	-0.59413
Upper	MIR	0.33739	-0.23875	0.11896	0.30810	0.31513	-0.25485
West	Residuals	0.45157	-0.37505	0.09673	0.43166	0.47889	-0.37607
	MIR	0.48570	-0.52721	0.08041	0.48248	0.55299	0.20777
Northern	Residuals	0.62385	-0.70276	0.01941	0.58662	0.66410	-0.28291
Brong	MIR	0.45313	-0.21375	0.03172	0.32966	0.48800	-0.05323
Ahafo	Residuals	0.55671	-0.35952	0.09767	0.44066	0.52513	-0.15010
	MIR	0.23463	-0.12400	-0.13836	0.12290	0.24697	-0.15814
Ashanti	Residuals	0.36898	-0.30664	-0.10452	0.28899	0.39366	-0.23722
	MIR	0.34222	-0.23523	0.22164	0.02103	0.28450	-0.15642
Eastern	Residuals	0.50095	-0.29716	0.00354	0.22781	0.46041	-0.21592
	MIR	0.21585	-0.03846	0.11174	0.27824	0.14384	-0.04284
Western	Residuals	0.41807	-0.03782	0.17156	0.29435	0.19618	-0.01222
	MIR	0.23317	0.04402	0.37522	0.10921	0.13675	0.13927
Central	Residuals	0.37440	0.05255	0.34972	0.10107	0.13518	0.07852
Greater	MIR	0.42891	-0.25737	-0.07888	0.15450	0.33715	-0.16853
Accra	Residuals	0.44835	-0.29100	0.19286	0.24283	0.35052	-0.17769
	MIR	0.29835	-0.23516	0.15384	0.18383	0.42778	-0.12820
Volta	Residuals	0.58054	-0.39501	0.10841	0.32747	0.53287	-0.21328

Table 4.4.2a: Cross-correlation analysis results of morbidity incidence rates for 0-4 year group and their residuals with climatic covariates in the month of incidence.

Region	Data (0-4)	Rainfall	MaxT	MinT	RH0600	RH1500	Sunshrs
Upper East	MIR	0.44853	-0.57040	-0.35826	0.53177	0.53625	-0.35787
	Residuals	0.48942	-0.68752	-0.26809	0.60782	0.61674	-0.41648
Upper West	MIR	0.44248	-0.50628	-0.08284	0.52973	0.53802	-0.37002
	Residuals	0.51795	-0.64743	-0.14107	0.64859	0.67758	-0.46419
Northern	MIR	0.49203	-0.65342	-0.15825	0.56514	0.59426	0.04485
	Residuals	0.51733	-0.70702	-0.22318	0.58344	0.59550	-0.25563
Brong Ahafo	MIR	0.22586	-0.34475	-0.10461	0.34493	0.52909	-0.11305
	Residuals	0.22407	-0.44395	-0.02470	0.39123	0.49593	-0.15184
Ashanti	MIR	0.18244	-0.15050	-0.15556	0.09606	0.26158	-0.19386
	Residuals	0.31245	-0.37249	-0.04866	0.18681	0.40668	-0.31949
Eastern	MIR	0.28202	-0.41649	-0.00500	0.20552	0.41118	-0.26115
	Residuals	0.31179	-0.49940	-0.21685	0.34313	0.51118	-0.32242
Western	MIR	0.15246	-0.08379	0.05382	0.25694	0.15420	-0.06976
	Residuals	0.24389	-0.20443	0.01882	0.24107	0.23527	-0.14161
Central	MIR	0.20810	-0.11843	0.24373	0.13012	0.23591	-0.01763
	Residuals	0.36230	-0.23500	0.14130	0.12880	0.31148	-0.24004
Greater Accra	MIR	0.10116	-0.23175	-0.12674	-0.0078	0.18473	-0.16534
	Residuals	0.07489	-0.27326	-0.24433	0.06614	0.18837	-0.17850
Volta	MIR	0.14527	-0.25426	-0.01523	0.21132	0.35776	-0.08600
	Residuals	0.33423	-0.43242	-0.19647	0.32049	0.42699	-0.17210

Table 4.4.2b: Cross-correlation analysis results of morbidity incidence rates for 0-4 year group and their residuals with climatic covariates in the month incidence prior to (lag 1).

Region	Data (0-4)	Rainf_1	MaxT_1	MinT_1	RH06_1	RH15_1	Sunsh_1
Upper East	MIR	0.64298	-0.65607	-0.19395	0.62833	0.67833	-0.48869
	Residuals	0.70797	-0.78181	-0.08187	0.71278	0.77732	-0.55706
Upper West	MIR	0.54980	-0.45458	0.11903	0.52971	0.55615	-0.45486
	Residuals	0.63745	-0.57207	0.00932	0.62889	0.68318	-0.55459
Northern	MIR	0.67370	-0.71520	0.10190	0.65140	0.73620	-0.07270
	Residuals	0.71216	-0.76944	0.06404	0.67600	0.75344	-0.37972
Brong Ahafo	MIR	0.56859	-0.29668	0.04198	0.44211	0.61177	-0.16370
	Residuals	0.61522	-0.38489	0.13972	0.50234	0.59318	-0.20817
Ashanti	MIR	0.23557	-0.08441	-0.09651	0.11827	0.23179	-0.14389
	Residuals	0.37145	-0.23864	0.07382	0.22454	0.34642	-0.19768
Eastern	MIR	0.45085	-0.32846	0.11820	0.17518	0.41430	-0.25700
	Residuals	0.51628	-0.37277	-0.05498	0.31131	0.50630	-0.30144
Western	MIR	0.21232	-0.03190	0.13496	0.27611	0.15196	-0.03410
	Residuals	0.41678	-0.01182	0.25837	0.29382	0.20252	0.01660
Central	MIR	0.22015	0.07147	0.38985	0.10159	0.11443	0.15602
	Residuals	0.34830	0.08700	0.36450	0.08610	0.10128	0.10170
Greater Accra	MIR	0.29865	-0.17830	-0.06057	0.10991	0.24573	-0.08446
	Residuals	0.31234	-0.21064	-0.16161	0.20447	0.26321	-0.08434
Volta	MIR	0.26552	-0.23710	0.11709	0.20734	0.39508	-0.13720
	Residuals	0.48688	0.37613	0.00667	0.33264	0.45897	0.20800

temperatures and number of sunshine hours (see Table 4.4.1 and 4.4.2). However, the morbidity incidence in Central Region exhibit direct linear relationships with minimum temperature and sunshine hours. Relatively, the correlations appear stronger in the three regions forming the northern zone (Upper East, Upper West and Northern) and weaker in Ashanti, Central and Western regions, although, statistically there are some significant relationships with the rainfall, minimum temperature and relative humidity at 1500 hours (p -values ≤ 0.05). The incidence rates among the young children correlate more highly with rainfall, temperature and relative humidity in the northern zone and Brong Ahafo Region, than in the other regions except Greater Accra Region.

Rainfall, temperature and relative humidity are highly correlated, as observed from Results A-5.1. However, relative humidity (at 1500 hours) exhibits stronger correlations with rainfall and maximum temperature, ranging mostly between -0.4 and -0.9. This is evidence of multicollinearity which affects the choice of the predictors and estimates of regression coefficients retained in the predictive model, though it does not reduce the predictive power or reliability of the model as a whole (Chatterjee & Hadi, 2006; Draper & Smith, 1981; Farrar & Glauber, 1967). The variations of the incidence rates from the model fitting of (4.4.2) are highly explained in the northern-zone regions and Brong Ahafo Region, the observed coefficient of determination (\hat{R}^2) values, ranging from 0.3052 to 0.720 (see Results A-5.2 and A-5.3 in Appendix A-5). Thus, the retained covariates can be very useful for predicting malaria risk in these regions, but differ between the total incidence rates and those of the 0-4 year group, unlike in the other regions which appeared to be modelled by same set of predictors. The morbidity incidence variations in the other regions, especially in Ashanti and Western, are poorly explained by the potential covariates. Rainfall and maximum temperature and relative humidity (at 15 hours) lagged by one month significantly relate with the morbidity incidence rates in most of the regions (p -value < 0.005). In particular, the incidence for regions in the coastal and forest zones (e.g. Greater Accra and Western) can be significantly (p -value < 0.005) predicted by only rainfall in the previous month whilst that for regions in the northern zone is strongly impacted by maximum temperature and/or relative humidity in the previous month (see Tables 4.4.3 and 4.4.4). However, rainfall which correlates positively (0.21232–0.72212) with the residuals across the country, proves to have no significant effect in the northern

Table 4.4.3: Multiple regression analysis results for the detrended morbidity incidence rates (total) with climatic covariates at lags 0 and 1 in the regions, neglecting interaction terms not to compound problem of multicollinearity among the covariates (Jaccard, et al., 1990). All predictor variables are retained at p -value < 0.05 .

Upper West Region (Total)				
Covariate	β -estimate	std error	t -statistic	p -value
Intercept	7.324	67.056	0.11	0.913
Rainfall	-0.226	0.130	-1.73	0.086
MinTemp_1	-5.166	3.027	-1.71	0.090
RH1500	3.062	0.601	5.09	1.2e-06
$SSE = 61.5$; $\hat{R}^2 = 0.305$ (0.289); $AIC = 1083$				
Northern Region (Total)				
Covariate	β -estimate	std error	t -statistic	p -value
Intercept	391.96	32.91	11.91	<2.0e-16
MaxTemp	-7.530	2.45	-3.07	0.00260
MaxTemp_1	-10.87	2.26	-4.80	4.4e-06
Sunshrs	3.950	1.84	2.14	0.0340
$SSE = 28.5$; $\hat{R}^2 = 0.532$ (0.521); $AIC = 882$				
Brong Ahafo Region (Total)				
Covariate	β -estimate	std error	t -statistic	p -value
Intercept	-111.92	87.108	-1.28	0.20072
Rainfall_1	0.1599	0.0457	3.50	0.00061
MaxTemp_1	-5.9272	2.4328	-2.44	0.01593
MinTemp	7.0121	3.2191	2.18	0.03084
RH1500_1	1.0199	0.3177	3.21	0.00160
Sunshrs	10.7022	3.0118	3.55	0.00050
$SSE = 31.2$; $\hat{R}^2 = 0.408$ (0.390); $AIC = 1155$				
Ashanti Region (Total)				
Covariate	β -estimate	std error	t -statistic	p -value
Intercept	-39.401	34.155	-1.15	0.2508
Rainfall_1	0.0799	0.0215	3.72	0.0003
MinTemp_1	3.1338	1.6874	1.86	0.0656
Sunshrs	-6.0406	1.2990	-4.65	8.2e-06
$SSE = 32.2$; $\hat{R}^2 = 0.367$ (0.341); $AIC = 915.4$				
Greater Accra Region (Total)				
Covariate	β -estimate	std error	t -statistic	p -value
Intercept	97.175	35.699	2.72	0.00740
Rainfall_1	0.0984	0.0247	3.98	0.00011
MaxTemp	-2.6224	1.2973	-2.02	0.04534
Sunshrs	-3.3279	1.5660	-2.13	0.03551
$SSE = 17.9$; $\hat{R}^2 = 0.315$ (0.298); $AIC = 759.2$				
Western Region (Total)				
Covariate	β -estimate	std error	t -statistic	p -value
Intercept	-357.785	252.624	-1.42	0.1592
Rainfall_1	0.07960	0.0286	2.78	0.0062
MaxTemp	-10.8348	4.7431	-2.28	0.0241
MaxTemp_1	5.53440	2.5887	2.14	0.0345
RH0600_1	4.96860	2.0702	2.40	0.0179
RH0600	-1.7423	0.9070	-1.92	0.0570
$SSE = 22.8$; $\hat{R}^2 = 0.243$ (0.206); $AIC = 826$				

Table 4.4.4: Multiple regression analysis results for the detrended morbidity incidence rates (0-4) with climatic covariates at lags 0 and 1 in the regions, neglecting interaction terms not to compound problem of multicollinearity among the covariates (Jaccard, et al., 1990). All predictor variables are retained at p -value < 0.05.

Upper West Region (0-4)				
Covariate	β -estimate	std error	t -statistic	p -value
Intercept	159.930	140.077	1.14	0.25571
Rainfall	-0.795	0.280	-2.84	0.00531
MinTemp_1	-22.717	5.958	-3.81	0.00021
RH1500	10.125	1.268	7.98	7.3e-13
$SSE = 132;$ $\hat{R}^2 = 0.539 (0.528);$ $AIC = 1284$				
Northern Region (0-4)				
Covariate	β -estimate	std error	t -statistic	p -value
Intercept	654.98	117.99	5.55	1.6e-07
MaxTemp_1	-30.18	5.06	-5.96	2.3e-08
MinTemp	-11.63	6.35	-1.83	0.06954
RH0600	3.520	1.04	3.40	0.00091
$SSE = 63.8;$ $\hat{R}^2 = 0.627 (0.618);$ $AIC = 1093$				
Brong Ahafo Region (0-4)				
Covariate	β -estimate	std error	t -statistic	p -value
Intercept	-526.868	170.619	-3.09	0.00238
Rainfall_1	0.3746	0.0923	4.06	7.7e-05
MaxTemp_1	-8.5882	4.7825	-1.80	0.07442
MinTemp	27.1362	6.9540	3.90	0.00014
RH1500_1	3.3678	0.6829	4.93	2.0e-06
Sunshrs_1	15.0853	6.1011	2.47	0.01446
$SSE = 61.1;$ $\hat{R}^2 = 0.507 (0.488);$ $AIC = 1380$				
Ashanti Region (0-4)				
Covariate	β -estimate	std error	t -statistic	p -value
Intercept	19.039	20.639	0.92	0.3580
Rainfall	0.0918	0.0541	1.70	0.0921
Rainfall_1	0.1703	0.0534	3.19	0.0018
Sunshrs	-8.5780	3.0515	-2.81	0.0057
$SSE = 44;$ $\hat{R}^2 = 0.219 (0.201);$ $AIC = 995.4$				
Greater Accra Region (0-4)				
Covariate	β -estimate	std error	t -statistic	p -value
Intercept	364.326	189.921	1.92	0.0573
Rainfall_1	0.1932	0.0666	2.90	0.0044
MinTemp_1	-7.7359	4.3666	-1.77	0.0789
RH0600	-3.6469	2.1979	-1.66	0.0995
RH1500	2.0327	1.4529	1.40	0.1642
$SSE = 47.3;$ $\hat{R}^2 = 0.137 (0.110);$ $AIC = 1015$				
Western Region (0-4)				
Covariate	β -estimate	std error	t -statistic	p -value
Intercept	-907.899	337.734	-2.69	0.0081
Rainfall_1	0.161	0.042	3.83	0.0002
MinTemp_1	13.938	5.962	2.34	0.0210
RH0600_1	6.021	3.329	1.81	0.0729
$SSE = 43.8;$ $\hat{R}^2 = 0.231 (0.213);$ $AIC = 994.4$				

zone, except in the under 5-year old group in Upper West Region (p -value = 0.00531) which rather decreases the residuals by 0.795 per unit change. This can be attributed to the effect of multicollinearity with the other covariates.

As noted above, relative humidity confounds with rainfall due to high collinearity between them whilst a similar stronger correlation exists between maximum temperature and sunshine hours. Thus, malaria risk in the regions can be significantly influenced by rainfall and maximum temperature lagged one month, confirming the earlier assertion of rainfall, temperature and humidity as the main contributors to malaria transmission in Ghana. The varied regression models established at the regions give an indication of the spatial distributions of the malaria morbidity incidence which could be attributed to the effect of variations in climatic conditions. This is explored further in section 4.5 via SARIMA predictive models and in section 4.5, using the space-time incidence data and the covariates observed at the district-month locations.

4.4.2 Correlation Analysis of Space-time Data

Cross-correlation analysis of the observed district-month (space-time) data is performed with the ultimate aim of identifying the potential climate variables which relate strongly with elevation and the morbidity incidence rates and then used for developing suitable linear models of coregionalisation (LMC) in chapter 5. Elevations of district locations of the observed monthly count cases of malaria morbidity were first extracted from the exhaustive information source, DEM (IntraSearch, 2011). The results by month (shown in Appendix B-3) indicate that elevations correlate significantly with the morbidity incidence rates and climatic covariates (p -value < 0.05), though not strongly with the former where correlation coefficients mostly range between 0.20000 and 0.40000. However, they relate more strongly with the climatic covariates, and are often used as proxy for atmospheric variables in meteorological studies (Goovaerts, 1999; Hudson & Wackernagel, 1994; Kyriakidis, Miller, & Kim, 2004; Spadavecchia & Williams, 2009). In particular, increasing elevation correlates highly with decreasing minimum temperature and relative humidity measured at 1500 hours with monthly observed spatial correlation coefficients ranging mostly between -0.10000 and -0.80000 but poorly with increasing maximum temperature. Rather, rainfall relates positively and negatively with elevation depending on the month of observation. Relative humidity (at 1500 hours) correlates

positively and highly with minimum temperature and negatively with maximum temperature which happens to be stronger from November to December (see the spatial correlation results in Appendix B-3).

Table 4.4.5: Correlation analysis of residuals for the observed the morbidity incidence rates with the climatic covariates observed at the district-month locations over the whole the study area in Ghana

Covariate	MIR	Rainfall	MaxT	MinT	RH0600	RH1500	Sunshr
MIR	1						
Rainfall	0.157	1					
MaxTemp	-0.102	-0.366	1				
MinTemp	-0.112	0.049	0.236	1			
RH0600	0.037	0.402	-0.578	0.131	1		
RH1500	0.056	0.495	-0.743	0.175	0.799	1	
Sunshrs	-0.020	-0.301	0.649	0.125	-0.413	-0.548	1
Covariate	Residuals	Rainf	MaxT	MinT	RH0600	RH1500	Sunshr
Residuals	1						
Rainfall	0.277	1					
MaxTemp	-0.332	-0.366	1				
MinTemp	-0.090	0.049	0.236	1			
RH0600	0.288	0.402	-0.578	0.131	1		
RH1500	0.321	0.495	-0.743	0.175	0.799	1	
Sunshrs	-0.194	-0.301	0.649	0.125	-0.413	-0.548	1
Covariate	Residuals	Rainf_1	MaxT_1	MinT_1	RH06_1	RH15_1	Sunsh_1
Residuals	1						
Rainfall_1	0.380	1					
MaxTemp_1	-0.283	-0.368	1				
MinTemp_1	0.026	0.049	0.234	1			
RH0600_1	0.318	0.402	-0.578	0.131	1		
RH1500_1	0.360	0.498	-0.745	0.176	0.798	1	
Sunshrs_1	-0.179	-0.300	0.649	0.125	-0.414	-0.550	1
Covariate	Residuals	Rainf_2	MaxT_2	MinT_2	RH06_2	RH15_2	Sunsh_2
Residuals	1						
Rainf_2	0.304	1					
MaxTemp_2	-0.160	-0.369	1				
MinTemp_2	0.150	0.049	0.232	1			
RH0600_2	0.266	0.403	-0.581	0.132	1		
RH1500_2	0.286	0.499	-0.748	0.178	0.799	1	
Sunshrs_2	-0.150	-0.300	0.651	0.124	-0.415	-0.550	1

Table 4.4.5 and Appendix B-4 give the spatial and temporal correlations between the detrended morbidity incidence rates (residuals) and potential climatic covariates for the study areas. Nationally, there is a significant effect of the climatic covariates on the residuals at the district-time locations. The residuals exhibit higher correlations with maximum temperature, relative humidity and rainfall (at lags 0 and 1) which is

consistent with the temporal correlations observed in the regions, where increase in rainfall/relative humidity (or maximum temperature) leads to increased (or decreased) risk of the disease. Similar and more variable correlations are observed in BAR and the vegetation zones (see Results B-4.1). However, as in the former, the effect of the potential covariates, rainfall, maximum temperature and relative humidity (at 1500 hours) is more pronounced in the northern savannah zone where the correlation coefficients between the morbidity risk (via residuals) and the three potential covariates are relatively stronger. Malaria morbidity risk as observed in the coastal and forest zones is poorly correlated with the covariates but significant increased risk of the disease can statistically be predicted by increasing rainfall and relative humidity. Temporally, the correlations of morbidity incidence with the potential covariates at the district weather locations are much stronger than in the spatial domain with higher correlation coefficient values mainly observed in the northern-zone regions and Brong Ahafo Region (see Results B-4.2).

4.5 Seasonal ARIMA Models of the Global MIR

The classical multiple regression analysis of the global (or regional) morbidity incidence rates conducted in the previous section appeared to be insufficient for explaining some of the interesting dynamics existing within the time series incidence data. The residuals obtained from such a modelling approach are likely to exhibit serial correlation, violating the underlying normality (white noise) assumption (Bepari & Mollik, 2009; Box & Pierce, 1970; Cowpertwait & Metcalfe, 2009; Shumway & Stoffer, 2011). Thus, the detrended incidence data arising from the fitting of the second order polynomial model in time (4.4.1) to the morbidity incidence data are further examined for the application of appropriate predictive and forecast models of the morbidity cases in the regions. The autoregressive integrated moving average (ARIMA) models of time series analysis, as discussed in section 2.5 of chapter 2, are capable of modelling the non-stationarity in the observed morbidity incidence data due to the large scale trend and seasonal effects, which are achieved through an integrated process of differencing (Box & Jenkins, 1976; Cowpertwait & Metcalfe, 2009). In this section the residual analysis of the detrended incidence time series data is performed and then followed by application of the multiplicative seasonal autoregressive integrated moving average (SARIMA) modelling of the morbidity incidence rates for

future forecasting in the regions. The SARIMA predictive model of the incidence rates (as outlined in section 2.5.3) is then extended to SARIMAX model to incorporate the effects of variation in rainfall, relative humidity and temperature as exogenous variables(X) to characterise the morbidity incidence in the regions.

4.5.1 Autocorrelation Analysis of the Detrended Incidence Rates

The monthly detrended incidence rates $R_t(\mathbf{u}_\alpha)$, by (4.4.1), in the regions are analysed using the autocorrelation functions (ACFs) and their partial autocorrelation functions (PACFs) coupled with Augmented Dickey-Fuller test (ADF) test for stationarity (Dickey & Fuller, 1979) and Q-Q plots via the Shapiro-Wilk test (Royston, 1982; Shapiro & Wilk, 1965). This gives a very useful visual impression of the correlations among close observed incidence rates of the disease and eventually leads to the accurate SARIMA model and other applicable methodology to achieve the desired prediction (Johnson & Wichern, 1992; Shumway & Stoffer, 2011). The time sequence and Q-Q plots as well as the autocorrelation functions of the residuals of the regions are produced in Figures 4.5.1 and 4.5.2 and Appendix C-1.

The analysis of the residuals, generally, indicates similar behaviour of the morbidity incidence in the regions with very strong serial correlations at lag 1. The time sequence plots of the residuals which centred at zero mostly show significant fluctuations but with some highly extreme values and also indicating the periodic cycles in the incidence data. The seasonal effects are further evidenced by autocorrelation and partial autocorrelation functions which are characterised by high spikes observed at lag 12 and its multiples (24, 36, ...), after which they decay exponentially and die out eventually. The residuals appear stationary (p -value < 0.05) by the ADF test (Dickey & Fuller, 1979) and also close to the normal but with pronounced outliers noticed in the tails of plots, especially in Upper West, Upper West, Greater Accra, Eastern and Ashanti regions. Shapiro-Wilk tests (Shapiro & Wilk, 1965) were performed which yielded p -values of mostly less 0.01, which implies that the detrended incidence data in the regions are not normally distributed but can be improved by differencing (or integration) (Cai, 2009; Cowpertwait & Metcalfe, 2009; Shumway & Stoffer, 2011). The modelling process is improved by the application of a multiplicative seasonal ARIMA modelling process (Box & Jenkins, 1976) with an alternative diagnostics procedure such as Ljung-Box Q-test (Ljung & Box, 1978) which uses a chi-

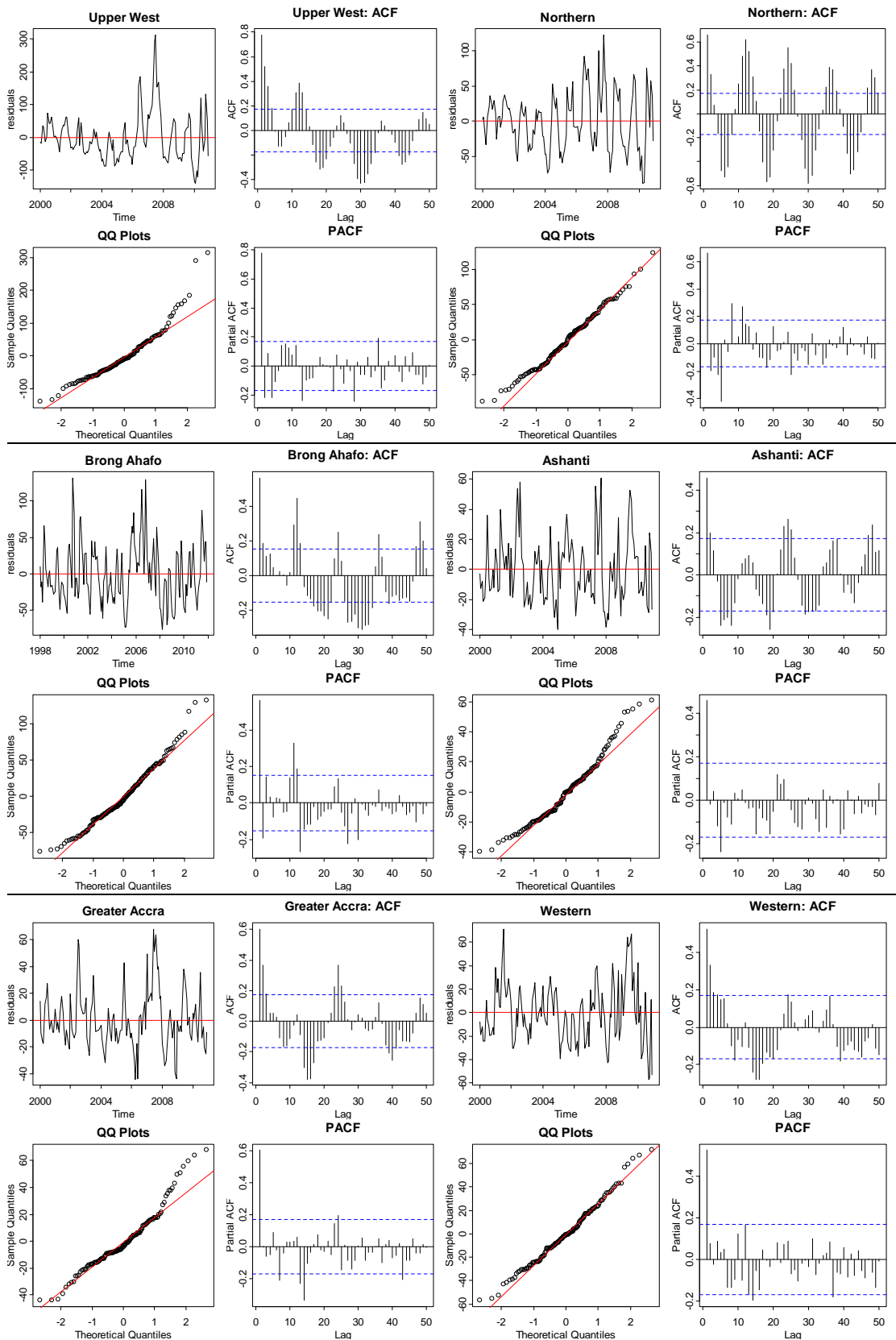


Figure 4.5.1: Time sequence and QQ plots (left), ACFs and PACFs (right) of residuals in Upper West, Northern (top), Brong Ahafo, Ashanti (middle), Greater Accra and Western (bottom) regions for regional total morbidity incidence rates

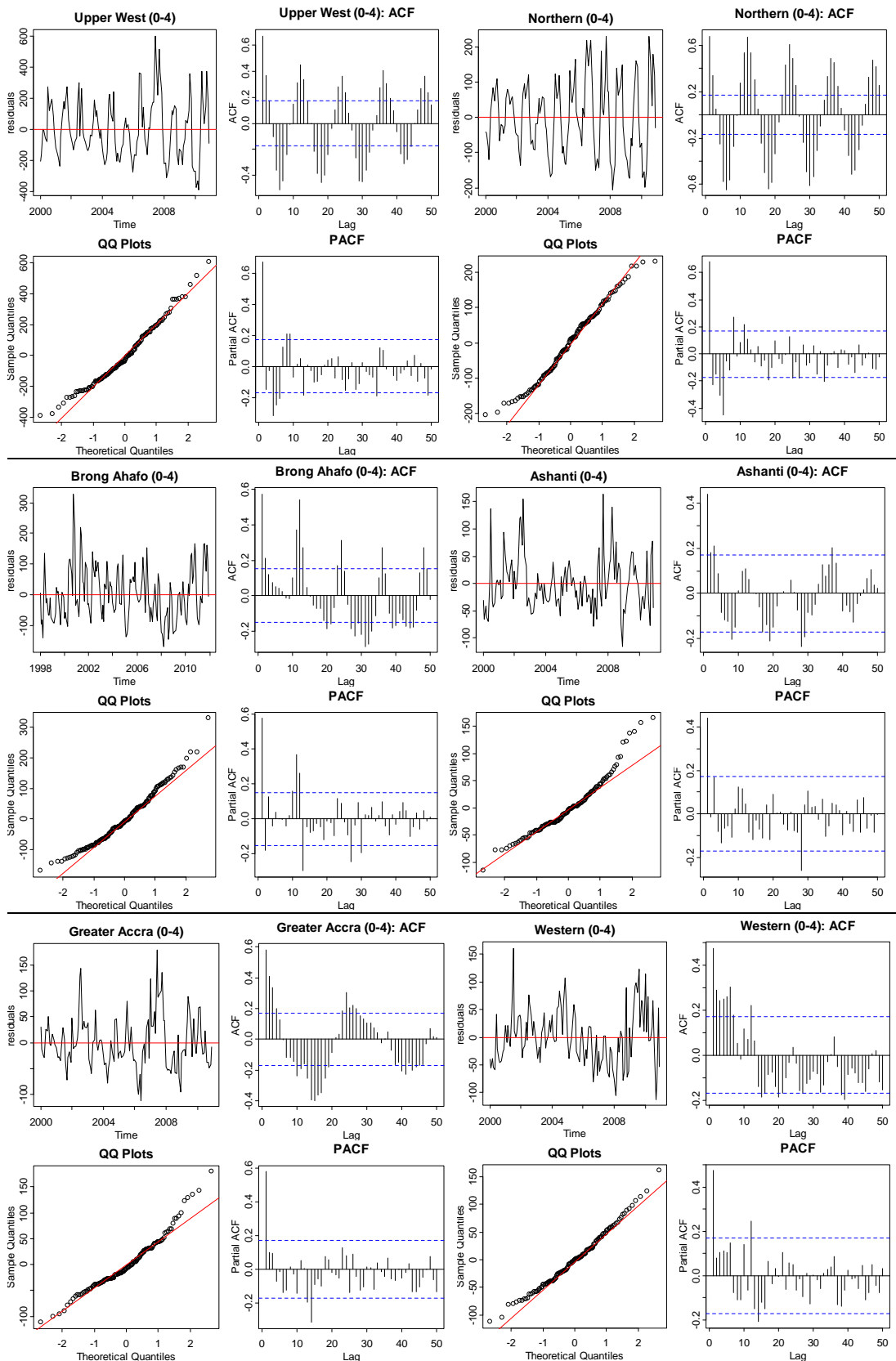


Figure 4.5.2: Time sequence and QQ plots (left), ACFs and PACFs (right) of residuals in Upper West, Northern (top), Brong Ahafo, Ashanti (middle), Greater Accra and Western (bottom) regions for the morbidity incidence rates of the 0-4 year old group

square distribution with heavier tails than the normal distribution to establish goodness-of-fit of the modeling. This methodology has extensively been applied to the morbidity incidence rates and the results are presented in section 4.5.2.

4.5.2 Multiplicative SARIMA Models of the Malaria Morbidity Incidence Rates

The multiplicative seasonal autoregressive integrated moving average (SARIMA) model of order $(p, d, q) \times (P, D, Q)$, introduced by Box and Jenkins (1976) and given in (2.5.8), was applied to time series morbidity incidence data $I_t(\mathbf{u}_\alpha)$ in the regions due to the strong autocorrelations exhibited by the detrended data as observed in previous section. Stationarity of the incidence time series data in each region was achieved by taking the first (or second) and seasonal order differences through the integrated process of the SARIMA model (2.5.8) to remove the linear (or quadratic) trend and seasonal effects within the data. This was further confirmed by ADF tests (Dickey & Fuller, 1979) conducted, which all proved statistically significant (p -value < 0.01), rejecting the non-stationarity of the differenced incidence data. The advantage of the differencing being, unlike the detrending, it does not require parameter estimation (Shumway & Stoffer, 2011).

The Box-Jenkins model-building is continued with parameter estimation by fitting a wide range of multiplicative models to the morbidity incidence rates data using the maximum likelihood estimation (MLE) method, by (2.5.9) and (2.5.10). The best-fitting models obtained were based on two main criteria of model adequacy, the Akaike information criterion (AIC) by Akaike (1974), which measures how the models fit to the incidence rates time series using the least value of AIC (2.5.11) and the Ljung-Box Q-test (Ljung & Box, 1978), which performed the diagnostics of the fitted models using the residuals via (2.5.12). In choosing the best-fitting morbidity incidence model of the disease for each region, two types of predictive models were developed, following Wangdi et al. (2010). Model I is the univariate SARIMA model used to provide forecasts of the morbidity incidence cases in the region. This model was developed based on the trend pattern of the morbidity incidence rates over the years and under the presumed stable environmental and socio-economic conditions such as climatic, vegetation, access to health care for treatment, intervention measures, population movement and poverty in the region. The potential impact of these factors

on malaria transmission is detailed in chapters 1 and 6. Model II is the multivariate SARIMA model which extends Model I to account for the effects of the potential climatic covariates as exogenous variables (hereafter and elsewhere referred to as SARIMAX) model. The exogenous variables included rainfall, temperature, relative humidity and number of sunshine hours, lagged one month to allow sufficient time for the development of the disease and its subsequent reporting (Wangdi et al., 2010). The parameter estimates for best-fitting predictive SARIMA and SARIMAX models for each region are presented in Appendix C-2 whilst Tables 4.5.1 and 4.5.2 list the summary results of the developed predictive models. The results of Ljung-Box Q-tests for model adequacy by residual analysis of the predictive models are shown in Appendix C-3, whilst results for some selected regions are given in Figures 4.5.3 and 4.5.4. All the multiplicative SARIMA and SARIMAX model-building procedures were carried out using functions and codes in the R program (R Development Core Team, 2011) as shown in Appendix H-1.3.

Overall, the SARIMA models for predicting the morbidity incidence rates vary (see the best-fitted models obtained as shown in Table 4.5.1 and 4.5.2) due to the different morbidity patterns of occurrence of the disease in the regions. The predictions are strongly influenced by both the seasonal and non-seasonal components of the autoregressive and moving average processes whose parameters are mostly found to be highly statistically significant (p -value < 0.01). The predictive models of the morbidity incidence for the 0-4 year olds are different from the total incidence except in three regions, namely, Upper East, Northern and Ashanti, which were modelled, in both cases by the predictive models, $ARIMA(1,1,1) \times (0,1,1)_{12}$, $ARIMA(1,1,4) \times (1,1,0)_{12}$ and $ARIMA(3,1,0) \times (3,2,1)_{12}$, respectively. The morbidity incidence rates among the vulnerable young children are estimated higher with the highest incidence cases mainly occurring in Upper East, Upper West, Brong Ahafo and Western regions. The SARIMA models developed for all the regions appear to provide adequately fits as evidenced by the Ljung-Box Q-tests for the model diagnostics (see Figures 4.5.3 and 4.5.4 Appendix C-3), where the time sequence plots of the standardised residuals show no obvious pattern, except for some few outliers which can be observed. In addition, the autocorrelation functions of the residuals do not indicate any apparent departure from the model assumptions, as evidenced by the high estimated p -values, which appear higher in most cases for the 0-4 year group predictions.

Table 4.5.1: Summary results of multiplicative SARIMA and SARIMAX predictive models of morbidity incidence rates (total) for the ten regions of Ghana with the potential exogenous variables (X). Also indicated are the AIC, MAE and RMSE values obtained for the models.

Region (Total)	SARIMA(X) Model	Exogenous Variables (X)	AIC	MAE	RMSE
Upper East	ARIMA(1,1,1)×(0,1,1) ₁₂	-	1225	27.17	37.32
	ARIMAX(1,1,1)×(0,1,1) ₁₂	MaxTemp; RH1500 Sunshrs	1216	26.90	36.74
Upper West	ARIMA(1,0,0)×(0,1,1) ₁₂	-	1239	27.35	38.32
	ARIMAX(1,0,0)×(0,1,1) ₁₂	Rainfall_1; Sunshrs_1	1226	26.24	37.22
Northern	ARIMA(1,1,4)×(1,1,0) ₁₂	-	1098	15.17	21.20
	ARIMAX(1,1,4)×(1,1,0) ₁₂	RH1500; Sunshrs_1	1081	14.29	20.05
Brong Ahafo	ARIMA(3,1,0)×(0,1,1) ₁₂	-	1465	17.33	23.96
	ARIMAX(3,1,0)×(0,1,1) ₁₂	Rainfall; RH1500_1	1447	16.97	22.37
Ashanti	ARIMA(3,1,0)×(3,2,1) ₁₂	-	1034	12.98	18.68
	ARIMAX(3,1,0)×(3,2,1) ₁₂	RH1500_1; MinTemp_1	1027	13.01	18.41
Eastern	ARIMA(1,1,2)×(0,1,1) ₁₂	-	1141	17.80	25.25
	ARIMAX(1,1,2)×(0,1,1) ₁₂	MinTemp_1; Sunshrs_1	1129	16.56	24.40
Western	ARIMA(0,1,1)×(2,1,2) ₁₂	-	1069	12.07	17.07
	ARIMAX(0,1,1)×(2,1,2) ₁₂	Rainfall; Rainfall_1 MaxTemp	1055	12.00	16.33
Central	ARIMA(0,0,2)×(1,1,0) ₁₂	-	1020	10.00	15.49
	ARIMAX(0,0,2)×(1,1,0) ₁₂	RH1500; MinTemp_1	1013	10.77	15.33
Greater Accra	ARIMA(0,1,1)×(2,1,0) ₁₂	-	1012	10.79	14.94
	ARIMAX(0,1,1)×(2,1,0) ₁₂	Rainfall_1; Sunshrs RH1500_1	1000	10.49	14.57
Volta	ARIMA(1,1,2)×(0,1,2) ₁₂	-	610	10.29	14.41
	ARIMAX(1,1,2)×(0,1,2) ₁₂	Rainfall_1; Sunshrs	600	9.94	13.67

Table 4.5.2: Summary results of multiplicative SARIMA and SARIMAX predictive models of morbidity incidence rates (0-4) for the ten regions of Ghana with the potential exogenous variables (X); Also indicated are the AIC, MAE and RMSE values obtained for the models.

Region (0-4)	SARIMA(X) Model	Exogenous Variables (X)	AIC	MAE	RMSE
Upper East	ARIMA(1,1,1)×(0,1,1) ₁₂	-	1517	88.74	124.70
	ARIMAX(1,1,1)×(0,1,1) ₁₂	MinTemp_1; RH1500	1506	88.65	122.80
Upper West	ARIMA(1,1,1)×(0,1,1) ₁₂	-	1487	78.70	108.60
	ARIMAX(1,1,1)×(0,1,1) ₁₂	Rainfall_1; Sunshrs_1	1470	76.94	105.40
Northern	ARIMA(1,1,4)×(1,1,0) ₁₂	-	1306	35.63	51.17
	ARIMAX(1,1,4)×(1,1,0) ₁₂	Sunshrs_1	1288	34.57	49.38
Brong Ahafo	ARIMA(0,1,2)×(0,1,1) ₁₂	-	1692	38.68	51.89
	ARIMAX(0,1,2)×(0,1,1) ₁₂	MaxTemp; RH1500_1	1672	36.62	49.75
Ashanti	ARIMA(3,1,0)×(3,2,1) ₁₂	-	1212	31.96	43.90
	ARIMAX(3,1,0)×(3,2,1) ₁₂	Rainfall, MaxTemp_1	1201	31.27	43.90
Eastern	ARIMA(0,1,2)×(0,1,1) ₁₂	-	1316	38.30	53.42
	ARIMAX(0,1,2)×(0,1,1) ₁₂	Rainfall_1; MinTemp_1	1304	37.43	52.07
Western	ARIMA(0,1,1)×(0,1,1) ₁₂	-	1232	26.77	37.80
	ARIMAX(0,1,1)×(0,1,1) ₁₂	RH0600; RH0600_1	1215	25.48	35.95
Central	ARIMA(0,1,3)×(0,1,2) ₁₂	-	1179	19.56	27.90
	ARIMAX(0,1,3)×(0,1,2) ₁₂	MaxTemp_1; MinT MinTemp_1	1169	19.97	27.26
Greater Accra	ARIMA(0,1,1)×(1,2,1) ₁₂	-	1184	29.13	42.98
	ARIMAX(0,1,1)×(1,2,1) ₁₂	Rainfall_1, RH1500_1; Sunshrs	1170	27.91	41.12
Volta	ARIMA(1,1,0)×(0,1,1) ₁₂	-	755	29.31	40.21
	ARIMAX(1,1,0)×(0,1,1) ₁₂	RH1500_1; Sunshrs_1	746	27.97	38.65

The SARIMAX models, which were established by fitting the already developed SARIMA models with the covariates as exogeneous variables to account for the effect of the climatic conditions, contribute to further predictions of the morbidity incidence rates and explanation of the variations in morbidity incidence in the various regions. The SARIMAX models showed different climatic predictors and significant impact on the morbidity incidence for the different regions. However, rainfall and number of sunshine hours (both lagged one month) which confound with maximum temperature are generally found to be significant predictors of the morbidity incidence for regions in the northern savannah zone whilst current or prior one month rainfall and relative humidity (or temperature) prove to be the important predictors of the incidence for regions in the other two vegetation zones. The effects of these potential predictors tend not to show any particular relationship as they are found to either increase or decrease the incidence rates per unit change of their observations. In particular, rainfall is observed to decrease morbidity whilst relative humidity appears to increase morbidity for regions in the northern zone. In contrast, the impact of some covariates is the opposite in some regions (Ashanti, Greater and Western) in the other two zones (see results in Appendix C-2).

The impact of the climatic covariates can further be observed by the significant reductions in the AIC, MAE and RMSE values, compared with those obtained by the SARIMA models (see Tables 4.5.1 and 4.5.2). The SARIMAX model diagnosis of the morbidity incidence rates also showed significant increase of the p -values. The parameters of both predictive SARIMA and SARIMAX models show that the morbidity incidence rates within the last four months and three seasons coupled with rainfall, maximum temperature and relative humidity in the preceding one month highly influence the morbidity incidence in the current month. This can be interpreted that the malaria morbidity incidence in the last few months and seasons and that of variations in climatic conditions affect the reported new morbidity incidence cases in the current month in the regions. The results can be used to provide an early warning system for malaria epidemics in the various regions and also serve a guide for further analysis in the following chapter.

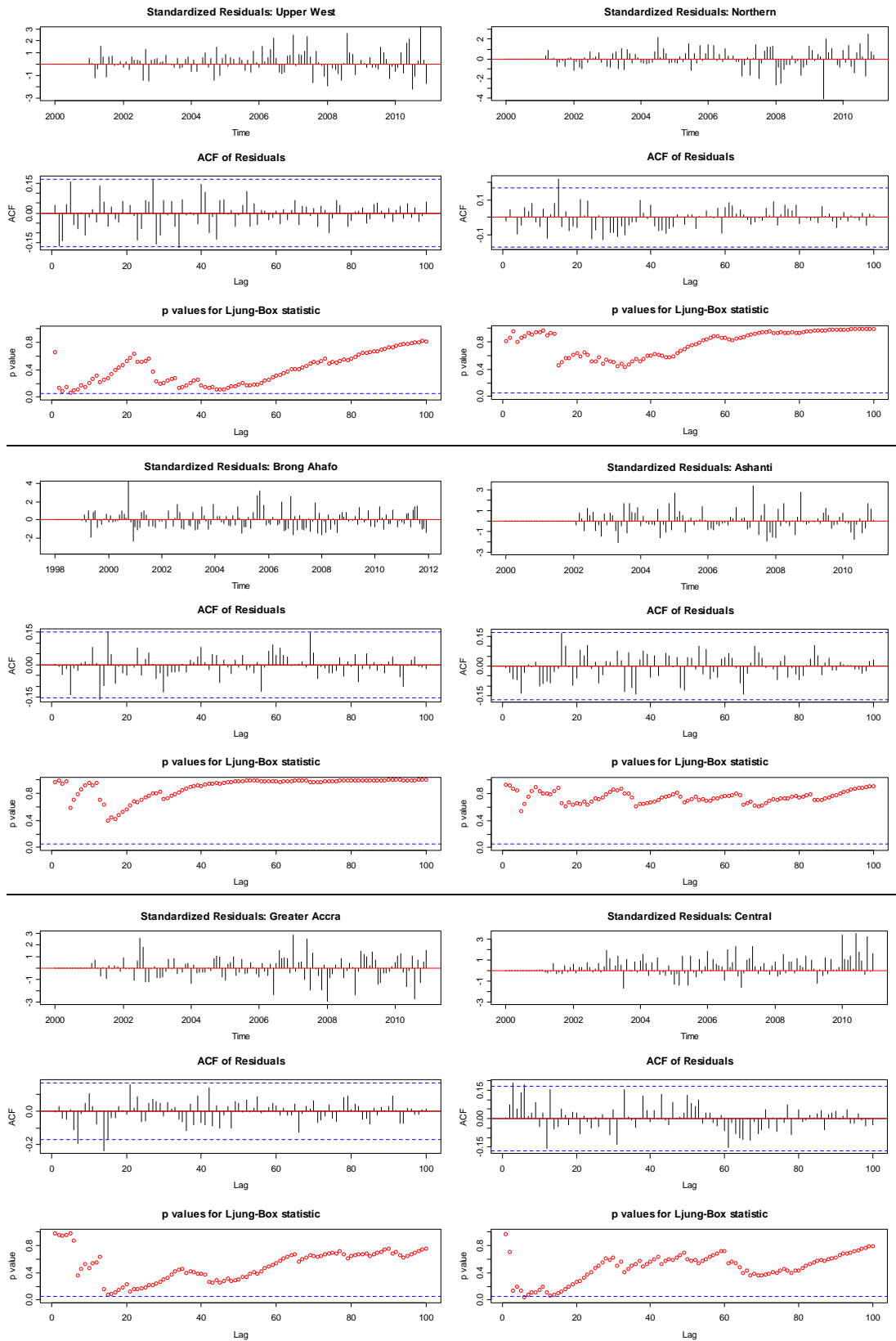


Figure 4.5.3: SARIMA model diagnostics of the morbidity incidence rates (total) by the Lyung-Box Q-test indicating the standardised residuals (top), ACF of residuals (middle) and the p-values (bottom) for Upper West, Northern, Brong Ahafo, Ashanti, Greater Accra and Central regions

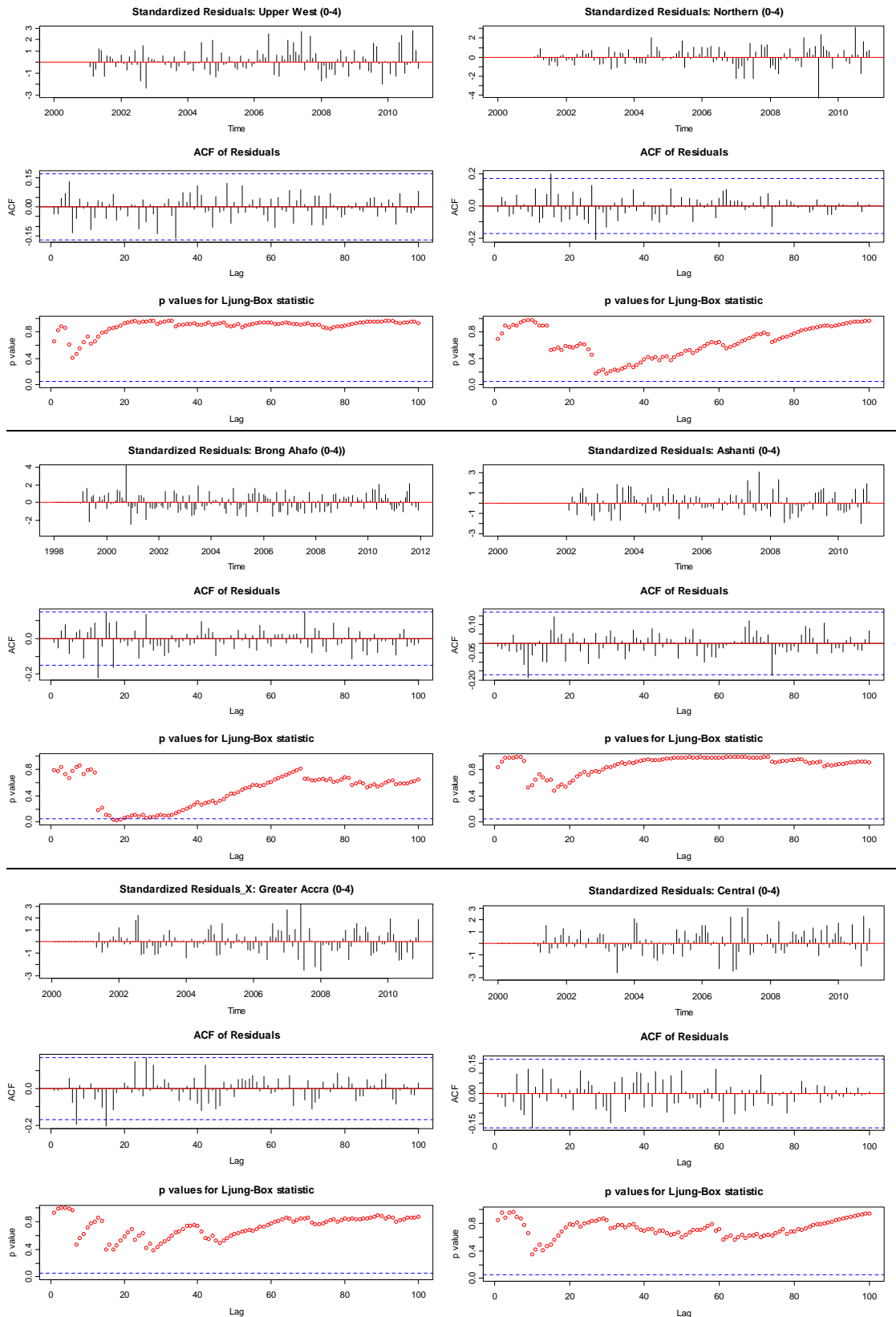


Figure 4.5.4: SARIMA model diagnostics of the morbidity incidence rates (0-4) by the Lyung-Box Q-test indicating the standardised residuals (top), ACF of residuals (middle) and the p-values (bottom) for Upper West, Northern, Brong Ahafo, Ashanti, Greater Accra and Central regions

4.5.3 SARIMA Predictive Model Forecast of MIR and Validation

The SARIMA models established in section 4.5.3 are used to make future forecasting of the morbidity incidence rates. A three-year forecast of the monthly morbidity incidence is proposed for the period 2011–2013/2014. The results of the forecasting when implemented will assist the monitoring of progress towards Ghana’s NMCP Strategy Plan 2008-2015 for achieving 75% reduction of morbidity cases by 2015. The forecast values are presented in Appendix C-5 whilst the graphs are displayed in Figures 4.5.5 and 4.5.6 and Appendix C-4. Tables 4.5.3 and 4.5.4 show the validation results for the 2011 (and 2012 for BAR) forecast values.

As observed from the forecast tables and figures, varied results have been produced across the country but followed similar seasonal and also trend behaviours, especially for regions in the same vegetation zone (see Appendix C-4). On the whole, the incidence rates for the northern zone are forecasted higher and appear to remain constant within the prediction period, except Upper East which appears to show a sharp increase. However, the forecasts for the regions in the forest zone (for example, Brong Ahafo and Ashanti) show gradual increase whilst the forecasts of morbidity incidence in Greater Accra, which is part of the coastal zone, decreases. The three regions (Central, Western and Volta) in both forest and coastal zones exhibit almost similar characteristics with their forecasted incidence rates following the same trend pattern as observed in the forest zone. The incidence rates among the most vulnerable people (0-4 year old children) are increasingly forecasted higher except in Greater Accra Region which decreases like the total incidence forecast.

The prediction performance of the models is assessed using the 2011 morbidity incidence rates as validation data which were not included in forecasting. Comparing the forecasted incidence values with the actual values for 2011, they are found to be very close (as clearly evidenced by the mean values in Tables 4.5.3 and 4.5.4 and graphs in Figures 4.5.5 and 4.5.6). The forecast estimates are all observed to lie within the 95% confidence interval values. The estimates also correlate very highly with the observed morbidity incidence with correlation coefficients for both the total and 0-4 year grouping incidence rates ranging between 0.771 and 0.989 (see Tables 4.5.3 and 4.5.4). However, the RMSE and MAE values for the regions in the northern savannah zone and Volta Region which falls in both the forest and coastal zones are higher, compared with the other regions. These forecast results as earlier indicated have policy

Table 4.5.3: Forecasted MIR values for 2011(and 2012 for BAR), compared with the observed sample and measures of prediction accuracy for the regional total incidence rates data

Region	MIR	Min	Max	Mean	StDev.	ME	MAE	RMSE	Corr.
Upper East	Sample	417	717	550.25	110.47	-	-	-	-
	Forecast	445.62	688.24	549.23	87.810	-1.023	28.418	31.828	0.970
Upper West	Sample	285	498	377.92	76.378	-	-	-	-
	Forecast	324.74	468.51	382.99	56.553	5.073	24.698	27.696	0.952
Northern	Sample	183	311	240.33	46.720	-	-	-	-
	Forecast	190.17	320.67	246.94	48.274	6.650	8.692	9.624	0.989
Brong Ahafo	Sample	229.00	346	284.67	38.070	-	-	-	-
	Forecast	243.09	320.20	282.18	30.059	-2.489	11.503	15.102	0.922
Ashanti	Sample	214.00	272	238.67	19.114	-	-	-	-
	Forecast	204.65	267.50	240.17	22.060	1.506	10.209	12.902	0.789
Eastern	Sample	255.00	391	307.83	44.022	-	-	-	-
	Forecast	272.31	365.01	314.23	32.558	6.402	15.352	16.844	0.953
Western	Sample	287.00	342	310.92	17.906	-	-	-	-
	Forecast	299.29	399.85	314.07	15.910	3.149	10.594	11.594	0.769
Central	Sample	151.0	223	182.42	23.434	-	-	-	-
	Forecast	147.55	203.75	168.59	19.101	-13.82	14.710	16.933	0.966
Greater Accra	Sample	90.00	124	106.67	9.1880	-	-	-	-
	Forecast	80.041	127.93	100.25	14.684	-6.418	8.575	10.198	0.858
Volta	Sample	240.0	370	295.08	44.570	-	-	-	-
	Forecast	256.30	383.62	315.29	44.353	20.208	20.208	21.908	0.980

Table 4.5.4: Forecasted MIR values for 2011 (and 2012 for BAR), compared with the observed sample and measures of prediction accuracy for the 0-4 year group incidence rates data

Region	MIR	Min	Max	Mean	StDev.	ME	MAE	RMSE	Corr.
Upper East	Sample	720	1951	1259.5	423.05	-	-	-	-
	Forecast	979.61	1717.6	1302.9	283.46	43.33	139.17	151.76	0.985
Upper West	Sample	575	1255	897.33	251.12	-	-	-	-
	Forecast	733.79	1140.6	925.52	164.89	28.167	94.667	111.32	0.937
Northern	Sample	311	703	500.00	146.31	-	-	-	-
	Forecast	365.54	712.60	527.99	129.59	27.958	36.445	43.950	0.975
Brong Ahafo	Sample	423	681	556.92	92.80	-	-	-	-
	Forecast	470.66	683.79	575.97	73.328	19.050	29.158	33.552	0.967
Ashanti	Sample	427	605	529.17	59.853	-	-	-	-
	Forecast	448.18	614.73	538.31	46.938	9.148	25.987	28.738	0.886
Eastern	Sample	453	686	565.92	84.305	-	-	-	-
	Forecast	478.64	660.13	557.95	61.526	-7.963	28.055	37.592	0.908
Western	Sample	591	717	655.17	37.479	-	-	-	-
	Forecast	615.75	721.13	676.13	31.169	20.966	31.118	31.118	0.771
Central	Sample	322	465	376.83	36.244	-	-	-	-
	Forecast	334.08	448.38	382.26	31.242	5.422	16.867	18.075	0.863
Greater Accra	Sample	215	325	273.50	35.019	-	-	-	-
	Forecast	234.97	316.43	297.50	29.494	5.994	9.470	10.931	0.970
Volta	Sample	486	673	576.08	63.189	-	-	-	-
	Forecast	544.32	704.68	619.76	55.574	43.675	43.675	46.656	0.966

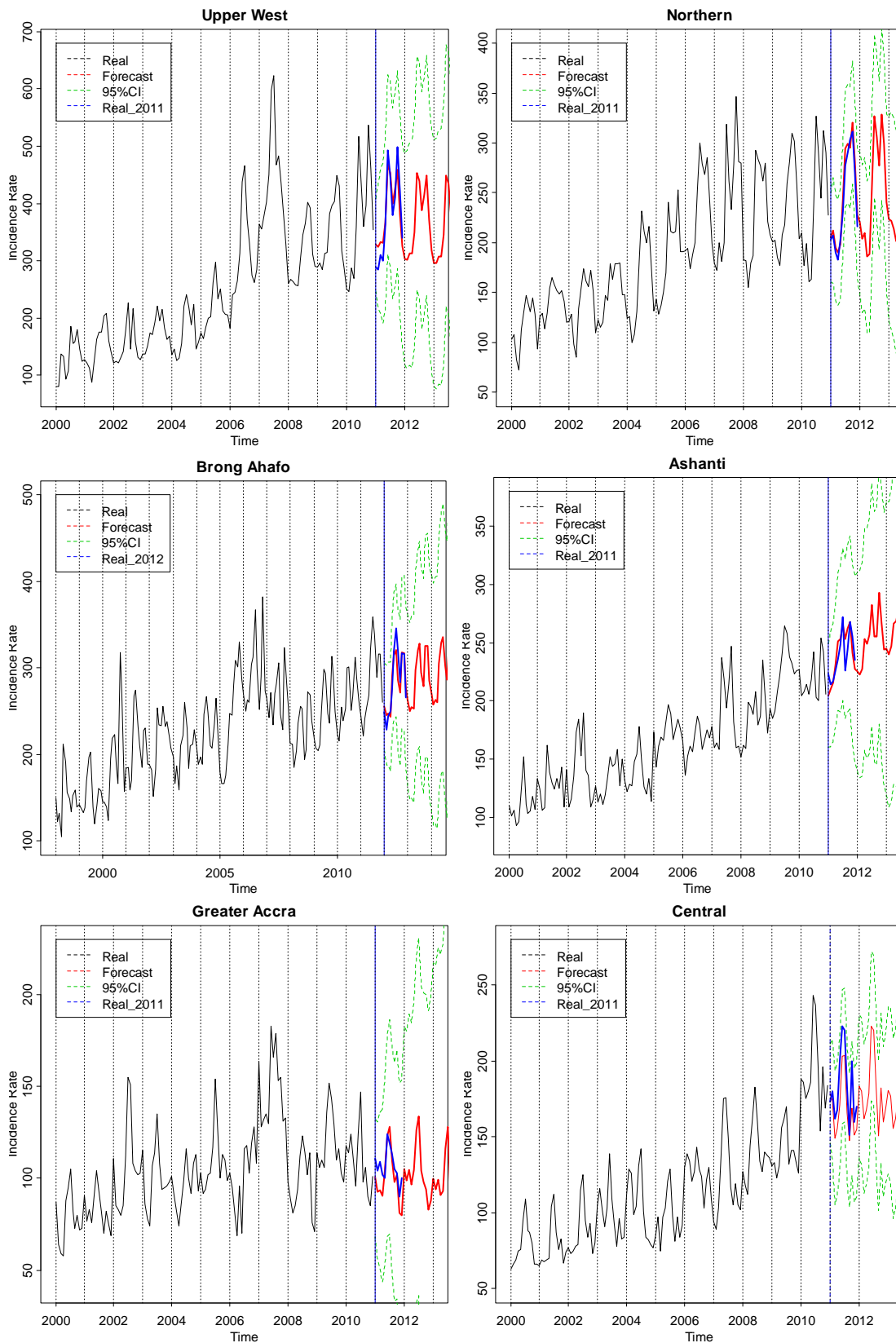


Figure 4.5.5: SARIMA model forecast of monthly morbidity incidence rates (total) for 2011–2013/2014 in Upper West, Northern, Brong Ahafo, Ashanti, Greater Accra and Central regions

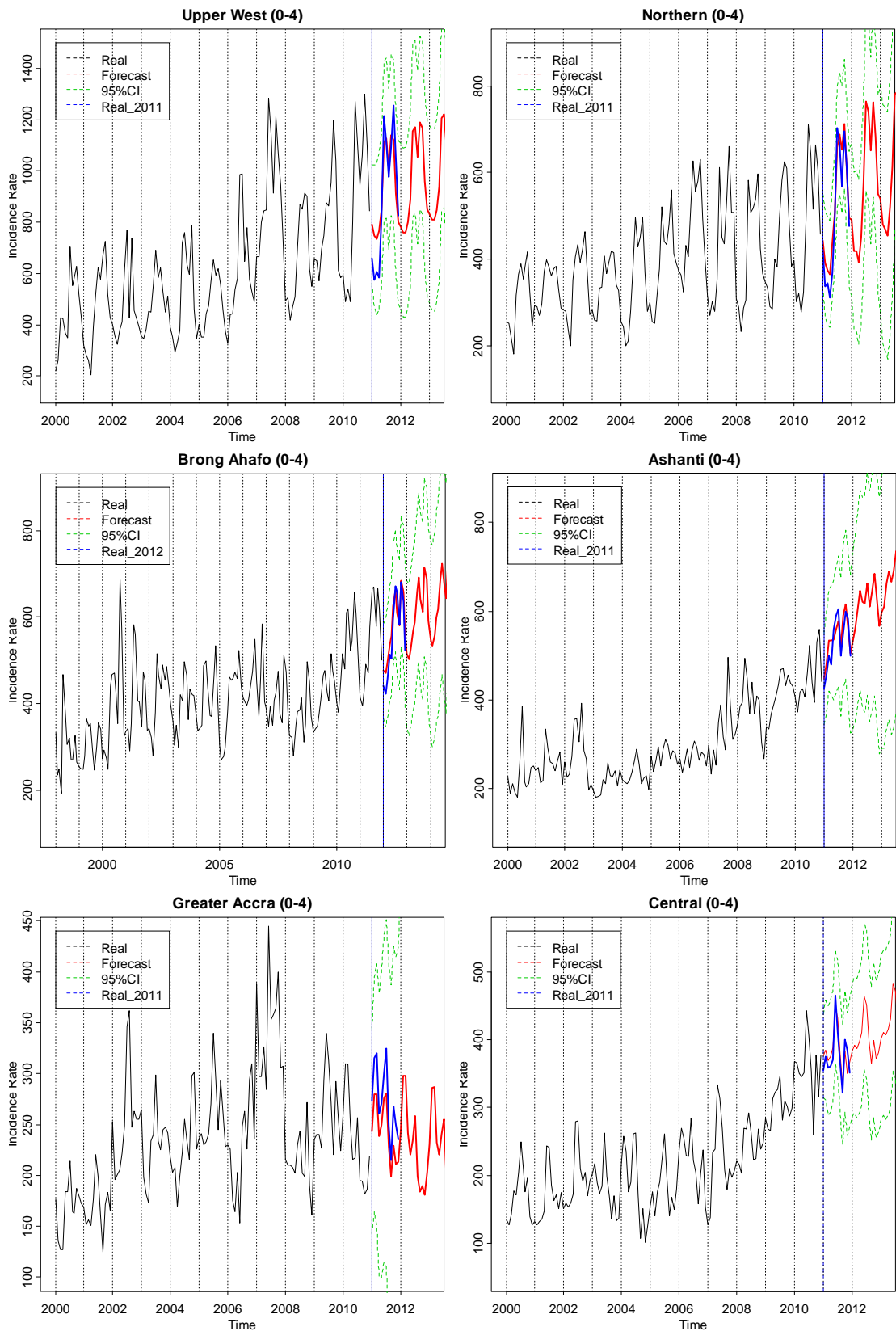


Figure 1 Figure 4.5.6: SARIMA model forecast monthly morbidity incidence rates (0-4) for 2011–2013/2014 in Upper West, Northern, Brong Ahafo, Ashanti, Greater Accra and Central regions

implications, as they will provide useful and reliable information for evaluation of reducing the morbidity cases of malaria in the country by 75% by the year 2015.

4.6 Chapter Summary

The exploratory analysis of the malaria morbidity cases carried out in this chapter aimed at establishing the distributional properties of the morbidity incidence rates for implementation of suitable predictive models of morbidity risk at both regional and district levels in Ghana. First, the study presented background information of the study area, highlighting on its geographical location and climatic conditions, and collection of the morbidity data, classified as regional (global) and space-time, together with the climatic covariates and elevation for the temporal and spatio-temporal analyses of morbidity incidence cases of the disease in the regions and at districts, respectively. The morbidity data were modelled as incidence rates, defined as the number of new cases per 10,000 resident people in a region or district and then considered as a realisation of random process occurring in space and by time as well.

The time sequence plots and smoothing analysis of the incidence rates revealed continuous upward trend coupled with fluctuating periodic cycles, an indication of non-stationarity of the incidence time series data observed in the regions and at districts. Multiple regression analysis of the global data was then explored to establish the potential effect of climatic covariates of which the classical linear regression model proved insufficient to account for the detailed dynamics existing within the incidence rates at the regions. Consequently, the multiplicative SARIMA models were fitted, taking into account of non-stationarity of the incidence data and effect of the covariates for the best-fitting predictive models for the future forecast of the malaria morbidity risk to be determined in each region. The fitted models produced varied morbidity incidence patterns in the regions with strong significant influence of both the seasonal and non-seasonal components coupled with significant effect of rainfall, maximum temperature and relative humidity in the month preceding incidence of the disease. The forecast values of the morbidity incidence rates which followed similar upward or downward trend showed very strong correlation with the observed and also found lying within 95% confidence interval estimates.

In the case of the space-time morbidity incidence data, the analysis was categorised into three studies, namely national, BAR and vegetation types (northern, forest and

coastal zones) to facilitate better description of local variation and quantification of the morbidity burden in a fine-scale. The cross-correlation analysis of the space-time incidence data sets revealed strong positive correlations of elevation of district locations with climatic covariates but with various significant effects of the covariates on the morbidity incidence. In the following chapter, spatio-temporal analysis of the morbidity incidence rates at the district locations is conducted, incorporating the effect of the potential climatic covariates via structural analysis of linear modelling of coregionalisation.

Chapter 5

Space-time Statistical Analysis of the Malaria Morbidity Incidence Rates

5.1 Introduction

In this chapter the theoretical framework of spatial and space-time statistical analysis presented in chapters 2 and 3 is applied to the counts malaria morbidity cases observed at the district health facilities over the period 1998-2011 in Ghana. The study seeks to model the spatial and spatio-temporal distributions of the monthly malaria morbidity incidence rates, incorporating climate effects with particular focus on delineating areas with high risk of malaria morbidity. Thus, the methodology is designed to characterise the correlation structure of the morbidity incidence of the disease spatially and temporally by using various semivariogram models, leading to the local prediction of the morbidity risk. The district-month morbidity incidence rates (MIR) data, as defined in (4.2.1), are assumed to be a realisation of the space-time random function (STRF), $\{I(\mathbf{u}, t) : (\mathbf{u}, t) \in \mathbf{D} \times \mathbf{T}\}$, where $\mathbf{D} \subseteq \mathbb{R}^2$ is the study area and $\mathbf{T} \subseteq \mathbb{R}$ is the temporal domain. The exploratory analysis conducted in Chapter 4 and a previous preliminary study (Appiah et al., 2011) of the observed space-time incidence data revealed some pertinent characteristics. These include non-stationarity due to the presence of a large-scale trend and annual periodicity as well as potential effects of rainfall, temperature and relative humidity on malaria incidence at the district-local level. As per the geostatistical conceptual framework discussed in chapter 3, the district-month MIR are modelled based on the assumption of stationarity of the STRF, characterised by a bounded semivariograms. Thus, following Kyriakidis and Journel (1999), the observed morbidity incidence rates $I(\mathbf{u}_\alpha, t)$ are modelled as joint single random function and also spatially correlated time series at each district location \mathbf{u}_α . The large-scale noise in the incidence rates is reduced by log-transformation, whilst the trend and seasonal cycles occurring in the temporal domain are removed, using the space-time trend model (5.2.1). The resulting trend coefficients (or parameters) are then regionalised (interpolated) in space to account for their spatio-temporal autocorrelations. The residuals independently obtained from the detrending and deseasonalising at the district-month locations are then modelled as a realisation of a stationary spatio-

temporal process, which eventually leads to the reconstruction of STRF at an unsampled spatial location \mathbf{u} at an instant time t (Kyriakidis & Journel, 1999, 2001; Kyriakidis et al., 2004).

The focus of the study is on Ghana as a whole, applying the geostatistical space-time methodological approaches, as stated above, to the morbidity incidence data at all district locations across the country. However, two other cases studies considering the morbidity incidence occurring only at district locations in Brong Ahafo Region (BAR) and the three vegetation (or malaria epidemiological) zones are investigated. These have been designed to facilitate detailed investigation of spatio-temporal dependence of the morbidity incidence at various local scales and to delimit areas of high risk due to the economic importance of these sub-areas. In Ghana, the predominantly vector *Anopheles* mosquito species which cause the disease are classified according to the vegetation types (northern savannah, tropical rainforest and coastal savanna) due to differences in distributions of their habitats in these zones (NMCP/GHS, 2009). The choice of the case study in BAR is informed by its central strategic position in the country, which exhibits both the northern savannah and tropical rainforest types of vegetation, despite its relatively limited availability of data in the spatial domain.

The detailed spatio-temporal analysis of the morbidity incidence data conducted in this chapter are structured into six main sections. Section 5.2 considers the global analysis of space-time trend model, estimating the incidence rates at the district locations across the country and its regionalisation at unsampled locations. The structural analysis of the district-month data is performed in section 5.3 to characterise the spatial and temporal autocorrelations of the observed morbidity incidence rates using space-time semivariograms models of log-transformation of the incidence data (logMIR) and residuals from detrending and deseasonalising of the observed incidence rates at the district-month data locations. Also presented in this section, are the generalised product-sum semivariogram models (De Iaco et al., 2001) of the space-time residuals and cross-validation of the space-time semivariogram models. Section 5.4 implements the space-time kriging techniques of the morbidity incidence rates, which are developed based on the semivariogram models to estimate the morbidity risk at the unsampled locations and explain its distribution patterns in space and time as well. These are the space-time lognormal ordinary kriging (STOLK), applied to logMIR and space-time ordinary kriging (STOK) to the residuals. The effect of the climatic

covariates on the malaria morbidity incidence is established in section 5.5, presenting the linear models of coregionalisation using the detrended incidence data and space-time ordinary co-kriging (STOCK) for the prediction of morbidity risk. Section 5.6 compares and validates the kriging estimates with a brief discussion of the results. The spatio-temporal modelling of the morbidity incidence in BAR and the vegetation zones are considered in sections 5.7 and 5.8, respectively, where the key results of the incidence data analysis are presented. Finally, the chapter is concluded in section 5.9, summarising the results of the data analysis.

All the space-time statistical analyses of the malaria morbidity incidence rates were implemented using the geostatistical software packages, ISATIS version 2013 (Geovariances, 2013) and modified GSLIB routines “GAMV” and “KT3D” programs (De Cesare et al., 2002). The pre-and post-processing of the data and results from the geostatistical software were done using Microsoft Excel 2010 and R version 2.13.2 (R Development Core Team, 2011).

5.2 Analysis of Space-time Global Trend Model of MIR

Following a series of smoothing analyses of the morbidity incidence rates performed at the 138 district-locations (\mathbf{u}_α, t), for $t = 1, \dots, 132$ in section 4.3.2 of chapter 4, an increasing linear or quadratic trend coupled with seasonal patterns of period 12 months were established (see Figure 4.3.4). The large-scale trend and seasonal variability are therefore removed or reduced prior to modelling of the spatio-temporal continuity and kriging of the malaria morbidity risk at the district-month locations where data were missing or unobserved. A case where the large-scale variation in the observed morbidity incidence rates is removed by detrending and deseasonalising is considered in this section. This leads to computation of the space-time trend model and analysis of its coefficients for the global trend surface of the morbidity risk to be estimated at the district locations. The resulting space-time residuals are regionalised spatially and temporally for further modelling procedures as presented in sections 5.3 and 5.4. Thus, in this section, the global estimates of the morbidity incidence rates are computed via the analysis of the space-time trend model (5.2.1).

5.2.1 Estimation of the Trend Model at District Locations

The observed space-time morbidity incidence rate data $\{I(\mathbf{u}_\alpha, t) : \alpha = 1, \dots, n; t = 1, \dots, T\}$ are independently detrended and deseasonalised at each district location \mathbf{u}_α which results in the decomposition of the morbidity incidence rates into a trend model $m(\mathbf{u}, t)$ and a stochastic component $R(\mathbf{u}, t)$. The deterministic trend function $m(\mathbf{u}, t)$ is modelled by fitting various polynomial functions coupled with a periodic (cosine and sine trigonometric functions) function in time t scales to the morbidity incidence data $I(u_\alpha, t)$, following (3.4.2). The following second order polynomial nested with the periodic function of cosine and sine is obtained as the best fitting model to obtain (5.2.1):

$$m(\mathbf{u}_\alpha, t) = b_0(\mathbf{u}_\alpha) + b_1(\mathbf{u}_\alpha)t + b_2(\mathbf{u}_\alpha)t^2 + b_3(\mathbf{u}_\alpha)\cos[(2\pi/\lambda)t] + b_4(\mathbf{u}_\alpha)\sin[(2\pi/\lambda)t] \quad (5.2.1)$$

where $\lambda = 12$ months, being the seasonal period of the morbidity incidence data. The model coefficients $b_0(\mathbf{u}_\alpha)$, $b_1(\mathbf{u}_\alpha)$, $b_2(\mathbf{u}_\alpha)$, $b_3(\mathbf{u}_\alpha)$ and $b_4(\mathbf{u}_\alpha)$ are computed by regressing the incidence data $\{I(\mathbf{u}_\alpha, t); t = 1, \dots, 132\}$, as response variable at each location (\mathbf{u}_α, t) , $\alpha = 1, \dots, 138$, on the second order polynomial and trigonometric basis functions of time t which spans 132 months from January 2000 to December 2010, following the OLS method (3.4.4). The computed trend coefficients are presented in Appendix D-1 together with the coefficients of determination (r^2). The temporal profiles of the morbidity incidence rates, superimposed with the estimated trend model (5.2.1), at selected district locations across the study area are presented in Figure 5.2.1 (and Appendix B-1). The base maps of the trend coefficients and coefficients of determination, which account for the proportion of the variation explained by the basis functions used in the model, are shown in Figure 5.2.2.

The morbidity incidence rate profiles at the district locations which have been superimposed with the trend model indicate varied temporal pattern of distributions, capturing various aspects of the incidence variability (see Figure 5.2.1). This is evidenced by the trend coefficients values which exhibit various negative and positive values (see Figure 5.2.2 and Tables D-1.1 and D-1.2 in Appendix D-1). The b_0 – values estimate the incidence rates at the onset of the study (January 2000 but 1998 for

BAR) which tend to be lower in the central and north-eastern parts of Ghana but relatively higher at district locations in the northern and some other parts. The negative values are associated with the district locations where there were no case-reports for the disease at the start of the study. The corresponding linear terms (b_1 – values) tend to be highly positive resulting in high correlations between the intercepts b_0 and the trend coefficients (b_1 and b_2), with the intercept estimates having a stronger negative correlation (-0.9585) with b_1 . The inverse relationship is inherent in any modelling procedure where a high intercept results in smaller slope or vice-versa (Kyriakidis & Journal, 2001).

As observed from the base maps in Figure 5.2.2 and the parameter tables in Appendix D-1, there are quite a number of negative b_1 and b_2 values which indicate the long-term decrease of the morbidity incidence rates at these locations whilst positive values indicate a long-term increase over the period of study 2000-2010. These are typically illustrated by the different temporal profiles of the incidence rates as shown by the graphs in Figure 5.2.1. Generally, there is an increased risk of malaria morbidity across the country, except in the north-west parts where the risk appeared to have been reduced over the years under study. The coefficients b_3 and b_4 are associated with amplitude and phase of the annual cycles in the time series data whilst the coefficients of determination (r^2) account for the proportion of the morbidity incidence's variation that can be explained by the trend model for the long-term trend and cycles in the incidence data. The coefficient of determination values, range from 0.195 to 0.912 with an average of 0.673, indicating that most of the districts' incidence rate profiles differ significantly from the spatial average profile. It is also observed from the base map (shown in Figure 5.2.2) that high values of r^2 are estimated in the northern (mostly at the district locations in the Upper East Region) and central parts of the country.

Further analysis of the trend coefficients by spatial regionalisation is considered. The regionalised coefficients of the trend model are presented in section 5.2.2 for the trend surfaces of the morbidity risk to be computed in section 5.2.3.

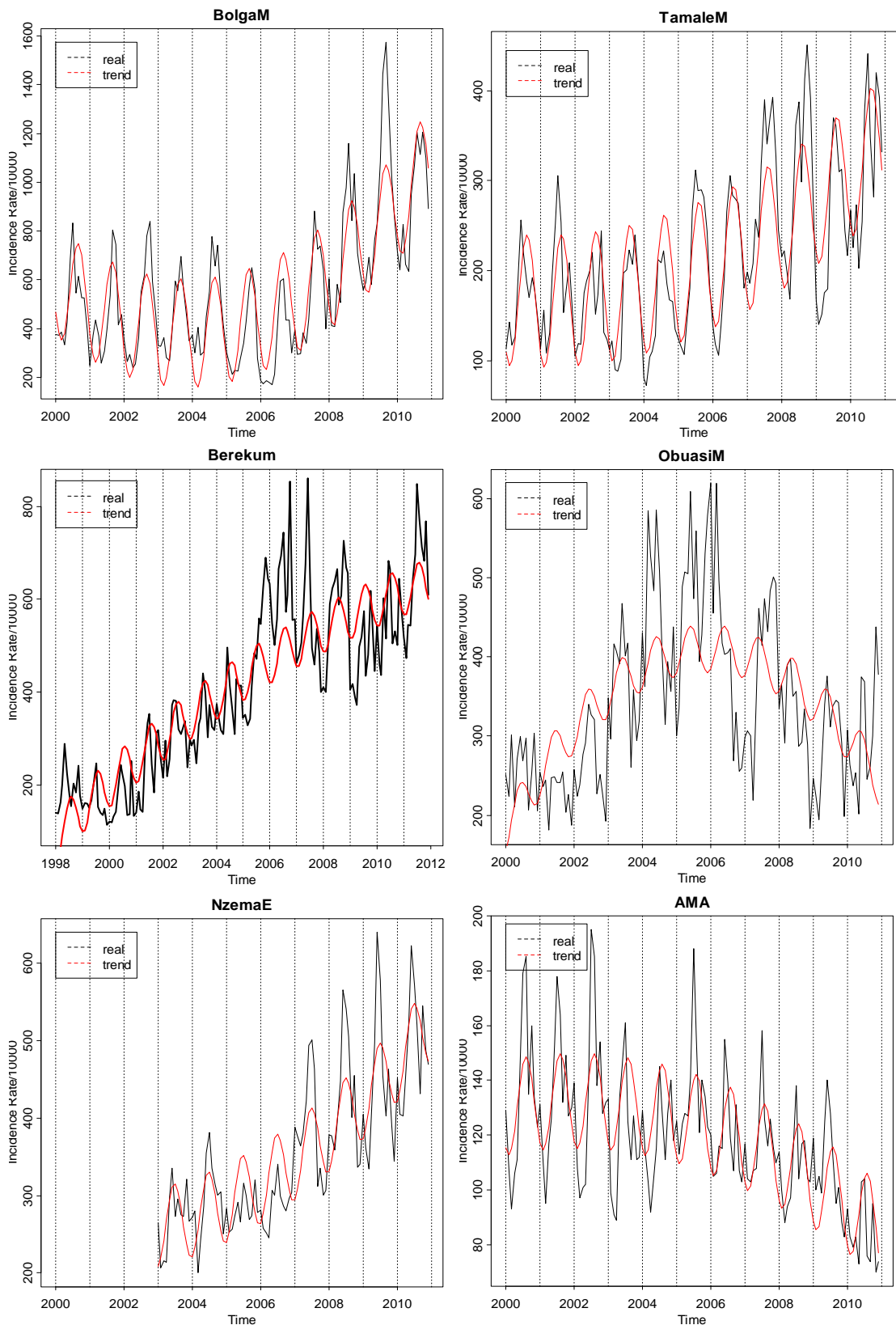


Figure 5.2.1: Temporal profiles of the morbidity incidence rates superimposed with the estimated trend model (5.2.1) at some district locations selected across the study area, Bolgantaga and Tamale municipals in Northern zone, Berekum and Kumasi (KMA) in forest zone and Nzema East and Accra (AMA) in coastal zone.

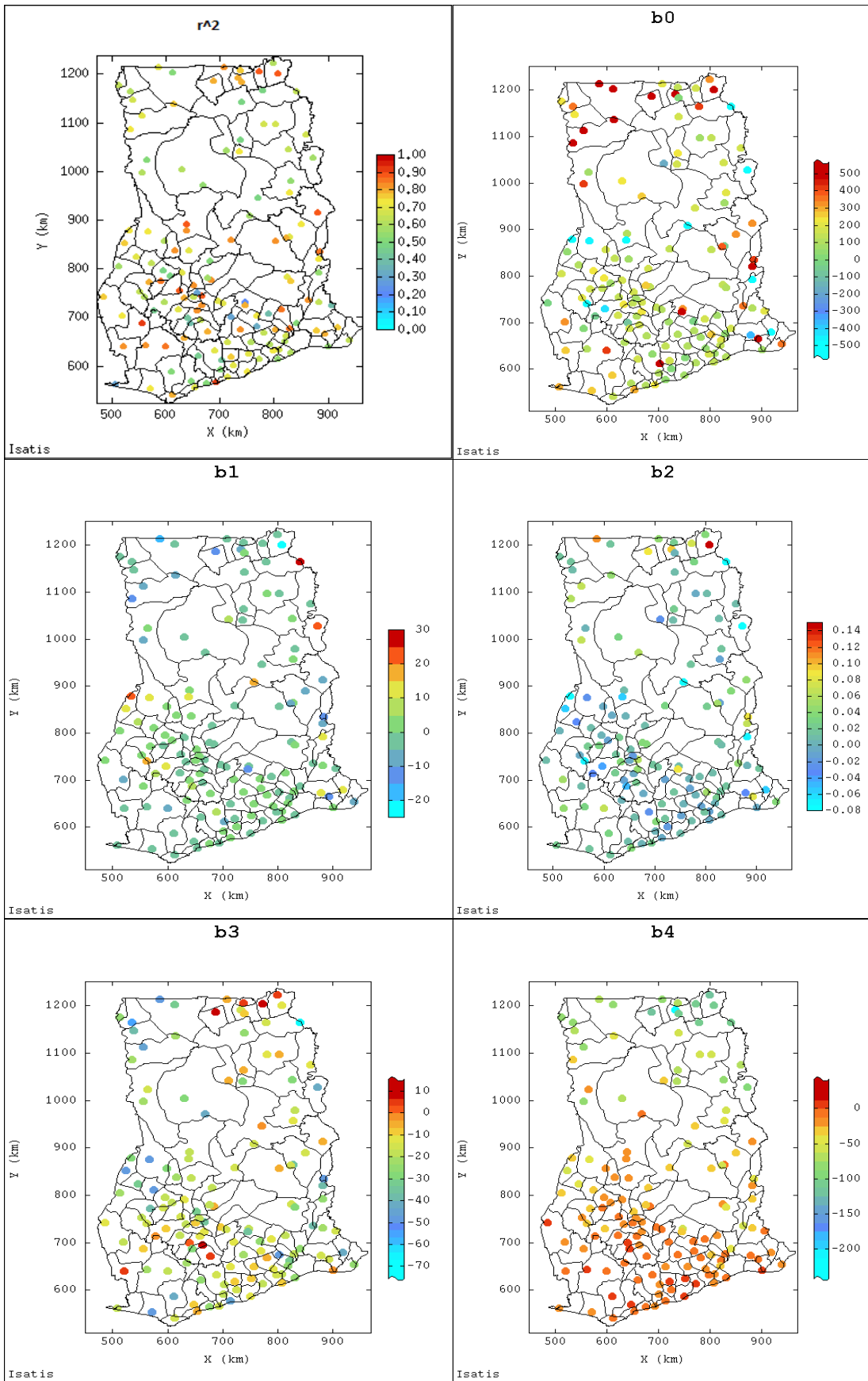


Figure 5.2.2: Base maps of coefficients of determination (r^2), being proportions of the observed incidence variations explained due to the basis functions (top left) and coefficients of the trend model (b_0 , b_1 , b_2 , b_3 and b_4).

5.2.2 Regionalisation of Trend Model Coefficients

The trend coefficients, $\{b_i(\mathbf{u}_\alpha); i = 1, \dots, 4\}$, computed from model (5.2.1) in section 5.2.1, are treated as precise data but then modelled as outcomes of random variables in space (Kyriakidis et al., 2004) to obtain their spatial correlation structures and pave the way for the estimation of morbidity risk in space and time. Models for the spatial continuity of the coefficients are then obtained by calculating the experimental semivariogram $\hat{\gamma}_s^{(i)}(\mathbf{h}_s)$ for each trend coefficient $b_i(u_\alpha)$ and fitting a nested model consisting of spherical and exponential functions with a nugget effect. The experimental semivariograms were computed using a spatial lag spacing of 30 km for 15 lags (see Table E-1.1 in Appendix E-1) with an angular tolerance of 90° and a tolerance of 50% at slicing of height 1.55, which produced the best smoothing for the model fitting. The results of the model parameters for this global analysis are as displayed in Table 5.2.1 and the fitted semivariogram models are shown in Figure 5.2.3. Cross-validation of the semivariogram models of the trend coefficients (based on search neighbourhoods of 150 and 200 km and other parameters as specified in Table E-4.3 in Appendix E-4) are conducted to assess the ordinary kriging (OK) performance of the spatial interpolation of the coefficients. However, kriging with a search radius of 200 km of data locations was chosen as it yielded the least mean and standardised mean errors.

The experimental semivariograms show a consistent autocorrelation pattern in structure (except for that of the sine coefficient (b_4)) and appeared to be characterised by similar short and long ranges from 50 to 250 km. The relative nugget effect values increase from 0.329 for the intercept (b_0) to 0.393 for b_2 . There are extremely high semivariance values for the long lags. This could be attributed to the nature of pairs of district locations at these separation distances, where a disproportionate number of these pairs are cross-type (that is, districts of the same status, either metropolitan, municipal or just ordinary district are rarely found so close together), as more commonly seen in most cases where large health facilities such as hospitals, at distant locations from each other, are surrounded by a number of smaller health facilities (Gething et al., 2007). These different facility types are more likely to have different morbidity incidence rate values than their spatial separations would otherwise suggest, resulting in a relatively larger semivariance values at the short and/or long lags

(Gething et al., 2007). This is the typical case for this study in Ghana. For example, each of the regional administrative capitals (such as Accra in Greater Accra Region or Sunyani in Brong Ahafo Region) is district location, which also serves as either municipal or metropolitan and mostly bordered with other smaller districts in the region.

Table 5.2.1: Spatial semivariogram model parameters of the regionalised trend model coefficients of morbidity incidence rates for the national study involving all the district locations

Coefficient b_i	Model $\gamma(h)$	Sill (c_s)	Range r_s (km)	Relative Nugget
(Intercept) b_0	<i>nugget</i>	25000	-	0.329
	<i>spherical</i>	21000	65	
	<i>exponential</i>	30000	200	
(t) b_1	<i>nugget</i>	15	-	0.357
	<i>spherical</i>	12	65	
	<i>exponential</i>	15	210	
(t^2) b_2	<i>nugget</i>	0.00055	-	0.393
	<i>spherical</i>	0.00030	65	
	<i>exponential</i>	0.00055	200	
(cos) b_3	<i>nugget</i>	55	-	0.297
	<i>spherical</i>	30	50	
	<i>exponential</i>	100	190	
(sin) b_4	<i>nugget</i>	50	-	0.110
	<i>spherical</i>	50	60	
	<i>exponential</i>	450	250	

The ordinary kriging (OK) technique was then used, as outlined in section 2.4.2 of chapter 2, to obtain the interpolated surfaces of $\{b_i(\mathbf{u}_\alpha)\}$ at unobserved locations \mathbf{u} by employing the modelled semivariograms and 8 to 20 closet neighbouring observations within the search circle radius of 200 km as inputs, following the Matheron estimator (2.3.16) and models (3.4.5) to obtain the optimal OK estimates of $\{b_i(\mathbf{u}_\alpha)\}$:

$$b_i^{ok}(\mathbf{u}) = \sum_{\alpha_i=1}^{n(\mathbf{u})} \lambda_{\alpha_i}^{ok}(\mathbf{u}) b_i(\mathbf{u}_\alpha), \quad i = 0, 1, \dots, 4, \quad (5.2.2)$$

which leads to the prediction of month by month spatial maps of the global trend surfaces of the morbidity risk. The grid interpolated surfaces of the estimated trend coefficients of the morbidity incidence are given in Figure 5.2.4. The results give a strong indication of linear rise of the morbidity incidence rates across the country. The

suurface of b_0 portrays a high incidence rates of the disease from onset of the study, especially in the northern parts whilst that of b_1 shows a pattern of high linear increase of incidence in the south-eastern and western through to the north-eastern parts of the country.

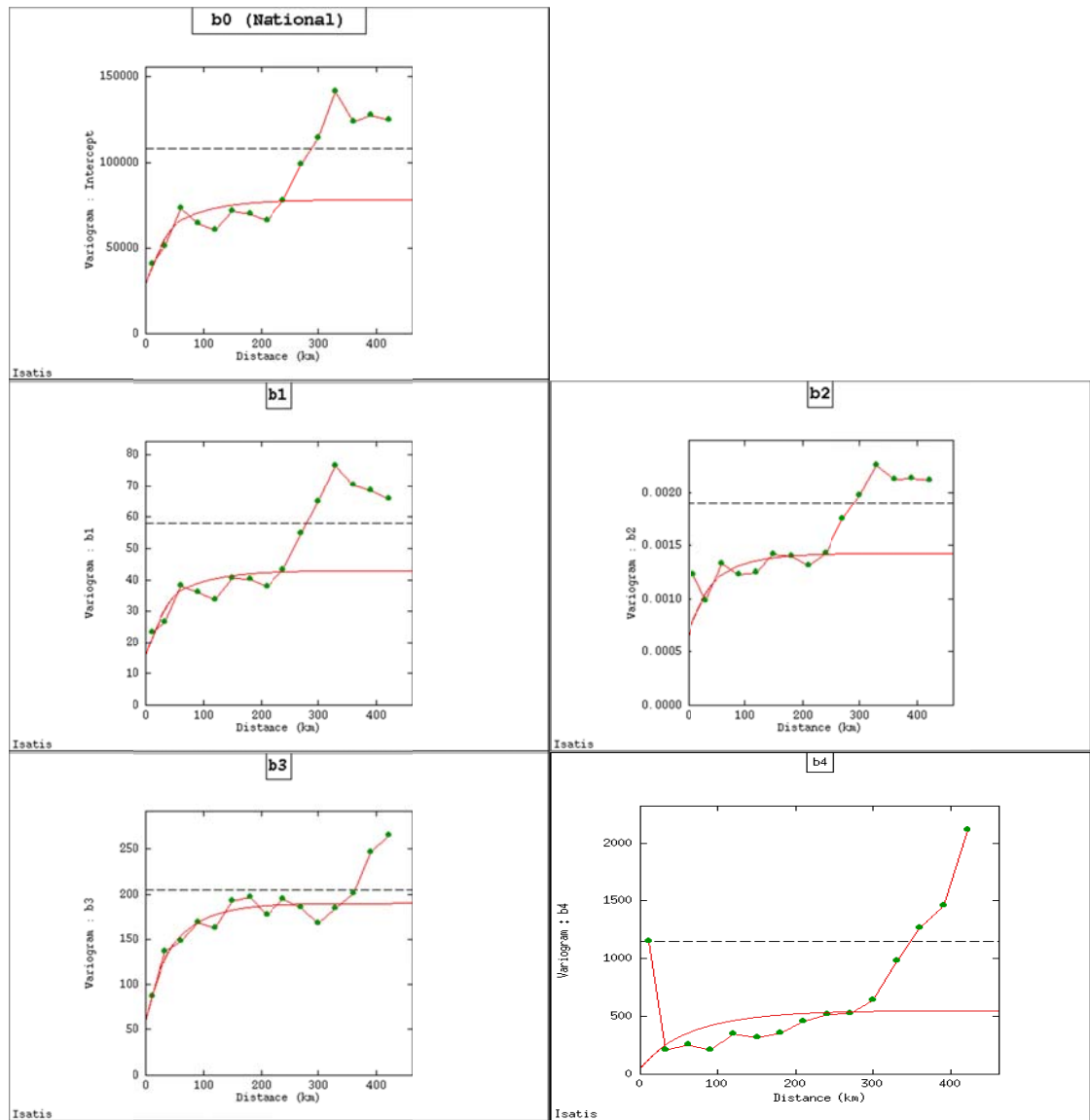


Figure 5.2.3: Spatial experimental semivariograms (dotted green) with fitted variogram models of trend model parameters (coefficients) of the morbidity incidence rates for the national study.

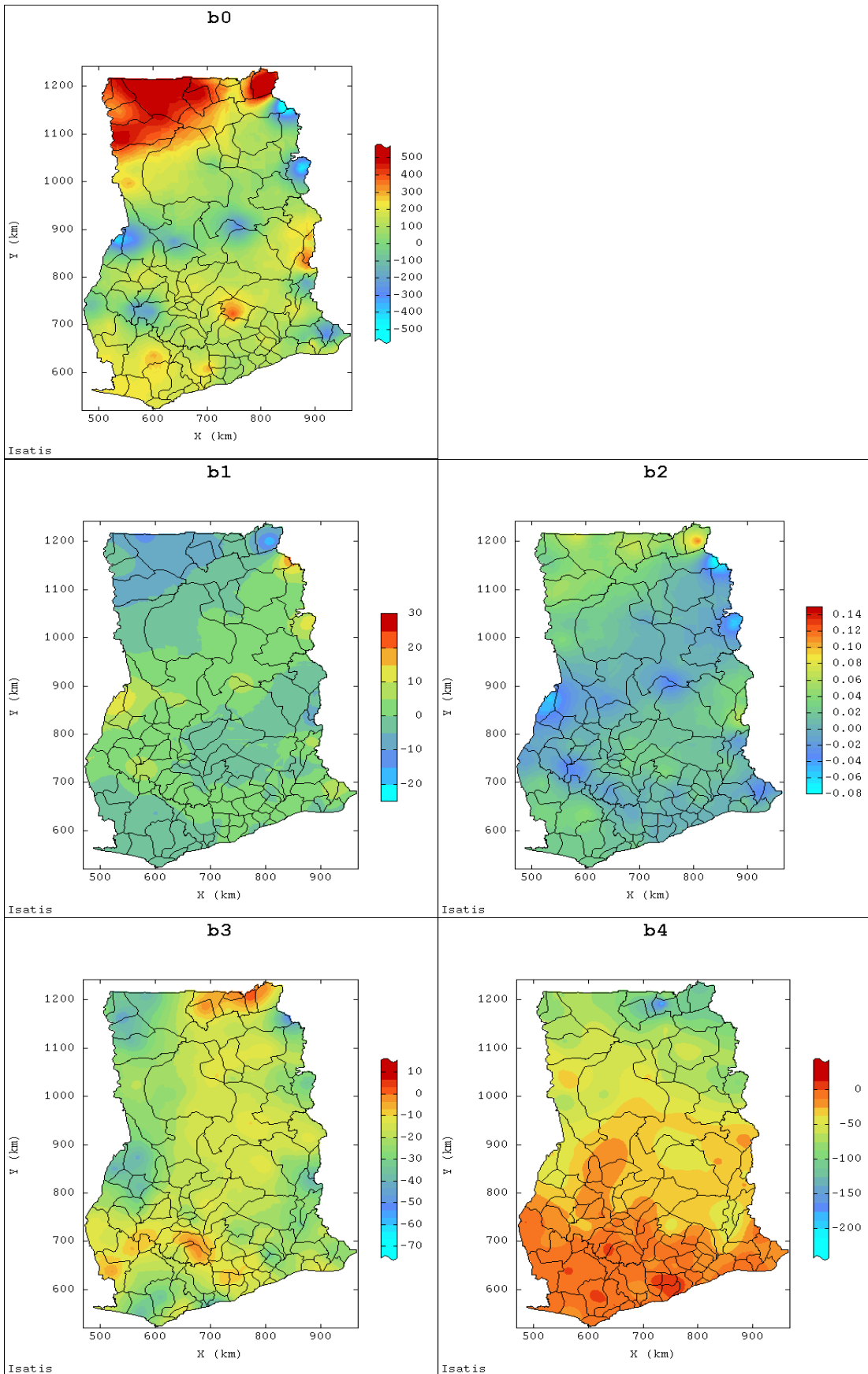


Figure 5.2.4: Spatial interpolated surfaces of trend model coefficients as computed by the optimal linear predictor (5.2.2).

5.2.3 Estimation of Global Trend Surfaces of MIR

The monthly global trend surfaces of the morbidity incidence rates are computed, following the optimal predictor (5.2.3), via a batch file looping in the ISATIS software program (Geovariances, 2013):

$$\hat{m}_{ok}(\mathbf{u}, t) = \sum_{i=0}^2 b_i^{ok}(\mathbf{u}) t^i + b_3^{ok}(\mathbf{u}) \cos[(2\pi/12)t] + b_4^{ok}(\mathbf{u}) \sin[(2\pi/12)t], \quad (5.2.3)$$

for each $t = 1, \dots, T$. The generated spatial maps for the estimated trend surfaces of the malaria morbidity risk at the district locations are labelled from “Month 1” (January 2000) to “Month 132” (December 2010), except BAR which produced 156 spatial maps, starting from January 1998 to December 2010. In the case of the national study, the trend surfaces can be interpreted as the average estimated risks of the morbidity for each district location for the total period of 132 months, starting from the year 2000. These estimates will provide the baseline for the space-time prediction process to be considered in the following sections. Figures 5.2.5 and 5.2.6 provide the spatial maps for some selected months for transition period from 2000–2004 to 2006–2010, whilst the other risk maps are shown in Appendix D-2.

As observed from the monthly spatial maps, the temporal trend surface profiles of the incidence rates follow similar distributional pattern of morbidity risk within the whole country. Generally, there have been varied spatial and temporal transmissions of malaria incidence over the years under review. There is also a transition of both high and low morbidity incidence which is observed from the period 2000–2005 to 2006–2010 in several parts of the country (see Figures 5.2.5 and 5.2.6 and Appendix D-2). This is particularly seen in the north-west, where the initially high risk of malaria morbidity has moved to the north-east, whilst suspected district locations in the west and central parts have consistently increased their incidence of the disease. There is also potentially increasing risk of malaria morbidity towards the coast and south-east locations. The rise in the risk of malaria morbidity during the period 2006–2010 appear to cover larger geographical area with locations of high incidence rates mostly found in the northern and western parts close to the borders with neighbouring countries. The temporal trend surfaces of the estimated incidence for months from May to November are observed higher for most parts of the country. These months are the typical rainy weather period during which breeding sites of mosquitoes increase resulting in high malaria transmission.

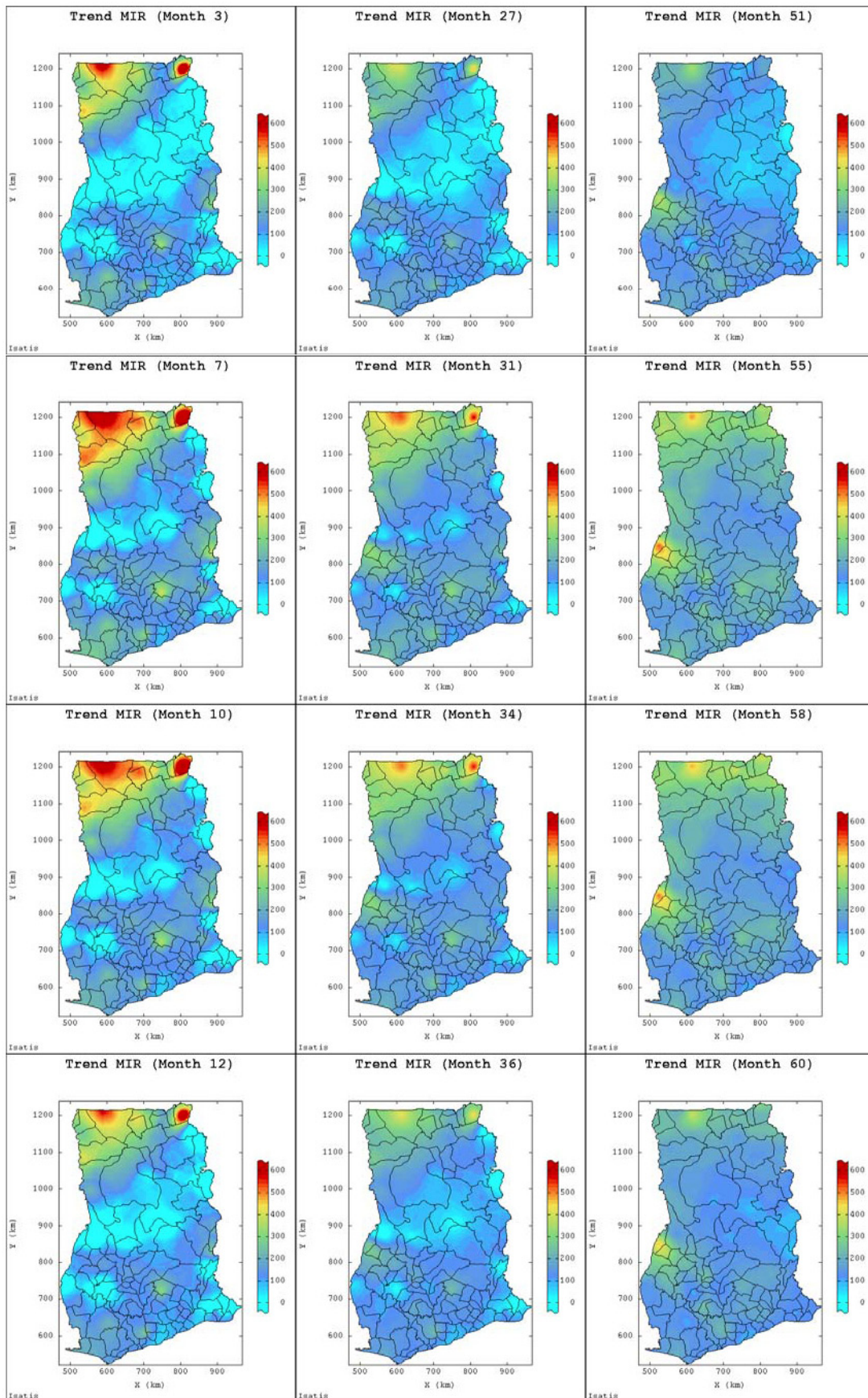


Figure 5.2.5: Estimated trend surfaces of the morbidity incidence rates for the selected months March, July, October and December (from top to bottom) for years 2000 (left), 2002 (middle) and 2004 (right).

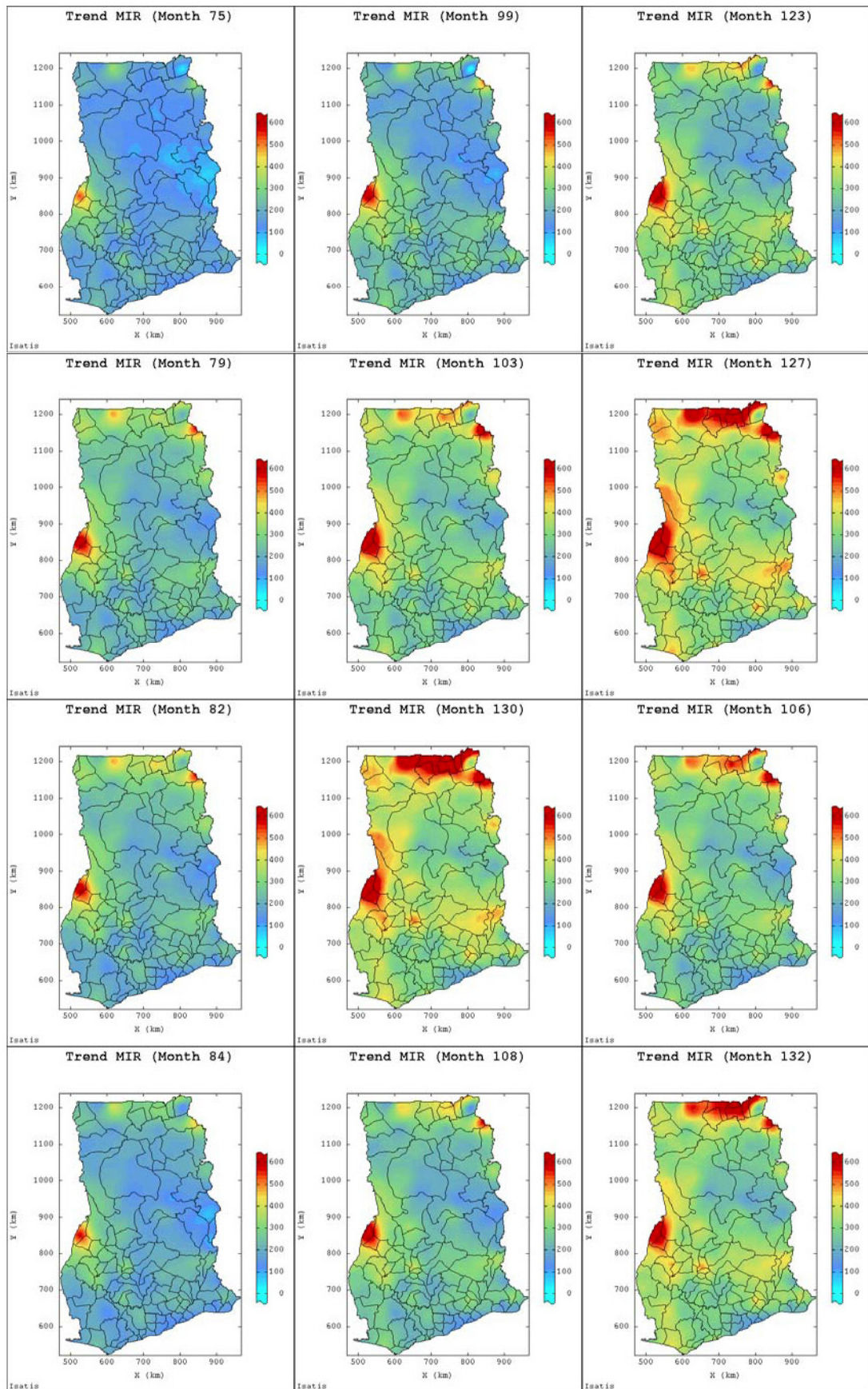


Figure 5.2.6: Estimated trend surfaces of the morbidity incidence rates for the selected months March, July, October and December (from top to bottom) for years 2006 (left), 2008 (middle) and 2010 (right).

5.3 Structural Analysis of Morbidity Incidence Rates

Structural analysis, as discussed in chapter 3, is one of the most important steps in geostatistical analysis. It is explored in this section for further investigation into the spatio-temporal correlations of the observed morbidity incidence rates (MIR). Space-time semivariogram models are used to characterise the correlations structure of the incidence rates at the district locations and over time across the whole study area. Initial exploration of the space-time data analysis indicated no obvious evidence of anisotropy in the spatial domain for short separation distances mostly less than 250 km (see variogram maps in Figure 4.3.3). Thus, all the experimental semivariograms were calculated and modelled as isotropic using a spatial angular tolerance of 90° and lag tolerance 50% at slicing height of 1.55 whilst the the temporal domain used an angular tolerance of 10° . The appropriate lag spacings in both domains for the construction of experimental space-time semivariograms for the whole study area in Ghana (national) and the two other studies in the Brong Ahafo Region and three vegetation zones are provided in the calculation parameter table in Appendix E-1. The structural analysis of the space-time data conducted in this section includes the variography of the log-transformed space-time MIR, residuals of the morbidity incidence rates and the generalised product-sum modelling of space-time semivariogram of the residuals.

5.3.1 Variography of Log-transformed Space-time MIR Data

The district-month morbidity incidence data $\{I(\mathbf{u}_\alpha, t); \alpha = 1, \dots, n; t = 1, \dots, T\}$, observed nationally and geo-referenced by the space-time coordinates (\mathbf{u}_α, t) , produced 14,568 sampled locations, representing 80% of the entire data locations. Initial exploration of the space-time morbidity incidence data sets showed highly positively skewed distributions, which were log-transformed to stabilise the variability and approximately tend to normality (see section 4.3.2 of chapter 4) and also allow space-time lognormal ordinary kriging (STLOK) to be used (Journel, 1980; Journel & Huijbregts, 1978). To account for the spatio-temporal distributions of the malaria risk at the district locations, the logMIR data, $Z(\mathbf{u}_\alpha, t) = \ln[I(\mathbf{u}_\alpha, t)]$ were first used to obtain the joint space-time experimental semivariogram, following (3.2.10) (Gething et al., 2007; Kyriakidis & Journel, 1999; Sherman, 2011), as presented in Chapter 3. Each district location is point-referenced by its spatial (\mathbf{u}_α) , being easting and northing (in kilometres), and temporal t locations, where the time (in months) is treated as the additional third

dimension. Ghana has a land area approximately of size 500 km by 750 km (see the elevation and vegetation zones maps in Figures 4.1.1 and 4.1.2, respectively), so choosing a lag spacing of 30 km for 15 lags with a tolerance of 50% and temporal lags for 70 months at 1 month spacing (as specified in Table E-1.1 in Appedix E-1) were sufficient to cover the required range and to calculate a smooth experimental semivariogram for the national data set, following (Cressie, 1993; Goovaerts, 1997). The resultant space-time experimental semivariogram was fitted using the nested model (5.3.1) comprising of two isotropic models, spherical (*sph*) and exponential (*exp*), and a periodic function, exponential-cosine (*cos exp*) of period 12 coupled with a nugget effect as denoted by (5.3.1):

$$\gamma_{st}(\mathbf{h}_s, h_t) = nug(h_0) + c_{s1} sph(h_s/r_{s1}) + c_{s2} \exp(h_s/r_{s2}) + c_t \cos \exp(h_t/r_t) \quad (5.3.1)$$

where $nug(h_0)$ represents the nugget effect in both spatial and temporal directions; c_{s1} and r_{s1} denote partial sill and range for spherical model structure respectively; c_{s2} and r_{s2} denote the respective sill and range for exponential model structure; and c_t and r_t are the sill and range of the exponential-cosine model used in the temporal domain. Although the exponential-cosine model is only semi-definite, when nested with a conditionally negative-definite model, it results in a valid semivariogram model (De Iaco et al., 2003). Also modelled by (5.3.1) for comparison with the same lag spacings is the experimental semivariogram for observed (untransformed) MIR (shown in Table E-1.2 in Appendix E-1). Table 5.3.1 presents the space-time semivariogram model parameters whilst the fitted experimental semivariograms are as shown in Figure 5.3.1.

The space-time experimental semivariogram of the log-transformed morbidity incidence rates shows that there is strong evidence of both spatial and temporal dependence of incidence of the disease at the local (district) levels across Ghana, as indicated by the smaller values of the nugget-to-sill ratios (relative nugget effects) values. As per (5.3.1), the experimental semivariogram in spatial domain is modelled as isotropic with the spherical and exponential functions nested with a nugget effect of 0.025. The space-time semivariogram model exhibits both short and long ranges; the range of the spatial autocorrelations varies from 35 to 250 km with a maximum sill of 0.208 compared with the semivariogram of the untransformed incidence data which has relatively a longer range of autocorrelation, varying between 30 and 300 km (see

Table E-1.2 in Appendix E-1). The temporal component which differs significantly in structure from the spatial is fitted using the exponential-cosine function of period 12 plus the same basic structures for the spatial domain modelling. It also exhibits a linear trend with annual cycles of the incidence rates until it attains its maximum sill of 0.228 at the shortest temporal range of correlations of 85 months (see Figure 5.3.1), providing further evidence of seasonality in the observed incidence rates of the disease.

Table 5.3.1: Space-time semivariogram model parameters of log-transformed malaria incidence rates data for the for the national study

Data	Model $\gamma(h)$	Sill c_s / c_t	Spatial range r_s (km)	Temporal range r_t (months)	Relative Nugget
LogMIR	<i>nugget</i>	0.025	-	-	0.120
	<i>spherical</i>	0.112	35	85	
	<i>exponential</i>	0.071	250	300	(0.110)
	<i>expcosine</i>	0.020	10000	400	

Note: In parentheses is relative nugget effect in the temporal domain.

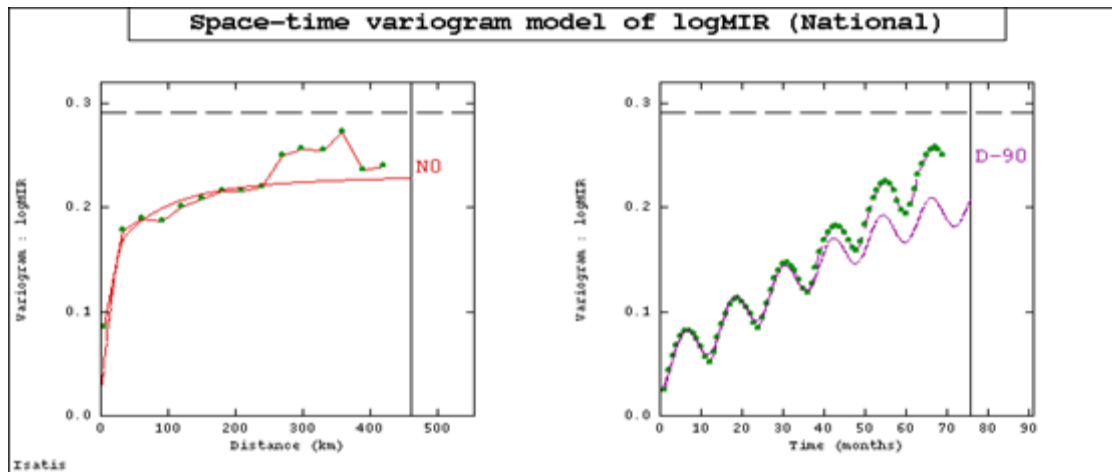


Figure 5.3.1: Space-time experimental semivariograms (dotted green) fitted with variogram models showing spatial (left) and temporal (right) autocorrelation of log-transformed malaria incidence rates for national study.

5.3.2 Variography of Space-time Residuals

The space-time residuals, $R(\mathbf{u}_\alpha, t)$ as per the temporal trend model (5.2.1), are considered as a space-time random function, $R = \{R(\mathbf{u}, t); (\mathbf{u}, t) \in \mathbf{D} \times \mathbf{T}\}$ where the spatio-temporal dependence of $I(\mathbf{u}, t)$ can be described by the semiovariogram of R . Following (3.2.10), the experimental semivariograms for the space-time residuals, were calculated using the lag spacing values as specified in Table E-1.1 in Appendix E-1. They were then fitted in both spatial and temporal domains with a nugget effect, two spherical variogram models and one exponential variogram model as denoted by

(5.3.2):

$$\gamma_{st}(\mathbf{h}_s, h_t) = \text{nug}(h_0) + c_{s1} \exp(h_s / r_{s1}) + c_{s2} \text{sph}(h_s / r_{s2}) + c_t \text{sph}(h_t / r_t) \quad (5.3.2)$$

The estimates of the model parameters and the space-time semivariogram model of the residuals produced for the national study are as shown in Table 5.3.2 and Figure 5.3.2, respectively.

The removal of the large-scale trend and variations in the temporal domain leads to the faster attainment of both sills of the semivariogram which then improves the modelling fitting with relatively fewer structures. The temporal range of correlation has reduced considerably with short and long ranges falling between 12 and 30 months whilst the sill continues to dominate that of the spatial (Table 5.3.2). The spatial range appears to remain the same as for the log-transformed modelling of the incidence rates, characterised with short and long ranges. Also, the variations in the residuals are observed to be much smaller in both domains with estimated total sills of 2950 spatially and 3700 temporally. The temporal correlation, by the relative nugget effect value of 0.351, is stronger compared with the spatial value of 0.441.

Table 5.3.2: Space-time semivariogram model parameters of residuals of observed morbidity incidence rates for the national study

Model	Sill	Spatial range	Temporal range	Relative Nugget
$\gamma(h)$		r_s (km)	r_t (months)	
<i>nugget</i>	1300	-	-	
<i>spherical</i>	800	35	12	0.441
<i>exponential</i>	850	250	15	(0.351)
<i>spherical</i>	750	10000	30	

Note: In parentheses is the relative nugget effect in the temporal domain.

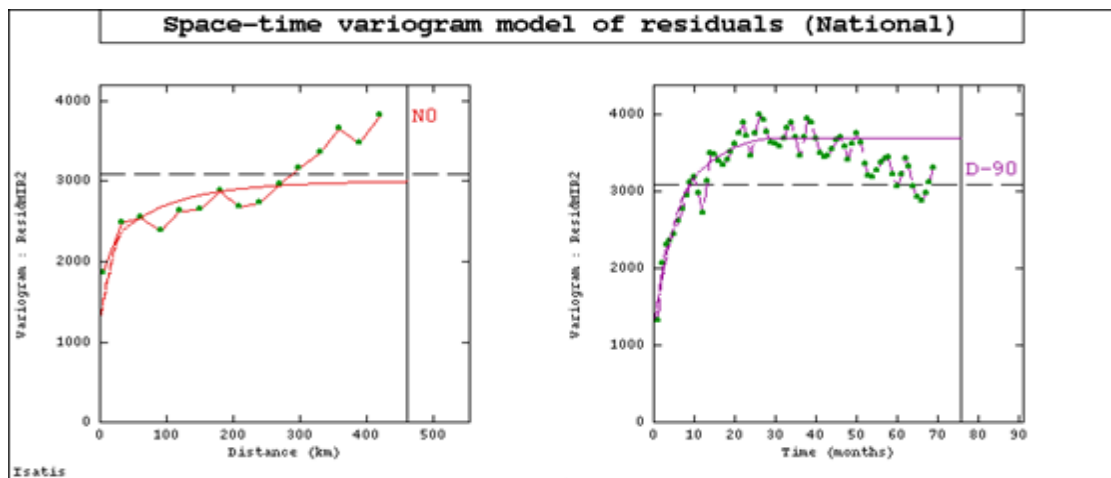


Figure 5.3.2: Space-time experimental semivariograms (dotted green) with fitted variogram models of residuals of observed morbidity incidence rates for national study.

5.3.3 Product-Sum Semivariogram Modelling of MIR

The generalised product-sum model (De Iaco et al., 2001; De Iaco & Posa, 2012), as given in (3.2.33), is considered and applied in this section to characterise the spatio-temporal continuity of the morbidity incidence rates. This choice, as already discussed in chapter 3, is informed by its relatively wide spread of application, efficiency and flexibility. Following the modelling procedure as outlined in sections 3.2.3 and 3.2.4, the space-time semivariograms of the residuals, $R(\mathbf{u}_\alpha, t)$ were estimated (including that for each other two case studies being investigated in this thesis, as presented in sections 5.7 and 5.8). The space-time experimental semivariograms were calculated using the spatial and temporal lag spacing values specified in Table E-1.1 in Appendix E-1. In each case study, the number of lags has been chosen to allow the maximum spatial lag distance (250–450 km) and the maximum temporal lag time (80–100 months) to be attained (Deutsch & Journel, 1998; Goovaerts, 1997). The marginal spatial and temporal semivariograms have also been obtained and modelled separately with nugget effects, using a single structure of an exponential model and/or a spherical model, respectively. The space-time experimental semivariogram surfaces were plotted and the global sills $C_{st}(\mathbf{0}, 0)$ determined by a visual inspection, which were then used to compute the space-time parameter k , following (3.2.32) for the generalised product-sum model to be obtained and space-time semivariogram surfaces plotted. The values of the global sills have all been chosen to be greater than both the total spatial and temporal sills but less than the their sum in order to satisfy condition (3.2.30) and ensure validity of fitting product-sum modelsto the space-time experimental semivariograms (De Iaco et al., 2001).

A modified GSLIB program, *gamvmod.exe* (De Cesare et al., 2002), as per the parameter file shown in Appendix H-2.1, was used to compute and model the experimental semivariograms of the malaria incidence data. This is complemented by the R version 2.13.2 (R Development Core Team, 2011) functions and code, which were used for the post-processing of the results generated. Table 5.3.3 provides the parameters of the marginal spatial and temporal semivariogram models as well as the space-time generalised product-sum semivariogram model of the residuals for the national study. Figure 5.3.3 displays graphs of the marginal semivariograms and the space-time semivariogram surfaces produced from the model fitting. In Appendix E-1

are the space-time experimental surface and its marginal semivariograms of the observed malaria incidence rates $I(\mathbf{u}_\alpha, t)$ together with their model parameters.

Table 5.3.3: Parameters of the marginal semivariograms and product-sum semivariogram models of the detrended and deseasonalised (residuals) of the observed malaria incidence rates for the national study

Model	Spatial		Temporal		Product-sum	
	Sill (RN)	Range	Sill (RN)	Range	Global Sill	k
<i>nugget</i>	1300 (0.481)	-	1300 (0.342)	-		2.583×10^{-4}
<i>exponential</i>	1400	110	-	-	3850	(2.667×10^{-4})
<i>exponential</i>	-	-	2500	16		

In parentheses are the relative nugget (RN) effects of marginal semivariograms and maximum k limit values for the product-sum model.

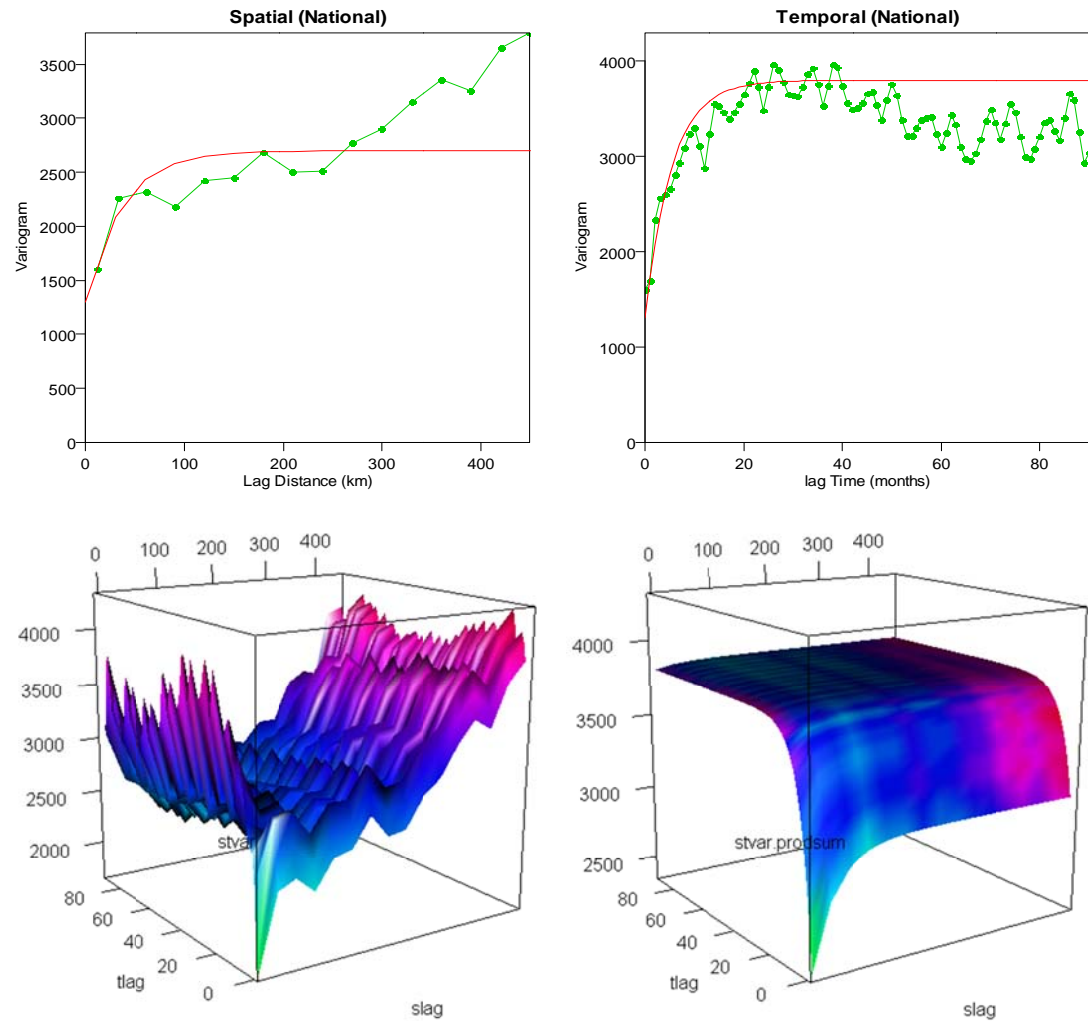


Figure 5.3.3: Marginal spatial and temporal semivariograms models (top) and space-time experimental semivariogram and product-sum models (bottom) of detrended MIR (residuals) for the national study.

The marginal temporal semivariograms of the observed morbidity incidence rates (as observed from Figure E-1.2 in Appendix E-1) produced continuous upward trend and seasonal variations in the incidence data (as opposed to the residuals). The generalised product-sum model, when applied to the detrended and deseasonalised space-time incidence rates (residuals) data, improved the model fit, using two exponential variogram models with nugget effects (see Table 5.3.3 and Figure 5.3.3). The nugget effects of the marginal semivariograms are comparable with the joint space-time semivariogram model of the residuals (in section 5.3.2) with same values. However, the relative nugget effect values for marginal spatial and temporal semivariogram models which are 0.481 and 0.342 respectively differ slightly in each domain from the joint modeling in section 5.3.2. The shapes of the marginal semivariograms are similar to the ones produced by the joint space-time modelling approach applied to the residuals incidence data. However, the product-sum semivariogram model used fewer basic structures to fit to the space-time experimental semivariograms, characterising the spatial continuity of the incidence of the disease with shorter ranges and smaller sills. It produced a global sill of 3850 whilst the range of the autocorrelation varies within 110 km and 16 months compared with the range of correlations of 35–250 km (spatially) and 12–30 months (temporally) of the joint model (5.3.2).

5.3.4 Neighbourhood Selection for the Space-time Models

Cross-validation of the semivariogram models established in the previous sections is performed in this section to ascertain the suitability of the space-time models for prediction of the malaria incidence rates and to select suitable search neighbourhoods for the subsequent space-time kriging process of the incidence rates at the district locations. Accordingly, the kriging processes were carried out using the various moving (search) neighbourhoods as specified in Table E-4.1 in Appendix E-4. Such a choice of a search neighbourhood is deemed convenient as it reasonably limits the stationarity assumption to small areas for the kriging techniques to be appropriately applied to the non-stationary morbidity incidence with varying mean but stationary semivariogram (Berterretche et al., 2005; De Iaco & Posa, 2011; Journel & Rossi, 1989). In the case of the national study the cross-validation processes were conducted using search neighbourhoods of radii varying between 100 and 250 km and within a period of 5 months with a minimum of 2 nodes and maximum of 20 nodes. ISATIS version 2013 and GSLIB software packages were used to produce the estimates of the

incidence rates.

The results included the kriging estimation errors, correlations between the estimates and the observed incidence rates and some graphical display of the estimates. The space-time model estimates which characterise the malaria morbidity risk at the district locations nationally are presented in Table 5.3.4. The graphical summaries of the models, consisting of the basemaps for the data; scatter plots of the true values versus the estimates; histograms of the standardised errors; and scatter plots of the standard errors against the estimated values are displayed in Figures E-4.1 and E-4.2 in Appendix E-4.

Table 5.3.4: Cross-validation estimates of the semivariogram models for different moving neighbourhoods within a period of 5 months with number of samples per angular sector for national study area.

Model	Neighbourhood		Error		Standardised Error		Corr. Coeff.
	Search radius	No. of samples	Mean	Variance	Mean	Variance	
STOLK (logMIR)	150km	2 – 10	0.00100	0.02646	0.00465	0.68618	0.953
		4 – 20	-0.00026	0.02576	-0.00144	0.67614	0.955
	200 km	2 – 10	-0.00064	0.02559	-0.00337	0.69091	0.950
		4 – 20	0.00012	0.02491	0.00048	0.64127	0.956
	250 km	2 – 10	-0.00698	0.04850	-0.00942	0.77435	0.912
		4 – 20	-0.00024	0.02640	-0.00126	0.65743	0.954
STROK (Residuals)	150 km	2 – 10	-0.03304	1716.087	-0.00059	0.89809	0.659
		4 – 20	0.07627	1702.647	0.00183	0.88422	0.662
	200 km	2 – 10	0.06859	1534.180	0.00137	0.74320	0.705
		4 – 20	0.01559	1567.302	0.00019	0.77644	0.698
	250 km	2 – 10	0.14966	1673.845	0.00266	0.75263	0.670
		4 – 20	0.06497	1567.370	0.00118	0.76538	0.699
STROK_PS (Residuals)	200 km	2 – 10	-0.04236	1808.373	-0.00080	0.81534	0.699
		4 – 20	-0.04236	1808.373	-0.00080	0.81534	0.699
	200 km	2 – 10	-0.04236	1808.373	-0.00080	0.81534	0.699
		4 – 20	-0.04236	1808.373	-0.00080	0.81534	0.699
	200 km	2 – 10	-0.04236	1808.373	-0.00080	0.81534	0.699
		4 – 20	-0.04236	1808.373	-0.00080	0.81534	0.699

Generally, the mean error and standardised mean error of the estimates for the space-time predictive models, namely space-time lognormal ordinary kriging (STLOK) and the space-time ordinary kriging of the residuals by the joint modelling of the semivariogram (STROK) and that via the generalised product-sum modelling approach (STROK_PS) were small in magnitude, with the latter two well-centred around zero. Also, the estimates exhibited strong positive correlations with the observed values for all the neighbourhoods, ranging from 0.659 to 0.956. However, kriging using the search radius of 150 km or 200 km with closet samples ranging from 8 to 20 produced better results with least standardised errors and/or stronger correlations (see Table 5.3.4). The variance of the standardised errors were higher and close to 1 (by Wackernagel (1998) criterion as cited by Goovaerts (2009)), especially for STROK and STROK_PS which were 0.77644 and 0.81534, respectively. The histograms of the standard errors appear normally distributed though there are some outliers, as quite a number of the plots are located outside the 99% confidence limits (see Figures E-4.1 and E-4.2 in Appendix E-4). This could be attributed to some effects of interventions which were not considered in this study. A moving neighbourhood of search radius 200 km was deemed most suitable and thus chosen for the space-time kriging process of the national malaria morbidity risk to be considered in the following section.

5.4 Applications of Space-time Kriging Techniques to Morbidity Incidence Rates

Spatial statistical analysis of the morbidity incidence rates is conducted within the framework of geostatistics to produce malaria morbidity risk maps of Ghana, with the ultimate aim of illustrating the patterns of morbidity risk over space and time. In this section the space-time ordinary kriging techniques employed for the interpolation process of the morbidity incidence rates include the space-time lognormal ordinary kriging (STLOK), applied to the log-transformed morbidity incidence rates data, $\{Z(\mathbf{u}_\alpha, t)\} = \{\ln(I(\mathbf{u}_\alpha, t))\}$ and space-time ordinary kriging (STOK) of the observed morbidity incidence rates via the residuals data $\{R(\mathbf{u}_\alpha, t); \alpha = 1, 2, \dots, 138; t = 1, 2, \dots, 132\}$ arising from the detrending and deseasonalising of $I(\mathbf{u}_\alpha, t)$, using two approaches: by the joint modelling of space-time semivariogram of the residuals (STROK) and generalised product-sum modelling of the space-time semivariogram of the residuals (STROK_PS).

5.4.1 Space-time Lognormal Ordinary Kriging of MIR

Following the variography of $\{\ln I(\mathbf{u}_\alpha, t)\}$ in section 5.3.1, the nested semivariogram models from (5.3.1) were used as inputs for the space-time lognormal ordinary kriging (STLOK) applied to the log-transformed incidence data for estimation of the morbidity risk $\{I(\mathbf{u}, t)\}$ at district-month locations where data were missing or unobserved. A grid file approximately coinciding with the DEM interpolation grid in Figure 4.1.1 was created (see Table E-4.2 in Appendix E-4) after which the optimal linear predictor (STLOK) in (3.3.6) was used to interpolate $\hat{Z}_{stlok}(\mathbf{u}, t)$ in log-transformed scale. It was then back-transformed following (3.3.7), yielding the result $\hat{I}_{stlok}(\mathbf{u}, t)$, as the estimated values of the morbidity incidence rates at the unsampled location (\mathbf{u}, t) to produce the monthly morbidity risk maps. A selection of the monthly morbidity risk maps estimated by STLOK nationally for the years in 2000, 2002, 2004, 2006, 2008 and 2010 are shown in Figures 5.4.1 and 5.4.2, with the spatial maps for all months made available by Results E-5.1 in Appendix E-5.

The monthly spatial maps display seasonality and increasing morbidity risk of the disease occurring over time, particularly from the initial years 2000–2004 to 2005–2010. The results also indicate spatial heterogeneity across the country with highly elevated cases occurring at locations near the borders with the two neighbouring countries in the north (Burkina Faso) and west (Cote d’Ivoire) (see Figure 5.4.2) which equally report high incidence cases of malaria (WHO, 2008). The results are consistent with the seasonal variations in the occurrence of the disease, where low incidence cases are mostly observed during the months from January to April, whilst the months May to December are associated with the high risk of incidence. Nationally, high morbidity incidence rates are estimated in the northernmost and western areas extending to central parts towards the east, which are all located within the northern and forest zones. The initial years (2000–2004) are characterised predominantly with low incidence rates, mostly in the central parts of the north and along the coast in the south. However, malaria morbidity risk estimates for the disease are high for the later years (2008–2010) and cover larger geographical areas. The risk surfaces, as also observed from the spatial maps, appear rough. They can be smoothed to increase the prediction accuracy by the space-time kriging techniques considered in the following sections.

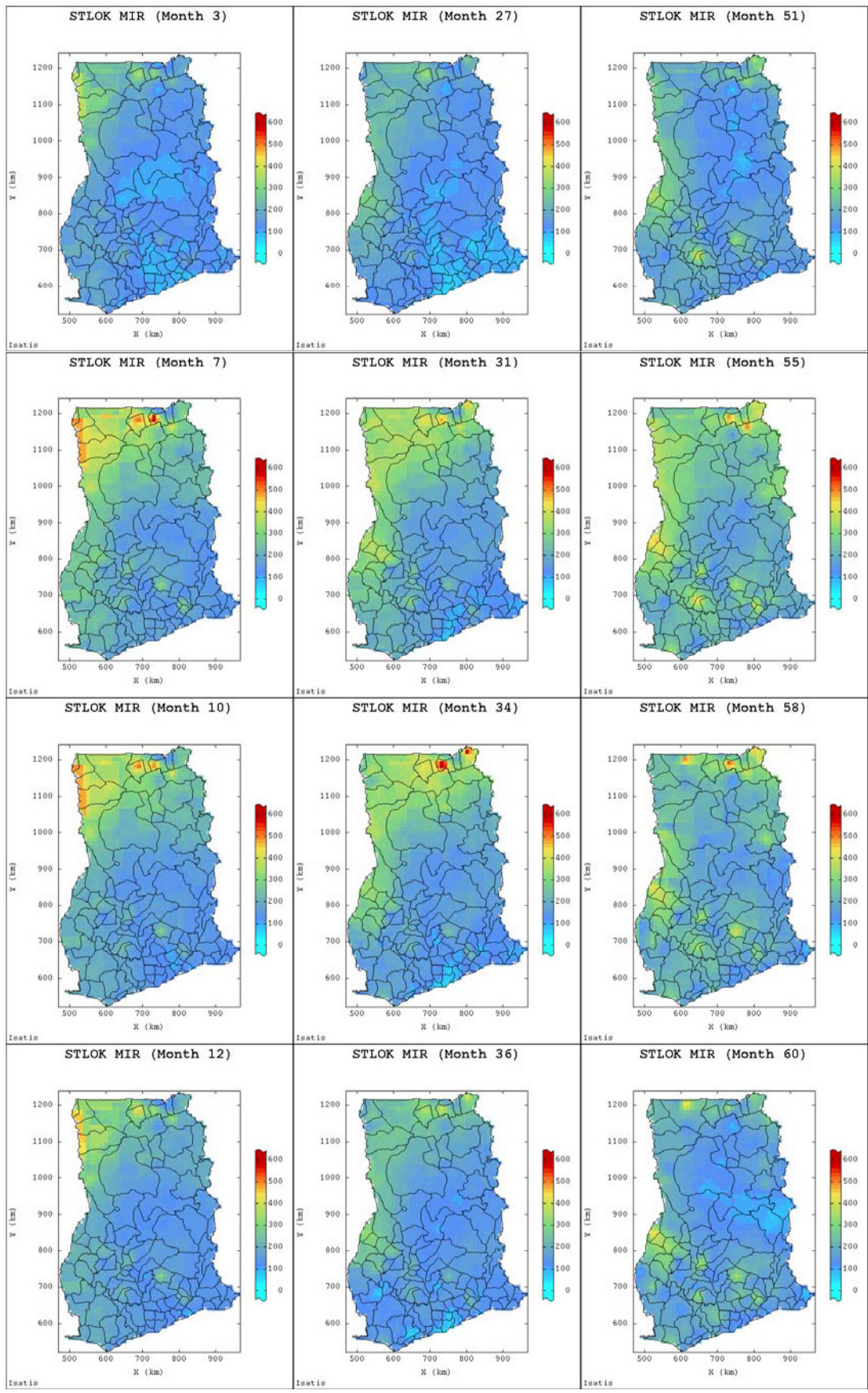


Figure 5.4.1: Morbidity incidence rates estimated by space-time log-normal ordinary kriging (STLOK) for the selected months March, July, October and December (from top to bottom) for years 2000 (left), 2002 (middle) and 2004 (right).

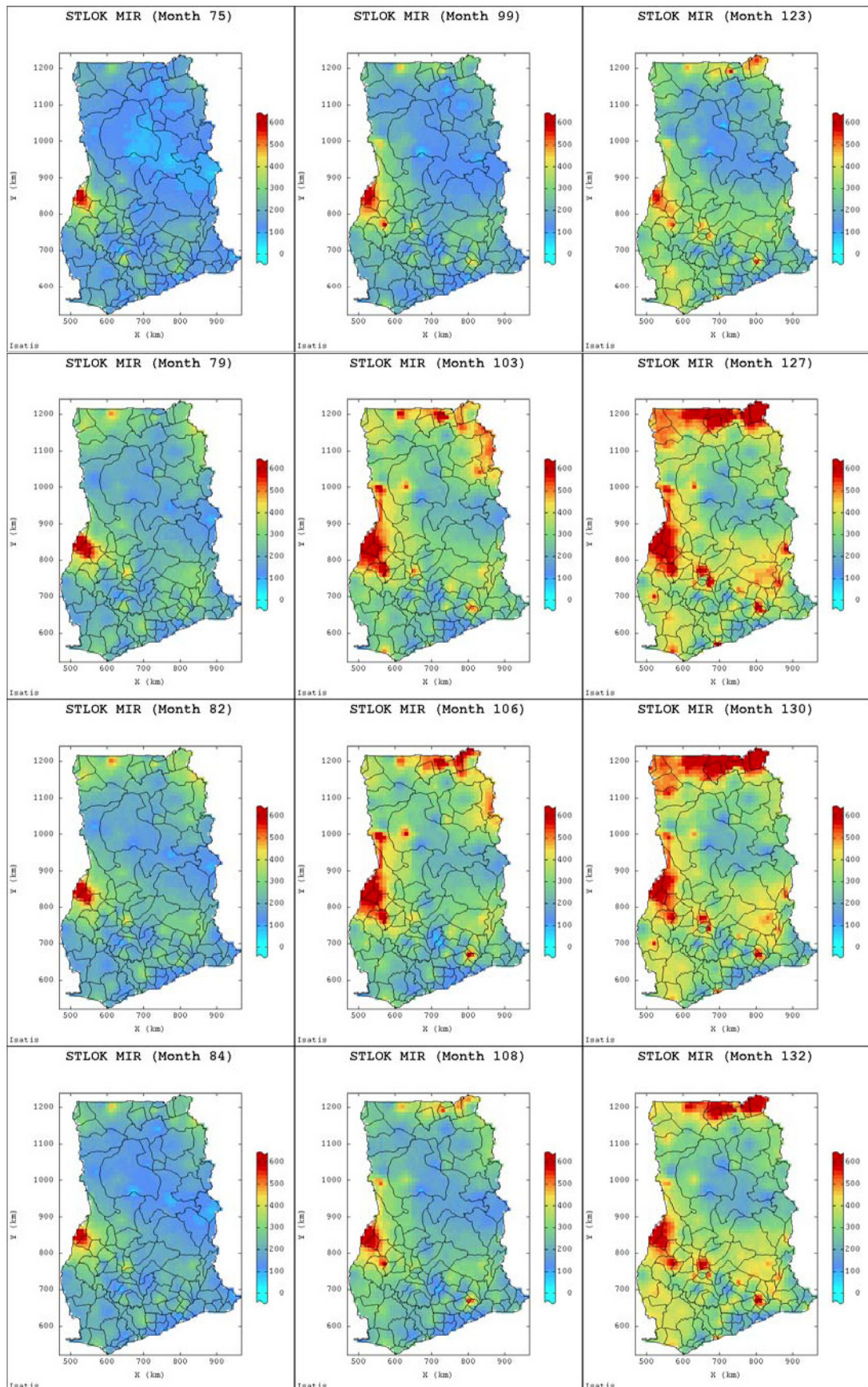


Figure 5.4.2: Morbidity incidence rates estimated by space-time lognormal ordinary (STLOK) for the selected months March, July, October and December (from top to bottom) for years 2006 (left), 2008 (middle) and 2010 (right).in 2000 (left) and 2005 (right).

5.4.2 Space-time Ordinary Kriging of Residuals

In this section the space-time ordinary kriging (STOK) is applied to account for the non-stationarity in the morbidity incidence data, as observed in the STLOK prediction in section 5.3.1. This is done by considering the incidence rates as a collection of finite number of spatially correlated time series at each district location. Thus, STOK is implemented using the joint space-time semivariogram model of the stationary random process $R(\mathbf{u}, t)$, which gave a better representation of the autocorrelation structure of the observed morbidity incidence rates (as was established section 5.3.2) and also a useful predictor of the morbidity risk at the district-month locations. The prediction process begins with the estimation of the monthly trend surfaces $\hat{m}_{ok}(\mathbf{u}, t)$, obtained by model (5.2.3) in section 5.2. The STOK technique using (3.3.2) was then applied to the space-time residuals $R(\mathbf{u}_\alpha, t)$, to interpolate at each grid node by applying the same search neighbourhoods as in the previous predictions to obtain $\hat{R}_{strok}(\mathbf{u}, t)$.

$$\hat{R}_{strok}(\mathbf{u}, t) = \sum_{\alpha=1}^n \sum_{t=1}^T \lambda_{\alpha t}^{stok} R(\mathbf{u}_\alpha, t) \quad (5.4.1)$$

The STOK estimates of the residuals $\hat{R}_{strok}(\mathbf{u}, t)$ obtained were added to the trend estimates $\hat{m}_{ok}(\mathbf{u}, t)$, which have been characterised spatially and temporally by the model (5.2.3), to obtain the monthly optimal prediction values of the morbidity incidence rates at the unsampled district locations (5.4.2):

$$\hat{I}_{strok}(\mathbf{u}, t) = \hat{m}_{ok}(\mathbf{u}, t) + \hat{R}_{strok}(\mathbf{u}, t), \text{ for each } t \in T. \quad (5.4.2)$$

A second modelling approach of generating the residual estimates $\hat{R}_{strok}(\mathbf{u}, t)$ is considered in section 5.4.3. Spatial maps of the estimated morbidity risk for the whole areas by the STOK model (5.4.2) are provided in Appendix E-5.2 whilst Figures 5.4.3 and 5.4.4 present the risk maps for the selected months in the years 2000, 2002, 2004, 2006, 2008 and 2010.

The spatial morbidity risk maps obtained by the STOK technique show similar spatial and temporal patterns as were estimated by the temporal trend model (5.2.3) and STLOK. However, the STOK results appear less variable as the spatial heterogeneity of morbidity risk of the disease tends to produce more smoothed surfaces spreading over larger geographical areas. The results also indicate transition

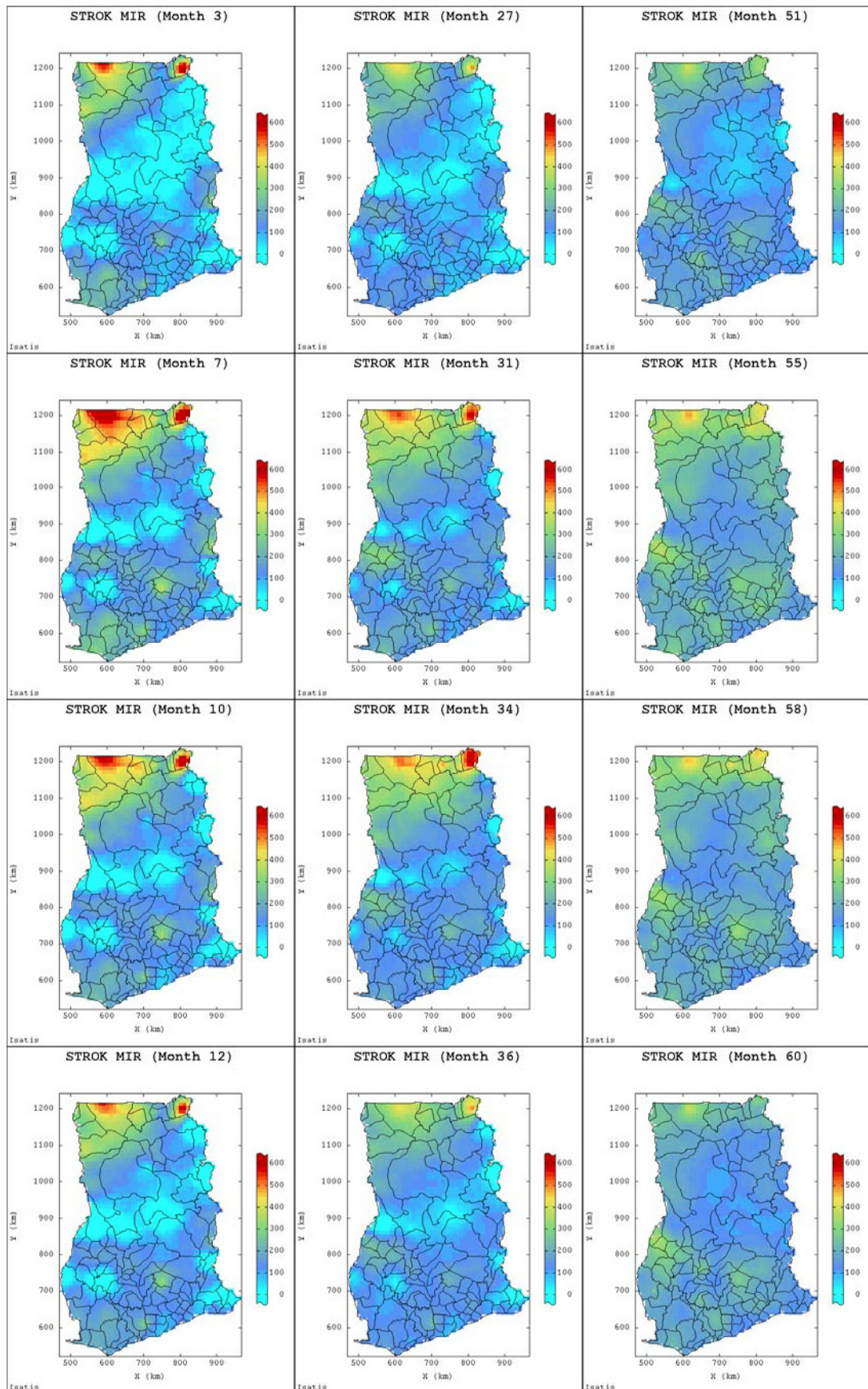


Figure 5.4.3: Morbidity incidence rates estimated by the space-time ordinary kriging of residuals (STROK) for the selected months March, July, October and December (from top to bottom) for years 2000 (left), 2002 (middle) and 2004 (right).

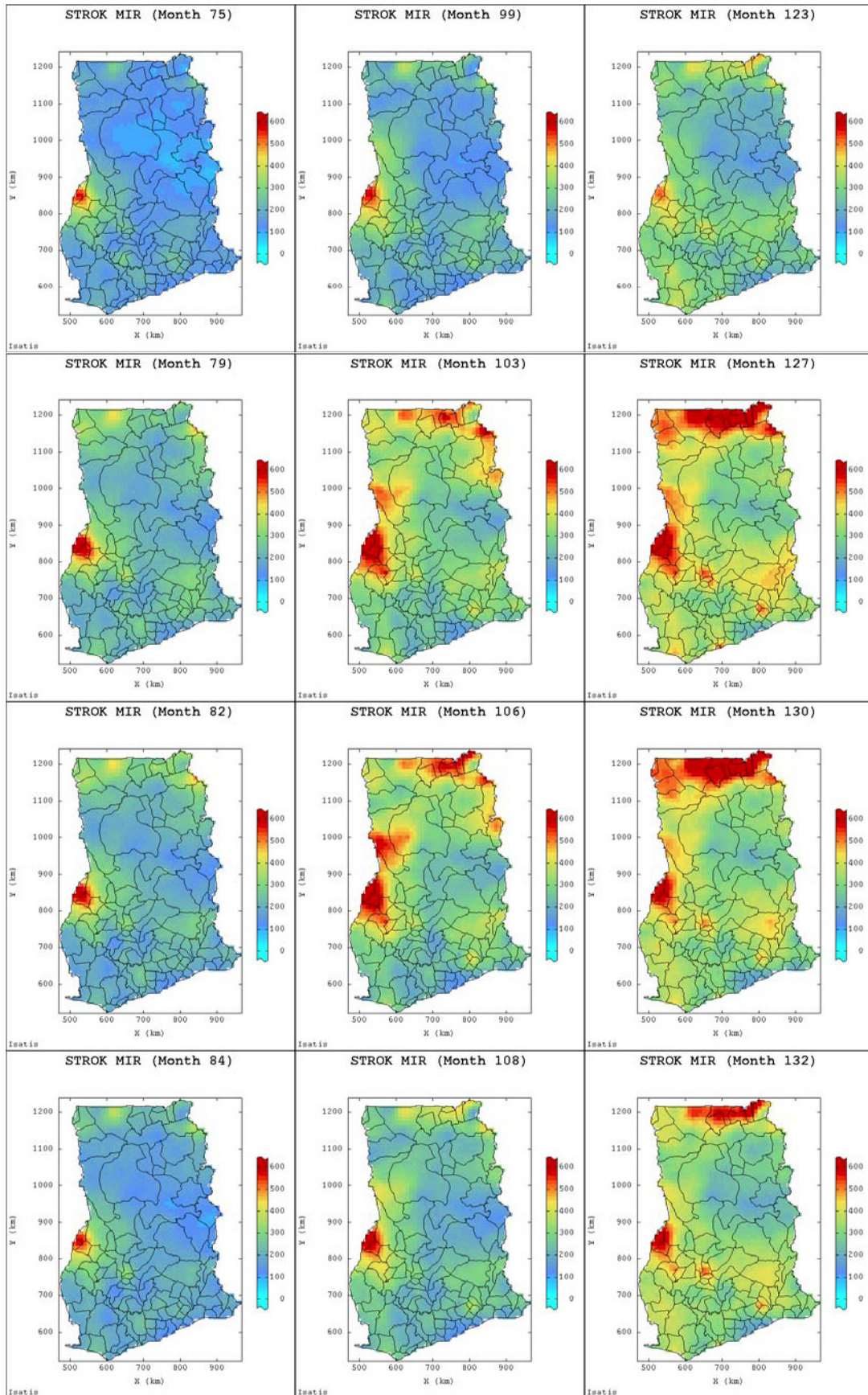


Figure 5.4.4: Morbidity incidence rates estimated by space-time ordinary kriging of residuals (STROK) for the selected months March, July, October and December (from top to bottom) for years 2006 (left), 2008 (middle) and 2010 (right).

of higher morbidity incidence rates from the upper western (north-western) to the upper eastern (north-eastern) parts of the country (see Figure 5.4.3). In addition, most parts of the country appear to have been underestimated for the months in 2000-2004. Morbidity incidence observed at the district-month locations during this period were, relatively low and appeared to confirm the wide-spread of under reporting of cases from the district to the CHIM data bases coupled with several missing records, which resulted in negative estimates.

5.4.3 Space-time Ordinary Kriging of Residuals using the Product-Sum Model

In section 5.4.2, a joint space-time semivariogram model constructed was used as input for the space-time ordinary kriging of residuals (STROK) estimates in (5.4.2). The second type of residual estimates is obtained in this section by the use of the generalised product-sum models to fit the space-time semivariograms of the residuals, as in section 5.3.3. Figures 5.4.5 and 5.4.6 provide risk maps generated by STROK via the generalised product-sum modeling approach (STROK_PS) for selected months.

The morbidity incidence rates which were estimated by the product-sum modelling of residuals exhibit similar distribution pattern as the previous estimates. However, the risk maps produced appeared more smoothed and regions of high morbidity risk of the disease have expanded further towards areas in the east and south. Like the previous predictions, the high risk areas are mainly observed in the north-eastern and western parts of the country bordering with the neighbouring countries. These high risk areas are mostly inhabited by people who engage in commercial activities such as fishing, farming, and trading. The areas are often liable to flooding from the two large rivers, Afram and Volta, resulting in suitable environmental conditions for mass breeding of mosquitoes. The west, east and north borders of Ghana with the neighbouring countries are well-known for their large movement of people across the border for commercial and business activities. The morbidity risk of the disease is seasonal. Predicted values are high from May to December, coinciding with the wet season during which the weather is relatively cool to support the *Anopheles* mosquito vector breeding and their survival. The months from January to April record lower numbers of incidence cases. Generally, this period is relatively dry and warm across the whole country which is often not very favourable for the agents of transmission of the disease.

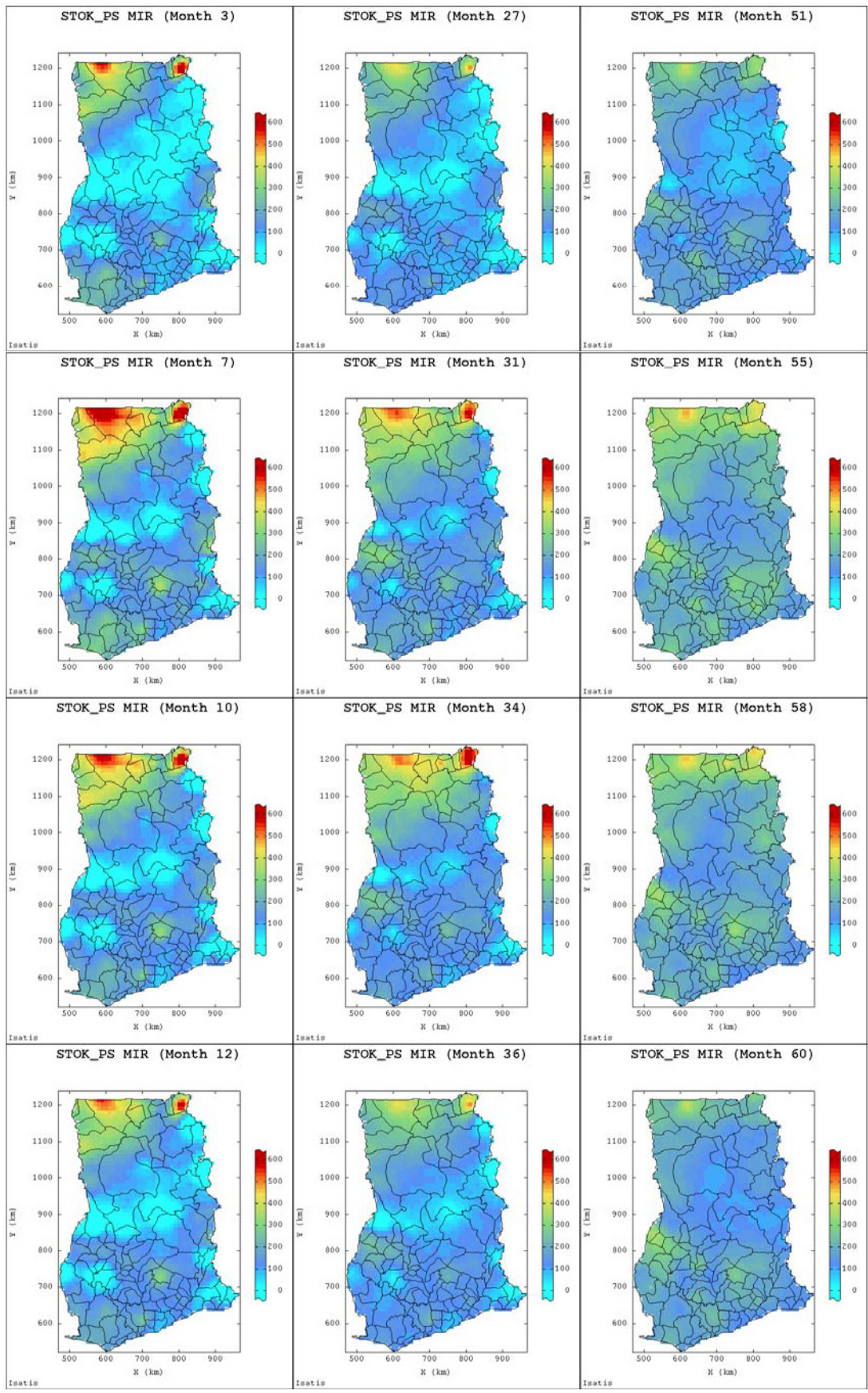


Figure 5.4.5: Malaria incidence rates estimated by the product-sum modelling of residuals (STOK_PS) for the selected months March, July, October and December (from top to bottom) for years 2000 (left), 2002 (middle) and 2004 (right) .

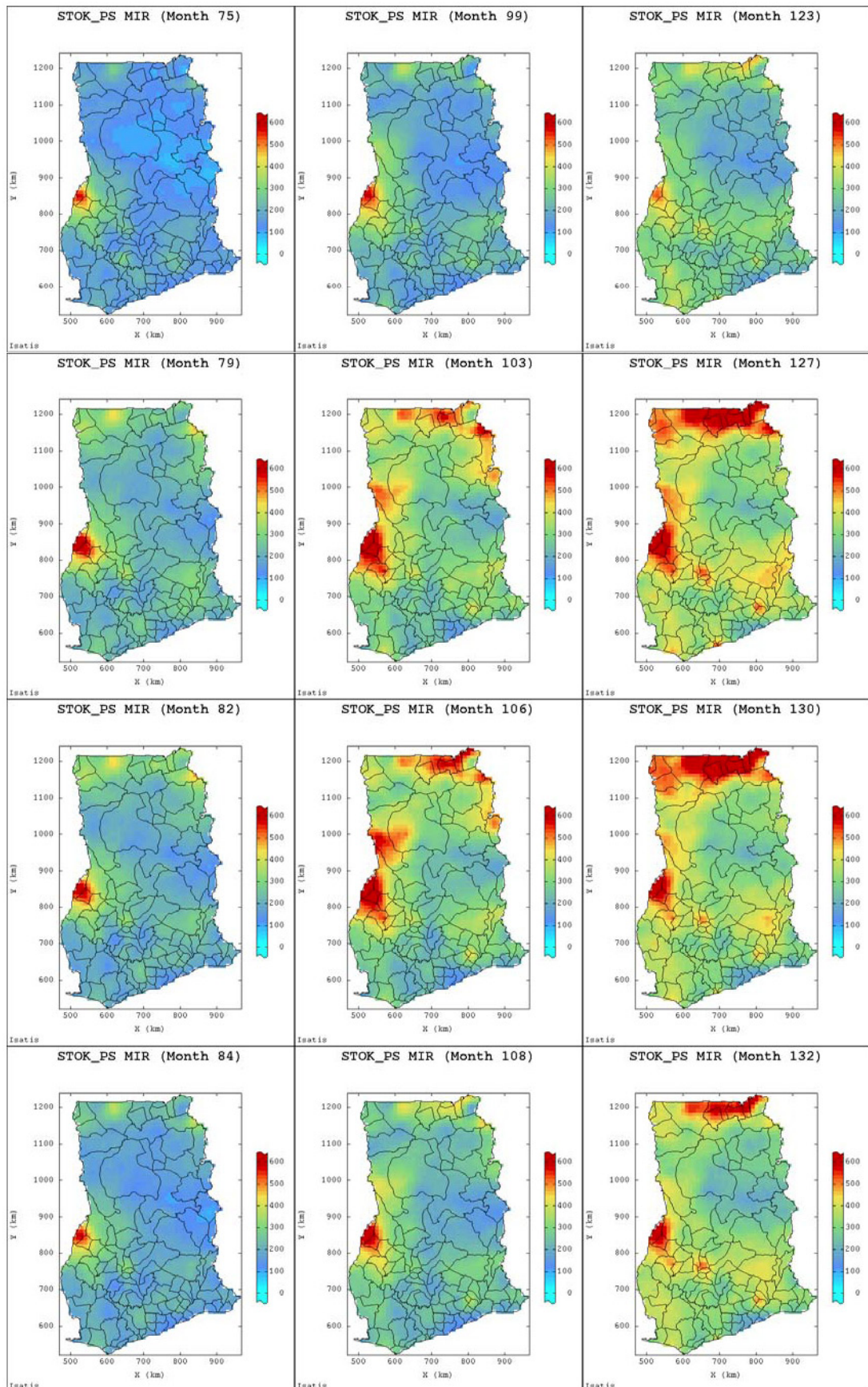


Figure 5.4.6: Malaria incidence rates estimated by the product-sum modelling of residuals (STOK_PS) for the selected months March, July, October and December (from top to bottom) for years 2006 (left), 2008 (middle) and 2010 (right) .

5.5 Space-Time Prediction of the MIR Accounting for Climatic Effects

Sections 5.2–5.4 focused on space-time and spatial structure of the morbidity incidence rates without considering the potential covariates. As an alternative way of characterising the patterns of local distribution of the incidence rates, the effect of climate is incorporated, taking into account their spatio-temporal autocorrelations. The multivariate analyses conducted in chapter 4 (sections 4.4 and 4.5) gave an indication that the malaria transmission, as observed at the various districts and regions, could be influenced by environmental factors that vary in space and by time. This relationship is further established by coregionalising the detrended morbidity incidence rates with the climatic covariates: total rainfall, relative humidity (at 1500 hours) and maximum temperature, identified as the potential climatic risk factors of the disease incidence at the local level. As was the case for the regional morbidity incidence rates, the district-month incidence data were detrended, following (4.4.1), which showed the presence of a higher degree of interdependence between the dispersed values of $I(\mathbf{u}_\alpha, t)$ and the potential covariates $Y_{t-1}(\mathbf{u}_\alpha, t)$ at different spatial and temporal scales. The ordinary cokriging (OCK) and space-time ordinary co-kriging (STOCK) techniques were then applied to the detrended morbidity incidence data (residuals), $R_d(\mathbf{u}_\alpha, t)$ via linear models of coregionalisation to account for the spatial and temporal continuity of the potential covariates into the optimal space-time predictions of malaria risk at the various district locations. The effect of climate on morbidity incidence is explored by first spatially interpolating the three potential but sparse covariates (total rainfall, temperature and relative humidity) available at only 77 district locations at the national level, taking advantage of the secondary and exhaustive data on elevation via the digital elevation model (DEM) of Ghana (IntraSearch, 2011). This is considered in the following section.

5.5.1 Interpolation of Climatic Covariates

This was achieved by using collocated cokriging via a linear model of coregionalisation (LMC) with elevation whose values were generated from the digital elevation map of Ghana. The elevation map (Figure 4.1.1), gridded on a denser and regular resolution consisting of 52×76 cells of size approximately 9.5×9.5 km², provided an exhaustive source of information on elevation at every location, from

which the elevation data were extracted for each of the 138 district-locations. Joint experimental semivariograms of total rainfall, temperature (maximum and minimum) and relative humidity with elevation were separately computed for each month t using an average lag spacing of 30 km for 15 lags. They were then modelled with nugget effects, nested with either one or two spherical models. Spatial maps of the interpolated values of the covariates, using DEM as the collocated variable were produced for each month, some of which are provided for the years 2000, 2005 and 2010 in Figures 5.5.1 and 5.5.2. The fitted linear models of coregionalisation for the multivariate semivariograms and their parameters are shown in Appendix E-2.

The results of the above linear models of coregionalisation indicate that elevation is able to account for the large-scale spatial variations with the potential covariates. The direct semivariogram and cross semivariogram models obtained from the interpolations of the three potential covariates are characterised by long range of correlations varying from 100 to 200 km. However, the linear coregionalisation models of maximum (or minimum) temperature and rainfall with elevation, relatively, appeared to have stronger correlations and smaller ranges, all varying from 100 to 180 km, whilst that of relative humidity (at 1500 hours) with elevation, fitted by one spherical model with nugget effect, have ranges of either 180 km or 200 km.

The monthly spatial maps of covariates arising from the collocated cokriging conform to the seasonal patterns of the climatic conditions in the country but with some variations though hardly to discern from the maps (see Figures 5.5.1 and 5.5.2). This is an indication of variations in the weather conditions over the years. The months from December to March are characterised with dry weather when virtually rainfall hardly occur across the country. High temperatures (exceeding 35°C) and low relative humidity (less than 40%) are recorded during this period, especially in the northern parts. The spatial maps also show the wet season occurring between May and November with high relative humidity and relatively low maximum temperatures of approximately 30°C. The central and south-west parts, which are mostly in the tropical rainforest zone, are observed with high amounts of rainfall and relatively humidity exceeding 300 mm and 75%, respectively.

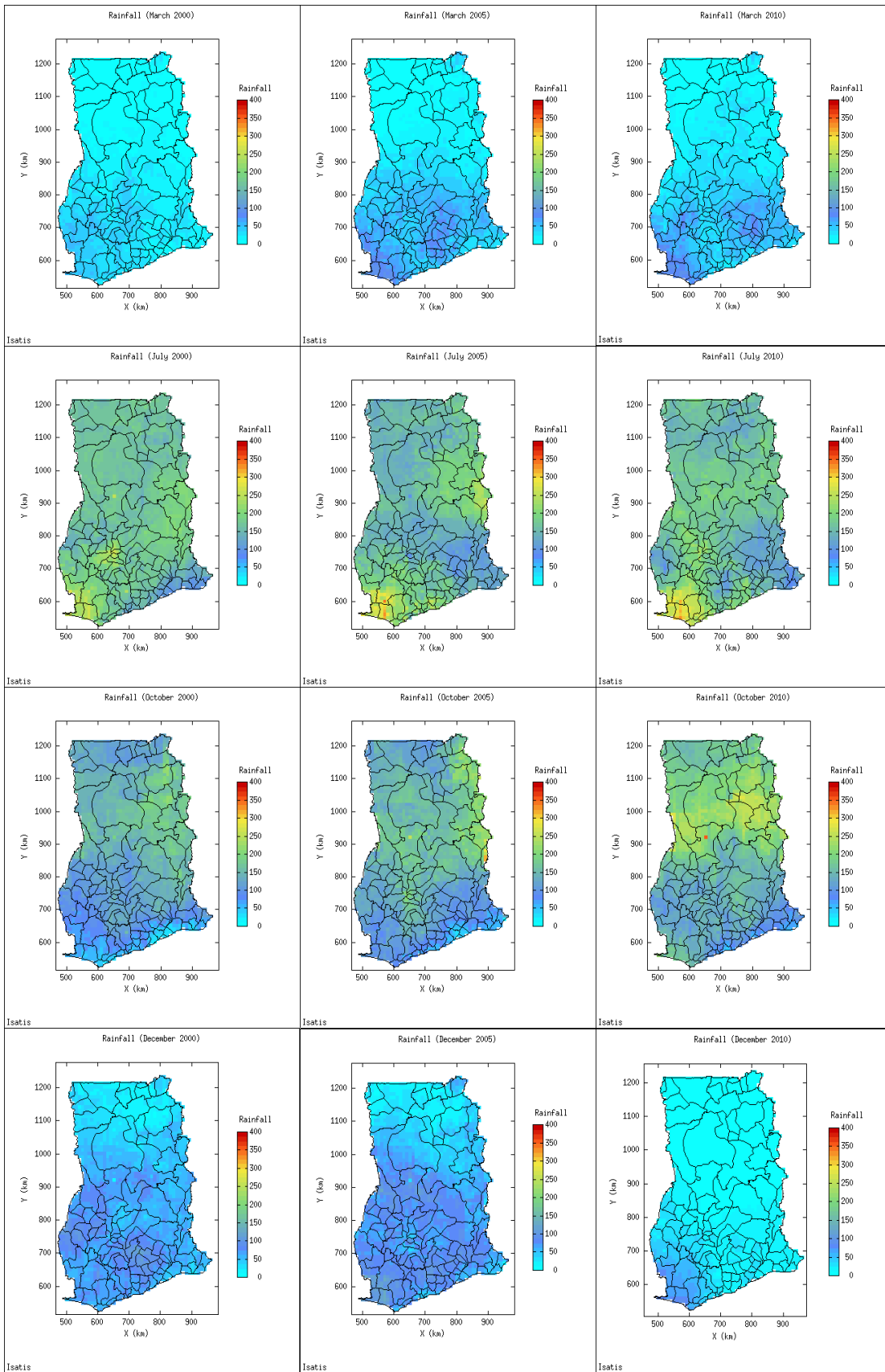


Figure 5.5.1: Spatial maps of total rainfall for March, July, October and December in 2000, 2005 and 2010.

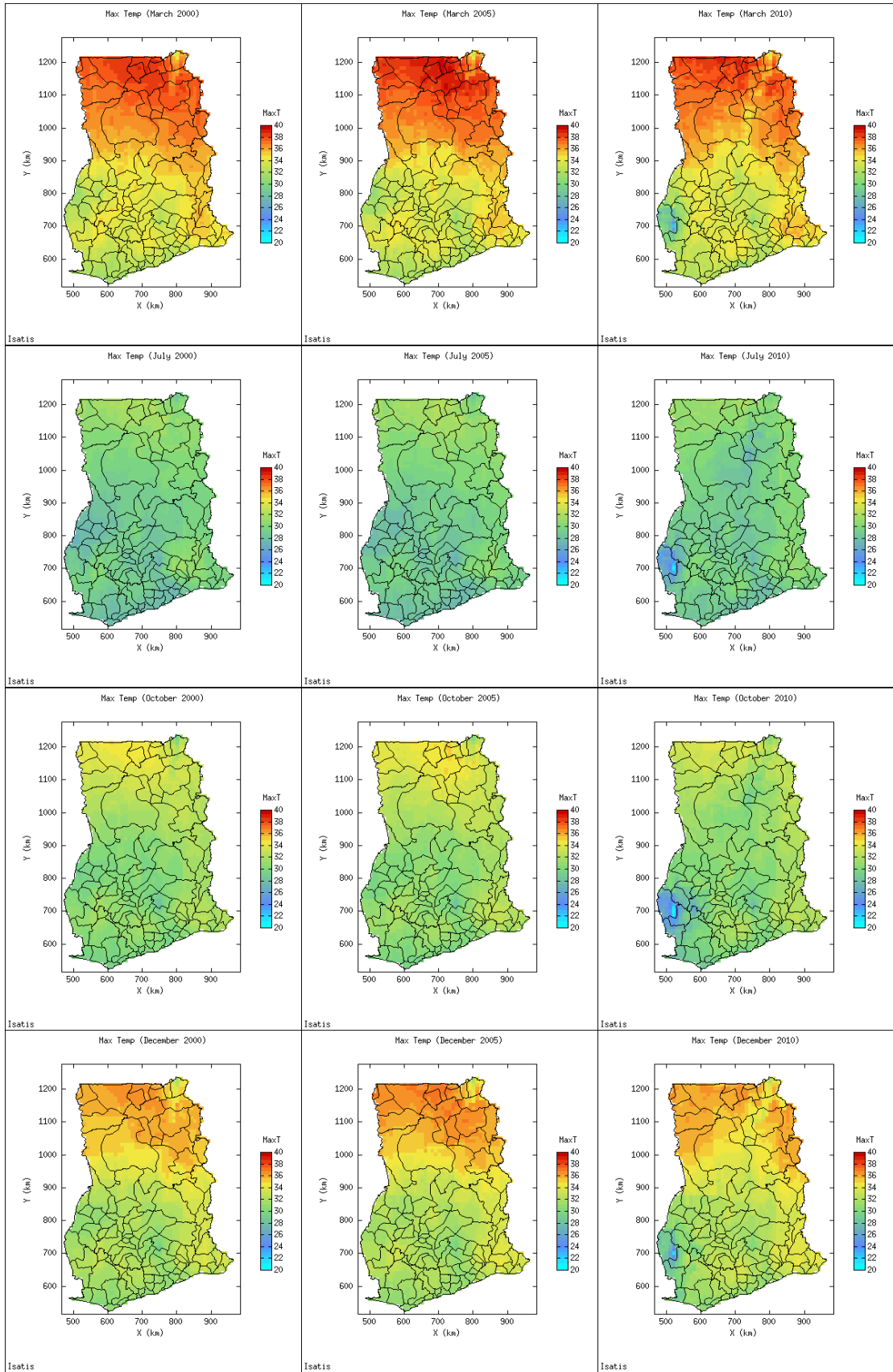


Figure 5.5.2: Spatial maps of maximum temperature for March, July, October and December in 2000, 2005 and 2010.

5.5.2 Linear Coregionalisation Models of MIR with Climate

Having incorporated elevation via the DEM to account for the sparse climatic data locations via LMC, the detrended district-month morbidity incidence data, $R_d(\mathbf{u}_\alpha, t)$ were coregionalised separately with the above potential covariates at the same or preceding month of incidence (lag $t - i$; $i = 0, 1$) and to avoid multicollinearity. The space-time experimental direct and cross semivariograms were computed using 15 lags at an average spacing of 30 km, following (3.3.8) to obtain a multivariate system of semivariograms $\hat{\gamma}_{IY_{t-i}}(\mathbf{h}_s, t)$. Rainfall, relative humidity (lagged one month) and maximum temperature at same month of incidence of the disease proved to have significantly and higher correlations with the detrended incidence rates (p -value < 0.01) and were considered for semivariogram model fitting. Consequently, a LMC was fitted, for each potential covariate $Y_{t-1}(\mathbf{u}_\alpha, t)$ to space-time experimental semivariogram in both space and time domains simultaneously using the linear combination of spherical and/or exponential models with nugget effect (5.5.1), following the procedure of Goovaerts (1997) and Goulard (1989) as given in (3.3.11).

$$\begin{aligned} \gamma_{ij}(\mathbf{h}_s, h_t) &= b_{ij}^0 + b_{ij}^1 \exp(h_s/r_1) + b_{ij}^2 \text{sph}(h_s/r_2) + b_{ij}^3 \text{cosexp}(h_t/r_t); \\ \text{for } i, j &= 1, 2 \end{aligned} \quad (5.5.1)$$

Also constructed were purely the spatial semivariogram models of the morbidity incidence rates $\gamma_{Y_{t-1}}^t(\mathbf{u}_\alpha)$ with each of the potential climatic covariates using same nested model (5.5.1) to investigate the spatial variations of the incidence data $I_t(\mathbf{u}_\alpha)$ for each month t . This was to compare the monthly OK spatial maps of malaria risk produced with that by the space-time kriging techniques. The model parameters and graphs of the space-time linear coregionalisation models fitted separately to the direct and cross experimental semivariograms of the morbidity incidence rates with the potential covariates are shown in Table 5.5.1 and Figures 5.5.3 and 5.5.4, respectively. However, the parameters and graphs relating to relative humidity which confounds with rainfall are presented in Table E-3.1 and Figure E-3-1, respectively in Appendix E-3. The results of purely spatial direct and cross semivariogram models for the months in 2010 are provided in Appendix E-2. The dashed red lines in the cross semivariograms, called hulls of perfect correlation, give the ranges within which the linear models of coregionalisation are assumed to be positive semidefinite and perfect

correlations exist (Wackernagel, 2003; Webster & Oliver, 2007).

As observed from the space-time semivariogram models, rainfall lagged by one month, relative humidity and maximum temperature correlate significantly with the detrended morbidity incidence rates, though not very strongly. Rainfall and relative humidity increase the spatial dependence of the disease, varying from 35 to 250 km, whilst maximum temperature decreases the spatial continuity and varies with same spatial range of correlations. However, the morbidity incidence due to effects of the covariates appeared to vary across the country in a different manner with varying temporal ranges. In particular, maximum temperature varies more continuously (20–200 months) compared with the other two covariates (10–100 months).

The total sills observed from the effect of rainfall in the preceding one month are comparable, being almost equal both spatially and temporally. In addition both multivariate space-time semivariograms have same nugget effect of 1500, unlike the effect of relative humidity which has a higher nugget effect and temporal sill of 1600 and 5000, respectively (see Appendix E-2).

Table 5.5.1: Parameters of space-time linear models of coregionalisation of detrended morbidity incidence rates with rainfall and (lagged one month) and current month maximum temperature for the national data set study

Variable	Spatial			Temporal
	$nug(h_0)$	$exp(h/35)$	$sph(h/250)$	$cosexp$ ($h/10 - 60$)
Residuals	1500	1100	500	1700
Rainfall_1	1500	1800	800	2900
Resid&Rainf_1	50	250	150	1700
Variable	$nug(h_0)$	$exp(h/35)$	$sph(h/250)$	$cosexp$ ($h/20 - 200$)
Residuals	1500	800	800	1780
MaxTemp	0.80	0.7	1	3.2
Resid& MaxT	-10	5	6	-57

In the purely spatial case, the direct semivariograms for the monthly morbidity incidence rates, rainfall (at lag 1), minimum temperature and relative humidity (at 1500 hours) are mostly observed to be unstable due to lack of sufficient data in the space domain. The correlations of the incidence rates with the lagged rainfall vary within short and long ranges from 60 to 260 km. However, the two other potential covariates differ with long ranges, mostly between 150 and 280 km. Generally, the

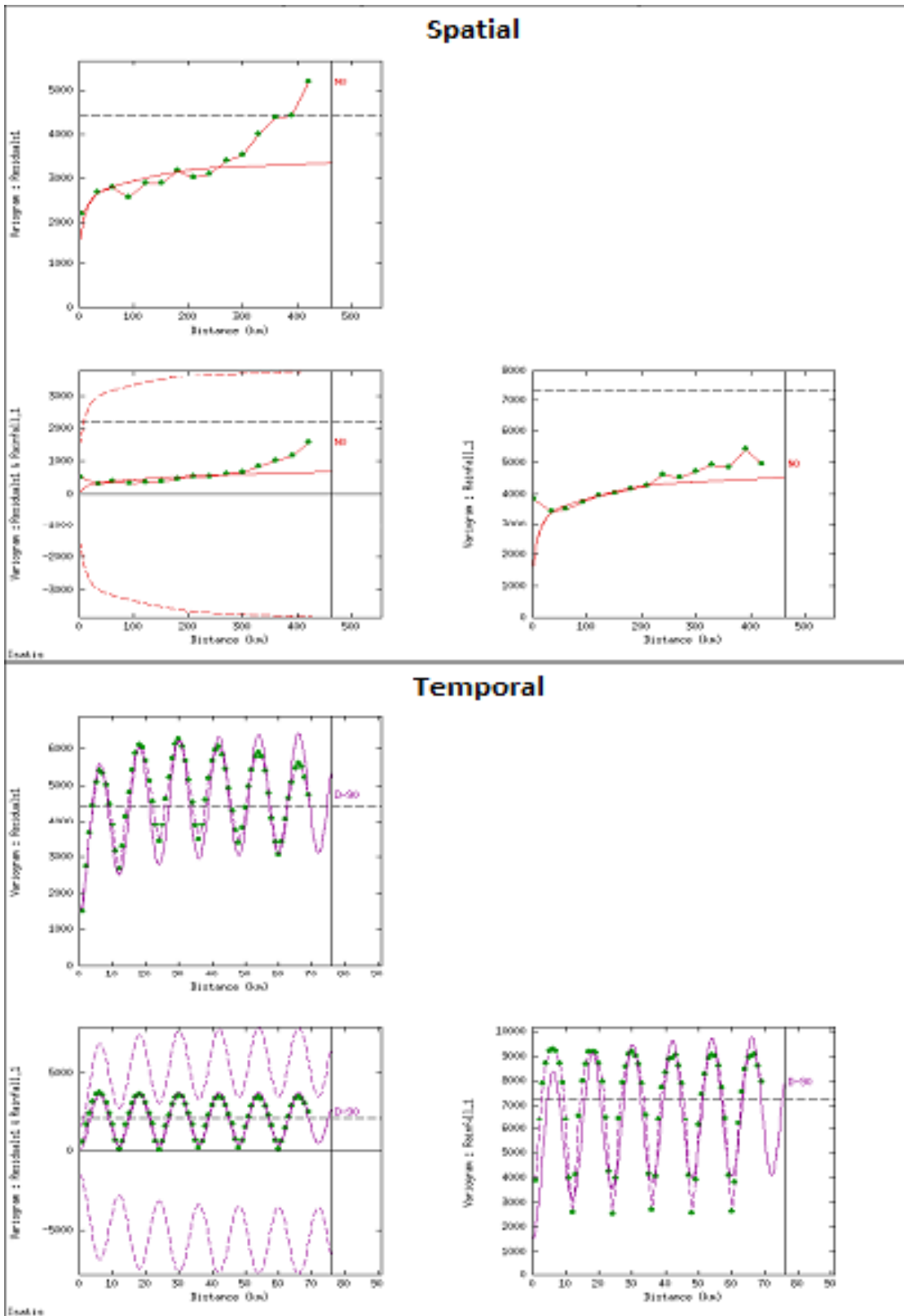


Figure 5.5.3: Space-time linear model of coregionalisation of detrended morbidity incidence rates (residuals) with lagged one month rainfall showing spatial (top) and temporal (bottom) correlations for the national study.

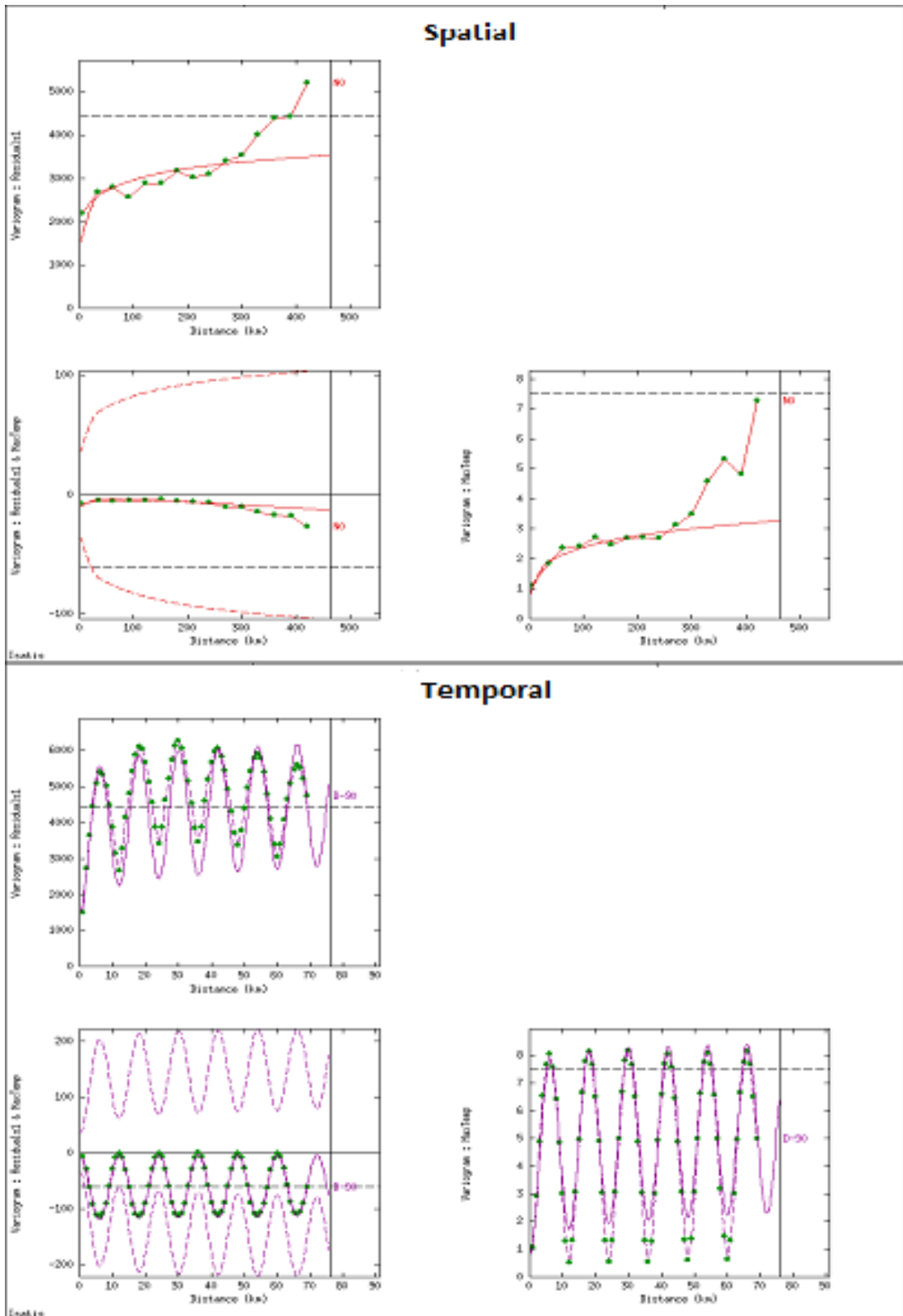


Figure 5.5.4: Space-time linear model of coregionalisation of detrended morbidity incidence rates (residuals) with maximum temperature showing spatial (top) and temporal (bottom) correlations for the national study

cross-correlations are not strong as they are mostly found farther from the hulls of correlation, unlike the cross-correlations of the LMC of elevation with the covariates which appeared relatively stronger (see figures in Appendix E-2). The graphs of the experimental semivariograms appear to be consistent (vary similarly) in structure across the different months. The monthly structural analysis also indicate higher variations in the incidence rates during the months, May–November but lower in August–September and December–April, compared with the variation of the covariates which appear to be more pronounced during the wet months in May–October/November. This coupled with the cross-correlation results affirms the extent of impact of the climatic covariates on the morbidity incidence.

5.5.3 Neighbourhood Selection for LMC Semivariograms

The cross-validation incidence estimates of the space-time models implementing the linear models of coregionalisation with the climatic covariates of rainfall and maximum temperature in the preceeding month are shown in Table 5.5.2. The graphical summary of the estimates are displayed in Figures E-4.1 and E-4.2 in Appendix E-4.

Table 5.5.2: Cross-validation estimates of the space-time ordinary co-kriging models for different moving neighbourhoods within a period of 5 months with number of samples per angular sector for national study area.

Model	Neighbourhood		Error		Standardised Error		Corr. Coeff.
	Search radius	No. of samples	Mean	Variance	Mean	Variance	
STOCK_	150km	2 – 10	-0.00311	1791.239	-0.00022	0.87176	0.773
		4 – 20	0.03225	1656.899	0.00059	0.82090	0.796
Rainf_1	200 km	2 – 10	0.01562	1619.344	0.00022	0.75910	0.804
		4 – 20	-0.09787	1613.111	-0.00217	0.77298	0.807
	250 km	2 – 10	0.04731	1765.041	0.00078	0.78352	0.781
		4 – 20	-0.06484	1626,582	-0.00154	0.77185	0.806
STOCK_	150km	2 – 10	-0.04981	1783.578	-0.00137	0.86111	0.773
		4 – 20	0.14297	1705.109	0.00293	0.78355	0.788
	200 km	2 – 10	0.04448	1607.926	0.00082	0.74133	0.803
		4 – 20	0.07958	1617.028	0.00148	0.76394	0.803
MaxT	250 km	2 – 10	0.09144	1760.469	0.00157	0.75691	0.779
		4 – 20	0.07882	1626.510	0.00141	0.75908	0.803

As observed for the STOLK and STOK models, the mean and standardised errors of the estimates for all the moving neighbourhoods tested are smaller with the search radius of 150 km or 200 km using a minimum of 8 and maximum of 20 sample observations producing the best results. However, kriging with the larger search radius (200 km) yielded more reliable estimates. For this moving neighbourhood, the mean errors for the STOCK estimates accounting for rainfall and maximum temperature in the previous month are -0.09787 and 0.07958, respectively, whilst that for the standardised mean errors are -0.00217 and 0.00148, respectively. In addition, the STOCK model influenced by rainfall (lagged one month) appeared more appropriate as it yields a higher standardised error variance of 0.77298 and relatively higher correlation coefficient of 0.807 between the observed and the estimated values of residuals.

5.5.4 Space-time Ordinary Co-kriging of MIR

In this section the space-time ordinary co-kriging (STOCK) of the morbidity incidence via the residuals with the main potential covariates is carried out. Following (3.3.15) in chapter 3 (section 3.3.3), the STOCK linear optimal predictor with each of potential covariates $Y_{t-i}(\mathbf{u}_\alpha)$; $i=0,1$ being rainfall (lagged one month) and maximum temperature were implemented. STOCK estimates of the residuals were computed by collocating with the interpolated covariates, using the grid cells and moving search neighbourhood as described in the previous sections. The kriged residuals $\hat{R}_{d,stock}(\mathbf{u}_\alpha, t)$ are then added to the estimated trend surface (5.5.2), following (5.2.3) and (5.4.2) to obtain the monthly climate induced spatial maps of the malaria morbidity risk.

$$\hat{m}_d^{ok}(\mathbf{u}, t) = \sum_{i=0}^2 a_i^{ok}(\mathbf{u}) t^i, \text{ for each } t = 1, 2, \dots, 132, \quad (5.5.2)$$

where $a_i, i=0,1,2$ are the trend coefficients and $a_i^{ok}(\mathbf{u}) = \sum_{\alpha=1}^{n(\mathbf{u})} \lambda_i^{ok}(\mathbf{u}) a_i(\mathbf{u}_\alpha)$. Figures

5.5.5–5.5.8 show selected spatial maps accounting for the effects of the two covariates.

Critical examination of the monthly spatial maps show smoothed surfaces, which confirms that the climatic covariates significantly impacted on the malaria morbidity incidence. Areas of high rainfall and low temperatures in the preceding month of are usually associated with high increased morbidity incidence rates of the disease, which

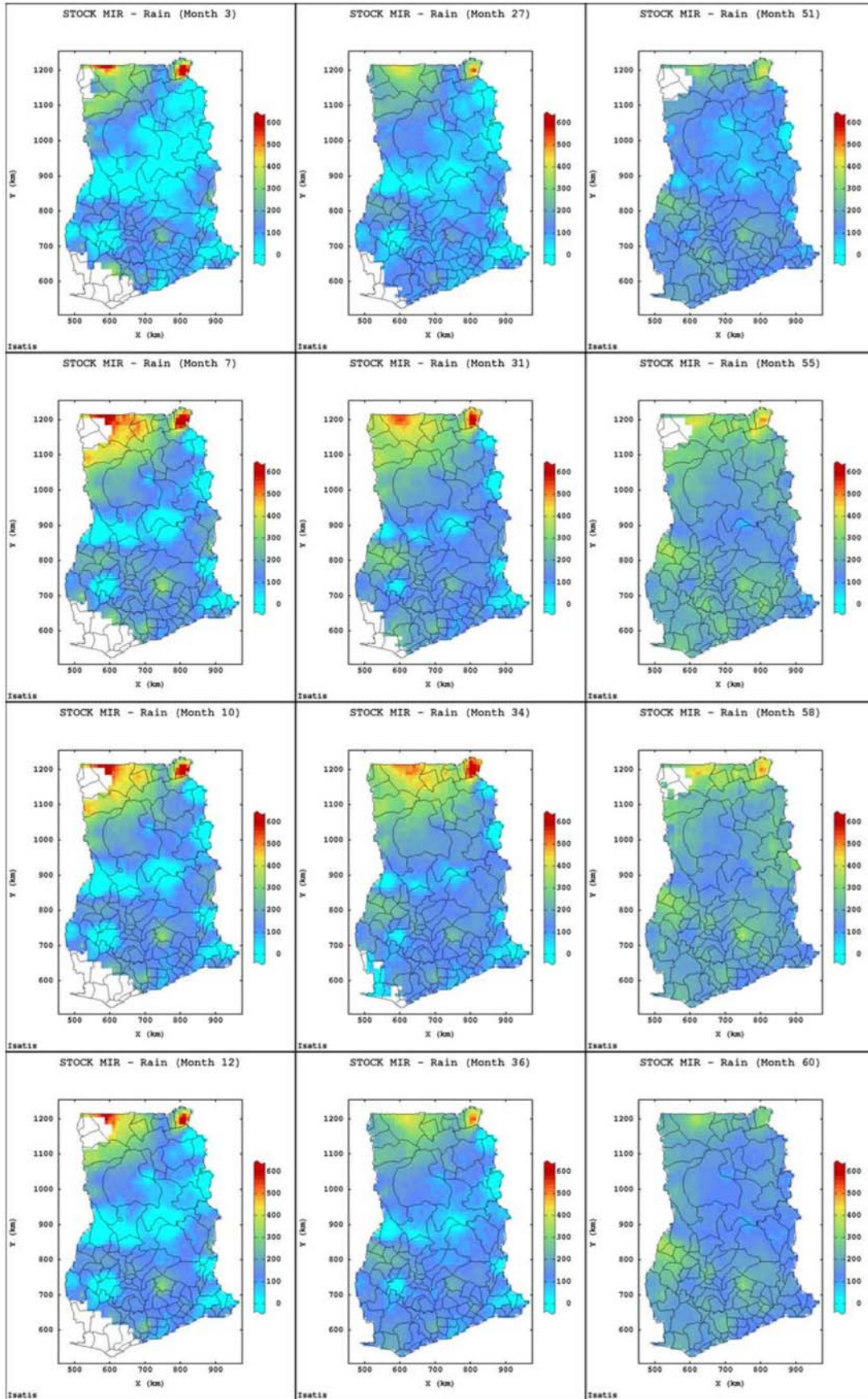


Figure 5.5.5: Selected monthly spatial maps of malaria incidence rates estimated by space-time ordinary cokriging, incorporating the effect of rainfall lagged one month (STOCK_Rain) for 2000-2004.

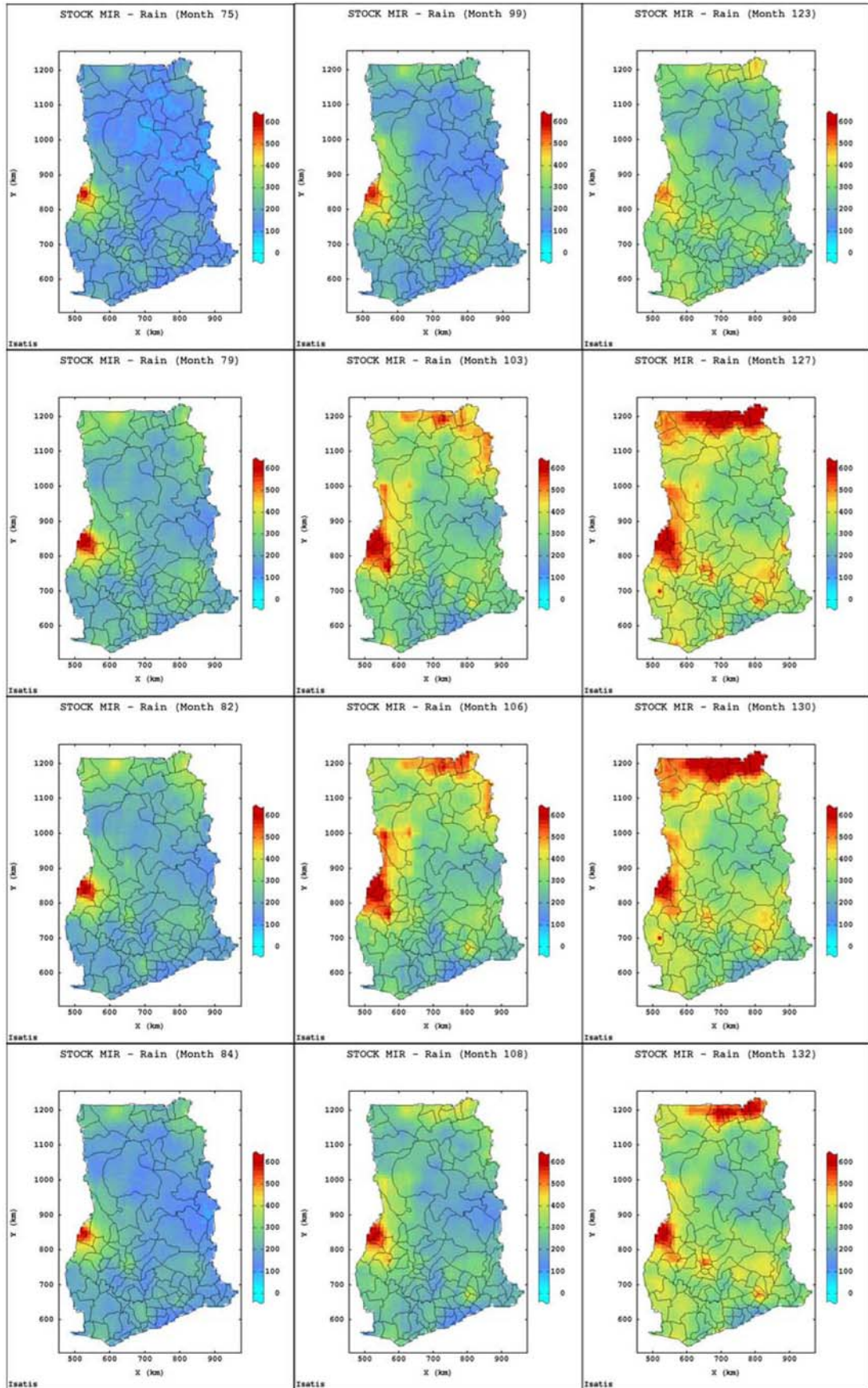


Figure 5.5.6: Selected monthly spatial maps of malaria incidence rates estimated by space-time ordinary cokriging, incorporating the effect of rainfall lagged one month (STOCK_Rain) for 2006-2010.

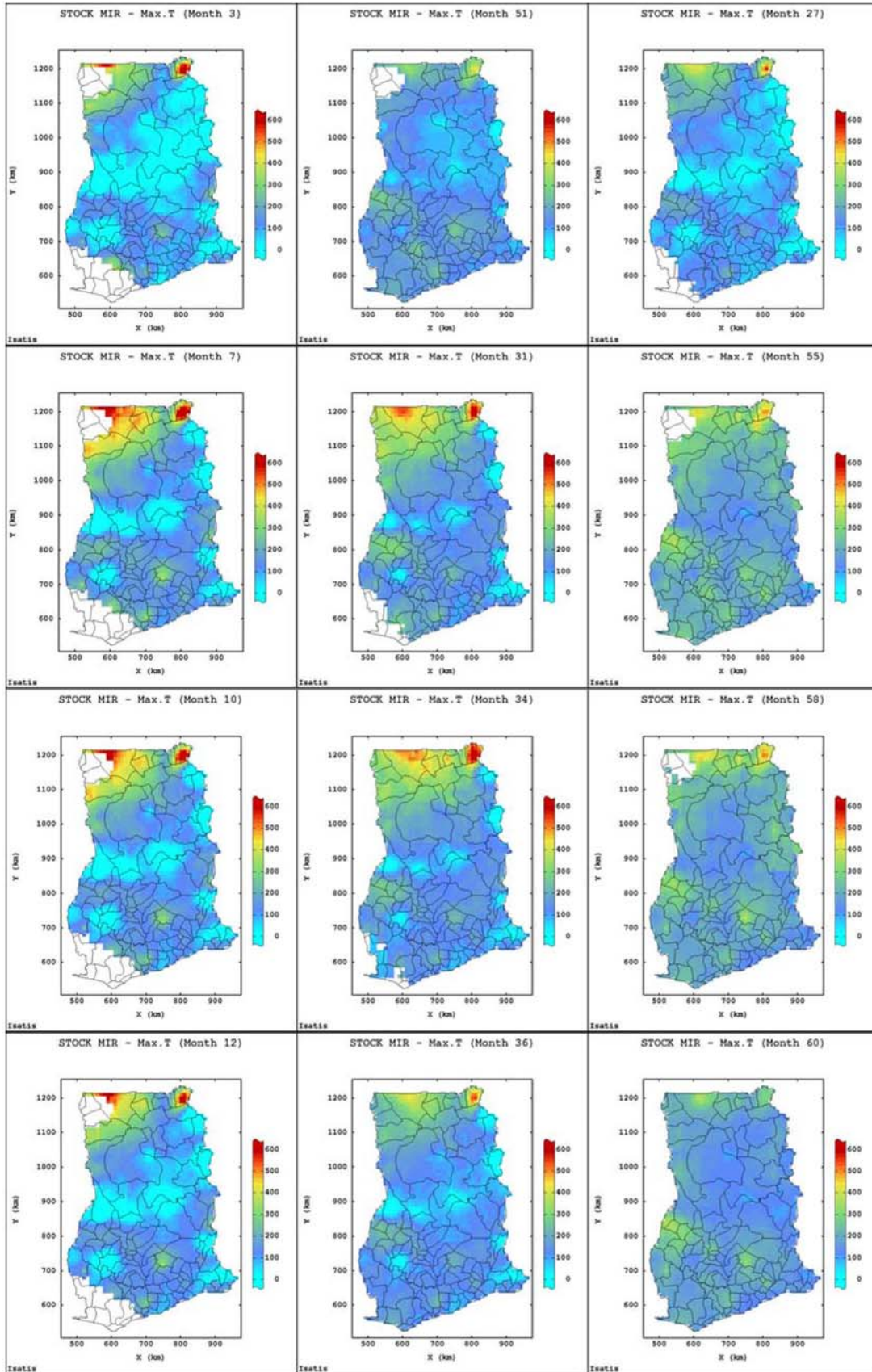


Figure 5.5.7: Selected monthly monthly spatial maps of malaria incidence rates estimated by space-time ordinary cokriging (STOCK_MaxT), incorporating the effect of maximum temperature 2000-2004.

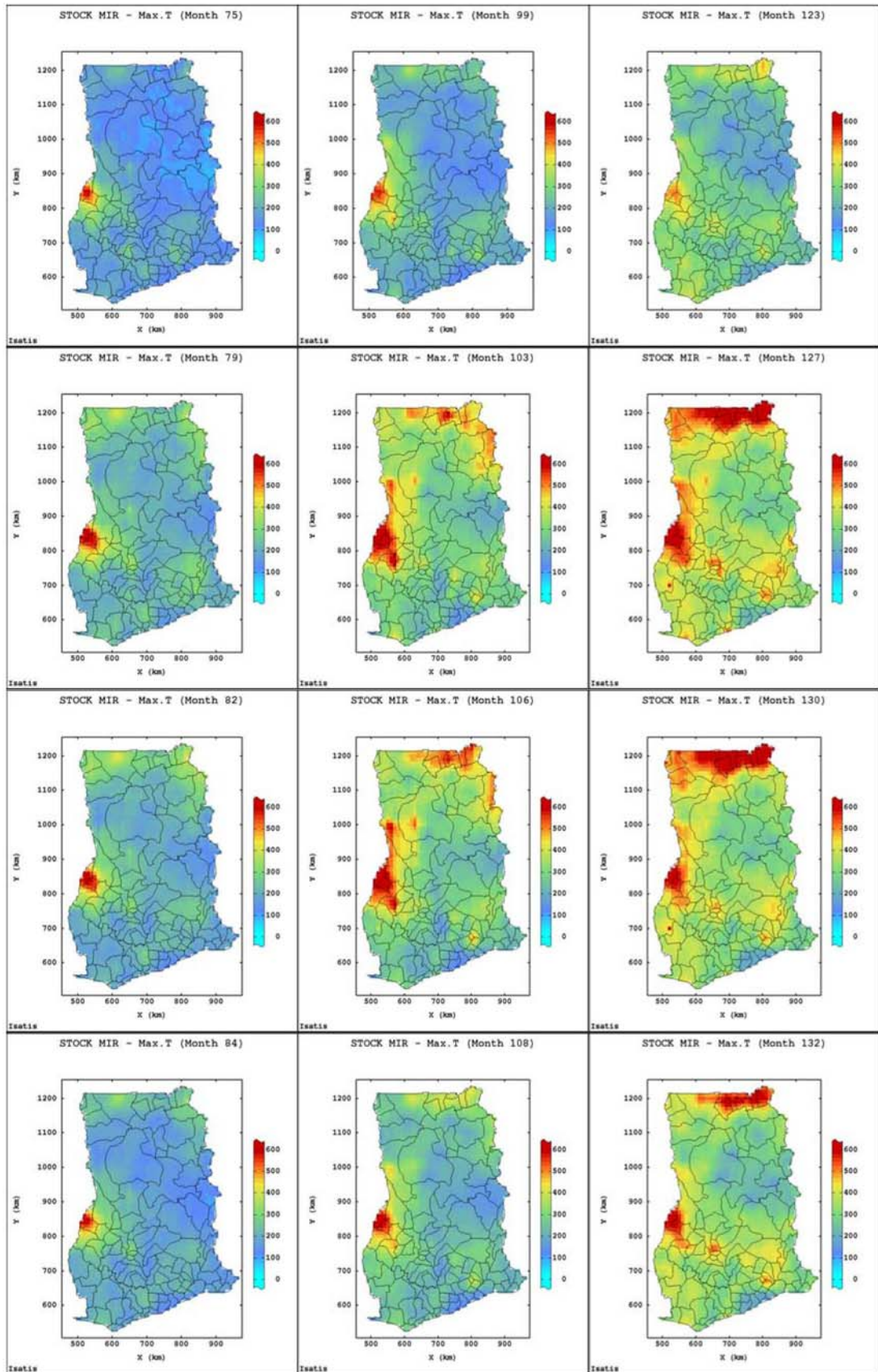


Figure 5.5.8: Selected monthly monthly spatial maps of malaria incidence rates estimated by space-time ordinary cokriging (STOCK_MaxT), incorporating the effect of maximum temperature 2006-2010.

vary across the country. These are often observed during the wet season (May-November) when temperatures are relatively low in the country. As identified by the other kriging techniques, the period from December to April is characterised by dry and warm weather conditions, which results in a significant reduction in the incidence of morbidity cases. High risk areas of malaria morbidity are consistently located in the northern, western and central parts towards east and the coast.

5.6 Comparison and Validation of Kriging Estimates

In this section the prediction estimates of the morbidity incidence rates by the various space-time kriging techniques implemented in the previous sections are compared. This is done by using prediction estimates at the unsampled locations and then making forward predictions (spatial forecasts) for the monthly 2011 incidence rates data in order to assess the overall prediction performance of the space-time kriging models. In all, five predictions have been made at the unsampled district-month locations, as per the trend and structural analyses of the morbidity incidence data conducted in sections 5.2 and 5.3, respectively. The space-time lognormal ordinary kriging (STOLK) estimates were obtained via the space-time variography of the log-transformed observed incidence rates. The space-time ordinary kriging (STOK) technique was used to produce two estimates, one based on the joint space-time semivariogram modelling of residuals (STROK) and the other, the generalised product-sum model fitting to the residuals (STROK_PS). The space-time ordinary co-kriging (STOCK) technique estimates, accounting for the rainfall and maximum temperature) are represented by STOCK_Rain and STOCK_MaxT, respectively.

5.6.1 Summary Statistics of Kriging Estimates

The summary statistics of the kriging estimates produced at the unsampled locations are given in Table 5.6.1. Generally, all the kriging techniques underestimate the sample mean value. Nationally, the predicted morbidity incidence rates range from 0 (-812.25) to 1197.89 cases per 10,000 resident people, compared with the observed sample values which vary from 42 to 1574 with an average of 240.94 per 10,000 residents population. However, they do not differ significantly from each other, except the estimates obtained through the residuals by STROK and STOK_PS, which have extreme high negative values, resulting from the detrending and deseasonalising of the observed incidence rates in section 5.2. Assuming non-negativity incidence rates may

tend to improve these prediction processes. As observed from the spatial risk maps, rainfall in the previous month leads to increased risk of the disease across the country. Its effect is measured by the STOCK_Rain estimates, which are more variable with a range of 0 (-812.25)–980.77 and records the highest mean incidence rates of 238.24. The decreasing effect of maximum temperature on morbidity incidence of the disease is evidenced by its relatively low values but highly variable as estimated by STOCK_MaxT, ranging from 0 (-808.33) to 973.75 with a standard deviation of 127.34.

Table 5.6.1: Summary statistics of kriging estimates of malaria morbidity incidence rates compared with the observed incidence data.

Kriging Estimate	National					
	Count	Min	Max	Mean	StdDev	CV
Sample	14568	42.00	1574.00	240.94	141.95	0.589
Trend	315216	-746.65	940.89	213.08	109.01	0.512
STOLK	315480	59.07	1197.89	228.98	92.69	0.405
STROK	314952	-754.37	979.95	213.41	111.37	0.523
STROK_PS	314952	-711.46	900.81	213.21	111.04	0.521
STOCK_Rain	308668	-812.25	980.77	238.24	126.84	0.581
STOCK_MaxT	308067	-808.33	973.75	211.19	127.34	0.584

5.6.2 Validation of Kriging Estimates

The forward predictions of the incidence data were done by following the Jackknife procedure. The observed malaria incidence rates data for 2011 were excluded from the structural analysis but used as input data for the predictions at the sampled locations to validate the estimates by the established space-time models. Table 5.6.2 shows the predicted estimates and their measures of prediction accuracy as well as the summary statistics of the sample data. Spatial maps of the observed and predicted values at the data locations as well as the grid estimates are also provided in Figures 5.6.1-5.6.3.

The results appear to reproduce the observed incidence rates as they are either predicted higher or lower and follow similar patterns as the observed incidence. The estimates produced by the models range from 65.01 to 1214 compared with that of the sample of 101–1209 with mean 387.93 and standard deviation of 173.16. As indicated from previous results in Table 5.6.1, the two kriging techniques of STOK (STROK and STOK_PS) prove to estimate close to the sample observations. The estimates correlate

strongly with the observed incidence data, the correlation coefficients being 0.785 and 0.876. They also performed better with lower MAE (84.85 and 75.36) and RMSE (120.68 and 117.23) values compared with the other techniques which have corresponding figures of 121.55–200.12 and 155.23–195.17. However, higher prediction accuracy is achieved by STROK_PS, which implemented the generalised product-sum modelling using the incidence residuals data. It yielded the smallest MAE and RMSE values. STLOK consistently produced the least variable estimates whilst STOCK estimates are more variable. They appeared to have performed equal, though the latter’s correlation with the observed incidence data is not very strong as the former but highly significant (p - value < 0.001).

Table 5.6.2: Prediction estimates for 2011 compared with the sample data and their measures of prediction accuracy in the national study

Kriging Estimate	National								
	Min	Max	Mean	Std.	CV	ME	MAE	RMSE	Corr.
Sample	101.00	1209.0	387.93	173.16	0.446	-	-	-	-
STOLK	124.31	688.70	314.94	77.16	0.145	-70.95	131.55	155.325	0.918
STROK	65.01	1204.0	345.52	167.77	0.486	-33.53	84.850	120.680	0.785
STROK_PS	54.83	1214.0	356.74	163.28	0.458	-31.18	75.358	117.231	0.876
STOCK_	210.12	905.76	401.15	211.54	0.527	12.15	200.12	195.165	0.643
Rain									
STOCK_	185.99	755.40	362.10	116.96	0.323	-24.23	155.56	161.430	0.618
MaxT									

Critical examination of the spatial maps of the predicted 2011 values (see Figures 5.6.1-5.6.3) shows that the high and low observed incidence rates are reproduced at the data locations and also follow similar distribution patterns as produced by the modelled data. The grid estimates appear to behave similarly, mimicking the high risky areas in the west and the low in the east. The incidence rates are predicted at larger geographical during the rainy season. The low incidence rates predicted in the east can be attributed to lack of sufficient data as that part of the region is sparsely populated. The west is part of the tropical rainforest area and predominantly made up of densely populated rural communities. Most people who live in these areas practice subsistence farming in food and economic crops and always exposed to the bites of mosquitoes. The area is also known for the exodus of people to and from an endemic neighbouring country, where there is high co-infection of the disease with HIV.

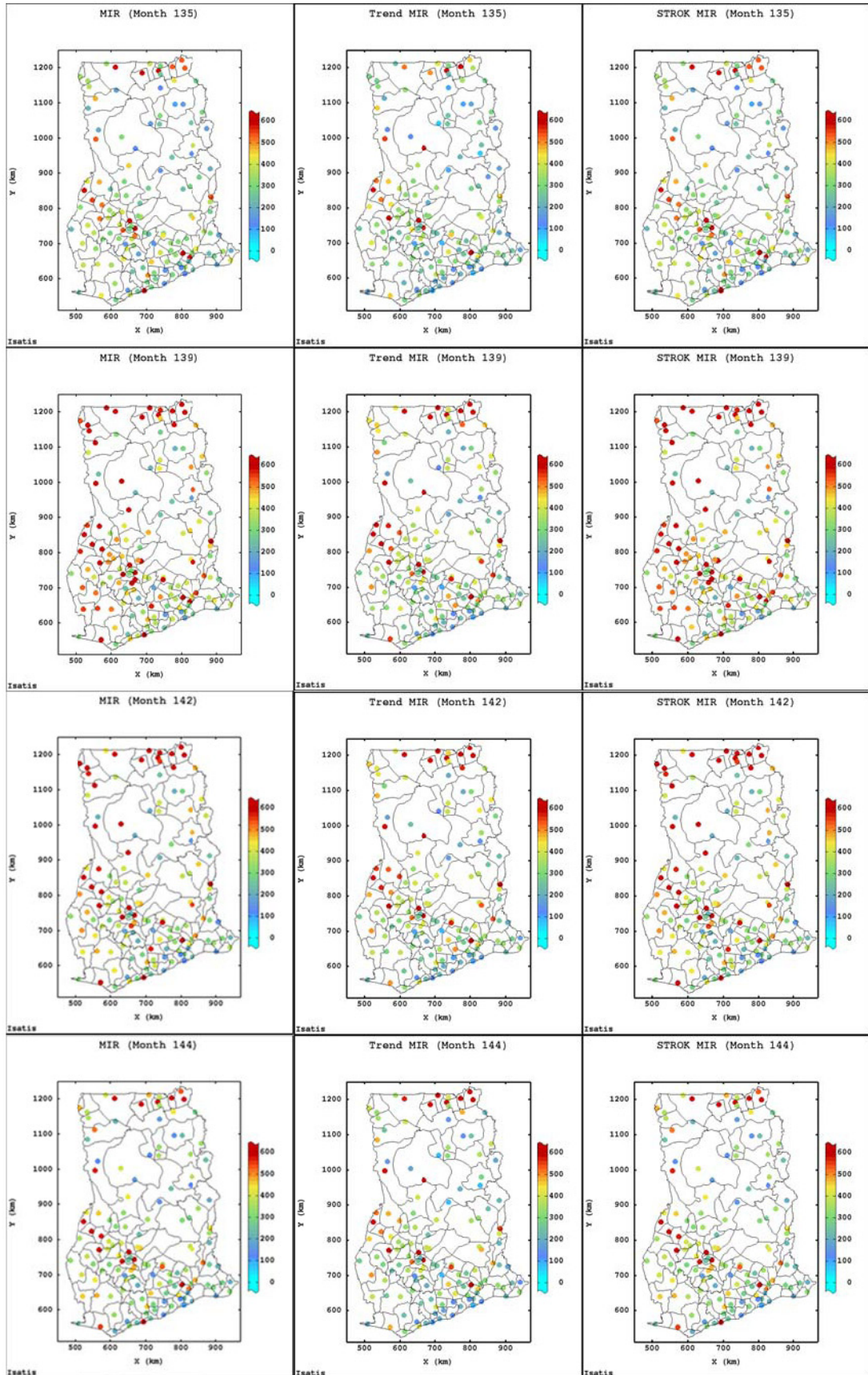


Figure 5.6.1: Posting of the observed malaria incidence rates (left) compared with the trend (with periodic cycles, shown middle) and STROK (right) estimates

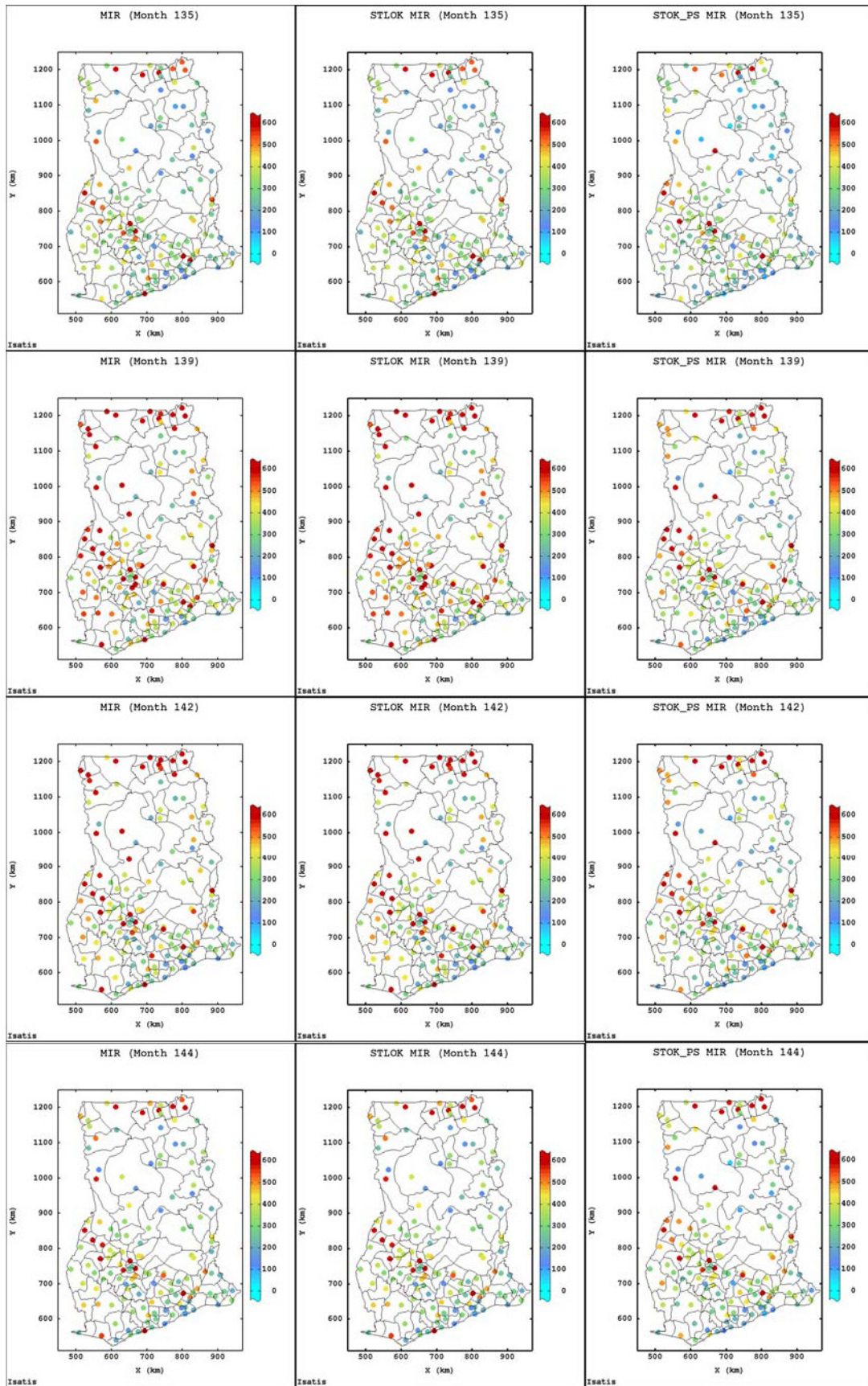


Figure 5.6.2: Posting of the observed malaria incidence rates (left) compared with STLOK (middle) and STROK_PS (right) estimates

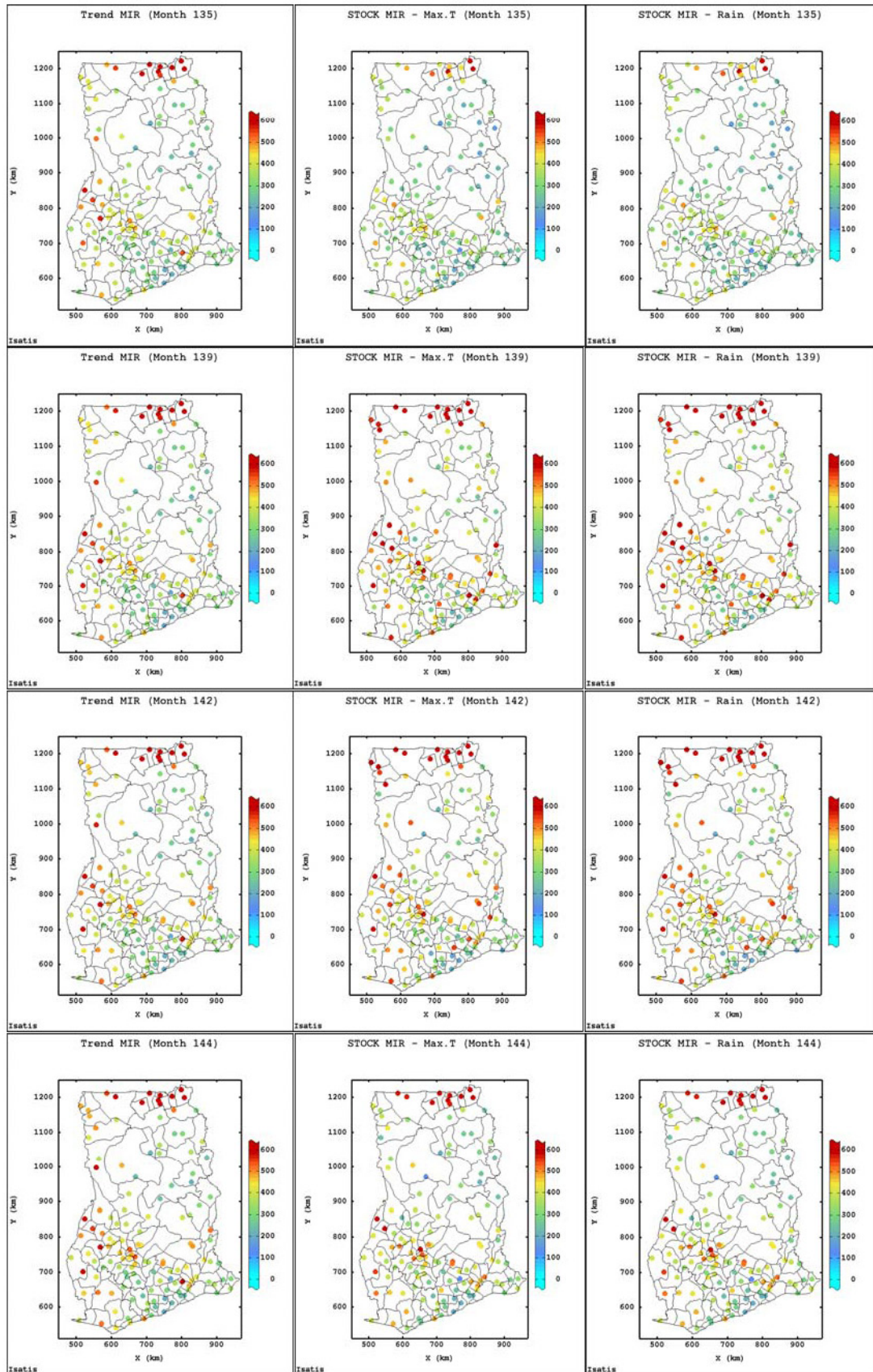


Figure 5.6.3: Posting of the trend (without period cyclest) of the observed malaria incidence rates (left) compared with STOCK_MaxT (middle) and STOCK_Rain (right) estimates

5.7 Malaria Morbidity Risk in Brong Ahafo Region

The estimation of the malaria morbidity incidence cases in the Brong Ahafo Region (BAR) is considered in this section. The analysis of the incidence data has been performed alongside with the national study. The main results of the space-time semivariogram models, characterising the spatio-temporal continuity of the disease coupled with the monthly spatial maps, estimating the morbidity risk at the district locations are presented and discussed. BAR has 19 district locations but with the larger temporal data set observed from 1998 to 2011 for modelling processes, which produced approximately 2,460 (83%) of the district-month data locations. As per the national study the various space-time semivariogram and kriging models have been developed to describe the spatio-temporal autocorrelation structures and estimate the morbidity incidence rates in the region. These include the space-time trend, space-time log-normal kriging, space-time ordinary kriging models. The results of estimation of the global trend surfaces for the morbidity incidence and space-time ordinary kriging via the residuals using the generalised product-sum modelling of semivariogram approach are presented and discussed. The detailed results of structural analysis and the optimal prediction process of the morbidity incidence are given in Appendix F.

5.7.1 Estimation of Trend Surfaces of MIR

The global trend surfaces for the morbidity incidence rates in BAR were estimated, following (5.2.1) and (5.2.3). The computed trend coefficients $\{b_i(\mathbf{u}_a); i = 1, \dots, 4\}$ and the spatial regionalised results are presented in Appendix D-1 and Table 5.7.1, respectively. The experimental semivariograms of the trend coefficients were modelled as per Table 5.7.1 and Figure F-1.1 in Appendix F-1. As for the national study the trend coefficients b_1 and b_2 are characterised by both negative and positive values, indicating rise and fall of the incidence at the various locations. Relatively, the coefficients of determination recorded for districts in the region are higher, ranging from 0.6306 to 0.9128 with an average of 0.7748. In addition, the spatial semivariogram models of the trend coefficients show substantial spatial correlations with shorter range from 50 to 140 km, despite the some extreme semivariance values (Figure F-1.1). The spatial continuity of the coefficients appears to vary similarly in both short and long ranges. However, values for the two parameters (nuggets and sills) differ remarkably, compared with the national trend parameters. The total sills for the

intercept(b_0) and the linear coefficient(b_1) are 260,000 and 76, respectively compared with the national trend coefficients which are modelled with much lower sills. The periodic coefficients (b_3 and b_4), rather have smaller sill values of 146.5 and 151, respectively. The extremely high semivariance values for the first lag of the trend coefficients for BAR could be attributed to the cross-type of pairs of district locations, (Gething et al., 2007), as earlier explained in section 5.2.2.

Table 5.7.1: Spatial semivariogram model parameters of the regionalised trend model coefficients of malaria incidence rates for BAR

Coefficient b_i	Model $\hat{\gamma}_s^{(i)}(\mathbf{h}_s)$	Sill (c_s)	Spatial Range (r_s in km)	Relative Nugget
(Intercept) b_0	<i>nugget</i>	25000	-	0.096
	<i>spherical</i>	35500	65	
	<i>spherical</i>	199500	110	
(t) b_1	<i>nugget</i>	2.5	-	0.033
	<i>spherical</i>	70	110	
	<i>spherical</i>	3.5	75	
(t ²) b_2	<i>nugget</i>	0.00015	-	0.117
	<i>spherical</i>	0.00005	50	
	<i>spherical</i>	0.00108	120	
(cos) b_3	<i>nugget</i>	1.50	-	0.010
	<i>spherical</i>	105	50	
	<i>spherical</i>	40	100	
(sin) b_4	<i>nugget</i>	1.00	-	0.007
	<i>sph(h/r)</i>	5.00	60	
	<i>sph(h/r)</i>	145	140	
R squared (\hat{R}^2)	<i>nugget</i>	0.0002	-	0.013
	<i>sph(h/r)</i>	0.0022	50	
	<i>sph(h/r)</i>	0.0125	115	

The estimation of the trend surfaces by (5.2.3) generated 156 spatial maps, indicating the monthly average risk estimates of the malaria morbidity in the region for the period 1998-2010. Figures 5.7.1 and 5.7.2 display spatial maps of the temporal surface profiles of the estimated risk for selected months in 2000, 2004, 2008 and 2010. High incidence of the disease in the region is consistently localised in the west and south-west, bordering with the neighbouring country, Cote d'Ivoire and has also been extended to the central part of the region in recent times. Consistently, the eastern part is observed with the least estimated morbidity risk. This part of the region is the least inhabited and has the fewer number of sample locations. As it pertains nationally, the

reported morbidity cases of malaria have risen sharply over the years but appear to be stabilising or increasing at large geographical areas towards the central parts of the region after 2008.

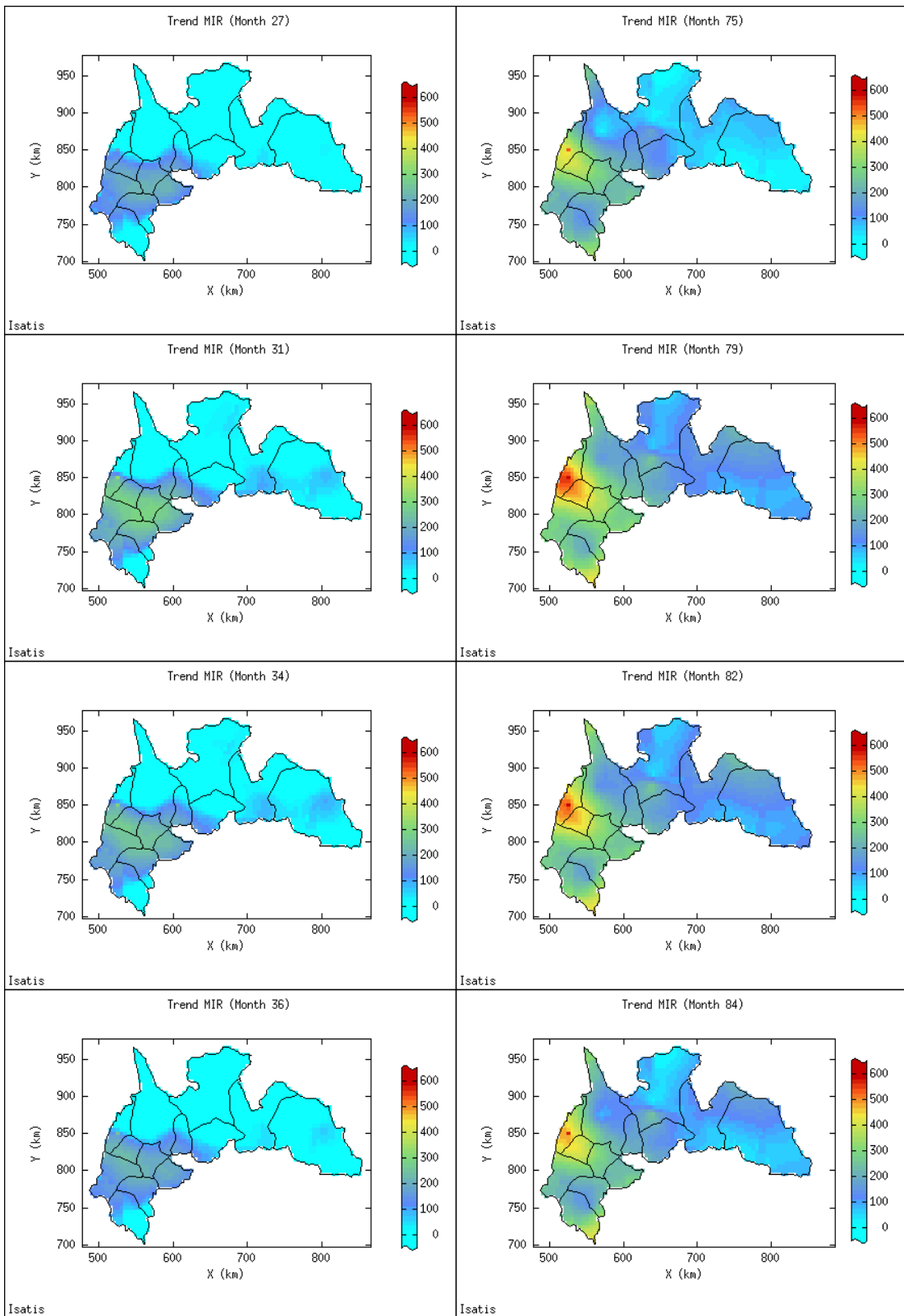


Figure 5.7.1: Estimated trend surfaces of the malaria morbidity incidence rates for the selected months, March, July, October and December in 2000 and 2004.

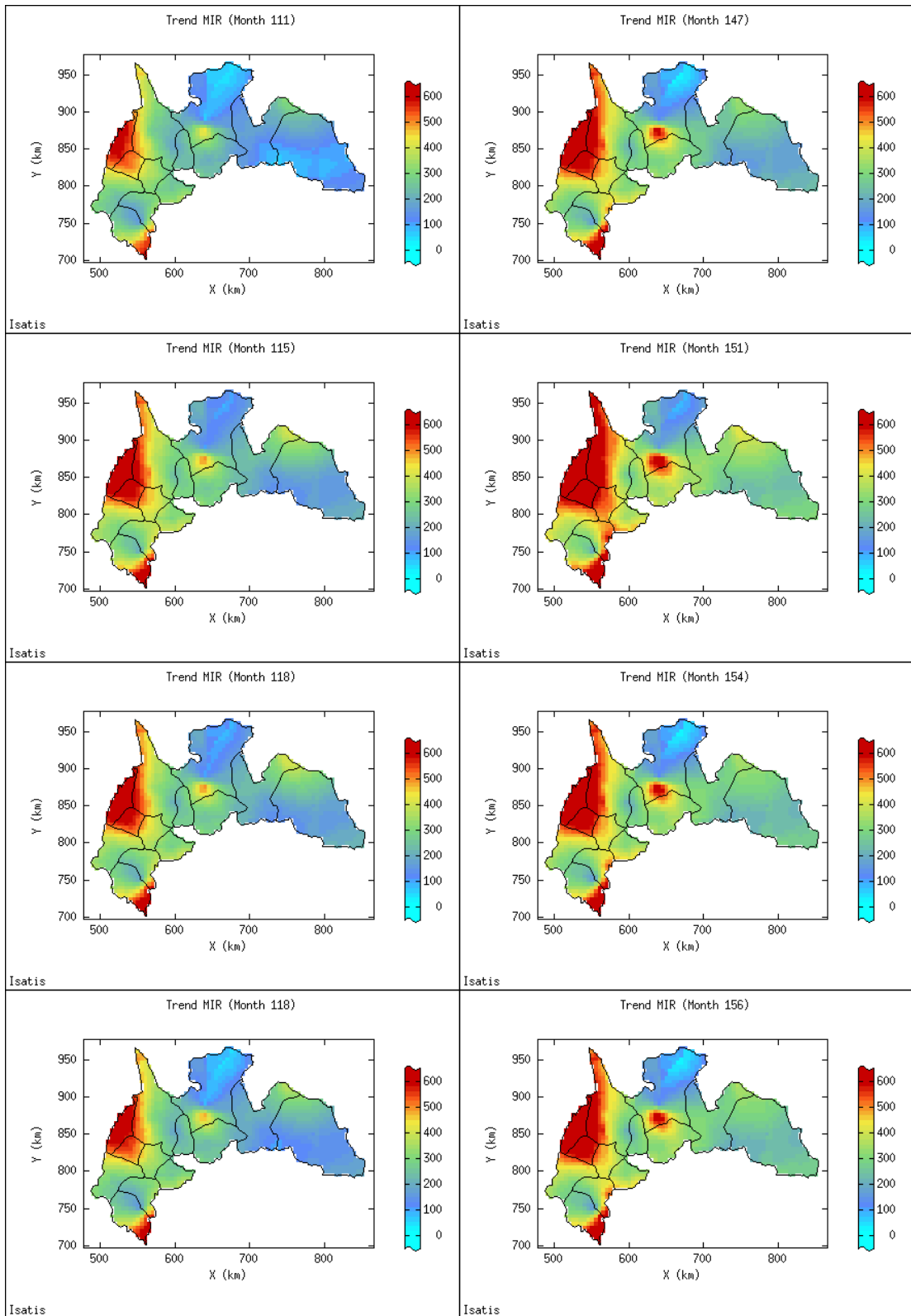


Figure 5.7.2: Estimated trend surfaces of the malaria morbidity incidence rates for the selected months, March, July, October and December in 2008 and 2010

5.7.2 Space-time Ordinary Kriging of MIR

The space-time ordinary kriging of the residuals (STROK) via the generalised product-sum (GPS) modelling of the space-time semivariogram of the residuals is among the various models considered for the estimation of morbidity risk in BAR. The GPS models produced better characterisation of the correlation structure of the morbidity incidence, as also observed by the national study. Table 5.7.2 provides the parameters of the marginal spatial and temporal semivariograms and the space-time generalised product-sum semivariogram models of the residuals. Figures 5.7.3 displays graphs of the marginal semivariograms and the space-time semivariogram surfaces whilst the modelling parameters for the non-stationary observed morbidity incidence rates are given in Table F-2.1 and the graphs shown in Figure F-2.1 in Appendix F-2.

The results indicate stronger autocorrelations of the incidence rates with smaller relative nugget effects of 0.128 spatially and 0.140 temporally, compared with the corresponding figures 0.302 and 0.255 by the joint modelling of the residuals (see Table F-1.3) and national study figures of 0.481 and 0.342 (see Table 5.3.3), respectively. The GPS modelling also provides better spatio-temporal continuity of the incidence with shorter ranges of 80 km and 18 months and global sill of 4800. The dissimilarity of the malaria morbidity incidence rates, as illustrated by the sills of semivariograms, are higher in the BAR, compared with that values which were obtained nationally. Following (5.4.1) and (5.4.2) the estimates of STROK are obtained for the temporal surface profiles and estimated risk of the morbidity incidence in BAR to be generated. Figures 5.7.4 and 5.7.5 display some of the spatial maps produced for 2000, 2004, 2008 and 2010.

High morbidity incidence of the disease in the region is consistently localised in the west and south-west, bordering with the neighbouring country, Cote d'Ivoire and in recent times been extended to the central part of the region. The eastern part of the region has the fewer number of sample locations, and consistently, as trend earlier observed by the global trend profiles, has the least estimated morbidity risk. As it pertains nationally, the reported morbidity cases of malaria have risen sharply over the years but appear to be stabilising or increasing at large geographical areas towards the central parts of the region after 2008.

Table 5.7.2: Parameters of the marginal semivariograms and product-sum semivariogram models of the detrended malaria incidence rates (residuals) for the study in BAR

Model	Spatial		Temporal		Product-sum	
	Sill (RN)	Range	Sill (RN)	Range	Global Sill	k
<i>nugget</i>	500 (0.128)	-	650 (0.140)	-		2.068×10^{-4}
<i>exponential</i>	3400	80	-	-	4800	(2.151×10^{-4})
<i>exponential</i>	-	-	4000	18		

In parentheses are the relative nugget (RN) effects of marginal semivariograms and maximum k limit values for the product-sum model.

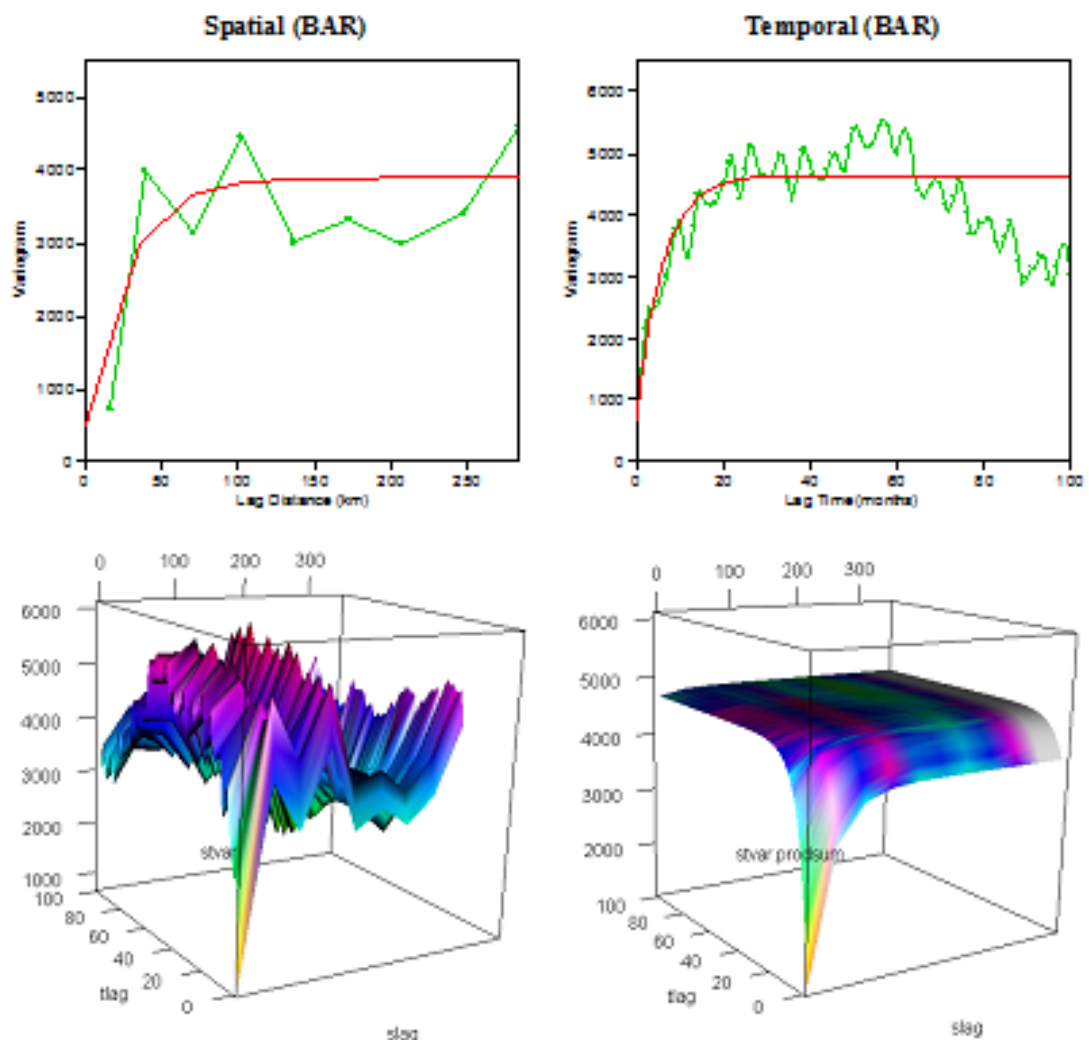


Figure 5.7.3: Marginal spatial and temporal semivariogram models of the residuals incidence rates (top) and space-time experimental semivariogram surfaces together with their product-sum models (bottom) for the study in Brong Ahafo Region

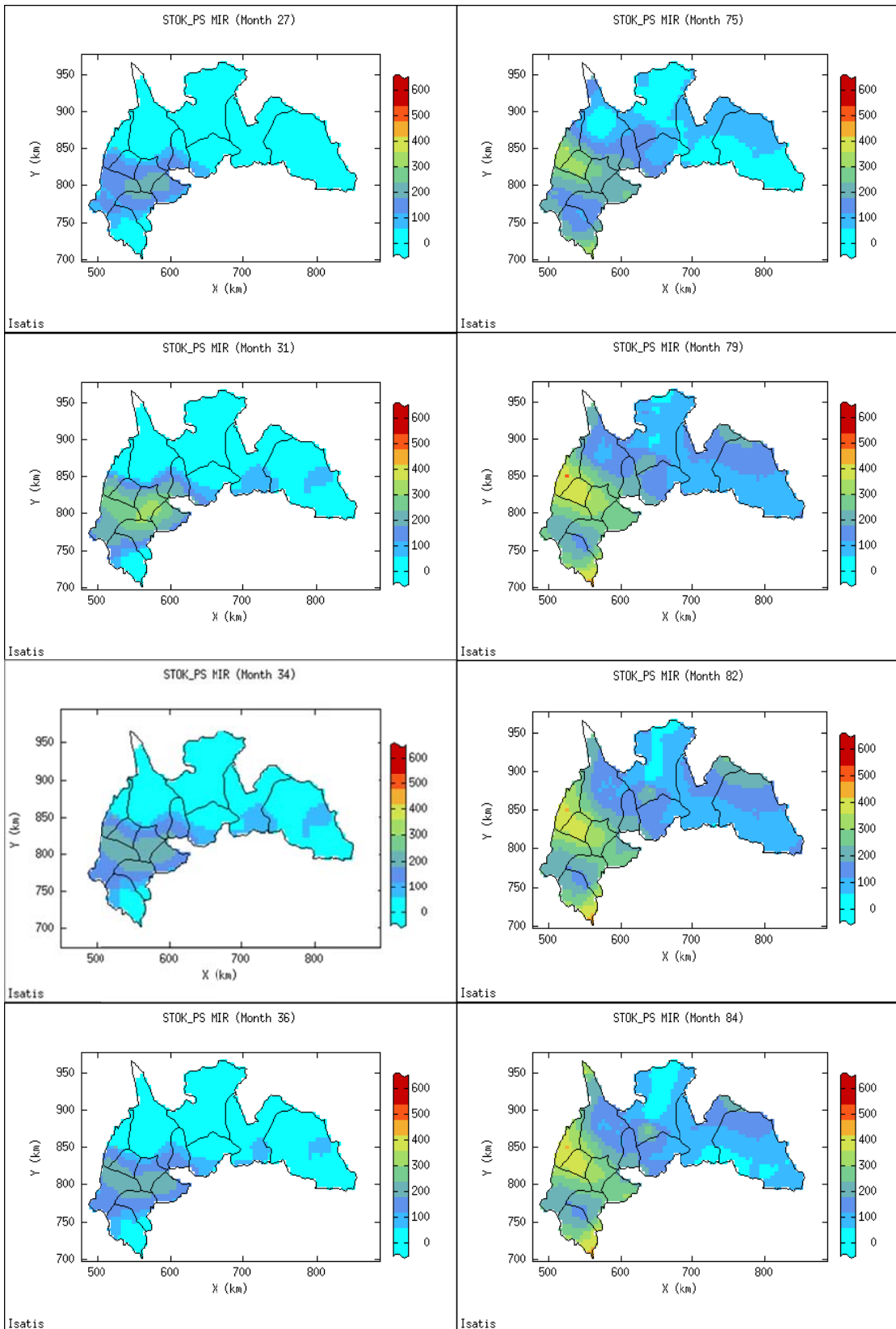


Figure 5.7.4: Monthly spatial maps of malaria risk estimated by space-time ordinary kriging by the generalised product-sum modelling of residuals (STOK_PS) in BAR for some selected months in 2000 and 2004.

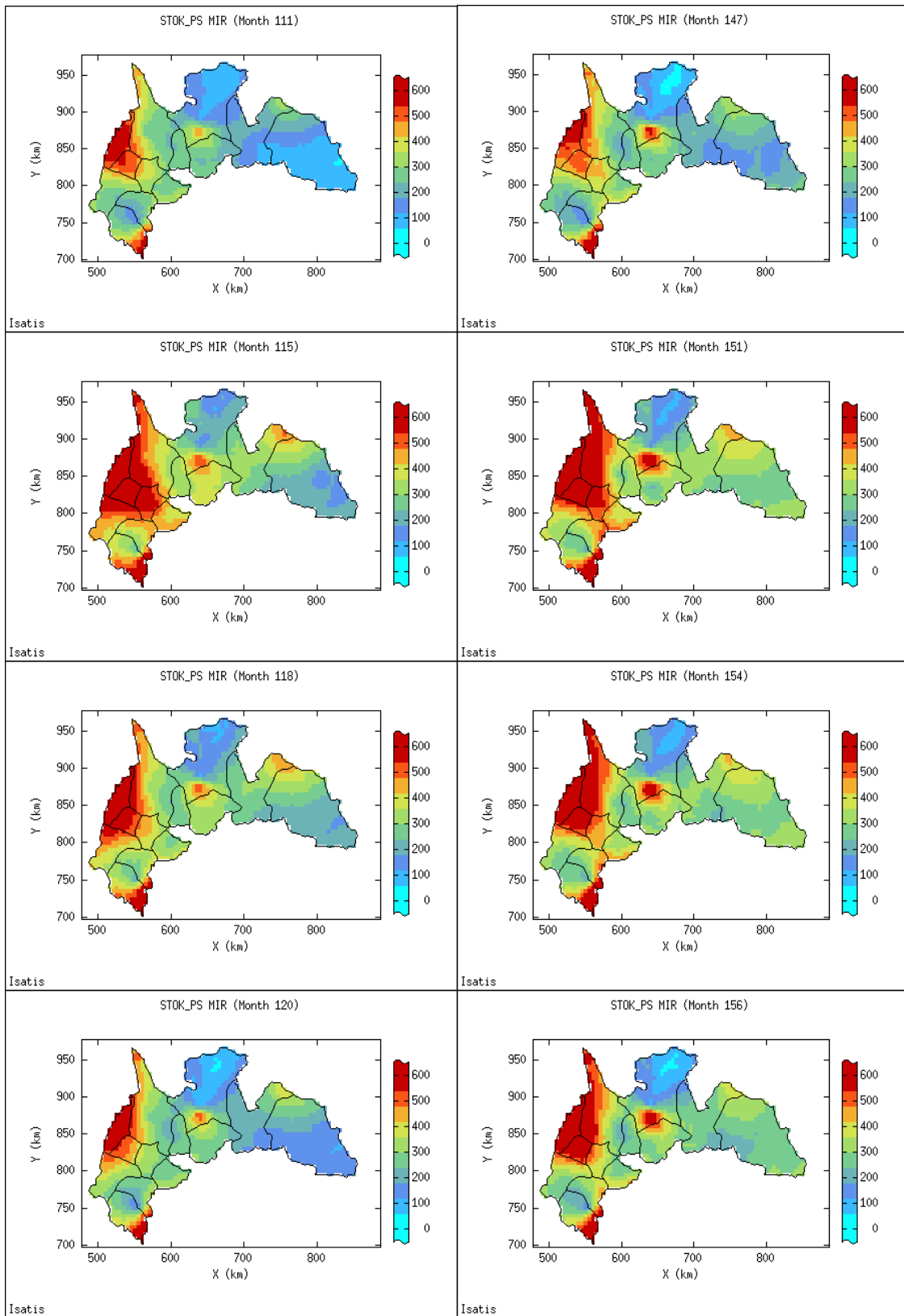


Figure 5.7.5: Monthly spatial maps of malaria risk estimated by space-time ordinary kriging by the generalised product-sum modelling of residuals (STROK_PS) in BAR for some selected months in 2008 and 2010.

5.7.3 Validation of Kriging Estimates

The space-time kriging estimates in the region by Tables 5.7.3 and 5.7.4 are summarised and validated by forward predictions of the 2011 incidence data. The estimates are higher and more variable due to the large extreme values, just like the observed incidence samples. The sample incidence data range from 64 to 1275 and record an average of 288 incidence cases with a standard deviation of 165.60. Malaria morbidity incidence in the region is predicted to occur from 0 (-1065.3) to 1275 cases per 10,000 resident people and as was the case for the national, the STOLK estimates are less variable and predict more close to the observed sample data (see Table 5.7.3).

Table 5.7.3: Summary statistics of kriging estimates of malaria incidence rates together with their prediction standard deviations compared with the observed incidence data.

Kriging Estimate	Brong Ahafo Region (BAR)					
	Count	Min	Max	Mean	StDev.	CV
Sample	2460	64.00	1275.00	288.33	165.60	0.574
STOLK	242553	76.20	1275.00	244.56	126.90	0.519
STROK	243204	-1065.3	1274.98	151.20	208.67	1.375
STOK_PS	242537	-1059.7	1274.98	152.43	208.65	1.369

As judged by the Jackknife prediction of the 2011 incidence data in the region (see Table 5.7.4), predictions by the space-time kriging techniques which employ variography of the residuals coupled with or without the generalised product-sum modelling approach appear more close to the samples. However, the latter technique (STOK_PS) proved more superior with least MAE and RMSE values of 44.732 and 56.663, respectively. This is further evidenced by the spatial maps which revealed detailed information (as observed from the national maps) regarding the dynamics of the incidence of the disease in the region.

Table 5.7.4: Prediction estimates for 2011 compared with the sample data and their measures of prediction accuracy in BAR

Kriging Estimate	Brong Ahafo Region (BAR)								
	Min	Max	Mean	Std.	CV	ME	MAE	RMSE	Corr.
Sample	144.00	940.00	434.99	156.68	0.360	-	-	-	-
STOLK	269.00	622.00	470.65	95.19	0.202	43.48	118.39	162.271	0.400
STROK	34.79	1077.1	461.76	205.46	0.445	-26.77	69.718	85.624	0.934
STOK_PS	127.44	926.49	442.20	161.80	0.366	-7.21	44.732	56.553	0.938

5.8 Malaria Morbidity Risk in the Vegetation Zones

Having holistically and exhaustively investigated the spatio-temporal distribution of malaria morbidity incidence rates in Ghana, the morbidity risk of the disease by vegetation types in the country, like in BAR, is considered because of their economic importance, as outlined in section 5.1. As was the case for the Brong Ahafo Region in section 5.7, results of the main space-time kriging models used to explore the spatio-temporal distributions of the malaria incidence rates in three vegetation (northern, forest and coastal) zones are presented in this section. These include the structural analysis of the incidence rates by the generalised product-sum modelling and the subsequent space-time kriging process of the incidence rates at the unsampled district-month locations. The results for the other space-time prediction models considered for the analysis, namely STLOK, STROK and STOCK, are presented in Appendix G.

5.8.1 Product-Sum Semivariogram Models of MIR

The results for the generalised product-sum modelling of space-time semivariograms of malaria incidence rates by the vegetation types, following the same procedure as in the previous sections, are as shown in Table 5.8.1 and Figures 5.8.1 and 5.8.2.

Table 5.8.1: Parameters of the marginal semivariograms and product-sum semivariogram models of the detrended malaria incidence rates (residuals) for the vegetation zones study

Zone	Model	Spatial		Temporal		Product-sum	
		Sill (RN)	Range	Sill (RN)	Range	Global Sill	k
Northern	<i>nugget</i>	1950 (0.448)	-	2200 (0.358)	-	6500	1.495×10^{-4} (1.626×10^{-4})
	<i>exponential</i>	2400	100	-	-		
	<i>exponential</i>	-	-	3950	16		
Forest	<i>nugget</i>	1500 (0.556)	-	1000 (0.286)	-	3550	2.804×10^{-4} (2.817×10^{-4})
	<i>exponential</i>	1200	55	-	-		
	<i>exponential</i>	-	-	2500	18		
Coastal	<i>nugget</i>	500 (0.364)	-	600 (0.364)	-	1750	5.620×10^{-4} (6.061×10^{-4})
	<i>exponential</i>	875	100	-	-		
	<i>exponential</i>	-	-	1050	16		

In parentheses are the relative nugget (RN) effects of marginal semivariograms and maximum k limit values for the product-sum model

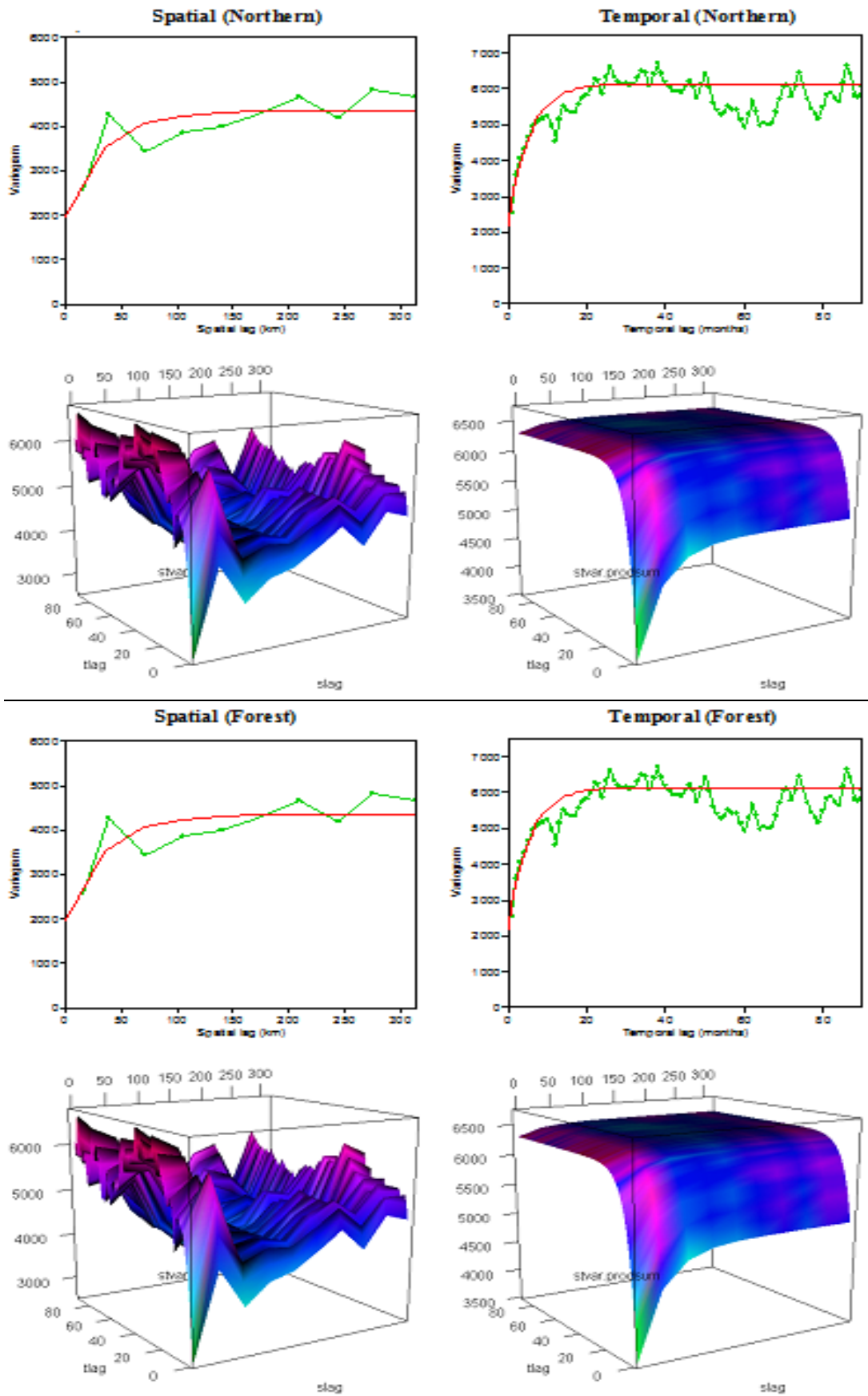


Figure 5.8.1: Marginal spatial and temporal semivariogram models of the residuals(top) and space-time experimental semivariogram surfaces together with their product-sum models (bottom) for the northern and forest zones.

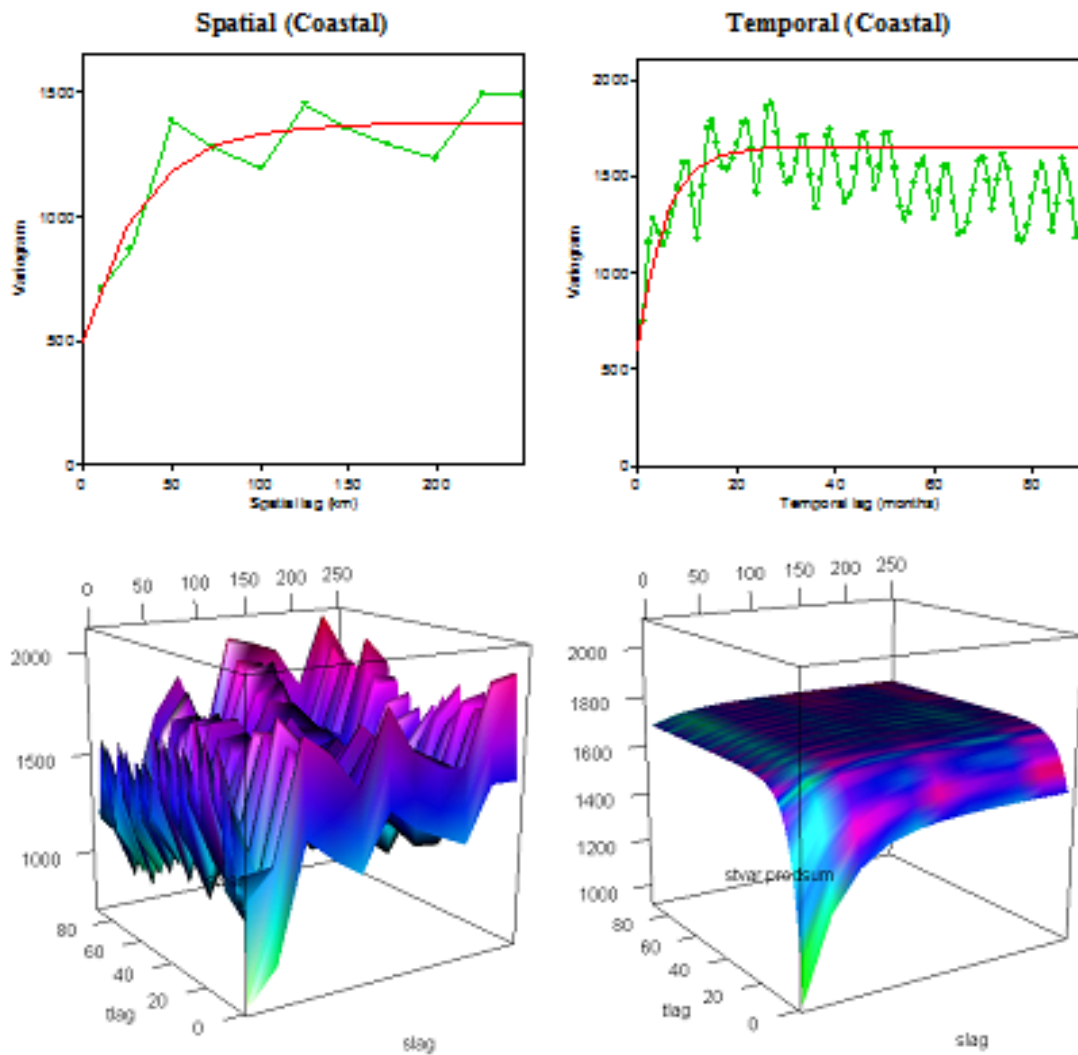


Figure 5.8.2: Marginal spatial and temporal semivariograms modelsof residuals (top) and space-time experimental semivariogram surfaces together with their product-sum models (bottom) for the coastal zone

The space-time semivariogram surfaces of both the observed incidence rates and the residuals for the three zones, generally appear to be similar but with varied global sills. As expected, they are highest in the northern zone but lowest in the coastal zone. The variography of the residuals, as evidenced in the two previous studies, provides a better representation of the correlation structure of disease's incidence in the three zones (see Figures 5.8.1 and 5.8.2 and Appendix G). The relative nugget effects of the residuals for zones vary from 0.364 to 0.556, spatially and 0.286 to 0.364, temporally, compared with the national study values of 0.481 and 0.342, respectively which are higher than the observed incidence rates, just like the previous modelling approaches. Malaria risk in the northern and forest zones appears to be spatially and temporally heterogeneous which in the latter case could be influenced by the high incidence in BAR. The ranges of the autocorrelation vary across the zones from 55 to 100 km, spatially and 16 to 18

months, temporally, with the shortest range in the spatial domain occurring in the forest zone. The global sill is highest (6500) in the northern zone and lowest (1750) in the coastal zone, with the forest zone recording a value (3550) between the two values. The marginal spatial semivariograms of the observed incidence rates show more continuity of the disease occurrence in the northern and coastal zones (100 km) than the forest zone (80 km). Contrary, the temporal dependence varies more continuously in the forest zone (85 months) than the other two zones (80 months); however, the morbidity incidence in the northern zone has very distinct seasonal variations (Table 5.8.1 and Figures G-2.1–G-2.3 in Appendix G-2).

5.8.2 Space-time Ordinary Kriging of MIR in the Northern Zone

As observed from the spatial maps in the national study, areas in the northern zone appeared highly risk of the malaria morbidity. In view of this only the spatial maps of the northern zone will be presented and compare (like the BAR) with the national risk maps. The STROK technique, utilising the generalised product-sum semivariogram models of the residuals developed in section 5.8.1, is then applied to obtain the morbidity incidence rate estimates at the unobserved district-month locations. Figures 5.8.3 and 5.8.4 present the spatial maps generated by STROK_PS for some selected months in 2000, 2002, 2008 and 2010.

The estimated incidence rates by the spatial maps follow similar pattern of distribution as observed from the national maps, revealing more details of the risk of the disease in the zone. The higher risk areas are mainly found at locations near the borders with the neighbouring countries Burkina Faso and La Cote d'Ivoire and the spatial range of incidence of the disease has expanded significantly over recent years. Also potential of high risk of the malaria morbidity are the other parts towards the east, where there has been significant transition of the disease from the north-west. The effects of the climatic covariates of rainfall and maximum temperature, which correlate highly with the morbidity incidence, contribute to the high morbidity cases in the zone. This is evidenced by the spatial maps generated by the STOCK_Rain and STOCK_MaxT techniques using the effects of rainfall and maximum temperature in the preceding one month. The morbidity incidence rate surfaces observed for the zone appeared more heterogeneous and relatively spread over larger geographical areas.

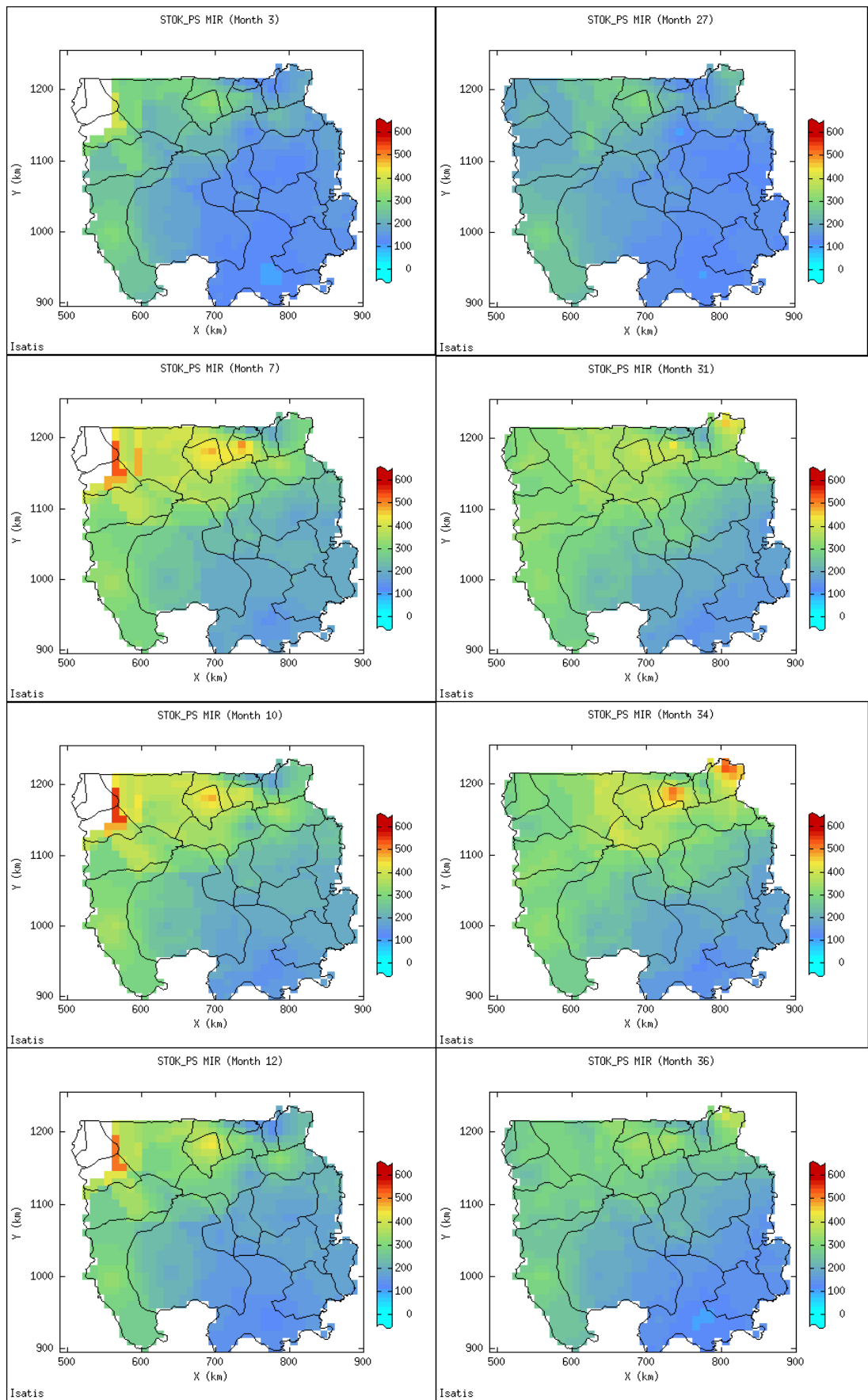


Figure 5.8.3: Monthly spatial maps of malaria risk estimated by space-time ordinary kriging by the generalised product-sum modelling of residuals (STOK_PS) in northern zone for some selected months in 2000 and 2002.

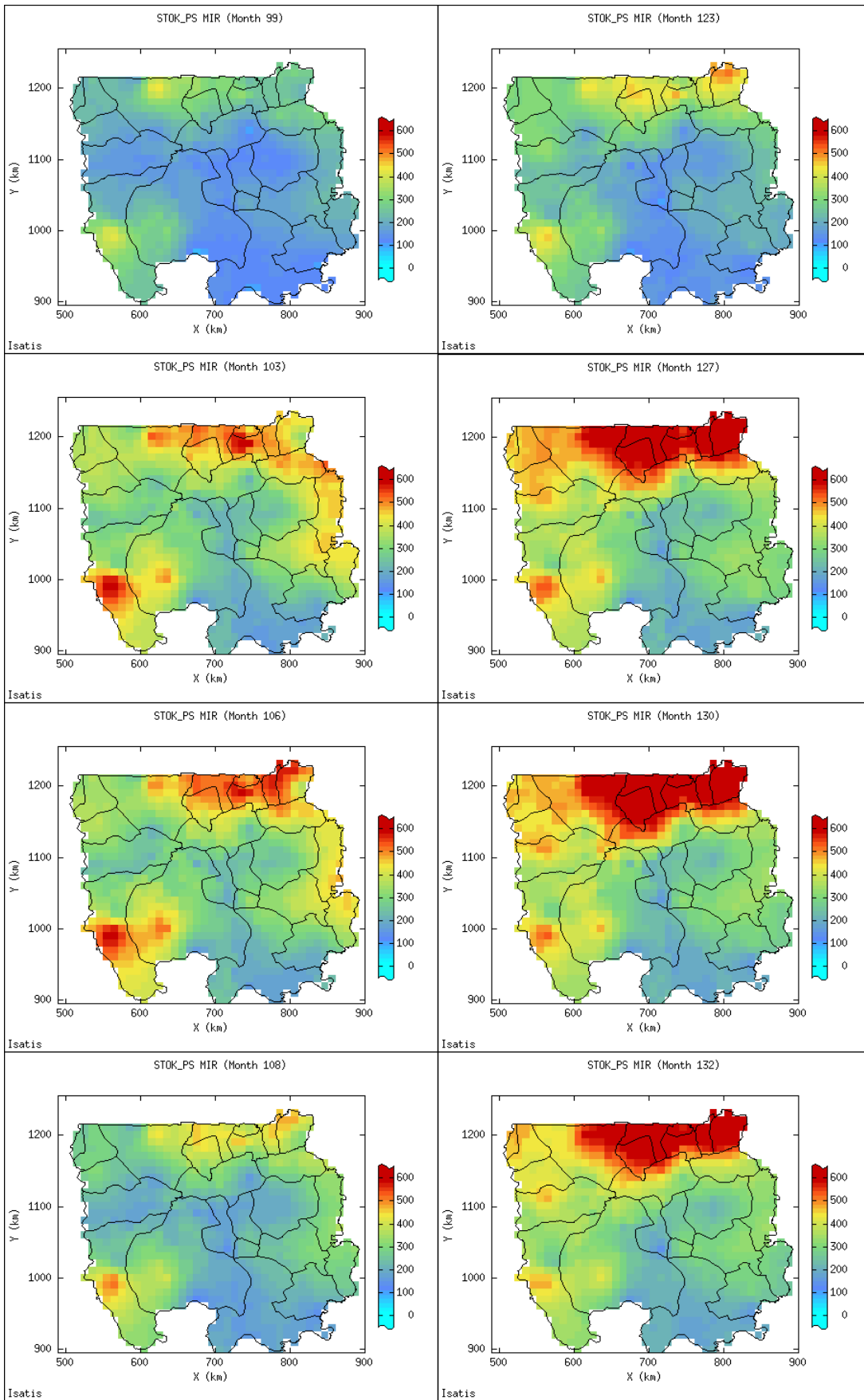


Figure 5.8.4: Monthly spatial maps of malaria risk estimated by space-time ordinary kriging by the generalised product-sum modelling of residuals (STOK_PS) in northern zone for some selected months in 2008 and 2010.

5.9 Chapter Summary

In this chapter, the malaria morbidity incidence rates observed at the district-month locations in Ghana have been modelled using geostatistical space-time kriging techniques. The analysis sought to describe the spatio-temporal distribution of the monthly malaria morbidity case reports from the district health facilities and to account for the environmental effect of rainfall, relative humidity and temperature, with particular attention to identifying areas with high risk of morbidity incidence in the country. This has been achieved by applying the geostatistical methodology to three different case studies, nationally, regionally (using BAR) and by vegetation (or malaria epidemiological) zones. For each case study, structural analysis was performed to develop semivariogram models to quantify the spatial and temporal correlations of the morbidity incidence rates leading to the predictions of incidence rates at unsampled locations. Three main kriging techniques STOLK, STROK and STOCK, based on the structural analysis were employed. STOLK was applied to the log-transformed morbidity incidence rates data; STROK used the detrended and deseasonalised incidence data coupled with the generalised product-sum model; and STOCK, which used the LMC to account for the potential influence of rainfall, temperature and relative humidity on morbidity incidence rates.

The space-time semivariogram models constructed showed spatial and temporal correlations of the incidence rates in short and long ranges. The semivariogram models fitted by the generalised product-sum model exhibited shorter ranges of autocorrelations and characterised the continuity of incidence rates with fewer basic structures of spherical and exponential variogram models. The LMC of morbidity incidence rates with the potential covariates accounted for significant spatial and temporal continuity of morbidity incidence in all the study areas, with rainfall lagged one month contributing to higher of the morbidity incidence variation with shorter range of correlation. The space-time kriging predictive models established increased risk of morbidity which is seasonal across the country. However, highly elevated incidence cases of the disease can be observed at locations near the borders with the neighbouring countries. Rainfall and maximum temperature contributed significantly to the increased morbidity incidence in Ghana. Validation analysis was conducted which proved the STROK techniques predicting the morbidity incidence rates of the disease with higher degree of accuracy.

Chapter 6

Conclusions and Recommendations

6.1 Summary of Analysis and Findings

Malaria is a highly endemic disease which poses serious threats to both the public health and socio-economic development of Ghana, in spite of high knowledge of its mode of transmission and prevention among the general population. Detailed knowledge of its distribution in space and time, coupled with accurate quantification of the disease (morbidity and mortality) burden has become important for the efficient management of malaria control programmes and public health planning in the country. Ghana's National Malaria Control Programme (NMCP) faces such challenges as often incomplete monthly case reports are recorded in the national data base. This raises concern about the annual estimates released on the disease burden. Spatial and temporal distributions of malaria incidence provide a rationale for interventions, making it possible to determine estimates at unsampled locations and time instances. In this thesis, the concepts of both geostatistical space-time statistical and time series SARIMA predictive models were studied and applied to the malaria morbidity case reports from the district and regional health facilities in Ghana. The purpose of the study was to explore both the spatial and temporal distributions of the malaria morbidity incidence cases as reported in the country over period 1998-2011 and to account for the potential influence of environmental variability. More specifically, the study sought:

- (i) To perform seasonal analysis of morbidity cases in the regions with the aim of establishing temporal distributional patterns and providing predictive models for seasonal forecasting of the malaria risk;
- (ii) To characterise the spatio-temporal continuity of the malaria incidence rates at the district-month locations across the country and to identify and account for potential climatic effects; and
- (iii) To produce evidence-based risk maps of malaria incidence, estimating its incidence rates and describing distributional patterns over space and time, with a particular focus on delineating areas with high risk of malaria infection in Ghana.

The monthly malaria morbidity count data considered for the study were new clinically diagnosed outpatient (non-laboratory confirmed) cases for the period 1998-2011. They were obtained from the data base of CHIM and complemented by the available records at Regional Health Information Units of GHS. As per reasons previously given in Chapter 4, the whole data set was classified as regional (global), comprising morbidity cases from all the 10 regions, and space-time (district-month), being the observed cases from the districts for the seasonal and spatio-temporal analyses performed at the regional and district levels, respectively. The analysis was pursued by first standardising the monthly case count data as incidence rates, in view of the high occurrence of malaria in all parts of the country. Thus, the morbidity incidence rate (MIR) was defined as the number of new morbidity cases per unit district or region resident population of 10,000. The MIR data together with the climatic covariates, collected from the Ghana Meteorological Agency (GMet), were considered as realisations of random processes occurring in space and/or time and modelled as per the various temporal and spatio-temporal techniques employed in this study.

Generally, the results showed varied spatial and temporal distribution of the morbidity incidence cases, which have increased over the years across the country. This could partly be attributed to the seasonal variability in environmental conditions such as rainfall and temperature which create favourable conditions for breeding of the *Anopheles* mosquito vector. This was evidenced by the significant impact of the weather variables considered in the analysis. Other possible causes which are widely believed to have links with malaria occurrence but were not investigated in this study include socio-economic and biological factors. In the following sections, the detailed summary of the research findings of the analyses conducted in chapters 4 and 5 together with the discussion are presented. Also, outlined in the chapter are the limitations of the research, the significant findings contributing to knowledge, and recommendations for possible future research and policy interventions for malaria control.

6.1.1 Seasonal Analysis of MIR at Regions

The time series plots coupled with the smoothing analyses were performed to examine the long-term trends and seasonal dynamics of the morbidity incidence rates at a regional level. The incidence rates showed a continuous upward trend, characterised by similar but strong seasonal variations. High and low peaks were observed, occurring

during the wet (May-November) and dry (December-April) seasons, respectively. The highest peaks of the incidence rates were observed between 2006 and 2009, after which they seemed to be levelling off. However, the seasonal variations in the three regions forming the northern savannah zone were very distinctive with continuous linear or exponential growth. For them, together with the Brong Ahafo region, the number of new incidence cases was highest, whilst the lowest incidence cases were observed in Greater Accra and Central regions. In all cases, the smoothing analyses showed that the female incidence rates were slightly higher than those for men whilst the monthly incidence rates for children up to age 4 were highest with high growth rates, as observed from the moving average and Holt-Winter's smoothing results. The predictive forecast of new incidence cases followed a similar trend pattern which appeared to be either increasing or stabilising in Brong Ahafo, Ashanti, Greater Accra, Northern and Upper West. The malaria morbidity incidence in these regions was strongly influenced by both seasonal and non-seasonal components of autoregressive and moving average processes and strongly influenced by the rainfall, temperature and relative humidity in the preceding month as evidenced by the significant reductions in the AIC, RMSE and MAE values. The forecasted values for 2011 appeared close to the observed, as they were all found lying within 95% confidence intervals of the estimates and also strongly correlate with the observed values with the correlations for both the total and the under 5 year groups ranging between 0.771 and 0.889.

6.1.2 Structural Analysis of Space-time MIR at District Locations

The space-time semivariogram models characterising the spatio-temporal continuity of the morbidity incidence rates indicated that the occurrence of the malaria morbidity cases was spatially and temporally correlated. Nationally, the spatial range of dependence varied from 35 to 250 km and the temporal range from 10 to 85 months. The range of spatial autocorrelation of the incidence in the Brong Ahafo Region was between 35 and 140 km, whilst that for temporal autocorrelation was between 20 and 80 months. The corresponding spatial and temporal ranges observed for the incidence rates in the malaria epidemiological (vegetation) zones were between 35 and 160 km and 6 to 100 months, respectively, with the incidence rates in the forest zone varying more continuously with longer ranges. However, the generalised product-sum semivariogram models which characterised the incidence rates with fewer basic structures exhibited shorter ranges of autocorrelations, mostly between 55 and 120 km

and 16 and 100 months. The relative nugget effect values arising from the product-sum modelling of the spatio-temporal semivariograms were much smaller, ranging from 0.098-0.354 (spatially) and 0.045-0.313 (temporally), compared with the corresponding joint space-time results of 0.302-0.441 and 0.255-0.370, respectively, which facilitated the space-time kriging at the district-month locations with increased higher precision.

Spatially and temporally, the morbidity incidence rates at the district locations correlated positively with rainfall and relative humidity and negatively with temperature. The LMC of the incidence rates with the climatic covariates separately showed that rainfall (lagged 1 month) and instantaneous maximum temperature and relative humidity (at 1500 hours) accounted for much of the spatial continuity of the morbidity incidence at the district locations. Rainfall in the preceding month of malaria incidence resulted in relatively longer ranges of correlation (35-280 km), compared with the other potential covariates which ranges were from 35 to 200 km. In the purely spatial case, rainfall and relative humidity increased the range of spatial dependence to between 60 and 260 km whilst temperature has rather longer range of continuity of 150-280 km. In the vegetation zones and BAR, the impact of potential covariates of rainfall, maximum temperature and relative humidity in the preceding month on the incidence rates followed the similar pattern and stronger effect of spatial and temporal correlations but with smaller range of correlations.

6.1.3 Prediction of Space-time MIR at District Locations

The space-time optimal predictions at the unsampled district locations were based on the spatio-temporal continuity of the malaria morbidity incidence rates. The results showed that malaria morbidity risk is seasonal and has increased across the country over the years, particularly from the period 1998/2000-2004 to 2005-2010. There has also been a spatial expansion and transition of high morbidity risk of the disease from areas in the north-west (Upper West Region) to the north-east (Upper East Region) parts. The morbidity incidence rates were found to be heterogeneous with highly elevated incidence rates at locations near the borders with neighbouring countries in the north (Burkina Faso), west (La Cote d'Ivoire) and central parts towards the east (with Republic of Togo). The effect of weather changes contributed significantly in the distribution of the morbidity cases reported from the district health facilities, as established by the seasonal variations. The incidence rates of the disease were

estimated to be high mostly in the wet season when temperatures were relatively low whilst low incidence rates were observed during the warm weather period in the dry season. The findings were in line with the space-time ordinary co-kriging (STOCK) results which established significant impact of rainfall and temperature on morbidity incidence at the district and regional locations. Whilst rainfall in the preceding month contributed to an increased risk of malaria morbidity across the whole study area of Ghana, the effect of maximum temperature was more pronounced in the northern, western, and at central parts towards the coast. Areas with high amount of rainfall (or relative humidity) coupled with low or decreasing maximum temperatures were found to be associated with an increased risk of malaria morbidity, mostly at the district locations in the south, through the central, to the north. The findings are also consistent with the different temporal profiles of the incidence rates and the results of the estimated trend model (5.5.1) which showed long-term increase or decrease of the incidence rates at the district locations with high variations.

The prediction of MIR in the Brong Ahafo Region, which was chosen for its strategic position in Ghana, consistently estimated higher incidence rates at locations in the west, close to the border with La Cote d'Ivoire. Lately, the high morbidity risk of the disease has also expanded to the central parts of the region, noted for commercial activities such as crop farming and inland fishing. As was the case for the national study, increased (or decreased) risk of malaria morbidity in the region was associated with high rainfall in the preceding month (or decreasing maximum temperature) which appeared stronger. The variations in the morbidity risk were estimated higher. In the vegetation zones, the space-time predictive kriging models produced results which affirmed the spatial heterogeneity of the morbidity incidence rates, which was strongly associated with the two potential risk factors in the preceding month. In particular, the incidence rates in the northern savannah zone were estimated to be high and found to be more variable due to favourable environmental conditions for the transmission of the disease in that part of the country, as discussed below in section 6.1.4.

Also of worthy of note are the monthly spatial maps produced by the STROK and STOCK techniques, which showed much smoother risk surfaces with detailed patterns of the morbidity incidence over larger locations across the country. The validation analysis proved the space-time ordinary kriging technique of residuals using the generalised product-sum modelling, as being more efficient for producing estimates

with least errors of estimation.

6.1.4 Discussion of Results

The intense malaria intervention activities over the years in Ghana do not appear to yield the much desired impact as recent national studies on the disease showed increased infant and maternal mortality rates across the country, far from the highly envisaged Millennium Development Goal-6 (MDG-6) reduction target of 75% by 2015 (MICS, 2011; UNICEF, 2012). This could be partly attributed, particularly, to persistent high level of transmission and lack of accurate information on new incidence cases of the disease to identify the high risk areas. Thus, baseline data and reliable monitoring of key malaria indicators are needed to measure whether the goals for morbidity and mortality reduction are being achieved. Data from health facilities become potentially useful for monitoring malaria patterns and trends, but have several limitations. The crucial factor affecting the representativeness of health facility records is the extent to which these statistics reflect the burden of disease in the population under investigation. In Ghana, severe malaria cases are only included in the health statistics that are also affected by the accessibility of hospital services and by the health-care seeking behaviour of the people. Demographic and health surveys and other sources indicate that less than 50% of malaria morbidity and mortality cases are seen in formal health facilities (GSS et al., 2004b), indicating that only a fraction of the total burden can be accounted for by health statistics. These raise concerns of both under and over reporting for the malaria morbidity data captured in the database of CHIM, on which this study's results were based. Despite these limitations, health statistics may be acceptable for monitoring trends if their low sensitivity remains consistent over time (Adams et al., 2004).

The study was carried out with the ultimate aim of updating the inadequacies of the national data base on the disease with the view of strengthening the country's malaria prevention and control measures. This has been achieved by the development of time series predictive SARIMA and geostatistical space-time kriging models of the malaria morbidity incidence rates at the regional and district levels of Ghana and to account for the characteristics of the underlying spatial continuity of the potential climatic covariates. The SARIMA models provided the temporal seasonal forecasts at the regions whilst the space-time models described the autocorrelation structure of the malaria incidence rates at the district locations and over time. The space-time models

were then used to produce monthly spatial maps estimating the malaria morbidity risk at locations where data were not available, and more importantly, highlight the high risk locations of the disease. In this way, the seasonal forecasts and spatial maps provide useful analytical tools for resource allocation to reduce the morbidity burden of the disease at the local level.

The time sequence plots and the smoothing analyses of the incidence rates in the regions have established varied demographic (age and sex) regional patterns of the disease's occurrence, which will enhance effective monitoring and reduction of new incidence cases. Generally, the results revealed a steady increase in new reports of the disease from onset of the study, characterised by similar seasonal patterns until 2009, after which seemed to be levelling off. The highest incidence rates were observed between 2006 and 2009, which appeared to be the “epidemic” or outbreak of the disease in all the regions. This period coincided with the introduction of free maternal care treatment and passage of the National Health Insurance Scheme (NHIS) bill in 2006 (PMI, 2013) and 2007, respectively in Ghana. The introduction of these two new policies requires that expectant mothers be treated and that health cost delivery be much more affordable in the country as opposed the previous “cash and carry” system which demanded largely unaffordable spot payments for treatment. These interventions, as already established elsewhere (Burgert et al., 2011; Landoh et al., 2012), could potentially contribute to the increased examination of morbidity cases. The decline observed in other time sequence plots of MIR (Greater Accra and Upper West regions) could be due to several combined factors including malaria interventions, notably the introduction of the policies on the use of insecticide treated nets (ITNs), anti-malarial drugs (ACTs) such as Artesunate+Amodiaquine to treat uncomplicated malaria cases and mass spraying of homes with insecticides through indoor residual spraying (IRS) to kill the female *Anopheles* mosquitoes, the main cause of the malaria in the country.

The findings of more malaria morbidity cases among females and in 0-4 year group are consistent with other recent studies in the country (Krefis et al., 2010; Kreuels et al., 2008) and elsewhere in Ethiopia (Woyessa, Deressa, Ali, & Lindtjørn, 2013), which linked malaria infections with demographic factors, such as sex and age. However, the results of these studies were based on clinical trials conducted in rural communities, contrary to this study which used morbidity cases from all regions in the country. The

results further reflect how highly vulnerable these people are to most of the severe clinical symptoms due to their low levels of immunity from the disease. The variability in climate played a prominent role as it contributed to the extreme dry and wet periods experienced in the country. The seasonal predictive models established for the incidence rates for the 0-4 year group and regional total significantly accounted for impact of rainfall, temperature, and relative humidity including the incidence rates in the preceding months. Rainfall, maximum temperatures and relative humidity (at 1500 hours) in the previous month variously proved to be important predictors of the increased malaria risk, especially in the most endemic regions. The finding agrees with several other studies including Yè, Louis, Simboro, and Sauerborn (2007) who established high risk of malaria infection with the same climatic conditions. This result has policy implication, as the lag one month effect of the climatic covariates appeared to be in agreement with the development of the malaria parasites in the mosquito vector, which was largely influenced by favourable weather conditions during this period. The dependence on rainfall and temperature in the previous month will aid in planning and serve as a valuable early warning tool to avert potential outbreak of the disease in the regions.

The space-time analysis of the study has shown remarkable spatio-temporal variation of the new malaria morbidity incidence rates at the district locations with increased spatial expansion of the incidence of the disease over the study period, coupled with high risk areas. The locations of high risk areas varied over time in each epidemiological zone and were mainly found close to the borders with neighbouring countries (in the north, west and east) and along the coast. These findings could be ascribed to the location which people live, an important risk factor, which is often associated with the local environmental conditions (Carter, Mendis, & Roberts, 2000). Consequently, the results serve as indicators of the potential changes of the malaria transmission patterns and increasingly risk for the low occurrence areas in the other parts of the country. The high risk areas identified in this study appear to be consistent with recent national health surveys (MICS, 2011), which used malaria parasite prevalence in children aged between 0.5 and 5 years (GHS, 2011). The regions in the northern savannah zone were found to have the highest prevalence rates of malaria (43.7–50.7%), followed by Brong Ahafo (37.1%) and Western (36.5%) in the forest zone, which border with Cote d'Ivoire in the western part of the country, whilst the

lowest (4.1%) was for the Greater Accra Region in the coastal zone, compared with the national prevalence rate of 27.5%. Ghana's three neighbouring countries, Burkina Faso, Cote d'Ivoire and Togo, are endemic countries with equally high reports of malaria morbidity and mortality cases (WHO, 2008, 2011). The frequent exodus of population across the borders puts susceptible resident locals at risk of the disease. Often, migrants to the high endemic areas tend to be biologically more vulnerable to malaria infections due to lack of immunity; they are also highly suspected carriers to the low risk regions (Ricci, 2012; Sachs & Malaney, 2002; Silal et al., 2013; Tumwiine et al., 2010). Baragatti et al. (2009) observed that travel outside urban areas increases the risk of being exposed to malaria transmission in their spatial analysis of malaria epidemiology in Burkina Faso, whilst other studies have associated significantly an increased risk of malaria with people engaged in regular farming activities or live close to forest areas, where mosquito breeding is very conducive (Klinkenberg et al., 2005; Kreuels et al., 2008; Ricci, 2012). In Ghana, like most typical SSA countries, many settlements (especially in rural and peri-urban areas) are surrounded by various vegetative covers where the *Anopheles* mosquito vectors are very predominant.

The short and long ranges of auto-correlation for the space-time semivariograms were indications of the spatial heterogeneity of the morbidity risk at the district locations, as observed in the monthly spatial maps. This finding is consistent with other studies (Kreuels et al., 2008; Lindsay et al., 1990; Reid et al., 2010), involving small-area variation in the disease risk and national mapping of the disease risk in Bangladesh. The study of Kreuels et al. (2008), conducted in a tropical forest area as in this thesis, concluded a marked morbidity risk which varies across the communities considered and over short distances. Reid et al. (2010) using a model-based geostatistical approach observed spatial autocorrelation of malaria prevalence within a range of 50 km. Spatial heterogeneity may also be due to the spatial (de Souza et al., 2010; WHO/VBCD, 1989) and temporal distributions of habitats of vector mosquitoes which differ according to the varying environmental local conditions, which can lead to the detection of high-risk groups for the selection of intervention measures (Carter et al., 2000; Coulibaly et al., 2013). This important result recognises differences in malaria infections at various district locations, which implies that health facilities in same district or districts close together might share similar conditions or common vector mosquito breeding places. Spatial homogeneity of the morbidity risk also suggests an

uneven application of malaria intervention activities with more focus on highly risk areas.

This study focused attention on the spatio-temporal structure of the malaria morbidity incidence rates, taking into account of spatial and temporal correlations with only climatic covariates of rainfall, temperature and relative humidity. Many studies have suggested the various negative effects of climate on human health including infectious diseases (Ricci, 2012). The one-month lagged effect of rainfall and maximum temperature on malaria morbidity incidence infection is consistent with the development of mosquitoes, the external period of incubation of malaria parasite in the host and the possible delay in the disease occurrence or reporting, as previously reported in several studies herein cited, including Kleinschmidt, Sharp, Clarke, Curtis, and Fraser (2001), Thomson et al. (2005) and Tian et al. (2008). Rainfall (which confounds with relative humidity) and temperature are important in the transmission of malaria infections, as mosquito larvae require suitable temperature and moderate amount of water for breeding. For example, the high-risk areas found in the various vegetation zones may be due to the wide presence of permanent breeding conditions provided by irrigation facilities and ponds resulting from rivers running off since the mosquito vectors are known to be associated with flooded areas and rainfall (de Souza et al., 2010; Klinkenberg et al., 2005). The forest and coastal zones in the western part of the country record high rainfall and low temperatures in Ghana. However, the study by Reid et al. (2010) in Bangladesh did not find a significant relationship with rainfall but rather established positive association with temperature and vegetation cover in the forest. The heavy rainfall typically associated with the tropical rainforest regions can destroy larvae of mosquitoes, leading to a decrease in transmission of the disease.

There are many other non-climatic factors, such as socio-economic, access to health care and intervention measures, known to have significant influence on the transmission of malaria (Huang, Zhou, Zhang, et al., 2011; Kurane, 2009). The high morbidity incidence which occurred at the district locations in the northern parts of the country could be also attributed to poverty, a socio-economic factor. This part of the country is considered as the most deprived, lacking the resources needed for the provision of social services and infrastructural developments, coupled with high malnutrition rates (Baird et al., 2002). Most malaria intervention activities in Ghana are piloted in suspected areas of high incidence of the disease. These studies include

Appawu et al. (2004), Baird et al. (2002) and Binka et al. (1998), one of which estimates malaria as accounting for over 25% of under-five mortality at the Kessena-Nakana district in the Upper East Region. Efforts to intensify malaria campaigns at these targeted areas will surely reduce malaria burden in the country. WHO recommends the stratification of malaria risk, making it possible to set up clinical trials, targeting high-risk areas on fine geographical scales (WHO, 1986, 2000). Thus, the spatial and temporal heterogeneities established in this study, become important tools for defining local patterns and predictors of the malaria morbidity transmission and infection in space and time. This will facilitate the selection of appropriate study population and allocation of intervention resources which will enhance the accuracy and efficacy of the analysis describing the impact of the study interventions (Coulibaly et al., 2013; Gaudart et al., 2006). In addition, the malaria vaccine trials currently being conducted at two sites (Agogo and Kintampo) in the forest zone (GHS, 2011) could be implemented and expanded in a sustained manner.

6.2 Limitations

The study has been conducted and achieved the targeted objectives, as outlined in sections 1.3 and 6.1. However, the following limitations must be noted that could have affected the findings obtained.

- Malaria morbidity cases considered for the study were clinically diagnosed cases as opposed to the confirmed. The reason was that malaria cases recorded by health facilities in Ghana only account for a small fraction (15%) of the actual infections, as most of these new cases are not microscopically tested or confirmed due to limited laboratory facilities (Agyepong & Kangeya-Kayonda, 2004; NMCP, 2008). However, the number of morbidity cases could equally be balanced by under reporting as large proportion of cases are not reported at the formal health centres. The under-reporting may also arise when people infected by the malaria parasites have subclinical infections and/or did not seek medical attention.
- The reported malaria morbidity cases were aggregated by regions and districts from the health centres, which might have prevented the analysis of incidence rates of the disease at a higher spatial resolution at health-facility levels. This might have led to locations of high risk of the disease being obscured or

wrongly sighted. However, this was the only highest resolution on occurrence of new cases that could be made available and easily collected.

- Different filing of records at the district and regional health offices coupled with inconsistency of reporting were often observed which severely impact on accuracy of the data base system of CHIM. As a routine, the districts were required to report monthly via their regional health information units, but whilst some reported by specific age groupings and sex, others submitted returns differently or just on the total cases. In many cases, the monthly reports on the disease were not received (or promptly), leading to missing records (or wrong recordings). Lack of logistics to facilitate collection and storing information at the district level constitutes yet another problem.
- There is also the possibility of variation in the quality of the CHIM data base system as awareness of malaria among the public and medical practitioners might have varied with time and places of health facilities, which according to Hu, Clements, Williams, and Tong (2011), invariably tend to affect the assessment of the spatio-temporal distribution of the disease.
- In the space-time analysis, the incidence rates of the disease could not be computed for sex and age since such demographic data on population were not available at the district level. However, accounting for the effect of age might have probably led to a negligible impact on the results, as previous studies elsewhere have shown that age distribution of cases follow age distribution of the population (Kleinschmidt, Sharp, et al., 2001).

6.3 Recommendations for Further Work

The following recommendations are made based upon the findings of the research.

- The study investigated the distribution patterns of malaria morbidity incidence spatially and temporal, focusing only on effect of climate variability but did not examine the other key environmental and socio-economic risk factors. Future research using similar methodology should determine the environmental factors, such as vegetation and mosquito density as realisation of random processes, which affect the transmission patterns of malaria. Another possible cause which will be worth investigating into to establish its effect is poverty, as it is widely assumed to have severe impact on malaria risk. However, poverty

encompasses several socio-economic factors including deprivation of economic opportunities and access to health services (Ricci, 2012). The impact of socio-economic factors (such family's income or financial situation) may be difficult to assess due to the lack of standardised economic data of income and tax in Ghana (Krefis et al., 2010).

- The malaria morbidity incidence time series data could seriously be affected by certain external factors such as the intervention policies of free maternal care treatment, passage of the National Health Insurance Scheme (NHIS) bill and use of insecticide treated nets (ITNs) and anti-malarial drugs (ACTs), as being speculated in this study. Though these interventions were not examined in this study, they appeared to have created more awareness for prompt treatments of the disease at the health facility centres, after which there was a substantial reduction of reported cases across most parts (regions) of the country. A further study testing these interventions explicitly will be needed to confirm the significant impact on the occurrence of the disease in the country. This will require adequate monthly time series data on such interventions activities and updates of the malaria morbidity data in Ghana.
- The study had been based on classical geostatistical modelling approach. The potential use of the model-based approaches such as Bayesian hierarchical and Poisson kriging modelling to account for the uncertainty of the model parameters (Beale et al., 2008) and also obtain more stable estimates of the disease risk at sparse data locations (Best, Richardson, & Thomson, 2005) is recommended for future studies. It will be worth comparing the estimates of the classical models obtained in this study with those that will be produced by these model-based methods. Also worth investigating into are the applications of other advanced time series models for further analysis of the regional data. These include the GARCH models which are very useful for analysing highly variable data and state-space models which consider the ARIMAX models as a vector with autocorrelated errors (Shumway & Stoffer, 2011).

6.4 Contributions to Knowledge

The thesis further builds on the preliminary analysis work of the malaria morbidity incidence data in Appiah et al. (2011) and a poster presentation for the ECU industry engagement 2011 (see Appendix I). In addition, the findings have the potential to

contribute to research in malaria epidemiology towards the quantification of malaria morbidity burden and consequently help in the review of the existing and also identify malaria control programmes needed to achieve significant reduction of the disease by 2015. The contributions of the findings of the study are summarised in the following:

- Review of literature on spatial statistical modelling indicates its wide applications to public health data, particularly, of the use of space-time models to quantify spatially and temporally the distribution burden of infectious diseases coupled with delineating the most endemic or areas, although not much has been documented in malaria epidemiological studies. The study appeared to be among the few applications (and first in Ghana) of geostatistical space-time kriging methodology to investigate the spatio-temporal variation of the malaria epidemics at both local and regional levels, taking into account of climatic effects. The generalised product-sum modelling of space-time semivariogram (De Iaco et al., 2001) has proved to be effective for this study.
- Delineating geographical areas of high risk of malaria forms an important basis for locating appropriate interventions for its control and means to monitoring their effectiveness. Such a result further supports stratification of malaria risk and other research studies on malaria vaccine trials (GHS, 2011; WHO, 2000), which can only be improved by such precise epidemiological modelling (Gaudart et al., 2006). It also provides a possibility for identifying socio-economical, ecological and biological factors with which the disease can be associated with.
- In this study an innovation to introduce geostatistical space-time modelling into the predictions of malaria morbidity incidence at unsampled locations in the face of under or over reporting coupled with missing or failure reports has been introduced. The findings will help to eradicate the inadequacies or incompleteness in the data base of CHIM. The study contributes to the efforts of NMCP in providing a complete morbidity data to WHO and also review of the current malaria intervention programmes to achieving its overall goal of 75% reduction of morbidity cases by 2015. WHO computes the disease burden of malaria annually for each of the endemic countries in the world. These findings will serve as a baseline for further research in estimation of the malaria morbidity burden in Ghana.

- Seasonal forecasting of the disease is also of immense contribution to knowledge in the area of malaria early warning system (MEWS). The lag effect of the climatic covariates on the morbidity incidence will aid in planning intervention programmes to avert possible future outbreak of the disease. The rainfall and maximum temperature in the preceding month contribute to the significant variation in the morbidity incidence and increased risk of malaria across the country. This has particularly been established during the months of June-December and in the northern most, western and southern parts which may be an important revelation for the NMCP in their malaria control activities.
- In spite of the limitations listed section 6.2 the study contributes to improving the data limitation problem, which in most studies have focused attention on survey data for the estimation of malaria morbidity and mortality burden. In contrast, this study employed available data on malaria morbidity cases from all public health facilities coupled with available data on rainfall, temperature, relative humidity and elevation across the country.

In conclusion, the study has established increased malaria morbidity risk both spatially and temporally in Ghana, which is seasonal, heterogeneous and varies according to changes in climatic conditions. The spatio-temporal distribution of malaria morbidity burden has been estimated for areas in the country where there were no detailed health outcomes. It has also been used to delimit areas of high morbidity risk of the disease. Thus, the study could be used as a platform to make health information on the disease available to the public health practitioners. In addition, the current malaria control efforts could be more beneficial through application of targeted interventions at the district locations of high morbidity cases by prioritising the most vulnerable (children less than 5 years of age) and also embarking on these interventions timely, especially during the wet weather periods which are associated with relatively low temperatures. This will require efficient early warning systems such as the methodology employed in this study to improve the effectiveness of the national malaria control programmes.

REFERENCES

- Abdi, H., & Williams. (2010). *Jackknife*. Encyclopedia of Research Design: Encyclopedia of Research Design.
- Adams, I., Darko, D., & Accorsi. (2004). Malaria: A burden explored. *Bulletin of Health Information*, 1(1), 28-34.
- Agyepong, I. A., & Kangeya-Kayonda, J. (2004). Providing practical estimates of malaria burden for health planners in resource - poor countries *American Journal of Tropical Medicine and Hygiene*, 71(Suppl 2), 162-167.
- Aiken, L. S., & West, S. G. (1991). *Multiple regression: Testing and interpreting interactions*. : . Newbury Park, CA: Sage, 212 pp.
- Akaike, H. (1974). A new look at statistical model identification. *IEEE Transactions on Automatic Control*, 19(6), 716-723.
- Ali, M., Goovaerts, P., Nazia, N., Haq, M. Z., Yunus, M., & Emch, M. (2006). Application of Poisson kriging to the mapping of cholera and dysentery incidence in an endemic area of Bangladesh. *International Journal of Health Geographics*, 5:45.
- AMMREN. (2008). An African Media & Malaria Research Network (AMMRN) Magazine, November 2008, 2.
- Anderson, R. M., & May, R. M. (1991). *Infectious diseases of humans*. Oxford, United Kingdom: Oxford University Press.
- Appawu, M., Owusu-Agyei, S., Dadzie, S., Asoala, V., Anto, F., Koram, K., . . . Fryauff, D. J. (2004). Malaria transmission dynamics at a site in northern Ghana proposed for testing malaria vaccines. *Tropical Medicine and International Health*, 9(1), 164-170.
- Appiah, S. K., Mueller, U., & Cross, J. (2011). *Spatio-temporal modelling of malaria incidence for evaluation of public health policy interventions in Ghana, West Africa*. Paper presented at the MODSIM 2011, 19th International Congress on Modelling and Simulation. Modelling and Simulation Society of Australia and New Zealand, F. Chan, D. Msrinova & R.S. Anderson (eds), December, 2011 Perth, Australia. www.mssanz.org.au/modsim2011/A10/appiah.pdf
- Armstrong, Chetboun, G., & Hubert, P. (1993). *Kriging the rainfall in Lesitho*. (Vol. 2). In: A. Soares (ed), Kluwer Academic Publishers, Dordrecht, 66-672 Geostatistics Tróia '92.
- Armstrong, A. C., & Delfiner, P. (1980). *Towards a variogram: A case study of coal*: Internal Note N-671, Centrede Geostatistique, Fontainebleau, France.
- Asenso-Okyere, W. K. (1994). Socio-economic factors in malaria control. *World Health Organization (WHO) Forum*, 15, 265-268.
- Baatuuwie, N. B., & Van Leeuwen, I. L. (2011). Evaluation of three classifiers in mapping forest strand types using medium resolution imagery: A case study in the Offinso Forest District, Ghana. *African Journal of Environmental Science and Technology* 5(1), 25-36.
- Bailey, T. C. (2001). Spatial statistical methods in health. *Cad. Saúde Pública, Rio de Janeiro*, 17(5), 1083-1098.
- Baird, J. K., Agyei, S. O., Utz, G. C., Koram, K., Barcus, M. J., Jones, T. R., . . . F.N., N. (2002). Seasonal malaria attacks rates in infants and young children in northern Ghana. *The American Journal of Tropical Medicine and Hygiene*, 66(3), 280-286.
- Banerjee, S., & Gelfand, A. E. (2003). On smoothness properties of spatial processes. *Journal of Multivariate Analysis*, 84, 84-100.

- Baragatti, M., Fournet, F., Henry, M., Assi, S., Ouedraogo, H., Rogier, C., & Salem, G. (2009). Social and environmental malaria risk factors in urban areas of Ouagadougou, Burkina Faso. *Malaria Journal*, 8(13).
- Beale, L., Abellan, J. J., Hodgson, S., & Jarup, L. (2008). Methodological issues and approaches to spatial epidemiology. *Environmental Health and Perspectives*, 116(8), 1105-1110. doi: 10.1289/ehp.10816
- Bell, D., Wongsrichanalai, C., & Barnwell, J. W. (2006). Ensuring quality and access for malaria diagnosis: how can it be achieved? *Nature Reviews Microbiology*, 4, S7-S20. doi: 10.1038/nrmicro1525
- Bepari, K., & Mollik, A. B. (2009). Seasonality in the monthly stock returns: Evidence from Bangladesh Dhaka Stock Exchange (DSE). *International Research Journal of Finance and Economics*, 24, 167-175.
- Berterretche, M., Hudak, A. T., W.B., C., Maieresperger, T. K., Gower, S. T., & Dungan, J. (2005). Comparison area index (CAI) with landsat ETM+ data over a boreal forest. *Remote Sensing of Environment*, 96, 49-61. doi: 10.1016/j.rse.2005.01.014
- Besag, J., York, J., & Mollié, A. (1991). Bayesian image restoration, with two applications in spatial statistics (with discussion). *Annals of Institute of Statistical Mathematics*, 43(1), 1-59.
- Best, N. G., Richardson, S., & Thomson, A. (2005). A comparison of Bayesian spatial models for disease mapping. *Statistical Methods for Medical Research*, 14, 35-59.
- Bi, P., Tong, S., Donald, K., Parton, K. A., & Ni, J. (2003). Climatic variables and transmission of malaria: A 12-year data analysis in Shchen County, China. *Public Health Reports*, 118, 65-71.
- Bingham, P., Verlander, N. Q., & Cheal, M. J. (2004). John Snow, William Farr and the 1849 outbreak of cholera that affected London: A reworking of the data highlights the importance of the water supply. *Journal of Royal Institute of Public Health*, 118, 387-394.
- Binka, F. N., Indome, F., & Smith, T. (1998). Impact of spatial distribution of permethrin-impregnated bed nets on child mortality in Northern Ghana. *American Journal of Tropical Medicine and Hygiene*, 59, 80-85.
- Binka, F. N., Kubaje, A., Abjuik, M., Williams, L. A., Lengeler, C., Maude, G. H., . . . Smith, P. G. (1996). Impact of permethrin impregnated bednets on child mortality in Kassena-Nankana district, Ghana: A case randomized controlled trial. *Tropical Medicine and International Health*, 1(2), 147-154.
- Box, G. E. P., & Cox, D. R. (1964). An analysis of transformations. *Journal of the Royal Statistical Society, Series B: Methodology*, 26(2), 211-252.
- Box, G. E. P., & Jenkins, G. M. (1976). *Time series analysis: Forecasting and control* (revised ed.). San Francisco: Holden-Day.
- Box, G. E. P., & Pierce, D. A. (1970). Distribution of residual correlations in autoregressive-integrated moving average time series models. *Journal of the American Statistical Association*, 65, 1509-1526.
- Brabin, B. J. (1991). The risks and severity of malaria in pregnant women (Vol. Applied Field Research in Malaria Reports, No. 1). Geneva, Switzerland: World Health Organization; 1991.
- Brockwell, P. J., & Davis, R. A. (1987). *Time series: Theory and methods*. New York: Springer-Verlag.
- Brockwell, P. J., & Davis, R. A. (2002). *Introduction to time series and forecasting* (second ed.). New York: Springer-Verlag.

- Bruno, F., & Cocchi, D. (2004). Non-separability in spatiotemporal covariance models arisen by non-stationarity in time *Atti della XLII Riunione Scientifica SIS-Bari, CLEUP Padova*, 157-160.
- Bruno, F., Guttorp, P., Sampson, P. D., & Cocchi, D. (2009). A simple non-separable, non-stationary spatial-temporal model for ozone *Environmental and Ecological Statistics*, 16(4), 515-529. doi: 10.1007/s/0651-008-0094-8
- Buckee, C. O., & Gupta, S. (2009). Modelling malaria population structure and its implications for control. *Modelling Parasite Transmission and Control* <http://www.landesbioscience.com/curie/chapter/4139/>.
- Burgert, C. R., Bigogo, G., Adazu, K., Odhiambo, F., Buehler, J., Breiman, R. F., . . . Feikin, D. R. (2011). Impact of implementation free high-quality health care on health facility attendance by sick children in rural western Kenya. *Tropical Medicine and International Health*, 16(6), 11-720. doi: 10.1111/j.1365-3156.2011.02772
- Buttafuoco, G., Caloiero, T., & Coscarelli, R. (2011). Spatial and temporal patterns of the mean annual precipitation at decadal time scale in southern Italy (Calabria region). *Theory and Applied Climatology*, 105, 431-444. doi: 10.1007/s00704-011-0398-8
- Cai, Z. (2009). *Analysis of time series with applications in finance*. Lecture notes. Department of Mathematics & Statistics and Economics, University of North Carolina, Charlotte, NC 28223, USA
- Carneiro, I., Roca-Feltrer, A., & Schellenberg, J. (2005). Estimates of the burden on malaria mortality in Africa in children under the age of five years. Child Health Epidemiology Reference Group (CHERG) working paper: Disease Control and Vector Biology Unit, Department of Infectious and Tropical Disease, London School of Hygiene and Tropical Medicine
- Carrat, F., & Valleron, A. J. (1992). Epidemiologic mapping using the "kriging" method application to an influenza-like illness epidemic in France *American Journal of Epidemiology*, 135(11), 293-1300.
- Carter, R., Mendis, K. N., & Roberts, D. (2000). Spatial targeting of interventions against malaria *Bulletin World Health Organization*, 78(12), 1401-1411.
- Caulfield, L. E., Richard, S. A., & Black, R. E. (2004). Undernutrition as an underlying cause of malaria morbidity and mortality in children less than five years old. *American Journal of Tropical Medicine and Hygiene*, 71(Suppl 2), 55-63.
- Chatterjee, & Hadi, A. S. (2006). *Regression analysis by example* (4th ed.). New Jersey: John Wiley and Sons, Inc.
- Chatterjee, C., & Sarkar, R. R. (2009). Multi-step polynomial regression method to model and forecast malaria incidence. *PLoS ONE*, 4(3), e726 doi: 10.1371/journal.pone.0004726
- Chilès, J. P., & Delfiner, P. (1999). *Geostatistics: Modelling spatial uncertainty*. New York John Wiley and Sons, Inc.
- Chilès, J. P., & Delfiner, P. (2012). *Geostatistics: Modelling with uncertainty* (second ed.). New Jersey: John Wiley and Sons, Inc.
- Chinery, W. A. (1999a). The breeding patterns of three major mosquito species in lentic-water habitats in Accra, Ghana. *Ghana Journal Science*, 39, 117-122.
- Chinery, W. A. (1999b). Environmental management for mosquito control in tropical urban areas. *Ghana Journal Science*, 39, 103-110.
- Christakos, G. (1984). On the problem of permissible covariance and variogram models. *Water Resources Research* 20, 251-265.

- Christakos, G. (1992). *Random field models in earth sciences*. San Diego: Academic Press.
- Christakos, G. (2012). *Modern spatiotemporal geostatistics* (revised ed.). Mineola, New York: Dover Publications Inc., In Press.
- Christakos, G., & Bogaert, P. (1996). Spatiotemporal analysis of spring water ion processes derived from measurement at the Dyle basin in Belgium. *IEEE Transactions on Geoscience and Remote Sensing*, 34(3), 626-642.
- Christakos, G., & Hristopulos, D. T. (1998). *Spatiotemporal environmental health modelling: A tractatus stochasticus* Boston: Kluwer Academic Publishers
- Cibulskis, R. E., Aregawi, M., Williams, R., Otten, M., & Dye, C. (2011). Worldwide incidence of malaria in 2009: Estimates, time trends, and a critique of methods. *PLoS Medicine*, 8(12), e1001142. doi: 10.1371/journal.pmed.1001142
- Cibulskis, R. E., Bell, D., Christophel, E.-M., Hill, J., Delacollette, C., Bakayaita, N., & Aregawi, M. W. (2007). Estimating trends in the burden of malaria at country level. *American Journal of Tropical Medicine and Hygiene*, 77(Suppl 6), 133-137.
- Coetzee, M., Craig, M., & le Sueur, D. (2000). Distribution of African malaria mosquitoes belonging to *Anopheles gambiae* complex *Parasitology Today*, 16(2), 74-77.
- Coulibaly, D., Rebaudet, S., Travassos, M., Tolo, Y., Laurens, M., Kone, A. K., . . . Doumbo, O. K. (2013). Spatio-temporal analysis of malaria within a transmission season in Bandiagara, Mali. *Malaria Journal*, 12(82). doi: 10.1186/1475-2875-12-82
- Cowpertwait, P. S. P., & Metcalfe, A. V. (2009). *Introductory time series with R*. New York: Springer.
- Craig, M. H., Kleinschmidt, I., Nawn, J. B., Le Saour, D., & Sharp, B. L. (2004). Exploring 30 years of malaria case data in KwaZulu-Natal, South Africa. Part I: The impact of climatic factors *Tropical Medicine and International Health*, 9(12), 1247-1257.
- Craig, M. H., Snow, R. W., & le Sueur, D. (1999). A climate-based distribution model of malaria transmission in Sub-Saharan Africa. *Parasitology Today*, 15(3), 105-111. doi: 10.1016/S0169-4758(99)01396-4
- Crawley, J., Chu, C., Mtove, G., & Nosten, F. (2010). Malaria in children. *Lancet*, 375, 1468-1481.
- Cressie, N. (1985). Fitting variogram models by weighted least squares. *International Association of Mathematical Geology*, 17(5), 563-586.
- Cressie, N. (1993). *Statistics for spatial data* (revised ed.). New York: John Wiley & Sons, Inc.
- Cressie, N., & Grondona, M. O. (1992). *A comparison of variogram estimation with covariogram estimation* In: K.V. Mardia (ed), *The Art of Statistical Science*, Chichester, UK: John Wiley & Sons, Inc.
- Cressie, N., & Hawkin, D. M. (1980). Robust estimation of variogram, I. *Journal of the International Association for Mathematical Geology*, 12, 112-125.
- Cressie, N., & Huang, H. C. (1999). Classes of nonseparable, spatial-temporal stationary covariance functions. *Journal of the American Statistical Association*, 94(448), 1330-1340.
- Cressie, N., & Kornak, J. (2003). Spatial statistics in presence of location error with an application to Remote Sensing of the environment. *Statistical Science*, 18(4), 436-456.

- Cressie, N., & Wikle, C. K. (2011). *Statistics for spatio-temporal data*. New Jersey: John Wiley & Sons, Inc.
- Crookston, B. T., Alder, S. C., Boakye, I., Merrill, R. M., Amuasi, J. H., Porucznik, C. A., . . . Ansong, D. (2010). Exploring the relationship between chronic undernutrition and asymptomatic malaria in Ghanaian children. *Malaria Journal*, 9(39). doi: 10.1186/1475-2875-9-39
- Cuzick, J., & Elliott, P. (1992). *Geographical and environmental epidemiology: methods for small-area studies*. Oxford, United Kingdom: Oxford University Press.
- Daley, D. J., & Gani, J. (2005). *Epidemic modelling and introduction*. New York: Cambridge University Press.
- Danuor, S. K., Tay, S. C. K., Annor, T., Forkuo, E. K., Bosompem, K. M., & Antwi, V. (2010). *The impact of climate variability on malaria incidence and prevalence in the forest zone of Ghana: A case study at two(2) hospitals located within the Kumasi Metropolitan Area of the Ashanti Region of Ghana*. Paper presented at the 2nd International Conference Climate, Sustainability and Development in Semi-arid Regions, August 16-20, 2010 Fortaleza-Ceara, Brazil.
- De Cesare, L., Myers, D. E., & Posa, D. (1997). Spatial-temporal modelling of SO₂ in Milan District In E.Y. Baafi and N.A. Schofield (eds.), *Geostatistics Wollongong '96, Volume 2*, Kluwer Academic Publishers, Dordrecht, 1031-1042.
- De Cesare, L., Myers, D. E., & Posa, D. (2001a). Product-sum covariance for space-time modelling: An environmental application. *Environmetrics*, 12, 11-23.
- De Cesare, L., Myers, D. E., & Posa, D. (2001b). Estimating and modelling space-time correlation structures. *Statistical and Probability Letters*, 51(1), 9-14.
- De Cesare, L., Myers, D. E., & Posa, D. (2002). FORTRAN 77 programs for space-time modelling. *Computers and Gostatistics*, 28, 205-212.
- De Iaco, S. (2010). Space-time correlation analysis: A comparative study *Journal of Applied Statistics*, 37(6), 1027-1041. doi: 10.1080/02664760903019422
- De Iaco, S., Maggio, S., Palma, M., & Posa, D. (2012). Towards an automatic procedure for modelling multivariate space-time data. *Computers and Geosciences*, 41, 1-11. doi: 10.1016/j.cageo.2011.08.008
- De Iaco, S., Myers, D. E., Palma, M., & Posa, D. (2010). FORTRAN programs for space-time multivariate modelling and prediction. *Computers and Geosciences*, 36(5), 636-646. doi: 10.1016/j.cageo.2009.10.004
- De Iaco, S., Myers, D. E., & Posa, D. (2001). Space-time analysis using a general product-sum model. *Statistics and Probability Letters*, 52(1), 21-28. doi: 10.1016/S0167-7152(00)00200-5
- De Iaco, S., Myers, D. E., & Posa, D. (2003). The linear coregionalisation model and the product-sum space-time variogram. *Mathematical Geology*, 35(1), 25-38.
- De Iaco, S., Myers, D. E., & Posa, D. (2011a). On strict positive definiteness of product and product-sum covariance models *Journal of Statistical Planning and Inference*, 141(3), 1132-1140. doi: 10.1016/j.jspi.2010.09.014
- De Iaco, S., Myers, D. E., & Posa, D. (2011b). Strict positive definiteness of a product of covariance functions *Communications in Statistics -Theory and Methods*, 40(24), 4400-4408. doi: 10.1080/03610926.2010.513790
- De Iaco, S., Palma, M., & Posa, D. (2005). Modelling and prediction of multivariate space-time random fields. *Computational Statistics and Data Analysis*, 48, 525-547.

- De Iaco, S., & Posa, D. (2011). Predicting spatio-temporal random field: Some computational aspects *Computers and Geosciences*. doi: 10.1016/j.cageo.2011.11.014
- De Iaco, S., & Posa, D. (2012). Predicting spatio-temporal random fields: Some computational aspects. *Computers and Geosciences*, 41, 12-24. doi: 10.1016/j.cageo.2011.11.014
- de Souza, D., Kelly-Hope, L., Lawson, B., Wilson, M., & Boakye, D. (2010). Environmental factors associated with the distribution of *anopheles gambiae* s.s in Ghana; an important vector of lymphatic filariasis and malaria. *PLoS ONE*, 5(3), e9927 doi: 10.1371/journal.pone.0009927
- Denham, A. (2012). *Geostatistical spatiotemporal modelling with application to the western king prawn of the shark bay managed prawn fishery* (PhD Thesis), School of Engineering, Faculty of Computing, Health and Science, Edith Cowan University, Perth, Western Australia.
- Deutsch, C., & Journel, A. (1998). *GSLIB: Geostatistical software library and user's guide* (second ed.). New York: Oxford University Press.
- Dhingra, N., Jha, P., Sharma, V. P., Cohen, A. A., Jotkar, R. M., Rodriguez, P. S., . . . Collaborators, f. t. M. D. S. (2010). Adult and child malaria mortality in India. *Lancet*, 376(9754), 1768–1774. doi: 10.1016/S0140-6736(10)60831-8.
- Dickey, D. A., & Fuller, W. (1979). Distribution of the estimators for autoregressive time series with unit root. *Journal of American Statistical Association*, 74, 427-431.
- Diggle, P. J., & Ribeiro Jr., P. J. (2007). *Model-based geostatistics*. New York: Springer-Verlag.
- Dimitrakopoulos, R., & Luo, X. (1994). Spatiotemporal modelling: Covariances and ordinary kriging systems. In: *Geostatistics for the next Century*, R. Dimitrakopoulos (ed), Dordrecht, Kluwer Academic Publishers, 88-93.
- Dimitrakopoulos, R., & Luo, X. (1997). *Joint space-time modelling in the presence of trends* (Vol. 1). In Geostatistics Wollongong '96, E. Baafi, N. Schofield (eds) Dordrecht: Kluwer Academic Publishers.
- Doudou, M. H., Mahamadou, A., Ouba, I., Lazoumar, R., Boubacar, B., Arzika2, I., . . . Fandeur, T. (2012). A refined estimate of the malaria burden in Niger. *Malaria Journal*, 11(9).
- Draper, N. R., & Smith, H. (1981). *Applied regression analysis* (2nd Ed.). New York: John Wiley and Sons, Inc, 706 pp.
- Elmatzoglou, I. (2006). *Spatio-temporal geostatistical models with an application in fish stock*. (MSc Thesis), Lancaster University, Lancaster.
- Farrar, D. E., & Glauber, R. R. (1967). Multicollinearity in regression analysis: The problem revisited. *The Review of Economics and Statistics*, 49(1), 319-330.
- Fernández-Cortés, A., Calaforra, J. M., Jiménez-Espinosa, R., & Sánchez-Martos, F. (2006). Geostatistical spatiotemporal analysis of air temperature as an aid to delineating thermal stability zones in a potential show cave: Implications for environmental management. *Journal of Environmental Management*, 81, 371-383. doi: 10.1016/j.jenvman.2005.11.011
- Fisher, R. A. (1935). *The design of experiments* (1st ed.). Edinburgh, UK: Oliver and Boyd.
- Fuentes, M. (2006). Testing for separability of spatial-temporal covariance functions *Journal of Statistical Planning and Inference*, 136, 447-466.
- Gallup, J. L., & Sachs, J. D. (2001). The economic burden of malaria *American Journal of Tropical Medicine and Hygiene*, 64(1,2), 85-96.

- Gaudart, J., Poudiogou, B., Dicko, A., Ranque, S., Toure, O., Sagara, I., . . . Doumbo, O. K. (2006). Space-time clustering of childhood malaria at the household level: a dynamic cohort in a Mali village. *BMC Public Health*, 6:286.
- Gaudart, J., Toure, O., Dessay, N., Lassane Dicko, A., Ranque, S., Forest, L., . . . Doumbo, O. K. (2009). Modelling malaria incidence with environmental dependency in a locality of Sudanese savannah area, Mali. *Malaria Journal*, 8:61.
- Gelfand, A. E., Diggle, P. J., Fuentes, M., & Guttorp, P. (Eds.). (2010). *Handbook of spatial statistics*. Boca Raton: Chapman and Hall/CRC.
- Gemperli, A. (2003). *Development of spatial statistical methods for modelling point-referenced spatial data in malaria epidemiology*. (PhD Thesis Publications), University of Basel Basel, Switzerland.
- Gemperli, A., Sogoba, N., Fonjo, E., Mabaso, M. L. H., Bagayo, M., & Briet, O. J. T. (2006). Mapping malaria transmission in West and Central Africa. *Tropical Medicine and International Health*, 11, 1032-1046.
- Geovariances. (2013). Isatis Software 2013: Release version 2013. Geovariances and Ecole des Mines de Paris, Paris, France.
- Gething, P. W. (2006). *Spatiotemporal modelling of Health Management Information System data to quantify malaria treatment burdens in the Kenyan Government's formal health sector*. (PhD Thesis), Faculty of Engineering and Mathematics, School of Electronics and Computer Science and School of Geography, University of Southampton, Southampton.
- Gething, P. W., Atkinson, P. M., Noor, A. M., Gikandi, Hay, S. I., & Nixon, M. S. (2007). A local space-time kriging approach applied to a national outpatient malaria data set. *Computers and Geosciences*, 33, 1337-1350. doi: 10.1016/j.cago.2007.05.006
- Gething, P. W., Noor, A. M., Gikandi, P. W., Hay, S. I., Nixon, M. S., Snow, R. W., & Atkinson, P. M. (2008). Developing geostatistical space-time models to predict outpatient treatment burdens from incomplete national data. *Geographical Analysis*, 40(2), 167-188. doi: 10.1111/j.1538-4632.2008.00718.x
- Gething, P. W., Noor, A. M., Gikandi, P. W., Ogara, E., Hay, S. I., Nixon, M. S., . . . Atkinson, P. M. (2006). Improving imperfect data from health management information systems in Africa using space-time geostatistics. *PLoS Medicine* 3(6), 271. doi: 10.1371/journal.pmed.0030271
- Ghana Web. (2013). Ghana: Country information on climate. Retrieved 17/12/2013, from <http://www.GhanaHomePage/geography/climate.php>
- GHS. (2007). Annual report of Ghana Health Service 2007. Accra: Ghana Health Service (GHS).
- GHS. (2011). Annual report of Ghana Health Services 2011. Accra: Ghana Health Services (GHS).
- GMAG. (2007). Ghana Malaria Advocacy Guide (GMAG): A guide to the promotion of advocacy for malaria control in Ghana. *MOH/GHS/NMCP/JHU/CCP*.
- GMP/WHO. (2012). Q and A on malaria mortality. Geneva, Switzerland: Global Malaria Project (GMP), World Health Organisation (WHO).
- Gneiting, T. (2001). Criteria of Pólya type for radial positive definite functions. *Proceedings of American Mathematical Society*, 129, 2309–2318, MR1823914.
- Gneiting, T., Genton, M. G., & Guttorp, P. (2007). *Geostatistical space-time models, stationary, separability and full symmetry* In: Statistics of Spatio-temporal Systems, B. Finkelstadt, W. Härdle & V. Isham (eds), Boca Raton Taylor and Francis.

- Gomez-Elipe, A., Otero, A., van Herp, M., & Aguirre-Jaime, A. (2007). Forecasting malaria incidence based on monthly case reports and environmental factors in Karuzi, Buurundi, 1997-2003. *Malaria Journal*, 6(129). doi: 10.1186/1475-2875-6-129
- Gómez-Hernández, J. J. (1996). *Geostatistics and hydrology: An overview, geographical information* Paper presented at the Second Joint European Conference and Exhibition on Geographical Information, Barcelona, Spain.
- Goodman, C., Coleman, P., & Mills, A. (2000). Economic analysis of malaria control in Sub-Saharan Africa *Global Forum for Health Research*.
- Goovaerts, P. (1997). *Geostatistics for natural resources evaluation*. New York: Oxford University Press, Inc.
- Goovaerts, P. (1999). Using elevation to aid the geostatistical mapping of rainfall erosivity. *Catena*, 34, 227-242.
- Goovaerts, P. (2009). AUTO-IK: A 2D indicator kriging program for the automated non-parametric modelling of local uncertainty in earth sciences. *Computational Geosciences*, 35(6), 1255-1270.
- Goovaerts, P., & Chiang, C. (1993). Patterns for mineralisable of nitrogen and selected soil properties. *Soil Science Society of America Journal*, 57(2), 372-381.
- Gosoniua, L., Vounatsou, P., Sogoba, N., & Smith, T. (2006). Bayesian modeling of geostatistical malaria risk data. *Geospatial Health*, 1, 127-139.
- Gosoniua, L., Vounatsou, P., Sgobab, N., Mairea, N., & Smith, T. (2009). Mapping malaria risk in West Africa using a Bayesian non-parametric non-stationary model *Computational statistical Data Analysis*, 53, 3358-3371.
- Goulard, M. (1989). *Inference in a coregionalisation model*. In: M. Armstrong (ed), *Geostatistics*, Dordrecht: Kluwer Publishers, 397-408.
- Gregori, P., Porcu, E., Mateu, J., & Sasvári, Z. (2008). On potentially negative space-time covariances obtained as sum of products of marginals. *Annals Institute of Statistical Mathematics*, 60, 865-882. doi: 10.1007/s10463-007-0122-8
- Griffith, D. A., & Heuvelink, G. B. M. (2010). Deriving space-time variograms from space-time autoregressive (STAR) model specifications. *The International Archives of the Photogrammetry, Remote Sensing and Spatial Information System Sciences*, 38(Part II), 15-20.
- GSMF. (2004). Public-commercial partnership for the sustainable marketing of insecticide treated nets (ITNs) in Ghana *GSMF, Ghana*.
- GSS. (2002). *2000 Population and Housing Census: Summary report of final results*. Accra: Ghana Statistical Service (GSS).
- GSS, NMIMR, & Macro, O. (2004a). *Ghana Demographic and Health Survey 2003 Calverton, Maryland*.
- GSS, NMIMR, & Macro, O. (2004b). *Ghana Demographic Health Survey (GDHS) 2003*. Calverton, Maryland: Ghana Statistical Service (GSS), Noguchi Memorial Institute for Medical Research (NMIMR) & ORC Macro.
- Guyatt, H. L., & Snow, R. W. (2004). Impact of malaria during pregnancy on low birth weight in Sub-Saharan Africa. *Clinical Microbiology Reviews*, 17(4), 760-769. doi: 10.1128/CMR.17.4.760-769.2004
- Hart, J. T. (1971). The inverse care law. *The Lancet*, 297(7696), 405-412. doi: 10.1016/S0140-6736(71)92410-X
- Hay, S. I., Guerra, C. A., Gething, P. W., Patil, A. P., Tatem, A. J., Noor, A. M., . . . Snow, R. W. (2009). A world malaria map: *Plasmodium falciparum* endemicity in 2007 *PLoS Med*, 6(3), e1000048. doi: 10.1371/journal.pmed.1000048

- Hay, S. I., Guerra, C. A., Tatem, A. J., Noor, A. M., & Snow, R. W. (2004). The global distribution and population at risk of malaria: Past, present and future. *Lancet Infectious Diseases*, 4(6), 327-336.
- Hay, S. I., Okiro, E. A., Gething, P. W., Patil, A. P., Tatem, A. J., Guerra, C. A., & Snow, R. W. (2010). Estimating the global clinical burden of *Plasmodium falciparum* malaria in 2007. *PLoS Medicine*, 7(6), e1000290. doi: 10.1371/journal.pmed.1000290
- Hellmuth, M. E., Moorhead, A., Thomson, M. C., & Williams, J. (Eds.). (2007). *Climate risk management in Africa: Learning from practice*. International Research Institute for Climate and Society (IRI), Columbia University, New York, USA
- Hengl, T. (2009). *A practical guide to geostatistics mapping*. Luxembourg: Office for Official Publications for European Communities.
- Hengl, T., & Reuter, H. (Eds.). (2008). *Geomorphometry: Concepts, software, applications of developments in soil science* (Vol. 33). Amsterdam: Elsevier.
- Holding, P. A., & Snow, R. W. (2001). Impact of Plasmodium falciparum malaria on performance and learning: review of the evidence *American Journal of Tropical Medicine and Hygiene*, 64(2), 68-75.
- Holt, C. C. (1957). *Forecasting trends and seasonals by exponentially weighted moving averages* Carnegie Institute of Technology. In: Office of Naval Research Memorandum No. 52, Pittsburgh, Pennsylvania.
- Holt, R. A. (2002). The Genome sequence of the malaria mosquitoes Anopheles gambiae. *Science*, 298, 129-149.
- Horvatic, D., Stanley, H. E., & Podobnik, B. (2011). Detrended cross-correlation analysis for non-stationary time series with periodic trends. *A Letters Journal Exploring Frontiers of Physics (EPL)*, 94. doi: 10.1209/0295-5075/94/18007
- Hu, W., Clements, A., Williams, G., & Tong, S. (2011). Spatial analysis of notified dengue fever infections. *Epidemiology and Infection*, 139, 291-399. doi: 10.1017/S0950268810000713
- Huang, F., Zhou, S., Zhang, S., Wang, H., & Tang, L. (2011). Temporal correlation analysis between malaria and meteorological factors in Motuo County, Tibet. *Malaria Journal*, 10(54). doi: 10.1186/1475-2875-10-54
- Huang, F., Zhou, S., Zhang, S., Zhang, H., & Li, W. (2011). Meteorological factors-based spatio-temporal mapping and predicting malaria in Central China. *American Journal of Tropical Medicine and Hygiene*, 85(3), 560-567. doi: 10.4269/ajtmh.2011.11-0156
- Hudson, G., & Wackernagel, H. (1994). Mapping temperature using kriging with external drift: Theory and an example from Scotland *International Journal of Climatology*, 14(1), 77-91.
- IntraSearch, M. (Cartographer). (2011). Digital elevation model (DEM) of Ghana. Retrieved from <http://www.mapmart.com/products/digitalelevationmodel.asp>
- Isaaks, E. H., & Srivastava, R. M. (1989). *An introduction to applied geostatistics*. New York: Oxford University Press, Inc.
- Jaccard, J., Wan, C. K., & Turrisi, R. (1990). The detection and interpretation of interaction effects between continuous variables in multiple regression. *Multivariate Behavioral Research*, 25(4), 467-478.
- Jian, X., Olea, R. A., & Yu, Y. S. (1996). Semivariogram modelling by weighted least squares *Computers and Geosciences*, 22(4), 387-397.

- Jobin, W. (2004). *Prediction of health hazards in tropical reservoirs and evaluation of low-cost methods for disease prevention*. Paper presented at the UNIHIDRO 2004, Beijing.
- Johnson, R. A., & Wichern, D. W. (1992). *Applied multivariate statistical analysis* (third ed.). Englewood Cliffs, New Jersey: Prentice-Hall.
- Journel, A. G. (1980). The lognormal approach to predict local distributions of selective mining unit grades. *Mathematical Geology*, *12*, 285-303.
- Journel, A. G., & Huijbregts, C. J. (1978). *Mining geostatistical*. New York: Academic Press.
- Journel, A. G., & Rossi, M. E. (1989). When do we need a trend model in kriging? *Mathematical Geology*, *21*(7), 715-739.
- Kazembe, L. N., Kleinschmidt, I., Holtz, T. H., & Sharp, B. L. (2006). Spatial analysis and mapping of malaria risk in Malawi using point-reference prevalence of infection data. *International Journal of Health Geographics*, *5*(41). doi: 10.1186/1476-072X-5-41
- Kleinschmidt, I. (2001). *Spatial statistical analysis, modelling and mapping of malaria in Africa*. (PhD Thesis), Swiss Tropical Institute, University of Basel, Basel
- Kleinschmidt, I., Bagayoko, M., Clarke, G. P. Y., Craig, M., & Le Sueur, D. (2000). A spatial statistical approach to malaria mapping. *International Journal of Epidemiology*, *29*(2), 355-361.
- Kleinschmidt, I., Omumbo, J., Briet, O., van de Giesen, N., Sogoba, N., Mensah, N. K., . . . Teuscher, T. (2001). An empirical malaria distribution map for West Africa. *Tropical Medicine and International Health*, *6*(10), 779-786.
- Kleinschmidt, I., Sharp, B. L., Clarke, G. P. Y., Curtis, B., & Fraser, C. (2001). Use of generalised linear mixed models in the spatial analysis of small area malaria incidence rates in KwaZulu Natal, South Africa. *American Journal of Epidemiology*, *153*(12), 1213-1221.
- Klinkenberg, E., McCall, P. J., Hastings, I. M., Wilson, M. D., Amerasinghe, F. P., & Donnelly, M. J. (2005). Malaria and irrigation crops, Accra, Ghana. *Emerging Infectious Diseases*, *11*(8), 1290-1293
- Korenromp, E. (2005). Malaria incidence estimates at country level for the year 2004. Proposed estimates and draft report. Geneva, Switzerland: World Health Organization (WHO)
- Krefis, A. C., Schwarz, N. G., Nkrumah, B., Acquah, S., Loag, W., Sarpong, N., . . . May, J. (2010). Principal component analysis of socioeconomic factors and their association with malaria in children from Ashanti Region, Ghana. *Malaria Journal*, *9*(201). doi: 10.1186/1475-2875-9-201
- Kreuels, B., Kobbe, R., Adjei, S., Kreuzberg, C., Von Reden, C., Bäter, K., . . . May, J. (2008). Spatial variation of malaria incidences in young children from geographically homogeneous area with high endemicity. *The Journal of Infectious Diseases*, *197*(1), 85-93. doi: 10.1086/524066
- Kurane, I. (2009). The emerging and forecasted effect of climate change on human health. *Journal of Health Science*, *55*(6), 865-869.
- Kyriakidis, P. C., & Journel, A. G. (1998). *Stochastic modelling of spatiotemporal distributions: Application to sulphate deposition trends over Europe* Paper presented at the Second European conference on Geostatistical for Environmental Applications Valencia, Spain, November 18-20, 1998.
- Kyriakidis, P. C., & Journel, A. G. (1999). Geostatistical space-time methods: A review. *Mathematical Geology*, *31*(6), 651-684.

- Kyriakidis, P. C., & Journel, A. G. (2001). Stochastic modelling of atmospheric pollution: A spatial time-series framework. Part II: Application to monitoring monthly sulfate deposition over Europe. *Atmospheric Environment*, *35*, 2339-2348.
- Kyriakidis, P. C., Miller, N. L., & Kim, J. (2004). A spatial time series framework for simulating daily precipitation at regional scales. *Journal of Hydrology*, *297*, 236-255. doi: 10.1016/j.jhydrol.2004.04.022
- Kyriakidis, P. C., Shortbridge, A. M., & Goodchild, M. F. (1999). Geostatistics for conflation and accuracy assessment of Digital Elevation Models (DEM). *International Journal of Geographical Information Science*, *13*(7), 677-708.
- Landoh, E. D., Tchamdja, P., Saka, B., Tint, K. S., Gitta, S. N., Wassawa, P., & de Jagger, C. (2012). Morbidity and mortality due to malaria in Est Mono district, Togo, from 2005 to 2010: A time series analysis. *Malaria Journal*, *11*(389). doi: 10.1186/1475-11389
- Lee, Y.-M., & Ellis, J. H. (1997). Estimation and simulation of lognormal random fields. *Computers and Geosciences*, *23*(1), 19-31.
- Li, B., Genton, M., & Sherman, M. (2007). A non-parametric assessment of properties of space-time covariance functions. *Journal of the American Statistical Association*, *102*, 736-829.
- Lin, H., L., L., Tian, L., Zhou, S., Wu, H., Y., B., . . . Liu, Q. (2009). Spatial and temporal distribution of falciparum malaria in China. *Malaria Journal*, *8*(130). doi: doi:10.1186/1475-2875-8-130
- Lindsay, S. W., Campbell, H., Adiamah, J. H., Greenwood, A. M., Bangali, J. E., & Greenwood, B. M. (1990). Malaria in a peri-urban area of The Gambia. *Annals of Tropical Medicine and Parasitology*, *84*(6), 553-562.
- Lindsey, C., & Sheather, S. J. (2010). Variable selection in linear regression. *Stata Journal*, *10*(4), 650-669.
- Liu, C., & Koike, K. (2007). Extending multivariate space-time geostatistics for environmental data analysis. *Mathematical Geology*, *39*(3), 289-305.
- Ljung, G. M., & Box, G. E. P. (1978). On a measure of a lack of fit in time series models. *Biometrika*, *65*(2), 297-303. doi: 10.1093/biomet/65.2.297
- Loevinshn, M. E. (1994). Climatic warning and increased malaria incidence in Rwanda *Lancet*, *343*, 714-718.
- Loevinsohn, M. E. (1994). Climatic warning and increased malaria incidence in Rwanda *Lancet*, *343*, 714-718.
- Lynch, C., & Hewitt, S. (2012). *Malaria in the Asia-Pacific: Burden, success and challenges*. Paper presented at the Malaria 2012: Saving Lives in the Asia-Pacific, Sydney, Australia.
- Lynch, M., Korenromp, E., Eisele, T., Newby, H., Steketee, R., Kachhur, S. P., . . . Cibulskis, R. (2012). New global estimates of malaria deaths. *The Lancet*, *380*(9841), 559. doi: 10.1016/S0140-6736(08)61345-8
- Ma, C. (2008). Recent developments on the construction of spatio-temporal covariance models. *Stochastic Environmental Research and Risk Assessment*, *22*, S39-S47.
- Mabaso, M. L. H. (2007). *Temporal variations in malaria risk in Africa*. (Ph.D. Thesis Publications), University of Basel, Basel, Switzerland.
- MARA Project. (1998). Towards an Atlas of malaria risk in Africa: First technical report of the MARA/ARMA Collaboration. Durban, South Africa: Mapping of Malaria Risk in Africa (MARA/ARMA) Collaboration.

- Matérn, B. (1960). *Spatial variation* (Vol. 49, No. 5). Stockholm: Meddelanden fran Statens Skogsforskningsinstitut, [2nd ed. (1986), Lectures notes in statistics, No. 36, Springer, New York]
- Matheron, G. (1962-1963). *Traité de Géostatistique appliquée: Mémoires du Bureau de Recherches Géologiques et Minières*, Editions Technip, Paris, Tome I, No. 14.
- Matheron, G. (1963). Principles of geostatistics. *Economic Geology*, 59, 1246-1266.
- McCormick, M. C. (1985). The contribution of low birth weight to infant mortality and childhood mortality. *The New England Journal of Medicine*, 312, 82-90.
- McKenzie, F. E., & Samba, E. (2004). The role of mathematical modelling in evidence-based malaria control *American Journal of Tropical Medicine and Hygiene*, 71(Suppl 2), 94-96.
- MICS. (2006). Multiple Indicator Cluster Survey (MICS) 2006 in Ghana (Vol. UNICEF/NACP/GSS): Ghana Statistical Services (GSS).
- MICS. (2011). Multiple Indicator Cluster Survey (MICS) with Malaria Biomarker Survey (Vol. GSS/UNICEF/GHS/PMI). Accra: Ghana Statistical Service (GSS).
- Militino, A. F., Dolores, M., & Ibáñez, B. (2008). Longitudinal analysis of spatially correlated data. *Stochastic Environmental Resource and Risk Assessment*, 22(Suppl 1), S49-S57. doi: 10.1007/s00477-007-0158-6
- Miller, R. G. (1974). The Jack-knife: A review *Biometrika*, 61, 1-15.
- Mitchell, M. V., Genton, M. G., & Gumpertz, M. L. (2005). Testing for separability of space-time covariances. *Environmetrics*, 16, 819-831.
- Mitchell, M. V., Genton, M. G., & Gumpertz, M. L. (2006). A likelihood ratio test for separability of covariances. *Journal of Multivariate Analysis*, 97, 1025-1043.
- Montalvo, J. G., & Reynal-Querol, M. (2007). Fighting against malaria: Prevent wars while waiting for the "Miraculous Vaccine". *The Review of Economics and Statistics*, 89(1), 165-177.
- Morris, J. H., Sherman, J., & Mansfield, E. R. (1986). Failures to detect moderating effects with ordinary least squares-moderated regression: Some reasons and a remedy. *Psychological Bulletin*, 99, 282-288.
- Murray, C. J. L., Rosenfeld, L. C., Lim, S. S., Andrews, K. G., Foreman, K. J., Haring, D., . . . Lopez, A. D. (2012). Global malaria mortality between 1980 and 2010: A systematic analysis. *The Lancet*, 379(9814), 413-431.
- Myers, D. E. (1991). *On variogram estimation*. In: The Frontiers of Statistical Scientific Theory and Industrial Applications, A. Öztürk, E. C. van der Meulen (eds.): American Science Press, 261-281.
- Nadine, R., Vounatsou, P., Miller, J. M., Gosoni, L., Chizema-Kawesha, Mukonka, V., & Steketee, R. W. (2010). Geostatistical patterns and predictors of malaria risk in Zambia: Bayesian geostatistical modelling of the 2006 Zambia national malaria indicator survey (ZMIS). *Malaria Journal*, 9(37). doi: 10.1186/1475-2875-9-37
- NDPC, & IMF. (2005). IMF Report 2005: Ghana Poverty Reduction Strategy 2004 Annual Report (Vol. No.06/226).
- NMCP. (2007). Ghana Malaria Advocacy Guide (GMAG): A guide to the promotion of advocacy for malaria control in Ghana *Malaria Watch*. Accra, Ghana: National Malaria Control Programme (NMCP).
- NMCP. (2008). Lunch of Ghana malaria advocacy campaign by National Malaria Control Programme (NMCP). *Malaria Watch*, 5, 9.

- NMCP/GHS. (2009). Epidemiological strata and predominant *Anopheles* species in Ghana. In: Training manual for management of malaria at health facilities in Ghana: Facilitators Guide. Accra: National Malaria Control Programme (NMCP)/Ghana Health Service (GHS).
- NMCP/GHS. (2010). National Malaria Control Strategy 2008-2015. Accra: National Malaria Control Programme (NMCP), Ghana Health Services (GHS).
- Nobre, A. A., Schmidt, A. M., & Lopes, H. F. (2005). Spatio-temporal models for mapping the incidence of malaria in Para. *Environmetrics*, 16, 291-304. doi: 10.1002/env.704
- Nochai, R., & Nochai, T. (2006). *ARIMA model for forecasting oil palm price*. Paper presented at the 2nd IMT-GT Regional Conference on Mathematics, Statistics and Applications, Universiti Sains Malaysia, Penang, June 13-15, 2006.
- Noor, A. M., Alegana, V. A., Gething, P. W., & Snow, R. W. (2009). A spatial national health facility database for public health sector planning in Kenya in 2008. *International Journal of Health Geographics*, 8(13). doi: 10.1186/1476-072X-8-13
- Nyakeriga, A. M., Troye-Blomberg, M., Chemtai, A. K., Marsh, K., & Williams, T. N. (2004). Malaria and nutritional status in children living on the coast of Kenya. *American Journal of Clinical and Nutrition*, 80, 1604-1610.
- Obiri-Danso, K., Okore-Hanson, A., & Jones, K. (2003). The microbiological quality of drinking water sold on the streets in Kumasi, Ghana. *Letters in Applied Microbiology*, 37, 334-335.
- Obiri-Danso, K., Weobong, C. A. A., & Jones, K. (2005). Aspects of health related microbiology of the Subin, an urban river in Kumasi, Ghana. *Journal of Water and Health*, 03(1).
- Oehlert, G. W. (1993). Regional trends in sulphate wet deposition. *Journal of Climate and Applied Meteorology*, 88(422), 390-399.
- Ofori, M. F., Ansah, E., Agyepong, I., Ofori-Adjei, D., Hviid, L., & Akanmori, B. D. (2009). Pregnancy-associated malaria in rural community of Ghana. *Ghana Medical Journal*, 43(1), 13-18.
- Okafor, E. E., & Amzat, J. (2007). Problems of malaria menace and behavioural intervention for its management in Sub-Saharan Africa. *Journal of Human and Ecology*, 21(2), 155-162.
- Okorosobo, T., Okorosobo, F., Mwabu, G., Orem, J. N., & Kirigia, J. M. (2011). Economic burden of malaria in six countries in Africa. *European Journal of Business and Management*, 3(6).
- Olea, R. A. (1999). *Geostatistics for engineers and earth scientists*. Boston: Kluwer Academic Publishers.
- Osei, F. B., & Duker, A. A. (2008). Spatial and demographic patterns of Cholera in Ashanti Region-Ghana. *Internal Journal of Health Geographics*, 7.44.
- Osei, F. B., Duker, A. A., Augustijn, E. W., & Stein, A. (2010). Spatial dependency of cholera prevalence on potential cholera reservoirs in an urban area, Kumasi, Ghana. *International Journal of Applied Earth Observation and Geoinformation*, 12(5), 331-339.
- Osnas, E. E., Heisey, D. M., Rolley, R. E., & Samuel, M. D. (2009). Spatial and temporal patterns of chronic wasting disease: fine-scale mapping of a wildlife epidemic in Wisconsin *Ecological Applications*, 19(5), 1311-1322.
- Patil, A. P., Okiro, E. A., Gething, P. W., Guerra, C. A., Sharma, S. K., & et al. (2009). Defining the relationship between *Plasmodium falciparum* parasite rate and

- clinical disease: Statistical methods for disease burden estimation. *Malaria Journal*, 8(186).
- Pfaff, B. (2008). *Analysis of integrated and cointegrated time series with R* (Second ed.). New York: Springer Science + Business Media
- PMI. (2009). President's Malaria Initiative (PMI) in Ghana: Malaria Operational Plan-Year Two (FY05).
- PMI. (2012). President's Malaria Initiative (IMI) in Ghana: Malaria Operational Plan-FY 2012 (Year 5). Accra: National Malaria Control Programme (NMCP), Ghana Health Services (GHS).
- PMI. (2013). President's Malaria Initiative (PMI) in Ghana: Malaria Operational Plan FY 2013. Accra: National Malaria Control Programme (NMCP), Ghana Health Services (GHS).
- Posa, D. (1993). A simple description of spatial-temporal processes *Computational statistical Data Analysis*, 15, 425-437.
- PSS/GSS. (2009). Population projections release 2009 Accra: Population Statistics Section (PSS), Ghana Statistical Service (GSS).
- Quenouille, M. H. (1956). Notes on bias in estimation. *Biometrika*, 43, 353-360.
- R Development Core Team. (2011). R: A language and environment for statistical computing. R Foundation for Statistical Computing, Vienna, Austria, ISBN 3-900051-07-0, <http://www.R-project.org/>.
- RBM/NMCP/GHS. (2010). *Roll Back Malaria (RBM) Strategic Plan for Ghana 2000-2010 (Draft 2)*. Accra.
- Reid, H., Haque, U., Clements, A. C. A., Tatem, A. J., Vallely, A., Ahmed, S. M., . . . Haque, R. (2010). Mapping malaria risk in Bangladesh using Bayesian geostatistical models. *American Journal of Tropical Medicine and and Hygiene* 83(4), 861-867. doi: 10.4269/ajtmh.2010.10-0154
- Reiner, R. C., Perkins, T. A., Barber, C. M., Niu, T., Chaves, L. F., Ellis, A. M., . . . Smith, D. L. (2013). A systematic review of mathematical models of mosquito-borne pathogen transmission: 1970-2010. *Journal of the Royal Statistical Society Interface*, 10(81), 20120921. doi: 10.1098/rsif.2012.0921
- Reiter, P. (2008). Global warming and malaria: Knowing the horse before hitching the cart. *Malaria Journal*, 7(suppl):53.
- Ricci, F. (2012). Social implications of malaria and their relationships with poverty. *Mediterranean Journal of Hematology and Infectious Diseases*, 4(1), e2012048. doi: 10.4048/MJHID.2012.048
- Rivoirard, J. (1990). Teacher's aid: A review of lognormal estimators for in situ reserves. *Mathematical Geology*, 22, 213-221.
- RMSC/FC. (2011). Vegetation zones and forest reserve map of Ghana Accra: GIS Department, Resource Management Support Centre (RMSC), Forestry Commission (FC), Ghana
- Rodriguez-Iturbe, I., & Mejia, J. M. (1974). The design of rainfall networks in time and space. *Water Resources and Research*, 10, 713-728. doi: 10.1029/WR010i004p00713
- Roth, C. (1998). Is lognormal kriging suitable for local estimation? *Mathematical Geology*, 30(8), 999-1009.
- Rouhani, S., & Hall, T. J. (1989). *Space-time kriging of groundwater data* (Vol. 2). In: M. Armstrong (ed), Dordrecht: Kluwer Academic Publications, 639-650.
- Rouhani, S., & Wackernagel, H. (1990). Multivariate geostatistical approach to space-time data analysis. *Water Resources and Research*, 26(4), 586-591. doi: 10.1029/WR026i004p00585

- Royston, P. (1982). An extension of Shapiro and Wilk's W test for normality to large samples. *Applied Statistics*, 31, 115-124.
- Sachs, J., & Malaney, P. (2002). The economic and social burden of malaria. *Nature*, 415(6872), 680-685. doi: 10.1038/415680a
- Saxena, R., Nagpal, B. N., Srivastava, A., Gupta, S. K., & Dash, A. P. (2009). Application of spatial technology in malaria research and control: some new insights. *Indian Journal of Medical Research*, 130, 125-132.
- Schabenberger, O., & Pierce, F. J. (2002). *Contemporary statistical models for the plant and soil sciences*. Boca Raton: CRC Press.
- Schantz-Dunn, J., & Nawal, N. M. (2009). Malaria and pregnancy: A global health perspective. *Review in Obstetrics Gynecology*, 2(3), 186-192.
- Schwarz, G. (1978). Estimating the dimension of a model. *Annals of Statistics*, 6, 461-464.
- Shapiro, S. S., & Wilk, M. B. (1965). An analysis of variance test for normality (complete samples). *Biometrika*, 52(2-4), 591-611. doi: 10.1093/biomet/52.3-4.591
- Sherman, M. (2011). *Spatial statistics and spatio-temporal data: Covariance functions and directional properties*. Chichester: John Wiley & Sons, Ltd
- Shumway, R. H., & Stoffer, D. S. (2011). *Time series analysis and its applications with R examples* (3rd ed.). New York: Springer.
- Silal, S. P., Barnes, K. L., Kok, G., Mabuza, A., & Little, F. (2013). Exploring the seasonality of reported treated malaria cases in Mpumalanga, South Africa. *PLoS ONE*, 8(10), e76640. doi: 10.1371/journal.pone.0076640
- Small, J., Goetz, S. J., & Hay, S. I. (2003). Climate suitability for malaria transmission in Africa, 1911-1995. *Proceedings of the National Academy of Sciences (PNAS)*, 100(26), 15341-15345 doi: 10.1073.pnas.2236969100
- Snepvangers, J. J. J. C., Heuvelink, G. B. M., & Huisman, J. A. (2003). Soil water content interpolation using spatio-temporal kriging with external driftal *Geoderma*, 112, 253-271.
- Snow, J. (1855). *On the mode of communication of cholera*. New Burlington Street, England: John Churchill.
- Snow, R. W., Craig, M. H., Deichmann, U., & Marsh, K. (1999). Estimating mortality, morbidity and disability due to malaria among Africa's non-pregnant population *Bulletin of the World Health Organization*, 77(8), 624-640.
- Snow, R. W., Guerra, C. A., Noor, A. M., Myint, H. Y., & Hay, S. I. (2005). The global distribution of clinical episodes of *Plasmodium falciparum* malaria. *Nature*, 434, 214-217.
- Spadavecchia, L., & Williams, M. (2009). Can spatio-temporal geostatistical methods improve high resolution regionalisation of meteorological variables? *Agricultural and Forest Meteorology*, 149, 1105-1117.
- Steketee, R. W. (2001). The burden of malaria in pregnancy in malaria endemic areas. *American Journal of Tropical Medicine and Hygiene*, 64(Suppl 1-2), 28-35.
- Thomson, M. C., Connor, S., D'Alessandro, U., Rowlington, B., Diggle, P., Cresswell, M., & Greenwood, B. (1999). Predicting malaria infection in Gambian children from satellite data and bed net use surveys: The importance of spatial correlation in the interpretation of results. *American Journal of Tropical Medicine and Hygiene*, 61, 2-8.
- Thomson, M. C., & Connor, S. J. (2001). A framework for field research in Africa in malaria early warning system (MEWS): Concepts, indicators and partners Roll Back Malaria/World Health Organization, <http://www.rbm.who.int>

- Thomson, M. C., Doblas-Reyes, F. J., Mason, S. J., Hagedorn, R., Connor, S. J., Phindela, T., . . . Palmer, T. N. (2006). Malaria early warnings based on seasonal climate forecasts from multi-model ensembles *Nature*, *439*, 576-597.
- Thomson, M. C., Mason, S. J., Phindela, T., & Connor, S. J. (2005). Use of rainfall and sea surface temperature monitoring for malaria early warning in Botswana. *The American Society of Tropical Medicine and Hygiene*, *73*(1), 214-221.
- Tian, L., Bi, Y., Ho, S. C., W., L., Liang, S., Goggins, W. B., . . . Sung, J. J. Y. (2008). One-year delayed effect of fog on malaria transmission: a time series analysis in the rain forest area of Mengla County, south-west China. *Malaria Journal*, *7*:110.
- Tobler, W. R. (1970). A computer movie simulating urban growth in the Detroit region. *Economic Geography*, *46*, 234-240.
- Tukey, J. W. (1958). Bias and confidence in not quite large samples (abstract). *Annals of Mathematical Statistics*, *29*(614).
- Tumwiine, J., Mugisha, J. Y. T., & Luboobi, L. S. (2010). A host-vector model for malaria with infective immigrants. *Journal of Mathematical Analysis and Applications*, *361*(1), 139-149. doi: 10.1016/j.jmaa.2009.09.005
- UNICEF. (2008). UNICEF Annual Report 2007. New York, USA: United Nations Children's Fund (UNICEF), http://www.unicef.org/publications/index_44268.html#
- UNICEF. (2012). UNICEF Annual Report 2012 for Ghana: West and Central Africa Regional Office (WCARO), United Nations Children's Fund (UNICEF), http://www.unicef.org/about/annualreport/files/Ghana_COAR_2012_2012.pdf.
- van Beers, W. C. M., & Kleijnen, J. P. C. (2003). Kriging for interpolation in radon simulation. *Journal of the Operational Research* *54*, 255-262. doi: 10.1057/palgrave.jors.2601492
- Vecchia, A. V. (1988). Estimation and model identification for continuous spatial processes *Journal of the Royal Statistical Society, Series B*, *50*, 297-312.
- Vercruysse, J., Jancloes, M., & Van de Velden, L. (1983). Epidemiology of seasonal falciparum malaria in an urban area of Senegal *Bulletin of World Health Organization*, *61*(5), 821-831.
- Wackernagel, H. (1998). *Multivariate geostatistics* (Second revised ed.). Berlin: Springer.
- Wackernagel, H. (2003). *Multivariate geostatistics: An introduction with applications* (third revised ed.). New York: Springer.
- Walter, S. D. (1992). The analysis of regional patterns in health data, Part I *American Journal of Epidemiology*, *136*, 730-741.
- Wangdi, K., Singhasivanon, P., Silawan, T., Lawpoolsri, S., White, N. J., & Kaewkungwal, J. (2010). Development of temporal modelling for forecasting and prediction of malaria infections using time-series and ARIMAX analyses: A case study in endemic districts of Bhutan. *Malaria Journal*, *9*(251). doi: 10.1186/1475-2875-9-251
- Watt, G. (2002). The inverse law today. *The Lancet*, *360*, 252-254. doi: 10.1016/S0140-6736(02)09466-7
- Webster, R., Atteia, O., & Dubios, J. P. (1994). Coregionalisation of trace metals in the soil in the Swiss Jura. *European Journal of Soil Science*, *45*, 205-218.
- Webster, R., & Oliver, M. A. (1992). Sample adequately to estimate variograms of soil properties *Journal of Soil Sciences* *43*, 177-192 [Application of geostatistical techniques to soil sciences].

- Webster, R., & Oliver, M. A. (2007). *Geostatistics for environmental scientists* (second ed.). Chichester: Wiley, Statistics in Practice
- Webster, R., Oliver, M. A., Munir, K. R., & Mann, J. R. (1994). Kriging the local risk of a rare disease from a register of diagnoses. *Geographical Analysis*, 26(2), 168-185.
- WHO. (1986). WHO Expert Committee Report on Malaria: 18th Report: World Health Organisation (WHO) Technical Report, 735.
- WHO. (2000). WHO Expert Committee Report on Malaria: 20th Report: World Health Organisation (WHO) Technical Report, 892.
- WHO. (2003). Climate change and human health, risks and responses. Geneva, Switzerland: World Health Organisation (WHO).
- WHO. (2008). World Malaria Report 2008 (Vol. WHO/HTM/GMP/2008.1). Geneva, Switzerland: World Health Organisation (WHO).
- WHO. (2011). World Malaria Report 2011. Geneva, Switzerland: World Health Organization (WHO).
- WHO. (2012). World Malaria Report 2012. Geneva, Switzerland: World Health Organization (WHO).
- WHO/UNICEF. (2003). Africa Malaria Report 2003 (Vol. WHO/CDS/MAL 2003). Geneva, Switzerland: World Health Organisation (WHO).
- WHO/UNICEF. (2005). Roll Back Malaria: World Malaria Report 2005. Geneva, Switzerland: World Health Organisation (WHO).
- WHO/VBCD. (1989). Geographical distribution of arthropod-borne diseases and their principal vectors (Vol. WHO/VBC/89.967, pp. WHO/VBC/89.967, 966-917). Geneva, Switzerland: World Health Organization (WHO), Vector Biology and Control Division (VBCD), WHO/VBC/89.967.
- Winters, P. R. (1960). Forecasting sales by exponentially weighted moving averages. *Management Sciences*, 6, 324-342.
- Woyessa, A., Deressa, W., Ali, A., & Lindtjörn. (2013). Malaria risk factors in Butajira area, south-central Ethiopia: A multilevel analysis *Malaria Journal*, 12(273).
- Yaglom, A. M. (1957). Some classes of random fields in n -dimensional space, related to stationary random processes *Theory of Probability and its Applications*, 2, 273-320.
- Yu, D. (2010). Exploring spatiotemporally varying regressed relationships: The geographically weighted panel regression analysis. *The International Archives of the Photogrammetry, Remote Sensing and Spatial Information System Sciences*, 38(Part II), 134-139.
- Yè, Y., Louis, V. R., Simboro, S., & Sauerborn, R. (2007). Effect of meteorological factors on clinical malaria risk among children: An assessment using village-based meteorological station and community-based parasitological survey *BMC Public Health*, 7(101). doi: 10.1186/1471-2458-7-101
- Zacarias, O. P., & Anderson, M. (2011). Spatial and temporal patterns of malaria incidence in Mozambique. *Malaria Journal*, 10(189). doi: 10.1186/147-2875-10-189
- Zhang, X., Zhang, T., Young, A. A., & Li, X. (2014). Applications and comparisons of four time series models in epidemiological surveillance data. *PLoS ONE*, 9(2), e88075. doi: 10.1371/journal.pone.0088075
- Zimmerman, D. L., & Zimmerman, M. B. (1991). A Monte Carlo comparison of spatial semivariogram estimators and corresponding ordinary kriging predictors. *Technometrics*, 33, 77-91.

Appendices

Appendix A: Exploratory Analysis of Regional Data

A-1: Summary Statistics of Monthly MIR for Age Groups

Table A-1.1: Summary statistics of monthly malaria incidence rates of age group (0-4) in the regions

Region		Min	Max	Mean	Q1	Med	Q3	StDev	CV
Ashanti	Total	181	496	288.6	229.8	267.5	334.2	77.823	0.270
	Male	177	502	289.1	236.8	268.5	319.5	75.428	0.261
	Female	179	497	288.0	226.0	265.5	335.2	81.843	0.284
Brong Ahafo	Total	191	686	390.0	334.5	382.0	454.0	85.480	0.219
	Male	207	637	407.5	350.8	402.0	471.2	85.832	0.211
	Female	175	735	373.1	319.8	369.5	432.5	86.669	0.232
Eastern	Total	154	611	316.4	252.0	299.0	357.0	91.829	0.290
	Male	162	625	321.8	257.8	298.5	360.2	95.226	0.296
	Female	143	598	311.0	249.5	289.5	347.8	90.611	0.291
Greater Accra	Total	125	445	235.8	197.5	230.0	265.5	60.933	0.258
	Male	127	402	242.2	201.0	237.5	270.2	61.073	0.252
	Female	124	511	229.2	191.2	222.5	257.0	61.923	0.270
Western	Total	126	673	301.1	208.0	269.0	352.8	129.47	0.430
	Male	124	714	312.3	217.5	285.0	370.0	135.44	0.434
	Female	129	633	290.4	195.0	263.0	339.2	124.79	0.430
Northern	Total	181	661	382.4	290.8	373.0	437.0	110.22	0.288
	Male	170	691	392.7	306.0	381.5	464.5	117.85	0.300
	Female	192	643	372.4	286.5	363.5	420.8	104.55	0.281
Upper West	Total	205	1285	585.0	422.2	555.0	700.2	224.56	0.384
	Male	215	1207	582.6	422.2	543.0	693.5	212.73	0.365
	Female	190	1371	588.3	404.5	543.5	703.5	241.32	0.411
Upper East	Total	284	1515	756.8	515.8	672.5	963.0	303.80	0.401
	Male	280	1523	734.9	506.8	674.9	934.5	288.37	0.392
	Female	268	1642	781.9	518.2	714.0	1006	328.00	0.419
Central	Total	101	347	207.1	162.0	202.0	250.5	56.798	0.274
	Male	98	333	200.6	156.8	194.5	255.8	56.902	0.284
	Female	105	373	214.0	168.2	208.0	263.0	58.095	0.271
Volta	Total	228	653	376.0	288.0	352.0	438.0	112.76	0.300
	Male	214	650	367.0	275.0	342.0	432.0	114.40	0.312
	Female	228	657	384.0	289.0	356.0	449.0	115.20	0.300

Table A1.2: Summary statistics of monthly malaria incidence rates of age group (5-14) in the regions

Region		Min	Max	Mean	Q1	Med	Q3	StDev	CV
Ashanti	Total	63	211	110.3	87.5	106.0	123.0	31.839	0.289
	Male	64	204	108.3	84.8	104.5	125.0	30.332	0.280
	Female	62	217	112.4	88.0	108.5	127.0	33.956	0.302
Brong Ahafo	Total	62	285	148.4	109.0	146.0	183.5	50.666	0.341
	Male	62	285	144.5	106.8	143.5	178.2	49.442	0.342
	Female	63	287	152.0	110.8	147.5	185.5	52.787	0.343
Eastern	Total	36	340	124.4	78.8	112.5	151.8	59.586	0.479
	Male	34	358	121.1	76.0	108.5	149.8	58.784	0.486
	Female	31	321	128.0	82.0	115.0	159.0	60.828	0.475
Greater Accra	Total	35	150	76.1	62.8	74.0	88.0	21.344	0.280
	Male	33	144	76.6	61.8	75.0	88.3	21.255	0.278
	Female	35	156	75.6	58.5	75.0	86.3	22.327	0.295
Western	Total	29	277	113.8	75.8	96.5	150.0	57.527	0.505
	Male	29	270	113.0	76.0	98.5	151.8	55.794	0.494
	Female	29	284	114.6	75.8	96.5	153.0	59.419	0.519
Northern	Total	34	246	111.6	71.0	100.0	141.0	49.917	0.447
	Male	36	244	112.7	72.8	102.5	140.2	50.129	0.445
	Female	32	249	110.6	69.5	98.5	142.2	50.096	0.453
Upper West	Total	30	441	139.5	69.8	101.0	194.2	85.811	0.615
	Male	31	420	137.0	72.0	100.0	187.2	81.946	0.598
	Female	28	464	142.2	66.8	102.5	210.2	90.547	0.637
Upper Eeast	Total	48	575	167.4	96.8	138.5	194.5	101.45	0.606
	Male	46	527	161.7	94.0	131.5	187.2	93.752	0.580
	Female	49	626	173.4	99.3	139.5	206.0	110.25	0.636
Central	Total	37	151	73.0	55.0	71.0	86.3	22.423	0.307
	Male	35	149	68.9	52.0	67.0	82.0	22.374	0.325
	Female	39	153	77.4	58.8	74.5	91.3	24.278	0.314

Table A-1.3: Summary statistics of monthly malaria incidence rates of age group (15-59) in Regions

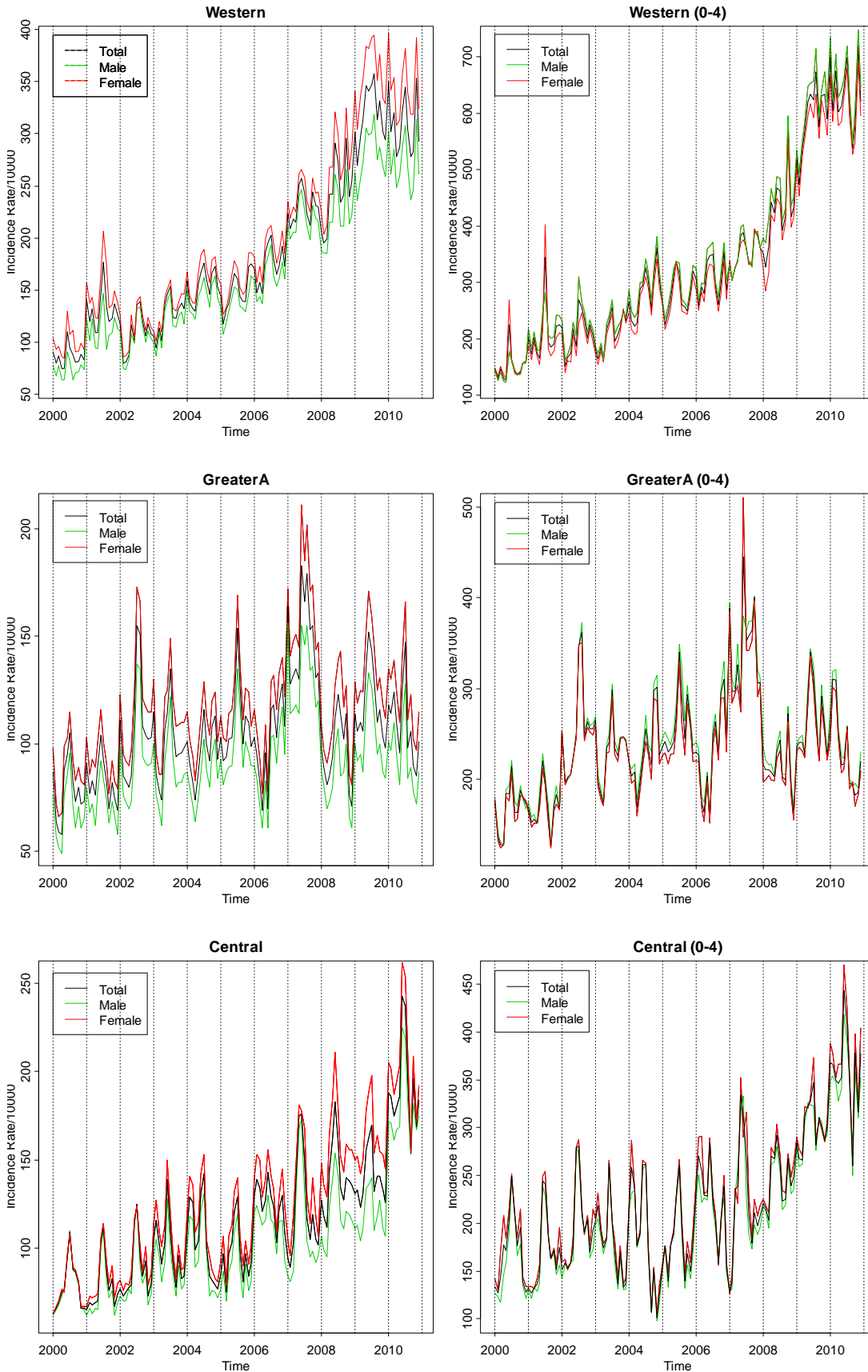
Region		Min	Max	Mean	Q1	Med	Q3	StDev	CV
Ashanti	Total	73	202	135.5	111.0	138.5	156.2	29.928	0.221
	Male	63	195	112.5	90.0	109.5	131.2	28.694	0.255
	Female	81	245	157.5	135.8	159.5	180.0	34.845	0.221
Brong Ahafo	Total	104	358	198.3	166.0	196.0	229.2	49.610	0.250
	Male	88	284	161.7	131.8	158.5	185.2	39.066	0.242
	Female	119	447	234.3	195.8	226.0	271.8	62.438	0.266
Eastern	Total	62	336	156.3	105.5	153.0	199.0	60.584	0.388
	Male	46	234	114.2	78.0	111.0	143.5	39.878	0.349
	Female	75	434	197.2	127.8	183.5	245.8	84.844	0.430
Greater Accra	Total	51	155	86.8	72.0	85.0	97.3	21.291	0.245
	Male	41	119	68.3	57.8	65.5	75.5	17.037	0.249
	Female	61	189	106.4	88.8	104.5	118.5	25.169	0.236
Western	Total	75	305	169.7	136.2	163.0	206.0	54.623	0.322
	Male	54	230	134.1	94.8	127.0	175.0	46.614	0.348
	Female	95	383	204.9	158.8	198.0	233.8	66.134	0.323
Northern	Total	56	277	144.4	103.0	138.0	179.2	50.587	0.350
	Male	47	277	118.9	87.0	111.5	145.5	42.788	0.360
	Female	64	319	169.3	119.8	163.5	214.5	60.170	0.355
Upper West	Total	45	524	173.8	94.0	134.5	231.8	97.781	0.563
	Male	46	602	200.3	89.5	159.5	292.8	126.13	0.630
	Female	44	453	149.7	97.8	123.0	182.5	74.922	0.500
Upper East	Total	86	472	189.8	131.8	162.5	236.8	80.598	0.425
	Male	74	461	161.7	111.5	140.0	195.0	68.755	0.425
	Female	93	507	215.0	149.2	180.5	261.0	93.289	0.434
Central	Total	49	159	91.7	71.0	91.0	114.0	25.257	0.275
	Male	46	144	77.6	63.0	73.5	91.0	19.373	0.250
	Female	47	191	105.2	77.8	105.5	131.0	33.023	0.314

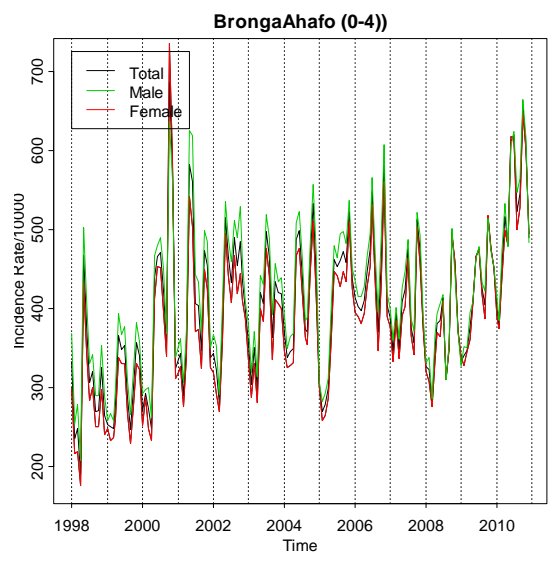
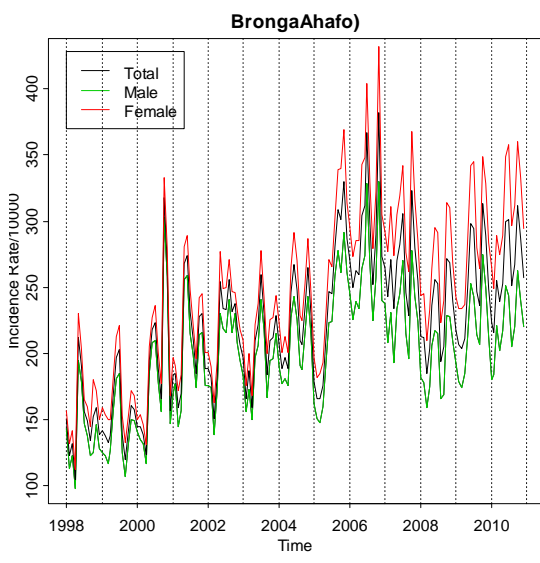
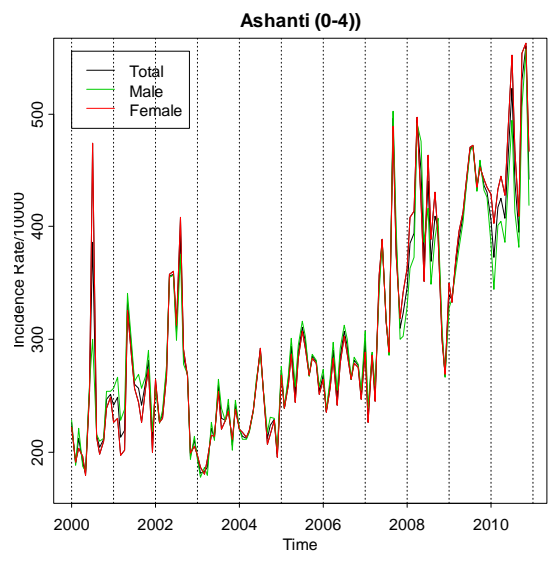
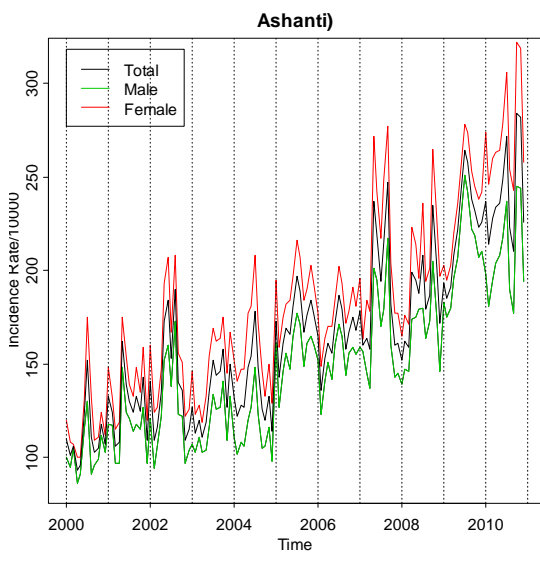
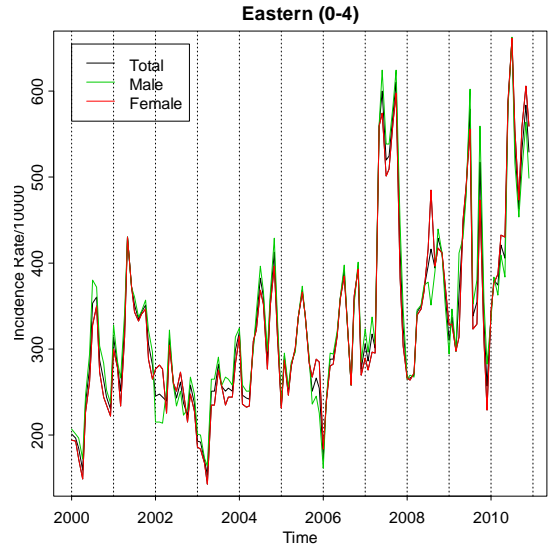
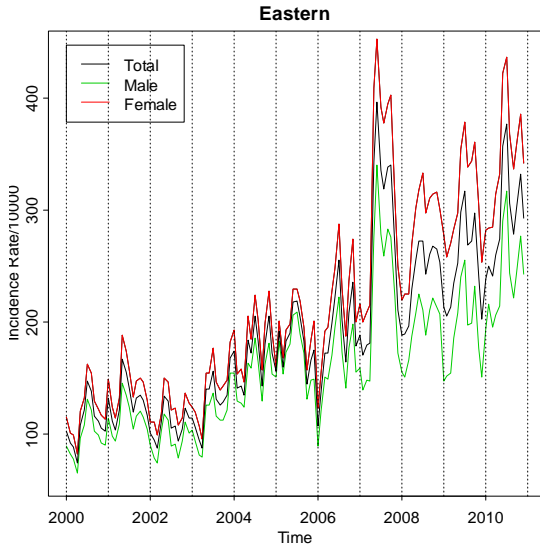
Table A-1.4: Summary statistics of monthly malaria incidence rates of age group (60+) in the regions

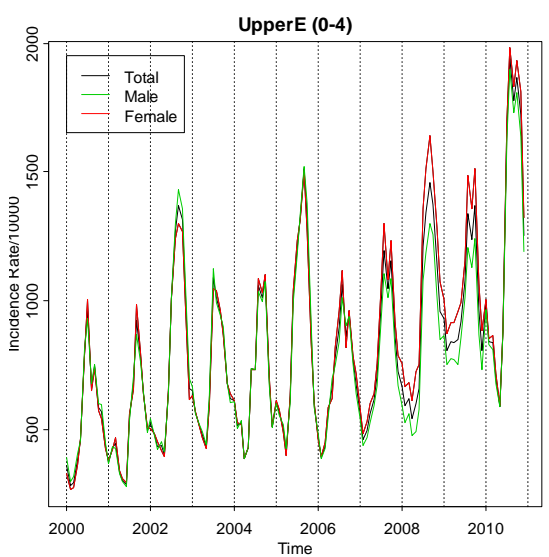
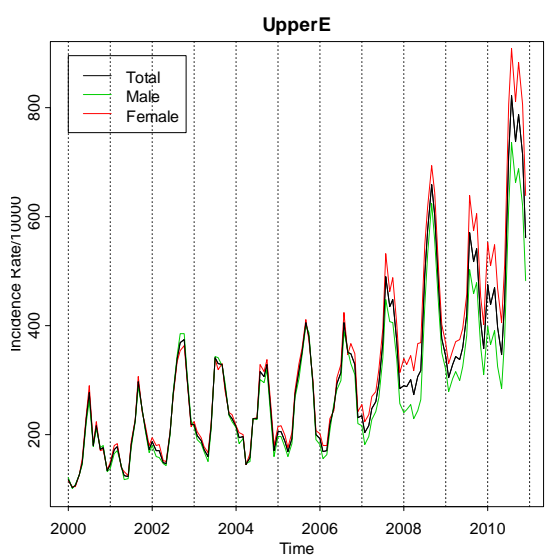
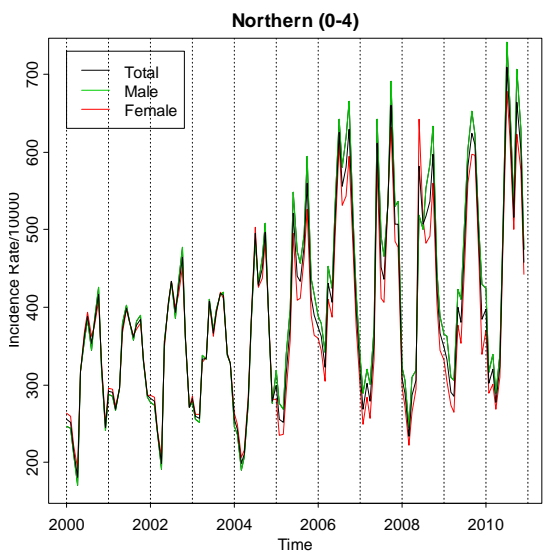
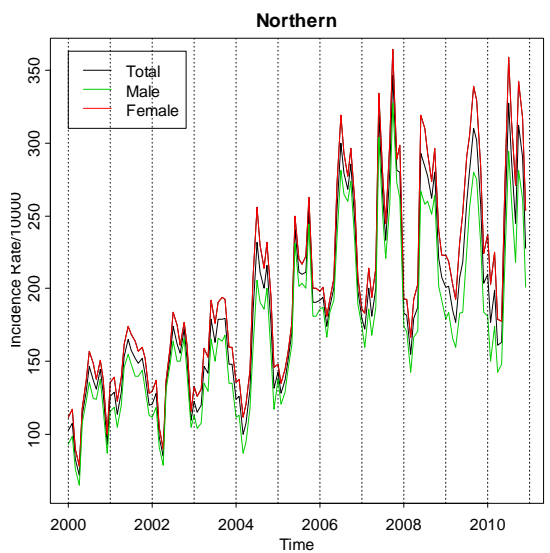
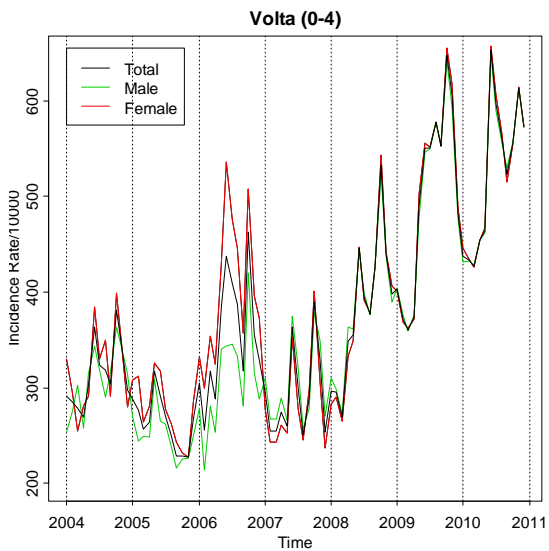
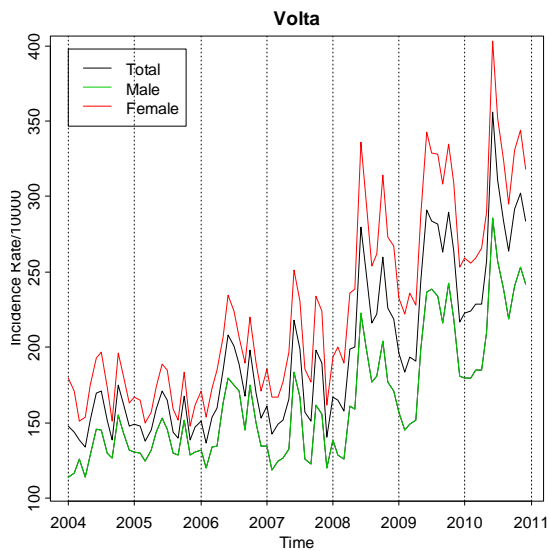
Region		Min	Max	Mean	Q1	Med	Q3	StDev	CV
Ashanti	Total	99	515	220.5	135.0	198.0	295.2	106.06	0.481
	Male	68	353	162.4	95.8	144.5	218.0	73.684	0.454
	Female	116	722	284.5	172.8	246.0	369.5	141.89	0.499
Brong Ahafo	Total	91	517	260.4	174.0	229.5	354.5	109.91	0.422
	Male	80	396	198.7	140.5	186.0	253.5	73.855	0.382
	Female	97	669	320.1	203.0	273.0	453.0	146.28	0.457
Eastern	Total	87	642	245.2	124.5	205.0	342.5	140.34	0.572
	Male	62	458	183.1	93.5	159.5	253.0	99.896	0.546
	Female	99	793	296.2	152.0	217.6	438.0	177.65	0.600
Greater Accra	Total	53	280	121.8	83.0	107.5	161.2	50.579	0.415
	Male	36	279	94.0	58.0	78.0	130.2	46.972	0.500
	Female	70	321	147.9	105.8	135.5	184.2	55.017	0.372
Western	Total	60	473	175.2	93.8	123.0	286.0	109.42	0.624
	Male	45	427	142.2	74.8	105.0	204.0	86.722	0.610
	Female	66	583	209.4	113.0	146.0	332.2	134.27	0.641
Northern	Total	52	470	227.3	121.0	198.0	323.2	115.10	0.506
	Male	42	406	185.7	97.0	170.5	253.8	98.755	0.532
	Female	63	539	271.0	148.5	245.0	392.2	134.43	0.496
Upper West	Total	60	879	313.8	137.8	255.0	472.2	185.82	0.592
	Male	51	847	280.1	121.8	223.0	419.2	170.11	0.607
	Female	67	910	347.4	161.0	245.0	534.5	222.51	0.641
Upper East	Total	61	483	168.3	110.0	130.0	216.8	84.619	0.503
	Male	65	431	147.6	106.5	123.0	171.8	65.101	0.441
	Female	57	542	188.3	115.5	144.5	254.0	105.54	0.561
Central	Total	60	313	129.4	87.0	107.0	166.5	55.574	0.429
	Male	59	288	114.9	78.0	96.5	152.0	45.831	0.399
	Female	61	332	140.1	89.8	116	174.2	65.261	0.466

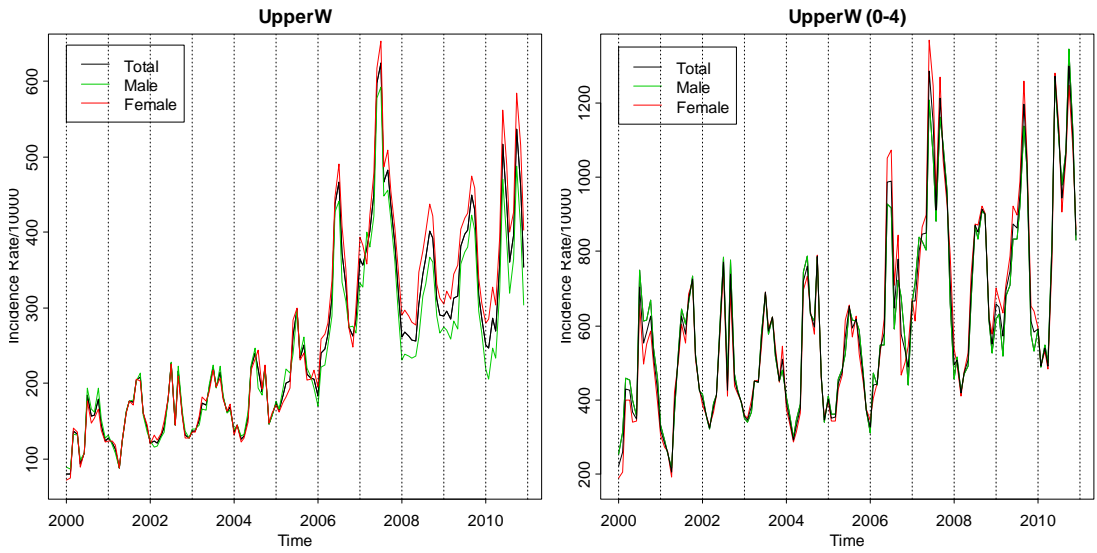
A-2: Time Sequence Plots of MIR

A-2.1: Time Sequence Plots of MIR by Regional Total and Sex

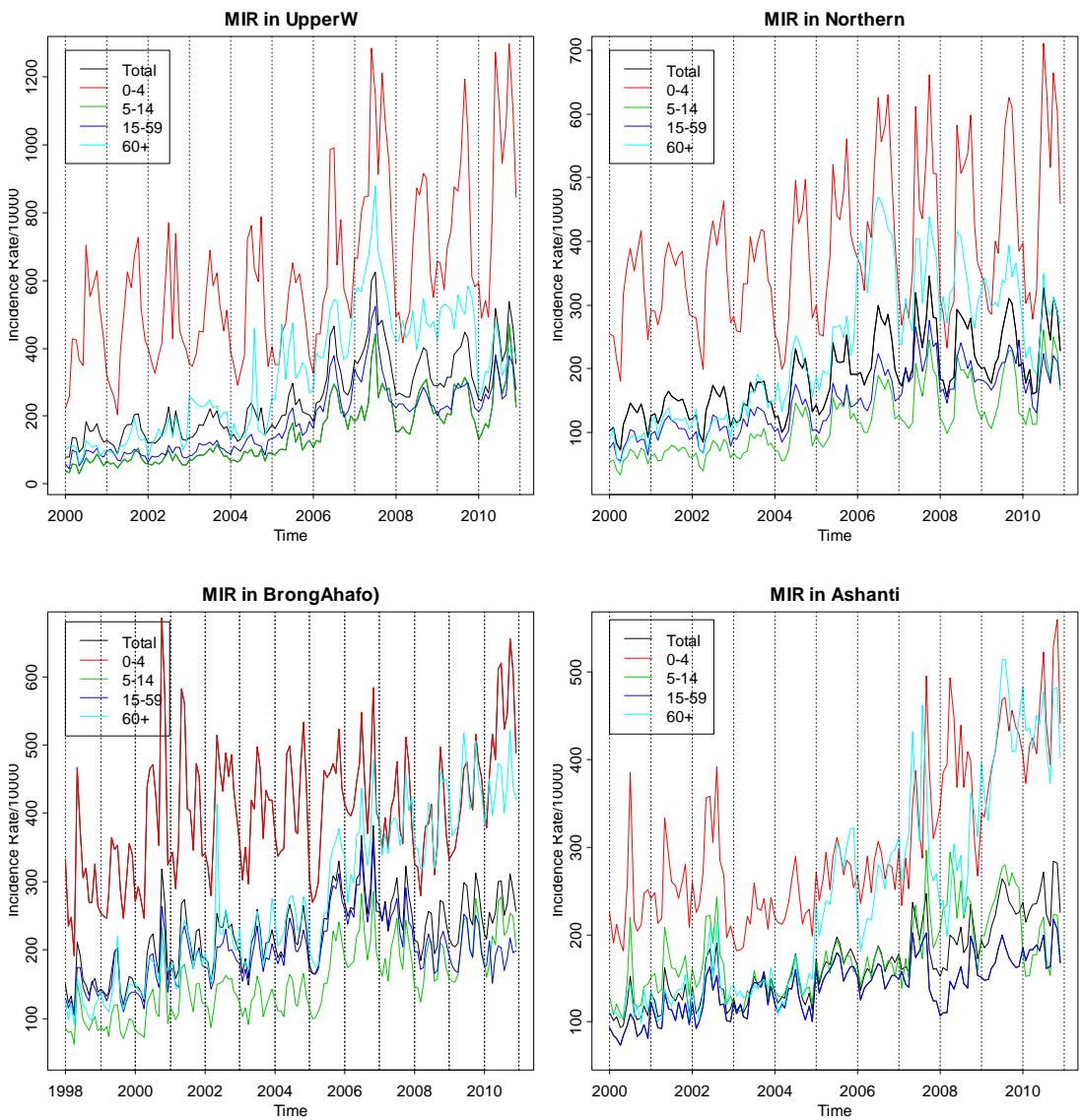




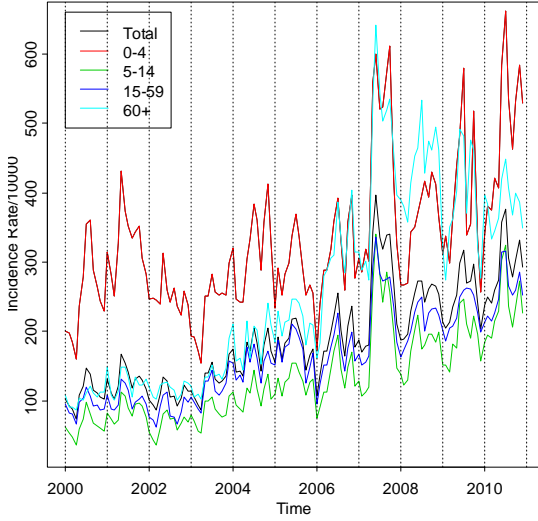




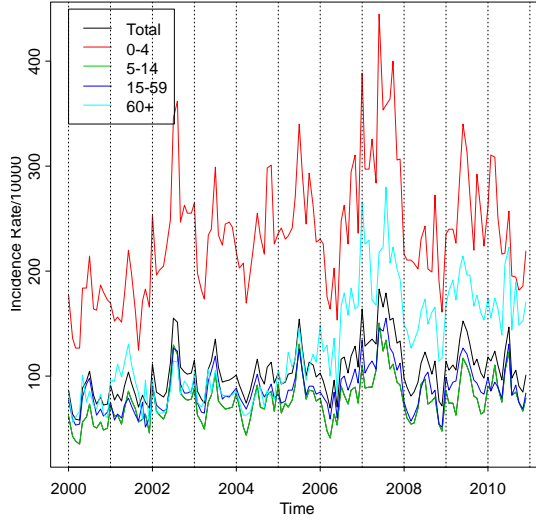
A-2.2: Time sequence plots of MIR by Age Groups and Regions



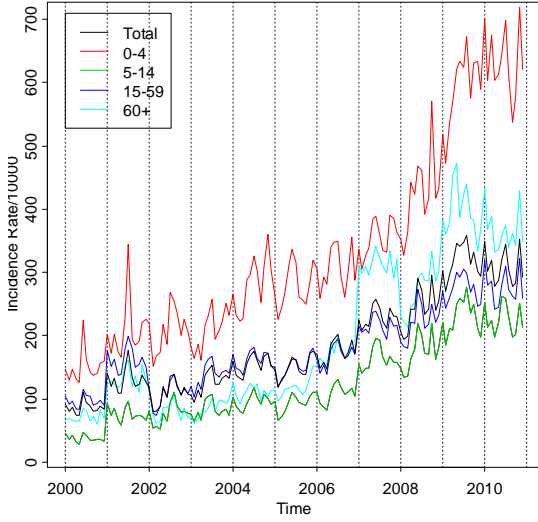
MIR in Eastern



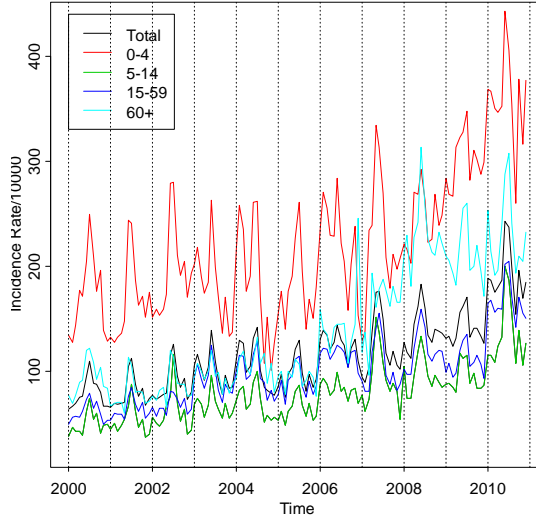
MIR in GreaterA



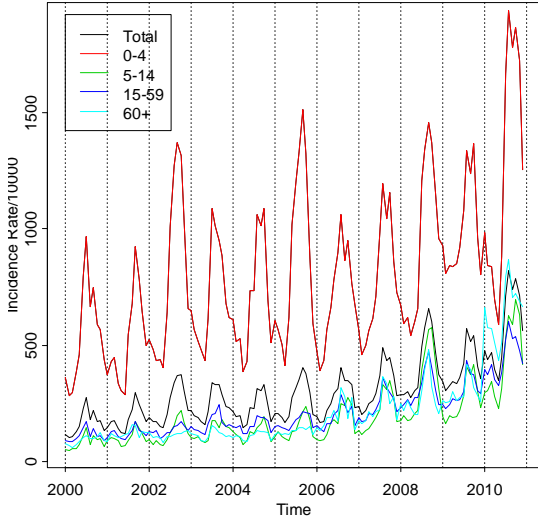
MIR in Western



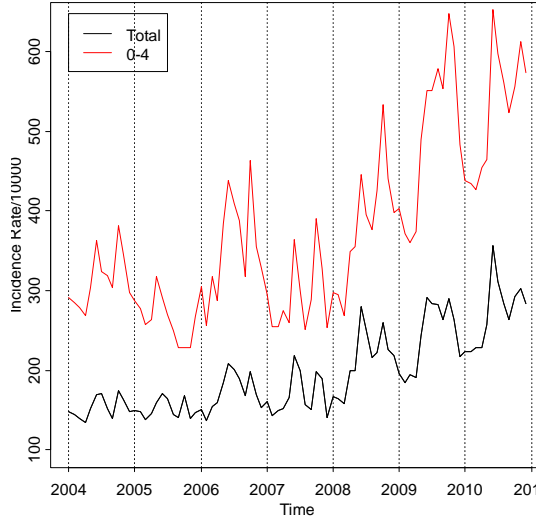
MIR in Central

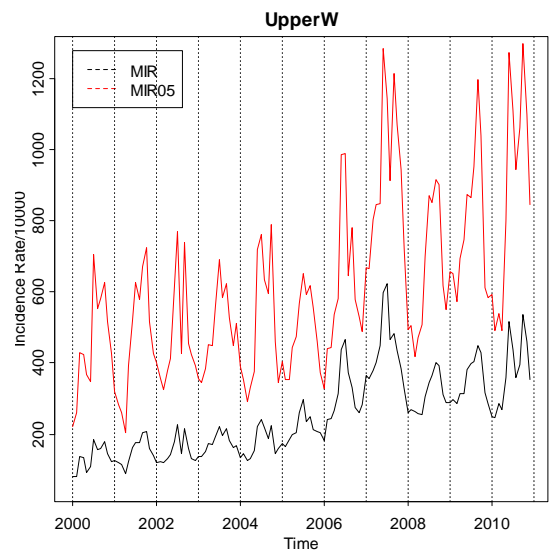
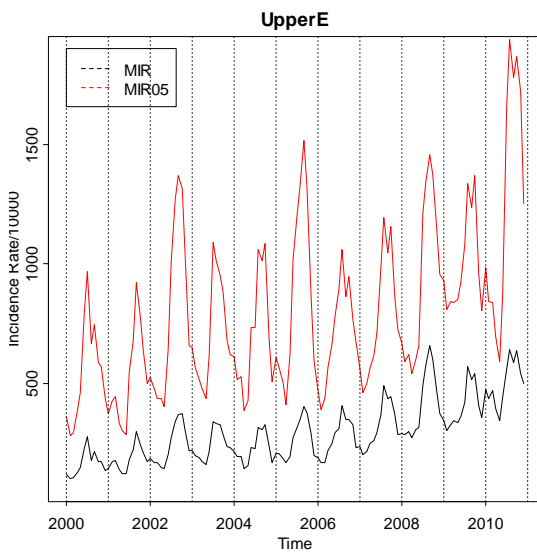
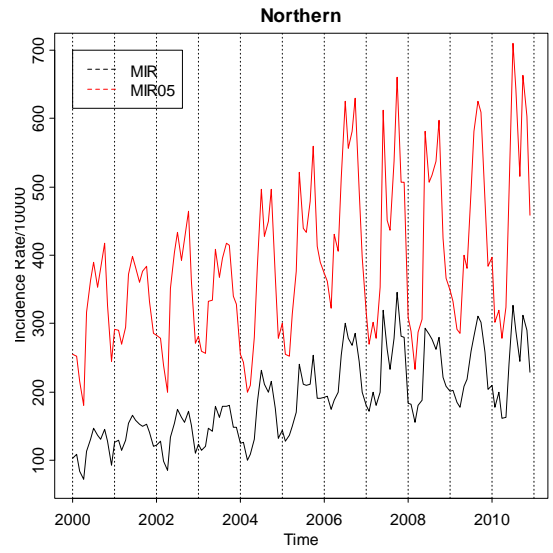
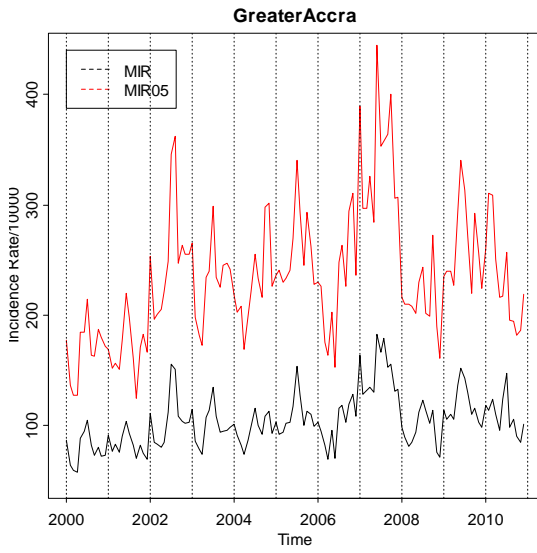
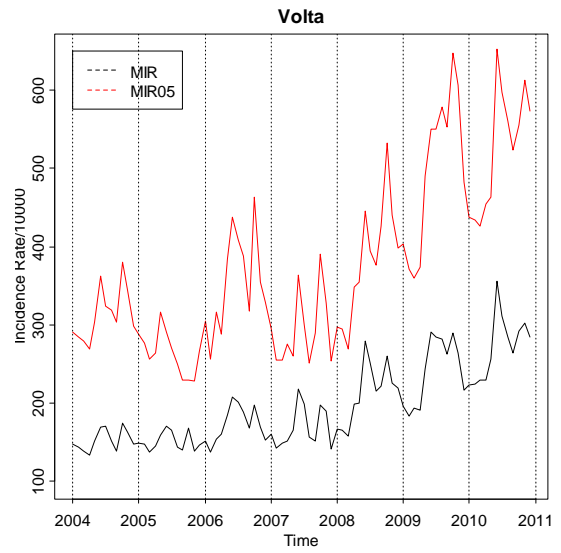
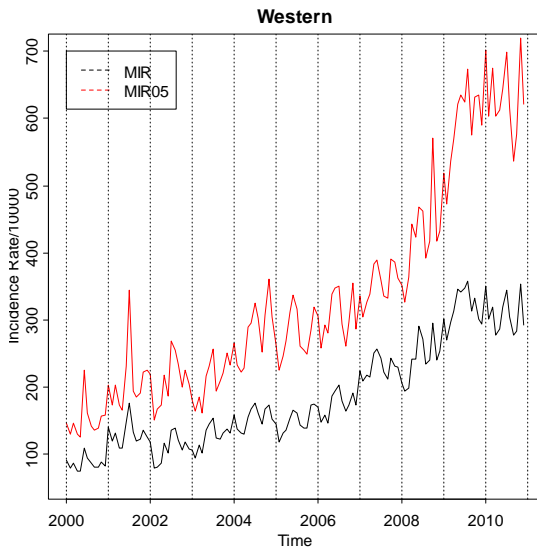


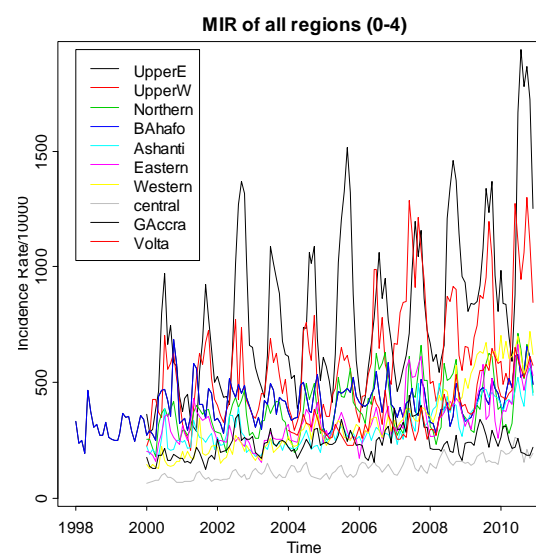
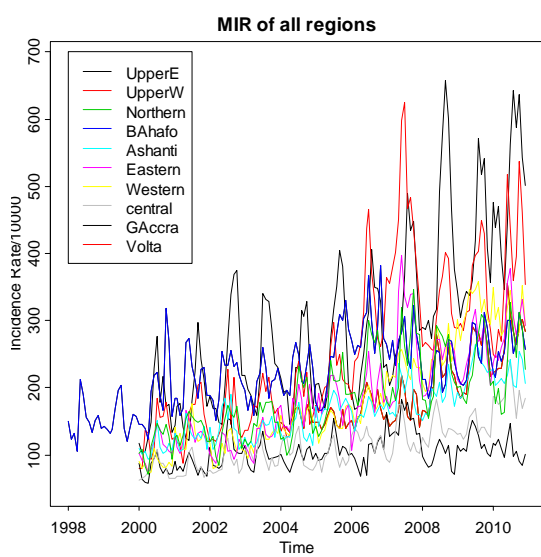
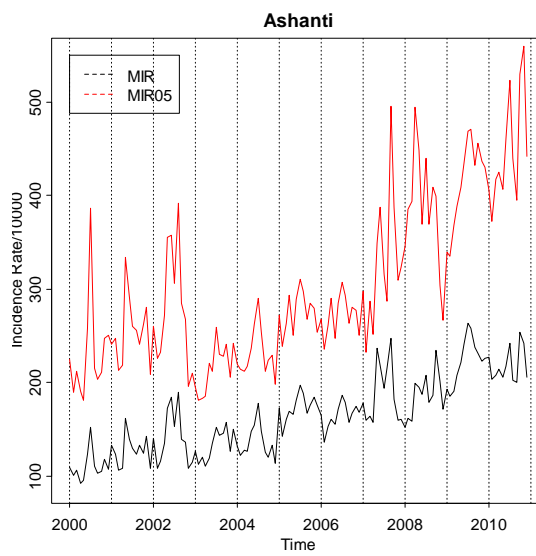
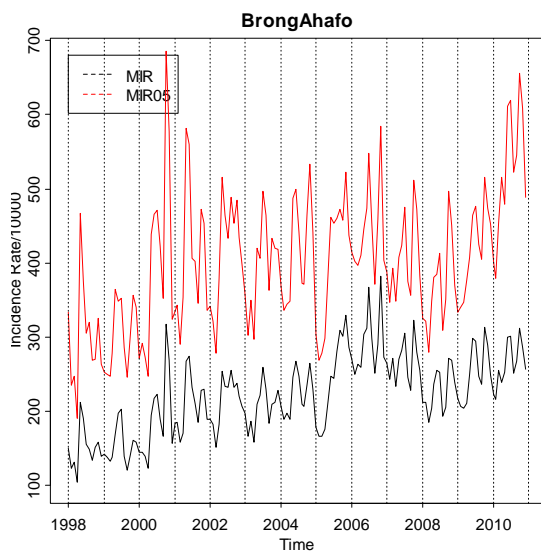
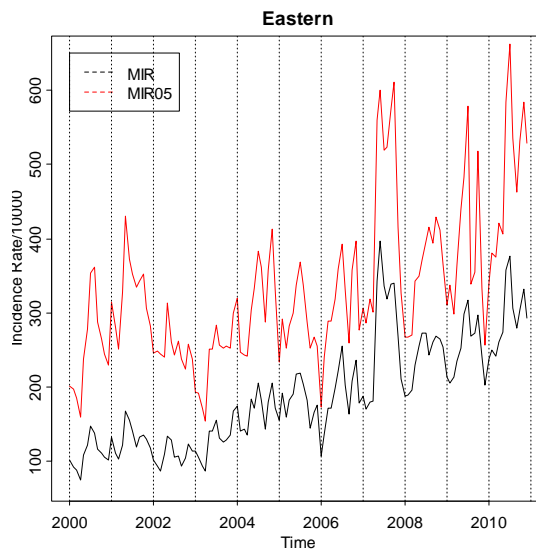
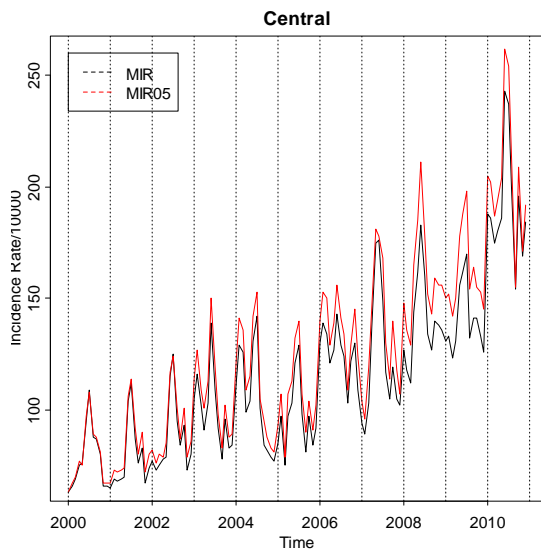
MIR in UpperE



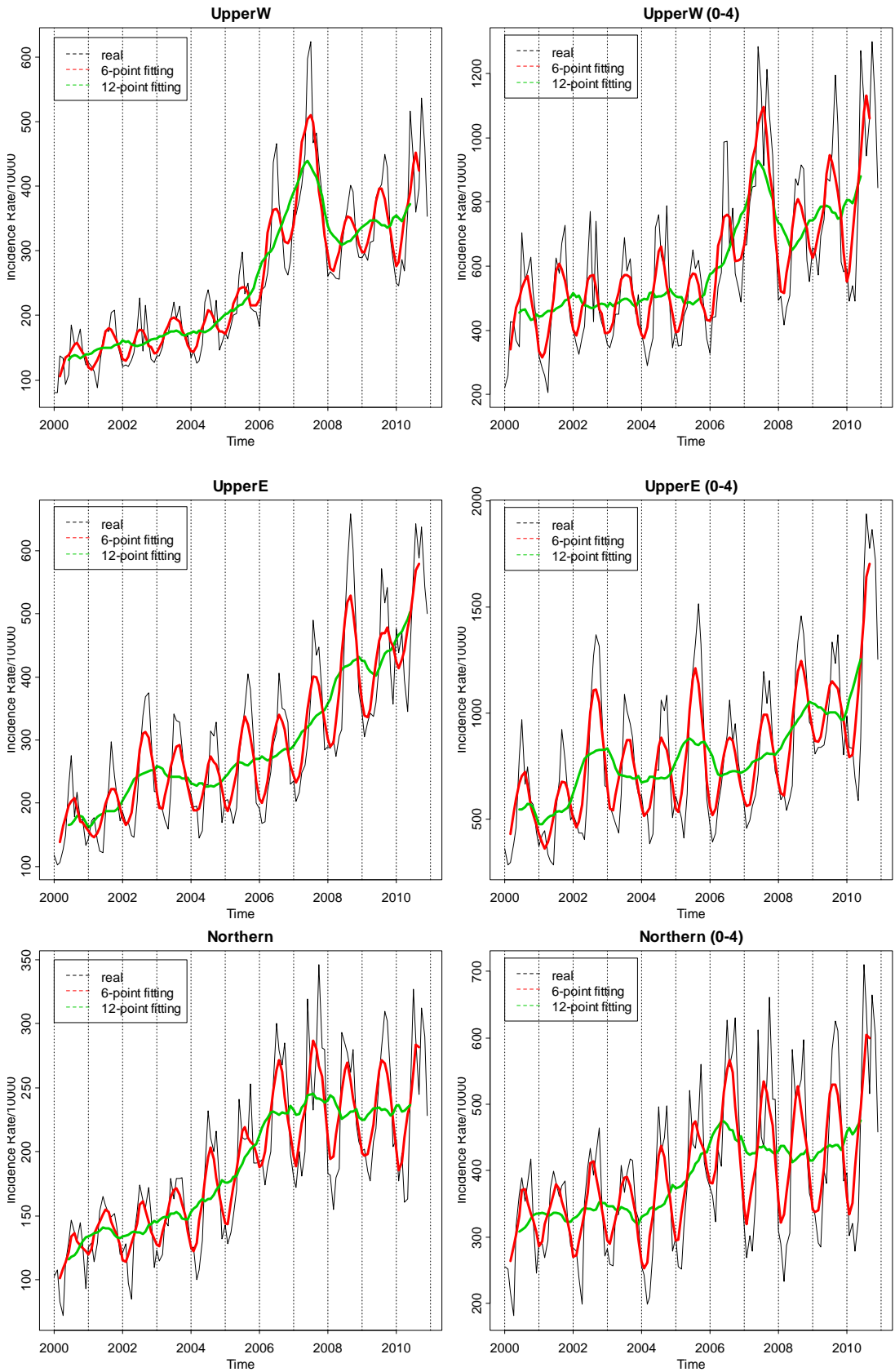
MIR in Volta

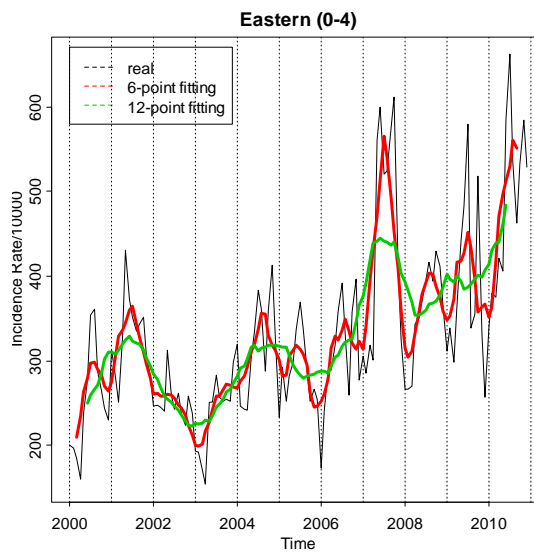
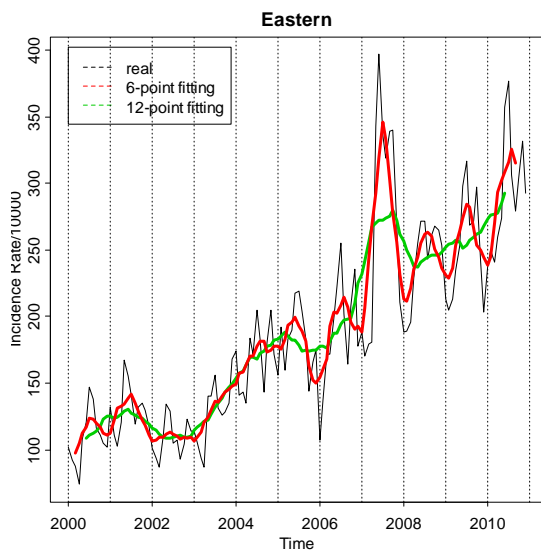
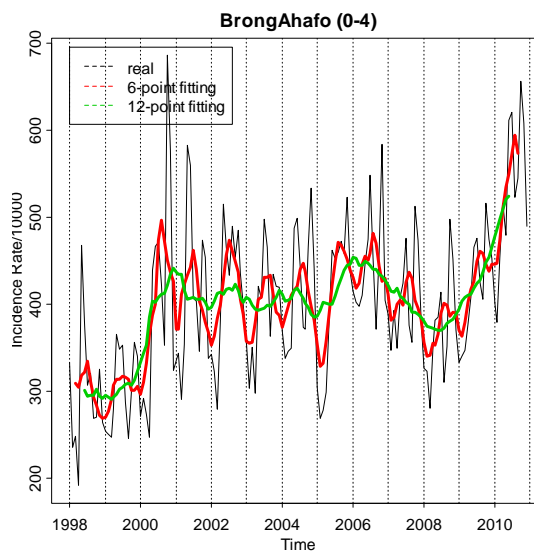
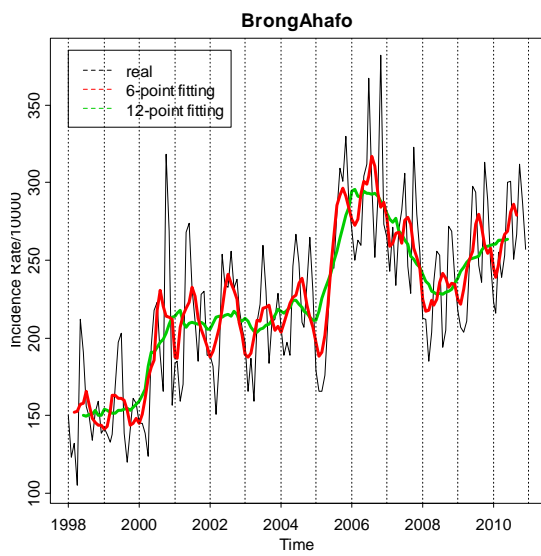
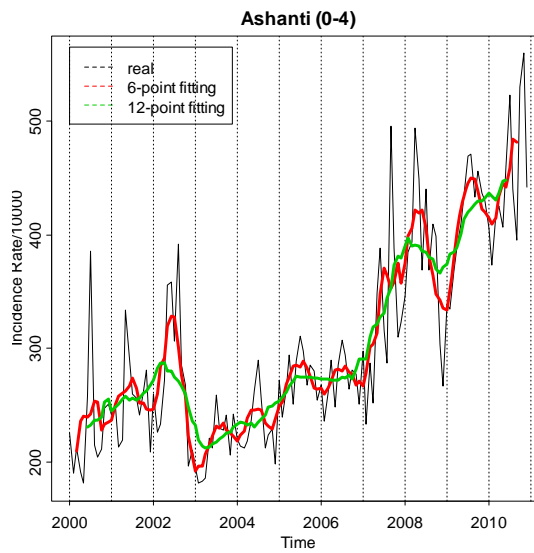
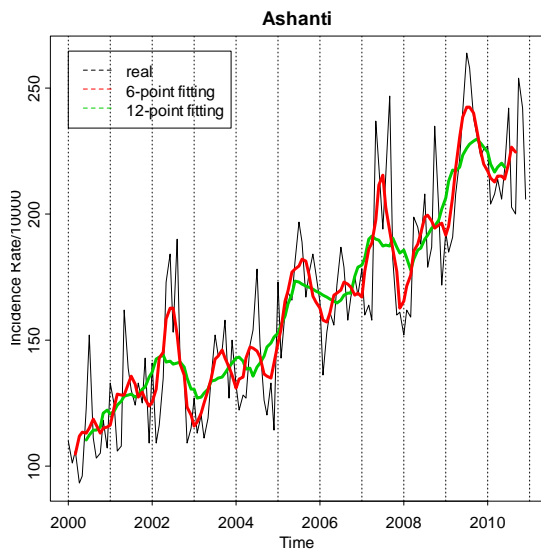


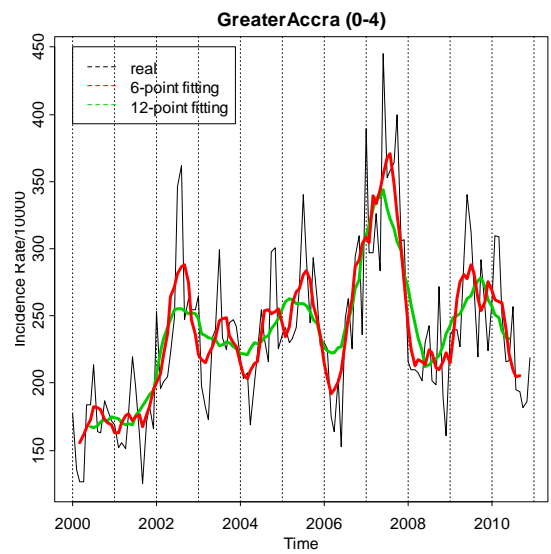
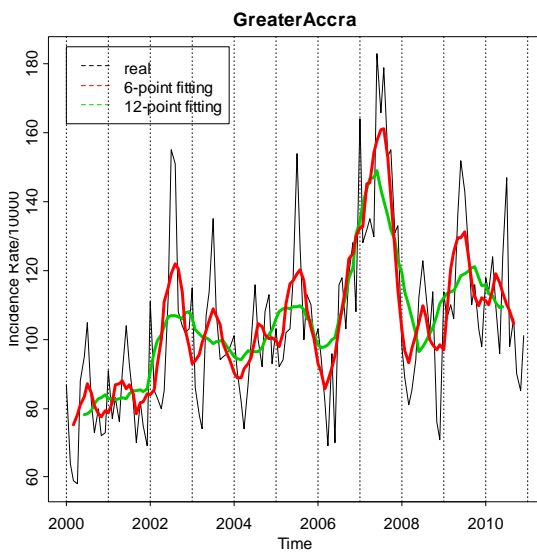
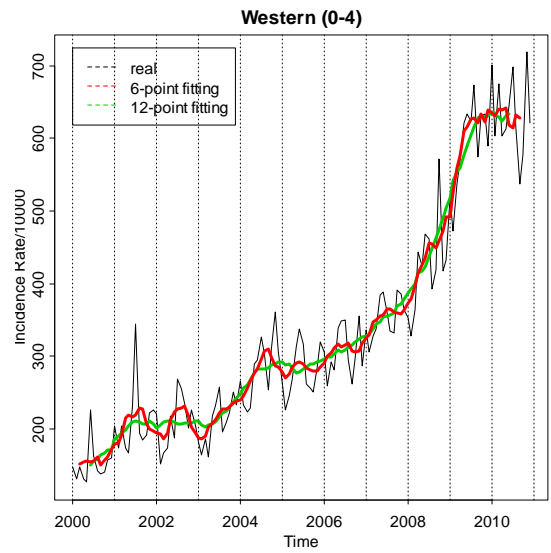
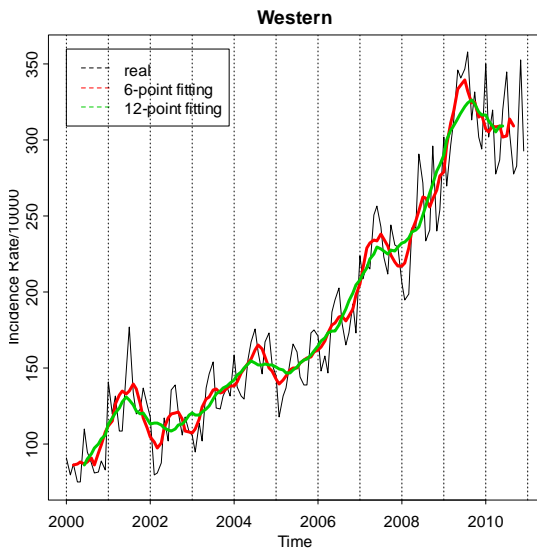
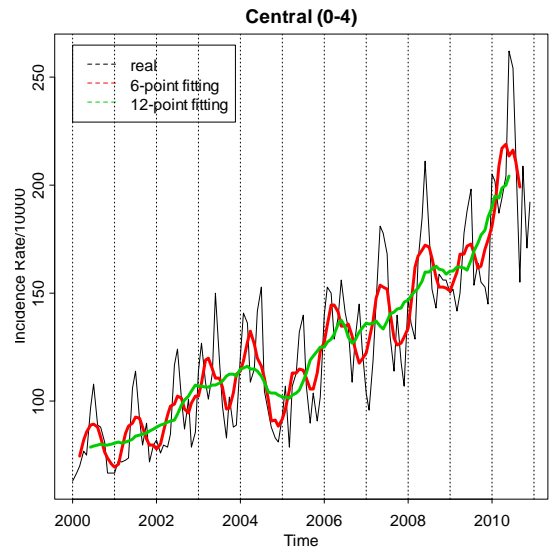
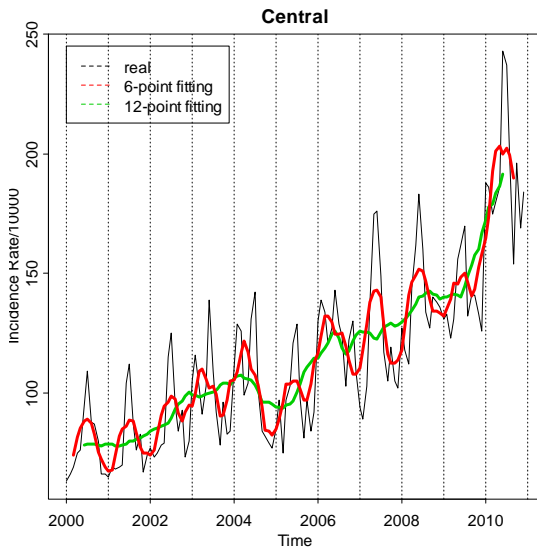


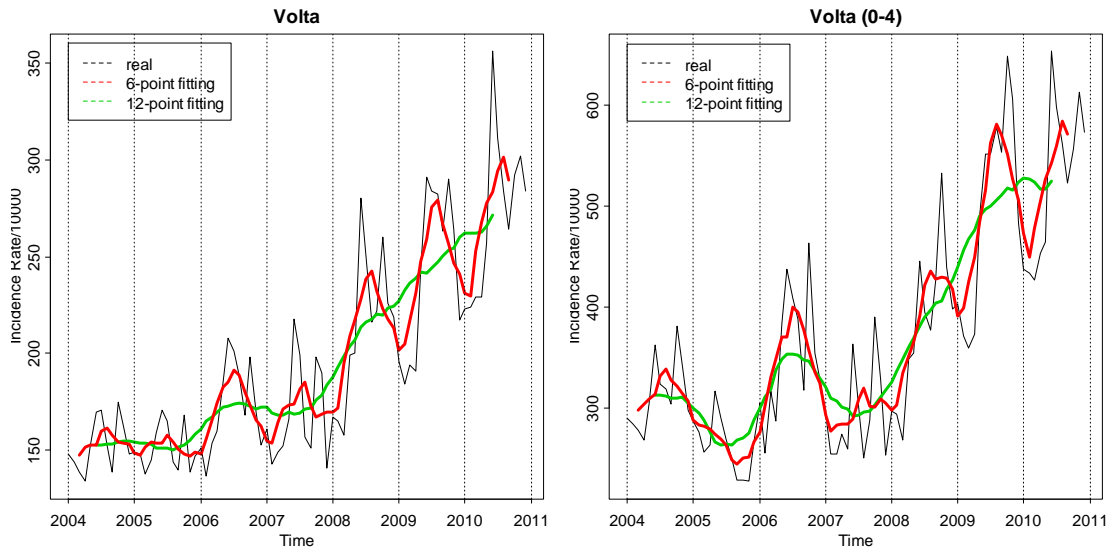


A-3: Smoothing Analysis of MIR









A-4: Holt-Winters Seasonal Decomposition of Regional MIR

Table A-4.1. Holt-Winters' seasonal decomposition components of malaria incidence rates (total) for the regions

Month	Upper West	Upper East	Northern	B. Ahafo	Ashanti
January	0.871655	0.933945	0.798768	0.896663	0.903082
February	0.904765	0.794230	0.744541	0.842107	0.838867
March	0.917928	0.813948	0.741003	0.875110	0.860415
April	0.853518	0.743936	0.700060	0.867786	0.914353
May	0.883255	0.728440	0.768882	1.007253	0.969000
June	1.075545	0.900800	1.054455	1.165803	1.014723
July	1.085521	1.150065	1.204889	1.205207	1.097901
August	1.019101	1.415770	1.133462	1.042299	1.006436
September	1.107718	1.356356	1.096492	0.977498	0.982698
October	1.122465	1.427843	1.234310	1.155185	1.049673
November	0.909005	1.141288	1.050640	1.130961	0.958573
December	0.845238	0.956704	0.868235	0.969106	0.864209
Month	Eastern	Western	Central	G. Accra	Volta
January	0.809170	0.955310	1.0359289	1.052247	0.943727
February	0.819776	0.835751	1.0151672	0.904334	0.924968
March	0.820277	0.890902	0.9546183	0.960912	0.928386
April	0.876343	0.882397	1.0226564	0.895993	0.957209
May	1.058103	0.969803	1.1048608	1.050543	1.064183
June	1.225875	1.056672	1.2729343	1.217151	1.262835
July	1.224988	1.078190	1.2180762	1.322008	1.120080
August	1.053184	0.977051	0.9911275	1.039689	0.992264
September	1.003100	0.894179	0.8843430	0.892876	0.920433
October	1.033448	0.941945	1.0020658	0.949713	1.080057
November	0.974604	0.945130	0.9094960	0.850986	1.019742
December	0.841334	0.854563	0.9030709	0.847510	0.913254

Table A-4.2: Holt-Winters' seasonal decomposition components of malaria incidence rates (0-4 year group) for regions

Month	Upper West	Upper East	Northern	B. Ahafo	Ashanti
January	0.796416	0.894403	0.772878	0.879058	0.877666
February	0.752038	0.705670	0.671653	0.840088	0.835674
March	0.732730	0.695095	0.639286	0.887506	0.915009
April	0.760370	0.632532	0.650991	0.965559	0.954643
May	0.906226	0.633704	0.789798	0.991015	0.954331
June	1.243180	0.881380	1.101185	1.160751	1.009482
July	1.236240	1.371960	1.257165	1.235958	1.091648
August	1.104160	1.548959	1.216681	1.093767	0.969167
September	1.273650	1.426993	1.186670	1.018860	0.957733
October	1.244670	1.491184	1.343708	1.239868	1.063113
November	0.931077	1.194678	1.077209	1.181847	0.971777
December	0.793648	0.888930	0.871861	0.982595	0.827666
Month	Eastern	Western	Central	G. Accra	Volta
January	0.740151	0.998694	1.028379	0.968577	0.937770
February	0.775859	0.867442	1.017701	0.868870	0.895658
March	0.752075	0.955189	0.962103	0.871682	0.877777
April	0.838074	0.945223	1.021605	0.850699	0.935334
May	0.973993	0.999255	1.111964	0.984229	1.069381
June	1.144929	1.054189	1.281663	1.201600	1.234542
July	1.211709	1.085799	1.234565	1.259587	1.073485
August	1.000080	0.967290	1.003956	1.000101	0.997357
September	0.954682	0.880846	0.881113	0.928979	0.961627
October	1.104985	0.966819	1.001550	1.072092	1.155821
November	0.954506	0.993454	0.900921	1.009257	1.077718
December	0.781972	0.910612	0.898104	0.949403	0.945356

A-5: Multiple Regression and Correlation Analysis of the Regional MIR Data with Climatic Covariates

Table A-5.1 Cross-correlation results of malaria incidence rates (total) and their detrended (residuals) with climatic covariates at same month of incidence.

Region	Data (Total)	Rainfall	MaxTemp	MinTemp	RH0600	RH1500	Sunshrs
Upper East	MIR	0.37517	-0.41299	-0.33456	0.40830	0.41626	-0.28713
	Residuals	0.51698	-0.68095	-0.22902	0.60715	0.62679	-0.44292
Upper West	MIR	0.29325	-0.29108	-0.00606	0.32827	0.32870	-0.23930
	Residuals	0.40126	-0.47068	-0.05591	0.48821	0.52229	-0.37294
Northern	MIR	0.36101	-0.48360	-0.08874	0.42511	0.45753	0.27157
	Residuals	0.45752	-0.65031	-0.21757	0.50955	0.52660	-0.2049
Brong Ahafo	MIR	0.15688	-0.25353	-0.09649	0.23809	0.40653	-0.05015
	Residuals	0.15053	-0.42017	-0.07398	0.31553	0.40983	-0.14929
Ashanti	MIR	0.14858	-0.18715	-0.23007	0.08023	0.25167	-0.22743
	Residuals	0.23776	-0.44149	-0.07784	0.21189	0.40956	-0.39887
Eastern	MIR	0.22215	-0.32198	0.11401	0.04429	0.28893	-0.19682
	Residuals	0.29221	-0.46909	-0.20356	0.25504	0.47270	-0.31009
Western	MIR	0.15543	-0.09984	0.02935	0.24307	0.14636	-0.09859
	Residuals	0.24507	-0.24988	-0.10537	0.19628	0.22637	-0.22165
Central	MIR	0.21676	-0.13425	0.22943	0.12558	0.24541	-0.02805
	Residuals	0.38345	-0.27906	0.10467	0.12685	0.34065	-0.24029
Greater Accra	MIR	0.15809	-0.40176	-0.25700	0.02224	0.28055	-0.33633
	Residuals	0.13479	-0.45900	-0.40380	-0.0918	0.28419	-0.37415
Volta	Total	0.20809	-0.32084	-0.00028	0.20879	0.42504	-0.16029
	Residuals	0.47196	-0.58961	-0.18044	0.35642	0.56342	-0.33388

Table A-5.2: Cross-correlation results of malaria incidence rates (total) and their detrended (residuals) with climatic covariates at previous month of incidence (lag 1).

Region	Data (Total)	Rainfall _1	MaxTemp _1	MinTemp _1	RH06_1	RH15_1	Sunshrs_1
Upper East	MIR	0.51606	-0.49244	-0.22680	0.47298	0.52387	-0.39751
	Residuals	0.72212	-0.79891	-0.07478	0.69590	0.78774	-0.59413
Upper West	MIR	0.33739	-0.23875	0.11896	0.30810	0.31513	-0.25485
	Residuals	0.45157	-0.37505	0.09673	0.43166	0.47889	-0.37607
Northern	MIR	0.48570	-0.52721	0.08041	0.48248	0.55299	0.20777
	Residuals	0.62385	-0.70276	0.01941	0.58662	0.66410	-0.28291
Brong Ahafo	MIR	0.45313	-0.21375	0.03172	0.32966	0.48800	-0.05323
	Residuals	0.55671	-0.35952	0.09767	0.44066	0.52513	-0.15010
Ashanti	MIR	0.23463	-0.12400	-0.13836	0.12290	0.24697	-0.15814
	Residuals	0.36898	-0.30664	-0.10452	0.28899	0.39366	-0.23722
Eastern	MIR	0.34222	-0.23523	0.22164	0.02103	0.28450	-0.15642
	Residuals	0.50095	-0.29716	0.00354	0.22781	0.46041	-0.21592
Western	MIR	0.21585	-0.03846	0.11174	0.27824	0.14384	-0.04284
	Residuals	0.41807	-0.03782	0.17156	0.29435	0.19618	-0.01222
Central	MIR	0.23317	0.04402	0.37522	0.10921	0.13675	0.13927
	Residuals	0.37440	0.05255	0.34972	0.10107	0.13518	0.07852
Greater Accra	MIR	0.42891	-0.25737	-0.07888	0.15450	0.33715	-0.16853
	Residuals	0.44835	-0.29100	0.19286	0.24283	0.35052	-0.17769
Volta	MIR	0.29835	-0.23516	0.15384	0.18383	0.42778	-0.12820
	Residuals	0.58054	-0.39501	0.10841	0.32747	0.53287	-0.21328

Table A-5.3: Cross-correlation results of observed malaria incidence rates (total) and their detrended (residuals) with climatic covariates at previous two months of incidence (lag 2).

Region	Data (Total)	Rainf_2	MaxT_2	MinT_2	RH06_2	RH15_2	Sunsh_2
Upper East	MIR	0.53744	-0.38402	-0.04811	0.45742	0.50068	-0.37052
	Residuals	0.72169	-0.60760	0.18392	0.65997	0.72592	-0.51783
Upper West	MIR	0.29138	-0.09228	0.24457	0.21429	0.21306	-0.19693
	Residuals	0.35739	-0.12515	0.27707	0.27774	0.29948	-0.25873
Northern	MIR	0.47521	-0.40645	0.29857	0.43278	0.50472	0.17633
	Residuals	0.59212	-0.51968	0.33339	0.51677	0.59381	-0.31318
Brong Ahafo	MIR	0.37469	-0.11514	0.14384	0.28093	0.41422	-0.13506
	Residuals	0.43709	-0.22111	0.25217	0.36846	0.42481	-0.26149
Ashanti	MIR	0.18445	0.02363	-0.08875	0.06045	0.14455	-0.05811
	Residuals	0.25874	-0.02452	0.22096	0.17927	0.20395	-0.03030
Eastern	MIR	0.31975	-0.11544	0.37804	-0.0231	0.19072	-0.13930
	Residuals	0.43019	-0.05569	0.29036	0.15202	0.26777	-0.14243
Western	MIR	0.15307	0.03115	0.16391	0.21639	0.09062	-0.01624
	Residuals	0.20836	0.13664	0.28728	0.16035	0.04245	0.10670
Central	MIR	0.10750	0.20827	0.47974	0.03157	0.00484	0.26401
	Residuals	0.13161	0.35002	0.53079	-0.0089	-0.0963	0.32934
Greater Accra	MIR	0.39398	-0.04220	0.12143	0.06939	0.21317	0.03100
	Residuals	0.40534	-0.04147	-0.04156	0.14277	0.20577	0.05422
Volta	MIR	0.22840	-0.11081	0.29524	0.09731	0.32077	-0.14384
	Residuals	0.41683	-0.14165	0.34479	0.18149	0.32018	-0.17789

Table A-5.4 Cross-correlation results of malaria incidence rates for 0-4 year group and their detrended (residuals) with climatic covariates at same month of incidence.

Region	Data (0-4)	Rainfall	MaxT	MinT	RH0600	RH1500	Sunshine
Upper East	MIR	0.44853	-0.57040	-0.35826	0.53177	0.53625	-0.35787
	Residuals	0.48942	-0.68752	-0.26809	0.60782	0.61674	-0.41648
Upper West	MIR	0.44248	-0.50628	-0.08284	0.52973	0.53802	-0.37002
	Residuals	0.51795	-0.64743	-0.14107	0.64859	0.67758	-0.46419
Northern	MIR	0.49203	-0.65342	-0.15825	0.56514	0.59426	0.04485
	Residuals	0.51733	-0.70702	-0.22318	0.58344	0.59550	-0.25563
Brong Ahafo	MIR	0.22586	-0.34475	-0.10461	0.34493	0.52909	-0.11305
	Residuals	0.22407	-0.44395	-0.02470	0.39123	0.49593	-0.15184
Ashanti	MIR	0.18244	-0.15050	-0.15556	0.09606	0.26158	-0.19386
	Residuals	0.31245	-0.37249	-0.04866	0.18681	0.40668	-0.31949
Eastern	MIR	0.28202	-0.41649	-0.00500	0.20552	0.41118	-0.26115
	Residuals	0.31179	-0.49940	-0.21685	0.34313	0.51118	-0.32242
Western	MIR	0.15246	-0.08379	0.05382	0.25694	0.15420	-0.06976
	Residuals	0.24389	-0.20443	0.01882	0.24107	0.23527	-0.14161
Central	MIR	0.20810	-0.11843	0.24373	0.13012	0.23591	-0.01763
	Residuals	0.36230	-0.23500	0.14130	0.12880	0.31148	-0.24004
Greater Accra	MIR	0.10116	-0.23175	-0.12674	-0.0078	0.18473	-0.16534
	Residuals	0.07489	-0.27326	-0.24433	0.06614	0.18837	-0.17850
Volta	MIR	0.14527	-0.25426	-0.01523	0.21132	0.35776	-0.08600
	Residuals	0.33423	-0.43242	-0.19647	0.32049	0.42699	-0.17210

Table A-5.5: Cross-correlation results of malaria incidence rates for 0-4 year group and their residuals with climatic covariates at same month of incidence at previous month of incidence (lag 1).

Region	Data (0-4)	Rainfall_1	MaxTemp_1	MinTemp_1	RH06_1	Rh15_1	Sunsh_1
Upper East	MIR	0.64298	-0.65607	-0.19395	0.62833	0.67833	-0.48869
	Residuals	0.70797	-0.78181	-0.08187	0.71278	0.77732	-0.55706
Upper West	MIR	0.54980	-0.45458	0.11903	0.52971	0.55615	-0.45486
	Residuals	0.63745	-0.57207	0.00932	0.62889	0.68318	-0.55459
Northern	MIR	0.67370	-0.71520	0.10190	0.65140	0.73620	-0.07270
	Residuals	0.71216	-0.76944	0.06404	0.67600	0.75344	-0.37972
Brong Ahafo	MIR	0.56859	-0.29668	0.04198	0.44211	0.61177	-0.16370
	Residuals	0.61522	-0.38489	0.13972	0.50234	0.59318	-0.20817
Ashanti	MIR	0.23557	-0.08441	-0.09651	0.11827	0.23179	-0.14389
	Residuals	0.37145	-0.23864	0.07382	0.22454	0.34642	-0.19768
Eastern	MIR	0.45085	-0.32846	0.11820	0.17518	0.41430	-0.25700
	Residuals	0.51628	-0.37277	-0.05498	0.31131	0.50630	-0.30144
Western	MIR	0.21232	-0.03190	0.13496	0.27611	0.15196	-0.03410
	Residuals	0.41678	-0.01182	0.25837	0.29382	0.20252	0.01660
Central	MIR	0.22015	0.07147	0.38985	0.10159	0.11443	0.15602
	Residuals	0.34830	0.08700	0.36450	0.08610	0.10128	0.10170
Greater Accra	MIR	0.29865	-0.17830	-0.06057	0.10991	0.24573	-0.08446
	Residuals	0.31234	-0.21064	-0.16161	0.20447	0.26321	-0.08434
Volta	MIR	0.26552	-0.23710	0.11709	0.20734	0.39508	-0.13720
	Residuals	0.48688	0.37613	0.00667	0.33264	0.45897	0.20800

Table A-5.6: Cross-correlation results of malaria incidence rates for 0-4 year group and their residuals with climatic covariates at same month of incidence at previous two months of incidence (lag 2).

Region	Data (0-4)	Rainfall_2	MaxTemp_2	MinTemp_2	RH06_2	RH15_2	Sunsh_2
Upper East	MIR	0.66777	-0.49934	0.06737	0.60717	0.64855	-0.45451
	Residuals	0.71951	-0.58724	0.21336	0.68192	0.72932	-0.49981
Upper West	MIR	0.48477	-0.23561	0.33513	0.40324	0.41644	-0.39142
	Residuals	0.53784	-0.28147	0.35058	0.46452	0.49256	-0.45392
Northern	MIR	0.64399	-0.55308	0.40834	0.57502	0.67599	-0.11822
	Residuals	0.66793	-0.58211	0.40537	0.59043	0.68442	-0.42219
Brong Ahafo	MIR	0.44221	-0.17128	0.15220	0.33979	0.47901	-0.26040
	Residuals	0.45870	-0.23963	0.26888	0.38012	0.44126	-0.31848
Ashanti	MIR	0.14887	0.04687	-0.05474	0.02417	0.11927	-0.06347
	Residuals	0.19849	0.00048	0.18150	0.06698	0.14966	-0.03130
Eastern	MIR	0.39753	-0.17152	0.33407	0.11051	0.29287	-0.22425
	Residuals	0.43350	-0.15642	0.22568	0.23538	0.34034	-0.23261
Western	MIR	0.13840	0.02116	0.16905	0.20950	0.09899	-0.02930
	Residuals	0.16703	0.11277	0.32506	0.13922	0.04512	0.07098
Central	MIR	0.09453	0.22647	0.45432	0.00188	-0.0256	0.26699
	Residuals	0.12253	0.34720	0.46750	-0.0484	-0.1224	0.31274
Greater Accra	MIR	0.25857	-0.09469	0.01309	0.05685	0.18023	0.00493
	Residuals	0.26370	-0.11141	-0.06972	0.13818	0.18615	0.01913
Volta	MIR	0.23232	-0.17792	0.23660	0.15493	0.34737	-0.21780
	Residuals	0.40107	-0.25627	0.20837	0.25963	0.36709	-0.28848

Results A-5.1: The following are the cross-correlation analysis results of malaria incidence rates with climatic covariates in the ten regions

```

-----
Upper East Region
  mir    mir    mir05  resid  resid05  rainf  rainf_1  maxT  maxT_1
mir      1.0000  0.8991  0.61543  0.55930  0.3682  0.52178 -0.41448 -0.4898
mir05    0.8991  1.0000  0.76000  0.83685  0.4429  0.64700 -0.57248 -0.6521
resid    0.6154  0.7600  1.00000  0.90891  0.5138  0.72448 -0.68185 -0.7968
resid05  0.5593  0.8369  0.90891  1.00000  0.4864  0.71044 -0.68825 -0.7798
rainf    0.3682  0.4429  0.51385  0.48643  1.0000  0.73114 -0.75029 -0.4424
rainf_1  0.5218  0.6470  0.72448  0.71044  0.7311  1.00000 -0.77941 -0.7498
maxT     -0.4145 -0.5725 -0.68185 -0.68825 -0.7503 -0.77941 1.00000 0.7441
maxT_1   -0.4898 -0.6521 -0.79677 -0.77976 -0.4424 -0.74976 0.74414 1.0000
minT     -0.3440 -0.3669 -0.23387 -0.27268 0.2212 -0.05424 0.31593 0.4360
minT_1   -0.2170 -0.1847 -0.06929 -0.07636 0.4411 0.21333 -0.05876 0.3223
rh0600   0.4019  0.5271  0.60469  0.60565  0.8215  0.84952 -0.71509 -0.5103
rh0600_1 0.4790  0.6323  0.69842  0.71515  0.5821  0.82201 -0.76642 -0.7138
rh1500   0.4106  0.5321  0.62459  0.61471  0.9125  0.85278 -0.81921 -0.5576
rh1500_1 0.5286  0.6812  0.78934  0.77900  0.6784  0.91325 -0.79962 -0.8177
sunsh    -0.2890 -0.3599 -0.44394 -0.41729 -0.7439 -0.55169 0.60171 0.4089
sunsh_1  -0.3943 -0.4848 -0.59193 -0.55503 -0.6086 -0.73874 0.51752 0.6023
  mir    minT  minT_1  rh0600  rh0600_1  rh1500  rh1500_1  sunsh  sunsh_1
mir      -0.34404 -0.21698 0.4019 0.4790 0.4106 0.5286 -0.2890 -0.3943
mir05    -0.36694 -0.18466 0.5271 0.6323 0.5321 0.6812 -0.3599 -0.4848
resid    -0.23387 -0.06929 0.6047 0.6984 0.6246 0.7893 -0.4439 -0.5919
resid05  -0.27268 -0.07636 0.6056 0.7151 0.6147 0.7790 -0.4173 -0.5550
rainf    0.22115 0.44112 0.8215 0.5821 0.9125 0.6784 -0.7439 -0.6086
rainf_1  -0.05424 0.21333 0.8495 0.8220 0.8528 0.9132 -0.5517 -0.7387
maxT     0.31593 -0.05876 -0.7151 -0.7664 -0.8192 -0.7996 0.6017 0.5175
maxT_1   0.43602 0.32228 -0.5103 -0.7138 -0.5576 -0.8177 0.4089 0.6023
minT     1.00000 0.72090 0.1986 -0.3023 0.1817 -0.1742 -0.2401 -0.1752
minT_1   0.72090 1.00000 0.5619 0.1936 0.4655 0.1786 -0.2166 -0.2300
rh0600   0.19865 0.56191 1.0000 0.8206 0.9465 0.8693 -0.5473 -0.6931
rh0600_1 -0.30227 0.19356 0.8206 1.0000 0.7379 0.9468 -0.3025 -0.5423
rh1500   0.18169 0.46547 0.9465 0.7379 1.0000 0.8295 -0.7099 -0.6993
rh1500_1 -0.17419 0.17861 0.8693 0.9468 0.8295 1.0000 -0.4651 -0.7063
sunsh    -0.24014 -0.21662 -0.5473 -0.3025 -0.7099 -0.4651 1.0000 0.5577
sunsh_1  -0.17518 -0.23004 -0.6931 -0.5423 -0.6993 -0.7063 0.5577 1.0000
>
Upper West Region
  mir    mir    mir05  resid  resid05  rainf  rainf_1  maxT  maxT_1
mir      1.000000  0.90363  0.62221  0.54094  0.2867  0.3374 -0.293043 -0.2387
mir05    0.903629  1.00000  0.69532  0.78182  0.4374  0.5498 -0.510756 -0.4546
resid    0.622214  0.69532  1.00000  0.88392  0.4010  0.4516 -0.470695 -0.3750
resid05  0.540937  0.78182  0.88392  1.00000  0.5146  0.6374 -0.649927 -0.5721
rainf    0.286661  0.43741  0.40103  0.51458  1.0000  0.6679 -0.784018 -0.4656
rainf_1  0.337393  0.54980  0.45157  0.63745  0.6679  1.0000 -0.786582 -0.7820
maxT     -0.293043 -0.51076 -0.47069 -0.64993 -0.7840 -0.7866 1.000000 0.7449
maxT_1   -0.238747 -0.45458 -0.37504 -0.57207 -0.4656 -0.7820 0.744949 1.0000
minT     -0.002332 -0.09299 -0.05729 -0.14810 0.1099 -0.1125 0.347326 0.4420
minT_1   0.118959 0.11903 0.09673 0.09321 0.3543 0.1038 -0.009497 0.3561
rh0600   0.321737 0.52545 0.48831 0.64603 0.7670 0.7922 -0.702324 -0.5208
rh0600_1 0.308108 0.52971 0.43166 0.62889 0.5638 0.7666 -0.760657 -0.7004
rh1500   0.322500 0.53415 0.52244 0.67537 0.8823 0.8361 -0.833141 -0.5932
rh1500_1 0.315128 0.55615 0.47889 0.68318 0.6417 0.8821 -0.804824 -0.8313
sunsh    -0.238175 -0.37030 -0.37265 -0.46405 -0.8071 -0.5971 0.685635 0.4757
sunsh_1  -0.254846 -0.45486 -0.37607 -0.55459 -0.6280 -0.8049 0.613988 0.6853
  mir    minT  minT_1  rh0600  rh0600_1  rh1500  rh1500_1  sunsh  sunsh_1
mir      -0.002332 0.118959 0.3217 0.3081 0.3225 0.3151 -0.2382 -0.25485
mir05    -0.092994 0.119034 0.5254 0.5297 0.5342 0.5561 -0.3703 -0.45486
resid    -0.057293 0.096728 0.4883 0.4317 0.5224 0.4789 -0.3726 -0.37607
resid05  -0.148097 0.093207 0.6460 0.6289 0.6754 0.6832 -0.4641 -0.55459
rainf    0.109905 0.354301 0.7670 0.5638 0.8823 0.6417 -0.8071 -0.62800
rainf_1  -0.112504 0.103830 0.7922 0.7666 0.8361 0.8821 -0.5971 -0.80491
maxT     0.347326 -0.009497 -0.7023 -0.7607 -0.8331 -0.8048 0.6856 0.61399
maxT_1   0.441989 0.356093 -0.5208 -0.7004 -0.5932 -0.8313 0.4757 0.68527
minT     1.000000 0.700880 0.1657 -0.3599 0.1204 -0.2469 -0.1938 -0.08275
minT_1   0.700880 1.000000 0.5233 0.1580 0.4047 0.1137 -0.2012 -0.18404
rh0600   0.165684 0.523345 1.0000 0.8134 0.9437 0.8582 -0.6000 -0.73798
rh0600_1 -0.359881 0.157960 0.8134 1.0000 0.7405 0.9436 -0.3428 -0.59592
rh1500   0.120421 0.404686 0.9437 0.7405 1.0000 0.8304 -0.7609 -0.76020
rh1500_1 -0.246900 0.113700 0.8582 0.9436 0.8304 1.0000 -0.5058 -0.75831
sunsh    -0.193773 -0.201216 -0.6000 -0.3428 -0.7609 -0.5058 1.0000 0.61267
sunsh_1  -0.082755 -0.184038 -0.7380 -0.5959 -0.7602 -0.7583 0.6127 1.00000
>

```

Northern Region

	mir	mir05	resid	resid05	rainf	rainf_1	maxT	maxT_1
mir	1.00000	0.9122	0.67685	0.63942	0.3554	0.485698	-0.4818	-0.5272
mir05	0.91219	1.0000	0.84036	0.87981	0.4882	0.673669	-0.6526	-0.7152
resid	0.67685	0.8404	1.00000	0.95207	0.4592	0.623851	-0.6513	-0.7028
resid05	0.63942	0.8798	0.95207	1.00000	0.5165	0.712161	-0.7066	-0.7694
rainf	0.35543	0.4882	0.45922	0.51646	1.0000	0.640992	-0.8298	-0.5763
rainf_1	0.48570	0.6737	0.62385	0.71216	0.6410	1.000000	-0.7682	-0.8303
maxT	-0.48179	-0.6526	-0.65133	-0.70658	-0.8298	-0.768195	1.0000	0.8016
maxT_1	-0.52721	-0.7152	-0.70276	-0.76944	-0.5763	-0.830342	0.8016	1.0000
minT	-0.09381	-0.1628	-0.21754	-0.22471	0.2366	0.009615	0.1262	0.3309
minT_1	0.08041	0.1019	0.01941	0.06404	0.3936	0.230986	-0.2581	0.1299
rh0600	0.42121	0.5626	0.51095	0.58274	0.7067	0.755332	-0.7131	-0.5916
rh0600_1	0.48248	0.6514	0.58662	0.67600	0.4570	0.709278	-0.7334	-0.7137
rh1500	0.45214	0.5908	0.52894	0.59503	0.8682	0.768513	-0.8697	-0.6405
rh1500_1	0.55299	0.7362	0.66410	0.75344	0.6652	0.873599	-0.8502	-0.8709
sunsh	0.26945	0.0415	-0.20486	-0.25719	-0.5355	-0.325020	0.5157	0.3739
sunsh_1	0.20777	-0.0727	-0.28291	-0.37972	-0.5027	-0.524380	0.4754	0.5128
	minT	minT_1	rh0600	rh0600_1	rh1500	rh1500_1	sunsh	sunsh_1
mir	-0.093807	0.08041	0.4212	0.4825	0.4521	0.55299	0.26945	0.20777
mir05	-0.162804	0.10195	0.5626	0.6514	0.5908	0.73621	0.04150	-0.07270
resid	-0.217543	0.01941	0.5109	0.5866	0.5289	0.66410	-0.20486	-0.28291
resid05	-0.224714	0.06404	0.5827	0.6760	0.5950	0.75344	-0.25719	-0.37972
rainf	0.236590	0.39364	0.7067	0.4570	0.8682	0.66523	-0.53553	-0.50268
rainf_1	0.009615	0.23099	0.7553	0.7093	0.7685	0.87360	-0.32502	-0.52438
maxT	0.126242	-0.25809	-0.7131	-0.7334	-0.8697	-0.85017	0.51572	0.47544
maxT_1	0.330889	0.12990	-0.5916	-0.7137	-0.6405	-0.87091	0.37393	0.51275
minT	1.000000	0.61857	0.3119	-0.2849	0.2941	-0.07511	-0.07123	-0.02315
minT_1	0.618571	1.00000	0.5761	0.3124	0.5222	0.29761	-0.09656	-0.05423
rh0600	0.311892	0.57611	1.0000	0.7079	0.8710	0.82294	-0.30165	-0.39500
rh0600_1	-0.284907	0.31240	0.7079	1.0000	0.6196	0.87191	-0.18353	-0.29852
rh1500	0.294085	0.52222	0.8710	0.6196	1.0000	0.83051	-0.44332	-0.42419
rh1500_1	-0.075113	0.29761	0.8229	0.8719	0.8305	1.00000	-0.32474	-0.44536
sunsh	-0.071230	-0.09656	-0.3016	-0.1835	-0.4433	-0.32474	1.00000	0.77517
sunsh_1	-0.023154	-0.05423	-0.3950	-0.2985	-0.4242	-0.44536	0.77517	1.00000

>

Brong Ahafo Region

	mir	mir05	resid	resid05	rainf	rainf_1	maxT	maxT_1
mir	1.00000	0.86846	0.71508	0.61201	0.1471	0.45313	-0.24952	-0.2138
mir05	0.86846	1.00000	0.73478	0.85499	0.2211	0.56859	-0.34260	-0.2967
resid	0.71508	0.73478	1.00000	0.85816	0.1536	0.55671	-0.42195	-0.3595
resid05	0.61201	0.85499	0.85816	1.00000	0.2257	0.61522	-0.44480	-0.3849
rainf	0.14713	0.22108	0.15356	0.22573	1.0000	0.44571	-0.44083	-0.2133
rainf_1	0.45313	0.56859	0.55671	0.61522	0.4457	1.00000	-0.57747	-0.4433
maxT	-0.24952	-0.34260	-0.42195	-0.44480	-0.4408	-0.57747	1.00000	0.8204
maxT_1	-0.21375	-0.29668	-0.35952	-0.38489	-0.2133	-0.44333	0.82041	1.0000
minT	-0.12009	-0.11874	-0.07154	-0.02453	0.1041	-0.08808	0.42689	0.5389
minT_1	0.03172	0.04198	0.09767	0.13972	0.2250	0.11444	0.04966	0.4116
rh0600	0.21824	0.34234	0.33437	0.40838	0.6058	0.59633	-0.61876	-0.4029
rh0600_1	0.32966	0.44211	0.44066	0.50234	0.3396	0.60950	-0.72800	-0.6083
rh1500	0.39546	0.52863	0.42225	0.50669	0.6562	0.66620	-0.75767	-0.5038
rh1500_1	0.48800	0.61177	0.52513	0.59318	0.3682	0.66666	-0.80729	-0.7533
sunsh	-0.04400	-0.10978	-0.15080	-0.15232	-0.3168	-0.23462	0.78083	0.6383
sunsh_1	-0.05323	-0.16370	-0.15010	-0.20817	-0.4132	-0.31959	0.65907	0.7814
	minT	minT_1	rh0600	rh0600_1	rh1500	rh1500_1	sunsh	sunsh_1
mir	-0.12009	0.03172	0.21824	0.3297	0.39546	0.48800	-0.0440	-0.05323
mir05	-0.11874	0.04198	0.34234	0.4421	0.52863	0.61177	-0.1098	-0.16370
resid	-0.07154	0.09767	0.33437	0.4407	0.42225	0.52513	-0.1508	-0.15010
resid05	-0.02453	0.13972	0.40838	0.5023	0.50669	0.59318	-0.1523	-0.20817
rainf	0.10409	0.22498	0.60578	0.3396	0.65621	0.36824	-0.3168	-0.41322
rainf_1	-0.08808	0.11444	0.59633	0.6095	0.66620	0.66666	-0.2346	-0.31959
maxT	0.42689	0.04966	-0.61876	-0.7280	-0.75767	-0.80729	0.7808	0.65907
maxT_1	0.53889	0.41161	-0.40293	-0.6083	-0.50385	-0.75333	0.6383	0.78138
minT	1.00000	0.50686	0.09753	-0.4222	-0.07984	-0.43211	0.3207	0.33176
minT_1	0.50686	1.00000	0.18269	0.1448	0.14221	-0.03627	0.2045	0.30633
rh0600	0.09753	0.18269	1.00000	0.5700	0.86251	0.60822	-0.4306	-0.45171
rh0600_1	-0.42223	0.14481	0.56995	1.0000	0.65312	0.86808	-0.3532	-0.42934
rh1500	-0.07984	0.14221	0.86251	0.6531	1.00000	0.77896	-0.5871	-0.55841
rh1500_1	-0.43211	-0.03627	0.60822	0.8681	0.77896	1.00000	-0.4932	-0.58759
sunsh	0.32065	0.20451	-0.43056	-0.3532	-0.58708	-0.49318	1.0000	0.68045
sunsh_1	0.33176	0.30633	-0.45171	-0.4293	-0.55841	-0.58759	0.6805	1.00000

>

Ashanti Region

	mir	mir05	resid	resid05	rainf	rainf_1	maxT	maxT_1
mir	1.0000	0.8833	0.5260	0.3783	0.1401	0.2346	-0.1831	-0.1240
mir05	0.8833	1.0000	0.4025	0.5502	0.1770	0.2356	-0.1474	-0.0844

resid	0.5260	0.4025	1.0000	0.7292	0.2376	0.3690	-0.4415	-0.3066
resid05	0.3783	0.5502	0.7292	1.0000	0.3092	0.3715	-0.3708	-0.2386
rainf	0.1401	0.1770	0.2376	0.3092	1.0000	0.3818	-0.3536	-0.1140
rainf_1	0.2346	0.2356	0.3690	0.3715	0.3818	1.0000	-0.4978	-0.3534
maxT	-0.1831	-0.1474	-0.4415	-0.3708	-0.3536	-0.4978	1.0000	0.7959
maxT_1	-0.1240	-0.0844	-0.3066	-0.2386	-0.1140	-0.3534	0.7959	1.0000
minT	-0.2231	-0.1504	-0.0792	-0.0444	0.0781	-0.0153	0.2921	0.3687
minT_1	-0.1384	-0.0965	0.1045	0.0738	0.0869	0.0730	0.0377	0.2941
rh0600	0.0769	0.0938	0.2116	0.1853	0.4474	0.4523	-0.4600	-0.2819
rh0600_1	0.1229	0.1183	0.2890	0.2245	0.1881	0.4497	-0.5579	-0.4608
rh1500	0.2447	0.2569	0.4100	0.4041	0.5907	0.6350	-0.8162	-0.5398
rh1500_1	0.2470	0.2318	0.3937	0.3464	0.2829	0.5956	-0.8556	-0.8168
sunsh	-0.2243	-0.1913	-0.3967	-0.3179	-0.2547	-0.1887	0.8249	0.6626
sunsh_1	-0.1581	-0.1439	-0.2372	-0.1977	-0.3169	-0.2502	0.6617	0.8253
	minT	minT_1	rh0600	rh0600_1	rh1500	rh1500_1	sunsh	sunsh_1
mir	-0.2231	-0.13836	0.07687	0.123	0.2447	0.2470	-0.224	-0.158
mir05	-0.1504	-0.09651	0.09377	0.118	0.2569	0.2318	-0.191	-0.144
resid	-0.0792	0.10452	0.21162	0.289	0.4100	0.3937	-0.397	-0.237
resid05	-0.0444	0.07382	0.18529	0.225	0.4041	0.3464	-0.318	-0.198
rainf	0.0781	0.08692	0.44743	0.188	0.5907	0.2829	-0.255	-0.317
rainf_1	-0.0153	0.07300	0.45228	0.450	0.6350	0.5956	-0.189	-0.250
maxT	0.2921	0.03769	-0.46002	-0.558	-0.8162	-0.8556	0.825	0.662
maxT_1	0.3687	0.29413	-0.28189	-0.461	-0.5398	-0.8168	0.663	0.825
minT	1.0000	0.46196	0.37239	-0.206	0.0268	-0.2640	0.313	0.268
minT_1	0.4620	1.00000	0.00137	0.369	0.1223	0.0204	0.165	0.314
rh0600	0.3724	0.00137	1.00000	0.317	0.6628	0.3962	-0.243	-0.273
rh0600_1	-0.2060	0.36859	0.31690	1.000	0.5108	0.6629	-0.229	-0.244
rh1500	0.0268	0.12227	0.66275	0.511	1.0000	0.7811	-0.614	-0.507
rh1500_1	-0.2640	0.02043	0.39617	0.663	0.7811	1.0000	-0.592	-0.616
sunsh	0.3125	0.16534	-0.24256	-0.229	-0.6137	-0.5915	1.000	0.681
sunsh_1	0.2684	0.31433	-0.27316	-0.244	-0.5070	-0.6160	0.681	1.000

Greater Accra Region

	mir	mir05	resid	resid05	rainf	rainf_1	maxT	maxT_1	minT
mir	1.0000	0.92874	0.8712	0.7979	0.1540	0.4289	-0.400	-0.257	-0.2577
mir05	0.9287	1.00000	0.7787	0.8486	0.0950	0.2987	-0.229	-0.178	-0.1274
resid	0.8712	0.77869	1.0000	0.9160	0.1401	0.4484	-0.463	-0.291	-0.4043
resid05	0.7979	0.84864	0.9160	1.0000	0.0794	0.3123	-0.276	-0.211	-0.2445
rainf	0.1540	0.09503	0.1401	0.0794	1.0000	0.2898	-0.172	0.165	-0.0629
rainf_1	0.4289	0.29865	0.4484	0.3123	0.2898	1.0000	-0.432	-0.172	-0.2768
maxT	-0.4001	-0.22891	-0.4629	-0.2763	-0.1715	-0.4320	1.000	0.783	0.8610
maxT_1	-0.2574	-0.17830	-0.2910	-0.2106	0.1654	-0.1723	0.783	1.000	0.7859
minT	-0.2577	-0.12744	-0.4043	-0.2445	-0.0629	-0.2768	0.861	0.786	1.0000
minT_1	-0.0789	-0.06057	-0.1929	-0.1616	0.2992	-0.0589	0.591	0.860	0.6739
rh0600	0.0253	-0.00371	0.0892	0.0638	0.2873	0.2878	-0.426	-0.338	-0.2074
rh0600_1	0.1545	0.10991	0.2428	0.2045	0.0311	0.2813	-0.359	-0.422	-0.4712
rh1500	0.2788	0.18200	0.2874	0.1910	0.3737	0.4521	-0.730	-0.481	-0.4125
rh1500_1	0.3371	0.24573	0.3505	0.2632	0.0785	0.3748	-0.699	-0.730	-0.6805
sunsh	-0.3387	-0.16825	-0.3734	-0.1774	-0.1106	-0.1679	0.598	0.265	0.4694
sunsh_1	-0.1685	-0.08446	-0.1777	-0.0843	0.1125	-0.1037	0.512	0.595	0.4057
	minT	rh0600	rh0600_1	rh1500	rh1500_1	sunsh	sunsh_1		
mir	-0.0789	0.02527	0.1545	0.279	0.3371	-0.3387	-0.1685		
mir05	-0.0606	-0.00371	0.1099	0.182	0.2457	-0.1682	-0.0845		
resid	-0.1929	0.08924	0.2428	0.287	0.3505	-0.3734	-0.1777		
resid05	-0.1616	0.06378	0.2045	0.191	0.2632	-0.1774	-0.0843		
rainf	0.2992	0.28729	0.0311	0.374	0.0785	-0.1106	0.1125		
rainf_1	-0.0589	0.28784	0.2813	0.452	0.3748	-0.1679	-0.1037		
maxT	0.5906	-0.42627	-0.3594	-0.730	-0.6990	0.5981	0.5121		
maxT_1	0.8597	-0.33798	-0.4223	-0.481	-0.7303	0.2654	0.5945		
minT	0.6739	-0.20737	-0.4712	-0.413	-0.6805	0.4694	0.4057		
minT_1	1.0000	-0.31007	-0.2055	-0.299	-0.4115	0.1306	0.4644		
rh0600	-0.3101	1.00000	0.1204	0.819	0.3171	0.1351	-0.0968		
rh0600_1	-0.2055	0.12044	1.0000	0.172	0.8157	-0.0381	0.1382		
rh1500	-0.2990	0.81942	0.1718	1.000	0.5162	-0.2497	-0.3398		
rh1500_1	-0.4115	0.31709	0.8157	0.516	1.0000	-0.2060	-0.2471		
sunsh	0.1306	0.13511	-0.0381	-0.250	-0.2060	1.0000	0.3659		
sunsh_1	0.4644	-0.09680	0.1382	-0.340	-0.2471	0.3659	1.0000		

Western Region

	mir	mir05	resid	resid05	rainf	rainf_1	maxT	maxT_1
mir	1.0000	0.9747	0.3239	0.2477	0.1477	0.224	-0.0971	-0.0420
mir05	0.9747	1.0000	0.2434	0.3090	0.1448	0.220	-0.0810	-0.0353
resid	0.3239	0.2434	1.0000	0.7800	0.2438	0.421	-0.2493	-0.0398
resid05	0.2477	0.3090	0.7800	1.0000	0.2392	0.422	-0.2028	-0.0150
rainf	0.1477	0.1448	0.2438	0.2392	1.0000	0.507	-0.1530	0.2054
rainf_1	0.2239	0.2201	0.4213	0.4219	0.5066	1.000	-0.5204	-0.1528
maxT	-0.0971	-0.0810	-0.2493	-0.2028	-0.1530	-0.520	1.0000	0.7980

maxT_1	-0.0420	-0.0353	-0.0398	-0.0150	0.2054	-0.153	0.7980	1.0000
minT	0.0182	0.0431	-0.1089	-0.0268	0.1996	-0.183	0.5273	0.4916
minT_1	0.1232	0.1457	0.1773	0.2665	0.4395	0.207	0.1984	0.5213
rh0600	0.2474	0.2613	0.1972	0.2438	0.3752	0.404	-0.5019	-0.3722
rh0600_1	0.2729	0.2710	0.2918	0.2894	0.1795	0.373	-0.5463	-0.5030
rh1500	0.1445	0.1524	0.2258	0.2341	0.4300	0.597	-0.8427	-0.5666
rh1500_1	0.1459	0.1539	0.1974	0.2041	0.1180	0.429	-0.8652	-0.8426
sunsh	-0.0944	-0.0655	-0.2208	-0.1389	-0.1718	-0.401	0.8406	0.5599
sunsh_1	-0.0480	-0.0391	-0.0152	0.0118	0.0797	-0.172	0.7119	0.8404
	minT	minT_1	rh0600	rh0600_1	rh1500	rh1500_1	sunsh	sunsh_1
mir	0.0182	0.1232	0.2474	0.2729	0.1445	0.146	-0.0944	-0.0480
mir05	0.0431	0.1457	0.2613	0.2710	0.1524	0.154	-0.0655	-0.0391
resid	-0.1089	0.1773	0.1972	0.2918	0.2258	0.197	-0.2208	-0.0152
resid05	-0.0268	0.2665	0.2438	0.2894	0.2341	0.204	-0.1389	0.0118
rainf	0.1996	0.4395	0.3752	0.1795	0.4300	0.118	-0.1718	0.0797
rainf_1	-0.1830	0.2073	0.4037	0.3732	0.5972	0.429	-0.4008	-0.1716
maxT	0.5273	0.1984	-0.5019	-0.5463	-0.8427	-0.865	0.8406	0.7119
maxT_1	0.4916	0.5213	-0.3722	-0.5030	-0.5666	-0.843	0.5599	0.8404
minT	1.0000	0.2793	0.0882	-0.4713	-0.1445	-0.521	0.4121	0.2643
minT_1	0.2793	1.0000	0.1007	0.0847	0.0224	-0.141	0.2040	0.4059
rh0600	0.0882	0.1007	1.0000	0.3941	0.7203	0.553	-0.2496	-0.2952
rh0600_1	-0.4713	0.0847	0.3941	1.0000	0.4231	0.721	-0.3563	-0.2514
rh1500	-0.1445	0.0224	0.7203	0.4231	1.0000	0.763	-0.6913	-0.5910
rh1500_1	-0.5210	-0.1410	0.5525	0.7211	0.7633	1.000	-0.5875	-0.6911
sunsh	0.4121	0.2040	-0.2496	-0.3563	-0.6913	-0.587	1.0000	0.5837
sunsh_1	0.2643	0.4059	-0.2952	-0.2514	-0.5910	-0.691	0.5837	1.0000

>

Eastern Region

	mir	mir05	resid	resid05	rainf	rainf_1	maxT	maxT_1
mir	1.0000	0.89997	0.53977	0.481	0.2134	0.3506	-0.319	-0.2396
mir05	0.9000	1.00000	0.69472	0.758	0.2733	0.4578	-0.414	-0.3321
resid	0.5398	0.69472	1.00000	0.911	0.2953	0.4992	-0.470	-0.2973
resid05	0.4814	0.75829	0.91062	1.000	0.3058	0.5207	-0.497	-0.3755
rainf	0.2134	0.27334	0.29531	0.306	1.0000	0.4242	-0.268	-0.0426
rainf_1	0.3506	0.45779	0.49919	0.521	0.4242	1.0000	-0.472	-0.2678
maxT	-0.3186	-0.41366	-0.47048	-0.497	-0.2677	-0.4718	1.000	0.7962
maxT_1	-0.2396	-0.33206	-0.29735	-0.376	-0.0426	-0.2678	0.796	1.0000
minT	0.1113	-0.00857	-0.20328	-0.220	0.1468	-0.0614	0.552	0.6387
minT_1	0.2238	0.12111	0.00393	-0.052	0.2806	0.1532	0.176	0.5483
rh0600	0.0395	0.20157	0.25597	0.341	0.4681	0.4503	-0.422	-0.2922
rh0600_1	0.0266	0.17945	0.22811	0.314	0.2065	0.4747	-0.527	-0.4253
rh1500	0.2820	0.40510	0.47599	0.508	0.5744	0.6192	-0.817	-0.5589
rh1500_1	0.2923	0.42056	0.45945	0.510	0.2324	0.5766	-0.841	-0.8164
sunsh	-0.1941	-0.25874	-0.31080	-0.321	-0.1499	-0.1002	0.786	0.6107
sunsh_1	-0.1597	-0.25954	-0.21620	-0.303	-0.2694	-0.1456	0.591	0.7860
	minT	minT_1	rh0600	rh0600_1	rh1500	rh1500_1	sunsh	sunsh_1
mir	0.11128	0.22383	0.0395	0.0266	0.2820	0.292	-0.194	-0.160
mir05	-0.00857	0.12111	0.2016	0.1794	0.4051	0.421	-0.259	-0.260
resid	-0.20328	0.00393	0.2560	0.2281	0.4760	0.459	-0.311	-0.216
resid05	-0.22034	-0.05196	0.3407	0.3140	0.5075	0.510	-0.321	-0.303
rainf	0.14680	0.28060	0.4681	0.2065	0.5744	0.232	-0.150	-0.269
rainf_1	-0.06139	0.15318	0.4503	0.4747	0.6192	0.577	-0.100	-0.146
maxT	0.55165	0.17580	-0.4220	-0.5271	-0.8167	-0.841	0.786	0.591
maxT_1	0.63871	0.54829	-0.2922	-0.4253	-0.5589	-0.816	0.611	0.786
minT	1.00000	0.59952	0.0791	-0.3801	-0.2293	-0.561	0.444	0.390
minT_1	0.59952	1.00000	-0.0917	0.0800	0.0496	-0.224	0.214	0.441
rh0600	0.07905	-0.09173	1.0000	0.3809	0.6989	0.445	-0.197	-0.319
rh0600_1	-0.38006	0.08004	0.3809	1.0000	0.5658	0.702	-0.199	-0.201
rh1500	-0.22928	0.04958	0.6989	0.5658	1.0000	0.780	-0.523	-0.517
rh1500_1	-0.56145	-0.22390	0.4454	0.7021	0.7798	1.000	-0.460	-0.522
sunsh	0.44358	0.21377	-0.1971	-0.1987	-0.5233	-0.460	1.000	0.620
sunsh_1	0.39028	0.44118	-0.3187	-0.2009	-0.5174	-0.522	0.620	1.000

Central Region

	mir	mir05	resid	resid05	rainf	rainf_1	maxT	maxT_1
mir	1.00000	0.93775	0.56795	0.4909	0.20393	0.2332	-0.1290	0.04402
mir05	0.93775	1.00000	0.54266	0.6224	0.19685	0.2215	-0.1136	0.07147
resid	0.56795	0.54266	1.00000	0.8706	0.37816	0.3744	-0.2764	0.05255
resid05	0.49091	0.62241	0.87056	1.0000	0.35341	0.3483	-0.2313	0.08700
rainf	0.20393	0.19685	0.37816	0.3534	1.00000	0.5448	-0.3482	-0.07644
rainf_1	0.23317	0.22150	0.37440	0.3483	0.54476	1.0000	-0.6124	-0.34613
maxT	-0.12897	-0.11362	-0.27636	-0.2313	-0.34824	-0.6124	1.0000	0.80640
maxT_1	0.04402	0.07147	0.05255	0.0870	-0.07644	-0.3461	0.8064	1.00000
minT	0.22204	0.23731	0.09946	0.1340	0.26172	-0.1567	0.5216	0.60851
minT_1	0.37522	0.38985	0.34972	0.3645	0.45974	0.2703	0.1172	0.51695
rh0600	0.11945	0.12472	0.12309	0.1234	0.49371	0.6038	-0.5274	-0.45482
rh0600_1	0.10921	0.10159	0.10107	0.0861	0.14562	0.5028	-0.5535	-0.53175

rh1500	0.23842	0.22962	0.33692	0.3060	0.62117	0.7134	-0.8682	-0.62508
rh1500_1	0.13675	0.11443	0.13518	0.1028	0.31481	0.6241	-0.8569	-0.86841
sunsh	-0.02895	-0.01833	-0.24134	-0.2022	-0.21926	-0.3296	0.8534	0.62155
sunsh_1	0.13927	0.15602	0.07852	0.1017	-0.14905	-0.2057	0.6765	0.85133
	minT	minT_1	rh0600	rh0600_1	rh1500	rh1500_1	sunsh	sunsh_1
mir	0.22204	0.37522	0.11945	0.10921	0.2384	0.1368	-0.02895	0.13927
mir05	0.23731	0.38985	0.12472	0.10159	0.2296	0.1144	-0.01833	0.15602
resid	0.09946	0.34972	0.12309	0.10107	0.3369	0.1352	-0.24134	0.07852
resid05	0.13402	0.36447	0.12342	0.08610	0.3060	0.1028	-0.20215	0.10166
rainf	0.26172	0.45974	0.49371	0.14562	0.6212	0.3148	-0.21926	-0.14905
rainf_1	-0.15666	0.27031	0.60380	0.50277	0.7134	0.6241	-0.32965	-0.20567
maxT	0.52157	0.11719	-0.52738	-0.55353	-0.8682	-0.8569	0.85340	0.67652
maxT_1	0.60851	0.51695	-0.45482	-0.53175	-0.6251	-0.8684	0.62155	0.85133
minT	1.00000	0.48348	0.08378	-0.55709	-0.1081	-0.5325	0.46371	0.36786
minT_1	0.48348	1.00000	0.10001	0.08822	0.1797	-0.1017	0.19925	0.46633
rh0600	0.08378	0.10001	1.00000	0.44660	0.7858	0.6219	-0.16158	-0.30478
rh0600_1	-0.55709	0.08822	0.44660	1.00000	0.4884	0.7884	-0.24939	-0.16414
rh1500	-0.10809	0.17970	0.78583	0.48845	1.0000	0.7939	-0.63400	-0.54925
rh1500_1	-0.53251	-0.10169	0.62188	0.78841	0.7939	1.0000	-0.54574	-0.63130
sunsh	0.46371	0.19925	-0.16158	-0.24939	-0.6340	-0.5457	1.00000	0.62896
sunsh_1	0.36786	0.46633	-0.30478	-0.16414	-0.5493	-0.6313	0.62896	1.00000

Volta Region

	mir	mir05	resid	resid05	rainf	rainf_1	maxT	maxT_1
mir	1.0000	0.9461	0.5172	0.43045	0.199	0.298	-0.31549	-0.235
mir05	0.9461	1.0000	0.4694	0.55990	0.138	0.266	-0.24938	-0.237
resid	0.5172	0.4694	1.0000	0.83672	0.473	0.581	-0.59009	-0.396
resid05	0.4305	0.5599	0.8367	1.00000	0.332	0.487	-0.43092	-0.376
rainf	0.1995	0.1377	0.4728	0.33208	1.000	0.427	-0.54245	-0.285
rainf_1	0.2984	0.2655	0.5805	0.48688	0.427	1.000	-0.64391	-0.545
maxT	-0.3155	-0.2494	-0.5901	-0.43092	-0.542	-0.644	1.00000	0.818
maxT_1	-0.2352	-0.2371	-0.3962	-0.37613	-0.285	-0.545	0.81835	1.000
minT	-0.0116	-0.0247	-0.1837	-0.20241	0.123	-0.144	0.44482	0.572
minT_1	0.1538	0.1171	0.0841	0.00667	0.341	0.125	0.00492	0.437
rh0600	0.2079	0.2104	0.3562	0.32000	0.464	0.541	-0.48596	-0.435
rh0600_1	0.1838	0.2073	0.3275	0.33264	0.162	0.477	-0.52206	-0.490
rh1500	0.4155	0.3496	0.5705	0.42748	0.705	0.716	-0.84756	-0.616
rh1500_1	0.4278	0.3951	0.5329	0.45897	0.409	0.710	-0.86963	-0.844
sunsh	-0.1628	-0.0877	-0.3343	-0.17292	-0.300	-0.178	0.73597	0.570
sunsh_1	-0.1282	-0.1372	-0.2133	-0.20800	-0.422	-0.281	0.59346	0.733
	minT	minT_1	rh0600	rh0600_1	rh1500	rh1500_1	sunsh	sunsh_1
mir	-0.0116	0.15384	0.208	0.1838	0.4155	0.42778	-0.1628	-0.1282
mir05	-0.0247	0.11709	0.210	0.2073	0.3496	0.39508	-0.0877	-0.1372
resid	-0.1837	0.08414	0.356	0.3275	0.5705	0.53287	-0.3343	-0.2133
resid05	-0.2024	0.00667	0.320	0.3326	0.4275	0.45897	-0.1729	-0.2080
rainf	0.1231	0.34115	0.464	0.1617	0.7052	0.40900	-0.2996	-0.4223
rainf_1	-0.1439	0.12533	0.541	0.4772	0.7162	0.70973	-0.1782	-0.2815
maxT	0.4448	0.00492	-0.486	-0.5221	-0.8476	-0.86963	0.7360	0.5935
maxT_1	0.5719	0.43720	-0.435	-0.4901	-0.6160	-0.84392	0.5697	0.7326
minT	1.0000	0.47420	0.240	-0.4336	-0.0205	-0.43518	0.3248	0.1731
minT_1	0.4742	1.00000	0.145	0.2448	0.2920	-0.00223	0.1654	0.3373
rh0600	0.2400	0.14472	1.000	0.2622	0.6808	0.54646	-0.0890	-0.3264
rh0600_1	-0.4336	0.24484	0.262	1.0000	0.4270	0.67646	-0.1121	-0.0965
rh1500	-0.0205	0.29196	0.681	0.4270	1.0000	0.81721	-0.4856	-0.5067
rh1500_1	-0.4352	-0.00223	0.546	0.6765	0.8172	1.00000	-0.4154	-0.4712
sunsh	0.3248	0.16536	-0.089	-0.1121	-0.4856	-0.41542	1.0000	0.6226
sunsh_1	0.1731	0.33726	-0.326	-0.0965	-0.5067	-0.47122	0.6226	1.0000

>

Results A-5.2: Stepwise regression analysis results of the detrended malaria incidence rates (residuals) with the climatic covariates to identify potential predictors for the total incidence data

=====

UPPER EAST REGION (TOTAL)

Coefficients:

	Estimate	Std. Error	t-value	Pr(> t)	
(Intercept)	456.366	105.293	4.33	2.9e-05	***
maxT_1	-13.809	2.609	-5.29	5.1e-07	***
rh1500_1	1.522	0.347	4.38	2.4e-05	***
sunsh	-6.133	4.150	-1.48	0.14	

Signif. codes: 0 '***' 0.001 '**' 0.01 '*' 0.05 '.' 0.1 ' ' 1

Residual standard error: 44.7 on 127 degrees of freedom

Multiple R-squared: 0.697, Adjusted R-squared: 0.69

F-statistic: 97.5 on 3 and 127 DF, **p-value:** <2e-16, **AIC**=1001

=====

UPPER WEST REGION (TOTAL)

Coefficients:

	Estimate	Std. Error	t-value	Pr(> t)	
(Intercept)	7.324	67.056	0.11	0.913	
rainf	-0.226	0.130	-1.73	0.086	.
minT_1	-5.166	3.027	-1.71	0.090	.
rh1500	3.062	0.601	5.09	1.2e-06	***

Signif. codes: 0 '***' 0.001 '**' 0.01 '*' 0.05 '.' 0.1 ' ' 1

Residual standard error: 61.5 on 127 degrees of freedom

Multiple R-squared: 0.305, Adjusted R-squared: 0.289

F-statistic: 18.6 on 3 and 127 DF, **p-value:** 4.66e-10, **AIC**=1083

=====

NORTHERN REGION (TOTAL)

Coefficients:

	Estimate	Std. Error	t-value	Pr(> t)	
(Intercept)	391.96	32.91	11.91	< 2e-16	***
maxT	-7.53	2.45	-3.07	0.0026	**
maxT_1	-10.87	2.26	-4.80	4.4e-06	***
sunsh	3.95	1.84	2.14	0.0340	*

Signif. codes: 0 '***' 0.001 '**' 0.01 '*' 0.05 '.' 0.1 ' ' 1

Residual standard error: 28.5 on 127 degrees of freedom

Multiple R-squared: 0.532, Adjusted R-squared: 0.521

F-statistic: 48.2 on 3 and 127 DF, **p-value:** < 2e-16, **AIC** = 882

=====

BRONG AHAFO REGION (TOTAL):

Coefficients:

	Estimate	Std. Error	t-value	Pr(> t)	
(Intercept)	-111.9148	87.1083	-1.28	0.20072	
rainf_1	0.1599	0.0457	3.50	0.00061	***
maxT_1	-5.9272	2.4328	-2.44	0.01593	*
minT	7.0121	3.2191	2.18	0.03084	*
rh1500_1	1.0199	0.3177	3.21	0.00160	**
sunsh_1	10.7022	3.0118	3.55	0.00050	***

Signif. codes: 0 '***' 0.001 '**' 0.01 '*' 0.05 '.' 0.1 ' ' 1

Residual standard error: 31.2 on 161 degrees of freedom

Multiple R-squared: 0.408, Adjusted R-squared: 0.39

F-statistic: 22.2 on 5 and 161 DF, **p-value:** < 2e-16, **AIC**=1155

ASHANTI REGION (TOTAL)

Coefficients:

	Estimate	Std. Error	t-value	Pr(> t)
(Intercept)	-39.4011	34.1551	-1.15	0.2508
rainf_1	0.0799	0.0215	3.72	0.0003 ***
minT_1	3.1338	1.6874	1.86	0.0656 .
sunsh	-6.0406	1.2990	-4.65	8.2e-06 ***

Signif. codes: 0 '***' 0.001 '**' 0.01 '*' 0.05 '.' 0.1 ' ' 1
Residual standard error: 18.8 on 127 degrees of freedom

Multiple R-squared: 0.267, **Adjusted R-squared:** 0.25

F-statistic: 15.4 on 3 and 127 DF, **p-value:** 1.3e-08, **AIC = 773**

=====
EASTERN REGION (TOTAL)

Coefficients:

	Estimate	Std. Error	t-value	Pr(> t)
(Intercept)	22.459	168.015	0.13	0.89388
rainf_1	0.235	0.066	3.56	0.00053 ***
maxT_1	8.085	3.978	2.03	0.04422 *
rh0600_1	-4.111	1.662	-2.47	0.01473 *
rh1500_1	2.271	0.766	2.97	0.00362 **
sunsh	-8.627	3.097	-2.79	0.00617 **

Signif. codes: 0 '***' 0.001 '**' 0.01 '*' 0.05 '.' 0.1 ' ' 1
Residual standard error: 32.2 on 125 degrees of freedom

Multiple R-squared: 0.367, **Adjusted R-squared:** 0.341

F-statistic: 14.5 on 5 and 125 DF, **p-value:** 3.55e-11, **AIC=915.4**

=====
GREATER ACCRA (TOTAL)

Coefficients:

	Estimate	Std. Error	t-value	Pr(> t)
(Intercept)	97.1748	35.6989	2.72	0.00740 **
rainf_1	0.0984	0.0247	3.98	0.00011 ***
maxT	-2.6224	1.2973	-2.02	0.04534 *
sunsh	-3.3279	1.5660	-2.13	0.03551 *

Signif. codes: 0 '***' 0.001 '**' 0.01 '*' 0.05 '.' 0.1 ' ' 1
Residual standard error: 17.9 on 127 degrees of freedom

Multiple R-squared: 0.315, **Adjusted R-squared:** 0.298

F-statistic: 19.4 on 3 and 127 DF, **p-value:** 1.99e-10, **AIC=759.2**

=====
WESTERN REGION (TOTAL)

Coefficients:

	Estimate	Std. Error	t-value	Pr(> t)
(Intercept)	-357.7847	252.6241	-1.42	0.1592
rainf_1	0.0796	0.0286	2.78	0.0062 **
maxT	-10.8348	4.7431	-2.28	0.0241 *
maxT_1	5.5344	2.5887	2.14	0.0345 *
minT	7.2975	4.9908	1.46	0.1462
rh0600_1	4.9686	2.0702	2.40	0.0179 *
rh1500	-1.7423	0.9070	-1.92	0.0570 .

Signif. codes: 0 '***' 0.001 '**' 0.01 '*' 0.05 '.' 0.1 ' ' 1
Residual standard error: 22.8 on 124 degrees of freedom

Multiple R-squared: 0.243, **Adjusted R-squared:** 0.206

F-statistic: 6.62 on 6 and 124 DF, **p-value:** 4.32e-06, **AIC = 826**

CENTRAL REGION (TOTAL)

Coefficients:

	Estimate	Std. Error	t-value	Pr(> t)	
(Intercept)	731.0402	216.5128	3.38	0.00099	***
rainf	0.0738	0.0353	2.09	0.03868	*
maxT	-22.1343	4.8601	-4.55	1.3e-05	***
maxT_1	5.2544	3.5621	1.48	0.14276	
minT	13.4920	4.2176	3.20	0.00176	**
minT_1	-5.9435	4.0206	-1.48	0.14192	
rh0600	-5.1561	1.4724	-3.50	0.00065	***
sunsh	10.1200	4.2183	2.40	0.01795	*
sunsh_1	6.1470	3.0875	1.99	0.04872	*

Signif. codes: 0 '***' 0.001 '**' 0.01 '*' 0.05 '.' 0.1 ' ' 1

Residual standard error: 17.2 on 122 degrees of freedom

Multiple R-squared: 0.388, Adjusted R-squared: 0.348

F-statistic: 9.69 on 8 and 122 DF, p-value: 2.47e-10, AIC = 753

=====

VOLTA REGION (TOTAL)

Coefficients:

	Estimate	Std. Error	t-value	Pr(> t)	
(Intercept)	46.8129	126.9155	0.37	0.7133	
rainf	0.1047	0.0518	2.02	0.0468	*
rainf_1	0.1534	0.0566	2.71	0.0083	**
maxT	-8.7985	2.9565	-2.98	0.0039	**
maxT_1	12.6829	4.4115	2.87	0.0052	**
minT_1	-11.8023	4.6682	-2.53	0.0135	*
rh1500_1	1.2114	0.7252	1.67	0.0989	.

Signif. codes: 0 '***' 0.001 '**' 0.01 '*' 0.05 '.' 0.1 ' ' 1

Residual standard error: 20.2 on 76 degrees of freedom

Multiple R-squared: 0.496, Adjusted R-squared: 0.457

F-statistic: 12.5 on 6 and 76 DF, p-value: 9.74e-10, AIC= 505.4

=====

Results A-5.3: Stepwise regression analysis results of the detrended malaria incidence rates (residuals) with the climatic covariates to identify potential predictors for the 0-4 year group incidence data

=====

UPPER EAST REGION (0-4)

Coefficients:

	Estimate	Std. Error	t value	Pr(> t)	
(Intercept)	2166.876	270.453	8.01	6.0e-13	***
maxT_1	-72.510	6.763	-10.72	< 2e-16	***
rh0600	4.173	0.882	4.73	5.8e-06	***

Signif. codes: 0 '***' 0.001 '**' 0.01 '*' 0.05 '.' 0.1 ' ' 1

Residual standard error: 173 on 128 degrees of freedom

Multiple R-squared: 0.666, Adjusted R-squared: 0.661

F-statistic: 128 on 2 and 128 DF, p-value: <2e-16, AIC=1354

=====

UPPER WEST REGION (0-4)

Coefficients:

	Estimate	Std. Error	t value	Pr(> t)	
(Intercept)	159.930	140.077	1.14	0.25571	
rainf	-0.795	0.280	-2.84	0.00531	**
minT	-22.717	5.958	-3.81	0.00021	***
rh1500	10.125	1.268	7.98	7.3e-13	***

 Signif. codes: 0 '***' 0.001 '**' 0.01 '*' 0.05 '.' 0.1 ' ' 1
 Residual standard error: 132 on 127 degrees of freedom
Multiple R-squared: 0.539, **Adjusted R-squared:** 0.528
F-statistic: 49.4 on 3 and 127 DF, **p-value:** <2e-16, **AIC=1284**
 =====

NORTHERN REGION (0-4)

Coefficients:

	Estimate	Std. Error	t-value	Pr(> t)
(Intercept)	654.98	117.99	5.55	1.6e-07 ***
maxT_1	-30.18	5.06	-5.96	2.3e-08 ***
minT	-11.63	6.35	-1.83	0.06954 .
rh0600	3.52	1.04	3.40	0.00091 ***

 Signif. codes: 0 '***' 0.001 '**' 0.01 '*' 0.05 '.' 0.1 ' ' 1
 Residual standard error: 63.8 on 127 degrees of freedom
Multiple R-squared: 0.627, **Adjusted R-squared:** 0.618
F-statistic: 71.1 on 3 and 127 DF, **p-value:** < 2e-16, **AIC = 1093**
 =====

BRONG AHAFO REGION (0-4)

Coefficients:

	Estimate	Std. Error	t-value	Pr(> t)
(Intercept)	-526.8675	170.6186	-3.09	0.00238 **
rainf_1	0.3746	0.0923	4.06	7.7e-05 ***
maxT_1	-8.5882	4.7825	-1.80	0.07442 .
minT	27.1362	6.9540	3.90	0.00014 ***
rh0600	-1.5070	0.9092	-1.66	0.09939 .
rh1500_1	3.3678	0.6829	4.93	2.0e-06 ***
sunsh_1	15.0853	6.1011	2.47	0.01446 *

 Signif. codes: 0 '***' 0.001 '**' 0.01 '*' 0.05 '.' 0.1 ' ' 1
 Residual standard error: 61.1 on 160 degrees of freedom
Multiple R-squared: 0.507, **Adjusted R-squared:** 0.488
F-statistic: 27.4 on 6 and 160 DF, **p-value:**< 2e-16, **AIC = 1380**
 =====

ASHANTI REGION (0-4)

Coefficients:

	Estimate	Std. Error	t-value	Pr(> t)
(Intercept)	19.0393	20.6388	0.92	0.3580
rainf	0.0918	0.0541	1.70	0.0921 .
rainf_1	0.1703	0.0534	3.19	0.0018 **
sunsh	-8.5780	3.0515	-2.81	0.0057 **

 Signif. codes: 0 '***' 0.001 '**' 0.01 '*' 0.05 '.' 0.1 ' ' 1
 Residual standard error: 44 on 127 degrees of freedom
Multiple R-squared: 0.219, **Adjusted R-squared:** 0.201
F-statistic: 11.9 on 3 and 127 DF, **p-value:** 6.45e-07, **AIC=995.4**
 =====

EASTERN REGION(0-4)

Coefficients:

	Estimate	Std. Error	t-value	Pr(> t)
(Intercept)	-71.328	66.999	-1.06	0.289
rainf_1	0.527	0.121	4.34	2.9e-05 ***
rh1500_1	1.534	0.763	2.01	0.046 *
sunsh	-13.007	5.606	-2.32	0.022 *

 Signif. codes: 0 '***' 0.001 '**' 0.01 '*' 0.05 '.' 0.1 ' ' 1
 Residual standard error: 64 on 127 degrees of freedom
Multiple R-squared: 0.364, **Adjusted R-squared:** 0.349
F-statistic: 24.2 on 3 and 127 DF, **p-value:** 1.81e-12, **AIC=1093**
 =====

GREATER ACCRA (0-4)

Coefficients:

	Estimate	Std. Error	t-value	Pr(> t)
(Intercept)	364.3263	189.9214	1.92	0.0573 .
rainf_1	0.1932	0.0666	2.90	0.0044 **
minT_1	-7.7359	4.3666	-1.77	0.0789 .
rh0600	-3.6469	2.1979	-1.66	0.0995 .
rh1500	2.0327	1.4529	1.40	0.1642

Signif. codes: 0 '***' 0.001 '**' 0.01 '*' 0.05 '.' 0.1 ' ' 1

Residual standard error: 47.3 on 126 degrees of freedom

Multiple R-squared: 0.137, Adjusted R-squared: 0.11

F-statistic: 5.01 on 4 and 126 DF, p-value:0.000887, AIC = 1015

WESTERN REGION (0-4)

Coefficients:

	Estimate	Std. Error	t-value	Pr(> t)
(Intercept)	-907.899	337.734	-2.69	0.0081 **
rainf_1	0.161	0.042	3.83	0.0002 ***
minT_1	13.938	5.962	2.34	0.0210 *
rh0600_1	6.021	3.329	1.81	0.0729 .

Signif. codes: 0 '***' 0.001 '**' 0.01 '*' 0.05 '.' 0.1 ' ' 1

Residual standard error: 43.8 on 127 degrees of freedom

Multiple R-squared: 0.231, Adjusted R-squared: 0.213

F-statistic: 12.7 on 3 and 127 DF, p-value: 2.48e-07, AIC=994.4

CENTRAL REGION (0-4)

Coefficients:

	Estimate	Std. Error	t-value	Pr(> t)
(Intercept)	640.1153	490.8003	1.30	0.1946
rainf	0.1076	0.0751	1.43	0.1546
maxT	-45.9009	10.6484	-4.31	3.3e-05 ***
maxT_1	24.2635	5.9619	4.07	8.4e-05 ***
minT	33.6520	11.2362	2.99	0.0033 **
minT_1	-20.0576	10.9603	-1.83	0.0697 .
rh0600	-10.0077	3.3990	-2.94	0.0039 **
rh0600_1	5.6120	2.9725	1.89	0.0614 .
sunsh	20.3145	8.9389	2.27	0.0248 *

Signif. codes: 0 '***' 0.001 '**' 0.01 '*' 0.05 '.' 0.1 ' ' 1

Residual standard error: 37.1 on 122 degrees of freedom

Multiple R-squared: 0.344, Adjusted R-squared: 0.301

F-statistic: 8.01 on 8 and 122 DF, p-value: 1.23e-08, AIC = 956

VOLTA REGION (0-4)

Coefficients:

	Estimate	Std. Error	t-value	Pr(> t)
(Intercept)	-161.871	228.137	-0.71	0.4801
rainf	0.235	0.123	1.91	0.0601 .
rainf_1	0.364	0.132	2.75	0.0074 **
minT_1	-9.910	6.857	-1.45	0.1524
rh0600_1	3.572	2.253	1.59	0.1168

Signif. codes: 0 '***' 0.001 '**' 0.01 '*' 0.05 '.' 0.1 ' ' 1

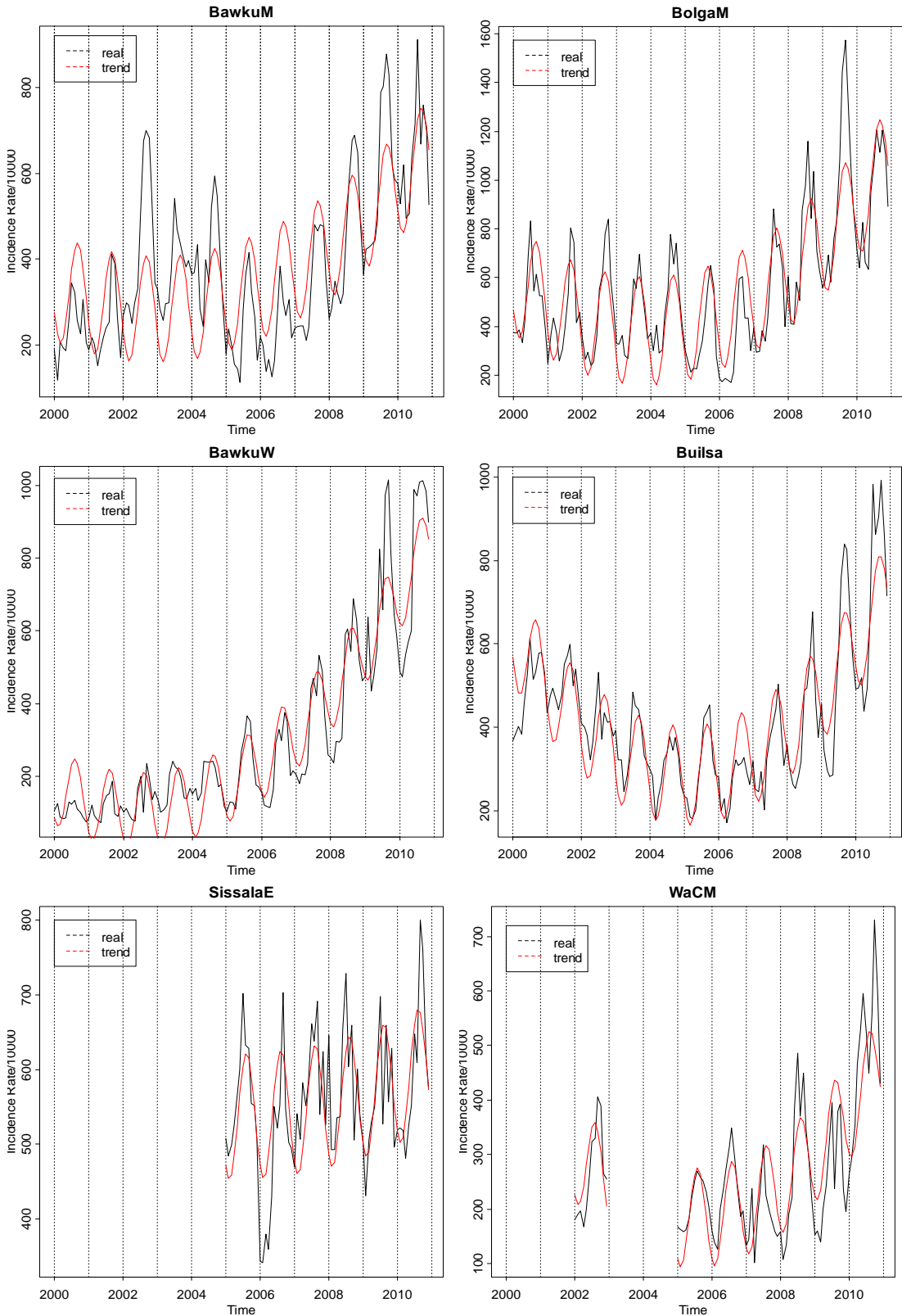
Residual standard error: 54.9 on 78 degrees of freedom

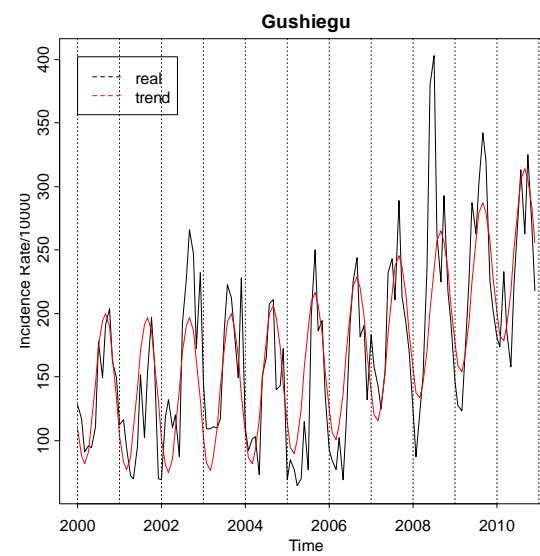
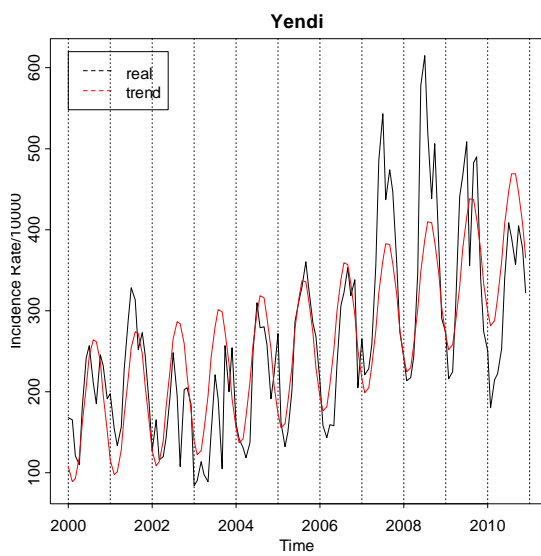
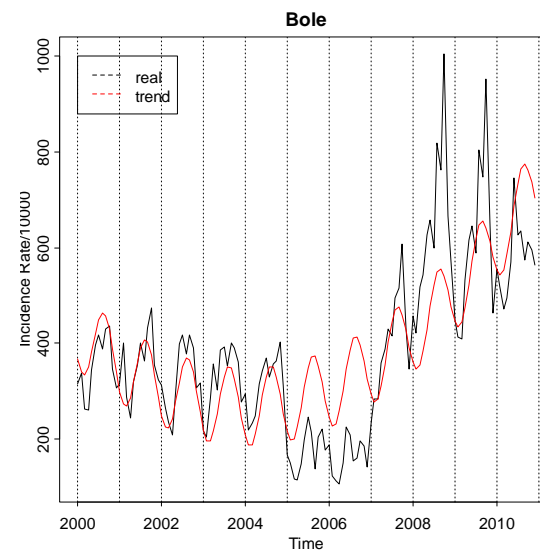
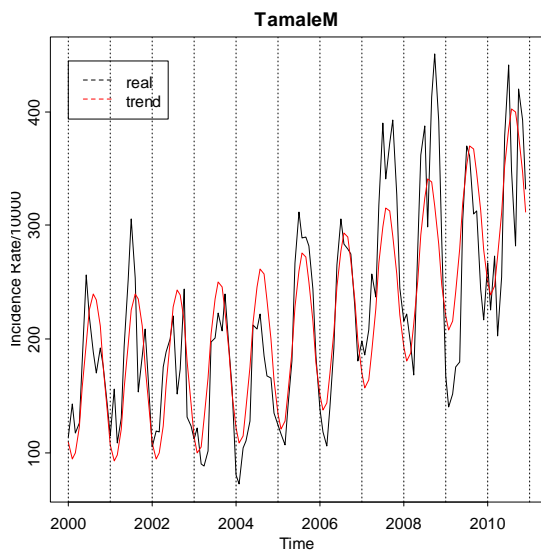
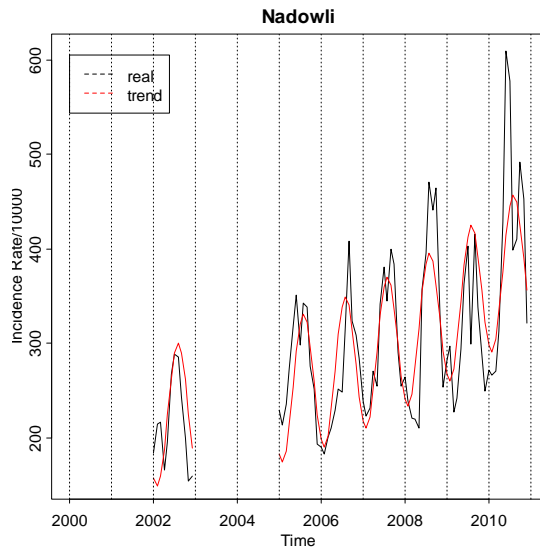
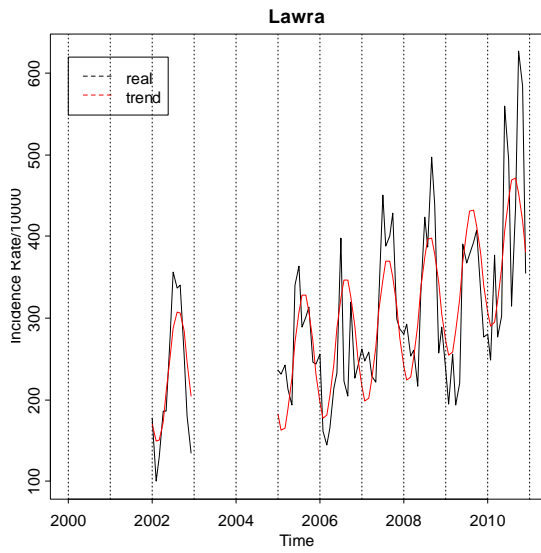
Multiple R-squared: 0.29, Adjusted R-squared: 0.253

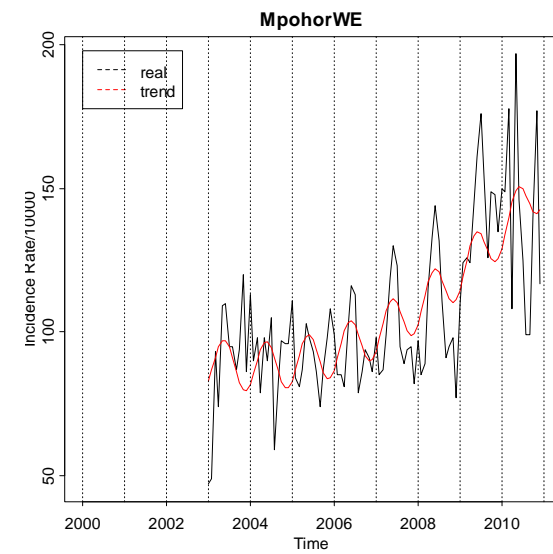
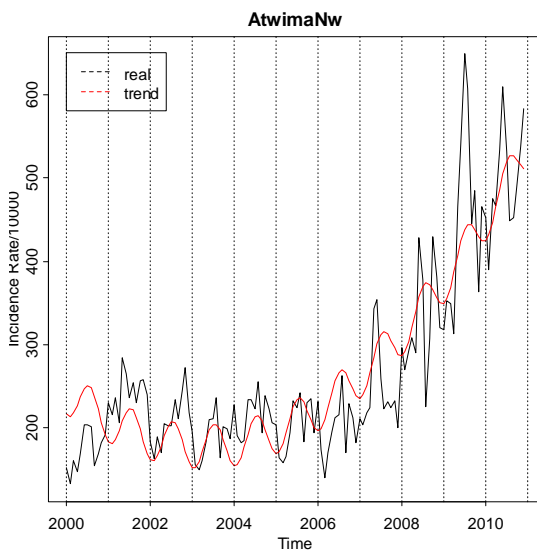
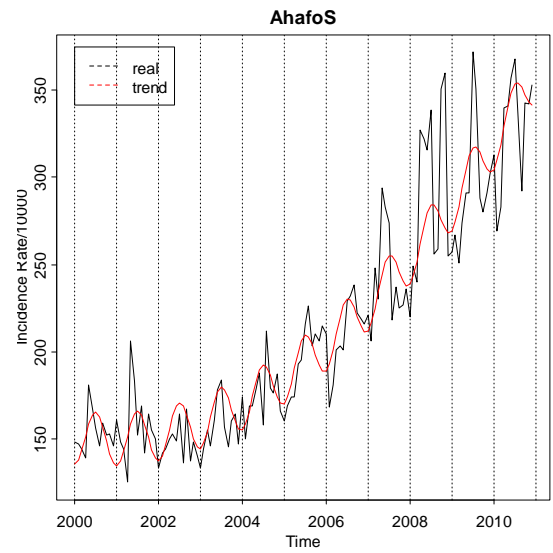
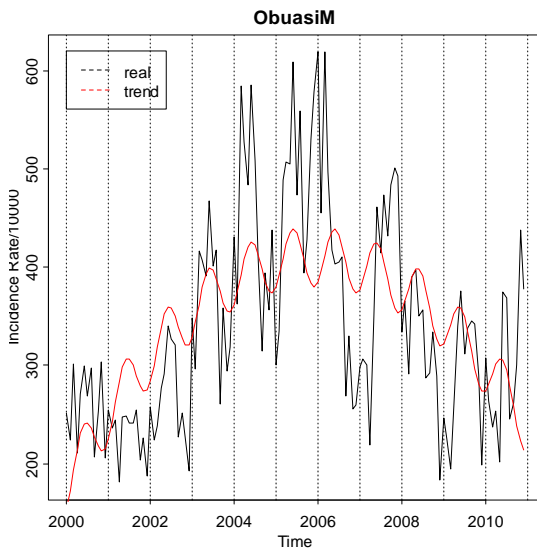
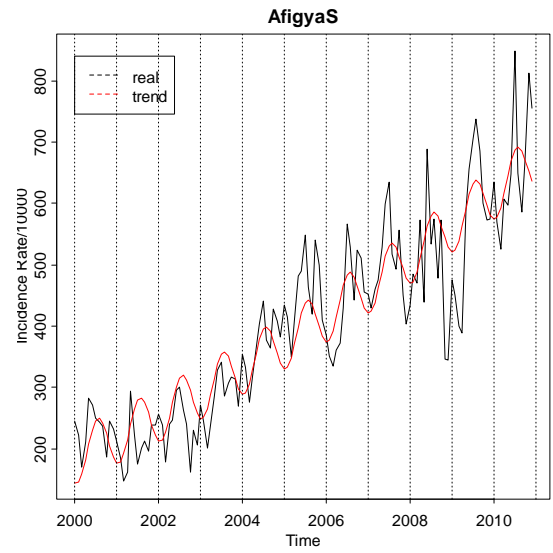
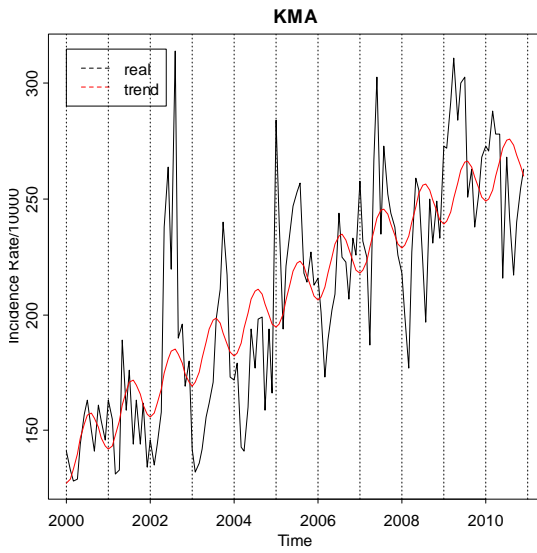
F-statistic: 7.96 on 4 and 78 DF, p-value: 1.97e-05, AIC=670

Appendix B: Exploratory Analysis of the Space-time MIR Data

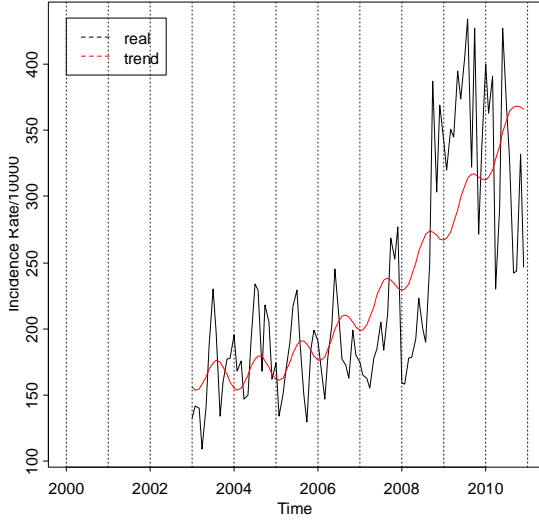
B-1: Temporal Profiles of MIR at District Locations



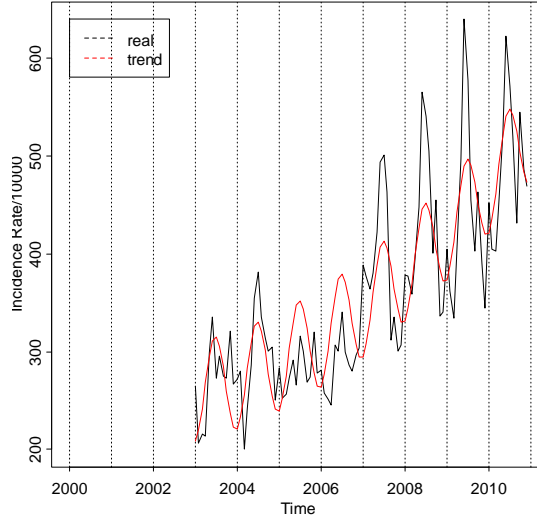




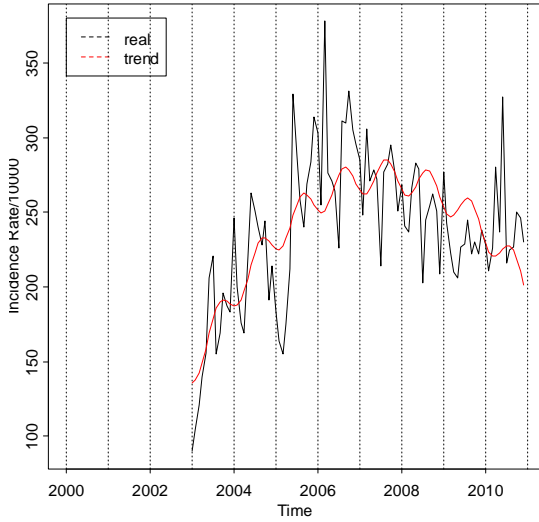
ShamaAW



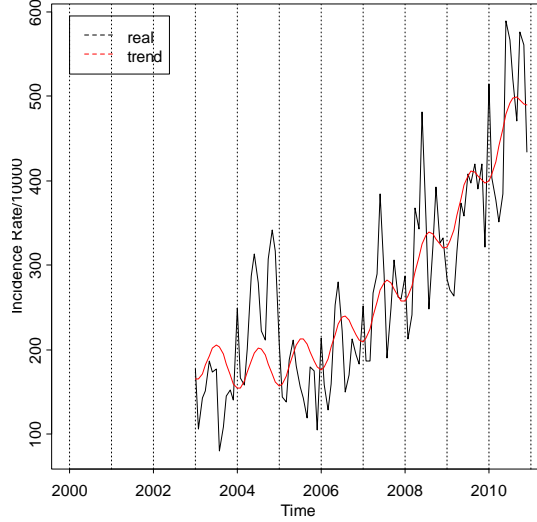
NzemaE



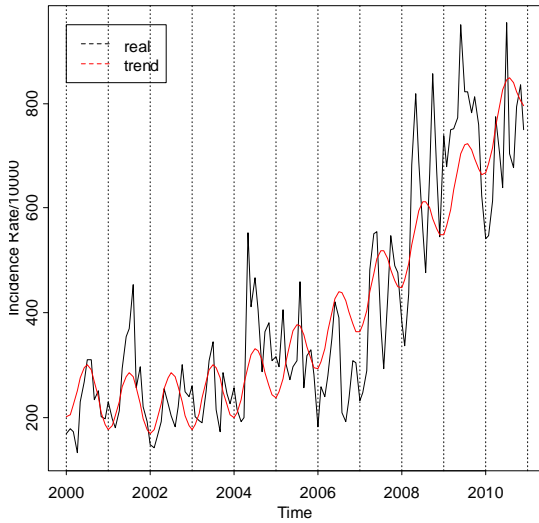
BibianiAB



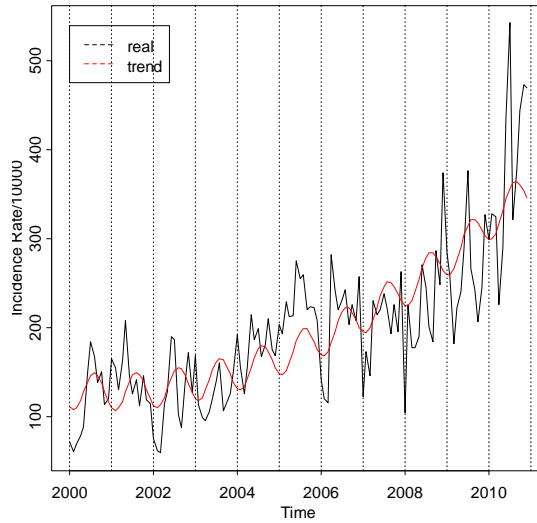
Juabeso

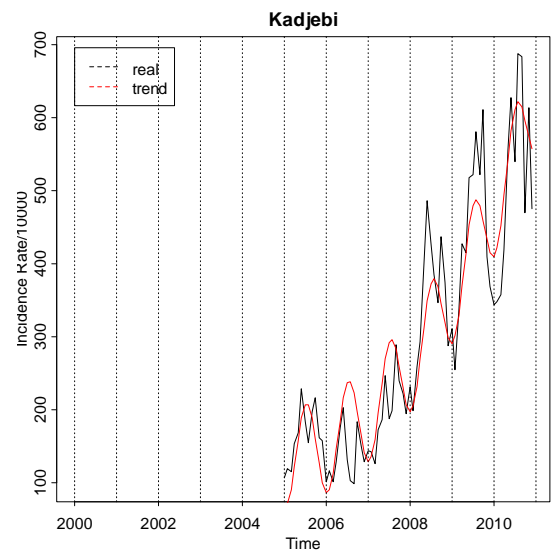
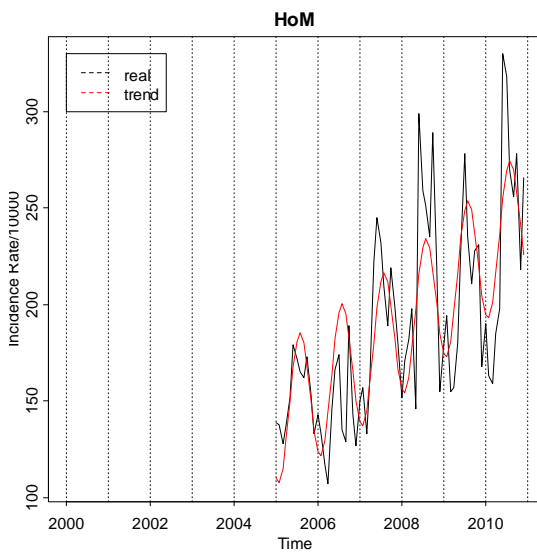
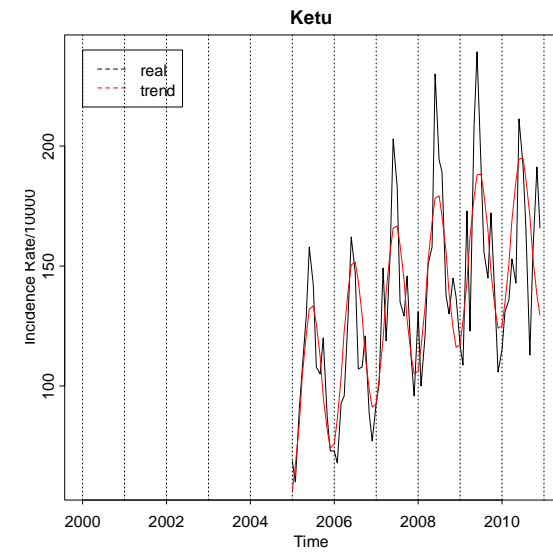
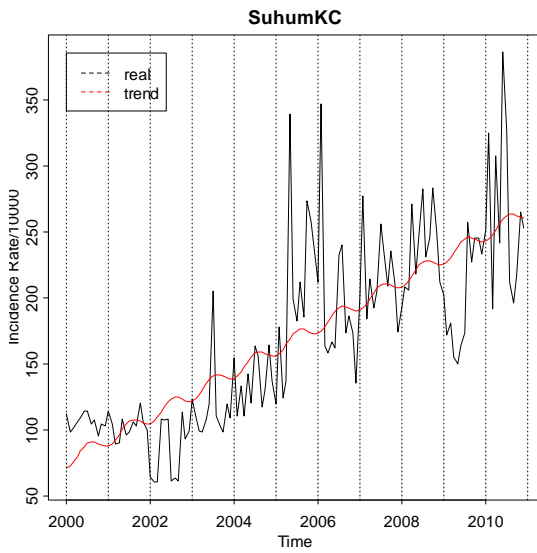
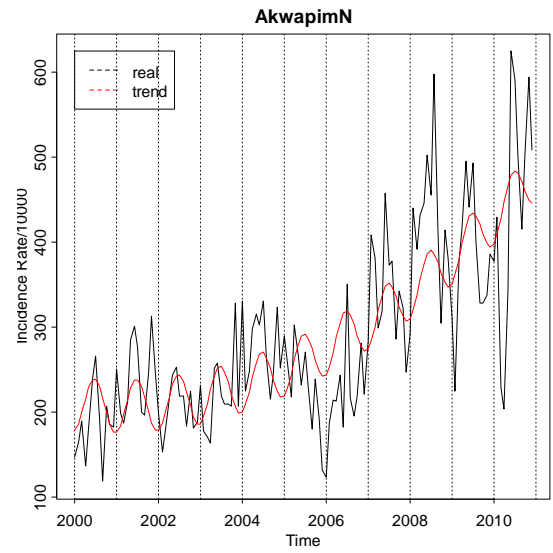
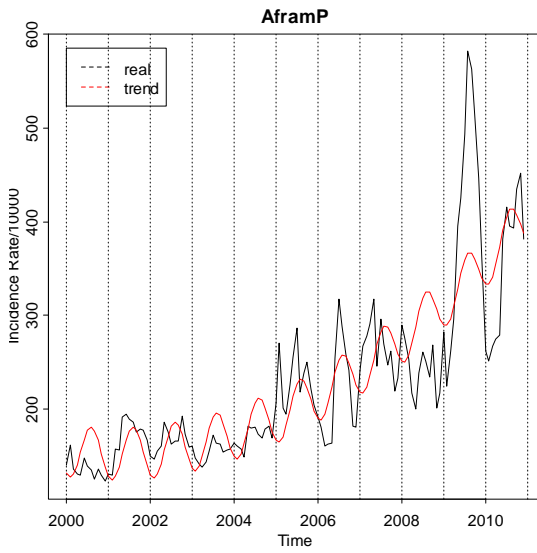


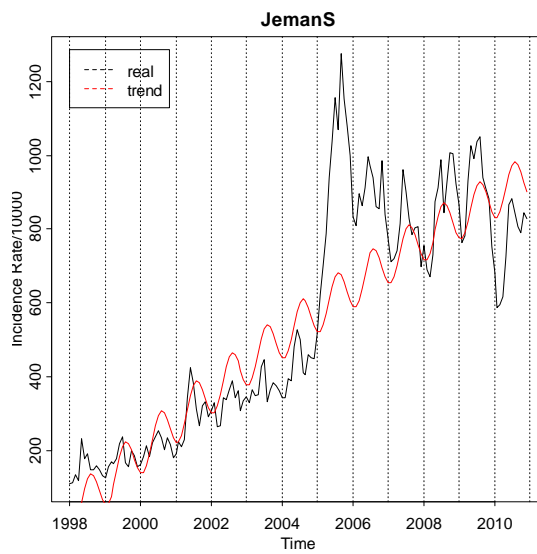
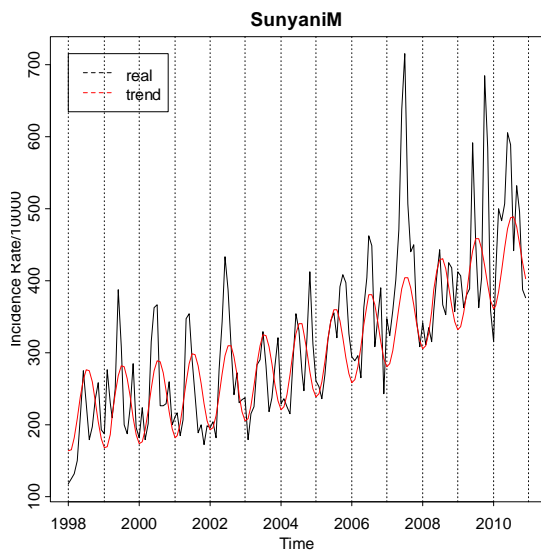
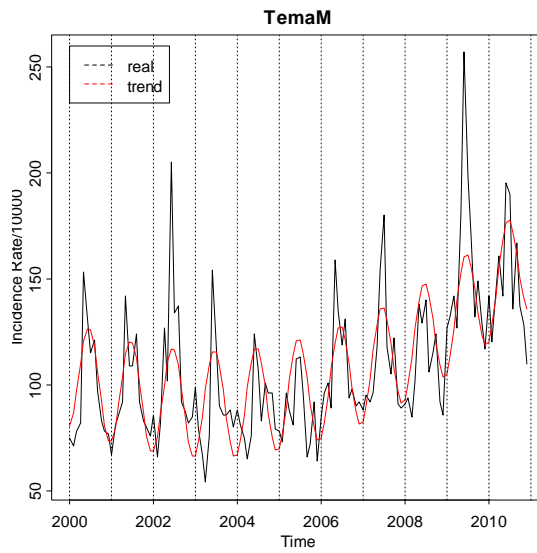
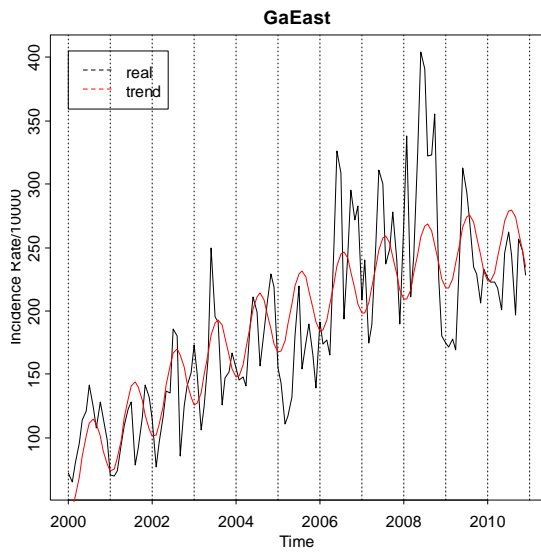
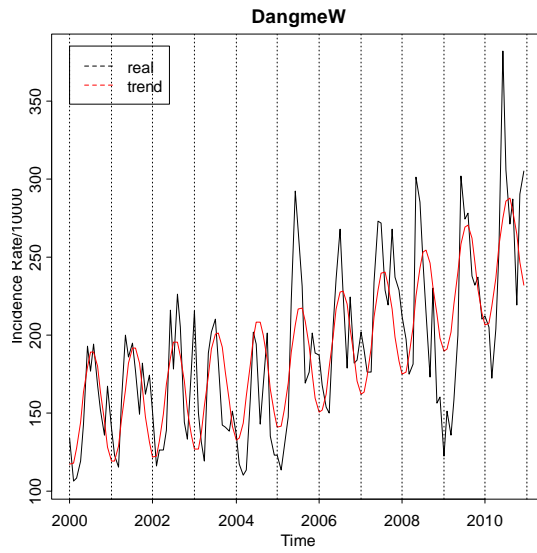
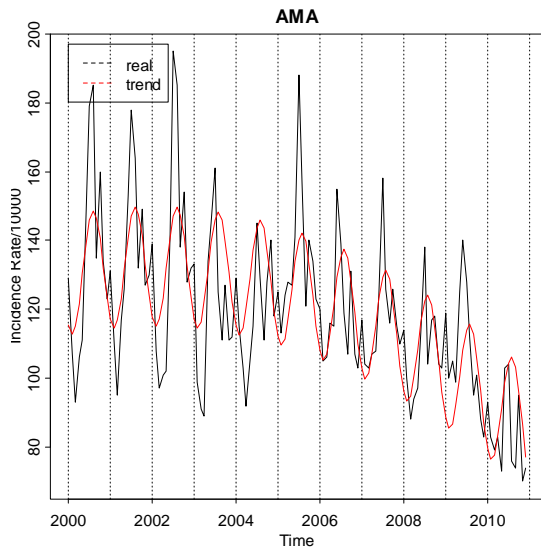
NewJuaben

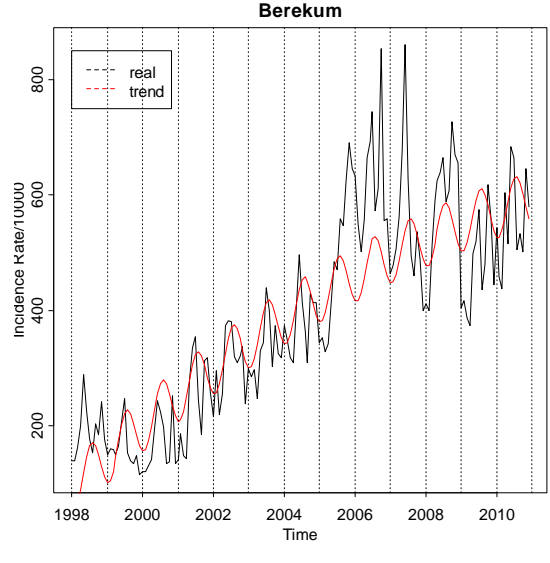
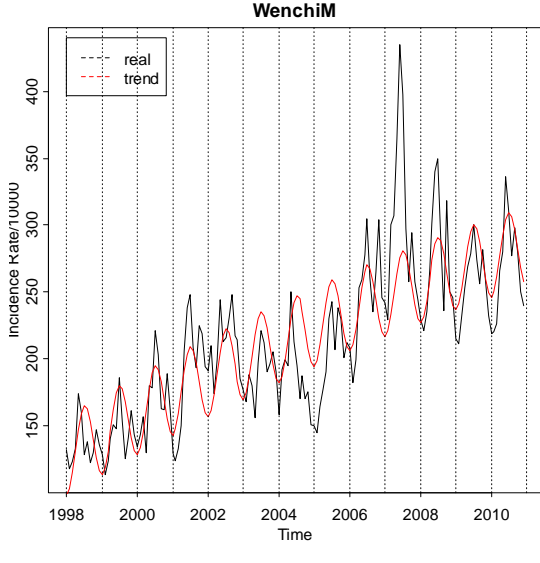
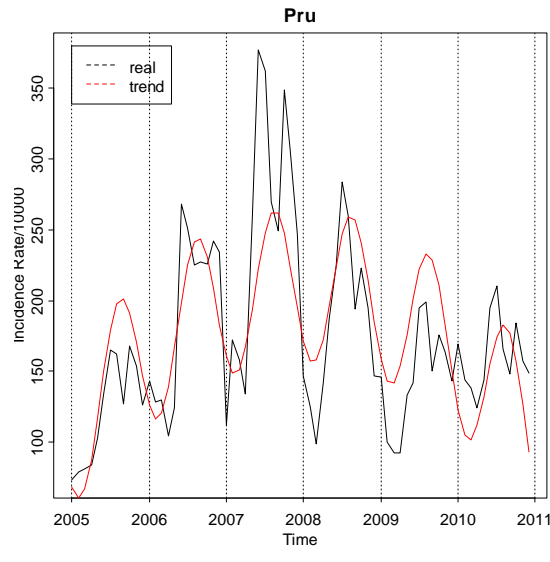
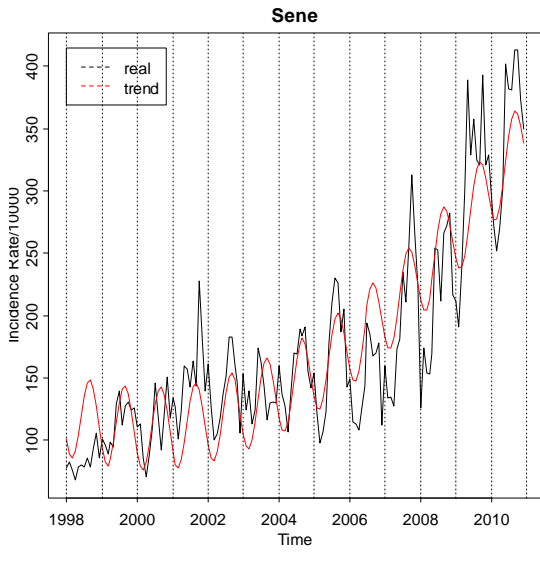
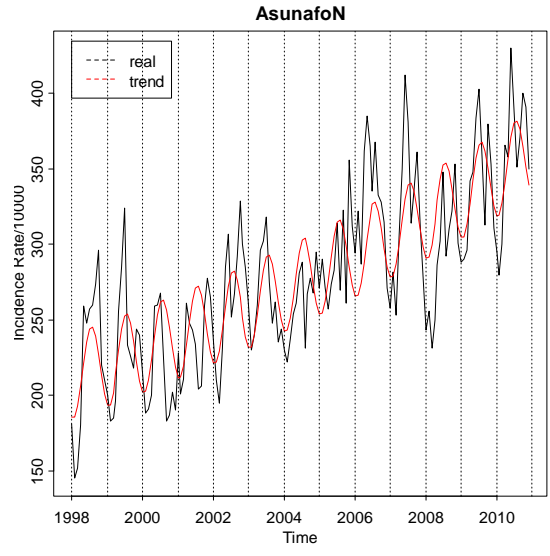
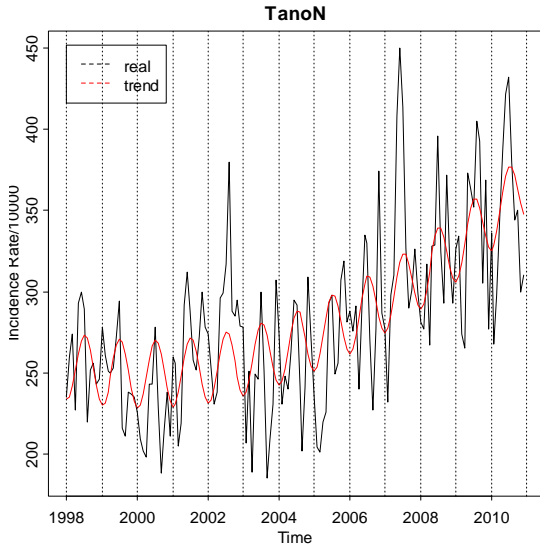


BirimS

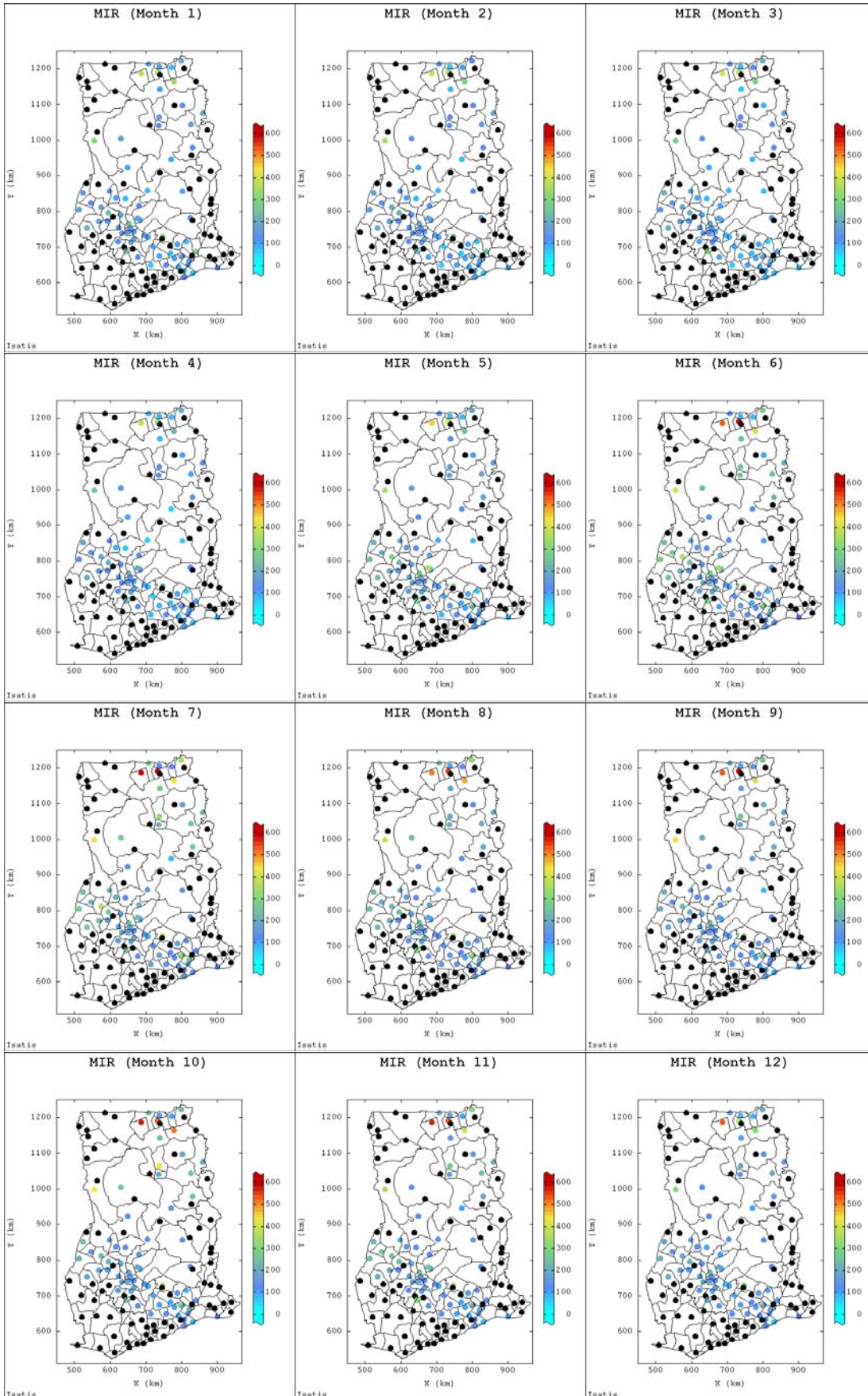


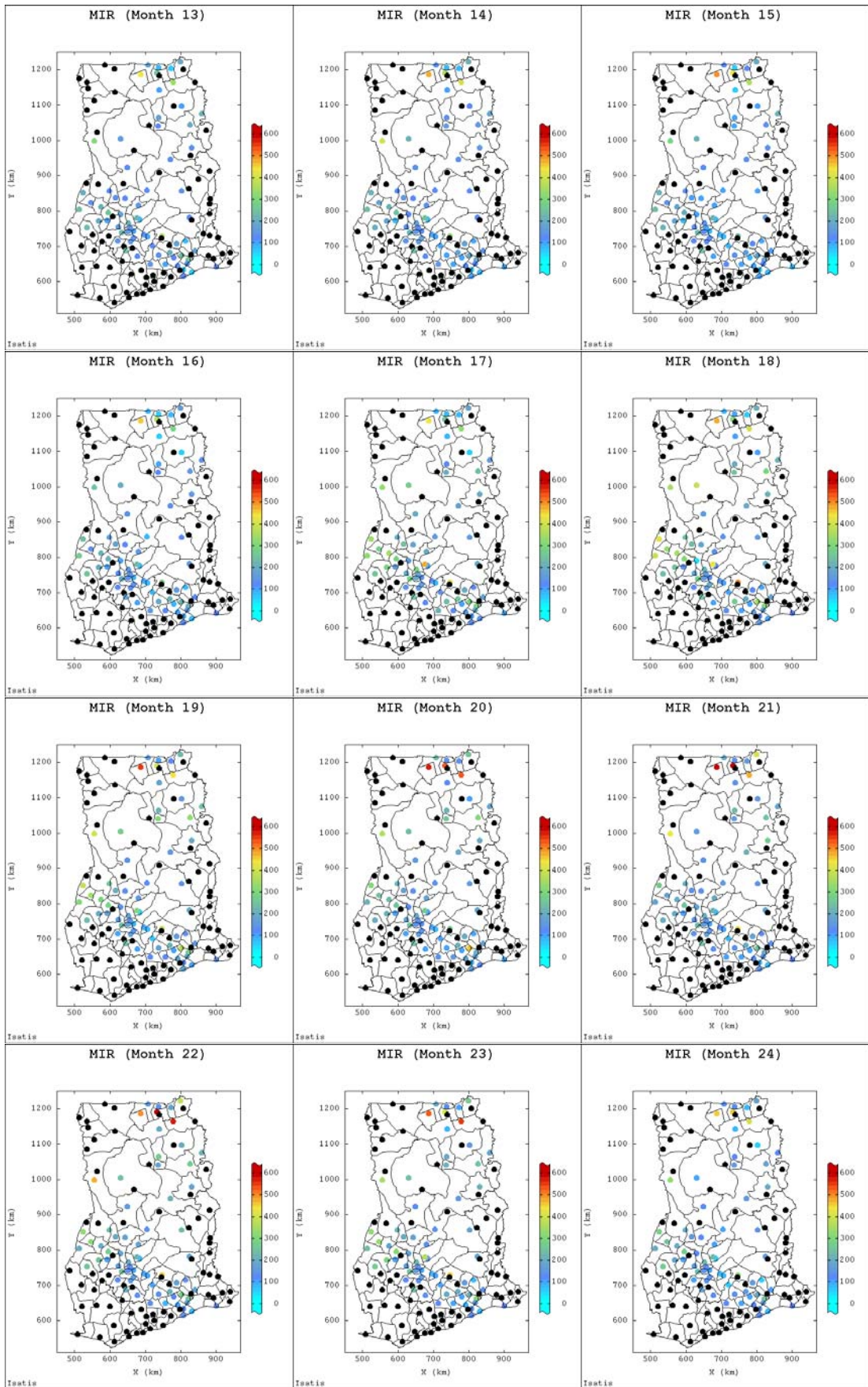


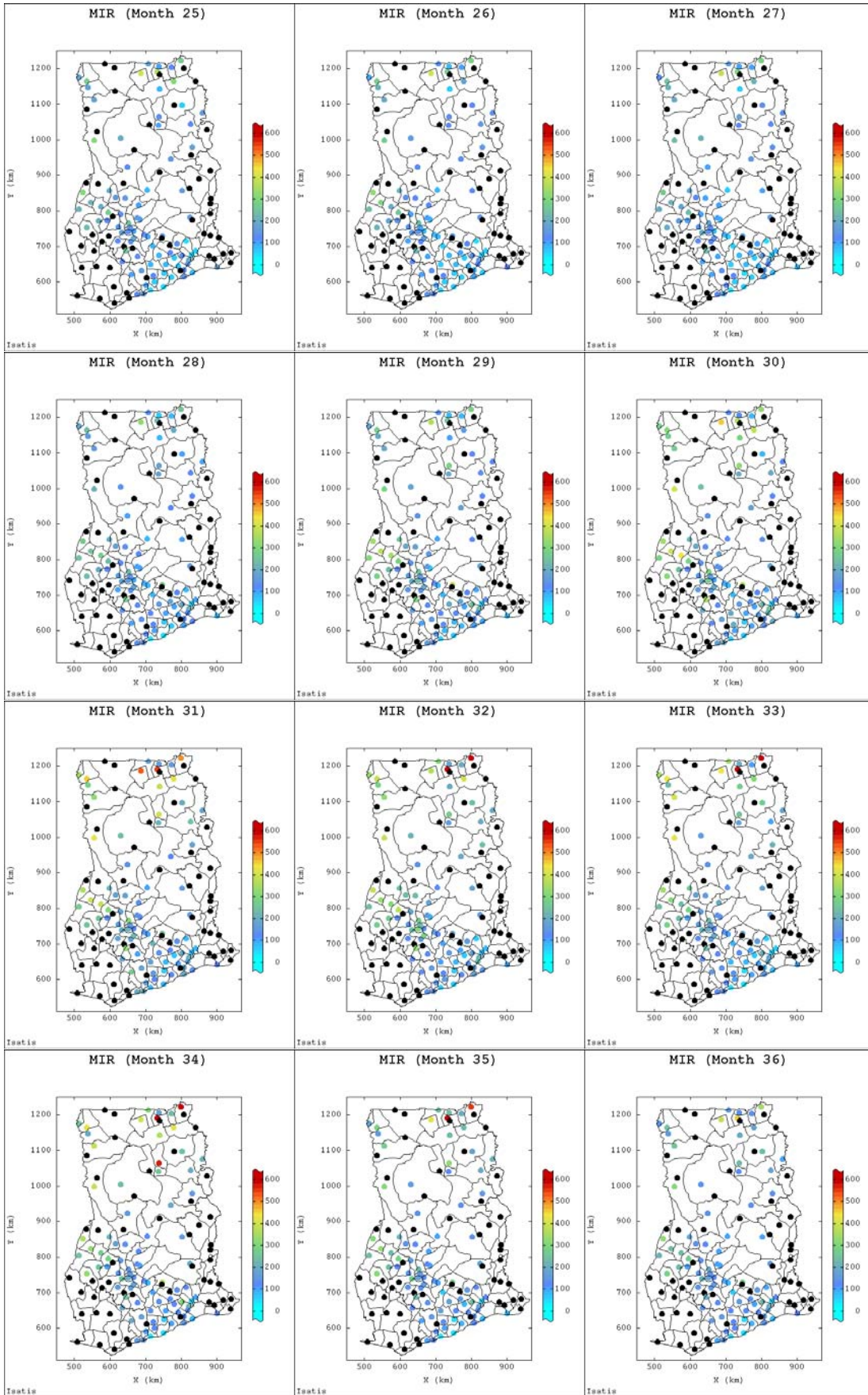


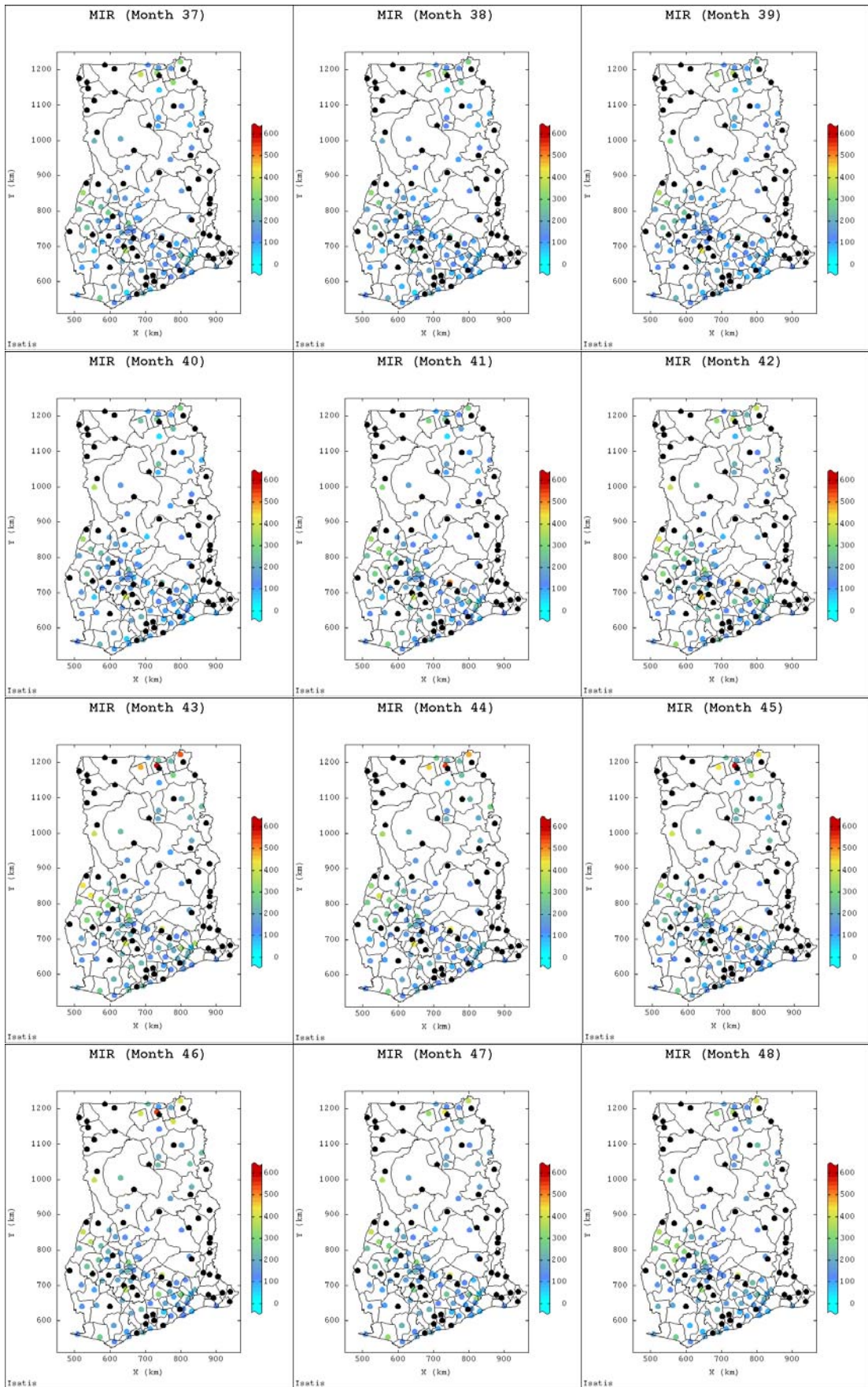


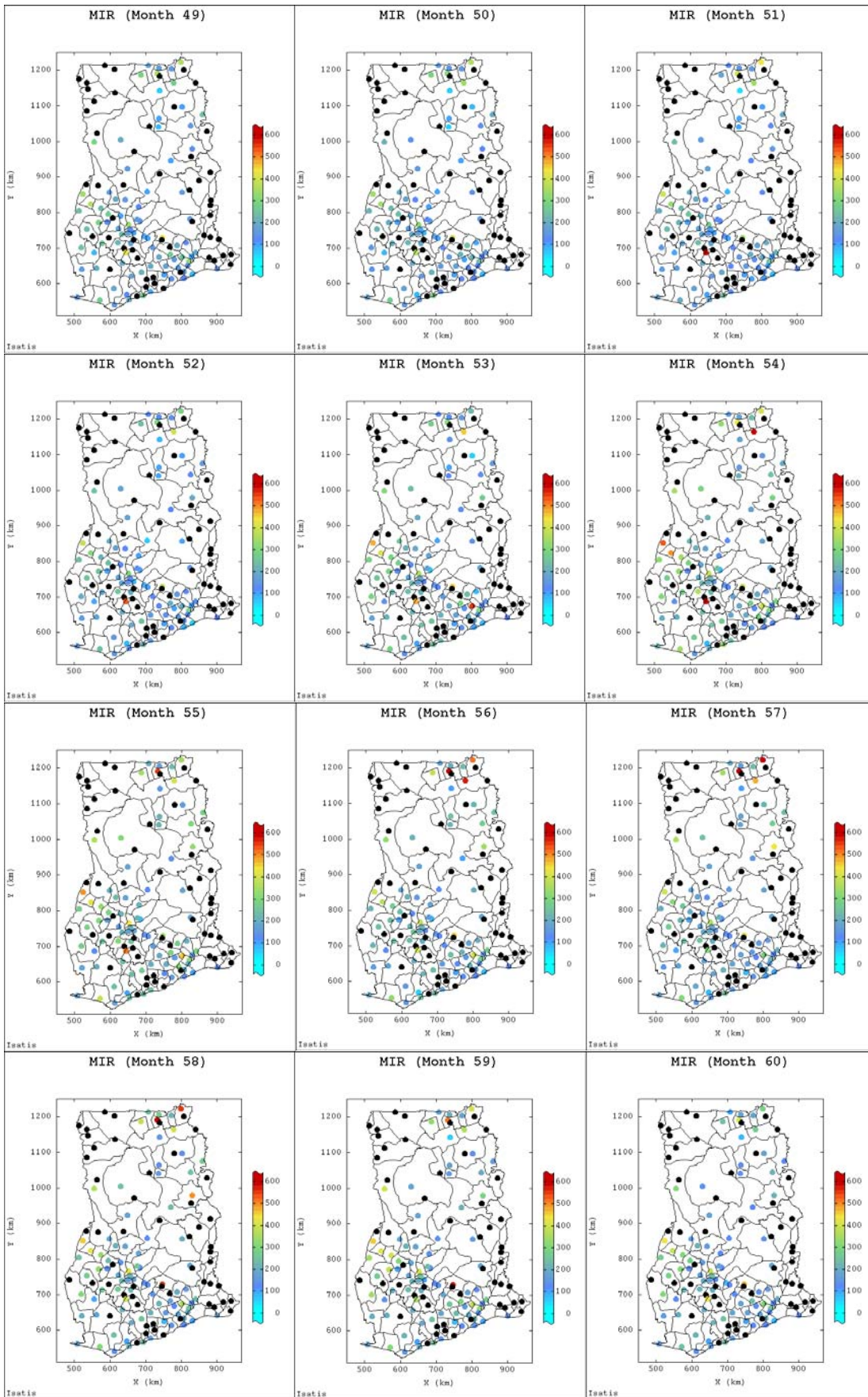
B-2: Post-plots of the observed MIR Data

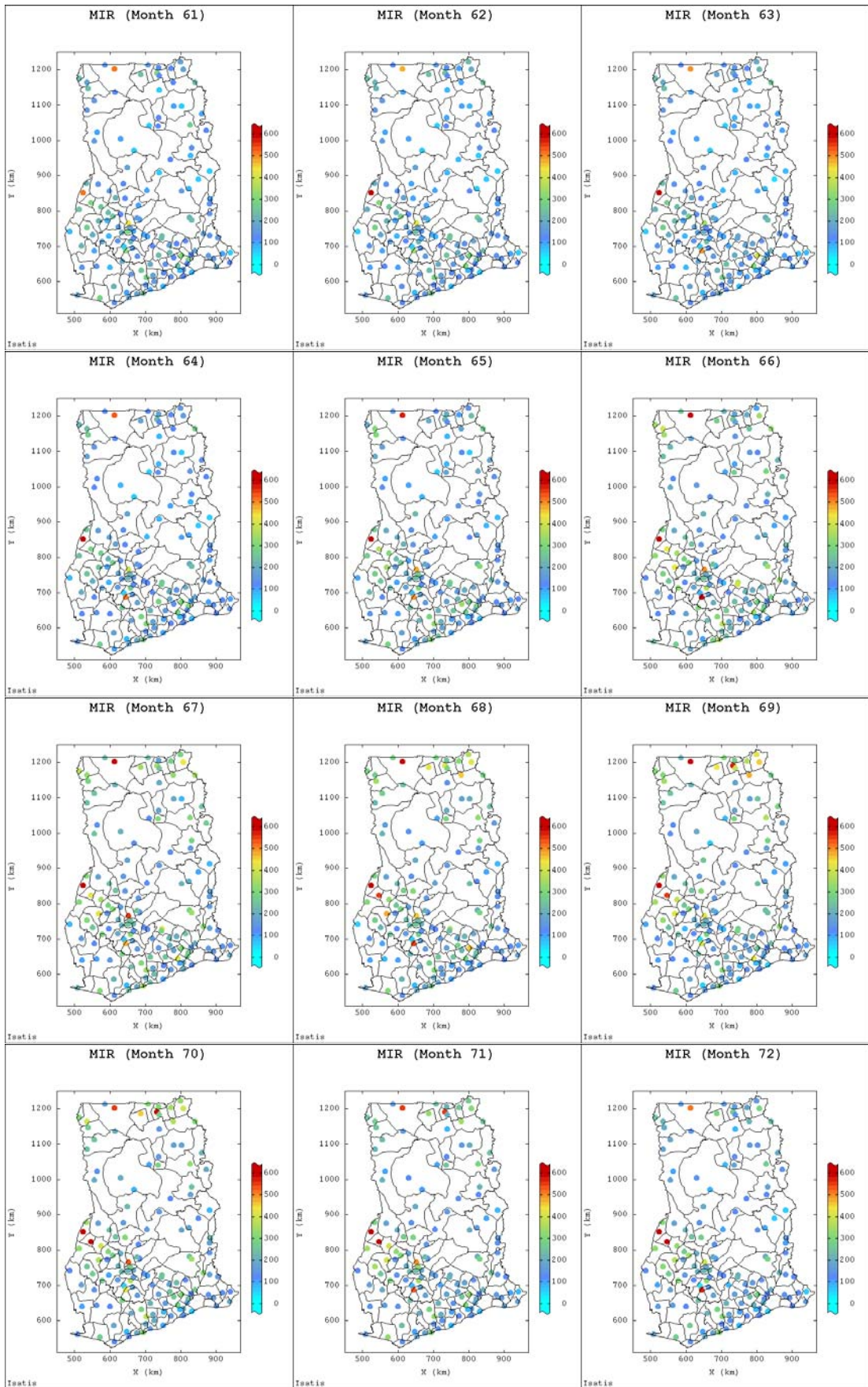


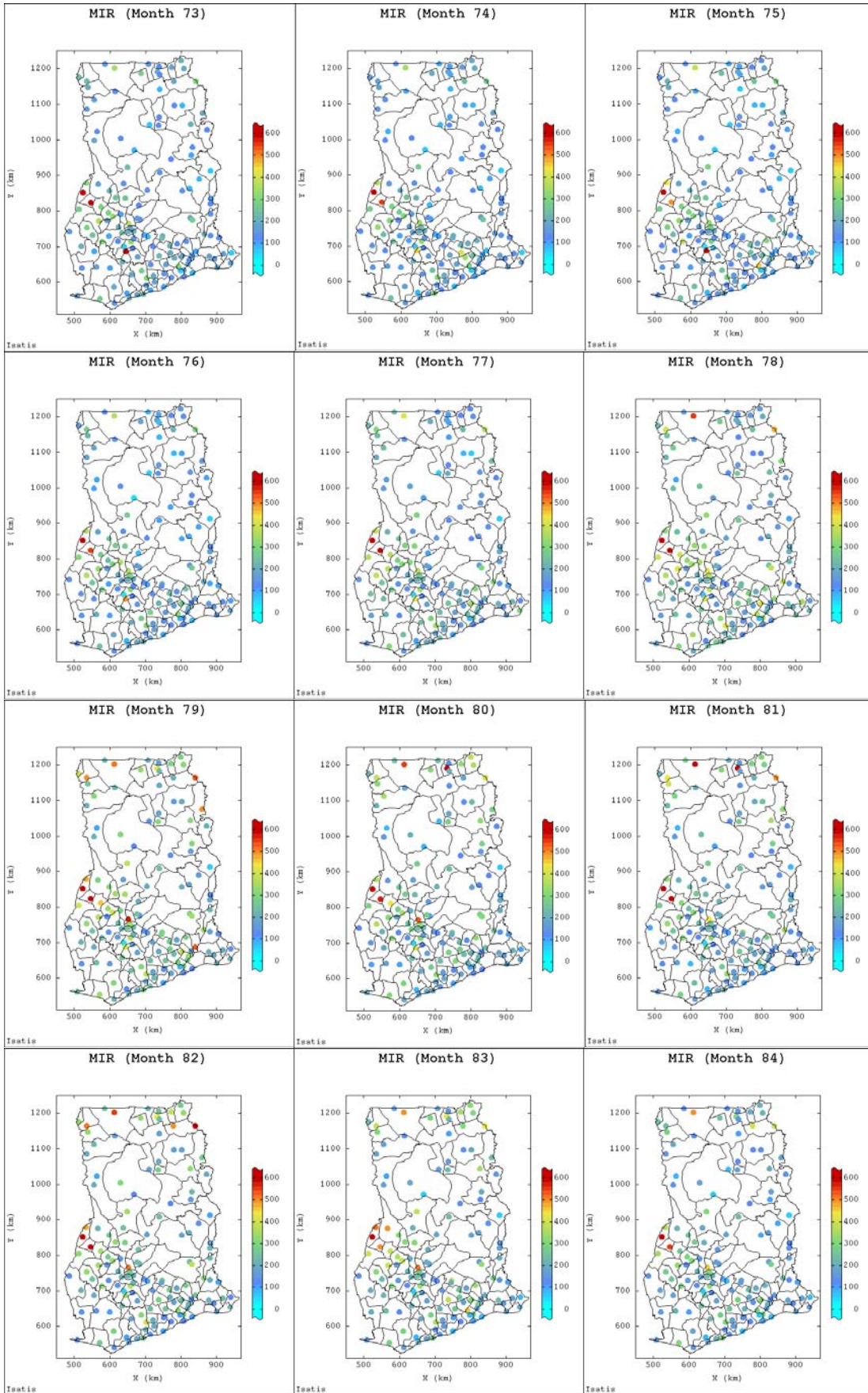


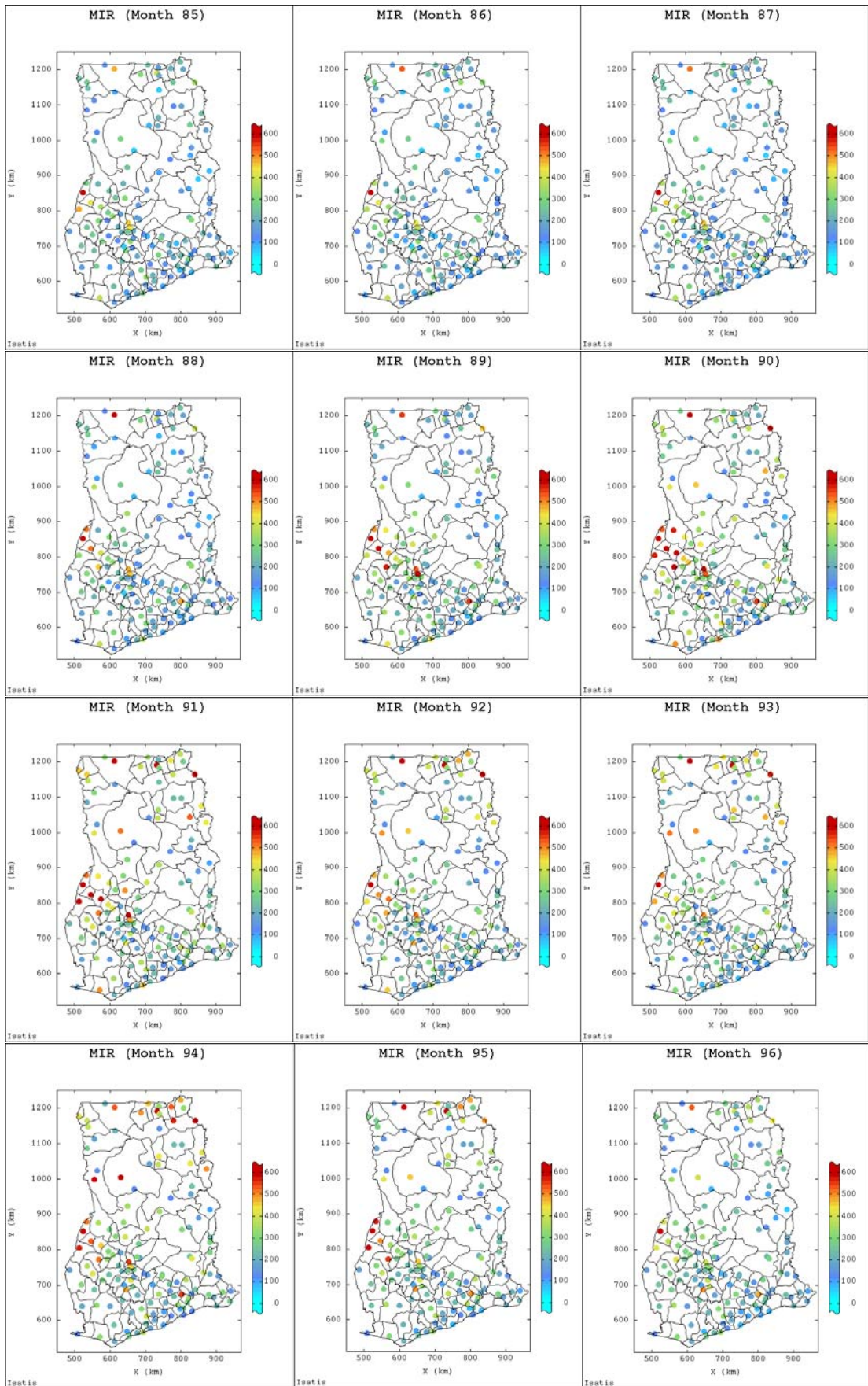


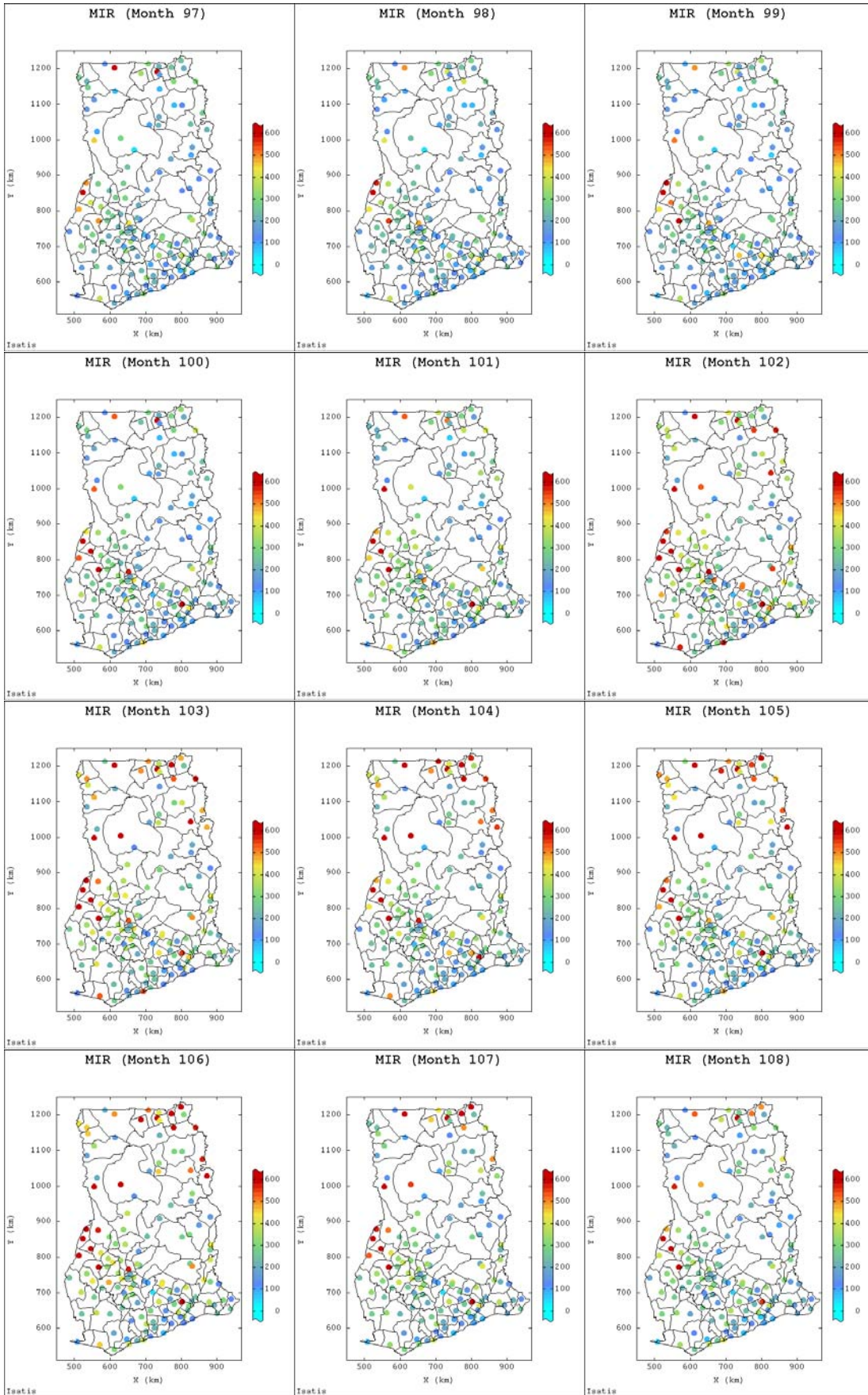


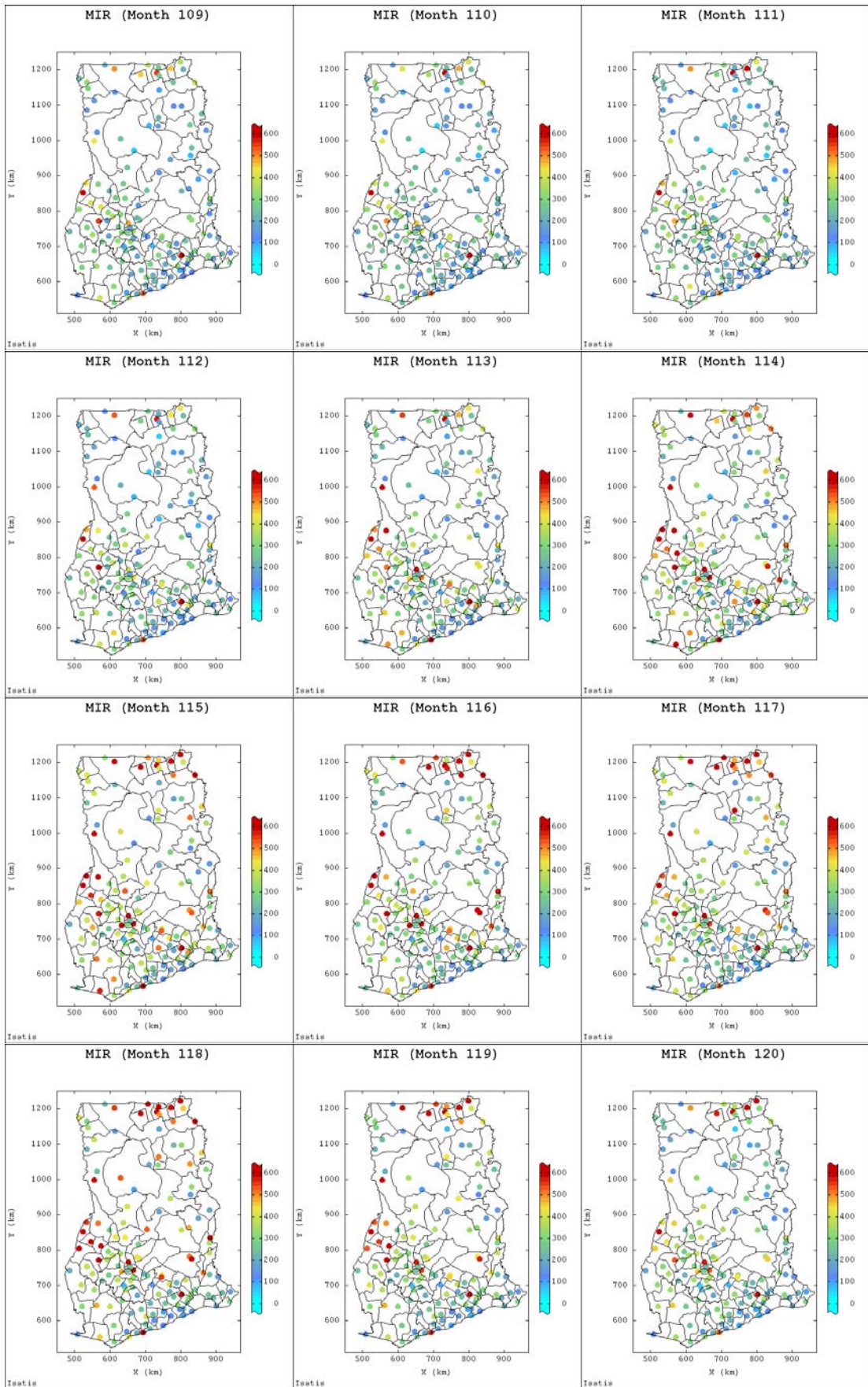


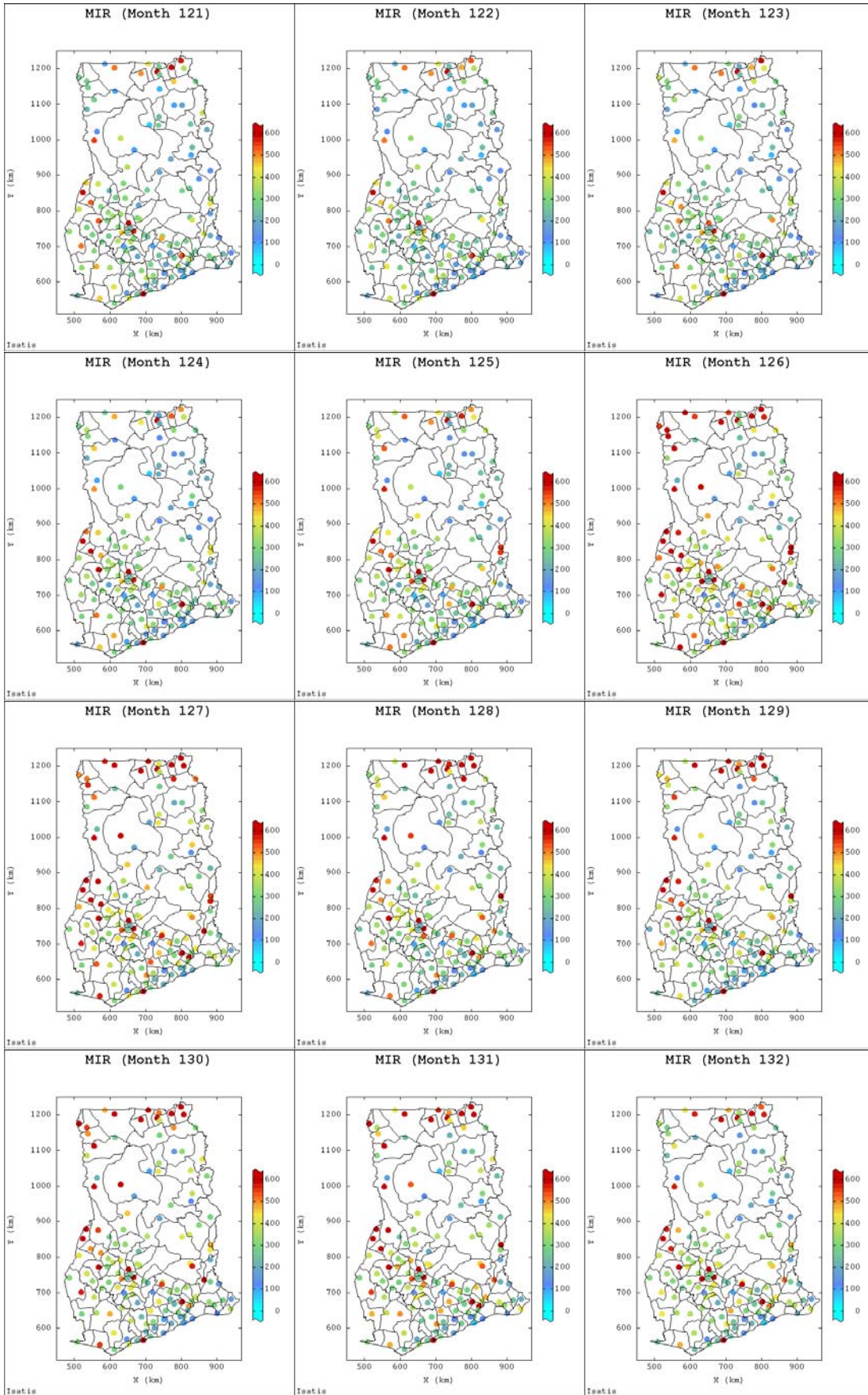












Appendix B-3: Monthly Spatial Correlation of MIR and Elevation with Climate Variables

Results B-3.1: The following gives month by month spatial correlations of elevation with MIR and climatic covariates over the whole the study area in Ghana

 Month: 1

	MIR	Rainf	MaxTemp	MinTemp	RH0600	RH1500	Sunsh
MIR	1.0000	0.0841	0.2337	-0.1844	-0.227	-0.238	0.4237
Rainf	0.0841	1.0000	-0.0462	-0.0271	0.204	0.103	0.0407
MaxTemp	0.2337	-0.0462	1.0000	-0.2506	-0.566	-0.668	0.4820
MinTemp	-0.1844	-0.0271	-0.2506	1.0000	0.396	0.545	-0.2275
RH0600	-0.2269	0.2044	-0.5662	0.3957	1.000	0.802	-0.5332
RH1500	-0.2381	0.1027	-0.6684	0.5451	0.802	1.000	-0.4122
Sunsh	0.4237	0.0407	0.4820	-0.2275	-0.533	-0.412	1.0000
Elevation	0.1145	0.1693	0.0840	-0.5358	-0.296	-0.414	0.1533

Elevation

MIR	0.114
Rainf	0.169
MaxTemp	0.084
MinTemp	-0.536
RH0600	-0.296
RH1500	-0.414
Sunsh	0.153
Elevation	1.000

 Month: 2

	MIR	Rainf	MaxTemp	MinTemp	RH0600	RH1500	Sunsh
MIR	1.0000	-0.0751	0.115	-0.273	-0.322	-0.375	0.385
Rainf	-0.0751	1.0000	-0.286	0.116	0.380	0.209	-0.331
MaxTemp	0.1147	-0.2859	1.000	-0.365	-0.511	-0.596	0.301
MinTemp	-0.2725	0.1165	-0.365	1.000	0.325	0.457	-0.340
RH0600	-0.3224	0.3805	-0.511	0.325	1.000	0.788	-0.758
RH1500	-0.3753	0.2087	-0.596	0.457	0.788	1.000	-0.543
Sunsh	0.3851	-0.3306	0.301	-0.340	-0.758	-0.543	1.000
Elevation	0.1144	-0.0449	0.118	-0.439	-0.383	-0.511	0.287

Elevation

MIR	0.1144
Rainf	-0.0449
MaxTemp	0.1183
MinTemp	-0.4387
RH0600	-0.3827
RH1500	-0.5109
Sunsh	0.2872
Elevation	1.0000

 Month: 3

	MIR	Rainf	MaxTemp	MinTemp	RH0600	RH1500	Sunsh
MIR	1.0000	-0.0672	0.2661	-0.2175	-0.3002	-0.372	0.3259
Rainf	-0.0672	1.0000	-0.4464	-0.1787	0.5416	0.458	-0.4328
MaxTemp	0.2661	-0.4464	1.0000	-0.0429	-0.7850	-0.758	0.3388
MinTemp	-0.2175	-0.1787	-0.0429	1.0000	-0.0177	0.255	-0.0533
RH0600	-0.3002	0.5416	-0.7850	-0.0177	1.0000	0.742	-0.4519
RH1500	-0.3718	0.4582	-0.7581	0.2553	0.7419	1.000	-0.3951
Sunsh	0.3259	-0.4328	0.3388	-0.0533	-0.4519	-0.395	1.0000
Elevation	0.1075	-0.0788	0.1747	-0.4693	-0.2351	-0.448	0.0826

Elevation

MIR	0.1075
Rainf	-0.0788
MaxTemp	0.1747
MinTemp	-0.4693
RH0600	-0.2351
RH1500	-0.4481
Sunsh	0.0826
Elevation	1.0000

 Month: 4

	MIR	Rainf	MaxTemp	MinTemp	RH0600	RH1500	Sunsh
MIR	1.000	-0.133	0.303	0.170	-0.321	-0.366	0.277
Rainf	-0.133	1.000	-0.534	-0.480	0.574	0.385	-0.432
MaxTemp	0.303	-0.534	1.000	0.596	-0.802	-0.837	0.508
MinTemp	0.170	-0.480	0.596	1.000	-0.646	-0.451	0.504
RH0600	-0.321	0.574	-0.802	-0.646	1.000	0.820	-0.541
RH1500	-0.366	0.385	-0.837	-0.451	0.820	1.000	-0.398

```

Sunsh      0.277 -0.432  0.508  0.504 -0.541 -0.398  1.000
Elevation  0.160  0.188  0.130 -0.284 -0.195 -0.331 -0.071
Elevation
MIR        0.160
Rainf      0.188
MaxTemp    0.130
MinTemp    -0.284
RH0600     -0.195
RH1500     -0.331
Sunsh      -0.071
Elevation  1.000

```

Month: 5

```

MIR      Rainf MaxTemp MinTemp RH0600 RH1500 Sunsh
MIR      1.000 -0.0710 0.1665  0.122 -0.205 -0.242  0.171
Rainf    -0.071  1.0000 -0.2670 -0.137  0.255  0.389 -0.129
MaxTemp  0.166 -0.2670  1.0000  0.475 -0.744 -0.796  0.519
MinTemp  0.122 -0.1369  0.4745  1.000 -0.567 -0.326  0.362
RH0600  -0.205  0.2551 -0.7437 -0.567  1.000  0.742 -0.631
RH1500  -0.242  0.3893 -0.7965 -0.326  0.742  1.000 -0.554
Sunsh    0.171 -0.1289  0.5188  0.362 -0.631 -0.554  1.000
Elevation 0.253 -0.0959  0.0973 -0.377 -0.112 -0.293  0.151
Elevation
MIR      0.2532
Rainf    -0.0959
MaxTemp  0.0973
MinTemp  -0.3771
RH0600  -0.1119
RH1500  -0.2928
Sunsh    0.1513
Elevation 1.0000

```

Month: 6

```

MIR      Rainf MaxTemp MinTemp RH0600 RH1500 Sunsh
MIR      1.0000 0.0374 0.1516 0.0909 -0.2413 -0.3306 0.3442
Rainf    0.0374 1.0000 -0.0946 -0.1093 0.0711 0.2302 -0.3004
MaxTemp  0.1516 -0.0946  1.0000  0.1401 -0.4924 -0.6029 0.4473
MinTemp  0.0909 -0.1093  0.1401  1.0000 -0.4068 0.0893 -0.0158
RH0600  -0.2413 0.0711 -0.4924 -0.4068  1.0000 0.4503 -0.3813
RH1500  -0.3306 0.2302 -0.6029 0.0893 0.4503 1.0000 -0.7353
Sunsh    0.3442 -0.3004 0.4473 -0.0158 -0.3813 -0.7353 1.0000
Elevation 0.1254 0.0183 0.1569 -0.5355 0.0190 -0.2721 0.1599
Elevation
MIR      0.1254
Rainf    0.0183
MaxTemp  0.1569
MinTemp  -0.5355
RH0600  0.0190
RH1500  -0.2721
Sunsh    0.1599
Elevation 1.0000

```

Month: 7

```

MIR      Rainf MaxTemp MinTemp RH0600 RH1500 Sunsh
MIR      1.0000 0.2996 0.285  0.187 -0.1747 -0.411 0.309
Rainf    0.2996 1.0000 0.334  -0.142 0.0697 -0.427 0.123
MaxTemp  0.2847 0.3339  1.000  0.209 -0.3304 -0.596 0.373
MinTemp  0.1871 -0.1423  0.209  1.000 -0.3476 -0.167 0.201
RH0600  -0.1747 0.0697 -0.330 -0.348  1.0000 0.362 -0.297
RH1500  -0.4105 -0.4272 -0.596 -0.167 0.3622  1.000 -0.275
Sunsh    0.3091 0.1227 0.373  0.201 -0.2972 -0.275 1.000
Elevation 0.0738 0.3668 0.134  -0.479 0.2059 -0.298 -0.076
Elevation
MIR      0.0738
Rainf    0.3668
MaxTemp  0.1342
MinTemp  -0.4790
RH0600  0.2059
RH1500  -0.2985
Sunsh    -0.0760
Elevation 1.0000

```

Month: 8

```

MIR      Rainf MaxTemp MinTemp RH0600 RH1500 Sunsh
MIR      1.0000 0.3250 0.244  0.0876 0.1124 -0.1578 0.4782
Rainf    0.3250 1.0000 0.556  0.0924 0.2061 -0.3988 0.5118
MaxTemp  0.2441 0.5556  1.000  0.3291 -0.1979 -0.5980 0.4761

```

MinTemp	0.0876	0.0924	0.329	1.0000	-0.4136	-0.0629	0.2467
RH0600	0.1124	0.2061	-0.198	-0.4136	1.0000	0.1987	-0.0538
RH1500	-0.1578	-0.3988	-0.598	-0.0629	0.1987	1.0000	-0.2998
Sunsh	0.4782	0.5118	0.476	0.2467	-0.0538	-0.2998	1.0000
Elevation	0.1097	0.2346	0.173	-0.4488	0.2386	-0.2531	0.0321

Elevation							
MIR	0.1097						
Rainf	0.2346						
MaxTemp	0.1730						
MinTemp	-0.4488						
RH0600	0.2386						
RH1500	-0.2531						
Sunsh	0.0321						
Elevation	1.0000						

Month: 9

	MIR	Rainf	MaxTemp	MinTemp	RH0600	RH1500	Sunsh
MIR	1.0000	0.0714	0.2181	-0.0232	0.1576	-0.1693	0.3480
Rainf	0.0714	1.0000	0.3805	-0.3063	0.4043	-0.4145	0.0327
MaxTemp	0.2181	0.3805	1.0000	0.2072	-0.2926	-0.5562	0.3526
MinTemp	-0.0232	-0.3063	0.2072	1.0000	-0.4865	0.1489	0.1253
RH0600	0.1576	0.4043	-0.2926	-0.4865	1.0000	0.0764	-0.2610
RH1500	-0.1693	-0.4145	-0.5562	0.1489	0.0764	1.0000	-0.1506
Sunsh	0.3480	0.0327	0.3526	0.1253	-0.2610	-0.1506	1.0000
Elevation	0.0727	0.3500	0.0683	-0.5102	0.2698	-0.2805	-0.0520

Elevation							
MIR	0.0727						
Rainf	0.3500						
MaxTemp	0.0683						
MinTemp	-0.5102						
RH0600	0.2698						
RH1500	-0.2805						
Sunsh	-0.0520						
Elevation	1.0000						

Month: 10

	MIR	Rainf	MaxTemp	MinTemp	RH0600	RH1500	Sunsh
MIR	1.0000	-0.215	0.3871	0.1253	-0.0982	-0.4655	0.153
Rainf	-0.2147	1.000	-0.4716	-0.5567	0.6314	0.3537	-0.311
MaxTemp	0.3871	-0.472	1.0000	0.3083	-0.5227	-0.7170	0.337
MinTemp	0.1253	-0.557	0.3083	1.0000	-0.3824	-0.0141	0.322
RH0600	-0.0982	0.631	-0.5227	-0.3824	1.0000	0.4671	-0.295
RH1500	-0.4655	0.354	-0.7170	-0.0141	0.4671	1.0000	-0.243
Sunsh	0.1531	-0.311	0.3367	0.3217	-0.2953	-0.2429	1.000
Elevation	0.0592	0.194	0.0204	-0.5429	0.0405	-0.2525	-0.215

Elevation							
MIR	0.0592						
Rainf	0.1942						
MaxTemp	0.0204						
MinTemp	-0.5429						
RH0600	0.0405						
RH1500	-0.2525						
Sunsh	-0.2153						
Elevation	1.0000						

Month: 11

	MIR	Rainf	MaxTemp	MinTemp	RH0600	RH1500	Sunsh
MIR	1.000	-0.2742	0.3331	-0.4165	-0.431	-0.505	0.3296
Rainf	-0.274	1.0000	-0.5707	0.0186	0.508	0.566	-0.6415
MaxTemp	0.333	-0.5707	1.0000	-0.2210	-0.721	-0.833	0.5509
MinTemp	-0.417	0.0186	-0.2210	1.0000	0.257	0.427	0.0438
RH0600	-0.431	0.5085	-0.7209	0.2572	1.000	0.792	-0.5384
RH1500	-0.505	0.5661	-0.8329	0.4273	0.792	1.000	-0.5107
Sunsh	0.330	-0.6415	0.5509	0.0438	-0.538	-0.511	1.0000
Elevation	0.170	-0.0833	0.0483	-0.5110	-0.136	-0.227	-0.1619

Elevation							
MIR	0.1699						
Rainf	-0.0833						
MaxTemp	0.0483						
MinTemp	-0.5110						
RH0600	-0.1356						
RH1500	-0.2265						
Sunsh	-0.1619						
Elevation	1.0000						

Month: 12

MIR	Rainf	MaxTemp	MinTemp	RH0600	RH1500	Sunsh
-----	-------	---------	---------	--------	--------	-------

MIR	1.000	-0.181	0.2670	-0.359	-0.308	-0.380	0.346
Rainf	-0.181	1.000	-0.5155	0.404	0.345	0.452	-0.305
MaxTemp	0.267	-0.515	1.0000	-0.559	-0.710	-0.777	0.553
MinTemp	-0.359	0.404	-0.5588	1.000	0.649	0.719	-0.418
RH0600	-0.308	0.345	-0.7097	0.649	1.000	0.813	-0.716
RH1500	-0.380	0.452	-0.7771	0.719	0.813	1.000	-0.637
Sunsh	0.346	-0.305	0.5534	-0.418	-0.716	-0.637	1.000
Elevation	0.120	-0.237	0.0775	-0.418	-0.249	-0.342	0.127

Elevation

MIR	0.1196
Rainf	-0.2370
MaxTemp	0.0775
MinTemp	-0.4176
RH0600	-0.2493
RH1500	-0.3419
Sunsh	0.1269
Elevation	1.0000

Month: 13

	MIR	Rainf	MaxTemp	MinTemp	RH0600	RH1500	Sunsh
MIR	1.000	-0.170	0.137	-0.245	-0.161	-0.293	0.278
Rainf	-0.170	1.000	-0.400	0.215	0.350	0.364	-0.435
MaxTemp	0.137	-0.400	1.000	-0.661	-0.676	-0.756	0.559
MinTemp	-0.245	0.215	-0.661	1.000	0.600	0.697	-0.538
RH0600	-0.161	0.350	-0.676	0.600	1.000	0.819	-0.712
RH1500	-0.293	0.364	-0.756	0.697	0.819	1.000	-0.619
Sunsh	0.278	-0.435	0.559	-0.538	-0.712	-0.619	1.000
Elevation	0.243	-0.129	0.217	-0.397	-0.302	-0.450	0.261

Elevation

MIR	0.243
Rainf	-0.129
MaxTemp	0.217
MinTemp	-0.397
RH0600	-0.302
RH1500	-0.450
Sunsh	0.261
Elevation	1.000

Month: 14

	MIR	Rainf	MaxTemp	MinTemp	RH0600	RH1500	Sunsh
MIR	1.000	-0.15095	0.144	-0.2952	-0.290	-0.436	0.472
Rainf	-0.151	1.00000	-0.460	0.0943	0.557	0.440	-0.463
MaxTemp	0.144	-0.45957	1.000	-0.3649	-0.622	-0.669	0.576
MinTemp	-0.295	0.09425	-0.365	1.0000	0.402	0.439	-0.316
RH0600	-0.290	0.55712	-0.622	0.4018	1.000	0.790	-0.834
RH1500	-0.436	0.44013	-0.669	0.4391	0.790	1.000	-0.698
Sunsh	0.472	-0.46266	0.576	-0.3163	-0.834	-0.698	1.000
Elevation	0.239	-0.00198	0.214	-0.4327	-0.325	-0.456	0.303

Elevation

MIR	0.23872
Rainf	-0.00198
MaxTemp	0.21397
MinTemp	-0.43273
RH0600	-0.32538
RH1500	-0.45565
Sunsh	0.30260
Elevation	1.00000

Month: 15

	MIR	Rainf	MaxTemp	MinTemp	RH0600	RH1500	Sunsh
MIR	1.0000	-0.148	0.276	0.0223	-0.295	-0.448	0.3490
Rainf	-0.1481	1.000	-0.559	-0.4477	0.521	0.426	-0.3784
MaxTemp	0.2762	-0.559	1.000	0.4581	-0.799	-0.834	0.5588
MinTemp	0.0223	-0.448	0.458	1.0000	-0.471	-0.268	0.4145
RH0600	-0.2951	0.521	-0.799	-0.4709	1.000	0.819	-0.6926
RH1500	-0.4477	0.426	-0.834	-0.2682	0.819	1.000	-0.5123
Sunsh	0.3490	-0.378	0.559	0.4145	-0.693	-0.512	1.0000
Elevation	0.1318	0.107	0.157	-0.3116	-0.180	-0.372	-0.0507

Elevation

MIR	0.1318
Rainf	0.1067
MaxTemp	0.1573
MinTemp	-0.3116
RH0600	-0.1797
RH1500	-0.3718
Sunsh	-0.0507
Elevation	1.0000

```

-----
Month: 16
      MIR   Rainf MaxTemp MinTemp RH0600 RH1500  Sunsh
MIR      1.000 -0.1324  0.169  0.138 -0.102 -0.259  0.211
Rainf    -0.132 1.0000  -0.573 -0.469  0.529  0.484 -0.477
MaxTemp  0.169 -0.5732  1.000  0.693 -0.786 -0.832  0.502
MinTemp  0.138 -0.4694  0.693  1.000 -0.637 -0.493  0.488
RH0600   -0.102 0.5293  -0.786 -0.637  1.000  0.852 -0.631
RH1500   -0.259 0.4838  -0.832 -0.493  0.852  1.000 -0.511
Sunsh    0.211 -0.4771  0.502  0.488 -0.631 -0.511  1.000
Elevation 0.204 0.0128  0.128 -0.265 -0.152 -0.319  0.109
      Elevation
MIR      0.2036
Rainf    0.0128
MaxTemp  0.1276
MinTemp  -0.2649
RH0600   -0.1523
RH1500   -0.3191
Sunsh    0.1093
Elevation 1.0000
-----

```

```

-----
Month: 17
      MIR   Rainf MaxTemp MinTemp RH0600  RH1500  Sunsh
MIR      1.00000 -0.2587 -0.0886 -0.1414  0.1042 -0.00438  0.114
Rainf    -0.25869 1.0000  -0.4772  0.0184  0.3422  0.58533 -0.418
MaxTemp  -0.08858 -0.4772  1.0000  0.5708 -0.7341 -0.80975  0.577
MinTemp  -0.14141 0.0184  0.5708  1.0000 -0.5452 -0.41791  0.420
RH0600   0.10418 0.3422  -0.7341 -0.5452  1.0000  0.79061 -0.603
RH1500   -0.00438 0.5853  -0.8097 -0.4179  0.7906  1.00000 -0.660
Sunsh    0.11446 -0.4178  0.5766  0.4199 -0.6026 -0.66010  1.000
Elevation 0.38710 -0.2857  0.0254 -0.3988 -0.0952 -0.22957  0.100
      Elevation
MIR      0.3871
Rainf    -0.2857
MaxTemp  0.0254
MinTemp  -0.3988
RH0600   -0.0952
RH1500   -0.2296
Sunsh    0.1003
Elevation 1.0000
-----

```

```

-----
Month: 18
      MIR   Rainf MaxTemp MinTemp RH0600  RH1500  Sunsh
MIR      1.0000  0.1707 -0.0738 -0.1566  0.0656 -0.1392  0.1522
Rainf    0.1707  1.0000 -0.1507  0.0318  0.1165  0.2828 -0.4073
MaxTemp  -0.0738 -0.1507  1.0000  0.2092 -0.4648 -0.6858  0.5672
MinTemp  -0.1566  0.0318  0.2092  1.0000 -0.3694  0.0485  0.0368
RH0600   0.0656  0.1165 -0.4648 -0.3694  1.0000  0.5013 -0.6791
RH1500   -0.1392 0.2828 -0.6858  0.0485  0.5013  1.0000 -0.6757
Sunsh    0.1522 -0.4073  0.5672  0.0368 -0.6791 -0.6757  1.0000
Elevation 0.2870 -0.2151  0.0632 -0.4416  0.0686 -0.3496  0.1991
      Elevation
MIR      0.2870
Rainf    -0.2151
MaxTemp  0.0632
MinTemp  -0.4416
RH0600   0.0686
RH1500   -0.3496
Sunsh    0.1991
Elevation 1.0000
-----

```

```

-----
Month: 19
      MIR   Rainf MaxTemp MinTemp RH0600  RH1500  Sunsh
MIR      1.0000  0.13536 0.1328 -0.0163  0.01248 -0.2811  0.1571
Rainf    0.1354  1.00000  0.1085  0.0825 -0.00881 -0.0248  0.0962
MaxTemp  0.1328  0.10849  1.0000  0.3444 -0.41023 -0.6632  0.3969
MinTemp  -0.0163  0.08245  0.3444  1.0000 -0.52403 -0.0190  0.2314
RH0600   0.0125 -0.00881 -0.4102 -0.5240  1.00000  0.3967 -0.4841
RH1500   -0.2811 -0.02477 -0.6632 -0.0190  0.39670  1.0000 -0.3436
Sunsh    0.1571  0.09623  0.3969  0.2314 -0.48414 -0.3436  1.0000
Elevation 0.1637 0.00315  0.0542 -0.4793  0.10295 -0.3669  0.0276
      Elevation
MIR      0.16366
Rainf    0.00315
MaxTemp  0.05419
MinTemp  -0.47932
RH0600   0.10295
-----

```

RH1500 -0.36693
Sunsh 0.02763
Elevation 1.00000

Month: 20

	MIR	Rainf	MaxTemp	MinTemp	RH0600	RH1500	Sunsh
MIR	1.0000	0.3969	0.3080	0.1217	0.2345	-0.2769	0.4274
Rainf	0.3969	1.0000	0.6058	0.2587	0.0955	-0.3533	0.5661
MaxTemp	0.3080	0.6058	1.0000	0.5061	-0.2708	-0.5833	0.3696
MinTemp	0.1217	0.2587	0.5061	1.0000	-0.4578	-0.0623	0.0264
RH0600	0.2345	0.0955	-0.2708	-0.4578	1.0000	0.3342	-0.0349
RH1500	-0.2769	-0.3533	-0.5833	-0.0623	0.3342	1.0000	-0.3069
Sunsh	0.4274	0.5661	0.3696	0.0264	-0.0349	-0.3069	1.0000
Elevation	0.0907	0.1546	0.0368	-0.4116	0.1346	-0.3989	0.1210

Elevation
MIR 0.0907
Rainf 0.1546
MaxTemp 0.0368
MinTemp -0.4116
RH0600 0.1346
RH1500 -0.3989
Sunsh 0.1210
Elevation 1.0000

Month: 21

	MIR	Rainf	MaxTemp	MinTemp	RH0600	RH1500	Sunsh
MIR	1.0000	0.1170	0.1774	-0.0708	0.279	-0.3516	0.3742
Rainf	0.1170	1.0000	0.1884	-0.4026	0.279	-0.3310	-0.0287
MaxTemp	0.1774	0.1884	1.0000	0.2711	-0.240	-0.6918	0.3451
MinTemp	-0.0708	-0.4026	0.2711	1.0000	-0.454	0.0728	0.1320
RH0600	0.2786	0.2794	-0.2401	-0.4542	1.000	0.2105	-0.2138
RH1500	-0.3516	-0.3310	-0.6918	0.0728	0.211	1.0000	-0.3204
Sunsh	0.3742	-0.0287	0.3451	0.1320	-0.214	-0.3204	1.0000
Elevation	0.1130	0.2696	0.0506	-0.4563	0.198	-0.2950	-0.0689

Elevation
MIR 0.1130
Rainf 0.2696
MaxTemp 0.0506
MinTemp -0.4563
RH0600 0.1979
RH1500 -0.2950
Sunsh -0.0689
Elevation 1.0000

Month: 22

	MIR	Rainf	MaxTemp	MinTemp	RH0600	RH1500	Sunsh
MIR	1.000	-0.164	0.2825	-0.125	-0.2814	-0.489	0.4689
Rainf	-0.164	1.000	-0.3643	-0.317	0.4180	0.335	-0.4456
MaxTemp	0.282	-0.364	1.0000	0.332	-0.6157	-0.825	0.5697
MinTemp	-0.125	-0.317	0.3317	1.000	-0.3904	-0.125	0.3585
RH0600	-0.281	0.418	-0.6157	-0.390	1.0000	0.707	-0.5124
RH1500	-0.489	0.335	-0.8252	-0.125	0.7071	1.000	-0.5017
Sunsh	0.469	-0.446	0.5697	0.358	-0.5124	-0.502	1.0000
Elevation	0.140	0.123	0.0507	-0.449	-0.0031	-0.172	-0.0385

Elevation
MIR 0.1396
Rainf 0.1226
MaxTemp 0.0507
MinTemp -0.4489
RH0600 -0.0031
RH1500 -0.1721
Sunsh -0.0385
Elevation 1.0000

Month: 23

	MIR	Rainf	MaxTemp	MinTemp	RH0600	RH1500	Sunsh
MIR	1.000	-0.1935	0.2079	-0.4262	-0.252	-0.382	0.3204
Rainf	-0.194	1.0000	-0.5460	0.0865	0.385	0.537	-0.3195
MaxTemp	0.208	-0.5460	1.0000	-0.2493	-0.724	-0.859	0.6218
MinTemp	-0.426	0.0865	-0.2493	1.0000	0.281	0.489	-0.1229
RH0600	-0.252	0.3848	-0.7245	0.2812	1.000	0.799	-0.5759
RH1500	-0.382	0.5372	-0.8590	0.4892	0.799	1.000	-0.5898
Sunsh	0.320	-0.3195	0.6218	-0.1229	-0.576	-0.590	1.0000
Elevation	0.290	-0.0819	0.0487	-0.4830	-0.146	-0.228	-0.0154

Elevation
MIR 0.2903
Rainf -0.0819

MaxTemp 0.0487
 MinTemp -0.4830
 RH0600 -0.1462
 RH1500 -0.2281
 Sunsh -0.0154
 Elevation 1.0000

 Month: 24

	MIR	Rainf	MaxTemp	MinTemp	RH0600	RH1500	Sunsh
MIR	1.0000	-0.15583	0.0999	-0.336	-0.236	-0.332	0.4131
Rainf	-0.1558	1.00000	-0.2831	0.293	0.413	0.430	-0.2410
MaxTemp	0.0999	-0.28310	1.0000	-0.397	-0.691	-0.743	0.6141
MinTemp	-0.3356	0.29339	-0.3966	1.000	0.620	0.760	-0.3332
RH0600	-0.2363	0.41271	-0.6913	0.620	1.000	0.823	-0.6383
RH1500	-0.3322	0.42971	-0.7435	0.760	0.823	1.000	-0.5389
Sunsh	0.4131	-0.24104	0.6141	-0.333	-0.638	-0.539	1.0000
Elevation	0.1852	0.00829	0.0313	-0.367	-0.199	-0.314	0.0997

Elevation
 MIR 0.18523
 Rainf 0.00829
 MaxTemp 0.03133
 MinTemp -0.36711
 RH0600 -0.19931
 RH1500 -0.31351
 Sunsh 0.09971
 Elevation 1.00000

 Month: 25

	MIR	Rainf	MaxTemp	MinTemp	RH0600	RH1500	Sunsh
MIR	1.000	-0.337	0.1408	-0.223	-0.356	-0.397	0.544
Rainf	-0.337	1.000	-0.3621	0.598	0.496	0.538	-0.391
MaxTemp	0.141	-0.362	1.0000	-0.463	-0.545	-0.644	0.301
MinTemp	-0.223	0.598	-0.4633	1.000	0.545	0.694	-0.471
RH0600	-0.356	0.496	-0.5454	0.545	1.000	0.772	-0.648
RH1500	-0.397	0.538	-0.6438	0.694	0.772	1.000	-0.592
Sunsh	0.544	-0.391	0.3009	-0.471	-0.648	-0.592	1.000
Elevation	0.267	-0.281	0.0912	-0.395	-0.275	-0.356	0.345

Elevation
 MIR 0.2672
 Rainf -0.2812
 MaxTemp 0.0912
 MinTemp -0.3946
 RH0600 -0.2754
 RH1500 -0.3558
 Sunsh 0.3451
 Elevation 1.0000

 Month: 26

	MIR	Rainf	MaxTemp	MinTemp	RH0600	RH1500	Sunsh
MIR	1.000	-0.2688	0.145	-0.340	-0.371	-0.483	0.411
Rainf	-0.269	1.0000	-0.563	0.132	0.471	0.509	-0.316
MaxTemp	0.145	-0.5635	1.000	-0.491	-0.650	-0.734	0.379
MinTemp	-0.340	0.1324	-0.491	1.000	0.434	0.616	-0.388
RH0600	-0.371	0.4706	-0.650	0.434	1.000	0.758	-0.633
RH1500	-0.483	0.5094	-0.734	0.616	0.758	1.000	-0.553
Sunsh	0.411	-0.3156	0.379	-0.388	-0.633	-0.553	1.000
Elevation	0.242	-0.0536	0.213	-0.472	-0.280	-0.463	0.175

Elevation
 MIR 0.2415
 Rainf -0.0536
 MaxTemp 0.2132
 MinTemp -0.4722
 RH0600 -0.2795
 RH1500 -0.4631
 Sunsh 0.1746
 Elevation 1.0000

 Month: 27

	MIR	Rainf	MaxTemp	MinTemp	RH0600	RH1500	Sunsh
MIR	1.00000	-0.00638	0.335	0.143	-0.437	-0.525	0.4308
Rainf	-0.00638	1.00000	-0.470	-0.584	0.383	0.214	-0.1994
MaxTemp	0.33535	-0.46968	1.000	0.473	-0.776	-0.809	0.3954
MinTemp	0.14338	-0.58439	0.473	1.000	-0.490	-0.247	0.3547
RH0600	-0.43711	0.38302	-0.776	-0.490	1.000	0.813	-0.4013
RH1500	-0.52526	0.21446	-0.809	-0.247	0.813	1.000	-0.3365
Sunsh	0.43077	-0.19939	0.395	0.355	-0.401	-0.336	1.0000
Elevation	0.22639	0.22333	0.129	-0.319	-0.205	-0.352	0.0942

Elevation
MIR 0.2264
Rainf 0.2233
MaxTemp 0.1287
MinTemp -0.3192
RH0600 -0.2055
RH1500 -0.3524
Sunsh 0.0942
Elevation 1.0000

Month : 28

	MIR	Rainf	MaxTemp	MinTemp	RH0600	RH1500	Sunsh
MIR	1.0000	-0.139	0.0830	0.0738	-0.206	-0.276	0.0913
Rainf	-0.1387	1.000	-0.6436	-0.3821	0.600	0.554	-0.5096
MaxTemp	0.0830	-0.644	1.0000	0.6204	-0.797	-0.843	0.4979
MinTemp	0.0738	-0.382	0.6204	1.0000	-0.591	-0.400	0.4835
RH0600	-0.2062	0.600	-0.7967	-0.5912	1.000	0.833	-0.5649
RH1500	-0.2764	0.554	-0.8429	-0.4003	0.833	1.000	-0.4263
Sunsh	0.0913	-0.510	0.4979	0.4835	-0.565	-0.426	1.0000
Elevation	0.3287	-0.131	0.0708	-0.2927	-0.169	-0.302	-0.0351

Elevation
MIR 0.3287
Rainf -0.1308
MaxTemp 0.0708
MinTemp -0.2927
RH0600 -0.1690
RH1500 -0.3017
Sunsh -0.0351
Elevation 1.0000

Month: 29

	MIR	Rainf	MaxTemp	MinTemp	RH0600	RH1500	Sunsh
MIR	1.0000	0.1328	-0.0125	-0.076	-0.0941	-0.230	0.0387
Rainf	0.1328	1.0000	-0.3768	-0.370	0.3036	0.323	-0.5491
MaxTemp	-0.0125	-0.3768	1.0000	0.555	-0.7093	-0.798	0.5562
MinTemp	-0.0760	-0.3703	0.5547	1.000	-0.4989	-0.338	0.5469
RH0600	-0.0941	0.3036	-0.7093	-0.499	1.0000	0.752	-0.6482
RH1500	-0.2305	0.3227	-0.7976	-0.338	0.7524	1.000	-0.4826
Sunsh	0.0387	-0.5491	0.5562	0.547	-0.6482	-0.483	1.0000
Elevation	0.3280	0.0118	0.0150	-0.390	-0.1229	-0.259	-0.0842

Elevation
MIR 0.3280
Rainf 0.0118
MaxTemp 0.0150
MinTemp -0.3898
RH0600 -0.1229
RH1500 -0.2594
Sunsh -0.0842
Elevation 1.0000

Month: 30

	MIR	Rainf	MaxTemp	MinTemp	RH0600	RH1500	Sunsh
MIR	1.0000	-0.286	0.0793	0.103	-0.2258	-0.371	0.409
Rainf	-0.2861	1.000	-0.3313	0.061	0.1406	0.562	-0.467
MaxTemp	0.0793	-0.331	1.0000	0.299	-0.5396	-0.717	0.553
MinTemp	0.1027	0.061	0.2991	1.000	-0.3411	-0.211	0.191
RH0600	-0.2258	0.141	-0.5396	-0.341	1.0000	0.608	-0.542
RH1500	-0.3706	0.562	-0.7166	-0.211	0.6078	1.000	-0.718
Sunsh	0.4088	-0.467	0.5532	0.191	-0.5420	-0.718	1.000
Elevation	0.2424	-0.357	0.0589	-0.425	-0.0992	-0.310	0.278

Elevation
MIR 0.2424
Rainf -0.3571
MaxTemp 0.0589
MinTemp -0.4249
RH0600 -0.0992
RH1500 -0.3100
Sunsh 0.2781
Elevation 1.0000

Month: 31

	MIR	Rainf	MaxTemp	MinTemp	RH0600	RH1500	Sunsh
MIR	1.000	0.14047	0.356	0.2270	-0.2547	-0.6065	0.51924
Rainf	0.140	1.00000	0.207	0.0837	0.0598	0.0529	-0.00229
MaxTemp	0.356	0.20674	1.000	0.2645	-0.4241	-0.6935	0.58173
MinTemp	0.227	0.08369	0.265	1.0000	0.0252	-0.1245	0.32328
RH0600	-0.255	0.05978	-0.424	0.0252	1.0000	0.5256	-0.40771

RH1500 -0.606 0.05286 -0.693 -0.1245 0.5256 1.0000 -0.60377
 Sunsh 0.519 -0.00229 0.582 0.3233 -0.4077 -0.6038 1.00000
 Elevation 0.153 0.03320 0.106 -0.3982 -0.1440 -0.3402 0.22213

Elevation
 MIR 0.1531
 Rainf 0.0332
 MaxTemp 0.1057
 MinTemp -0.3982
 RH0600 -0.1440
 RH1500 -0.3402
 Sunsh 0.2221
 Elevation 1.0000

 Month: 32

	MIR	Rainf	MaxTemp	MinTemp	RH0600	RH1500	Sunsh
MIR	1.0000	0.3598	0.16805	0.11377	0.0681	-0.28249	0.3622
Rainf	0.3598	1.0000	0.38377	0.12644	0.1787	-0.08094	0.3484
MaxTemp	0.1681	0.3838	1.00000	0.33011	-0.3248	-0.56586	0.2690
MinTemp	0.1138	0.1264	0.33011	1.00000	0.0520	0.00864	0.4188
RH0600	0.0681	0.1787	-0.32482	0.05198	1.0000	0.35594	-0.0509
RH1500	-0.2825	-0.0809	-0.56586	0.00864	0.3559	1.00000	0.0350
Sunsh	0.3622	0.3484	0.26896	0.41885	-0.0509	0.03497	1.0000
Elevation	0.2347	0.1080	0.00117	-0.39239	-0.0322	-0.27811	-0.1183

Elevation
 MIR 0.23467
 Rainf 0.10796
 MaxTemp 0.00117
 MinTemp -0.39239
 RH0600 -0.03221
 RH1500 -0.27811
 Sunsh -0.11828
 Elevation 1.00000

 Month: 33

	MIR	Rainf	MaxTemp	MinTemp	RH0600	RH1500	Sunsh
MIR	1.0000	0.1955	0.2281	0.07118	-0.0589	-0.42351	0.4467
Rainf	0.1955	1.0000	0.0409	-0.43368	0.2634	-0.38412	-0.1231
MaxTemp	0.2281	0.0409	1.0000	0.12645	-0.3464	-0.68544	0.3804
MinTemp	0.0712	-0.4337	0.1265	1.00000	-0.1137	0.00634	0.2759
RH0600	-0.0589	0.2634	-0.3464	-0.11371	1.0000	0.28354	-0.3698
RH1500	-0.4235	-0.3841	-0.6854	0.00634	0.2835	1.00000	-0.2625
Sunsh	0.4467	-0.1231	0.3804	0.27594	-0.3698	-0.26247	1.0000
Elevation	0.2127	0.4342	0.0116	-0.44020	0.0685	-0.26551	-0.0682

Elevation
 MIR 0.2127
 Rainf 0.4342
 MaxTemp 0.0116
 MinTemp -0.4402
 RH0600 0.0685
 RH1500 -0.2655
 Sunsh -0.0682
 Elevation 1.0000

 Month: 34

	MIR	Rainf	MaxTemp	MinTemp	RH0600	RH1500	Sunsh
MIR	1.0000	0.0519	0.196	0.0455	-0.3192	-0.5407	0.357
Rainf	0.0519	1.0000	-0.316	-0.1810	0.2723	0.2065	-0.378
MaxTemp	0.1962	-0.3162	1.000	0.1548	-0.4321	-0.7054	0.478
MinTemp	0.0455	-0.1810	0.155	1.0000	-0.1579	0.0335	0.261
RH0600	-0.3192	0.2723	-0.432	-0.1579	1.0000	0.5452	-0.446
RH1500	-0.5407	0.2065	-0.705	0.0335	0.5452	1.0000	-0.483
Sunsh	0.3574	-0.3784	0.478	0.2608	-0.4463	-0.4827	1.000
Elevation	0.1794	0.1159	-0.022	-0.4733	-0.0837	-0.2260	-0.104

Elevation
 MIR 0.1794
 Rainf 0.1159
 MaxTemp -0.0220
 MinTemp -0.4733
 RH0600 -0.0837
 RH1500 -0.2260
 Sunsh -0.1035
 Elevation 1.0000

 Month: 35

	MIR	Rainf	MaxTemp	MinTemp	RH0600	RH1500	Sunsh
MIR	1.000	-0.312	0.23814	-0.2018	-0.421	-0.542	0.2948
Rainf	-0.312	1.000	-0.45466	0.2317	0.486	0.610	-0.5063

MaxTemp 0.238 -0.455 1.00000 -0.1732 -0.668 -0.752 0.5444
 MinTemp -0.202 0.232 -0.17322 1.0000 0.338 0.464 0.0807
 RH0600 -0.421 0.486 -0.66754 0.3375 1.000 0.831 -0.4523
 RH1500 -0.542 0.610 -0.75191 0.4637 0.831 1.000 -0.4568
 Sunsh 0.295 -0.506 0.54439 0.0807 -0.452 -0.457 1.0000
 Elevation 0.224 -0.341 0.00369 -0.4987 -0.161 -0.232 -0.0263

Elevation
 MIR 0.22366
 Rainf -0.34063
 MaxTemp 0.00369
 MinTemp -0.49866
 RH0600 -0.16101
 RH1500 -0.23218
 Sunsh -0.02626
 Elevation 1.00000

 Month: 36

	MIR	Rainf	MaxTemp	MinTemp	RH0600	RH1500	Sunsh
MIR	1.000	-0.2018	0.22063	-0.202	-0.295	-0.482	0.4626
Rainf	-0.202	1.0000	-0.53102	0.202	0.396	0.485	-0.3868
MaxTemp	0.221	-0.5310	1.00000	-0.483	-0.700	-0.730	0.5802
MinTemp	-0.202	0.2016	-0.48255	1.000	0.511	0.667	-0.2890
RH0600	-0.295	0.3957	-0.69998	0.511	1.000	0.841	-0.6674
RH1500	-0.482	0.4851	-0.73021	0.667	0.841	1.000	-0.6083
Sunsh	0.463	-0.3868	0.58024	-0.289	-0.667	-0.608	1.0000
Elevation	0.233	-0.0953	-0.00484	-0.448	-0.292	-0.375	0.0902

Elevation
 MIR 0.23312
 Rainf -0.09533
 MaxTemp -0.00484
 MinTemp -0.44787
 RH0600 -0.29212
 RH1500 -0.37483
 Sunsh 0.09020
 Elevation 1.00000

 Month : 37

	MIR	Rainf	MaxTemp	MinTemp	RH0600	RH1500	Sunsh
MIR	1.00000	-0.138	0.00524	-0.041	-0.0697	-0.191	0.401
Rainf	-0.13830	1.000	-0.21946	0.413	0.4720	0.499	-0.474
MaxTemp	0.00524	-0.219	1.00000	-0.400	-0.5659	-0.626	0.471
MinTemp	-0.04098	0.413	-0.40043	1.000	0.5059	0.690	-0.417
RH0600	-0.06971	0.472	-0.56595	0.506	1.0000	0.777	-0.690
RH1500	-0.19074	0.499	-0.62641	0.690	0.7765	1.000	-0.664
Sunsh	0.40100	-0.474	0.47138	-0.417	-0.6902	-0.664	1.000
Elevation	0.12532	-0.123	0.07687	-0.421	-0.3184	-0.432	0.283

Elevation
 MIR 0.1253
 Rainf -0.1234
 MaxTemp 0.0769
 MinTemp -0.4213
 RH0600 -0.3184
 RH1500 -0.4321
 Sunsh 0.2826
 Elevation 1.0000

 Month : 38

	MIR	Rainf	MaxTemp	MinTemp	RH0600	RH1500	Sunsh
MIR	1.0000	-0.1831	0.0602	-0.0527	-0.196	-0.270	0.2842
Rainf	-0.1831	1.0000	-0.4421	-0.1757	0.563	0.319	-0.4097
MaxTemp	0.0602	-0.4421	1.0000	-0.1177	-0.699	-0.713	0.4177
MinTemp	-0.0527	-0.1757	-0.1177	1.0000	0.168	0.407	0.0877
RH0600	-0.1965	0.5635	-0.6992	0.1677	1.000	0.756	-0.3694
RH1500	-0.2701	0.3190	-0.7126	0.4069	0.756	1.000	-0.2339
Sunsh	0.2842	-0.4097	0.4177	0.0877	-0.369	-0.234	1.0000
Elevation	0.1637	0.0207	0.1338	-0.4683	-0.263	-0.472	-0.0624

Elevation
 MIR 0.1637
 Rainf 0.0207
 MaxTemp 0.1338
 MinTemp -0.4683
 RH0600 -0.2630
 RH1500 -0.4719
 Sunsh -0.0624
 Elevation 1.0000

 Month : 39

	MIR	Rainf	MaxTemp	MinTemp	RH0600	RH1500	Sunsh
MIR	1.0000	-0.1022	0.0853	-0.0709	-0.170	-0.2598	0.385
Rainf	-0.1022	1.0000	-0.5921	-0.5161	0.518	0.4314	-0.357
MaxTemp	0.0853	-0.5921	1.0000	0.2950	-0.756	-0.8000	0.466
MinTemp	-0.0709	-0.5161	0.2950	1.0000	-0.283	-0.0588	0.146
RH0600	-0.1696	0.5183	-0.7562	-0.2830	1.000	0.8208	-0.581
RH1500	-0.2598	0.4314	-0.8000	-0.0588	0.821	1.0000	-0.520
Sunsh	0.3852	-0.3569	0.4663	0.1462	-0.581	-0.5198	1.000
Elevation	0.1386	-0.0155	0.1477	-0.3914	-0.211	-0.4153	0.144

Elevation

MIR	0.1386
Rainf	-0.0155
MaxTemp	0.1477
MinTemp	-0.3914
RH0600	-0.2111
RH1500	-0.4153
Sunsh	0.1441
Elevation	1.0000

Month: 40

	MIR	Rainf	MaxTemp	MinTemp	RH0600	RH1500	Sunsh
MIR	1.000000	0.000949	-0.0187	-0.0063	-0.100	-0.191	0.206
Rainf	0.000949	1.000000	-0.5798	-0.3711	0.546	0.488	-0.410
MaxTemp	-0.018740	-0.579771	1.0000	0.5464	-0.801	-0.791	0.443
MinTemp	-0.006298	-0.371148	0.5464	1.0000	-0.515	-0.306	0.308
RH0600	-0.100315	0.546273	-0.8014	-0.5152	1.000	0.834	-0.555
RH1500	-0.191233	0.487557	-0.7915	-0.3057	0.834	1.000	-0.482
Sunsh	0.206364	-0.410415	0.4430	0.3083	-0.555	-0.482	1.000
Elevation	0.153387	-0.064850	0.0993	-0.2998	-0.220	-0.352	0.126

Elevation

MIR	0.1534
Rainf	-0.0648
MaxTemp	0.0993
MinTemp	-0.2998
RH0600	-0.2204
RH1500	-0.3517
Sunsh	0.1259
Elevation	1.0000

Month : 41

	MIR	Rainf	MaxTemp	MinTemp	RH0600	RH1500	Sunsh
MIR	1.0000	0.2649	-0.2255	-0.0753	0.082	-0.0177	0.0794
Rainf	0.2649	1.0000	-0.2811	-0.0811	0.153	0.2035	-0.2665
MaxTemp	-0.2255	-0.2811	1.0000	0.4123	-0.735	-0.7598	0.5696
MinTemp	-0.0753	-0.0811	0.4123	1.0000	-0.379	-0.2562	0.4365
RH0600	0.0820	0.1527	-0.7349	-0.3794	1.000	0.7978	-0.7010
RH1500	-0.0177	0.2035	-0.7598	-0.2562	0.798	1.0000	-0.6506
Sunsh	0.0794	-0.2665	0.5696	0.4365	-0.701	-0.6506	1.0000
Elevation	0.2437	0.0858	0.0814	-0.3858	-0.179	-0.3417	0.0895

Elevation

MIR	0.2437
Rainf	0.0858
MaxTemp	0.0814
MinTemp	-0.3858
RH0600	-0.1795
RH1500	-0.3417
Sunsh	0.0895
Elevation	1.0000

Month : 42

	MIR	Rainf	MaxTemp	MinTemp	RH0600	RH1500	Sunsh
MIR	1.0000	0.0204	-0.0765	0.042021	0.0134	-0.1110	0.116317
Rainf	0.0204	1.0000	-0.1473	0.028207	0.0257	0.2334	-0.295281
MaxTemp	-0.0765	-0.1473	1.0000	0.214915	-0.5581	-0.6290	0.492556
MinTemp	0.0420	0.0282	0.2149	1.000000	-0.1100	0.0618	0.000932
RH0600	0.0134	0.0257	-0.5581	-0.110027	1.0000	0.6093	-0.497681
RH1500	-0.1110	0.2334	-0.6290	0.061773	0.6093	1.0000	-0.653141
Sunsh	0.1163	-0.2953	0.4926	0.000932	-0.4977	-0.6531	1.000000
Elevation	0.1548	-0.2340	0.0551	-0.437082	-0.2087	-0.3687	0.197578

Elevation

MIR	0.1548
Rainf	-0.2340
MaxTemp	0.0551
MinTemp	-0.4371
RH0600	-0.2087
RH1500	-0.3687
Sunsh	0.1976

```

Elevation      1.0000
-----
Month : 43
      MIR   Rainf MaxTemp MinTemp  RH0600  RH1500  Sunsh
MIR      1.00000 0.1927  0.0825  0.0904 -0.00056 -0.2648  0.1360
Rainf    0.19270 1.0000  0.4331  0.1542  0.06581 -0.4503  0.0383
MaxTemp  0.08254 0.4331  1.0000  0.1805 -0.21124 -0.5820  0.3360
MinTemp  0.09035 0.1542  0.1805  1.0000 -0.09772 -0.0827  0.3023
RH0600   -0.00056 0.0658 -0.2112 -0.0977  1.00000  0.3369 -0.1567
RH1500   -0.26475 -0.4503 -0.5820 -0.0827  0.33689  1.0000 -0.1844
Sunsh    0.13599 0.0383  0.3360  0.3023 -0.15670 -0.1844  1.0000
Elevation 0.16293 0.1443 -0.0188 -0.4306 -0.07869 -0.3415 -0.0714
      Elevation
MIR      0.1629
Rainf    0.1443
MaxTemp  -0.0188
MinTemp  -0.4306
RH0600   -0.0787
RH1500   -0.3415
Sunsh    -0.0714
Elevation 1.0000
-----
Month : 44
      MIR   Rainf MaxTemp MinTemp  RH0600  RH1500  Sunsh
MIR      1.0000  0.3074  0.1935  0.1032  0.0493 -0.2421  0.301210
Rainf    0.3074  1.0000  0.5518  0.1734  0.0051 -0.3756  0.318496
MaxTemp  0.1935  0.5518  1.0000  0.1805 -0.3232 -0.5664  0.334132
MinTemp  0.1032  0.1734  0.1805  1.0000 -0.0196 -0.0199  0.280356
RH0600   0.0493  0.0051 -0.3232 -0.0196  1.0000  0.4408 -0.019672
RH1500  -0.2421 -0.3756 -0.5664 -0.0199  0.4408  1.0000 -0.154055
Sunsh    0.3012  0.3185  0.3341  0.2804 -0.0197 -0.1541  1.000000
Elevation 0.1613  0.1144  0.0929 -0.3768 -0.1000 -0.3836  0.000296
      Elevation
MIR      0.161280
Rainf    0.114433
MaxTemp  0.092875
MinTemp  -0.376816
RH0600   -0.100048
RH1500   -0.383558
Sunsh    0.000296
Elevation 1.000000
-----
Month : 45
      MIR   Rainf MaxTemp MinTemp  RH0600  RH1500  Sunsh
MIR      1.0000  0.360  0.1132 -0.0822  0.1473 -0.2967  0.390
Rainf    0.3604  1.000  0.1808 -0.4435  0.2086 -0.4038  0.147
MaxTemp  0.1132  0.181  1.0000  0.1020 -0.3509 -0.6916  0.410
MinTemp  -0.0822 -0.443  0.1020  1.0000 -0.2511  0.0467  0.255
RH0600   0.1473  0.209 -0.3509 -0.2511  1.0000  0.2311 -0.203
RH1500  -0.2967 -0.404 -0.6916  0.0467  0.2311  1.0000 -0.318
Sunsh    0.3897  0.147  0.4099  0.2547 -0.2032 -0.3180  1.000
Elevation 0.1789  0.366 -0.0351 -0.4733  0.0366 -0.3129 -0.102
      Elevation
MIR      0.1789
Rainf    0.3660
MaxTemp  -0.0351
MinTemp  -0.4733
RH0600   0.0366
RH1500  -0.3129
Sunsh    -0.1025
Elevation 1.0000
-----
Month : 46
      MIR   Rainf MaxTemp MinTemp  RH0600  RH1500  Sunsh
MIR      1.0000 -0.2036  0.1819 -0.0397 -0.134 -0.3790  0.186
Rainf    -0.2036  1.0000 -0.4192 -0.0779  0.208  0.3722 -0.583
MaxTemp  0.1819 -0.4192  1.0000  0.2393 -0.459 -0.7233  0.589
MinTemp  -0.0397 -0.0779  0.2393  1.0000 -0.120  0.0335  0.332
RH0600   -0.1344  0.2078 -0.4594 -0.1198  1.000  0.5057 -0.422
RH1500  -0.3790  0.3722 -0.7233  0.0335  0.506  1.0000 -0.460
Sunsh    0.1857 -0.5829  0.5895  0.3323 -0.422 -0.4603  1.000
Elevation 0.1680 -0.0303  0.0041 -0.4601 -0.153 -0.2916 -0.081
      Elevation
MIR      0.1680
Rainf    -0.0303
MaxTemp  0.0041
MinTemp  -0.4601

```

RH0600 -0.1530
 RH1500 -0.2916
 Sunsh -0.0810
 Elevation 1.0000

 Month : 47

	MIR	Rainf	MaxTemp	MinTemp	RH0600	RH1500	Sunsh
MIR	1.0000	-0.0136	0.0798	-0.1187	-0.3023	-0.339	0.162
Rainf	-0.0136	1.0000	-0.5333	-0.0813	0.4460	0.556	-0.587
MaxTemp	0.0798	-0.5333	1.0000	-0.0422	-0.6637	-0.796	0.608
MinTemp	-0.1187	-0.0813	-0.0422	1.0000	0.0352	0.219	0.126
RH0600	-0.3023	0.4460	-0.6637	0.0352	1.0000	0.802	-0.562
RH1500	-0.3391	0.5561	-0.7959	0.2187	0.8018	1.000	-0.599
Sunsh	0.1621	-0.5868	0.6077	0.1261	-0.5619	-0.599	1.000
Elevation	0.2221	-0.0389	0.0126	-0.4407	-0.1834	-0.241	-0.101

Elevation
 MIR 0.2221
 Rainf -0.0389
 MaxTemp 0.0126
 MinTemp -0.4407
 RH0600 -0.1834
 RH1500 -0.2411
 Sunsh -0.1006
 Elevation 1.0000

 Month : 48

	MIR	Rainf	MaxTemp	MinTemp	RH0600	RH1500	Sunsh
MIR	1.0000	-0.073	-0.0442	-0.202	-0.180	-0.326	0.349
Rainf	-0.0730	1.000	-0.3861	0.433	0.499	0.556	-0.398
MaxTemp	-0.0442	-0.386	1.0000	-0.447	-0.701	-0.760	0.630
MinTemp	-0.2023	0.433	-0.4471	1.000	0.478	0.686	-0.387
RH0600	-0.1797	0.499	-0.7013	0.478	1.000	0.870	-0.687
RH1500	-0.3257	0.556	-0.7603	0.686	0.870	1.000	-0.719
Sunsh	0.3488	-0.398	0.6297	-0.387	-0.687	-0.719	1.000
Elevation	0.2701	-0.247	-0.0271	-0.430	-0.273	-0.337	0.195

Elevation
 MIR 0.2701
 Rainf -0.2475
 MaxTemp -0.0271
 MinTemp -0.4302
 RH0600 -0.2733
 RH1500 -0.3373
 Sunsh 0.1953
 Elevation 1.0000

 Month : 49

	MIR	Rainf	MaxTemp	MinTemp	RH0600	RH1500	Sunsh
MIR	1.0000	0.07919	-0.0958	-0.0218	-0.0276	-0.0976	0.184
Rainf	0.0792	1.00000	-0.4315	0.0997	0.3471	0.3793	-0.259
MaxTemp	-0.0958	-0.43150	1.0000	-0.4342	-0.6455	-0.6834	0.621
MinTemp	-0.0218	0.09971	-0.4342	1.0000	0.4618	0.6653	-0.555
RH0600	-0.0276	0.34713	-0.6455	0.4618	1.0000	0.8345	-0.793
RH1500	-0.0976	0.37927	-0.6834	0.6653	0.8345	1.0000	-0.773
Sunsh	0.1845	-0.25913	0.6215	-0.5552	-0.7934	-0.7731	1.000
Elevation	0.2104	-0.00441	0.0779	-0.4099	-0.2934	-0.4226	0.240

Elevation
 MIR 0.21040
 Rainf -0.00441
 MaxTemp 0.07787
 MinTemp -0.40988
 RH0600 -0.29335
 RH1500 -0.42257
 Sunsh 0.24037
 Elevation 1.00000

 Month : 50

	MIR	Rainf	MaxTemp	MinTemp	RH0600	RH1500	Sunsh
MIR	1.0000	0.2150	-0.2604	-0.180	-0.0192	-0.0725	0.296
Rainf	0.2150	1.0000	-0.4647	0.030	0.5712	0.5077	-0.437
MaxTemp	-0.2604	-0.4647	1.0000	-0.248	-0.4233	-0.5843	0.278
MinTemp	-0.1795	0.0300	-0.2476	1.000	0.1759	0.4391	-0.201
RH0600	-0.0192	0.5712	-0.4233	0.176	1.0000	0.8032	-0.513
RH1500	-0.0725	0.5077	-0.5843	0.439	0.8032	1.0000	-0.506
Sunsh	0.2963	-0.4367	0.2776	-0.201	-0.5128	-0.5058	1.000
Elevation	0.2308	0.0358	0.0506	-0.506	-0.3089	-0.4407	0.123

Elevation
 MIR 0.2308

Rainf 0.0358
 MaxTemp 0.0506
 MinTemp -0.5061
 RH0600 -0.3089
 RH1500 -0.4407
 Sunsh 0.1227
 Elevation 1.0000

 Month : 51

	MIR	Rainf	MaxTemp	MinTemp	RH0600	RH1500	Sunsh
MIR	1.0000	0.0810	-0.1378	-0.1548	-0.0706	-0.1574	0.2791
Rainf	0.0810	1.0000	-0.5109	-0.6073	0.5513	0.4066	-0.0516
MaxTemp	-0.1378	-0.5109	1.0000	0.2793	-0.7307	-0.7824	0.0073
MinTemp	-0.1548	-0.6073	0.2793	1.0000	-0.3003	-0.0229	-0.1634
RH0600	-0.0706	0.5513	-0.7307	-0.3003	1.0000	0.8345	-0.0250
RH1500	-0.1574	0.4066	-0.7824	-0.0229	0.8345	1.0000	-0.0457
Sunsh	0.2791	-0.0516	0.0073	-0.1634	-0.0250	-0.0457	1.0000
Elevation	0.1831	0.1162	0.0833	-0.4088	-0.2293	-0.3777	0.0514

Elevation
 MIR 0.1831
 Rainf 0.1162
 MaxTemp 0.0833
 MinTemp -0.4088
 RH0600 -0.2293
 RH1500 -0.3777
 Sunsh 0.0514
 Elevation 1.0000

 Month : 52

	MIR	Rainf	MaxTemp	MinTemp	RH0600	RH1500	Sunsh
MIR	1.0000	0.119	-0.1435	-0.0283	0.0623	-0.0813	0.1783
Rainf	0.1185	1.000	-0.1319	-0.4525	0.2090	-0.1044	-0.1785
MaxTemp	-0.1435	-0.132	1.0000	0.4724	-0.7684	-0.7877	0.3971
MinTemp	-0.0283	-0.453	0.4724	1.0000	-0.5026	-0.2279	0.3269
RH0600	0.0623	0.209	-0.7684	-0.5026	1.0000	0.7962	-0.4483
RH1500	-0.0813	-0.104	-0.7877	-0.2279	0.7962	1.0000	-0.3166
Sunsh	0.1783	-0.179	0.3971	0.3269	-0.4483	-0.3166	1.0000
Elevation	0.2066	0.293	0.0722	-0.3444	-0.1848	-0.3271	-0.0666

Elevation
 MIR 0.2066
 Rainf 0.2932
 MaxTemp 0.0722
 MinTemp -0.3444
 RH0600 -0.1848
 RH1500 -0.3271
 Sunsh -0.0666
 Elevation 1.0000

 Month : 53

	MIR	Rainf	MaxTemp	MinTemp	RH0600	RH1500	Sunsh
MIR	1.00000	0.00461	-0.1545	-0.0723	0.173	0.00811	0.0525
Rainf	0.00461	1.00000	-0.2190	-0.3203	0.429	0.46103	-0.2894
MaxTemp	-0.15449	-0.21896	1.0000	0.3381	-0.631	-0.69550	0.4201
MinTemp	-0.07227	-0.32035	0.3381	1.0000	-0.384	-0.09716	0.3035
RH0600	0.17286	0.42932	-0.6312	-0.3840	1.000	0.64047	-0.5644
RH1500	0.00811	0.46103	-0.6955	-0.0972	0.640	1.00000	-0.4437
Sunsh	0.05254	-0.28939	0.4201	0.3035	-0.564	-0.44372	1.0000
Elevation	0.21412	-0.23065	0.0328	-0.3784	-0.162	-0.35108	-0.0377

Elevation
 MIR 0.2141
 Rainf -0.2306
 MaxTemp 0.0328
 MinTemp -0.3784
 RH0600 -0.1624
 RH1500 -0.3511
 Sunsh -0.0377
 Elevation 1.0000

 Month : 54

	MIR	Rainf	MaxTemp	MinTemp	RH0600	RH1500	Sunsh
MIR	1.0000	0.1051	-0.0562	0.0784	0.0802	-0.1556	0.1873
Rainf	0.1051	1.0000	-0.1607	0.2271	0.0161	0.3358	-0.2025
MaxTemp	-0.0562	-0.1607	1.0000	0.0896	-0.4269	-0.6480	0.5662
MinTemp	0.0784	0.2271	0.0896	1.0000	0.0370	0.0606	-0.0155
RH0600	0.0802	0.0161	-0.4269	0.0370	1.0000	0.5943	-0.3881
RH1500	-0.1556	0.3358	-0.6480	0.0606	0.5943	1.0000	-0.6240
Sunsh	0.1873	-0.2025	0.5662	-0.0155	-0.3881	-0.6240	1.0000

Elevation 0.1523 -0.2046 0.0933 -0.4545 -0.2235 -0.3993 0.2359
 Elevation
 MIR 0.1523
 Rainf -0.2046
 MaxTemp 0.0933
 MinTemp -0.4545
 RH0600 -0.2235
 RH1500 -0.3993
 Sunsh 0.2359
 Elevation 1.0000

Month : 55

	MIR	Rainf	MaxTemp	MinTemp	RH0600	RH1500	Sunsh
MIR	1.00000	0.168	0.1205	0.00802	0.2110	-0.211	0.1930
Rainf	0.16761	1.000	0.2665	0.11605	-0.1235	-0.222	0.2560
MaxTemp	0.12053	0.267	1.0000	0.08375	-0.2080	-0.562	0.3790
MinTemp	0.00802	0.116	0.0838	1.00000	0.1151	0.163	0.2116
RH0600	0.21097	-0.123	-0.2080	0.11511	1.0000	0.404	-0.0105
RH1500	-0.21051	-0.222	-0.5617	0.16281	0.4042	1.000	-0.1125
Sunsh	0.19302	0.256	0.3790	0.21158	-0.0105	-0.112	1.0000
Elevation	0.15110	0.163	0.0699	-0.44172	-0.1010	-0.386	-0.0545

Elevation
 MIR 0.1511
 Rainf 0.1631
 MaxTemp 0.0699
 MinTemp -0.4417
 RH0600 -0.1010
 RH1500 -0.3864
 Sunsh -0.0545
 Elevation 1.0000

Month : 56

	MIR	Rainf	MaxTemp	MinTemp	RH0600	RH1500	Sunsh
MIR	1.0000	0.2501	0.1765	0.0477	0.193561	-0.0352	0.2598
Rainf	0.2501	1.0000	0.4668	0.0284	0.075068	-0.0774	0.4409
MaxTemp	0.1765	0.4668	1.0000	0.1391	-0.215970	-0.4384	0.4000
MinTemp	0.0477	0.0284	0.1391	1.0000	0.102165	0.1500	0.2699
RH0600	0.1936	0.0751	-0.2160	0.1022	1.000000	0.2030	0.2470
RH1500	-0.0352	-0.0774	-0.4384	0.1500	0.202969	1.0000	0.0979
Sunsh	0.2598	0.4409	0.4000	0.2699	0.247037	0.0979	1.0000
Elevation	0.1611	0.2388	0.0615	-0.4258	0.000973	-0.1670	-0.0607

Elevation
 MIR 0.161084
 Rainf 0.238756
 MaxTemp 0.061464
 MinTemp -0.425803
 RH0600 0.000973
 RH1500 -0.166967
 Sunsh -0.060694
 Elevation 1.000000

Month : 57

	MIR	Rainf	MaxTemp	MinTemp	RH0600	RH1500	Sunsh
MIR	1.0000	0.1469	0.0164	-0.0730	0.0227	-0.193	0.1669
Rainf	0.1469	1.0000	0.1207	-0.2856	0.1582	-0.140	0.0237
MaxTemp	0.0164	0.1207	1.0000	0.0101	-0.2558	-0.659	0.4576
MinTemp	-0.0730	-0.2856	0.0101	1.0000	0.0343	0.123	0.3330
RH0600	0.0227	0.1582	-0.2558	0.0343	1.0000	0.255	-0.3001
RH1500	-0.1926	-0.1400	-0.6587	0.1225	0.2550	1.000	-0.3088
Sunsh	0.1669	0.0237	0.4576	0.3330	-0.3001	-0.309	1.0000
Elevation	0.1644	0.2249	0.0178	-0.4858	-0.0438	-0.253	-0.1000

Elevation
 MIR 0.1644
 Rainf 0.2249
 MaxTemp 0.0178
 MinTemp -0.4858
 RH0600 -0.0438
 RH1500 -0.2525
 Sunsh -0.1000
 Elevation 1.0000

Month : 58

	MIR	Rainf	MaxTemp	MinTemp	RH0600	RH1500	Sunsh
MIR	1.000	-0.24749	0.1826	-0.0340	-0.238	-0.3119	0.3364
Rainf	-0.247	1.00000	-0.6265	-0.2098	0.424	0.5227	-0.6394
MaxTemp	0.183	-0.62653	1.0000	0.2293	-0.538	-0.8408	0.7295
MinTemp	-0.034	-0.20978	0.2293	1.0000	-0.207	-0.0543	0.3665

RH0600	-0.238	0.42374	-0.5384	-0.2073	1.000	0.5800	-0.5987
RH1500	-0.312	0.52267	-0.8408	-0.0543	0.580	1.0000	-0.7201
Sunsh	0.336	-0.63936	0.7295	0.3665	-0.599	-0.7201	1.0000
Elevation	0.200	-0.00147	0.0266	-0.5099	-0.119	-0.2563	-0.0344
Elevation							
MIR		0.19988					
Rainf		-0.00147					
MaxTemp		0.02656					
MinTemp		-0.50994					
RH0600		-0.11907					
RH1500		-0.25631					
Sunsh		-0.03445					
Elevation		1.00000					

Month : 59

	MIR	Rainf	MaxTemp	MinTemp	RH0600	RH1500	Sunsh
MIR	1.00000	0.00271	-0.0323	-0.104	-0.125	-0.219	0.0712
Rainf	0.00271	1.00000	-0.3478	0.192	0.451	0.491	-0.3748
MaxTemp	-0.03225	-0.34778	1.0000	-0.115	-0.670	-0.720	0.4540
MinTemp	-0.10416	0.19176	-0.1152	1.000	0.262	0.471	-0.1884
RH0600	-0.12508	0.45097	-0.6698	0.262	1.000	0.818	-0.5730
RH1500	-0.21939	0.49127	-0.7196	0.471	0.818	1.000	-0.5613
Sunsh	0.07122	-0.37480	0.4540	-0.188	-0.573	-0.561	1.0000
Elevation	0.28284	-0.12425	-0.0356	-0.541	-0.185	-0.295	-0.0904
Elevation							
MIR		0.2828					
Rainf		-0.1243					
MaxTemp		-0.0356					
MinTemp		-0.5408					
RH0600		-0.1854					
RH1500		-0.2954					
Sunsh		-0.0904					
Elevation		1.0000					

Month : 60

	MIR	Rainf	MaxTemp	MinTemp	RH0600	RH1500	Sunsh
MIR	1.00000	0.1567	-0.1257	-0.0153	0.0764	0.00737	0.0257
Rainf	0.15666	1.0000	-0.4493	0.2636	0.3508	0.52215	-0.2033
MaxTemp	-0.12567	-0.4493	1.0000	-0.2787	-0.5430	-0.63929	0.5250
MinTemp	-0.01528	0.2636	-0.2787	1.0000	0.5382	0.68723	-0.1497
RH0600	0.07639	0.3508	-0.5430	0.5382	1.0000	0.76765	-0.5615
RH1500	0.00737	0.5221	-0.6393	0.6872	0.7676	1.00000	-0.4122
Sunsh	0.02566	-0.2033	0.5250	-0.1497	-0.5615	-0.41223	1.0000
Elevation	0.24422	0.0566	-0.0582	-0.4537	-0.2484	-0.29847	-0.0553
Elevation							
MIR		0.2442					
Rainf		0.0566					
MaxTemp		-0.0582					
MinTemp		-0.4537					
RH0600		-0.2484					
RH1500		-0.2985					
Sunsh		-0.0553					
Elevation		1.0000					

Month : 61

	MIR	Rainf	MaxTemp	MinTemp	RH0600	RH1500	Sunsh
MIR	1.0000	-0.0446	-0.2154	0.046	-0.0629	-0.0441	0.0736
Rainf	-0.0446	1.0000	-0.4202	0.152	0.2724	0.3054	-0.1917
MaxTemp	-0.2154	-0.4202	1.0000	-0.396	-0.4461	-0.5643	0.1934
MinTemp	0.0460	0.1519	-0.3964	1.000	0.4064	0.6460	-0.5432
RH0600	-0.0629	0.2724	-0.4461	0.406	1.0000	0.7907	-0.6722
RH1500	-0.0441	0.3054	-0.5643	0.646	0.7907	1.0000	-0.6252
Sunsh	0.0736	-0.1917	0.1934	-0.543	-0.6722	-0.6252	1.0000
Elevation	0.1724	-0.0276	-0.0559	-0.472	-0.3824	-0.4640	0.3555
Elevation							
MIR		0.1724					
Rainf		-0.0276					
MaxTemp		-0.0559					
MinTemp		-0.4718					
RH0600		-0.3824					
RH1500		-0.4640					
Sunsh		0.3555					
Elevation		1.0000					

Month : 62

	MIR	Rainf	MaxTemp	MinTemp	RH0600	RH1500	Sunsh
MIR	1.0000	0.2019	-0.1484	-0.1333	-0.113	-0.127	0.0137

Rainf	0.2019	1.0000	-0.4644	-0.0840	0.519	0.362	-0.2649
MaxTemp	-0.1484	-0.4644	1.0000	-0.0505	-0.600	-0.631	0.1055
MinTemp	-0.1333	-0.0840	-0.0505	1.0000	0.172	0.491	-0.3016
RH0600	-0.1126	0.5193	-0.6002	0.1716	1.000	0.725	-0.4975
RH1500	-0.1269	0.3618	-0.6306	0.4910	0.725	1.000	-0.3261
Sunsh	0.0137	-0.2649	0.1055	-0.3016	-0.498	-0.326	1.0000
Elevation	0.1974	0.0326	0.1141	-0.4373	-0.260	-0.439	0.1275

Elevation	
MIR	0.1974
Rainf	0.0326
MaxTemp	0.1141
MinTemp	-0.4373
RH0600	-0.2599
RH1500	-0.4389
Sunsh	0.1275
Elevation	1.0000

Month : 63

	MIR	Rainf	MaxTemp	MinTemp	RH0600	RH1500	Sunsh
MIR	1.0000	-0.0179	-0.0139	-0.0252	-0.184	-0.133	0.0283
Rainf	-0.0179	1.0000	-0.7629	-0.5849	0.739	0.713	-0.5905
MaxTemp	-0.0139	-0.7629	1.0000	0.5558	-0.760	-0.779	0.4873
MinTemp	-0.0252	-0.5849	0.5558	1.0000	-0.578	-0.335	0.3247
RH0600	-0.1840	0.7387	-0.7596	-0.5780	1.000	0.819	-0.6563
RH1500	-0.1330	0.7134	-0.7787	-0.3352	0.819	1.000	-0.5506
Sunsh	0.0283	-0.5905	0.4873	0.3247	-0.656	-0.551	1.0000
Elevation	0.1865	-0.1334	0.1260	-0.2557	-0.256	-0.364	0.2089

Elevation	
MIR	0.186
Rainf	-0.133
MaxTemp	0.126
MinTemp	-0.256
RH0600	-0.256
RH1500	-0.364
Sunsh	0.209
Elevation	1.000

Month : 64

	MIR	Rainf	MaxTemp	MinTemp	RH0600	RH1500	Sunsh
MIR	1.0000	0.0311	-0.0748	-0.0499	-0.0369	-0.0542	-0.1149
Rainf	0.0311	1.0000	-0.3283	-0.3748	0.2870	0.2460	-0.1015
MaxTemp	-0.0748	-0.3283	1.0000	0.5537	-0.7854	-0.7636	0.4629
MinTemp	-0.0499	-0.3748	0.5537	1.0000	-0.5847	-0.3227	0.4160
RH0600	-0.0369	0.2870	-0.7854	-0.5847	1.0000	0.8144	-0.5875
RH1500	-0.0542	0.2460	-0.7636	-0.3227	0.8144	1.0000	-0.4308
Sunsh	-0.1149	-0.1015	0.4629	0.4160	-0.5875	-0.4308	1.0000
Elevation	0.1938	0.0134	0.0904	-0.2915	-0.1852	-0.3357	-0.0049

Elevation	
MIR	0.1938
Rainf	0.0134
MaxTemp	0.0904
MinTemp	-0.2915
RH0600	-0.1852
RH1500	-0.3357
Sunsh	-0.0049
Elevation	1.0000

Month : 65

	MIR	Rainf	MaxTemp	MinTemp	RH0600	RH1500	Sunsh
MIR	1.0000	0.0464	-0.0279	0.0404	-0.0615	-0.0651	-0.0422
Rainf	0.0464	1.0000	-0.5586	-0.2302	0.3922	0.4775	-0.4242
MaxTemp	-0.0279	-0.5586	1.0000	0.4220	-0.7528	-0.7699	0.6631
MinTemp	0.0404	-0.2302	0.4220	1.0000	-0.4532	-0.2470	0.3084
RH0600	-0.0615	0.3922	-0.7528	-0.4532	1.0000	0.7878	-0.6812
RH1500	-0.0651	0.4775	-0.7699	-0.2470	0.7878	1.0000	-0.7226
Sunsh	-0.0422	-0.4242	0.6631	0.3084	-0.6812	-0.7226	1.0000
Elevation	0.2096	-0.1025	0.0896	-0.3446	-0.1858	-0.3348	0.1695

Elevation	
MIR	0.2096
Rainf	-0.1025
MaxTemp	0.0896
MinTemp	-0.3446
RH0600	-0.1858
RH1500	-0.3348
Sunsh	0.1695
Elevation	1.0000

Month : 66

	MIR	Rainf	MaxTemp	MinTemp	RH0600	RH1500	Sunsh
MIR	1.0000	-0.045	0.0485	0.05853	-0.0655	-0.08075	0.0829
Rainf	-0.0450	1.000	-0.1493	0.23542	0.1140	0.30827	-0.2490
MaxTemp	0.0485	-0.149	1.0000	0.25040	-0.5880	-0.67370	0.5614
MinTemp	0.0585	0.235	0.2504	1.00000	-0.2544	0.00301	0.0248
RH0600	-0.0655	0.114	-0.5880	-0.25436	1.0000	0.55834	-0.4628
RH1500	-0.0807	0.308	-0.6737	0.00301	0.5583	1.00000	-0.7390
Sunsh	0.0829	-0.249	0.5614	0.02478	-0.4628	-0.73899	1.0000
Elevation	0.1715	-0.389	0.1199	-0.39482	-0.1174	-0.38973	0.2693
Elevation							
MIR	0.171						
Rainf	-0.389						
MaxTemp	0.120						
MinTemp	-0.395						
RH0600	-0.117						
RH1500	-0.390						
Sunsh	0.269						
Elevation	1.000						

Month : 67

	MIR	Rainf	MaxTemp	MinTemp	RH0600	RH1500	Sunsh
MIR	1.0000	0.0936	0.0532	0.02783	0.14673	-0.20349	0.1705
Rainf	0.0936	1.0000	0.3884	0.27394	0.13850	-0.32309	0.3609
MaxTemp	0.0532	0.3884	1.0000	0.18998	-0.25013	-0.55898	0.2978
MinTemp	0.0278	0.2739	0.1900	1.00000	-0.00343	0.00539	0.1446
RH0600	0.1467	0.1385	-0.2501	-0.00343	1.00000	0.31272	0.1058
RH1500	-0.2035	-0.3231	-0.5590	0.00539	0.31272	1.00000	-0.0426
Sunsh	0.1705	0.3609	0.2978	0.14461	0.10584	-0.04257	1.0000
Elevation	0.2247	-0.0679	0.0850	-0.44564	-0.03546	-0.36154	-0.0858
Elevation							
MIR	0.2247						
Rainf	-0.0679						
MaxTemp	0.0850						
MinTemp	-0.4456						
RH0600	-0.0355						
RH1500	-0.3615						
Sunsh	-0.0858						
Elevation	1.0000						

Month : 68

	MIR	Rainf	MaxTemp	MinTemp	RH0600	RH1500	Sunsh
MIR	1.0000	0.2423	0.0740	0.0623	0.1112	-0.157	0.129
Rainf	0.2423	1.0000	0.4596	0.1889	0.0253	-0.206	0.322
MaxTemp	0.0740	0.4596	1.0000	0.2167	-0.1826	-0.512	0.328
MinTemp	0.0623	0.1889	0.2167	1.0000	-0.0488	-0.103	0.271
RH0600	0.1112	0.0253	-0.1826	-0.0488	1.0000	0.460	0.174
RH1500	-0.1574	-0.2065	-0.5117	-0.1034	0.4605	1.000	0.146
Sunsh	0.1289	0.3215	0.3280	0.2713	0.1737	0.146	1.000
Elevation	0.2776	0.1958	0.0976	-0.4215	0.0849	-0.292	-0.165
Elevation							
MIR	0.2776						
Rainf	0.1958						
MaxTemp	0.0976						
MinTemp	-0.4215						
RH0600	0.0849						
RH1500	-0.2925						
Sunsh	-0.1647						
Elevation	1.0000						

Month: 69

	MIR	Rainf	MaxTemp	MinTemp	RH0600	RH1500	Sunsh
MIR	1.0000	0.06278	0.104	-0.0243	0.187	-0.2628	0.27148
Rainf	0.0628	1.00000	0.127	-0.3920	0.285	-0.2794	0.00381
MaxTemp	0.1040	0.12722	1.000	0.1649	-0.205	-0.6719	0.47507
MinTemp	-0.0243	-0.39203	0.165	1.0000	-0.121	-0.0184	0.19281
RH0600	0.1869	0.28532	-0.205	-0.1209	1.000	0.2699	-0.03798
RH1500	-0.2628	-0.27943	-0.672	-0.0184	0.270	1.0000	-0.33049
Sunsh	0.2715	0.00381	0.475	0.1928	-0.038	-0.3305	1.00000
Elevation	0.2527	0.36189	0.069	-0.4850	0.071	-0.3325	-0.01047
Elevation							
MIR	0.2527						
Rainf	0.3619						
MaxTemp	0.0690						
MinTemp	-0.4850						
RH0600	0.0710						
RH1500	-0.3325						

```

Sunsh      -0.0105
Elevation  1.0000
-----
Month data1[, 5]: 70
      MIR  Rainf MaxTemp  MinTemp RH0600  RH1500  Sunsh
MIR      1.0000 -0.1264  0.2828 -0.01886 -0.175 -0.39040  0.1814
Rainf    -0.1264 1.0000 -0.4128 -0.10877  0.288  0.41523 -0.5066
MaxTemp  0.2828 -0.4128  1.0000  0.08253 -0.461 -0.76472  0.5233
MinTemp  -0.0189 -0.1088  0.0825  1.00000 -0.120 -0.00631  0.3900
RH0600   -0.1753 0.2882 -0.4614 -0.11970  1.000  0.56178 -0.3985
RH1500   -0.3904 0.4152 -0.7647 -0.00631  0.562  1.00000 -0.4741
Sunsh     0.1814 -0.5066  0.5233  0.38996 -0.398 -0.47409  1.0000
Elevation 0.2539 0.0599  0.0605 -0.46477 -0.127 -0.26560 -0.0986
      Elevation
MIR      0.2539
Rainf    0.0599
MaxTemp  0.0605
MinTemp  -0.4648
RH0600   -0.1275
RH1500   -0.2656
Sunsh    -0.0986
Elevation 1.0000
-----
Month : 71
      MIR  Rainf MaxTemp  MinTemp RH0600 RH1500  Sunsh
MIR      1.00000 -0.184  0.1315 -0.0664 -0.254 -0.223  0.00344
Rainf    -0.18409 1.000 -0.5313  0.2522  0.478  0.647 -0.50707
MaxTemp  0.13153 -0.531  1.0000 -0.3846 -0.713 -0.783  0.48833
MinTemp  -0.06643 0.252 -0.3846  1.0000  0.315  0.597 -0.15223
RH0600   -0.25435 0.478 -0.7131  0.3150  1.000  0.787 -0.49252
RH1500   -0.22263 0.647 -0.7833  0.5966  0.787  1.000 -0.48509
Sunsh     0.00344 -0.507  0.4883 -0.1522 -0.493 -0.485  1.00000
Elevation 0.22365 -0.149  0.0744 -0.4731 -0.195 -0.298 -0.06384
      Elevation
MIR      0.2236
Rainf    -0.1493
MaxTemp  0.0744
MinTemp  -0.4731
RH0600   -0.1947
RH1500   -0.2980
Sunsh    -0.0638
Elevation 1.0000
-----
Month : 72
      MIR  Rainf MaxTemp  MinTemp RH0600 RH1500  Sunsh
MIR      1.0000 -0.0636  0.0312 -0.0147 -0.182 -0.129 -0.1211
Rainf    -0.0636 1.0000 -0.4340  0.0250  0.396  0.356 -0.3992
MaxTemp  0.0312 -0.4340  1.0000 -0.4067 -0.771 -0.800  0.6785
MinTemp  -0.0147 0.0250 -0.4067  1.0000  0.397  0.579 -0.1898
RH0600   -0.1815 0.3958 -0.7712  0.3970  1.000  0.855 -0.7041
RH1500   -0.1295 0.3565 -0.7998  0.5789  0.855  1.000 -0.6194
Sunsh    -0.1211 -0.3992  0.6785 -0.1898 -0.704 -0.619  1.0000
Elevation 0.1927 0.0733  0.0553 -0.4642 -0.247 -0.286  0.0312
      Elevation
MIR      0.1927
Rainf    0.0733
MaxTemp  0.0553
MinTemp  -0.4642
RH0600   -0.2475
RH1500   -0.2857
Sunsh     0.0312
Elevation 1.0000
-----
Month: 73
      MIR  Rainf MaxTemp  MinTemp RH0600 RH1500  Sunsh
MIR      1.0000 0.0717 -0.0887 -0.0402 -0.0859 -0.0856 -0.0501
Rainf    0.0717 1.0000 -0.3389 -0.0124  0.3100  0.1770 -0.2120
MaxTemp  -0.0887 -0.3389  1.0000 -0.4653 -0.7490 -0.7849  0.6326
MinTemp  -0.0402 -0.0124 -0.4653  1.0000  0.4735  0.6299 -0.3863
RH0600   -0.0859 0.3100 -0.7490  0.4735  1.0000  0.8478 -0.6664
RH1500   -0.0856 0.1770 -0.7849  0.6299  0.8478  1.0000 -0.6343
Sunsh    -0.0501 -0.2120  0.6326 -0.3863 -0.6664 -0.6343  1.0000
Elevation 0.1265 0.2677  0.1358 -0.5005 -0.2500 -0.3731  0.2255
      Elevation
MIR      0.127
Rainf    0.268
MaxTemp  0.136

```

MinTemp -0.501
 RH0600 -0.250
 RH1500 -0.373
 Sunsh 0.225
 Elevation 1.000

 Month: 74

	MIR	Rainf	MaxTemp	MinTemp	RH0600	RH1500
MIR	1.000000	0.161	-0.1620	0.01637	0.0190	-0.000479
Rainf	0.160593	1.000	-0.4136	-0.17306	0.4181	0.249288
MaxTemp	-0.162023	-0.414	1.0000	-0.08147	-0.7434	-0.769449
MinTemp	0.016366	-0.173	-0.0815	1.00000	0.0502	0.270477
RH0600	0.019007	0.418	-0.7434	0.05015	1.0000	0.815424
RH1500	-0.000479	0.249	-0.7694	0.27048	0.8154	1.000000
Sunsh	-0.054077	-0.476	0.5507	-0.00476	-0.6533	-0.558090
Elevation	0.205275	0.166	0.1303	-0.50357	-0.2324	-0.371282

	Sunsh	Elevation
MIR	-0.05408	0.205
Rainf	-0.47625	0.166
MaxTemp	0.55071	0.130
MinTemp	-0.00476	-0.504
RH0600	-0.65329	-0.232
RH1500	-0.55809	-0.371
Sunsh	1.00000	0.147
Elevation	0.14734	1.000

 Month: 75

	MIR	Rainf	MaxTemp	MinTemp	RH0600	RH1500	Sunsh
MIR	1.0000	0.138	-0.0875	-0.0819	0.0388	-0.0112	-0.1160
Rainf	0.1375	1.000	-0.6498	-0.6375	0.6038	0.5022	-0.6547
MaxTemp	-0.0875	-0.650	1.0000	0.5404	-0.8003	-0.8367	0.5850
MinTemp	-0.0819	-0.637	0.5404	1.0000	-0.5554	-0.4281	0.5798
RH0600	0.0388	0.604	-0.8003	-0.5554	1.0000	0.8735	-0.5451
RH1500	-0.0112	0.502	-0.8367	-0.4281	0.8735	1.0000	-0.4674
Sunsh	-0.1160	-0.655	0.5850	0.5798	-0.5451	-0.4674	1.0000
Elevation	0.2157	0.100	0.1380	-0.2267	-0.2261	-0.3323	-0.0952

	Elevation
MIR	0.2157
Rainf	0.1002
MaxTemp	0.1380
MinTemp	-0.2267
RH0600	-0.2261
RH1500	-0.3323
Sunsh	-0.0952
Elevation	1.0000

 Month: 76

	MIR	Rainf	MaxTemp	MinTemp	RH0600	RH1500	Sunsh
MIR	1.0000	0.106	-0.1530	-0.158	0.182	0.0632	-0.1881
Rainf	0.1061	1.000	-0.4397	-0.453	0.420	0.2920	-0.2991
MaxTemp	-0.1530	-0.440	1.0000	0.533	-0.790	-0.8243	0.6304
MinTemp	-0.1585	-0.453	0.5331	1.000	-0.575	-0.4645	0.6174
RH0600	0.1821	0.420	-0.7903	-0.575	1.000	0.8762	-0.7492
RH1500	0.0632	0.292	-0.8243	-0.464	0.876	1.0000	-0.6976
Sunsh	-0.1881	-0.299	0.6304	0.617	-0.749	-0.6976	1.0000
Elevation	0.2225	0.124	0.0789	-0.272	-0.164	-0.2964	0.0115

	Elevation
MIR	0.2225
Rainf	0.1244
MaxTemp	0.0789
MinTemp	-0.2723
RH0600	-0.1639
RH1500	-0.2964
Sunsh	0.0115
Elevation	1.0000

 Month: 77

	MIR	Rainf	MaxTemp	MinTemp	RH0600	RH1500	Sunsh
MIR	1.0000	-0.0389	-0.0179	0.0324	0.197	0.0603	-0.141
Rainf	-0.0389	1.0000	-0.2927	-0.3055	0.484	0.6670	-0.568
MaxTemp	-0.0179	-0.2927	1.0000	0.2725	-0.423	-0.5909	0.385
MinTemp	0.0324	-0.3055	0.2725	1.0000	-0.301	-0.2236	0.156
RH0600	0.1965	0.4839	-0.4230	-0.3007	1.000	0.7680	-0.648
RH1500	0.0603	0.6670	-0.5909	-0.2236	0.768	1.0000	-0.732
Sunsh	-0.1408	-0.5685	0.3848	0.1559	-0.648	-0.7316	1.000
Elevation	0.2130	-0.2515	0.0395	-0.2934	-0.269	-0.3253	0.265

Elevation

MIR 0.2130
 Rainf -0.2515
 MaxTemp 0.0395
 MinTemp -0.2934
 RH0600 -0.2687
 RH1500 -0.3253
 Sunsh 0.2654
 Elevation 1.0000

 Month: 78

	MIR	Rainf	MaxTemp	MinTemp	RH0600	RH1500	Sunsh
MIR	1.0000	0.0505	-0.0785	0.0311	0.191	-0.0130	-0.0215
Rainf	0.0505	1.0000	-0.4041	0.0391	0.223	0.4124	-0.3207
MaxTemp	-0.0785	-0.4041	1.0000	0.1585	-0.616	-0.7362	0.6433
MinTemp	0.0311	0.0391	0.1585	1.0000	-0.095	-0.0412	0.2280
RH0600	0.1914	0.2229	-0.6158	-0.0950	1.000	0.6304	-0.5223
RH1500	-0.0130	0.4124	-0.7362	-0.0412	0.630	1.0000	-0.5977
Sunsh	-0.0215	-0.3207	0.6433	0.2280	-0.522	-0.5977	1.0000
Elevation	0.1618	-0.2704	0.0418	-0.3407	-0.199	-0.3088	0.0859

Elevation

MIR	0.1618
Rainf	-0.2704
MaxTemp	0.0418
MinTemp	-0.3407
RH0600	-0.1990
RH1500	-0.3088
Sunsh	0.0859
Elevation	1.0000

 Month: 79

	MIR	Rainf	MaxTemp	MinTemp	RH0600	RH1500	Sunsh
MIR	1.00000	-0.00517	0.0298	-0.0748	0.0182	-0.209	0.0813
Rainf	-0.00517	1.00000	0.2569	-0.0747	-0.2220	-0.362	0.2750
MaxTemp	0.02980	0.25685	1.0000	0.3742	-0.3695	-0.613	0.5117
MinTemp	-0.07477	-0.07475	0.3742	1.0000	-0.2449	0.123	0.2205
RH0600	0.01820	-0.22201	-0.3695	-0.2449	1.0000	0.422	-0.1492
RH1500	-0.20915	-0.36200	-0.6129	0.1235	0.4219	1.000	-0.3520
Sunsh	0.08134	0.27495	0.5117	0.2205	-0.1492	-0.352	1.0000
Elevation	0.25198	0.09936	0.1022	-0.3834	-0.1204	-0.417	0.0701

Elevation

MIR	0.2520
Rainf	0.0994
MaxTemp	0.1022
MinTemp	-0.3834
RH0600	-0.1204
RH1500	-0.4167
Sunsh	0.0701
Elevation	1.0000

 Month: 80

	MIR	Rainf	MaxTemp	MinTemp	RH0600	RH1500	Sunsh
MIR	1.0000	0.1525	0.2027	-0.0820	0.0514	-0.386	0.15392
Rainf	0.1525	1.0000	0.4114	0.0319	0.1764	-0.319	0.35163
MaxTemp	0.2027	0.4114	1.0000	0.2952	-0.0734	-0.561	0.37050
MinTemp	-0.0820	0.0319	0.2952	1.0000	-0.2219	0.120	0.23467
RH0600	0.0514	0.1764	-0.0734	-0.2219	1.0000	0.262	0.09301
RH1500	-0.3855	-0.3194	-0.5609	0.1196	0.2620	1.000	-0.21524
Sunsh	0.1539	0.3516	0.3705	0.2347	0.0930	-0.215	1.00000
Elevation	0.2515	0.0950	0.1707	-0.3562	-0.0478	-0.433	0.00955

Elevation

MIR	0.25152
Rainf	0.09500
MaxTemp	0.17066
MinTemp	-0.35617
RH0600	-0.04785
RH1500	-0.43284
Sunsh	0.00955
Elevation	1.00000

 Month: 81

	MIR	Rainf	MaxTemp	MinTemp	RH0600	RH1500	Sunsh
MIR	1.0000	0.3219	0.161	-0.0835	0.21082	-0.206	0.24327
Rainf	0.3219	1.0000	0.460	-0.2771	-0.01152	-0.438	0.24527
MaxTemp	0.1610	0.4601	1.000	0.1568	-0.11627	-0.511	0.41222
MinTemp	-0.0835	-0.2771	0.157	1.0000	-0.23656	0.220	0.13446
RH0600	0.2108	-0.0115	-0.116	-0.2366	1.00000	0.276	-0.00624
RH1500	-0.2060	-0.4383	-0.511	0.2203	0.27613	1.000	-0.14168

```

Sunsh      0.2433  0.2453  0.412  0.1345 -0.00624 -0.142  1.00000
Elevation  0.2853  0.3700  0.135 -0.5352 -0.08046 -0.398 -0.01373
Elevation
MIR        0.2853
Rainf      0.3700
MaxTemp    0.1348
MinTemp    -0.5352
RH0600     -0.0805
RH1500     -0.3983
Sunsh      -0.0137
Elevation   1.0000

```

Month: 82

```

MIR        1.00000  0.04175  0.1157 -0.0900  0.07157 -0.1715 -0.00667
Rainf      0.04175  1.00000 -0.2322 -0.1620 -0.00672  0.1452 -0.53940
MaxTemp    0.11565 -0.23221  1.0000  0.3401 -0.16449 -0.6378  0.56436
MinTemp    -0.08998 -0.16196  0.3401  1.0000 -0.09859  0.0789  0.45809
RH0600     0.07157 -0.00672 -0.1645 -0.0986  1.00000  0.3277 -0.22293
RH1500    -0.17154  0.14516 -0.6378  0.0789  0.32766  1.0000 -0.31320
Sunsh      -0.00667 -0.53940  0.5644  0.4581 -0.22293 -0.3132  1.00000
Elevation  0.27162  0.18614  0.0412 -0.4456 -0.03321 -0.2835 -0.18145
Elevation
MIR        0.2716
Rainf      0.1861
MaxTemp    0.0412
MinTemp    -0.4456
RH0600     -0.0332
RH1500     -0.2835
Sunsh      -0.1814
Elevation  1.0000

```

Month: 83

```

MIR        1.0000  0.0654 -0.0630 -0.122 -0.160 -0.154 -0.0484
Rainf      0.0654  1.0000 -0.5387  0.429  0.458  0.577 -0.5118
MaxTemp    -0.0630 -0.5387  1.0000 -0.545 -0.667 -0.722  0.6383
MinTemp    -0.1216  0.4286 -0.5447  1.000  0.543  0.782 -0.5173
RH0600     -0.1598  0.4581 -0.6668  0.543  1.000  0.767 -0.7056
RH1500    -0.1543  0.5766 -0.7223  0.782  0.767  1.000 -0.6814
Sunsh      -0.0484 -0.5118  0.6383 -0.517 -0.706 -0.681  1.0000
Elevation  0.3225 -0.2630  0.0595 -0.418 -0.229 -0.396  0.1054
Elevation
MIR        0.3225
Rainf      -0.2630
MaxTemp    0.0595
MinTemp    -0.4184
RH0600     -0.2286
RH1500     -0.3956
Sunsh      0.1054
Elevation  1.0000

```

Month: 84

```

MIR        1.0000  0.119 -0.0710 -0.105 -0.124 -0.115 -0.0405
Rainf      0.1185  1.000 -0.5568  0.347  0.413  0.457 -0.5096
MaxTemp    -0.0710 -0.557  1.0000 -0.589 -0.662 -0.722  0.6476
MinTemp    -0.1051  0.347 -0.5885  1.000  0.652  0.765 -0.4915
RH0600     -0.1240  0.413 -0.6625  0.652  1.000  0.817 -0.7468
RH1500    -0.1154  0.457 -0.7222  0.765  0.817  1.000 -0.6758
Sunsh      -0.0405 -0.510  0.6476 -0.491 -0.747 -0.676  1.0000
Elevation  0.2406 -0.101  0.0742 -0.391 -0.272 -0.380  0.0636
Elevation
MIR        0.2406
Rainf      -0.1009
MaxTemp    0.0742
MinTemp    -0.3911
RH0600     -0.2721
RH1500     -0.3797
Sunsh      0.0636
Elevation  1.0000

```

datal[, 5]: 85

```

MIR        1.00000 -0.0617 -0.0102 -0.183 -0.175 -0.229  0.00702
Rainf      -0.06173  1.0000 -0.1379  0.137  0.251  0.132  0.08960
MaxTemp    -0.01025 -0.1379  1.0000 -0.466 -0.516 -0.660  0.26028

```



```

MinTemp -0.18260 0.1371 -0.4657 1.000 0.561 0.685 -0.31910
RH0600 -0.17528 0.2514 -0.5164 0.561 1.000 0.812 -0.32359
RH1500 -0.22934 0.1323 -0.6599 0.685 0.812 1.000 -0.26395
Sunsh 0.00702 0.0896 0.2603 -0.319 -0.324 -0.264 1.00000
Elevation 0.22722 0.1178 0.1064 -0.415 -0.381 -0.430 0.21402

```

```

Elevation
MIR 0.227
Rainf 0.118
MaxTemp 0.106
MinTemp -0.415
RH0600 -0.381
RH1500 -0.430
Sunsh 0.214
Elevation 1.000

```

Month: 86

```

MIR Rainf MaxTemp MinTemp RH0600 RH1500 Sunsh
MIR 1.0000 0.0931 -0.0367 -0.0467 -0.143 -0.144 0.0203
Rainf 0.0931 1.0000 -0.4909 0.1338 0.517 0.354 -0.3861
MaxTemp -0.0367 -0.4909 1.0000 -0.2969 -0.625 -0.691 0.5046
MinTemp -0.0467 0.1338 -0.2969 1.0000 0.380 0.615 -0.1596
RH0600 -0.1426 0.5172 -0.6250 0.3798 1.000 0.735 -0.5874
RH1500 -0.1443 0.3542 -0.6915 0.6153 0.735 1.000 -0.3984
Sunsh 0.0203 -0.3861 0.5046 -0.1596 -0.587 -0.398 1.0000
Elevation 0.2641 -0.0448 0.1702 -0.5187 -0.276 -0.461 0.1748

```

```

Elevation
MIR 0.2641
Rainf -0.0448
MaxTemp 0.1702
MinTemp -0.5187
RH0600 -0.2757
RH1500 -0.4608
Sunsh 0.1748
Elevation 1.0000

```

Month: 87

```

MIR Rainf MaxTemp MinTemp RH0600 RH1500 Sunsh
MIR 1.0000 -0.0128 0.0533 -0.0394 -0.145 -0.162 0.0431
Rainf -0.0128 1.0000 -0.6392 -0.1854 0.636 0.604 -0.3613
MaxTemp 0.0533 -0.6392 1.0000 0.1601 -0.789 -0.784 0.4558
MinTemp -0.0394 -0.1854 0.1601 1.0000 -0.227 0.121 0.1213
RH0600 -0.1451 0.6355 -0.7889 -0.2269 1.000 0.790 -0.4943
RH1500 -0.1618 0.6037 -0.7840 0.1210 0.790 1.000 -0.4386
Sunsh 0.0431 -0.3613 0.4558 0.1213 -0.494 -0.439 1.0000
Elevation 0.3056 -0.1896 0.2040 -0.3612 -0.254 -0.503 0.2038

```

```

Elevation
MIR 0.306
Rainf -0.190
MaxTemp 0.204
MinTemp -0.361
RH0600 -0.254
RH1500 -0.503
Sunsh 0.204
Elevation 1.000

```

Month: 88

```

MIR Rainf MaxTemp MinTemp RH0600 RH1500 Sunsh
MIR 1.0000 -0.0793 0.0570 0.0161 -0.0162 -0.0938 -0.0447
Rainf -0.0793 1.0000 -0.2129 -0.6208 0.2608 0.1074 -0.4172
MaxTemp 0.0570 -0.2129 1.0000 0.5756 -0.6457 -0.6779 -0.1406
MinTemp 0.0161 -0.6208 0.5756 1.0000 -0.3759 -0.1605 0.1999
RH0600 -0.0162 0.2608 -0.6457 -0.3759 1.0000 0.7588 -0.0665
RH1500 -0.0938 0.1074 -0.6779 -0.1605 0.7588 1.0000 0.1976
Sunsh -0.0447 -0.4172 -0.1406 0.1999 -0.0665 0.1976 1.0000
Elevation 0.2354 0.2231 0.0877 -0.3764 -0.2277 -0.3070 -0.1031

```

```

Elevation
MIR 0.2354
Rainf 0.2231
MaxTemp 0.0877
MinTemp -0.3764
RH0600 -0.2277
RH1500 -0.3070
Sunsh -0.1031
Elevation 1.0000

```

data1[, 5]: 89

```

MIR Rainf MaxTemp MinTemp RH0600 RH1500 Sunsh

```

MIR	1.0000	0.117	-0.1247	-0.1337	0.0762	-0.1006	-0.2273
Rainf	0.1174	1.000	-0.2524	-0.1335	0.2256	0.2468	-0.1909
MaxTemp	-0.1247	-0.252	1.0000	0.5763	-0.6001	-0.5303	0.4085
MinTemp	-0.1337	-0.133	0.5763	1.0000	-0.3462	-0.0176	0.1546
RH0600	0.0762	0.226	-0.6001	-0.3462	1.0000	0.6894	-0.4834
RH1500	-0.1006	0.247	-0.5303	-0.0176	0.6894	1.0000	-0.4281
Sunsh	-0.2273	-0.191	0.4085	0.1546	-0.4834	-0.4281	1.0000
Elevation	0.2534	-0.118	0.0184	-0.4135	-0.2857	-0.4303	0.0872
Elevation	0.2534						
MIR	0.2534						
Rainf	-0.1175						
MaxTemp	0.0184						
MinTemp	-0.4135						
RH0600	-0.2857						
RH1500	-0.4303						
Sunsh	0.0872						
Elevation	1.0000						

Month: 90

	MIR	Rainf	MaxTemp	MinTemp	RH0600	RH1500	Sunsh
MIR	1.00000	-0.00302	-0.108	-0.0754	0.0813	-0.1437	0.0795
Rainf	-0.00302	1.00000	-0.381	0.2099	0.1511	0.5343	-0.5586
MaxTemp	-0.10824	-0.38133	1.000	0.3540	-0.5624	-0.6739	0.5998
MinTemp	-0.07535	0.20993	0.354	1.0000	-0.3707	-0.0578	0.0473
RH0600	0.08133	0.15110	-0.562	-0.3707	1.0000	0.5782	-0.5071
RH1500	-0.14373	0.53430	-0.674	-0.0578	0.5782	1.0000	-0.7988
Sunsh	0.07952	-0.55859	0.600	0.0473	-0.5071	-0.7988	1.0000
Elevation	0.25122	-0.33511	0.164	-0.4514	-0.1920	-0.3850	0.3565
Elevation	0.251						
MIR	0.251						
Rainf	-0.335						
MaxTemp	0.164						
MinTemp	-0.451						
RH0600	-0.192						
RH1500	-0.385						
Sunsh	0.357						
Elevation	1.000						

Month: 91

	MIR	Rainf	MaxTemp	MinTemp	RH0600	RH1500	Sunsh
MIR	1.0000	0.0147	0.0335	0.0267	-0.0267	-0.210	0.0242
Rainf	0.0147	1.0000	0.1885	0.4572	-0.3070	0.017	0.1112
MaxTemp	0.0335	0.1885	1.0000	0.4562	-0.4444	-0.672	0.3735
MinTemp	0.0267	0.4572	0.4562	1.0000	-0.3391	-0.144	0.3445
RH0600	-0.0267	-0.3070	-0.4444	-0.3391	1.0000	0.464	-0.3055
RH1500	-0.2102	0.0170	-0.6722	-0.1438	0.4643	1.000	-0.3183
Sunsh	0.0242	0.1112	0.3735	0.3445	-0.3055	-0.318	1.0000
Elevation	0.2641	-0.1232	0.1615	-0.4539	-0.1602	-0.323	-0.1012
Elevation	0.264						
MIR	0.264						
Rainf	-0.123						
MaxTemp	0.161						
MinTemp	-0.454						
RH0600	-0.160						
RH1500	-0.323						
Sunsh	-0.101						
Elevation	1.000						

Month: 92

	MIR	Rainf	MaxTemp	MinTemp	RH0600	RH1500	Sunsh
MIR	1.0000	0.3355	0.150	0.0299	0.0514	-0.2111	0.1959
Rainf	0.3355	1.0000	0.296	0.1388	0.0551	-0.3695	0.2940
MaxTemp	0.1502	0.2956	1.000	0.4206	-0.1985	-0.4406	0.2705
MinTemp	0.0299	0.1388	0.421	1.0000	-0.2096	0.1142	0.2252
RH0600	0.0514	0.0551	-0.198	-0.2096	1.0000	0.3026	0.0279
RH1500	-0.2111	-0.3695	-0.441	0.1142	0.3026	1.0000	-0.0292
Sunsh	0.1959	0.2940	0.271	0.2252	0.0279	-0.0292	1.0000
Elevation	0.2366	0.0862	0.100	-0.4618	-0.0709	-0.3714	-0.0911
Elevation	0.2366						
MIR	0.2366						
Rainf	0.0862						
MaxTemp	0.1001						
MinTemp	-0.4618						
RH0600	-0.0709						
RH1500	-0.3714						
Sunsh	-0.0911						
Elevation	1.0000						

```

-----
Month: 93
      MIR  Rainf MaxTemp MinTemp  RH0600 RH1500  Sunsh
MIR    1.0000  0.1528  0.1722  -0.168  0.0516 -0.337  0.154
Rainf  0.1528  1.0000  0.0488  -0.502  0.1990 -0.206 -0.240
MaxTemp 0.1722  0.0488  1.0000  0.252 -0.2637 -0.621  0.364
MinTemp -0.1675 -0.5018  0.2521  1.000 -0.2009  0.229  0.174
RH0600  0.0516  0.1990 -0.2637  -0.201  1.0000  0.191 -0.172
RH1500 -0.3371 -0.2063 -0.6212  0.229  0.1910  1.000 -0.248
Sunsh   0.1538 -0.2399  0.3642  0.174 -0.1725 -0.248  1.000
Elevation 0.2588  0.5181  0.0847  -0.527  0.0135 -0.318 -0.140
      Elevation
MIR    0.2588
Rainf  0.5181
MaxTemp 0.0847
MinTemp -0.5271
RH0600  0.0135
RH1500 -0.3183
Sunsh  -0.1403
Elevation 1.0000
-----

```

```

-----
Month: 94
      MIR  Rainf MaxTemp MinTemp  RH0600 RH1500  Sunsh
MIR    1.0000 -0.202  0.1932 -0.1946 -0.1007 -0.3528  0.0801
Rainf  -0.2016  1.000 -0.4933 -0.2967  0.1595  0.3955 -0.6206
MaxTemp 0.1932 -0.493  1.0000  0.3631 -0.3933 -0.7278  0.6033
MinTemp -0.1946 -0.297  0.3631  1.0000 -0.0785  0.0416  0.2701
RH0600 -0.1007  0.159 -0.3933 -0.0785  1.0000  0.4930 -0.3923
RH1500 -0.3528  0.395 -0.7278  0.0416  0.4930  1.0000 -0.5259
Sunsh   0.0801 -0.621  0.6033  0.2701 -0.3923 -0.5259  1.0000
Elevation 0.2455 -0.123  0.0628 -0.5090 -0.1510 -0.3071  0.0133
      Elevation
MIR    0.2455
Rainf  -0.1231
MaxTemp 0.0628
MinTemp -0.5090
RH0600 -0.1510
RH1500 -0.3071
Sunsh   0.0133
Elevation 1.0000
-----

```

```

-----
Month: 95
      MIR  Rainf MaxTemp MinTemp  RH0600 RH1500  Sunsh
MIR    1.0000  0.0918  0.1166 -0.4465 -0.223 -0.296  0.01930
Rainf  0.0918  1.0000 -0.4008 -0.0199  0.443  0.439 -0.49529
MaxTemp 0.1166 -0.4008  1.0000 -0.0353 -0.585 -0.790  0.62607
MinTemp -0.4465 -0.0199 -0.0353  1.0000  0.158  0.422 -0.06255
RH0600 -0.2231  0.4433 -0.5850  0.1584  1.000  0.718 -0.60954
RH1500 -0.2964  0.4387 -0.7897  0.4216  0.718  1.000 -0.64951
Sunsh   0.0193 -0.4953  0.6261 -0.0625 -0.610 -0.650  1.00000
Elevation 0.2559 -0.1379  0.0561 -0.5437 -0.213 -0.288  0.00709
      Elevation
MIR    0.25587
Rainf  -0.13789
MaxTemp 0.05607
MinTemp -0.54367
RH0600 -0.21268
RH1500 -0.28809
Sunsh   0.00709
Elevation 1.00000
-----

```

```

-----
Month: 96
      MIR  Rainf MaxTemp MinTemp  RH0600 RH1500  Sunsh
MIR    1.0000 -0.095  0.0340  -0.249  -0.186 -0.262 -0.0151
Rainf  -0.0950  1.000 -0.4480  0.387  0.451  0.599 -0.3259
MaxTemp 0.0340 -0.448  1.0000  -0.500 -0.673 -0.698  0.5714
MinTemp -0.2494  0.387 -0.4997  1.000  0.637  0.786 -0.4764
RH0600 -0.1864  0.451 -0.6732  0.637  1.000  0.841 -0.7629
RH1500 -0.2623  0.599 -0.6977  0.786  0.841  1.000 -0.6400
Sunsh  -0.0151 -0.326  0.5714  -0.476 -0.763 -0.640  1.0000
Elevation 0.2379 -0.302  0.0487  -0.459 -0.265 -0.385  0.0483
      Elevation
MIR    0.2379
Rainf  -0.3021
MaxTemp 0.0487
MinTemp -0.4593
RH0600 -0.2650
-----

```

RH1500 -0.3850
 Sunsh 0.0483
 Elevation 1.0000

 Month: 97

	MIR	Rainf	MaxTemp	MinTemp	RH0600	RH1500	Sunsh
MIR	1.00000	-0.00868	0.0205	-0.213	-0.193	-0.264	0.121
Rainf	-0.00868	1.00000	-0.2378	0.417	0.403	0.425	-0.472
MaxTemp	0.02046	-0.23780	1.0000	-0.264	-0.286	-0.418	0.188
MinTemp	-0.21259	0.41653	-0.2640	1.000	0.334	0.570	-0.511
RH0600	-0.19327	0.40307	-0.2859	0.334	1.000	0.793	-0.709
RH1500	-0.26353	0.42462	-0.4184	0.570	0.793	1.000	-0.739
Sunsh	0.12068	-0.47198	0.1881	-0.511	-0.709	-0.739	1.000
Elevation	0.27060	-0.19057	0.0518	-0.395	-0.398	-0.458	0.295

Elevation

MIR	0.2706
Rainf	-0.1906
MaxTemp	0.0518
MinTemp	-0.3951
RH0600	-0.3980
RH1500	-0.4583
Sunsh	0.2953
Elevation	1.0000

 Month : 98

	MIR	Rainf	MaxTemp	MinTemp	RH0600	RH1500	Sunsh
MIR	1.0000	0.0942	0.0809	-0.327	-0.159	-0.256	0.0257
Rainf	0.0942	1.0000	-0.1245	-0.213	0.342	0.165	-0.2332
MaxTemp	0.0809	-0.1245	1.0000	-0.169	-0.688	-0.723	0.2057
MinTemp	-0.3266	-0.2130	-0.1685	1.000	0.150	0.435	-0.1422
RH0600	-0.1594	0.3420	-0.6878	0.150	1.000	0.787	-0.4483
RH1500	-0.2556	0.1646	-0.7227	0.435	0.787	1.000	-0.3575
Sunsh	0.0257	-0.2332	0.2057	-0.142	-0.448	-0.358	1.0000
Elevation	0.3056	0.0283	0.2137	-0.411	-0.325	-0.475	0.3053

Elevation

MIR	0.3056
Rainf	0.0283
MaxTemp	0.2137
MinTemp	-0.4107
RH0600	-0.3254
RH1500	-0.4754
Sunsh	0.3053
Elevation	1.0000

 Month : 99

	MIR	Rainf	MaxTemp	MinTemp	RH0600	RH1500	Sunsh
MIR	1.0000	0.200	0.064	-0.2577	-0.119	-0.1744	-0.0713
Rainf	0.2000	1.000	-0.446	-0.5515	0.443	0.2554	-0.1681
MaxTemp	0.0640	-0.446	1.000	0.3699	-0.770	-0.7672	0.4456
MinTemp	-0.2577	-0.551	0.370	1.0000	-0.305	-0.0375	0.2215
RH0600	-0.1185	0.443	-0.770	-0.3049	1.000	0.7908	-0.5749
RH1500	-0.1744	0.255	-0.767	-0.0375	0.791	1.0000	-0.4389
Sunsh	-0.0713	-0.168	0.446	0.2215	-0.575	-0.4389	1.0000
Elevation	0.3131	0.197	0.178	-0.3506	-0.247	-0.4191	0.1515

Elevation

MIR	0.313
Rainf	0.197
MaxTemp	0.178
MinTemp	-0.351
RH0600	-0.247
RH1500	-0.419
Sunsh	0.152
Elevation	1.000

 Month : 100

	MIR	Rainf	MaxTemp	MinTemp	RH0600	RH1500	Sunsh
MIR	1.0000	0.0649	0.076	-0.164	-0.0542	-0.136	0.0493
Rainf	0.0649	1.0000	-0.552	-0.540	0.5008	0.343	-0.3580
MaxTemp	0.0760	-0.5516	1.000	0.640	-0.8092	-0.833	0.6407
MinTemp	-0.1643	-0.5400	0.640	1.000	-0.5519	-0.344	0.4193
RH0600	-0.0542	0.5008	-0.809	-0.552	1.0000	0.852	-0.6111
RH1500	-0.1361	0.3432	-0.833	-0.344	0.8523	1.000	-0.6258
Sunsh	0.0493	-0.3580	0.641	0.419	-0.6111	-0.626	1.0000
Elevation	0.2919	0.1662	0.139	-0.224	-0.2064	-0.319	0.1668

Elevation

MIR	0.292
Rainf	0.166

MaxTemp 0.139
 MinTemp -0.224
 RH0600 -0.206
 RH1500 -0.319
 Sunsh 0.167
 Elevation 1.000

 Month: 101

	MIR	Rainf	MaxTemp	MinTemp	RH0600	RH1500	Sunsh
MIR	1.00000	0.00602	0.0428	-0.120	0.0167	-0.0771	0.0643
Rainf	0.00602	1.00000	-0.4511	-0.321	0.4027	0.5011	-0.3755
MaxTemp	0.04283	-0.45105	1.0000	0.607	-0.7068	-0.7731	0.6525
MinTemp	-0.12041	-0.32142	0.6072	1.000	-0.5089	-0.3572	0.4269
RH0600	0.01667	0.40271	-0.7068	-0.509	1.0000	0.7871	-0.7006
RH1500	-0.07709	0.50113	-0.7731	-0.357	0.7871	1.0000	-0.6949
Sunsh	0.06435	-0.37551	0.6525	0.427	-0.7006	-0.6949	1.0000
Elevation	0.25115	-0.21124	0.1141	-0.227	-0.2745	-0.3341	0.0898

Elevation
 MIR 0.2511
 Rainf -0.2112
 MaxTemp 0.1141
 MinTemp -0.2269
 RH0600 -0.2745
 RH1500 -0.3341
 Sunsh 0.0898
 Elevation 1.0000

 Month : 102

	MIR	Rainf	MaxTemp	MinTemp	RH0600	RH1500	Sunsh
MIR	1.0000	-0.0201	0.121	-0.0674	-0.082	-0.200	0.177
Rainf	-0.0201	1.0000	-0.176	-0.2163	0.222	0.233	-0.237
MaxTemp	0.1211	-0.1761	1.000	0.4095	-0.578	-0.705	0.481
MinTemp	-0.0674	-0.2163	0.410	1.0000	-0.412	-0.186	0.178
RH0600	-0.0820	0.2222	-0.578	-0.4122	1.000	0.700	-0.584
RH1500	-0.1999	0.2325	-0.705	-0.1865	0.700	1.000	-0.669
Sunsh	0.1771	-0.2365	0.481	0.1783	-0.584	-0.669	1.000
Elevation	0.2366	-0.0331	0.156	-0.3771	-0.220	-0.333	0.244

Elevation
 MIR 0.2366
 Rainf -0.0331
 MaxTemp 0.1559
 MinTemp -0.3771
 RH0600 -0.2203
 RH1500 -0.3330
 Sunsh 0.2445
 Elevation 1.0000

 Month : 103

	MIR	Rainf	MaxTemp	MinTemp	RH0600	RH1500	Sunsh
MIR	1.00000	0.0814	0.0921	-0.1200	0.00513	-0.2656	0.1470
Rainf	0.08145	1.0000	0.2700	0.0971	-0.01840	-0.2272	0.1192
MaxTemp	0.09209	0.2700	1.0000	0.4044	-0.34287	-0.5951	0.3566
MinTemp	-0.12000	0.0971	0.4044	1.0000	-0.36529	-0.0186	0.3486
RH0600	0.00513	-0.0184	-0.3429	-0.3653	1.00000	0.2878	-0.2424
RH1500	-0.26559	-0.2272	-0.5951	-0.0186	0.28779	1.0000	-0.1874
Sunsh	0.14705	0.1192	0.3566	0.3486	-0.24240	-0.1874	1.0000
Elevation	0.30648	0.0245	0.0740	-0.4508	-0.12315	-0.2751	-0.0284

Elevation
 MIR 0.3065
 Rainf 0.0245
 MaxTemp 0.0740
 MinTemp -0.4508
 RH0600 -0.1232
 RH1500 -0.2751
 Sunsh -0.0284
 Elevation 1.0000

 Month : 104

	MIR	Rainf	MaxTemp	MinTemp	RH0600	RH1500	Sunsh
MIR	1.0000	0.254	0.1607	-0.0514	0.1727	-0.1645	0.0804
Rainf	0.2538	1.000	0.2950	0.1472	0.1548	-0.2197	0.1443
MaxTemp	0.1607	0.295	1.0000	0.4129	-0.1655	-0.4732	0.1543
MinTemp	-0.0514	0.147	0.4129	1.0000	-0.2062	-0.0459	0.4365
RH0600	0.1727	0.155	-0.1655	-0.2062	1.0000	0.2315	-0.0672
RH1500	-0.1645	-0.220	-0.4732	-0.0459	0.2315	1.0000	0.3027
Sunsh	0.0804	0.144	0.1543	0.4365	-0.0672	0.3027	1.0000
Elevation	0.2866	0.239	0.0849	-0.3648	-0.0517	-0.2579	-0.0957

Elevation
MIR 0.2866
Rainf 0.2393
MaxTemp 0.0849
MinTemp -0.3648
RH0600 -0.0517
RH1500 -0.2579
Sunsh -0.0957
Elevation 1.0000

Month : 105

	MIR	Rainf	MaxTemp	MinTemp	RH0600	RH1500	Sunsh
MIR	1.0000	0.3422	0.0815	-0.1810	0.226	-0.1812	0.2251
Rainf	0.3422	1.0000	0.3069	-0.3380	0.154	-0.3972	-0.0245
MaxTemp	0.0815	0.3069	1.0000	0.3077	-0.261	-0.6446	0.2634
MinTemp	-0.1810	-0.3380	0.3077	1.0000	-0.213	0.0969	0.3571
RH0600	0.2264	0.1543	-0.2606	-0.2126	1.000	0.2936	-0.1068
RH1500	-0.1812	-0.3972	-0.6446	0.0969	0.294	1.0000	0.0339
Sunsh	0.2251	-0.0245	0.2634	0.3571	-0.107	0.0339	1.0000
Elevation	0.2996	0.4807	0.0393	-0.4765	-0.053	-0.2593	-0.1019

Elevation
MIR 0.2996
Rainf 0.4807
MaxTemp 0.0393
MinTemp -0.4765
RH0600 -0.0530
RH1500 -0.2593
Sunsh -0.1019
Elevation 1.0000

Month : 106

	MIR	Rainf	MaxTemp	MinTemp	RH0600	RH1500	Sunsh
MIR	1.0000	-0.0755	0.19313	-0.2962	-0.0977	-0.3889	0.207
Rainf	-0.0755	1.0000	-0.35239	-0.3341	0.3266	0.2571	-0.441
MaxTemp	0.1931	-0.3524	1.00000	0.3397	-0.3962	-0.7514	0.483
MinTemp	-0.2962	-0.3341	0.33969	1.0000	-0.2437	0.0745	0.426
RH0600	-0.0977	0.3266	-0.39623	-0.2437	1.0000	0.4564	-0.453
RH1500	-0.3889	0.2571	-0.75135	0.0745	0.4564	1.0000	-0.333
Sunsh	0.2065	-0.4408	0.48339	0.4259	-0.4533	-0.3326	1.000
Elevation	0.2703	0.1877	0.00158	-0.5174	-0.0792	-0.2708	-0.199

Elevation
MIR 0.27026
Rainf 0.18766
MaxTemp 0.00158
MinTemp -0.51736
RH0600 -0.07917
RH1500 -0.27079
Sunsh -0.19941
Elevation 1.00000

Month : 107

	MIR	Rainf	MaxTemp	MinTemp	RH0600	RH1500	Sunsh
MIR	1.000	-0.291	0.178	-0.502	-0.246	-0.343	0.1031
Rainf	-0.291	1.000	-0.523	0.365	0.429	0.636	-0.4652
MaxTemp	0.178	-0.523	1.000	-0.297	-0.694	-0.800	0.5780
MinTemp	-0.502	0.365	-0.297	1.000	0.326	0.600	-0.2280
RH0600	-0.246	0.429	-0.694	0.326	1.000	0.817	-0.6472
RH1500	-0.343	0.636	-0.800	0.600	0.817	1.000	-0.6245
Sunsh	0.103	-0.465	0.578	-0.228	-0.647	-0.624	1.0000
Elevation	0.313	-0.375	0.081	-0.462	-0.209	-0.314	0.0502

Elevation
MIR 0.3134
Rainf -0.3745
MaxTemp 0.0810
MinTemp -0.4621
RH0600 -0.2088
RH1500 -0.3138
Sunsh 0.0502
Elevation 1.0000

Month : 108

	MIR	Rainf	MaxTemp	MinTemp	RH0600	RH1500	Sunsh
MIR	1.0000	-0.150	0.0459	-0.4285	-0.237	-0.315	0.1257
Rainf	-0.1504	1.000	-0.5042	0.3909	0.549	0.622	-0.3636
MaxTemp	0.0459	-0.504	1.0000	-0.1925	-0.746	-0.746	0.5494
MinTemp	-0.4285	0.391	-0.1925	1.0000	0.325	0.585	-0.0335
RH0600	-0.2372	0.549	-0.7460	0.3245	1.000	0.878	-0.6446

RH1500 -0.3146 0.622 -0.7465 0.5850 0.878 1.000 -0.5079
 Sunsh 0.1257 -0.364 0.5494 -0.0335 -0.645 -0.508 1.0000
 Elevation 0.2915 -0.230 0.0648 -0.4568 -0.258 -0.373 -0.0755
 Elevation
 MIR 0.2915
 Rainf -0.2296
 MaxTemp 0.0648
 MinTemp -0.4568
 RH0600 -0.2582
 RH1500 -0.3733
 Sunsh -0.0755
 Elevation 1.0000

 Month : 109

	MIR	Rainf	MaxTemp	MinTemp	RH0600	RH1500	Sunsh
MIR	1.0000	0.0888	-0.106	-0.182	-0.0568	-0.0778	0.124
Rainf	0.0888	1.0000	-0.285	0.360	0.3907	0.4321	-0.293
MaxTemp	-0.1065	-0.2848	1.000	-0.376	-0.6151	-0.6669	0.518
MinTemp	-0.1822	0.3603	-0.376	1.000	0.5000	0.7271	-0.413
RH0600	-0.0568	0.3907	-0.615	0.500	1.0000	0.8086	-0.729
RH1500	-0.0778	0.4321	-0.667	0.727	0.8086	1.0000	-0.680
Sunsh	0.1238	-0.2934	0.518	-0.413	-0.7286	-0.6798	1.000
Elevation	0.2245	-0.2280	0.163	-0.505	-0.3440	-0.5334	0.195
Elevation							
MIR	0.225						
Rainf	-0.228						
MaxTemp	0.163						
MinTemp	-0.505						
RH0600	-0.344						
RH1500	-0.533						
Sunsh	0.195						
Elevation	1.000						

 Month : 110

	MIR	Rainf	MaxTemp	MinTemp	RH0600	RH1500	Sunsh
MIR	1.00000	0.1453	-0.0393	-0.2900	-0.0511	-0.0543	-0.00477
Rainf	0.14528	1.0000	-0.2350	-0.1136	0.3479	0.1890	-0.34290
MaxTemp	-0.03930	-0.2350	1.0000	0.1122	-0.6517	-0.6801	0.41167
MinTemp	-0.29003	-0.1136	0.1122	1.0000	0.0788	0.3857	0.19485
RH0600	-0.05111	0.3479	-0.6517	0.0788	1.0000	0.7726	-0.51942
RH1500	-0.05428	0.1890	-0.6801	0.3857	0.7726	1.0000	-0.25788
Sunsh	-0.00477	-0.3429	0.4117	0.1949	-0.5194	-0.2579	1.00000
Elevation	0.25135	0.0889	0.1366	-0.4591	-0.2462	-0.4457	-0.05755
Elevation							
MIR	0.2514						
Rainf	0.0889						
MaxTemp	0.1366						
MinTemp	-0.4591						
RH0600	-0.2462						
RH1500	-0.4457						
Sunsh	-0.0575						
Elevation	1.0000						

 Month : 111

	MIR	Rainf	MaxTemp	MinTemp	RH0600	RH1500	Sunsh
MIR	1.0000	0.0739	-0.0165	-0.230	-0.0962	-0.083	0.122
Rainf	0.0739	1.0000	-0.4119	-0.673	0.4370	0.179	-0.446
MaxTemp	-0.0165	-0.4119	1.0000	0.554	-0.7259	-0.764	0.370
MinTemp	-0.2301	-0.6730	0.5544	1.000	-0.4243	-0.157	0.266
RH0600	-0.0962	0.4370	-0.7259	-0.424	1.0000	0.821	-0.538
RH1500	-0.0830	0.1795	-0.7643	-0.157	0.8206	1.000	-0.451
Sunsh	0.1221	-0.4458	0.3700	0.266	-0.5375	-0.451	1.000
Elevation	0.2743	0.3171	0.1380	-0.319	-0.2350	-0.395	0.063
Elevation							
MIR	0.274						
Rainf	0.317						
MaxTemp	0.138						
MinTemp	-0.319						
RH0600	-0.235						
RH1500	-0.395						
Sunsh	0.063						
Elevation	1.000						

 Month : 112

	MIR	Rainf	MaxTemp	MinTemp	RH0600	RH1500	Sunsh
MIR	1.00000	-0.00438	-0.00862	-0.148	-0.0226	-0.0303	-0.0672
Rainf	-0.00438	1.00000	-0.48453	-0.326	0.5242	0.4936	-0.3384

MaxTemp	-0.00862	-0.48453	1.00000	0.588	-0.7267	-0.7795	0.4616
MinTemp	-0.14770	-0.32619	0.58813	1.000	-0.5113	-0.2891	0.5824
RH0600	-0.02255	0.52421	-0.72665	-0.511	1.0000	0.8167	-0.5288
RH1500	-0.03030	0.49365	-0.77948	-0.289	0.8167	1.0000	-0.3868
Sunsh	-0.06716	-0.33841	0.46164	0.582	-0.5288	-0.3868	1.0000
Elevation	0.25850	-0.14628	0.14311	-0.290	-0.2668	-0.3919	-0.1384

Elevation

MIR	0.258
Rainf	-0.146
MaxTemp	0.143
MinTemp	-0.290
RH0600	-0.267
RH1500	-0.392
Sunsh	-0.138
Elevation	1.000

Month : 113

	MIR	Rainf	MaxTemp	MinTemp	RH0600	RH1500	Sunsh
MIR	1.00000	0.2718	-0.0199	-0.163	0.0393	-0.00835	-0.00197
Rainf	0.27179	1.0000	-0.3460	-0.191	0.2979	0.32136	-0.33491
MaxTemp	-0.01986	-0.3460	1.0000	0.539	-0.6676	-0.72337	0.35270
MinTemp	-0.16315	-0.1913	0.5391	1.000	-0.3587	-0.14930	0.16620
RH0600	0.03935	0.2979	-0.6676	-0.359	1.0000	0.75921	-0.42012
RH1500	-0.00835	0.3214	-0.7234	-0.149	0.7592	1.00000	-0.46527
Sunsh	-0.00197	-0.3349	0.3527	0.166	-0.4201	-0.46527	1.00000
Elevation	0.23890	-0.0885	0.1282	-0.429	-0.2708	-0.40241	0.13700

Elevation

MIR	0.2389
Rainf	-0.0885
MaxTemp	0.1282
MinTemp	-0.4292
RH0600	-0.2708
RH1500	-0.4024
Sunsh	0.1370
Elevation	1.0000

Month : 114

	MIR	Rainf	MaxTemp	MinTemp	RH0600	RH1500	Sunsh
MIR	1.0000	0.0818	0.0741	-0.0908	-0.0489	-0.0345	0.0720
Rainf	0.0818	1.0000	-0.2253	-0.0637	0.1352	0.4754	-0.3653
MaxTemp	0.0741	-0.2253	1.0000	0.3393	-0.5393	-0.6160	0.5283
MinTemp	-0.0908	-0.0637	0.3393	1.0000	-0.1518	0.0917	0.0025
RH0600	-0.0489	0.1352	-0.5393	-0.1518	1.0000	0.5921	-0.6820
RH1500	-0.0345	0.4754	-0.6160	0.0917	0.5921	1.0000	-0.7638
Sunsh	0.0720	-0.3653	0.5283	0.0025	-0.6820	-0.7638	1.0000
Elevation	0.2121	-0.1781	0.1637	-0.5273	-0.2296	-0.3988	0.2708

Elevation

MIR	0.212
Rainf	-0.178
MaxTemp	0.164
MinTemp	-0.527
RH0600	-0.230
RH1500	-0.399
Sunsh	0.271
Elevation	1.000

Month : 115

	MIR	Rainf	MaxTemp	MinTemp	RH0600	RH1500	Sunsh
MIR	1.0000	0.0652	0.2106	-0.1435	-0.0448	-0.185	0.2634
Rainf	0.0652	1.0000	0.0611	0.1031	-0.2496	0.196	0.1164
MaxTemp	0.2106	0.0611	1.0000	0.2590	-0.2476	-0.594	0.4847
MinTemp	-0.1435	0.1031	0.2590	1.0000	-0.0786	0.156	0.0687
RH0600	-0.0448	-0.2496	-0.2476	-0.0786	1.0000	0.272	-0.3168
RH1500	-0.1852	0.1963	-0.5936	0.1564	0.2722	1.000	-0.2969
Sunsh	0.2634	0.1164	0.4847	0.0687	-0.3168	-0.297	1.0000
Elevation	0.2769	-0.0794	0.1419	-0.5591	-0.0995	-0.397	0.0785

Elevation

MIR	0.2769
Rainf	-0.0794
MaxTemp	0.1419
MinTemp	-0.5591
RH0600	-0.0995
RH1500	-0.3974
Sunsh	0.0785
Elevation	1.0000

Month : 116

	MIR	Rainf	MaxTemp	MinTemp	RH0600	RH1500	Sunsh
MIR	1.0000	0.286	0.231	-0.0600	0.1380	0.00462	0.1287
Rainf	0.28585	1.000	0.539	0.2247	0.0250	-0.22423	0.4269
MaxTemp	0.23109	0.539	1.000	0.3816	-0.2221	-0.44282	0.2396
MinTemp	-0.05999	0.225	0.382	1.0000	-0.1077	0.29022	-0.0275
RH0600	0.13803	0.025	-0.222	-0.1077	1.0000	0.36127	-0.0492
RH1500	0.00462	-0.224	-0.443	0.2902	0.3613	1.00000	-0.0168
Sunsh	0.12869	0.427	0.240	-0.0275	-0.0492	-0.01679	1.0000
Elevation	0.26577	0.110	0.102	-0.4837	-0.0289	-0.38471	0.1109

Elevation	
MIR	0.2658
Rainf	0.1099
MaxTemp	0.1022
MinTemp	-0.4837
RH0600	-0.0289
RH1500	-0.3847
Sunsh	0.1109
Elevation	1.0000

Month : 117

	MIR	Rainf	MaxTemp	MinTemp	RH0600	RH1500	Sunsh
MIR	1.0000	0.290	0.2636	-0.102	0.0764	-0.251	0.255
Rainf	0.2901	1.000	0.3186	-0.114	0.2126	-0.409	0.290
MaxTemp	0.2636	0.319	1.0000	0.294	-0.2346	-0.665	0.359
MinTemp	-0.1022	-0.114	0.2944	1.000	-0.2486	0.105	0.251
RH0600	0.0764	0.213	-0.2346	-0.249	1.0000	0.260	-0.211
RH1500	-0.2509	-0.409	-0.6652	0.105	0.2603	1.000	-0.170
Sunsh	0.2547	0.290	0.3591	0.251	-0.2106	-0.170	1.000
Elevation	0.2676	0.266	0.0533	-0.534	0.0799	-0.316	-0.186

Elevation	
MIR	0.2676
Rainf	0.2662
MaxTemp	0.0533
MinTemp	-0.5340
RH0600	0.0799
RH1500	-0.3159
Sunsh	-0.1859
Elevation	1.0000

Month : 118

	MIR	Rainf	MaxTemp	MinTemp	RH0600	RH1500	Sunsh
MIR	1.0000	0.1299	0.184	-0.221	-0.0718	-0.3319	0.0595
Rainf	0.1299	1.0000	-0.076	-0.440	0.3625	-0.0528	-0.4924
MaxTemp	0.1836	-0.0760	1.000	0.289	-0.4248	-0.7305	0.3887
MinTemp	-0.2214	-0.4403	0.289	1.000	-0.3427	0.1152	0.3614
RH0600	-0.0718	0.3625	-0.425	-0.343	1.0000	0.4856	-0.4332
RH1500	-0.3319	-0.0528	-0.730	0.115	0.4856	1.0000	-0.3620
Sunsh	0.0595	-0.4924	0.389	0.361	-0.4332	-0.3620	1.0000
Elevation	0.2810	0.2642	0.037	-0.575	0.0420	-0.2199	-0.2820

Elevation	
MIR	0.281
Rainf	0.264
MaxTemp	0.037
MinTemp	-0.575
RH0600	0.042
RH1500	-0.220
Sunsh	-0.282
Elevation	1.000

Month : 119

	MIR	Rainf	MaxTemp	MinTemp	RH0600	RH1500	Sunsh
MIR	1.0000	0.0563	0.1566	-0.4213	-0.206	-0.309	-0.0243
Rainf	0.0563	1.0000	-0.5782	-0.0242	0.487	0.506	-0.5607
MaxTemp	0.1566	-0.5782	1.0000	-0.0972	-0.654	-0.792	0.4355
MinTemp	-0.4213	-0.0242	-0.0972	1.0000	0.236	0.495	-0.0244
RH0600	-0.2057	0.4869	-0.6541	0.2360	1.000	0.788	-0.4870
RH1500	-0.3094	0.5059	-0.7923	0.4945	0.788	1.000	-0.4404
Sunsh	-0.0243	-0.5607	0.4355	-0.0244	-0.487	-0.440	1.0000
Elevation	0.3198	0.0493	0.0520	-0.6089	-0.172	-0.297	-0.0265

Elevation	
MIR	0.3198
Rainf	0.0493
MaxTemp	0.0520
MinTemp	-0.6089
RH0600	-0.1715
RH1500	-0.2965
Sunsh	-0.0265

```

Elevation      1.0000
-----
Month : 120
      MIR    Rainf  MaxTemp  MinTemp  RH0600  RH1500  Sunsh
MIR      1.0000 -0.0638  0.0976  -0.197  -0.0884 -0.189  0.0856
Rainf    -0.0638 1.0000 -0.4211  0.577  0.4901  0.670 -0.3606
MaxTemp  0.0976 -0.4211 1.0000 -0.386  -0.6482 -0.677  0.4851
MinTemp  -0.1969 0.5774 -0.3859  1.000  0.6611  0.785 -0.4477
RH0600   -0.0884 0.4901 -0.6482  0.661  1.0000  0.813 -0.6415
RH1500   -0.1893 0.6701 -0.6773  0.785  0.8134  1.000 -0.5604
Sunsh    0.0856 -0.3606 0.4851  -0.448  -0.6415 -0.560  1.0000
Elevation 0.3086 -0.2965 0.0641  -0.529  -0.2242 -0.393  0.0602
      Elevation
MIR      0.3086
Rainf    -0.2965
MaxTemp  0.0641
MinTemp  -0.5292
RH0600   -0.2242
RH1500   -0.3929
Sunsh    0.0602
Elevation 1.0000
-----
Month : 121
      MIR    Rainf  MaxTemp  MinTemp  RH0600  RH1500  Sunsh
MIR      1.0000 -0.0358 -0.1714 -0.3182 -0.157  -0.111  0.113
Rainf    -0.0358 1.0000 -0.2920  0.3302  0.445  0.314 -0.426
MaxTemp  -0.1714 -0.2920 1.0000 -0.0819 -0.356  -0.358  0.539
MinTemp  -0.3182 0.3302 -0.0819  1.0000  0.625  0.683 -0.320
RH0600   -0.1569 0.4451 -0.3561  0.6253  1.000  0.728 -0.692
RH1500   -0.1109 0.3143 -0.3576  0.6827  0.728  1.000 -0.429
Sunsh    0.1134 -0.4263 0.5391  -0.3195 -0.692  -0.429  1.000
Elevation 0.2413 -0.1131 0.0880  -0.4688 -0.267  -0.498  0.112
      Elevation
MIR      0.241
Rainf    -0.113
MaxTemp  0.088
MinTemp  -0.469
RH0600   -0.267
RH1500   -0.498
Sunsh    0.112
Elevation 1.000
-----
Month : 122
      MIR    Rainf  MaxTemp  MinTemp  RH0600  RH1500  Sunsh
MIR      1.00000 0.0408 -0.0152 -0.214  -0.047  -0.0365  0.00386
Rainf    0.04084 1.0000 -0.1595  0.149  0.503  0.4087 -0.07013
MaxTemp  -0.01517 -0.1595 1.0000 0.208  -0.314  -0.2414  0.55514
MinTemp  -0.21410 0.1487 0.2081  1.000  0.427  0.5856  0.17599
RH0600   -0.04702 0.5032 -0.3136  0.427  1.000  0.6637 -0.49884
RH1500   -0.03647 0.4087 -0.2414  0.586  0.664  1.0000 -0.09448
Sunsh    0.00386 -0.0701 0.5551  0.176  -0.499  -0.0945  1.00000
Elevation 0.23610 -0.0410 0.1439  -0.481  -0.287  -0.4076  0.09166
      Elevation
MIR      0.2361
Rainf    -0.0410
MaxTemp  0.1439
MinTemp  -0.4805
RH0600   -0.2870
RH1500   -0.4076
Sunsh    0.0917
Elevation 1.0000
-----
Month : 123
      MIR    Rainf  MaxTemp  MinTemp  RH0600  RH1500  Sunsh
MIR      1.0000 0.0411 0.0626 -0.1457 -0.1616 -0.132  0.0402
Rainf    0.0411 1.0000 -0.4829 -0.2413 0.6120 0.463 -0.3888
MaxTemp  0.0626 -0.4829 1.0000 0.5267 -0.5486 -0.355 0.2532
MinTemp  -0.1457 -0.2413 0.5267 1.0000 -0.0771 0.230 -0.0240
RH0600   -0.1616 0.6120 -0.5486 -0.0771 1.0000 0.699 -0.2911
RH1500   -0.1325 0.4628 -0.3549 0.2297 0.6989 1.000 -0.4650
Sunsh    0.0402 -0.3888 0.2532 -0.0240 -0.2911 -0.465 1.0000
Elevation 0.2367 -0.0799 0.1144 -0.4099 -0.2680 -0.351 0.1346
      Elevation
MIR      0.2367
Rainf    -0.0799
MaxTemp  0.1144
MinTemp  -0.4099

```

RH0600 -0.2680
 RH1500 -0.3513
 Sunsh 0.1346
 Elevation 1.0000

 Month : 124

	MIR	Rainf	MaxTemp	MinTemp	RH0600	RH1500	Sunsh
MIR	1.00000	0.253	-0.0385	-0.1223	-0.0656	-0.00208	-0.0873
Rainf	0.25299	1.000	-0.3532	-0.4798	0.3421	0.27302	-0.4256
MaxTemp	-0.03845	-0.353	1.0000	0.6078	-0.3056	-0.33741	0.4511
MinTemp	-0.12231	-0.480	0.6078	1.0000	-0.2405	0.01729	0.4733
RH0600	-0.06556	0.342	-0.3056	-0.2405	1.0000	0.70384	-0.2016
RH1500	-0.00208	0.273	-0.3374	0.0173	0.7038	1.00000	-0.2611
Sunsh	-0.08727	-0.426	0.4511	0.4733	-0.2016	-0.26109	1.0000
Elevation	0.27159	0.189	0.0582	-0.3395	-0.2124	-0.35635	-0.1180

Elevation
 MIR 0.2716
 Rainf 0.1890
 MaxTemp 0.0582
 MinTemp -0.3395
 RH0600 -0.2124
 RH1500 -0.3563
 Sunsh -0.1180
 Elevation 1.0000

 Month : 125

	MIR	Rainf	MaxTemp	MinTemp	RH0600	RH1500	Sunsh
MIR	1.0000	0.1887	0.0619	-0.1377	-0.0817	-0.0748	0.0708
Rainf	0.1887	1.0000	-0.1969	-0.0195	0.3108	0.5074	-0.1897
MaxTemp	0.0619	-0.1969	1.0000	0.5718	-0.0264	-0.2994	0.5432
MinTemp	-0.1377	-0.0195	0.5718	1.0000	0.0268	0.2238	0.3133
RH0600	-0.0817	0.3108	-0.0264	0.0268	1.0000	0.6477	-0.2492
RH1500	-0.0748	0.5074	-0.2994	0.2238	0.6477	1.0000	-0.3438
Sunsh	0.0708	-0.1897	0.5432	0.3133	-0.2492	-0.3438	1.0000
Elevation	0.3000	-0.2453	0.0718	-0.4073	-0.1452	-0.3791	0.0919

Elevation
 MIR 0.3000
 Rainf -0.2453
 MaxTemp 0.0718
 MinTemp -0.4073
 RH0600 -0.1452
 RH1500 -0.3791
 Sunsh 0.0919
 Elevation 1.0000

 Month : 126

	MIR	Rainf	MaxTemp	MinTemp	RH0600	RH1500	Sunsh
MIR	1.0000	-0.0675	0.1000	-0.11543	-0.2377	-0.1766	0.13316
Rainf	-0.0675	1.0000	-0.1408	0.07534	0.1399	0.3875	-0.30948
MaxTemp	0.1000	-0.1408	1.0000	0.45045	0.3732	-0.0691	0.43619
MinTemp	-0.1154	0.0753	0.4505	1.00000	0.1966	0.3700	0.00582
RH0600	-0.2377	0.1399	0.3732	0.19658	1.0000	0.5507	-0.11177
RH1500	-0.1766	0.3875	-0.0691	0.36999	0.5507	1.0000	-0.55306
Sunsh	0.1332	-0.3095	0.4362	0.00582	-0.1118	-0.5531	1.00000
Elevation	0.3123	-0.2616	0.0675	-0.46300	-0.0295	-0.3134	0.22422

Elevation
 MIR 0.3123
 Rainf -0.2616
 MaxTemp 0.0675
 MinTemp -0.4630
 RH0600 -0.0295
 RH1500 -0.3134
 Sunsh 0.2242
 Elevation 1.0000

 Month : 127

	MIR	Rainf	MaxTemp	MinTemp	RH0600	RH1500	Sunsh
MIR	1.0000	0.1710	0.1126	-0.112	-0.0745	-0.1700	0.1417
Rainf	0.1710	1.0000	0.0741	-0.188	0.0769	-0.1608	0.1649
MaxTemp	0.1126	0.0741	1.0000	0.436	0.4950	0.0779	0.2822
MinTemp	-0.1115	-0.1879	0.4363	1.000	0.2890	0.4005	0.2928
RH0600	-0.0745	0.0769	0.4950	0.289	1.0000	0.4984	0.0560
RH1500	-0.1700	-0.1608	0.0779	0.401	0.4984	1.0000	0.0816
Sunsh	0.1417	0.1649	0.2822	0.293	0.0560	0.0816	1.0000
Elevation	0.2762	0.3454	0.0370	-0.454	-0.0300	-0.4168	-0.0824

Elevation
 MIR 0.2762

Rainf 0.3454
 MaxTemp 0.0370
 MinTemp -0.4543
 RH0600 -0.0300
 RH1500 -0.4168
 Sunsh -0.0824
 Elevation 1.0000

 Month : 128

	MIR	Rainf	MaxTemp	MinTemp	RH0600	RH1500	Sunsh
MIR	1.0000	0.28830	0.1031	-0.11683	-0.0834	-0.1036	0.2744
Rainf	0.2883	1.00000	0.2914	0.00619	0.0396	-0.2882	0.5020
MaxTemp	0.1031	0.29138	1.0000	0.45632	0.5202	0.0957	0.2309
MinTemp	-0.1168	0.00619	0.4563	1.00000	0.3756	0.3836	0.0568
RH0600	-0.0834	0.03963	0.5202	0.37561	1.0000	0.5740	0.1430
RH1500	-0.1036	-0.28821	0.0957	0.38357	0.5740	1.0000	-0.0272
Sunsh	0.2744	0.50196	0.2309	0.05675	0.1430	-0.0272	1.0000
Elevation	0.2645	0.31321	0.0432	-0.44143	-0.0513	-0.2643	0.0932

Elevation
 MIR 0.2645
 Rainf 0.3132
 MaxTemp 0.0432
 MinTemp -0.4414
 RH0600 -0.0513
 RH1500 -0.2643
 Sunsh 0.0932
 Elevation 1.0000

 Month : 129

	MIR	Rainf	MaxTemp	MinTemp	RH0600	RH1500	Sunsh
MIR	1.0000	0.03017	0.1398	-0.158	-0.0772	-0.2419	0.14030
Rainf	0.0302	1.00000	0.0956	-0.190	0.1613	-0.0660	0.00501
MaxTemp	0.1398	0.09560	1.0000	0.411	0.5744	0.0490	0.26075
MinTemp	-0.1577	-0.18976	0.4112	1.000	0.3752	0.3849	0.20663
RH0600	-0.0772	0.16131	0.5744	0.375	1.0000	0.5502	0.22443
RH1500	-0.2419	-0.06601	0.0490	0.385	0.5502	1.0000	0.05827
Sunsh	0.1403	0.00501	0.2608	0.207	0.2244	0.0583	1.00000
Elevation	0.3146	0.36255	-0.0397	-0.500	-0.0369	-0.1787	-0.25665

Elevation
 MIR 0.3146
 Rainf 0.3625
 MaxTemp -0.0397
 MinTemp -0.5004
 RH0600 -0.0369
 RH1500 -0.1787
 Sunsh -0.2567
 Elevation 1.0000

 Month : 130

	MIR	Rainf	MaxTemp	MinTemp	RH0600	RH1500	Sunsh
MIR	1.00000	0.0314	0.15586	-0.181	-0.1813	-0.3074	0.00289
Rainf	0.03137	1.0000	-0.17014	-0.167	0.2178	0.2636	-0.29058
MaxTemp	0.15586	-0.1701	1.00000	0.365	0.4538	-0.1306	0.43484
MinTemp	-0.18144	-0.1668	0.36493	1.000	0.3401	0.3996	0.33637
RH0600	-0.18129	0.2178	0.45383	0.340	1.0000	0.5062	0.12550
RH1500	-0.30739	0.2636	-0.13062	0.400	0.5062	1.0000	-0.05076
Sunsh	0.00289	-0.2906	0.43484	0.336	0.1255	-0.0508	1.00000
Elevation	0.29214	0.0751	-0.00502	-0.488	-0.0805	-0.3016	-0.18806

Elevation
 MIR 0.29214
 Rainf 0.07505
 MaxTemp -0.00502
 MinTemp -0.48794
 RH0600 -0.08048
 RH1500 -0.30163
 Sunsh -0.18806
 Elevation 1.00000

 Month : 131

	MIR	Rainf	MaxTemp	MinTemp	RH0600	RH1500	Sunsh
MIR	1.000	-0.111	0.1655	-0.33579	-0.355	-0.336	0.18719
Rainf	-0.111	1.000	-0.4488	0.30742	0.458	0.662	-0.52603
MaxTemp	0.165	-0.449	1.0000	0.10938	-0.232	-0.413	0.57280
MinTemp	-0.336	0.307	0.1094	1.00000	0.480	0.548	0.00519
RH0600	-0.355	0.458	-0.2317	0.47962	1.000	0.726	-0.35493
RH1500	-0.336	0.662	-0.4135	0.54837	0.726	1.000	-0.49671
Sunsh	0.187	-0.526	0.5728	0.00519	-0.355	-0.497	1.00000

```

Elevation  0.290 -0.252  0.0629 -0.50358 -0.198 -0.369 -0.01069
Elevation
MIR        0.2902
Rainf     -0.2522
MaxTemp   0.0629
MinTemp   -0.5036
RH0600    -0.1982
RH1500    -0.3693
Sunsh     -0.0107
Elevation  1.0000

```

Month : 132

```

MIR      Rainf  MaxTemp  MinTemp  RH0600  RH1500  Sunsh
MIR      1.0000 -0.0224  0.0869  -0.182  -0.191  -0.174  0.0917
Rainf   -0.0224  1.0000  -0.3161  0.445  0.401  0.550 -0.2340
MaxTemp  0.0869 -0.3161  1.0000  -0.107  -0.417  -0.370  0.5597
MinTemp -0.1819  0.4453  -0.1069  1.000  0.640  0.749 -0.1221
RH0600  -0.1912  0.4007  -0.4172  0.640  1.000  0.784 -0.4888
RH1500  -0.1739  0.5505  -0.3702  0.749  0.784  1.000 -0.2969
Sunsh   0.0917 -0.2340  0.5597  -0.122  -0.489  -0.297  1.0000
Elevation 0.2794 -0.1637  0.0165  -0.444  -0.255  -0.383 -0.1036

```

```

Elevation
MIR      0.2794
Rainf    -0.1637
MaxTemp  0.0165
MinTemp  -0.4441
RH0600  -0.2546
RH1500  -0.3835
Sunsh    -0.1036
Elevation  1.0000

```

B-4: Cross-correlation Analysis of MIR with Covariates

Results B-4.1: Spatial correlations of residuals (detrended MIR) with climatic covariates at the study areas (national, BAR and vegetation zones)

National

```

Residuals  1.00000  0.27652 -0.3233 -0.09078  0.2876  0.3207 -0.1942
Rainfall   0.27652  1.00000 -0.3660  0.04911  0.4017  0.4950 -0.3010
MaxTemp    -0.32333  -0.36602  1.0000  0.23637 -0.5782 -0.7429  0.6486
MinTemp    -0.09078  0.04911  0.2364  1.00000  0.1307  0.1750  0.1248
RH0600     0.28756  0.40171 -0.5782  0.13069  1.0000  0.7986 -0.4125
RH1500     0.32072  0.49502 -0.7429  0.17501  0.7986  1.0000 -0.5477
Sunshrs   -0.19417  -0.30103  0.6486  0.12478 -0.4125 -0.5477  1.0000

```

National

```

Resid1  Rainf_1  MaxT_1  MinT_1  RH0600_1  RH1500_1  Sunsh_1
Residuals  1.00000  0.37981 -0.2827  0.02564  0.3179  0.3597 -0.1790
Rainfall_1 0.37981  1.00000 -0.3685  0.04868  0.4017  0.4978 -0.2996
MaxTemp_1 -0.28272  -0.36849  1.0000  0.23382 -0.5781 -0.7451  0.6494
MinTemp_1  0.02564  0.04868  0.2338  1.00000  0.1308  0.1765  0.1251
RH0600_1  0.31792  0.40171 -0.5781  0.13077  1.0000  0.7979 -0.4135
RH1500_1  0.35967  0.49783 -0.7451  0.17649  0.7979  1.0000 -0.5495
Sunshrs_1 -0.17896  -0.29958  0.6494  0.12512 -0.4135 -0.5495  1.0000

```

BAR

```

Residuals1  Rainf_1  MaxT_1  MinT_1  RH0600_1  RH1500_1  Sunsh_1
Residuals1  1.0000  0.37562 -0.2066  0.04910  0.2892  0.3591 -0.1322
Rainf_1     0.3756  1.00000 -0.3059  0.09534  0.4944  0.5876 -0.1823
MaxT_1     -0.2066 -0.30594  1.0000  0.14057 -0.5576 -0.7073  0.7326
MinT_1     0.0491  0.09534  0.1406  1.00000  0.1817 -0.0473  0.1601
RH0600_1  0.2892  0.49440 -0.5576  0.18166  1.0000  0.8295 -0.3795
RH1500_1  0.3591  0.58757 -0.7073 -0.04730  0.8295  1.0000 -0.5851
Sunsh_1   -0.1322 -0.18235  0.7326  0.16007 -0.3795 -0.5851  1.0000

```

BAR

	Residuals1	Rainfall	MaxTemp	MinTemp	RH0600	RH1500	Sunshrs
Residuals1	1.00000	0.1973	-0.3109	-0.07303	0.2564	0.35191	-0.2079
Rainfall	0.19726	1.0000	-0.3070	0.09700	0.4947	0.58820	-0.1868
MaxTemp	-0.31088	-0.3070	1.0000	0.14022	-0.5580	-0.70691	0.7324
MinTemp	-0.07303	0.0970	0.1402	1.00000	0.1815	-0.04862	0.1583
RH0600	0.25640	0.4947	-0.5580	0.18145	1.0000	0.82942	-0.3803
RH1500	0.35191	0.5882	-0.7069	-0.04862	0.8294	1.00000	-0.5856
Sunshrs	-0.20789	-0.1868	0.7324	0.15832	-0.3803	-0.58564	1.0000

Coastal Zone

	Residuals1	Rainfall_1	MaxTemp_1	MinTemp_1	RH0600_1	RH1500_1	Sunshrs_1
Residuals1	1.00000	0.34471	-0.07103	0.04277	0.06322	0.14283	-0.06689
Rainfall_1	0.34471	1.00000	-0.17565	-0.02775	0.16894	0.28063	-0.19057
MaxTemp_1	-0.07103	-0.17565	1.00000	0.53391	-0.24067	-0.72198	0.51424
MinTemp_1	0.04277	-0.02775	0.53391	1.00000	-0.26482	-0.07982	0.47082
RH0600_1	0.06322	0.16894	-0.24067	-0.26482	1.00000	0.45509	-0.06434
RH1500_1	0.14283	0.28063	-0.72198	-0.07982	0.45509	1.00000	-0.19825
Sunshrs_1	-0.06689	-0.19057	0.51424	0.47082	-0.06434	-0.19825	1.00000

Forest Zone

	Residuals1	Rainfall_1	MaxTemp_1	MinTemp_1	RH0600_1	RH1500_1	Sunshrs_1
Residuals1	1.00000	0.31626	-0.1944	0.027956	0.2175	0.325050	-0.1237
Rainfall_1	0.31626	1.00000	-0.2736	0.092644	0.3830	0.548638	-0.1821
MaxTemp_1	-0.19441	-0.27356	1.0000	0.331797	-0.3047	-0.632470	0.6111
MinTemp_1	0.02796	0.09264	0.3318	1.000000	0.1500	-0.003617	0.1827
RH0600_1	0.21749	0.38301	-0.3047	0.150003	1.0000	0.713302	-0.2310
RH1500_1	0.32505	0.54864	-0.6325	-0.003617	0.7133	1.000000	-0.5051
Sunshrs_1	-0.12372	-0.18210	0.6111	0.182747	-0.2310	-0.505144	1.0000

Northern Zone

	Residuals1	Rainfall_1	MaxTemp_1	MinTemp_1	RH0600_1	RH1500_1	Sunshrs_1
Residuals1	1.00000	0.5091	-0.5066	0.02884	0.4735	0.5572	-0.38908
Rainfall_1	0.50910	1.0000	-0.7267	0.13411	0.6713	0.8181	-0.66400
MaxTemp_1	-0.50664	-0.7267	1.0000	0.30293	-0.6529	-0.7785	0.63546
MinTemp_1	0.02884	0.1341	0.3029	1.00000	0.1372	0.1924	-0.09998
RH0600_1	0.47353	0.6713	-0.6529	0.13723	1.0000	0.8655	-0.48115
RH1500_1	0.55717	0.8181	-0.7785	0.19242	0.8655	1.0000	-0.68671
Sunshrs_1	-0.38908	-0.6640	0.6355	-0.09998	-0.4811	-0.6867	1.00000

Results B-4.2: Temporal correlations of residuals (detrended MIR) with climatic covariates at the district weather locations across the country

Accra MA

	Residuals1	Rainfall_1	MaxTemp_1	MinTemp_1	RH0600_1	RH1500_1	Sunshrs_1
Residuals1	1.0000	0.48149	-0.5194	-0.41905	0.3562	0.5929	-0.26465
Rainfall_1	0.4815	1.00000	-0.1609	-0.08735	0.3053	0.3950	-0.09171
MaxTemp_1	-0.5194	-0.16093	1.0000	0.85388	-0.3632	-0.7036	0.65791
MinTemp_1	-0.4190	-0.08735	0.8539	1.00000	-0.1255	-0.4008	0.51295
RH0600_1	0.3562	0.30533	-0.3632	-0.12553	1.0000	0.7730	0.11470
RH1500_1	0.5929	0.39495	-0.7036	-0.40075	0.7730	1.0000	-0.29355
Sunshrs_1	-0.2646	-0.09171	0.6579	0.51295	0.1147	-0.2935	1.00000

AframP/KwahuN

	Residuals1	Rainfall_1	MaxTemp_1	MinTemp_1	RH0600_1	RH1500_1	Sunshrs_1
Residuals1	1.00000	0.09881	-0.3403	-0.16938	0.07786	0.24128	-0.33138
Rainfall_1	0.09881	1.00000	-0.2353	0.19748	0.44379	0.59125	-0.03923
MaxTemp_1	-0.34029	-0.23534	1.0000	0.50665	-0.43934	-0.78061	0.74018
MinTemp_1	-0.16938	0.19748	0.5066	1.00000	0.31211	0.02926	0.33140
RH0600_1	0.07786	0.44379	-0.4393	0.31211	1.00000	0.80156	-0.10203
RH1500_1	0.24128	0.59125	-0.7806	0.02926	0.80156	1.00000	-0.46702
Sunshrs_1	-0.33138	-0.03923	0.7402	0.33140	-0.10203	-0.46702	1.00000

Agona

	Residuals1	Rainfall_1	MaxTemp_1	MinTemp_1	RH0600_1	RH1500_1	Sunshrs_1
Residuals1	1.00000	-0.03041	0.2497	0.19773	-0.059534	-0.1377	0.268052
Rainfall_1	-0.03041	1.00000	-0.3162	0.05947	0.317587	0.5319	-0.115339
MaxTemp_1	0.24974	-0.31621	1.0000	0.62247	-0.229991	-0.8256	0.768020
MinTemp_1	0.19773	0.05947	0.6225	1.00000	0.067073	-0.2585	0.517336
RH0600_1	-0.05953	0.31759	-0.2300	0.06707	1.000000	0.4502	-0.005548
RH1500_1	-0.13772	0.53193	-0.8256	-0.25853	0.450194	1.0000	-0.483958
Sunshrs_1	0.26805	-0.11534	0.7680	0.51734	-0.005548	-0.4840	1.000000

Ahafo AnoN

	Residuals1	Rainfall_1	MaxTemp_1	MinTemp_1	RH0600_1	RH1500_1	Sunshrs_1
Residuals1	1.00000	0.38406	-0.09409	0.22424	0.2178	0.26433	-0.01956
Rainfall_1	0.38406	1.00000	-0.22414	0.28570	0.5541	0.55266	-0.07899
MaxTemp_1	-0.09409	-0.22414	1.00000	0.50368	-0.5434	-0.85253	0.85829
MinTemp_1	0.22424	0.28570	0.50368	1.00000	0.2728	-0.06598	0.42993
RH0600_1	0.21776	0.55408	-0.54339	0.27277	1.00000	0.84670	-0.33303
RH1500_1	0.26433	0.55266	-0.85253	-0.06598	0.8467	1.00000	-0.67200
Sunshrs_1	-0.01956	-0.07899	0.85829	0.42993	-0.3330	-0.67200	1.00000

Ahanta W

	Residuals1	Rainfall_1	MaxTemp_1	MinTemp_1	RH0600_1	RH1500_1	Sunshrs_1
Residuals1	1.0000000	0.22098	-0.0002829	0.02541	-0.01678	0.2482	-0.01101
Rainfall_1	0.2209808	1.00000	-0.0891678	0.25199	-0.19075	0.3142	-0.11589
MaxTemp_1	-0.0002829	-0.08917	1.0000000	0.72092	-0.44479	-0.7866	0.71385
MinTemp_1	0.0254097	0.25199	0.7209154	1.00000	-0.50721	-0.3624	0.48955
RH0600_1	-0.0167768	-0.19075	-0.4447859	-0.50721	1.00000	0.4765	-0.11146
RH1500_1	0.2481821	0.31417	-0.7865915	-0.36237	0.47652	1.0000	-0.57916
Sunshrs_1	-0.0110056	-0.11589	0.7138454	0.48955	-0.11146	-0.5792	1.00000

Akatsi

	Residuals1	Rainfall_1	MaxTemp_1	MinTemp_1	RH0600_1	RH1500_1	Sunshrs_1
Residuals1	1.00000	0.44454	-0.3772	-0.06113	0.21673	0.4164	-0.40401
Rainfall_1	0.44454	1.00000	-0.1866	0.02962	0.25318	0.3517	0.04789
MaxTemp_1	-0.37722	-0.18665	1.0000	0.74454	-0.33948	-0.5073	0.65360
MinTemp_1	-0.06113	0.02962	0.7445	1.00000	0.14080	-0.2379	0.48823
RH0600_1	0.21673	0.25318	-0.3395	0.14080	1.00000	0.5158	0.07528
RH1500_1	0.41645	0.35165	-0.5073	-0.23792	0.51582	1.0000	-0.22512
Sunshrs_1	-0.40401	0.04789	0.6536	0.48823	0.07528	-0.2251	1.00000

Akwapim S

	Residuals1	Rainfall_1	MaxTemp_1	MinTemp_1	RH0600_1	RH1500_1	Sunshrs_1
Residuals1	1.00000	0.19094	-0.1511	-0.1228	-0.03962	0.2018	-0.02003
Rainfall_1	0.19094	1.00000	-0.2669	-0.1173	0.20684	0.4062	-0.08847
MaxTemp_1	-0.15105	-0.26690	1.0000	0.7627	-0.22090	-0.7824	0.76909
MinTemp_1	-0.12276	-0.11726	0.7627	1.0000	-0.15122	-0.5583	0.71922
RH0600_1	-0.03962	0.20684	-0.2209	-0.1512	1.00000	0.3938	-0.10534
RH1500_1	0.20178	0.40624	-0.7824	-0.5583	0.39383	1.0000	-0.45898
Sunshrs_1	-0.02003	-0.08847	0.7691	0.7192	-0.10534	-0.4590	1.00000

Amansie E/BM

	Residuals1	Rainfall_1	MaxTemp_1	MinTemp_1	RH0600_1	RH1500_1	Sunshrs_1
Residuals1	1.00000	0.3099	-0.1517	-0.053994	0.274998	0.2911	-0.05876
Rainfall_1	0.30993	1.0000	-0.2946	0.155639	0.513650	0.5911	-0.14818
MaxTemp_1	-0.15169	-0.2946	1.0000	0.657207	-0.498926	-0.8013	0.88117
MinTemp_1	-0.05399	0.1556	0.6572	1.000000	0.007197	-0.2839	0.57648
RH0600_1	0.27500	0.5136	-0.4989	0.007197	1.000000	0.8488	-0.36196
RH1500_1	0.29111	0.5911	-0.8013	-0.283865	0.848803	1.0000	-0.66901
Sunshrs_1	-0.05876	-0.1482	0.8812	0.576483	-0.361958	-0.6690	1.00000

Aowin S

	Residuals1	Rainfall_1	MaxTemp_1	MinTemp_1	RH0600_1	RH1500_1	Sunshrs_1
Residuals1	1.00000	0.21418	-0.1043	0.06434	0.40557	0.15085	0.17983
Rainfall_1	0.21418	1.00000	-0.1635	0.07073	0.36229	0.43417	-0.11970
MaxTemp_1	-0.10426	-0.16353	1.0000	0.47010	-0.37240	-0.77538	0.74862
MinTemp_1	0.06434	0.07073	0.4701	1.00000	0.12364	-0.03121	0.32568
RH0600_1	0.40557	0.36229	-0.3724	0.12364	1.00000	0.64092	-0.07116
RH1500_1	0.15085	0.43417	-0.7754	-0.03121	0.64092	1.00000	-0.60496
Sunshrs_1	0.17983	-0.11970	0.7486	0.32568	-0.07116	-0.60496	1.00000

Asante AN

	Residuals1	Rainfall_1	MaxTemp_1	MinTemp_1	RH0600_1	RH1500_1	Sunshrs_1
Residuals1	1.00000	0.2597	-0.1868	-0.06508	0.1353	0.2095	-0.1072
Rainfall_1	0.25968	1.0000	-0.2407	0.15406	0.4604	0.5077	-0.1091
MaxTemp_1	-0.18684	-0.2407	1.0000	0.57061	-0.5424	-0.8561	0.8719
MinTemp_1	-0.06508	0.1541	0.5706	1.00000	0.2366	-0.1403	0.5055
RH0600_1	0.13532	0.4604	-0.5424	0.23660	1.0000	0.8307	-0.3879
RH1500_1	0.20950	0.5077	-0.8561	-0.14031	0.8307	1.0000	-0.6939
Sunshrs_1	-0.10721	-0.1091	0.8719	0.50549	-0.3879	-0.6939	1.0000

Assin N

	Residuals1	Rainfall_1	MaxTemp_1	MinTemp_1	RH0600_1	RH1500_1	Sunshrs_1
Residuals1	1.00000	0.3382	-0.07242	0.33150	0.3625	0.35319	0.0908
Rainfall_1	0.33818	1.0000	-0.40432	0.21946	0.5239	0.63742	-0.2277
MaxTemp_1	-0.07242	-0.4043	1.00000	0.40129	-0.4917	-0.82523	0.8051
MinTemp_1	0.33150	0.2195	0.40129	1.00000	0.3285	0.08481	0.3741
RH0600_1	0.36248	0.5239	-0.49168	0.32852	1.0000	0.81708	-0.1541

RH1500_1	0.35319	0.6374	-0.82523	0.08481	0.8171	1.00000	-0.5288
Sunshrs_1	0.09080	-0.2277	0.80513	0.37413	-0.1541	-0.52876	1.0000

Asunafo N

	Residuals1	Rainfall_1	MaxTemp_1	MinTemp_1	RH0600_1	RH1500_1	Sunshrs_1
Residuals1	1.0000	0.49093	-0.2273	-0.03800	0.44251	0.4777	-0.11054
Rainfall_1	0.4909	1.00000	-0.2108	0.15889	0.49106	0.5582	-0.09839
MaxTemp_1	-0.2273	-0.21076	1.0000	0.62552	-0.45287	-0.7279	0.85599
MinTemp_1	-0.0380	0.15889	0.6255	1.00000	0.02697	-0.2337	0.48978
RH0600_1	0.4425	0.49106	-0.4529	0.02697	1.00000	0.8679	-0.38826
RH1500_1	0.4777	0.55821	-0.7279	-0.23369	0.86785	1.0000	-0.64050
Sunshrs_1	-0.1105	-0.09839	0.8560	0.48978	-0.38826	-0.6405	1.00000

Asuogyaman

	Residuals1	Rainfall_1	MaxTemp_1	MinTemp_1	RH0600_1	RH1500_1	Sunshrs_1
Residuals1	1.00000	0.37096	-0.3868	-0.01304	0.29561	0.45995	-0.15536
Rainfall_1	0.37096	1.00000	-0.2494	0.22722	0.40115	0.56658	0.06008
MaxTemp_1	-0.38679	-0.24941	1.0000	0.51520	-0.44666	-0.75275	0.62382
MinTemp_1	-0.01304	0.22722	0.5152	1.00000	-0.19873	-0.05219	0.34180
RH0600_1	0.29561	0.40115	-0.4467	-0.19873	1.00000	0.70672	0.08125
RH1500_1	0.45995	0.56658	-0.7528	-0.05219	0.70672	1.00000	-0.24561
Sunshrs_1	-0.15536	0.06008	0.6238	0.34180	0.08125	-0.24561	1.00000

Atebubu A

	Residuals1	Rainfall_1	MaxTemp_1	MinTemp_1	RH0600_1	RH1500_1	Sunshrs_1
Residuals1	1.0000	0.41677	-0.4245	-0.11262	0.3110	0.49799	-0.3470
Rainfall_1	0.4168	1.00000	-0.3517	0.07645	0.5016	0.61632	-0.1429
MaxTemp_1	-0.4245	-0.35173	1.0000	0.24431	-0.5364	-0.76828	0.7711
MinTemp_1	-0.1126	0.07645	0.2443	1.00000	0.2330	-0.04882	0.2502
RH0600_1	0.3110	0.50160	-0.5364	0.23304	1.0000	0.81543	-0.2267
RH1500_1	0.4980	0.61632	-0.7683	-0.04882	0.8154	1.00000	-0.5411
Sunshrs_1	-0.3470	-0.14295	0.7711	0.25023	-0.2267	-0.54114	1.0000

Awutu ES

	Residuals1	Rainfall_1	MaxTemp_1	MinTemp_1	RH0600_1	RH1500_1	Sunshrs_1
Residuals1	1.00000	0.30554	0.05224	0.3196	-0.084492	0.1033	0.059416
Rainfall_1	0.30554	1.00000	-0.10295	0.1900	0.070034	0.3312	-0.174617
MaxTemp_1	0.05224	-0.10295	1.00000	0.6830	-0.375953	-0.8161	0.707841
MinTemp_1	0.31960	0.18998	0.68301	1.0000	-0.105576	-0.2430	0.476539
RH0600_1	-0.08449	0.07003	-0.37595	-0.1056	1.000000	0.6040	-0.006835
RH1500_1	0.10329	0.33117	-0.81612	-0.2430	0.603995	1.0000	-0.531306
Sunshrs_1	0.05942	-0.17462	0.70784	0.4765	-0.006835	-0.5313	1.000000

Bawku M

	Residuals1	Rainfall_1	MaxTemp_1	MinTemp_1	RH0600_1	RH1500_1	Sunshrs_1
Residuals1	1.0000	0.31662	-0.6309	-0.25971	0.5514	0.6048	-0.4556
Rainfall_1	0.3166	1.00000	-0.3504	-0.05305	0.5182	0.5056	-0.2351
MaxTemp_1	-0.6309	-0.35038	1.0000	0.16299	-0.8635	-0.8421	0.5000
MinTemp_1	-0.2597	-0.05305	0.1630	1.00000	-0.2384	-0.1934	0.1676
RH0600_1	0.5514	0.51816	-0.8635	-0.23839	1.0000	0.9183	-0.4805
RH1500_1	0.6048	0.50558	-0.8421	-0.19339	0.9183	1.0000	-0.6619
Sunshrs_1	-0.4556	-0.23512	0.5000	0.16763	-0.4805	-0.6619	1.0000

Berekum

	Residuals1	Rainfall_1	MaxTemp_1	MinTemp_1	RH0600_1	RH1500_1	Sunshrs_1
Residuals1	1.0000	0.3719	-0.2082	0.13229	0.2960	0.38228	-0.1678
Rainfall_1	0.3719	1.0000	-0.3078	0.23648	0.5208	0.59352	-0.2034
MaxTemp_1	-0.2082	-0.3078	1.0000	0.36851	-0.6084	-0.77560	0.7480
MinTemp_1	0.1323	0.2365	0.3685	1.00000	0.1609	0.02959	0.2437
RH0600_1	0.2960	0.5208	-0.6084	0.16094	1.0000	0.87697	-0.3951
RH1500_1	0.3823	0.5935	-0.7756	0.02959	0.8770	1.00000	-0.6171
Sunshrs_1	-0.1678	-0.2034	0.7480	0.24370	-0.3951	-0.61707	1.0000

Bibiani AB

	Residuals1	Rainfall_1	MaxTemp_1	MinTemp_1	RH0600_1	RH1500_1	Sunshrs_1
Residuals1	1.00000	0.17532	-0.1691	0.1279	0.02385	0.3099	-0.10506
Rainfall_1	0.17532	1.00000	-0.1325	0.2257	0.47061	0.4860	0.04609
MaxTemp_1	-0.16911	-0.13248	1.0000	0.2256	-0.33447	-0.6850	0.54961
MinTemp_1	0.12792	0.22570	0.2256	1.0000	0.45220	0.2091	0.20778
RH0600_1	0.02385	0.47061	-0.3345	0.4522	1.00000	0.6564	-0.02305
RH1500_1	0.30986	0.48596	-0.6850	0.2091	0.65644	1.0000	-0.45319
Sunshrs_1	-0.10506	0.04609	0.5496	0.2078	-0.02305	-0.4532	1.00000

Birim S

	Residuals1	Rainfall_1	MaxTemp_1	MinTemp_1	RH0600_1	RH1500_1	Sunshrs_1
Residuals1	1.00000	0.15920	-0.1509	0.08156	0.2912	0.2922	0.01311
Rainfall_1	0.15920	1.00000	-0.1395	0.09841	0.3967	0.3842	0.13858

MaxTemp_1	-0.15092	-0.13947	1.0000	0.33727	-0.1520	-0.8090	0.63604
MinTemp_1	0.08156	0.09841	0.3373	1.00000	0.2040	0.1020	0.18384
RH0600_1	0.29121	0.39674	-0.1520	0.20398	1.0000	0.5087	0.16492
RH1500_1	0.29223	0.38418	-0.8090	0.10197	0.5087	1.0000	-0.44176
Sunshrs_1	0.01311	0.13858	0.6360	0.18384	0.1649	-0.4418	1.00000

Bole

	Residuals1	Rainfall_1	MaxTemp_1	MinTemp_1	RH0600_1	RH1500_1	Sunshrs_1
Residuals1	1.0000	0.3781	-0.4351	0.1154	0.3481	0.3962	-0.3379
Rainfall_1	0.3781	1.0000	-0.7274	0.4347	0.6212	0.7740	-0.6577
MaxTemp_1	-0.4351	-0.7274	1.0000	-0.1431	-0.6960	-0.8358	0.7794
MinTemp_1	0.1154	0.4347	-0.1431	1.0000	0.4591	0.5535	-0.3264
RH0600_1	0.3481	0.6212	-0.6960	0.4591	1.0000	0.8365	-0.4686
RH1500_1	0.3962	0.7740	-0.8358	0.5535	0.8365	1.0000	-0.7153
Sunshrs_1	-0.3379	-0.6577	0.7794	-0.3264	-0.4686	-0.7153	1.0000

Bolga M

	Residuals1	Rainfall_1	MaxTemp_1	MinTemp_1	RH0600_1	RH1500_1	Sunshrs_1
Residuals1	1.00000	0.6787	-0.6968	0.06629	0.7345	0.7179	-0.5644
Rainfall_1	0.67869	1.0000	-0.6990	0.25474	0.7660	0.8411	-0.7409
MaxTemp_1	-0.69683	-0.6990	1.0000	0.30334	-0.6721	-0.7074	0.5710
MinTemp_1	0.06629	0.2547	0.3033	1.00000	0.3364	0.3773	-0.3282
RH0600_1	0.73449	0.7660	-0.6721	0.33641	1.0000	0.9530	-0.5954
RH1500_1	0.71791	0.8411	-0.7074	0.37735	0.9530	1.0000	-0.7242
Sunshrs_1	-0.56442	-0.7409	0.5710	-0.32821	-0.5954	-0.7242	1.0000

Builsa

	Residuals1	Rainfall_1	MaxTemp_1	MinTemp_1	RH0600_1	RH1500_1	Sunshrs_1
Residuals1	1.00000	0.6570	-0.7138	-0.04641	0.6704	0.6657	-0.4812
Rainfall_1	0.65701	1.0000	-0.7690	0.25998	0.7940	0.8824	-0.7829
MaxTemp_1	-0.71378	-0.7690	1.0000	0.26033	-0.6872	-0.7640	0.6339
MinTemp_1	-0.04641	0.2600	0.2603	1.00000	0.3356	0.3617	-0.2988
RH0600_1	0.67039	0.7940	-0.6872	0.33562	1.0000	0.9484	-0.5747
RH1500_1	0.66571	0.8824	-0.7640	0.36169	0.9484	1.0000	-0.7146
Sunshrs_1	-0.48117	-0.7829	0.6339	-0.29884	-0.5747	-0.7146	1.0000

Cape CoastM

	Residuals1	Rainfall_1	MaxTemp_1	MinTemp_1	RH0600_1	RH1500_1	Sunshrs_1
Residuals1	1.00000	0.45331	0.01894	0.15933	0.08912	0.1256	-0.09993
Rainfall_1	0.45331	1.00000	-0.05631	0.22235	0.17777	0.2908	-0.13374
MaxTemp_1	0.01894	-0.05631	1.00000	0.62552	-0.30898	-0.8320	0.72864
MinTemp_1	0.15933	0.22235	0.62552	1.00000	0.04887	-0.1960	0.39990
RH0600_1	0.08912	0.17777	-0.30898	0.04887	1.00000	0.5680	0.01985
RH1500_1	0.12560	0.29075	-0.83197	-0.19604	0.56799	1.0000	-0.58428
Sunshrs_1	-0.09993	-0.13374	0.72864	0.39990	0.01985	-0.5843	1.00000

Dangme E

	Residuals1	Rainfall_1	MaxTemp_1	MinTemp_1	RH0600_1	RH1500_1	Sunshrs_1
Residuals1	1.000000	0.17773	0.0438	-0.11383	-0.05691	-0.1031	0.002471
Rainfall_1	0.177734	1.00000	-0.1969	-0.06829	0.28455	0.3841	-0.118453
MaxTemp_1	0.043805	-0.19688	1.0000	0.76479	-0.35718	-0.6955	0.645114
MinTemp_1	-0.113825	-0.06829	0.7648	1.00000	-0.08727	-0.2600	0.467586
RH0600_1	-0.056913	0.28455	-0.3572	-0.08727	1.00000	0.8007	0.127811
RH1500_1	-0.103112	0.38413	-0.6955	-0.26003	0.80068	1.0000	-0.267822
Sunshrs_1	0.002471	-0.11845	0.6451	0.46759	0.12781	-0.2678	1.000000

Dangme W

	Residuals1	Rainfall_1	MaxTemp_1	MinTemp_1	RH0600_1	RH1500_1	Sunshrs_1
Residuals1	1.00000	0.47766	-0.38580	-0.26455	0.00117	0.43817	-0.13587
Rainfall_1	0.47766	1.00000	-0.14871	-0.05668	0.01817	0.36318	-0.01399
MaxTemp_1	-0.38580	-0.14871	1.00000	0.88814	-0.05243	-0.70214	0.54948
MinTemp_1	-0.26455	-0.05668	0.88814	1.00000	0.03306	-0.41155	0.46435
RH0600_1	0.00117	0.01817	-0.05243	0.03306	1.00000	0.09619	-0.10459
RH1500_1	0.43817	0.36318	-0.70214	-0.41155	0.09619	1.00000	-0.24714
Sunshrs_1	-0.13587	-0.01399	0.54948	0.46435	-0.10459	-0.24714	1.00000

Dayi S

	Residuals1	Rainfall_1	MaxTemp_1	MinTemp_1	RH0600_1	RH1500_1	Sunshrs_1
Residuals1	1.0000	0.4583	-0.5802	0.25184	0.16294	0.6071	-0.43681
Rainfall_1	0.4583	1.0000	-0.3410	0.32352	0.26164	0.5931	-0.15913
MaxTemp_1	-0.5802	-0.3410	1.0000	-0.01830	-0.38610	-0.7423	0.64760
MinTemp_1	0.2518	0.3235	-0.0183	1.00000	0.21170	0.4624	0.03445
RH0600_1	0.1629	0.2616	-0.3861	0.21170	1.00000	0.5516	-0.08329
RH1500_1	0.6071	0.5931	-0.7423	0.46243	0.55161	1.0000	-0.46461
Sunshrs_1	-0.4368	-0.1591	0.6476	0.03445	-0.08329	-0.4646	1.00000

Dormaa

	Residuals ₁	Rainfall ₁	MaxTemp ₁	MinTemp ₁	RH0600 ₁	RH1500 ₁	Sunshrs ₁
Residuals ₁	1.00000	0.37755	-0.112807	-0.092516	0.2706	0.30577	-0.09769
Rainfall ₁	0.37755	1.00000	-0.178154	0.153252	0.4821	0.53501	-0.09174
MaxTemp ₁	-0.11281	-0.17815	1.000000	0.002084	-0.3894	-0.65527	0.74838
MinTemp ₁	-0.09252	0.15325	0.002084	1.000000	0.1746	0.04255	0.18809
RH0600 ₁	0.27064	0.48208	-0.389430	0.174633	1.0000	0.86504	-0.37234
RH1500 ₁	0.30577	0.53501	-0.655265	0.042546	0.8650	1.00000	-0.65617
Sunshrs ₁	-0.09769	-0.09174	0.748379	0.188094	-0.3723	-0.65617	1.00000

E Gonja

	Residuals ₁	Rainfall ₁	MaxTemp ₁	MinTemp ₁	RH0600 ₁	RH1500 ₁	Sunshrs ₁
Residuals ₁	1.00000	0.28580	-0.3526	-0.07129	0.2755	0.2997	-0.19256
Rainfall ₁	0.28580	1.00000	-0.7844	0.05847	0.6204	0.8212	-0.70031
MaxTemp ₁	-0.35263	-0.78442	1.0000	0.22926	-0.6821	-0.8743	0.71671
MinTemp ₁	-0.07129	0.05847	0.2293	1.00000	0.2155	0.1499	-0.04316
RH0600 ₁	0.27553	0.62041	-0.6821	0.21548	1.0000	0.8205	-0.41121
RH1500 ₁	0.29967	0.82116	-0.8743	0.14987	0.8205	1.0000	-0.69340
Sunshrs ₁	-0.19256	-0.70031	0.7167	-0.04316	-0.4112	-0.6934	1.00000

Ejura Sekyered

	Residuals ₁	Rainfall ₁	MaxTemp ₁	MinTemp ₁	RH0600 ₁	RH1500 ₁	Sunshrs ₁
Residuals ₁	1.0000	0.3804	-0.41586	0.22121	0.1860	0.4750	-0.39161
Rainfall ₁	0.3804	1.0000	-0.34463	0.12238	0.3644	0.5548	-0.27569
MaxTemp ₁	-0.4159	-0.3446	1.00000	-0.06763	-0.2993	-0.7469	0.79274
MinTemp ₁	0.2212	0.1224	-0.06763	1.00000	0.3280	0.1091	0.01015
RH0600 ₁	0.1860	0.3644	-0.29926	0.32800	1.0000	0.4833	-0.20558
RH1500 ₁	0.4750	0.5548	-0.74688	0.10913	0.4833	1.0000	-0.68432
Sunshrs ₁	-0.3916	-0.2757	0.79274	0.01015	-0.2056	-0.6843	1.00000

Fanteakwa

	Residuals ₁	Rainfall ₁	MaxTemp ₁	MinTemp ₁	RH0600 ₁	RH1500 ₁	Sunshrs ₁
Residuals ₁	1.00000	0.1469	-0.07479	-0.09600	0.09936	0.15363	-0.05682
Rainfall ₁	0.14691	1.0000	-0.13073	0.15970	0.26644	0.45287	-0.23853
MaxTemp ₁	-0.07479	-0.1307	1.00000	0.03709	-0.17227	-0.46706	0.45716
MinTemp ₁	-0.09600	0.1597	0.03709	1.00000	0.08445	0.00989	-0.03458
RH0600 ₁	0.09936	0.2664	-0.17227	0.08445	1.00000	0.44674	-0.21275
RH1500 ₁	0.15363	0.4529	-0.46706	0.00989	0.44674	1.00000	-0.55985
Sunshrs ₁	-0.05682	-0.2385	0.45716	-0.03458	-0.21275	-0.55985	1.00000

Ga West M

	Residuals ₁	Rainfall ₁	MaxTemp ₁	MinTemp ₁	RH0600 ₁	RH1500 ₁	Sunshrs ₁
Residuals ₁	1.0000000	0.30399	-0.08561	0.04247	-0.0006084	0.1656	-0.29004
Rainfall ₁	0.3039864	1.00000	-0.09560	0.06421	0.3058876	0.3745	-0.03944
MaxTemp ₁	-0.0856098	-0.09560	1.00000	0.87841	-0.3782201	-0.7412	0.60681
MinTemp ₁	0.0424668	0.06421	0.87841	1.00000	-0.1318058	-0.4413	0.47998
RH0600 ₁	-0.0006084	0.30589	-0.37822	-0.13181	1.0000000	0.7812	0.08030
RH1500 ₁	0.1655957	0.37454	-0.74119	-0.44129	0.7812034	1.0000	-0.31965
Sunshrs ₁	-0.2900383	-0.03944	0.60681	0.47998	0.0803040	-0.3197	1.00000

Garu Temp

	Residuals ₁	Rainfall ₁	MaxTemp ₁	MinTemp ₁	RH0600 ₁	RH1500 ₁	Sunshrs ₁
Residuals ₁	1.0000	0.73489	-0.7650	-0.17294	0.7107	0.7931	-0.4966
Rainfall ₁	0.7349	1.00000	-0.8201	0.02674	0.7488	0.8674	-0.7723
MaxTemp ₁	-0.7650	-0.82007	1.0000	0.36280	-0.7088	-0.8392	0.6474
MinTemp ₁	-0.1729	0.02674	0.3628	1.00000	0.1690	0.1159	-0.1959
RH0600 ₁	0.7107	0.74875	-0.7088	0.16895	1.0000	0.9320	-0.5630
RH1500 ₁	0.7931	0.86736	-0.8392	0.11593	0.9320	1.0000	-0.7241
Sunshrs ₁	-0.4966	-0.77227	0.6474	-0.19586	-0.5630	-0.7241	1.0000

Ho M

	Residuals ₁	Rainfall ₁	MaxTemp ₁	MinTemp ₁	RH0600 ₁	RH1500 ₁	Sunshrs ₁
Residuals ₁	1.0000	0.5711	-0.5377	-0.28488	0.14786	0.5163	-0.39618
Rainfall ₁	0.5711	1.0000	-0.4512	-0.15407	0.37491	0.6164	-0.19814
MaxTemp ₁	-0.5377	-0.4512	1.0000	0.75984	-0.50017	-0.8076	0.66643
MinTemp ₁	-0.2849	-0.1541	0.7598	1.00000	-0.07138	-0.3483	0.53602
RH0600 ₁	0.1479	0.3749	-0.5002	-0.07138	1.00000	0.6967	-0.04279
RH1500 ₁	0.5163	0.6164	-0.8076	-0.34831	0.69666	1.0000	-0.39790
Sunshrs ₁	-0.3962	-0.1981	0.6664	0.53602	-0.04279	-0.3979	1.00000

Hohoe

	Residuals ₁	Rainfall ₁	MaxTemp ₁	MinTemp ₁	RH0600 ₁	RH1500 ₁	Sunshrs ₁
Residuals ₁	1.00000	0.4418	-0.4246	-0.05516	0.10541	0.3518	-0.3035
Rainfall ₁	0.44175	1.0000	-0.6317	0.00760	0.46381	0.6330	-0.3486
MaxTemp ₁	-0.42455	-0.6317	1.0000	0.50316	-0.51814	-0.7701	0.7254
MinTemp ₁	-0.05516	0.0076	0.5032	1.00000	0.07422	-0.1528	0.3312
RH0600 ₁	0.10541	0.4638	-0.5181	0.07422	1.00000	0.5315	-0.1337
RH1500 ₁	0.35179	0.6330	-0.7701	-0.15281	0.53152	1.0000	-0.4652

Sunshrs_1	-0.30346	-0.3486	0.7254	0.33121	-0.13369	-0.4652	1.0000

Juabeso							
	Residuals1	Rainfall_1	MaxTemp_1	MinTemp_1	RH0600_1	RH1500_1	Sunshrs_1
Residuals1	1.00000	0.24987	-0.0470246	0.01795	0.1013	0.1991748	0.02677
Rainfall_1	0.24987	1.00000	0.0105312	0.18706	0.3388	0.5477733	0.03563
MaxTemp_1	-0.04702	0.01053	1.0000000	0.90528	0.6758	-0.0007085	0.68803
MinTemp_1	0.01795	0.18706	0.9052842	1.00000	0.8728	0.3504617	0.45246
RH0600_1	0.10131	0.33880	0.6757511	0.87284	1.0000	0.7055800	0.20811
RH1500_1	0.19917	0.54777	-0.0007085	0.35046	0.7056	1.0000000	-0.36037
Sunshrs_1	0.02677	0.03563	0.6880258	0.45246	0.2081	-0.3603676	1.00000

Kasena-N							
	Residuals1	Rainfall_1	MaxTemp_1	MinTemp_1	RH0600_1	RH1500_1	Sunshrs_1
Residuals1	1.00000	0.6390	-0.6968	-0.09476	0.5813	0.6292	-0.4395
Rainfall_1	0.63896	1.0000	-0.7723	0.15989	0.7521	0.8644	-0.6846
MaxTemp_1	-0.69680	-0.7723	1.0000	0.31393	-0.6729	-0.7982	0.5333
MinTemp_1	-0.09476	0.1599	0.3139	1.00000	0.2307	0.2155	-0.2874
RH0600_1	0.58130	0.7521	-0.6729	0.23071	1.0000	0.9172	-0.4888
RH1500_1	0.62916	0.8644	-0.7982	0.21550	0.9172	1.0000	-0.6401
Sunshrs_1	-0.43948	-0.6846	0.5333	-0.28740	-0.4888	-0.6401	1.0000

Kintampo NM							
	Residuals1	Rainfall_1	MaxTemp_1	MinTemp_1	RH0600_1	RH1500_1	Sunshrs_1
Residuals1	1.00000	0.39842	-0.1961	0.09534	0.3235	0.37458	-0.1100
Rainfall_1	0.39842	1.00000	-0.5487	0.05618	0.5889	0.64504	-0.3916
MaxTemp_1	-0.19611	-0.54870	1.0000	0.35190	-0.6092	-0.77494	0.7081
MinTemp_1	0.09534	0.05618	0.3519	1.00000	0.1395	-0.02382	0.2419
RH0600_1	0.32348	0.58892	-0.6092	0.13946	1.0000	0.85111	-0.4445
RH1500_1	0.37458	0.64504	-0.7749	-0.02382	0.8511	1.00000	-0.5283
Sunshrs_1	-0.10997	-0.39160	0.7081	0.24191	-0.4445	-0.52834	1.0000

Kpandu/DN							
	Residuals1	Rainfall_1	MaxTemp_1	MinTemp_1	RH0600_1	RH1500_1	Sunshrs_1
Residuals1	1.00000	0.517483	-0.4628	-0.082729	0.4092	0.5635	-0.1846
Rainfall_1	0.51748	1.000000	-0.5559	0.003475	0.5243	0.6503	-0.4051
MaxTemp_1	-0.46284	-0.555908	1.0000	0.592863	-0.3795	-0.7472	0.5959
MinTemp_1	-0.08273	0.003475	0.5929	1.000000	0.2737	-0.1882	0.2696
RH0600_1	0.40919	0.524334	-0.3795	0.273680	1.0000	0.6239	-0.1807
RH1500_1	0.56355	0.650264	-0.7472	-0.188224	0.6239	1.0000	-0.4256
Sunshrs_1	-0.18460	-0.405086	0.5959	0.269562	-0.1807	-0.4256	1.0000

Krachi/W							
	Residuals1	Rainfall_1	MaxTemp_1	MinTemp_1	RH0600_1	RH1500_1	Sunshrs_1
Residuals1	1.0000	0.63124	-0.6698	0.10121	0.45549	0.6345	-0.4399
Rainfall_1	0.6312	1.00000	-0.7933	0.09818	0.49440	0.7824	-0.6406
MaxTemp_1	-0.6698	-0.79326	1.0000	0.17426	-0.58546	-0.8332	0.7625
MinTemp_1	0.1012	0.09818	0.1743	1.00000	0.09505	0.2880	0.1244
RH0600_1	0.4555	0.49440	-0.5855	0.09505	1.00000	0.7410	-0.2024
RH1500_1	0.6345	0.78244	-0.8332	0.28804	0.74099	1.0000	-0.5589
Sunshrs_1	-0.4399	-0.64064	0.7625	0.12443	-0.20242	-0.5589	1.0000

Kumasi MA							
	Residuals1	Rainfall_1	MaxTemp_1	MinTemp_1	RH0600_1	RH1500_1	Sunshrs_1
Residuals1	1.00000	0.235437	-0.1813	-0.109933	0.1523	0.26090	-0.06793
Rainfall_1	0.23544	1.000000	-0.3134	0.009587	0.3579	0.49918	-0.13918
MaxTemp_1	-0.18129	-0.313371	1.0000	0.520341	-0.4029	-0.77975	0.78137
MinTemp_1	-0.10993	0.009587	0.5203	1.000000	0.3129	-0.05506	0.45135
RH0600_1	0.15226	0.357931	-0.4029	0.312913	1.0000	0.76871	-0.27791
RH1500_1	0.26090	0.499175	-0.7797	-0.055063	0.7687	1.00000	-0.58861
Sunshrs_1	-0.06793	-0.139179	0.7814	0.451354	-0.2779	-0.58861	1.00000

Kwaebirem							
	Residuals1	Rainfall_1	MaxTemp_1	MinTemp_1	RH0600_1	RH1500_1	Sunshrs_1
Residuals1	1.00000	0.4169	-0.04769	0.25777	0.05454	0.2144	-0.06792
Rainfall_1	0.41685	1.0000	-0.18330	0.33557	0.31722	0.4904	-0.01190
MaxTemp_1	-0.04769	-0.1833	1.00000	0.18901	-0.18911	-0.8309	0.73432
MinTemp_1	0.25777	0.3356	0.18901	1.00000	0.15570	0.2509	0.05112
RH0600_1	0.05454	0.3172	-0.18911	0.15570	1.00000	0.3730	0.13558
RH1500_1	0.21442	0.4904	-0.83088	0.25092	0.37296	1.0000	-0.52451
Sunshrs_1	-0.06792	-0.0119	0.73432	0.05112	0.13558	-0.5245	1.00000

Kwahu S							
	Residuals1	Rainfall_1	MaxTemp_1	MinTemp_1	RH0600_1	RH1500_1	Sunshrs_1
Residuals1	1.0000	0.2748	-0.3565	-0.2416	0.3309	0.4688	-0.2754
Rainfall_1	0.2748	1.0000	-0.2823	-0.1643	0.3673	0.5504	-0.3496
MaxTemp_1	-0.3565	-0.2823	1.0000	0.8792	-0.4918	-0.7702	0.7439

MinTemp_1	-0.2416	-0.1643	0.8792	1.0000	-0.2444	-0.4911	0.6947
RH0600_1	0.3309	0.3673	-0.4918	-0.2444	1.0000	0.8012	-0.3567
RH1500_1	0.4688	0.5504	-0.7702	-0.4911	0.8012	1.0000	-0.5877
Sunshrs_1	-0.2754	-0.3496	0.7439	0.6947	-0.3567	-0.5877	1.0000

Kwahu W

	Residuals1	Rainfall_1	MaxTemp_1	MinTemp_1	RH0600_1	RH1500_1	Sunshrs_1
Residuals1	1.0000	0.4368	-0.2454	-0.1449	0.2666	0.4489	-0.2164
Rainfall_1	0.4368	1.0000	-0.2963	-0.1143	0.4293	0.6244	-0.3318
MaxTemp_1	-0.2454	-0.2963	1.0000	0.8748	-0.5374	-0.8164	0.6501
MinTemp_1	-0.1449	-0.1143	0.8748	1.0000	-0.3745	-0.5585	0.5992
RH0600_1	0.2666	0.4293	-0.5374	-0.3745	1.0000	0.7980	-0.4235
RH1500_1	0.4489	0.6244	-0.8164	-0.5585	0.7980	1.0000	-0.5645
Sunshrs_1	-0.2164	-0.3318	0.6501	0.5992	-0.4235	-0.5645	1.0000

Lawra

	Residuals1	Rainfall_1	MaxTemp_1	MinTemp_1	RH0600_1	RH1500_1	Sunshrs_1
Residuals1	1.00000	0.6006	-0.6293	-0.03183	0.6000	0.6532	-0.5213
Rainfall_1	0.60057	1.0000	-0.7845	0.10143	0.7734	0.8861	-0.8132
MaxTemp_1	-0.62926	-0.7845	1.0000	0.35609	-0.7004	-0.8313	0.6853
MinTemp_1	-0.03183	0.1014	0.3561	1.00000	0.1580	0.1137	-0.1840
RH0600_1	0.60000	0.7734	-0.7004	0.15796	1.0000	0.9436	-0.5959
RH1500_1	0.65317	0.8861	-0.8313	0.11370	0.9436	1.0000	-0.7583
Sunshrs_1	-0.52134	-0.8132	0.6853	-0.18404	-0.5959	-0.7583	1.0000

Manya K

	Residuals1	Rainfall_1	MaxTemp_1	MinTemp_1	RH0600_1	RH1500_1	Sunshrs_1
Residuals1	1.00000	0.2259	-0.2816	-0.03152	-0.05164	0.2208	-0.1197
Rainfall_1	0.22592	1.0000	-0.1579	0.22809	0.32093	0.5187	0.1009
MaxTemp_1	-0.28162	-0.1579	1.0000	0.52093	-0.26365	-0.7154	0.5409
MinTemp_1	-0.03152	0.2281	0.5209	1.00000	-0.06616	-0.0434	0.2857
RH0600_1	-0.05164	0.3209	-0.2636	-0.06616	1.00000	0.6063	0.3044
RH1500_1	0.22082	0.5187	-0.7154	-0.04340	0.60632	1.0000	-0.1946
Sunshrs_1	-0.11968	0.1009	0.5409	0.28570	0.30441	-0.1946	1.0000

Mfantsiman M

	Residuals1	Rainfall_1	MaxTemp_1	MinTemp_1	RH0600_1	RH1500_1	Sunshrs_1
Residuals1	1.000000	0.4881	-0.09244	0.281750	-0.003264	0.2703	-0.16895
Rainfall_1	0.488104	1.0000	-0.08230	0.160888	0.116012	0.3060	-0.16927
MaxTemp_1	-0.092442	-0.0823	1.00000	0.600940	-0.278464	-0.7939	0.67263
MinTemp_1	0.281750	0.1609	0.60094	1.000000	0.007816	-0.2338	0.43737
RH0600_1	-0.003264	0.1160	-0.27846	0.007816	1.000000	0.5864	0.06626
RH1500_1	0.270306	0.3060	-0.79394	-0.233753	0.586420	1.0000	-0.49455
Sunshrs_1	-0.168954	-0.1693	0.67263	0.437366	0.066262	-0.4946	1.00000

N Juaben

	Residuals1	Rainfall_1	MaxTemp_1	MinTemp_1	RH0600_1	RH1500_1	Sunshrs_1
Residuals1	1.0000	0.26752	-0.1806	0.19044	0.1203	0.3137	-0.11590
Rainfall_1	0.2675	1.00000	-0.2531	0.25212	0.2405	0.5479	-0.05036
MaxTemp_1	-0.1806	-0.25311	1.0000	0.08270	-0.1958	-0.7670	0.79565
MinTemp_1	0.1904	0.25212	0.0827	1.00000	0.1550	0.3776	0.02675
RH0600_1	0.1203	0.24046	-0.1958	0.15500	1.0000	0.4568	0.02450
RH1500_1	0.3137	0.54785	-0.7670	0.37757	0.4568	1.0000	-0.53694
Sunshrs_1	-0.1159	-0.05036	0.7956	0.02675	0.0245	-0.5369	1.00000

Nadowli

	Residuals1	Rainfall_1	MaxTemp_1	MinTemp_1	RH0600_1	RH1500_1	Sunshrs_1
Residuals1	1.0000	0.6831	-0.6001	0.1700	0.5880	0.6776	-0.5531
Rainfall_1	0.6831	1.0000	-0.8175	0.1852	0.7918	0.9085	-0.8150
MaxTemp_1	-0.6001	-0.8175	1.0000	0.2842	-0.7150	-0.8336	0.6998
MinTemp_1	0.1700	0.1852	0.2842	1.0000	0.2518	0.2246	-0.2116
RH0600_1	0.5880	0.7918	-0.7150	0.2518	1.0000	0.9427	-0.5769
RH1500_1	0.6776	0.9085	-0.8336	0.2246	0.9427	1.0000	-0.7406
Sunshrs_1	-0.5531	-0.8150	0.6998	-0.2116	-0.5769	-0.7406	1.0000

Nanumba N

	Residuals1	Rainfall_1	MaxTemp_1	MinTemp_1	RH0600_1	RH1500_1	Sunshrs_1
Residuals1	1.00000	0.5889	-0.6018	0.01487	0.5279	0.6276	-0.45803
Rainfall_1	0.58887	1.0000	-0.8260	0.11027	0.7203	0.8841	-0.72722
MaxTemp_1	-0.60180	-0.8260	1.0000	0.25889	-0.7328	-0.8888	0.69497
MinTemp_1	0.01487	0.1103	0.2589	1.00000	0.1879	0.1532	-0.03178
RH0600_1	0.52789	0.7203	-0.7328	0.18791	1.0000	0.8977	-0.36655
RH1500_1	0.62761	0.8841	-0.8888	0.15317	0.8977	1.0000	-0.63108
Sunshrs_1	-0.45803	-0.7272	0.6950	-0.03178	-0.3666	-0.6311	1.00000

Nkwanta

	Residuals1	Rainfall_1	MaxTemp_1	MinTemp_1	RH0600_1	RH1500_1	Sunshrs_1
--	------------	------------	-----------	-----------	----------	----------	-----------

Residuals1	1.00000	0.52971	-0.5490	0.06596	0.33572	0.5526	-0.4998
Rainfall_1	0.52971	1.00000	-0.7581	0.06671	0.51246	0.7854	-0.6070
MaxTemp_1	-0.54904	-0.75807	1.0000	0.22815	-0.65766	-0.8881	0.7098
MinTemp_1	0.06596	0.06671	0.2282	1.00000	0.05225	0.1763	0.1985
RH0600_1	0.33572	0.51246	-0.6577	0.05225	1.00000	0.7990	-0.2180
RH1500_1	0.55261	0.78536	-0.8881	0.17629	0.79900	1.0000	-0.5433
Sunshrs_1	-0.49981	-0.60698	0.7098	0.19850	-0.21798	-0.5433	1.0000

 maindata[, 1]: North T

	Residuals1	Rainfall_1	MaxTemp_1	MinTemp_1	RH0600_1	RH1500_1	Sunshrs_1
Residuals1	1.0000000	0.49928	-0.0666	0.0006472	0.37093	0.2049	0.16390
Rainfall_1	0.4992841	1.00000	-0.1612	0.0697537	0.41410	0.3476	0.16391
MaxTemp_1	-0.0665982	-0.16122	1.0000	0.7512466	-0.35068	-0.7122	0.55901
MinTemp_1	0.0006472	0.06975	0.7512	1.0000000	-0.12132	-0.4666	0.44411
RH0600_1	0.3709268	0.41410	-0.3507	-0.1213200	1.00000	0.3992	0.04559
RH1500_1	0.2048677	0.34759	-0.7122	-0.4666280	0.39921	1.0000	-0.14936
Sunshrs_1	0.1639043	0.16391	0.5590	0.4441052	0.04559	-0.1494	1.00000

 Nzema E

	Residuals1	Rainfall_1	MaxTemp_1	MinTemp_1	RH0600_1	RH1500_1	Sunshrs_1
Residuals1	1.00000	0.528084	-0.05786	0.03466	-0.122348	0.1300	-0.20821
Rainfall_1	0.52808	1.000000	-0.14043	-0.01067	0.007503	0.3431	-0.37608
MaxTemp_1	-0.05786	-0.140428	1.00000	0.54066	-0.271947	-0.7866	0.77449
MinTemp_1	0.03466	-0.010667	0.54066	1.00000	-0.230877	-0.2155	0.40666
RH0600_1	-0.12235	0.007503	-0.27195	-0.23088	1.000000	0.4115	-0.08531
RH1500_1	0.13002	0.343090	-0.78662	-0.21554	0.411479	1.0000	-0.66958
Sunshrs_1	-0.20821	-0.376080	0.77449	0.40666	-0.085306	-0.6696	1.00000

 Obuasi M

	Residuals1	Rainfall_1	MaxTemp_1	MinTemp_1	RH0600_1	RH1500_1	Sunshrs_1
Residuals1	1.0000000	0.1591	0.0007732	0.19702	0.09179	0.12113	0.08713
Rainfall_1	0.1591262	1.0000	-0.5857434	0.15693	0.52569	0.75177	-0.43843
MaxTemp_1	0.0007732	-0.5857	1.0000000	0.38760	-0.55612	-0.83328	0.87196
MinTemp_1	0.1970234	0.1569	0.3875974	1.00000	0.18933	0.03453	0.39816
RH0600_1	0.0917917	0.5257	-0.5561204	0.18933	1.00000	0.81433	-0.34367
RH1500_1	0.1211288	0.7518	-0.8332820	0.03453	0.81433	1.00000	-0.65943
Sunshrs_1	0.0871329	-0.4384	0.8719595	0.39816	-0.34367	-0.65943	1.00000

 Offinso

	Residuals1	Rainfall_1	MaxTemp_1	MinTemp_1	RH0600_1	RH1500_1	Sunshrs_1
Residuals1	1.00000	0.3559	-0.2853	-0.04055	0.3214	0.36974	-0.1344
Rainfall_1	0.35594	1.0000	-0.3239	0.22870	0.5432	0.60493	-0.1773
MaxTemp_1	-0.28525	-0.3239	1.0000	0.35207	-0.5592	-0.80363	0.8301
MinTemp_1	-0.04055	0.2287	0.3521	1.00000	0.1592	-0.03824	0.2801
RH0600_1	0.32143	0.5432	-0.5592	0.15915	1.0000	0.86714	-0.3206
RH1500_1	0.36974	0.6049	-0.8036	-0.03824	0.8671	1.00000	-0.6090
Sunshrs_1	-0.13441	-0.1773	0.8301	0.28005	-0.3206	-0.60904	1.0000

 Pru

	Residuals1	Rainfall_1	MaxTemp_1	MinTemp_1	RH0600_1	RH1500_1	Sunshrs_1
Residuals1	1.00000	0.3971	-0.4798	-0.08878	0.4490	0.5765	-0.2847
Rainfall_1	0.39711	1.0000	-0.3141	0.24727	0.4877	0.5507	-0.1651
MaxTemp_1	-0.47984	-0.3141	1.0000	0.36712	-0.5835	-0.8167	0.7413
MinTemp_1	-0.08878	0.2473	0.3671	1.00000	0.1688	0.0208	0.1730
RH0600_1	0.44903	0.4877	-0.5835	0.16875	1.0000	0.8670	-0.3862
RH1500_1	0.57646	0.5507	-0.8167	0.02080	0.8670	1.0000	-0.6405
Sunshrs_1	-0.28465	-0.1651	0.7413	0.17302	-0.3862	-0.6405	1.0000

 Saboba-C

	Residuals1	Rainfall_1	MaxTemp_1	MinTemp_1	RH0600_1	RH1500_1	Sunshrs_1
Residuals1	1.00000	0.5899	-0.5678	0.0216465	0.5295	0.6253	-0.3140104
Rainfall_1	0.58992	1.0000	-0.7630	0.1262847	0.6808	0.8406	-0.5777282
MaxTemp_1	-0.56775	-0.7630	1.0000	0.2911355	-0.6823	-0.8644	0.6105292
MinTemp_1	0.02165	0.1263	0.2911	1.0000000	0.2105	0.1525	-0.0004526
RH0600_1	0.52947	0.6808	-0.6823	0.2104922	1.0000	0.9111	-0.2174262
RH1500_1	0.62534	0.8406	-0.8644	0.1525494	0.9111	1.0000	-0.4819505
Sunshrs_1	-0.31401	-0.5777	0.6105	-0.0004526	-0.2174	-0.4820	1.0000000

 Sawla TK

	Residuals1	Rainfall_1	MaxTemp_1	MinTemp_1	RH0600_1	RH1500_1	Sunshrs_1
Residuals1	1.0000	0.5266	-0.46516	0.31317	0.3746	0.5200	-0.4234
Rainfall_1	0.5266	1.0000	-0.69095	0.38347	0.6214	0.7884	-0.6312
MaxTemp_1	-0.4652	-0.6909	1.00000	-0.01908	-0.7023	-0.8588	0.7992
MinTemp_1	0.3132	0.3835	-0.01908	1.00000	0.3663	0.4659	-0.2235
RH0600_1	0.3746	0.6214	-0.70229	0.36635	1.0000	0.8653	-0.4784
RH1500_1	0.5200	0.7884	-0.85878	0.46590	0.8653	1.0000	-0.7523
Sunshrs_1	-0.4234	-0.6312	0.79917	-0.22348	-0.4784	-0.7523	1.0000

Sefwi Wi

	Residuals1	Rainfall_1	MaxTemp_1	MinTemp_1	RH0600_1	RH1500_1	Sunshrs_1
Residuals1	1.0000	0.45252	-0.19426	0.21575	0.3319	0.36723	-0.03740
Rainfall_1	0.4525	1.00000	-0.03394	0.29735	0.2485	0.27587	0.01140
MaxTemp_1	-0.1943	-0.03394	1.00000	0.14624	-0.4862	-0.77699	0.82157
MinTemp_1	0.2157	0.29735	0.14624	1.00000	0.2337	-0.01626	0.05797
RH0600_1	0.3319	0.24852	-0.48623	0.23371	1.0000	0.74064	-0.21262
RH1500_1	0.3672	0.27587	-0.77699	-0.01626	0.7406	1.00000	-0.57916
Sunshrs_1	-0.0374	0.01140	0.82157	0.05797	-0.2126	-0.57916	1.00000

Sekyere E

	Residuals1	Rainfall_1	MaxTemp_1	MinTemp_1	RH0600_1	RH1500_1	Sunshrs_1
Residuals1	1.00000	0.2938	-0.1432	-0.08769	0.2474	0.24268	-0.09018
Rainfall_1	0.29380	1.0000	-0.3116	0.14088	0.5096	0.59346	-0.22566
MaxTemp_1	-0.14316	-0.3116	1.0000	0.12777	-0.4813	-0.79086	0.84157
MinTemp_1	-0.08769	0.1409	0.1278	1.00000	0.3517	0.08597	0.18321
RH0600_1	0.24738	0.5096	-0.4813	0.35167	1.0000	0.71553	-0.30188
RH1500_1	0.24268	0.5935	-0.7909	0.08597	0.7155	1.00000	-0.63066
Sunshrs_1	-0.09018	-0.2257	0.8416	0.18321	-0.3019	-0.63066	1.00000

Sekyere W/Mam

	Residuals1	Rainfall_1	MaxTemp_1	MinTemp_1	RH0600_1	RH1500_1	Sunshrs_1
Residuals1	1.00000	0.30986	-0.2801	0.02521	0.3176	0.4290	-0.09001
Rainfall_1	0.30986	1.00000	-0.3256	-0.04509	0.3841	0.4982	-0.20119
MaxTemp_1	-0.28011	-0.32565	1.0000	0.16241	-0.5121	-0.7733	0.69055
MinTemp_1	0.02521	-0.04509	0.1624	1.00000	0.2283	-0.1043	0.29217
RH0600_1	0.31761	0.38410	-0.5121	0.22832	1.0000	0.5677	-0.15162
RH1500_1	0.42896	0.49819	-0.7733	-0.10426	0.5677	1.0000	-0.46351
Sunshrs_1	-0.09001	-0.20119	0.6906	0.29217	-0.1516	-0.4635	1.00000

Sene

	Residuals1	Rainfall_1	MaxTemp_1	MinTemp_1	RH0600_1	RH1500_1	Sunshrs_1
Residuals1	1.0000	0.4748	-0.5791	-0.14869	0.4968	0.55132	-0.4301
Rainfall_1	0.4748	1.0000	-0.5014	0.11755	0.5905	0.62839	-0.3351
MaxTemp_1	-0.5791	-0.5014	1.0000	0.41576	-0.5917	-0.78790	0.7674
MinTemp_1	-0.1487	0.1176	0.4158	1.00000	0.1474	-0.09953	0.2956
RH0600_1	0.4968	0.5905	-0.5917	0.14737	1.0000	0.74739	-0.3772
RH1500_1	0.5513	0.6284	-0.7879	-0.09953	0.7474	1.00000	-0.5493
Sunshrs_1	-0.4301	-0.3351	0.7674	0.29559	-0.3772	-0.54928	1.0000

Shama AE

	Residuals1	Rainfall_1	MaxTemp_1	MinTemp_1	RH0600_1	RH1500_1	Sunshrs_1
Residuals1	1.00000	0.21021	-0.1522	0.03172	0.19914	0.2418	-0.06278
Rainfall_1	0.21021	1.00000	-0.1110	0.18367	-0.05971	0.3381	-0.17362
MaxTemp_1	-0.15220	-0.11097	1.0000	0.72526	-0.48171	-0.7646	0.71477
MinTemp_1	0.03172	0.18367	0.7253	1.00000	-0.35416	-0.2232	0.47598
RH0600_1	0.19914	-0.05971	-0.4817	-0.35416	1.00000	0.5424	-0.11825
RH1500_1	0.24179	0.33806	-0.7646	-0.22320	0.54238	1.0000	-0.52369
Sunshrs_1	-0.06278	-0.17362	0.7148	0.47598	-0.11825	-0.5237	1.00000

Sissala E

	Residuals1	Rainfall_1	MaxTemp_1	MinTemp_1	RH0600_1	RH1500_1	Sunshrs_1
Residuals1	1.0000	0.5535	-0.5495	0.2001	0.6118	0.6507	-0.4434
Rainfall_1	0.5535	1.0000	-0.7082	0.1351	0.7013	0.8312	-0.6834
MaxTemp_1	-0.5495	-0.7082	1.0000	0.3150	-0.6079	-0.7642	0.5672
MinTemp_1	0.2001	0.1351	0.3150	1.0000	0.2464	0.2180	-0.2687
RH0600_1	0.6118	0.7013	-0.6079	0.2464	1.0000	0.9373	-0.4859
RH1500_1	0.6507	0.8312	-0.7642	0.2180	0.9373	1.0000	-0.6643
Sunshrs_1	-0.4434	-0.6834	0.5672	-0.2687	-0.4859	-0.6643	1.0000

Sunyani M

	Residuals1	Rainfall_1	MaxTemp_1	MinTemp_1	RH0600_1	RH1500_1	Sunshrs_1
Residuals1	1.00000	0.47999	-0.18537	0.14647	0.2911	0.39022	-0.09624
Rainfall_1	0.47999	1.00000	-0.21019	0.03185	0.4336	0.53465	-0.08637
MaxTemp_1	-0.18537	-0.21019	1.00000	0.01029	-0.4885	-0.64882	0.72814
MinTemp_1	0.14647	0.03185	0.01029	1.00000	0.2678	-0.08425	0.25846
RH0600_1	0.29111	0.43361	-0.48850	0.26785	1.0000	0.79080	-0.19786
RH1500_1	0.39022	0.53465	-0.64882	-0.08425	0.7908	1.00000	-0.55620
Sunshrs_1	-0.09624	-0.08637	0.72814	0.25846	-0.1979	-0.55620	1.00000

Tamale M

	Residuals1	Rainfall_1	MaxTemp_1	MinTemp_1	RH0600_1	RH1500_1	Sunshrs_1
Residuals1	1.0000	0.6237	-0.5981	0.1562	0.6447	0.6796	-0.4348
Rainfall_1	0.6237	1.0000	-0.7679	0.1933	0.6963	0.8144	-0.7064
MaxTemp_1	-0.5981	-0.7679	1.0000	0.1123	-0.7008	-0.8531	0.6566
MinTemp_1	0.1562	0.1933	0.1123	1.0000	0.3086	0.2986	-0.1785

RH0600_1	0.6447	0.6963	-0.7008	0.3086	1.0000	0.9136	-0.4439
RH1500_1	0.6796	0.8144	-0.8531	0.2986	0.9136	1.0000	-0.6227
Sunshrs_1	-0.4348	-0.7064	0.6566	-0.1785	-0.4439	-0.6227	1.0000

Techiman M

	Residuals1	Rainfall_1	MaxTemp_1	MinTemp_1	RH0600_1	RH1500_1	Sunshrs_1
Residuals1	1.0000	0.4887	-0.3558	0.15307	0.40232	0.4266	-0.1591
Rainfall_1	0.4887	1.0000	-0.2887	0.18889	0.47267	0.5339	-0.1442
MaxTemp_1	-0.3558	-0.2887	1.0000	0.45552	-0.52493	-0.7106	0.7430
MinTemp_1	0.1531	0.1889	0.4555	1.00000	0.04733	-0.1488	0.3222
RH0600_1	0.4023	0.4727	-0.5249	0.04733	1.00000	0.8622	-0.3298
RH1500_1	0.4266	0.5339	-0.7106	-0.14882	0.86216	1.0000	-0.5874
Sunshrs_1	-0.1591	-0.1442	0.7430	0.32223	-0.32981	-0.5874	1.0000

Tema M

	Residuals1	Rainfall_1	MaxTemp_1	MinTemp_1	RH0600_1	RH1500_1	Sunshrs_1
Residuals1	1.000000	0.459029	-0.0978	-0.001564	0.1585	0.2107	-0.105785
Rainfall_1	0.459029	1.000000	-0.1330	-0.057161	0.2691	0.2787	-0.007515
MaxTemp_1	-0.097796	-0.133025	1.0000	0.793683	-0.4909	-0.7363	0.401901
MinTemp_1	-0.001564	-0.057161	0.7937	1.000000	-0.3628	-0.4808	0.280678
RH0600_1	0.158481	0.269117	-0.4909	-0.362843	1.0000	0.8056	0.169761
RH1500_1	0.210725	0.278708	-0.7363	-0.480827	0.8056	1.0000	-0.122929
Sunshrs_1	-0.105785	-0.007515	0.4019	0.280678	0.1698	-0.1229	1.000000

Twifo HLD

	Residuals1	Rainfall_1	MaxTemp_1	MinTemp_1	RH0600_1	RH1500_1	Sunshrs_1
Residuals1	1.00000	0.3221	-0.07456	0.36617	0.3568	0.34165	0.1100
Rainfall_1	0.32205	1.0000	-0.41446	0.20679	0.5140	0.63508	-0.2505
MaxTemp_1	-0.07456	-0.4145	1.00000	0.40101	-0.4856	-0.82447	0.8051
MinTemp_1	0.36617	0.2068	0.40101	1.00000	0.3315	0.08345	0.3761
RH0600_1	0.35677	0.5140	-0.48562	0.33151	1.0000	0.81607	-0.1448
RH1500_1	0.34165	0.6351	-0.82447	0.08345	0.8161	1.00000	-0.5234
Sunshrs_1	0.11003	-0.2505	0.80506	0.37605	-0.1448	-0.52341	1.0000

Upper D

	Residuals1	Rainfall_1	MaxTemp_1	MinTemp_1	RH0600_1	RH1500_1	Sunshrs_1
Residuals1	1.00000	0.4269	-0.04143	0.32031	0.2023	0.26154	0.1149
Rainfall_1	0.42695	1.0000	-0.59649	0.13770	0.5146	0.75008	-0.4527
MaxTemp_1	-0.04143	-0.5965	1.00000	0.39148	-0.5530	-0.83426	0.8723
MinTemp_1	0.32031	0.1377	0.39148	1.00000	0.1854	0.02467	0.4007
RH0600_1	0.20230	0.5146	-0.55302	0.18543	1.0000	0.81339	-0.3411
RH1500_1	0.26154	0.7501	-0.83426	0.02467	0.8134	1.00000	-0.6605
Sunshrs_1	0.11490	-0.4527	0.87233	0.40066	-0.3411	-0.66046	1.0000

Wa C/M

	Residuals1	Rainfall_1	MaxTemp_1	MinTemp_1	RH0600_1	RH1500_1	Sunshrs_1
Residuals1	1.00000	0.57205	-0.5274	0.04441	0.5666	0.62447	-0.54951
Rainfall_1	0.57205	1.00000	-0.7604	0.01424	0.7400	0.84986	-0.70613
MaxTemp_1	-0.52740	-0.76043	1.0000	0.39685	-0.7324	-0.86024	0.71084
MinTemp_1	0.04441	0.01424	0.3968	1.00000	0.0772	-0.01724	-0.02418
RH0600_1	0.56664	0.74003	-0.7324	0.07720	1.0000	0.93353	-0.59631
RH1500_1	0.62447	0.84986	-0.8602	-0.01724	0.9335	1.00000	-0.75040
Sunshrs_1	-0.54951	-0.70613	0.7108	-0.02418	-0.5963	-0.75040	1.00000

Wa E

	Residuals1	Rainfall_1	MaxTemp_1	MinTemp_1	RH0600_1	RH1500_1	Sunshrs_1
Residuals1	1.0000	0.71083	-0.6236	0.16510	0.7432	0.7926	-0.63292
Rainfall_1	0.7108	1.00000	-0.7324	0.08369	0.7295	0.8402	-0.62040
MaxTemp_1	-0.6236	-0.73241	1.0000	0.29372	-0.6998	-0.8181	0.63018
MinTemp_1	0.1651	0.08369	0.2937	1.00000	0.2015	0.1415	-0.07243
RH0600_1	0.7432	0.72946	-0.6998	0.20153	1.0000	0.9386	-0.52982
RH1500_1	0.7926	0.84020	-0.8181	0.14153	0.9386	1.0000	-0.70156
Sunshrs_1	-0.6329	-0.62040	0.6302	-0.07243	-0.5298	-0.7016	1.00000

Wassa AE

	Residuals1	Rainfall_1	MaxTemp_1	MinTemp_1	RH0600_1	RH1500_1	Sunshrs_1
Residuals1	1.000000	0.43830	0.02234	0.1968	0.2496	0.1857	-0.004177
Rainfall_1	0.438296	1.00000	-0.10042	0.1934	0.2007	0.3688	-0.038095
MaxTemp_1	0.022344	-0.10042	1.00000	0.5864	-0.4710	-0.8390	0.833712
MinTemp_1	0.196801	0.19338	0.58640	1.0000	-0.1150	-0.1737	0.435394
RH0600_1	0.249562	0.20066	-0.47103	-0.1150	1.0000	0.6939	-0.184166
RH1500_1	0.185650	0.36878	-0.83895	-0.1737	0.6939	1.0000	-0.657896
Sunshrs_1	-0.004177	-0.03809	0.83371	0.4354	-0.1842	-0.6579	1.000000

Wassa W

	Residuals1	Rainfall_1	MaxTemp_1	MinTemp_1	RH0600_1	RH1500_1	Sunshrs_1
Residuals1	1.000000	0.342383	0.0876	0.29088	0.038297	0.1922	-0.003598
Rainfall_1	0.342383	1.000000	-0.1188	0.04865	-0.001424	0.3696	-0.272917
MaxTemp_1	0.087601	-0.118774	1.0000	0.70028	-0.367511	-0.7896	0.761862
MinTemp_1	0.290880	0.048648	0.7003	1.00000	-0.299647	-0.2633	0.471617
RH0600_1	0.038297	-0.001424	-0.3675	-0.41211	1.000000	0.4616	-0.040759
RH1500_1	0.192236	0.369641	-0.7896	-0.26326	0.461572	1.0000	-0.618869
Sunshrs_1	-0.003598	-0.272917	0.7619	0.47162	-0.040759	-0.6189	1.000000

Wenchi M

	Residuals1	Rainfall_1	MaxTemp_1	MinTemp_1	RH0600_1	RH1500_1	Sunshrs_1
Residuals1	1.0000	0.40859	-0.2091	0.15738	0.3038	0.31903	-0.1512
Rainfall_1	0.4086	1.00000	-0.4200	0.09787	0.5502	0.64425	-0.2951
MaxTemp_1	-0.2091	-0.41995	1.0000	0.41211	-0.5752	-0.79713	0.7786
MinTemp_1	0.1574	0.09787	0.4121	1.00000	0.1707	-0.03074	0.2329
RH0600_1	0.3038	0.55024	-0.5752	0.17074	1.0000	0.87963	-0.4291
RH1500_1	0.3190	0.64425	-0.7971	-0.03074	0.8796	1.00000	-0.6270
Sunshrs_1	-0.1512	-0.29506	0.7786	0.23290	-0.4291	-0.62700	1.0000

West Gonja

	Residuals1	Rainfall_1	MaxTemp_1	MinTemp_1	RH0600_1	RH1500_1	Sunshrs_1
Residuals1	1.0000	0.4972	-0.4609	0.1656	0.3778	0.4702	-0.3923
Rainfall_1	0.4972	1.0000	-0.7792	0.4887	0.7134	0.8775	-0.7131
MaxTemp_1	-0.4609	-0.7792	1.0000	-0.1155	-0.7365	-0.8764	0.8274
MinTemp_1	0.1656	0.4887	-0.1155	1.0000	0.4006	0.5151	-0.2837
RH0600_1	0.3778	0.7134	-0.7365	0.4006	1.0000	0.8678	-0.4998
RH1500_1	0.4702	0.8775	-0.8764	0.5151	0.8678	1.0000	-0.7652
Sunshrs_1	-0.3923	-0.7131	0.8274	-0.2837	-0.4998	-0.7652	1.0000

West Mamp

	Residuals1	Rainfall_1	MaxTemp_1	MinTemp_1	RH0600_1	RH1500_1	Sunshrs_1
Residuals1	1.0000	0.5600	-0.5493	0.2131	0.6165	0.6364	-0.3990
Rainfall_1	0.5600	1.0000	-0.8011	0.2570	0.7765	0.8808	-0.7855
MaxTemp_1	-0.5493	-0.8011	1.0000	0.2004	-0.6962	-0.8094	0.6672
MinTemp_1	0.2131	0.2570	0.2004	1.0000	0.3466	0.3522	-0.2659
RH0600_1	0.6165	0.7765	-0.6962	0.3466	1.0000	0.9368	-0.5354
RH1500_1	0.6364	0.8808	-0.8094	0.3522	0.9368	1.0000	-0.6934
Sunshrs_1	-0.3990	-0.7855	0.6672	-0.2659	-0.5354	-0.6934	1.0000

Yendi M

	Residuals1	Rainfall_1	MaxTemp_1	MinTemp_1	RH0600_1	RH1500_1	Sunshrs_1
Residuals1	1.00000	0.5734	-0.6187	0.02006	0.5721	0.5956	-0.3824
Rainfall_1	0.57340	1.0000	-0.7474	0.18391	0.6051	0.8156	-0.6826
MaxTemp_1	-0.61866	-0.7474	1.0000	0.18899	-0.6157	-0.8242	0.6417
MinTemp_1	0.02006	0.1839	0.1890	1.00000	0.2893	0.2510	-0.1050
RH0600_1	0.57210	0.6051	-0.6157	0.28933	1.0000	0.8269	-0.3701
RH1500_1	0.59564	0.8156	-0.8242	0.25097	0.8269	1.0000	-0.6221
Sunshrs_1	-0.38244	-0.6826	0.6417	-0.10499	-0.3701	-0.6221	1.0000

Appendix C: SARIMA Model Fitting and Forecast of MIR at the Regions

C-1: Autocorrelation Analysis of Detrended MIR Data

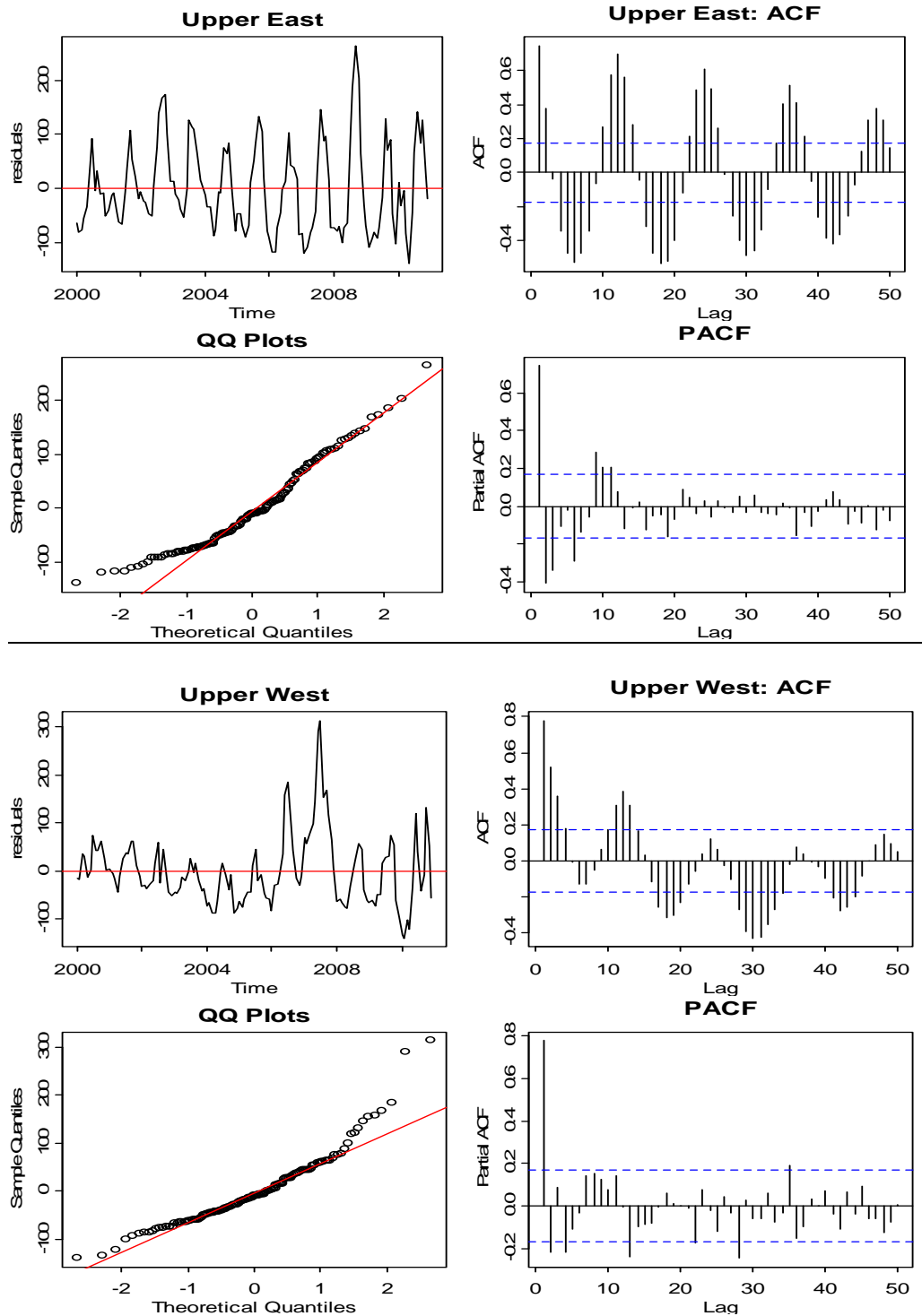


Figure C-1.1: Time and QQ plots (left), ACF and PACF (right) of detrended MIR (total) in Upper East Region (top) and Upper West Region (bottom)

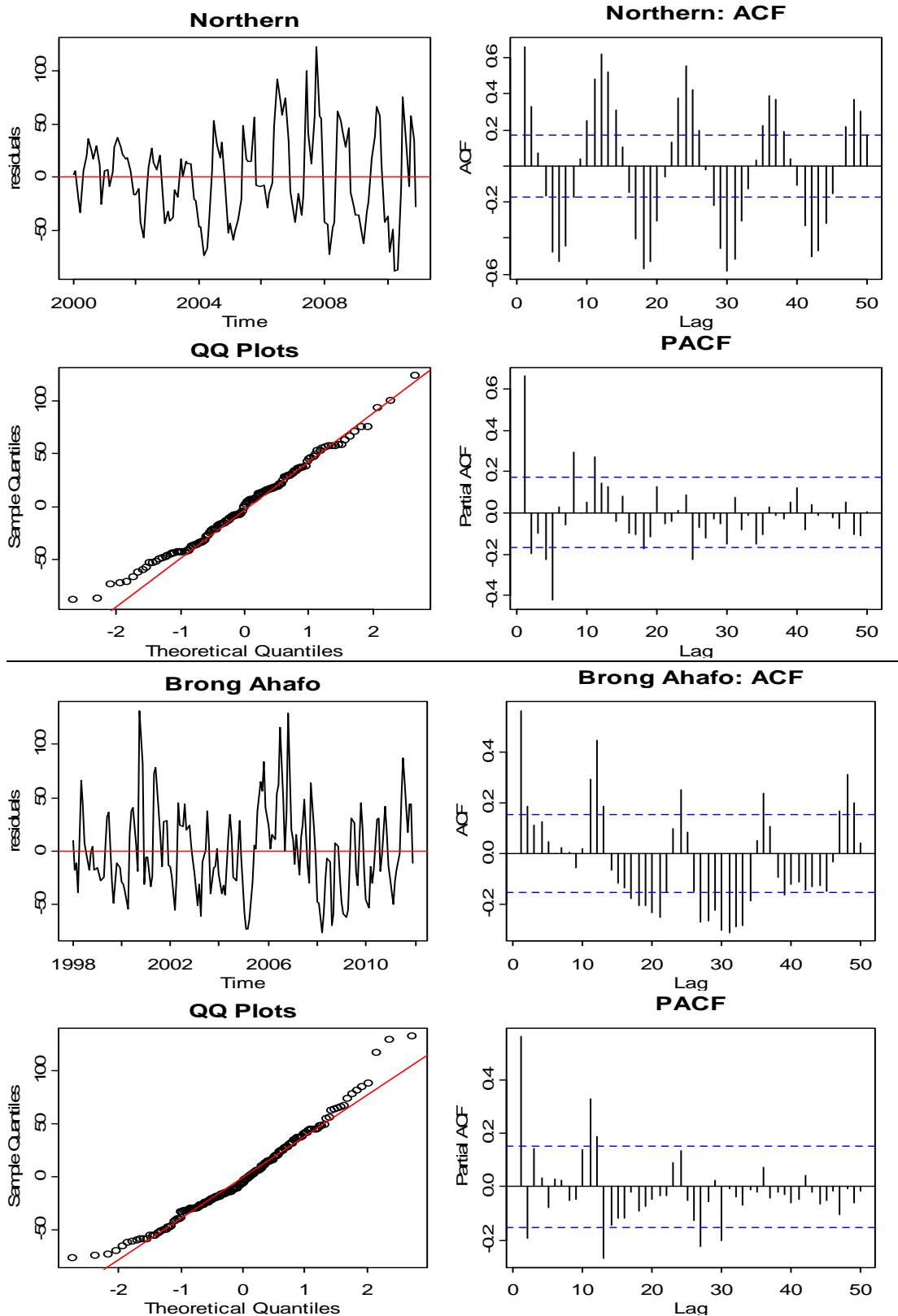


Figure C-1.2: Time and QQ plots (left), ACF and PACF (right) of detrended MIR (total) in Northern Region (top) and Brong Ahafo Region (bottom)

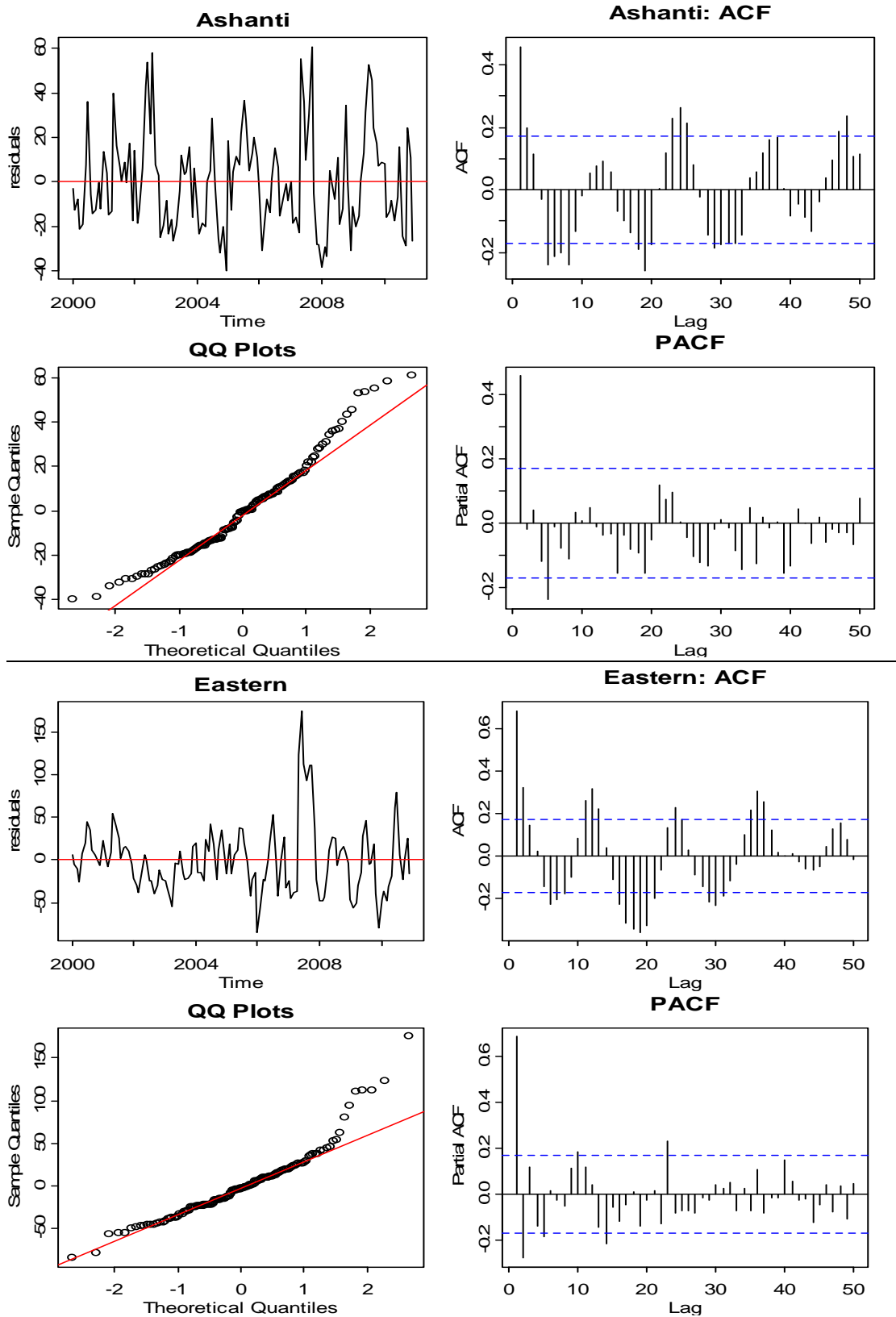


Figure C-1.3: Time and QQ plots (left), ACF and PACF (right) of detrended MIR (total) in Ashanti Region (top) and Eastern Region (bottom)

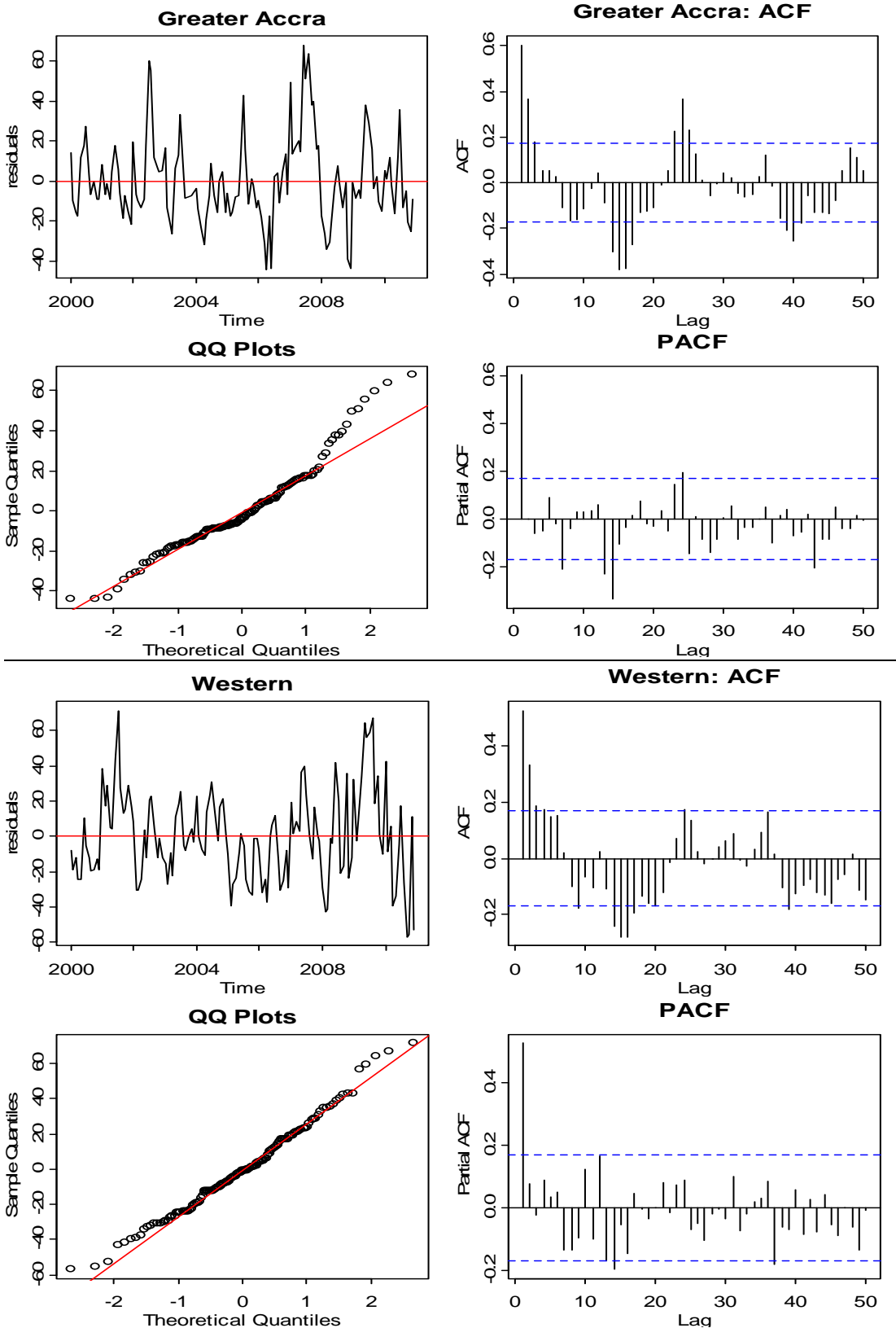


Figure C-1.4: Time and QQ plots (left), ACF and PACF (right) of detrended MIR (total) in Greater Accra Region (top) and Western Region (bottom)

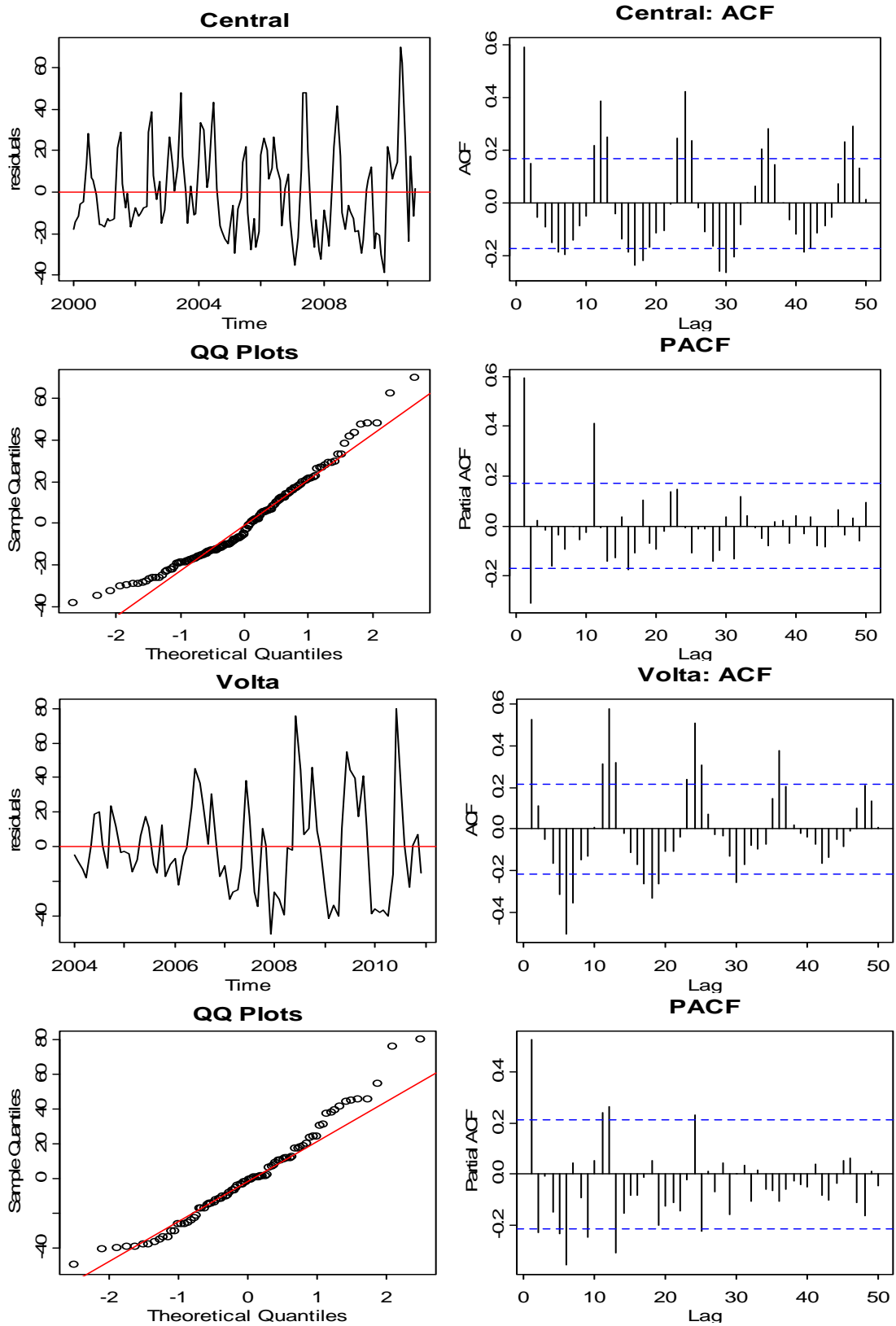


Figure C-1.5: Time and QQ plots (left), ACF and PACF (right) of detrended MIR (total) in Central Region (top) and Volta Region (bottom)

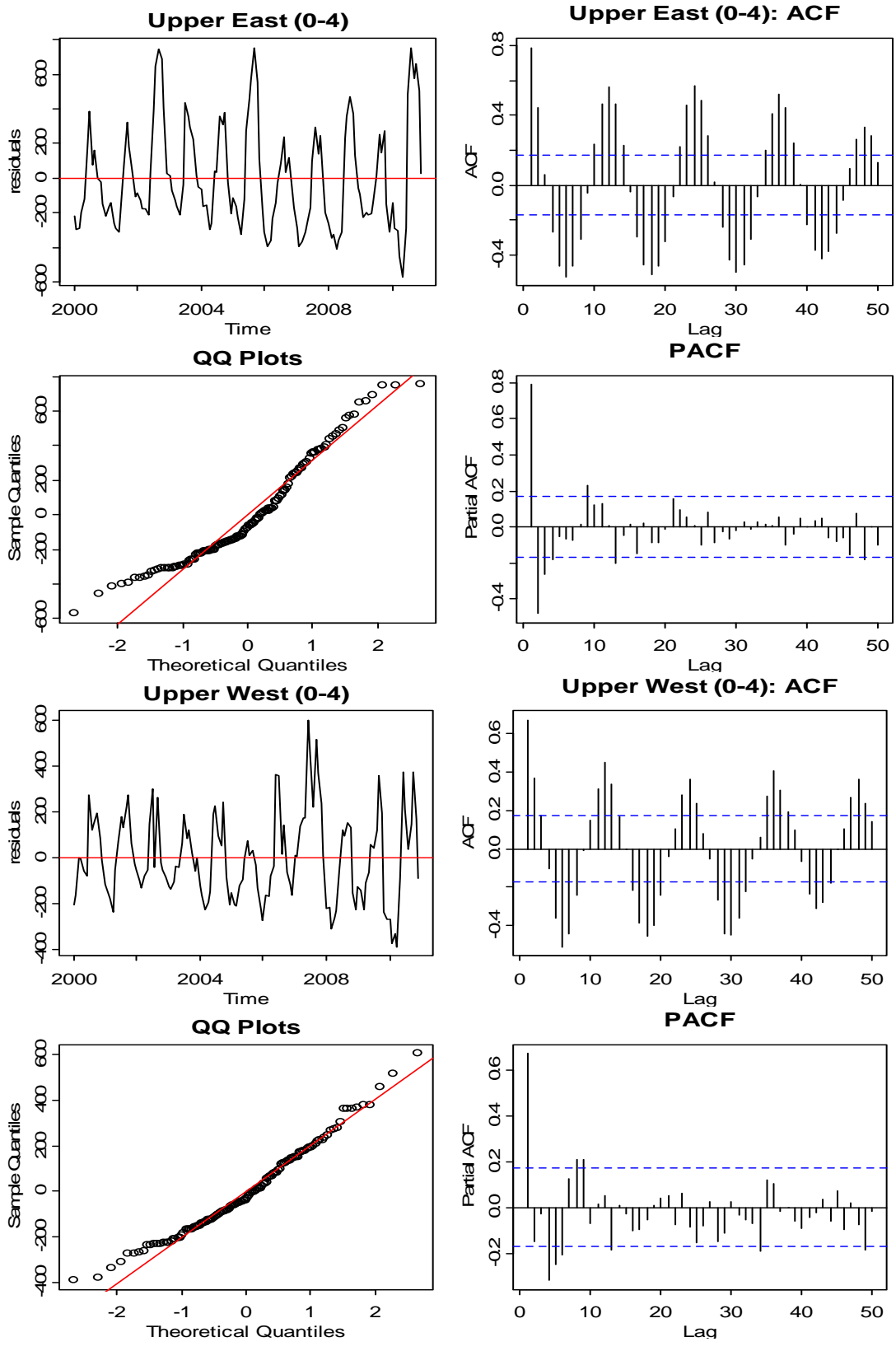


Figure C-1.6: Time and QQ plots (left), ACF and PACF (right) of detrended MIR (0-4) in Upper west Region (top) and Volta Region (bottom)

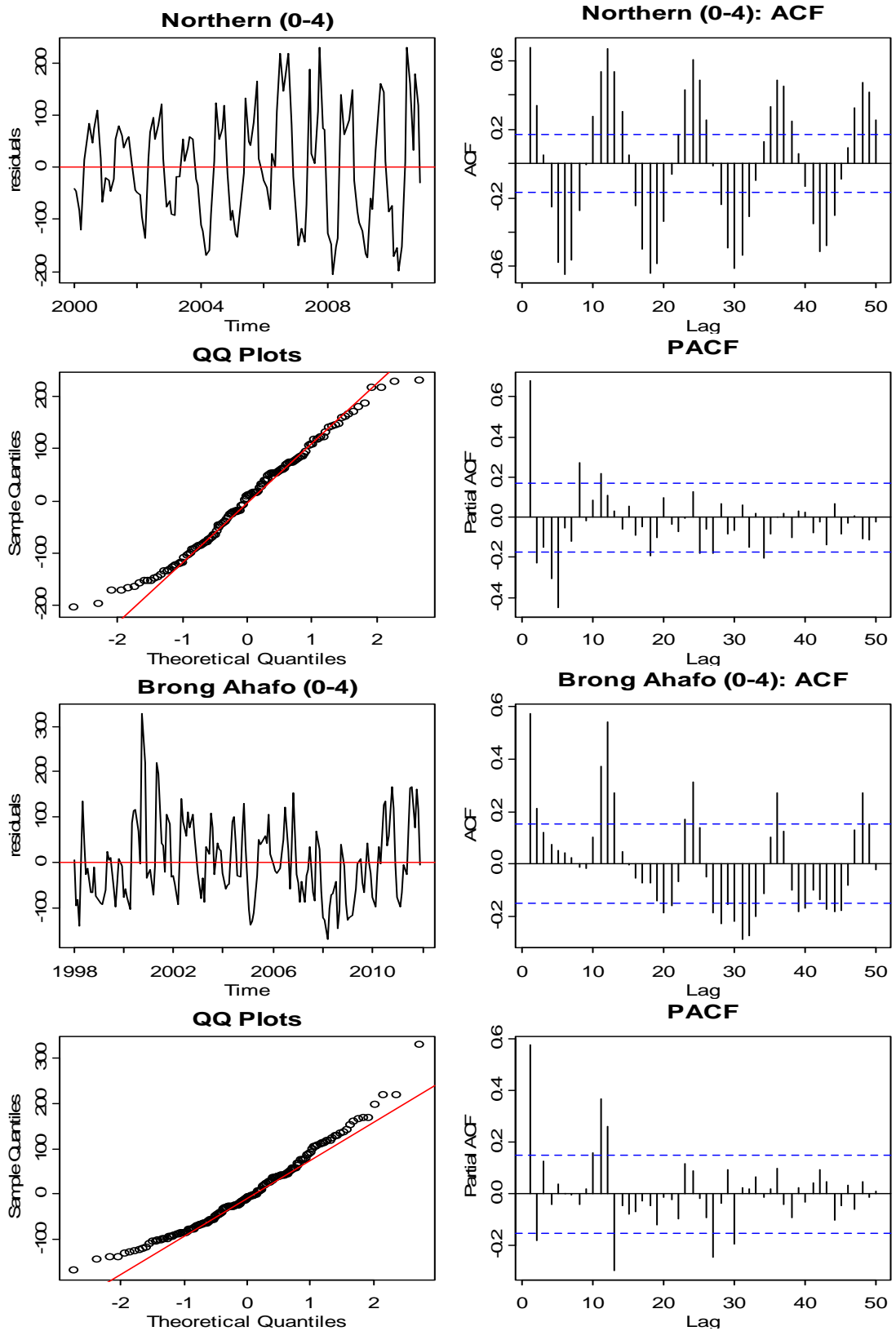


Figure C-1.7: Time and QQ plots (left), ACF and PACF (right) of detrended MIR (0-4) in Northern Region (top) and Brong Ahafo Region (bottom)

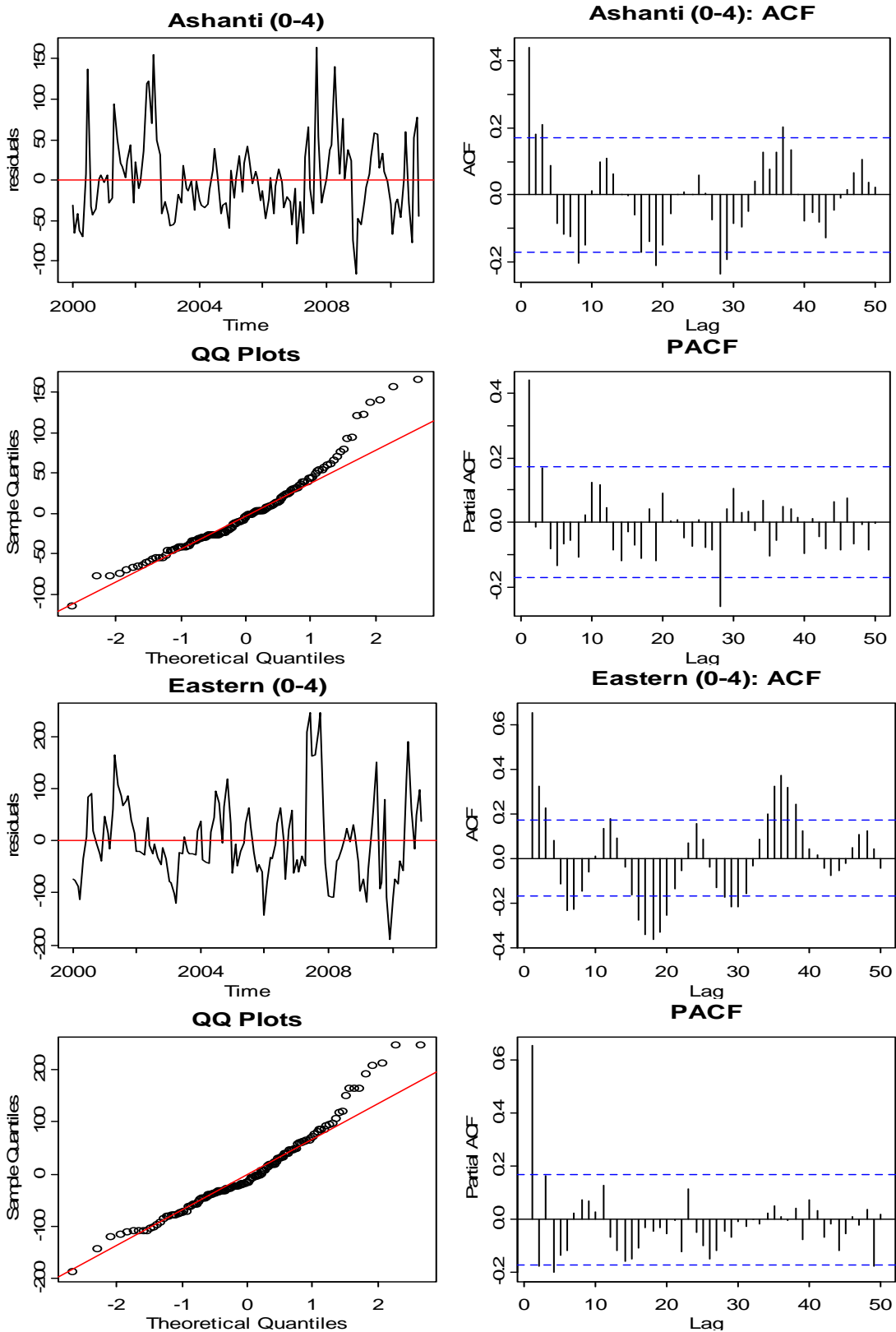


Figure C-1.8: Time and QQ plots (left), ACF and PACF (right) of detrended MIR (0-4) in Ashanti Region (top) and Eastern Region (bottom)

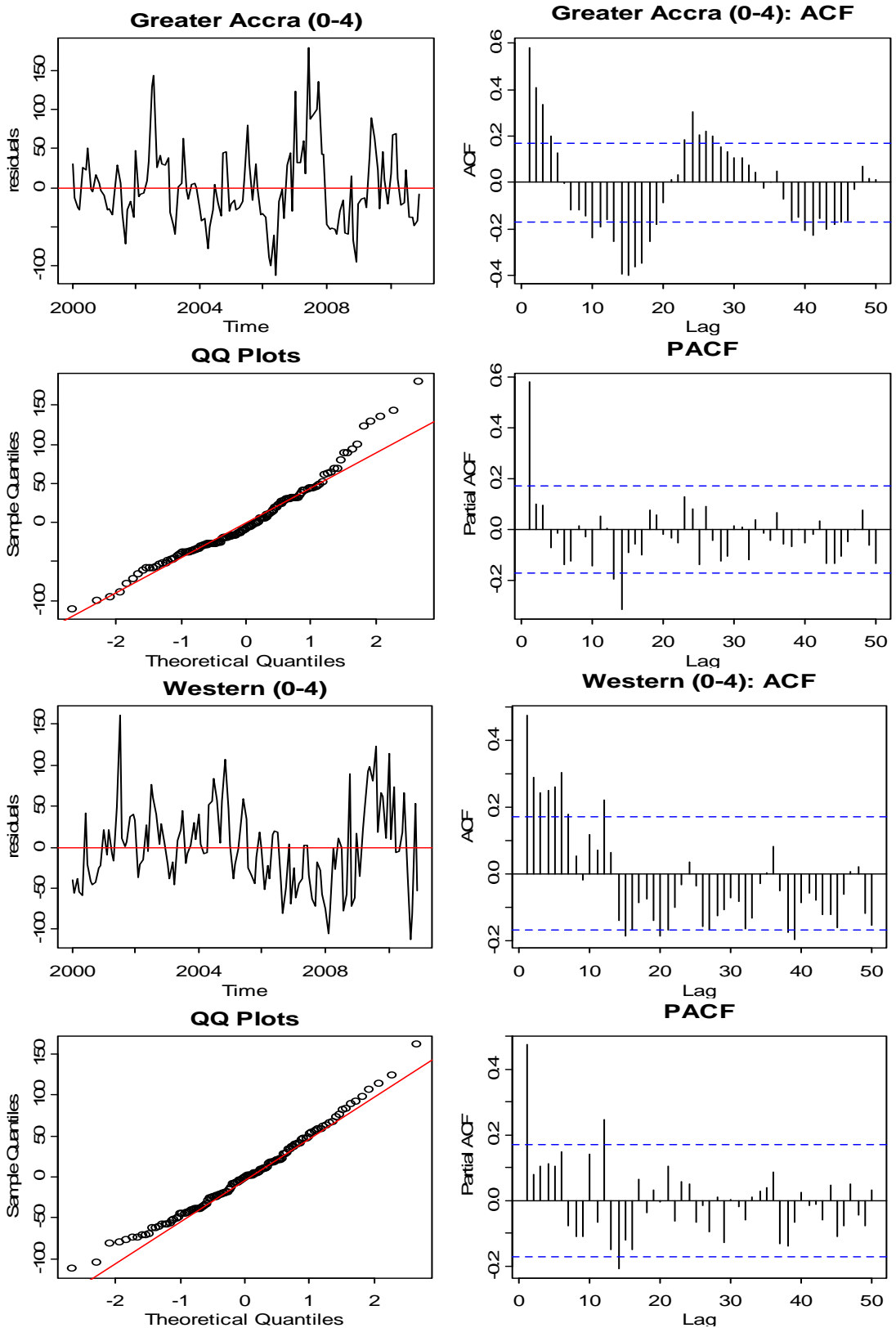


Figure C-1.9: Time and QQ plots (left), ACF and PACF (right) of detrended MIR (0-4) in Greater Accra Region (top) and Western Region (bottom)

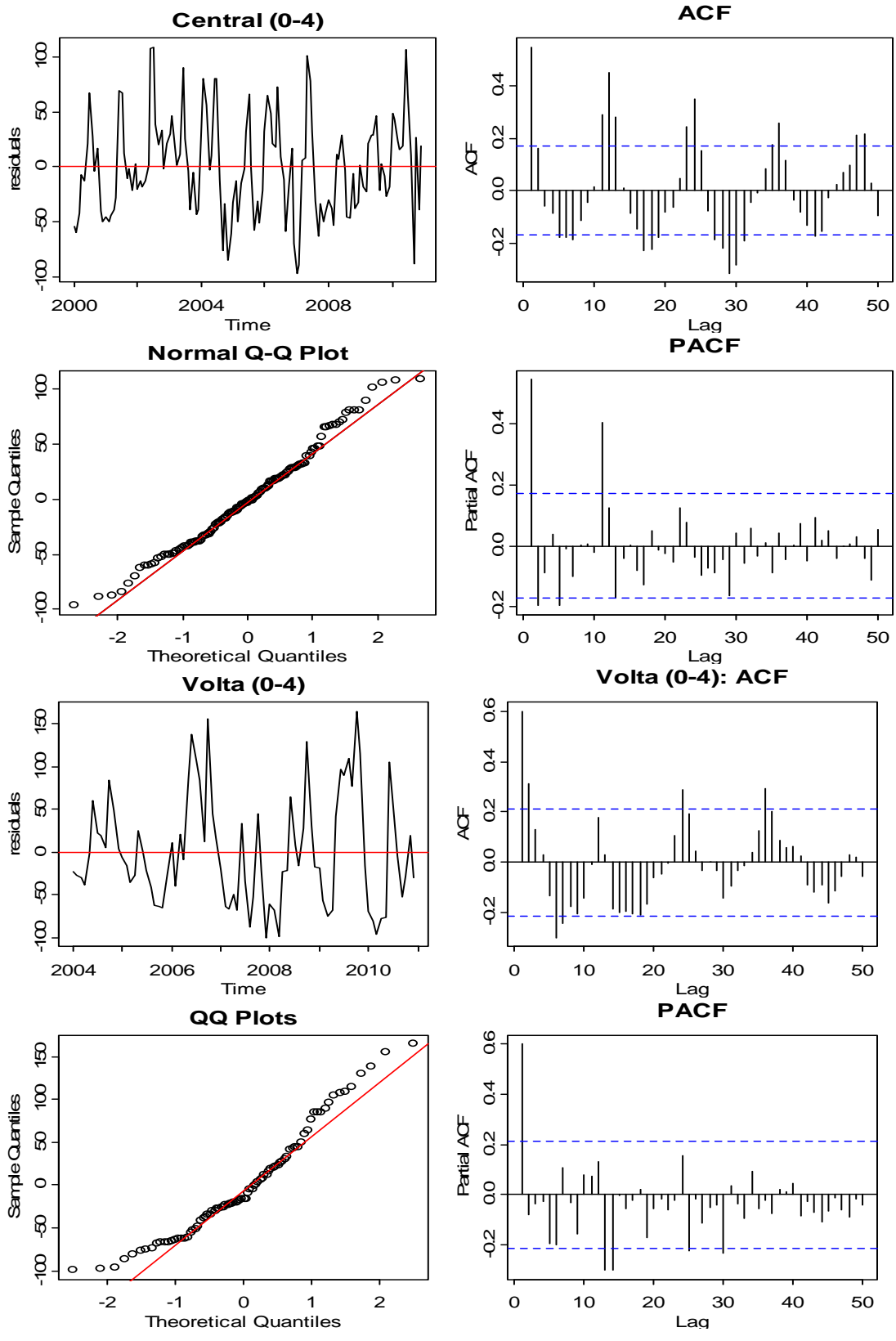


Figure C-1.10: Time and QQ plots (left), ACF and PACF (right) of detrended MIR (0-4) in Central Region (top) and Volta Region (bottom)

C-2: SARIMA Predictive Models of MIR at the Regions

Results C-2.1: Results of multiplicative SARIMA and SARIMAX models of morbidity incidence rates (Total) for the regions

=====

Upper East (Total):

ARIMA(1,1,1)(0,1,1)[12]

Coefficients:

	ar1	ma1	sma1
	0.594	-0.920	-0.653
s.e.	0.094	0.047	0.087

sigma^2 estimated as 1545: log likelihood=-609.7

AIC=1225; AICc=1226; BIC=1237 mae = 27.17; rmse = 37.32

Box-Pierce test X-squared = 9.091, df = 24, p-value = 0.8069

ARIMA(1,1,1)(0,1,1)[12]

Coefficients:

	ar1	ma1	sma1	maxT	rh1500	sunsh
	0.596	-0.919	-0.671	-5.806	1.915	5.636
s.e.	0.097	0.050	0.088	4.806	1.001	5.651

sigma^2 estimated as 1475: log likelihood=-602.2

AIC=1216 AICc=1217 BIC=1236

ARIMA(1,1,1)(0,1,1)[12]

Coefficients:

	ar1	ma1	sma1	rh1500
	0.597	-0.922	-0.668	1.968
s.e.	0.095	0.048	0.089	0.967

sigma^2 estimated as 1499: log likelihood=-603.1

AIC=1214 AICc=1215 BIC=1228; maex= 26.9; msex= 36.74

Box-Pierce test: X-squared = 7.156, df = 12, p-value = 0.8471

=====

Upper West (Total):

ARIMA(1,0,0)(0,1,1)[12]

Coefficients:

	ar1	sma1
	0.900	-0.636
s.e.	0.046	0.107

sigma^2 estimated as 1615: log likelihood=-617.3

AIC=1239 AICc=1239 BIC=1247; mae = 27.35; rmse= 38.32

Box-Pierce test: X-squared = 31.08, df = 30, p-value = 0.4115

ARIMA(1,0,0)(0,1,1)[12]

Coefficients:

	ar1	sma1	rainf_1	sunsh_1
	0.910	-0.652	-0.149	-12.954
s.e.	0.044	0.109	0.075	5.812

sigma^2 estimated as 1525: log likelihood=-609

AIC=1226 AICc=1226 BIC=1240; mae=26.24; rmse=37.22

Box-Pierce test: X-squared = 23.85, df = 24, p-value = 0.4702

=====

Northern (Total):

ARIMA(1,1,4)(1,1,0)[12]

Coefficients:

	ar1	ma1	ma2	ma3	ma4	sar1
	-0.819	0.448	-0.781	-0.491	0.288	-0.612
s.e.	0.074	0.104	0.087	0.087	0.095	0.072

sigma^2 estimated as 499: log likelihood=-543

AIC=1098 AICc=1099 BIC=1117; mae= 15.17; rmse=21.2

Box-Pierce test: X-squared = 20.1, df = 24, p-value = 0.691

ARIMA(1,1,4)(1,1,0)[12]

Coefficients:

	ar1	ma1	ma2	ma3	ma4	sar1	rh1500	sunsh_1
	-0.798	0.404	-0.860	-0.494	0.345	-0.630	0.588	7.663
s.e.	0.079	0.106	0.089	0.085	0.094	0.073	0.457	2.264

sigma^2 estimated as 446: log likelihood=-532.5

AIC=1081 AICc=1083 BIC=1106; mae=14.29; rmse=20.05

Box-Pierce test: X-squared = 22.43, df = 24, p-value = 0.5538

=====
Brong Ahafo (Total)

ARIMA(3,1,0)(0,1,1)[12]

Coefficients:

	ar1	ar2	ar3	sma1
	-0.442	-0.462	-0.176	-0.898
s.e.	0.079	0.079	0.080	0.109

sigma^2 estimated as 622: log likelihood=-728.4

AIC=1465 AICc=1465 BIC=1480; mae=17.33; rmse=23.96

Box-Pierce test: X-squared = 4.901, df = 12, p-value = 0.9612

ARIMA(3,1,0)(0,1,1)[12]

Coefficients:

	ar1	ar2	ar3	sma1	rainf	rh1500_1
	-0.365	-0.438	-0.111	-0.836	-0.129	0.68
s.e.	0.081	0.078	0.083	0.083	0.039	0.40

sigma^2 estimated as 592: log likelihood=-717.5

AIC=1447 AICc=1448 BIC=1468; mae=16.97; rmse=22.37

Box-Pierce test: X-squared = 17.87, df = 24, p-value = 0.8095

=====
Ashanti (Total)

ARIMA(3,1,0)(3,2,1)[12]

Coefficients:

	ar1	ar2	ar3	sar1	sar2	sar3	sma1
	-0.488	-0.472	-0.213	-0.884	-0.588	-0.313	-0.988
s.e.	0.097	0.100	0.099	0.110	0.146	0.122	0.151

sigma^2 estimated as 430: log likelihood=-509.9

AIC=1034 AICc=1035 BIC=1055; mae=12.98; rmse=18.68

Box-Pierce test: X-squared = 17.84, df = 24, p-value = 0.8106

ARIMA(3,1,0)(3,2,1)[12]

Coefficients:

	ar1	ar2	ar3	sar1	sar2	sar3	sma1	rh1500_1	minT_1
	-0.505	-0.504	-0.204	-0.892	-0.612	-0.338	-0.988	-0.657	2.944
Se	0.10	0.102	0.103	0.109	0.146	0.123	0.153	0.521	2.279

sigma^2 estimated as 419: log likelihood=-504.4

AIC=1027 AICc=1029 BIC=1054; mae=13.01; rmse=18.41

Box-Pierce test: X-squared = 17.33, df = 24, p-value = 0.8343

```

=====
Eastern (Total):
ARIMA(1,1,2)(0,1,1)[12]
Coefficients:
      ar1      ma1      ma2      sma1
      0.231  -0.386  -0.353  -0.823
s.e.  0.388   0.373   0.111   0.106
sigma^2 estimated as 707:  log likelihood=-566.3
AIC=1141  AICc=1141  BIC=1155; mae=17.8; rmse=25.25
Box-Pierce test: X-squared = 28.46, df = 24, p-value = 0.241

ARIMA(1,1,2)(0,1,1)[12]
Coefficients:
      ar1      ma1      ma2      sma1  minT_1  sunsh_1
      0.367  -0.472  -0.381  -0.846  -10.538  -7.767
s.e.  0.234   0.235   0.117   0.115   4.496   5.377
sigma^2 estimated as 661:  log likelihood=-558.6
AIC=1129  AICc=1130  BIC=1149; mae=16.56; rmse=24.4
Box-Pierce test: X-squared = 26.39, df = 24, p-value = 0.3336
=====
Greater Accra (Total)
ARIMA(0,1,1)(2,1,0)[12]
Coefficients:
      ma1      sar1      sar2
      -0.375  -0.808  -0.385
s.e.  0.090   0.089   0.096
sigma^2 estimated as 255:  log likelihood=-503
AIC=1012  AICc=1012  BIC=1023; mae=10.79; rmse=14.94
Box-Pierce test: X-squared = 26.93, df = 24, p-value = 0.3075

ARIMA(0,1,1)(2,1,0)[12]
Coefficients:
      ma1      sar1      sar2  rainf_1  rh1500_1  sunsh
      -0.390  -0.797  -0.375   0.042   0.591  -4.131
s.e.  0.092   0.093   0.100   0.022   0.345   1.638

sigma^2 estimated as 236:  log likelihood=-494.1
AIC=1000  AICc=1001  BIC=1020; mae=10.49; rmse=14.57
Box-Pierce test: X-squared = 25.48, df = 24, p-value = 0.3802
=====
Central (Total):
ARIMA(0,0,2)(1,1,0)[12]
Coefficients:
      ma1      ma2      sar1
      0.742   0.536  -0.496
s.e.  0.080   0.072   0.093
sigma^2 estimated as 264:  log likelihood=-507
AIC=1020  AICc=1020  BIC=1031; mae=10.76; rmse=15.49
Box-Pierce test: X-squared = 17.12, df = 12, p-value = 0.145

ARIMA(0,0,2)(1,1,0)[12]
Coefficients:
      ma1      ma2      sar1  minT_1  rh0600
      0.682   0.545  -0.495   5.531   0.854
s.e.  0.086   0.072   0.091   3.084   0.832

```

sigma^2 estimated as 259: log likelihood=-501.6
 AIC=1013 AICc=1014 BIC=1030; mae=10.77; rmse=15.33
 Box-Pierce test: X-squared = 17.02, df = 12, p-value = 0.1488
 =====

Western (Total):

ARIMA(0,1,1)(2,1,2)[12]

Coefficients:

	ma1	sar1	sar2	sma1	sma2
	-0.479	-0.666	-0.201	-0.375	-0.625
s.e.	0.091	0.314	0.122	0.461	0.383

sigma^2 estimated as 323: log likelihood=-529.3
 AIC=1069 AICc=1069 BIC=1085; mae=12.07; rmse=17.07
 Box-Pierce test: X-squared = 11.7, df = 24, p-value = 0.9831

ARIMA(0,1,1)(2,1,2)[12]

Coefficients:

	ma1	sar1	sar2	sma1	sma2	rainf	rainf_1	maxT
	-0.431	-0.360	-0.210	-0.617	-0.383	-0.047	0.075	-8.183
s.e.	0.098	0.368	0.125	0.411	0.371	0.030	0.029	4.344

sigma^2 estimated as 296: log likelihood=-519.5
 AIC=1055 AICc=1057 BIC=1080; mae=12; rmse=16.33
 Box-Pierce test: X-squared = 14.32, df = 24, p-value = 0.939
 =====

Volta(Total):

ARIMA(1,1,2)(0,1,2)[12]

Coefficients:

	ar1	ma1	ma2	sma1	sma2
	-0.695	0.329	-0.511	-0.625	0.381
s.e.	0.154	0.171	0.122	0.132	0.184

sigma^2 estimated as 246: log likelihood=-299.8
 AIC=609.7 AICc=611 BIC=623.2; mae=10.29; rmse=14.41
 Box-Pierce test: X-squared = 20.4, df = 24, p-value = 0.674

ARIMA(1,1,2)(0,1,2)[12]

Coefficients:

	ar1	ma1	ma2	sma1	sma2	rainf_1	sunsh
	-0.732	0.467	-0.533	-0.614	0.370	-0.060	-5.037
s.e.	0.102	0.146	0.141	0.133	0.173	0.022	3.594

sigma^2 estimated as 222: log likelihood=-293.1
 AIC=600.1 AICc=602.5 BIC=618.1; mae=9.944; rmse=13.67
 Box-Pierce test: X-squared = 18.4, df = 24, p-value = 0.7829
 =====

Results C-2.2: Results of multiplicative SARIMA and SARIMAX models of morbidity incidence rates (0-4) for the regions

=====

Upper East (0-4):

ARIMA(1,1,1)(0,1,1)[12]

Coefficients:

	ar1	ma1	sma1
	0.733	-0.960	-0.753
s.e.	0.087	0.059	0.104

sigma^2 estimated as 17257: log likelihood=-755.4

AIC=1517 AICc=1517 BIC=1528; mae05=88.74; rmse05=124.7

Box-Pierce test: X-squared = 3.35, df = 12, p-value = 0.9925

ARIMA(1,1,1)(0,1,1)[12]

Coefficients:

	ar1	ma1	sma1	minT_1	rh1500
	0.743	-0.974	-0.770	-24.97	4.777
s.e.	0.086	0.077	0.104	21.05	3.227

sigma^2 estimated as 16729: log likelihood=-748

AIC=1506 AICc=1507 BIC=1523; mae=88.65; rmse=122.8

Box-Pierce test: X-squared = 4.378, df = 12, p-value = 0.9756

Upper West (0-4):

ARIMA(1,1,1)(0,1,1)[12]

Coefficients:

	ar1	ma1	sma1
	0.627	-0.966	-0.810
s.e.	0.095	0.067	0.103

sigma^2 estimated as 13083: log likelihood=-740.6

AIC=1487 AICc=1488 BIC=1498; mae=78.7; rmse=108.6

Box-Pierce test: X-squared = 12.74, df = 24, p-value = 0.9702

ARIMA(1,1,1)(0,1,1)[12]

Coefficients:

	ar1	ma1	sma1	rainf_1	sunsh_1
	0.641	-0.960	-0.785	-0.601	-45.21
s.e.	0.097	0.065	0.101	0.252	18.81

sigma^2 estimated as 12339: log likelihood=-730.2

AIC=1470 AICc=1471 BIC=1487; mae=76.94; rmse=105.4

Box-Pierce test: X-squared = 16.11, df = 24, p-value = 0.884

Northern (0-4):

ARIMA(1,1,4)(1,1,0)[12]

Coefficients:

	ar1	ma1	ma2	ma3	ma4	sar1
	-0.858	0.400	-0.852	-0.349	0.336	-0.576
s.e.	0.068	0.107	0.097	0.091	0.087	0.076

sigma^2 estimated as 2905: log likelihood=-646.8

AIC=1306 AICc=1307 BIC=1325; mae=35.63; rmse=51.17

Box-Pierce test: X-squared = 18.86, df = 24, p-value = 0.7592

```

ARIMA(1,1,4)(1,1,0)[12]
Coefficients:
      ar1      ma1      ma2      ma3      ma4      sar1      sunsh_1
      -0.807  0.285  -0.891  -0.315  0.361  -0.566  18.393
s.e.    0.102  0.125  0.092  0.085  0.084  0.080  5.838
sigma^2 estimated as 2707:  log likelihood=-637.2
AIC=1288  AICc=1290  BIC=1310; mae=34.57; rmse=49.38
Box-Pierce test: X-squared = 19.09, df = 24, p-value = 0.7473
=====

```

Brong Ahafo (0-4):

```

ARIMA(0,1,2)(0,1,1)[12]
Coefficients:
      ma1      ma2      sma1
      -0.431  -0.284  -0.720
s.e.    0.082  0.082  0.072
sigma^2 estimated as 2918:  log likelihood=-843
AIC=1692  AICc=1692  BIC=1704; mae=38.68; rmse=51.89
Box-Pierce test: X-squared = 30.44, df = 24, p-value = 0.1706

```

```

ARIMA(0,1,2)(0,1,1)[12]
Coefficients:
      ma1      ma2      sma1      maxT      rh1500_1
      -0.365  -0.376  -0.704  11.995      2.490
s.e.    0.082  0.087  0.074  8.129      0.838
sigma^2 estimated as 2684:  log likelihood=-831
AIC=1672  AICc=1673  BIC=1690; mae= 36.62; rmse=49.75
Box-Pierce test: X-squared = 26.62, df = 24, p-value = 0.3226
=====

```

Ashanti (0-4):

```

ARIMA(3,1,0)(3,2,1)[12]
Coefficients:
      ar1      ar2      ar3      sar1      sar2      sar3      sma1
      -0.549  -0.548  -0.204  -0.683  -0.564  -0.314  -0.975
s.e.    0.095  0.102  0.106  0.122  0.140  0.135  0.214
sigma^2 estimated as 2378:  log likelihood=-598.8
AIC=1212  AICc=1213  BIC=1233; mae=31.96; rmse=43.9
Box-Pierce test: X-squared = 16.64, df = 24, p-value = 0.8637

```

```

ARIMA(3,1,0)(3,2,1)[12]
Coefficients:
      ar1      ar2      ar3      sar1      sar2      sar3      sma1      rainf      maxT_1
      -0.606  -0.578  -0.224  -0.745  -0.634  -0.304  -0.976  0.145-18.035
s.e.    0.102  0.109  0.110  0.129  0.148  0.136  0.211  0.093  8.773
sigma^2 estimated as 2237:  log likelihood=-591.5
AIC=1201  AICc=1203  BIC=1228; mae=31.27; rmse=43.9
Box-Pierce test: X-squared = 19.16, df = 24, p-value = 0.7436
=====

```

Eastern (0-4):

ARIMA(0,1,2)(0,1,1)[12]
Coefficients:
 ma1 ma2 sma1
 -0.196 -0.370 -0.814
s.e. 0.087 0.091 0.097
sigma^2 estimated as 3165: log likelihood=-655.1
AIC=1316 AICc=1316 BIC=1327; mae=38.3; rmse=53.42
Box-Pierce test: X-squared = 10.38, df = 24, p-value = 0.9928

ARIMA(1,1,2)(0,1,1)[12]
Coefficients:
 ar1 ma1 ma2 sma1 rainf_1 minT_1
 -0.240 0.037 -0.427 -0.784 0.179 -19.878
s.e. 0.225 0.208 0.090 0.097 0.110 9.837
sigma^2 estimated as 3009: log likelihood=-645.9
AIC=1304 AICc=1305 BIC=1323; mae=37.43; rmse=52.07
Box-Pierce test: X-squared = 10.74, df = 24, p-value = 0.9907
=====

Greater Accra(0-4):

ARIMA(0,1,1)(1,2,1)[12]
Coefficients:
 ma1 sar1 sma1
 -0.439 -0.529 -0.991
s.e. 0.088 0.080 0.136
sigma^2 estimated as 2279: log likelihood=-589.1
AIC=1184 AICc=1185 BIC=1195; mae=29.13; rmse=42.98
Box-Pierce test: X-squared = 24.91, df = 24, p-value = 0.4104

ARIMA(0,1,1)(1,2,1)[12]
Coefficients:
 ma1 sar1 sma1 rainf_1 rh1500_1 sunsh
 -0.455 -0.534 -0.989 0.089 2.027 -11.694
s.e. 0.086 0.083 0.143 0.067 0.982 4.564
sigma^2 estimated as 2090: log likelihood=-579.2
AIC=1170 AICc=1172 BIC=1189; mae=27.91; rmse=41.12
Box-Pierce test: X-squared = 26.93, df = 24, p-value = 0.3077
=====

Central (0-4):

ARIMA(0,1,3)(0,1,2)[12]
Coefficients:
 ma1 ma2 ma3 sma1 sma2
 -0.354 -0.113 -0.285 -0.845 -0.155
s.e. 0.089 0.098 0.085 0.261 0.106
sigma^2 estimated as 863: log likelihood=-584.5
AIC=1179 AICc=1180 BIC=1196; mae=19.56; rmse=27.9
Box-Pierce test: X-squared = 10.51, df = 12, p-value = 0.5715

ARIMA(0,1,3)(0,1,2)[12]
Coefficients:
 ma1 ma2 ma3 sma1 sma2 maxT_1 minT minT_1
 -0.406 -0.095 -0.252 -0.809 -0.191 -20.69 13.378 15.922
s.e. 0.093 0.097 0.092 0.268 0.114 10.75 7.214 7.314
sigma^2 estimated as 825: log likelihood=-576.7
AIC=1169 AICc=1171 BIC=1194; mae=19.97; rmse=27.26
Box-Pierce test: X-squared = 8.737, df = 12, p-value = 0.7252
=====

Western (0-4):

```

ARIMA(0,1,1)(0,1,1)[12]
Coefficients:
      ma1      sma1
      -0.619  -0.815
s.e.    0.068   0.120
sigma^2 estimated as 1585:  log likelihood=-614
AIC=1232  AICc=1232  BIC=1240; mae=26.77; rmse=37.8
Box-Pierce test: X-squared = 20.17, df = 24, p-value = 0.6872

```

```

ARIMA(0,1,1)(0,1,1)[12]
Coefficients:
      ma1      sma1  rh0600  rh0600_1
      -0.629  -0.838  10.590   7.878
s.e.    0.063   0.133   3.663   3.502
sigma^2 estimated as 1434:  log likelihood=-603.7
AIC=1215  AICc=1216  BIC=1229; mae=25.48; rmse=35.95
Box-Pierce test: X-squared = 18.67, df = 24, p-value = 0.7692
=====

```

Volta (0-4):

```

ARIMA(1,1,0)(0,1,1)[12]
Coefficients:
      ar1      sma1
      -0.250  -0.816
s.e.    0.115   0.253
sigma^2 estimated as 1913:  log likelihood=-375.2
AIC=754.5  AICc=754.8  BIC=761.2; mae=29.31; rmse=40.21
Box-Pierce test: X-squared = 14.52, df = 24, p-value = 0.9339

```

```

ARIMA(1,1,0)(0,1,1)[12]
Coefficients:
      ar1      sma1  rh1500_1  sunsh_1
      -0.229  -0.879   -2.450   -13.79
s.e.    0.116   0.403    1.814    12.54
sigma^2 estimated as 1771:  log likelihood=-368.9
AIC=745.7  AICc=746.7  BIC=757; mae=27.97; rmse=38.65
Box-Pierce test: X-squared = 14.92, df = 24, p-value = 0.9229
=====

```

C-3: Results of SARIMA Model Diagnosis by Lyung-Box Q-Test

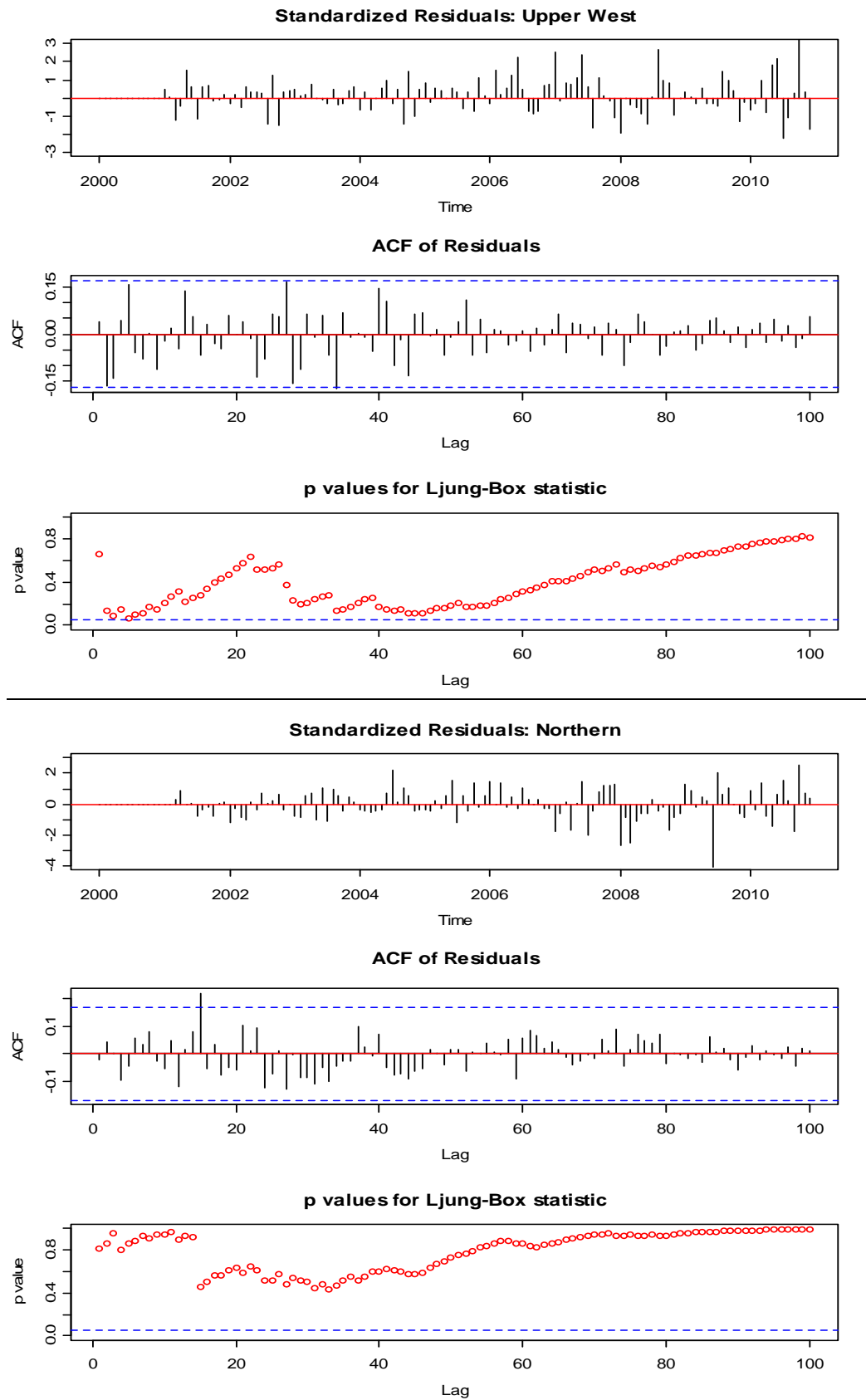


Figure C-3.1a: SARIMA model diagnostics of the morbidity incidence rates (total) by the Lyung-Box Q-test indicating the standardised residuals (top), ACF of residuals (middle) and the p-values (bottom) for Upper West and Northern regions

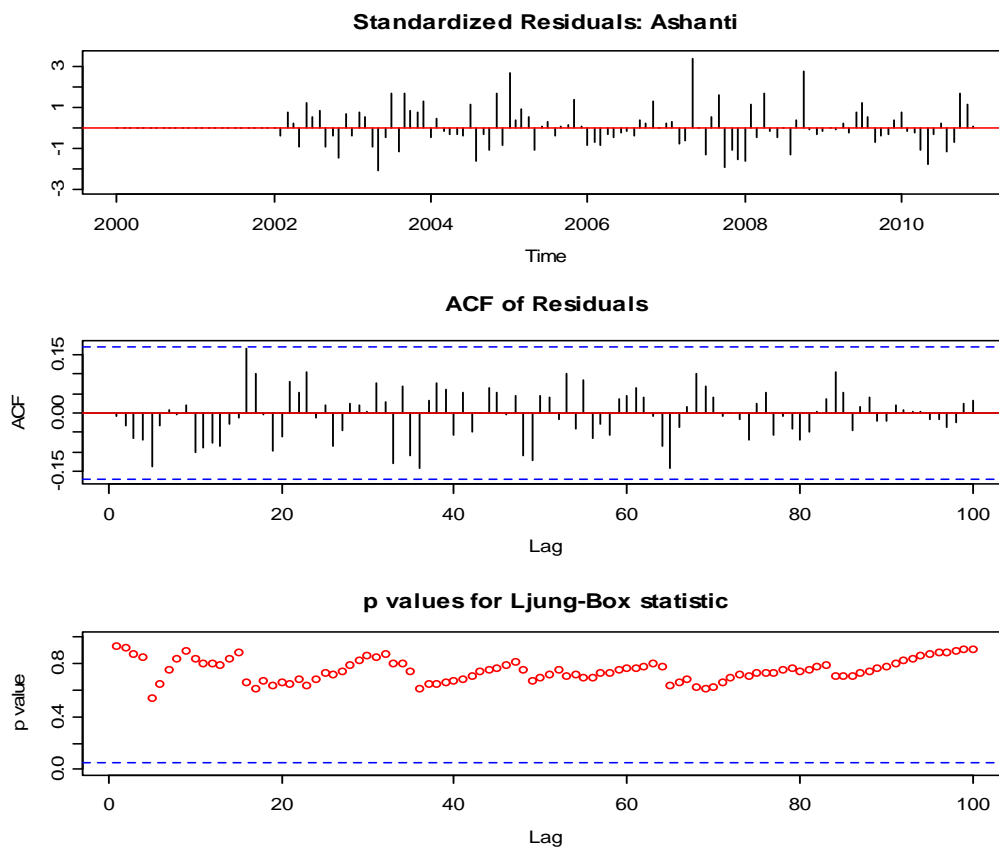
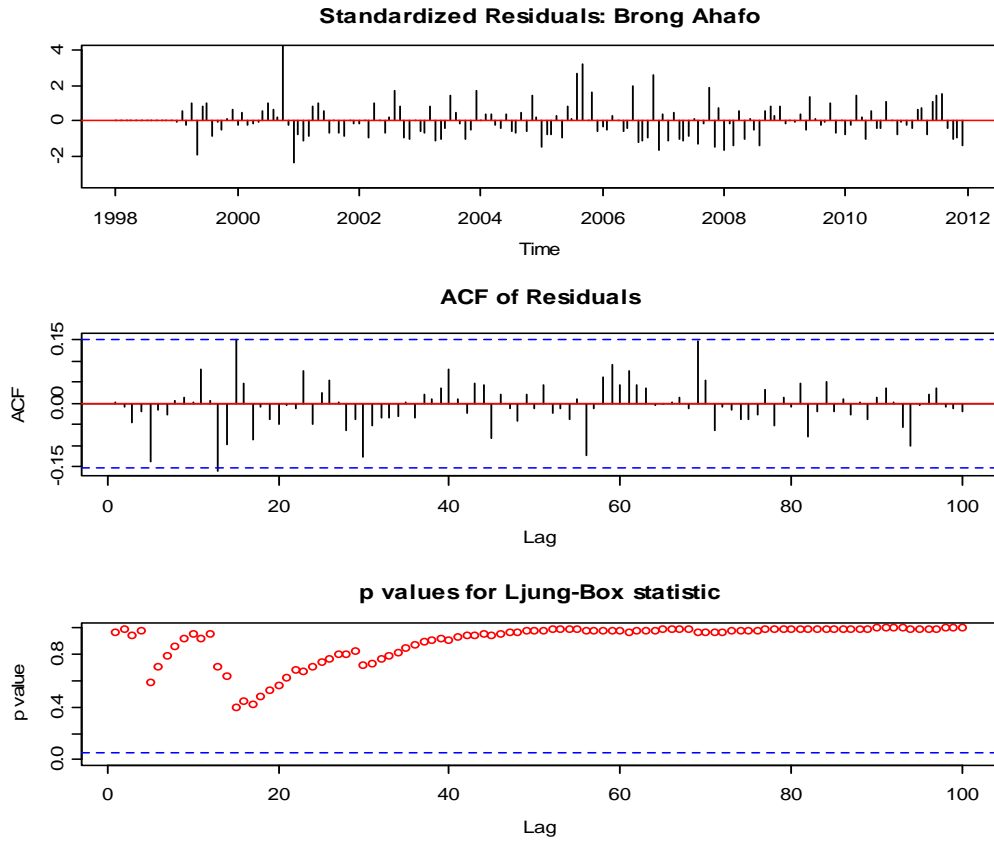


Figure C-3.1b: SARIMA model diagnostics of the morbidity incidence rates (total) by the Lyung-Box Q-test indicating the standardised residuals (top), ACF of residuals (middle) and the p-values (bottom) for Brong Ahafo and Ashanti regions

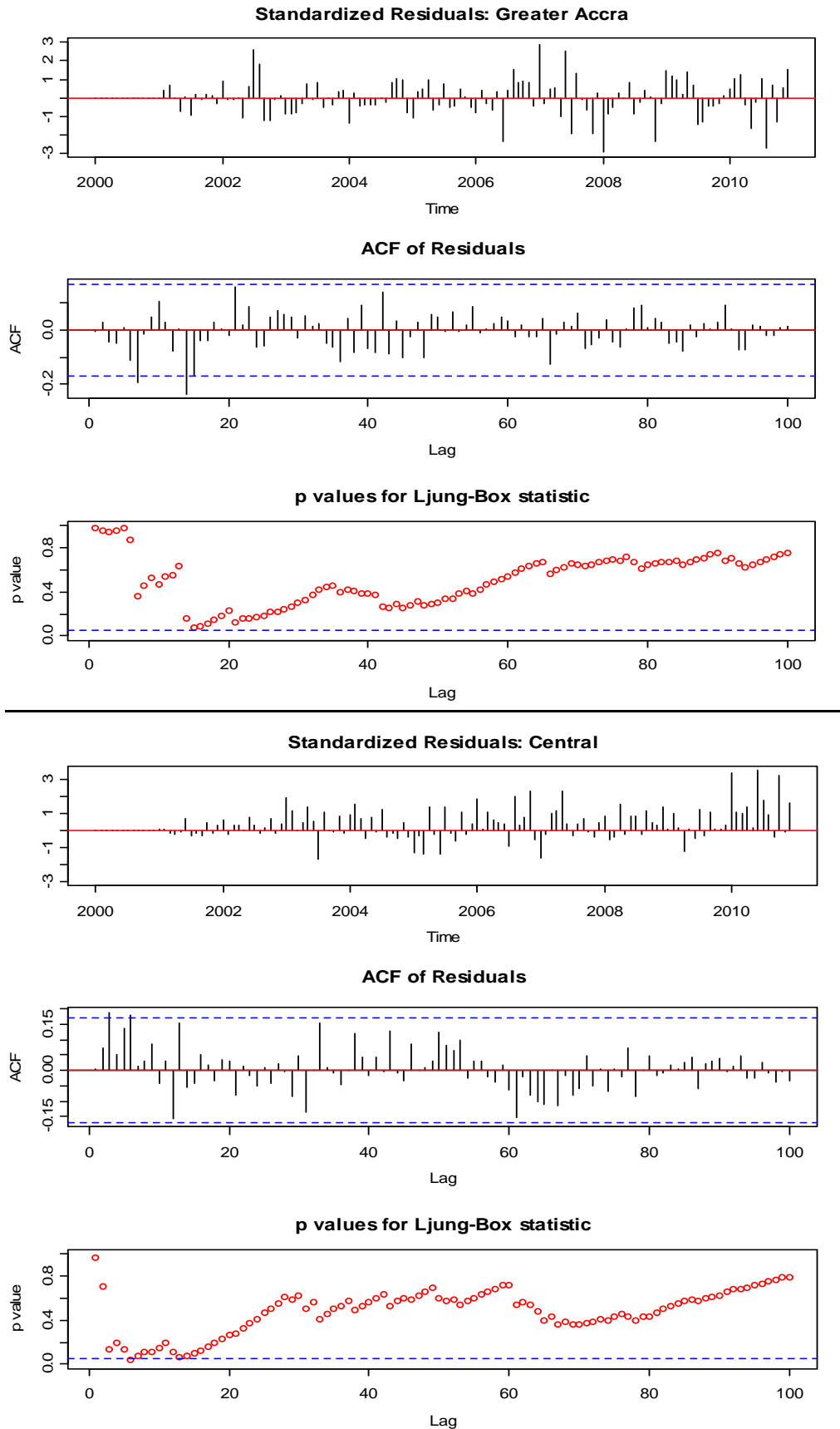


Figure C-3.1c: SARIMA model diagnostics of the morbidity incidence rates (total) by the Lyung-Box Q-test indicating the standardised residuals (top), ACF of residuals (middle) and the p-values (bottom) for Greater Accra and Central regions

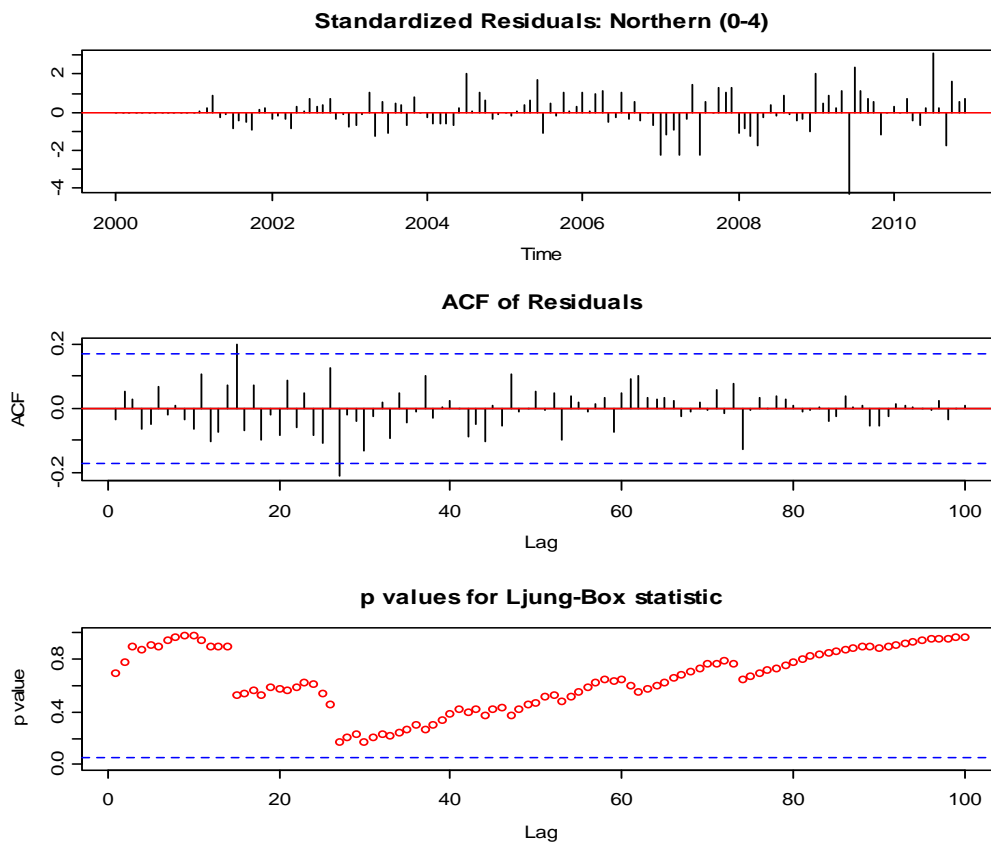
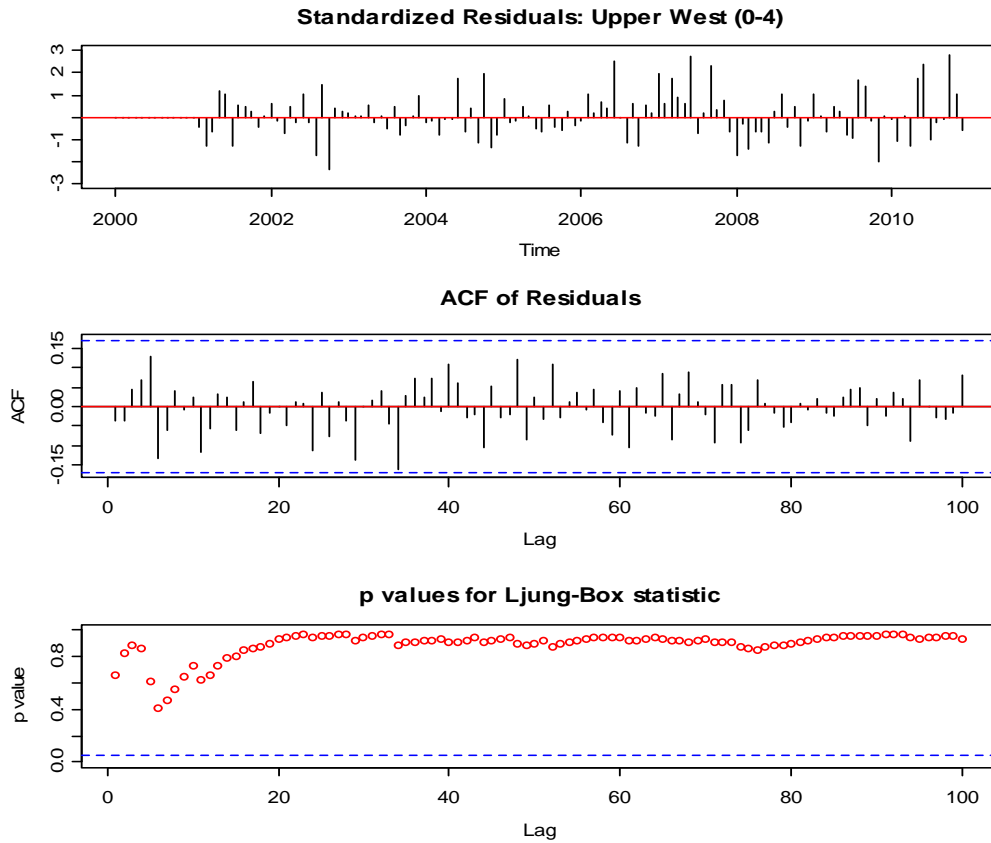


Figure C-3.2a: SARIMA model diagnostics of the morbidity incidence rates (0-4) by the Lyung-Box Q-test indicating the standardised residuals (top), ACF of residuals (middle) and the p-values (bottom) for Upper West and Northern regions

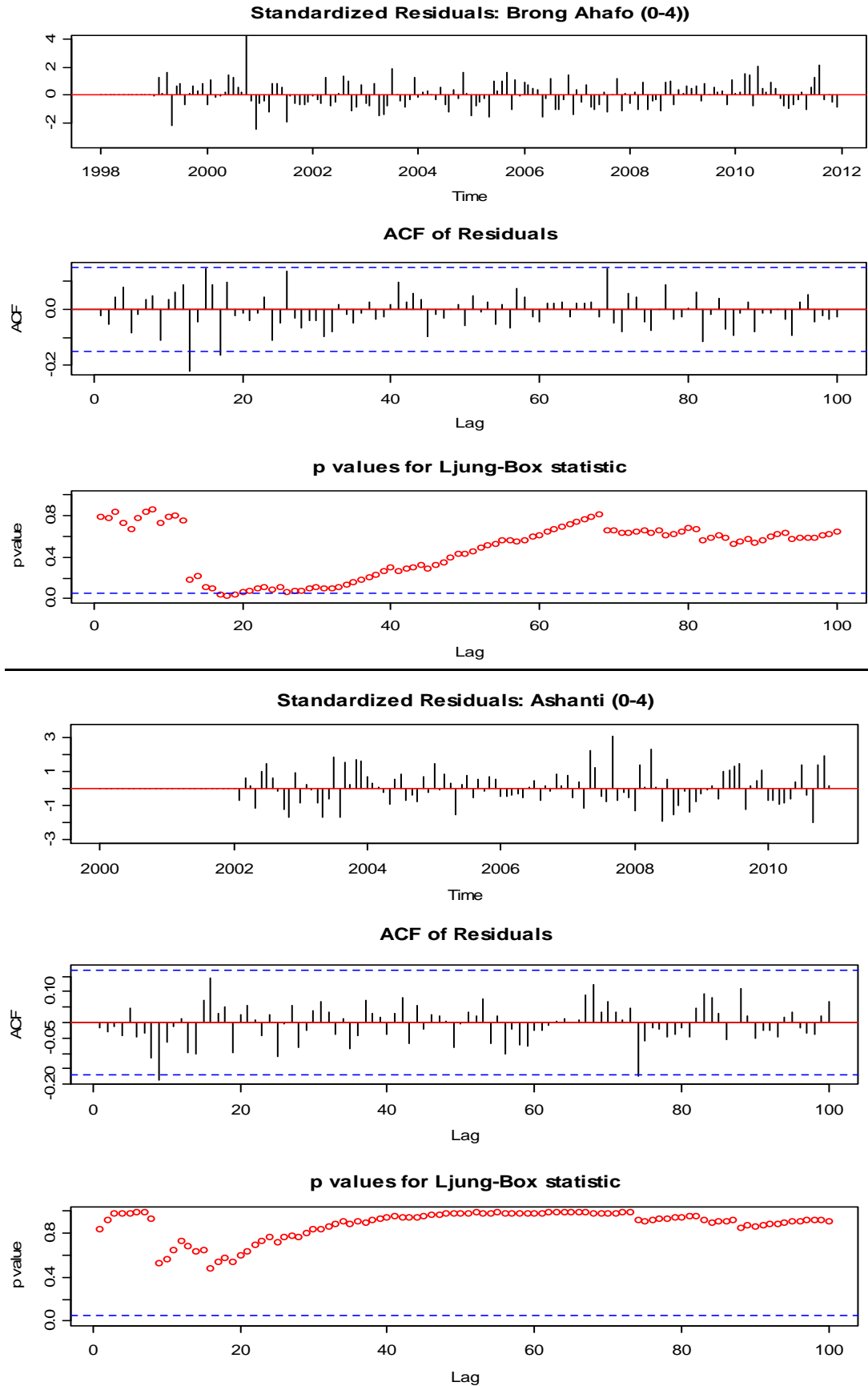


Figure C-3.2b: SARIMA model diagnostics of the morbidity incidence rates (0-4) by the Lyung-Box Q-test indicating the standardised residuals (top), ACF of residuals (middle) and the p-values (bottom) for Brong Ahafo and Ashanti regions

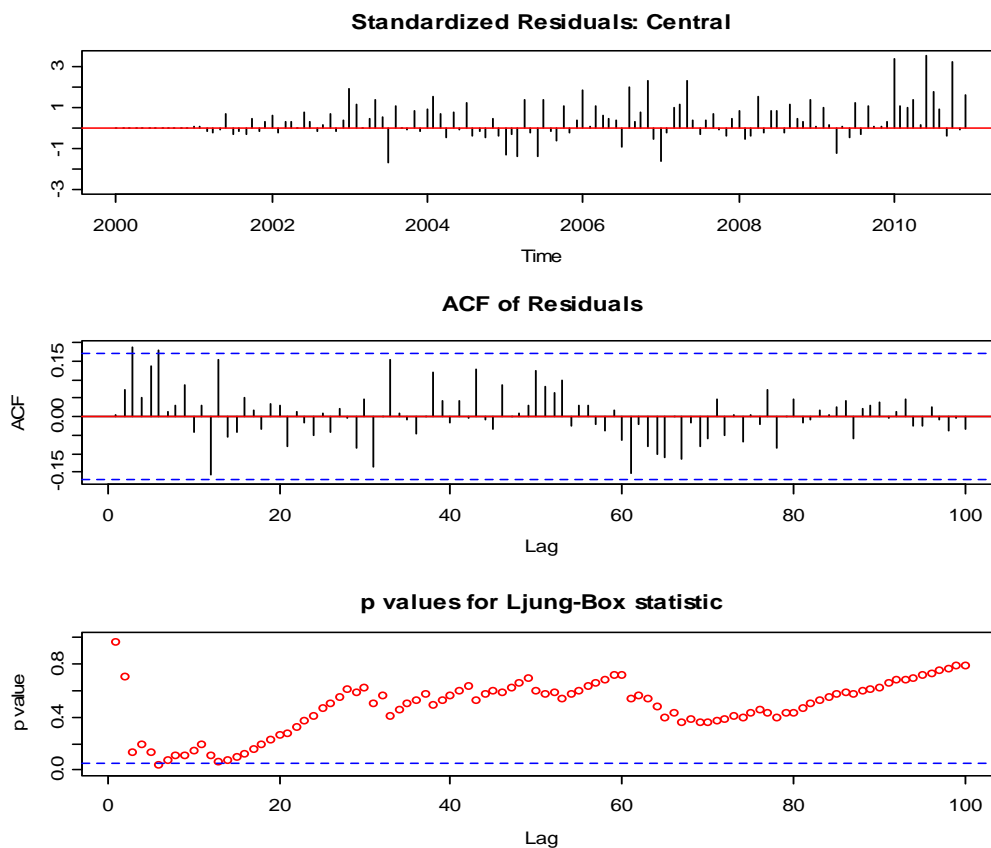
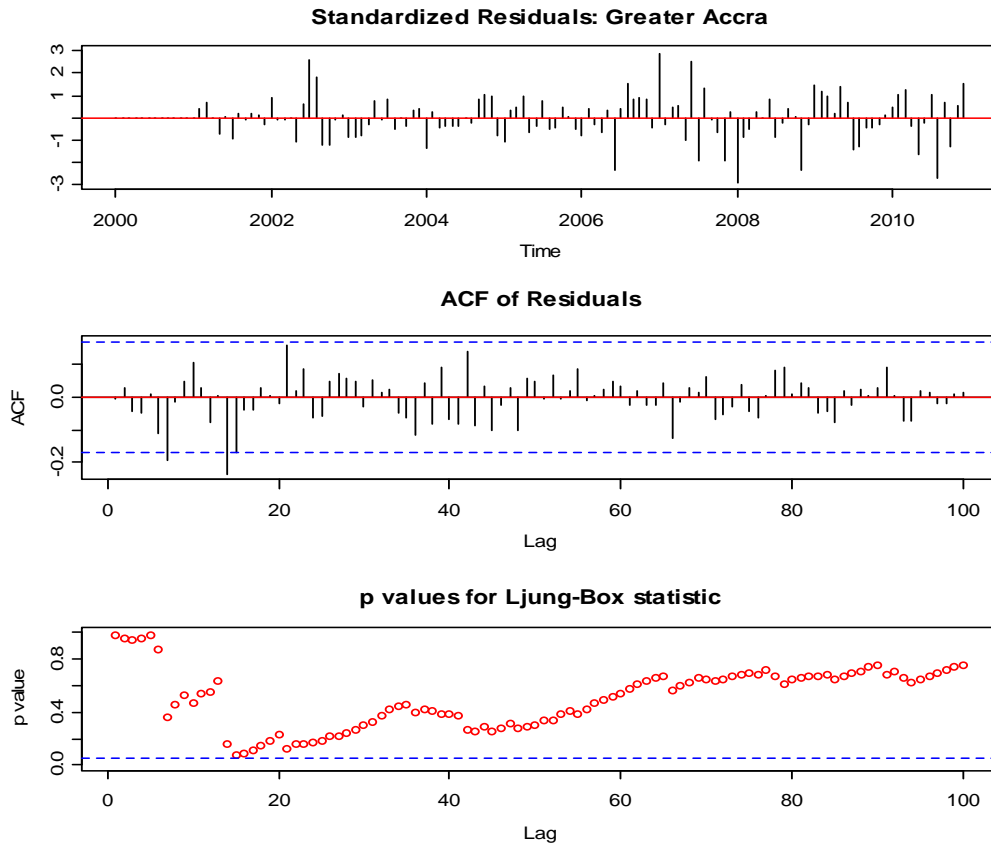


Figure C-3.2c: SARIMA model diagnostics of the morbidity incidence rates (0-4) by the Lyung-Box Q-test indicating the standardised residuals (top), ACF of residuals (middle) and the p-values (bottom) for Greater Accra and Central regions

C-4: Graphs of SARIMA Model Forecasting of MIR for 2011-2014

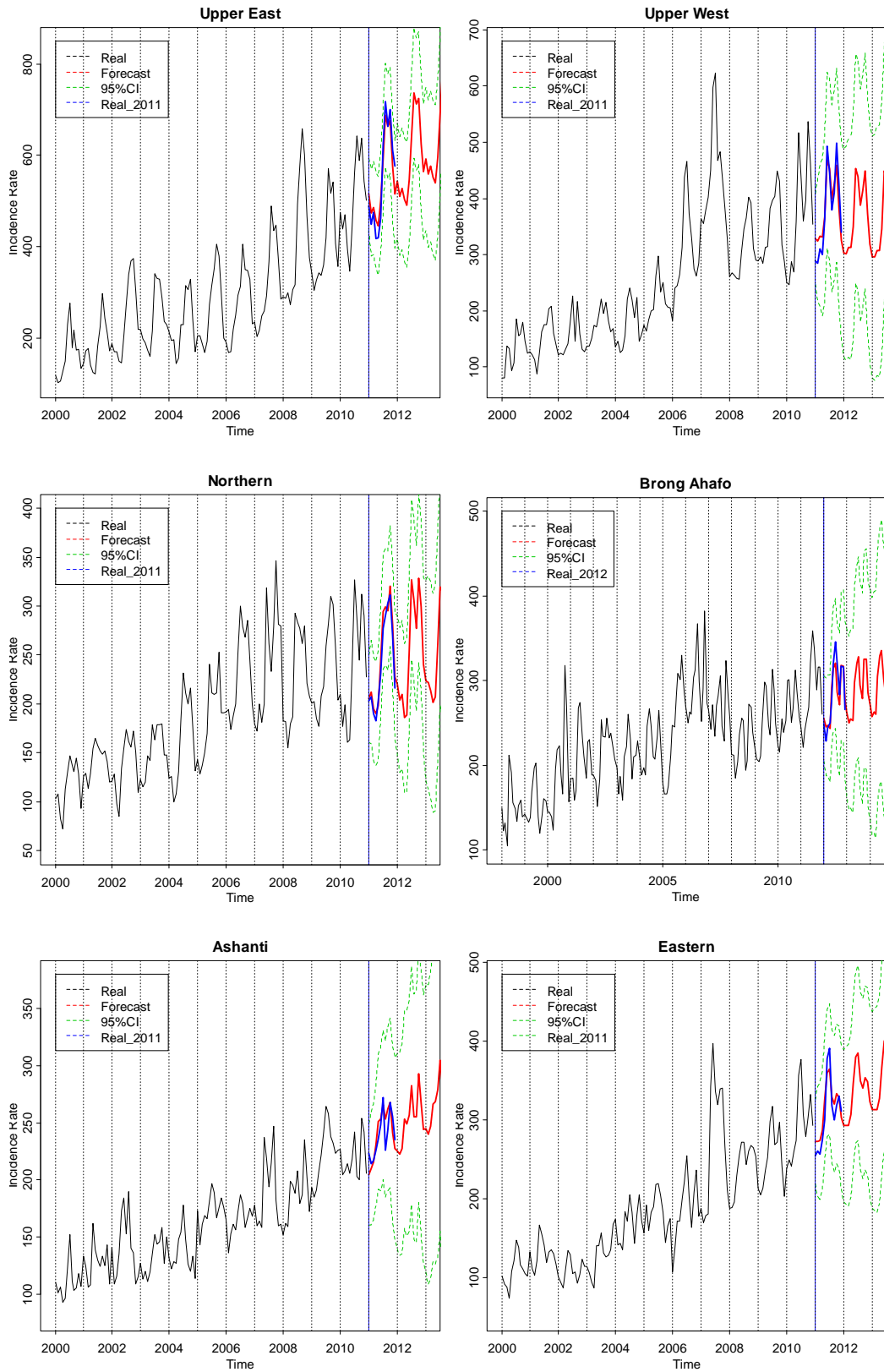


Figure C-4.1a: SARIMA model forecast of monthly morbidity incidence rates (total) for 2011-2013/14 in Upper East, Upper West, Northern, Brong Ahafo, Ashanti and Eastern regions

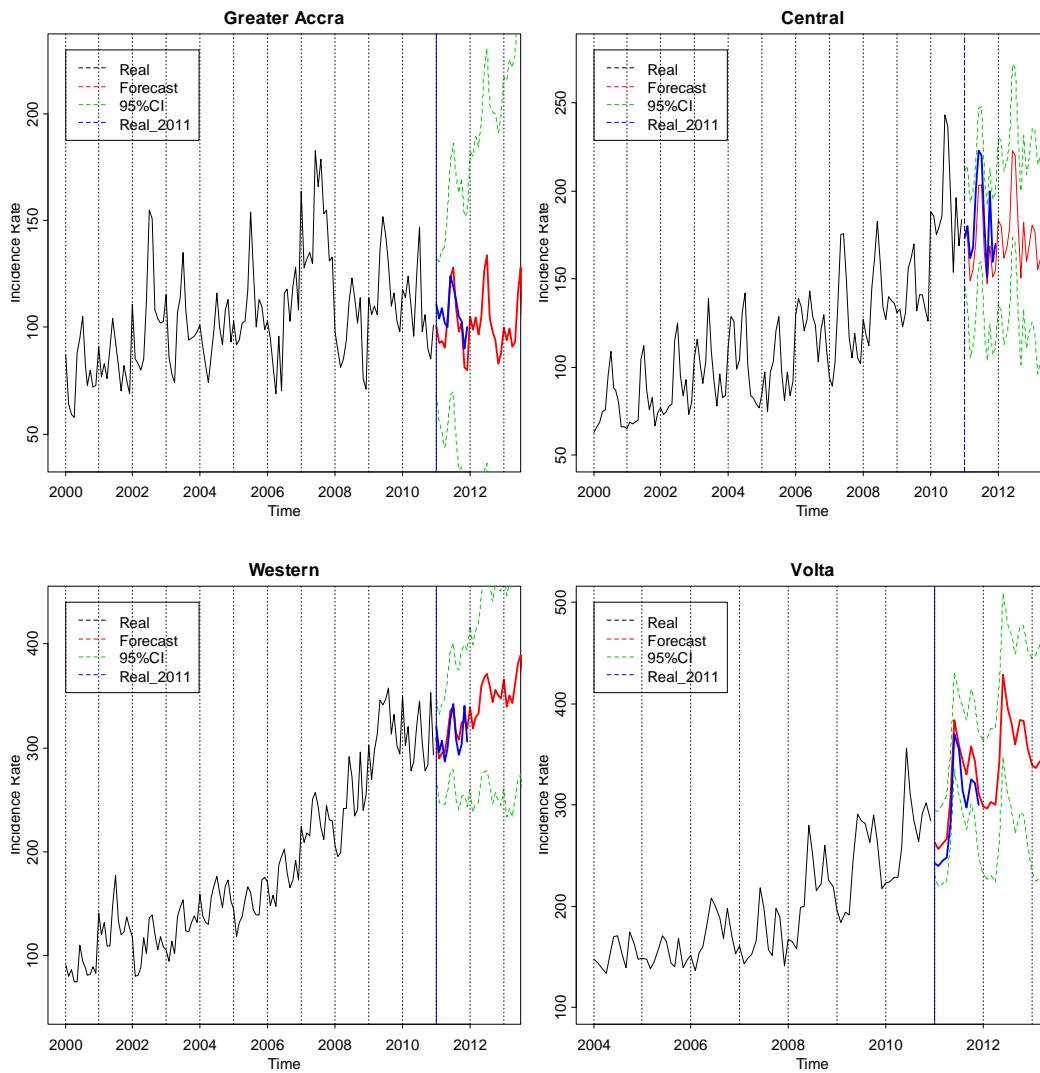


Figure C-4.1b: SARIMA model forecast of monthly morbidity incidence rates (total) for 2011-2013 in Greater Accra, Central, Western and Volta regions

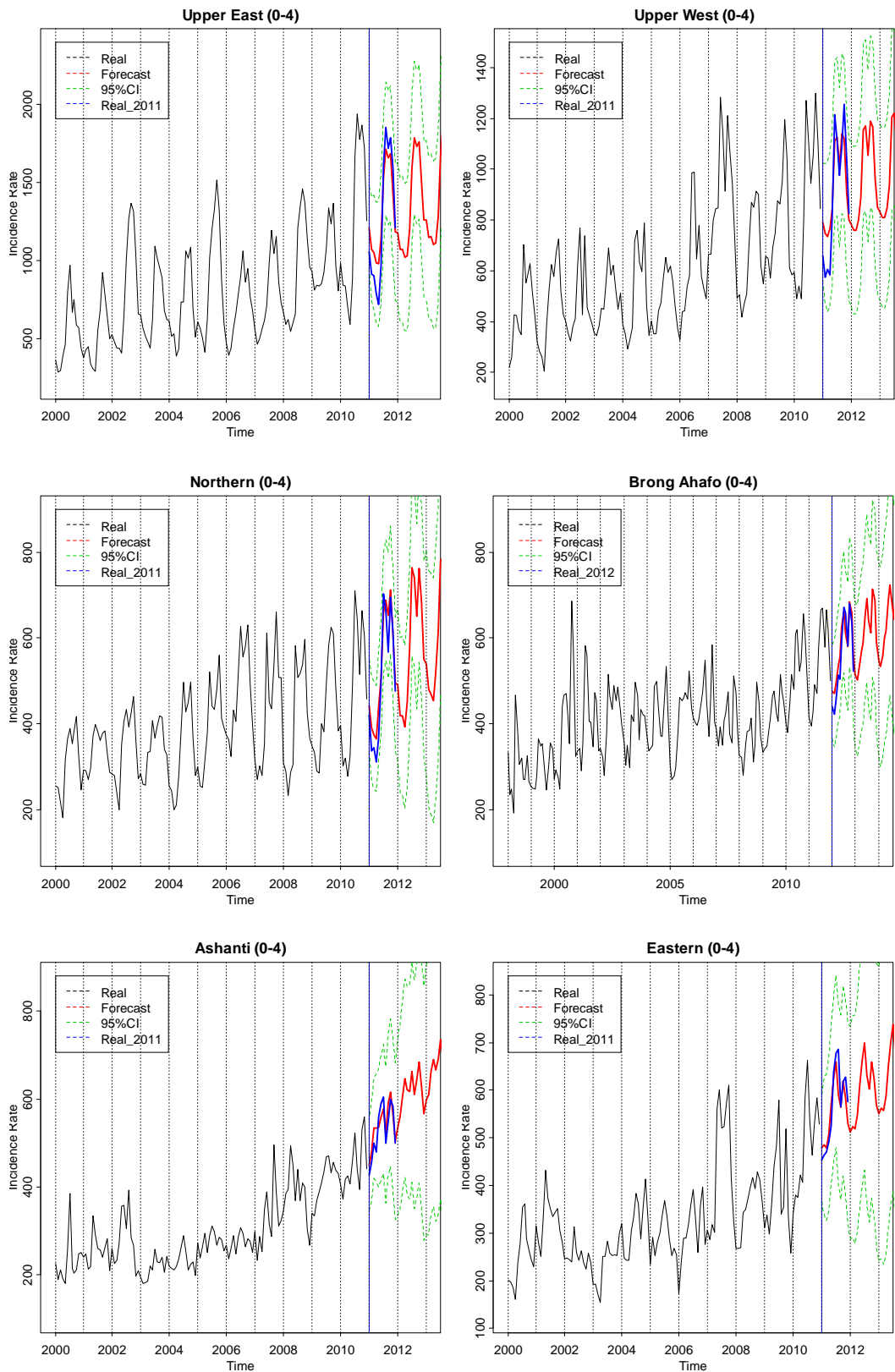


Figure C-4.2a: SARIMA model forecast of monthly morbidity incidence rates (0-4 year group) for 2011-2013/14 in Upper West, Northern, Brong Ahafo, Ashanti, Eastern regions

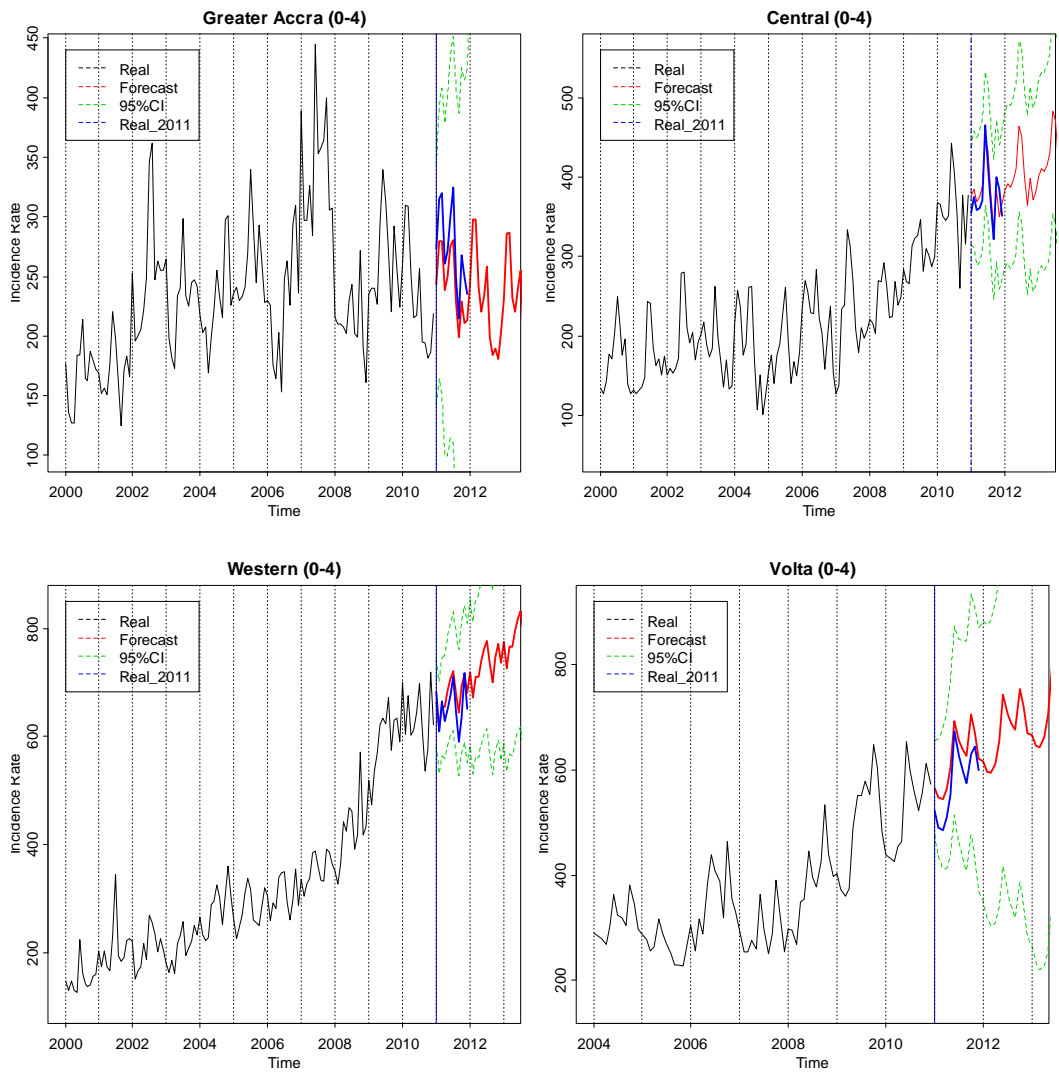


Figure C-4.2b: SARIMA model forecast of monthly morbidity incidence rates (0-4 year group) for 2011-2013 in Greater Accra, Central, Western and Volta regions

C-5: SARIMA Model Forecast Values for 2011-2014/2014

Table C-5.1: SARIMA three-year forecast of monthly morbidity incidence rates for the period 2011-2013 in Upper East Region

Month	Upper East Region (Total)				(0-4)			
	Prediction	Std Error	Lower	Upper	Prediction	Std Error	Lower	Upper
133	515.118	39.312	436.494	593.742	1210.369	131.513	947.342	1473.395
134	474.367	47.41	379.547	569.186	1069.946	166.246	737.455	1402.438
135	485.699	51.036	383.626	587.772	1050.18	184.435	681.31	1419.051
136	458.099	53.023	352.052	564.146	984.482	195.179	594.125	1374.84
137	445.615	54.299	337.017	554.212	979.612	202.019	575.573	1383.651
138	498.973	55.232	388.51	609.436	1143.357	206.654	730.05	1556.665
139	592.726	55.986	480.753	704.699	1529.081	209.977	1109.128	1949.035
140	688.241	56.643	574.954	801.528	1717.587	212.49	1292.606	2142.567
141	663.499	57.244	549.012	777.987	1657.43	214.488	1228.454	2086.405
142	676.641	57.81	561.021	792.261	1686.762	216.148	1254.465	2119.058
143	576.791	58.355	460.081	693.5	1424.934	217.583	989.767	1860.1
144	514.956	58.885	397.185	632.726	1181.436	218.866	743.704	1619.169
145	543.206	62.691	417.824	668.587	1179.043	225.772	727.499	1630.587
146	510.844	64.962	380.92	640.769	1068.84	230.626	607.588	1530.093
147	527.157	66.533	394.092	660.223	1071.221	234.26	602.7	1539.741
148	502.514	67.751	367.011	638.016	1021.752	237.122	547.509	1495.995
149	491.786	68.781	354.224	629.347	1028.774	239.478	549.818	1507.731
150	546.186	69.703	406.78	685.591	1201.235	241.497	718.242	1684.229
151	640.557	70.56	499.436	781.678	1593.346	243.285	1106.776	2079.916
152	736.44	71.378	593.684	879.196	1786.532	244.913	1296.706	2276.357
153	711.916	72.169	567.577	856.255	1729.805	246.429	1236.948	2222.662
154	725.187	72.942	579.303	871.071	1761.65	247.865	1265.92	2257.381
155	625.414	73.701	478.013	772.815	1501.664	249.246	1003.171	2000.157
156	563.624	74.448	414.728	712.521	1259.517	250.589	758.338	1760.695
157	591.901	78.275	435.351	748.452	1258.112	257.32	743.472	1772.753
158	559.556	80.719	398.119	720.994	1148.635	262.241	624.154	1673.116
159	575.879	82.502	410.874	740.883	1151.546	266.067	619.411	1683.681
160	551.241	83.943	383.354	719.128	1102.467	269.186	564.095	1640.839
161	540.516	85.196	370.124	710.908	1109.775	271.833	566.109	1653.441
162	594.918	86.339	422.241	767.595	1282.444	274.159	734.126	1830.763
163	689.291	87.414	514.462	864.119	1674.708	276.263	1122.183	2227.234
164	785.174	88.447	608.28	962.068	1868.006	278.21	1311.587	2424.426
165	760.651	89.45	581.75	939.551	1811.362	280.046	1251.271	2371.453
166	773.922	90.433	593.057	954.787	1843.268	281.803	1279.662	2406.873
167	674.149	91.398	491.352	856.946	1583.326	283.504	1016.319	2150.333
168	612.36	92.351	427.658	797.061	1341.211	285.166	770.879	1911.543

Lower and upper values are 95% confidence intervals of forecasted values

C-5.2: SARIMA three-year forecast of monthly morbidity incidence rates for the period 2011-2013 in Upper West Region

Month	Upper West Region (Total)				(0-4)			
	Prediction	Std Error	Lower	Upper	Prediction	Std Error	Lower	Upper
133	328.206	40.192	247.822	408.59	792.352	114.784	562.783	1021.921
134	324.739	54.086	216.568	432.91	747.292	137.638	472.016	1022.568
135	333.161	63.146	206.87	459.453	733.793	147.01	439.773	1027.814
136	330.711	69.632	191.447	469.976	765.818	151.447	462.925	1068.712
137	366.348	74.479	217.391	515.306	848.614	153.797	541.019	1156.209
138	468.512	78.188	312.136	624.888	1112.022	155.19	801.642	1422.402
139	452.833	81.071	290.69	614.976	1126.957	156.112	814.734	1439.18
140	399.937	83.336	233.264	566.609	1006.577	156.789	692.999	1320.155
141	425.688	85.129	255.431	595.945	1140.649	157.335	825.98	1455.319
142	458.65	86.555	285.541	631.759	1119.357	157.809	803.739	1434.975
143	381.22	87.694	205.832	556.608	911.327	158.246	594.835	1227.819
144	325.867	88.607	148.653	503.081	801.43	158.666	484.097	1118.762
145	302.873	92.355	118.164	487.582	783.257	162.207	458.844	1107.67
146	301.927	95.285	111.356	492.497	759.806	164.21	431.386	1088.227
147	312.619	97.597	117.425	507.813	759.853	165.51	428.832	1090.874
148	312.213	99.432	113.348	511.078	800.368	166.446	467.476	1133.26
149	349.691	100.896	147.899	551.483	888.486	167.183	554.12	1222.851
150	453.512	102.067	249.377	657.647	1155.229	167.807	819.615	1490.843
151	439.325	103.007	233.31	645.34	1172.255	168.366	835.523	1508.988
152	387.774	103.763	180.247	595.3	1053.186	168.888	715.41	1390.962
153	414.735	104.372	205.99	623.48	1188.08	169.39	849.299	1526.86
154	448.787	104.864	239.06	658.514	1167.302	169.885	827.532	1507.072
155	372.339	105.26	161.818	582.859	959.595	170.381	618.832	1300.358
156	317.869	105.581	106.708	529.031	849.9	170.887	508.127	1191.674
157	295.671	107.852	79.966	511.375	831.854	174.563	482.728	1180.981
158	295.441	109.66	76.122	514.761	808.483	176.708	455.067	1161.899
159	306.779	111.104	84.571	528.987	808.579	178.15	452.279	1164.88
160	306.954	112.261	82.432	531.476	849.126	179.221	490.683	1207.569
161	344.955	113.191	118.574	571.337	937.263	180.087	577.089	1297.437
162	449.248	113.939	221.369	677.126	1204.019	180.834	842.35	1565.688
163	435.485	114.542	206.4	664.57	1221.052	181.513	858.026	1584.079
164	384.316	115.029	154.257	614.374	1101.988	182.152	737.683	1466.293
165	411.621	115.422	180.776	642.466	1236.885	182.771	871.343	1602.426
166	445.983	115.74	214.503	677.464	1216.109	183.381	849.347	1582.871
167	369.814	115.997	137.819	601.808	1008.403	183.994	640.414	1376.392
168	315.596	116.205	83.185	548.006	898.709	184.62	529.469	1267.949

Lower and upper values are 95% confidence intervals of forecasted values

C-5.3: SARIMA three-year forecast of monthly morbidity incidence rates for the period 2011-2013 in Northern Region

Month	Northern Region (Total)				(0-4)			
	Prediction	Std Error	Lower	Upper	Prediction	Std Error	Lower	Upper
133	205.274	22.331	160.611	249.936	442.151	53.897	334.357	549.944
134	212.017	26.384	159.249	264.784	391.301	61.314	268.672	513.93
135	195.206	26.6	142.006	248.405	373.163	61.478	250.206	496.119
136	190.17	26.624	136.921	243.419	365.54	61.866	241.808	489.272
137	197.961	28.239	141.484	254.439	439.617	65.986	307.646	571.589
138	243.746	28.362	187.022	300.47	508.597	66.623	375.351	641.844
139	294.563	29.52	235.523	353.603	658.746	69.853	519.041	798.452
140	299.477	29.744	239.988	358.965	688.463	70.694	547.076	829.851
141	295.165	30.643	233.879	356.45	653.112	73.349	506.414	799.81
142	320.667	30.945	258.776	382.557	712.598	74.341	563.915	861.28
143	281.586	31.687	218.213	344.96	608.169	76.608	454.953	761.384
144	227.443	32.044	163.356	291.53	494.408	77.705	338.997	649.819
145	219.876	35.426	149.025	290.728	491.757	87.65	316.457	667.057
146	204.278	36.955	130.368	278.188	418.403	91.444	235.515	601.291
147	209.597	37.71	134.177	285.017	418.569	93.406	231.757	605.382
148	185.716	38.142	109.433	261.999	393.298	94.959	203.379	583.217
149	188.87	39.351	110.169	267.572	449.335	98.573	252.189	646.481
150	254.657	39.874	174.91	334.405	575.251	100.282	374.688	775.814
151	326.89	40.897	245.095	408.685	764.868	103.425	558.018	971.719
152	305.523	41.478	222.567	388.48	740.015	105.231	529.553	950.476
153	277.038	42.381	192.276	361.799	650.834	108.038	434.759	866.91
154	328.344	42.995	242.355	414.334	762.199	109.897	542.406	981.993
155	299.389	43.814	211.761	387.018	682.637	112.455	457.726	907.548
156	240.707	44.444	151.819	329.595	550.93	114.337	322.256	779.604
157	223.639	51.135	121.37	325.909	540.127	131.096	277.935	802.318
158	221.898	54.316	113.267	330.529	480.211	138.012	204.187	756.236
159	213.522	55.363	102.796	324.249	469.426	140.525	188.377	750.476
160	201.299	56.023	89.252	313.345	454.671	143.013	168.646	740.697
161	207.192	58.058	91.076	323.308	520.811	148.545	223.72	817.901
162	260.817	58.876	143.065	378.568	614.164	151.253	311.657	916.671
163	319.873	60.575	198.722	441.024	780.816	156.078	468.661	1092.972
164	314.648	61.494	191.661	437.635	787.601	158.919	469.763	1105.439
165	300.915	62.977	174.961	426.868	729.286	163.234	402.818	1055.754
166	336.463	63.953	208.557	464.368	810.887	166.145	478.598	1143.177
167	301.28	65.289	170.701	431.858	716.875	170.083	376.71	1057.04
168	245.401	66.293	112.815	377.986	595.613	173.018	249.577	941.648

Lower and upper values are 95% confidence intervals of forecasted values

C-5.4: SARIMA three-year forecast of monthly morbidity incidence rates for the period 2012-2014 in Brong Ahafo Region

Month	Brong Ahafo Region (Total)				(0-4)			
	Prediction	Std Error	Lower	Upper	Prediction	Std Error	Lower	Upper
169	255.799	25.098	205.604	305.995	475.327	54.023	367.282	583.372
170	245.582	28.739	188.104	303.061	470.661	62.146	346.369	594.953
171	247.288	29.655	187.979	306.597	495.028	64.021	366.985	623.07
172	243.089	31.62	179.849	306.329	536.126	65.843	404.44	667.812
173	289.782	34.741	220.301	359.264	555.756	67.616	420.525	690.988
174	314.046	36.876	240.294	387.798	624.88	69.343	486.194	763.567
175	320.2	38.493	243.215	397.185	661.281	71.029	519.224	803.338
176	286.344	40.308	205.727	366.96	609.941	72.675	464.591	755.291
177	271.367	42.21	186.948	355.787	580.132	74.285	431.562	728.702
178	317.51	43.904	229.702	405.317	683.788	75.861	532.067	835.509
179	317.352	45.473	226.405	408.299	657.745	77.404	502.937	812.553
180	277.771	47.047	183.677	371.864	560.935	78.918	403.1	718.771
181	263.028	49.38	164.269	361.788	515.757	84.61	346.537	684.978
182	249.914	51.217	147.479	352.348	501.981	87.944	326.093	677.869
183	254.882	52.796	149.289	360.475	526.348	90.121	346.106	706.589
184	252.432	54.438	143.556	361.308	567.446	92.246	382.953	751.939
185	297.355	56.126	185.103	409.608	587.076	94.324	398.428	775.725
186	321.02	57.707	205.606	436.434	656.2	96.357	463.487	848.914
187	327.949	59.211	209.527	446.37	692.601	98.348	495.906	889.297
188	294.338	60.703	172.932	415.744	641.261	100.299	440.663	841.859
189	279.001	62.175	154.652	403.35	611.452	102.213	407.025	815.878
190	325.053	63.598	197.857	452.249	715.108	104.092	506.924	923.293
191	325.059	64.982	195.094	455.023	689.065	105.938	477.19	900.94
192	285.51	66.348	152.814	418.206	592.255	107.752	376.752	807.759
193	270.694	68.314	134.065	407.322	547.077	113.238	320.602	773.553
194	257.568	69.922	117.725	397.411	533.301	116.718	299.864	766.737
195	262.57	71.34	119.889	405.25	557.668	119.159	319.349	795.986
196	260.123	72.813	114.497	405.749	598.766	121.551	355.663	841.868
197	305.031	74.333	156.366	453.696	618.396	123.897	370.602	866.19
198	328.695	75.777	177.142	480.248	687.52	126.199	435.122	939.919
199	335.63	77.165	181.301	489.96	723.921	128.46	467.001	980.841
200	302.02	78.549	144.922	459.118	672.581	130.682	411.217	933.945
201	286.68	79.923	126.835	446.525	642.772	132.867	377.039	908.505
202	332.732	81.261	170.211	495.253	746.428	135.016	476.397	1016.46
203	332.739	82.569	167.601	497.877	720.385	137.131	446.122	994.648
204	293.19	83.868	125.455	460.926	623.575	139.215	345.145	902.006

Lower and upper values are 95% confidence intervals of forecasted values

C-5.5: SARIMA three-year forecast of monthly morbidity incidence rates for the period 2011-2013 in Ashanti Region

Month	Ashanti Region (Total)				(0-4)			
	Prediction	Std Error	Lower	Upper	Prediction	Std Error	Lower	Upper
133	204.647	22.028	160.59	248.704	448.179	51.439	345.301	551.057
134	210.007	24.72	160.568	259.447	480.224	56.398	367.427	593.021
135	215.731	25.457	164.817	266.646	533.478	57.355	418.768	648.188
136	230.786	26.991	176.804	284.767	534.054	61.54	410.975	657.133
137	250.987	29.644	191.698	310.276	535.011	67.803	399.406	670.617
138	253.094	31.411	190.272	315.915	558.974	71.041	416.892	701.056
139	265.568	32.709	200.15	330.986	577.493	73.632	430.228	724.758
140	253.241	34.185	184.871	321.61	518.617	77.172	364.274	672.961
141	262.184	35.777	190.63	333.738	589.975	80.699	428.577	751.372
142	267.497	37.178	193.141	341.853	614.733	83.547	447.639	781.827
143	240.967	38.452	164.063	317.87	564.485	86.274	391.938	737.032
144	227.364	39.752	147.861	306.867	504.547	89.196	326.155	682.938
145	225.101	42.708	139.685	310.517	534.154	100.123	333.909	734.399
146	222.634	44.532	133.571	311.697	560.459	105.09	350.279	770.64
147	227.027	45.959	135.11	318.945	604.761	108.382	387.996	821.525
148	252.885	47.52	157.845	347.925	647.102	112.97	421.162	873.042
149	249.209	49.234	150.741	347.678	620.504	118.122	384.26	856.748
150	256.416	50.774	154.869	357.964	616.491	122.185	372.122	860.86
151	282.628	52.193	178.243	387.014	661.817	125.913	409.99	913.643
152	255.333	53.626	148.081	362.586	610.805	129.947	350.91	870.699
153	255.526	55.064	145.397	365.655	644.041	133.939	376.163	911.918
154	293.027	56.425	180.177	405.877	683.866	137.582	408.702	959.029
155	267.062	57.725	151.612	382.512	628.843	141.063	346.718	910.968
156	244.09	59.036	126.017	362.163	566.892	144.637	277.619	856.166
157	244.925	63.217	118.492	371.359	598.188	153.848	290.492	905.885
158	240.086	65.496	109.094	371.079	609.283	158.945	291.393	927.173
159	247.109	67.15	112.809	381.409	662.525	162.781	336.964	988.087
160	266.725	69.057	128.611	404.839	689.327	167.554	354.22	1024.435
161	268.217	71.267	125.683	410.751	666.931	172.758	321.416	1012.446
162	279.288	73.208	132.871	425.704	690.551	177.166	336.219	1044.882
163	304.9	74.969	154.962	454.837	734.82	181.291	372.239	1097.401
164	281.914	76.777	128.361	435.467	690.816	185.644	319.528	1062.103
165	280.523	78.615	123.292	437.753	699.59	189.989	319.612	1079.569
166	306.908	80.345	146.218	467.599	769.409	194.035	381.34	1157.478
167	283.401	81.992	119.418	447.384	739.423	197.895	343.633	1135.213
168	265.6	83.668	98.264	432.936	665.396	201.871	261.653	1069.138

Lower and upper values are 95% confidence intervals of forecasted values

C-5.6: SARIMA three-year forecast of monthly morbidity incidence rates for the period 2011-2013 in Eastern Region

Month	Eastern Region (Total)				(0-4)			
	Prediction	Std Error	Lower	Upper	Prediction	Std Error	Lower	Upper
133	272.314	26.679	218.955	325.673	478.638	56.406	365.825	591.451
134	272.711	34.921	202.869	342.552	484.627	72.363	339.901	629.353
135	273.357	36.981	199.395	347.32	479.122	76.397	326.328	631.917
136	286.753	38.252	210.249	363.257	509.172	80.229	348.714	669.629
137	326.655	39.349	247.957	405.353	571.224	83.885	403.453	738.995
138	359.542	40.387	278.767	440.316	623.669	87.389	448.89	798.447
139	365.006	41.393	282.221	447.792	660.131	90.758	478.615	841.647
140	329.266	42.373	244.519	414.012	591.144	94.006	403.132	779.156
141	320.17	43.331	233.508	406.833	563.473	97.146	369.182	757.764
142	333.297	44.269	244.76	421.835	619.765	100.187	419.392	820.139
143	328.868	45.188	238.491	419.244	584.532	103.138	378.255	790.808
144	302.88	46.093	210.695	395.065	529.941	106.015	317.91	741.972
145	292.657	48.154	196.349	388.965	511.577	111.737	288.104	735.05
146	292.828	49.911	193.007	392.65	523.818	116.529	290.76	756.877
147	293.423	51.163	191.097	395.749	518.314	120.113	278.088	758.54
148	306.807	52.294	202.219	411.395	548.363	123.593	301.178	795.549
149	346.706	53.381	239.943	453.468	610.416	126.977	356.461	864.37
150	379.592	54.442	270.708	488.476	662.861	130.274	402.313	923.409
151	385.056	55.481	274.093	496.019	699.322	133.489	432.344	966.301
152	349.316	56.502	236.312	462.319	630.335	136.629	357.077	903.593
153	340.22	57.504	225.213	455.227	602.665	139.698	323.269	882.061
154	353.347	58.489	236.369	470.325	658.957	142.701	373.555	944.359
155	348.918	59.46	229.998	467.837	623.724	145.642	332.439	915.008
156	322.93	60.421	202.089	443.771	569.133	148.537	272.06	866.206
157	312.707	62.401	187.904	437.51	550.768	153.821	243.127	858.409
158	312.878	64.121	184.636	441.121	563.01	158.371	246.269	879.751
159	313.473	65.4	182.672	444.273	557.506	161.922	233.662	881.35
160	326.857	66.572	193.712	460.001	587.555	165.397	256.76	918.35
161	366.755	67.706	231.344	502.167	649.607	168.801	312.005	987.21
162	399.642	68.816	262.009	537.275	702.052	172.138	357.777	1046.328
163	405.106	69.909	265.289	544.923	738.514	175.411	387.693	1089.336
164	369.366	70.984	227.398	511.333	669.527	178.624	312.279	1026.775
165	360.27	72.043	216.184	504.356	641.857	181.78	278.297	1005.417
166	373.397	73.087	227.223	519.571	698.149	184.883	328.384	1067.914
167	368.967	74.119	220.73	517.205	662.915	187.934	287.048	1038.783
168	342.98	75.143	192.694	493.266	608.325	190.949	226.426	990.224

Lower and upper values are 95% confidence intervals of forecasted values

C-5.7: SARIMA three-year forecast of monthly morbidity incidence rates for the period 2011-2013 in Western Region

Month	Western Region (Total)				(0-4)			
	Prediction	Std Error	Lower	Upper	Prediction	Std Error	Lower	Upper
133	309.352	18.865	271.622	347.082	663.257	39.907	583.444	743.07
134	289.294	21.257	246.779	331.808	615.755	42.7	530.356	701.154
135	294.923	23.407	248.11	341.736	654.203	45.321	563.561	744.844
136	295.845	25.375	245.096	346.594	654.732	47.798	559.135	750.328
137	312.617	27.2	258.216	367.018	684.051	50.154	583.743	784.358
138	335.614	28.911	277.792	393.436	707.714	52.403	602.908	812.521
139	339.853	30.526	278.801	400.906	721.129	54.56	612.008	830.249
140	313.696	32.06	249.576	377.816	678.948	56.635	565.678	792.218
141	308.065	33.524	241.017	375.112	644.63	58.636	527.357	761.903
142	323.642	34.926	253.789	393.494	692.376	60.572	571.232	813.519
143	327.026	36.274	254.477	399.575	715.66	62.447	590.765	840.554
144	318.857	37.574	243.709	394.006	681.134	64.268	552.598	809.669
145	338.868	39.108	260.653	417.083	718.955	68.18	582.594	855.316
146	318.324	40.417	237.491	399.158	671.454	70.525	530.403	812.504
147	329.738	41.685	246.369	413.107	709.901	72.795	564.311	855.49
148	333.5	42.915	247.67	419.331	710.43	74.996	560.439	860.421
149	359.373	44.112	271.15	447.596	739.749	77.134	585.482	894.016
150	367.592	45.276	277.04	458.145	763.413	79.214	604.985	921.84
151	370.847	46.412	278.024	463.671	776.827	81.241	614.345	939.309
152	359.299	47.52	264.259	454.339	734.646	83.219	568.208	901.083
153	343.537	48.603	246.331	440.743	700.328	85.151	530.027	870.63
154	356.196	49.662	256.871	455.52	748.074	87.04	573.995	922.153
155	350.047	50.7	248.648	451.447	771.358	88.888	593.582	949.135
156	347.278	51.716	243.845	450.71	736.832	90.699	555.433	918.231
157	365.74	52.445	260.85	470.631	774.653	94.256	586.142	963.165
158	339.895	53.245	233.405	446.385	727.152	96.538	534.075	920.229
159	349.946	54.033	241.88	458.012	765.599	98.768	568.063	963.136
160	343.176	54.81	233.557	452.796	766.128	100.949	564.231	968.026
161	361.422	55.576	250.271	472.573	795.447	103.083	589.281	1001.614
162	381.499	56.331	268.837	494.161	819.111	105.174	608.762	1029.46
163	389.589	57.077	275.436	503.742	832.525	107.225	618.076	1046.975
164	365.522	57.812	249.898	481.147	790.344	109.237	571.871	1008.818
165	352.207	58.539	235.129	469.285	756.027	111.212	533.602	978.451
166	364.681	59.257	246.167	483.194	803.772	113.153	577.466	1030.079
167	378.292	59.966	258.36	498.223	827.057	115.062	596.933	1057.18
168	361.492	60.667	240.159	482.825	792.53	116.939	558.652	1026.408

Lower and upper values are 95% confidence intervals of forecasted values

C-5.8: SARIMA three-year forecast of monthly morbidity incidence rates for the period 2011-2013 in Central Region

Month	Central Region (Total)				(0-4)			
	Prediction	Std Error	Lower	Upper	Prediction	Std Error	Lower	Upper
133	178.327	16.246	145.835	210.818	375.904	30.752	314.401	437.408
134	173.927	20.227	133.473	214.382	384.78	36.59	311.6	457.959
135	149.192	22.024	105.144	193.241	369.344	40.083	289.177	449.511
136	155.681	22.024	111.633	199.73	375.429	40.799	293.832	457.027
137	171.111	22.024	127.062	215.159	388.699	41.501	305.696	471.702
138	202.799	22.024	158.751	246.848	448.376	42.193	363.991	532.761
139	203.748	22.024	159.699	247.796	431.619	42.873	345.874	517.364
140	165.748	22.024	121.699	209.796	378.999	43.542	291.915	466.082
141	147.548	22.024	103.5	191.597	334.085	44.201	245.683	422.487
142	168.703	22.024	124.655	212.752	383.22	44.851	293.519	472.922
143	151.133	22.024	107.085	195.182	349.733	45.506	258.721	440.744
144	155.214	22.024	111.166	199.263	366.876	46.153	274.57	459.182
145	183.128	23.495	136.137	230.118	383.395	48.578	286.239	480.552
146	179.919	24.267	131.386	228.452	392.264	50.114	292.037	492.491
147	162.001	24.66	112.68	211.322	387.58	51.412	284.755	490.405
148	167.751	24.66	118.43	217.071	396.338	52.261	291.816	500.861
149	178.500	24.66	129.18	227.821	410.936	53.096	304.743	517.129
150	222.751	24.66	173.43	272.072	463.583	53.919	355.745	571.42
151	220.251	24.66	170.93	269.572	451.494	54.729	342.036	560.951
152	182.251	24.66	132.93	231.572	398.358	55.527	287.305	509.412
153	150.75	24.66	101.429	200.071	364.031	56.314	251.404	476.659
154	182.251	24.66	132.93	231.572	399.31	57.09	285.131	513.489
155	160	24.66	110.68	209.321	371.41	57.881	255.648	487.173
156	169.501	24.66	120.18	218.822	380.622	58.667	263.287	497.957
157	180.745	27.506	125.732	235.758	401.655	60.041	281.573	521.737
158	176.945	28.953	119.039	234.851	410.32	61.08	288.16	532.48
159	155.644	29.682	96.281	215.007	407.216	62.042	283.132	531.3
160	161.761	29.682	102.397	221.124	415.974	62.847	290.279	541.668
161	174.833	29.682	115.47	234.196	430.571	63.642	303.287	557.856
162	212.849	29.682	153.486	272.212	483.218	64.428	354.363	612.074
163	212.06	29.682	152.697	271.423	471.129	65.204	340.722	601.536
164	174.06	29.682	114.697	233.423	417.994	65.97	286.053	549.934
165	149.161	29.682	89.798	208.524	383.667	66.728	250.211	517.123
166	175.527	29.682	116.164	234.89	418.946	67.477	283.991	553.901
167	155.6	29.682	96.236	214.963	391.046	68.251	254.544	527.547
168	162.41	29.682	103.047	221.774	400.258	69.024	262.21	538.306

Lower and upper values are 95% confidence intervals of forecasted values

C-59: SARIMA three-year forecast of monthly morbidity incidence rates for the period 2011-2013 in Greater Region

Month	Greater Accra Region (Total)				(0-4)			
	Prediction	Std Error	Lower	Upper	Prediction	Std Error	Lower	Upper
133	100.465	15.967	68.532	132.398	279.149	55.139	168.871	389.426
134	92.848	18.826	55.196	130.499	316.273	77.753	160.766	471.779
135	93.381	21.305	50.772	135.991	316.429	95.136	126.156	506.701
136	90.541	23.524	43.494	137.588	275.036	109.801	55.434	494.637
137	104.019	25.551	52.918	155.121	284.641	122.725	39.191	530.092
138	123.091	27.428	68.234	177.948	309.764	134.413	40.939	578.589
139	127.926	29.185	69.555	186.297	315.893	145.162	25.569	606.217
140	109.558	30.843	47.873	171.244	263.24	155.169	-47.098	573.577
141	98.008	32.415	33.178	162.839	234.966	164.568	-94.17	564.102
142	102.096	33.915	34.267	169.926	263.997	173.459	-82.92	610.914
143	81.012	35.351	10.31	151.714	245.825	181.915	-118.005	609.656
144	80.041	36.731	6.578	153.503	248.771	189.996	-131.22	628.762
145	104.951	38.976	26.999	182.903	300.947	209.164	-117.382	719.276
146	98.718	40.749	17.221	180.215	355.106	226.32	-97.534	807.745
147	104.593	42.447	19.699	189.487	355.302	242.263	-129.225	839.828
148	96.582	44.08	8.422	184.742	298.64	257.22	-215.801	813.081
149	104.784	45.655	13.474	196.093	277.514	271.354	-265.194	820.223
150	126.454	47.177	32.1	220.808	290.478	284.788	-279.098	860.053
151	133.656	48.652	36.352	230.959	314.927	297.615	-280.304	910.157
152	104.385	50.083	4.219	204.55	255.919	309.912	-363.906	875.743
153	97.86	51.474	-5.088	200.808	240.87	321.74	-402.609	884.35
154	94.179	52.829	-11.479	199.837	246.242	333.148	-420.053	912.537
155	83.015	54.15	-25.285	191.315	238.066	344.177	-450.289	926.42
156	87.679	55.439	-23.2	198.557	260.139	354.864	-449.59	969.867
157	99.927	58.681	-17.436	217.289	320.444	380.406	-440.368	1081.257
158	93.967	60.951	-27.934	215.868	376.679	403.643	-430.606	1183.964
159	99.168	63.138	-27.109	225.445	377.493	425.612	-473.731	1228.717
160	91.041	65.253	-39.464	221.547	322.055	446.502	-570.949	1215.059
161	92.934	67.301	-41.668	227.537	309.178	466.457	-623.736	1242.092
162	115.94	69.289	-22.637	254.517	328.754	485.593	-642.431	1299.94
163	128.219	71.221	-14.223	270.66	344.519	504.002	-663.486	1352.524
164	95.972	73.102	-50.232	242.176	287.281	521.763	-756.245	1330.807
165	92.909	74.936	-56.963	242.781	264.503	538.939	-813.374	1342.38
166	87.777	76.726	-65.675	241.229	279.686	555.583	-831.481	1390.853
167	74.785	78.475	-82.166	231.735	264.862	571.744	-878.625	1408.35
168	81.425	80.186	-78.948	241.798	280.616	587.46	-894.304	1455.535

Lower and upper values are 95% confidence intervals of forecasted values

C-5.10: SARIMA three-year forecast of monthly morbidity incidence rates for the period 2011-2013 in Volta Region

Month	Volta Region (Total)				(0-4)			
	Prediction	Std Error	Lower	Upper	Prediction	Std Error	Lower	Upper
133	263.184	15.69	231.803	294.565	566.351	44.413	477.524	655.177
134	256.296	18.579	219.138	293.453	547.639	55.414	436.812	658.467
135	261.969	19.497	222.975	300.963	544.32	66.026	412.268	676.372
136	267.006	21.358	224.29	309.721	563.504	74.827	413.85	713.158
137	306.71	22.405	261.9	351.519	605.744	82.77	440.203	771.285
138	383.622	23.833	335.957	431.288	693.238	89.998	513.241	873.235
139	358.838	24.891	309.056	408.62	655.807	96.692	462.424	849.191
140	344.265	26.096	292.072	396.457	638.479	102.95	432.58	844.378
141	329.838	27.12	275.598	384.078	626.398	108.849	408.7	844.095
142	357.772	28.192	301.388	414.156	704.677	114.444	475.789	933.564
143	342.812	29.166	284.479	401.144	670.378	119.779	430.819	909.937
144	311.185	30.149	250.887	371.484	620.562	124.881	370.801	870.324
145	298.231	33.004	232.224	364.239	616.367	132.658	351.051	881.684
146	296.714	34.894	226.927	366.502	597.042	139.116	318.811	875.274
147	302.784	36.234	230.317	375.251	593.876	145.449	302.979	884.773
148	299.729	37.823	224.082	375.376	613.022	151.478	310.066	915.978
149	342.006	39.147	263.712	420.3	655.271	157.286	340.7	969.843
150	428.445	40.562	347.321	509.569	742.763	162.884	416.995	1068.532
151	395.226	41.838	311.55	478.902	705.333	168.297	368.739	1041.927
152	381.271	43.138	294.996	467.546	688.005	173.541	340.922	1035.087
153	360.02	44.357	271.305	448.734	675.923	178.631	318.66	1033.186
154	384.313	45.573	293.167	475.459	754.202	183.58	387.042	1121.363
155	383.164	46.737	289.689	476.638	719.904	188.401	343.102	1096.706
156	357.157	47.887	261.382	452.931	670.088	193.093	283.902	1056.274
157	338.825	52.812	233.201	444.448	665.893	199.941	266.01	1065.775
158	336.267	55.774	224.718	447.815	646.568	205.794	234.979	1058.157
159	343.06	57.72	227.62	458.501	643.402	211.617	220.169	1066.635
160	339.502	60.171	219.159	459.845	662.547	217.251	228.046	1097.049
161	382.129	62.139	257.851	506.407	704.797	222.75	259.296	1150.297
162	468.325	64.304	339.716	596.933	792.289	228.115	336.058	1248.519
163	435.275	66.224	302.827	567.722	754.859	233.357	288.144	1221.574
164	421.202	68.207	284.788	557.615	737.53	238.484	260.561	1214.499
165	400.032	70.054	259.925	540.139	725.449	243.503	238.442	1212.456
166	424.269	71.907	280.454	568.084	803.728	248.421	306.887	1300.569
167	423.159	73.677	275.804	570.514	769.429	253.245	262.94	1275.919
168	397.125	75.432	246.262	547.988	719.613	257.969	203.676	1235.551

Lower and upper values are 95% confidence intervals of forecasted values

Appendix D: Global Trend Analysis of the Space-time Morbidity Incidence Rates

D-1: Trend Model Coefficients

Table D-1.1: Trend model parameters (coefficients and coefficient of determination) of the observed morbidity incidence rates for national data set

District	Region	Easting	Northing	b0	b1	b2	b3	b4	r2
Abura AK	Central	702	590	119.451	0.234	0.004	-19.994	-23.176	0.513
Accra MA	GAccra	808	613	129.879	0.207	-0.004	-8.304	-15.235	0.546
Adaklu-A	Volta	907	723	194.384	-1.792	0.014	-14.121	-1.629	0.382
Adansi N	Ashanti	664	693	157.945	-1.805	0.024	8.532	-13.767	0.642
Adansi S	Ashanti	678	669	105.475	0.906	-0.001	3.567	-4.761	0.804
Afigya S	Ashanti	653	763	184.714	2.601	0.008	-30.026	-33.02	0.833
AframP	Eastern	826	780	156.203	-0.522	0.018	-13.959	-24.259	0.711
Agona	Central	753	623	13.825	2.023	-0.009	-7.824	9.424	0.691
Ahafo-AnoN	Ashanti	592	772	136.078	-1.8	0.029	-14.827	-12.028	0.852
Ahafo-AnoS	Ashanti	625	753	151.232	-0.29	0.014	-13.566	-6.914	0.887
Ahanta W	Western	614	539	152.341	-1.34	0.02	-14.538	-7.967	0.789
AjumakoEE	Central	726	599	9.365	3.582	-0.016	-16.172	-4.337	0.718
Akatsi	Volta	919	677	-496.05	13.061	-0.055	-40.607	-19.978	0.770
Akwapim N	Eastern	822	660	212.562	-0.71	0.021	-31.141	-5.346	0.662
Akwapim S	Eastern	793	642	60.681	3.463	-0.011	-10.977	-12.935	0.612
Amansie C	Ashanti	641	697	-68.402	2.53	-0.009	0.141	0.717	0.421
Amansie E	Ashanti	659	712	110.012	2.513	-0.002	-10.987	-12.373	0.835
AmansieW	Ashanti	623	713	162.573	-1.669	0.026	-17.092	-9.229	0.708
AowinS	Western	522	638	273.125	-4.876	0.043	4.755	-4.392	0.820
AsanteAN	Ashanti	697	730	140.244	-1.759	0.02	-8.934	-7.175	0.696
AsanteAS	Ashanti	707	726	115.897	-1.322	0.019	-14.439	-6.79	0.710
AsikumaOB	Central	722	616	156.876	-0.983	0.016	-8.887	8.505	0.763
Assin N	Central	690	630	33.673	5.241	-0.027	-16.5	-7.413	0.717
Assin S	Central	704	609	594.672	-6.669	0.041	-18.242	-19.055	0.434
AsunafoN	BAhafo	553	751	214.361	1.203	-0.001	-18.201	-17.431	0.652
AsunafoS	BAhafo	562	739	-478.97	15.101	-0.069	-15.328	-28.137	0.623
Asuogyaman	Eastern	842	685	158.565	-0.627	0.015	-24.974	-39.031	0.526
Asutifi	BAhafo	569	770	168.758	1.286	0.023	-36.801	-31.072	0.792
Atebubu-A	BAhafo	722	856	129.754	-1.795	0.03	-16.324	-36.088	0.831
Atiwa	Eastern	768	701	-0.687	2.826	0	-25.08	-8.956	0.728
Atwima M	Ashanti	598	728	-436.83	10.536	-0.039	-9.493	-35.838	0.623
Atwima Nw	Ashanti	634	737	246.597	-3.389	0.042	-19.511	-18.741	0.786
Awutu ES	Central	774	611	113.889	-0.593	0.011	-18.707	1.152	0.635
Bawku M	UEast	800	1221	337.385	-2.946	0.04	4.014	-123.68	0.620
Bawku W	UEast	773	1202	179.406	-4.564	0.073	10.252	-103.34	0.897
Berekum	BAhafo	547	822	105.337	7.631	-0.033	-31.521	-44.348	0.710
Bia	Western	486	740	-29.526	1.465	0.007	-12.198	3.083	0.779
BibianiAB	Western	578	712	-36.136	6.272	-0.032	-3.329	-11.071	0.444

BirimN	Eastern	721	699	83.403	1.256	-0.009	-12.399	-8.945	0.282
BirimS	Eastern	715	647	129.706	-0.36	0.016	-10.36	-18.364	0.669
Bole	Northern	557	996	433.26	-6.676	0.067	-23.301	-79.243	0.618
BolgaM	UEast	734	1190	600.736	-9.234	0.097	-13.46	-222.36	0.791
Bongo	UEast	739	1204	125.65	-0.825	0.022	4.73	-71.228	0.771
BosomtweK	Ashanti	668	722	224.303	-4.211	0.044	-12.39	-23.819	0.825
Builsa	UEast	688	1184	632.889	-11.25	0.091	7.424	-118.58	0.806
Bunkpru-Y	Northern	842	1162	-1329.4	36.69	-0.185	-71.55	-108.51	0.648
CapeCoast	Central	694	565	239.961	-3.581	0.021	-14.02	-21.896	0.906
C Gonja	Northern	669	969	254.687	-4.03	0.059	-43.235	-2.43	0.549
DangmeE	GAccra	902	639	89.428	1.398	-0.003	-2.335	2.559	0.545
DangmeW	GAccra	820	649	153.03	0.03	0.006	-26.15	-25.98	0.611
DayiS	Volta	865	734	352.258	-4.504	0.043	-39.343	-60.902	0.840
Dormaa	BAhafo	514	803	181.59	2.068	0.001	-20.069	-27.449	0.577
East Gonja	Northern	772	944	162.12	-1.515	0.018	-2.206	-25.797	0.483
East Akim	Eastern	770	680	116.728	2.047	-0.01	-11.471	-0.894	0.324
East Mamp	Northern	779	1163	413.591	-3.777	0.033	-15.974	-105.54	0.496
Ejisu Juaben	Ashanti	668	742	161.682	-4.073	0.061	-33.649	-13.904	0.901
Ejura Sekye	Ashanti	682	814	158.127	-0.91	0.012	-19.718	-30.684	0.514
Fanteakwa	Eastern	790	705	164.034	-1.029	0.013	-13.009	-6.82	0.388
Ga East	GAccra	809	632	67.256	2.658	-0.009	-18.536	-20.908	0.662
Ga WestM	GAccra	799	630	173.631	-2.654	0.02	-14.806	-3.028	0.749
Garu Temp	UEast	808	1198	1894.53	-38.28	0.217	-12.218	-102.42	0.885
Gomoa	Central	751	585	62.581	-0.155	0.007	-13.267	0.783	0.747
Gushiegu	Northern	804	1095	143.962	-0.618	0.011	-4.343	-60.674	0.670
HoM	Volta	883	729	94.583	0.462	0.005	-20.171	-29.239	0.654
Hohoe	Volta	883	790	-558.22	14.885	-0.067	-24.404	-35.95	0.560
JamanN	BAhafo	534	877	-737.62	21.24	-0.088	-27.908	-35.625	0.743
JamanS	BAhafo	525	850	35.023	13.902	-0.058	-48.758	-51.957	0.756
Jasikan	Volta	883	818	486.47	-9.677	0.07	-37.391	-20.444	0.732
Jirapa-L	UWest	535	1162	374.594	-2.276	0.018	-54.567	-83.985	0.613
Jomoro	Western	508	560	304.57	-4.174	0.027	-16.78	-12.82	0.297
Juabeso	Western	520	700	319.916	-5.438	0.052	-18.755	-15.177	0.737
Kadjebi	Volta	885	832	436.987	-10.32	0.088	-49.799	-45.607	0.870
Karaga	Northern	781	1095	62.519	1.583	-0.007	-10.994	-54.156	0.666
Kasena-N	UEast	709	1211	214.574	-3.369	0.047	-3.648	-87.109	0.839
Keta	Volta	940	652	349.373	-5.428	0.042	-24.962	-20.544	0.651
Ketu	Volta	829	863	-55.039	2.995	-0.01	-33.606	-8.748	0.695
KintampoN	BAhafo	640	889	113.058	0.72	0.012	-17.129	-14.696	0.879
KintampoS	BAhafo	638	875	-534.03	13.621	-0.054	-19.129	-17.79	0.843
KEEA	Central	676	563	116.973	0.997	0	-24.982	-4.484	0.503
Kpandu	Volta	832	773	101.592	2.153	0.007	-28.66	-49.562	0.755
KrachiE	Volta	851	888	313.538	-5.799	0.04	-13.459	-33.061	0.742
Krachi/W	Volta	824	861	390.092	-7.275	0.052	-15.289	-55.083	0.801
KumasiMA	Ashanti	652	740	137.144	1.231	-0.002	-8.362	-7.384	0.628
Kwabre	Ashanti	658	749	86.044	3.622	-0.019	-18.264	-13.562	0.286

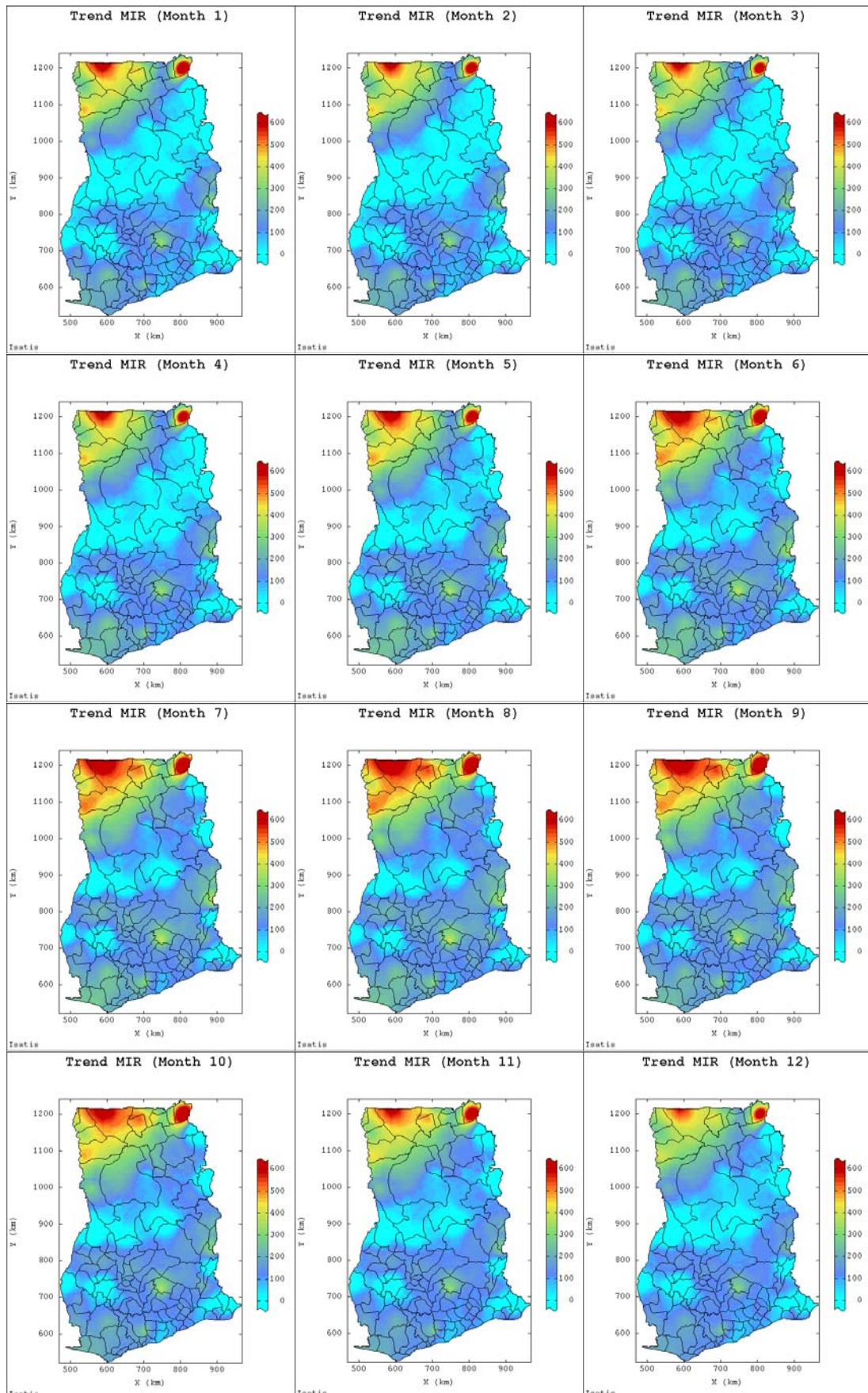
Kwaebirem	Eastern	739	673	123.941	0.6	0.016	-20.707	-10.763	0.824
KwahuS	Eastern	748	728	339.798	-0.918	0.009	-19.487	-51.488	0.199
KwahuW	Eastern	747	722	674.778	-12.71	0.091	-36.32	-36.145	0.805
Lawra	UWest	514	1174	248.795	-1.231	0.018	-23.564	-78.102	0.628
ManyaK	Eastern	814	713	66.415	1.16	0.011	-18.157	-17.264	0.854
Mfantsiman	Central	715	575	35.417	1.815	-0.002	-44.461	-7.218	0.696
MpohorEW	Western	648	567	110.96	-0.924	0.009	-8.507	1.944	0.516
New Juaben	Eastern	803	672	260.693	-2.738	0.054	-49.174	-28.751	0.792
Nadowli	UWest	539	1145	225.323	-0.413	0.013	-38.226	-64.181	0.681
NanumbaN	Northern	832	978	196.314	-0.94	0.014	-17.737	-58.389	0.560
NanumbaS	Northern	829	955	63.207	1.619	-0.01	-11.77	-40.377	0.745
Nkoranza	BAhafo	643	835	82.782	2.034	0.002	-17.46	-22.527	0.705
Nkwanta	Volta	882	912	321.916	-6.66	0.045	-6.08	-17.057	0.885
North T	Volta	879	671	-373.94	10.04	-0.035	-15.24	-7.674	0.780
Nzema E	Western	572	551	255.847	-0.678	0.02	-47.5	-18.611	0.743
Obuasi M	Ashanti	645	685	172.329	6.621	-0.046	-29.917	1.526	0.386
Offinso	Ashanti	631	789	167.443	-1.584	0.024	-13.061	-22.847	0.702
Pru	BAhafo	757	907	-547.51	15.71	-0.081	-15.35	-52.217	0.565
Saboba-C	Northern	860	1073	170.209	-0.02	0.013	-11.804	-69.84	0.660
Savelugu-N	Northern	738	1062	243.328	-2.552	0.026	-5.794	-72.218	0.485
Sawla TK	Northern	565	1022	75.668	0.312	0.003	-14.479	-20.344	0.511
SefwiWi	Western	557	685	19.566	1.006	0.013	-7.027	-13.564	0.912
Sekyere E	Ashanti	685	775	153.871	-2.915	0.037	-4.067	-12.367	0.830
SekyereW	Ashanti	677	778	272.594	-3.748	0.035	-18.142	-34.584	0.589
Sene	BAhafo	803	854	151.508	-1.542	0.024	-4.592	-36.963	0.834
Shama AE	Western	654	554	286.055	-4.472	0.041	-6.075	-12.01	0.718
Sissala E	UWest	613	1200	601.217	-1.954	0.015	-30.842	-78.459	0.527
Sissala W	UWest	587	1211	989.445	-19.32	0.112	-46.7	-66.354	0.713
South T	Volta	894	663	663.642	-12.89	0.079	-16.557	-9.568	0.793
Suhum KC	Eastern	782	667	74.365	1.406	0	-3.343	-3.355	0.639
Sunyani M	BAhafo	575	809	230.005	0.753	0.01	-48.144	-32.193	0.654
Tain	BAhafo	568	874	-438.06	10.786	-0.026	-48.887	-40.104	0.735
Talensi N	UEast	740	1181	14.47	2.316	0.001	-8.271	-109.55	0.796
Tamale M	Northern	737	1038	168.717	-0.37	0.013	-28.65	-68.351	0.741
Tano N	BAhafo	596	794	240.985	0.244	0.005	-17.768	-15.934	0.498
Tano S	BAhafo	608	783	82.834	4.162	-0.015	-17.024	-14.546	0.491
Techiman	BAhafo	617	836	128.872	1.711	-0.001	-20.108	-19.131	0.827
Tema M	GAccra	832	624	105.775	-0.713	0.009	-24.647	-6.242	0.617
Tolon K	Northern	712	1040	-163.84	5.652	-0.028	-3.908	-30.874	0.573
Twifo HLD	Central	661	619	172.535	-0.463	0.009	-24.391	-12.326	0.466
UpperD	Central	635	656	123.683	1.252	0.002	-20.763	-4.509	0.785
Wa CM	UWest	556	1111	489.012	-9.073	0.068	-43.927	-79.889	0.699
Wa E	UWest	615	1135	543.133	-8.877	0.048	-21.939	-49.991	0.750
Wa W	UWest	536	1084	632.886	-10.23	0.057	-21.328	-36.453	0.719
Wassa AE	Western	601	638	409.913	-9.051	0.069	-19.728	-6.067	0.854
Wassa AW	Western	563	641	119.667	-1.015	0.03	-22.246	2.557	0.838

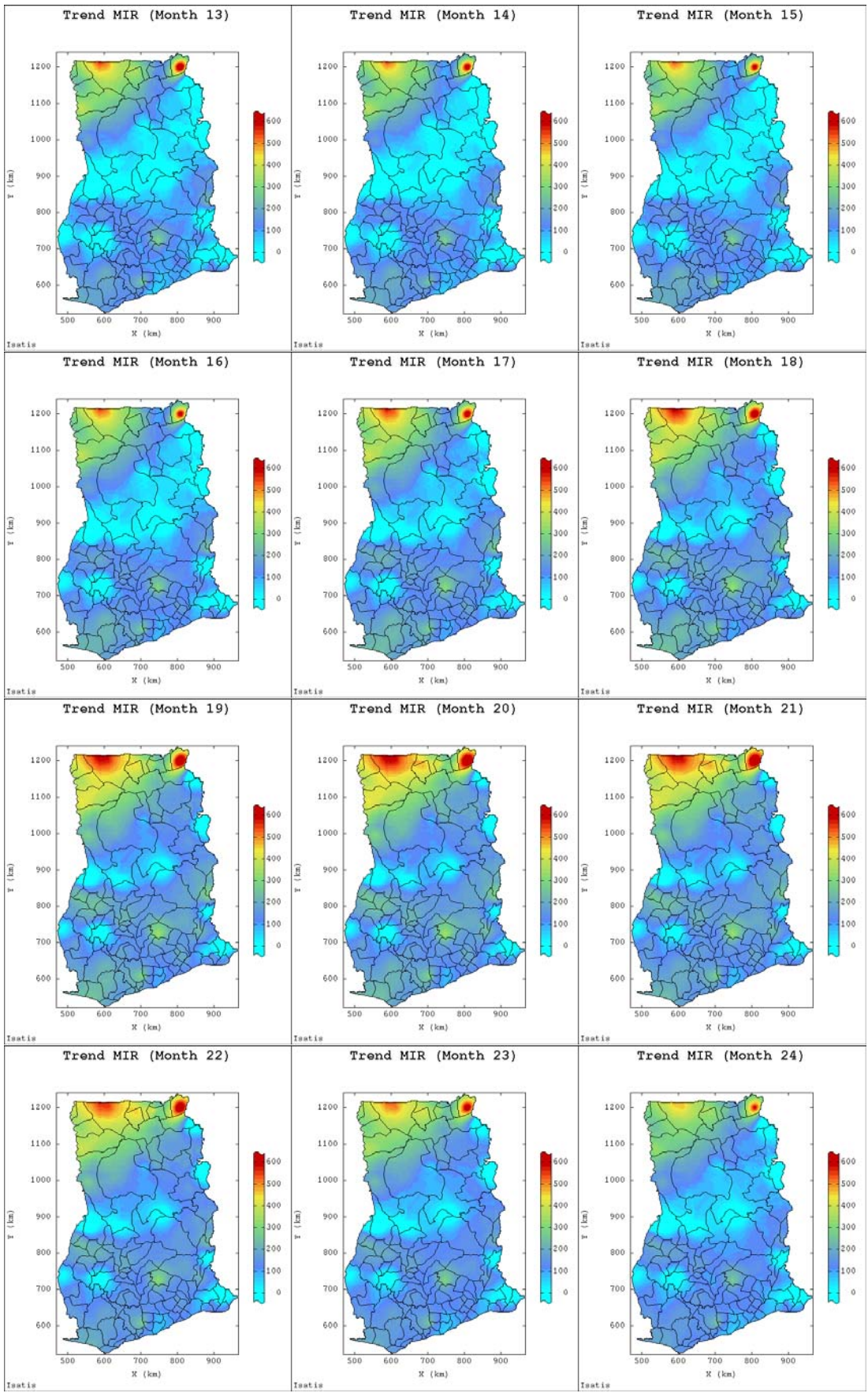
Wassa W	Western	611	585	256.24	-2.865	0.031	-43.19	3.508	0.521
Wenchi M	BAhafo	599	854	159.756	1.144	-0.002	-27.876	-17.97	0.611
West Akim	Eastern	758	647	104.364	0.76	0.002	-8.258	-17.382	0.597
West Gonja	Northern	630	1002	219.24	-2.052	0.032	-28.454	-70.23	0.612
West Mamp	Northern	740	1141	161.64	-1.524	0.012	-24.164	-56.281	0.474
YendiM	Northern	827	1042	173.837	0.586	0.008	-29.267	-82.193	0.655
YiloK	Eastern	830	674	47.326	0.276	0.014	-18.849	-7.124	0.864
Zabzugu-T	Northern	873	1026	-822.14	21.267	-0.102	-41.173	-93.087	0.573

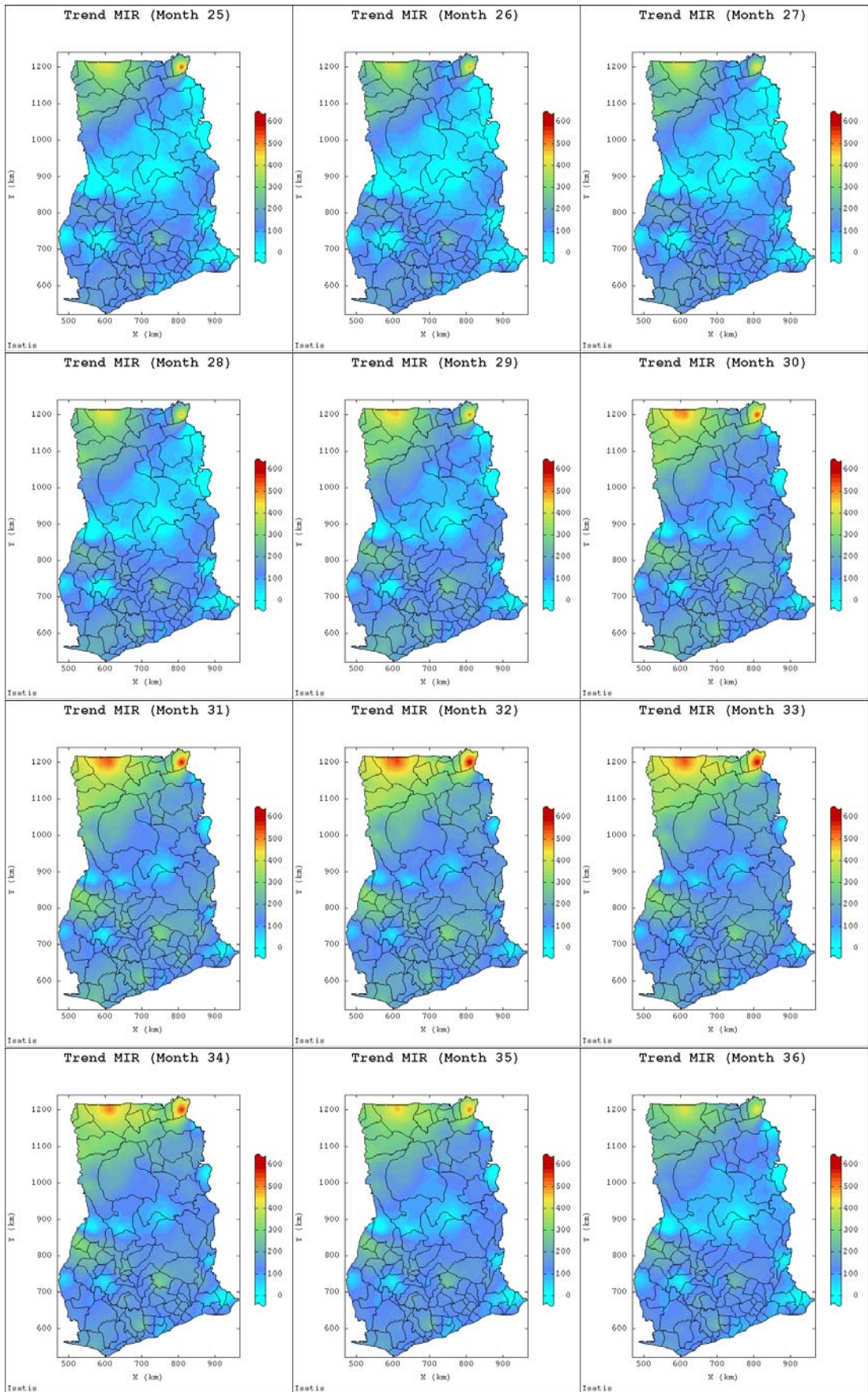
Table D-1.2: Trend model parameters (coefficients and coefficient of determination) of the morbidity incidence rates in the Brong Ahafo Region (BAR)

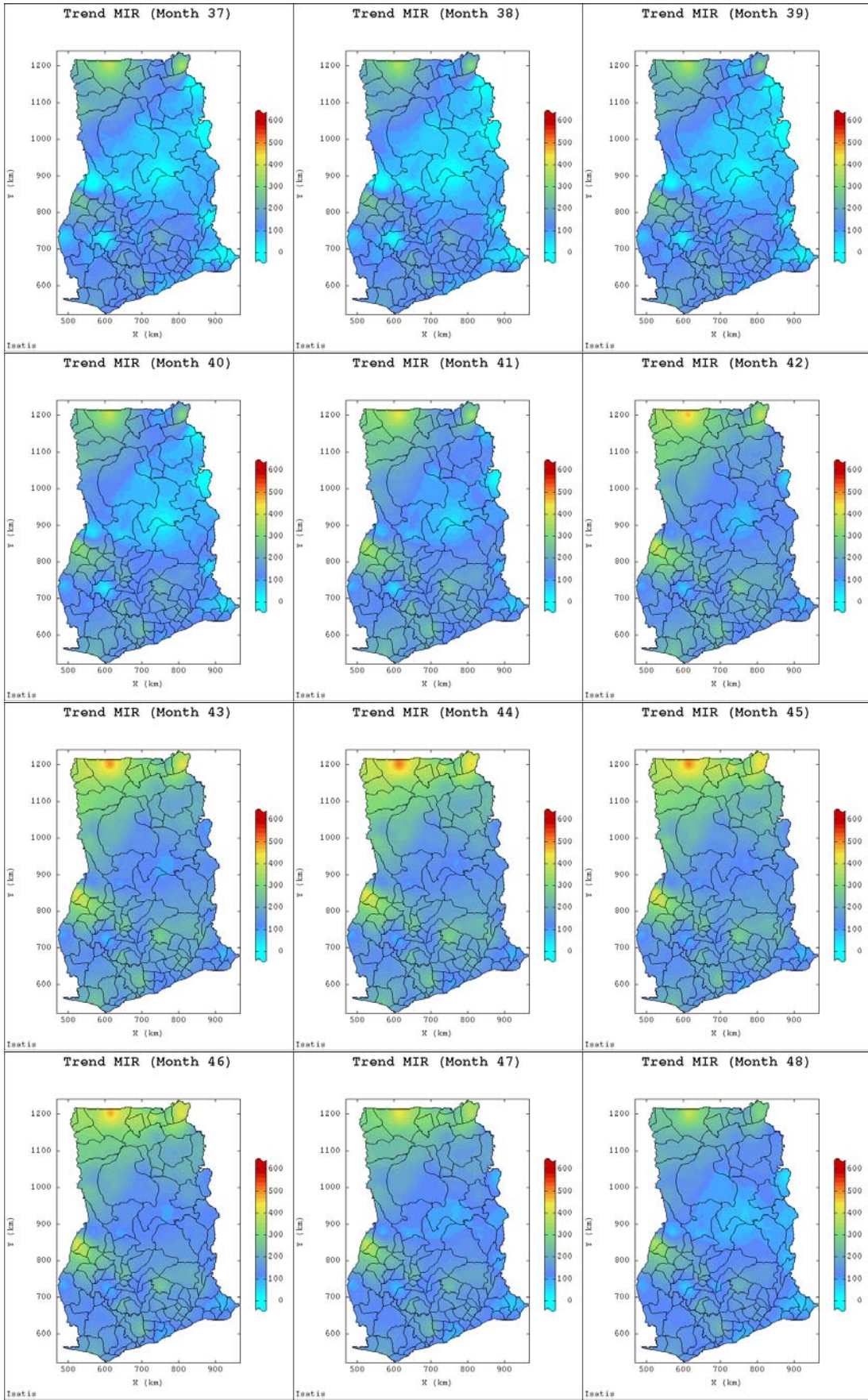
District	Easting	Northing	b0	b1	b2	b3	b4	r2
AsunafoN	553	751	220.459	0.26267	0.00482	-19.1186	-23.2182	0.7263
AsunafoS	562	739	-532.583	12.16728	-0.04172	-17.7041	-25.3032	0.598
Asutifi	569	770	170.516	0.05211	0.02198	-37.3104	-36.3335	0.8352
Atebubu-A	722	856	129.385	-1.68734	0.02112	-12.9405	-37.0225	0.8448
Berekum	547	822	87.331	4.86291	-0.00953	-34.0656	-38.5031	0.7674
Dormaa	514	803	121.136	2.53462	-0.00275	-23.9288	-27.5754	0.6658
JamanN	534	877	-1603.84	30.98441	-0.11214	-24.3842	-42.5845	0.6984
JamanS	525	850	-25.965	10.07292	-0.02703	-47.6843	-51.2202	0.7861
KintampoN	640	889	122.832	-0.73863	0.01872	-20.1328	-17.1375	0.8939
KintampoS	638	875	-627.332	11.5834	-0.03424	-19.9187	-24.3242	0.8184
Nkoranza	643	835	68.23	1.31974	0.00444	-18.7974	-21.2822	0.7755
Pru	757	907	-394.78	9.31415	-0.03658	-13.932	-50.5875	0.4458
Sene	803	854	115.05	-0.50877	0.0119	-5.55188	-35.7083	0.8248
SunyaniM	575	809	235.316	-0.76951	0.01833	-44.3107	-31.3293	0.7673
Tain	568	874	-475.129	7.83097	-0.00784	-53.1852	-43.3579	0.805
TanoN	596	794	267.663	-1.00944	0.01171	-16.7548	-14.7742	0.6474
TanoS	608	783	150.894	1.7267	-0.00133	-23.5633	-14.8137	0.5651
TechimanM	617	836	113.979	0.91517	0.00445	-24.29	-16.3283	0.8508
WenchiM	599	854	126.325	1.32379	-0.00212	-23.3759	-17.5812	0.6846

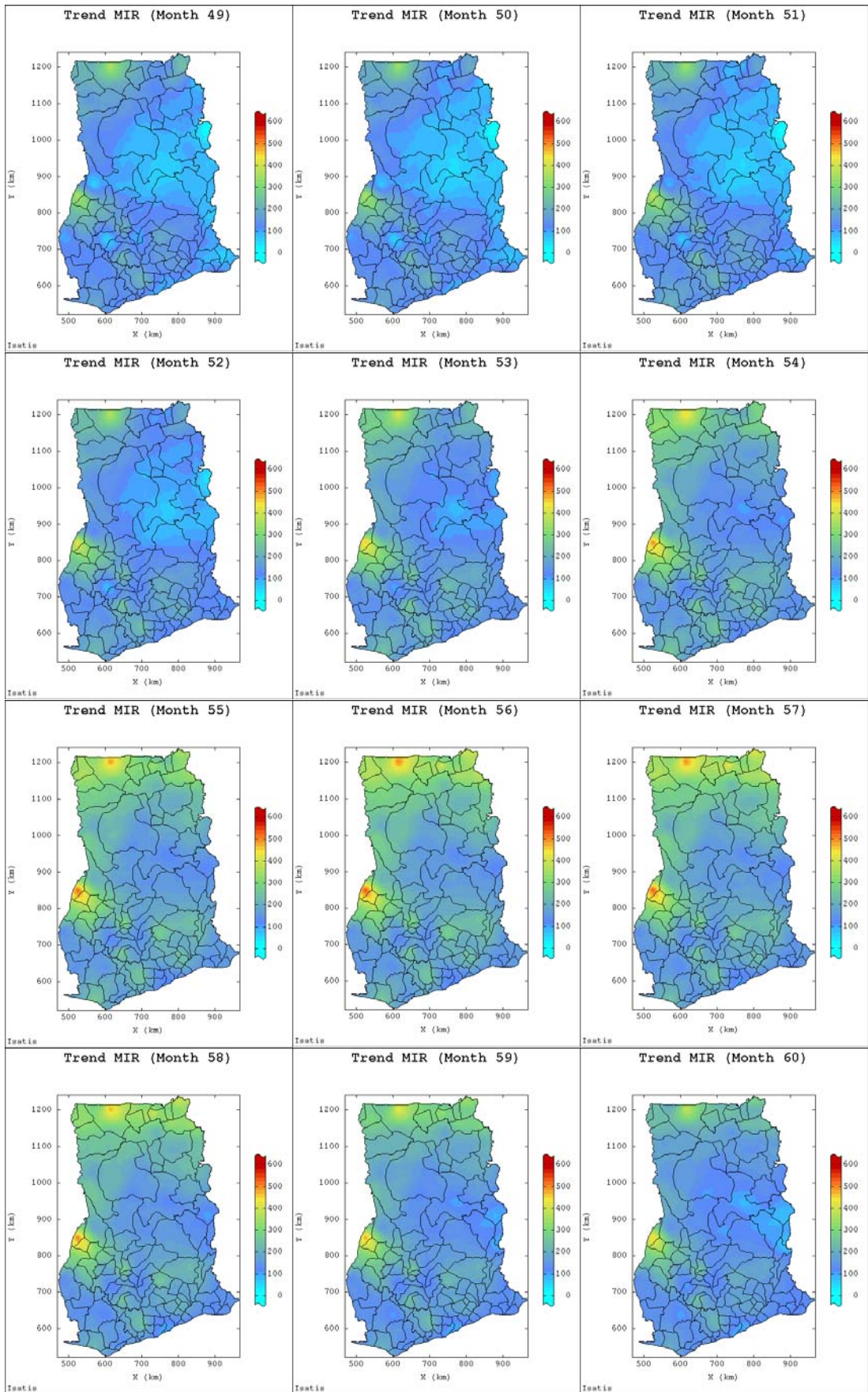
D-2: Spatial Maps of Trend Surfaces of MIR for Month 1-132

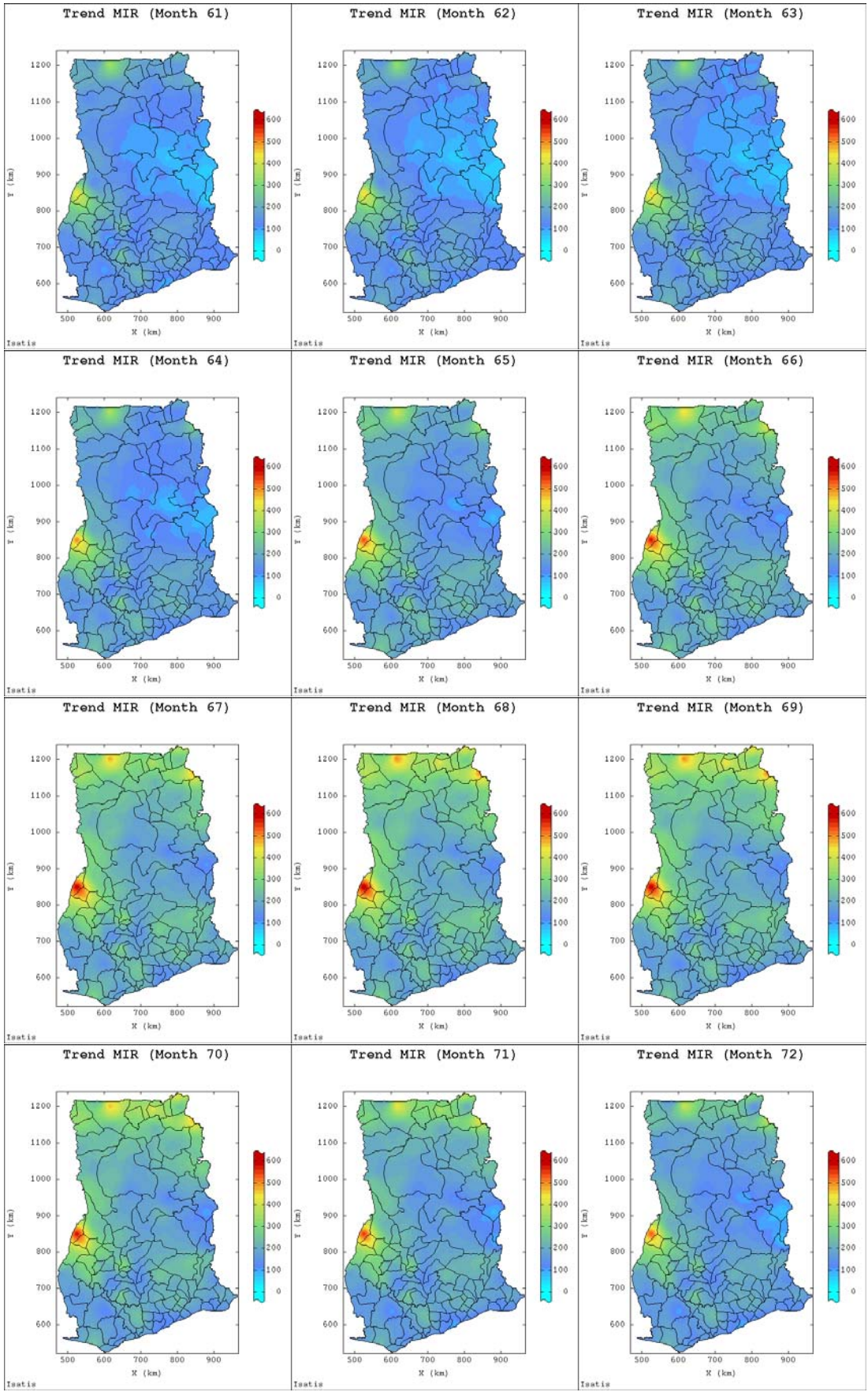


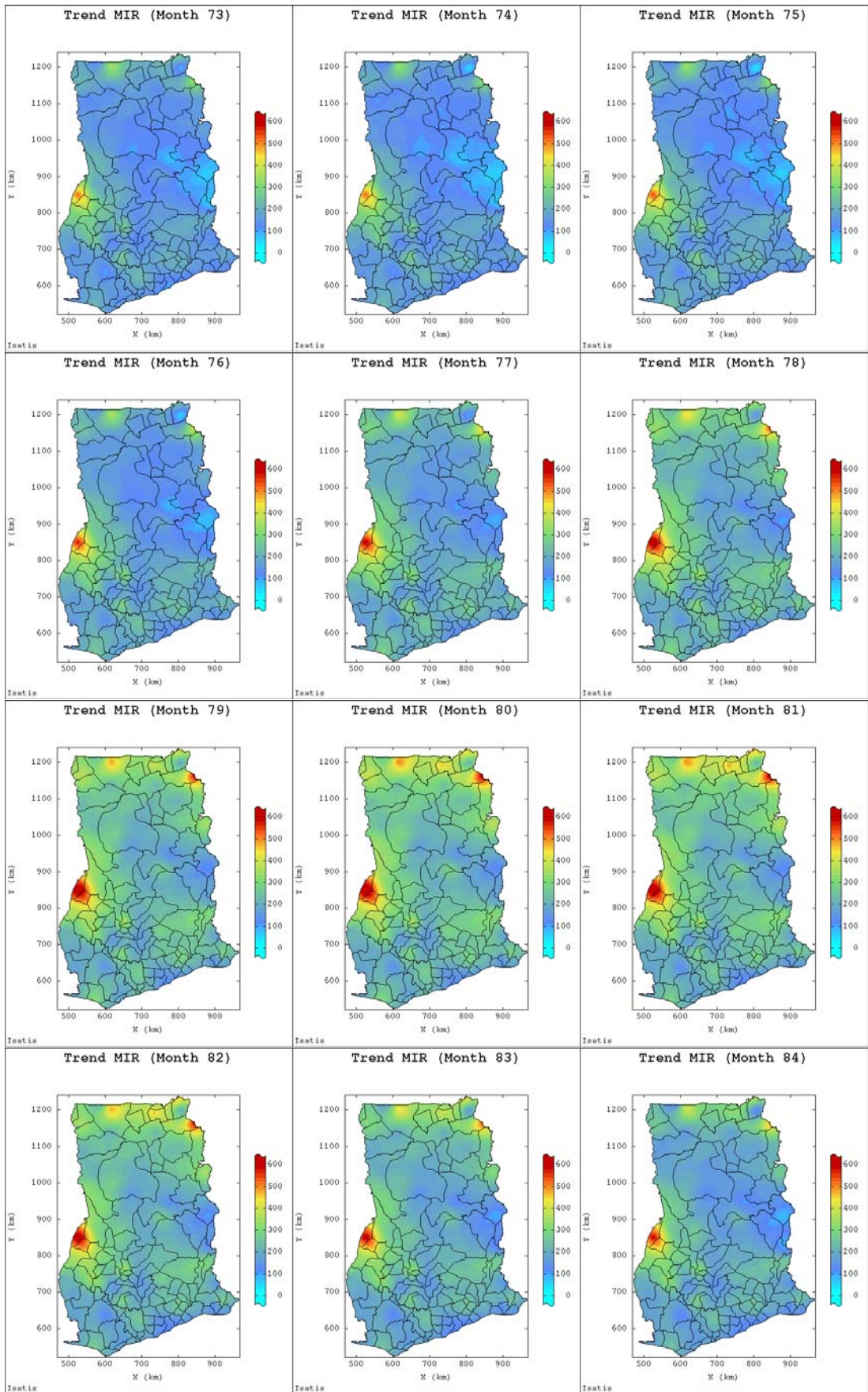


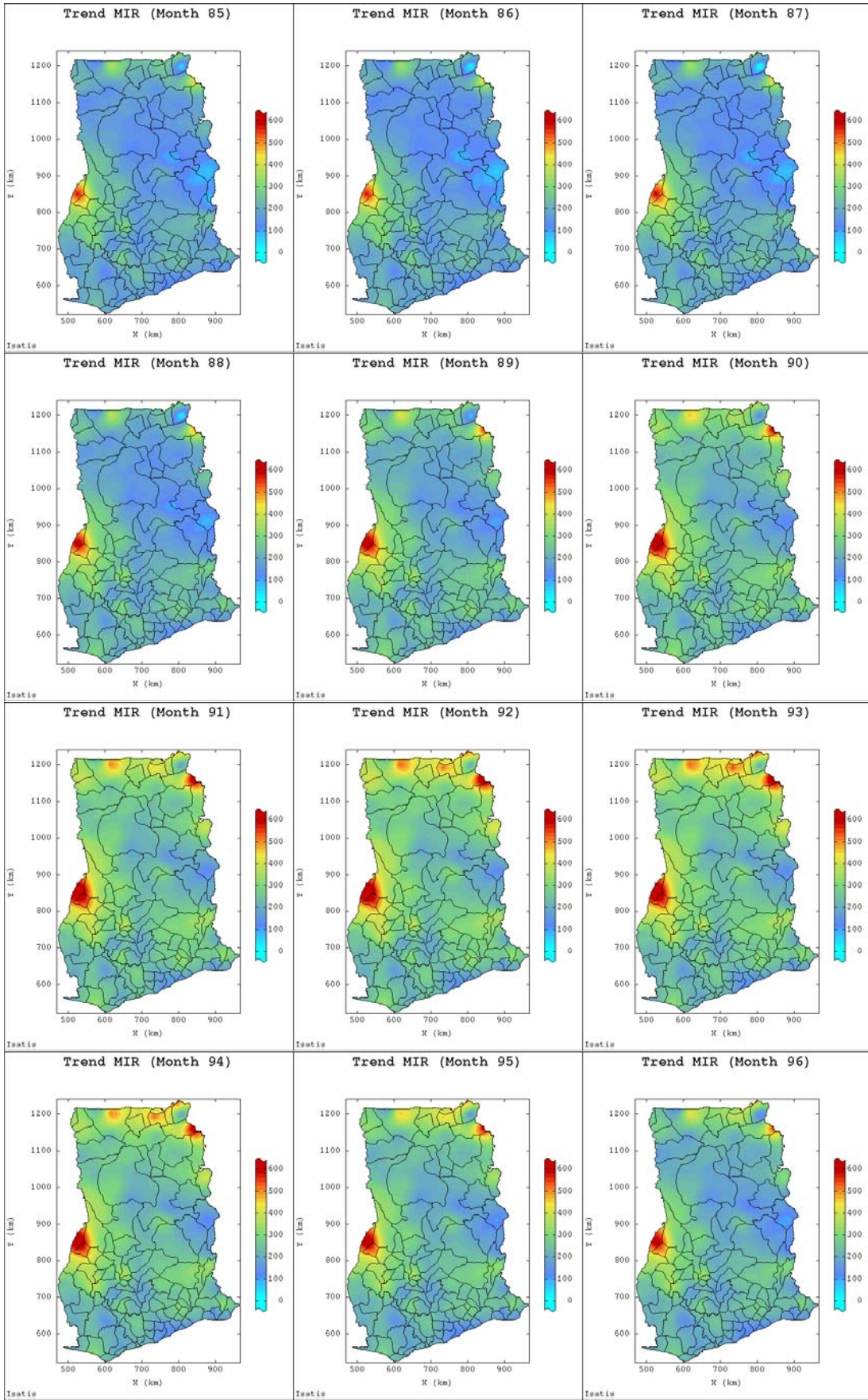


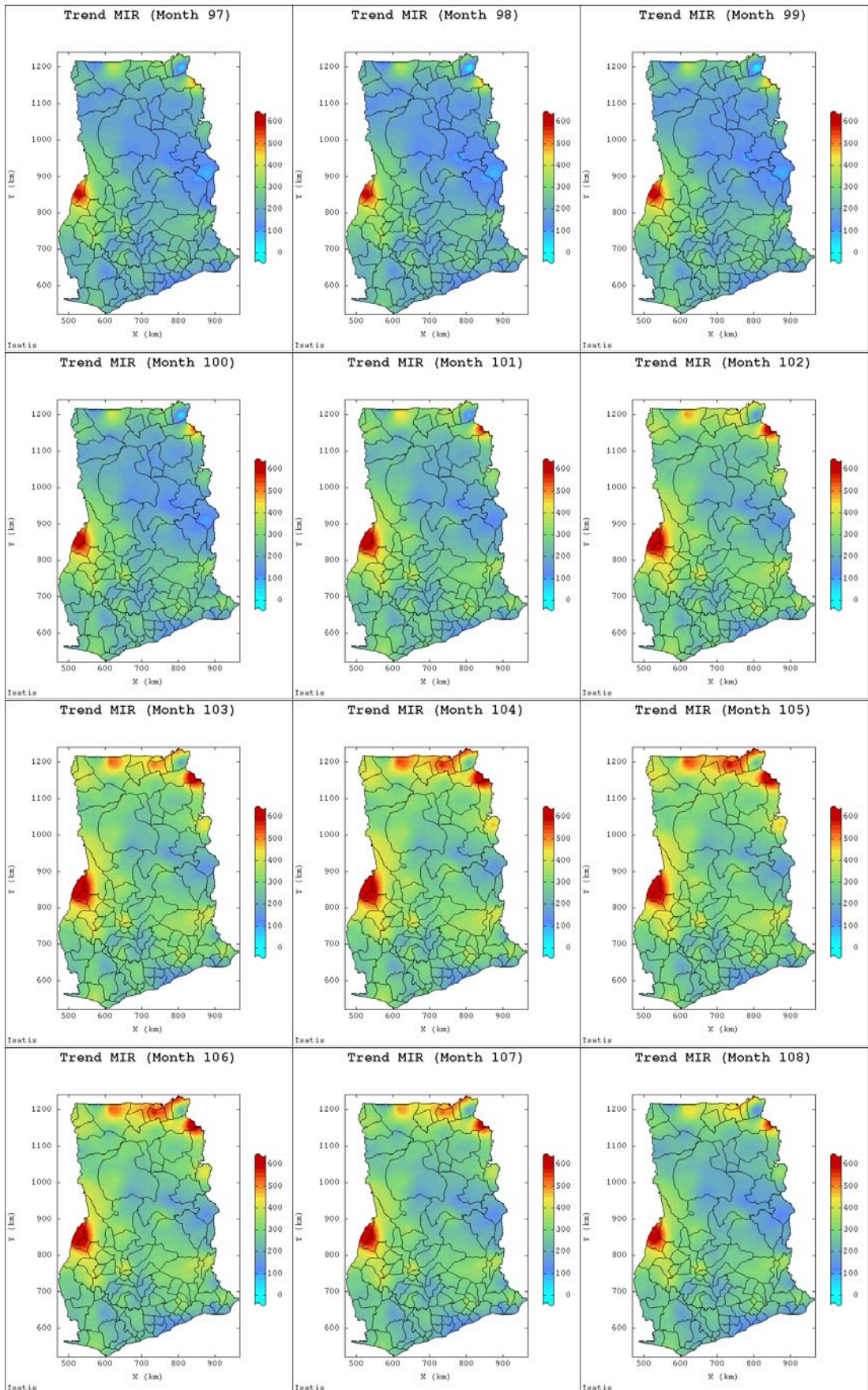


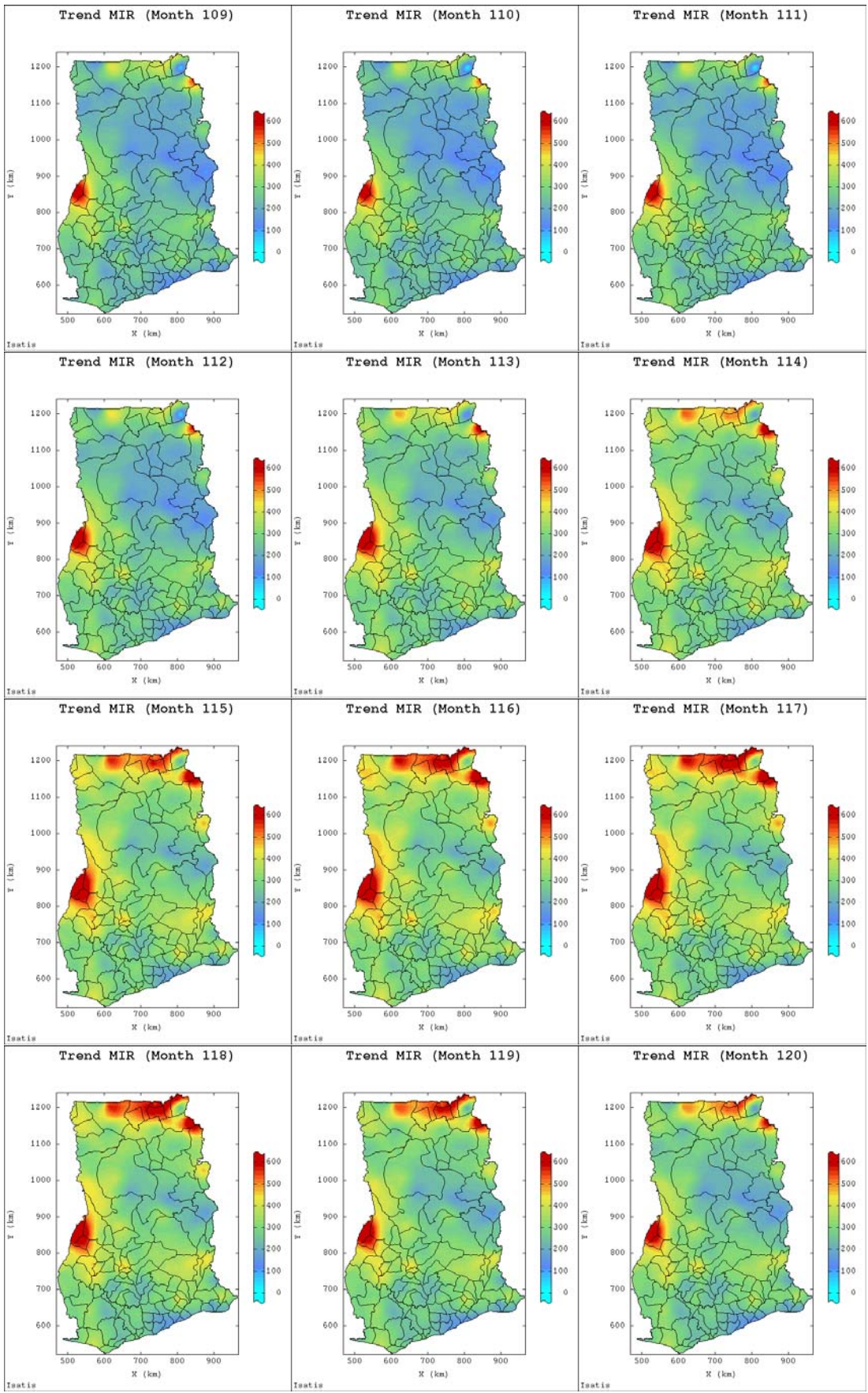


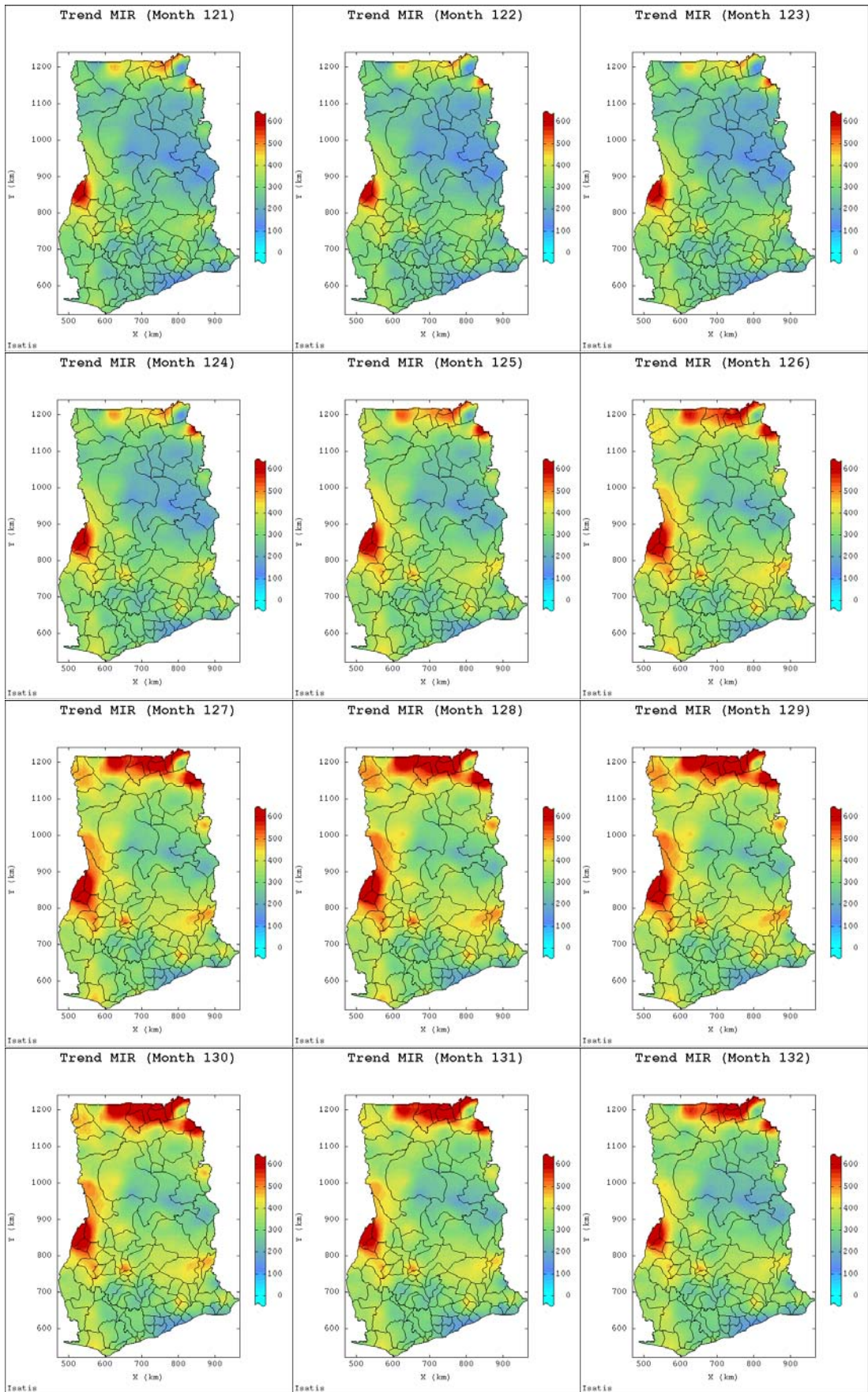












Appendix E: Space-time Prediction of the Morbidity Incidence Rates (MIR) at National Level

E-1: Space-time Semivariogram Models of MIR

Table E-1.1: Calculation parameters for the space-time experimental semivariograms of log-transformed morbidity incidence rates at district locations for the whole of Ghana (nationai), vegetation zones (northern, forest and coastal) and Brong Ahafo Region (BAR)

Study	Spatial spacing (km)		Temporal spacing (months)	
	Lag	No. of lags	Lag	No. of Lags
	h_s	n_s	h_t	n_t
National	30	15	1	70
BAR	35	8	1	80
Northern Zone	40	8	1	70
Forest Zone	30	10	1	70
Coastal Zone	25	10	1	70

Table E-1.2: Space-time semivariogram model parameters of log-transformed morbidity incidence rates compared with the untransformed malaria incidence rates data

Data	Model $\gamma(h)$	Sill c_s / c_t	Spatial range r_s (km)	Temporal range r_t (months)	Relative Nugget
LogMIR	<i>nugget</i>	0.025	-	-	0.120 (0.110)
	<i>spherical</i>	0.112	35	85	
	<i>exponential</i>	0.071	250	300	
	<i>expcosine</i>	0.020	1000	400	
MIR	<i>nugget</i>	1500	-	-	0.097 (0.088)
	<i>spherical</i>	7500	30	85	
	<i>exponential</i>	6500	300	250	
	<i>expcosine</i>	1600	1000	500	

Note: In parentheses are relative nugget effects in the temporal domain.

Table E-1.3: Parameters of the marginal semivariograms and product-sum semivarigram models of the observed malaria incidence rates for the national study

Study	Model	Spatial		Temporal		Product-sum	
		Sill (RN)	Range	Sill (RN)	Range	Global Sill	k
National	<i>nugget</i>	5000	-	5000	-	28000 (4.878 × 10 ⁻⁵)	2.471 × 10 ⁻⁵ (4.878 × 10 ⁻⁵)
	<i>spherical</i>	-	-	15500	100		
	<i>exponential</i>	10200	120	-	-		
	<i>expcosine</i>	-	-	-	-		

In parentheses are the relative nugget (RN) effects of marginal semivariograms and maximum k limit values for the product-sum model.

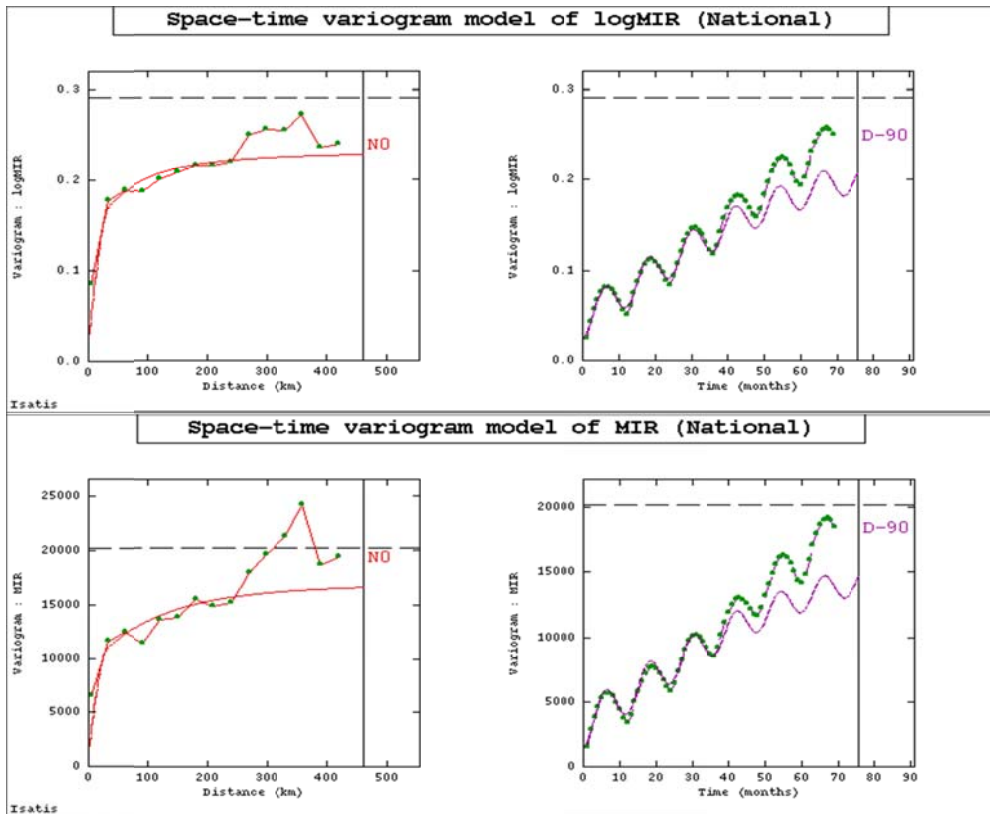


Figure E-1.1: Space-time semivariogram model of the log-transformed malaria incidence rates (top) compared with the observed incidence data model (bottom)

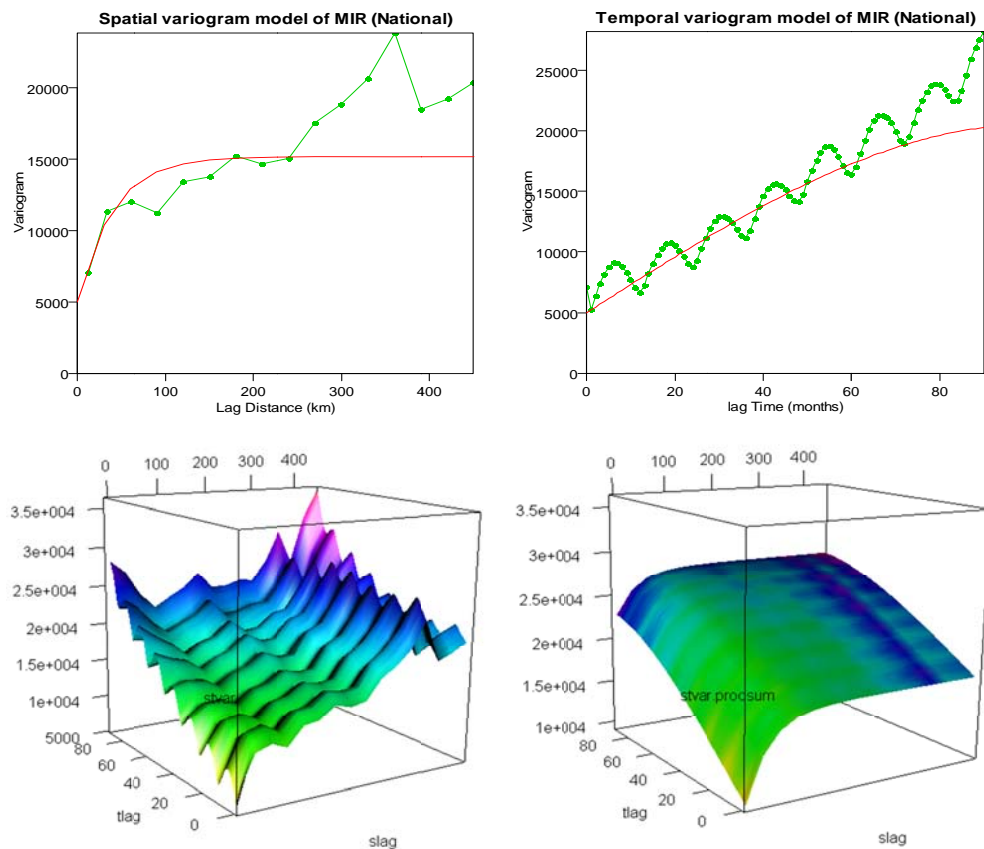


Figure E-1.2: Marginal spatial and temporal semivariograms models (left) and space-time experimental semivariogram and its product-sum model of (right) of the observed MIR for the national study.

E-2: LMC of MIR with Monthly Climatic Covariates

Table E-2.1: Parameters for linear coregionalisation model of minimum temperature with elevation for the months in 2010

Month	Variable	$nug(h)$	$sph_1(h/100-180)$		$sph_2(h/170-180)$	
		b_{ij}^0	b_{ij}^1	r_{ij}^1	b_{ij}^2	r_{ij}^2
January	Min Temp	1.35	0.55	120	2.05	170
	Elevation	2000	2500	120	4500	170
	MinT and Elevation	25	-25	120	-85	170
February	Min Temp	1.75	0.50	110	1.65	170
	Elevation	2000	2500	110	4500	170
	MinT and Elevation	25	-35	110	-85	170
March	Min Temp	0.95	1.05	150	1.75	190
	Elevation	2200	2000	150	5800	190
	MinT and Elevation	25	-35	150	-100	190
April	Min Temp	0.95	1.70	120	1.15	180
	Elevation	2200	2300	120	5000	180
	MinT and Elevation	25	-35	120	-75	180
May	Min Temp	0.95	1.15	180	-	-
	Elevation	2200	7700	180	-	-
	MinT and Elevation	10	-105	180	-	-
June	Min Temp	0.85	1.55	150	0.45	180
	Elevation	2200	2200	150	5500	180
	MinT and Elevation	15	-55	150	-48	180
July	Min Temp	0.75	0.05	120	2.15	180
	Elevation	2200	2000	120	5200	180
	MinT and Elevation	10	-5	120	-105	180
August	Min Temp	0.85	2.10	170	-	-
	Elevation	2200	7500	170	-	-
	MinT and Elevation	20	-115	170	-	-
September	Min Temp	0.50	2.30	150	0.25	180
	Elevation	2200	2000	150	5500	180
	MinT and Elevation	10	-65	150	-35	180
October	Min Temp	0.85	2.20	170	-	-
	Elevation	2200	7500	170	-	-
	MinT and Elevation	15	-115	170	-	-
November	Min Temp	0.50	1.00	145	0.35	170
	Elevation	2200	2200	145	5700	170
	MinT and Elevation	15	-40	145	-40	170
December	Min Temp	1.00	2.00	180	-	-
	Elevation	2300	7850	180	-	-
	MinT and Elevation	10	-95	180	-	-

Table E-2.2: Parameters for linear coregionalisation model of malaria incidence rates with relative humidity (at 1500 hours) for the months in 2010

Month	Variable	$nug(h_0)$	$sph(h/180 - 200)$	
		b_{ij}^0	b_{ij}^1	r_{ij}^1
January	RH1500	35	160	185
	Elevation	2300	7800	185
	RH1500 and Elevation	235	-880	185
February	RH1500	105	150	200
	Elevation	2500	7950	200
	RH1500 and Elevation	375	-950	200
March	RH1500	75	95	200
	Elevation	2500	7900	200
	RH1500 and Elevation	250	-650	200
April	RH1500	25	45	195
	Elevation	2500	7780	195
	RH1500 and Elevation	200	-480	195
May	RH1500	7.50	40	200
	Elevation	2500	7900	200
	RH1500 and Elevation	100	-335	200
June	RH1500	5,50	23	190
	Elevation	2450	7700	190
	RH1500 and Elevation	90	-225	190
July	RH1500	5.0	23.5	190
	Elevation	2450	7750	190
	RH1500 and Elevation	50	-260	190
August	RH1500	3.0	28	185
	Elevation	2350	7750	185
	1500 and Elevation	60	-195	185
September	RH1500	11.5	15.5	190
	Elevation	2470	7750	190
	RH1500 and Elevation	110	-190	190
October	RH1500	11.5	24.5	180
	Elevation	2250	7755	180
	RH1500 and Elevation	80	-250	180
November	RH1500	14	55	200
	Elevation	2550	7800	200
	RH1500 and Elevation	100	-400	200
December	RH1500	10	100	195
	Elevation	2550	7680	195
	RH1500 and Elevation	140	-550	195

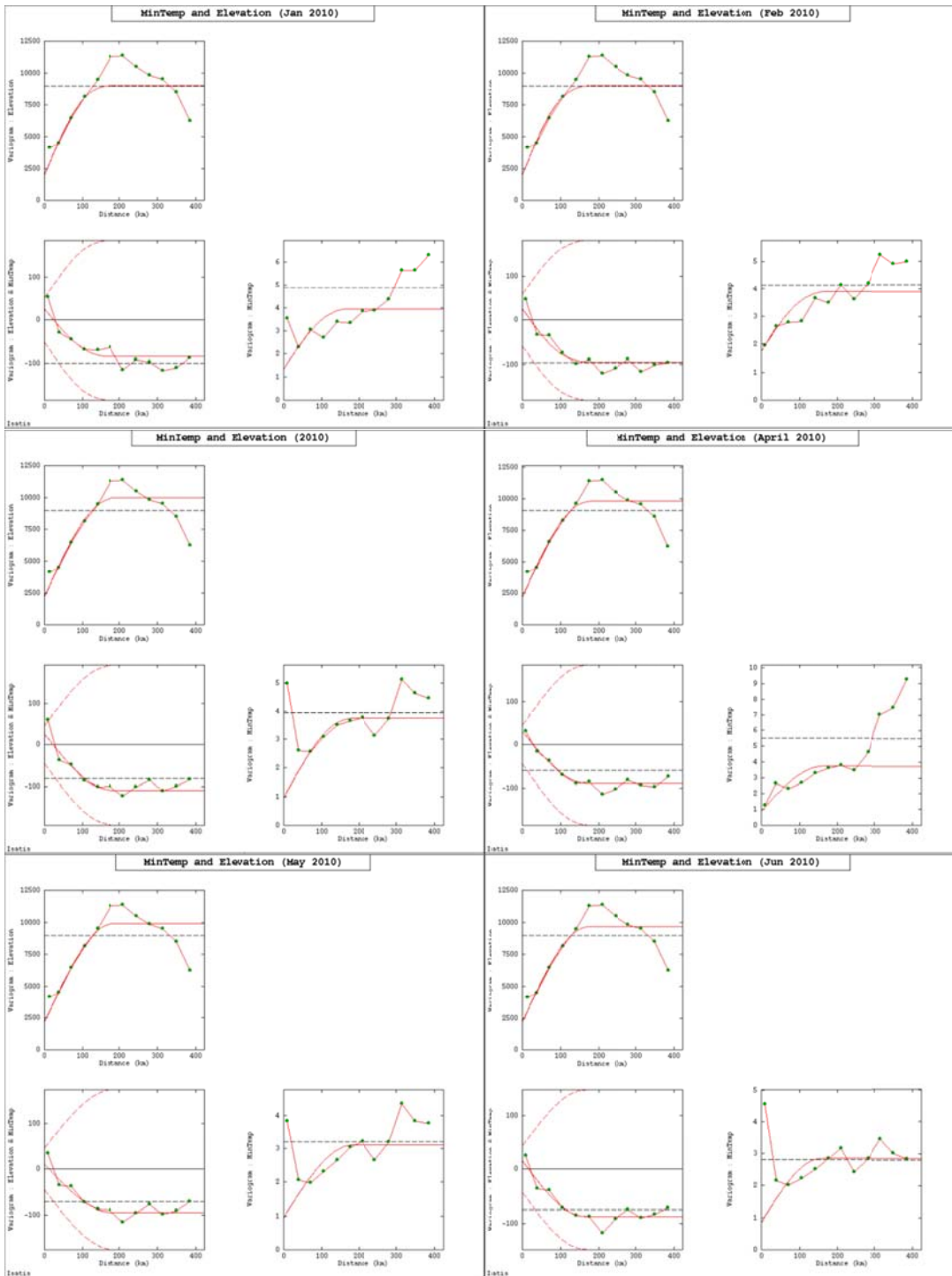


Figure E-2.1a: Linear coregionalisation model of elevation with minimum temperature for January – June 2010

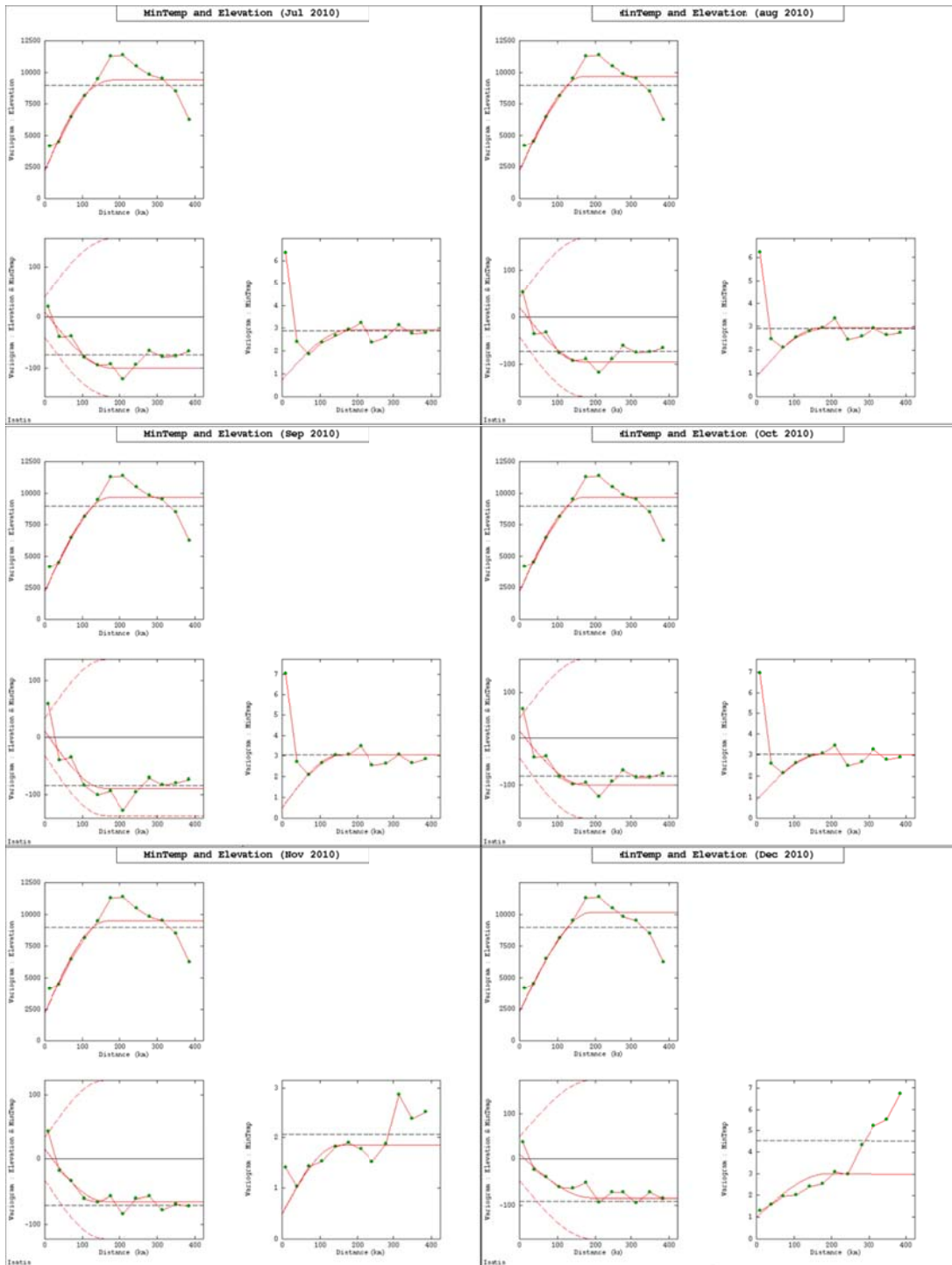


Figure E-2.1b: Linear coregionalisation model of elevation with minimum temperature for July – December 2010

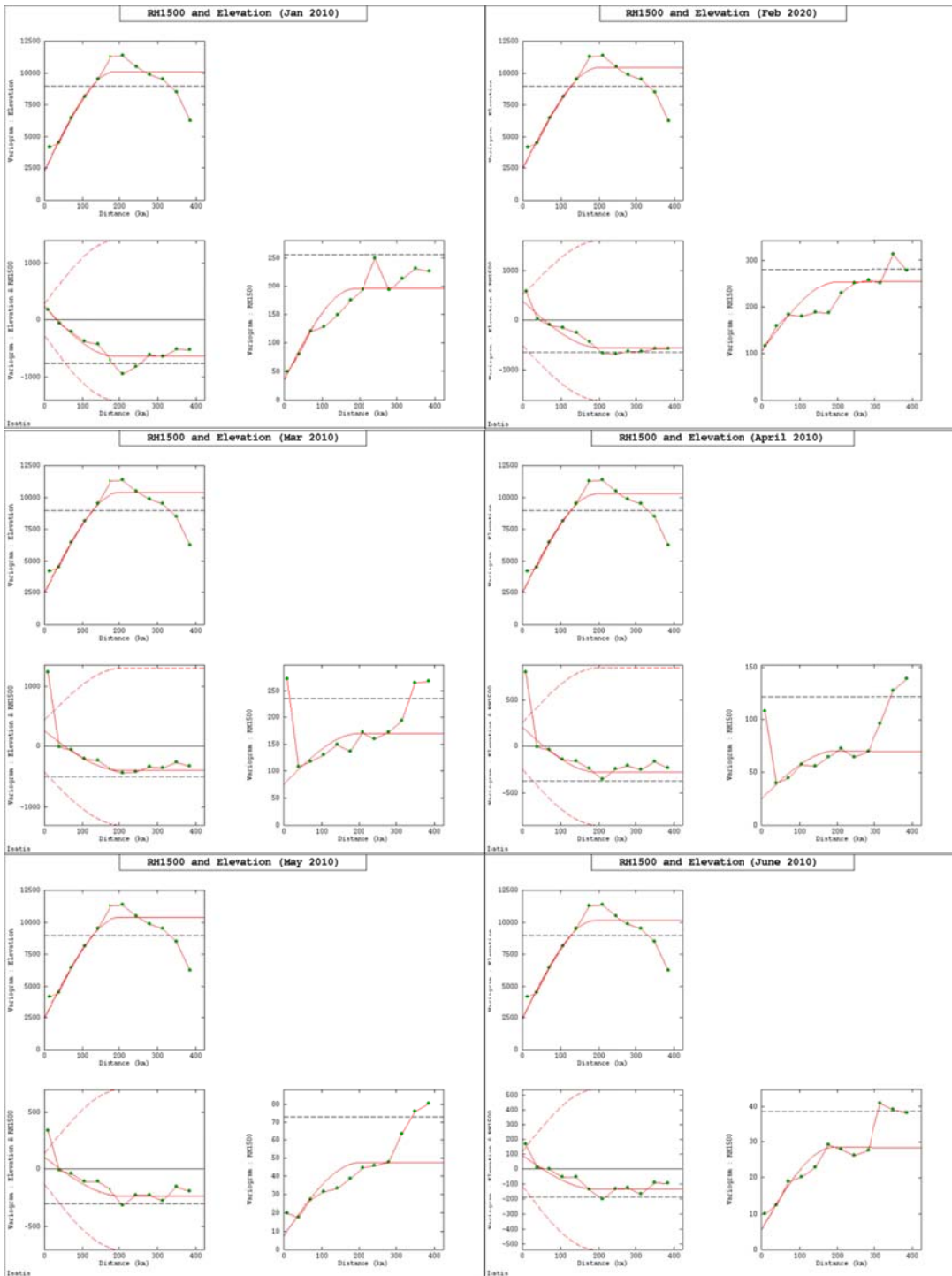


Figure E-2.2a: Linear coregionalisation model of elevation with relative humidity (at 1500 hours) for January –June 2010

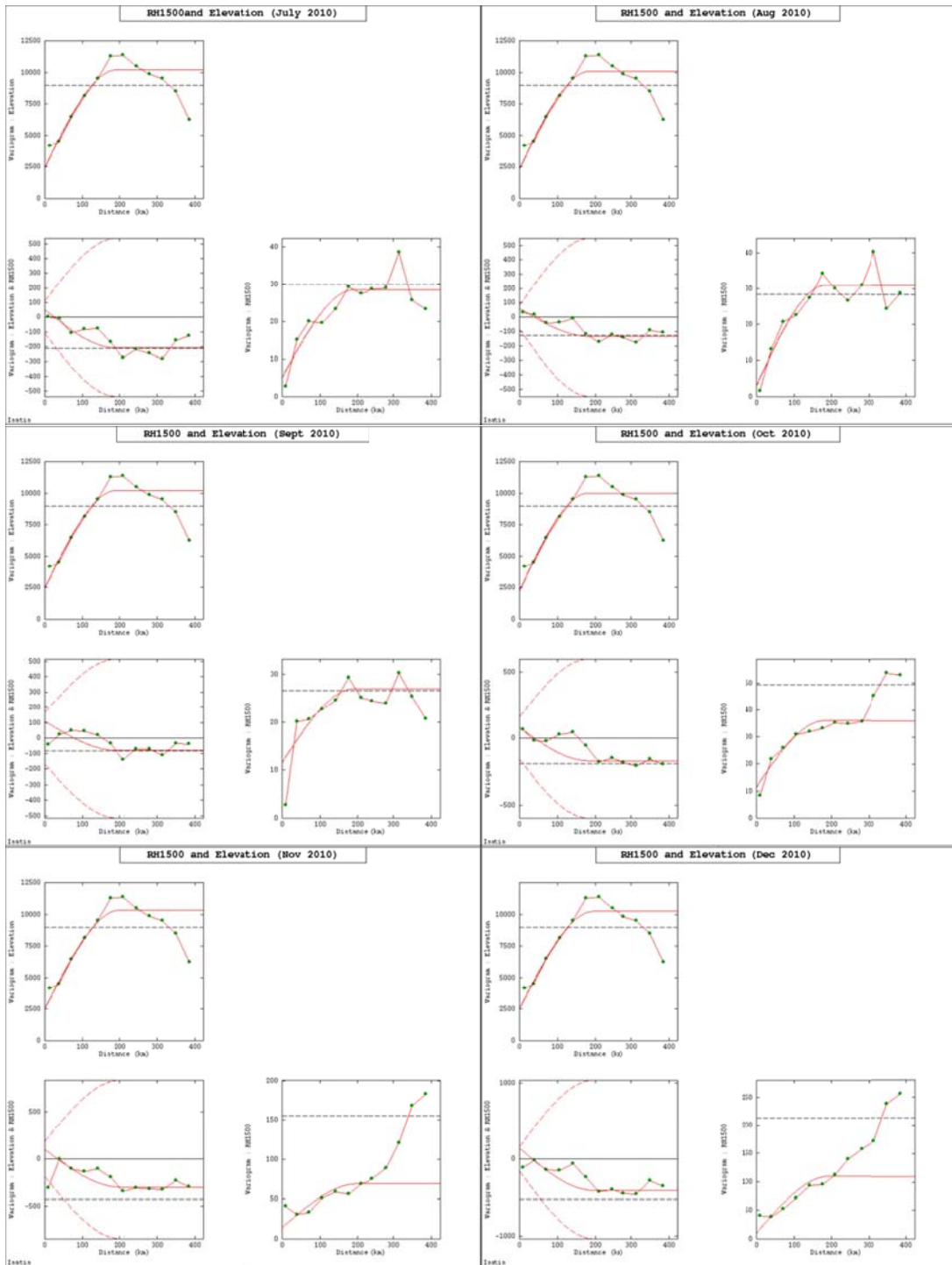


Figure E-2.2b: Linear coregionalisation model of elevation with relative humidity (at 1500 hours) for July –Dec 2010

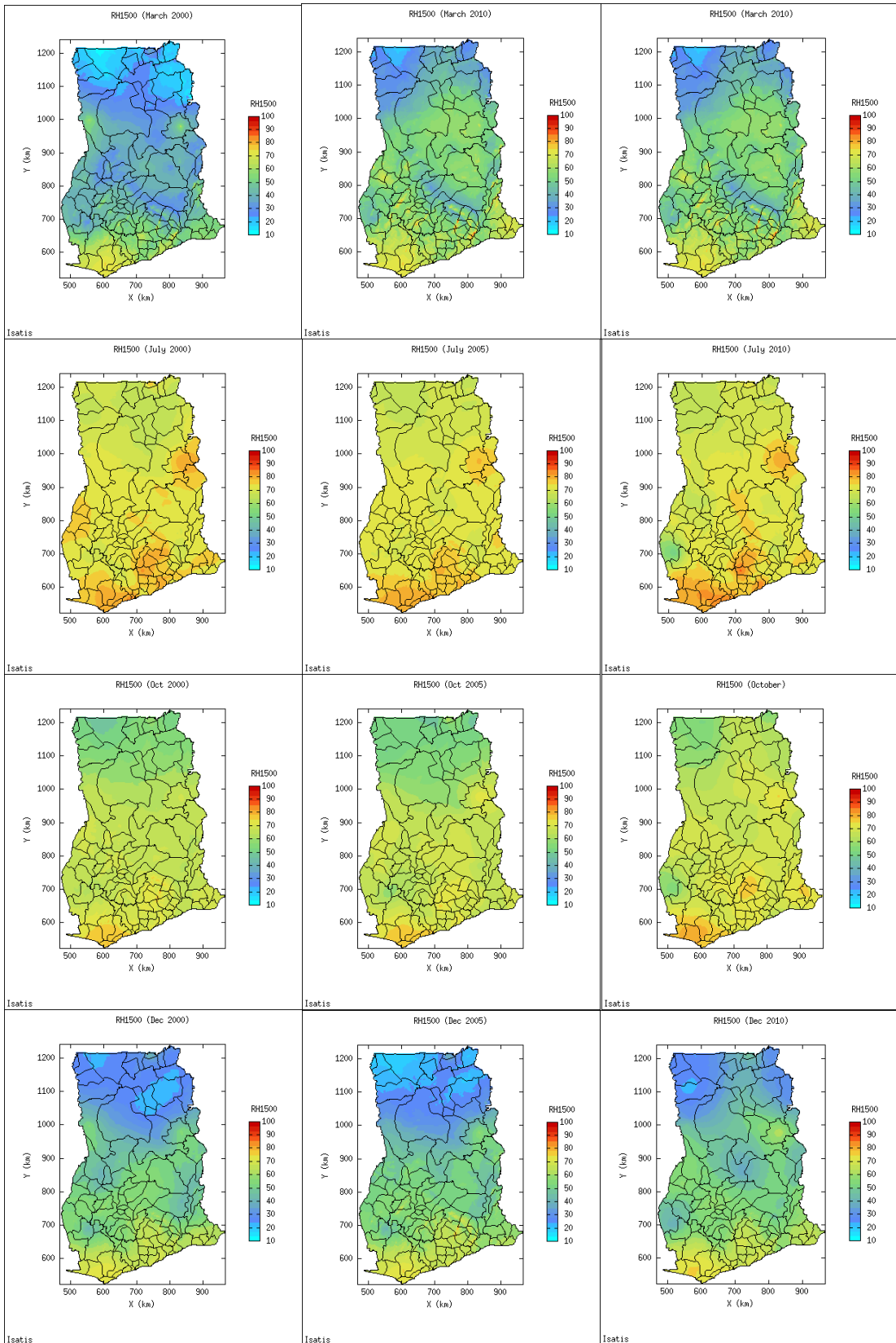


Figure E-2.3: Spatial maps of relative humidity (at 1500 hours) resulting from interpolations for March, July, October and December in 2000, 2005 and 2010.

Table E-2.3: Fitted parameters of linear models of coregionalisation of morbidity incidence rates with lagged one month rainfall for the months in 2010.

Month	Variable	$nug(h_0)$			$sph(h/60-100)$		$exp(h/150-260)$	
		b_{ij}^0	b_{ij}^1	r_{ij}^1	b_{ij}^1	r_{ij}^2		
January	MIR	5000	7500	60	4800	200		
	Rainfall_1	100	150	60	50	200		
	MIR and Rainf_1	-300	400	60	200	200		
February	MIR	5000	1000	100	9000	200		
	Rainfall_1	200	4800	100	100	200		
	MIR and Rainf_1	800	-600	100	-450	200		
March	MIR	2500	7000	60	8000	200		
	Rainfall_1	200	350	60	300	200		
	MIR and Rainf_1	-500	800	60	200	200		
April	MIR	4000	4000	100	12500	200		
	Rainfall_1	200	900	100	600	200		
	MIR and Rainf_1	-800	1000	100	800	200		
May	MIR	7000	5000	100	10500	250		
	Rainfall_1	500	200	100	3100	250		
	MIR and Rainf_1	1000	1000	100	200	250		
June	MIR	8000	11000	60	12000	200		
	Rainfall_1	180	1000	60	3550	200		
	MIR and Rainf_1	-1200	1200	60	1500	200		
July	MIR	7000	8000	100	22000	150		
	Rainfall_1	3800	1600	100	1600	150		
	MIR and Rainf_1	-4200	1800	100	700	150		
August	MIR	6000	11500	80	13000	220		
	Rainfall_1	300	2200	80	2200	220		
	MIR and Rainf_1	-1100	2000	80	600	220		
September	MIR	6000	10000	100	12000	230		
	Rainfall_1	700	1500	100	2850	230		
	MIR and Rainf_1	1800	-3500	100	2000	230		
October	MIR	6000	16000	100	7500	200		
	Rainfall_1	400	1900	100	3000	200		
	MIR and Rainf_1	1300	-2800	100	600	200		
November	MIR	6000	16000	100	9000	200		
	Rainfall_1	400	3000	100	2000	200		
	MIR and Rainf_1	-1500	2700	100	500	200		
December	MIR	6500	9000	100	9500	260		
	Rainfall_1	150	700	100	1600	260		
	MIR and Rainf_1	-800	1800	100	500	260		

Table E-2.4: Fitted parameters of linear models of coregionalisation of morbidity incidence rates with minimum temperature for the months in 2010.

Month	Variable	$nug(h_0)$			$sph(h/150)$		$exp(h/200 - 280)$	
		b_{ij}^0	b_{ij}^1	r_{ij}^1	b_{ij}^1	r_{ij}^2		
January	MIR	4500	1500	150	11500	220		
	Min Temp	1.00	0.95	150	2.00	220		
	MIR and MinT	-2.50	-35	150	-25	220		
February	MIR	4500	4500	150	5500	200		
	Min Temp	1.75	1.00	150	1.10	200		
	MIR and MinT	-10	-60	150	20	200		
March	MIR	4000	7200	150	5500	220		
	MinTemp	0.55	2.05	150	1.15	220		
	MIR and MinT	5	-100	150	50	220		
April	MIR	6000	5000	150	9000	200		
	MinTemp	0.50	5.50	150	9.50	200		
	MIR and MinT	10	-65	150	-35	200		
May	MIR	8000	5500	150	8500	200		
	MinTemp	0.35	0.75	150	2.15	200		
	MIR and MinT	0	-35	150	-10	200		
June	MIR	5000	7000	150	19000	200		
	MinTemp	0.65	0.75	150	1.50	200		
	MIR and MinT	15	-40	150	-10	200		
July	MIR	12000	12000	150	14000	200		
	MinTemp	0.15	1.05	150	1.75	200		
	MIR and MinT	25	-45	150	-30	200		
August	MIR	5000	6500	150	1850	220		
	MinTemp	0.50	1.05	150	1.50	220		
	MIR and MinT	10	-60	150	20	220		
September	MIR	5000	8500	150	14500	280		
	MinTemp	0.30	1.85	150	1.15	280		
	MIR and MinT	25	-20	150	-45	280		
October	MIR	5500	10500	150	14000	200		
	MinTemp	0.50	1.75	150	0.85	200		
	MIR and MinT	30	-40	150	-50	200		
November	MIR	12500	8000	150	11500	200		
	MinTemp	0.45	0.75	150	0.70	200		
	MIR and MinT	10	-75	150	10	200		
December	MIR	7000	6500	150	12000	200		
	MinTemp	0.55	0.25	150	2.25	200		
	MIR and MinT	30	-40	150	-60	200		

Table E-2.5: Fitted parameters of linear models of coregionalisation of morbidity incidence rates with relative humidity (at 1500 hours) for the months in 2010.

Month	Variable	$nug(h_0)$			$sph(h/150)$		$exp(h/200 - 250)$	
		b_{ij}^0	b_{ij}^1	r_{ij}^1	b_{ij}^1	r_{ij}^2		
January	MIR	4000	2500	150	11000	220		
	RH1500	10	30	150	155	220		
	MIR and RH1500	-180	180	150	80	220		
February	MIR	4500	5000	150	5200	220		
	RH1500	100	40	150	115	220		
	MIR and RH1500	140	-200	150	20	220		
March	MIR	4000	2000	150	10800	200		
	RH1500	40	35	150	90	200		
	MIR and RH1500	250	-80	150	-200	200		
April	MIR	6000	6000	150	8000	200		
	RH1500	15	25	150	28	200		
	MIR and RH1500	-50	250	150	-50	200		
May	MIR	7000	4000	150	11000	200		
	RH1500	2.5	12	150	28	200		
	MIR and RH1500	30	-180	150	150	200		
June	MIR	6000	5500	150	2000	200		
	RH1500	4	4	150	19	200		
	MIR and RH1500	-130	150	150	80	200		
July	MIR	12500	9000	150	16500	200		
	RH1500	1	4	150	25	200		
	MIR and RH1500	80	-180	150	80	200		
August	MIR	4000	8000	150	17500	200		
	RH1500	1	12.15	150	17.55	200		
	MIR and RH1500	-60	10	150	65	200		
September	MIR	6000	5000	150	17500	280		
	RH1500	9	11.5	150	6	280		
	MIR and RH1500	10	-220	150	120	280		
October	MIR	6500	8000	150	15500	200		
	RH1500	5.5	6.5	150	24.5	200		
	MIR and RH1500	70	-220	150	120	200		
November	MIR	12000	8500	150	12000	220		
	RH1500	8.50	20	150	35	220		
	MIR and RH1500	100	-250	150	-20	220		
December	MIR	10000	6000	150	9000	240		
	RH1500	10	25	150	80	240		
	MIR and RH1500	80	-350	150	160	240		

Table E-2.6: Fitted parameters of linear models of coregionalisation of morbidity incidence rates with lagged one month rainfall for the months in 2010 in BAR.

Month	Variable	$nug(h_0)$	$exp(h/100)$	
		b_{ij}^0	b_{ij}^1	r_{ij}^1
January	MIR	2000	14500	100
	Rainfall_1	40	70	100
	MIR and Rainf_1	-100	-250	100
February	MIR	2500	10200	100
	Rainfall_1	5	250	100
	MIR and Rainf_1	100	-1000	100
March	MIR	3000	10000	100
	Rainfall_1	20	240	100
	MIR and Rainf_1	-200	750	100
April	MIR	5500	12000	100
	Rainfall_1	20	550	100
	MIR and Rainf_1	-250	2300	100
May	MIR	5000	15000	100
	Rainfall_1	50	1250	100
	MIR and Rainf_1	-500	1650	100
June	MIR	4000	28000	100
	Rainfall_1	10	430	100
	MIR and Rainf_1	-200	800	100
July	MIR	5000	24500	100
	Rainfall_1	200	4000	100
	MIR and Rainf_1	-1000	2000	100
August	MIR	4500	22500	100
	Rainfall_1	500	7500	100
	MIR and Rainf_1	-1200	1500	100
September	MIR	2000	20000	100
	Rainfall_1	300	2800	100
	MIR and Rainf_1	-500	2000	100
October	MIR	4000	2000	100
	Rainfall_1	200	6500	100
	MIR and Rainf_1	-600	3600	100
November	MIR	9000	21500	100
	Rainfall_1	200	20000	100
	MIR and Rainf_1	1200	1800	100
December	MIR	3000	22500	100
	Rainfall_1	100	600	100
	MIR and Rainf_1	-500	900	100

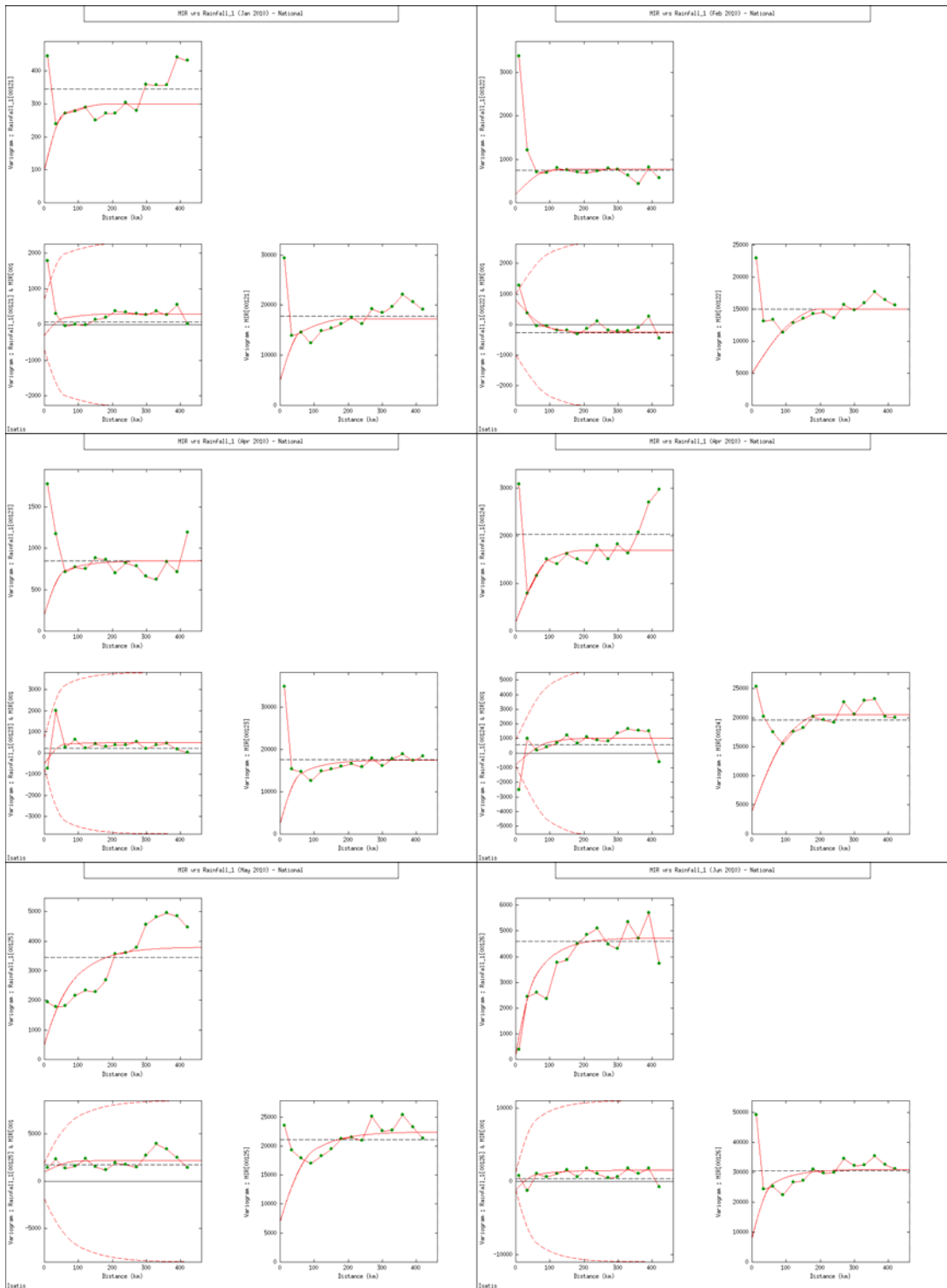


Figure E-2.4a: Linear coregionalisation modelling of morbidity incidence rates with rainfall in the previous month for January-June 2010.

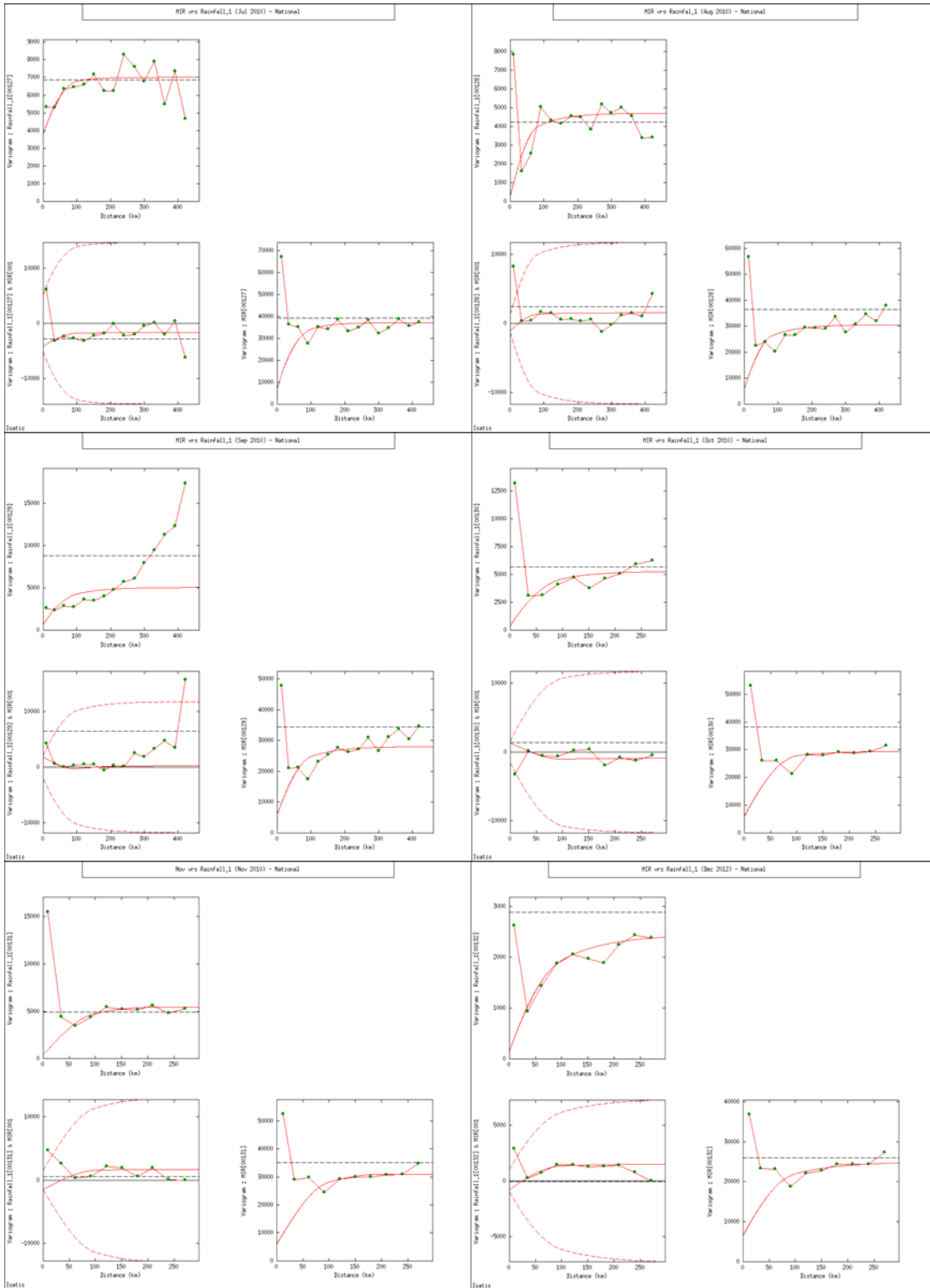


Figure E-2.4b: Linear coregionalisation modelling of morbidity incidence rates with rainfall in the previous month for July-December 2010.

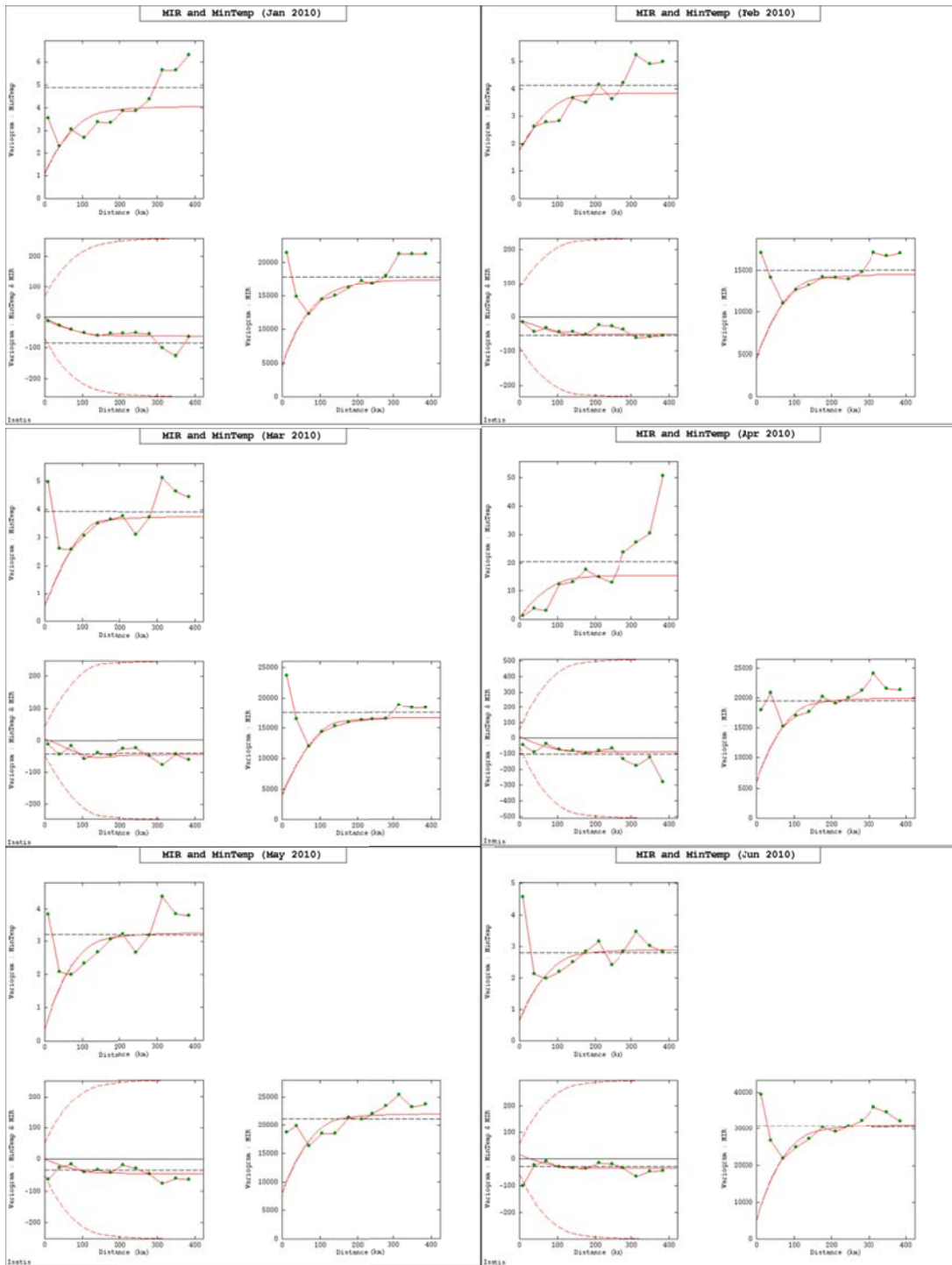


Figure E-2.5a: Linear coregionalisation model of morbidity incidence rates with minimum temperature for January –June 2010.

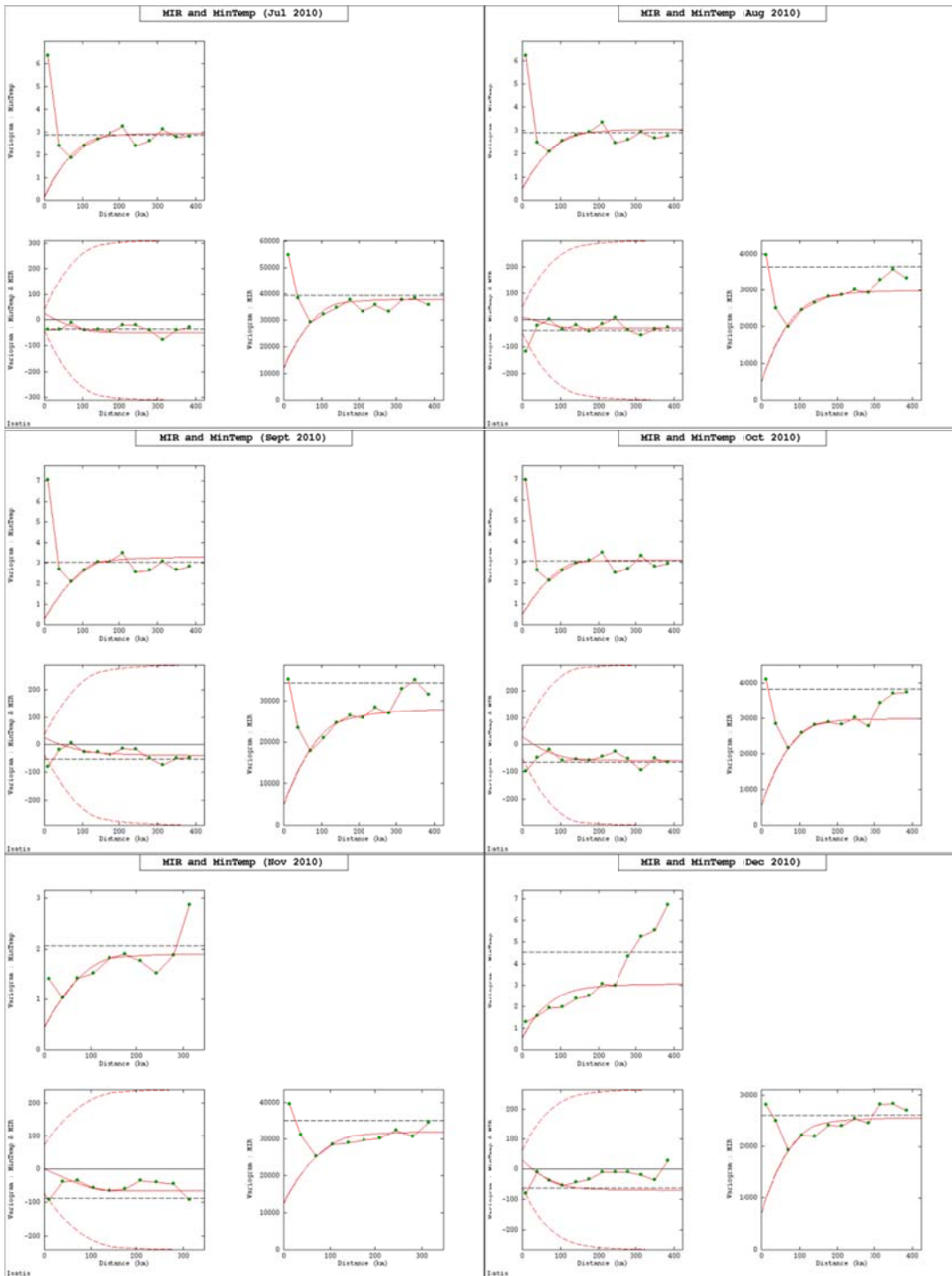


Figure E-2.5b: Linear coregionalisation model of malaria incidence rates with minimum temperature for July–December 2010.

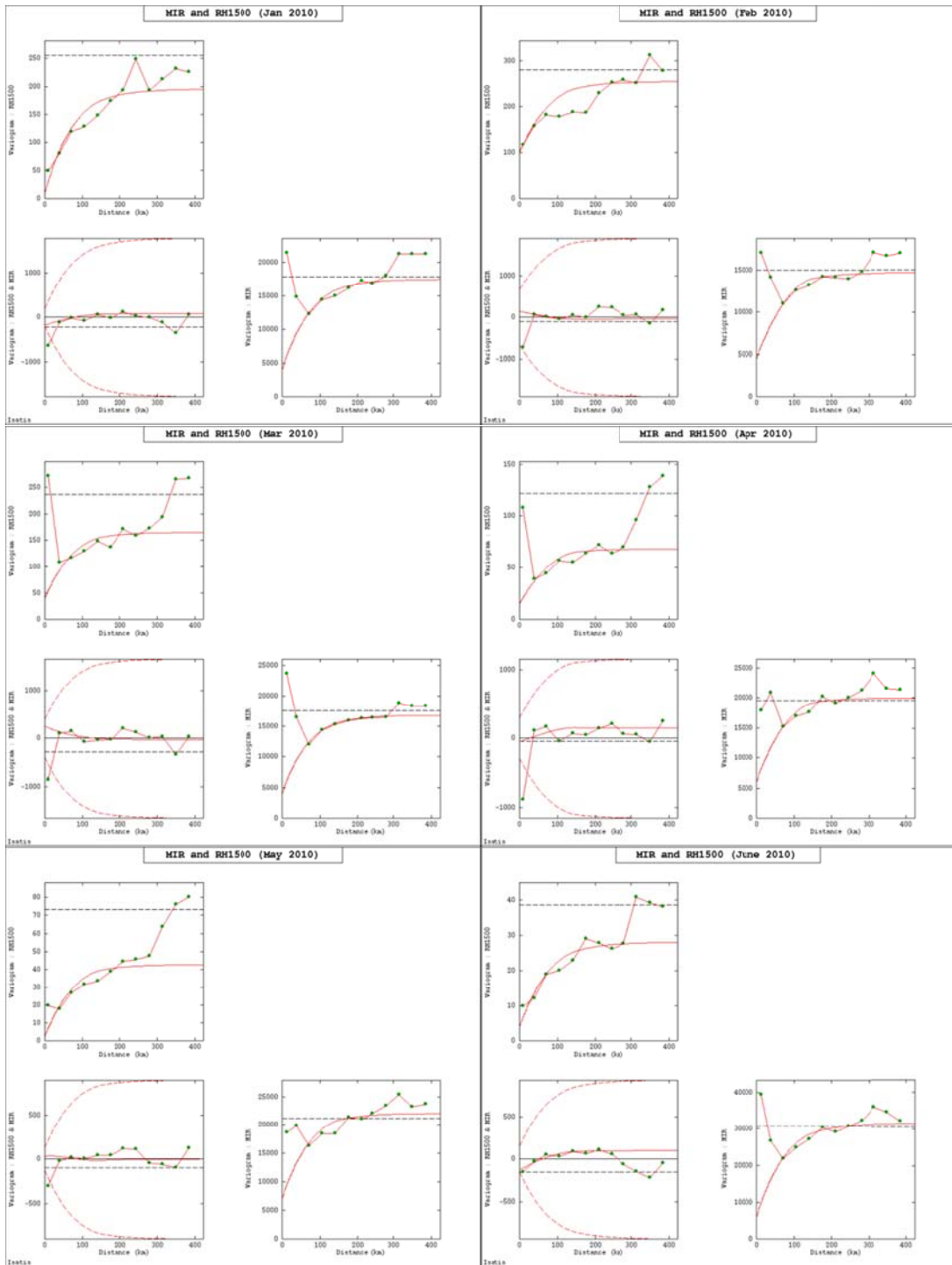


Figure E-2.6a: Linear coregionalisation model of malaria incidence rates with relative humidity (at 1500 hours) for January–June 2010.

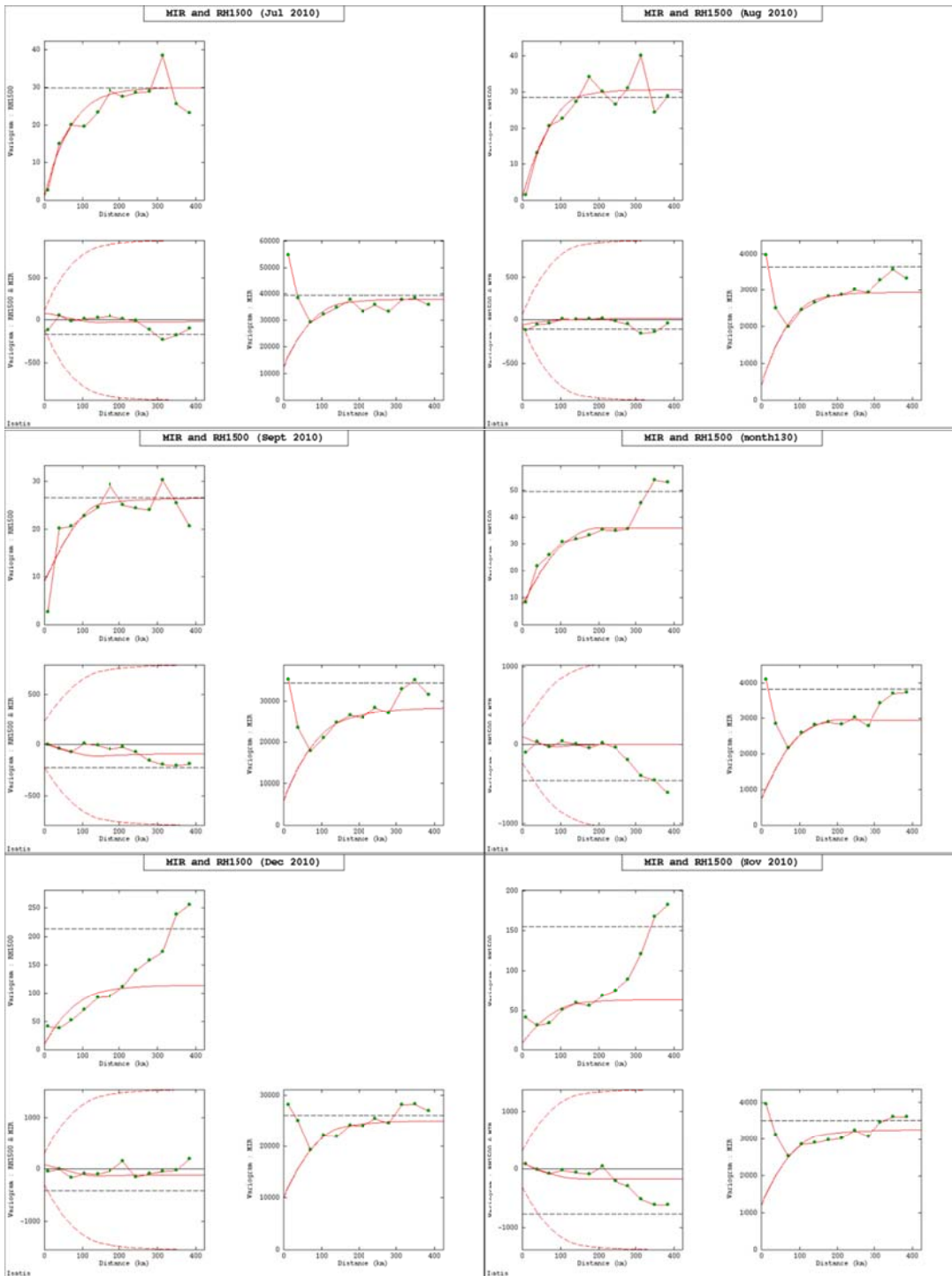


Figure E-2.6b: Linear coregionalisation model of malaria incidence rates with relative humidity (at 1500 hours) for July–December 2010.

E-3: Space-time LMC of Residuals with Potential Climate Covariates:

Table E-3.1: Parameters of space-time linear models of coreginalation of detrended morbidity incidence rates with lagged one month rainfall and relative humidity (1500), and current maximum temperature for the national data set study

Variable	Spatial			Temporal
	$nug(h_0)$	$exp(h/35)$	$sph(h/250)$	$cosexp$ ($h/10 - 60$)
Residuals	1500	1100	500	1700
Rainfall_1	1500	1800	800	2900
Resid & Rainf_1	50	250	150	1700
Variable	$nug(h_0)$	$exp(h/35)$	$sph(h/250)$	$cosexp$ ($h/20 - 200$)
Residuals	1500	800	800	1780
MaxTemp	0.80	0.7	1	3.2
MIR & MaxT	-10	5	6	-57
Variable	$nug(h_0)$	$exp(h/40)$	$sph(h/250)$	$cosexp$ ($h/10 - 100$)
Residuals	1600	1100	300	2000
Residuals	25	10	45	150
RH1500_1	10	20	10	400

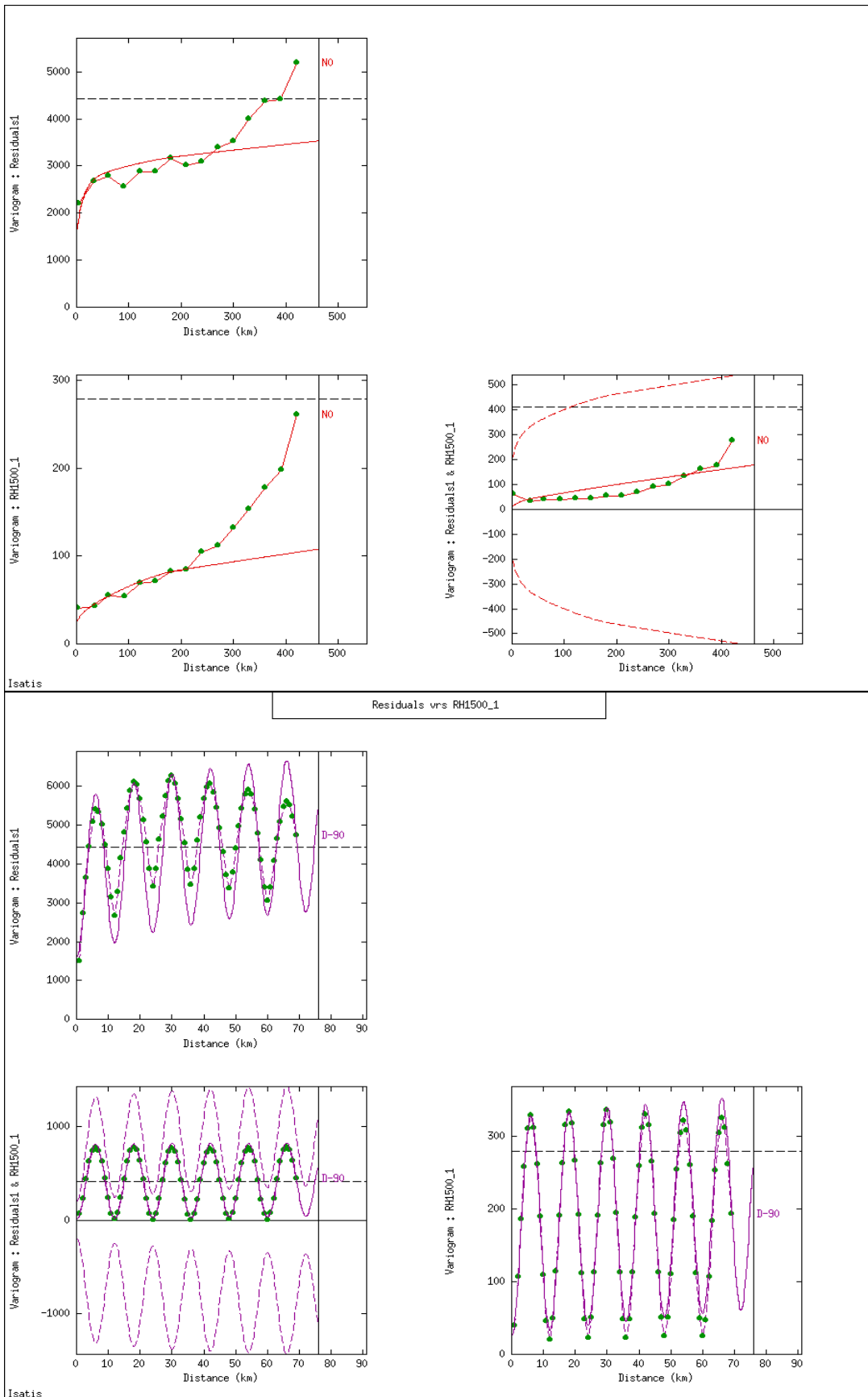


Figure E-3.1: Space-time linear model of coregionalisation of detrended malaria incidence rates (residuals) with relative humidity (at 1500 hours) showing spatial (top) and temporal (bottom) correlations (bottom) for the national study

E-4: Cross-Validation and Kriging Parameters

Table E-4.1: Search neighbourhood parameters for STLOK containing minimum and maximum number of samples per angular sector of spatial and temporal radii in kilometres and months, respectively for the four study areas.

Study	Radius		Min no. of samples/ Sector	Max no. of samples/ sector	No. of angular sectors
	Spatial (km)	Temporal (months)			
National	200	5	2	5	4
BAR	120	5	2	5	4
Northern	150	5	2	5	4
Forest	150	5	2	5	4
Coastal	100	5	2	5	4

Table E-4.2: Parameters for construction of grid for the interpolation of malaria risk in the four study areas (National BAR, Northern, Forest and the Coastal zones).

Study	Parameter	Spatial (km)		Temporal:
		Easting	Northing	Time (months)
National	Origin	470	520	1
	Mesh	10	10	1
	No. of nodes	52	76	132
BAR	Origin	480	700	1
	Mesh	5	5	1
	No. of nodes	82	56	156
Northern	Origin	500	900	1
	Mesh	10	10	1
	No. of nodes	40	38	132
Forest	Origin	470	550	1
	Mesh	10	10	1
	No. of nodes	45	43	132
Coastal	Origin	470	520	1
	Mesh	10	10	1
	No. of nodes	51	20	132

Table E-4.3: Cross-validation OK estimates of trend coefficients for different moving neighbourhoods for national study.

Model	Neighbourhood		Error		Standardised Error		Corr. Coeff.
	Search radius	No. of samples	Mean	Variance	Mean	Variance	
b_0		2 – 10	4.39400	119934.0	0.01024	1.94663	0.078
	150 km	4 – 20	4.05250	117924.1	0.009460	1.94456	0.070
		2 – 10	4.29200	118959.9	0.00996	1.94568	0.078
	200 km	4 – 20	3.84338	117919.0	0.00877	1.94886	0.065
b_1		2 – 10	-0.07135	62.08536	-0.00726	1.78990	0.120
	150 km	4 – 20	-0.07737	61.53279	-0.00875	1.78925	0.110
		2 – 10	-0.07307	62.09028	-0.00767	1.79024	0.121
	200 km	4 – 20	-0.07661	61.8193	-0.00876	1.80192	0.0100
b_2		2 – 10	0.00035	0.00198	0.00658	1.72048	0.139
	150 km	4 – 20	0.00032	0.00195	0.00061	1.71327	0.131
		2 – 10	0.00041	0.00198	0.00830	1.72250	0.139
	200 km	4 – 20	0.00034	0.00197	0.00673	1.73219	0.118
b_3		2 – 10	0.08497	180.4835	0.00579	1.29820	0.330
	150 km	4 – 20	0.14344	1773.294	0.01069	1.25832	0.360
		2 – 10	0.12873	179.7913	0.00935	1.239454	0.330
	200 km	4 – 20	0.17835	172.9653	0.01348	1.25959	0.357
b_4		2 – 10	-0.36076	454.9101	-0.01065	2.02104	0.787
	150 km	4 – 20	-0.34218	450.333	-0.01024	2.00930	0.789
		2 – 10	-0.39153	454.765	-0.01242	2.02062	0.788
	200 km	4 – 20	-0.31621	448.076	-0.00895	2.00448	0.790

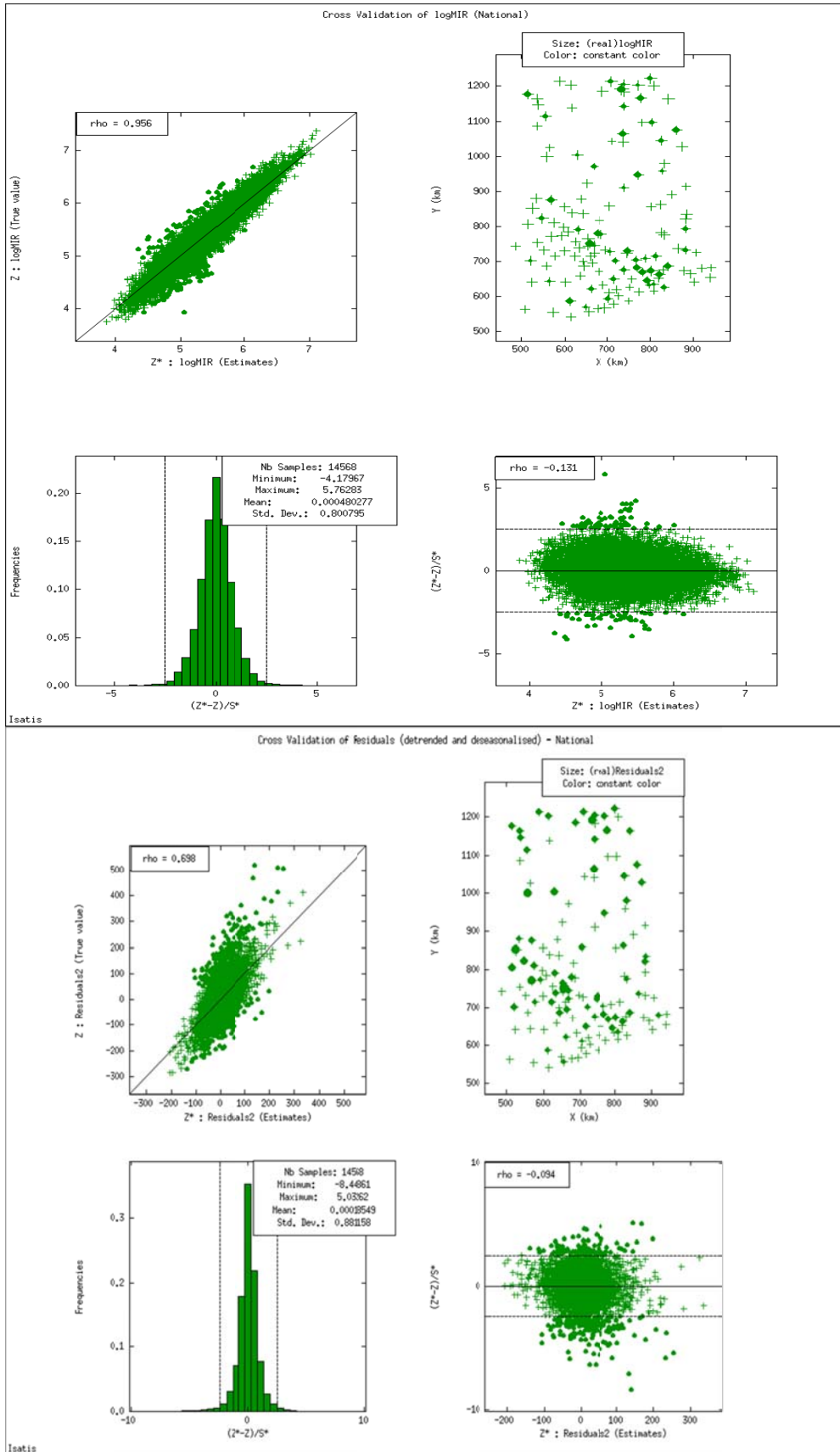


Figure E-4.1: Cross-validation summary of the STLOK and STOK estimates using a search neighbourhood of radius 200 km using 8 to 20 closest samples.

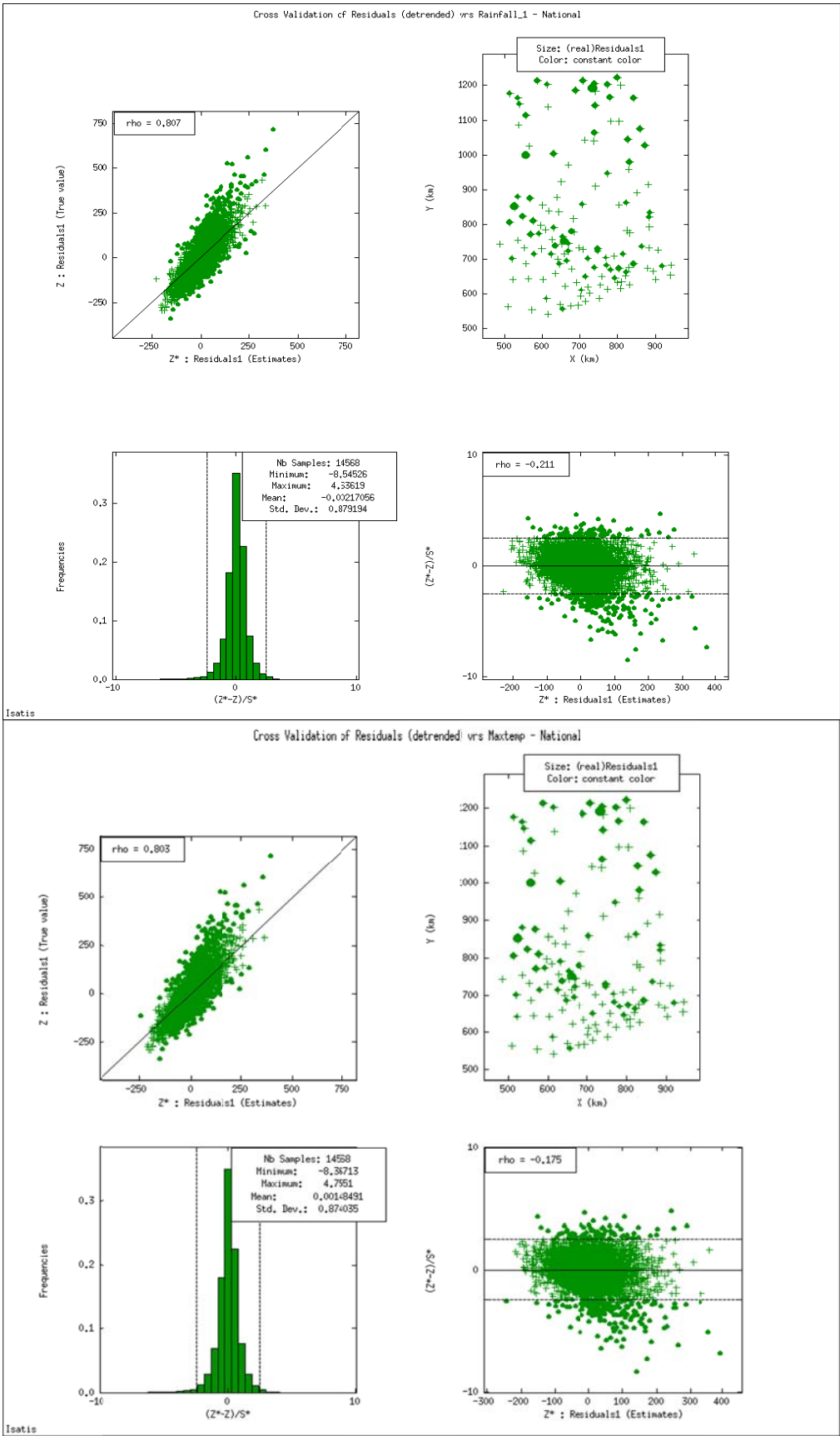


Figure E-4.2: Cross-validation summary of the STOCK technique accounting for the effect of preceding one month rainfall (top) and maximum temperature (bottom).

E-5: Spatial Maps of Morbidity Incidence Rates

Spatial maps of monthly morbidity incidence rates (MIR) from January 2000 (month 1) to December 2010 (month 132) have been produced by each of the following space-time kriging techniques:

E-5.1: Space-time lognormal ordinary kriging (STLOK) of MIR.

E-5.2: Space-time ordinary kriging of MIR via the joint modelling semivariogram of residuals (STROK)

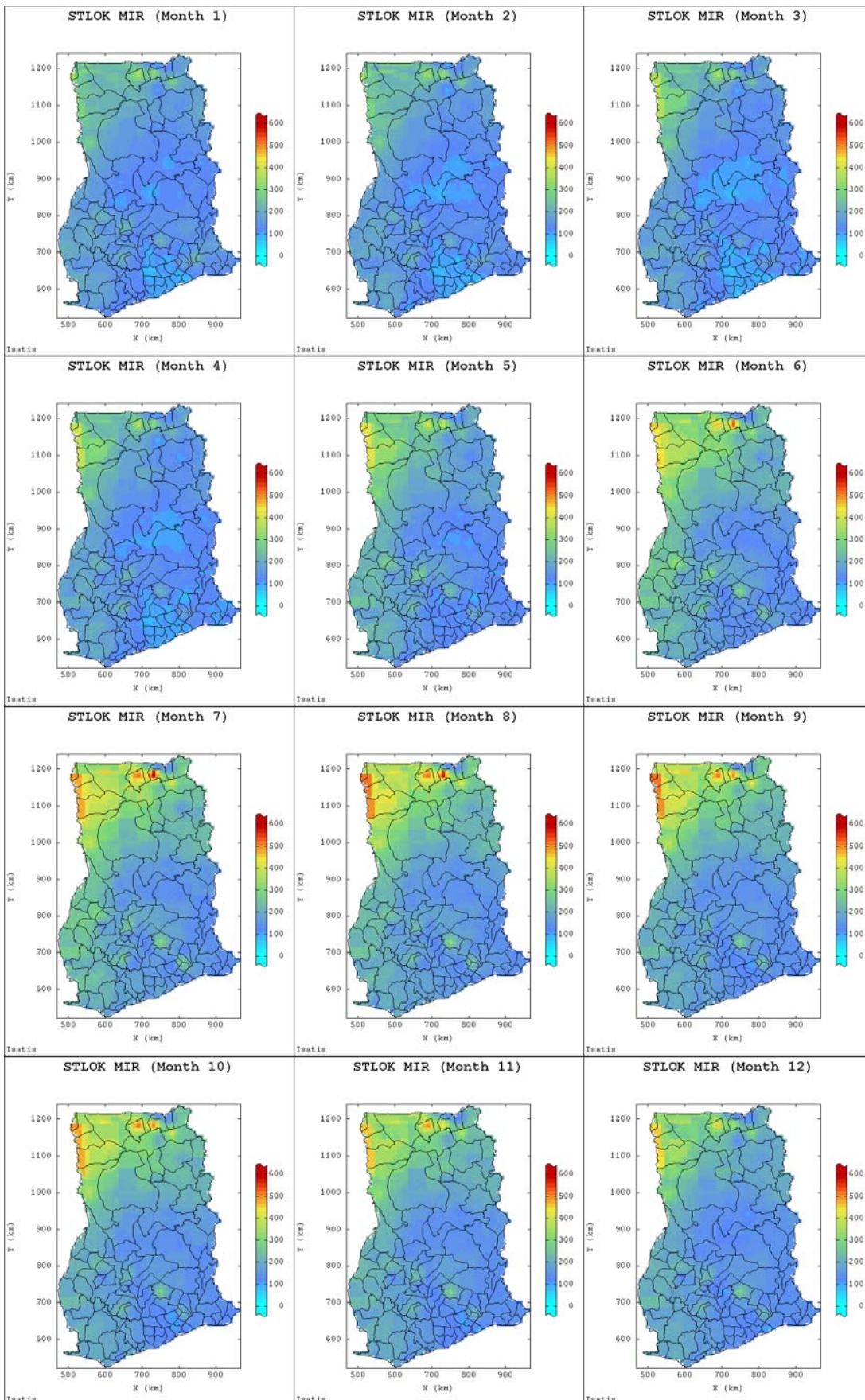
E-5.3: Space-time ordinary kriging of MIR via the generalised product-sum modelling of residuals (STROK_GPS)

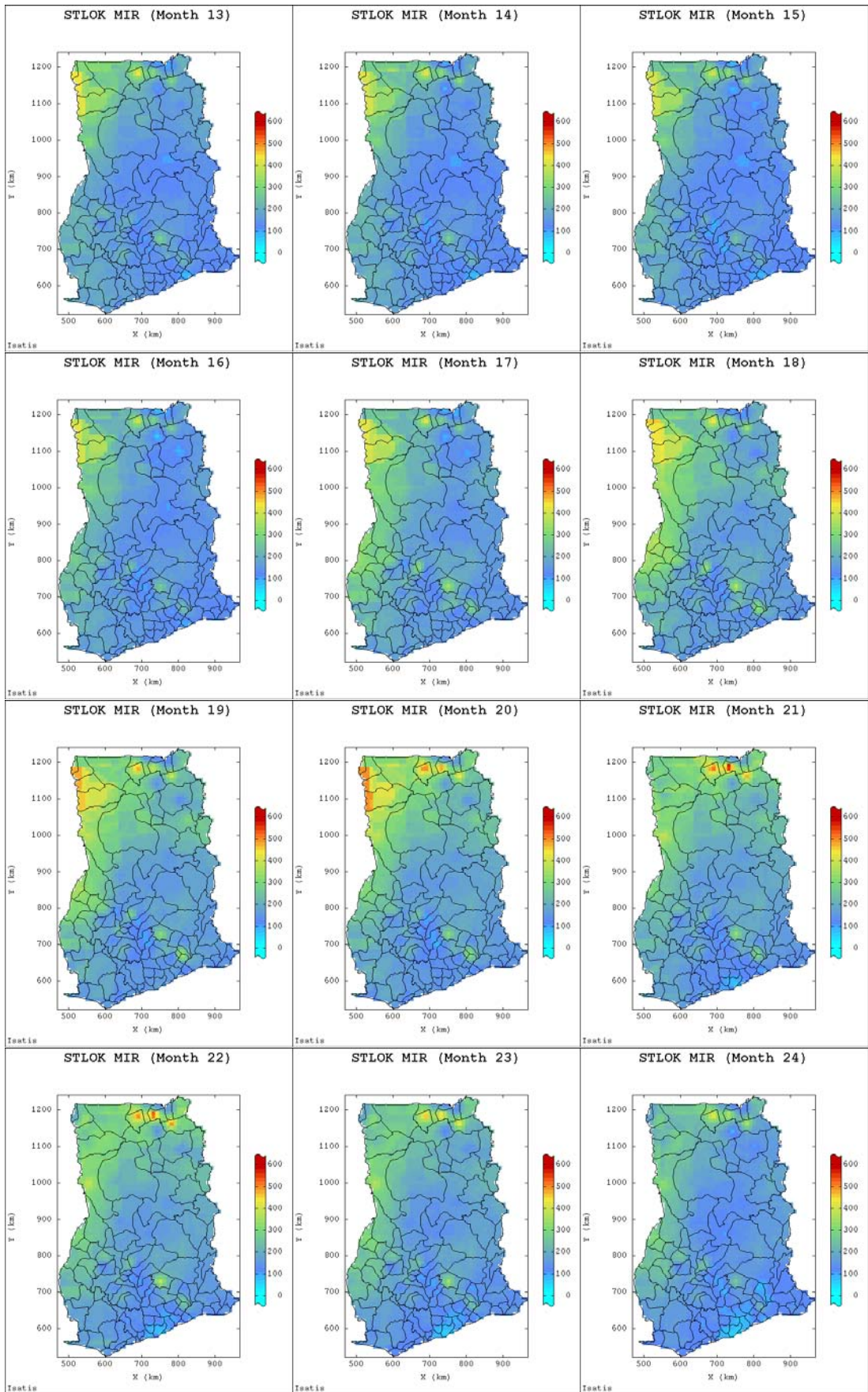
E-5.4: Space-time ordinary co-kriging of MIR accounting for the effect of rainfall (STOCK_Rainfall)

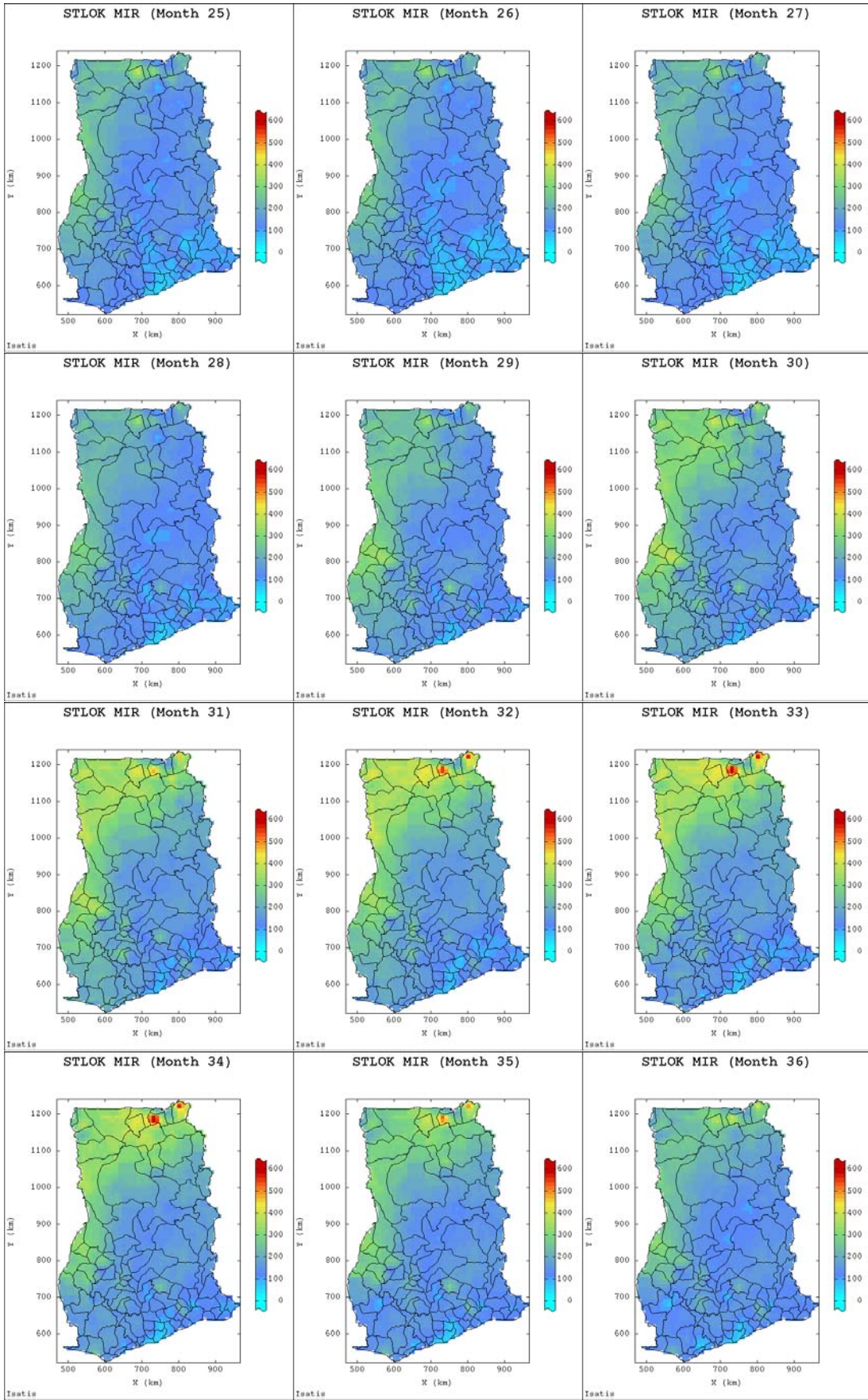
E-5.5: Space-time ordinary co-kriging of MIR accounting for the effect of maximum temperature (STOCK_MaxT)

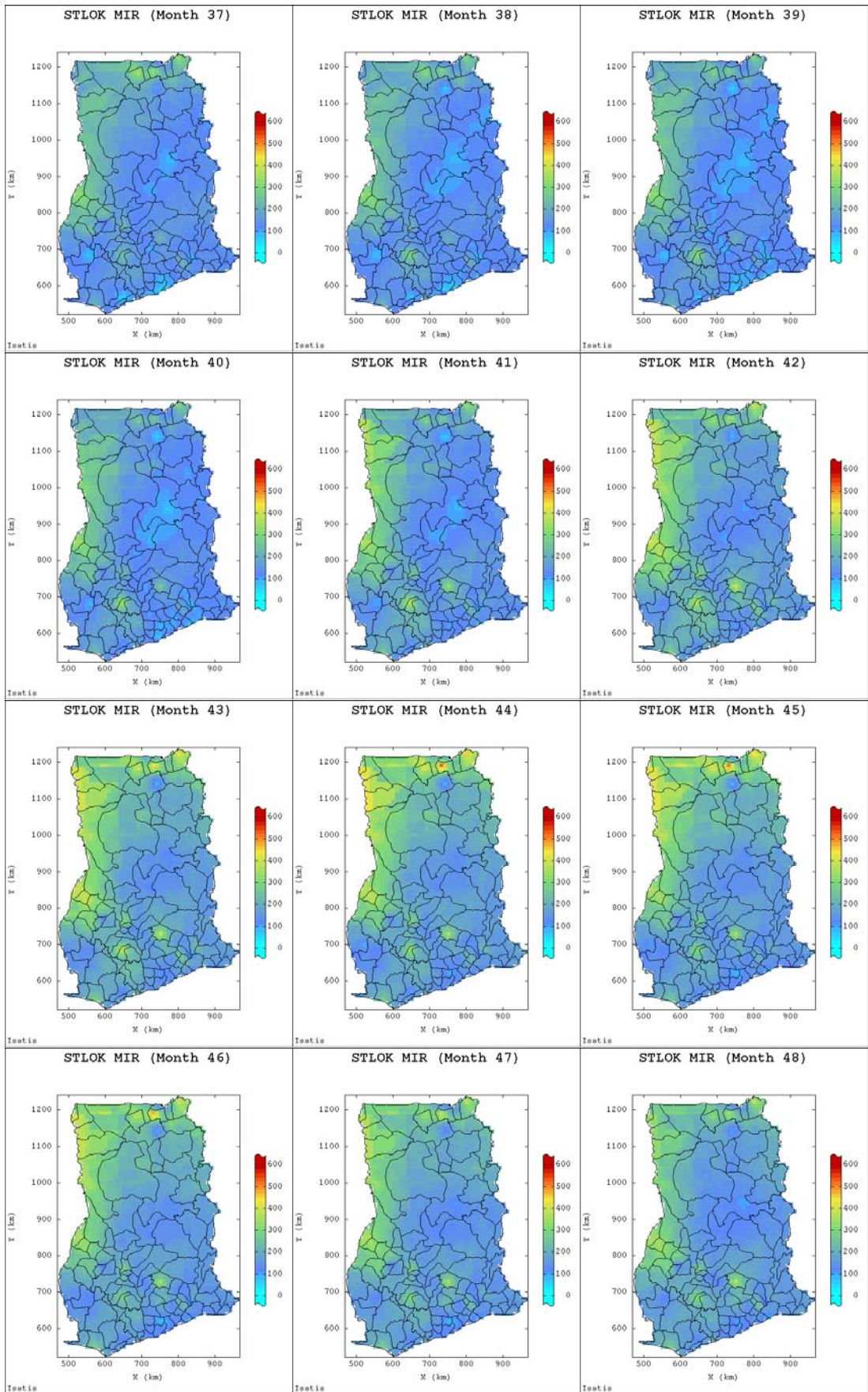
E-5.6: Jackknife Predictions of Space-time MIR Data for 2011

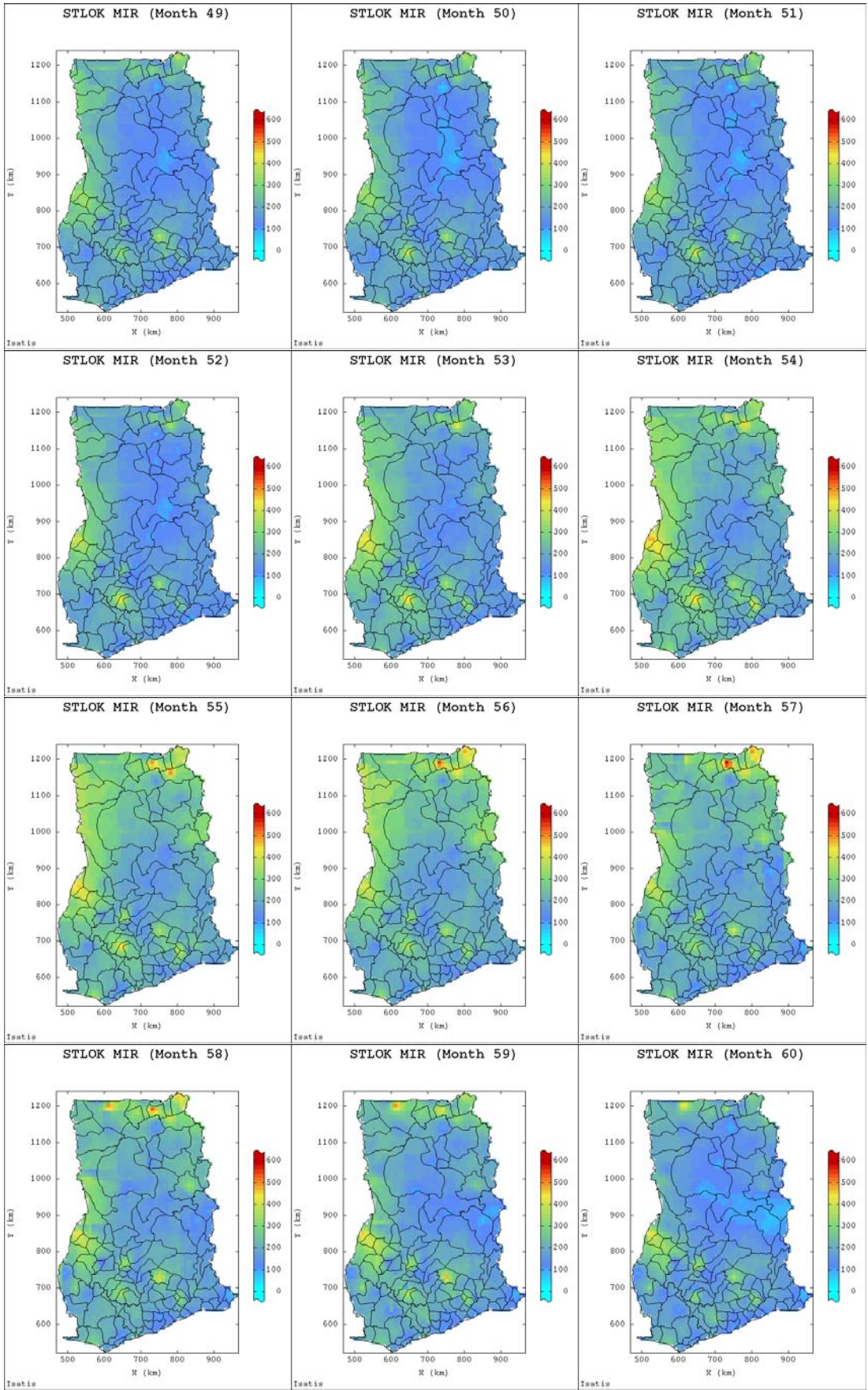
E-5.1: STLOK Produced Spatial Maps of MIR

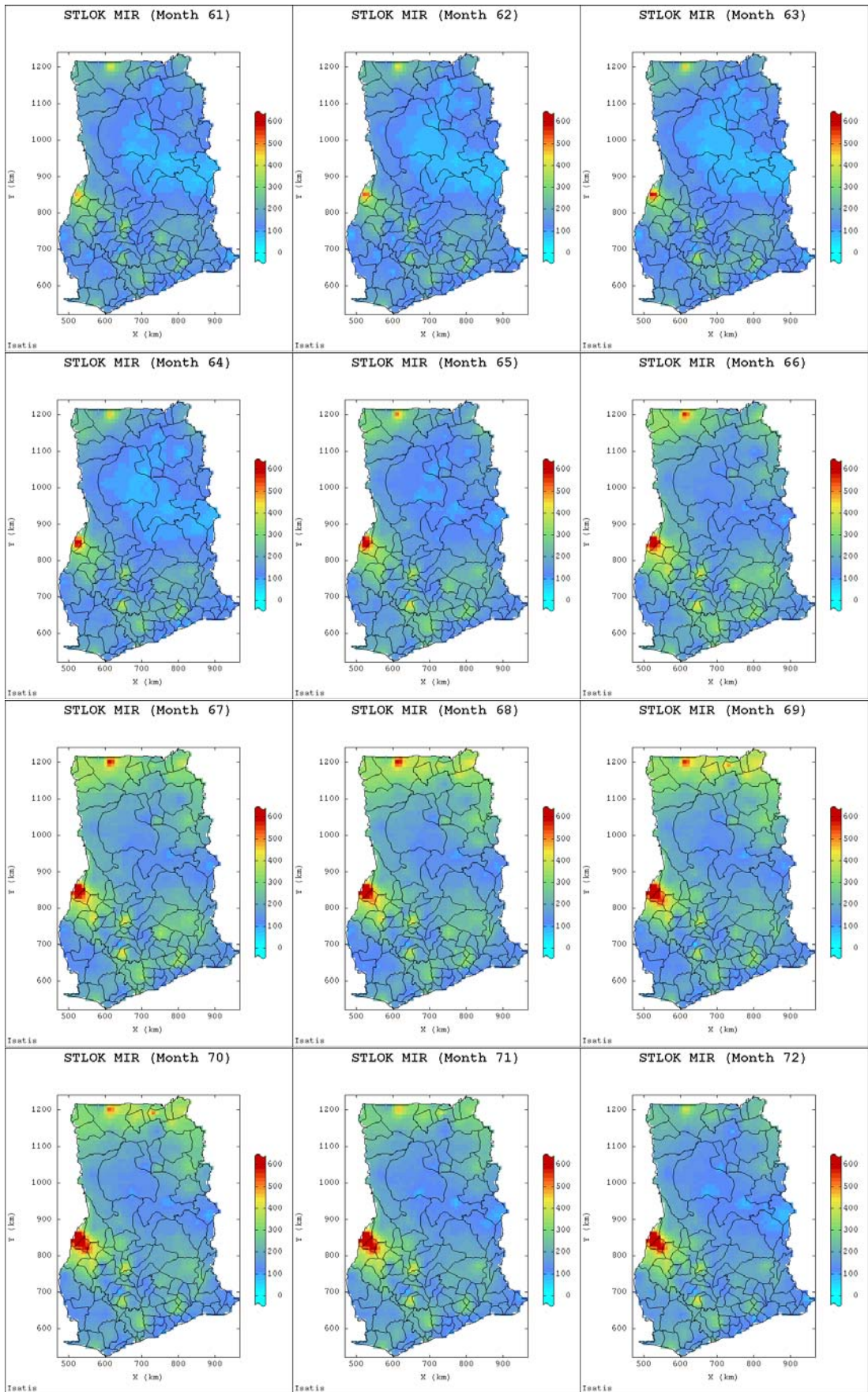


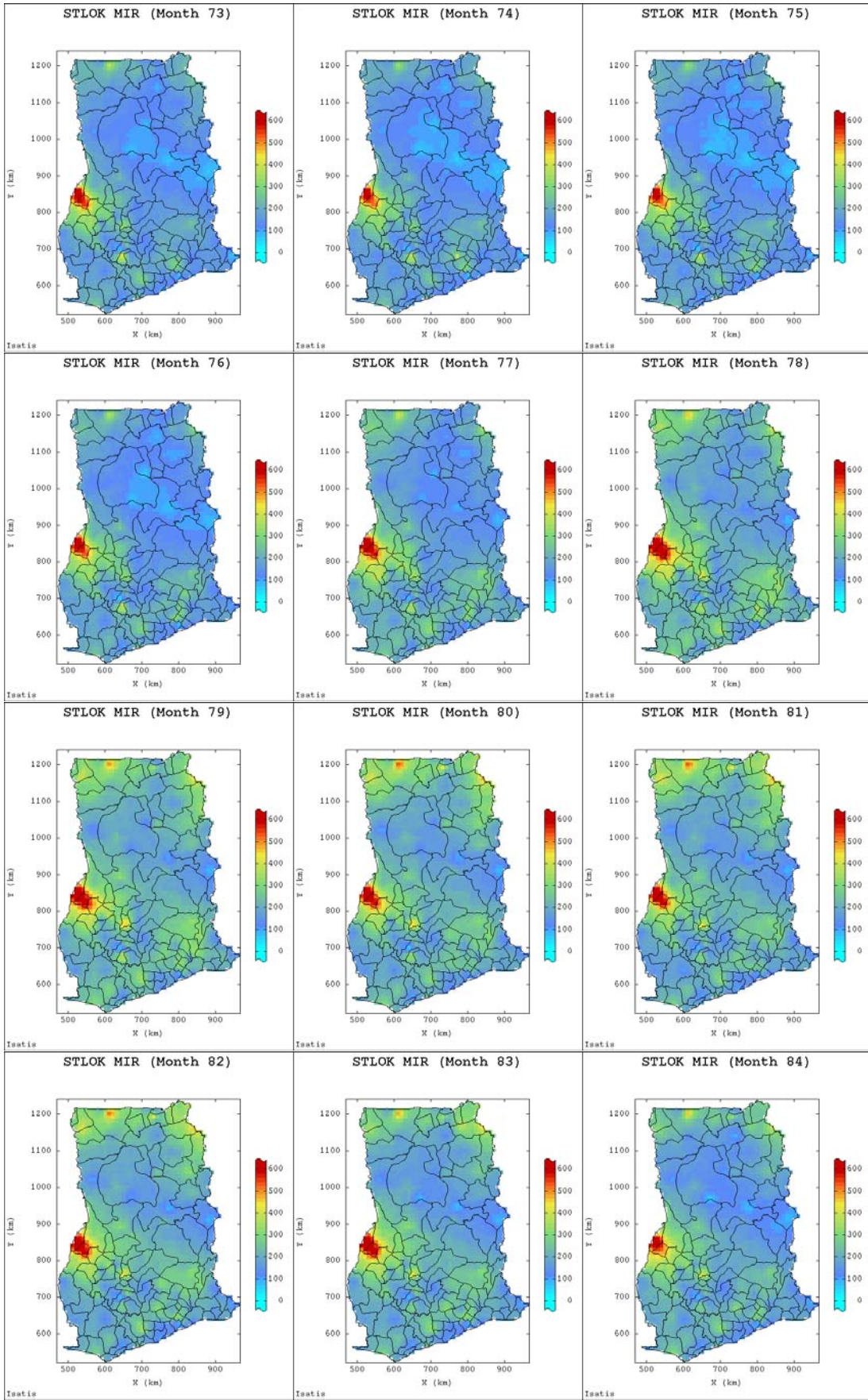


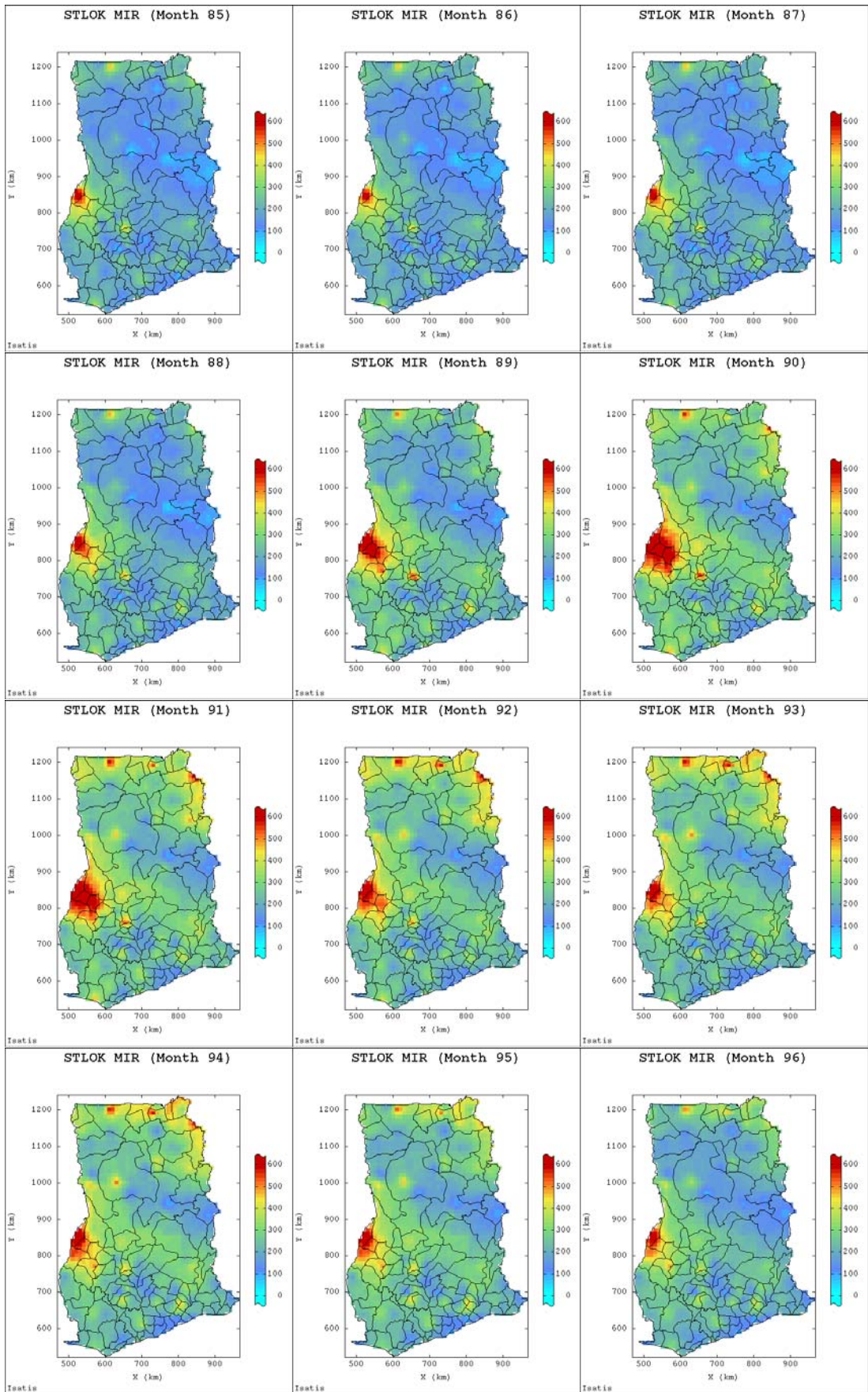


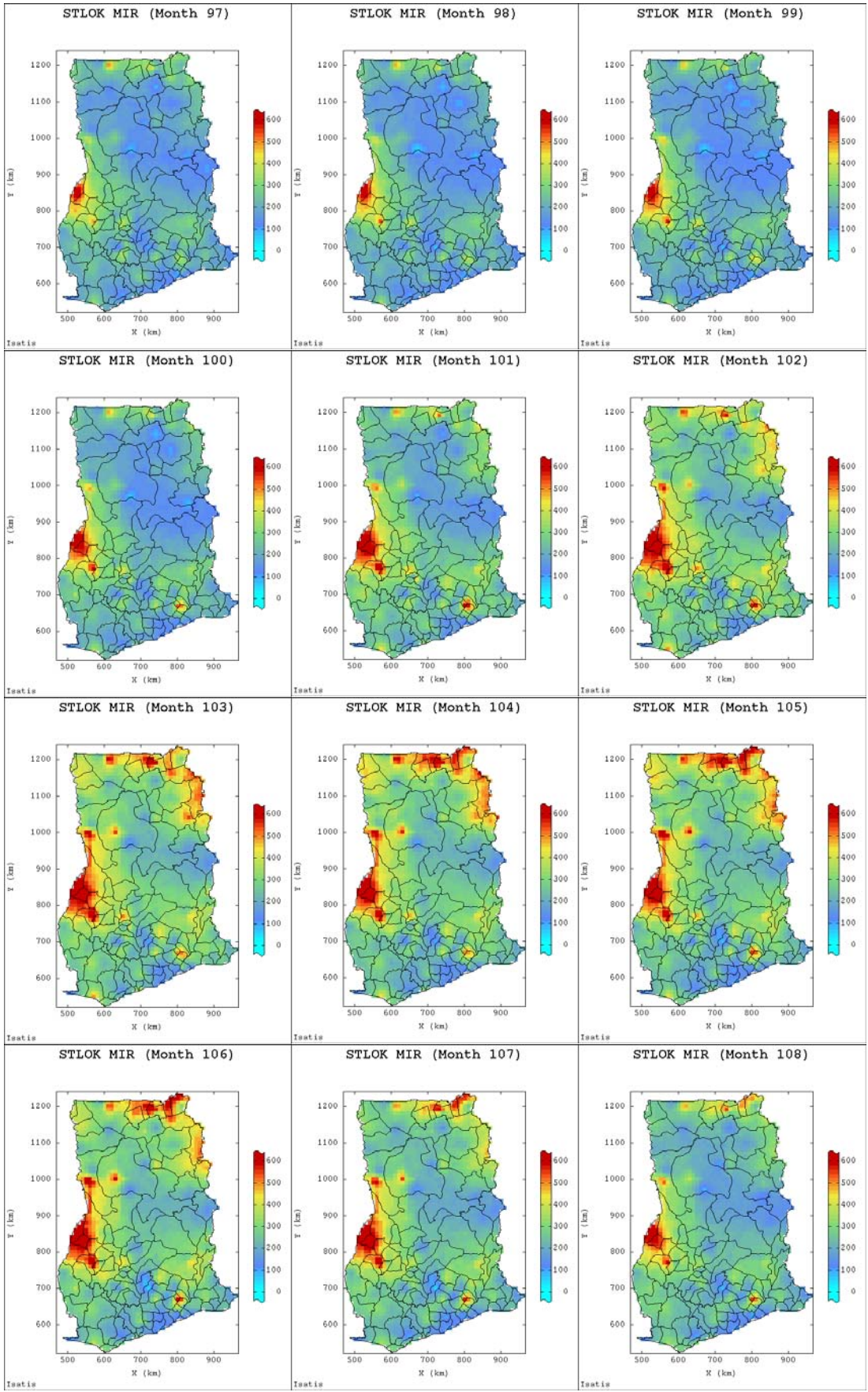


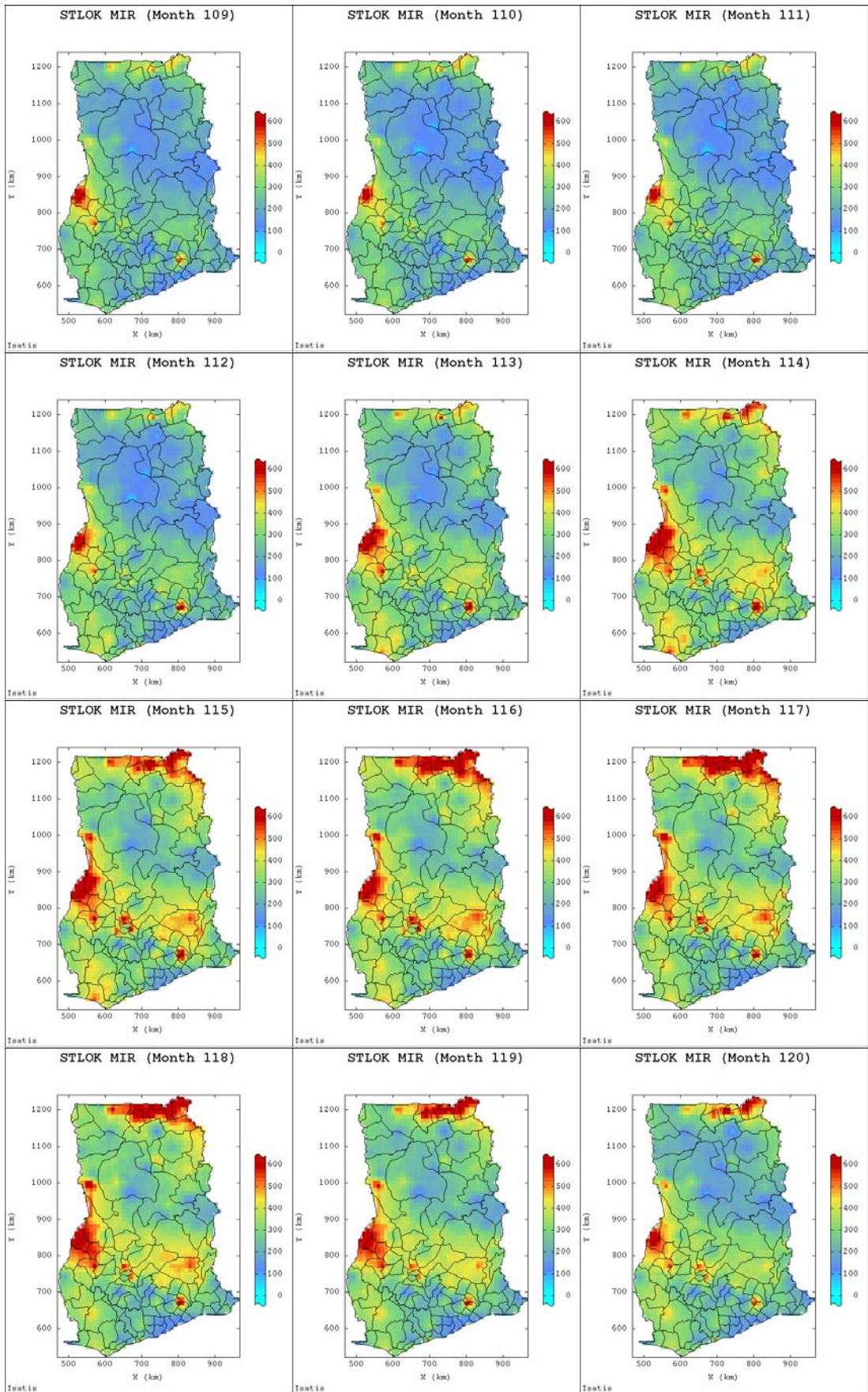


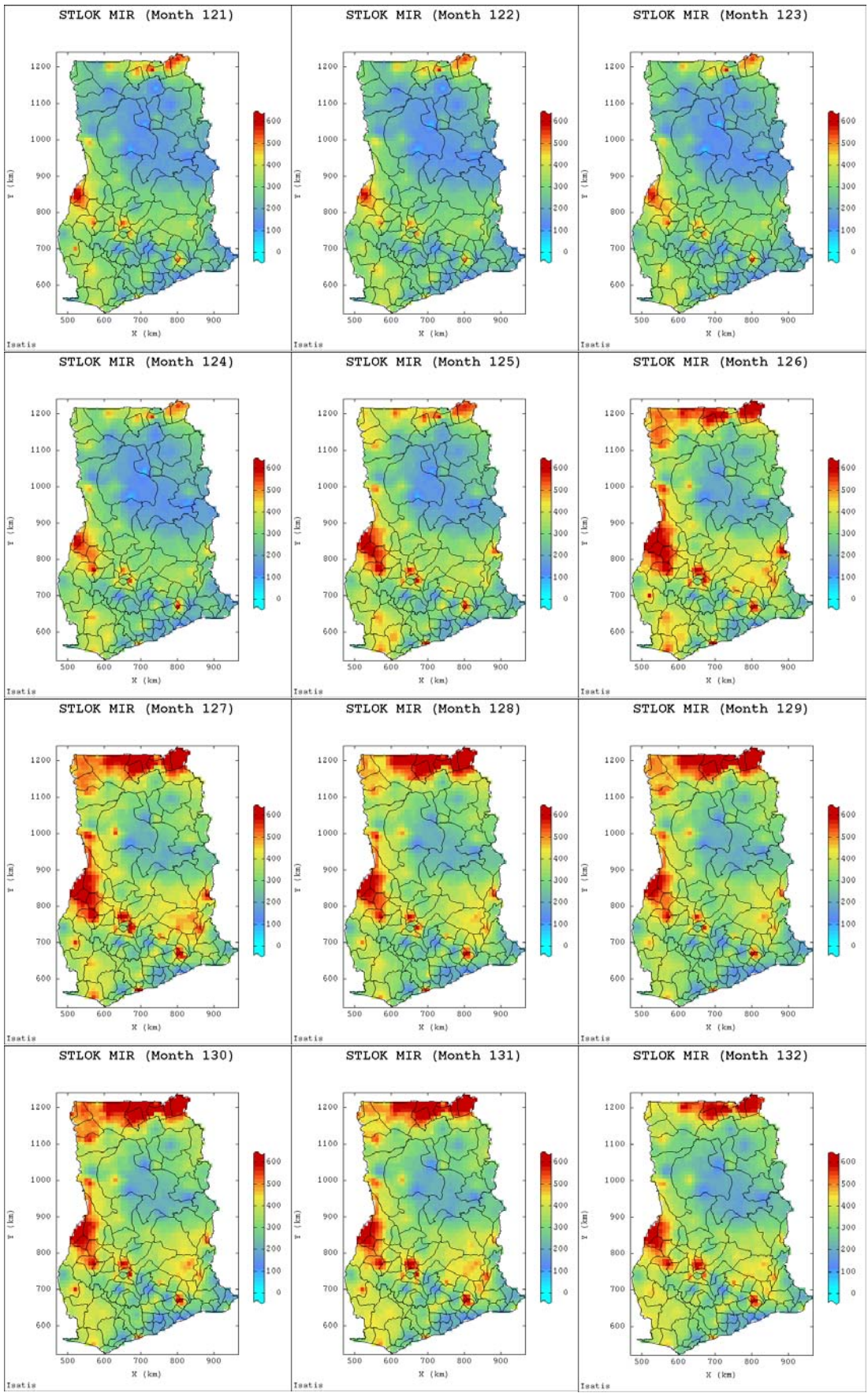




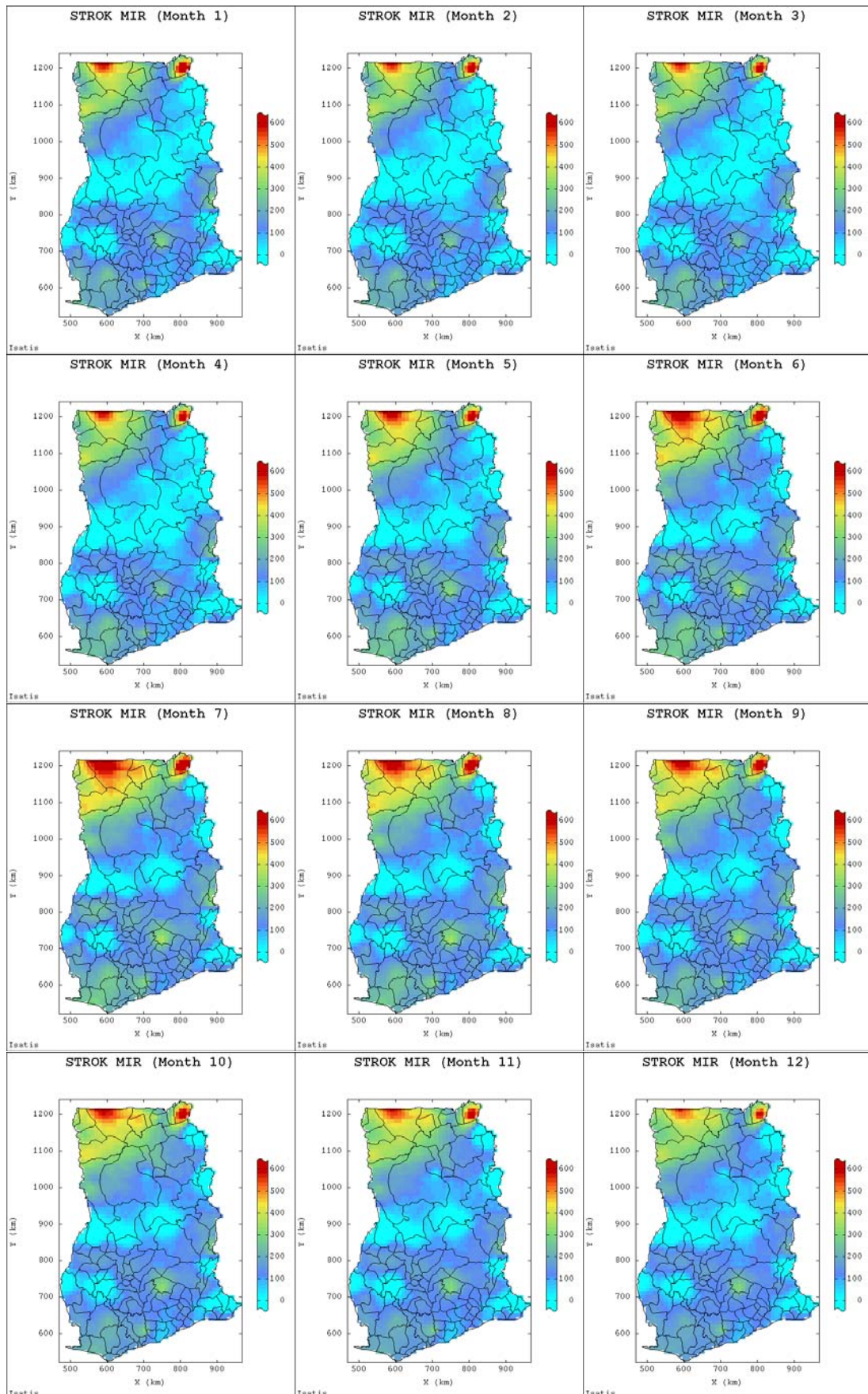


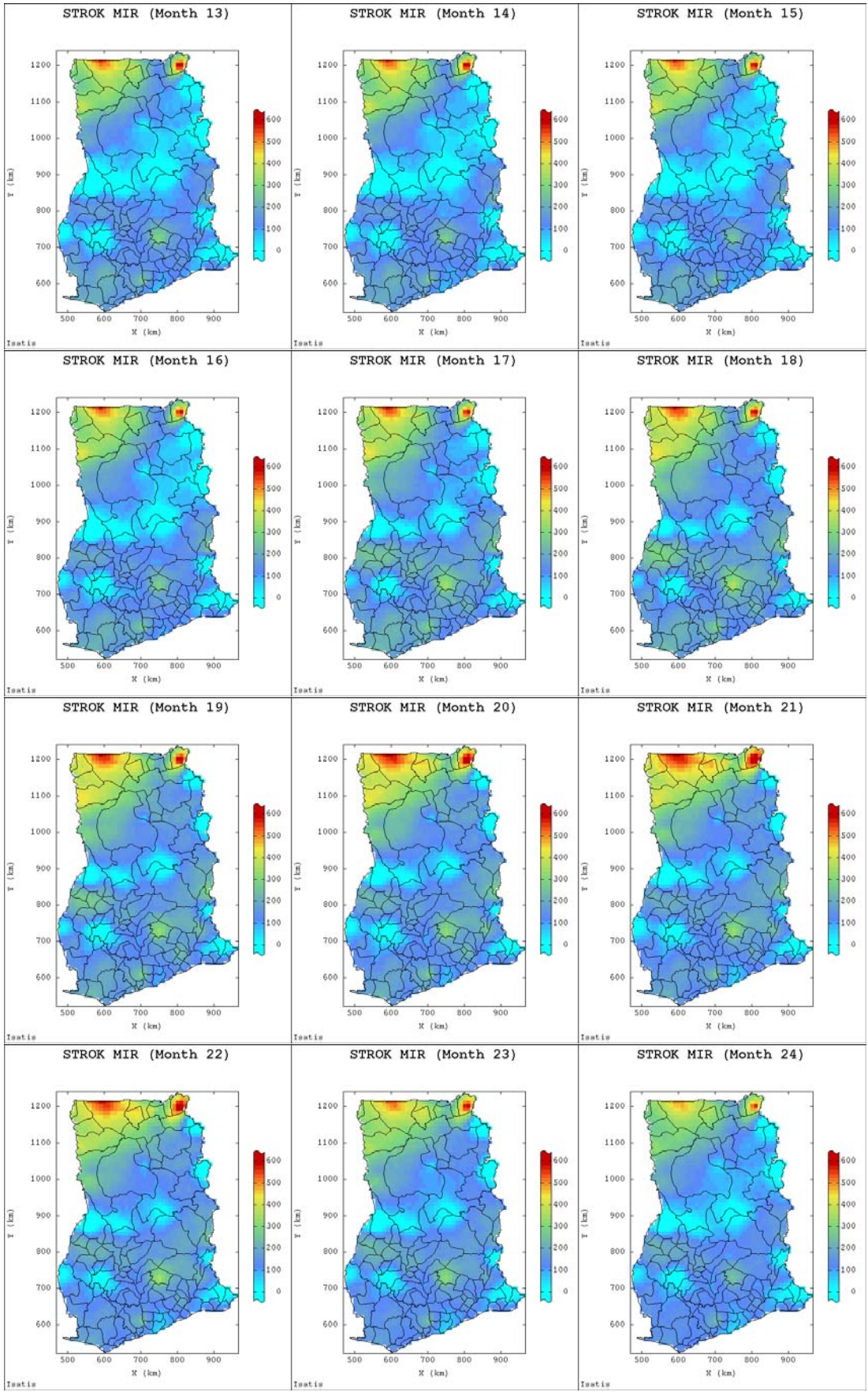


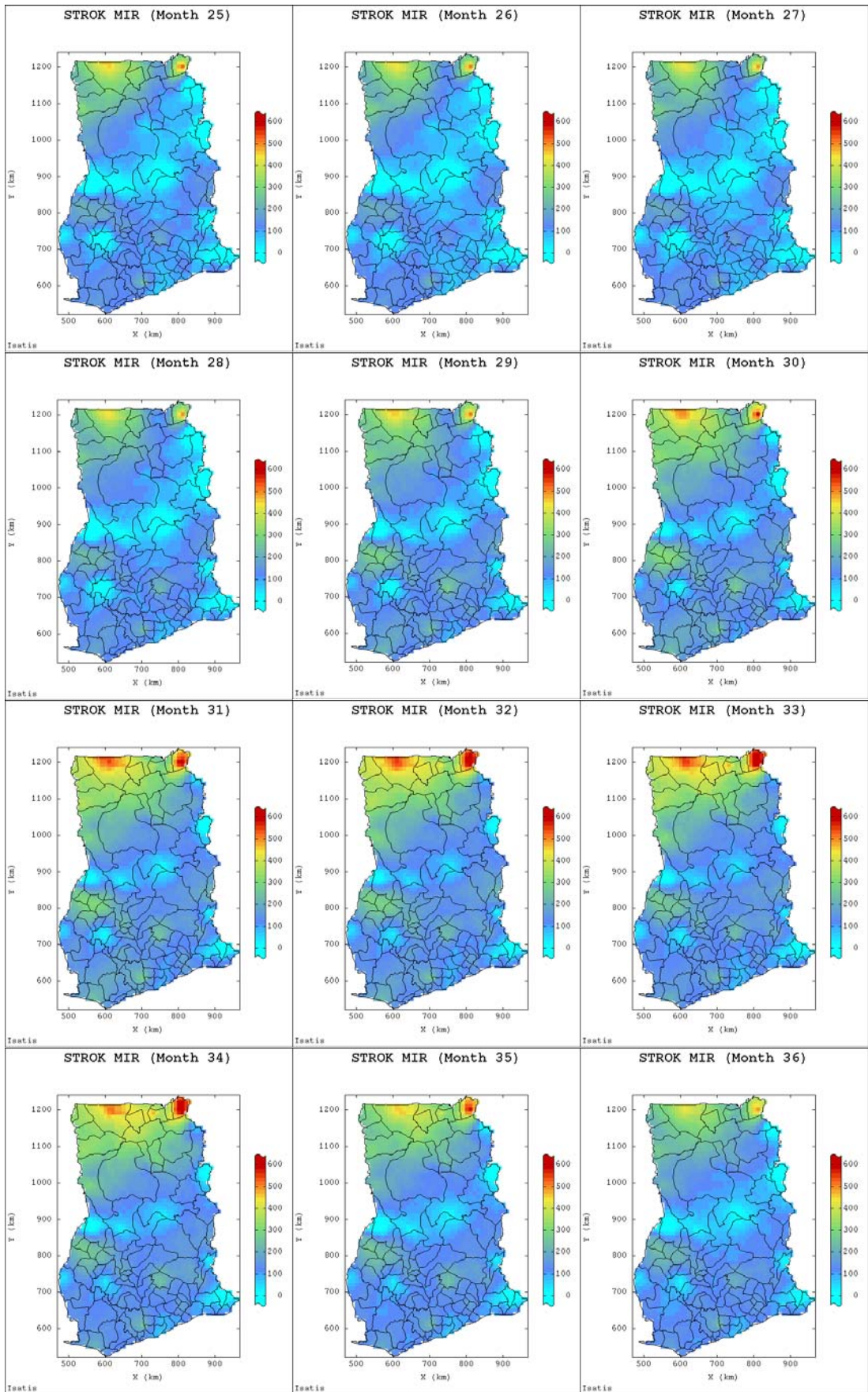


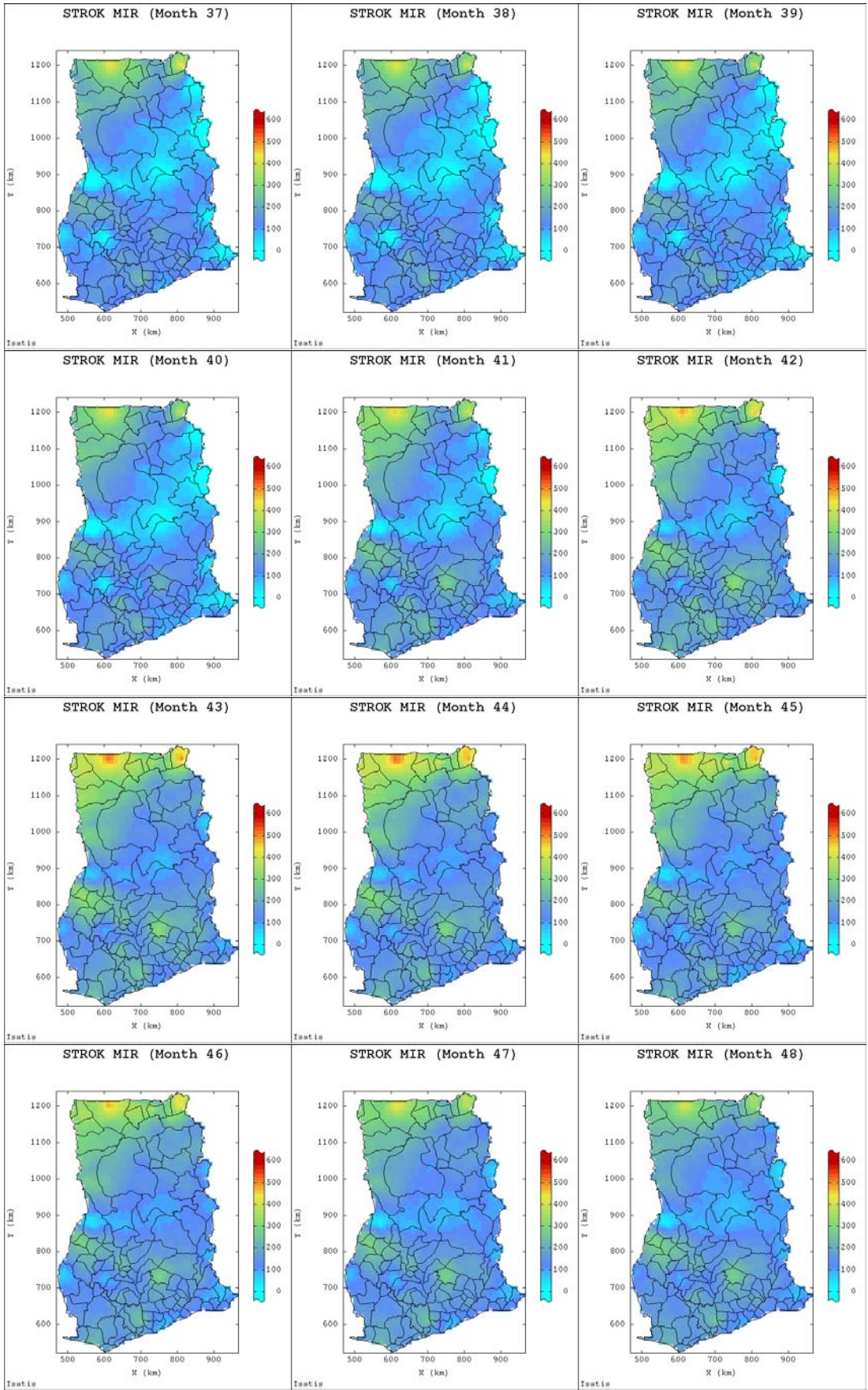


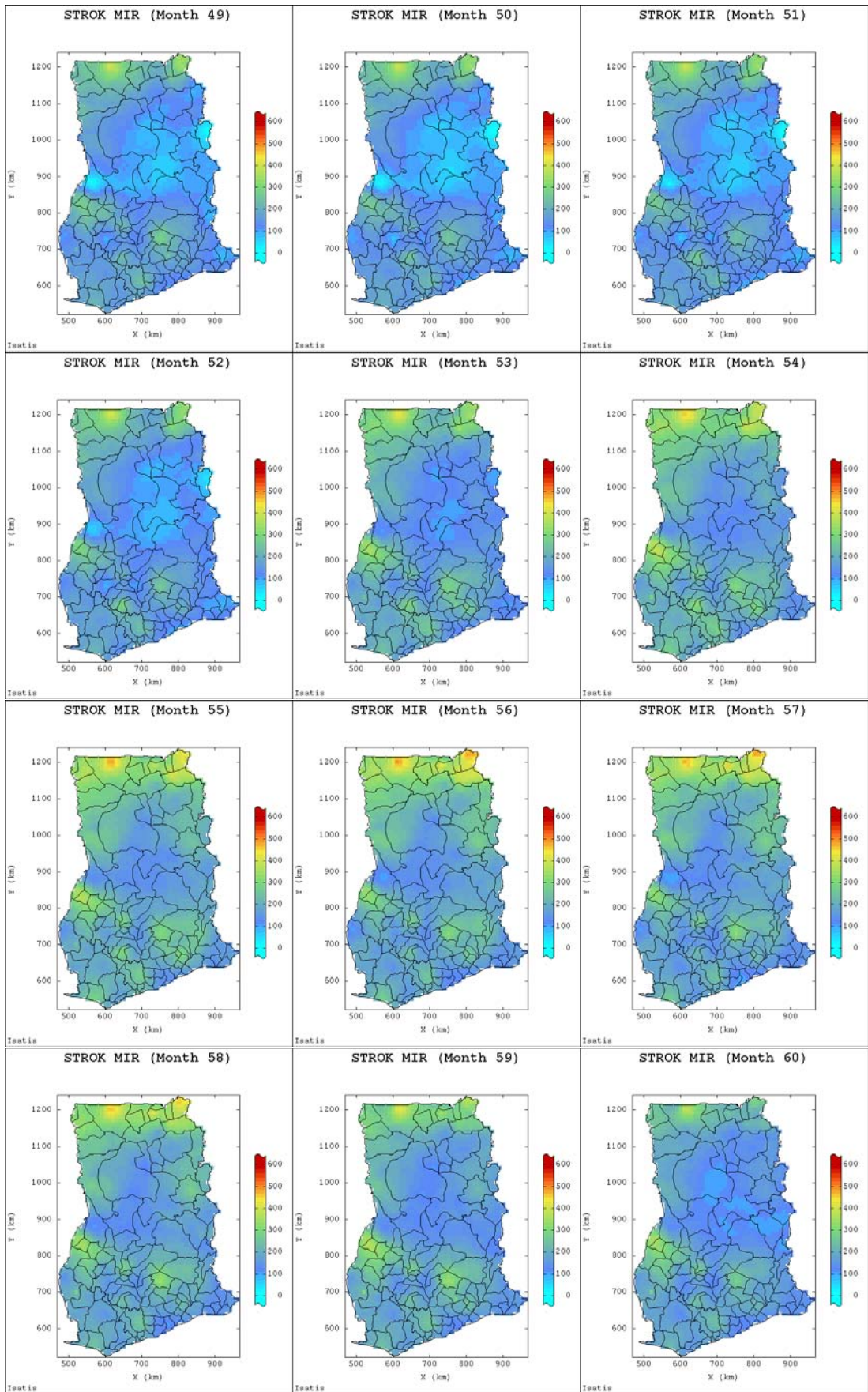
E-5.2 STROK Produced Spatial Maps

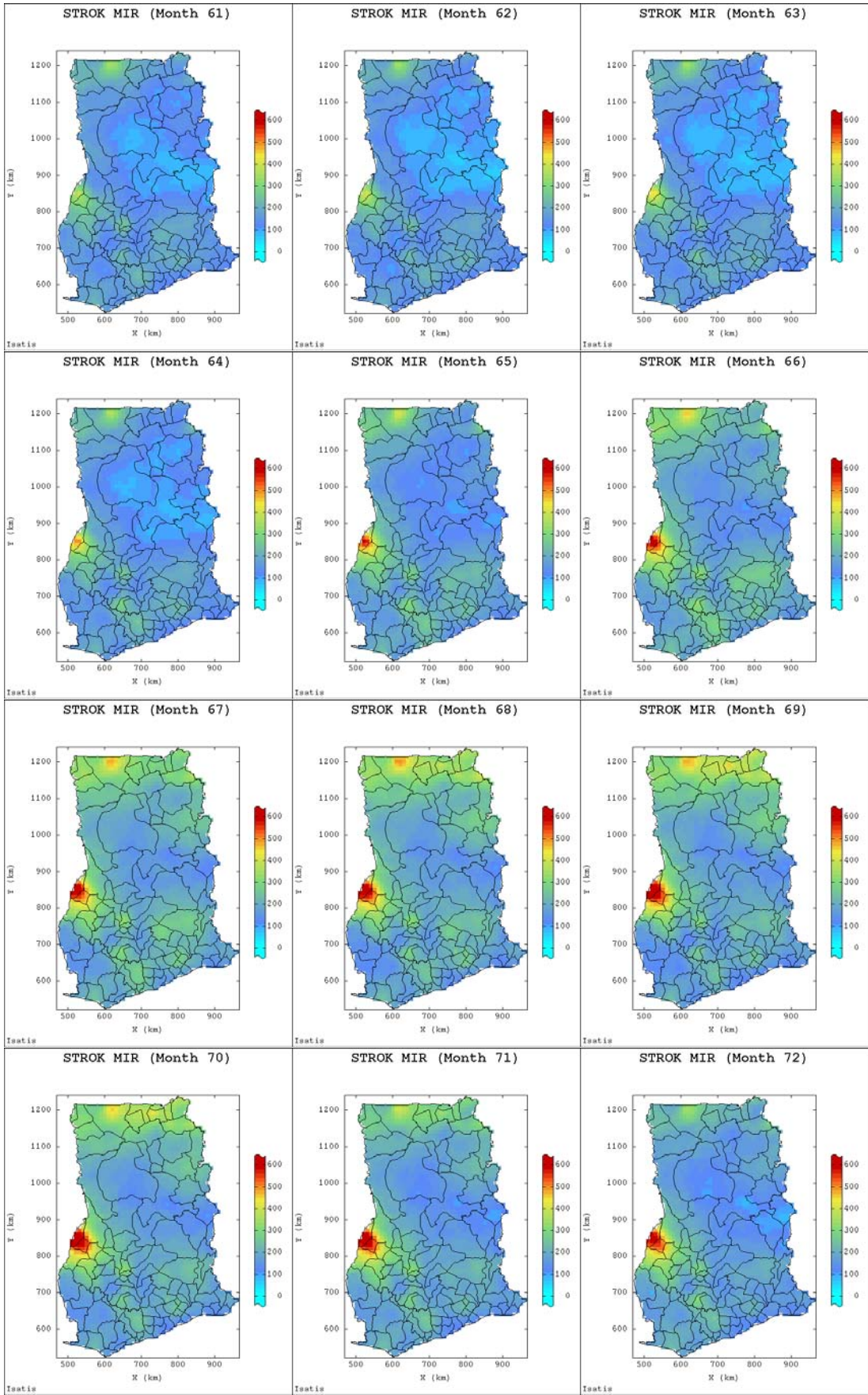


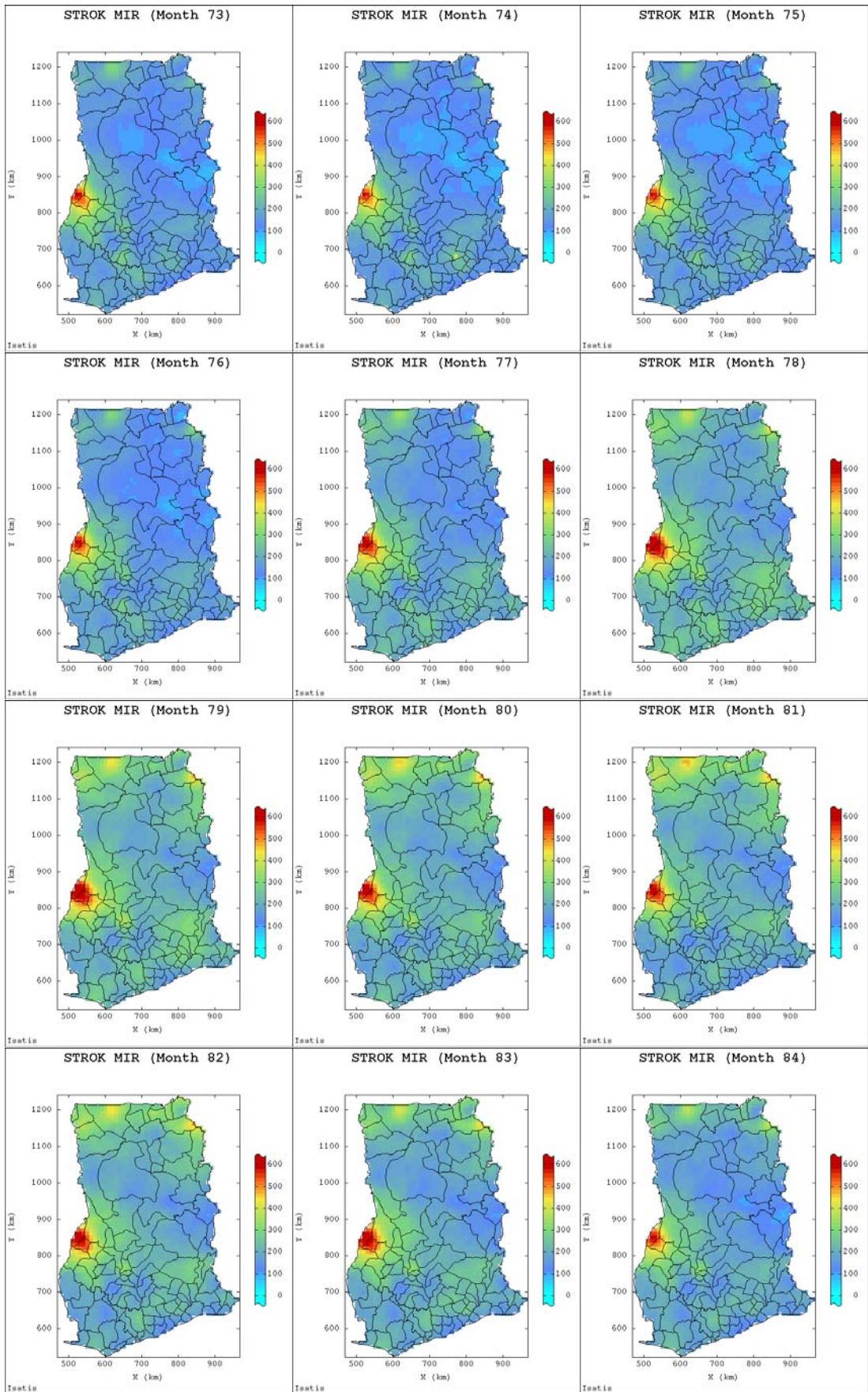


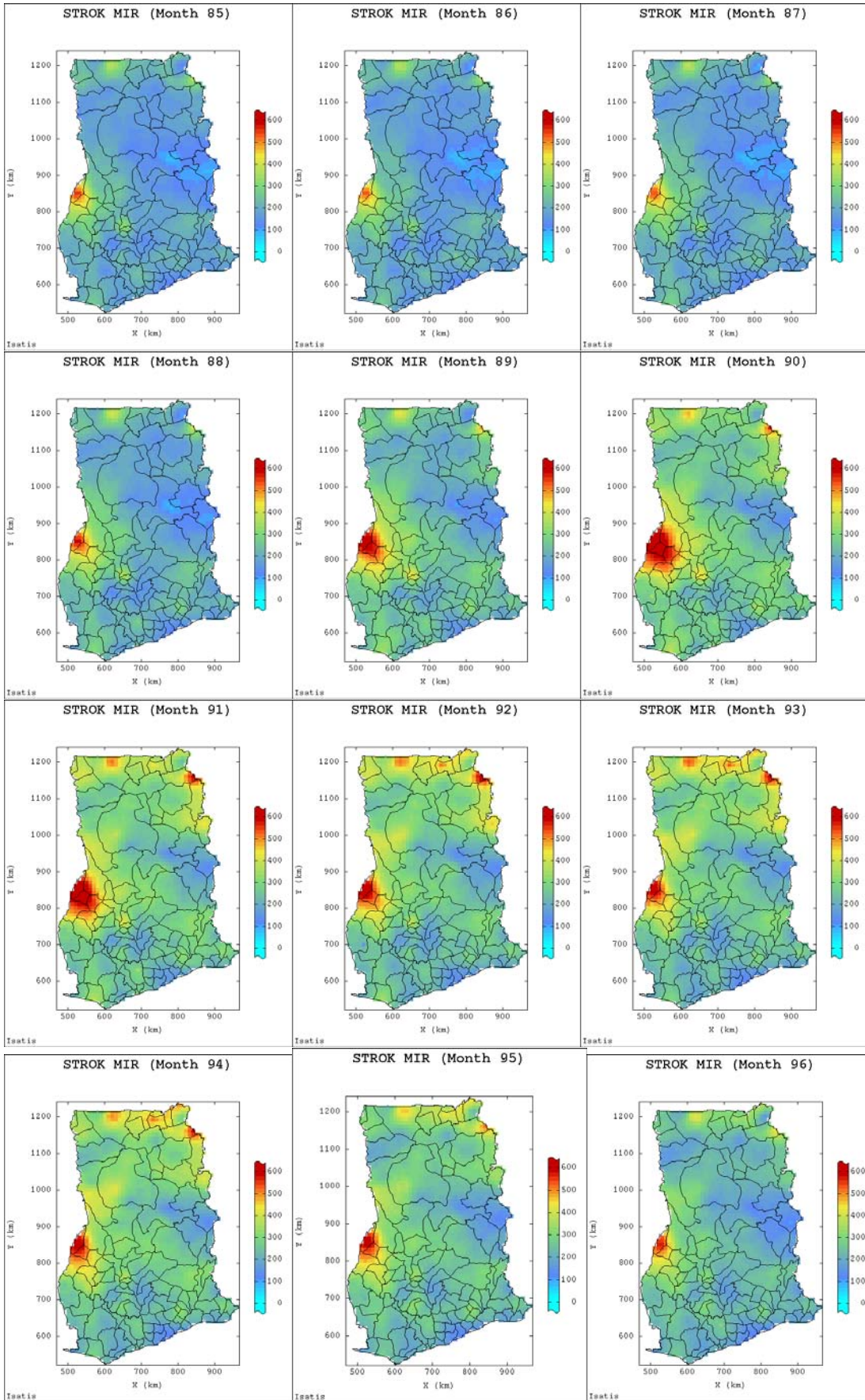


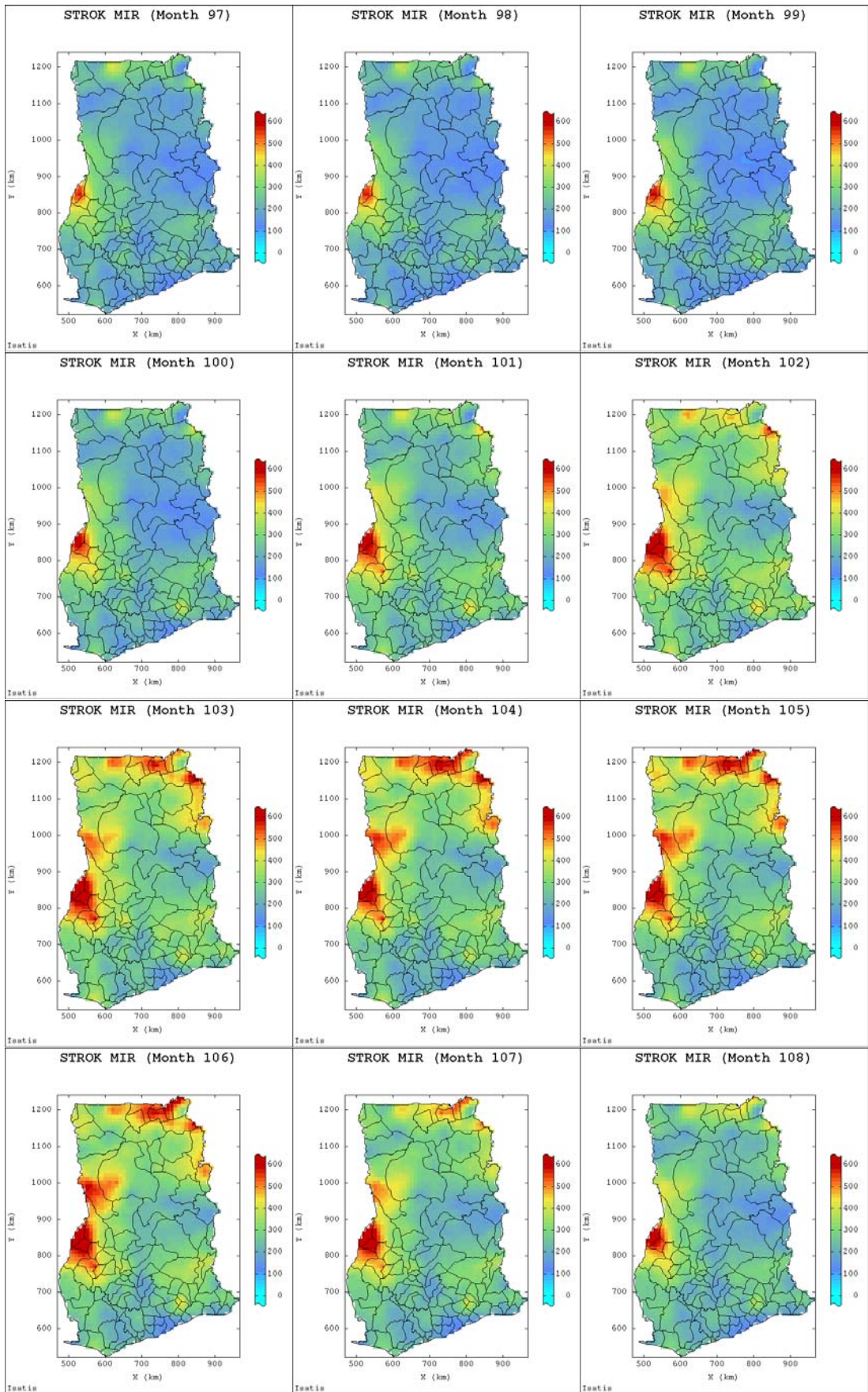


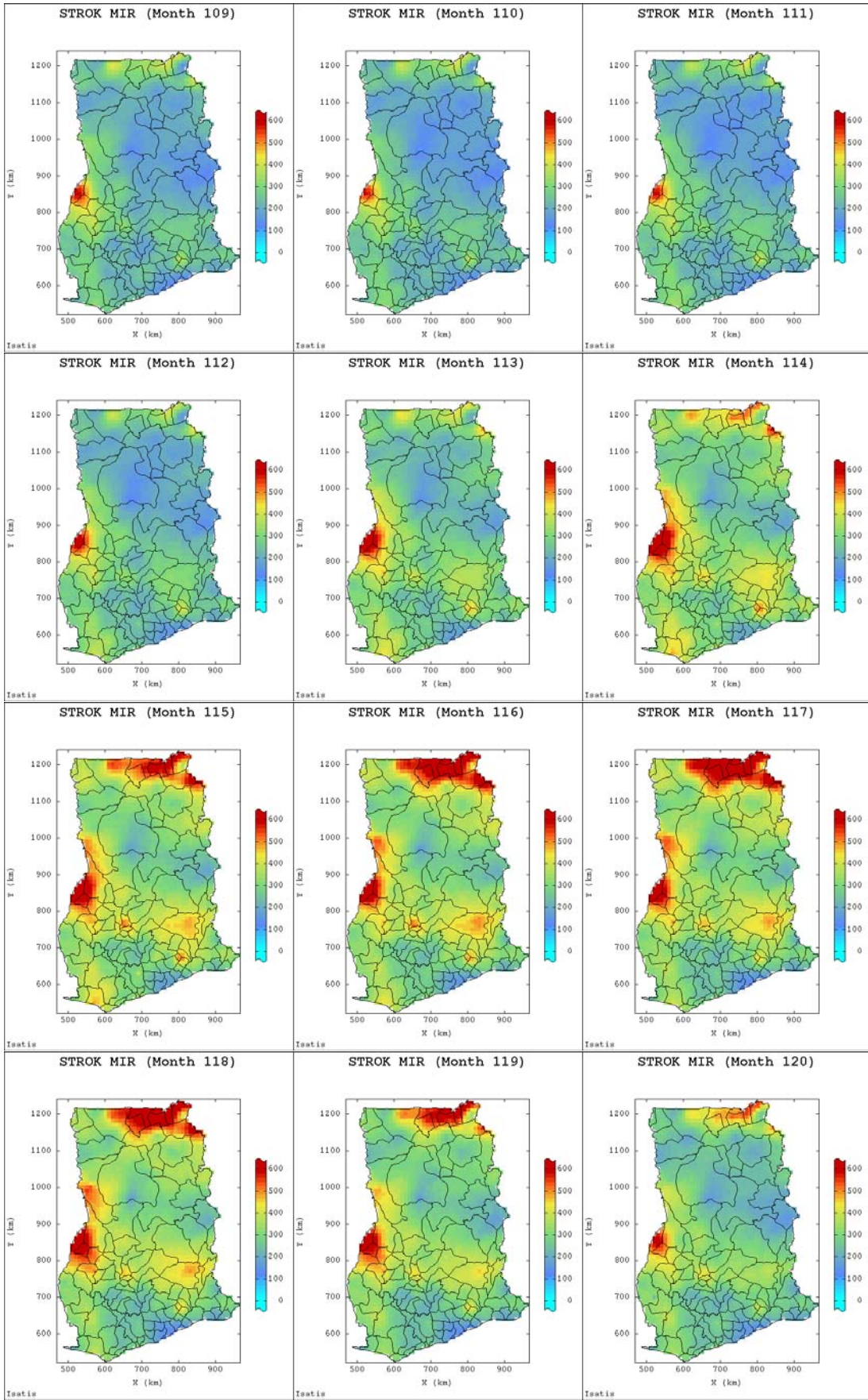


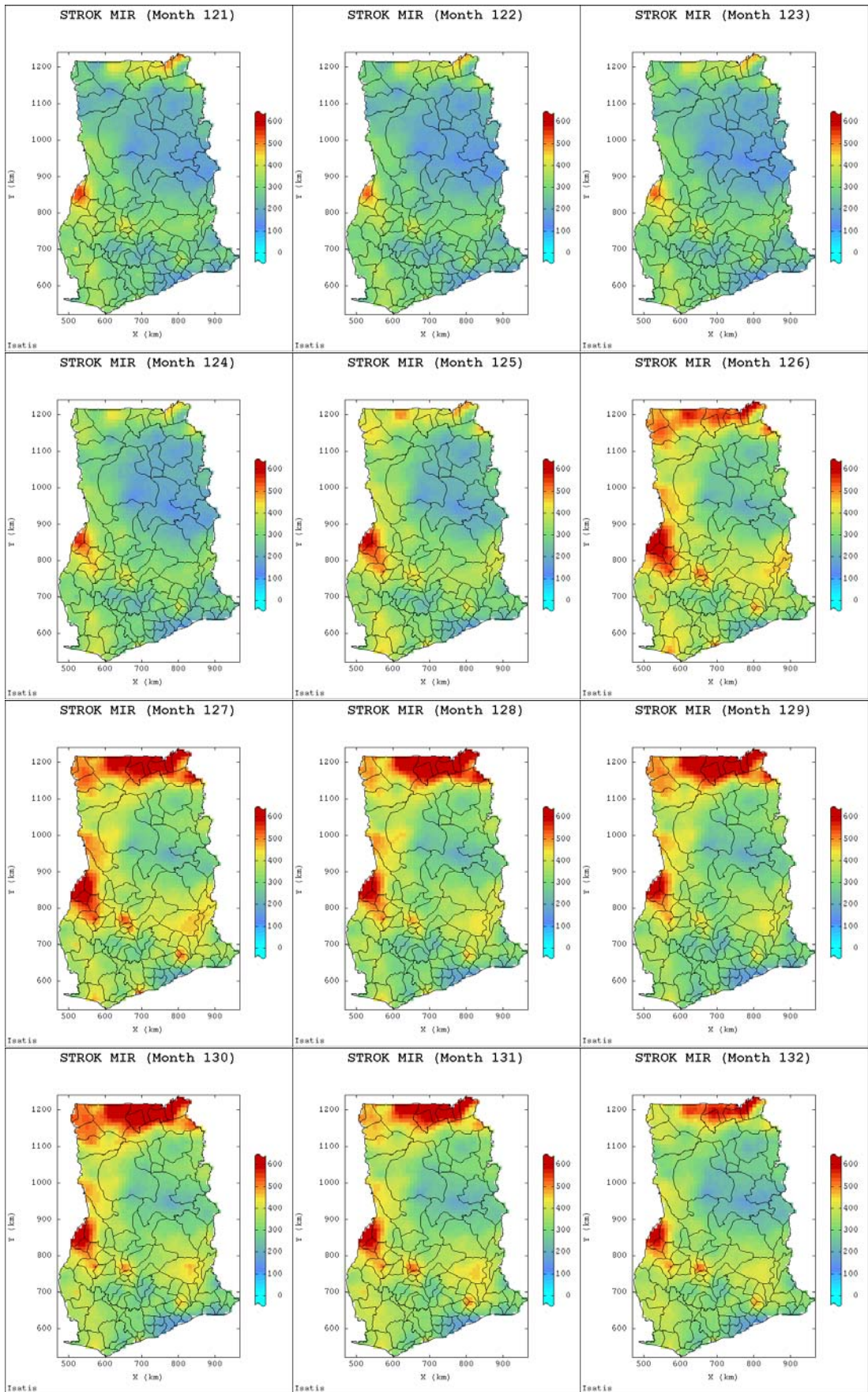




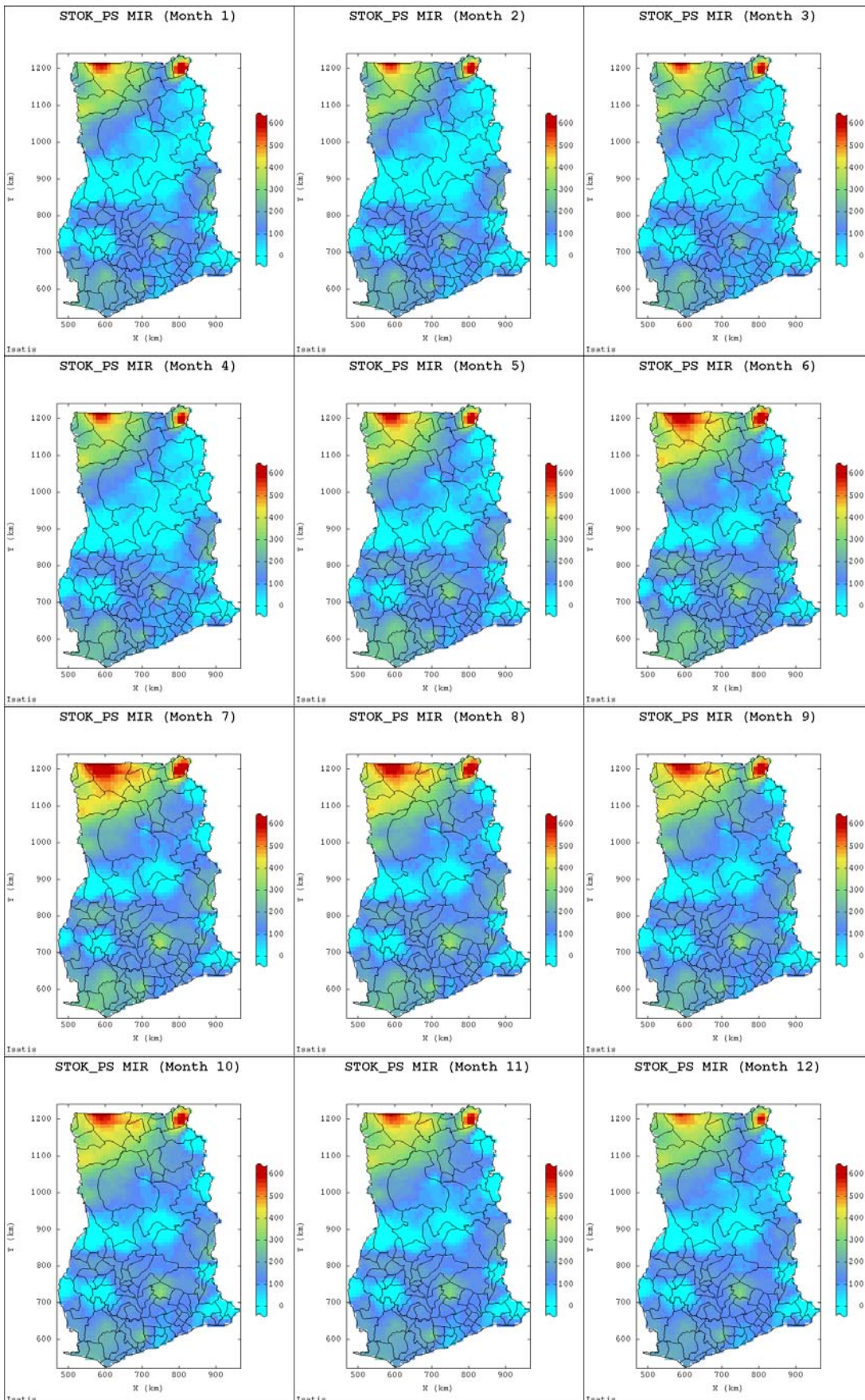


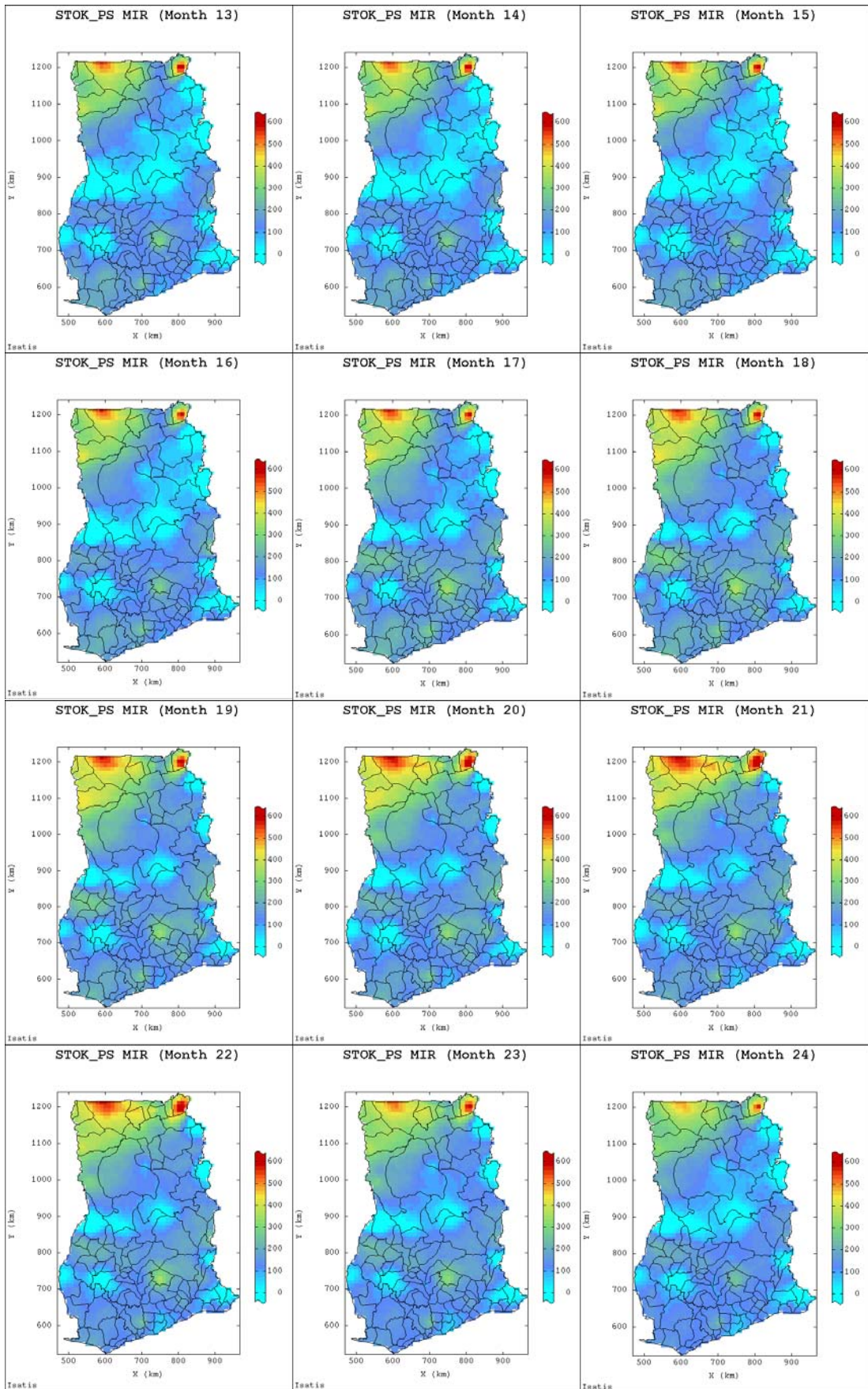


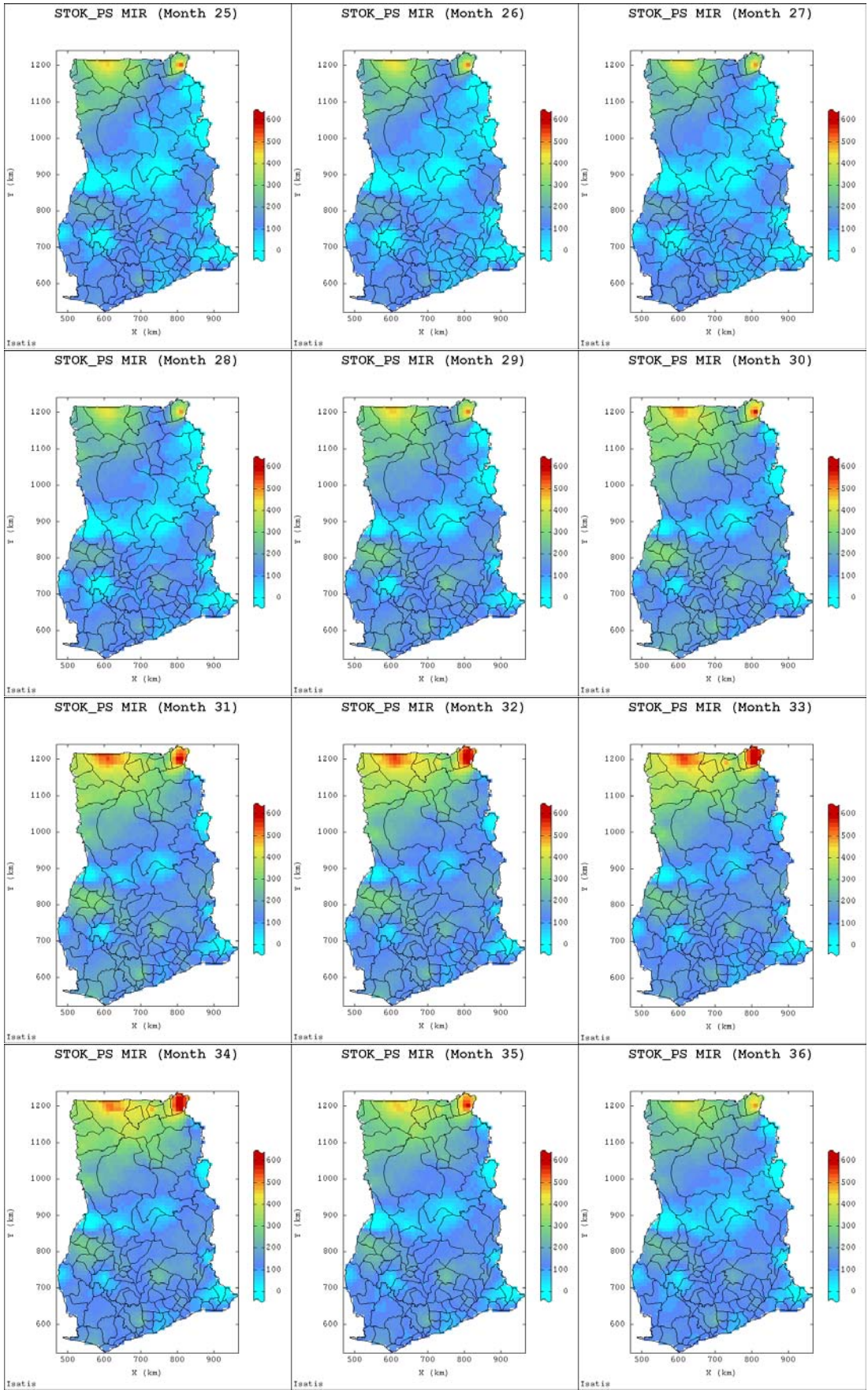


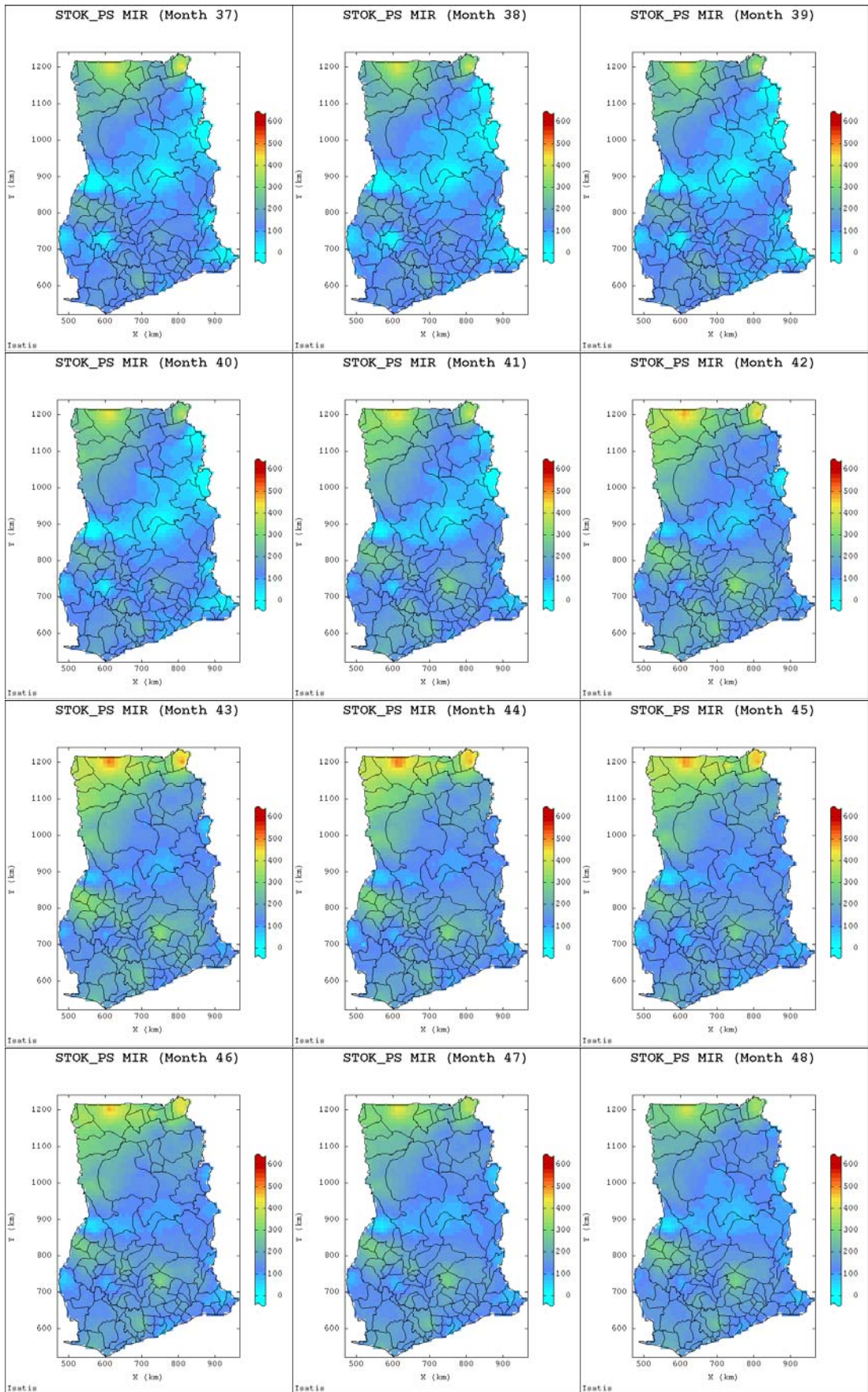


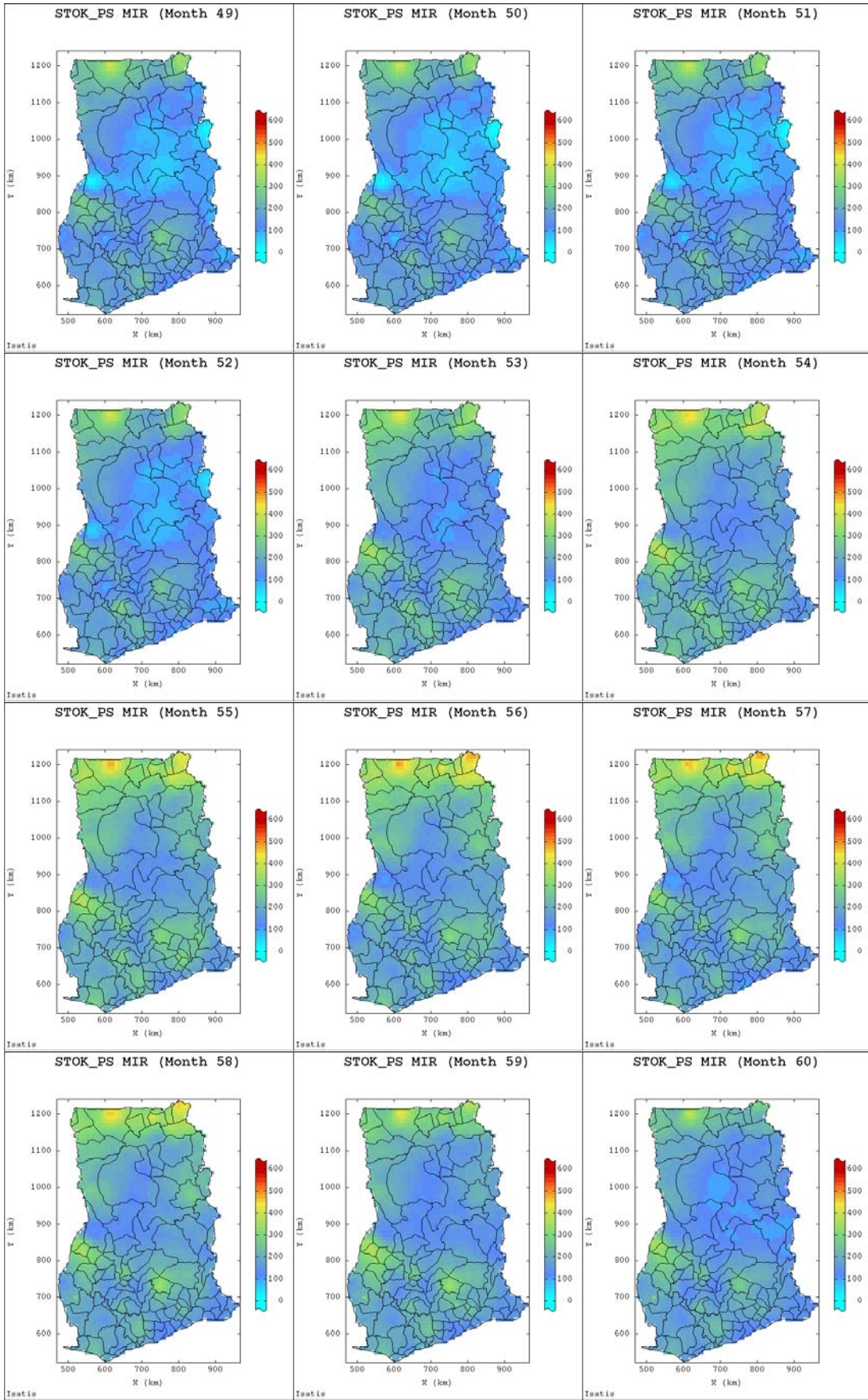
E-5.3 STOK_PS Produced Spatial Maps

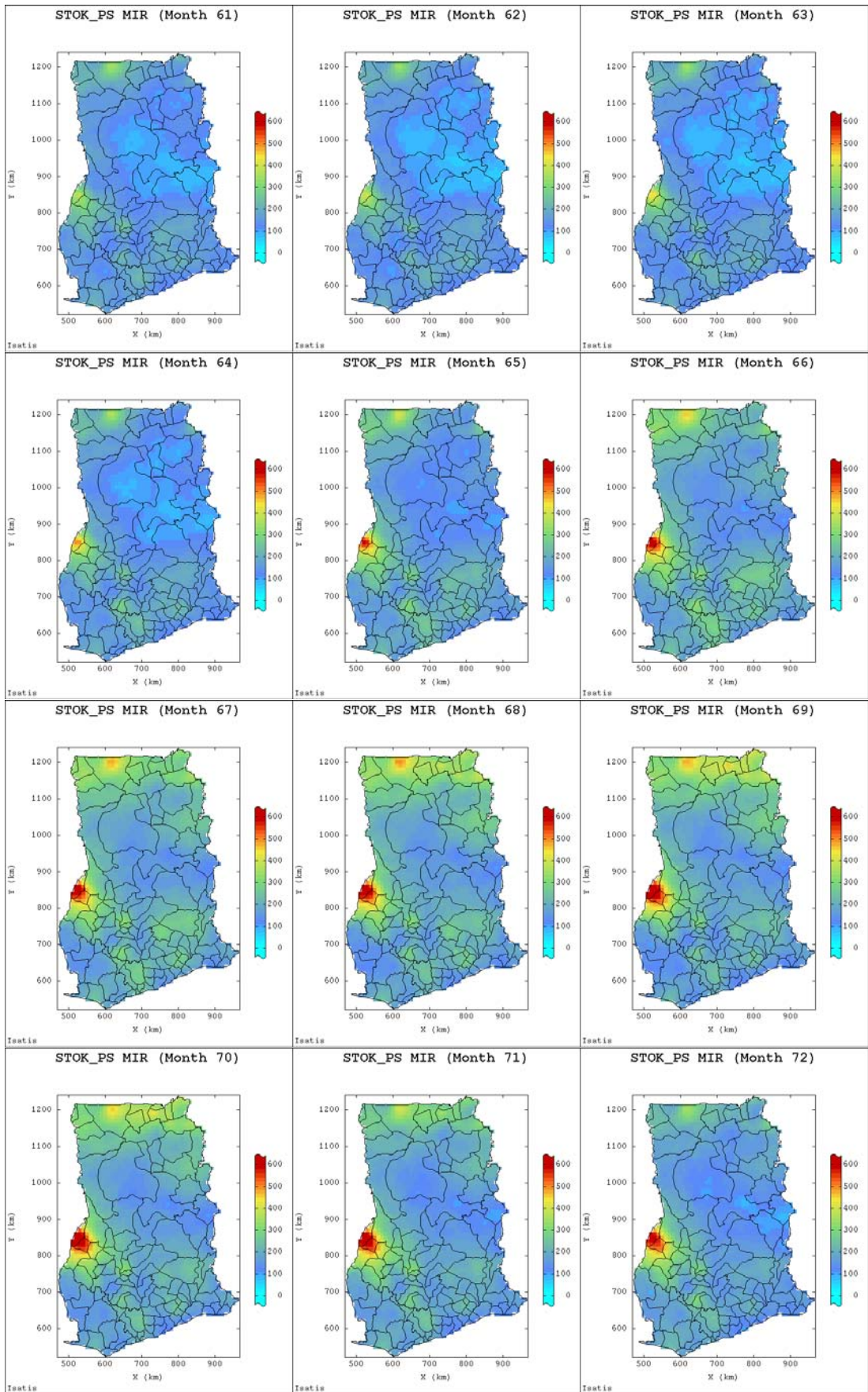


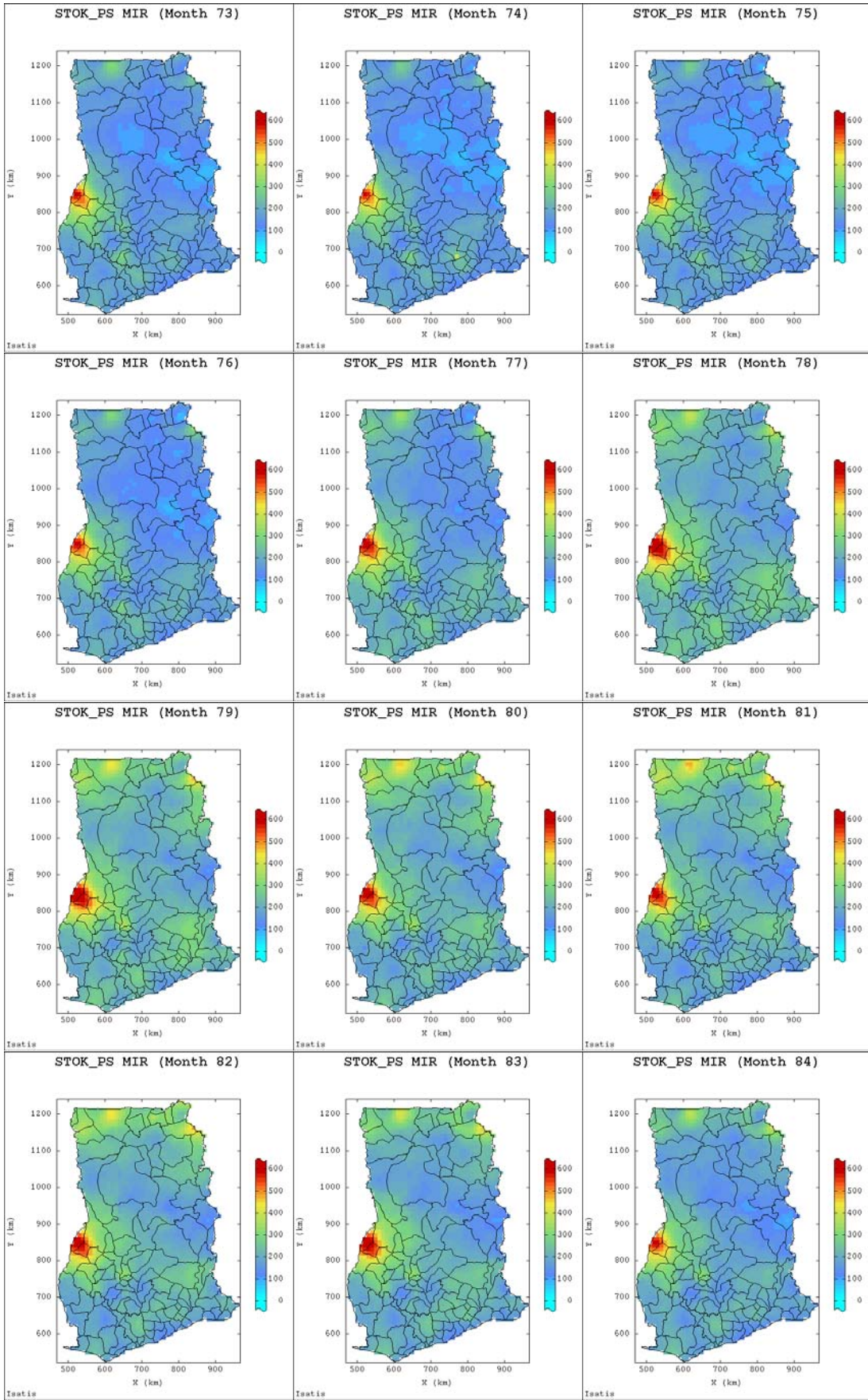


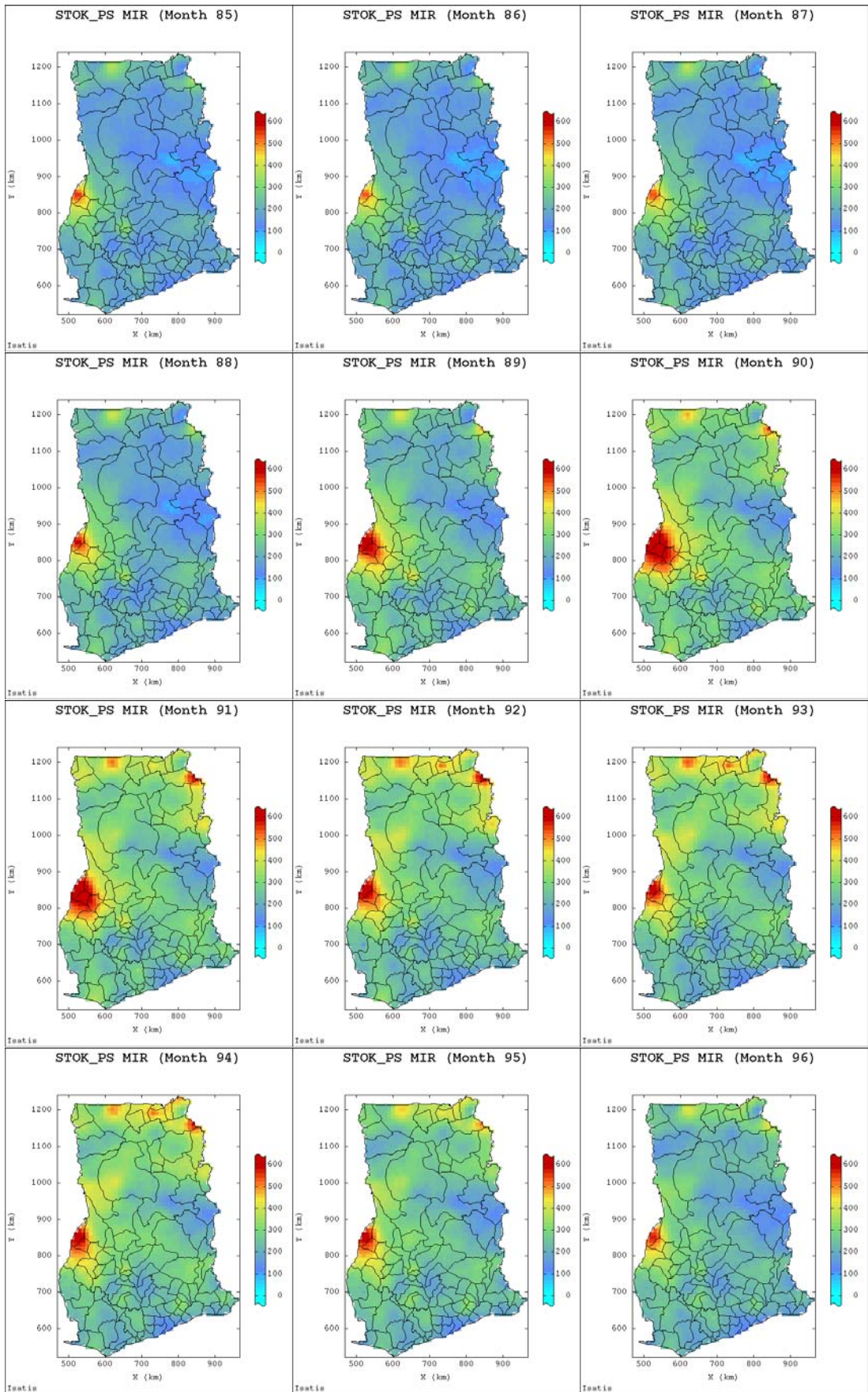


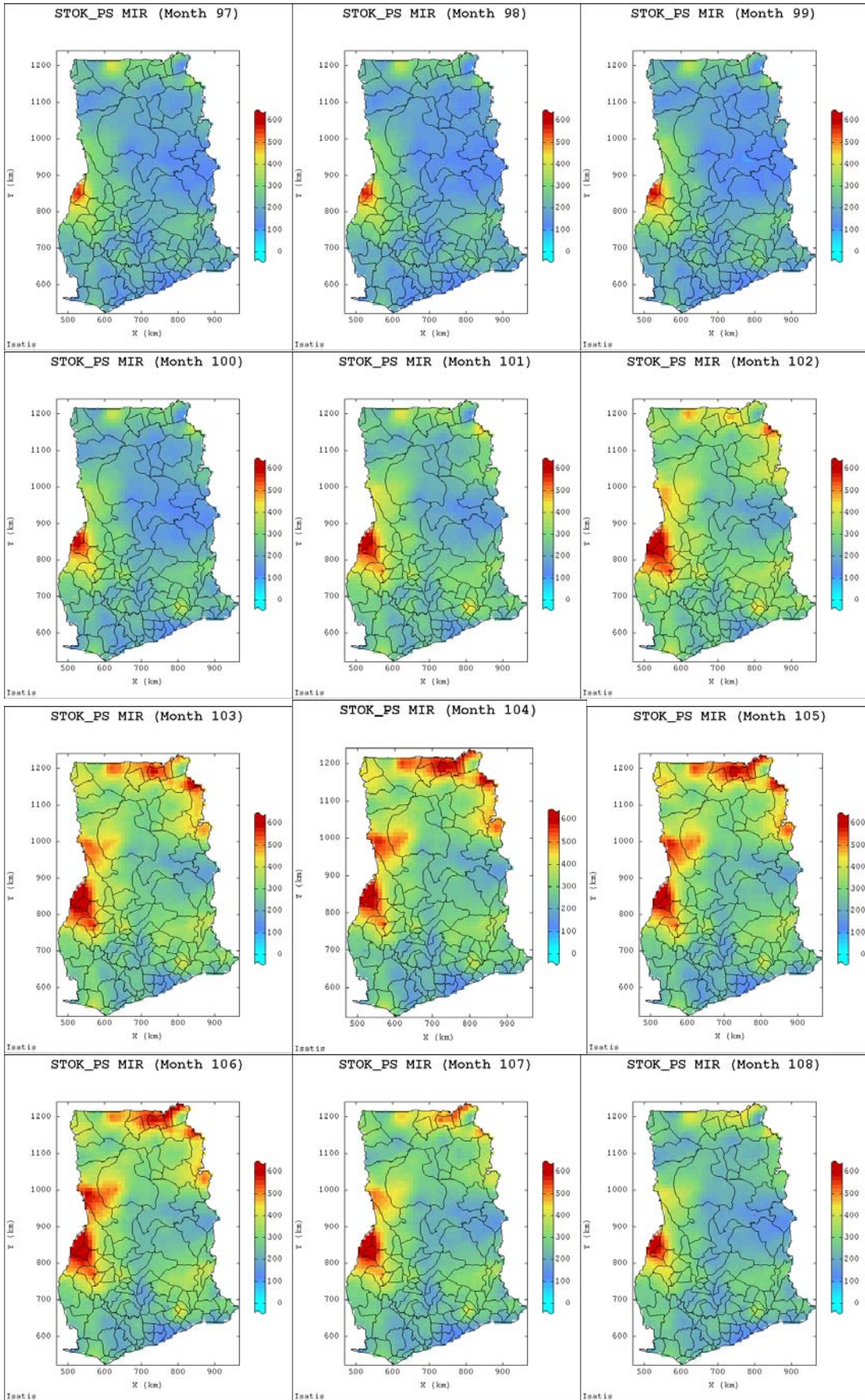


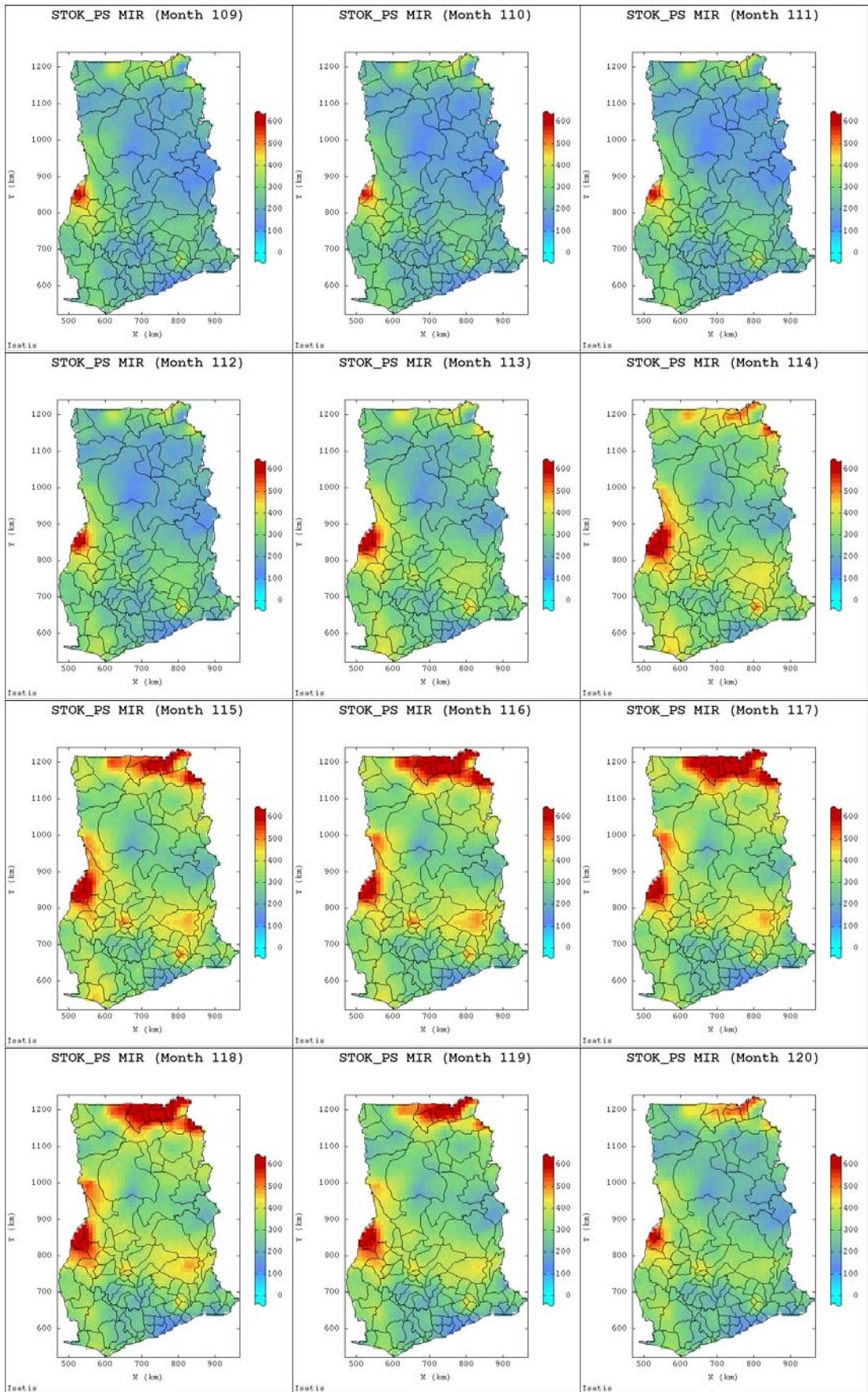


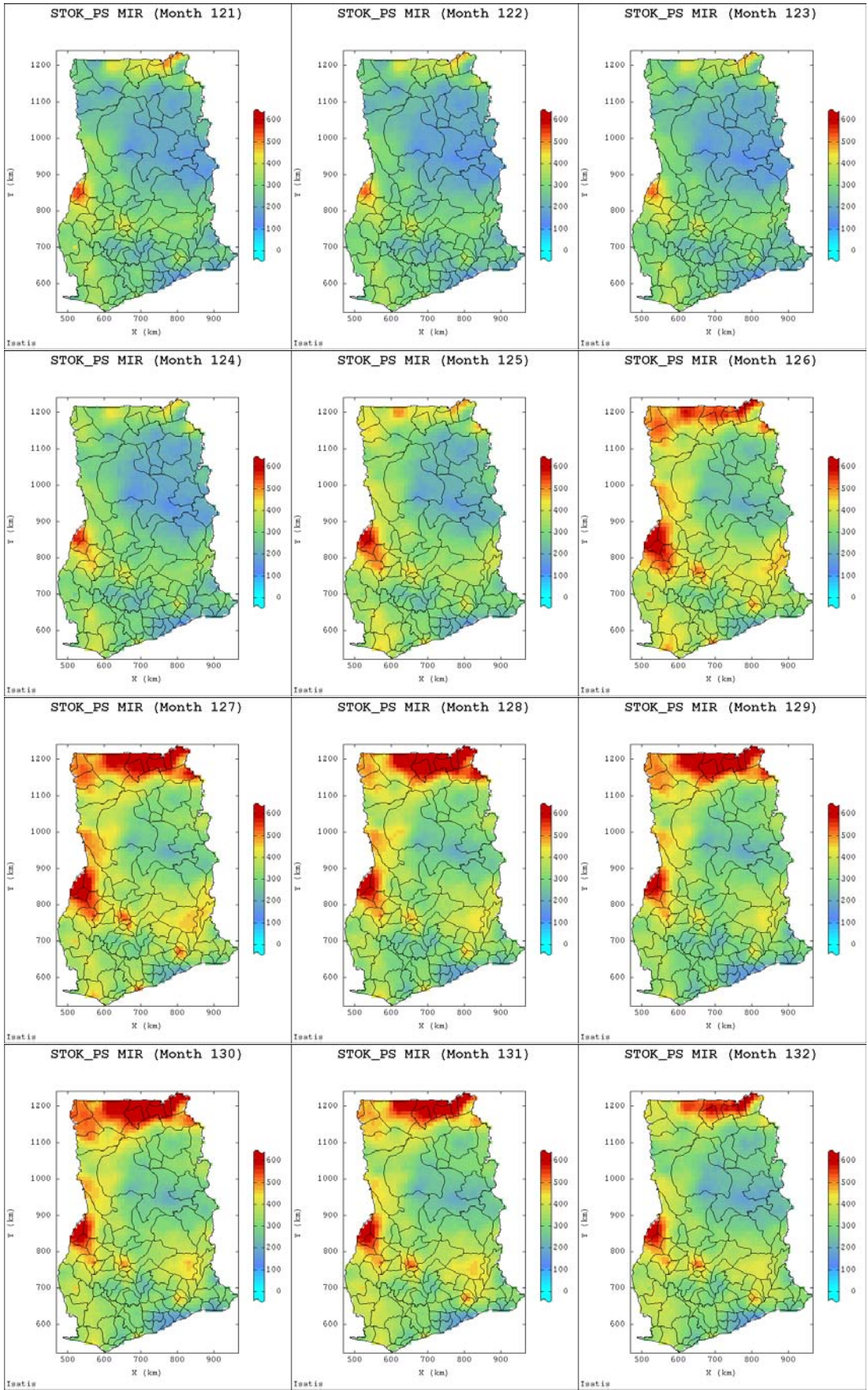




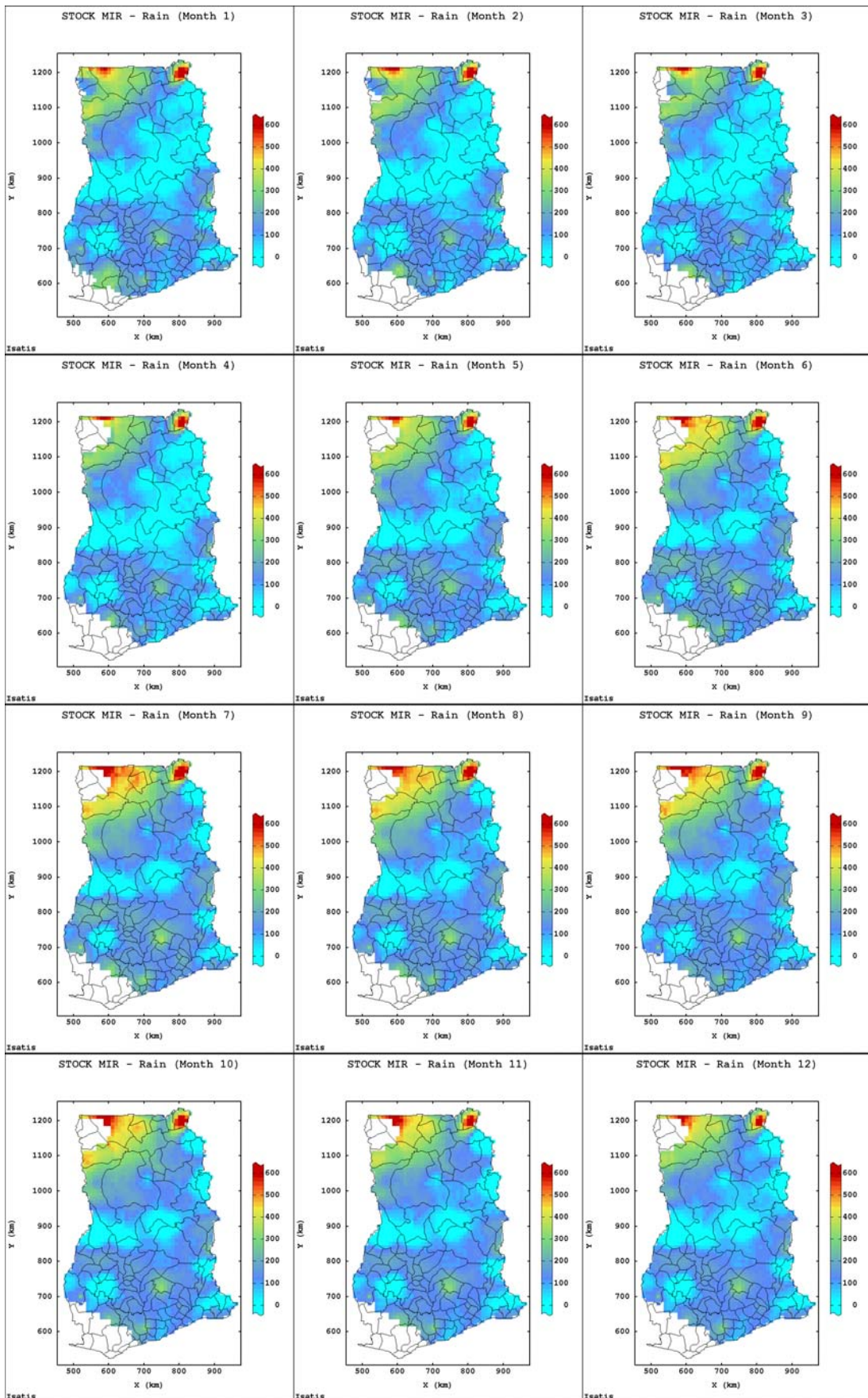


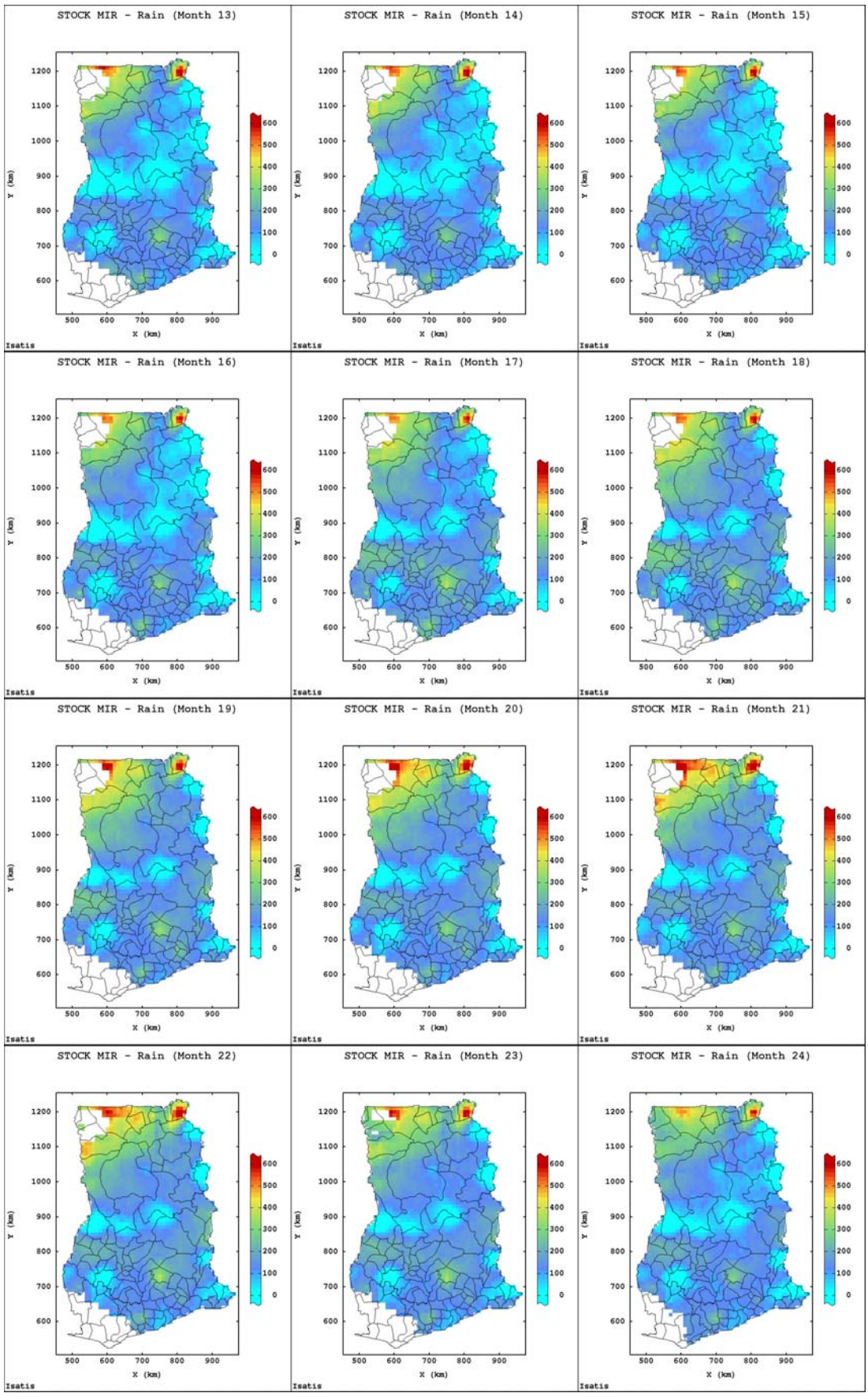


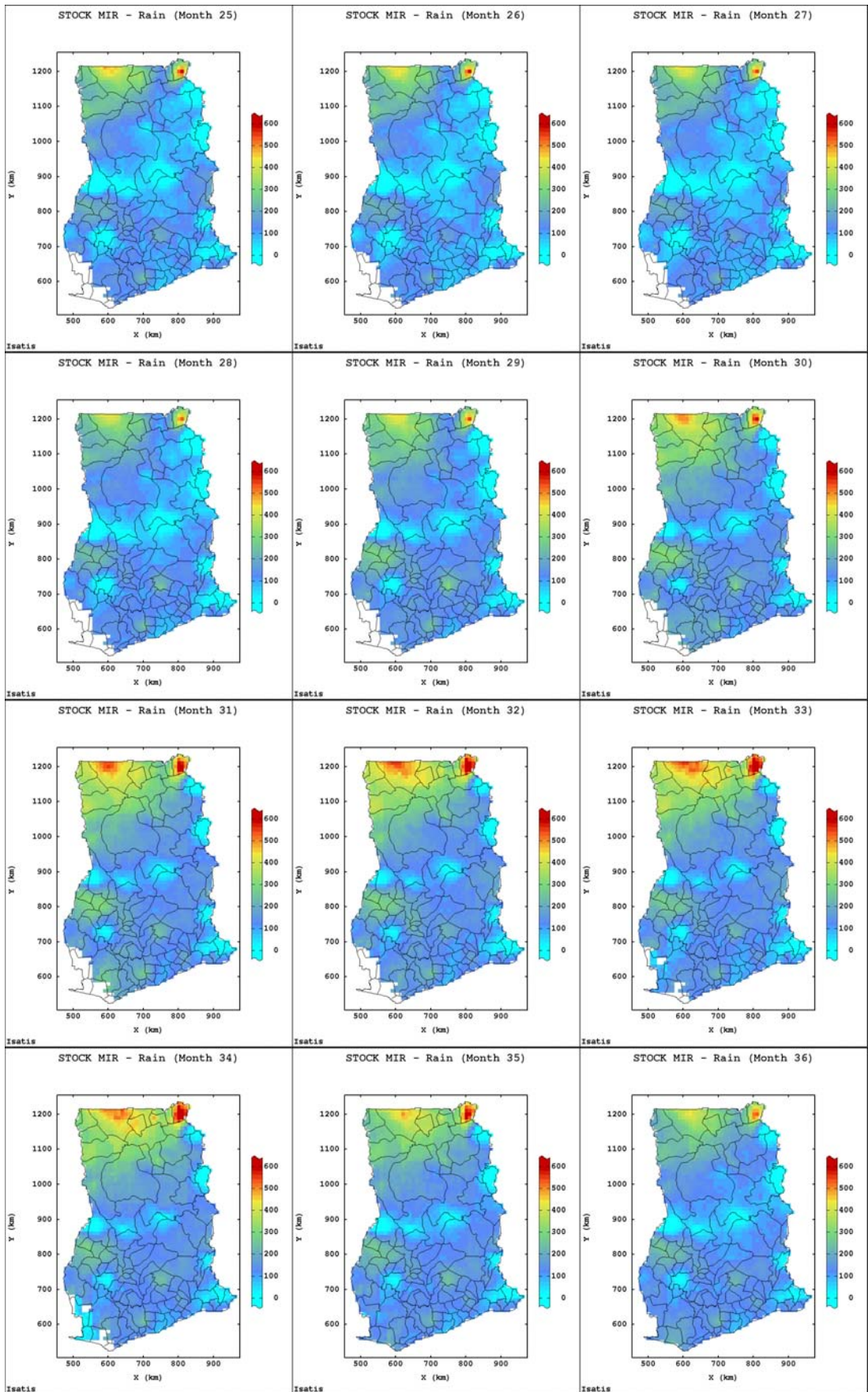


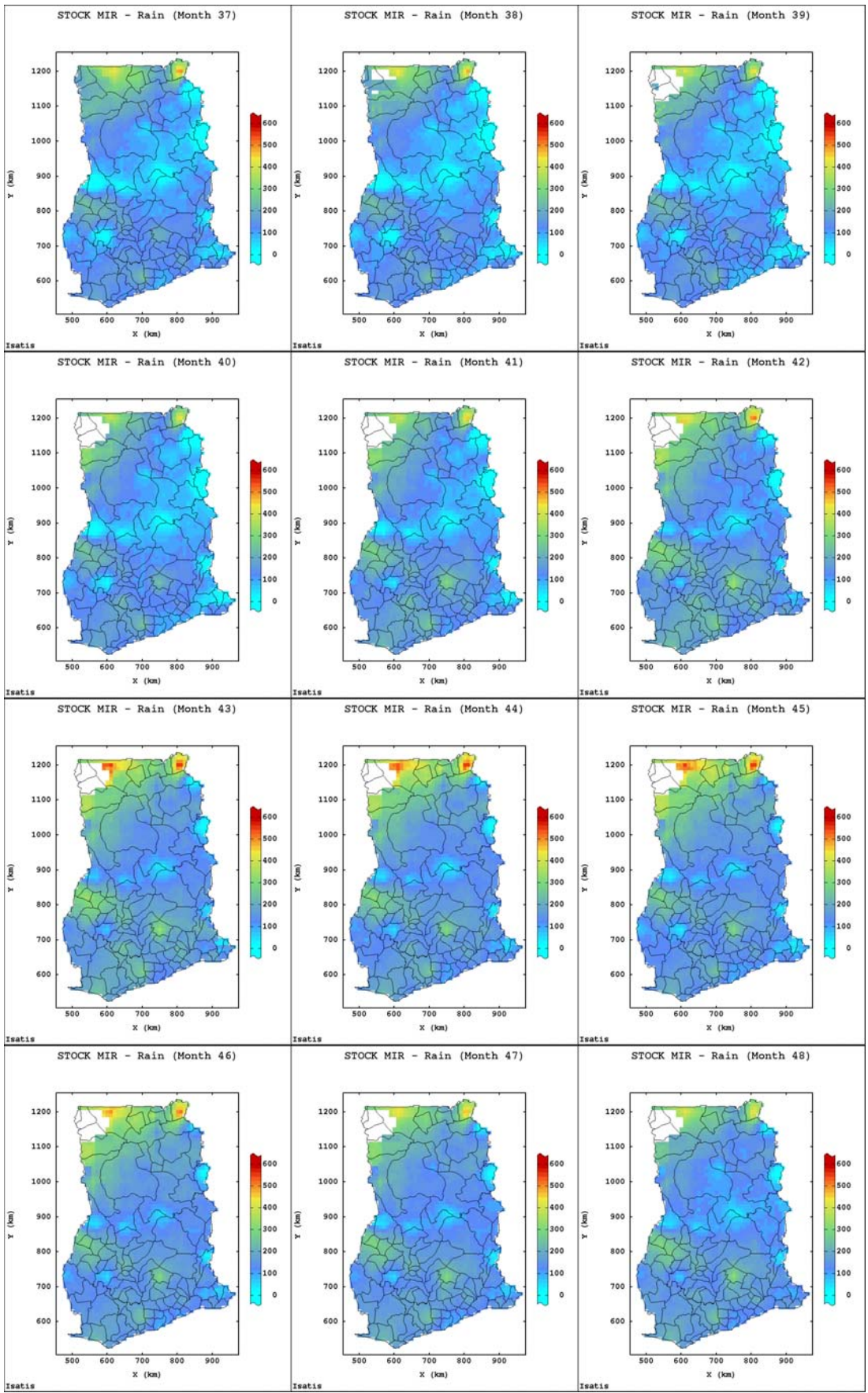


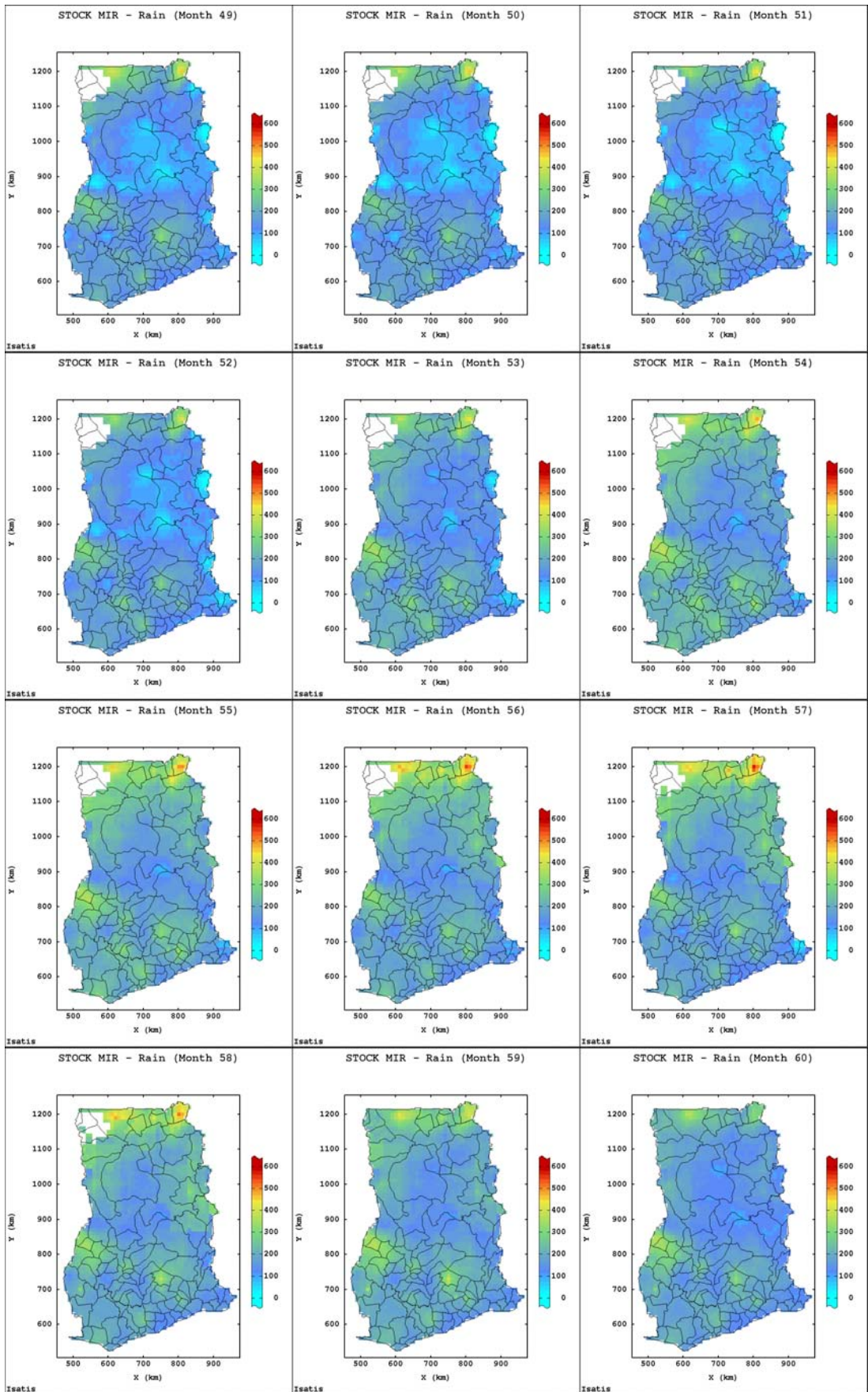
E-5.4 STOCK_Rain Produced Spatial Maps

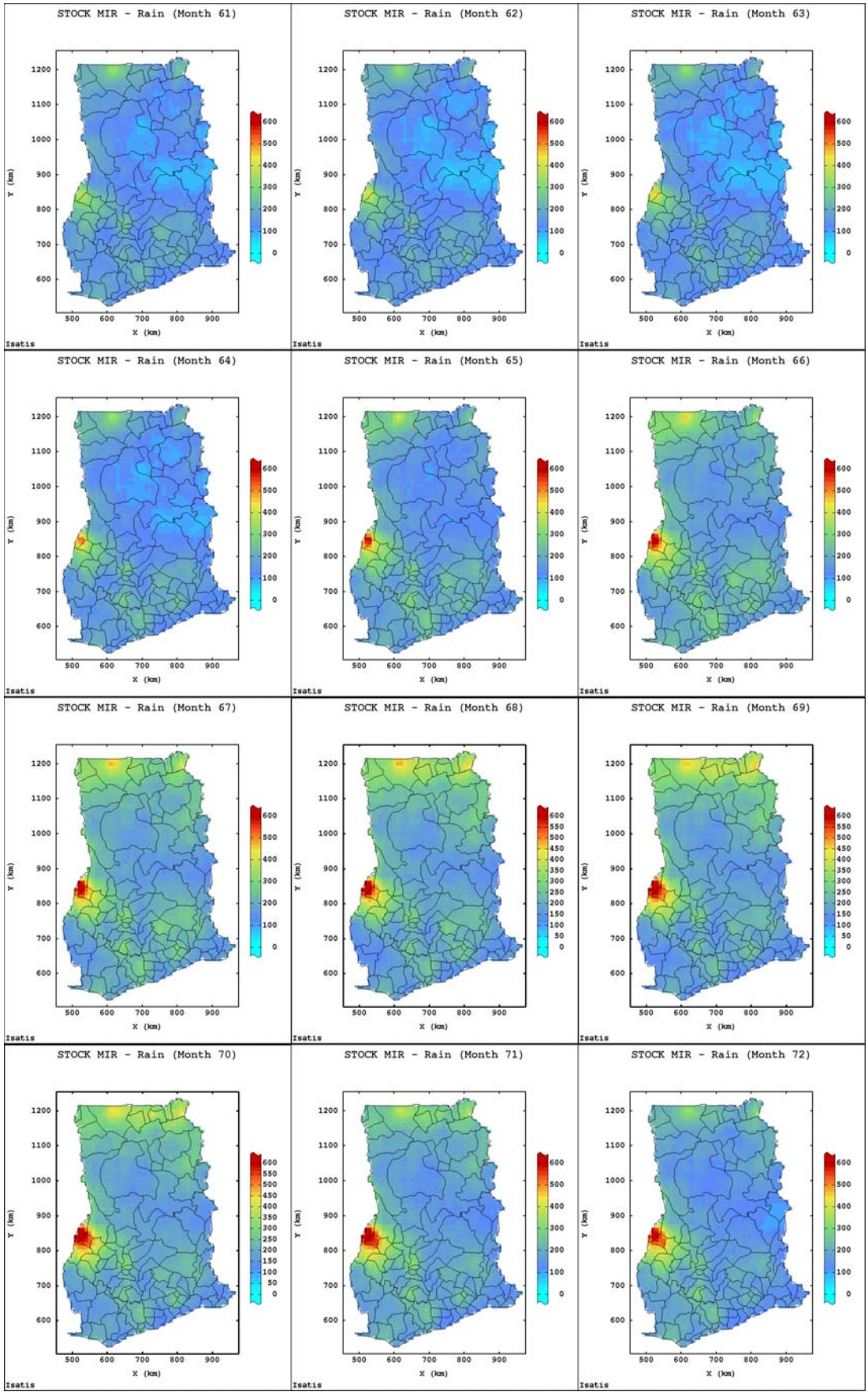


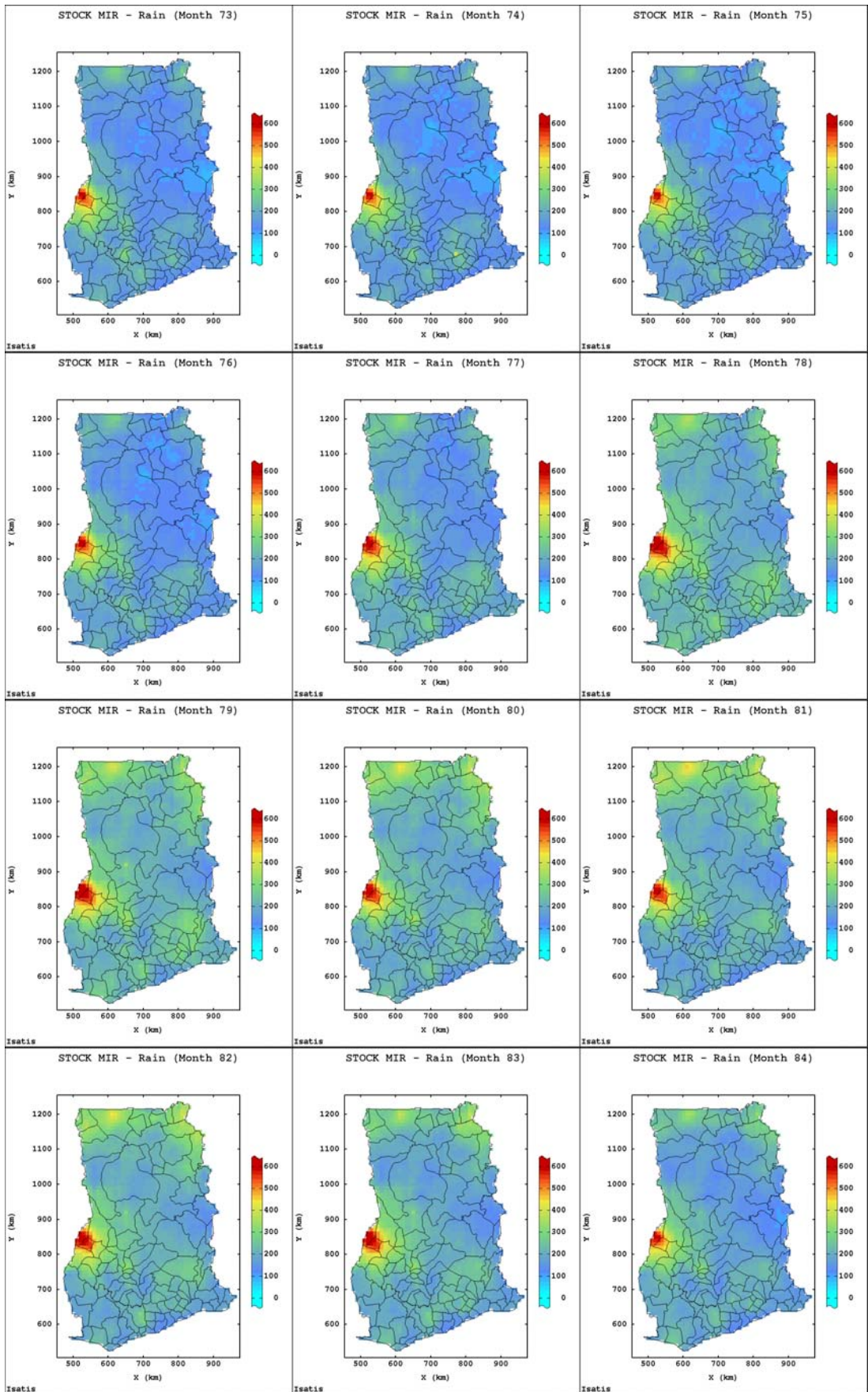


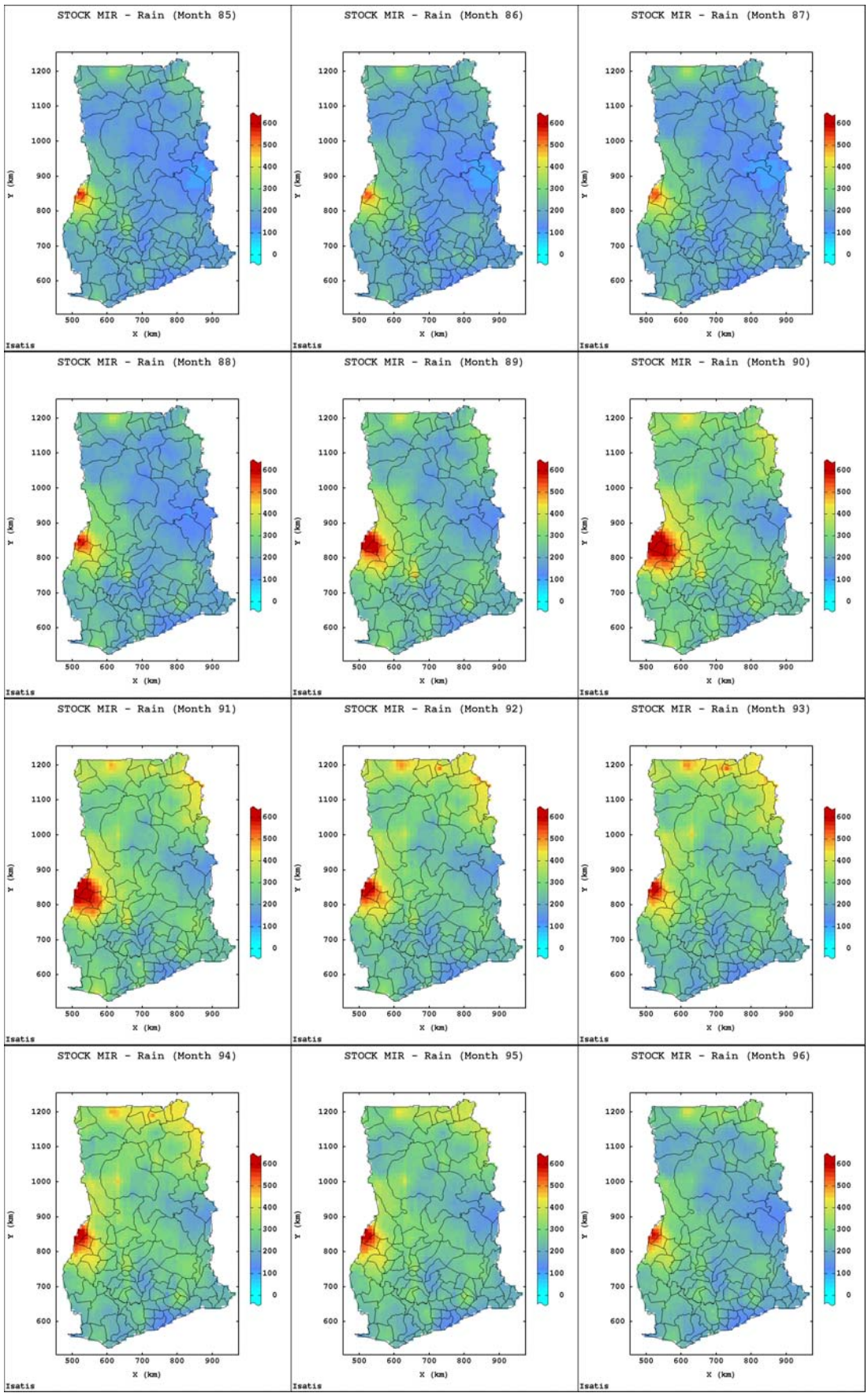


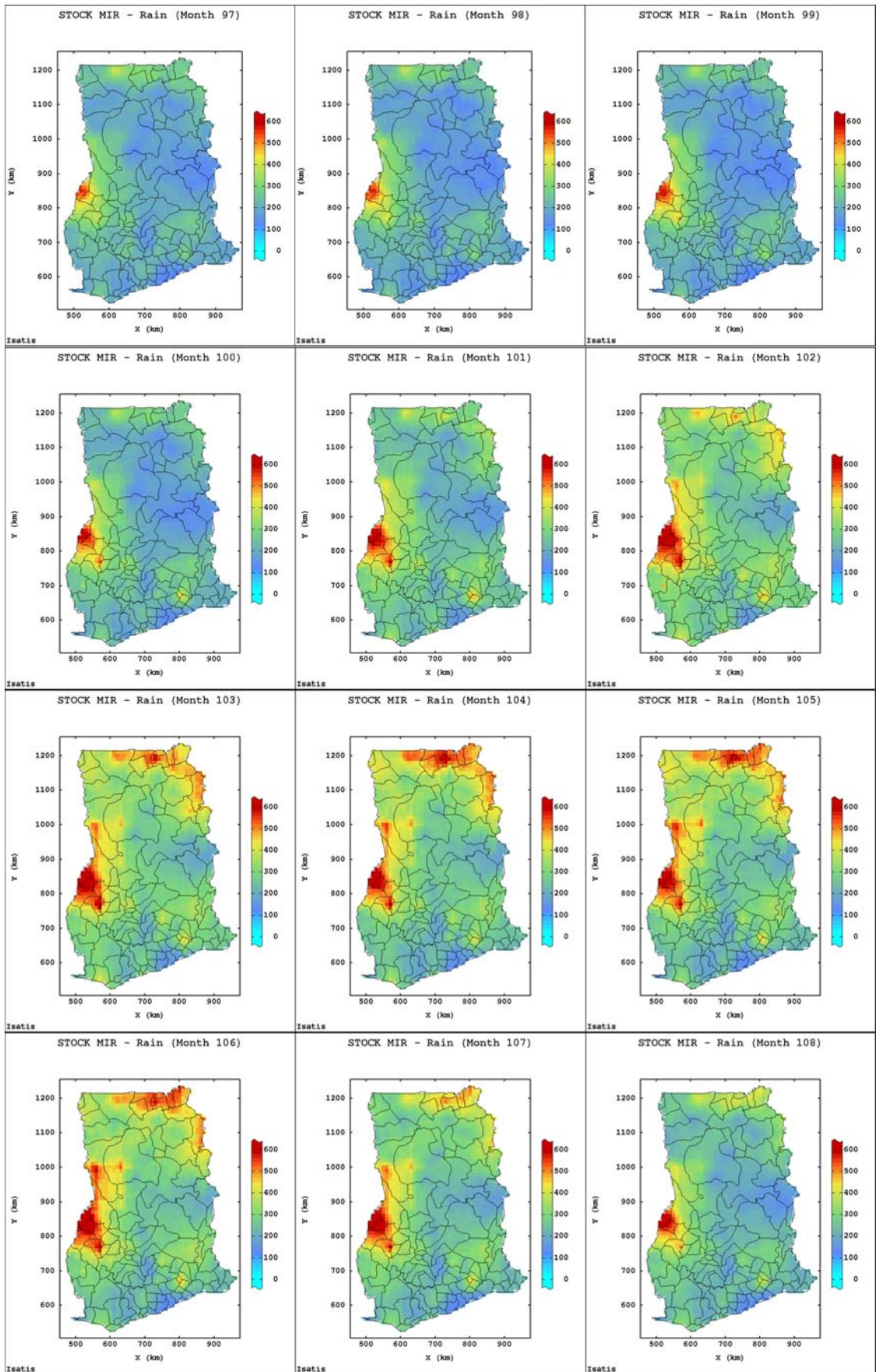


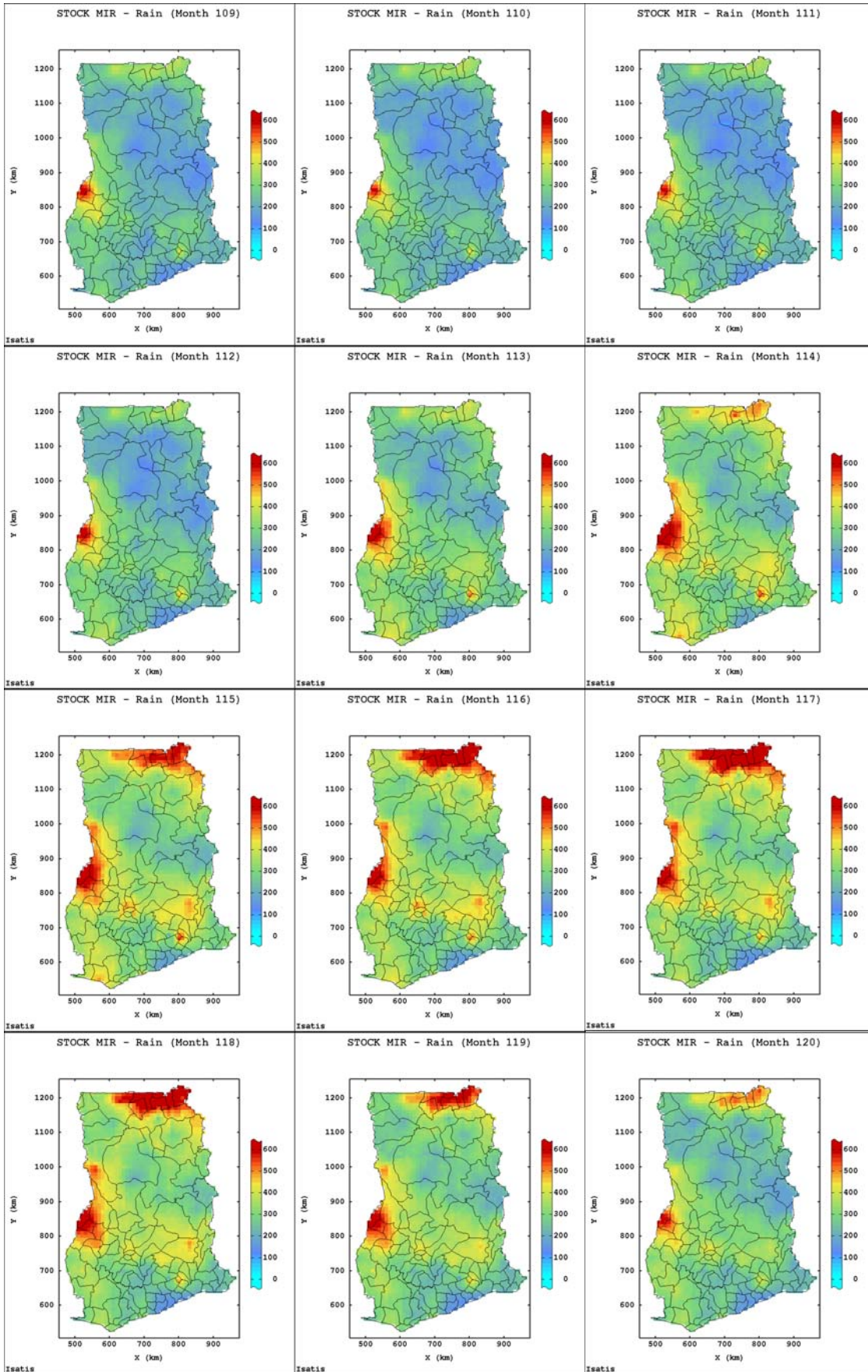


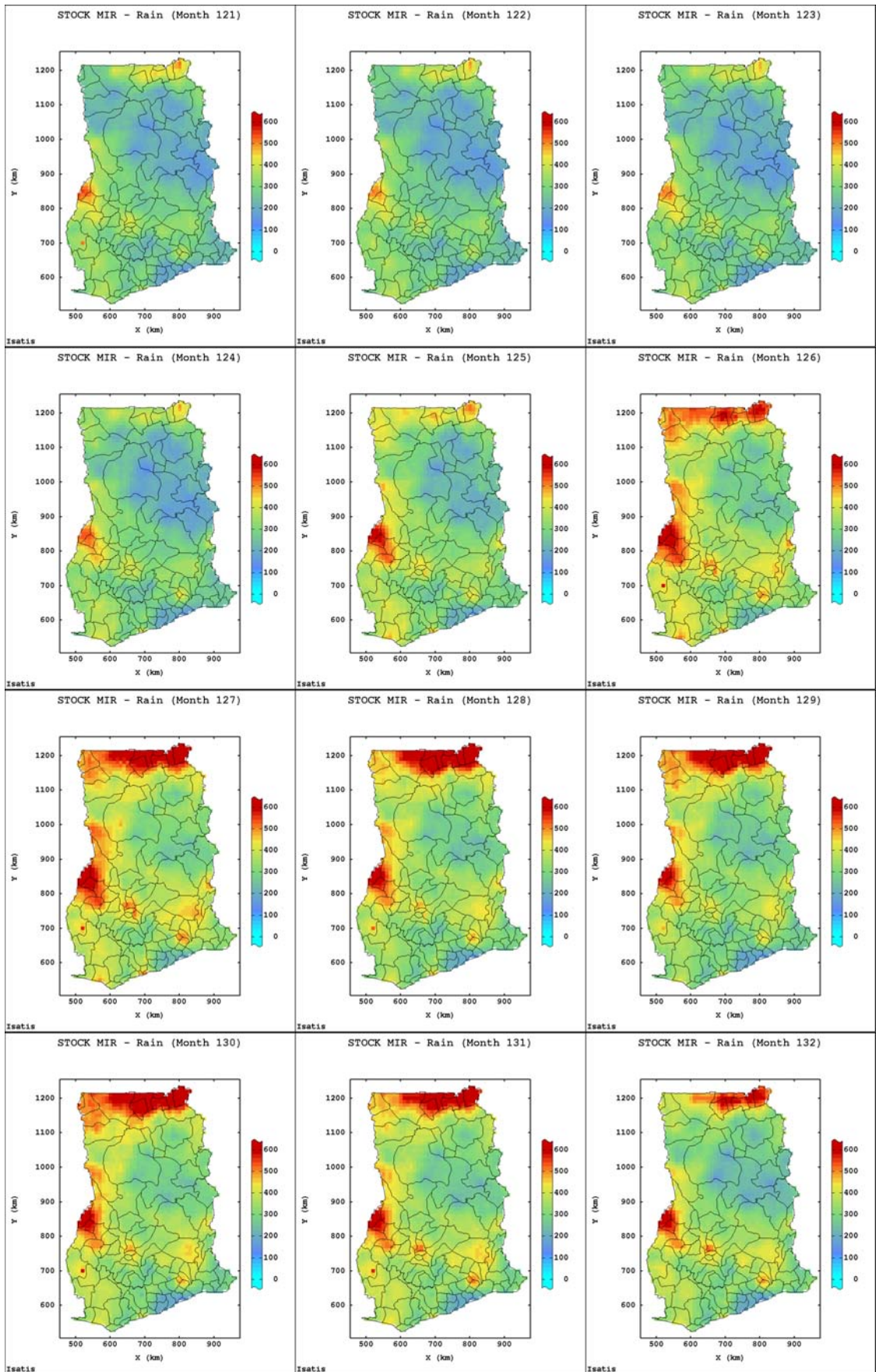




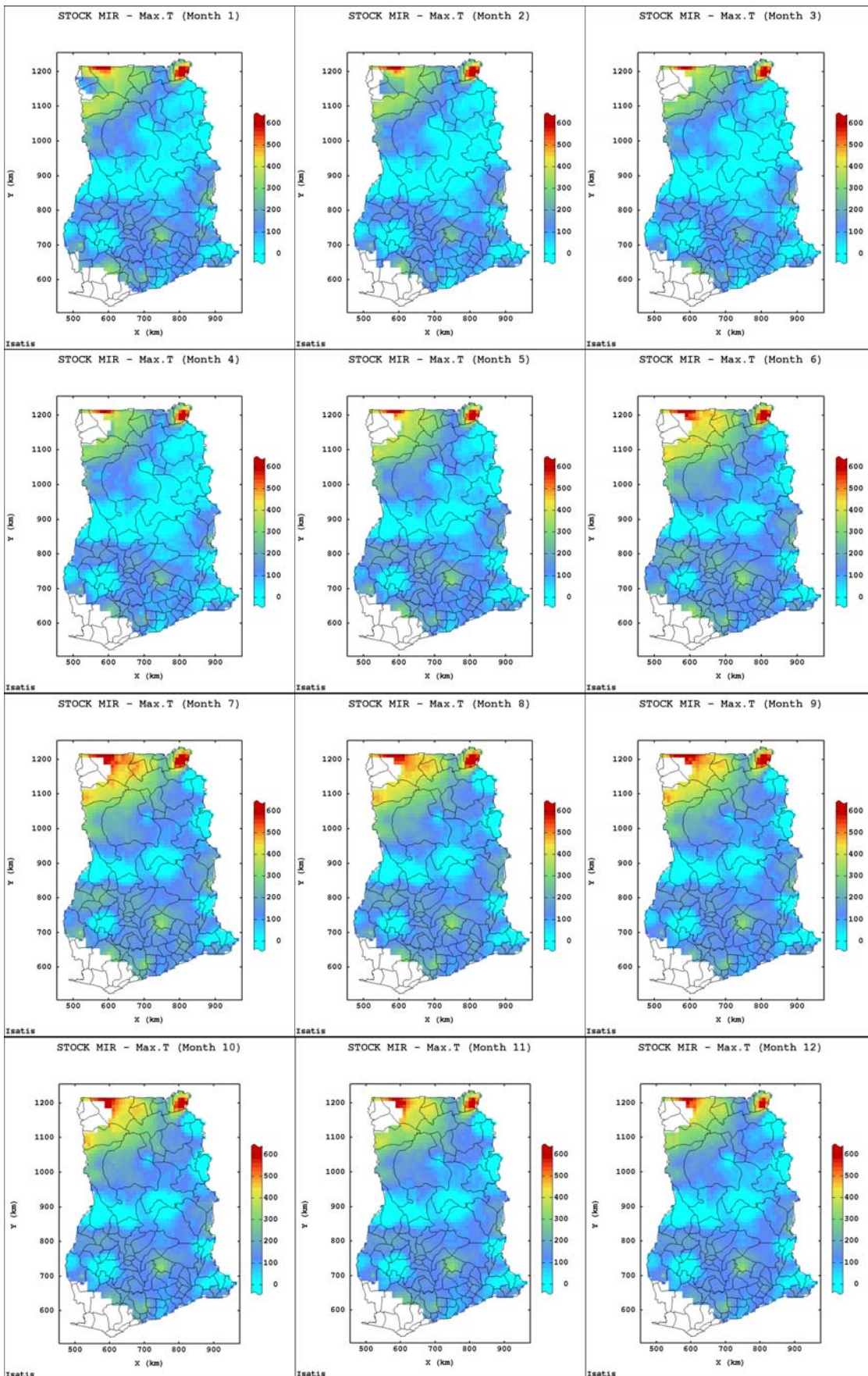


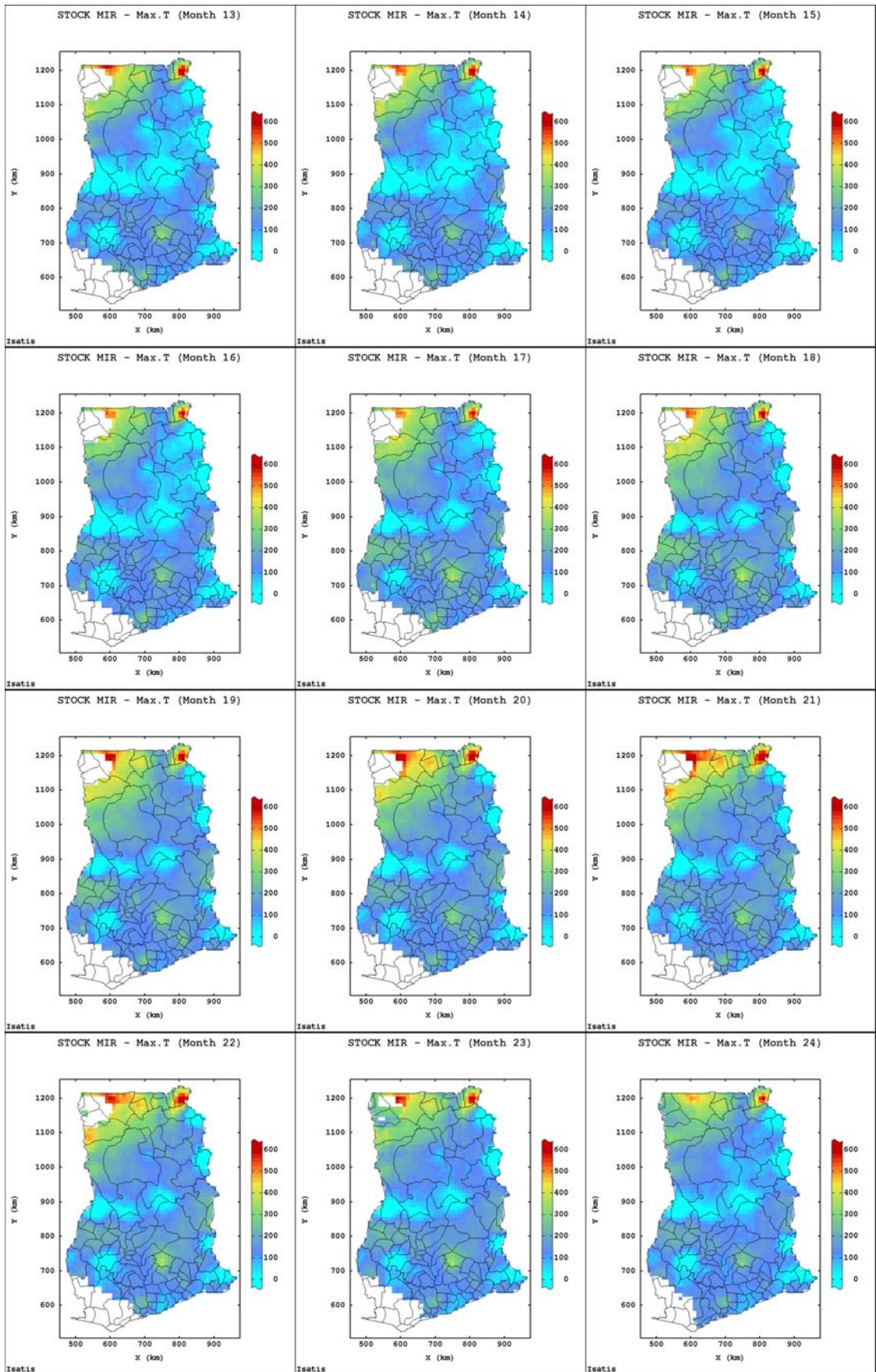


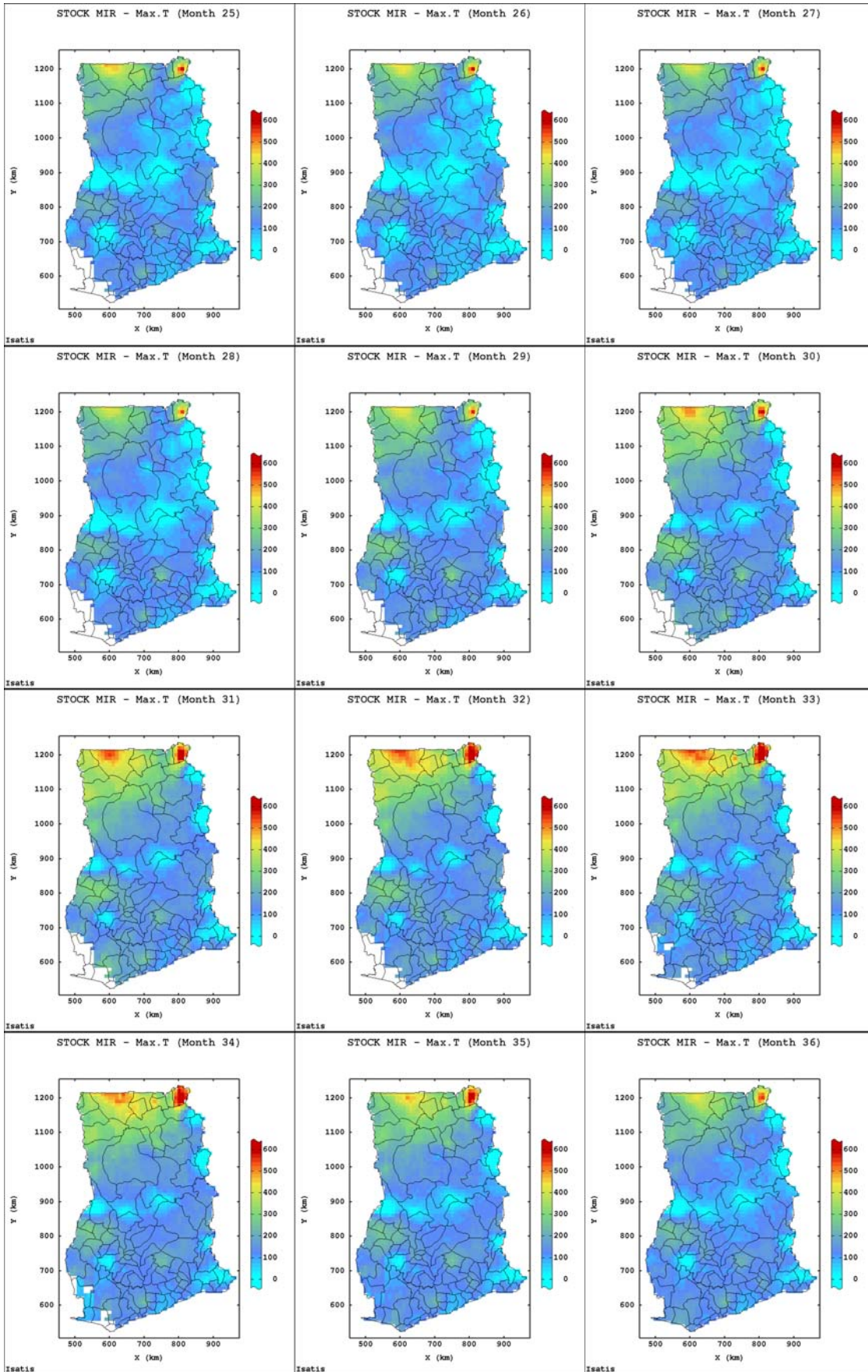


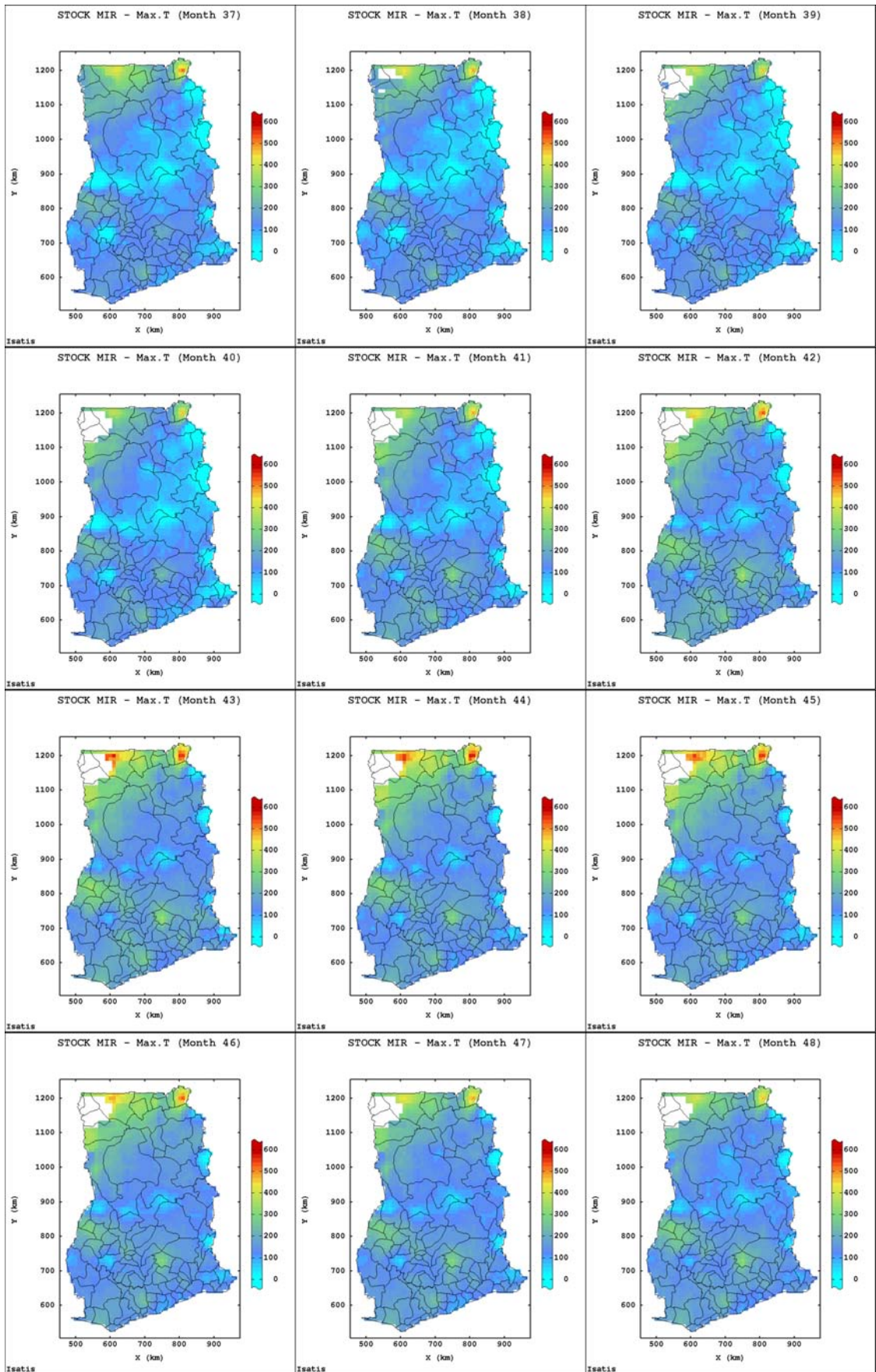


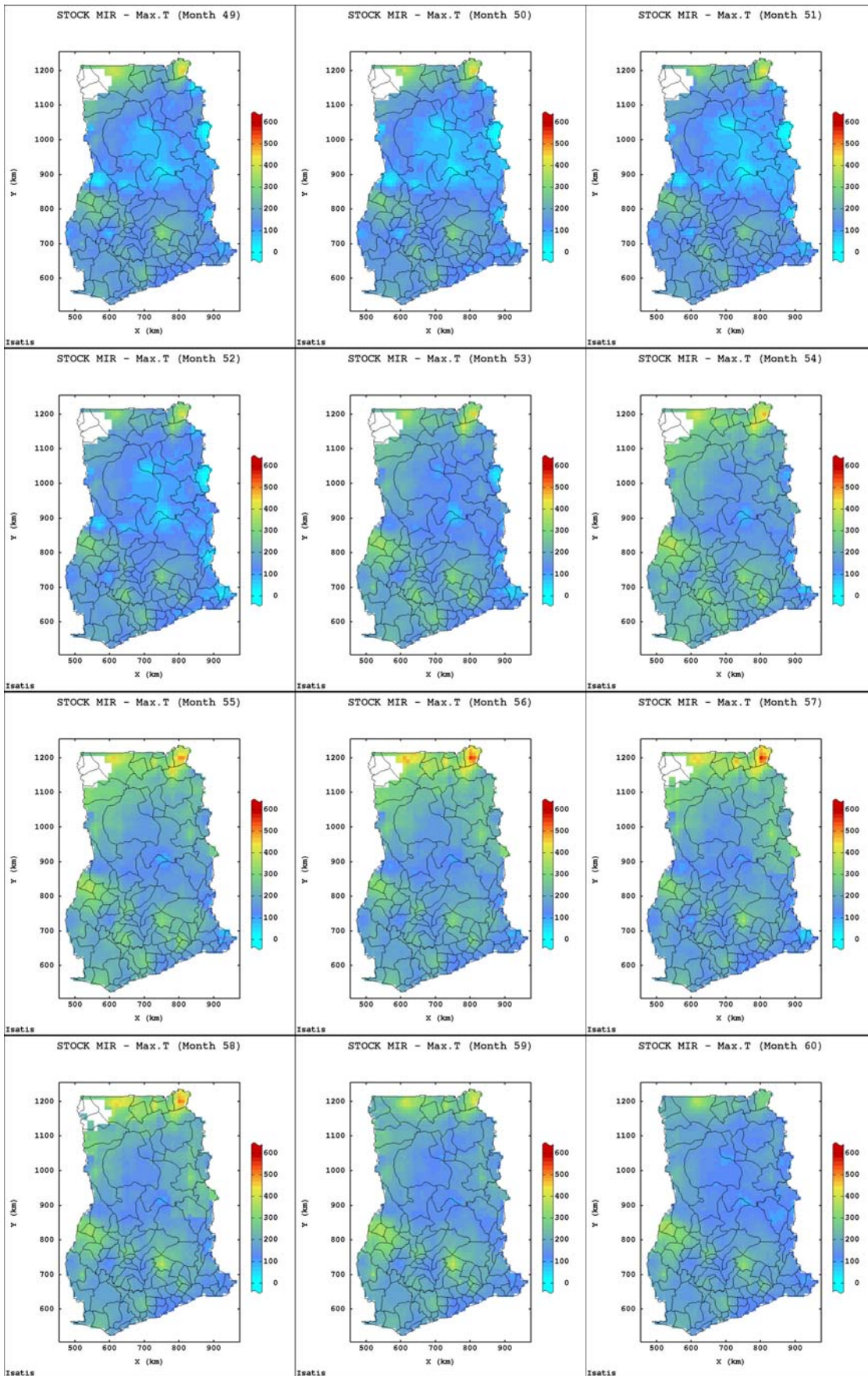
E-5.5 STOCK_MaxT Produced Spatial Maps

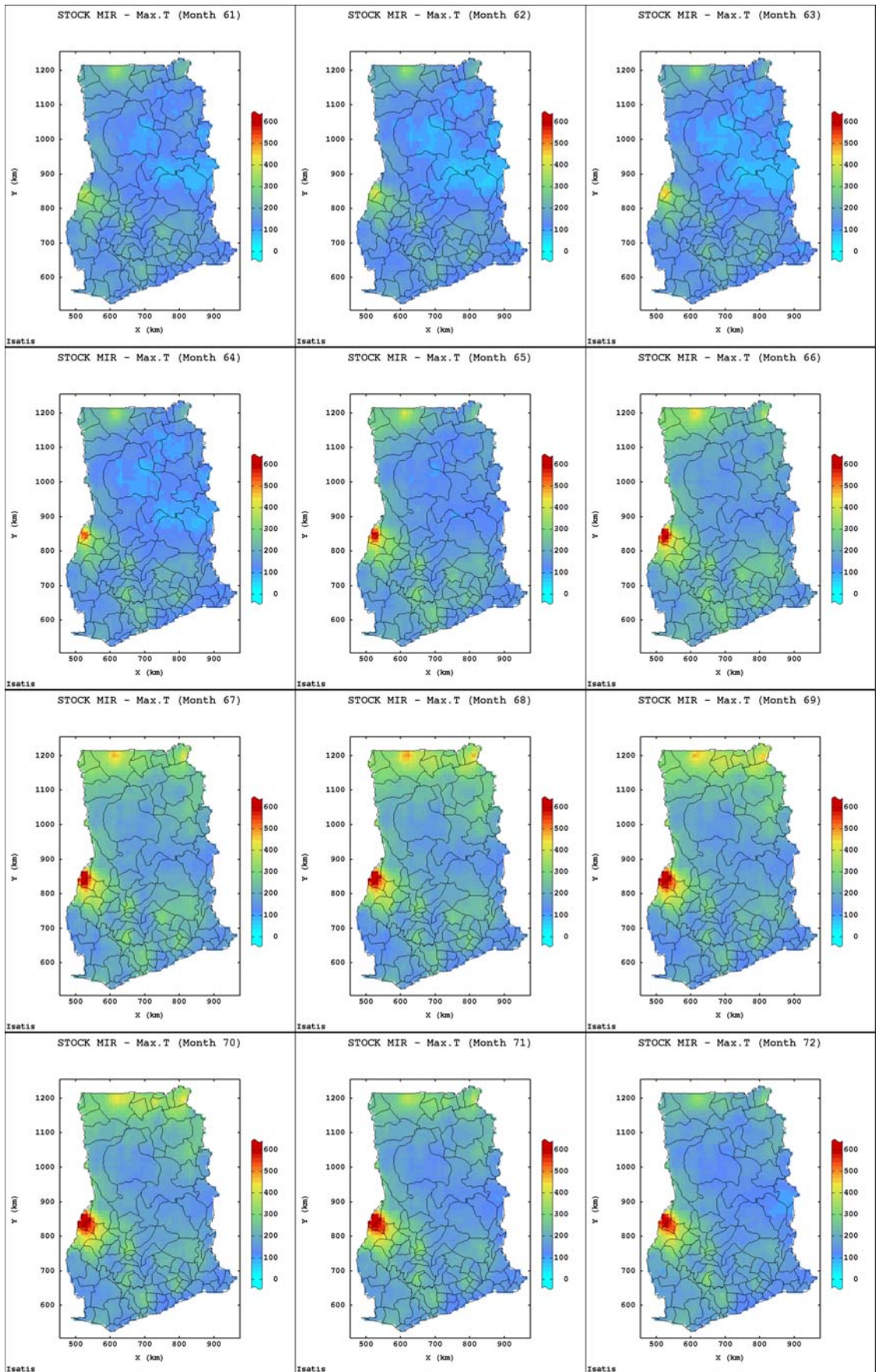


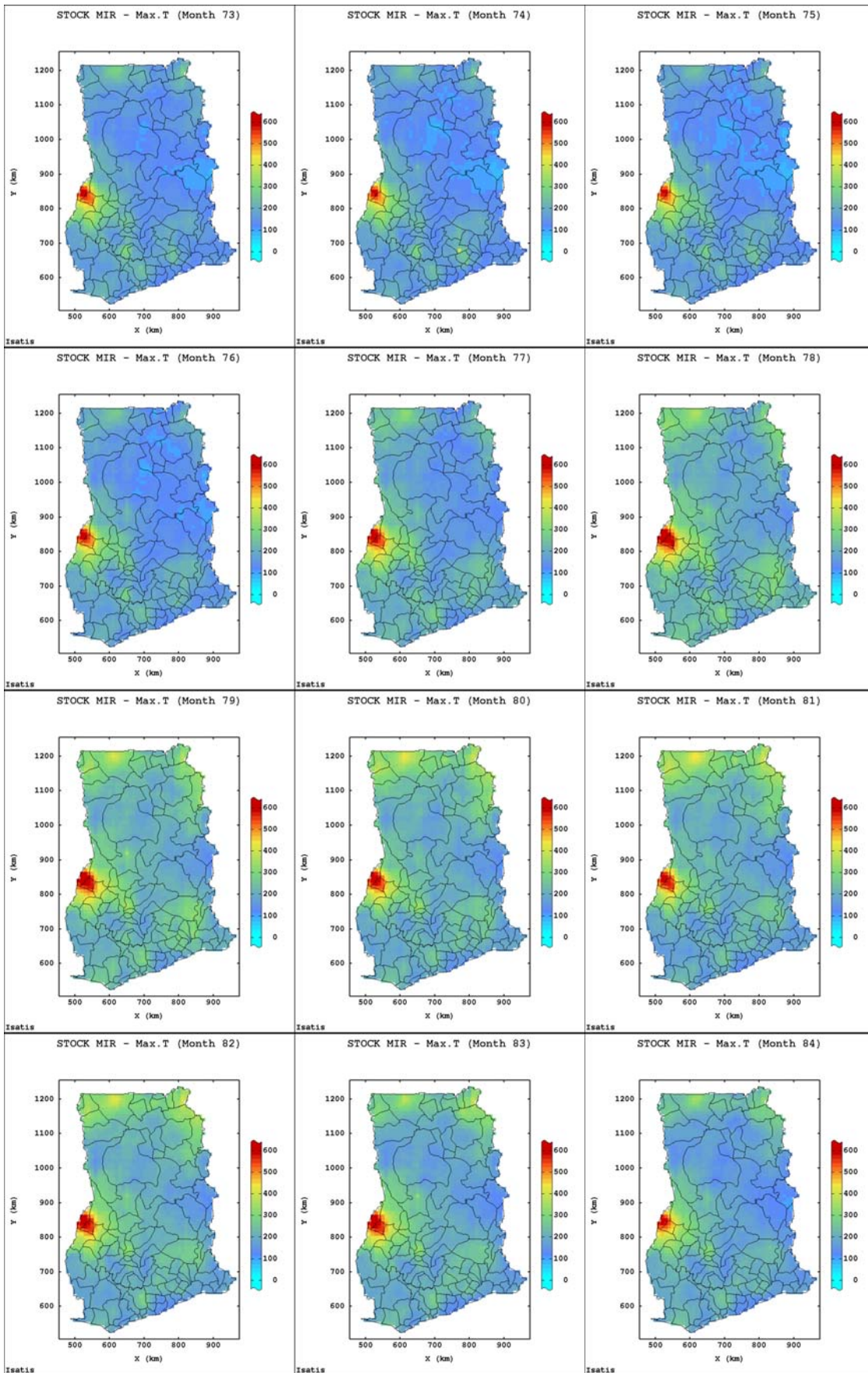


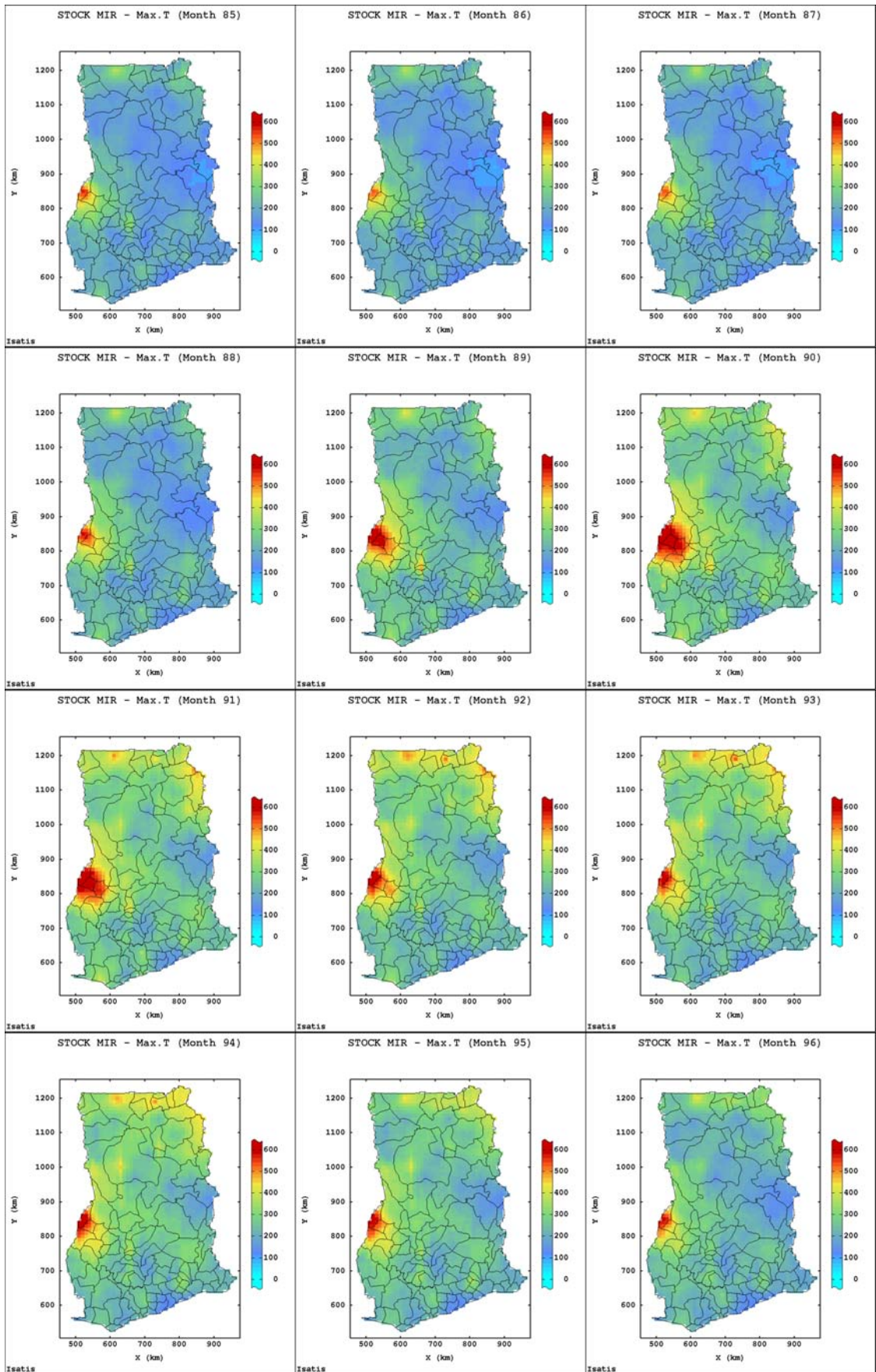


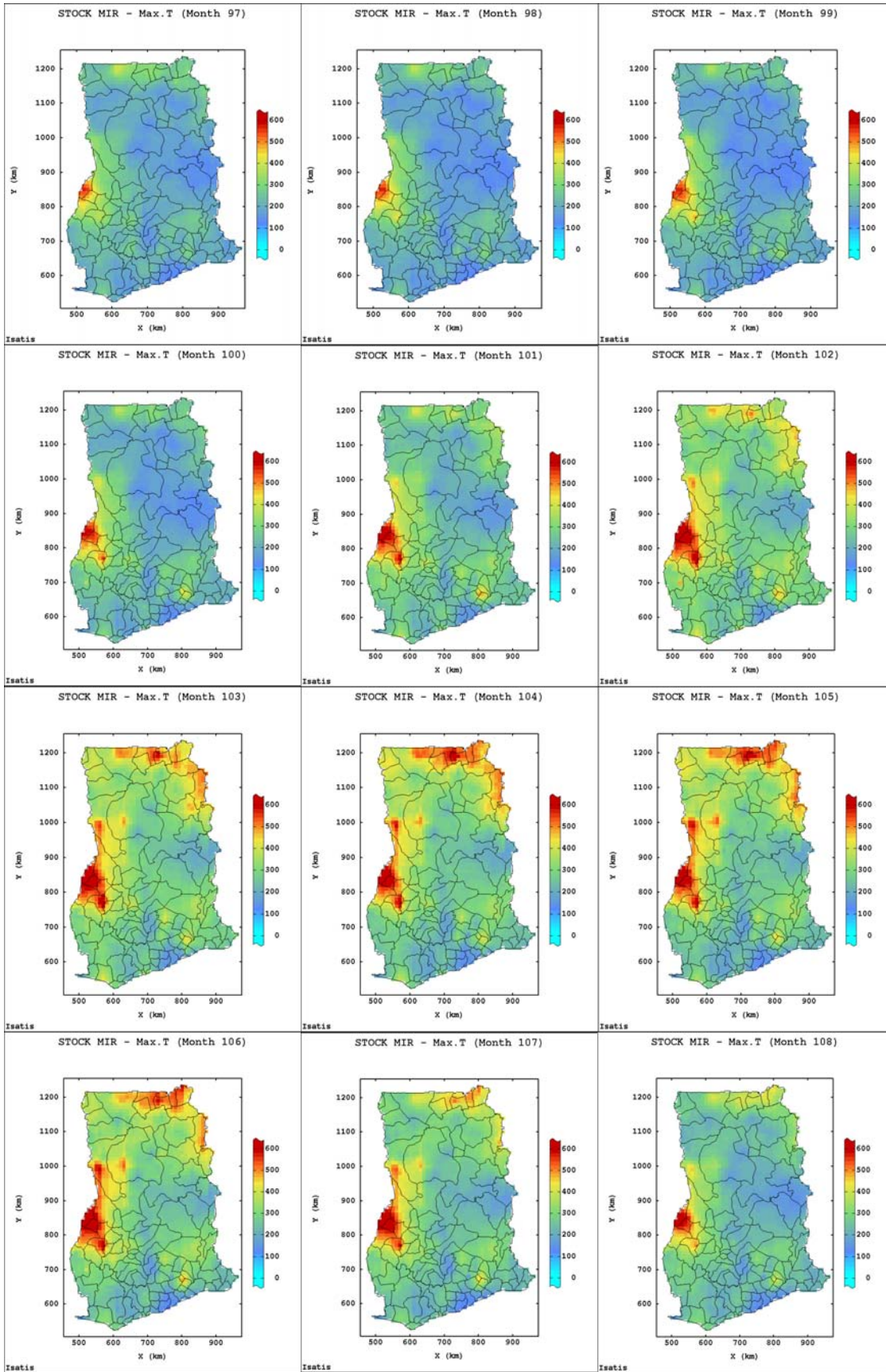


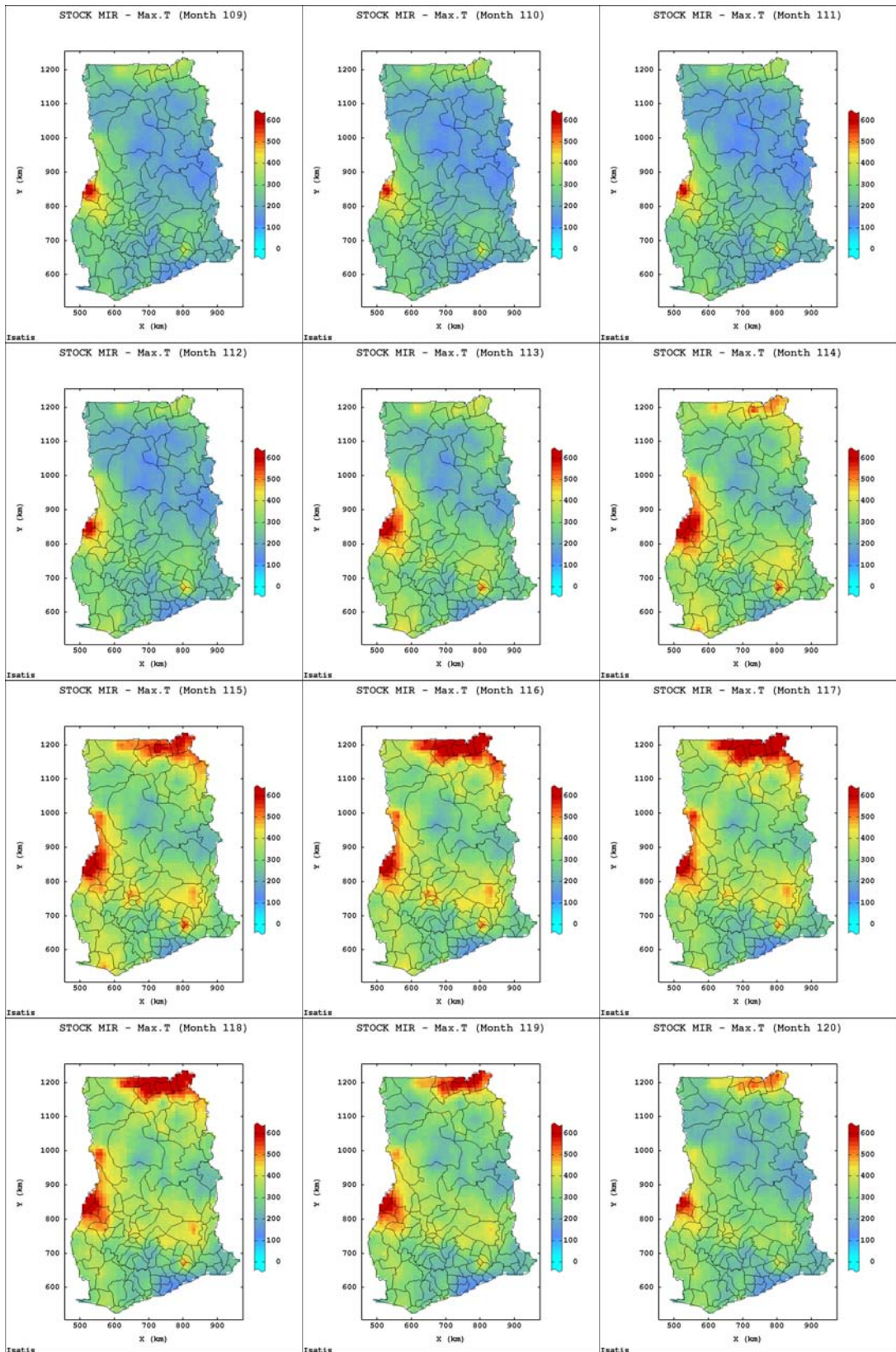


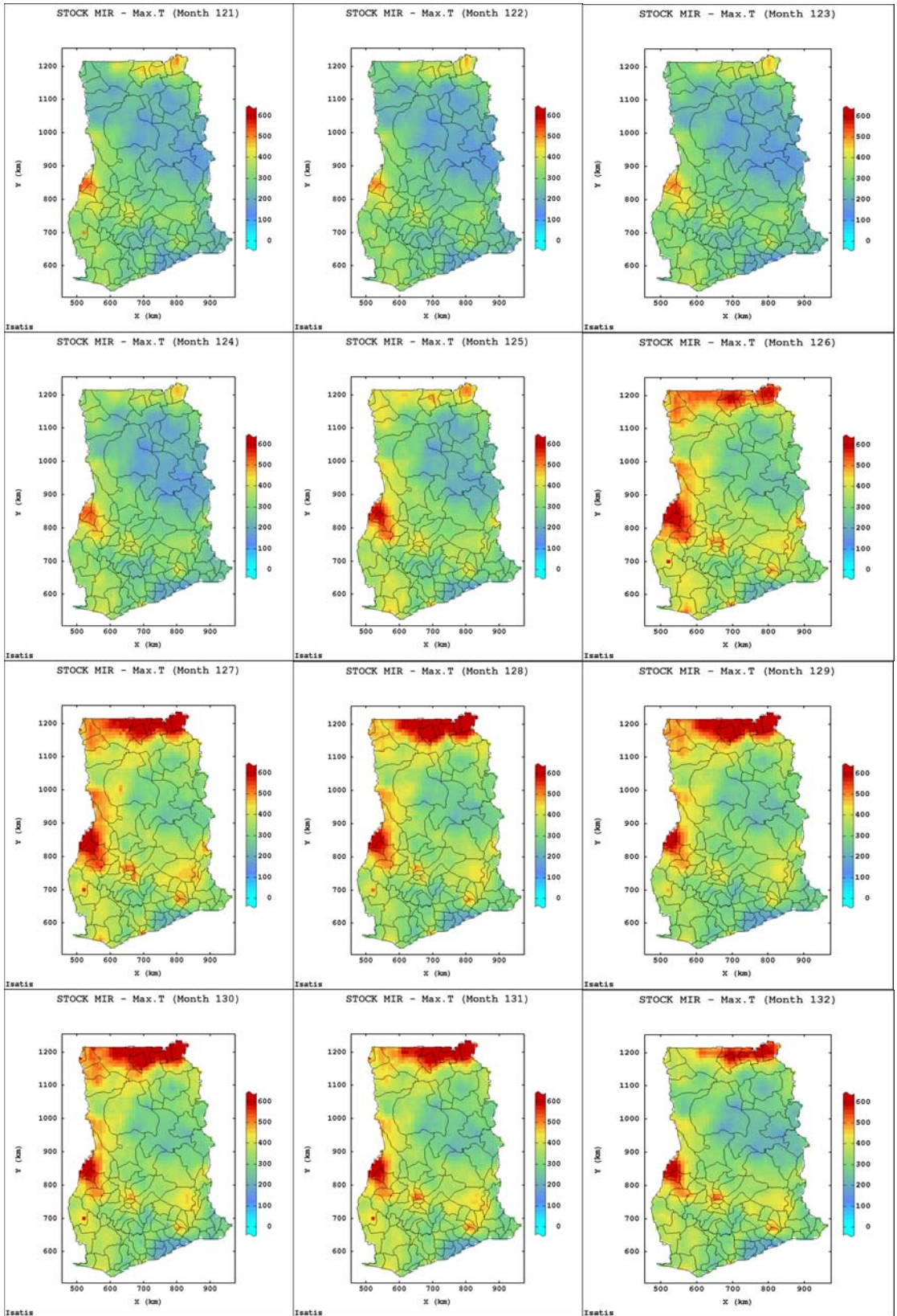






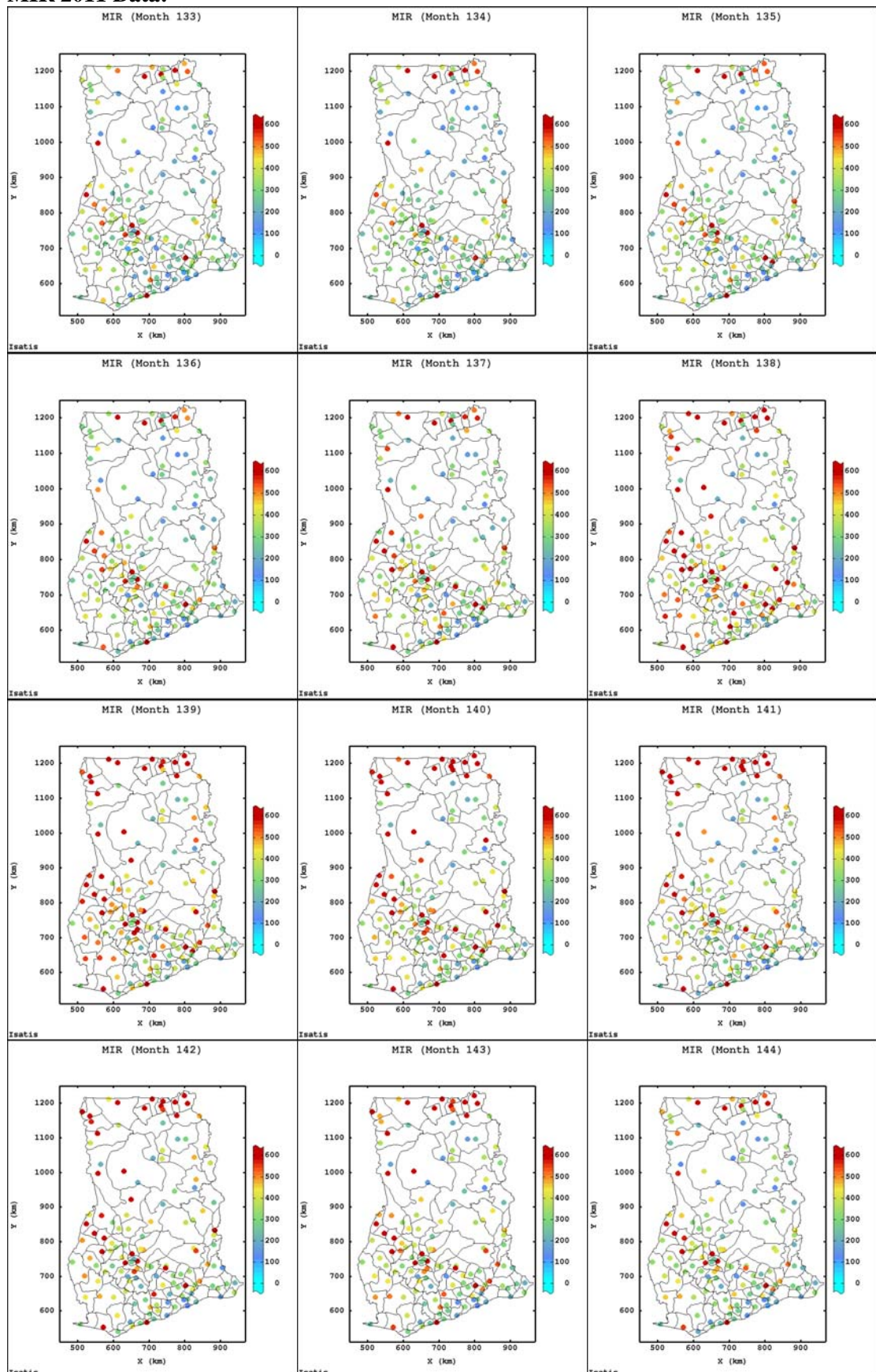




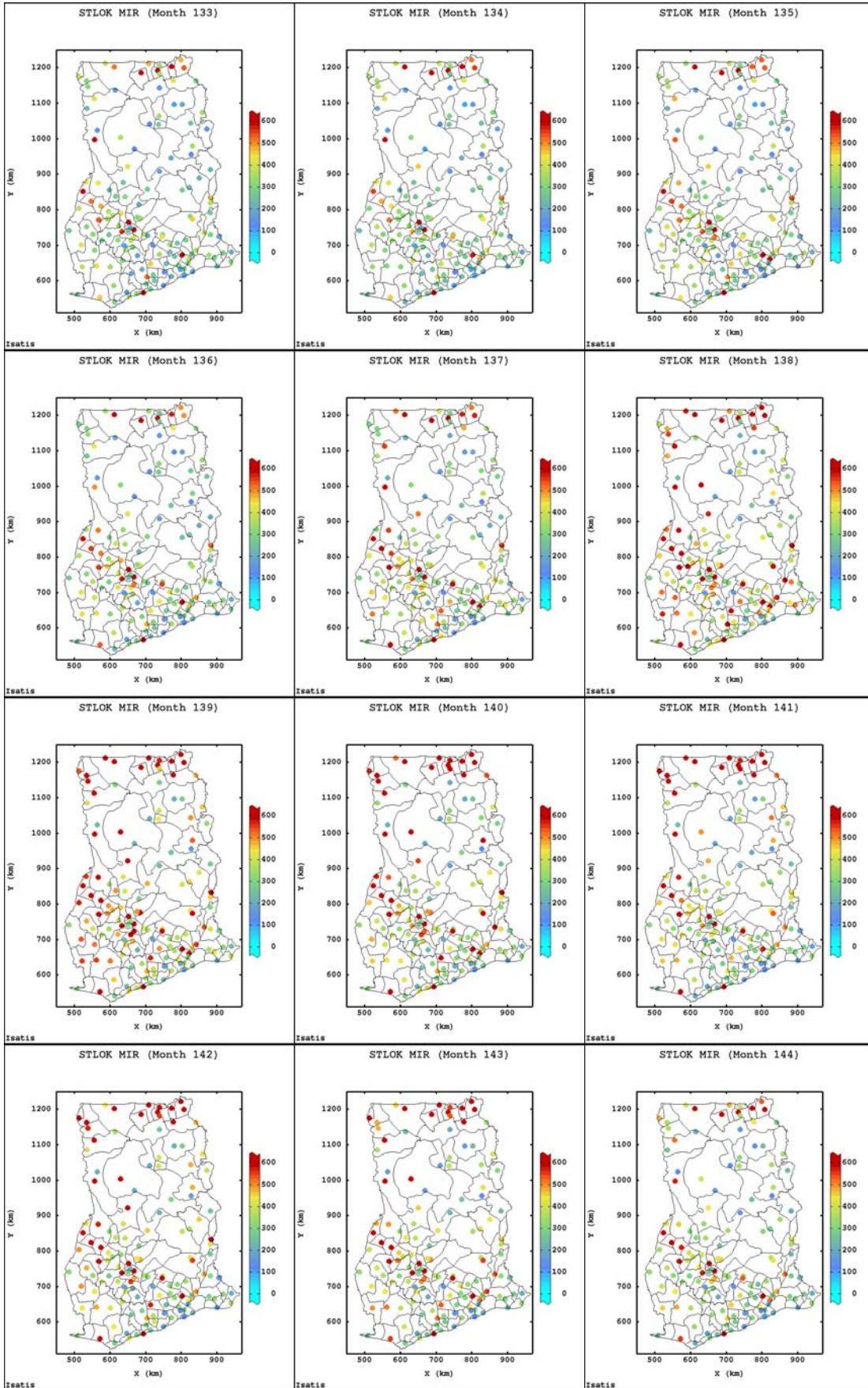


E-5.6: Jackknife Method Predictions for 2011 MIR Data

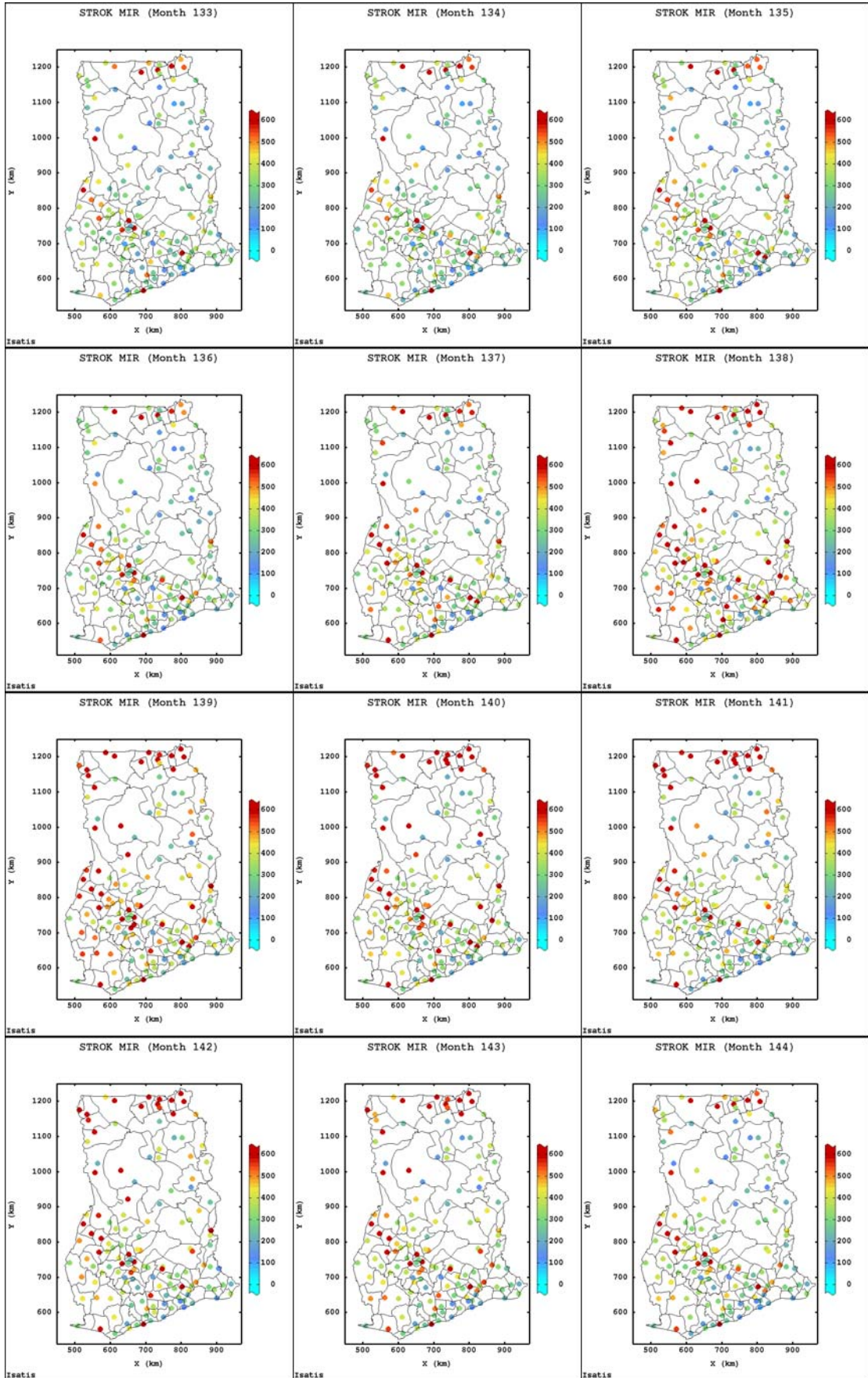
MIR 2011 Data:



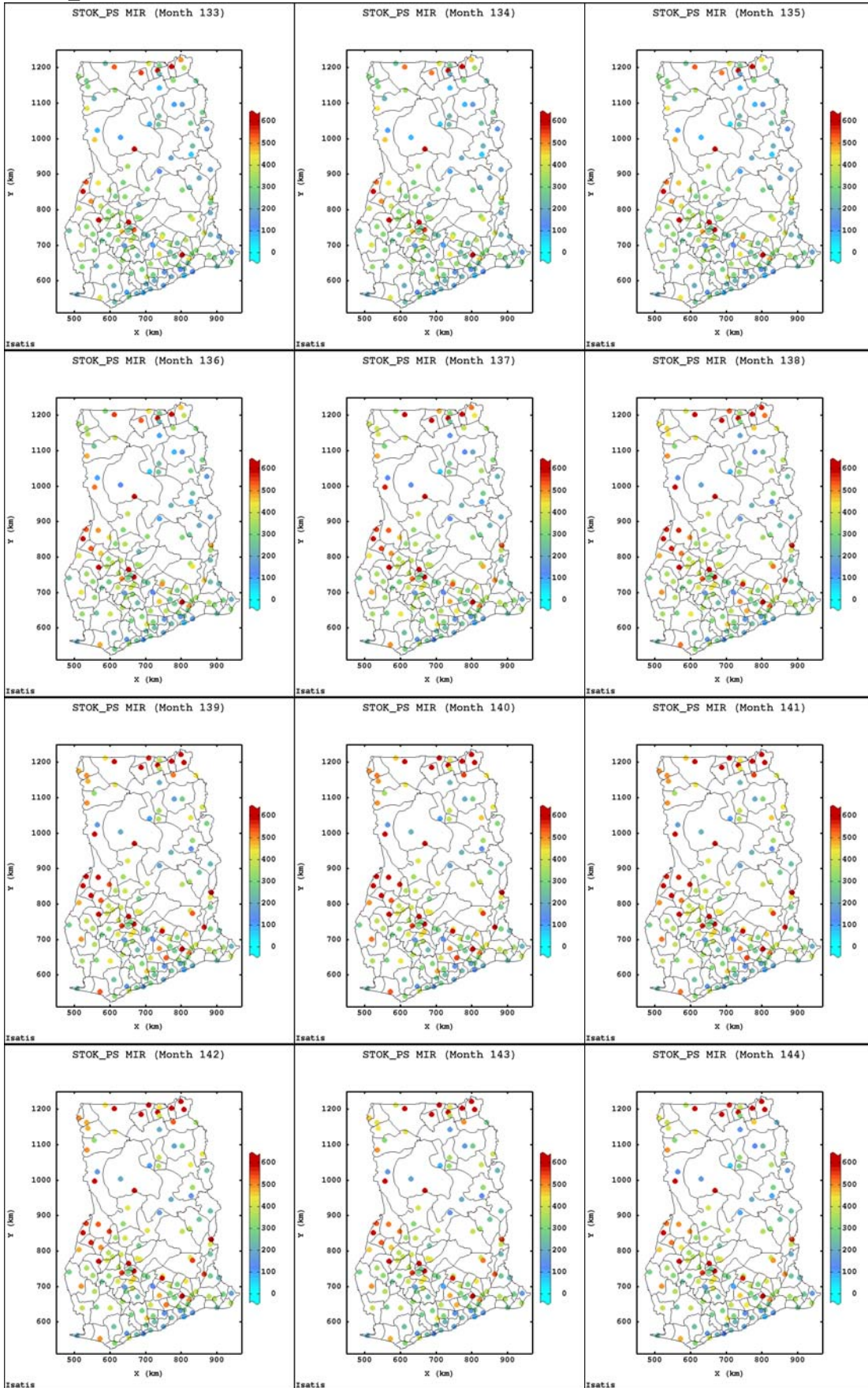
STLOK Estimates:



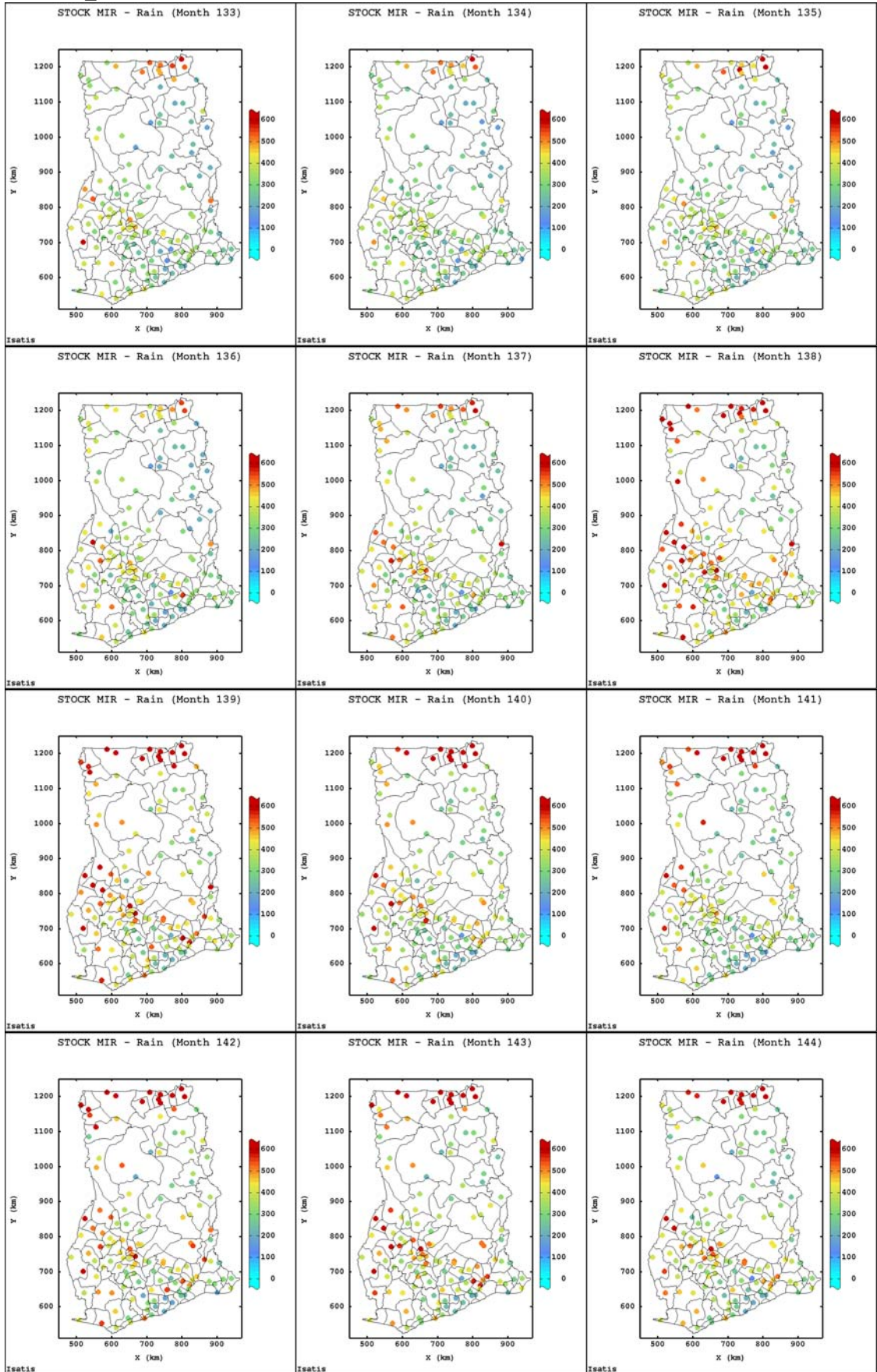
STROK Estimates:



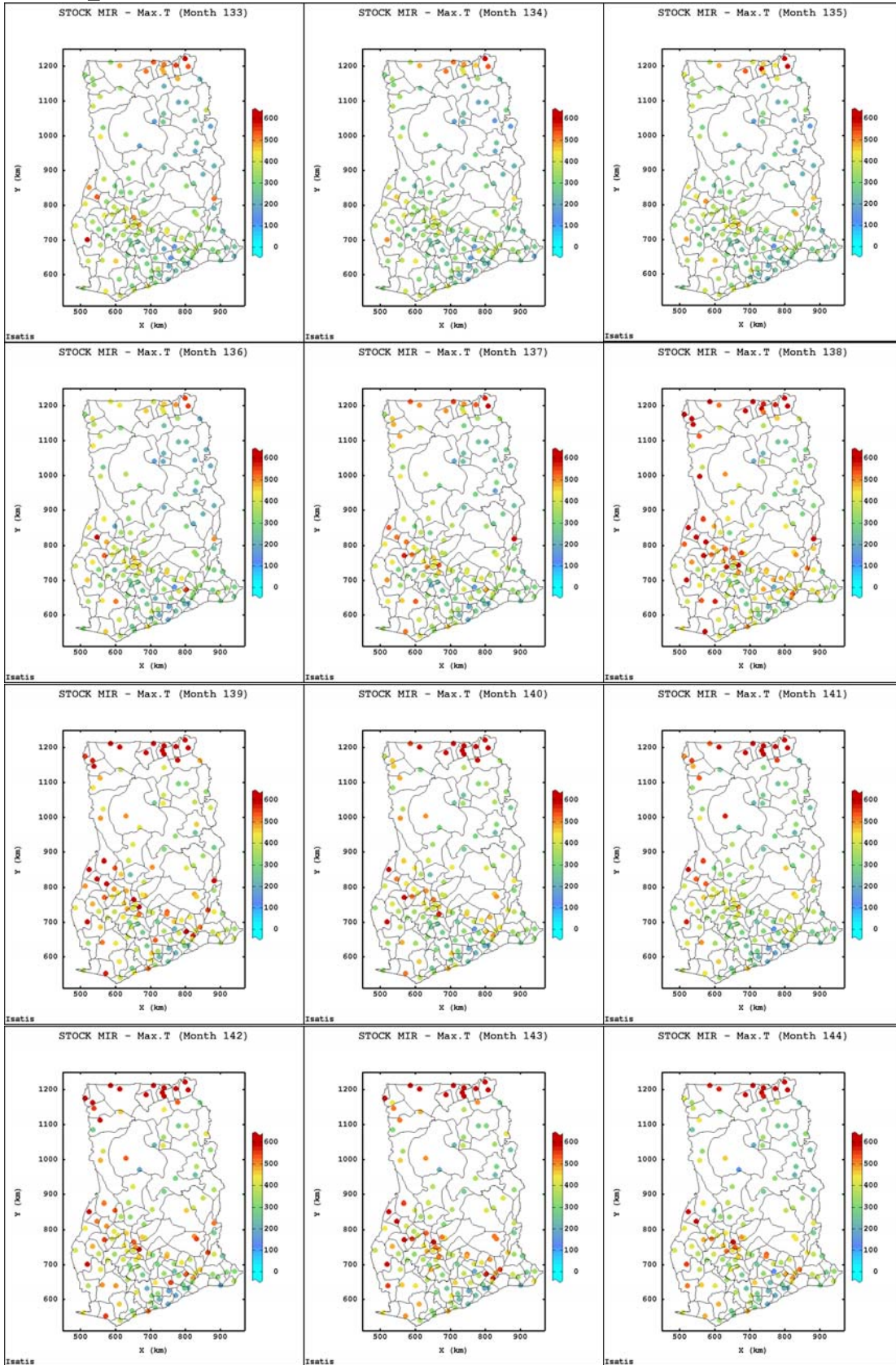
STOK_PS Estimates:



STOCK_Rain Estimates:



STOCK_MaxT Estimates:



Appendix F: Estimation of Malaria Risk in BAR

F-1: Space-time Semivariogram Models of MIR

Table F-1.1: Spatial semivariogram model parameters of the regionalised trend model coefficients of malaria incidence rates for BAR

Coefficient	Model $\hat{\gamma}_s^{(i)}(\mathbf{h}_s)$	Sill (c_s)	Spatial Range (r_s in km)	Relative Nugget
(Intercept) b_0	<i>nugget</i>	25000	-	0.096
	<i>spherical</i>	35500	65	
	<i>spherical</i>	199500	110	
(t) b_1	<i>nugget</i>	2.5	-	0.033
	<i>spherical</i>	70	110	
	<i>spherical</i>	3.5	75	
(t ²) b_2	<i>nugget</i>	0.00015	-	0.117
	<i>spherical</i>	0.00005	50	
	<i>spherical</i>	0.00108	120	
(cos) b_3	<i>nugget</i>	1.50	-	0.010
	<i>spherical</i>	105	50	
	<i>spherical</i>	40	100	
(sin) b_4	<i>nugget</i>	1.00	-	0.007
	<i>sph(h/r)</i>	5.00	60	
	<i>sph(h/r)</i>	145	140	
R squared (\hat{R}^2)	<i>nugget</i>	0.0002	-	0.013
	<i>sph(h/r)</i>	0.0022	50	
	<i>sph(h/r)</i>	0.0125	115	

Table F-1.2: Space-time semivariogram model parameters of log-transformed malaria incidence rates for the for case study in BAR

Study	Model $\gamma(h)$	Sill c_s/c_t	Spatial range r_s (km)	Temporal range r_t (months)	Relative nugget
BAR	<i>nugget</i>	0.025	-	-	0.095
	<i>exponential</i>	0.018	35	80	
	<i>spherical</i>	0.220	140	130	(0.090)
	<i>expcosine</i>	0.014	10000	400	

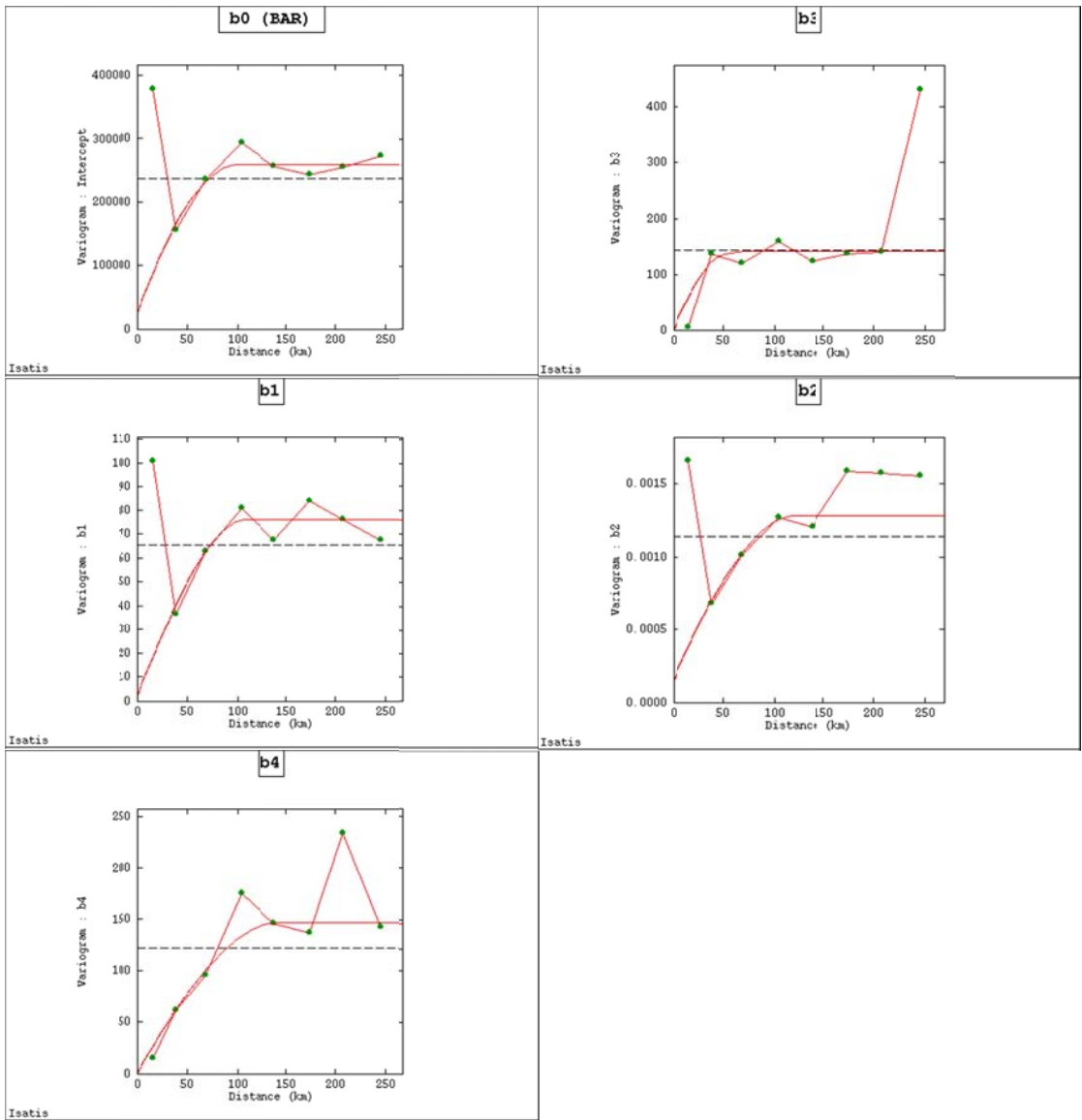


Figure F-1.1: Spatial experimental semivariograms (dotted green) with fitted variogram models of trend model parameters (coefficients) for Brong Ahafo Region

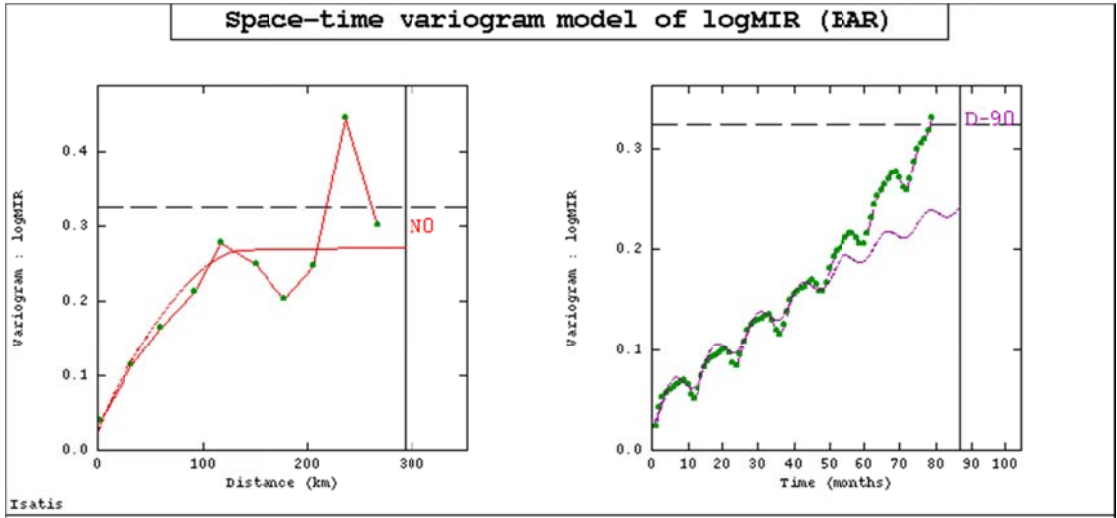


Figure F-1.2: Space-time experimental semivariograms (dotted green) fitted with variogram models showing spatial (left) and temporal (right) autocorrelation of log-transformed malaria incidence rates for national and BAR

Table F.1.3: Space-time semivariogram model parameters of residuals of malaria incidence rates for the BAR study area

Model $\gamma(h)$	Sill	Spatial range r_s (km)	Temporal range r_t (months)	Relative nugget
<i>nugget</i>	1300	-	-	0.302
<i>spherical</i>	2050	45	20	(0.255)
<i>exponential</i>	1000	120	25	
<i>spherical</i>	750	10000	36	

Note: In parentheses is the relative nugget effect in the temporal domain.

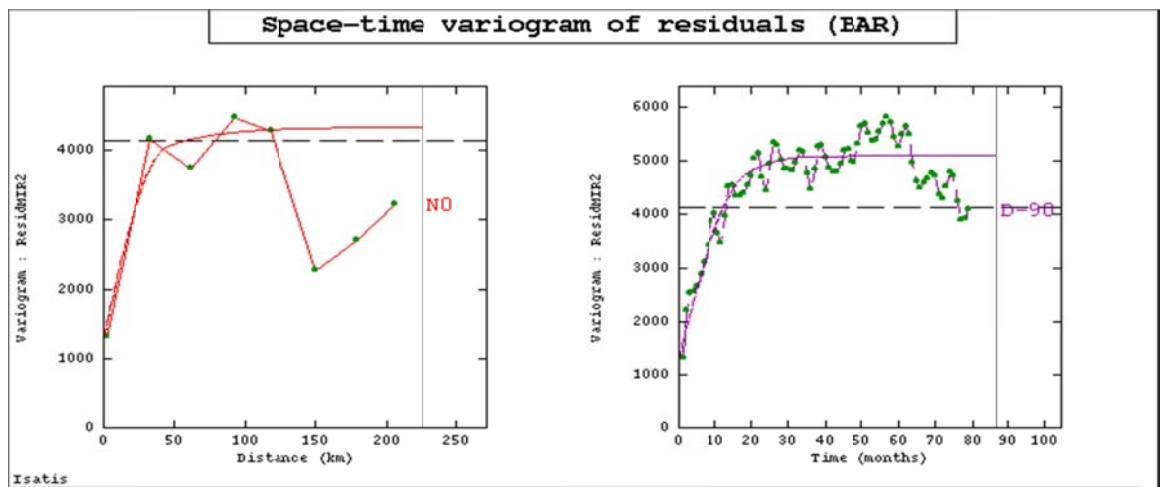


Figure F_1.3: Spatial experimental semivariograms (dotted green) with fitted variogram models of residuals of malaria incidence rates for regional study in BAR

F-2: Product-Sum Semivariogram Models of MIR

Table F-2.1: Parameters of the marginal semivariograms and generalised product-sum semivariogram models of the observed malaria incidence rates for the BAR study

Study	Model	Spatial		Temporal		Product-sum	
		Sill	Ran ge	Sill	Range	Global sill	k
BAR	<i>nugget</i>	2000 (0.098)	-	1000 (0.050)	-		1.219×10^{-6}
	<i>spherical</i>	-		19100	80	40000	(4.902×10^{-5})
	<i>exponential</i>	18400	100	-	-		

In parentheses are the relative nugget (RN) effects of marginal semivariograms and maximum k limit values for the product-sum model.

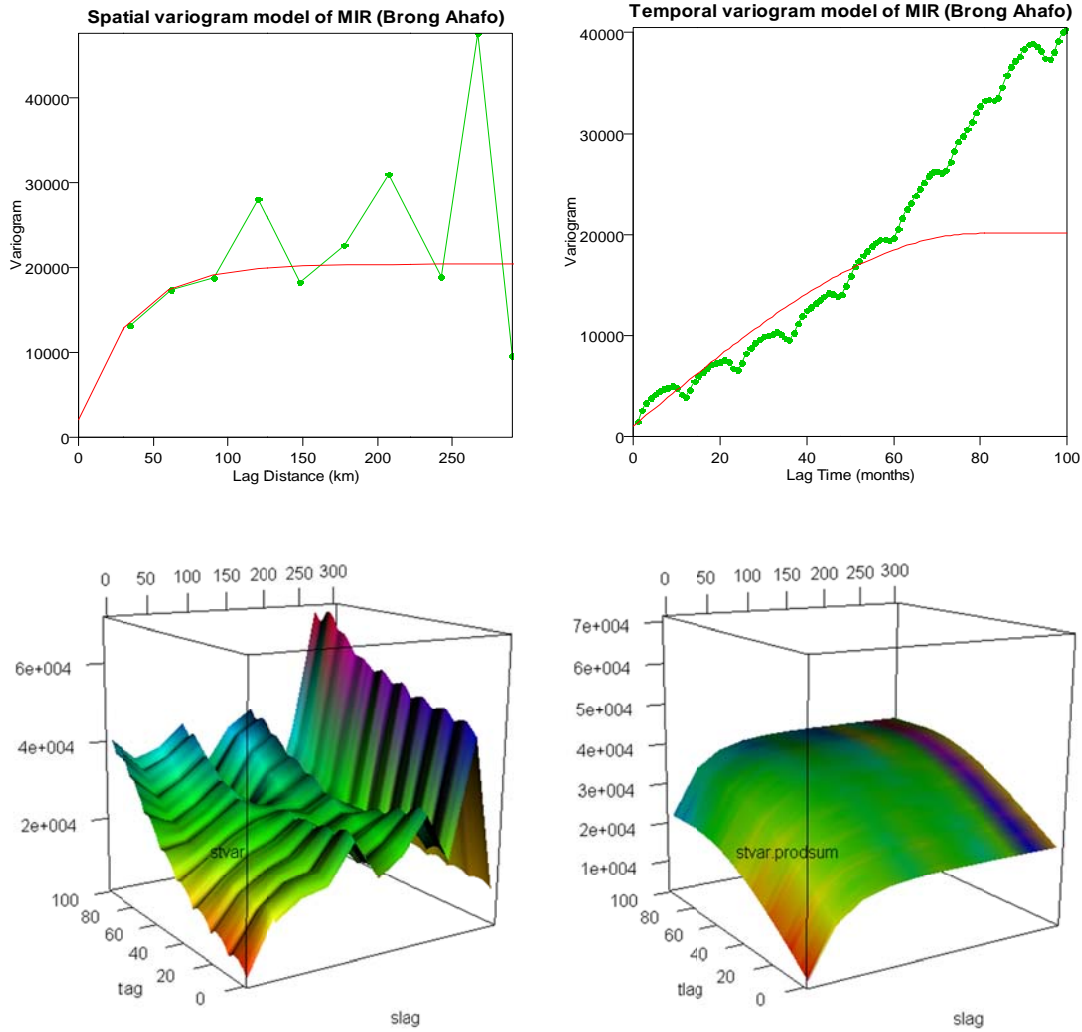


Figure F-2.1: Marginal spatial and temporal semivariograms models of malaria incidence rates (top) and space-time experimental semivariogram surfaces together with their product-sum models (bottom) for Brong Ahafo

Table F-2.2: Parameters of the marginal semivariograms and product-sum semivariogram models of the detrended malaria incidence rates (residuals) for the study in BAR

Study	Model	Spatial		Temporal		Product-sum	
		Sill (RN)	Range	Sill (RN)	Range	Global Sill	k
	<i>nugget</i>	500 (0.128)	-	650 (0.140)	-		2.068×10^{-4}
BAR	<i>exponential</i>	3400	80	-	-	4800	(2.151×10^{-4})
	<i>exponential</i>	-	-	4000	18		

In parentheses are the relative nugget (RN) effects of marginal semivariograms and maximum k limit values for the product-sum model.

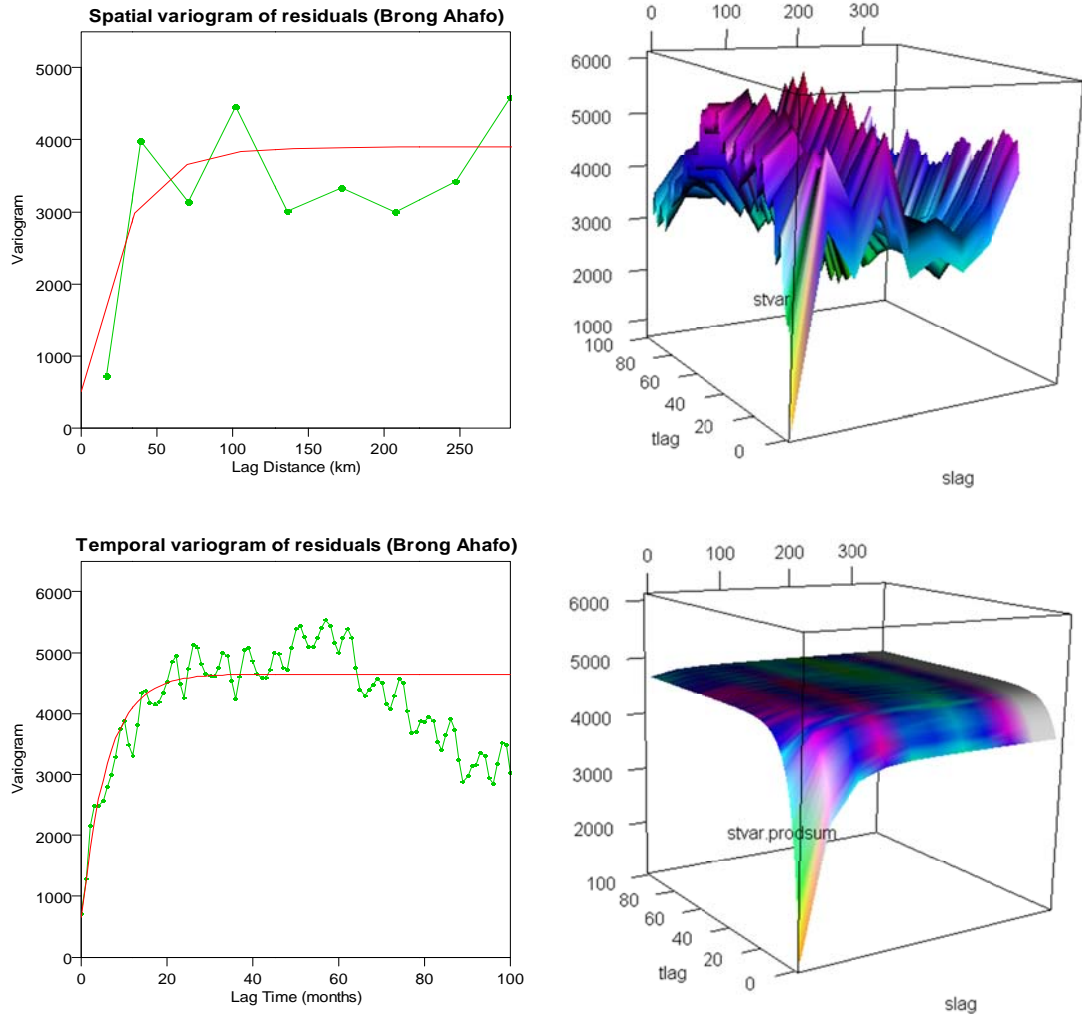


Figure F-2.2: Marginal spatial and temporal semivariogram models of the residuals incidence rates (left) and space-time experimental semivariogram surfaces together with their product-sum models (right) for the study in Brong Ahafo Region

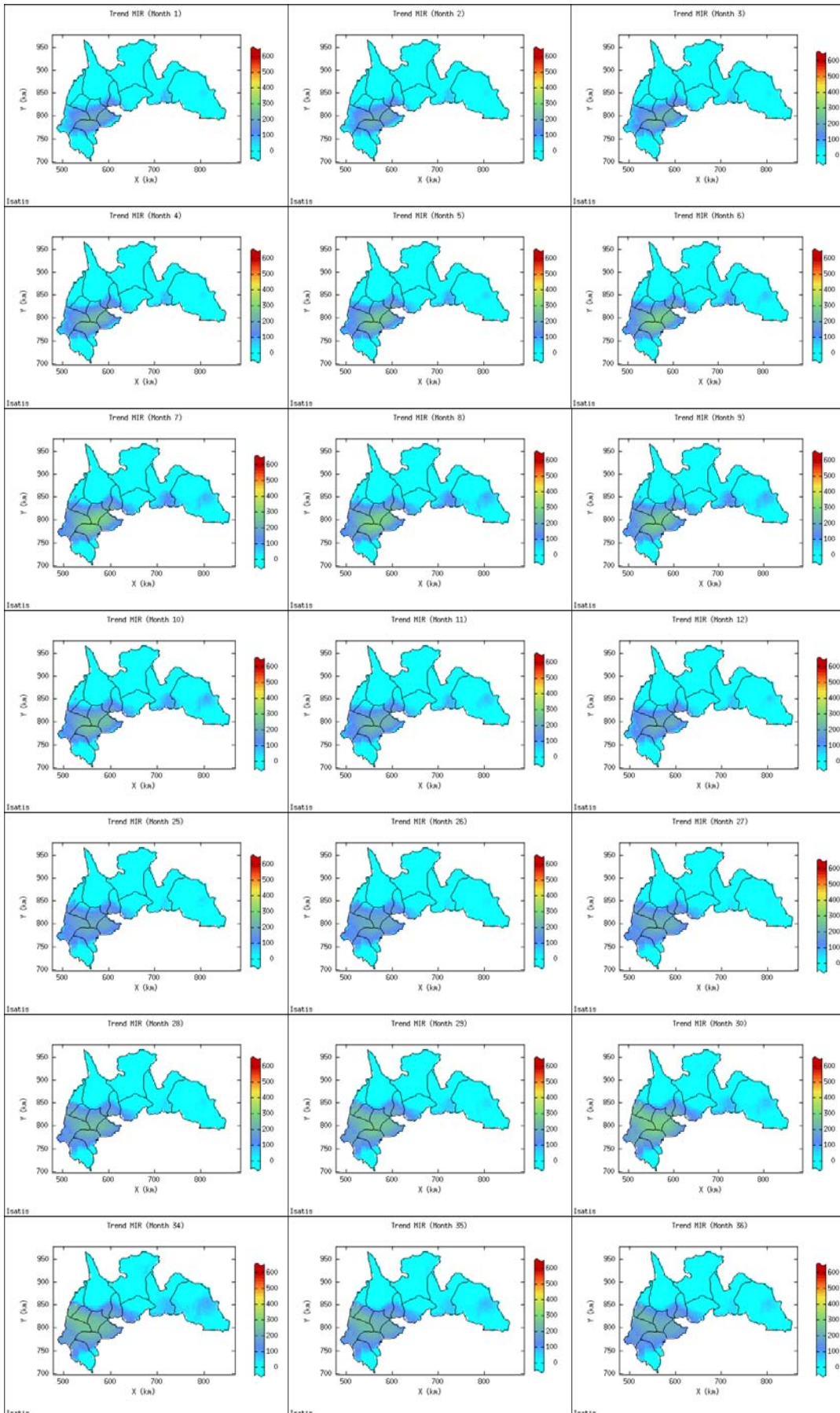
F-3: Spatial Maps of MIR

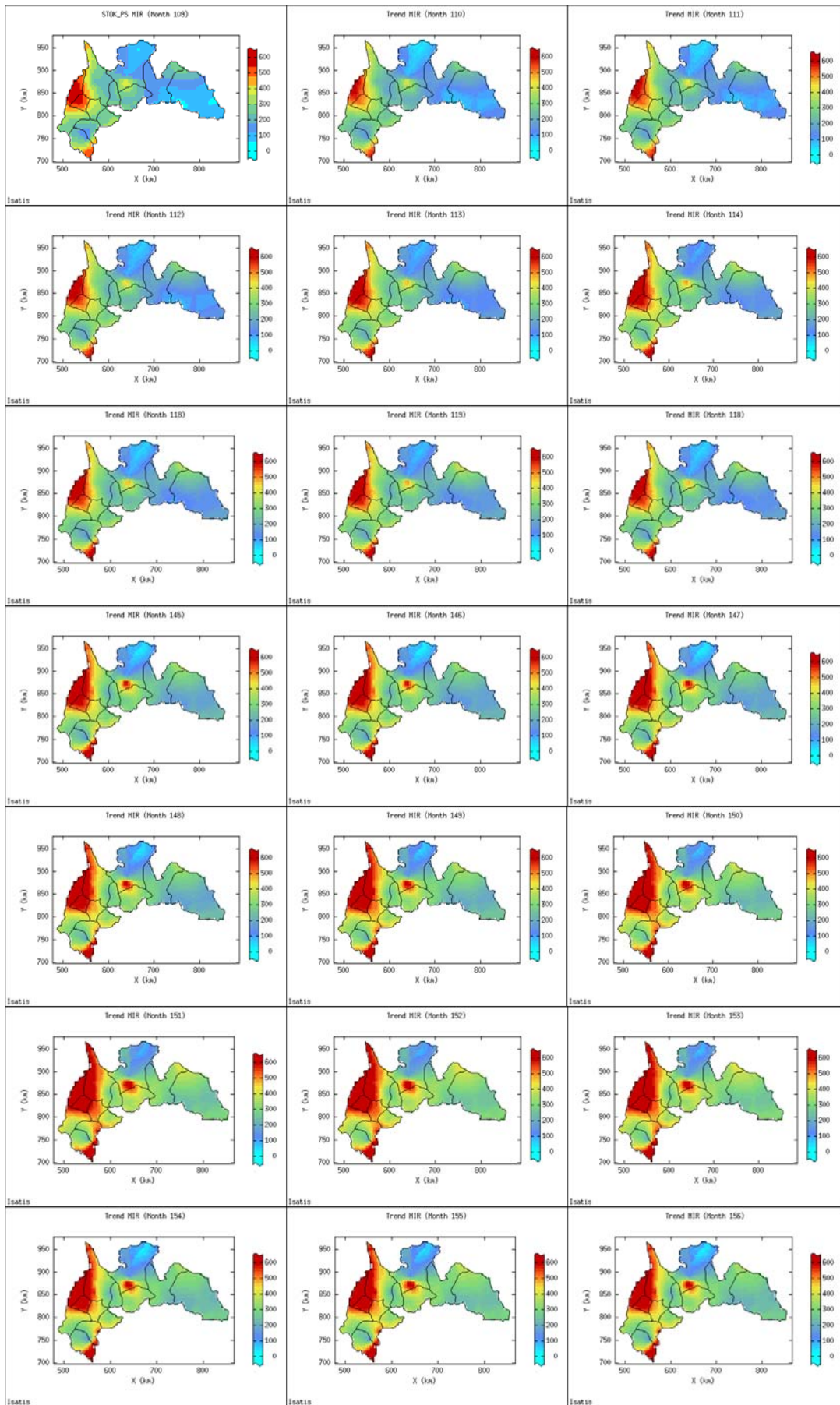
The monthly morbidity risk maps produced by each of the following space-time kriging techniques for the years 1998, 2004 and 2010:

F-3.1: Space-time trend model estimating the average morbidity risk

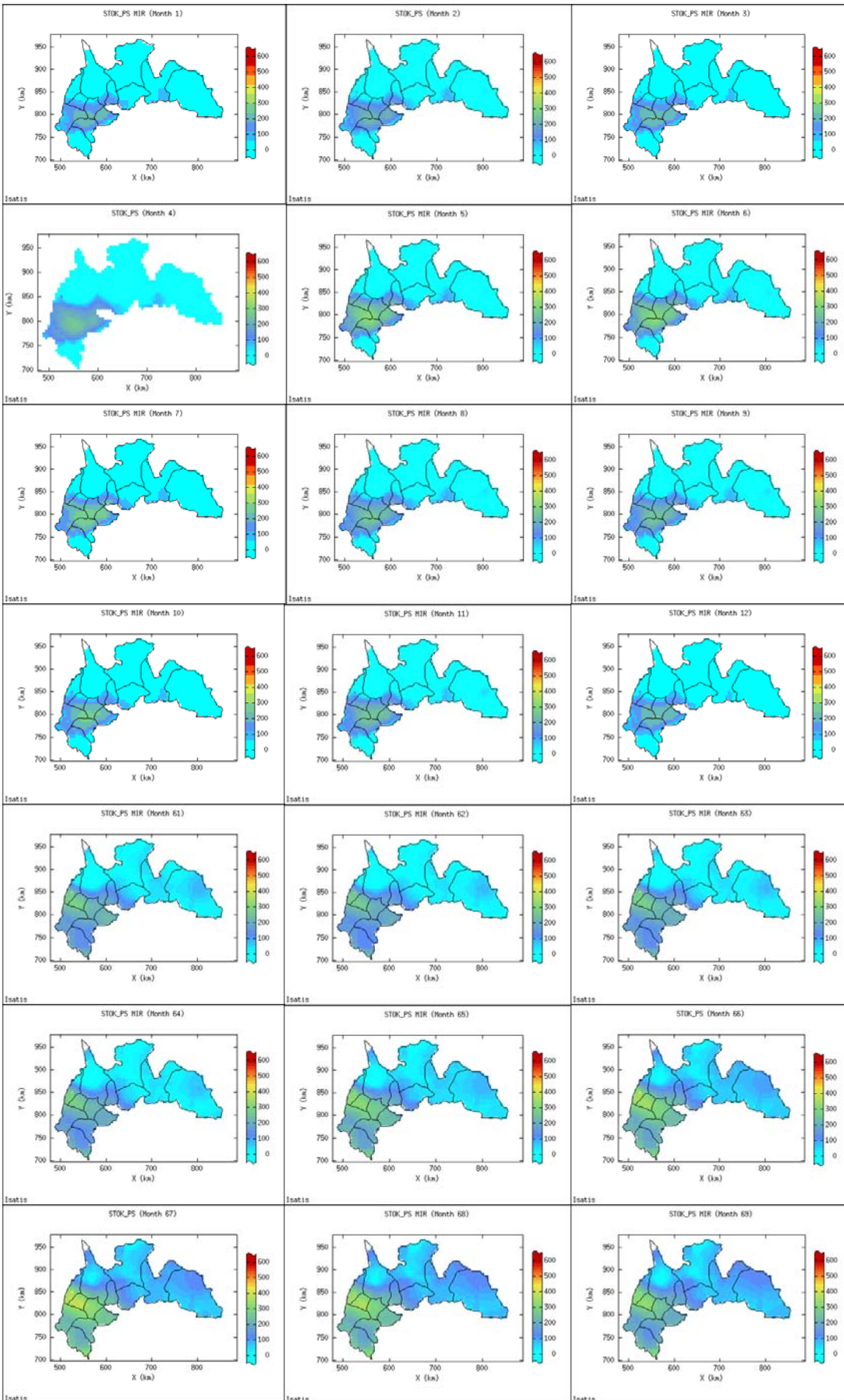
F-3.2: Space-time ordinary kriging of MIR via the generalised product-sum modelling

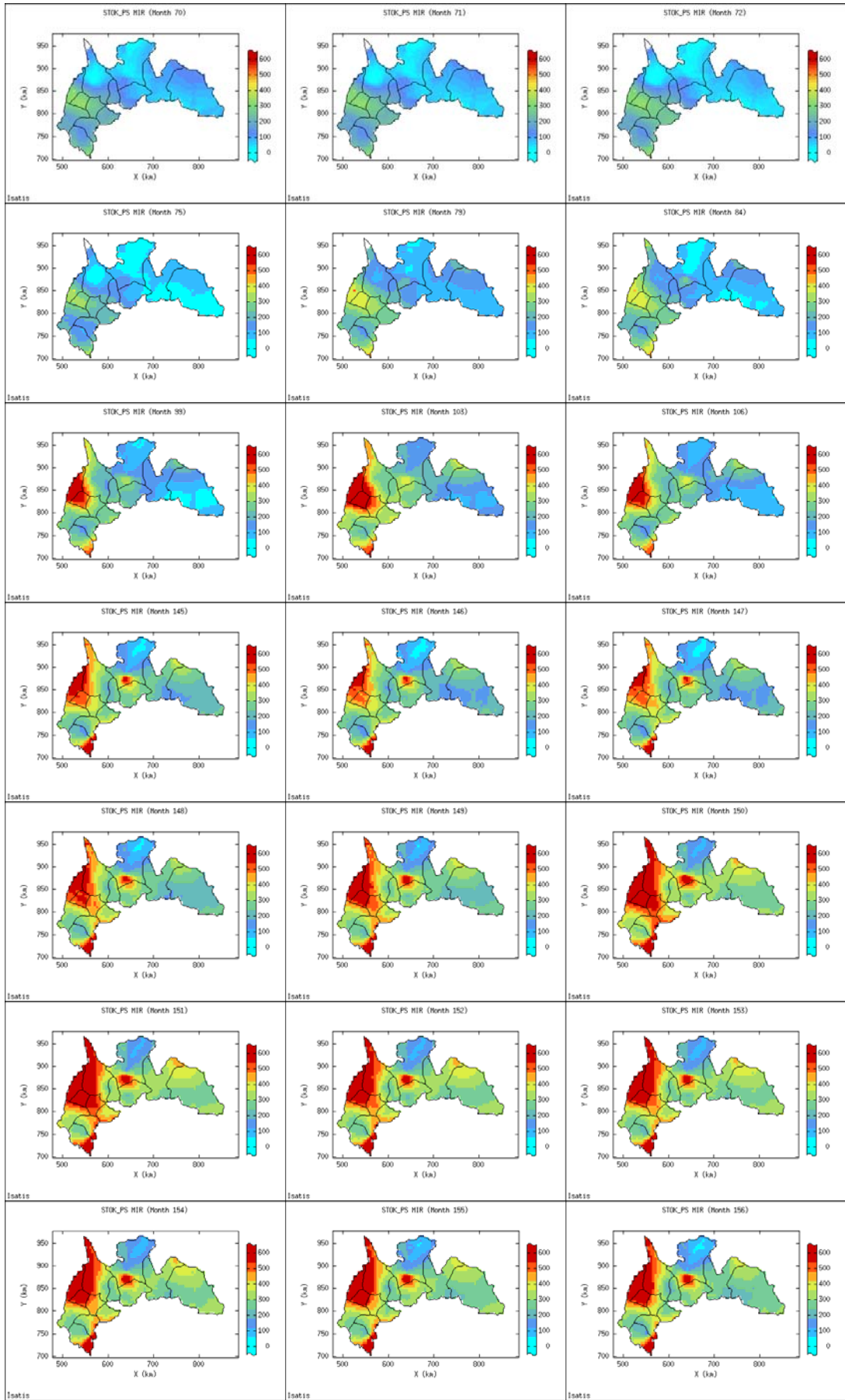
F-3.1: Trend Model produced maps





F-3.2: STROK_PS produced maps





Appendix G: Estimation of Malaria Risk in the Vegetation Zones

G-1: Space-time Semivariogram Models of MIR

Table G-1.1: Space-time semivariogram model parameters of log-transformed malaria incidence rates for the for the vegetation types (northern, forest and coastal)

Zone	Model $\gamma(h)$	Sill c_s/c_t	Spatial range r_s (km)	Temporal range r_t (months)	Relative Nugget
Northern	<i>nugget</i>	0.035	-		
	<i>spherical</i>	0.100	30	100	0.115
	<i>exponential</i>	0.170	170	350	(0.096)
	<i>expcosine</i>	0.058	10000	450	
Forest	<i>nugget</i>	0.020	-	-	
	<i>spherical</i>	0.115	35	90	0.105
	<i>exponential</i>	0.055	180	200	(0.100)
	<i>expcosine</i>	0.010	10000	200	
Coastal	<i>nugget</i>	0.020	-		
	<i>spherical</i>	0.072	30	75	0.125
	<i>exponential</i>	0.068	100	300	(0.118)
	<i>expcosine</i>	0.010	1000	300	

Note: In parentheses are relative nugget effects in the temporal domain.

Table G-1.2: Space-time semivariogram model parameters of residuals of malaria incidence rates for the study in the vegetation types

Zone	Model $\gamma(h)$	Sill	Spatial range r_s (km)	Temporal range r_t (months)	Relative nugget
Northern	<i>nugget</i>	1950	-	-	
	<i>spherical</i>	1500	35	6	0.386
	<i>exponential</i>	1600	140	20	(0.317)
	<i>spherical</i>	1100	10000	30	
Forest	<i>nugget</i>	1200	-	-	
	<i>exponential</i>	1350	40	15	0.436
	<i>spherical</i>	200	160	30	(0.343)
	<i>spherical</i>	750	10000	20	
Coastal	<i>nugget</i>	600	-	-	
	<i>spherical</i>	650	50	10	0.400
	<i>exponential</i>	250	120	20	(0.370)
	<i>spherical</i>	120	10000	15	

Note: In parentheses are relative nugget effects in the temporal domain.

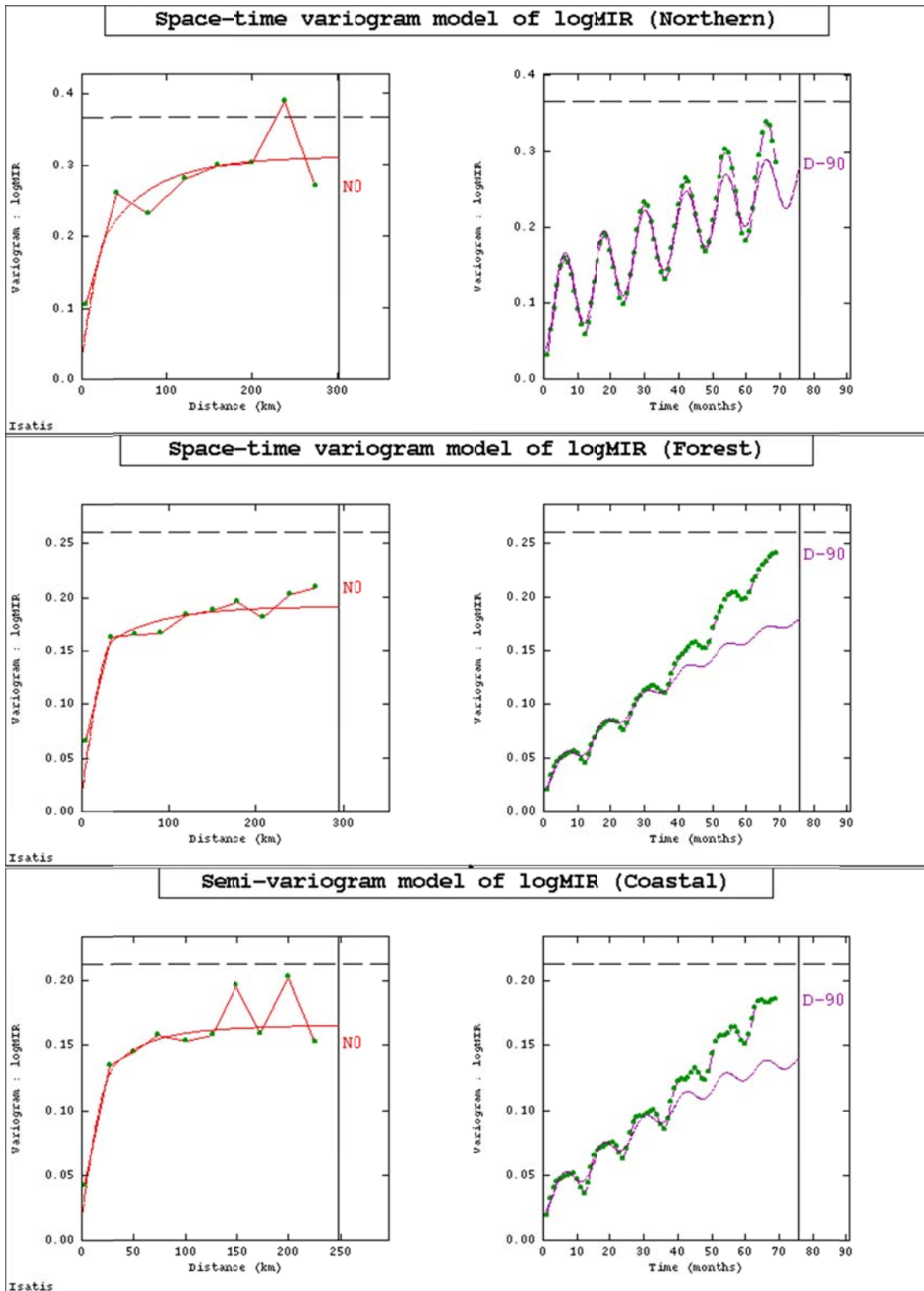


Figure G-1.1: Space-time experimental semivariograms (dotted green) with fitted variogram models showing spatial (left) and temporal (right) autocorrelation of log-transformed malaria incidence rates for the three epidemiological zones: northern savannah (top), rain forest (middle) and coastal savannah (bottom).

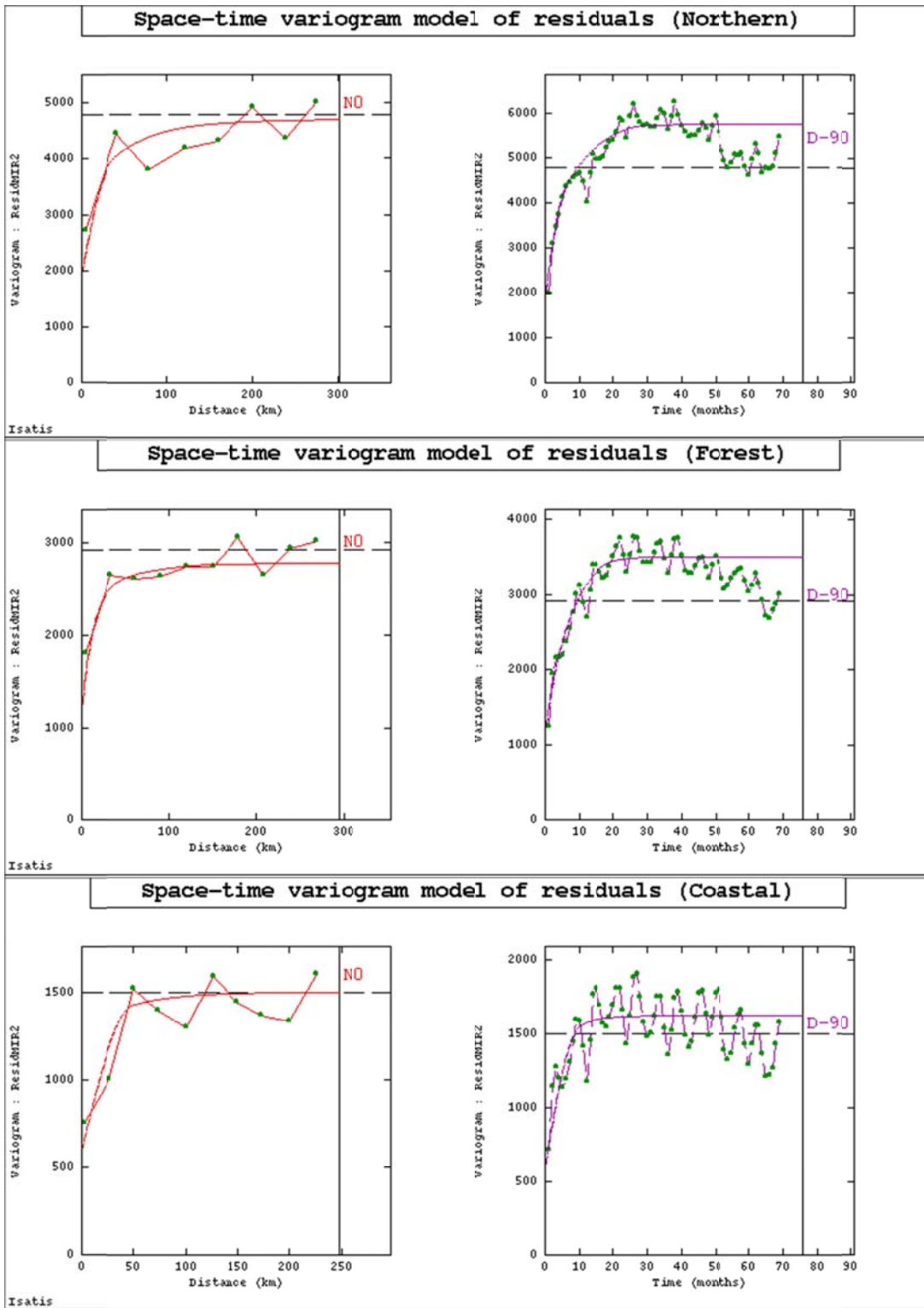


Figure G-1.2: Spatial experimental semivariograms (dotted green) with fitted variogram models of residuals of malaria incidence rates at the three epidemiological zones (northern, forest and coastal).

G-2: Product-sum Semivariogram Models of MIR

Table G-2.1: Parameters of the marginal semivariograms and generalised product-sum semivariogram models of the malaria incidence rates for the study data sets

Zone	Model	Spatial		Temporal		Product-sum	
		Sill	Range	Sill	Range	Global Sill	k
Northern	<i>nugget</i>	8500	-	10800	-	55000	4.227×10^{-6} (2.899×10^{-5})
	<i>spherical</i>	-	-	23700	80		
	<i>exponential</i>	15500	100	-	-		
Forest	<i>expcosine</i>	-	-	-	-	26000	1.713×10^{-5} (6.534×10^{-5})
	<i>nugget</i>	3000	-	1300	-		
	<i>spherical</i>	-	-	14000	85		
	<i>exponential</i>	11500	80	-	-		
Coastal	<i>expcosine</i>	-	-	-	-	15000	1.563×10^{-5} (1.250×10^{-4})
	<i>nugget</i>	2700	-	1000	-		
	<i>spherical</i>	-	-	7000	80		
	<i>exponential</i>	5300	100	-	-		
	<i>expcosine</i>	-	-	-	-		

In parentheses are the relative nugget (RN) effects of marginal semivariograms and maximum k limit values for the product-sum model

Table G-2.2: Parameters of the marginal semivariograms and product-sum semivariogram models of the detrended and deseasonalised malaria incidence rates (residuals) for the study in vegetation zones

Study	Model	Spatial		Temporal		Product-sum	
		Sill	Range	Sill	Range	Global sill	k
Northern	<i>nugget</i>	1950	-	2200	-	6500	1.495×10^{-4} (1.626×10^{-4})
	<i>exponential</i>	2400	100	-	-		
	<i>exponential</i>	-	-	3950	16		
Forest	<i>nugget</i>	1500	-	1000	-	3550	2.804×10^{-4} (2.817×10^{-4})
	<i>exponential</i>	1200	55	-	-		
	<i>exponential</i>	-	-	2500	18		
Coastal	<i>nugget</i>	500	-	600	-	1750	5.620×10^{-4} (6.061×10^{-4})
	<i>exponential</i>	875	100	-	-		
	<i>exponential</i>	-	-	1050	16		

In parenthesis are the maximum limit values of k

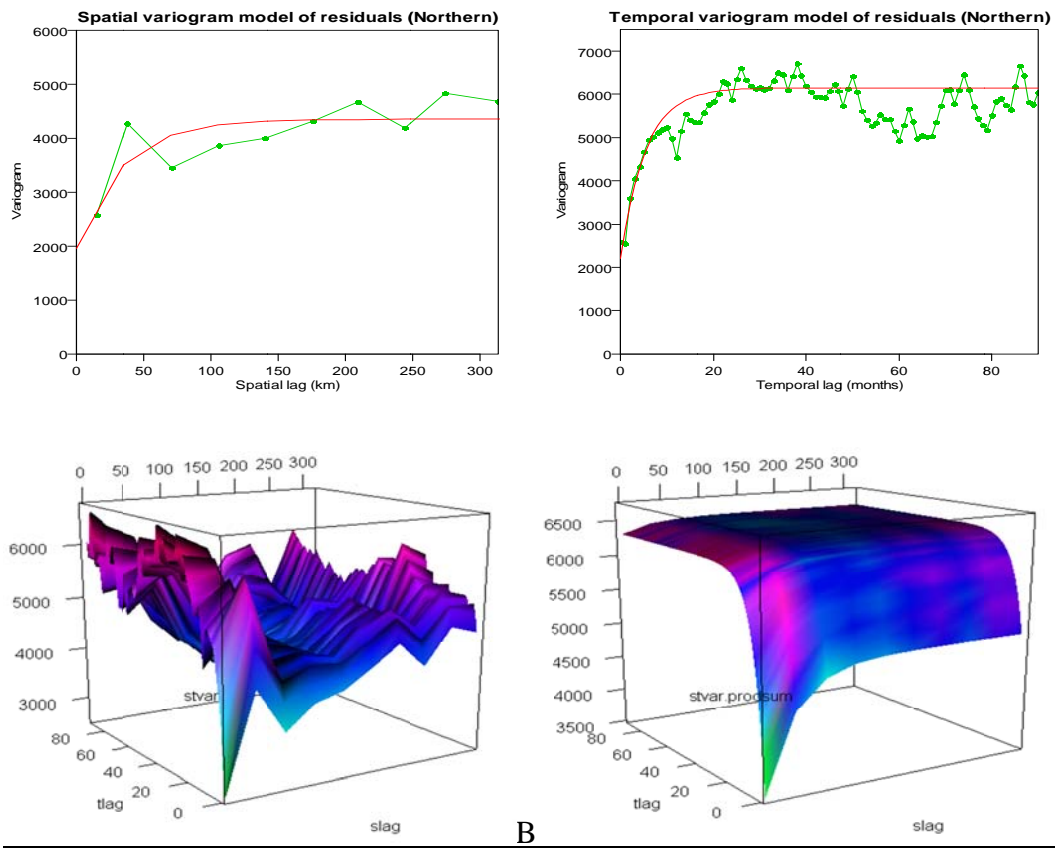
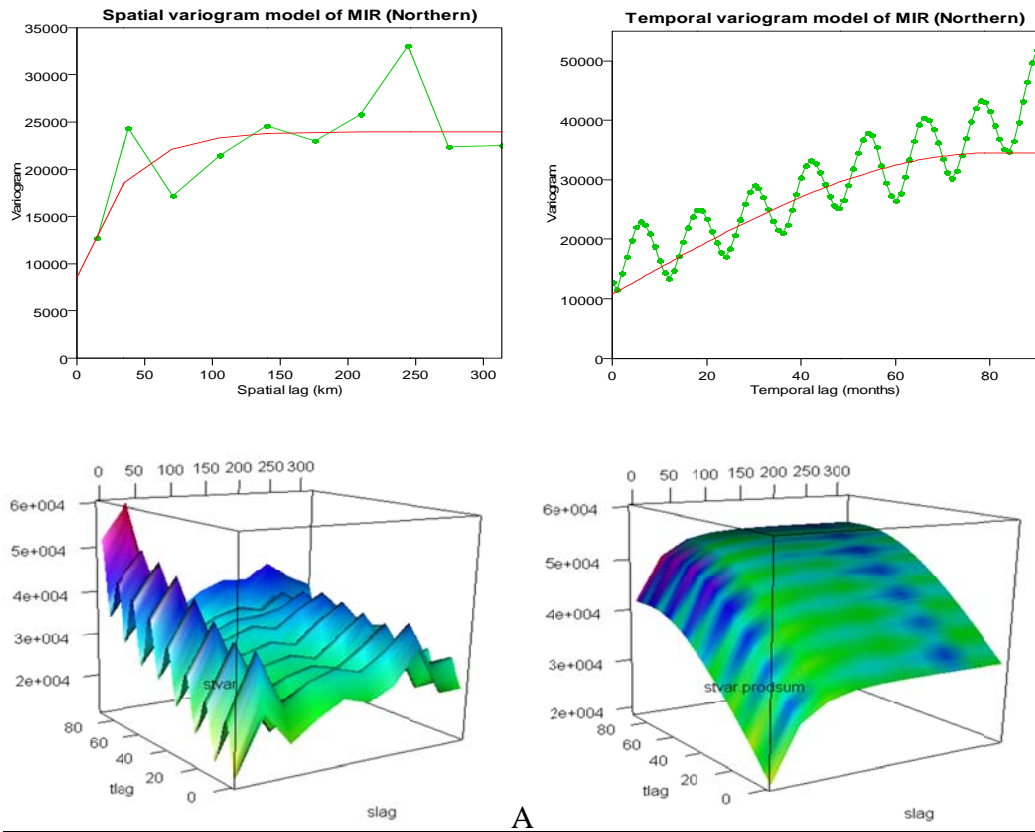


Figure G-2.1: Marginal spatial and temporal semivariograms models and space-time experimental semivariogram surfaces together with their product-sum models of observed malaria incidence rates (top two) and the residuals of incidence rates (top bottom) for the northern savannah zone

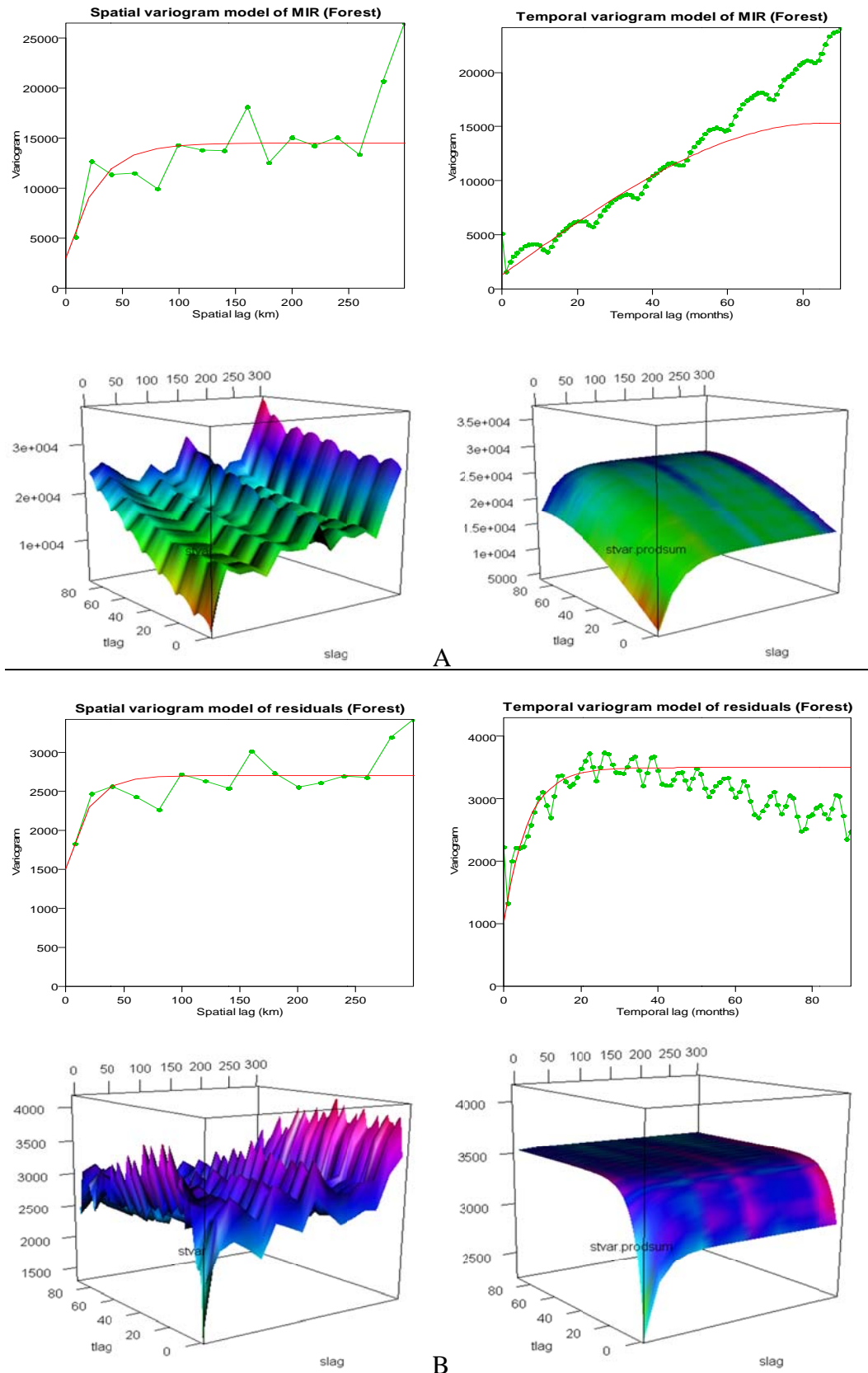
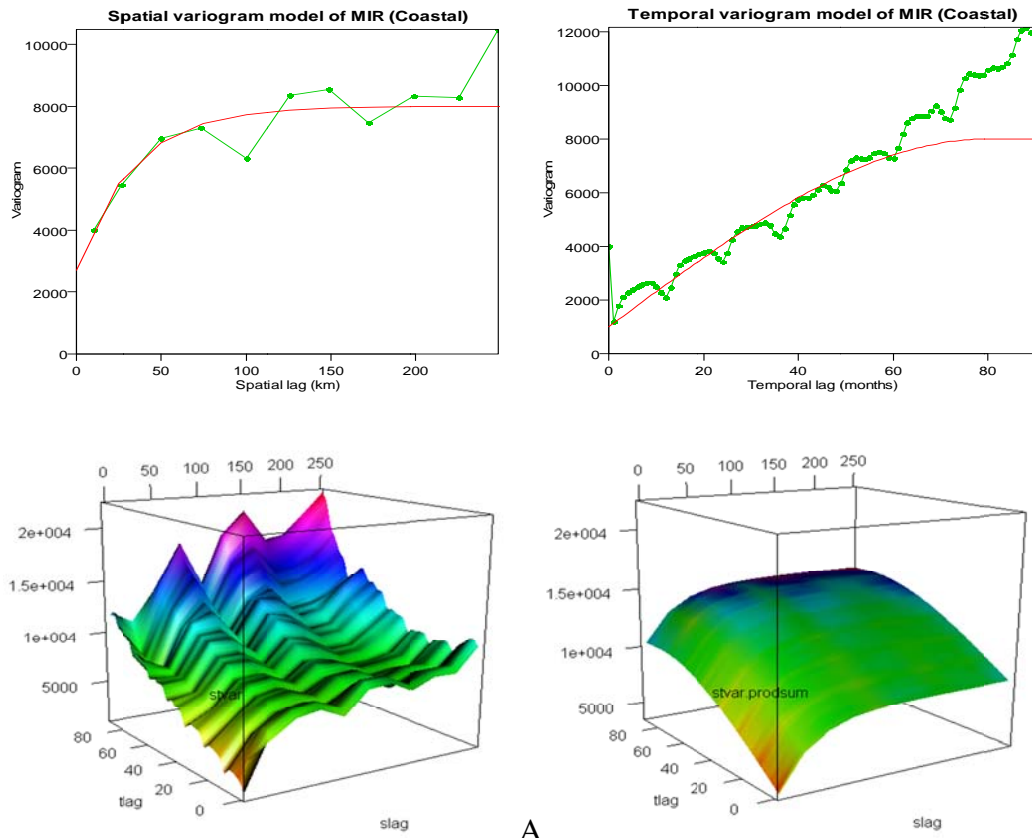
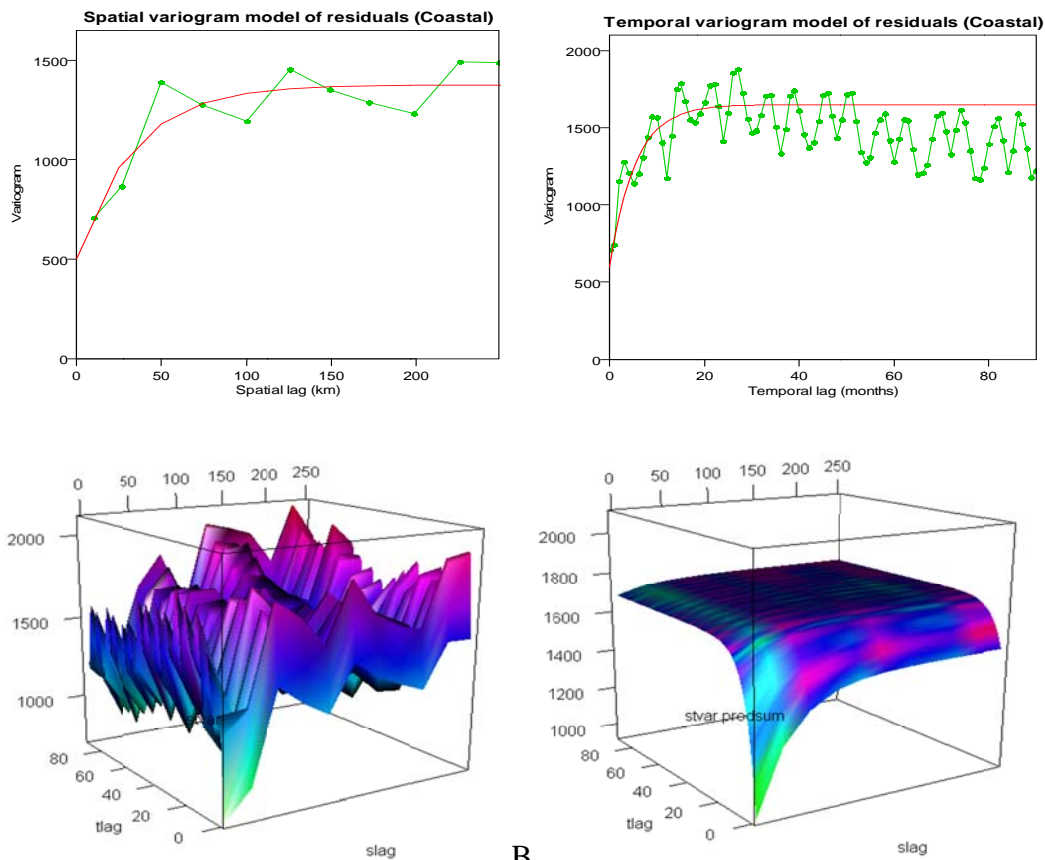


Figure G-2.2: Marginal spatial and temporal semivariograms models and space-time experimental semivariogram surfaces together with their product-sum models of observed malaria incidence rates (top two) and the residuals of incidence rates (bottom two) for the tropical forest zone



A



B

Figure G-2.3: Marginal spatial and temporal semivariograms models and space-time experimental semivariogram surfaces together with their product-sum models of observed malaria incidence rates (top two) and the residuals of incidence rates (bottom two) for the coastal savannah/mangrove zone

G-3: Space-time LMC of Residuals with Potential Climate Covariates

Table G-3.1: Parameters of space-time linear models of coreginalination of detrended malaria incidence rates (residuals) with lagged one month rainfall, maximum temperature and relative humidity (at 1500 hours) for the vegetation zones study

Northern	Spatial			Temporal
Variable	$nug(h_0)$	$exp(h/40)$	$sph(h/170)$	$cosexp$ ($h/10-100$)
Residuals	2600	2800	500	4200
Rainfall_1	1500	1200	150	5000
Resid & Rainf_1	450	250	50	3900
Variable	$nug(h_0)$	$exp(h/40)$	$sph(h/170)$	$cosexp$ ($h/10-200$)
Residuals	2600	2800	500	4500
MaxTemp_1	1.50	1	0.4	5.5
Resid & MaxT_1	-30	15	10	-150
Variable	$nug(h_0)$	$exp(h/40)$	$sph(h/250)$	$cosexp$ ($h/10-100$)
Residuals	2600	2800	500	4500
RH1500_1	40	8	5	3300
Resid & RH1500_1	85	50	-50	1100
Forest	Spatial			Temporal
Variable	$nug(h_0)$	$exp(h/45)$	$sph(h/180)$	$cosexp$ ($h/10-80$)
Residuals	1300	1350	250	1000
Rainfall_1	2000	1150	450	2700
Resid & Rainf_1	180	150	30	1000
Variable	$nug(h_0)$	$exp(h/45)$	$sph(h/180)$	$cosexp$ ($h/10-80$)
Residuals	1300	1200	300	300
RH1500_1	20	20	5	110
Resid & RH1500_1	-10	30	-5	35
Coastal	Spatial			Temporal
Variable	$nug(h_0)$	$exp(h/50)$	$sph(h/120)$	$cosexp$ ($h/6-100$)
Residuals	600	580	200	520
Rainfall_1	1500	2100	1000	3000
Resid & Rainf_1	500	-500	200	850

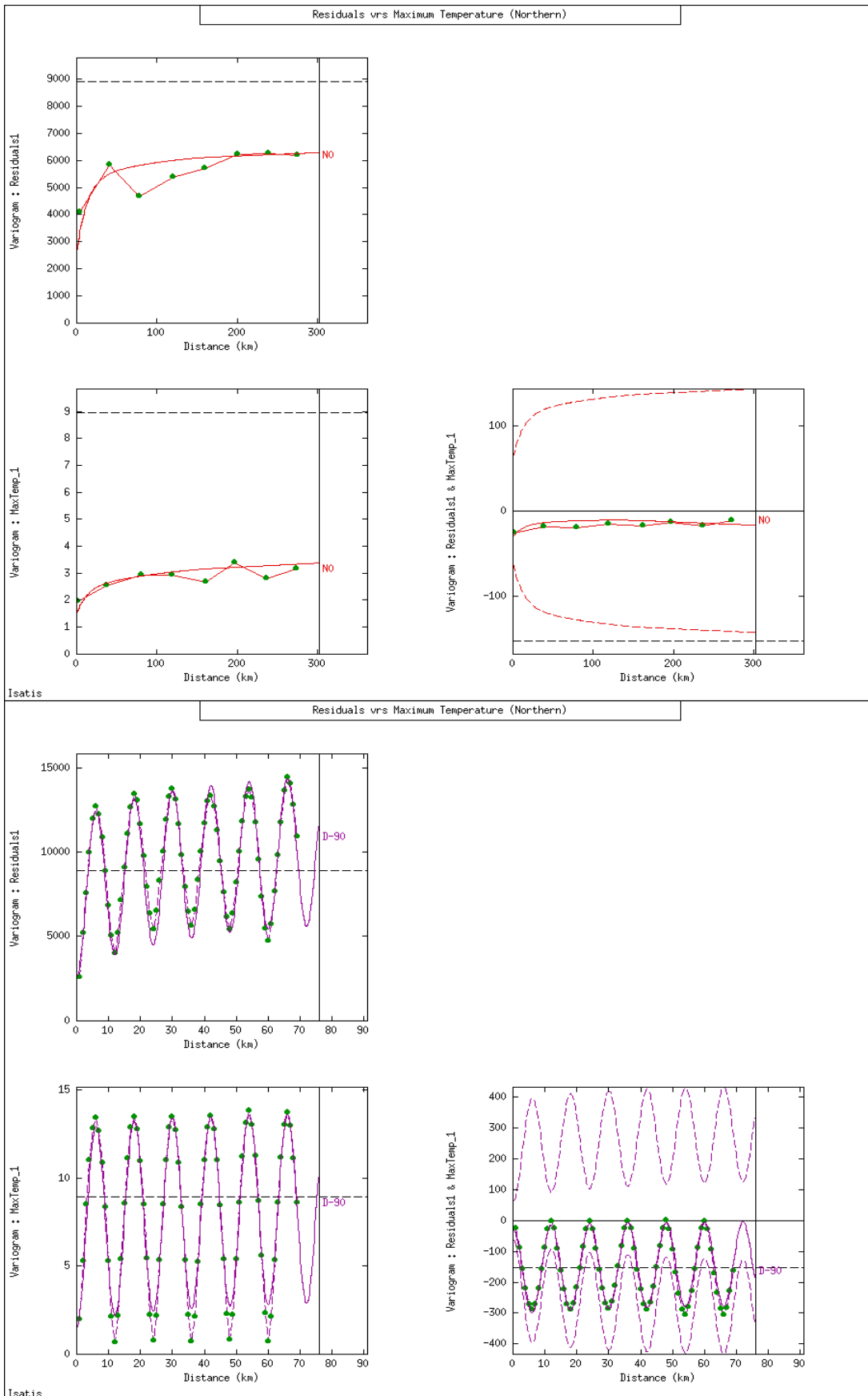


Figure G-3.1a: Space-time linear model of coregionalisation of detrended MIR (residuals) with lagged 1 maximum temperature in the northern zone.

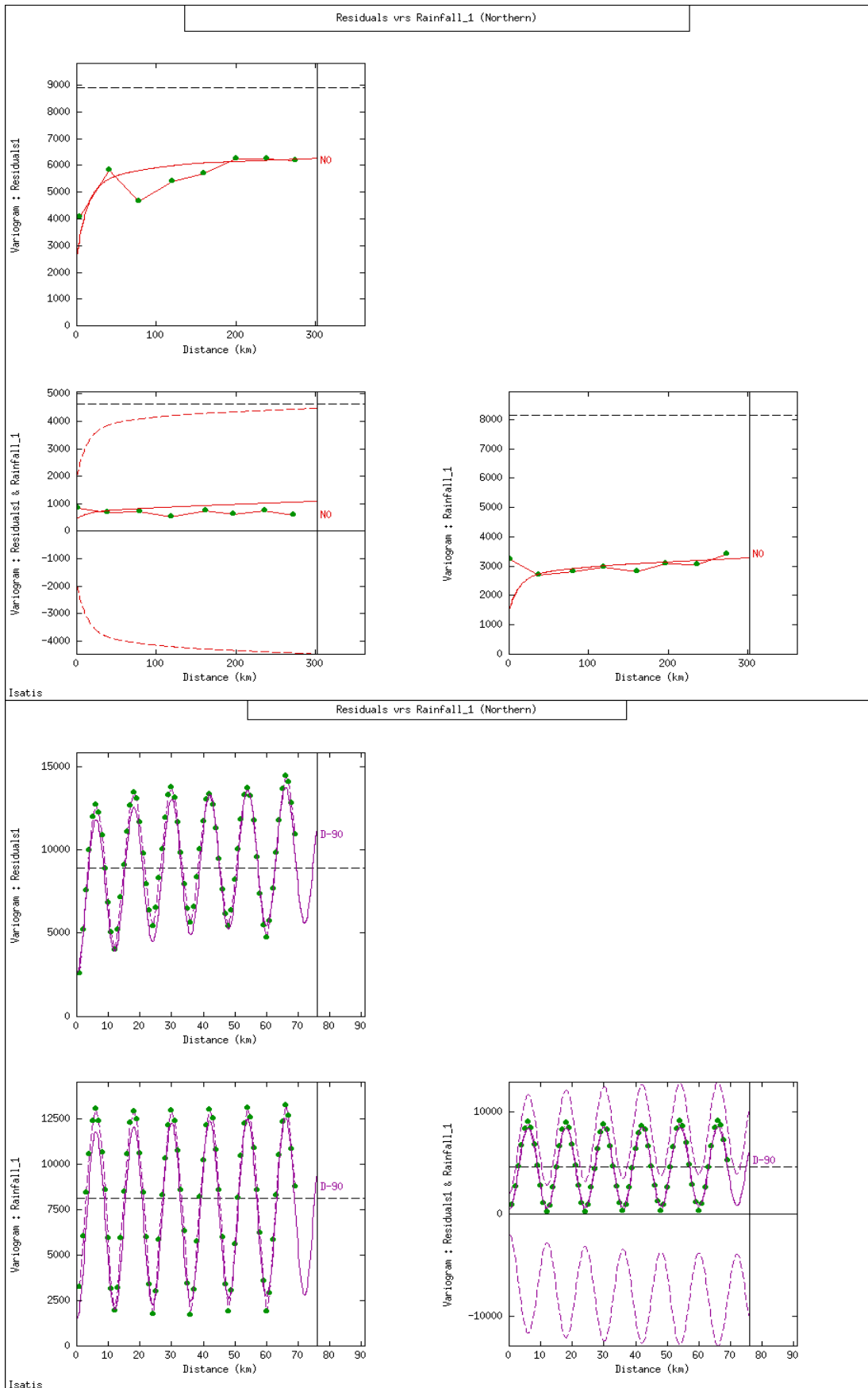


Figure G-3.1b: Space-time linear model of coregionalisation of detrended MIR (residuals) with lagged 1 month rainfall in the northern zone.

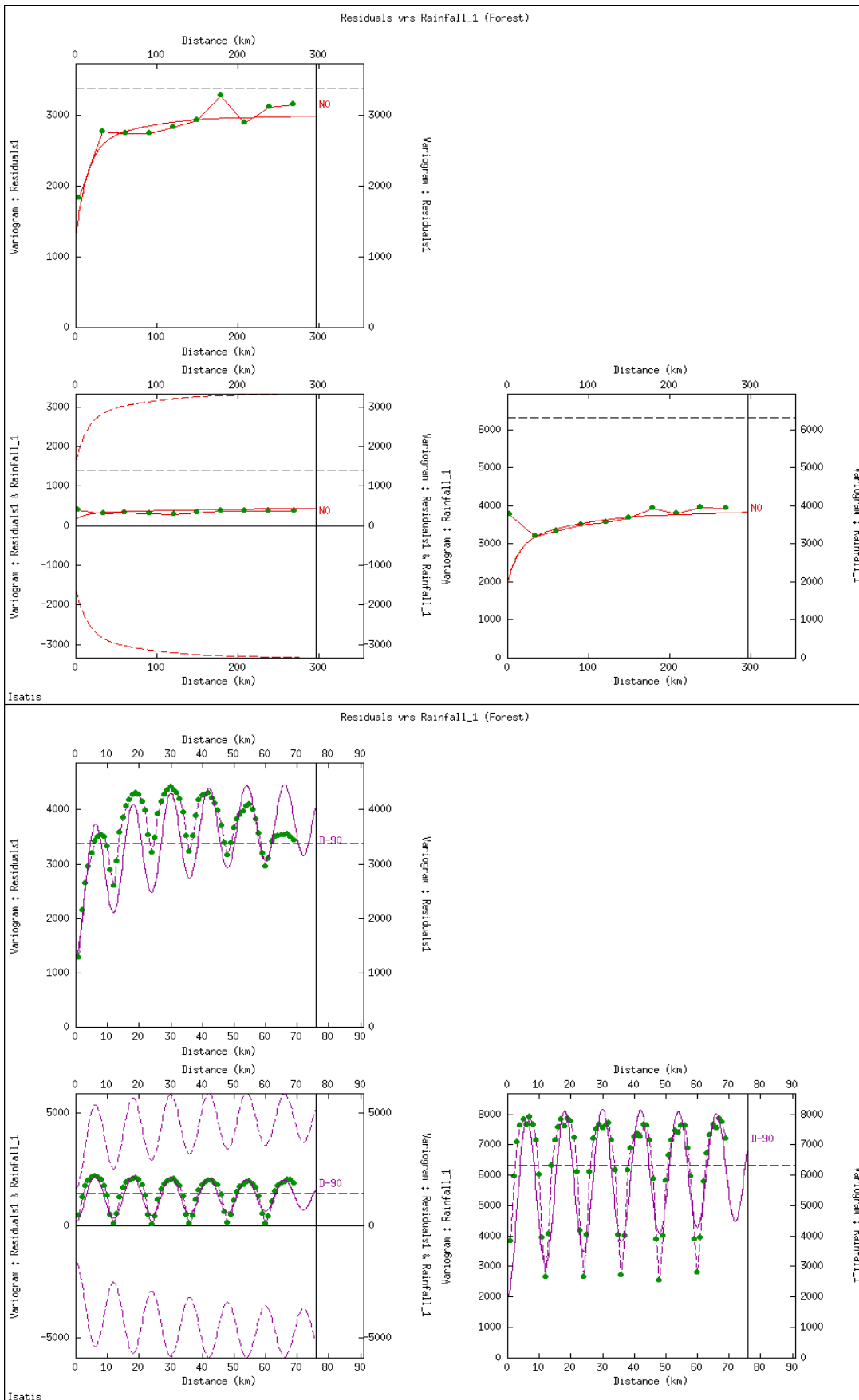


Figure G-3.2: Space-time linear model of coregionalisation of detrended MIR (residuals) with lagged 1 month rainfall in the forest zone.

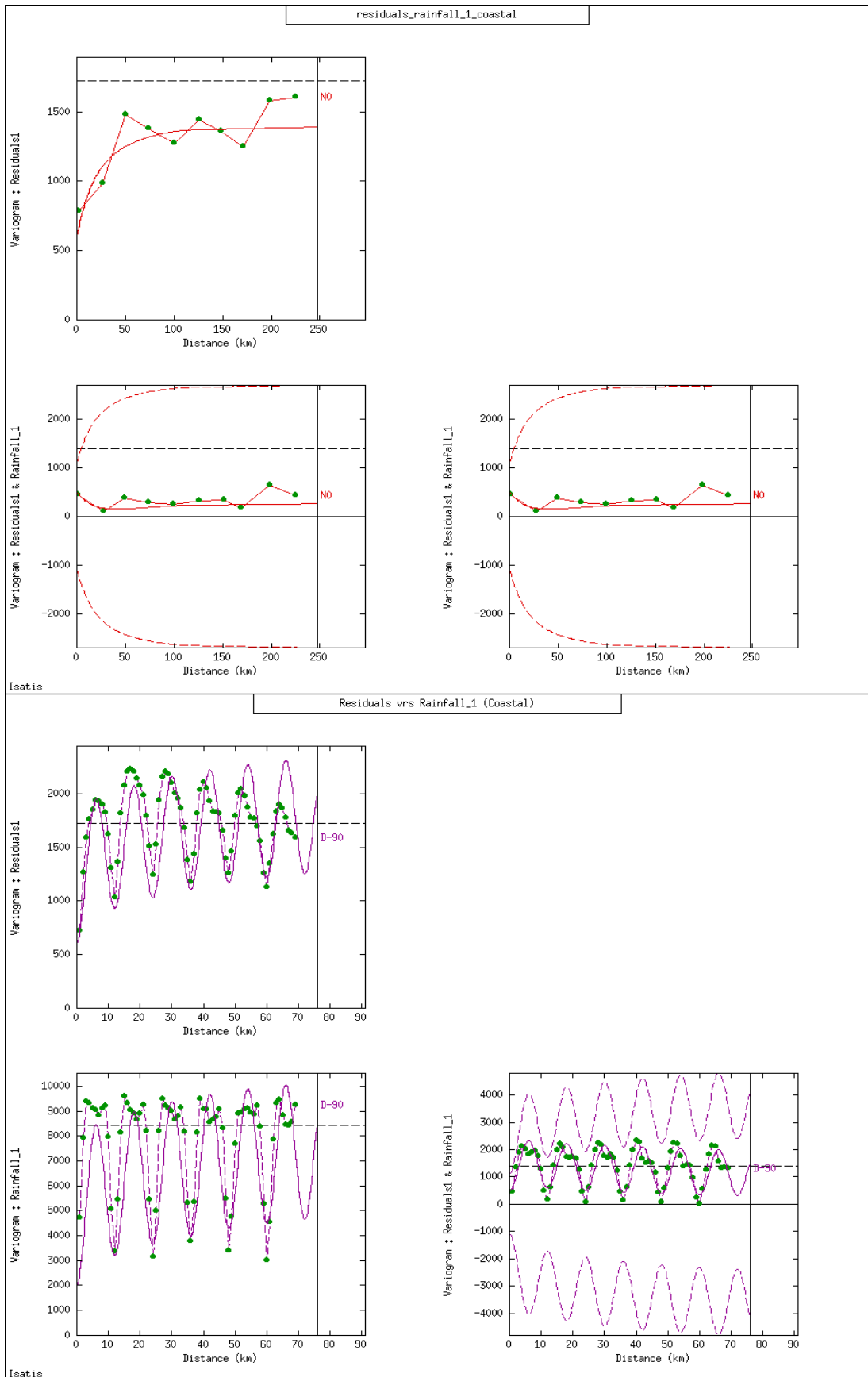


Figure G-3.3: Space-time linear model of coregionalisation of detrended MIR (residuals) with lagged 1 month rainfall in the coastal zone.

Appendix H: Programme Codes for Data Analysis

H-1: R Codes for Detrending and Deseasonalising and SARIMA Model Fitting

H-1.1: Code to detrend and deseasonalise MIR

```
*****
rm(list=ls())head
setwd("C:/Analysis/Regression")
options(digits=4)
maindat=read.csv("MainData144.csv",header=T,na="N/A")
main=split(maindat,maindat$District)
for(i in 1:length(main)){
  mir.k=main[[i]]$MIR
  t=1:length(mir.k)
  t2=t^2
  cost=cos((2*pi)/12*t)
  sint=sin((2*pi)/12*t)
  fac=gl(12,1,length=length(mir.k),label=c("jan","feb","mar","apr","may","jun","jul","aug","sep","oct","nov","dec"))
  fit1=lm(mir.k~t+t2,na.action=na.exclude)
  fit2=lm(mir.k~t+t2+cost+sint,na.action=na.exclude)
  fit3=lm(mir.k~t+t2+fac,na.action=na.exclude)
  residuals1=residuals(fit1)
  residuals2=residuals(fit2)
  residuals3=residuals(fit3)
  trend1=fitted(fit1)
  trend2=fitted(fit2)
  trend3=fitted(fit3)
  rsquare1=summary(fit1)$r.squared
  rsquare2=summary(fit2)$r.squared
  rsquare3=summary(fit3)$r.squared
  coeffit1=coef(fit1)
  coeffit2=coef(fit2)
  coeffit3=coef(fit3)
  main[[i]]=data.frame(residuals1,residuals2,residuals3,trend1,trend2,trend3,main[[i]])
}
maindata=do.call("rbind",main)
write.csv(maindata,file="MainData132_1.csv")
```

H-1.2: Regression Analysis of the Residuals with the Climatic Covariates

```
*****
```

Data input:

```
baregdata=read.csv("BAREgData.csv",header=T,na="N/A")
bar=ts(baregdata,start=c(1998,1),freq=12)
barregdata2011= read.csv("BAREgData2011.csv",header=T,na="N/A")
bar2011=ts(baregdata2011,start=c(2011,1),freq=12)
mir=bar[,1]
mir05=bar[,2]
rainf=bar[,3]
maxT=bar[,4]
minT=bar[,5]
rh0600=bar[,7]
rh1500=bar[,8]
```

```

sunsh=bar[,9]
rainf_1=lag(rainf,-1)
rainf_2=lag(rainf,-2)
maxT_1=lag(maxT,-1)
maxT_2=lag(maxT,-2)
minT_1=lag(minT,-1)
minT_2=lag(minT,-2)
rh0600_1=lag(rh0600,-1)
rh0600_2=lag(rh0600,-2)
rh1500_1=lag(rh1500,-1)
rh1500_2=lag(rh1500,-2)
sunsh_1=lag(sunsh,-1)
sunsh_2=lag(sunsh,-2)

```

Multiple linear regression model:

```

t=1:length(mir)
t2=t^2
fit=lm(mir~t+t2,na.action=na.exclude)
res=residuals(fit)
t=1:length(mir05)
t2=t^2
fit05=lm(mir05~t+t2,na.action=na.exclude)
res05=residuals(fit05)
resbar=data.frame(res,res05)
resba=ts(resbar,start=c(1998,1),freq=12)
resid=resba[,1]
resid05=resba[,2]
badata2=ts.intersect(mir,mir05,resid,resid05,rainf,rainf_1,rainf_2,maxT,maxT_1,maxT_2,minT,minT_1,
,minT_2,rh0600,rh0600_1,rh0600_2,rh1500,rh1500_1,rh1500_2,sunsh,sunsh_1,sunsh_2)
badata1=ts.intersect(mir,mir05,resid,resid05,rainf,rainf_1,maxT,maxT_1,minT,minT_1,rh0600,rh0600_
1,rh1500,rh1500_1,sunsh,sunsh_1)
badata0=ts.intersect(mir,mir05,resid,resid05,rainf,maxT,minT,rh0600,rh1500,sunsh)
modelbar3=dynlm(resid~rainf_1+rainf_2+maxT_1+maxT_2+minT_1+minT_2+rh0600_1+rh0600_2+r
h1500_1+rh1500_2+sunsh_1+sunsh_2,data=badata2,na.action=na.exclude)
modelbar3_05=dynlm(resid05~rainf_1+rainf_2+maxT_1+maxT_2+minT_1+minT_2+rh0600_1+rh060
0_2+rh1500_1+rh1500_2+sunsh_1+sunsh_2,data=badata2,na.action=na.exclude)
modelbar2=dynlm(resid~rainf+rainf_1+rainf_2+maxT+maxT_1+maxT_2+minT+minT_1+minT_2+rh0
600+rh0600_1+rh0600_2+rh1500+rh1500_1+rh1500_2+sunsh+sunsh_1+sunsh_2,data=badata
2,na.action=na.exclude)
modelbar2_05=dynlm(resid05~rainf+rainf_1+rainf_2+maxT+maxT_1+maxT_2+minT+minT_1+minT_
2+rh0600+rh0600_1+rh0600_2+rh1500+rh1500_1+rh1500_2+sunsh+sunsh_1+sunsh_2,data=
badata2,na.action=na.exclude)
modelbar1=dynlm(resid~rainf+rainf_1+maxT+maxT_1+minT+minT_1+rh0600+rh0600_1+rh1500+rh1
500_1+sunsh+sunsh_1,data=badata1,na.action=na.exclude)
modelbar1_05=dynlm(resid05~rainf+rainf_1+maxT+maxT_1+minT+minT_1+rh0600+rh0600_1+rh15
00+rh1500_1+sunsh+sunsh_1,data=badata1,na.action=na.exclude)
modelbar0=dynlm(resid~rainf+maxT+minT+rh0600+rh1500+sunsh,data=badata0,na.action=na.exclude
)
modelbar0_05=dynlm(resid05~rainf+maxT+minT+rh0600+rh1500+sunsh,data=badata0,na.action=na.e
xclude)
options(digits=4)
cor(badata2)

```

H-1-3: Autocorrelation Analysis of Residuals and SARIMA Model fitting

Residuals Analysis:

```
par(mfrow=c(2,2),mex=0.5)
plot(residbar,main="Residuals: Brong Ahafo",ylab="residuals")
qqnorm(residbar,main="Q-Q Plot",col=2)
qqline(residbar,main="Q-Q Plot")
acf(as.vector(residbar),lag.max=50,main="ACF")
pacf(as.vector(residbar),lag.max=50,main="PACF")
```

SARIMA Model fitting:

```
modelbar=arima(mir,order=c(3,1,0),seasonal=list(order=c(0,1,1),period=12))
residbar=modelbar$residual
mae=sum(abs(residbar))/length(residbar)
rmse=sqrt(sum(residbar^2)/length(residbar))
Box.test(residbar,lag=12)
Box.test(residbar,lag=100)
Shapiro.test(residbar)
cor(badata2)
summary(step(modelbar2))
badata=ts.intersect(mir,mir05,resid,resid05,maxT,maxT_1,rh0600,rh0600_1,rh1500,rh1500_1,sunsh)
summary(step(modelbar2))
```

Lyung-Box Q-Test:

```
{
  oldpar<-par(mfrow=c(3,1),mex=0.8)
  on.exit(par(oldpar))
  rs<-modelbarx$residuals
  stdres<-rs/sqrt(modelbar05x$sigma2)
  plot(stdres,type="h",main="Standardized Residuals_X: Brong
  Ahafo",ylab="",xlab="Time",ylim=c(-3,4))
  abline(h=0,col=2)
  acf(as.vector(modelbarx$residuals),lag.max=100,plot=TRUE,main="ACF of
  Residuals",xlab="Lag",na.action=na.pass)
  abline(h=0,col=2)
  nlag<-100
  pval<-numeric(nlag)
  for (i in 1:nlag)
  pval[i]<-Box.test(rs,i,type="Ljung-Box")$p.value
  plot(1:nlag,pval,xlab="Lag",ylab="p value",ylim=c(0,1),col=2,main="p values for Ljung-Box
  statistic")
  abline(h=0.05,lty=2,col="blue")
}
tsdiag(modelbar,gof.lag=100)
```

Model Forecast:

```
par(mfrow=c(1,1),mex=0.5)
modelbar05=arima(mir05,order=c(0,1,2),seasonal=list(order=c(0,1,1),period=12))
modelbar05_pr=predict(modelbar05,n.ahead=36)
U=modelbar05_pr$pred+2*modelbar05_pr$se
L=modelbar05_pr$pred-2*modelbar05_pr$se
plot(mir05,main="Brong Ahafo (0-4)",xlim=c(1998,2014),ylim=c(100,900),ylab="Incidence Rate")
lines(U,col=3,lty=2)
lines(L,col=3,lty=2)
lines(modelbar05_pr$pred,col=2,lwd=2)
lines(bar2011[,2],col=4,lwd=2)
abline(v=2011,col=4,lty=1)
abline(v=seq(1998,2014,1),lty="dotted")
legend(1998,400,c("Real","Forecast","95% CI","Real_2011"),col=c(1,2,3,4),lty=2)
```

H-2: GSLIB Programmes for Generalised Product-sum Modelling of Semivariograms

H-2.1: Parameter file for GAMV executable programme for the experimental semivariograms of MIR and the residuals

Parameters for GAMV:

START OF PARAMETERS:

```

forest.dat          \data file
1 2 3              \column for x,y,t coordinates
1 6               \nvar; column numbers...
-9000.0 1.0e21    \tmin, tmax (trimming limits)
national.var       \output file for variograms
15               \nlag - the number of spatial lags
30               \xlag - unit separation distance
15               \xltol- lag tolerance
90               \ntlag - the number of temporal lags
1               \tlag - unit separation distance
1               \ndir - number of directions
0.0 90.0 15000 0 0 0 \azm,atol,bandh,dip,dtol,bandv
0               \standardize sills? (0=no, 1=yes)
1               \number of variograms
1 1 1            \tail, head, variogram type
  
```

H-2.2: Parameter file for K2ST executable programme for the estimation of malaria morbidity incidence rates

Parameters for KT3D:

START OF PARAMETERS:

```

national.dat       \data file
1 2 3 6 0         \columns for X,Y,Z,var,sec var
-2000.0 1.0e21    \trimming limits
2               \option:0=grid,1=cross,2=jackknife
national2011.dat  \file with jackknife data
1 2 3 6 0         \columns for X,Y,Z,vr and sec var
2               \debugging level:0,1,2,3
national.dbg      file for debugging output
nationalOK.dat    file for debugging output
nationalOK.dat    file for kriged output
52 470 10        \nx,xmn,xsiz
76 520 10        \ny,ymn,ysiz
12 133 1         \nz,zmn,zsiz
1 1 1            \x,y and z block discretization
8 20             \min,max data for kriging
0               \max per octant(0-> not used)
200 200 15       \maximum search radii
0.0 0.0 0.0      \angles for search ellipsoid
1 0              \0=SK,1=OK,2=non-st SK,3=exdrift
0 0 0 0 0 0 0 0  \drift:x,y,z,xx,yy,zz,xy,xz,zy
0               \0,variable;1,estimate trend
  
```

nodata.dat	\gridded file with drift/mean
0	\column number in gridded file
2 5000	\nst,spatial nugget effect
2 10200 0.0 0.0 0.0	\it,cc,ang1,ang2,ang3
120 120 120	\a_hmax,a_hmin, a_vert
6 15500 0.0 0.0 0.0	\it,cc,ang1,ang2,ang3
100 100 100	\a_hmax,a_hmin,a_vert
5000 28000	\temporal nugget,global sill
1	\0=product,1=sum-product

Appendix I: Supporting Conference Publication and Poster Presentation

The following peer-reviewed conference and poster presentations support the work in the thesis.

I-1: Conference Presentation:

Appiah, S. K., Mueller, U., & Cross, J. (2011). Spatio-temporal modelling of malaria incidence for evaluation of public health policy interventions in Ghana, West Africa. Paper presented at the MODSIM 2011, 19th International Congress on Modelling and Simulation. Modelling and Simulation Society of Australia and New Zealand, F. Chan, D. Msrinova & R.S. Anderson (eds), December, 2011 Perth, Australia. www.mssanz.org.au/modsim2011/A10/appiah.pdf

I-2: Poster Presentation:

Appiah, S. K., Mueller, U., & Cross, J. (2011). Exploratory analysis of malaria risk in Ghana, West Africa. ECU industry engagement 2011, Perth, WA

Exploratory Analysis of Malaria Risk in Ghana, West Africa

Simon K. Appiah, Ute Mueller and Jim Cross
School of Engineering, Edith Cowan University, Western Australia

Background

Ghana's malaria risk poses a serious threat to health delivery system. Malaria is the leading cause of morbidity and mortality (38.6% of all outpatient illness), most vulnerable children under 5 years and pregnant women.

Spatial and temporal statistical models are applied to monthly morbidity cases reported from local health facilities; geostatistical space-time lognormal kriging is used to estimate malaria incidence rates (MIR) at unobserved locations.

The Results serve baseline for resource allocation for the disease's prevention.

Method

Ghana (in West Africa) has 10 administrative regions each subdivided into districts. Time series were considered for them individually.

Modelling was done using monthly MIR (number of morbidity cases per resident population of 10,000).

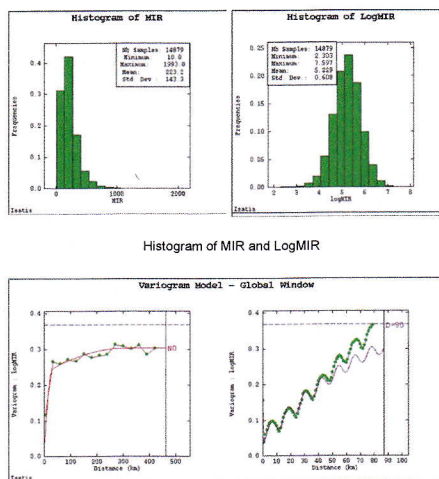
Time series moving average smoothing were used for behaviour and trend pattern of global incidence at regions.

Lognormal kriging was employed to interpolate disease risk.

Results

Malaria risk maps indicate varied spatial and temporal distribution with elevated

numbers of cases in the northern and central parts of the country.



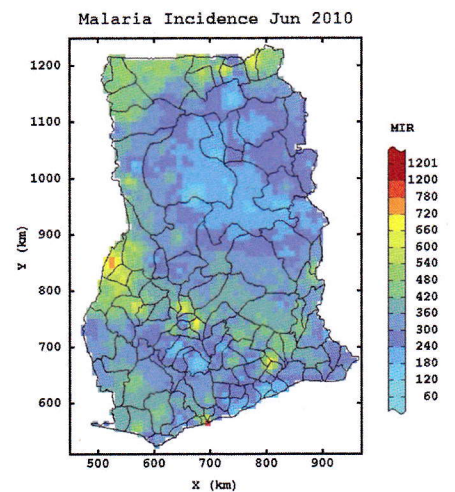
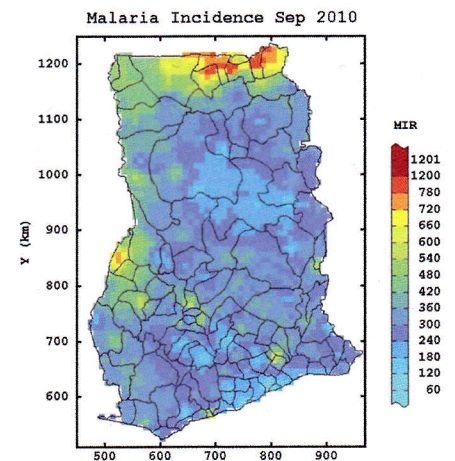
Variography of spatial and temporal directions of MIR

Conclusions

Time series and spatial maps of malaria incidence provide useful analytical tools for resource allocation to reduce the disease at the local level in Ghana.

Time series plots indicate that malaria incidence has been increasing until 2009 but is now levelling off in the regions of Ghana. Seasonal patterns over the years are similar for the regions.

Spatial maps indicate that the distribution of malaria incidence across Ghana is heterogeneous, with elevated incidence values in the northern and central parts.



Acknowledgements

Centre for Health Information and Management of Ghana Health Service for the data and Edith Cowan University for financial support.

